Philip G. Burke

SPRINGER SERIES ON ATOMIC, OPTICAL, AND PLASMA PHYSICS 61

R-Matrix Theory of Atomic Collisions

Application to Atomic, Molecular and Optical Processes

Springer

Springer Series on
ATOMIC, OPTICAL, AND PLASMA PHYSICS 61

Springer Series on

ATOMIC, OPTICAL, AND PLASMA PHYSICS

The Springer Series on Atomic, Optical, and Plasma Physics covers in a comprehensive manner theory and experiment in the entire field of atoms and molecules and their interaction with electromagnetic radiation. Books in the series provide a rich source of new ideas and techniques with wide applications in fields such as chemistry, materials science, astrophysics, surface science, plasma technology, advanced optics, aeronomy, and engineering. Laser physics is a particular connecting theme that has provided much of the continuing impetus for new developments in the field. The purpose of the series is to cover the gap between standard undergraduate textbooks and the research literature with emphasis on the fundamental ideas, methods, techniques, and results in the field.

Please view available titles in *Springer Series on Atomic, Optical, and Plasma Physics* on series homepage http://www.springer.com/series/411

Philip G. Burke

R-Matrix Theory of Atomic Collisions

Application to Atomic, Molecular and Optical Processes

With 110 Figures

Springer

Professor Philip G. Burke
School of Mathematics and Physics
David Bates Building
Queen's University
Belfast BT7 1NN, UK
p.burke@qub.ac.uk

Springer Series on Atomic, Optical, and Plasma Physics ISSN 1615-5653

ISBN 978-3-642-15930-5 e-ISBN 978-3-642-15931-2
DOI 10.1007/978-3-642-15931-2
Springer Heidelberg Dordrecht London New York

Cover design: Integra Software Services Pvt. Ltd., Pondicherry

Printed on acid-free paper

Springer is part of Springer Science+Business Media (www.springer.com)

To my wife Val

Preface

Research on processes which occur when electrons, positrons and photons collide with atoms, ions and molecules has seen a rapid increase in interest, both experimentally and theoretically, in recent years. This is partly because these processes provide an ideal means of investigating the dynamics of many-particle systems at a fundamental level and partly because a detailed understanding of these processes is required in many fields, particularly in the analysis of astronomical observations, in plasma physics including controlled thermonuclear fusion, in the interaction of super intense lasers with atoms and molecules, in atmospheric physics and chemistry including global warming, in isotope separation, in electrical discharges in gases and in electron surface interaction processes.

In recent years a number of important advances have been made in both experiment and theory. On the experimental side these advances include the absolute measurement of cross sections, the development of coincidence techniques, the use of polarized beams and targets, the development of very high resolution electron beams, the application of new light sources, the development of femtosecond and attosecond laser beams and a rapidly increasing number of studies using high-resolution positron and positronium beams. On the theoretical side these advances include the development of methods which allow highly accurate excitation and ionization cross sections to be calculated at intermediate energies, the increasing ability to determine accurate low-energy cross sections for electron and positron collisions with complex atoms and molecules and the development of non-perturbative approaches for studying multiphoton processes for many-electron targets. Many of these theoretical advances have been made possible by the increasing availability of high-performance parallel computers and the development of general computer programs which can take advantage of these facilities.

This monograph describes a generalized R-matrix theory of atomic collisions and its application to the ab initio study of atomic, molecular and optical collision processes. R-matrix theory was first introduced by Wigner and Eisenbud in the late 1940s in an analysis of nuclear resonance reactions. These resonances were described in terms of temporary compound states formed by the colliding nuclei, which were contained in an internal region of configuration space. The R-matrix, which represents the complexity of the compound states, relates the radial components of the wave function to their derivatives on the boundary of the internal

region. In the external region it was assumed that the colliding nuclei were weakly interacting and hence the complexity of the collision process was represented by the R-matrix. In early work the R-matrix was represented by a few parameters used to fit the experimental observations and in later work it was calculated directly using nuclear model potentials. This theory has been widely used in nuclear physics and developments have been reviewed by many authors.

The realization that R-matrix theory could be developed and applied as an ab initio approach to study atomic, molecular and optical collision processes began to emerge in the 1960s as a result of new resonance phenomena observed using high-resolution electron spectrometers and synchrotron radiation sources. In the analysis of these experiments it became clear that processes such as resonant electron – atom collisions and photoionization could be understood and predicted using R-matrix theory. Following the ideas introduced by Wigner and Eisenbud, configuration space describing the collision process is partitioned into three regions by spheres of radii a_0 and a_p. In the internal region, where the colliding atomic or molecular systems interact strongly, the resulting compound system behaves in a similar way to a bound state. Consequently, configuration interaction approaches, developed over many years to study bound-state problems, can often be extended to provide an ab initio treatment of the compound system yielding the R-matrix on the boundary of the internal region. In the the external and asymptotic regions, where the colliding systems are weakly interacting, the solution of the coupled equations describing their relative motion can be rapidly obtained using standard methods, yielding the scattering amplitudes and cross sections.

The monograph commences by presenting an overview of collision theory in Part I. As well as giving a self-contained summary of this theory it also provides an introduction to the basic concepts and notation required in Part II. After an introductory chapter on potential scattering, Chap. 2 presents an overview of multichannel collision theory with emphasis on electron collisions with atoms and atomic ions. Chapter 3 then provides an overview of resonance theory and threshold behaviour. In these chapters quantities such as the K-matrix, S-matrix, scattering amplitudes and cross sections, as well as resonance and threshold behaviour, are introduced.

Part II then turns to a detailed discussion of R-matrix theory of atomic, molecular and optical collisions and its applications. It commences in Chap. 4 with a review of R-matrix theory in potential scattering which sets the scene for the later chapters which develop and apply multichannel R-matrix theory to a wide range of collision processes. One of the first detailed applications of R-matrix theory in atomic, molecular and optical physics, in the early 1970s, was to electron collisions with atoms and atomic ions, which is reviewed in Chap. 5. More general aspects of R-matrix theory are also presented in this chapter including multichannel variational principles for the R-matrix and the inclusion of relativistic effects. Then in subsequent chapters the theory and application of R-matrix theory to a wide range of collision processes are discussed including electron collisions at intermediate energies, positron collisions with atoms and ions, photoionization, photorecombination and atoms in fields, multiphoton processes using Floquet and time-dependent theory, electron, positron and photon collisions with molecules and electron collisions with transition metal

oxides and electron transport in semiconductor devices. For all of these applications general computer programs have been developed and those that have been published or are generally available are briefly reviewed.

The monograph concludes with six appendices which summarize basic mathematical results and computational methods which are used in Parts I and II.

Finally, I wish to recognize my great indebtedness to Sir Harrie Massey and Richard Buckingham who introduced me to collision theory and the crucial role of scientific computing when I was a graduate student at University College London in the 1950s. Also, this monograph could not have been written without the inspiring atmosphere that Sir David Bates established in the Department of Applied Mathematics and Theoretical Physics at the Queen's University of Belfast where I have been privileged to work for the last 43 years. I also wish to take this opportunity to acknowledge two leading scientists and friends who made crucial contributions to the research discussed in this monograph. First, Ugo Fano for his incisive comments and encouragement over many years, particularly in the 1960s when it was clear there was a need for an ab initio theory which could accurately describe and predict the wide range of atomic, molecular and optical resonance phenomena being observed. Second, Mike Seaton for his support and encouragement over many years and for showing that the R-matrix approach could be used to calculate the vast amount of data required in the analysis of astronomical observations. I would also like to acknowledge long-term collaborations with Cliff Noble, Jonathan Tennyson, Klaus Bartschat and Charles Joachain. Throughout my years at Queen's University, in addition to many collaborators worldwide, I have been fortunate to interact and to work with many outstanding members of staff and graduate students. In particular it is a pleasure to mention Alan Hibbert, Derek Robb, Donald Allison, John Mitchell, Keith Berrington, Ken Taylor, Arthur Kingston, Ken Bell, Stan Scott, Penny Scott, Kevin Dunseath, James Walters, Robin Reid, Patrick Norrington, Charles Gillan, Katrina Higgins, Hugo van der Hart, Cathy Ramsbottom, David Glass and James Colgan who played a major role in the development of the theory, computational methods and computer programs and in the calculations discussed in this monograph.

Belfast, UK
March 2011

Philip G. Burke

Contents

Units

Atomic units (a.u.) will be used throughout this monograph. They are such that $\hbar = m = e = 1$, where $\hbar$ is Planck's constant h divided by 2π, m is the mass of the electron and $-e$ is the charge of the electron. Thus the atomic unit of length $a_0 = \hbar^2/me^2 \approx 5.292 \times 10^{-9}$ cm, which is the radius of the first Bohr orbit of the hydrogen atom with infinite nuclear mass. Using this unit of length, collision cross sections, which have the dimension of an area, are then expressed, either in units of $a_0^2 \approx 2.800 \times 10^{-17}\,\mathrm{cm}^2$ or in units of $\pi a_0^2 \approx 8.797 \times 10^{-17}\,\mathrm{cm}^2$. The atomic unit of time is given by $\hbar^3/me^4 = 2.419 \times 10^{-17}$ s, while the unit of velocity is $e^2/\hbar = 2.188 \times 10^8\,\mathrm{cm\,s}^{-1}$. The atomic unit of energy is $e^2/a_0 \approx 27.21$ eV, which is twice the ionization energy of the hydrogen atom in its ground state and twice the Rydberg unit of energy. The fine-structure constant $\alpha = e^2/\hbar c \approx 1/137$ is dimensionless, where c is the velocity of light in a vacuum.

Part I
Collision Theory

Chapter 1
Potential Scattering

In this chapter we introduce the basic concepts of atomic collision theory by considering potential scattering. While being of interest in its own right, this chapter also provides a basis for our treatment of electron and positron collisions with atoms, ions and molecules in later chapters in this monograph. We commence in Sect. 1.1 by considering the solution of the non-relativistic time-independent Schrödinger equation for a short-range spherically symmetric potential. This enables us to define the scattering amplitude and various cross sections and to obtain explicit expressions for these quantities in terms of the partial wave phase shifts. We also introduce and define the K-matrix, S-matrix and T-matrix in terms of the partial wave phase shifts and we obtain an integral expression for the K-matrix and the phase shift. In Sect. 1.2 we extend this discussion to consider the situation where a long-range Coulomb potential is present in addition to a short-range potential. We obtain expressions for the scattering amplitude and the differential cross section for pure Coulomb scattering and where both a Coulomb potential and a short-range potential are present. In Sect. 1.3 we turn our attention to the analytic properties of the partial wave S-matrix in the complex momentum plane and we discuss the connection between poles in the S-matrix and bound states and resonances. In Sect. 1.4 we extend this discussion of analytic properties to consider the analytic behaviour of the phase shift and the scattering amplitude in the neighbourhood of threshold energy both for short-range potentials and for potentials behaving asymptotically as r^{-s} where $s \geq 2$. Also in this section, we consider the threshold behaviour when a Coulomb potential is present in addition to a short-range potential, corresponding to electron scattering by a positive or negative ion. Next in Sect. 1.5 we derive variational principles first obtained by Kohn for the partial wave phase shift and for the S-matrix. We conclude this chapter by considering in Sect. 1.6 relativistic scattering of an electron by a spherically symmetric potential. This situation occurs for relativistic electron scattering energies or when an electron is scattered by heavy atoms or ions. In this case the time-independent Dirac equation, which takes into account both the spin and the relativistic behaviour of the scattered electron must be solved. Finally we note that some of these topics have been discussed in greater detail in monographs devoted to potential scattering by Burke [158] and Burke and Joachain [171].

P.G. Burke, *R-Matrix Theory of Atomic Collisions*, Springer Series on Atomic, Optical, and Plasma Physics 61, DOI 10.1007/978-3-642-15931-2_1,

1.1 Scattering by a Short-Range Potential

We initiate our discussion of potential scattering by considering the solution of the non-relativistic time-independent Schrödinger equation describing the motion of a particle of unit mass in a potential $V(\mathbf{r})$. We write this equation in atomic units as

$$\left(-\frac{1}{2}\nabla^2 + V(\mathbf{r})\right)\psi(\mathbf{r}) = E\psi(\mathbf{r})\,, \tag{1.1}$$

where E is the total energy and $\psi(\mathbf{r})$ is the wave function describing the motion of the scattered particle. We assume in this section that the potential $V(\mathbf{r})$ is short range, vanishing faster than r^{-1} at large distances. We also assume that the potential is less singular than r^{-2} at the origin.

The solution of (1.1), corresponding to the particle incident on the scattering centre in the z-direction and scattered in the direction $\Omega \equiv (\theta, \phi)$ defined by the polar angles θ and ϕ, has the asymptotic form

$$\psi(\mathbf{r}) \underset{r\to\infty}{\sim} \mathrm{e}^{\mathrm{i}kz} + f(\theta,\phi)\frac{\mathrm{e}^{\mathrm{i}kr}}{r}\,, \tag{1.2}$$

where $f(\theta, \phi)$ is the scattering amplitude and the wave number k of the scattered particle is related to the total energy E by

$$k^2 = 2E\,. \tag{1.3}$$

If the potential behaves as r^{-1} at large distances, corresponding to a long-range Coulomb potential, then logarithmic phase factors must be included in the exponentials in (1.2) to allow for the distortion caused by the Coulomb potential. We consider this possibility in Sect. 1.2.

The differential cross section can be obtained from (1.2) by calculating the outward flux of particles scattered through a spherical surface $r^2\mathrm{d}\Omega$ for large r divided by the incident flux and by the element of solid angle $\mathrm{d}\Omega$. This gives

$$\frac{\mathrm{d}\sigma}{\mathrm{d}\Omega} = |f(\theta,\phi)|^2\,, \tag{1.4}$$

in units of a_0^2 per steradian. The total cross section is then obtained by integrating the differential cross section over all scattering angles giving

$$\sigma_{\mathrm{tot}} = \int_0^{2\pi}\int_0^{\pi} |f(\theta,\phi)|^2 \sin\theta \mathrm{d}\theta\mathrm{d}\phi\,, \tag{1.5}$$

in units of a_0^2. A further cross section, of importance in the study of the motion of electron swarms in gases, is the momentum transfer cross section defined by

$$\sigma_M = \int_0^{2\pi}\int_0^{\pi} |f(\theta,\phi)|^2 (1-\cos\theta)\sin\theta \mathrm{d}\theta\mathrm{d}\phi\,. \tag{1.6}$$

In order to determine the scattering amplitude it is necessary to solve (1.1) for $\psi(\mathbf{r})$ subject to the asymptotic boundary condition (1.2). For low and intermediate energy scattering this is most conveniently achieved by making a partial wave analysis. This method was originally used in the treatment of scattering of sound waves by Rayleigh [779] and was first applied to the problem of scattering of electrons by atoms by Faxén and Holtsmark [314].

We consider the case of a spherically symmetric "reduced" potential $U(r) = 2V(r)$. We can expand the wave function $\psi(\mathbf{r})$ as

$$\psi(\mathbf{r}) = \sum_{\ell=0}^{\infty} B_\ell(k) r^{-1} u_\ell(r) P_\ell(\cos\theta)\,, \tag{1.7}$$

where ℓ is the orbital angular momentum quantum number of the particle, $P_\ell(\cos\theta)$ are Legendre polynomials defined in Appendix B and the coefficients $B_\ell(k)$ are determined below by requiring that the asymptotic boundary condition (1.2) is satisfied. The equation satisfied by the reduced radial wave function $u_\ell(r)$, which does not include the r^{-1} factor in (1.7), is determined by substituting (1.7) into (1.1), premultiplying by $P_\ell(\cos\theta)$ and integrating with respect to $\cos\theta$. We find that $u_\ell(r)$ satisfies the radial Schrödinger equation

$$\left(\frac{\mathrm{d}^2}{\mathrm{d}r^2} - \frac{\ell(\ell+1)}{r^2} - U(r) + k^2\right) u_\ell(r) = 0\,. \tag{1.8}$$

We note that the effective potential in this equation is the sum of the reduced potential $U(r)$ and the repulsive centrifugal barrier term $\ell(\ell+1)/r^2$. We also remark that since we are considering real potentials $U(r)$, as well as real energies and angular momenta, there is no loss of generality in assuming that $u_\ell(r)$ is real.

We look for a solution of (1.8) satisfying the boundary conditions

$$\begin{aligned} u_\ell(0) &\underset{r\to 0}{\sim} n r^{\ell+1}\,, \\ u_\ell(r) &\underset{r\to\infty}{\sim} s_\ell(kr) + c_\ell(kr)\tan\delta_\ell(k)\,, \end{aligned} \tag{1.9}$$

where n is a normalization factor and $s_\ell(kr)$ and $c_\ell(kr)$ are solutions of (1.8) in the absence of the potential $U(r)$, which are, respectively, regular and irregular at the origin. We show in Appendix C.2 that they can be written for integral values of ℓ in terms of spherical Bessel and Neumann functions $j_\ell(kr)$ and $n_\ell(kr)$ as follows:

$$s_\ell(kr) = kr j_\ell(kr) = \left(\frac{\pi kr}{2}\right)^{\frac{1}{2}} J_{\ell+\frac{1}{2}}(kr) \underset{r\to\infty}{\sim} \sin(kr - \tfrac{1}{2}\ell\pi) \tag{1.10}$$

and

$$c_\ell(kr) = -kr n_\ell(kr) = (-1)^\ell \left(\frac{\pi kr}{2}\right)^{\frac{1}{2}} J_{-\ell-\frac{1}{2}}(kr) \underset{r\to\infty}{\sim} \cos(kr - \tfrac{1}{2}\ell\pi)\,. \tag{1.11}$$

The remaining quantity in (1.9) is the partial wave phase shift $\delta_\ell(k)$ which is a real function of the wave number k when the reduced potential $U(r)$, energy E and angular momentum ℓ are real.

It is also convenient to introduce the S-matrix, whose matrix elements are defined in terms of the phase shifts. We first note that (1.8) satisfied by $u_\ell(r)$ is homogeneous so that $u_\ell(r)$ is only defined up to an arbitrary multiplicative complex normalization factor N. Hence it follows from (1.9) that

$$u_\ell^N(r) \underset{r\to\infty}{\sim} N[s_\ell(kr) + c_\ell(kr)\tan\delta_\ell(k)] \tag{1.12}$$

is also a solution of (1.8) for arbitrary N. If we choose $N = -2\mathrm{i}\cos\delta_\ell \exp(\mathrm{i}\delta_\ell)$ then we can rewrite (1.12) as

$$u_\ell(r) \underset{r\to\infty}{\sim} \exp(-\mathrm{i}\theta_\ell) - \exp(\mathrm{i}\theta_\ell)S_\ell(k)\,, \tag{1.13}$$

where $\theta_\ell = kr - \frac{1}{2}\ell\pi$. The quantity $S_\ell(k)$ in (1.13) is then a diagonal element of the S-matrix defined by

$$S_\ell(k) = \exp[2\mathrm{i}\delta_\ell(k)] = \frac{1 + \mathrm{i}K_\ell(k)}{1 - \mathrm{i}K_\ell(k)}\,, \tag{1.14}$$

where we have also introduced the K-matrix, whose diagonal elements are defined by

$$K_\ell(k) = \tan\delta_\ell(k)\,. \tag{1.15}$$

We see from (1.9) that the phase shift, and hence the K-matrix, is a measure of the departure of the radial wave function from the form it has when the potential $U(r)$ is zero.

We can obtain useful integral expressions for the K-matrix and the phase shift. We consider the solution $v_\ell(r)$ of the radial Schrödinger equation, obtained from (1.8) by setting the potential $U(r) = 0$. Hence $v_\ell(r)$ satisfies the equation

$$\left(\frac{\mathrm{d}^2}{\mathrm{d}r^2} - \frac{\ell(\ell+1)}{r^2} + k^2\right) v_\ell(r) = 0\,. \tag{1.16}$$

We choose $v_\ell(r)$ to be the regular solution of this equation, given by

$$v_\ell(r) = s_\ell(r)\,, \tag{1.17}$$

where $s_\ell(r)$ is defined by (1.10). We then premultiply (1.8) by $v_\ell(r)$, premultiply (1.16) by $u_\ell(r)$ and then integrate the difference of these two equations from $r = 0$ to ∞. We obtain

$$\int_0^\infty \left(v_\ell(r) \frac{\mathrm{d}^2 u_\ell}{\mathrm{d}r^2} - u_\ell(r) \frac{\mathrm{d}^2 v_\ell}{\mathrm{d}r^2} \right) \mathrm{d}r = \int_0^\infty v_\ell(r) U(r) u_\ell(r) \mathrm{d}r \,. \tag{1.18}$$

The left-hand side of this equation can be evaluated using Green's formula and the boundary conditions satisfied by $u_\ell(r)$ and $v_\ell(r)$, given by (1.9) and (1.10), yielding the result $-k \tan \delta_\ell(k)$. We then substitute for $v_\ell(r)$ in terms of $j_\ell(kr)$ on the right-hand side of (1.18) using (1.10) and (1.17). Combining these results we find that (1.18) reduces to

$$K_\ell(k) = \tan \delta_\ell(k) = -\int_0^\infty j_\ell(kr) U(r) u_\ell(r) r \mathrm{d}r \,, \tag{1.19}$$

which is an exact integral expression for the K-matrix element and the phase shift. If the potential $U(r)$ is weak or the scattered particle is moving fast, the distortion of $u_\ell(r)$ in (1.19) will be small. In this case $u_\ell(r)$ can be replaced by $v_\ell(r)$ and, after using (1.10) and (1.17), we find that (1.19) reduces to

$$K_\ell^B(k) = \tan \delta_\ell^B(k) = -k \int_0^\infty U(r) j_\ell^2(kr) r^2 \mathrm{d}r \,. \tag{1.20}$$

This is the first Born approximation for the K-matrix element and the phase shift which we will use when we discuss effective range theory for long-range potentials, in Sect. 1.4.2.

We will also need to consider solutions of (1.8) satisfying the following orthonormality relation

$$\int_0^\infty \left[u_\ell^N(k, r) \right]^* u_\ell^N(k', r) \mathrm{d}r = \delta(E - E') \,, \tag{1.21}$$

where we have displayed explicitly the dependence of the solution $u_\ell^N(r)$ on the wave number k and where $[u_\ell^N(k, r)]^*$ is the complex conjugate of $u_\ell^N(k, r)$. Also in (1.21) we have introduced the Dirac δ-function [263], which can be defined by the relations

$$\delta(x) = 0 \text{ for } x \neq 0 \,, \quad \int_{-\infty}^\infty \delta(x) \mathrm{d}x = 1 \,. \tag{1.22}$$

Of particular importance in applications are the following three solutions satisfying (1.21), corresponding to different choices of the normalization factor N in (1.12). Using (C.53) and (C.54) we define the real solution

$$u_\ell(k, r) \underset{r \to \infty}{\sim} \left(\frac{2}{\pi k} \right)^{\frac{1}{2}} [\sin \theta_\ell + \cos \theta_\ell K_\ell(k)] \left[1 + K_\ell^2(k) \right]^{-\frac{1}{2}} \,, \tag{1.23}$$

the outgoing wave solution

$$u_\ell^+(k, r) \underset{r \to \infty}{\sim} \left(\frac{2}{\pi k} \right)^{\frac{1}{2}} \left[\sin \theta_\ell + (2\mathrm{i})^{-1} \exp(\mathrm{i}\theta_\ell) T_\ell(k) \right] \tag{1.24}$$

and the ingoing wave solution

$$u_\ell^-(k,r) \underset{r\to\infty}{\sim} \left(\frac{2}{\pi k}\right)^{\frac{1}{2}} \left[\sin\theta_\ell - (2\mathrm{i})^{-1}\exp(-\mathrm{i}\theta_\ell)T_\ell^*(k)\right], \tag{1.25}$$

where in (1.24) and (1.25) we have introduced the T-matrix element $T_\ell(k)$ which is related to the K-matrix and the S-matrix elements by

$$T_\ell(k) = \frac{2\mathrm{i}K_\ell(k)}{1-\mathrm{i}K_\ell(k)} = S_\ell(k) - 1\,. \tag{1.26}$$

It is clear that if the reduced potential $U(r)$ is zero so that there is no scattering, then the phase shift $\delta_\ell(k) = 0$ and hence $S_\ell(k) = 1$ and $T_\ell(k) = 0$.

We are now in a position to determine an expression for the scattering amplitude in terms of the phase shifts. To achieve this we expand the plane wave term in (1.2) in partial waves and equate it with the asymptotic form of (1.7). The required expansion of the plane wave term in terms of Legendre polynomials, discussed in Appendix B.1, is

$$\mathrm{e}^{\mathrm{i}kz} = \sum_{\ell=0}^{\infty}(2\ell+1)\mathrm{i}^\ell j_\ell(kr)P_\ell(\cos\theta)\,. \tag{1.27}$$

Since the second term in (1.2) contributes only to the outgoing spherical wave in (1.7), we can determine the coefficients $B_\ell(k)$ by equating the coefficients of the ingoing wave $\mathrm{e}^{-\mathrm{i}kr}$ in (1.7) and (1.27). Using (1.9), (1.10), and (1.11) we find that

$$B_\ell(k) = k^{-1}(2\ell+1)\mathrm{i}^\ell\cos\delta_\ell(k)\exp[\mathrm{i}\delta_\ell(k)]\,. \tag{1.28}$$

Substituting this result into (1.7) and comparing with (1.2), then gives the following expression for the scattering amplitude:

$$f(\theta,\phi) = \frac{1}{2\mathrm{i}k}\sum_{\ell=0}^{\infty}(2\ell+1)\{\exp[2\mathrm{i}\delta_\ell(k)]-1\}P_\ell(\cos\theta)\,. \tag{1.29}$$

We notice that the scattering amplitude does not depend on the azimuthal angle ϕ since we have restricted our consideration to an incident beam in the z-direction scattering from a spherically symmetric potential. Also, for short-range potentials considered in this section, $\delta_\ell(k)$ tends rapidly to zero as ℓ tends to ∞ and hence the summation in (1.29) gives accurate results at low energies when only a few terms are retained.

An expression for the total cross section is obtained by substituting (1.29) into (1.5). We obtain

$$\sigma_{\mathrm{tot}} = \sum_{\ell=0}^{\infty}\sigma_\ell = \frac{4\pi}{k^2}\sum_{\ell=0}^{\infty}(2\ell+1)\sin^2\delta_\ell(k)\,, \tag{1.30}$$

where σ_ℓ is called the partial wave cross section. Also substituting (1.29) into (1.6) yields the following expression for the momentum transfer cross section:

$$\sigma_M = \frac{4\pi}{k^2}\sum_{\ell=0}^{\infty}(\ell+1)\sin^2[\delta_{\ell+1}(k)-\delta_\ell(k)]\,. \tag{1.31}$$

Finally, we observe that the imaginary part of the scattering amplitude in the forward direction can be related to the total cross section. Since $P_\ell(1) = 1$ we obtain from (1.29)

$$\mathrm{Im}\, f(\theta=0,\phi) = \frac{1}{k}\sum_{\ell=0}^{\infty}(2\ell+1)\sin^2\delta_\ell(k)\,. \tag{1.32}$$

Comparing this result with (1.30) gives immediately

$$\sigma_{\mathrm{tot}} = \frac{4\pi}{k}\mathrm{Im}\, f(\theta=0,\phi)\,, \tag{1.33}$$

which is known as the optical theorem [316]. This result, which can be generalized to multichannel collisions, can be shown to be a direct consequence of conservation of probability.

We conclude our discussion of scattering by a short-range potential by observing that the procedure of adopting a partial wave analysis of the wave function and the scattering amplitude is appropriate at low and intermediate energies when only a relatively small number of partial wave phase shifts are significantly different from zero. This situation is relevant to our discussion of R-matrix theory of atomic collisions in Part II of this monograph. On the other hand, at high energies this procedure breaks down because of the large number of partial waves which are required to determine the cross section accurately. It is then necessary to obtain a solution of the Schrödinger equation (1.1) which directly takes account of the boundary condition of the problem. This is the basis of the procedure introduced by Lippmann and Schwinger [600]. In this procedure the Schrödinger equation (1.1) is written in the form

$$(E-H_0)\psi(\mathbf{r}) = V(\mathbf{r})\psi(\mathbf{r})\,. \tag{1.34}$$

We can then solve this equation to yield a solution with the required asymptotic form by introducing the Green's function for the operator on the left-hand side. We obtain the formal solution

$$\psi^{\pm} = \phi + \frac{1}{E-H_0\pm \mathrm{i}\epsilon}V\psi^{\pm}\,, \tag{1.35}$$

where the term $\pm\mathrm{i}\epsilon$ in the denominator defines the contour of integration past the singularity $E = H_0$ and ϕ is the solution of the free-particle wave equation

$$(E-H_0)\phi = 0\,. \tag{1.36}$$

The Lippmann–Schwinger equation (1.35) is the basic integral equation of time-independent scattering theory and an iterative solution of this equation yields the Born series expansion. The solution of this equation is discussed in detail in the monographs by Burke [158] and Burke and Joachain [171].

1.2 Scattering by a Coulomb Potential

The discussion in the previous section must be modified when a long-range Coulomb potential is present in addition to the short-range potential $V(\mathbf{r})$.

We consider first scattering by a pure Coulomb potential acting between a particle of unit mass and charge number Z_1 and a particle of infinite mass and charge number Z_2. The time-independent Schrödinger equation is then

$$\left(-\frac{1}{2}\nabla^2 + V_c(\mathbf{r})\right)\psi_c(\mathbf{r}) = E\psi_c(\mathbf{r})\,, \tag{1.37}$$

where the Coulomb potential

$$V_c(\mathbf{r}) = \frac{Z_1 Z_2}{r}\,, \tag{1.38}$$

in atomic units. The solution of (1.37) was obtained by Gordon [403] and Temple [913] by introducing parabolic coordinates

$$\zeta = r - z, \quad \xi = r + z, \quad \phi = \tan^{-1}\frac{y}{x}\,. \tag{1.39}$$

In these coordinates the Laplacian becomes

$$\nabla^2 = \frac{4}{\zeta+\xi}\left[\frac{\partial}{\partial\zeta}\left(\zeta\frac{\partial}{\partial\zeta}\right) + \frac{\partial}{\partial\xi}\left(\xi\frac{\partial}{\partial\xi}\right)\right] + \frac{1}{\zeta\xi}\frac{\partial^2}{\partial\phi^2}\,. \tag{1.40}$$

The solution of (1.37), corresponding to an incident wave in the z-direction and an outgoing scattered wave, can then be written as

$$\psi_c(\mathbf{r}) = \exp(-\tfrac{1}{2}\pi\eta)\Gamma(1+\mathrm{i}\eta)\mathrm{e}^{\mathrm{i}kz}\,{}_1F_1(-\mathrm{i}\eta;\,1;\,\mathrm{i}k\zeta)\,, \tag{1.41}$$

where

$$\eta = \frac{\beta}{2k} = \frac{Z_1 Z_2}{k}\,, \tag{1.42}$$

and $\Gamma(z)$ is the gamma function. Also the function ${}_1F_1$ is defined by

$$\begin{aligned} {}_1F_1(a;b;z) &= 1 + \frac{a}{b}z + \frac{a(a+1)}{b(b+1)}\frac{z^2}{2!} + \cdots \\ &= \sum_{n=0}^{\infty}\frac{\Gamma(a+n)\Gamma(b)}{\Gamma(a)\Gamma(b+n)}\frac{z^n}{n!} \end{aligned} \tag{1.43}$$

and is related to the confluent hypergeometric function $M_{k,m}(z)$, defined by Whittaker and Watson [964], by

$$M_{k,m}(z) = z^{m+1/2} \exp(-\tfrac{1}{2}z)\ {}_1F_1(\tfrac{1}{2} + m - k; 2m + 1; z)\,. \tag{1.44}$$

The asymptotic form of ${}_1F_1$ can be obtained by writing

$${}_1F_1(a; b; z) = W_1(a; b; z) + W_2(a; b; z)\,, \tag{1.45}$$

where

$$W_1(a; b; z) \underset{|z|\to\infty}{\sim} \frac{\Gamma(b)}{\Gamma(b-a)}(-z)^{-a} v(a; a - b + 1; -z), \quad -\pi < \arg(-z) < \pi \tag{1.46}$$

and

$$W_2(a; b; z) \underset{|z|\to\infty}{\sim} \frac{\Gamma(b)}{\Gamma(a)} \mathrm{e}^z z^{a-b} v(1 - a; b - a; z), \quad -\pi < \arg(z) < \pi\,, \tag{1.47}$$

where v has the asymptotic expansion

$$\begin{aligned} v(\alpha; \beta; z) &= 1 + \frac{\alpha\beta}{z} + \frac{\alpha(\alpha+1)\beta(\beta+1)}{2!z^2} + \cdots \\ &= \sum_{n=0}^{\infty} \frac{\Gamma(n+\alpha)\Gamma(n+\beta)}{\Gamma(\alpha)\Gamma(\beta)} \frac{(z)^{-n}}{n!}\,. \end{aligned} \tag{1.48}$$

The W_1 term corresponds to the Coulomb-modified incident wave and the W_2 term to the outgoing scattered wave in $\psi_c(\mathbf{r})$. Thus we can write

$$\psi_c(\mathbf{r}) \underset{|r-z|\to\infty}{\sim} I + f_c(\theta) J\,, \tag{1.49}$$

where

$$I = \exp[\mathrm{i}kz + \mathrm{i}\eta \ln(k\zeta)] \left(1 + \frac{\eta^2}{\mathrm{i}k\zeta} + \cdots\right) \tag{1.50}$$

and

$$J = r^{-1} \exp[\mathrm{i}kr - \mathrm{i}\eta \ln(2kr)] \left(1 + \frac{(1+\mathrm{i}\eta)^2}{\mathrm{i}k\zeta} + \cdots\right). \tag{1.51}$$

The Coulomb scattering amplitude is then given by

$$f_c(\theta) = -\frac{\eta}{2k \sin^2(\theta/2)} \exp[-\mathrm{i}\eta \ln \sin^2(\theta/2) + 2\mathrm{i}\sigma_0]\,, \tag{1.52}$$

where

$$\sigma_0 = \arg \Gamma(1 + \mathrm{i}\eta)\,, \tag{1.53}$$

and the differential cross section is given by

$$\frac{\mathrm{d}\sigma_c}{\mathrm{d}\Omega} = |f_c(\theta)|^2 = \frac{\eta^2}{4k^2 \sin^4(\theta/2)} = \frac{(Z_1 Z_2)^2}{16E^2 \sin^4(\theta/2)}\,. \tag{1.54}$$

This result was first obtained by Rutherford [802] using classical mechanics to describe the scattering of α-particles by nuclei. Since the differential cross section diverges like θ^{-4} at small θ, the total Coulomb cross section obtained by integrating over all scattering angles is infinite. A further difference from the result obtained in Sect. 1.1 for scattering by short-range potentials is the distortion of both the incident and scattered waves, defined by (1.50) and (1.51), by logarithmic phase factors. These phase factors are a direct consequence of the long-range nature of the Coulomb potential. However, we see that they do not affect the form of the differential cross section for scattering by a pure Coulomb potential given by (1.54).

For electron–ion scattering problems of practical interest, the interaction potential experienced by the scattered electron is not pure Coulombic but is modified at short distances by the interaction of the scattered electron with the target electrons. In this case it is appropriate at low scattering energies to make a partial wave analysis of the scattering wave function in spherical polar coordinates, as in Sect. 1.1 where we considered short-range potentials.

We commence our discussion by making a partial wave analysis of the pure Coulomb scattering problem. Following (1.7) we expand the wave function in (1.37) in partial waves as

$$\psi_c(\mathbf{r}) = \sum_{\ell=0}^{\infty} B_\ell^c(k) r^{-1} u_\ell^c(r) P_\ell(\cos\theta)\,, \tag{1.55}$$

where $u_\ell^c(r)$ satisfies the radial Schrödinger equation

$$\left(\frac{\mathrm{d}^2}{\mathrm{d}r^2} - \frac{\ell(\ell+1)}{r^2} - U_c(r) + k^2\right) u_\ell^c(r) = 0\,, \tag{1.56}$$

and where

$$U_c(r) = 2V_c(r) = \frac{2Z_1 Z_2}{r} \tag{1.57}$$

is the reduced Coulomb potential. Equation (1.56) is the Coulomb wave equation that has been discussed extensively in the literature (e.g. by Yost et al. [984], Hull and Breit [479], Fröberg [343] and Chap. 14 of Abramowitz and Stegun [1]). The

solutions of this equation, which are regular and irregular at the origin, known as Coulomb wave functions, are defined, respectively, by

$$\begin{aligned} F_\ell(\eta, kr) &= C_\ell(\eta)\mathrm{e}^{\mathrm{i}kr}(kr)^{\ell+1}\ {}_1F_1(\ell+1+\mathrm{i}\eta; 2\ell+2; -2\mathrm{i}kr) \\ &\underset{r\to\infty}{\sim} \sin(kr - \tfrac{1}{2}\ell\pi - \eta\ln 2kr + \sigma_\ell) \end{aligned} \tag{1.58}$$

and

$$\begin{aligned} G_\ell(\eta, kr) &= \mathrm{i}C_\ell(\eta)\mathrm{e}^{\mathrm{i}kr}(kr)^{\ell+1}\,[W_1(\ell+1+\mathrm{i}\eta; 2\ell+2; -2\mathrm{i}kr) \\ &\quad - W_2(\ell+1+\mathrm{i}\eta; 2\ell+2; -2\mathrm{i}kr)] \\ &\underset{r\to\infty}{\sim} \cos(kr - \tfrac{1}{2}\ell\pi - \eta\ln 2kr + \sigma_\ell)\,, \end{aligned} \tag{1.59}$$

where η is defined by (1.42). Also in (1.58) and (1.59)

$$\begin{aligned} C_\ell(\eta) &= \frac{2^\ell \exp(-\frac{1}{2}\pi\eta)|\Gamma(\ell+1+\mathrm{i}\eta)|}{\Gamma(2\ell+2)} \\ &= C_0(\eta)\frac{2^\ell}{\Gamma(2\ell+2)}\prod_{s=1}^{\ell}(s^2+\eta^2)^{1/2}\,, \end{aligned} \tag{1.60}$$

with

$$C_0(\eta) = \left(\frac{2\pi\eta}{\mathrm{e}^{2\pi\eta}-1}\right)^{1/2}, \tag{1.61}$$

and σ_ℓ is the Coulomb phase shift

$$\sigma_\ell = \arg\Gamma(\ell+1+\mathrm{i}\eta)\,. \tag{1.62}$$

In order to determine the coefficients $B_\ell^c(k)$ in (1.55), we choose $u_\ell^c(r)$ to be the regular Coulomb wave function $F_\ell(\eta, kr)$ and require that $\psi_c(\mathbf{r})$ has the normalization defined by (1.41). Using the orthogonality properties of the Legendre polynomials and matching $\psi_c(\mathbf{r})$, given by (1.41) and (1.55), in the neighbourhood of $r = 0$ gives

$$B_\ell^c(k) = k^{-1}(2\ell+1)\mathrm{i}^\ell\exp(\mathrm{i}\sigma_\ell)\,, \tag{1.63}$$

so that

$$\psi_c(\mathbf{r}) = \sum_{\ell=0}^{\infty}(2\ell+1)\mathrm{i}^\ell\exp(\mathrm{i}\sigma_\ell)(kr)^{-1}F_\ell(\eta, kr)P_\ell(\cos\theta)\,. \tag{1.64}$$

This equation reduces to the expansion of the plane wave given by (1.27) when $\eta = 0$.

We now define the Coulomb S-matrix, in analogy with our discussion of scattering by a short-range potential, by considering the asymptotic form of the ℓth partial wave component of $\psi_c(\mathbf{r})$. From (1.58) and (1.64) this component has the asymptotic form

$$F_\ell(\eta, kr) \underset{r\to\infty}{\sim} N\left[\exp(-\mathrm{i}\theta_\ell^c) - \exp(\mathrm{i}\theta_\ell^c) S_\ell^c(k)\right], \tag{1.65}$$

where the normalization factor $N = -\exp(-\mathrm{i}\sigma_\ell)/2\mathrm{i}$, the phase factor $\theta_\ell^c = kr - \frac{1}{2}\ell\pi - \eta \ln 2kr$ and the Coulomb S-matrix $S_\ell^c(k)$ is given by

$$S_\ell^c(k) = \exp(2\mathrm{i}\sigma_\ell) = \frac{\Gamma(\ell + 1 + \mathrm{i}\eta)}{\Gamma(\ell + 1 - \mathrm{i}\eta)}. \tag{1.66}$$

It follows from the asymptotic properties of the Gamma function that the Coulomb S-matrix is analytic in the entire complex k-plane except for poles where $\ell+1+\mathrm{i}\eta = -\bar{n}$ with $\bar{n} = 0, 1, 2, \ldots$. Using (1.42) we see that the corresponding values of k are given by

$$k_{\bar{n}} = -\mathrm{i}\frac{Z_1 Z_2}{\bar{n} + \ell + 1}, \quad \bar{n} = 0, 1, 2, \ldots. \tag{1.67}$$

Thus for an attractive Coulomb potential ($Z_1 Z_2 < 0$) the poles of $S_\ell^c(k)$ lie on the positive imaginary axis of the complex k-plane. At these poles it follows from (1.65) that the wave function decays exponentially asymptotically and hence these poles correspond to the familiar bound states with energies

$$E_n = -\frac{1}{2}\frac{Z_1^2 Z_2^2}{n^2}, \quad n = \ell + 1,\ \ell + 2, \ldots, \tag{1.68}$$

where we have introduced the principal quantum number $n = \bar{n} + \ell + 1$. The location of poles in the S-matrix in the complex k-plane, corresponding to bound states and resonances, is discussed further in Sect. 1.3.

We now consider the situation where an additional short-range potential $V(r)$, which vanishes asymptotically faster than r^{-1}, is added to the Coulomb potential. Again, carrying out a partial wave analysis as in (1.7), we expand the total wave function as follows:

$$\psi(\mathbf{r}) = \sum_{\ell=0}^{\infty} B_\ell^s(k) r^{-1} u_\ell^s(r) P_\ell(\cos\theta), \tag{1.69}$$

where $u_\ell^s(r)$ satisfies the radial Schrödinger equation

$$\left(\frac{\mathrm{d}^2}{\mathrm{d}r^2} - \frac{\ell(\ell+1)}{r^2} - U(r) - U_c(r) + k^2\right) u_\ell^s(r) = 0, \tag{1.70}$$

where $U(r) = 2V(r)$ and, following (1.57), the reduced Coulomb potential $U_c(r) = 2V_c(r) = 2Z_1Z_2/r$. For large r, the potential $U(r)$ can be neglected compared with $U_c(r)$ and (1.70) then reduces to the Coulomb equation (1.56). The solution of (1.70) that is regular at the origin can thus be written asymptotically as a linear combination of the regular and irregular Coulomb wave functions $F_\ell(\eta, kr)$ and $G_\ell(\eta, kr)$. Hence, in analogy with (1.9), we look for a solution satisfying the boundary conditions

$$\begin{aligned} u_\ell^s(0) &\underset{r\to 0}{\sim} nr^{\ell+1}\,, \\ u_\ell^s(r) &\underset{r\to\infty}{\sim} F_\ell(\eta, kr) + G_\ell(\eta, kr)\tan\delta_\ell(k)\,. \end{aligned} \tag{1.71}$$

The quantity $\delta_\ell(k)$ defined by these equations is the phase shift due to the short-range potential $V(r)$ in the presence of the Coulomb potential $V_c(r)$. We note that $\delta_\ell(k)$ vanishes when the short-range potential is not present and contains all the information necessary to describe the non-Coulombic part of the scattering.

The coefficients $B_\ell^s(k)$ in (1.69) are determined by equating the coefficients of the ingoing wave in (1.49) and (1.69). This gives

$$B_\ell^s(k) = k^{-1}(2\ell+1)\mathrm{i}^\ell \cos\delta_\ell(k)\exp\{\mathrm{i}[\sigma_\ell + \delta_\ell(k)]\}\,. \tag{1.72}$$

Substituting this result into (1.69) then gives

$$\begin{aligned} \psi(\mathbf{r}) \underset{r\to\infty}{\sim} \psi_c(\mathbf{r}) + (2kr)^{-1}\sum_{\ell=0}^{\infty}(2\ell+1)\mathrm{i}^\ell \exp(2\mathrm{i}\sigma_\ell)\{\exp[2\mathrm{i}\delta_\ell(k)] - 1\}H_\ell^+(\eta, kr) \\ \times\, P_\ell(\cos\theta)\,, \end{aligned} \tag{1.73}$$

where we have defined the function

$$H_\ell^+(\eta, \rho) = \exp(\mathrm{i}\sigma_\ell)\,[F_\ell(\eta, \rho) + \mathrm{i}G_\ell(\eta, \rho)]\,. \tag{1.74}$$

We then find that

$$\psi(\mathbf{r}) \underset{r\to\infty}{\sim} \exp[\mathrm{i}(kz + \eta\ln k\zeta)] + \big[f_c(\theta) + f_s(\theta)\big]\frac{\exp[\mathrm{i}(kr - \eta\ln 2kr)]}{r}\,, \tag{1.75}$$

where $f_c(\theta)$ is the Coulomb scattering amplitude given by (1.52) and $f_s(\theta)$ is the scattering amplitude arising from the additional short-range potential $V(r)$. We find that

$$f_s(\theta) = \frac{1}{2\mathrm{i}k}\sum_{\ell=0}^{\infty}(2\ell+1)\exp(2\mathrm{i}\sigma_\ell)\{\exp[2\mathrm{i}\delta_\ell(k)] - 1\}P_\ell(\cos\theta)\,, \tag{1.76}$$

which is analogous to the result given by (1.29) when there is only a short-range potential.

The differential cross section can be obtained in the usual way from (1.75) by calculating the outward flux of particles scattered through a spherical surface $r^2 \mathrm{d}\Omega$ for large r per unit solid angle divided by the incident flux. This gives

$$\begin{aligned} \frac{\mathrm{d}\sigma}{\mathrm{d}\Omega} &= |f_c(\theta) + f_s(\theta)|^2 \\ &= |f_c(\theta)|^2 + |f_s(\theta)|^2 + 2\mathrm{Re}\left[f_c^*(\theta) f_s(\theta)\right] . \end{aligned} \tag{1.77}$$

At small scattering angles the Coulomb scattering amplitude will dominate the differential cross section giving a θ^{-4} singularity in the forward direction. However, at larger scattering angles $f_s(\theta)$ becomes relatively more important and information on the phase of $f_s(\theta)$ can be obtained from intermediate angles when the interference term in (1.77) involving both $f_c(\theta)$ and $f_s(\theta)$ is important.

Finally we remark that, as is the case for pure Coulomb scattering, because of the divergence in the forward direction the total cross section obtained by integrating (1.77) over all scattering angles is infinite.

1.3 Analytic Properties of the *S*-Matrix

In this section we consider the analytic properties of the partial wave S-matrix, defined by (1.14), in the complex momentum plane. We show that the poles in the S-matrix lying on the positive imaginary k-axis correspond to bound states while poles lying in the lower half k-plane close to the positive real k-axis correspond to resonances. We also derive an expression for the behaviour of the phase shift and the cross section when the energy of the scattered particle is in the neighbourhood of these poles.

We consider the solution $u_\ell(r)$ of the radial Schrödinger equation (1.8) describing the scattering of a particle by a spherically symmetric reduced potential $U(r)$ which we assume is less singular than r^{-2} at the origin and vanishes faster than r^{-3} at infinity. Hence we assume

$$\int_0^\infty r|U(r)|\mathrm{d}r < \infty \tag{1.78}$$

and

$$\int_0^\infty r^2|U(r)|\mathrm{d}r < \infty , \tag{1.79}$$

so that the solution $u_\ell(r)$ satisfies the boundary conditions (1.9).

Following Jost [515], we introduce two solutions $f_\ell(\pm k, r)$ of (1.8) defined by the relations

$$\lim_{r\to\infty} \mathrm{e}^{\pm \mathrm{i}kr} f_\ell(\pm k, r) = 1 . \tag{1.80}$$

These boundary conditions define $f_\ell(k,r)$ uniquely only in the lower half k-plane and $f_\ell(-k,r)$ uniquely only in the upper half k-plane. If the potential satisfies inequalities (1.78) and (1.79) then $f_\ell(k,r)$ is an analytic function of k when $\mathrm{Im}\, k < 0$ for all r, while $f_\ell(-k,r)$ is correspondingly an analytic function of k when $\mathrm{Im}\, k > 0$ [52]. These regions of analyticity can be extended if we impose stronger conditions on the potential. Thus if

$$I(\mu) = \int_0^\infty \mathrm{e}^{\mu r}|U(r)|\mathrm{d}r < \infty, \quad \mu \text{ real} > 0\,, \tag{1.81}$$

then $f_\ell(k,r)$ is analytic for $\mathrm{Im}\, k < \mu/2$ while $f_\ell(-k,r)$ is analytic for $\mathrm{Im}\, k > -\mu/2$. Further, if the potential can be written as a superposition of Yukawa potentials

$$U(r) = \int_{\mu_0}^\infty \rho(\mu)\frac{\mathrm{e}^{-\mu r}}{r}\mathrm{d}\mu\,, \tag{1.82}$$

where $\rho(\mu)$ is a weight function and $\mu_0 > 0$, then $f_\ell(k,r)$ will be analytic in the complex k-plane apart from a branch cut on the positive imaginary k-axis from $k = \mathrm{i}\mu_0/2$ to $\mathrm{i}\infty$ while $f_\ell(-k,r)$ will be analytic in the complex k-plane apart from a branch cut from $k = -\mathrm{i}\mu_0/2$ to $-\mathrm{i}\infty$. These branch cuts are called Yukawa cuts. Finally, if the potential vanishes identically beyond a certain distance a_0 then $I(\mu)$ defined by (1.81) is finite for all μ so that $f_\ell(\pm k,r)$ are analytic functions of k in the open k-plane for all fixed values of r, that is, they are entire functions of k.

We can express the physical solution of (1.8), defined by the boundary conditions (1.9), as a linear combination of $f_\ell(\pm k,r)$. Let us normalize this solution so that it satisfies

$$\lim_{r\to 0} r^{-l-1}u_\ell(r) = 1\,. \tag{1.83}$$

From a theorem proved by Poincaré [749], the absence of a k-dependence in this boundary condition implies that this solution is an entire function of k. The Jost functions [515] are then defined by

$$\tilde{f}_\ell(\pm k) = W[f_\ell(\pm k,r), u_\ell(r)]\,, \tag{1.84}$$

where the Wronskian $W[f,g] = fg' - f'g$ and where the primes denote the derivatives with respect to r. It is straightforward to show from the differential equation (1.8) satisfied by $f_\ell(\pm k,r)$ and $u_\ell(r)$ that the Wronskian is independent of r. It is also convenient to introduce other Jost functions by the equation

$$f_\ell(\pm k) = \frac{k^\ell \exp(\pm\frac{1}{2}\mathrm{i}\ell\pi)}{(2\ell+1)!!}\tilde{f}_\ell(\pm k)\,. \tag{1.85}$$

The functions $f_\ell(+k)$ and $f_\ell(-k)$ are continuous at $k = 0$ and approach unity at large $|k|$ for $\mathrm{Im}\, k \le 0$ and ≥ 0, respectively.

We now use the relations

$$W[f_\ell(\pm k, r),\, f_\ell(\mp k, r)] = \pm 2\mathrm{i}k\,,$$
$$W[f_\ell(\pm k, r),\, f_\ell(\pm k, r)] = 0\,, \tag{1.86}$$

which follow from (1.80) and the definition of the Wronskian, to write $u_\ell(r)$ in the form

$$u_\ell(r) = \frac{1}{2\mathrm{i}k}[\tilde{f}_\ell(k) f_\ell(-k, r) - \tilde{f}_\ell(-k) f_\ell(k, r)]\,. \tag{1.87}$$

Comparing this equation with the asymptotic form (1.13) and using (1.80) then yields the following expression for the S-matrix elements:

$$S_\ell(k) = \mathrm{e}^{\mathrm{i}\pi\ell}\frac{\tilde{f}_\ell(k)}{\tilde{f}_\ell(-k)} = \frac{f_\ell(k)}{f_\ell(-k)}\,. \tag{1.88}$$

This equation relates the analytic properties of the S-matrix with the simpler analytic properties of the Jost functions.

In order to study the analytic properties of the Jost functions further we return to (1.8) satisfied by the functions $f_\ell(\pm k, r)$. In particular we consider

$$\left(\frac{\mathrm{d}^2}{\mathrm{d}r^2} - \frac{\ell(\ell+1)}{r^2} - U(r) + k^2\right) f_\ell(-k, r) = 0\,. \tag{1.89}$$

We now take the complex conjugate of this equation, which gives

$$\left(\frac{\mathrm{d}^2}{\mathrm{d}r^2} - \frac{\ell(\ell+1)}{r^2} - U(r) + k^{*2}\right) f_\ell^*(-k, r) = 0\,, \tag{1.90}$$

where we have assumed that r, ℓ and $U(r)$ are real but k can take complex values. In addition, it follows from (1.89) that $f_\ell(k^*, r)$ is a solution of

$$\left(\frac{\mathrm{d}^2}{\mathrm{d}r^2} - \frac{\ell(\ell+1)}{r^2} - U(r) + k^{*2}\right) f_\ell(k^*, r) = 0\,. \tag{1.91}$$

Now from (1.80)

$$f_\ell^*(-k, r) \underset{r\to\infty}{\sim} \exp(-\mathrm{i}k^* r) \tag{1.92}$$

and

$$f_\ell(k^*, r) \underset{r\to\infty}{\sim} \exp(-\mathrm{i}k^* r)\,, \tag{1.93}$$

so that $f_\ell^*(-k,r)$ and $f_\ell(k^*,r)$ satisfy the same boundary conditions. Since these functions also satisfy the same differential equation, namely (1.90) and (1.91), respectively, they are equal for all r, for all points in the upper half k-plane and for all other points which admit an analytic continuation from the upper half k-plane. Hence in this region

$$f_\ell^*(-k,r) = f_\ell(k^*,r) \tag{1.94}$$

and thus from (1.84) the Jost functions satisfy

$$\tilde{f}_\ell^*(-k) = \tilde{f}_\ell(k^*)\,. \tag{1.95}$$

Combining this result with (1.88) we find that the S-matrix satisfies the following symmetry relation

$$S_\ell(k)S_\ell(-k) = \mathrm{e}^{2\mathrm{i}\pi\ell}\,\frac{\tilde{f}_\ell(k)}{\tilde{f}_\ell(-k)}\,\frac{\tilde{f}_\ell(-k)}{\tilde{f}_\ell(k)} = \mathrm{e}^{2\mathrm{i}\pi\ell} \tag{1.96}$$

and the unitarity relation

$$S_\ell(k)S_\ell^*(k^*) = \frac{\tilde{f}_\ell(k)}{\tilde{f}_\ell(-k)}\,\frac{\tilde{f}_\ell^*(k^*)}{\tilde{f}_\ell^*(-k^*)} = 1\,. \tag{1.97}$$

Also, from (1.96) and (1.97) we obtain the reflection relation

$$S_\ell(k) = \mathrm{e}^{2\mathrm{i}\pi\ell}\,S_\ell^*(-k^*)\,. \tag{1.98}$$

From (1.97), it follows that if k is real then the S-matrix has unit modulus and can thus be expressed in terms of a real phase shift $\delta_\ell(k)$ as

$$S_\ell(k) = \exp[2\mathrm{i}\delta_\ell(k)]\,, \tag{1.99}$$

in agreement with (1.14). In addition it follows from (1.98) that if the S-matrix has a pole at the point k, then it also has a pole at the point $-k^*$ and from (1.96) and (1.97) it has zeros at the points $-k$ and k^*. Thus the poles and zeros of the S-matrix are symmetrically situated with respect to the imaginary k-axis.

In order to determine the physical significance of poles in the S-matrix we note from (1.84) that the Jost functions $\tilde{f}_\ell(\pm k)$ are finite for all finite k. Hence it follows from (1.88) that a pole in the S-matrix must correspond to a zero in $\tilde{f}_\ell(-k)$ rather than a pole in $\tilde{f}_\ell(k)$. Substituting this result into (1.87) and using (1.80) shows that the physical solution of (1.8) corresponding to a pole in the S-matrix has the following asymptotic form:

$$u_\ell(r) \underset{r\to\infty}{\sim} N\mathrm{e}^{\mathrm{i}kr}\,, \tag{1.100}$$

where N is a normalization factor. When k is in the upper half k-plane, it follows from (1.100) that the corresponding wave function vanishes exponentially and hence is normalizable. Since the Hamiltonian is hermitian, all normalizable wave functions must correspond to real energy eigenvalues and hence the corresponding value of k^2 must be real. This shows that if a pole in the S-matrix occurs in the upper half k-plane in the region of analyticity connected to the physical real k-axis it must lie on the positive imaginary axis. If we write $k = \mathrm{i}\kappa$, where κ is real and positive, then (1.100) becomes

$$u_\ell(r) \underset{r\to\infty}{\sim} N\mathrm{e}^{-\kappa r}\,, \tag{1.101}$$

which clearly corresponds to a bound state with binding energy $-\kappa^2/2$. In the lower half k-plane the wave function defined by (1.100) diverges exponentially and thus cannot be normalized. The above arguments based on the hermiticity of the Hamiltonian then break down and the corresponding poles are then no longer confined to the imaginary k-axis.

We present in Fig. 1.1 a possible distribution of S-matrix poles in the complex k-plane. For potentials satisfying (1.78) and (1.79), only a finite number of bound states can be supported and these give rise to the poles lying on the positive imaginary axis in this figure. However, an infinite number of poles can occur in the lower half k-plane. If they do not lie on the negative imaginary k-axis, they occur in pairs symmetric with respect to this axis, as discussed above. If they lie on the negative imaginary k-axis, they are often referred to as virtual state poles. Poles lying in the lower half k-plane and close to the real positive k-axis give rise to resonance effects in the cross section which will be discussed below. The corresponding resonance states, defined by the outgoing wave boundary condition (1.100), are often called Siegert states [876]. Poles lying in the lower half k-plane and far away from the real positive k-axis contribute to the smooth "background" or "non-resonant" scattering. The distribution of poles in the complex k-plane has been discussed in detail in a few cases, most notably by Nussenzveig [700] for scattering by a square well potential.

We now consider an isolated pole in the S-matrix which lies in the lower half k-plane close to the positive real k-axis. We show that this pole gives rise to

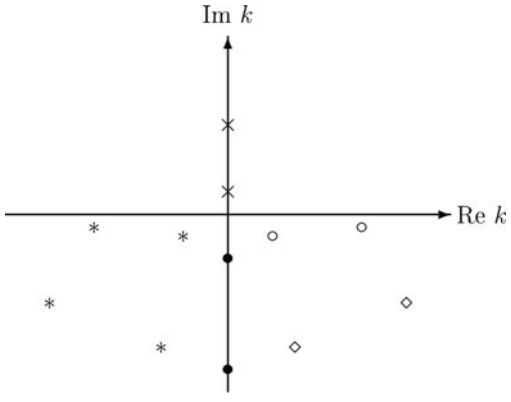

Fig. 1.1 Distribution of S-matrix poles in the complex k-plane. $\times$, poles corresponding to bound states; $\circ$, poles corresponding to resonances; $\diamond$, poles corresponding to background scattering; $*$, conjugate poles required by the symmetry and unitarity relations; $\bullet$, poles corresponding to virtual states

resonance scattering at the nearby real energy. We assume that the pole occurs at the complex energy

$$E = E_r - \tfrac{1}{2}\mathrm{i}\Gamma\,, \tag{1.102}$$

where E_r, the resonance position, and Γ, the resonance width, are both real positive numbers and where from (1.3) we remember that $E = \frac{1}{2}k^2$. Now from the unitarity relation (1.97) we see that corresponding to this pole there is a zero in the S-matrix at a complex energy in the upper half k-plane given by

$$E = E_r + \tfrac{1}{2}\mathrm{i}\Gamma\,. \tag{1.103}$$

For energies E on the real axis in the neighbourhood of this pole, the S-matrix can be written in the following form which is both unitary and explicitly contains the pole and zero:

$$S_\ell(k) = \exp\left[2\mathrm{i}\delta_\ell^0(k)\right]\frac{E - E_r - \frac{1}{2}\mathrm{i}\Gamma}{E - E_r + \frac{1}{2}\mathrm{i}\Gamma}\,. \tag{1.104}$$

The quantity $\delta_\ell^0(k)$ in this equation is called the "background" or "non-resonant" phase shift. Provided that the energy E_r is not close to threshold, $E = 0$, nor to another resonance then the background phase shift is slowly varying with energy. Comparing (1.99) and (1.104) we obtain the following expression for the phase shift:

$$\delta_\ell(k) = \delta_\ell^0(k) + \delta_\ell^r(k)\,, \tag{1.105}$$

where we have written

$$\delta_\ell^r(k) = \tan^{-1}\frac{\frac{1}{2}\Gamma}{E_r - E}\,. \tag{1.106}$$

The quantity $\delta_\ell^r(k)$ is called the "resonant" phase shift which we see from (1.106) increases through π radians as the energy E increases from well below to well above the resonance position E_r. It is also clear from (1.106) that the rapidity of this increase is inversely proportional to Γ, the resonance width.

If the background phase shift $\delta_\ell^0(k)$ is zero then we obtain from (1.30) and (1.106) the following expression for the partial wave cross section:

$$\sigma_\ell = \frac{4\pi}{k^2}(2\ell+1)\frac{\frac{1}{4}\Gamma^2}{(E - E_r)^2 + \frac{1}{4}\Gamma^2}\,. \tag{1.107}$$

This expression is called the Breit–Wigner one-level resonance formula first derived to describe nuclear resonance reactions [135]. We see that at the energy $E = E_r$ the

partial wave cross section σ_ℓ reaches its maximum value $4\pi(2\ell+1)/k^2$ allowed by unitarity and decreases to zero well below and well above this energy.

If the background phase shift $\delta_\ell^0(k)$ is non-zero then the partial wave cross section can be written as

$$\sigma_\ell = \frac{4\pi}{k^2}(2\ell+1)\sin^2\delta_\ell(k) = \frac{4\pi}{k^2}(2\ell+1)\frac{(\epsilon+q)^2}{1+\epsilon^2}\sin^2\delta_\ell^0(k)\,, \tag{1.108}$$

where ϵ is the reduced energy

$$\epsilon = \frac{E-E_r}{\frac{1}{2}\Gamma} \tag{1.109}$$

and q is the resonance shape parameter or line profile index

$$q = -\cot\delta_\ell^0(k)\,. \tag{1.110}$$

The line profile index was introduced by Fano [301] to describe resonant atomic photoionization processes. It follows from (1.108) that the partial wave cross section is zero when $\epsilon = -q$ and achieves its unitarity limit $4\pi(2\ell+1)/k^2$ when $\epsilon = q^{-1}$. In Fig. 1.2 we illustrate the total phase shift $\delta_\ell(k)$ and the partial wave cross section σ_ℓ for s-wave scattering for four different values of the background phase shift,

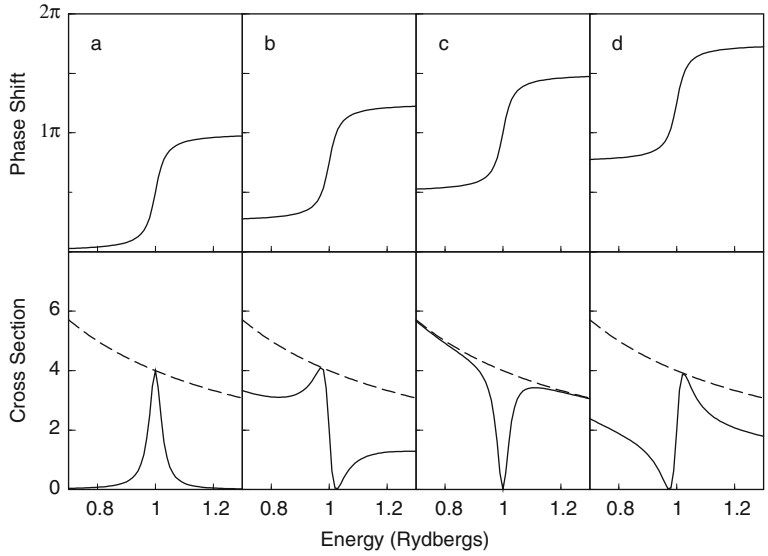

Fig. 1.2 The total phase shift $\delta_\ell(k)$ and the partial wave cross section σ_ℓ for s-wave resonance scattering with $k_r^2 = 2E_r = 1.0$ and $\Gamma = 0.05$ for four different values of the background phase shift. Case (**a**), $\delta_0^0(k) = 0$ giving $q = \infty$; case (**b**), $\delta_0^0(k) = \pi/4$ giving $q = -1$; case (**c**), $\delta_0^0(k) = \pi/2$ giving $q = 0$; case (**d**), $\delta_0^0(k) = 3\pi/4$ giving $q = 1$. The *cross section* is given in πa_0^2 units and the *dashed lines* are the s-wave unitarity limit $4k^{-2}$

which we assume is energy independent. Case (a) with $q = \infty$ corresponds to a standard Breit–Wigner resonance given by (1.107), where the non-resonant background scattering is zero. Case (c) with $q = 0$ corresponds to a window resonance where the background scattering has its maximum value allowed by unitarity. Finally, cases (b) and (d) are intermediate cases where the resonance shapes are asymmetric.

When several resonance poles lie in the lower half k-plane and close to the positive real k-axis their effects on the cross section may overlap. In the case of n resonances we must replace (1.104) by

$$S_\ell(k) = \exp\left[2\mathrm{i}\delta_\ell^0(k)\right] \prod_{j=1}^{n} \frac{E - E_j - \frac{1}{2}\mathrm{i}\Gamma_j}{E - E_j + \frac{1}{2}\mathrm{i}\Gamma_j}\,, \tag{1.111}$$

where the position of the jth pole is $E = E_j - \frac{1}{2}\mathrm{i}\Gamma_j$. The total phase shift is then given by

$$\delta_\ell(k) = \delta_\ell^0(k) + \sum_{j=1}^{n} \tan^{-1} \frac{\frac{1}{2}\Gamma_j}{E_j - E}\,. \tag{1.112}$$

In this case the total phase shift increases through $n\pi$ radians as the energy increases from below all the resonances to above all the resonances, provided that the non-resonant phase shift $\delta_\ell^0(k)$ is slowly varying over this range. The corresponding cross section will achieve its unitarity limit n times where the total phase shift goes through an half odd integral multiple of π radians and will have n zeros where it goes through an integral multiple of π radians.

1.4 Effective Range Theory

In this section we consider the analytic behaviour of the phase shift and the scattering amplitude in the neighbourhood of threshold energy. We show that there is a close relationship between the low-energy scattering amplitude and the bound-state spectrum at negative energies. We consider first the analytic properties for short-range potentials, where the potential vanishes faster than any inverse power of the distance. We then extend our discussion to the situation where the potential behaves asymptotically as r^{-s} where $s \geq 2$, which is relevant for low-energy electron scattering by neutral atoms. Finally, we consider scattering by a Coulomb potential which is relevant to electron–ion scattering.

1.4.1 Short-Range Potentials

We commence by considering the solution of the radial Schrödinger equation (1.8) where we assume that the potential $U(r)$ satisfies the condition

$$U(r) = 0, \quad r \geq a\,, \tag{1.113}$$

for some finite radius a. It follows from (1.9) and (1.15) that the solution which is regular at the origin satisfies the asymptotic boundary condition

$$u_\ell(r) = s_\ell(kr) + c_\ell(kr)K_\ell(k), \quad r \geq a. \tag{1.114}$$

In order to determine the analytic properties of the K-matrix $K_\ell(k)$ we relate it to the R-matrix $R_\ell(E)$ which we introduce in Sect. 4.1 and which is defined on the boundary $r = a$ by

$$u_\ell(a) = R_\ell(E)\left(a\frac{\mathrm{d}u_\ell}{\mathrm{d}r} - bu_\ell\right)_{r=a}, \tag{1.115}$$

where b is an arbitrary constant. Substituting (1.114) for $u_\ell(r)$ into (1.115) then yields

$$[K_\ell(k)]^{-1} = \frac{c_\ell(ka) - R_\ell(E)[kac'_\ell(ka) - bc_\ell(ka)]}{-s_\ell(ka) + R_\ell(E)[kas'_\ell(ka) - bs_\ell(ka)]}, \tag{1.116}$$

where $s'_\ell(kr)$ and $c'_\ell(kr)$ are the derivatives of $s_\ell(kr)$ and $c_\ell(kr)$ with respect to the argument kr.

The analytic properties of the R-matrix are discussed in Sect. 4.1, where we show that it is a real meromorphic function of the energy with simple poles only on the real energy axis. The analytic properties of the functions $s_\ell(kr)$ and $c_\ell(kr)$ and their derivatives are related to those of the spherical Bessel and Neumann functions $j_\ell(kr)$ and $n_\ell(kr)$ defined by (1.10) and (1.11). These functions are discussed in Appendix C.2, where we show that they can be expanded about $z = 0$ as follows:

$$\begin{aligned} j_\ell(z) &= [(2\ell+1)!!]^{-1}z^\ell + O(z^{\ell+2}), \\ n_\ell(z) &= -[(2\ell-1)!!]z^{-\ell-1} + O(z^{-\ell+1}). \end{aligned} \tag{1.117}$$

Hence $k^{-\ell-1}s_\ell(kr)$, $k^{-\ell}s'_\ell(kr)$, $k^\ell c_\ell(kr)$ and $k^{\ell+1}c'_\ell(kr)$ are entire functions of k^2, that is they are analytic functions of k^2 for fixed r. It follows from (1.116) that the M-matrix, which is defined by the equation

$$M_\ell(k^2) = k^{2\ell+1}\,[K_\ell(k)]^{-1}, \tag{1.118}$$

is a real analytic function of k^2 which can be expanded in a power series in k^2 about $k^2 = 0$. It is also useful to express the T-matrix element defined by (1.26) in terms of $M_\ell(k^2)$. We find using (1.118) that

$$T_\ell(k) = \frac{2\mathrm{i}k^{2\ell+1}}{M_\ell(k^2) - \mathrm{i}k^{2\ell+1}}. \tag{1.119}$$

We will see in Chap. 3 that this result generalizes in a straightforward way to multichannel scattering. Also, remembering from (1.15) that $K_\ell(k) = \tan\delta_\ell(k)$, it follows that we can expand $k^{2\ell+1}\cot\delta_\ell(k)$ about zero energy in the form

$$k^{2\ell+1}\cot\delta_\ell(k) = -\frac{1}{a_\ell} + \frac{1}{2}r_{e\ell}k^2 + O(k^4)\,, \tag{1.120}$$

where a_ℓ is called the "scattering length" and $r_{e\ell}$ is called the "effective range". This "effective range expansion" or "Blatt–Jackson expansion" was first derived by Blatt and Jackson [115] and by Bethe [104].

We can obtain a simple physical picture of the s-wave scattering length a_0 in terms of the zero-energy wave function. If we adopt the following normalization of the s-wave reduced radial wave function

$$u_0(r) \underset{r\to\infty}{\sim} \sin kr + \cos kr\tan\delta_0(k), \quad r \geq a\,, \tag{1.121}$$

then in the limit as the energy tends to zero, we find using (1.120) that

$$\lim_{k\to 0} u_0(r) = k(r - a_0), \quad r \geq a\,. \tag{1.122}$$

It follows that the s-wave scattering length a_0 is the intercept of the extrapolation of the asymptote of the zero-energy s-wave reduced radial wave function with the r-axis.

As an example of the relationship between the s-wave scattering length and the zero-energy wave function we consider the solution of (1.8) for a square-well potential. We consider the solution of the equation

$$\left(\frac{\mathrm{d}^2}{\mathrm{d}r^2} - U(r) + k^2\right)u(r) = 0\,, \tag{1.123}$$

where the range $r = a$ of the potential $U(r)$ is taken to equal 1 so that

$$\begin{aligned} U(r) &= -A, \quad r < 1, \\ U(r) &= 0, \quad r \geq 1\,, \end{aligned} \tag{1.124}$$

and the energy $E = \frac{1}{2}k^2 = 0$. Also the sign of the potential strength A is chosen so that it is positive for attractive potentials and negative for repulsive potentials.

We show in Fig. 1.3, three examples of the solution $u(r)$ of (1.123) and (1.124) for three different potential strengths. The first example, shown in Fig. 1.3a, corresponds to a repulsive potential where the scattering length $a_0 = 0.5$, the second example, shown in Fig. 1.3b, corresponds to a weak attractive potential which does not support a bound state where $a_0 = -1$ and the third example, shown in Fig. 1.3c, corresponds to a stronger attractive potential which supports one bound state where $a_0 = 2$.

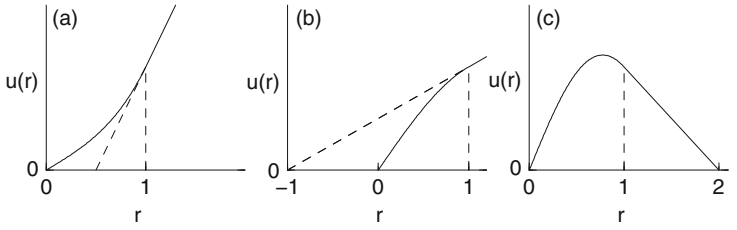

Fig. 1.3 The s-wave zero-energy reduced radial wave function $u(r)$, represented by the *full lines*, showing the scattering length a_0 for three square-well potentials with unit radius: (**a**) a repulsive potential with potential strength $A = -3.667$, giving $a_0 = 0.5$; (**b**) a weak attractive potential with potential strength $A = 1.359$, giving $a_0 = -1$; (**c**) a stronger attractive potential with potential strength $A = 4.116$, giving $a_0 = 2$. Also, represented by the *dashed lines* in (**a**) and (**b**) are the extrapolations of $u(r)$ for $r \geq 1$ back to its intercept $r = a_0$ with the r-axis

The relationship between the s-wave scattering length a_0 and the potential strength A is obtained by solving (1.123) and (1.124) subject to the condition that the solution $u(r)$ and its derivative are continuous on the boundary $r = 1$. We can show that the relationship for repulsive potentials $A < 0$ is

$$a_0 = 1 - \alpha^{-1} \tanh \alpha, \quad \text{where } \alpha^2 = -A\,, \tag{1.125}$$

and the relationship for attractive potentials $A > 0$ is

$$a_0 = 1 - \alpha^{-1} \tan \alpha, \quad \text{where } \alpha^2 = A\,. \tag{1.126}$$

The dependence of the scattering length a_0 on the potential strength A, given by (1.125) and (1.126), is shown in Fig. 1.4 for A in the range $-30 < A < 30$, where we have indicated by crosses on this figure the (A, a_0) values corresponding to the three solutions shown in Fig. 1.3. For an infinitely strong repulsive potential, or hard-core potential, where $A = -\infty$, the scattering length equals the range of the potential, which is unity in this example. As the potential strength increases towards attractive values, the scattering length decreases and passes through zero when $A = 0$, becoming infinitely negative when the asymptote of the solution $u(r)$ is parallel to the r-axis. We see from (1.126) that this occurs when $A = (\pi/2)^2$. A further increase in the potential strength leads to a large positive scattering length, resulting in the support of a bound state. The scattering length again decreases with increasing attraction, becoming infinitely negative again when $A = (3\pi/2)^2$. We see from (1.126) that this process is repeated with each new branch, corresponding to a new state becoming bound, occurring when $A = [(2n+1)\pi/2]^2$, $n = 0, 1, 2, \ldots$. Finally we observe that the same general picture occurs for square-well potentials of arbitrary range a, the strength of the potential where the asymptotes of the solution $u(r)$ are parallel to the r-axis then being given by $A = [(2n+1)\pi/(2a)]^2$, $n = 0, 1, 2, \ldots$.

We now discuss the relationship between the scattering length and effective range and the low-energy behaviour of the S-matrix, T-matrix and cross section. Provided

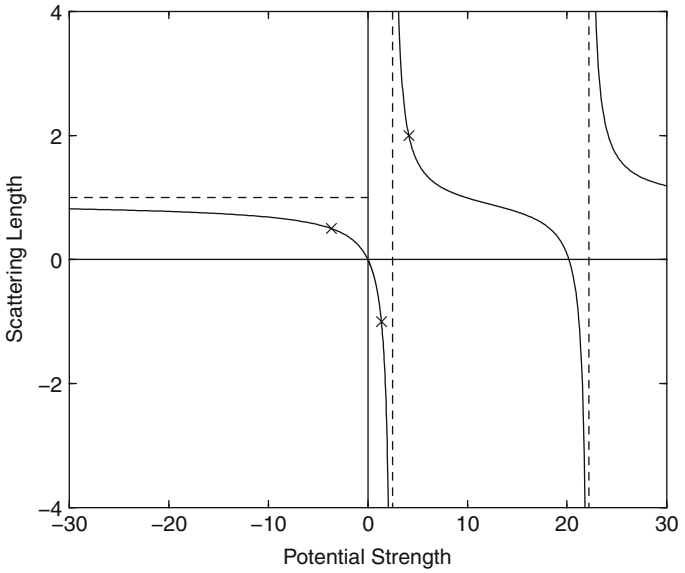

Fig. 1.4 The dependence of the scattering length a_0 on the potential strength A for a square-well potential with unit range. The scattering length and potential strength corresponding to Fig. 1.3a–c is marked by *crosses* on this figure

that the p-wave scattering length a_1 is non-singular then the s-wave partial wave cross section dominates low-energy scattering. It follows from (1.30) and (1.120) that the low-energy s-wave cross section

$$\sigma_0 = \frac{4\pi}{k^2}\sin^2\delta_0(k) = \frac{4\pi}{k^2}\frac{1}{1+\cot^2\delta_0(k)} = \frac{4\pi a_0^2}{k^2a_0^2 + (1-\frac{1}{2}r_{e0}k^2a_0)^2}\,. \quad (1.127)$$

The zero-energy cross section is thus $4\pi a_0^2$. Also, when an s-wave bound state occurs at zero energy then the scattering length and hence the cross section is infinite. We now determine the behaviour of the cross section when an s-wave bound state occurs close to zero energy. It follows from (1.15) and (1.26) that

$$T_\ell(k) = S_\ell(k) - 1 = \frac{2\mathrm{i}}{\cot\delta_\ell(k) - \mathrm{i}}\,. \quad (1.128)$$

Hence a pole in the S- and T-matrices occurs when $\cot\delta_\ell(k) = \mathrm{i}$. However, we saw in Sect. 1.3, see Fig. 1.1, that a bound-state pole in the S-matrix and hence in the T-matrix must lie on the imaginary k-axis, so that

$$k_b = \mathrm{i}\kappa_b\,, \quad (1.129)$$

where κ_b is real and positive. Combining (1.128) and (1.129) we obtain the following condition

$$k_b \cot \delta_0(k_b) = -\kappa_b \,, \tag{1.130}$$

for an s-wave bound state. By comparing this equation with the effective range expansion (1.120) we find that the scattering length is related to the position of the pole in the S- and T-matrices by

$$\kappa_b = a_0^{-1} \,, \tag{1.131}$$

where we have retained only the first term on the right-hand side of (1.120). Substituting this result into (1.127) gives the following expression for the low-energy s-wave cross section:

$$\sigma_0 = \frac{4\pi}{k^2 + \kappa_b^2} \,. \tag{1.132}$$

As we have already remarked, the s-wave cross section is infinite at zero energy when the bound-state pole occurs at zero energy. Also, since this cross section is independent of the sign of κ_b, it is not possible to distinguish by measuring the cross section alone, whether the pole in Fig. 1.1 corresponds to a bound state with positive κ_b or a virtual state with negative κ_b.

In the case of non-zero partial waves we obtain the following expression for the T-matrix by combining (1.120) and (1.128)

$$T_\ell(k) = \frac{2\mathrm{i}k^{2\ell+1}}{-a_\ell^{-1} + \frac{1}{2} r_{e\ell} k^2 - \mathrm{i}k^{2\ell+1}} \,, \tag{1.133}$$

which can be written in the form

$$T_\ell(k) = \frac{\mathrm{i}\Gamma}{E_r - E - \frac{1}{2}\mathrm{i}\Gamma} \,, \tag{1.134}$$

where the resonance position is given by

$$E_r = \frac{1}{a_\ell r_{e\ell}} \tag{1.135}$$

and the resonance width by

$$\Gamma = -\frac{2}{r_{e\ell}} k^{2\ell+1} \,. \tag{1.136}$$

It follows that the effective range $r_{e\ell}$, corresponding to a low-energy resonance with $l \geq 1$, must be negative and its width energy dependent. This type of resonance is

caused by the repulsive angular momentum barrier $\ell(\ell+1)r^{-2}$ which inhibits its decay.

Finally, we can show that although we have derived the effective range expansion (1.120) for a finite range potential satisfying (1.120), it is valid if the potential falls off as fast as, or faster than, an exponential.

1.4.2 Long-Range Potentials

We now consider modifications that have to be made to the effective range expansion (1.120) when the potential $U(r)$ in the radial Schrödinger equation (1.8) behaves asymptotically as follows:

$$U(r) = \frac{A}{r^s}, \quad r \geq a, \quad s \geq 2\,. \tag{1.137}$$

We can determine the required modifications by considering the first Born approximation for the phase shift given by (1.20), that is by

$$\tan\delta_\ell^B(k) = -k\int_0^\infty U(r)\,j_\ell^2(kr)r^2\mathrm{d}r\,, \tag{1.138}$$

which is applicable here since the coefficients in the effective range expansion arise from the long-range tail of the potential where it is weak. In the limit as $k \to 0$ we can use the power series expansion (C.33) for the spherical Bessel function $j_\ell(kr)$ in (1.138). It follows that the first term in the expansion of the integral in (1.138) only converges for large r if $s > 2\ell+3$, which gives rise to the first term in the effective range expansion (1.120). If $s \leq 2\ell+3$ the integral diverges and the first term in the effective range expansion is no longer defined. In a similar way, the second term in the expansion of the integral in (1.138) only converges for large r if $s > 2\ell+5$ and consequently if $s \leq 2\ell+5$ the second term in the effective range expansion is not defined. Summarizing these results for the terms in the effective range expansion (1.120) we obtain

$$\begin{aligned} &\text{scattering length } a_\ell \text{ defined if } s > 2\ell+3 \\ &\text{effective range } r_{e\ell} \text{ defined if } \quad s > 2\ell+5\,, \end{aligned} \tag{1.139}$$

and so on for higher terms in the effective range expansion.

An important example of long-range potentials occurs in elastic electron scattering by an atom in a non-degenerate s-wave ground state such as atomic hydrogen or the inert gases. We discuss this polarization potential in detail in Sect. 2.2.2, see (2.19), where we show that $U(r)$ has the asymptotic form

$$U(r) = 2V_p(r) \underset{r\to\infty}{\sim} -\frac{\alpha}{r^4}\,, \tag{1.140}$$

where α is the dipole polarizability. The radial Schrödinger equation (1.8) then becomes

$$\left(\frac{\mathrm{d}^2}{\mathrm{d}r^2} - \frac{\ell(\ell+1)}{r^2} + \frac{\alpha}{r^4} + k^2\right) u_\ell(r) = 0, \quad r \geq a\,, \tag{1.141}$$

where a is the radius beyond which the potential achieves its asymptotic form. In order to obtain the threshold behaviour of the phase shift we use the Born approximation (1.138), where we consider the contribution to this integral arising from $r \geq a$. Calling this contribution I_ℓ we obtain, after writing $x = kr$,

$$I_\ell = \frac{\pi\alpha k^2}{2} \int_{ka}^{\infty} J^2_{\ell+\frac{1}{2}}(x) x^{-3} \mathrm{d}x\,, \tag{1.142}$$

where for $\ell \geq 1$, the contribution to the integral from $r < a$ behaves as $k^{2\ell+1}$ for small k and can therefore be neglected compared with I_ℓ as $k \to 0$. Also, for $\ell \geq 1$ the integral in (1.142) converges at its lower limit for all $k \geq 0$. Carrying out this integral we find that

$$k^2 \cot \delta_\ell(k) = \frac{8(\ell+\frac{3}{2})(\ell+\frac{1}{2})(\ell-\frac{1}{2})}{\pi\alpha} + \text{ higher order terms}, \quad \ell \geq 1\,. \tag{1.143}$$

It follows in accord with (1.139) that the scattering length is not defined in the presence of a long-range polarization potential when $\ell \geq 1$.

For s-wave scattering in a long-range polarization potential, the contribution to the integral from $r < a$ dominates (1.142) and hence (1.143) is no longer applicable. In this case O'Malley et al. [704] transformed (1.141) into a modified form of Mathieu's equation. Replacing $s_\ell(kr)$ and $c_\ell(kr)$ in (1.114) by the appropriate regular and irregular solutions of this equation and using the known analytic behaviour of the Mathieu functions they obtained

$$k \cot \delta_0(k) = -\frac{1}{a_0} + \frac{\pi\alpha}{3a_0^2}k + \frac{2\alpha}{3a_0}k^2 \ln\left(\frac{\alpha k^2}{16}\right) + O(k^2), \quad \ell = 0\,. \tag{1.144}$$

This equation differs from (1.120) due to the presence of terms containing k and $k^2 \ln k$. Hence the scattering length a_0 is defined but the effective range is not, in accord with (1.139).

The low-energy behaviour of the total cross section in the presence of a long-range polarization potential can be obtained by substituting the above result into (1.30). We obtain

$$\sigma_{\mathrm{tot}}(k) = 4\pi\left(a_0 + \frac{\pi\alpha}{3}k + \cdots\right)^2, \tag{1.145}$$

where we have omitted higher order terms in k and higher partial wave contributions. It follows that the derivative of the total cross section with respect to energy is infinite at threshold, whereas in the absence of the polarization potential it is finite. Also, if the scattering length a_0 is negative, then the total cross section will decrease from threshold and in the absence of significant contributions from higher terms in the expansion (1.145) will become zero when $k = k_0$ where

$$k_0 = -\frac{3a_0}{\pi\alpha}\,. \tag{1.146}$$

This leads to the Ramsauer minimum which occurs, for example, in the total cross section for low-energy electron scattering from the heavier inert gases Ar, Kr and Xe where the scattering length a_0 is negative. On the other hand, if a_0 is positive, as is the case for electron scattering by He and Ne, there is no low-energy minimum in the cross section.

Levy and Keller [588] have considered the general case of potentials whose behaviour at large distances is given by (1.137). They found that

$$\tan\delta_\ell(k) = \tfrac{1}{2}\pi A k^{s-2}\frac{2^{1-s}\Gamma(s-1)\Gamma(\ell+\frac{3}{2}-\frac{1}{2}s)}{\Gamma^2(\frac{1}{2}s)\Gamma(\ell+\frac{1}{2}+\frac{1}{2}s)}, \quad 2 < s < 2\ell+3 \tag{1.147}$$

and

$$\tan\delta_\ell(k) = -\frac{Ak^{2\ell+1}\ln k}{[(2\ell+1)!!]^2}, \quad s = 2\ell+3\,. \tag{1.148}$$

By considering the contribution from higher angular momenta we find that the total threshold cross section is finite if $s > 2$ while the differential cross section is finite if $s > 3$.

Another long-range potential of interest is a dipole potential which falls off asymptotically as r^{-2} and is less singular than r^{-2} at the origin. This occurs in many applications, for example, in the scattering of electrons by polar molecules or by hydrogen atoms in degenerate excited states. The radial Schrödinger equation then has the asymptotic form

$$\left(\frac{\mathrm{d}^2}{\mathrm{d}r^2} - \frac{\ell(\ell+1)}{r^2} - \frac{A}{r^2} + k^2\right) u_\ell(r) = 0, \quad r \geq a\,. \tag{1.149}$$

This equation has analytic solutions which we can obtain by combining the r^{-2} terms as follows:

$$\lambda(\lambda+1) = \ell(\ell+1) + A\,, \tag{1.150}$$

which has the solution

$$\lambda = -\tfrac{1}{2} \pm \tfrac{1}{2}\left[(2\ell+1)^2 + 4A\right]^{1/2}\,. \tag{1.151}$$

Using this definition, (1.149) reduces to the standard form

$$\left(\frac{\mathrm{d}^2}{\mathrm{d}r^2} - \frac{\lambda(\lambda+1)}{r^2} + k^2\right) u_\ell(r) = 0, \quad r \geq a\,. \tag{1.152}$$

where λ is in general a non-integral quantity. In analogy with (1.10) and (1.11) we can define two linearly independent solutions of (1.152) by

$$s_\lambda(kr) = krj_\lambda(kr) \underset{r\to\infty}{\sim} \sin(kr - \tfrac{1}{2}\lambda\pi) \tag{1.153}$$

and

$$c_\lambda(kr) = -krn_\lambda(kr) \underset{r\to\infty}{\sim} \cos(kr - \tfrac{1}{2}\lambda\pi)\,, \tag{1.154}$$

where it is convenient to choose the upper positive sign in (1.151) so that $\lambda \to \ell$ in the limit $A \to 0$.

The solution of the radial Schrödinger equation, corresponding to a dipole potential $U(r)$, which is regular at the origin can be written in analogy with (1.114) by

$$u_\ell(r) = s_\lambda(kr) + c_\lambda(kr)K_\lambda(k), \quad r \geq a\,, \tag{1.155}$$

which defines the K-matrix $K_\lambda(k)$. We can relate the physical K-matrix $K_\ell(k)$, defined by (1.9) and (1.15), to $K_\lambda(k)$, defined by (1.155). We find that

$$K_\ell(k) = \frac{\sin\tau + \cos\tau\, K_\lambda(k)}{\cos\tau - \sin\tau\, K_\lambda(k)}\,, \tag{1.156}$$

where

$$\tau = \tfrac{1}{2}\pi(\ell - \lambda)\,. \tag{1.157}$$

It follows that when $A = 0$ then $\ell = \lambda$ and $K_\ell(k) = K_\lambda(k)$.

In order to determine the analytic behaviour of $K_\lambda(k)$ in the neighbourhood of threshold energy, we proceed as in the derivation of (1.118) by relating $K_\lambda(k)$ to the R-matrix on the boundary $r = a$. We substitute $u_\ell(r)$, given by (1.155), into (1.115) which yields (1.116) with ℓ replaced everywhere by λ. We then use the analytic properties of the functions $s_\lambda(kr)$ and $c_\lambda(kr)$ and their derivatives, which are related to those of the spherical Bessel and Neumann functions $j_\lambda(kr)$ and $n_\lambda(kr)$ through (1.10) and (1.11). In this way we can show that the M-matrix, which is defined by the equation

$$M_\lambda(k^2) = k^{2\lambda+1}\,[K_\lambda(k)]^{-1}\,, \tag{1.158}$$

is an analytic function of k^2 in the neighbourhood of threshold which is a real analytic function when λ is real. We can also express the T-matrix $T_\ell(k)$ defined by (1.26) in terms of the M-matrix, using (1.156) and (1.158). We find that

$$T_\ell(k) = \frac{2\mathrm{i}\mathrm{e}^{2\mathrm{i}\tau}k^{2\lambda+1}}{M_\lambda(k^2) - \mathrm{i}k^{2\lambda+1}} + \mathrm{e}^{2\mathrm{i}\tau} - 1\,, \tag{1.159}$$

which reduces to (1.119) in the limit $A \to 0$ so that $\tau \to 0$.

An important feature of scattering by a dipole potential occurs for strong attractive potentials where

$$A < -\tfrac{1}{4}(2\ell+1)^2\,. \tag{1.160}$$

In this case, the argument of the square root in (1.151) becomes negative and λ, which then becomes complex, can be written as

$$\lambda = -\tfrac{1}{2} + \mathrm{i}\,\mathrm{Im}\,\lambda\,, \tag{1.161}$$

where $\mathrm{Im}\,\lambda$ can be positive or negative. The factor $k^{2\lambda+1}$ in (1.159) can then be written as

$$k^{2\lambda+1} = k^{2\mathrm{i}\,\mathrm{Im}\lambda} = \exp(2\mathrm{i}\,\mathrm{Im}\,\lambda\ln k)\,. \tag{1.162}$$

We see immediately that this gives rise to an infinite number of oscillations in the partial wave cross section as the collision energy tends to zero. Also, if we consider complex values of k defined by

$$k = |k|\mathrm{e}^{\mathrm{i}\phi}\,, \tag{1.163}$$

then the denominator $D_\lambda(k) = M_\lambda(k^2) - \mathrm{i}k^{2\lambda+1}$ in (1.159) can be written as

$$D_\lambda(k) = M_\lambda(k^2) - \exp(-2\phi\mathrm{Im}\,\lambda)\exp\left[2\mathrm{i}\left(\mathrm{Im}\,\lambda\ln|k| + \frac{\pi}{4}\right)\right]\,. \tag{1.164}$$

It follows that $D_\lambda(k)$ has zeros along lines in the complex k-plane given by

$$|M_\lambda(k^2)| = \exp(-2\phi\mathrm{Im}\,\lambda)\,, \tag{1.165}$$

which gives

$$\phi = -\frac{\ln|M_\lambda(k^2)|}{2\,\mathrm{Im}\,\lambda}\,. \tag{1.166}$$

Also as $|k| \to 0$ then the quantity

$$\theta = \mathrm{Im}\,\lambda\ln|k| + \tfrac{1}{4}\pi \tag{1.167}$$

in (1.164) will increase or decrease through π radians an infinite number of times. Hence the T-matrix has an infinite number of poles converging to the origin along two lines in the now infinite sheeted complex k-plane, where these two lines correspond to the positive and negative values of $\mathrm{Im}\,\lambda$ in (1.167). These lines of poles correspond to bound states, resonances or virtual states depending on the value of ϕ and whether they lie on the physical sheet of the complex k-plane.

We will see when we discuss multichannel effective range theory in Sect. 3.3 that the oscillatory behaviour of the cross section above threshold and the infinite series of bound states below threshold apply in certain circumstances both to electron scattering by polar molecules and by atomic hydrogen in degenerate excited states. The above discussion provides an introduction to these more complicated and realistic situations.

We conclude this section by considering the properties of the total and momentum transfer cross sections at finite energies in the presence of a long-range r^{-2} potential. For high angular momentum ℓ the radial wave function in (1.155) is accurately represented by the first term $s_\lambda(kr)$. Hence the corresponding phase shift is given by

$$\delta_\ell = \tfrac{1}{2}\pi(\ell - \lambda)\,. \tag{1.168}$$

For large ℓ we find by expanding the square root in (1.151) and choosing the upper sign in this equation that

$$\delta_\ell \underset{\ell\to\infty}{\sim} -\frac{\pi A}{2(2\ell+1)} + O(\ell^{-3})\,. \tag{1.169}$$

The total cross section, defined by (1.30), then becomes

$$\sigma_{\rm tot} = \sigma_1 + \sigma_2, \tag{1.170}$$

where

$$\sigma_1 = \frac{4\pi}{k^2}\sum_{\ell=0}^{L}(2\ell+1)\sin^2\delta_\ell \tag{1.171}$$

and

$$\sigma_2 = \frac{4\pi}{k^2}\sum_{\ell=L+1}^{\infty}(2\ell+1)\sin^2\delta_\ell \approx \frac{\pi^3 A^2}{k^2}\sum_{\ell=L+1}^{\infty}\frac{1}{(2\ell+1)}\,. \tag{1.172}$$

In (1.171) and (1.172) L is the value of ℓ where the phase shift δ_ℓ can be accurately represented by the first term on the right-hand side of (1.169). It follows that σ_2, and hence the total cross section $\sigma_{\rm tot}$, diverges logarithmically with ℓ. Also the scattering amplitude, defined by (1.29), and hence the differential cross section, defined by (1.4), diverge in the forward direction. Since the contribution to the differential cross section in the forward direction arising from the short-range component of the potential $U(r)$ is negligible compared with that arising from the long-range r^{-2} component, the corresponding angular distribution is energy independent. In practice, the divergence in the forward direction is cut off either because of the Debye screening of the dipole potential at large distances if the scattering process occurs

in a plasma or because of the molecular rotational splitting or the fine-structure splitting of the target levels.

Finally, we remark that the momentum transfer cross section defined by (1.6) remains finite in the forward direction. This follows immediately by substituting the asymptotic expansion for the phase shift given by (1.169) into (1.31). This result can also be seen to follow from (1.6), where the factor $(1 - \cos\theta)$ cuts off the divergence in the scattering amplitude in the forward direction.

1.4.3 Coulomb Potential

Finally in this section we consider electron or positron scattering by a positive or negative ion. In this case we consider the solution of the radial Schrödinger equation (1.70), where we assume that the short-range part of the potential $U(r)$ vanishes for $r \geq a$. Hence the total potential reduces in this region to the Coulomb potential alone given by

$$U_c(r) = \frac{2Z_1 Z_2}{r}, \quad r \geq a\,, \tag{1.173}$$

where Z_1 and Z_2 are the charge numbers corresponding to the incident particle and the ion, respectively, and where we assume that the ion has infinite mass. The solution of (1.70) which is regular at the origin can be written as follows:

$$u_\ell(r) = F_\ell(\eta, kr) + G_\ell(\eta, kr)K_\ell(k), \quad r \geq a\,, \tag{1.174}$$

where $F_\ell(\eta, kr)$ and $G_\ell(\eta, kr)$ are the regular and irregular Coulomb wave functions, defined by (1.58) and (1.59), respectively, η is defined by (1.42) and $K_\ell(k)$ is the K-matrix.

In order to derive an effective range expansion we commence from (1.115) which defines the R-matrix $R_\ell(E)$ in terms of the radial wave function $u_\ell(r)$ and its derivative $\mathrm{d}u_\ell(r)/\mathrm{d}r$ on the boundary $r = a$ of the internal region. We then substitute $u_\ell(r)$, defined by (1.174), into (1.115) and set the arbitrary constant $b = 0$. After re-arranging terms and using the Wronskian relation $F'_\ell G_\ell - G'_\ell F_\ell = 1$ we obtain

$$[K_\ell(k)]^{-1} = -\frac{G_\ell}{F_\ell} + \frac{1}{F'_\ell F_\ell} + \frac{1}{\sqrt{\rho}F'_\ell}\left[R_\ell(E) - \rho^{-1}\frac{F_\ell}{F'_\ell}\right]\frac{1}{F'_\ell\sqrt{\rho}}\,, \tag{1.175}$$

where $\rho = ka$ and F_ℓ, G_ℓ and F'_ℓ and G'_ℓ are defined by

$$\begin{aligned} F_\ell &= F_\ell(\eta, ka), \qquad G_\ell = G_\ell(\eta, ka), \\ F'_\ell &= \frac{1}{k}\left.\frac{\mathrm{d}F_\ell(\eta, kr)}{\mathrm{d}r}\right|_{r=a}, \quad G'_\ell = \frac{1}{k}\left.\frac{\mathrm{d}G_\ell(\eta, kr)}{\mathrm{d}r}\right|_{r=a}. \end{aligned} \tag{1.176}$$

It follows from (1.175) that the analytic behaviour of $K_\ell(k)$ in the complex energy plane can be obtained in terms of the analytic properties of F_ℓ, G_ℓ, F'_ℓ and $R_\ell(E)$, where we remember that $R_\ell(E)$ is a real meromorphic function of the energy with simple poles only on the real energy axis.

The Coulomb wave functions, which were introduced and discussed in Sect. 1.2, can be written as follows:

$$F_\ell(\eta, kr) = C_\ell(\eta)(kr)^{\ell+1}\Phi_\ell(\eta, kr) \tag{1.177}$$

and

$$G_\ell(\eta, kr) = \frac{(kr)^{-\ell}}{(2\ell+1)C_\ell(\eta)} \times \left[\Psi_\ell(\eta, kr) + (kr)^{2\ell+1}\, p_\ell(\eta)\left(\ln(2kr) + \frac{q_\ell(\eta)}{p_\ell(\eta)}\right)\Phi_\ell(\eta, kr)\right], \tag{1.178}$$

where $\Phi_\ell(\eta, kr)$ and $\Psi_\ell(\eta, kr)$ are entire functions of k^2 and $C_\ell(\eta)$ is defined by (1.60) and (1.61). Also in (1.178)

$$p_\ell(\eta) = 2\eta(2\ell+1)\frac{C_\ell^2(\eta)}{C_0^2(\eta)}, \tag{1.179}$$

and

$$\frac{q_\ell(\eta)}{p_\ell(\eta)} = f(\eta), \tag{1.180}$$

is a rational function of η^2 which tends to a constant as $|\eta^2| \to \infty$. Finally

$$f(\eta) = \frac{1}{2}[\psi(\mathrm{i}\eta) + \psi(-\mathrm{i}\eta)], \tag{1.181}$$

where $\psi(z)$ is the Psi (digamma) function which is defined in terms of the gamma function $\Gamma(z)$ by

$$\psi(z) = \frac{\mathrm{d}\Gamma(z)}{\mathrm{d}z}. \tag{1.182}$$

Using these properties of the Coulomb wave functions, it then follows from (1.175) that the M-matrix, defined by

$$M_\ell(k^2) = k^{2\ell+1}[(2\ell+1)!!]^2 C_\ell^2(\eta)[K_\ell(k)]^{-1} + h_\ell(\eta), \tag{1.183}$$

is a real analytic function of k^2, where

$$h_\ell(\eta) = k^{2\ell+1}[(2\ell+1)!!]^2\left[2\eta\tau\frac{C_\ell^2(\eta)}{C_0^2(\eta)} - \mathrm{i}C_\ell^2(\eta)\right] \tag{1.184}$$

and

$$\tau = \ln k + f(\eta) + \frac{\mathrm{i}\pi}{\mathrm{e}^{2\pi\eta} - 1}\,. \tag{1.185}$$

Hence $M_\ell(k^2)$ can be expanded in a power series in k^2 giving the following effective range expansion for a Coulomb potential

$$k^{2\ell+1}[(2\ell+1)!!]^2 C_\ell^2(\eta)\cot\delta_\ell(k) + h_\ell(\eta) = -\frac{1}{a_\ell} + \frac{1}{2}r_{e\ell}k^2 + O(k^4)\,, \tag{1.186}$$

where we have expressed $K_\ell(k)$ in (1.183) in terms of the phase shift $\delta_\ell(k)$ using (1.15) and where a_ℓ is the scattering length and $r_{e\ell}$ is the effective range. Equation (1.186) was first derived for s-wave scattering by Bethe [104]. It is also convenient to rewrite this effective range expansion for the T-matrix, defined by (1.26), in terms of the M-matrix. We find that

$$T = \frac{2\mathrm{i}k^{2\ell+1}[(2\ell+1)!!]^2 C_\ell^2(\eta)}{M_\ell(k^2) - k^{2\ell+1}[(2\ell+1)!!]^2 p_\ell(\eta)\tau(2\ell+1)^{-1}}\,. \tag{1.187}$$

In the limit $\eta \to 0$, corresponding to short-range potentials, we can show that

$$[(2\ell+1)!!]^2 C_\ell^2(\eta) \to 1, \quad (2\ell+1)!!]^2 p_\ell(\eta)\tau \to \mathrm{i}, \quad h_\ell(\eta) \to 0\,. \tag{1.188}$$

Hence (1.186) reduces to the effective range expansion (1.120) and (1.187) reduces to (1.119). We will consider the generalization of (1.187) to multichannel scattering by a Coulomb potential in Sect. 3.3.3.

When the Coulomb potential is attractive, corresponding to electron scattering by positive ions or positron scattering by negative ions, we can relate the energies of the bound states to the positive energy scattering phase shift. We have shown in Sect. 1.3 that the poles of the S-matrix, and hence the T-matrix, which lie on the imaginary axis in the complex k-plane, correspond to bound states. It follows from (1.187) that these poles occur when

$$M_\ell(k^2) = k^{2\ell+1}[(2\ell+1)!!]^2 p_\ell(\eta)\tau(2\ell+1)^{-1}\,. \tag{1.189}$$

The branches of the function τ in (1.189) for negative energies, corresponding to positive imaginary k, give rise to an infinite number of solutions of (1.189) converging onto zero energy. These solutions correspond to the Rydberg series of bound states. The relationship between positive and negative energies is obtained using Stirling's series for the Psi functions in the definition of $f(\eta)$ given by (1.181). We find that

$$\tau = \ln z + \frac{\mathrm{i}\pi}{\mathrm{e}^{2\pi\eta} - 1} + \chi(k^2), \quad k^2 > 0 \tag{1.190}$$

and

$$\tau = \ln z + \pi \cot\left(\frac{\pi z}{\kappa}\right) + \chi(k^2), \quad k^2 < 0\,, \tag{1.191}$$

where $k = \mathrm{i}\kappa$ below threshold and $z = -Z_1 Z_2$. Also in (1.190) and (1.191) $\chi(k^2)$ is a real analytic function of k^2 which has the following representation in the neighbourhood of $k^2 = 0$:

$$\chi(k^2) = \sum_{r=1}^{\infty} \frac{B_r}{2r(2r-1)^2} \left(\frac{k}{z}\right)^{2r}, \tag{1.192}$$

where B_r are Bernoulli numbers. Hence, using (1.191), we see from (1.189) that the bound-state energies are given by the solutions of

$$M_\ell(k^2) = k^{2\ell+1}[(2\ell+1)!!]^2 2\eta \frac{C_\ell^2(\eta)}{C_0^2(\eta)} \left[\ln z + \pi \cot\left(\frac{\pi z}{\kappa_b}\right) + \chi(k^2)\right], \tag{1.193}$$

where we have substituted for $p_\ell(\eta)$ in (1.189) using (1.179). Since $M_\ell(k^2)$, $k^{2\ell+1}[(2\ell+1)!!]^2 2\eta C_\ell^2(\eta)/C_0^2(\eta)$ and $\chi(k^2)$ in (1.193) are analytic functions of energy then $\cot(\pi z/\kappa_b)$, where $k^2 = -\kappa_b^2$ are the bound-state energy solutions of (1.193), can be fitted by an analytic function of energy and extrapolated to positive energies.

At positive energies it follows from (1.183) that

$$\cot\delta_\ell(k) = \frac{M_\ell(k^2) - h_\ell(\eta)}{k^{2\ell+1}[(2\ell+1)!!]^2 C_\ell^2(\eta)}\,, \tag{1.194}$$

where we have rewritten $[K_\ell(k)]^{-1}$ in (1.183) as $\cot\delta_\ell(k)$. We then substitute for $M_\ell(k^2)$, defined by (1.193), and $h_\ell(\eta)$, defined by (1.184), in (1.194) yielding

$$\cot\delta_\ell(k) = \frac{2\eta}{C_0^2(\eta)} \left[\ln z + \pi \cot\left(\frac{\pi z}{k}\right) + \chi(k^2)\right] - \frac{2\eta\tau}{C_0^2(\eta)} + \mathrm{i}\,. \tag{1.195}$$

Finally, we substitute for τ, defined by (1.190), in (1.195) yielding the final result

$$\frac{\cot\delta_\ell(k)}{\mathrm{e}^{2\pi\eta} - 1} = \cot\left(\frac{\pi z}{\kappa_b}\right). \tag{1.196}$$

We interpret this equation by extrapolating $\cot(\pi z/\kappa_b)$ on the right-hand side, which is defined at the bound-state energies $k^2 = -\kappa_b^2$, to positive energies, where it is defined in terms of the phase shift $\delta_\ell(k)$, given by the expression on the left-hand side.

We can rewrite (1.196) in a more convenient form by introducing effective quantum numbers ν_n and associated quantum defects μ_n of the bound states by the equation

$$-\kappa_b^2 = -\frac{z^2}{\nu_n^2} = -\frac{z^2}{(n-\mu_n)^2}, \quad n = \ell+1,\ \ell+2,\ \ldots, \tag{1.197}$$

where μ_n is a slowly varying function of energy which is zero when the non-Coulombic part of the potential vanishes. Substituting (1.197) into (1.196) gives

$$\frac{\cot\delta_\ell(k)}{1-\mathrm{e}^{2\pi\eta}} = \cot[\pi\mu(k^2)]\,, \tag{1.198}$$

where $\mu(k^2)$ is an analytic function of energy which assumes the values μ_n at the bound-state energies. For small positive energies the factor $\exp(2\pi\eta)$ is negligibly small and (1.198) then reduces to

$$\delta_\ell(k) = \pi\mu(k^2)\,. \tag{1.199}$$

This result enables bound-state energies, which are often accurately known from spectroscopic observations, to be extrapolated to positive energies to yield electron–ion scattering phase shifts and hence the corresponding partial wave cross sections.

Equations (1.198) and (1.199) were first derived by Seaton [851, 852] and are the basis of single-channel quantum defect theory. The foundations of modern quantum defect theory were laid by Hartree [443], who considered bound-state solutions of the Schrödinger equation (1.8). Further interest in this theory was stimulated by the work of Bates and Damgaard [75], whose Coulomb approximation provided a powerful method for the computation of bound–bound oscillator strengths for simple atomic systems. An interest in quantum defect theory also arose in solid state physics discussed by Kuhn and van Vleck [551], which led to developments in the mathematical theory described in a review article by Ham [440]. In recent years quantum defect theory has been extended to multichannel scattering by Seaton [854] and co-workers, and a comprehensive review of the theory and applications has been written by Seaton [859]. We review multichannel quantum defect theory in Sect. 3.3.4.

We show in Fig. 1.5 an application of single-channel quantum defect theory to e^-–He^+ $^1\mathrm{S}^\mathrm{e}$ and $^3\mathrm{S}^\mathrm{e}$ scattering carried out by Seaton [855]. In this work

$$Y(k^2) = A^{-1}(k^2,\ell)\tan[\pi\mu(k^2)]\,, \tag{1.200}$$

rather than $\cot[\pi\mu(k^2)]$, was used in the extrapolation of the quantum defects, where $A(k^2,\ell)$ is an analytic function of energy defined by

$$A(k^2,\ell) = \prod_{s=0}^{\ell}\left(1+\frac{s^2k^2}{z^2}\right), \tag{1.201}$$

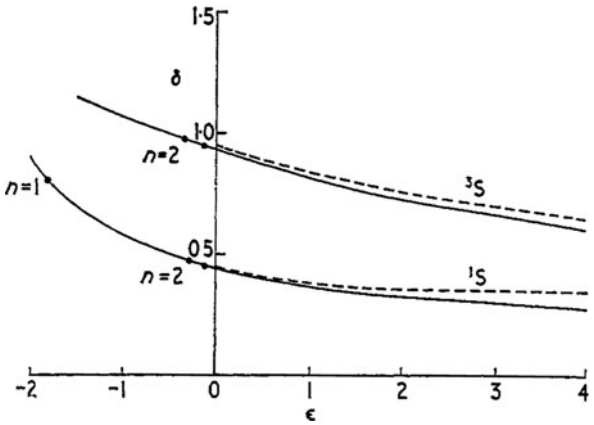

Fig. 1.5 Phase shifts δ in radians versus energy ϵ in Rydbergs for e^-–He^+ $^1S^e$ and $^3S^e$ scattering. *Full lines*, extrapolations using single-channel quantum defect theory; *broken lines*, polarized orbital calculations by Sloan [880]. The *points* at negative energies correspond to the experimental bound-state energies of He (Fig. 1 from [855])

which in the present application equals unity, since the angular momentum ℓ of the scattered electron is zero. A least-squares fit was then made to the bound-state data and the positive energy phase shifts determined using a re-arrangement of (1.198) for $\tan\delta_\ell(k)$. We see in Fig. 1.5 that the phase shifts obtained by extrapolation from the experimental bound-state energies are in excellent agreement with polarized orbital phase shift calculations by Sloan [880] close to threshold and remain good up to quite high energies. This agreement provides experimental confirmation of the accuracy of the theoretical phase shift calculations at low energies.

An important feature of the phase shift for electron scattering from positive ions, which is apparent from Fig. 1.5, is that it does not tend to $n\pi$ radians at threshold energy. This is in contrast to the phase shift for scattering by neutral targets which tends to a multiple of π radians as the scattering energy tends to zero. This is because the attractive Coulomb potential $U_c(r)$ pulls the scattered electron into a region where the short-range part of the potential $U(r)$ in (1.70) is effective, even for non-zero angular momenta. This effect is the same as that which causes the quantum defect μ_n in (1.197) to be non-zero at threshold.

When the Coulomb potential $U_c(r)$ is repulsive, which is the situation when electrons scatter from negative ions or positrons scatter from positive ions, the scattered electron or positron is kept away from the target at low energies and the phase shift vanishes rapidly as the energy tends to zero. In this case $\eta = Z_1 Z_2/k$ is positive and large. It follows from (1.61) that the quantity $[C_0(\eta)]^2$, which in this context is called the Coulomb penetration factor, is given to a good approximation by

$$[C_0(\eta)]^2 \approx 2\pi\eta \exp(-2\pi\eta)\,. \tag{1.202}$$

The factor $\exp(-2\pi\eta)$ in (1.202) is called the Gamow factor [361]. It then follows from (1.186) and (1.202) that

$$\delta_\ell(k) \underset{k\to 0}{\sim} \exp\left(-\frac{2\pi Z_1 Z_2}{k}\right), \quad Z_1 Z_2 > 0\,, \tag{1.203}$$

which applies for all angular momenta. It is clear that the Gamow factor strongly inhibits scattering at low energies when the Coulomb potential is repulsive.

The case when the potential $U(r)$ in (1.70) has a long-range component, falling off asymptotically as r^{-s} where $s > 1$, in addition to the Coulomb potential $U_c(r)$, has been considered by Berger and Spruch [91]. When the Coulomb potential is attractive the threshold behaviour of the phase shift is left unmodified, since the electron is pulled into the region where the short-range component of $U(r)$ is dominant. However, when the Coulomb potential is repulsive, the tail of $U(r)$ is important at low energies since this is the only part of the potential seen by the scattered electron. An important example of this situation is when the leading non-Coulombic component of the potential is due to the polarization of the ion so that $s = 4$. In this case we find that

$$\tan\delta_\ell(k) = \frac{1}{15}\alpha^2 k^5\,, \tag{1.204}$$

where α is the dipole polarizability. Clearly this contribution to the phase shift will dominate the contribution arising from (1.203) at sufficiently low energies.

1.5 Variational Principles

Variational principles were introduced in scattering theory by Hulthén [480, 481], Tamm [909–911], Schwinger [841] and Kohn [542]. In this section we derive Kohn variational principles for the partial wave phase shift and for the S-matrix which have been widely used in electron scattering. This section thus provides an introduction to multichannel variational principles discussed in Sects. 2.4 and 5.2. For specialized treatments of variational principles in scattering see, for example, Demkov [259], Moiseiwitsch [656] and Nesbet [678].

We commence by considering the radial Schrödinger equation (1.8) or (1.70), which we rewrite as

$$L_\ell u_\ell(r) = 0\,, \tag{1.205}$$

which defines the operator L_ℓ. We consider a solution $u_\ell(r)$ of (1.205) satisfying the boundary conditions

$$\begin{aligned} u_\ell(0) &\underset{r\to 0}{\sim} nr^{\ell+1}, \\ u_\ell(r) &\underset{r\to\infty}{\sim} \sin(\theta_\ell + \tau) + \cos(\theta_\ell + \tau)\tan(\delta_\ell - \tau)\,, \end{aligned} \tag{1.206}$$

where n is a normalization factor and where in the case of a long-range Coulomb potential

$$\theta_\ell = kr - \tfrac{1}{2}\ell\pi - \eta\ln 2kr + \sigma_\ell\,, \tag{1.207}$$

with η defined by (1.42) and σ_ℓ defined by (1.62). Also in (1.71) τ is a fixed constant chosen so that $0 \leq \tau \leq \pi$. We note that the solution defined by the boundary conditions (1.206) differs only by a normalization factor $\cos\delta_\ell/\cos(\delta_\ell - \tau)$ from the solution defined by the boundary conditions given by (1.71).

We now consider the functional

$$I_\ell[u_\ell^t] = \int_0^\infty u_\ell^t(r) L_\ell u_\ell^t(r) \mathrm{d}r \,, \tag{1.208}$$

where $u_\ell^t(r)$ is a trial function satisfying the same boundary conditions (1.206) as $u_\ell(r)$ with the phase shift δ_ℓ replaced by a trial phase shift δ_ℓ^t. It is clear from (1.205) and (1.208) that $I_\ell[u_\ell] = 0$. We then find using Green's theorem that

$$\int_0^\infty [u_\ell(r) L_\ell u_\ell^t(r) - u_\ell^t(r) L_\ell u_\ell(r)] \mathrm{d}r = \left[u_\ell \frac{\mathrm{d}u_\ell^t}{\mathrm{d}r} - u_\ell^t \frac{\mathrm{d}u_\ell}{\mathrm{d}r} \right]_0^\infty . \tag{1.209}$$

It follows using the boundary conditions satisfied by u_ℓ and u_ℓ^t that

$$I_\ell[u_\ell^t] - I_\ell[\Delta u_\ell] = k[\tan(\delta_\ell - \tau) - \tan(\delta_\ell^t - \tau)] \,, \tag{1.210}$$

where we have written

$$\Delta u_\ell(r) = u_\ell^t(r) - u_\ell(r) \,. \tag{1.211}$$

Relation (1.210) was first obtained by Kato [525] and is referred to as the Kato identity. If the trial function $u_\ell^t(r)$ is sufficiently close to the exact solution $u_\ell(r)$ then the functional $I_\ell[\Delta u_\ell]$, which is second order of smallness, can be neglected. Equation (1.210) can then be written as

$$\delta[I_\ell + k \tan(\delta_\ell - \tau)] = 0 \,, \tag{1.212}$$

where

$$\delta I_\ell = I_\ell[u_\ell^t] - I_\ell[u_\ell] = I_\ell[u_\ell^t] \tag{1.213}$$

is the change in I_ℓ under the variation $\delta u_\ell^t(r) = u_\ell^t(r) - u_\ell(r)$ and

$$\delta[\tan(\delta_\ell - \tau)] = \tan(\delta_\ell^t - \tau) - \tan(\delta_\ell - \tau) \,. \tag{1.214}$$

Equation (1.212) is known as the Kohn variational principle [542].

The Kohn variational principle (1.212) is clearly satisfied by the exact solution of the differential equation (1.205). It can also be used as the basis for obtaining approximate solutions of (1.205). Thus if we start from a trial function $u_\ell^t(r)$ which depends on n parameters $c_1, c_2, \ldots, c_n$ as well as the phase shift through the quantity λ_ℓ^t defined by

$$\lambda_\ell^t = \tan(\delta_\ell^t - \tau) \,, \tag{1.215}$$

then taking the variation in (1.212) with respect to these $n+1$ parameters yields the equations

$$\frac{\delta I_\ell}{\delta \lambda_\ell^{\mathrm{t}}} = -k \tag{1.216}$$

and

$$\frac{\delta I_\ell}{\delta c_i} = 0, \quad i = 1, \ldots, n\,. \tag{1.217}$$

If the trial function $u_\ell^t(r)$ depends linearly on the parameters $c_1, c_2, \ldots, c_n$ and λ_ℓ^t then (1.216) and (1.217) are a set of $n+1$ linear simultaneous equations which can be solved to yield these parameters. We can then use the variational principle (1.212) to obtain an improved estimate for λ_ℓ which is correct up to terms of second order in the error in the trial function. It is given by

$$[\lambda_\ell] = \lambda_\ell^t + \frac{1}{k} I_\ell[u_\ell^t]\,, \tag{1.218}$$

where the symbol $[\lambda_\ell]$ means that this quantity is the variational estimate of λ_ℓ. The corresponding phase shift, correct up to terms of second order, is then obtained from the variational estimate using the equation

$$[\lambda_\ell] = \tan(\delta_\ell - \tau)\,. \tag{1.219}$$

It follows from the above discussion that different choices of τ in the range $0 \leq \tau \leq \pi$ will yield different variational estimates for the phase shift. Kohn chose $\tau = 0$ so that the trial function satisfied the asymptotic boundary condition

$$u_\ell^t(r) \underset{r\to\infty}{\sim} \sin\theta_\ell + \cos\theta_\ell \tan\delta_\ell^t(k)\,. \tag{1.220}$$

Equation (1.218) then becomes

$$[\tan\delta_\ell] = \tan\delta_\ell^t + \frac{1}{k} I_\ell[u_\ell^t]\,, \tag{1.221}$$

which gives the Kohn variational estimate for $\tan\delta_\ell$ and hence, from (1.15), for the K-matrix. On the other hand Rubinow [800] took $\tau = \pi/2$ so that the trial function satisfied the asymptotic boundary condition

$$u_\ell^t(r) \underset{r\to\infty}{\sim} \cos\theta_\ell + \sin\theta_\ell \cot\delta_\ell^t(k)\,. \tag{1.222}$$

In this case (1.218) yields

$$[\cot\delta_\ell] = \cot\delta_\ell^t - \frac{1}{k} I_\ell[u_\ell^t]\,. \tag{1.223}$$

This approach is often called the Rubinow or inverse Kohn variational principle since it gives a variational estimate for $\cot \delta_\ell = (\tan \delta_\ell)^{-1}$.

It is also often useful to adopt the S-matrix form of the Kohn variational principle. In this case, the solution of (1.205) is chosen to satisfy the asymptotic boundary condition

$$u_\ell(r) \underset{r\to\infty}{\sim} \exp(-\mathrm{i}\theta_\ell) - \exp(\mathrm{i}\theta_\ell) S_\ell(k)\,, \tag{1.224}$$

where the S-matrix $S_\ell(k)$ is defined in terms of the phase shift $\delta_\ell(k)$ by (1.14). We also introduce a trial function $u_\ell^t(r)$ satisfying the asymptotic boundary condition

$$u_\ell^t(r) \underset{r\to\infty}{\sim} \exp(-\mathrm{i}\theta_\ell) - \exp(\mathrm{i}\theta_\ell) S_\ell^t(k)\,. \tag{1.225}$$

As before we consider the variation

$$\delta I_\ell = I_\ell[u_\ell^t] - I_\ell[u_\ell]\,, \tag{1.226}$$

which can be simplified using the boundary conditions satisfied by $u_\ell(r)$ and $u_\ell^t(r)$. Neglecting terms of second order in $\Delta u_\ell(r) = u_\ell^t(r) - u_\ell(r)$ we obtain the S-matrix form of the Kohn variational principle

$$\delta[I_\ell + 2\mathrm{i}k S_\ell] = 0\,, \tag{1.227}$$

where we have written

$$\delta S_\ell = S_\ell^t - S_\ell\,. \tag{1.228}$$

Again if the trial function $u_\ell^t(r)$ depends linearly on n parameters $c_1, c_2, \ldots, c_n$ as well as on the S-matrix S_ℓ^t, then taking the variation in (1.227) with respect to these $n+1$ parameters yields the $n+1$ coupled linear simultaneous equations

$$\frac{\delta I_\ell}{\delta S_\ell^t} = -2\mathrm{i}k \tag{1.229}$$

and

$$\frac{\delta I_\ell}{\delta c_i} = 0, \quad i = 1, \ldots, n\,. \tag{1.230}$$

Equations (1.229) and (1.230) can be solved to yield these $n+1$ parameters. The variational principle (1.227) can then be used to obtain an improved estimate for λ_ℓ which is correct up to terms of second order in the error in the trial function. We find that

$$[S_\ell] = S_\ell^t + \frac{1}{2\mathrm{i}k} I_\ell[u_\ell^t]\,, \tag{1.231}$$

which can be used instead of the Kohn variational estimate for $\tan\delta_\ell$ given by (1.221) or the inverse Kohn variational estimate for $\cot\delta_\ell$ given by (1.223).

In concluding this discussion of variational principles in potential scattering we stress that they are not extremum principles but are only stationary principles. Consequently the variational estimate can lead to misleading results if poor trial functions are used. Indeed, it was shown by Schwartz [838, 839] that anomalous singularities can arise in $[\tan\delta_\ell]$ and in $[\cot\delta_\ell]$ which can invalidate the variational estimate in these cases if care is not taken, even if the number n of trial functions is large. A detailed discussion of these anomalous singularities and methods for avoiding them has been given, for example by Nesbet [675, 676, 678], Burke and Joachain [171] and Cooper et al. [229] and will not be considered further here. However, we remark that the R-matrix method, discussed in Chap. 4 and in later chapters, provides a variational procedure for solving (1.205) which enables phase shifts and S-matrices to be obtained which do not have these singularities.

1.6 Relativistic Scattering: The Dirac Equation

We conclude this chapter on potential scattering by considering relativistic scattering of an electron by a spherically symmetric potential. This situation occurs for relativistic electron scattering energies or for electron collisions with heavy atoms and ions. The wave equation which must then be solved is the time-independent Dirac equation, which takes into account both the spin and the relativistic behaviour of the scattered electron. We consider first the separation of the Dirac equation in spherical polar coordinates which yields two coupled first-order differential equations satisfied by the radial functions describing the motion of the scattered electron. We then derive expressions for the phase shifts, scattering matrix and cross sections in terms of the asymptotic solution of these coupled equations.

The time-independent Dirac equation describing the motion of an electron in a potential $V(\mathbf{r})$ is (see [110, 171, 263, 411]),

$$[\mathrm{c}\boldsymbol{\alpha}\cdot\mathbf{p}+\beta'\mathrm{c}^2+V(\mathbf{r})]\psi(\mathbf{x})=E\psi(\mathbf{x})\,, \tag{1.232}$$

in atomic units, where c is the velocity of light in vacuum, $\mathbf{x}\equiv(\mathbf{r},\sigma)$ represents the space and spin coordinates of the scattered electron and $\mathbf{p}=-\mathrm{i}\nabla$ is the electron momentum operator. Also in (1.232), $\beta'=\beta-I_4$ and $\boldsymbol{\alpha}$ and β are the 4×4 Dirac matrices defined by

$$\boldsymbol{\alpha}=\begin{pmatrix}0 & \boldsymbol{\sigma}\\ \boldsymbol{\sigma} & 0\end{pmatrix},\quad \beta=\begin{pmatrix}I_2 & 0\\ 0 & -I_2\end{pmatrix}, \tag{1.233}$$

where the components of $\boldsymbol{\sigma}$, σ_x, σ_y and σ_z, are 2×2 Pauli spin matrices [723] defined by

$$\sigma_x=\begin{pmatrix}0 & 1\\ 1 & 0\end{pmatrix},\quad \sigma_y=\begin{pmatrix}0 & -\mathrm{i}\\ \mathrm{i} & 0\end{pmatrix},\quad \sigma_z=\begin{pmatrix}1 & 0\\ 0 & -1\end{pmatrix}, \tag{1.234}$$

and I_2 and I_4 are 2×2 and 4×4 unit matrices, respectively. Finally, the choice of β' in (1.232) is made so that the energy E in this equation does not include the electron rest mass and hence reduces in the non-relativistic limit to the energy E in (1.1).

We consider the solution of (1.232) for the case where the potential $V(\mathbf{r})$ is spherically symmetric and hence depends only on the radial variable r and not on the angular variables. We then separate the angular variables in (1.232) from the radial variable using the identity

$$\begin{aligned}\boldsymbol{\alpha}\cdot\mathbf{p} &= \alpha_r p_r + \mathrm{i}r^{-1}\alpha_r(\boldsymbol{\Sigma}\cdot\mathbf{L}+I_4)\\ &= \alpha_r p_r + \mathrm{i}r^{-1}\alpha_r\beta K\,,\end{aligned} \tag{1.235}$$

where the radial momentum operator p_r and the radial velocity operator α_r are defined by

$$p_r = -\mathrm{i}\frac{1}{r}\frac{\partial}{\partial r}r, \quad \alpha_r = r^{-1}\boldsymbol{\alpha}\cdot\mathbf{r}\,, \tag{1.236}$$

and where the operator K is defined by

$$K = \beta(\boldsymbol{\Sigma}\cdot\mathbf{L}+I_4)\,, \tag{1.237}$$

with

$$\boldsymbol{\Sigma} = \begin{pmatrix}\boldsymbol{\sigma} & 0\\ 0 & \boldsymbol{\sigma}\end{pmatrix}, \quad \mathbf{L} = \begin{pmatrix}\boldsymbol{\ell} & 0\\ 0 & \boldsymbol{\ell}\end{pmatrix}. \tag{1.238}$$

The operator K can be shown to commute with the Dirac Hamiltonian and hence its eigenvalues are constants of the motion. Furthermore, since

$$\boldsymbol{\Sigma}\cdot\mathbf{L} = 2\mathbf{S}\cdot\mathbf{L} = \mathbf{J^2}-\mathbf{L^2}-\mathbf{S^2} = \mathbf{J^2}-\mathbf{L^2}-\frac{3}{4}I_4\,, \tag{1.239}$$

then we may rewrite the operator K as

$$K = \beta\left(\mathbf{J^2}-\mathbf{L^2}+\frac{1}{4}I_4\right). \tag{1.240}$$

Also it follows from (1.237) that

$$K^2 = \left(\mathbf{L}+\frac{1}{2}\boldsymbol{\Sigma}\right)^2+\frac{1}{4}I_4\,. \tag{1.241}$$

Since $(\mathbf{L}+\frac{1}{2}\boldsymbol{\Sigma})^2$ is the square of the total angular momentum operator, which has the eigenvalues $j(j+1)$, then the eigenvalues of K^2 are $(j+\frac{1}{2})^2\equiv\kappa^2$ where κ is given by

$$\kappa = \pm 1,\ \pm 2,\ \pm 3,\ \ldots\,. \tag{1.242}$$

Using the above equations, the Dirac equation (1.232) can be written as

$$H\psi(\mathbf{x}) = [\mathrm{c}\alpha_r p_r + \mathrm{i}\mathrm{c}r^{-1}\alpha_r\beta K + \beta'\mathrm{c}^2 + V(r)]\psi(\mathbf{x}) = E\psi(\mathbf{x})\,. \tag{1.243}$$

The solution of (1.243) can be written as a four-component spinor in the form

$$\psi(\mathbf{x}) = \frac{1}{r}\begin{pmatrix} p_\kappa(r)\eta_{\kappa m}(\hat{\mathbf{r}},\sigma) \\ \mathrm{i}q_\kappa(r)\eta_{-\kappa m}(\hat{\mathbf{r}},\sigma)\end{pmatrix}, \tag{1.244}$$

where $p_\kappa(r)$ and $q_\kappa(r)$ are radial functions which depend on κ as described below, and the factor i is introduced so that the radial equations satisfied by $p_\kappa(r)$ and $q_\kappa(r)$, derived below, are real, and hence these functions can be chosen to be real. The spin–angle functions $\eta_{\kappa m}(\hat{\mathbf{r}},\sigma)$ in (1.244) are two-component spinors defined by

$$\eta_{\kappa m}(\hat{\mathbf{r}},\sigma) \equiv \mathcal{Y}_{\ell\frac{1}{2}jm}(\hat{\mathbf{r}},\sigma) = \sum_{m_\ell m_s}(\ell m_\ell \tfrac{1}{2} m_s|jm)Y_{\ell m_\ell}(\theta,\phi)\chi_{\frac{1}{2}m_s}(\sigma)\,, \tag{1.245}$$

where $(\ell m_\ell \frac{1}{2} m_s|jm)$ are Clebsch–Gordan coefficients defined in Appendix A.1, $Y_{\ell m_\ell}(\theta,\phi)$ are spherical harmonics defined in Appendix B.3 and $\chi_{\frac{1}{2}m_s}(\sigma)$ are the usual two-component Pauli spin functions given by

$$\chi_{\frac{1}{2}\frac{1}{2}}(\sigma) = \begin{pmatrix}1\\0\end{pmatrix}, \quad \chi_{\frac{1}{2}-\frac{1}{2}}(\sigma) = \begin{pmatrix}0\\1\end{pmatrix}. \tag{1.246}$$

It then follows from Appendices A and B that the functions $\mathcal{Y}_{\ell\frac{1}{2}jm}(\hat{\mathbf{r}},\sigma)$ defined by (1.245) are simultaneous eigenfunctions of $\mathbf{J}^2$ and $\mathbf{L}^2$ belonging to the eigenvalues $j(j+1)$ and $\ell(\ell+1)$, respectively. Hence

$$\begin{aligned}\left(\mathbf{J}^2 - \mathbf{L}^2 + \tfrac{1}{4}I_2\right)\mathcal{Y}_{\ell\frac{1}{2}jm}(\hat{\mathbf{r}},\sigma) &= \left[j(j+1) - \ell(\ell+1) + \tfrac{1}{4}\right]\mathcal{Y}_{\ell\frac{1}{2}jm}(\hat{\mathbf{r}},\sigma) \\ &= \left[(j+\tfrac{1}{2})^2 - \ell(\ell+1)\right]\mathcal{Y}_{\ell\frac{1}{2}jm}(\hat{\mathbf{r}},\sigma)\,. \end{aligned} \tag{1.247}$$

Using this result and the definition of K given by (1.240) and $\psi(\mathbf{x})$ given by (1.244), we find that

$$K\psi(\mathbf{x}) = -\kappa\psi(\mathbf{x})\,, \tag{1.248}$$

where the eigenvalue κ is then defined by

$$\kappa = \ell(\ell+1) - (j+\tfrac{1}{2})^2\,. \tag{1.249}$$

Hence the eigenvalue κ is related to the orbital and total angular momentum quantum numbers ℓ and j by the equations

$$\begin{aligned} \kappa &= \ell \quad \text{when} \quad j = \ell - \tfrac{1}{2}, \\ \kappa &= -\ell - 1 \quad \text{when} \quad j = \ell + \tfrac{1}{2}\,. \end{aligned} \tag{1.250}$$

Table 1.1 Relationship of κ to the usual spectroscopic notations ℓ and j

κ negative		κ positive	
$\kappa = -1$	$s_{1/2}$	$\kappa = +1$	$p_{1/2}$
$\kappa = -2$	$p_{3/2}$	$\kappa = +2$	$d_{3/2}$
$\kappa = -3$	$d_{5/2}$	$\kappa = +3$	$f_{5/2}$
$\vdots$	$\vdots$	$\vdots$	$\vdots$

This relationship is given explicitly in Table 1.1.

Using the above results for the eigenvalues of the K operator, we can now simplify the Dirac equation defined by (1.243). Substituting (1.244) into (1.243) and using (1.233) and (1.248) we obtain the following coupled equations

$$c\sigma_r(p_r + ir^{-1}\kappa)ir^{-1}q_\kappa(r)\eta_{-\kappa m}(\hat{\mathbf{r}},\sigma) + [V(r) - E]r^{-1}p_\kappa(r)\eta_{\kappa m}(\hat{\mathbf{r}},\sigma) = 0\,, \tag{1.251}$$

and

$$c\sigma_r(p_r - ir^{-1}\kappa)r^{-1}p_\kappa(r)\eta_{\kappa m}(\hat{\mathbf{r}},\sigma) + [-2c^2 + V(r) - E]ir^{-1}q_\kappa(r)\eta_{-\kappa m}(\hat{\mathbf{r}},\sigma) = 0\,. \tag{1.252}$$

These equations can be simplified using the identity

$$\sigma_r\eta_{\pm\kappa m}(\hat{\mathbf{r}},\sigma) = -\eta_{\mp\kappa m}(\hat{\mathbf{r}},\sigma)\,, \tag{1.253}$$

which follows since $\sigma_r = \boldsymbol{\sigma}\cdot\hat{\mathbf{r}}$ is a pseudo-scalar operator and hence it changes the sign of the parity but leaves the total angular momentum and its z-component unaltered. Projecting (1.251) onto the function $\eta_{\kappa m}(\hat{\mathbf{r}},\sigma)$ and (1.252) onto the function $\eta_{-\kappa m}(\hat{\mathbf{r}},\sigma)$ and using (1.236) we find that the time-independent Dirac equation reduces to the following coupled first-order differential equations satisfied by the functions $p_\kappa(r)$ and $q_\kappa(r)$

$$\left(\frac{d}{dr} + \frac{\kappa}{r}\right)p_\kappa(r) - \frac{1}{c}[2c^2 + E - V(r)]q_\kappa(r) = 0 \tag{1.254}$$

and

$$\left(\frac{d}{dr} - \frac{\kappa}{r}\right)q_\kappa(r) + \frac{1}{c}[E - V(r)]\,p_\kappa(r) = 0\,, \tag{1.255}$$

which must be solved for each κ. The coupled Eqs. (1.254) and (1.255) take the place of the radial Schrödinger equation (1.8) in non-relativistic theory. We thus see that the Dirac equation for a spherically symmetric potential can be separated without approximation in spherical polar coordinates. We also note from these equations that for scattering energies $E \ll c^2$, the ratio $p_\kappa/q_\kappa \approx c$. Hence p_κ is often referred to as the "large component" and q_κ as the "small component" of the Dirac wave function.

It is instructive at this point to consider the non-relativistic limit of the coupled differential equations (1.254) and (1.255). In this limit

$$|E - V(r)| \ll 2c^2\,, \tag{1.256}$$

and hence (1.254) can be rewritten as

$$\left(\frac{\mathrm{d}}{\mathrm{d}r} + \frac{\kappa}{r}\right) p_\kappa(r) - 2cq_\kappa(r) = 0\,. \tag{1.257}$$

Substituting for $q_\kappa(r)$ from (1.257) into (1.255) then gives

$$\frac{1}{2}\left(\frac{\mathrm{d}}{\mathrm{d}r} - \frac{\kappa}{r}\right)\left(\frac{\mathrm{d}}{\mathrm{d}r} + \frac{\kappa}{r}\right) p_\kappa(r) + [E - V(r)]\, p_\kappa(r) = 0\,, \tag{1.258}$$

which can be rewritten as

$$\left(\frac{\mathrm{d}^2}{\mathrm{d}r^2} - \frac{\kappa(\kappa+1)}{r^2} - 2V(r) + 2E\right) p_\kappa(r) = 0\,. \tag{1.259}$$

It follows from (1.250) that $\kappa = \ell$ or $-\ell - 1$, so that in both cases

$$\kappa(\kappa+1) = \ell(\ell+1)\,. \tag{1.260}$$

Also we remember from Sect. 1.1 that $k^2 = 2E$ and the reduced potential $U(r) = 2V(r)$. Hence (1.259) can be written as

$$\left(\frac{\mathrm{d}^2}{\mathrm{d}r^2} - \frac{\ell(\ell+1)}{r^2} - U(r) + k^2\right) p_\kappa(r) = 0\,, \tag{1.261}$$

which is the usual form of the radial Schrödinger equation given by (1.8).

The coupled equations (1.254) and (1.255) can be reduced to Schrödinger form even when (1.256) is not satisfied. This occurs for relativistic electron scattering energies or when the potential $V(r)$ corresponds to electron collisions with heavy target atoms or ions with large nuclear charge number Z. Taking the derivative of (1.254), substituting for $\mathrm{d}q_\kappa/\mathrm{d}r$ from (1.255) and eliminating $q_\kappa(r)$ then yields

$$\frac{\mathrm{d}^2 p_\kappa}{\mathrm{d}r^2} - \frac{A'(r)}{A(r)}\frac{\mathrm{d}p_\kappa}{\mathrm{d}r} + \left(A(r)B(r) - \frac{A'(r)}{A(r)}\frac{\kappa}{r} - \frac{\kappa(\kappa+1)}{r^2}\right) p_\kappa = 0\,, \tag{1.262}$$

where we have written

$$\begin{aligned} A(r) &= \frac{1}{c}[2c^2 + E - V(r)]\,, \\ A'(r) &= \frac{\mathrm{d}A}{\mathrm{d}r}\,, \\ B(r) &= \frac{1}{c}\,[E - V(r)]\,. \end{aligned} \tag{1.263}$$

We then make the substitution

$$p_\kappa(r) = [A(r)]^{1/2}\, \tilde{p}_\kappa(r) \tag{1.264}$$

in (1.262), which gives the following equation for $\tilde{p}_\kappa(r)$:

$$\left(\frac{\mathrm{d}^2}{\mathrm{d}r^2} - \frac{\kappa(\kappa+1)}{r^2} - U_\kappa(r) + k_r^2\right)\tilde{p}_\kappa(r) = 0\,, \tag{1.265}$$

where

$$k_r^2 = \frac{1}{\mathrm{c}^2} E(E + 2\mathrm{c}^2) \tag{1.266}$$

and

$$U_\kappa(r) = \frac{2(E+\mathrm{c}^2)V(r)}{\mathrm{c}^2} - \frac{[V(r)]^2}{\mathrm{c}^2} + \frac{\kappa}{r}\frac{A'(r)}{A(r)} + \frac{3}{4}\frac{[A'(r)]^2}{[A(r)]^2} - \frac{1}{2}\frac{A''(r)}{A(r)}\,. \tag{1.267}$$

After substituting for $\kappa(\kappa+1)$ from (1.260), we see that (1.265) has the same form as the non-relativistic Schrödinger equation (1.8). Also, for low-energy electron collisions with light atoms or ions, the terms involving $[V(r)]^2$, $A'(r)$ and $A''(r)$ in (1.267) can be neglected and we obtain

$$A(r) = 2\mathrm{c}, \quad k^2 = 2E, \quad U_\kappa(r) = U(r)\,. \tag{1.268}$$

Hence (1.265) reduces to the non-relativistic Schrödinger equation (1.261) or (1.8) as expected.

However, for relativistic electron scattering energies or for electron collisions with heavy atoms or ions all the terms in the potential $U_\kappa(r)$ given by (1.267) are appreciable. Hence the Dirac equations (1.254) and (1.255) or the equivalent relativistic Schrödinger equation (1.265) gives different results from the non-relativistic Schrödinger equation (1.8) or (1.261) for the same potential $U(r) = 2V(r)$. In particular, the term containing κ in $U_\kappa(r)$ corresponds to a spin–orbit interaction, since from (1.250), $\kappa = \ell$ when $j = \ell - 1/2$ and $\kappa = -\ell - 1$ when $j = \ell + 1/2$. We will see later in this section that this spin–orbit term in $U_\kappa(r)$ gives rise to spin polarization effects in electron collisions with heavy atoms or ions even for low electron scattering energies.

We conclude our discussion of the equivalent relativistic Schrödinger equation (1.265) by noting that although it has the same form as the non-relativistic Schrödinger equation, there are two other fundamental differences. First, the k_r^2 term, defined by (1.266), depends on E^2 as well as upon E and second the relativistic potential $U_\kappa(r)$, defined by (1.267), depends on the energy E as well as upon the radius r. However, for low-energy electron collisions with heavy atoms or ions, where the electron scattering energy $E \ll \mathrm{c}^2$, these differences become insignificant and we obtain in this limit

$$k_r^2 \to k^2 = 2E \tag{1.269}$$

and

$$U_\kappa(r) \to U_{\kappa 0}(r) = 2V(r) - \frac{[V(r)]^2}{c^2} + \frac{\kappa}{r}\frac{A'(r)}{A(r)} + \frac{3}{4}\frac{[A'(r)]^2}{[A(r)]^2} - \frac{1}{2}\frac{A''(r)}{A(r)}\,. \quad (1.270)$$

The corresponding relativistic Schrödinger equation (1.265) then reduces to the standard non-relativistic Schrödinger equation form, as shown in our discussion leading to (1.261), where $k^2 = 2E$ and the potential does not depend on energy. We will see in Sects. 4.6 and 5.5 that this result has important implications for the R-matrix method of solving the Dirac equation describing low-energy electron collisions with heavy atoms or ions.

We now derive expressions for the scattering amplitudes and cross sections by considering the asymptotic form of the solution of the Dirac equation. We commence by noting that it is only necessary to know the "large components" of the Dirac four-component spinor in order to determine the scattering matrix (see, for example, [171]). Thus if the Dirac four-component spinor, given by (1.244), is written in terms of two-component spinors as follows

$$\psi = \begin{pmatrix} \psi_A \\ \psi_B \end{pmatrix}, \quad (1.271)$$

then we need to only consider the two-component spinor ψ_A containing the "large component" $p_\kappa(r)$. In analogy with (1.2), we write the asymptotic form of ψ_A corresponding to a plane wave and outgoing spherical wave as

$$\psi_A(\mathbf{x}) \underset{r\to\infty}{\sim} \chi_{\frac{1}{2}m_s}(\sigma)\mathrm{e}^{\mathrm{i}kz} + \sum_{m_s'=\pm\frac{1}{2}} \chi_{\frac{1}{2}m_s'}(\sigma) M_{m_s'm_s}(\theta,\phi)\frac{\mathrm{e}^{\mathrm{i}kr}}{r}, \quad m_s = \pm\tfrac{1}{2}\,, \quad (1.272)$$

where we have assumed that the potential $V(r)$ is short range, vanishing faster than r^{-1} at large distances. Equation (1.272) then defines the scattering matrix $M_{m_s'm_s}(\theta,\phi)$, where the wave number k of the scattered electron is related to the incident electron energy E by (1.266).

In order to determine the scattering matrix, we expand $\psi_A(\mathbf{x})$ in terms of the spin–angle functions $\eta_{\kappa m}(\hat{\mathbf{r}},\sigma) \equiv \mathcal{Y}_{\ell\frac{1}{2}jm}(\hat{\mathbf{r}},\sigma)$ defined by (1.245). We write

$$\psi_A(\mathbf{x}) = \sum_{\ell=0}^{\infty} \sum_{j=\ell-\frac{1}{2}}^{\ell+\frac{1}{2}} B_{\ell j}(k) r^{-1} p_{\ell j}(r) \mathcal{Y}_{\ell\frac{1}{2}jm_s}(\hat{\mathbf{r}},\sigma)\,, \quad (1.273)$$

where the radial functions $p_{\ell j}(r)$ can be identified with the radial functions $p_\kappa(r)$ which satisfy (1.262). Also from (1.264) and (1.265), and the result that $A(r)$ tends to a constant as $r \to \infty$, it follows that the radial functions $\tilde{p}_\kappa(r)$ and hence the radial functions $p_{\ell j}(r)$ can be chosen to vanish at the origin and to satisfy the asymptotic boundary conditions

$$p_{\ell j}(r) \underset{r\to\infty}{\sim} \sin\left[kr - \tfrac{1}{2}\ell\pi + \delta_{\ell j}(k)\right], \quad j = \ell \pm \tfrac{1}{2}\,. \quad (1.274)$$

In this equation we have introduced the phase shifts $\delta_{\ell j}(k)$ which depend on j as well as on ℓ because of the κ dependence of $U_\kappa(r)$ in (1.265).

The scattering amplitudes and cross sections can be obtained, as in Sect. 1.1, by equating (1.272) with the asymptotic form of (1.273). We first express the incident plane wave term in (1.272) in terms of the spin–angle function $\mathcal{Y}_{\ell\frac{1}{2}jm}$. To achieve this we note from (1.27) that

$$\chi_{\frac{1}{2}m_s}(\sigma)\mathrm{e}^{\mathrm{i}kz} = \chi_{\frac{1}{2}m_s}(\sigma)\sum_{\ell=0}^{\infty}(2\ell+1)\mathrm{i}^\ell j_\ell(kr)P_\ell(\cos\theta)\,. \tag{1.275}$$

Using (B.47) and the inverse of (1.245), which from Appendix A.1 is

$$Y_{\ell m}(\theta,\phi)\chi_{\frac{1}{2}m_s}(\sigma) = \sum_{j=\ell-\frac{1}{2}}^{\ell+\frac{1}{2}}\left(\ell m_\ell \tfrac{1}{2}m_s|jm_\ell+m_s\right)\mathcal{Y}_{\ell\frac{1}{2}jm_\ell+m_s}(\hat{\mathbf{r}},\sigma)\,, \tag{1.276}$$

enables us to rewrite (1.275) as

$$\chi_{\frac{1}{2}m_s}(\sigma)\mathrm{e}^{\mathrm{i}kz} = \sum_{\ell=0}^{\infty}\sum_{j=\ell-\frac{1}{2}}^{\ell+\frac{1}{2}}[4\pi(2\ell+1)]^{1/2}\ \mathrm{i}^\ell j_\ell(kr)\left(\ell 0\tfrac{1}{2}m_s|jm_s\right)\mathcal{Y}_{\ell\frac{1}{2}jm_s}(\hat{\mathbf{r}},\sigma)\,. \tag{1.277}$$

The coefficient $B_{\ell j}(k)$ in (1.273) is then determined by equating the ingoing wave terms in (1.273) and (1.277). We find using (1.274) that

$$B_{\ell j}(k) = k^{-1}[4\pi(2\ell+1)]^{1/2}\,\mathrm{i}^\ell\exp[\mathrm{i}\delta_{\ell j}(k)]\left(\ell 0\tfrac{1}{2}m_s|jm_s\right)\,. \tag{1.278}$$

The second term on the right-hand side of (1.272) can now be obtained by subtracting (1.277) from the asymptotic form of (1.273). Calling this term $\psi_{\mathrm{sc}}(\mathbf{x})$ we find that

$$\psi_{\mathrm{sc}}(\mathbf{x}) \underset{r\to\infty}{\sim} \frac{1}{2\mathrm{i}k}\sum_{\ell=0}^{\infty}\sum_{j=\ell-\frac{1}{2}}^{\ell+\frac{1}{2}}[4\pi(2\ell+1)]^{1/2}\{\exp[2\mathrm{i}\delta_{\ell j}(k)]-1\}\left(\ell 0\tfrac{1}{2}m_s|jm_s\right)$$
$$\times\,\mathcal{Y}_{\ell\frac{1}{2}jm_s}(\hat{\mathbf{r}},\sigma)\frac{\mathrm{e}^{\mathrm{i}kr}}{r}\,. \tag{1.279}$$

The scattering matrix $M_{m_s'm_s}(\theta,\phi)$ is determined by substituting for the spin–angle function $\mathcal{Y}_{\ell\frac{1}{2}jm_s}(\hat{\mathbf{r}},\sigma)$ from (1.245) and comparing with (1.272). We obtain

$$M_{m_s' m_s}(\theta,\phi) = \frac{1}{2\mathrm{i}k}\sum_{\ell=0}^{\infty}\sum_{j=\ell-\frac{1}{2}}^{\ell+\frac{1}{2}}[4\pi(2\ell+1)]^{1/2}\left\{\exp\left[2\mathrm{i}\delta_{\ell j}(k)\right]-1\right\}\left(\ell 0\tfrac{1}{2}m_s|jm_s\right)$$
$$\times\left(\ell m_s - m_s'\tfrac{1}{2}m_s'|jm_s\right)Y_{\ell m_s - m_s'}(\theta,\phi)\,. \tag{1.280}$$

We can write this result as a 2×2 matrix in spin space using the explicit forms for the Clebsch–Gordan coefficients and for the spherical harmonics defined in Appendices A and B, respectively. We find that

$$\mathbf{M}(\theta,\phi) = \begin{pmatrix} f(\theta) & h(\theta)\mathrm{e}^{-\mathrm{i}\phi} \\ -h(\theta)\mathrm{e}^{\mathrm{i}\phi} & f(\theta)\end{pmatrix}, \tag{1.281}$$

where the direct scattering amplitude $f(\theta)$ is given by

$$f(\theta) = \frac{1}{2\mathrm{i}k}\sum_{\ell=0}^{\infty}\left[(\ell+1)\{\exp[2\mathrm{i}\delta_{\ell\ell+\frac{1}{2}}(k)]-1\}+\ell\{\exp[2\mathrm{i}\delta_{\ell\ell-\frac{1}{2}}(k)]-1\}\right]$$
$$\times P_\ell(\cos\theta)\,, \tag{1.282}$$

and the spin-flip scattering amplitude $h(\theta)$ is given by

$$h(\theta) = \frac{1}{2\mathrm{i}k}\sum_{\ell=1}^{\infty}\left\{\exp[2\mathrm{i}\delta_{\ell\ell+\frac{1}{2}}(k)]-\exp[2\mathrm{i}\delta_{\ell\ell-\frac{1}{2}}(k)]\right\}P_\ell^1(\cos\theta)\,. \tag{1.283}$$

We note that if the spin–orbit coupling term in the potential is negligible so that the interaction potential is the same for $j=\ell+\frac{1}{2}$ and $j=\ell-\frac{1}{2}$, then $\delta_{\ell\ell+\frac{1}{2}}(k)=\delta_{\ell\ell-\frac{1}{2}}(k)$. The spin-flip amplitude $h(\theta)$ then vanishes and the direct scattering amplitude $f(\theta)$ reduces to the familiar form given by (1.29) where $\delta_\ell(k)=\delta_{\ell\ell+\frac{1}{2}}(k)=\delta_{\ell\ell-\frac{1}{2}}(k)$.

We can rewrite the scattering matrix (1.281) in terms of the 2×2 unit matrix I_2 and the Pauli spin matrices given in (1.234) as

$$\mathbf{M}(\theta,\phi) = f(\theta)I_2 - \mathrm{i}h(\theta)\sin\phi\,\sigma_x + \mathrm{i}h(\theta)\cos\phi\,\sigma_y\,. \tag{1.284}$$

This expression can be further simplified if we define the (x,z) plane to be the plane of scattering, with the z-axis being the incident beam direction and the y-axis being normal to this plane. Then $\phi=0$ and we obtain

$$\mathbf{M} = f(\theta)I_2 + \mathrm{i}h(\theta)\sigma_y\,. \tag{1.285}$$

If we introduce a unit vector $\hat{\mathbf{n}}$ normal to the scattering plane defined by the incident and scattered electron vectors $\mathbf{k}_i$ and $\mathbf{k}_f$, respectively, so that

$$\hat{\mathbf{n}} = \frac{\mathbf{k}_i \times \mathbf{k}_f}{|\mathbf{k}_i \times \mathbf{k}_f|}\,, \tag{1.286}$$

then the scattering matrix can be written as

$$\mathbf{M} = f(\theta) I_2 + \mathrm{i} h(\theta) \boldsymbol{\sigma} \cdot \hat{\mathbf{n}}\,. \tag{1.287}$$

We note that the scattering matrix $\mathbf{M}$ is a scalar and hence is independent of the particular coordinate system which we have used to obtain it. In fact the expression given by (1.287) is the most general scalar which can be formed in the case of spin $\frac{1}{2}$ particles scattered from a spin zero target under the assumptions of rotational invariance, time-reversal invariance and parity conservation.

Having determined the scattering matrix, we can now calculate the cross sections. The differential cross section for a transition from a state denoted by $(\mathbf{k}, m_s)$ to a state denoted by $(\mathbf{k}', m_s')$ is

$$\frac{\mathrm{d}\sigma_{m_s' m_s}}{\mathrm{d}\Omega} = |\langle \chi_{\frac{1}{2} m_s'} | \mathbf{M} | \chi_{\frac{1}{2} m_s} \rangle|^2 = |M_{m_s' m_s}(\theta, \phi)|^2\,. \tag{1.288}$$

If the spin orientation of the final state is not measured, then the differential cross section for scattering from a pure initial spin state $\chi_{\frac{1}{2} m_s}$ is

$$\begin{aligned} \frac{\mathrm{d}\sigma_{m_s}}{\mathrm{d}\Omega} &= \sum_{m_s' = \pm\frac{1}{2}} |\langle \chi_{\frac{1}{2} m_s'} | \mathbf{M} | \chi_{\frac{1}{2} m_s} \rangle|^2 \\ &= \sum_{m_s' = \pm\frac{1}{2}} \langle \chi_{\frac{1}{2} m_s} | \mathbf{M}^+ | \chi_{\frac{1}{2} m_s'} \rangle \langle \chi_{\frac{1}{2} m_s'} | \mathbf{M} | \chi_{\frac{1}{2} m_s} \rangle \\ &= \langle \chi_{\frac{1}{2} m_s} | \mathbf{M}^+ \mathbf{M} | \chi_{\frac{1}{2} m_s} \rangle\,, \end{aligned} \tag{1.289}$$

where $\mathbf{M}^+$ is the hermitian conjugate of $\mathbf{M}$. Using (1.287) and the identity

$$(\boldsymbol{\sigma} \cdot \mathbf{V}_1)(\boldsymbol{\sigma} \cdot \mathbf{V}_2) = \mathbf{V}_1 \cdot \mathbf{V}_2 + \mathrm{i} \boldsymbol{\sigma} \cdot (\mathbf{V}_1 \times \mathbf{V}_2)\,, \tag{1.290}$$

where $\mathbf{V}_1$ and $\mathbf{V}_2$ are any two vectors, then we find that

$$\begin{aligned} \frac{\mathrm{d}\sigma_{m_s}}{\mathrm{d}\Omega} &= |f(\theta)|^2 + |h(\theta)|^2 + \mathrm{i}[f^*(\theta) h(\theta) - f(\theta) h^*(\theta)] \\ &\quad \times \langle \chi_{\frac{1}{2} m_s} | \boldsymbol{\sigma} \cdot \hat{\mathbf{n}} | \chi_{\frac{1}{2} m_s} \rangle\,. \end{aligned} \tag{1.291}$$

This result can be rewritten as

$$\frac{\mathrm{d}\sigma_{m_s}}{\mathrm{d}\Omega} = \left[|f(\theta)|^2 + |h(\theta)|^2 \right] \left[1 + S(\theta) \mathbf{P}_i \cdot \hat{\mathbf{n}} \right]\,, \tag{1.292}$$

where the real function

$$S(\theta) = \mathrm{i}\frac{f^*(\theta)h(\theta) - f(\theta)h^*(\theta)}{|f(\theta)|^2 + |h(\theta)|^2} \tag{1.293}$$

is called the Sherman function [871] and

$$\mathbf{P}_i = \langle \chi_{\frac{1}{2}m_s} | \boldsymbol{\sigma} | \chi_{\frac{1}{2}m_s} \rangle \tag{1.294}$$

is the initial electron spin polarization vector. Since we are considering a pure initial spin state we have $|\mathbf{P}_i| = 1$. However, (1.292) remains valid for any degree of polarization of the incident electron beam where $0 \leq |\mathbf{P}_i| \leq 1$. Spin and relativistic effects in potential scattering are discussed further by Burke and Joachain [171] and a discussion of polarization phenomena in atomic collisions using a density matrix approach has been given by Blum [119]. We refer to these texts for a more detailed presentation of these phenomena.

Chapter 2
Multichannel Collision Theory

In this chapter we introduce the basic concepts of multichannel collision theory and we apply this theory for illustrative purposes to non-relativistic electron collisions with multi-electron atoms and atomic ions. This chapter thus provides an introduction to our discussion of resonances and threshold behaviour presented in Chap. 3 and to R-matrix theory and applications, presented in Chap. 4 and later chapters in this monograph. We will be mainly concerned in this chapter with low-energy elastic scattering and excitation processes. However, we will show in Chap. 6 that the theory and methods developed in this chapter are the basis of R-matrix methods which enable accurate excitation and ionization processes to be calculated at intermediate energies.

We commence our discussion of multichannel collision theory in Sect. 2.1 by considering the solution of the time-independent Schrödinger equation describing low-energy electron collisions with multi-electron atoms and atomic ions which contain N electrons and have nuclear charge number Z. We define the scattering amplitude in terms of the asymptotic form of the solution of the Schrödinger equation. The differential and total cross sections are then defined in terms of this scattering amplitude. In Sect. 2.2 we consider the atomic or ionic target eigenstates which take part in the collision process. In order to obtain accurate scattering amplitudes and cross sections it is necessary to represent the target by accurate wave functions. We therefore give a brief overview in this section of representations of the target eigenstates, used in most practical applications, where electron exchange and correlation effects are both accurately represented. We also introduce the concept of pseudostates, which enable long-range polarization effects to be accurately included in low-energy electron–atom collisions. A discussion of the further role of pseudostates in representing inelastic effects due to excitation of high-lying bound states and continuum states at incident electron energies close to and above the ionization threshold is reserved for Chap. 6.

In Sect. 2.3 we turn our attention to the derivation of the close coupling equations that can yield accurate low- and intermediate-energy solutions of the time-independent Schrödinger equation describing electron–atom and electron–ion collisions. We commence by showing that the wave function can be expanded in terms of an antisymmetrized sum over target eigenstates and pseudostates multiplied by functions representing the motion of the scattered electron. This close coupling

P.G. Burke, *R-Matrix Theory of Atomic Collisions*, Springer Series on Atomic, Optical, and Plasma Physics 61, DOI 10.1007/978-3-642-15931-2_2,

expansion is then substituted into the Schrödinger equation leading to the close coupling equations which are a set of coupled second-order integrodifferential equations satisfied by functions representing the radial motion of the scattered electron. Finally in this section we examine the form of the local and non-local potentials that occur in these close coupling equations. In Sect. 2.4 we examine the asymptotic form of the solution of the close coupling equations which enables us to define the K-matrix which is a generalization of the expression for this quantity in potential scattering given in Chap. 1. We show that the solution of the close coupling equations satisfies the Kohn variational principle, and hence the corresponding K-matrix is correct to second order in the error in the collision wave function. We also show from general considerations that the K-matrix is real and symmetric. Finally, in Sect. 2.5 we define the multichannel S- and T-matrices in terms of the K-matrix, which in turn leads to the derivation of expressions for the differential and total cross sections. In this section we also summarize the angular momentum transfer formalism, which enables several qualitative features of angular distributions to be simply understood, and we define the collision strength and the effective collision strength which have been widely used in plasma physics and astrophysics applications.

2.1 Wave Equation and Cross Section

We illustrate multichannel collision theory in this chapter by considering non-relativistic low-energy elastic and inelastic electron collisions with multi-electron atoms and atomic ions represented by the equation

$$\mathrm{e}^- + A_i \rightarrow A_j + \mathrm{e}^-, \tag{2.1}$$

where A_i and A_j are the initial and final bound states of the target. The time-independent Schrödinger equation satisfied by the wave function Ψ describing process (2.1) is

$$H_{N+1}\Psi = E\Psi, \tag{2.2}$$

where H_{N+1} is the non-relativistic Hamiltonian defined in atomic units by

$$H_{N+1} = \sum_{i=1}^{N+1}\left(-\frac{1}{2}\nabla_i^2 - \frac{Z}{r_i}\right) + \sum_{i>j=1}^{N+1}\frac{1}{r_{ij}} \tag{2.3}$$

and E is the total energy. It then follows that (2.2) and (2.3) describe the collision of an electron with an atom or atomic ion containing N electrons and with nuclear charge number Z, where we limit ourselves in this chapter to low Z atomic targets so that relativistic effects are negligible. In (2.3) we have taken the origin of coordinates to be the target nucleus, which we assume has infinite mass. Also ∇_i^2 is the Laplacian operator defined in spherical polar coordinates in Appendix B.3 and we

have written $r_{ij} = |\mathbf{r}_i - \mathbf{r}_j|$ where $\mathbf{r}_i$ and $\mathbf{r}_j$ are the vector coordinates of the ith and jth electrons.

In order to define the scattering amplitude and cross sections we first rewrite H_{N+1} in terms of the target Hamiltonian H_N as follows:

$$H_{N+1} = H_N - \frac{1}{2}\nabla_{N+1}^2 - \frac{Z}{r_{N+1}} + \sum_{i=1}^{N} \frac{1}{r_{iN+1}}, \tag{2.4}$$

where H_N is defined by (2.3) with $N+1$ replaced by N. We next introduce a set of target eigenstates, and possibly pseudostates, Φ_i, and their corresponding energies e_i which satisfy the equation

$$\langle \Phi_i | H_N | \Phi_j \rangle = e_i \delta_{ij}, \tag{2.5}$$

where the integration in this equation is carried out over the space and spin coordinates of the N target electrons. We then look for the solution of (2.2) corresponding to the process represented by (2.1), where an electron in spin state $\chi_{\frac{1}{2}m_i}$ collides with a target atom or ion in state Φ_i and is scattered into spin state $\chi_{\frac{1}{2}m_j}$, leaving the atom or ion in state Φ_j allowed by the conservation relations, where the z-axis is chosen to lie along the incident beam direction. The asymptotic form of the wave function in the case of a neutral target where $N = Z$ is then

$$\Psi_i \underset{r\to\infty}{\sim} \Phi_i \chi_{\frac{1}{2}m_i} \exp(\mathrm{i}k_i z) + \sum_j \Phi_j \chi_{\frac{1}{2}m_j} f_{ji}(\theta, \phi) \frac{\exp(\mathrm{i}k_j r)}{r}, \tag{2.6}$$

where r, θ and ϕ are the radial and spherical polar coordinates of the scattered electron and where $f_{ji}(\theta, \phi)$ is the scattering amplitude for a transition from state $\Phi_i \chi_{\frac{1}{2}m_i}$ to state $\Phi_j \chi_{\frac{1}{2}m_j}$ corresponding to the scattering angles θ, ϕ. The direction of spin quantization is usually taken to be the incident beam direction and the wave numbers k_i and k_j, for the incident and scattered electrons, are related to the total energy E of the system and to the target eigenenergies e_i and e_j by the equation

$$E = e_i + \frac{1}{2}k_i^2 = e_j + \frac{1}{2}k_j^2. \tag{2.7}$$

The outgoing wave term in (2.6) contains contributions from all target states that are energetically allowed, that is for which $k_j^2 \geq 0$. The remaining states, for which $k_j^2 < 0$, can only occur virtually during the collision process. These virtual states play an important role when the scattered electron lies within the target charge cloud and we will see that they can give rise to resonances in the collision process.

If the incident electron energy is high enough then continuum states of the target can be excited and contribute to the asymptotic form in (2.6). These terms correspond to ionizing collisions. We will consider this possibility in Sect. 3.3.5 when

we discuss the threshold behaviour of ionization and in Chap. 6 when we discuss intermediate-energy electron–atom collisions.

We also note that when the target is an atomic ion, logarithmic phase factors must be included in the exponentials in (2.6) to allow for the long-range distortion caused by the Coulomb potential. This introduces no essential complications so we will not consider these factors further here, but will return to consider their effect on the cross section in Sect. 2.5.

The differential cross section for a transition from an initial atomic state Φ_i to a final atomic state Φ_j, with the scattered electron spin magnetic quantum number changing from m_i to m_j and its wave number changing from k_i to k_j, can be obtained by calculating the incident and scattered fluxes in (2.6). We obtain

$$\frac{\mathrm{d}\sigma_{ji}}{\mathrm{d}\Omega} = \frac{k_j}{k_i} \left| f_{ji}(\theta, \phi) \right|^2 \tag{2.8}$$

in units of a_0^2/steradian, where a_0 is the Bohr radius of the hydrogen atom in its ground state. The total cross section is then obtained by averaging over the initial spin states, summing over the final spin states and integrating over all scattering angles.

2.2 Target Eigenstates and Pseudostates

In order to calculate the wave function Ψ in (2.2) describing the collision process and hence the scattering amplitude and cross sections we must first consider how the target eigenstates, and possibly pseudostates, Φ_j, are represented in the theory. In this section we give a brief overview of the representations that are adopted for these target states in non-relativistic electron–atom and electron–ion collision calculations.

2.2.1 Target Eigenstates

For multi-electron atoms and ions, the target eigenstates are not known exactly. Hence in most electron collision calculations they are written as configuration interaction expansions in terms of sums over an orthonormal set of target basis configurations ϕ_i in the form

$$\Phi_j(\mathbf{X}_N) = \sum_i \phi_i(\mathbf{X}_N) c_{ij}, \tag{2.9}$$

as discussed by Hartree [445], Froese Fischer et al. [346, 349], Hibbert [465] and Cowan [233]. In this equation $\mathbf{X}_N \equiv \mathbf{x}_1, \ldots, \mathbf{x}_N$, where $\mathbf{x}_i \equiv \mathbf{r}_i \sigma_i$, $i = 1, \ldots, N$, represent the space and spin coordinates of the N target electrons and the expansion coefficients c_{ij} are obtained by diagonalizing the target Hamiltonian in (2.5) in

this basis. These calculations can be carried out using one of a number of atomic multiconfiguration atomic structure programs, which we refer to in Sect. 5.1.1. We assume in the following discussion that the atomic orbitals for each orbital angular momentum are constrained to be orthogonal, corresponding to most atomic structure and collision programs. However, we observe that non-orthogonal orbitals are finding increasing use in atomic structure and collision calculations considered in later chapters.

The basis configurations ϕ_i in (2.9) are constructed from N one-electron orbital and spin functions which have the form

$$u_{n\ell m_\ell m_i}(\mathbf{r}, \sigma) = r^{-1} P_{n\ell}(r) Y_{\ell m_\ell}(\theta, \phi) \chi_{\frac{1}{2} m_i}(\sigma), \tag{2.10}$$

where the reduced radial orbitals $P_{n\ell}(r)$ satisfy the orthonormality relations

$$\int_0^\infty P_{n\ell}(r) P_{n'\ell}(r) \mathrm{d}r = \delta_{nn'}, \tag{2.11}$$

for each orbital angular momentum ℓ. Also $Y_{\ell m_\ell}(\theta, \phi)$ are spherical harmonics, which are defined and discussed in Appendices B.3 and B.4, and and $\chi_{\frac{1}{2} m_i}(\sigma)$ are electron spin eigenfunctions. In the absence of relativistic terms in the Hamiltonian, the orbital and spin angular momenta of the one-electron functions are coupled together to yield completely antisymmetrized configurations, which are eigenfunctions of the square of the total N-electron target orbital and spin angular momentum operators $\mathbf{L^2}$ and $\mathbf{S^2}$ and their z-components L_z and S_z as well as the total target parity operator π. We can write these basis configurations more explicitly as

$$\phi_i(\mathbf{X}_N) \equiv \phi_i(1\mathrm{s}^{N_{1i}} 2\mathrm{s}^{N_{2i}} 2\mathrm{p}^{N_{3i}} \ldots \beta_i L_i S_i M_{L_i} M_{S_i} \pi_i \mid \mathbf{X}_N), \tag{2.12}$$

where the N_{ji} are the occupation numbers of the target shells, which satisfy

$$\sum_j N_{ji} = N, \quad \text{all } i. \tag{2.13}$$

Also in (2.12), β_i denotes the coupling of the target shells, L_i and S_i are the total target orbital and spin angular momentum quantum numbers, M_{L_i} and M_{S_i} are the corresponding magnetic quantum numbers in some preferred direction and π_i is the total target parity quantum number. Each target eigenstate Φ_j involves a summation over basis configurations ϕ_i that have the same total orbital, spin and parity quantum numbers but differ in the occupation numbers or the coupling. We can thus write these target eigenstates more explicitly as

$$\Phi_j(\alpha_j L_j S_j M_{L_j} M_{S_j} \pi_j \mid \mathbf{X}_N), \tag{2.14}$$

where the quantity α_j serves to distinguish different target states with the same total target orbital, spin and parity quantum numbers.

The basis configurations in (2.9) usually include the Hartree–Fock configuration of the target ground state or a low-lying excited state. Hence the reduced radial orbitals $P_{n\ell}(r)$ include the self-consistent field (SCF) orbitals. Additional "physical orbitals" are then included to represent the other target states of interest in the calculation and possibly further "pseudo-orbitals" are included to represent additional correlation and polarization effects. These orbitals are either expressed in analytical form as a sum of Slater-type orbitals (STOs) defined by

$$P_{n\ell}(r) = \sum_j b_j \frac{(2\xi_j)^{k_j+1/2}}{\sqrt{(2k_j)!}} r^{k_j} \exp(-\xi_j r), \tag{2.15}$$

where $k_j \geq \ell+1$ and the coefficients b_j, k_j and ξ_j depend on n and ℓ, or the orbitals are tabulated at a grid of points.

As an example, we consider the target eigenstates that have been adopted in several studies of low-energy electron collisions with Be-like ions C^{2+} and O^{4+}. In this case electron collisional excitation cross sections between the following six target eigenstates are important in many applications (see, for example, [97])

$$1s^2 2s^2\ {}^1S^e;\ 1s^2 2s2p\ {}^3P^o,\ {}^1P^o;\ 1s^2 2p^2\ {}^3P^e,\ {}^1D^e,\ {}^1S^e. \tag{2.16}$$

Accurate low-energy excitation cross sections can then be obtained using the following physical orbitals and pseudo-orbitals in the representation of the target eigenstates

$$1s,\ 2s,\ 2p,\ \overline{3s},\ \overline{3p},\ \overline{3d}, \tag{2.17}$$

where we distinguish the $\overline{3s}$, $\overline{3p}$ and $\overline{3d}$ pseudo-orbitals from the 1s, 2s and 2p physical orbitals by placing a bar over the pseudo-orbitals.

The target eigenstates are constructed by diagonalizing the target Hamiltonian matrix, defined in (2.5), in the basis of configurations defined by (2.9). These configurations are constructed from the physical and pseudo-orbitals assuming that the 1s orbital remains doubly occupied. Configurations where one or two electrons are excited out of the 1s orbital correspond to high-energy excitations which are not important in low-energy electron collisions. A list of configurations that can be constructed from the orbital basis defined by (2.17) for each target eigenstate is given in Table 2.1, where we find it convenient to put these configurations into categories depending on whether zero, one or two electrons are excited from physical to pseudo-orbitals.

The choice of the physical and pseudo-orbitals is not unique and care must be taken in choosing them. One appropriate choice is to take the 1s and 2s orbitals to be the Hartree–Fock orbitals from the $1s^2 2s^2\ {}^1S^e$ ground state and the 2p orbital to be the Hartree–Fock orbital from the $1s^2 2s2p\ {}^3P^o$ first excited state. The $\overline{3s}$, $\overline{3p}$ and $\overline{3d}$ pseudo-orbitals, which are orthogonal to the physical orbitals with the same angular symmetry, can then be chosen to optimize the energies of the remaining

Table 2.1 Configuration basis which represent the lowest six Be-like ion target eigenstates

Target state symmetry	Zero-electron excitations	One-electron excitations	Two-electron excitations
$^1S^e$	$1s^2 2s^2$ $1s^2 2p^2$	$1s^2 2s\overline{3s}$ $1s^2 2p\overline{3p}$	$1s^2\overline{3s}^2$ $1s^2\overline{3p}^2$ $1s^2\overline{3d}^2$
$^3P^o, ^1P^o$	$1s^2 2s2p$	$1s^2 2s\overline{3p}$ $1s^2 2p\overline{3s}$ $1s^2 2p\overline{3d}$	$1s^2\overline{3s}\ \overline{3p}$ $1s^2\overline{3p}\ \overline{3d}$
$^3P^e$	$1s^2 2p^2$	$1s^2 2p\overline{3p}$	$1s^2\overline{3p}^2$ $1s^2\overline{3d}^2$
$^1D^e$	$1s^2 2p^2$	$1s^2 2s\overline{3d}$ $1s^2 2p\overline{3p}$	$1s^2\overline{3s}\ \overline{3d}$ $1s^2\overline{3p}^2$ $1s^2\overline{3d}^2$

four excited states in (2.16). If we assume that the target eigenstates Φ_j in (2.9) are expanded in terms of zero-electron and one-electron excitation configurations from Table 2.1, then the six target eigenstates in (2.16) are expanded as follows:

$$
\begin{aligned}
\Phi_1 &= \left[c_{11}1s^2 2s^2 + c_{21}1s^2 2p^2 + c_{31}1s^2 2s\overline{3s} + c_{41}1s^2 2p\overline{3p}\right] {}^1S^e,\\
\Phi_2 &= \left[c_{12}1s^2 2s2p + c_{22}1s^2 2s\overline{3p} + c_{32}1s^2 2p\overline{3s} + c_{42}1s^2 2p\overline{3d}\right] {}^3P^o,\\
\Phi_3 &= \left[c_{13}1s^2 2s2p + c_{23}1s^2 2s\overline{3p} + c_{33}1s^2 2p\overline{3s} + c_{43}1s^2 2p\overline{3d}\right] {}^1P^o,\\
\Phi_4 &= \left[c_{14}1s^2 2p^2 + c_{24}1s^2 2p\overline{3p}\right] {}^3P^e,\\
\Phi_5 &= \left[c_{15}1s^2 2p^2 + c_{25}1s^2 2s\overline{3d} + c_{35}1s^2 2p\overline{3p}\right] {}^1D^e,\\
\Phi_6 &= \left[c_{16}1s^2 2p^2 + c_{26}1s^2 2s^2 + c_{36}1s^2 2s\overline{3s} + c_{46}1s^2 2p\overline{3p}\right] {}^1S^e,
\end{aligned}
\tag{2.18}
$$

where the dominant configuration is the first configuration in the list in each case. The coefficients defining the pseudo-orbitals in (2.15) can be determined by minimizing the energies of the excited states defined by (2.18) using an atomic structure program (e.g. [464], or an equivalent program). For example, the $\overline{3s}$ pseudo-orbital could be chosen to allow for the difference of the 2s orbital in the $1s^2 2s^2\ {}^1S^e$ ground state and in the $1s^2 2s2p\ {}^3P^o$ and $1s^2 2s2p\ {}^1P^o$ excited states. Thus the $\overline{3s}$ pseudo-orbital coefficients could be optimized on a linear combination of the $1s^2 2s2p\ {}^3P^o$ and $1s^2 2s2p\ {}^1P^o$ excited state energies. Also the $\overline{3p}$ pseudo-orbital could be chosen to allow for the difference of the 2p orbital in the $1s^2 2s2p\ {}^3P^o$ first excited state

and in the $1s^2 2p^2\ {}^3P^e$ and $1s^2 2p^2\ {}^1S^e$ excited states. Thus the $\overline{3p}$ pseudo-orbital coefficients could be optimized on a linear combination of the $1s^2 2p^2\ {}^3P^e$ and $1s^2 2p^2\ {}^1S^e$ excited state energies. Finally, the $\overline{3d}$ pseudo-orbital coefficients could be optimized on the $1s^2 2p^2\ {}^1D^e$ excited state energy.

We see from Table 2.1 that in addition to the zero-electron and one-electron excitation configurations, which we included in expansions (2.18) of the target eigenstates, we could also include two-electron excitation configurations. This would improve the target eigenstates by including additional electron–electron correlation effects. However, it is important to ensure that the correlation effects included in the target states balance those included in the collision wave function in order to obtain accurate collision results. We will see in Chap. 6, where we discuss electron collisions at intermediate energies, that the inclusion of two-electron excitation configurations in the collision wave function can give rise to unphysical or pseudo-resonances at these energies. We will therefore defer further discussion of this point until that chapter.

2.2.2 Target Pseudostates

In certain circumstances determination of target states which are not eigenstates of the target Hamiltonian is required to obtain accurate electron–atom collision cross sections. These states, which are usually called pseudostates, are found to be particularly useful in low-energy electron–atom and electron–molecule collisions, where the long-range polarization potential gives an important contribution to the cross section. We will see in Chaps. 6 and 11 that target pseudostates can also be used to represent the ionization continuum in electron–atom and electron–molecule collisions at intermediate energies.

For an atom in a non-degenerate S-state, the long-range polarization potential has the asymptotic form

$$V_p(r) \underset{r\to\infty}{\sim} -\frac{\alpha}{2r^4}, \tag{2.19}$$

where the quantity α which appears in this equation is the dipole polarizability. This is defined by the expression (see [243])

$$\alpha = 2\sum_k \int \frac{|\langle \Phi_0 | D_N | \Phi_k \rangle|^2}{e_k - e_0} \mathrm{d}k, \tag{2.20}$$

where the summation and integration in this equation are taken over all target eigenstates Φ_k, including the continuum, which are coupled to the ground state Φ_0 by the dipole operator

$$D_N = \sum_{i=1}^{N} z_i, \tag{2.21}$$

and where the eigenenergies e_k are defined by

$$e_k = \langle \Phi_k | H_N | \Phi_k \rangle. \tag{2.22}$$

It was shown by Castillejo et al. [205] that in the case of electron collisions with atomic hydrogen in its ground state, 65.8% of the dipole polarizability comes from including the 2p state in expansion (2.20) while 81.4% of the dipole polarizability comes from the sum over all bound states, the remaining 18.6% coming from the continuum terms in the expansion. In this case, Damburg and Karule [245] showed that a p-wave pseudostate denoted by $\overline{2\mathrm{p}}$ enables expansion (2.20) to be replaced by a single term. This polarized pseudostate has the same range as the 1s ground state orbital and has the reduced radial form

$$P_{\overline{2\mathrm{p}}}(r) = \left(\frac{8}{129}\right)^{1/2} \left(2r^2 + r^3\right) \mathrm{e}^{-r}. \tag{2.23}$$

The corresponding pseudostate energy e^p, defined by

$$e^p = \langle \Phi^p | H_N | \Phi^p \rangle, \tag{2.24}$$

has the value $-7/86$ a.u., where Φ^p is the pseudostate wave function. Clearly this energy is not an eigenenergy of the target Hamiltonian. However, if this polarized pseudostate, as well as the ground target eigenstate, is included in the close coupling expansion of the collision wave function, as discussed in Sect. 2.3 and Chaps. 5 and 6, then the full long-range part of the polarization potential given by (2.19) is represented in the collision process. Elastic e^-–H collision calculations including this pseudostate were first carried out at energies below the 2s and 2p excitation threshold by Burke et al. [177].

In the case of multi-electron atoms and atomic ions, the polarized pseudostates, like the target eigenstates, cannot be written down exactly. In this case a variational principle [166, 167, 941] can be used to calculate these pseudostates. We consider the following inhomogeneous equation for the unnormalized pseudostate $\widetilde{\Phi}^p$

$$(H_N - e_0)\widetilde{\Phi}^p = D_N \Phi_0. \tag{2.25}$$

This equation has the formal solution

$$|\widetilde{\Phi}^p\rangle = \sum_k \int \frac{\langle \Phi_k | D_N | \Phi_0 \rangle}{e_k - e_0} |\Phi_k\rangle \, \mathrm{d}k, \tag{2.26}$$

where the spectral representation of the Green's function $(H_N - e_0)^{-1}$ has been used, which involves a summation over the discrete spectrum and an integration over the continuum spectrum of H_N. Substituting (2.26) into (2.20) then gives

$$\alpha = 2\langle \Phi_0 | D_N | \widetilde{\Phi}^p \rangle. \tag{2.27}$$

In order to write this equation in the form of (2.20) containing a single term we normalize $\widetilde{\Phi}^p$ by introducing the constant n_p defined by

$$n_p = \langle \widetilde{\Phi}^p | \widetilde{\Phi}^p \rangle. \tag{2.28}$$

The normalized pseudostate Φ^p is then given by

$$\Phi^p = n_p^{-1/2} \widetilde{\Phi}^p. \tag{2.29}$$

Substituting this result into (2.27) then gives

$$\alpha = 2 n_p^{1/2} \langle \Phi_0 | D_N | \Phi^p \rangle. \tag{2.30}$$

The final step is to eliminate $n_p^{1/2}$ from this equation. To do this we project (2.25) onto $\widetilde{\Phi}^p$ yielding

$$\langle \widetilde{\Phi}^p | H_N - e_0 | \widetilde{\Phi}^p \rangle = \langle \widetilde{\Phi}^p | D_N | \Phi_0 \rangle, \tag{2.31}$$

which gives, after using (2.29)

$$n_p^{1/2} \langle \Phi^p | H_N - e_0 | \Phi^p \rangle = \langle \Phi^p | D_N | \Phi_0 \rangle. \tag{2.32}$$

Substituting this result for $n_p^{1/2}$ into (2.30) then gives

$$\alpha = 2 \frac{|\langle \Phi_0 | D_N | \Phi^p \rangle|^2}{e^p - e_0}, \tag{2.33}$$

where the energy e^p of the polarized pseudostate is given by (2.24). If we include the ground state Φ_0 and the polarized pseudostate Φ^p in the close coupling expansion of the wave function describing electron collisions with atomic hydrogen, as discussed in Sect. 2.3 and Chaps. 5 and 6, then the full long-range part of the dipole polarization potential given by (2.19) is represented in the collision process. In this way we have replaced the summation and integration in the expression for the dipole polarizability given by (2.20) by a single pole term given by (2.33).

The problem of calculating polarized pseudostates for complex targets reduces to solving the inhomogeneous equation (2.25) to obtain $\widetilde{\Phi}^p$ and then normalizing this solution using (2.29) to give the required polarized pseudostate Φ^p. We can solve (2.25) by introducing a trial function $\widetilde{\Phi}_{\rm t}^p$ and considering the variational functional

$$J[\widetilde{\Phi}_{\rm t}^p] = \langle \widetilde{\Phi}_{\rm t}^p | H_N - e_0 | \widetilde{\Phi}_{\rm t}^p \rangle - 2 \langle \widetilde{\Phi}_{\rm t}^p | D_N | \Phi_0 \rangle. \tag{2.34}$$

The first-order variation δJ of the functional J with respect to small variations $\delta \widetilde{\Phi}_{\rm t}^p$ in the trial function $\widetilde{\Phi}_{\rm t}^p$ is

$$\delta J[\widetilde{\Phi}_{\rm t}^{p}] = 2\langle \delta\widetilde{\Phi}_{\rm t}^{p}\,|H_N - e_0|\,\widetilde{\Phi}_{\rm t}^{p}\rangle - 2\langle \delta\widetilde{\Phi}_{\rm t}^{p}\,|D_N|\,\Phi_0\rangle, \tag{2.35}$$

which is zero when $\widetilde{\Phi}_{\rm t}^{p}$ is an exact solution of (2.25). We construct a trial function in analogy with the target eigenstates given by (2.9), by expanding $\widetilde{\Phi}_{\rm t}^{p}$ in terms of a sum of orthonormal basis configurations $\widetilde{\phi}_j$ with the appropriate symmetry as follows:

$$\widetilde{\Phi}_{\rm t}^{p}(\mathbf{X}_N) = \sum_{j=1}^{m} \widetilde{\phi}_j(\mathbf{X}_N) b_j. \tag{2.36}$$

Substituting this expansion into (2.34) and varying the coefficients b_j leads to the system of m linear simultaneous equations

$$\sum_{j=1}^{m} \left(\langle \widetilde{\phi}_i\,|H_N|\,\widetilde{\phi}_j\rangle - e_0\delta_{ij}\right) b_j = \langle \widetilde{\phi}_i\,|D_N|\,\Phi_0\rangle, \quad i = 1,\ldots,m, \tag{2.37}$$

which can be solved to yield the coefficients b_j, and hence $\widetilde{\Phi}_{\rm t}^{p}$ and the normalized polarized pseudostate Φ^p can be constructed.

Also we see from (2.34) that the second-order variation $\delta^2 J[\widetilde{\Phi}_{\rm t}^{p}]$ satisfies

$$\delta^2 J[\widetilde{\Phi}_{\rm t}^{p}] = \langle \delta\widetilde{\Phi}_{\rm t}^{p}\,|H_N - e_0|\,\delta\widetilde{\Phi}_{\rm t}^{p}\rangle \geq 0, \tag{2.38}$$

since e_0 is the lowest eigenvalue of H_N so that $H_N - e_0$ is a positive definite operator. Hence the minimum value of J is obtained when $\widetilde{\Phi}_{\rm t}^{p}$ is the exact solution of (2.25). Further at the minimum $J_{\rm min}$ of J we have

$$\begin{aligned} J_{\rm min} &= \langle \widetilde{\Phi}^{p}\,|H_N - e_0|\,\widetilde{\Phi}^{p}\rangle - 2\langle \widetilde{\Phi}^{p}\,|D_N|\,\Phi_0\rangle \\ &= -\langle \widetilde{\Phi}^{p}\,|D_N|\,\Phi_0\rangle \\ &= -\frac{1}{2}\alpha, \end{aligned} \tag{2.39}$$

which follows from (2.25), (2.27) and (2.34). Hence in constructing the polarized pseudostate it is possible to improve this state by varying the radial orbitals used in the definition of the basis configurations in (2.36) to minimize J or to maximize α.

As an example of the above theory we consider the calculation of the polarized pseudostate required to represent low-energy elastic electron collisions with neon. In this case a reasonably good approximation for the elastic collision process is obtained by representing the neon ground state by the Hartree–Fock $1s^2 2s^2 2p^6\ {}^1S^e$ configuration and the polarized pseudostate, which has ${}^1P^o$ symmetry, by a linear combination of the following basis configurations:

$$\begin{aligned} &1s^2 2s^2 2p^5 \overline{js}\ {}^1P^o, \quad j = 1,\ldots,n, \\ &1s^2 2s^2 2p^5 \overline{jd}\ {}^1P^o, \quad j = 3,\ldots,n, \\ &1s^2\ 2s\ 2p^6 \overline{jp}\ {}^1P^o, \quad j = 2,\ldots,n. \end{aligned} \tag{2.40}$$

The additional polarized pseudo-orbitals $\overline{j\mathrm{s}}$, $\overline{j\mathrm{p}}$ and $\overline{j\mathrm{d}}$ must satisfy the usual orthonormality relations given by (2.11) but are not physical. Indeed, like the $\overline{2\mathrm{p}}$ orbital representing the polarized pseudostate in atomic hydrogen given by (2.23), their range is determined by the range of the ground state of the target atom whose polarizability they are representing rather than by the range of the excited states. In a study carried out by Burke and Mitchell [166], the $\overline{j\mathrm{s}}$, $\overline{j\mathrm{p}}$ and $\overline{j\mathrm{d}}$ polarized pseudo-orbitals were expanded in terms of basis orbitals with the following reduced radial form:

$$P_{\overline{j\ell}}(r) = \sum_{i=\ell+1}^{n} a_{ij\ell}\, r^i \mathrm{e}^{-\beta r}. \tag{2.41}$$

In this equation, β is a range parameter and the coefficients $a_{ij\ell}$ were chosen so that these pseudo-orbitals were orthogonal to the 1s, 2s and 2p Hartree–Fock orbitals of the same angular symmetry and orthonormal to each other. Equation (2.37) was then solved for a series of values of this range parameter. Figure 2.1 shows the variation of the dipole polarizability with the range parameter β for three expansions including all configurations in (2.40) with $n = 4$, 5 and 6, respectively. For example, when $n = 4$ six basis configurations corresponding to the pseudo-orbitals $\overline{3\mathrm{s}}$, $\overline{4\mathrm{s}}$, $\overline{3\mathrm{p}}$, $\overline{4\mathrm{p}}$, $\overline{3\mathrm{d}}$ and $\overline{4\mathrm{d}}$ are retained in expansion (2.36). Also shown in Fig. 2.1 is the experimental value of the dipole polarizability determined from experimental data by Dalgarno and Kingston [242]. As the number of terms in the basis increases the curves become flatter and converge towards the experimental value. However, this calculation does not give a rigorous lower bound on the exact dipole polarizability

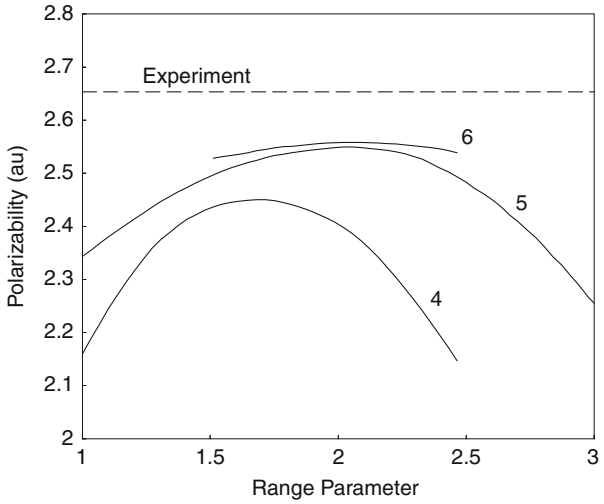

Fig. 2.1 The variation of the dipole polarizability with the range parameter β in expansion (2.41) compared with experiment for neon. The *curves* are labelled by the value of n defined by (2.40) (modified from Fig. 2 in [166])

since an exact target ground state was not used. Polarized pseudostates of this type have been used in electron–neon elastic scattering calculations by Blum and Burke [120] and Fon and Berrington [327].

The above theory can be modified in a straightforward way so that pseudostates can be calculated which represent higher multipole polarizabilities of the target and also which represent the dipole polarizabilities of excited states of the target. In addition, pseudostates can be chosen which allow in an average way for the loss of flux into the infinite number of high-lying Rydberg states and continuum states of the target, thus representing ionization in electron–atom collisions. We will discuss the construction and application of such pseudostates when we consider electron–atom collisions at intermediate energies in Chap. 6.

2.3 Close Coupling Equations

In the previous section we showed how accurate wave functions can be obtained for the target eigenstates and pseudostates which occur in electron collisions with multi-electron atoms or atomic ions. We turn our attention in this section to the determination of the electron–atom or electron–ion collision wave function Ψ that satisfies the non-relativistic Schrödinger equation (2.2). In Sect. 2.3.1 we review the foundations of the method which involves the solution of a set of "close coupling equations" also known as "coupled ID equations" which enables accurate excitation and ionization cross sections to be determined at low and intermediate energies. Then in Sect. 2.3.2 we describe the explicit form of the close coupling equations which must be solved in practical calculations.

2.3.1 Foundations of the Method

The foundations of methods for solving the Schrödinger equation (2.2) to obtain accurate elastic scattering, excitation and ionization cross sections for low- and intermediate-energy electron–atom and electron–ion collisions were laid by Massey and Mohr [642, 643] and Mott and Massey [665]. They introduced the following "close coupling" expansion of the total wave function describing electron collisions with an N-electron atom or atomic ion

$$\Psi(\mathbf{X}_{N+1}) = \sum_i \int \Phi_i(\mathbf{X}_N) F_i(\mathbf{x}_{N+1}), \tag{2.42}$$

where $\mathbf{X}_{N+1} \equiv \mathbf{x}_1, \ldots, \mathbf{x}_{N+1}$ and where $\mathbf{x}_i \equiv \mathbf{r}_i \sigma_i$, $i = 1, \ldots, N+1$, represent the space and spin coordinates of the $N+1$ electrons. The summation in (2.42) goes over the bound target eigenstates and the integration goes over the continuum target eigenstates, which are described by $\Phi_i(\mathbf{X}_N)$, and the functions $F_i(\mathbf{x}_{N+1})$ describe the corresponding motion of the scattered electron. We now substitute expansion

(2.42) into the Schrödinger equation (2.2) and project onto the target eigenstates $\Phi_i(\mathbf{X}_N)$ to yield the following infinite set of coupled second-order partial differential equations satisfied by the functions $F_i(\mathbf{x}_{N+1})$

$$(\nabla^2 + k_i^2)F_i(\mathbf{x}_{N+1}) = 2\sum_j \int V_{ij}(\mathbf{x}_{N+1})F_j(\mathbf{x}_{N+1}). \tag{2.43}$$

Here k_i^2 is defined by (2.5) and (2.7) and the potential matrix $V_{ij}(\mathbf{x}_{N+1})$ is defined by

$$V_{ij}(\mathbf{x}_{N+1}) = \langle \Phi_i(\mathbf{X}_N) \left| \sum_{i=1}^{N} \frac{1}{r_{iN+1}} - \frac{Z}{r_{N+1}} \right| \Phi_j(\mathbf{X}_N)\rangle, \tag{2.44}$$

where the integration in this matrix element goes over the space and spin coordinates of the N target electrons.

Although the solution of Schrödinger's equation (2.2) given by (2.42) and (2.43) in principle gives an accurate description of the collision, one question which arises is how can electron exchange, which is implicit in the theory, be calculated. The importance of exchange is well known in many applications, for example in "forbidden transitions" between the $1s^2 2s^2 2p^2\ ^3P^e$, $^1D^e$ and $^1S^e$ terms of O III (O^{2+}) which give rise to prominent lines in the spectra of many gaseous nebulae and active galactic nuclei [709]. On examining expansion (2.42) we see that electron exchange arises from the continuum terms in the expansion. In this case the incident electron labelled $N+1$ is captured into a bound eigenstate and one of the target electrons labelled $1, \ldots, N$ is ejected into a continuum state. While this process can be calculated using perturbation theory the resultant cross section can be significantly in error (e.g. [77]). On the other hand, the corresponding solution of the coupled equations (2.43) gives rise to difficulties owing to singularities which occur in integration over the continuum terms in the expansion corresponding to electron exchange. In nuclear structure and collisions these singularities were avoided in early work by Wheeler [960, 961], by expanding the total wave function in antisymmetric resonating groups of nucleons. We now discuss how these difficulties are resolved in electron–atom multichannel collision theory.

In electron–atom collisions the difficulties owing to singularities arising in the continuum due to electron exchange were overcome in a fundamental paper by Seaton [848], who extended the Hartree–Fock equations for bound states, in which electron exchange is treated using explicitly antisymmetric wave functions, to the treatment of continuum states. In this paper expansion (2.42) is replaced by the close coupling expansion

$$\Psi(\mathbf{X}_{N+1}) = \mathcal{A}\sum_i \Phi_i(\mathbf{X}_N)F_i(\mathbf{x}_{N+1}), \tag{2.45}$$

where the summation in this equation is now restricted to a finite number of bound antisymmetric target eigenstates $\Phi_i(\mathbf{X}_N)$ which satisfy (2.5). In addition $\mathcal{A}$ is the antisymmetrization operator which ensures that each term in expansion (2.45) is antisymmetric with respect to interchange of the space and spin coordinates of any pair of the $N+1$ electrons. We find that $\mathcal{A}$ is defined by

$$\mathcal{A} = (N+1)^{-1/2}\left(1 - \sum_{i=1}^{N} P_{iN+1}\right), \tag{2.46}$$

where P_{iN+1} is the operator which interchanges the space and spin coordinates of electrons labelled i and $N+1$. It follows that the total wave function $\Psi(\mathbf{X}_{N+1})$ defined by (2.45) is antisymmetric with respect to interchange of the space and spin coordinates of any pair of the $N+1$ electrons, in accordance with the Pauli exclusion principle.

Following Burke and Seaton [164], we consider first the uniqueness of the solution defined by (2.45) and (2.46). In the case where $N = 1$, corresponding to electron collisions with hydrogenic targets, (2.45) becomes, after using (2.46),

$$\Psi(\mathbf{x}_1, \mathbf{x}_2) = \frac{1}{\sqrt{2}} \sum_i \left[\Phi_i(\mathbf{x}_1) F_i(\mathbf{x}_2) - \Phi_i(\mathbf{x}_2) F_i(\mathbf{x}_1)\right]. \tag{2.47}$$

We now write

$$F_i(\mathbf{x}) = \overline{F}_i(\mathbf{x}) + \sum_j b_{ij} \Phi_j(\mathbf{x}), \tag{2.48}$$

where the summation in this equation goes over the same set of bound target eigenstates $\Phi_i(\mathbf{x})$ which are retained in (2.47). In this way we have defined a new function $\overline{F}_i(\mathbf{x})$ for any given set of coefficients b_{ij}. Substituting (2.48) into the right-hand side of (2.47) then gives

$$\begin{aligned}\Psi(\mathbf{x}_1, \mathbf{x}_2) = {} & \frac{1}{\sqrt{2}} \sum_i \left[\Phi_i(\mathbf{x}_1) \overline{F}_i(\mathbf{x}_2) - \Phi_i(\mathbf{x}_2) \overline{F}_i(\mathbf{x}_1)\right] \\ & + \frac{1}{\sqrt{2}} \sum_{ij} \Phi_i(\mathbf{x}_1) \Phi_j(\mathbf{x}_2)(b_{ij} - b_{ji}).\end{aligned} \tag{2.49}$$

We see that if

$$b_{ij} = b_{ji}, \tag{2.50}$$

then the second summation on the right-hand side of (2.49) vanishes and hence the wave function $\Psi(\mathbf{x}_1, \mathbf{x}_2)$ is unaltered by the transformation defined by (2.48). It follows that the functions $F_i(\mathbf{x})$ defined by (2.48) are not unique and that different functions defined by this equation will yield the same wave function

$\Psi(\mathbf{x}_1, \mathbf{x}_2)$ provided that the coefficients b_{ij} satisfy the symmetry relations given by (2.50).

On the other hand, the asymptotic form of the functions $F_i(\mathbf{x})$ is unique since the bound target eigenstates $\Phi_i(\mathbf{x})$ retained in (2.47) vanish asymptotically. Hence the scattering amplitudes and cross sections which are determined from the asymptotic form of the functions $F_i(\mathbf{x})$ are not modified by transformation (2.48).

We now consider three different procedures for choosing the coefficients b_{ij} in (2.48):

i. We may use expansion (2.47) without introducing explicit conditions which suffice to define $F_i(\mathbf{x})$ uniquely. This may lead to loss of accuracy in the numerical solution of the coupled integrodifferential equations, which we will see below are satisfied by the functions $F_i(\mathbf{x})$.
ii. We may introduce conditions which are sufficient to define the functions $F_i(\mathbf{x})$ uniquely, but which do not change the form of (2.47). Thus, for example, we could impose the orthogonality conditions

$$\langle \Phi_i | F_j \rangle = 0, \quad i \leq j, \tag{2.51}$$

where we list the states in some definite order. This procedure has been widely discussed [161, 164, 289, 848] and was shown by Norcross [692] to improve the accuracy of the numerical integrations.
iii. We may impose the orthogonality conditions

$$\langle \Phi_i | F_j \rangle = 0, \quad \text{all } i, \ j, \tag{2.52}$$

and replace (2.47) by

$$\begin{aligned} \Psi(\mathbf{x}_1, \mathbf{x}_2) \ &= \frac{1}{\sqrt{2}} \sum_i [\Phi_i(\mathbf{x}_1) F_i(\mathbf{x}_2) - \Phi_i(\mathbf{x}_2) F_i(\mathbf{x}_1)] \\ &\quad + \frac{1}{\sqrt{2}} \sum_{i \leq j} \left[\Phi_i(\mathbf{x}_1)\Phi_j(\mathbf{x}_2) - \Phi_i(\mathbf{x}_2)\Phi_j(\mathbf{x}_1)\right] c_{ij}. \end{aligned} \tag{2.53}$$

We then have to solve for the functions $F_i(\mathbf{x})$ and for the coefficients c_{ij}, subject to the orthogonality conditions (2.52). This method has the advantage of being easy to generalize to the case of electron collisions with atoms and ions containing many electrons and has been adopted in many recent theoretical developments, which we discuss in Sect. 2.3.2 and in Chap. 5.

Returning to (2.45), we now substitute this expansion into the Schrödinger equation (2.2) and project onto the target eigenstates Φ_i to yield the following set of coupled second-order integrodifferential equations, satisfied by the functions $F_i(\mathbf{x})$

$$(\nabla^2 + k_i^2) F_i(\mathbf{x}) = 2 \sum_j \left[V_{ij}(\mathbf{x}) F_j(\mathbf{x}) + \int K_{ij}(\mathbf{x}, \mathbf{x}') F_j(\mathbf{x}') \mathrm{d}\mathbf{x}' \right]. \tag{2.54}$$

In this equation the potential matrix elements $V_{ij}(\mathbf{x})$ coupling the target states are the same as in (2.43) and the new exchange kernel $K_{ij}(\mathbf{x}, \mathbf{x}')$ arises from the operator P_{iN+1} in (2.46) and gives rise to electron exchange in the collision. The solution of (2.54) now yields both the direct and exchange scattering amplitudes for transitions between the target states Φ_i retained in the original expansion (2.45).

However, we observe that an exact solution of these coupled equations will not yield an exact solution of the original Schrödinger equation (2.2) because of the truncation of expansion (2.45) to a finite number of bound target eigenstates. In many cases of interest, involving transitions between strongly coupled low-energy eigenstates, the resultant solution will be accurate. However, the omission from the expansion of an infinite number of bound target eigenstates lying close to the ionization threshold, as well as all the continuum target eigenstates can lead to substantial errors for some transitions, particularly for incident-electron energies close to and above the ionization threshold, often referred to as "intermediate energies". In addition, since the continuum eigenstates are omitted from expansion (2.45), the possibility of determining ionization resulting from the excitation of these continuum eigenstates is not included in the calculation.

We now consider a straightforward extension of the close coupling expansion (2.45) which has enabled accurate ionization cross sections as well as excitation cross sections to be determined at intermediate energies. We observed in Sect. 2.2.2 that an effective way of representing the long-range polarization potential, where a substantial contribution to this potential comes from intermediate target eigenstates lying in the continuum, is to introduce a quadratically integrable polarized pseudostate which has a substantial overlap with the continuum. This pseudostate replaces the usual integral expression for the dipole polarizability, given by (2.20), by a single pole term, given by (2.33). In an analogous way, including a finite number of discrete quadratically integrable target pseudostates in the expansion has been found to be an effective way of representing the continuum in electron collisions. In this approach the eigenstate close coupling expansion (2.45) is replaced by the following "close coupling with pseudostates" expansion suggested by Burke and Schey [160]

$$\Psi(\mathbf{X}_{N+1}) = \mathcal{A}\sum_i \Phi_i(\mathbf{X}_N)F_i(\mathbf{x}_{N+1}) + \mathcal{A}\sum_i \Phi_i^p(\mathbf{X}_N)G_i(\mathbf{x}_{N+1}). \tag{2.55}$$

The first summation in this equation goes over a finite number of bound target eigenstates $\Phi_i(\mathbf{X}_N)$, as in (2.45), and the second summation goes over a finite number of suitably chosen quadratically integrable target pseudostates $\Phi_i^p(\mathbf{X}_N)$ representing the highly excited and continuum target eigenstates. The functions $F_i(\mathbf{x})$ and $G_i(\mathbf{x})$ represent the corresponding motion of the scattered electron. The pseudostates are chosen to be orthogonal to the bound target eigenstates retained in the first expansion in (2.55) and to diagonalize the target Hamiltonian H_N as follows:

$$\langle \Phi_i^p | H_N | \Phi_j^p \rangle = e_i^p \delta_{ij}, \tag{2.56}$$

where the pseudostate energies e_i^p partially span the energy range, including the continuum, which is omitted from the first expansion. Substituting expansion (2.55) into the Schrödinger equation (2.2) and projecting onto the target eigenstates $\Phi_i(\mathbf{X}_N)$ and onto the target pseudostates $\Phi_i^p(\mathbf{X}_N)$ then yields a set of coupled second-order integrodifferential equations satisfied by the functions $F_i(\mathbf{x})$ and $G_i(\mathbf{x})$ which have the same form as (2.54).

We will consider in detail the choice and role of pseudostates in the close coupling expansion when we discuss electron collisions at low and intermediate energies in Chaps. 5 and 6, respectively. We will see in these chapters that approaches based on the close coupling with pseudostates expansion, including the R-Matrix with PseudoStates (RMPS) method, introduced by Bartschat et al. [70, 71] and discussed in Sect. 6.2, and the convergent close coupling (CCC) method, introduced by Bray and Stelbovics [126–128] and reviewed in Sect. 6.1, yield accurate cross sections over a wide range of electron collision energies.

2.3.2 Derivation of the Close Coupling Equations

We now turn our attention to determine the explicit form of the close coupling equations which must be solved in practical calculations. We first observe that in order to minimize the computational effort we must use the symmetry of the Hamiltonian to separate these equations into uncoupled blocks, corresponding to the conserved quantum numbers, which can be solved independently. In addition, in order to make the solution of these coupled equations tractable for electron collisions with multi-electron atoms and ions, a partial wave analysis must also be carried out. In this way we obtain sets of coupled second-order integrodifferential equations which are satisfied by the wave functions representing the radial motion of the scattered electron. We will then examine the detailed form of these close coupling equations including the local direct and the non-local exchange and correlation potentials that arise. In this way we provide the basis of the R-matrix theory approach for solving these equations which we will discuss in Chap. 5.

Following Burke [159] the required close coupling with pseudostates expansion, which replaces (2.55), has the following form for each set of conserved quantum numbers represented by Γ

$$\begin{aligned}\Psi_{jE}^{\Gamma}(\mathbf{X}_{N+1}) &= \mathcal{A}\sum_{i=1}^{n}\overline{\Phi}_i^{\Gamma}(\mathbf{X}_N;\hat{\mathbf{r}}_{N+1}\sigma_{N+1})r_{N+1}^{-1}F_{ij}^{\Gamma}(r_{N+1}) \\ &\quad+\sum_{i=1}^{m}\chi_i^{\Gamma}(\mathbf{X}_{N+1})c_{ij}^{\Gamma},\end{aligned} \tag{2.57}$$

where j labels the linearly independent solutions of the Schrödinger equation (2.2), which we will discuss in detail in Sect. 2.4 when we consider the asymptotic boundary conditions satisfied by the functions $F_{ij}^{\Gamma}(r_{N+1})$. The conserved quantum numbers represented by Γ in (2.57) correspond to the eigenvalues of the complete set of

operators which commute with the Hamiltonian. In the case of the non-relativistic Hamiltonian defined by (2.3) these conserved quantum numbers are given by

$$\Gamma \equiv \alpha \; L \; S \; M_L \; M_S \; \pi, \tag{2.58}$$

where L and S are the total orbital and spin angular momentum quantum numbers, M_L and M_S are the corresponding magnetic quantum numbers in some preferred direction z, π is the total parity quantum number and α represents any further quantum numbers which are conserved in the collision. Also, the channel functions $\overline{\Phi}_i^{\Gamma}(\mathbf{X}_N; \hat{\mathbf{r}}_{N+1}\sigma_{N+1})$ in (2.57) are obtained by coupling the target eigenstates and pseudostates retained in the expansion with the spin–angle functions of the scattered electron to form eigenfunctions of the square of the total orbital and spin angular momentum operators $\mathbf{L^2}$ and $\mathbf{S^2}$ and their z-components as well as the parity operator π. Hence the channel functions can be written as follows:

$$\begin{aligned}\overline{\Phi}_i^{\Gamma}(\mathbf{X}_N; \hat{\mathbf{r}}_{N+1}\sigma_{N+1}) \; = \; & \sum_{M_{L_i} m_{\ell_i}} \sum_{M_{S_i} m_i} (L_i M_{L_i} \ell_i m_{\ell_i} | L M_L) \\ & \times (S_i M_{S_i} \tfrac{1}{2} m_i | S M_S) \Phi_i(\mathbf{X}_N) \\ & \times Y_{\ell_i m_{\ell_i}}(\theta_{N+1}, \phi_{N+1}) \chi_{\frac{1}{2} m_i}(\sigma_{N+1}),\end{aligned} \tag{2.59}$$

where $\Phi_i(\mathbf{X}_N)$ are the antisymmetric target eigenstates and pseudostates, discussed above, $Y_{\ell_i m_{\ell_i}}(\theta_{N+1}, \phi_{N+1})$ are spherical harmonics, defined in Appendix B.3, which describe the angular motion of the scattered electron, $\chi_{\frac{1}{2} m_i}(\sigma_{N+1})$ are electron spin functions which describe the spin motion of the scattered electron and $(abcd|ef)$ are Clebsch–Gordan coefficients defined in Appendix A.1. Returning to (2.57), the reduced radial functions $F_{ij}^{\Gamma}(r_{N+1})$ describe the radial motion of the scattered electron in the ith channel and the $\chi_i^{\Gamma}(\mathbf{X}_{N+1})$ are quadratically integrable functions which vanish at large distances from the nucleus. These quadratically integrable functions are usually constructed from the same set of physical and pseudo-orbitals used to construct the target eigenstates and pseudostates $\Phi_i(\mathbf{X}_N)$ and are antisymmetric with respect to interchange of the space and spin coordinates of any pair of the $N + 1$ electrons. We discuss the reasons for the inclusion of these quadratically integrable functions in the expansion of the wave function below. Finally, the antisymmetrization operator $\mathcal{A}$ defined by (2.46) ensures that the total wave function is explicitly antisymmetric with respect to interchange of the space and spin coordinates of any pair of the $N + 1$ electrons, in accordance with the Pauli exclusion principle.

We observe that in order to obtain accurate scattering amplitudes we must include in the first expansion on the right-hand side of (2.57) all the target states of physical interest. By this we mean that we must include both the initial and final target eigenstates corresponding to the scattering amplitude of interest, as well as all other target eigenstates that are expected to play an important role as intermediate states in the transitions of interest. In particular, if one term of a target configuration

is included in this expansion then all other terms corresponding to this configuration are normally strongly coupled to this configuration and should also be included. For example, if we are considering electron collisions with atomic oxygen in its $1s^2 2s^2 2p^4\ {}^3P^e$ ground state, then the other $1s^2 2s^2 2p^4\ {}^1D^e$ and $1s^2 2s^2 2p^4\ {}^1S^e$ terms corresponding to this ground state configuration will be strongly coupled and must also be included to obtain accurate results. We may also need to include pseudostates in this expansion, either to accurately represent polarization effects at low energies, as discussed in Sect. 2.2.2, or to represent the highly excited and continuum states of the target in order to obtain accurate excitation and ionization cross sections at intermediate energies, as discussed later in this section and in Chap. 6.

The second expansion on the right-hand side of (2.57), over the quadratically integrable functions $\chi_i^{\Gamma}(\mathbf{X}_{N+1})$, is included for two reasons. First, as discussed in Sect. 2.3.1, the reduced radial functions $F_{ij}^{\Gamma}(r)$ are in many calculations constrained to be orthogonal to the physical orbitals and pseudo-orbitals with the same angular symmetry which are used in the construction of the target states $\Phi_i(\mathbf{X}_N)$. For example, in electron collisions with atomic oxygen the p-wave reduced radial function is constrained to be orthogonal to the 2p orbital in the target. However, this constraint means that the $1s^2 2s^2 2p^5\ {}^2P^o$ configuration, which plays an important role as an intermediate state in ${}^2P^o$ electron collisions with the $1s^2 2s^2 2p^4\ {}^3P^e$, ${}^1D^e$ and ${}^1S^e$ target states, is not represented in the first expansion. This configuration must therefore be included in the second expansion for completeness, to ensure that the ${}^2P^o$ collision wave function represents this possibility. This example also re-emphasizes the importance of including all three target state terms belonging to the $1s^2 2s^2 2p^4$ configuration in the first expansion in (2.57), since they are strongly coupled through the $1s^2 2s^2 2p^5\ {}^2P^o$ intermediate quadratically integrable function and their omission would lead to inconsistencies, including the appearance of low-energy pseudoresonances in the cross sections, as pointed out by Gorczyca et al. [398].

The second reason for including quadratically integrable functions in the second expansion in (2.57) is to represent short-range electron–electron correlation effects, which may be difficult to represent accurately by including a finite expansion over target states and pseudostates in the first expansion in (2.57). In the case of one-electron targets, such as H and He^+, highly accurate electron collision phase shifts and cross sections have been obtained at low energies by Schwartz [838, 839], Burke and Taylor [162] and Armstead [24], by taking the terms in the second expansion to be Hylleraas-type functions. In the case of multi-electron targets these correlation effects are usually included by the introduction of additional contracted pseudo-orbitals with approximately the same range as the Hartree–Fock orbitals used to construct the target wave functions, but with more nodes. Additional $(N+1)$-electron quadratically integrable functions, constructed from the physical orbitals and the pseudo-orbitals, must then be included in the second expansion in (2.57) for consistency. Finally, we note that the inclusion of quadratically integrable functions in the second expansion in (2.57), to represent short-range electron–electron correlation effects, gives rise to unphysical pseudoresonances at intermediate energies. We discuss the role of these pseudoresonances later in this section and in Chap. 6.

We now derive coupled second-order integrodifferential equations satisfied by the reduced radial functions $F_{ij}^{\Gamma}(r_{N+1})$ in (2.57). These equations are obtained by substituting the representation for $\Psi_{jE}^{\Gamma}(\mathbf{X}_{N+1})$ given by (2.57) into the Schrödinger equation (2.2) and projecting onto the channel functions $\overline{\Phi}_i^{\Gamma}$, defined by (2.59) and onto the quadratically integrable functions $\chi_i^{\Gamma}(\mathbf{X}_{N+1})$. In this way we obtain the following set of $n + m$ coupled equations

$$\langle r_{N+1}^{-1}\overline{\Phi}_i^{\Gamma}(\mathbf{X}_N;\hat{\mathbf{r}}_{N+1}\sigma_{N+1})|(H_{N+1}-E)|\Psi_{jE}^{\Gamma}(\mathbf{X}_{N+1})\rangle' = 0, \quad i = 1,\ldots,n, \tag{2.60}$$

and

$$\langle \chi_i^{\Gamma}(\mathbf{X}_{N+1})|(H_{N+1}-E)|\Psi_{jE}^{\Gamma}(\mathbf{X}_{N+1})\rangle = 0, \quad i = 1,\ldots,m, \tag{2.61}$$

subject to the orthogonality constraints

$$\langle F_{ij}^{\Gamma}(r)|P_{n_s\ell_i}(r)\rangle = 0, \quad \text{all } n_s. \tag{2.62}$$

The prime on the Dirac bracket in (2.60) and later equations means that the integration is carried out over the space and spin coordinates of all $N + 1$ electrons except the radial coordinate r_{N+1} of the scattered electron. In (2.61) the integration is carried out over the space and spin coordinates of all $N + 1$ electrons. Finally, the orthogonality constraints (2.62) are required to ensure that the reduced radial functions $F_{ij}^{\Gamma}(r)$ are orthogonal to all the physical and pseudo-orbitals $P_{n_s\ell_i}(r)$ of the same angular symmetry ℓ_i, which are used to construct the target states retained in expansion (2.57), as discussed above.

We now eliminate the expansion coefficients c_{ij}^{Γ} in (2.57) between (2.60) and (2.61), by substituting the expression for these coefficients obtained from (2.61) into (2.60). After writing the Hamiltonian H_{N+1} in terms of H_N using (2.4), we find that the reduced radial functions $F_{ij}^{\Gamma}(r)$ satisfy the following set of n coupled second-order integrodifferential equations which are called the "close coupling equations" or "coupled ID equations"

$$\begin{aligned}
&\left(\frac{\mathrm{d}^2}{\mathrm{d}r^2} - \frac{\ell_i(\ell_i+1)}{r^2} + \frac{2(Z-N)}{r} + k_i^2\right) F_{ij}^{\Gamma}(r) \\
&= 2\sum_{i'=1}^{n}\left\{V_{ii'}^{\Gamma}(r)F_{i'j}^{\Gamma}(r) + \int_0^{\infty}\left[W_{ii'}^{\Gamma}(r,r') + X_{ii'}^{\Gamma}(r,r')\right]F_{i'j}^{\Gamma}(r')\mathrm{d}r'\right\} \\
&\quad + \sum_{n_s}\lambda_{in_sj}P_{n_s\ell_i}(r), \quad i = 1,\ldots,n.
\end{aligned} \tag{2.63}$$

In (2.63) ℓ_i is the orbital angular momentum of the scattered electron, k_i^2 is the wave number squared of the scattered electron, $V_{ii'}^{\Gamma}(r)$, $W_{ii'}^{\Gamma}(r,r')$ and $X_{ii'}^{\Gamma}(r,r')$ are the local direct, non-local exchange and non-local correlation potentials, respectively,

$\lambda_{in_s j}$ are Lagrange multipliers which are chosen so that the orthogonality constraints defined by (2.62) are satisfied and j labels the linearly independent solutions of these equations.

After writing H_{N+1} in terms of H_N using (2.4), we find that the channel wave numbers squared k_i^2 in (2.63) are given by

$$k_i^2 = 2\left(E - \overline{e}_i^{\Gamma}\right), \quad i = 1, \ldots, n, \tag{2.64}$$

where the channel energies $\overline{e}_i^{\Gamma}$ are defined by

$$\overline{e}_i^{\Gamma} = \langle r_{N+1}^{-1} \overline{\Phi}_i^{\Gamma}(\mathbf{X}_N; \hat{\mathbf{r}}_{N+1}\sigma_{N+1}) | H_N | r_{N+1}^{-1} \overline{\Phi}_i^{\Gamma}(\mathbf{X}_N; \hat{\mathbf{r}}_{N+1}\sigma_{N+1}) \rangle, \quad i = 1, \ldots, n, \tag{2.65}$$

where the channel functions $\overline{\Phi}_i^{\Gamma}$ are defined by (2.59). The local direct potential $V_{ii'}^{\Gamma}(r)$ in (2.63), which arises from the direct terms in the first expansion in (2.57), has the explicit form

$$V_{ii'}^{\Gamma}(r_{N+1}) = \langle r_{N+1}^{-1} \overline{\Phi}_i^{\Gamma}(\mathbf{X}_N; \hat{\mathbf{r}}_{N+1}\sigma_{N+1}) \left| \sum_{k=1}^{N} \frac{1}{r_{kN+1}} - \frac{N}{r_{N+1}} \right| \times r_{N+1}^{-1} \overline{\Phi}_{i'}^{\Gamma}(\mathbf{X}_N; \hat{\mathbf{r}}_{N+1}\sigma_{N+1}) \rangle', \quad i,\ i' = 1, \ldots, n, \tag{2.66}$$

where the term $-N/r_{N+1}$ is included in this definition so that the long-range Coulomb potential in electron collisions with atomic ions is included on the left-hand side of (2.63). The non-local exchange potential $W_{ii'}^{\Gamma}(r, r')$ in (2.63), which arises from the exchange terms in the first expansion in (2.57) has the explicit form:

$$W_{ii'}^{\Gamma}(r_{N+1}, r_N) = -N \langle r_{N+1}^{-1} \overline{\Phi}_i^{\Gamma}(\mathbf{x}_1, \ldots, \mathbf{x}_N; \hat{\mathbf{r}}_{N+1}\sigma_{N+1}) \left| \frac{1}{r_{N\,N+1}} \right| \times r_{N+1}^{-1} \overline{\Phi}_{i'}^{\Gamma}(\mathbf{x}_1, \ldots, \mathbf{x}_{N-1}, \mathbf{x}_{N+1}; \hat{\mathbf{r}}_N\sigma_N) \rangle'', \quad i,\ i' = 1, \ldots, n, \tag{2.67}$$

where the double prime on the Dirac bracket means that the integration is carried out over the space and spin coordinates of all $N + 1$ electrons except the radial coordinates r_{N+1} and r_N of the incident and scattered electrons. Finally, the non-local correlation potential $X_{ii'}^{\Gamma}(r, r')$ in (2.63) arises from the quadratically integrable functions $\chi_i^{\Gamma}(\mathbf{X}_{N+1})$ in expansion (2.57). We can choose these functions without approximation to diagonalize H_{N+1} as follows:

$$\langle \chi_k^{\Gamma}(\mathbf{X}_{N+1}) | H_{N+1} | \chi_{k'}^{\Gamma}(\mathbf{X}_{N+1}) \rangle = \mathcal{E}_k \delta_{kk'}, \quad k,\ k' = 1, \ldots, m. \tag{2.68}$$

We then define the radial functions

$$U_{ik}^{\Gamma}(r_{N+1}) = \langle r_{N+1}^{-1} \overline{\Phi}_i^{\Gamma}(\mathbf{X}_N; \hat{\mathbf{r}}_{N+1}\sigma_{N+1}) \,|(H_{N+1} - E)|\, \chi_k^{\Gamma}(\mathbf{X}_{N+1})\rangle', \quad i = 1, \ldots, n, \quad k = 1, \ldots, m. \tag{2.69}$$

The elimination of expansion coefficients c_{ij}^{Γ} in (2.57) between (2.60) and (2.61) then yields the following expression for the correlation potential:

$$X_{ii'}^{\Gamma}(r_{N+1}, r_N) = -\sum_{k=1}^{m} U_{ik}^{\Gamma}(r_{N+1}) \frac{1}{\mathcal{E}_k - E} U_{i'k}^{\Gamma}(r_N), \quad i,\ i' = 1, \ldots, n. \tag{2.70}$$

Explicit forms for the potentials $V_{ii'}^{\Gamma}(r)$, $W_{ii'}^{\Gamma}(r, r')$ and $X_{ii'}^{\Gamma}(r, r')$ have been given in a few simple cases, for example, for e^- – H collisions by Percival and Seaton [726] and for electron collisions with atoms or ions with open $2p^q$ and $3p^q$ shells by Henry et al. [455]. However, it is not feasible or necessary to write down the explicit form of these potentials for electron collisions with general atoms and atomic ions. Instead, they are constructed as part of R-matrix computer programs for solving the close coupling equations (2.63) that we refer to in Sect. 5.1.1. Numerical methods for solving (2.63) have been discussed by Burke and Seaton [164] and the R-matrix approach for their solution will be presented in Chap. 5.

Nevertheless, certain general statements can be made about the form of potentials $V_{ii'}^{\Gamma}(r)$, $W_{ii'}^{\Gamma}(r, r')$ and $X_{ii'}^{\Gamma}(r, r')$ which are important in understanding the physical properties of the solution of the close coupling equations (2.63). First, we observe that the phases of the angular integrals in (2.66), (2.67) and (2.69) can be chosen so that these potentials are real. Also, it follows from these equations that the potentials satisfy the following symmetry relations:

$$V_{ii'}^{\Gamma}(r) = V_{i'i}^{\Gamma}(r), \quad W_{ii'}^{\Gamma}(r, r') = W_{i'i}^{\Gamma}(r', r), \quad X_{ii'}^{\Gamma}(r, r') = X_{i'i}^{\Gamma}(r', r), \quad i,\ i' = 1, \ldots, n. \tag{2.71}$$

These reality and symmetry conditions follow from the time-reversal invariance and hermiticity of the Hamiltonian which we will see in Sects. 2.4 and 2.5 lead to the reality and symmetry of the K-matrix and to the unitarity and symmetry of the S-matrix.

We also mention here some further properties of the potentials $V_{ii'}^{\Gamma}(r)$, $W_{ii'}^{\Gamma}(r, r')$ and $X_{ii'}^{\Gamma}(r, r')$. We will see when we discuss Feshbach projection operator theory of resonances in Sect. 3.2.5 that we can divide Hilbert space spanned by the eigensolutions of the Schrödinger equation into two mutually orthogonal spaces by two projection operators P and Q, where the "optical potential" corresponding to scattering in Q-space is represented by the sum of pole terms in the expression defined by (3.108). We can relate Feshbach theory directly to the close coupling with pseudostates expansion (2.57), where P-space corresponds to the space spanned by those target states in this expansion which give rise to channels which are open at the energy under consideration, while Q-space corresponds to the remaining target

states and pseudostates in this expansion, together with the quadratically integrable functions representing short-range electron–electron correlation effects included in the second expansion in (2.57). It is important to emphasize that the quadratically integrable functions included to remove the orthogonality constraints imposed on the radial functions $F_{ij}^{\Gamma}(r_{N+1})$ in (2.57) must be regarded as part of P-space and must therefore be carefully chosen for this purpose, as discussed by Gorczyca et al. [398]. As a result of this choice of P- and Q-spaces, we will show in our discussion of Feshbach projection operator theory that the poles in the optical potential give rise to resonances. Also, since the resonances arise from pseudostates and quadratically integrable functions representing the effect of physical states not explicitly included in the first expansion, they are unphysical pseudoresonances and the corresponding T-matrix must be averaged over energy to obtain physically meaningful results at intermediate energies. We will consider this averaging procedure in the context of intermediate energy collisions in Chap. 6.

We consider next the asymptotic form of the direct potential $V_{ii'}^{\Gamma}(r)$ defined by (2.66). This potential can be simplified at large distances using (B.49) which can be written as

$$\frac{1}{r_{kN+1}} = \sum_{\lambda=0}^{\infty} \frac{r_<^{\lambda}}{r_>^{\lambda+1}} P_{\lambda}(\cos\theta_{kN+1}), \tag{2.72}$$

where θ_{kN+1} is the angle between the unit vectors $\hat{\mathbf{r}}_{\mathbf{k}}$ and $\hat{\mathbf{r}}_{\mathbf{N+1}}$, $P_{\lambda}(x)$ is a Legendre polynomial and $r_<$ and $r_>$ are the smaller and larger of the two scalar distances r_k and r_{N+1}. We now observe that the integral over r_k, $k = 1, \ldots, N$ in (2.66) involves the target states and pseudostates $\Phi_i(\mathbf{X}_N)$ and $\Phi_{i'}(\mathbf{X}_N)$, retained in the original expansion (2.57) which vanish exponentially at large r_k. Hence we can choose a value of the radial distance, say a_0, beyond which all the target states and pseudostates are effectively zero. The corresponding contributions to the integrals over $r_k > a_0$, $k = 1, \ldots, N$ in (2.66) are then zero. It follows that when the scattered electron coordinate $r_{N+1} \geq a_0$, then $r_<^{\lambda}/r_>^{\lambda+1}$ in (2.72) can be replaced by $r_k^{\lambda}/r_{N+1}^{\lambda+1}$. Hence (2.66) can be rewritten as

$$V_{ii'}^{\Gamma}(r) = \sum_{\lambda=1}^{\lambda_{\max}} \alpha_{ii'\lambda}^{\Gamma} r^{-\lambda-1}, \quad r \geq a_0, \quad i,\ i' = 1, \ldots, n, \tag{2.73}$$

where the long-range potential coefficients $\alpha_{ii'\lambda}^{\Gamma}$ are defined by

$$\begin{aligned}\alpha_{ii'\lambda}^{\Gamma} = \langle r_{N+1}^{-1} \overline{\Phi}_i^{\Gamma}(\mathbf{X}_N; \hat{\mathbf{r}}_{N+1}\sigma_{N+1}) | \sum_{k=1}^{N} r_k^{\lambda} P_{\lambda}(\cos\theta_{kN+1}) | \\ \times r_{N+1}^{-1} \overline{\Phi}_{i'}^{\Gamma}(\mathbf{X}_N; \hat{\mathbf{r}}_{N+1}\sigma_{N+1}) \rangle', \quad i,\ i' = 1, \ldots, n, \\ \lambda = 1, \ldots, \lambda_{\max}.\end{aligned} \tag{2.74}$$

We derive an explicit expression for these coefficients in Appendix D.1; see (D.12) and (D.21).

The leading term in the expansion of the potential matrix $V^{\Gamma}_{ii'}(r)$ in inverse powers of r behaves as r^{-2} since we remember that we have included the Coulomb potential $(Z-N)/r$ between the scattered electron and the target on the left-hand side of (2.63). The upper limit $\lambda_{\max}$ in the summation over λ in (2.73) results from the triangular relations satisfied by the angular momentum quantum numbers which arise in the integral in (2.74). We will see in Chaps. 3 and 5 that the long-range potentials given by (2.73) play a crucial role in many low-energy electron–atom collision cross sections. In particular, the leading dipole potential terms behaving as r^{-2}, which from (2.74) can be seen to couple target states between which optically allowed transitions occur, give rise in second order to the long-range polarization potential defined by (2.19) and (2.20). Also, we will see in Sect. 3.3.2 that the long-range dipole potential which couples degenerate or almost degenerate target states of neutral atoms gives rise to resonances which lie below the thresholds for exciting these degenerate states. It follows that these long-range potentials must be accurately represented in any computational approach which is adopted in the low-energy electron collision region.

Finally we consider the asymptotic forms of the non-local exchange and correlation potentials $W^{\Gamma}_{ii'}(r,r')$ and $X^{\Gamma}_{ii'}(r,r')$ in (2.63). We see from the definition of $W^{\Gamma}_{ii'}(r,r')$, given by (2.67), that its behaviour as $r \to \infty$ and $r' \to \infty$ is determined by the asymptotic behaviour of the channel functions $\overline{\Phi}^{\Gamma}_{i}(\mathbf{x}_1,\ldots,\mathbf{x}_N;\hat{\mathbf{r}}_{N+1}\sigma_{N+1})$ and $\overline{\Phi}^{\Gamma}_{i'}(\mathbf{x}_1,\ldots,\mathbf{x}_{N-1},\mathbf{x}_{N+1};\hat{\mathbf{r}}_N\sigma_N)$, respectively. It then follows from (2.59), defining these functions in terms of the target states and pseudostates, that the first channel function vanishes exponentially as $r_N \to \infty$ and the second as $r_{N+1} \to \infty$. Hence $W^{\Gamma}_{ii'}(r,r')$ vanishes exponentially as $r \to \infty$ or as $r' \to \infty$. In a similar way we can see from the definition of $X^{\Gamma}_{ii'}(r_{N+1},r_N)$, given by (2.70), that its behaviour as $r_N \to \infty$ and $r_{N+1} \to \infty$ is determined by the asymptotic behaviour of the radial functions $U^{\Gamma}_{i'k}(r_N)$ and $U^{\Gamma}_{ik}(r_{N+1})$, respectively. It then follows from (2.69), defining these radial functions, that the first radial function vanishes exponentially as $r_N \to \infty$ and the second as $r_{N+1} \to \infty$. Hence $X^{\Gamma}_{ii'}(r,r')$ vanishes exponentially as $r \to \infty$ or as $r' \to \infty$. We then find that the radius a_0 where $V^{\Gamma}_{ii'}(r)$ achieves its asymptotic form given by (2.73) can also be chosen so that

$$W^{\Gamma}_{ii'}(r,r') \simeq 0, \quad X^{\Gamma}_{ii'}(r,r') \simeq 0, \quad r \geq a_0 \ \text{ or } \ r' \geq a_0. \tag{2.75}$$

The close coupling equations (2.63) then reduce to coupled second-order differential equations given by

$$\left(\frac{\mathrm{d}^2}{\mathrm{d}r^2} - \frac{\ell_i(\ell_i+1)}{r^2} + \frac{2(Z-N)}{r} + k_i^2\right) F^{\Gamma}_{ij}(r)$$
$$= 2\sum_{i'=1}^{n}\sum_{\lambda=1}^{\lambda_{\max}} \alpha^{\Gamma}_{ii'\lambda} r^{-\lambda-1} F^{\Gamma}_{i'j}(r), \quad r \geq a_0, \quad i = 1,\ldots,n, \tag{2.76}$$

which can be solved in a straightforward way in the region $r \geq a_0$ to yield the K-matrix, S-matrix and cross sections as discussed in Sects. 2.4 and 2.5. This result is of crucial importance in the development of the R-matrix approach for solving the coupled integrodifferential equations (2.63) which we discuss in Chap. 5.

We conclude this section by considering, as an example, the number of coupled channels and quadratically integrable functions which arise in the close coupling expansion (2.57) for electron collisions with Be-like ions. We consider the example where the six target eigenstates given by (2.16) are retained in the close coupling expansion (2.57), where these target eigenstates are represented by (2.18) in terms of three physical orbitals and three pseudo-orbitals 1s, 2s, 2p, $\overline{3s}$, $\overline{3p}$ and $\overline{3d}$.

We give in Table 2.2 the orbital angular momenta ℓ_i of the scattered electron which are coupled to each of these six target states for total spin $S = 1/2$ and for each L and π combination with $L \leq 4$. We also give the total number of channels which are coupled to these target states for each L and π combination. We see that the number of coupled channels for $L \geq 2$ equals 10 when $\pi = (-1)^L$ and equals 6 when $\pi = (-1)^{L+1}$. We also note that if the total spin $S = 3/2$, then only the two triplet target states $1s^2 2s2p\ ^3P^o$ and $1s^2 2p^2\ ^3P^e$ are coupled where the orbital angular momenta l_i of the coupled channels are given by the corresponding rows in Table 2.2.

We next consider the quadratically integrable functions which must be included in expansion (2.57) for electron collisions with Be-like ions. We give in Table 2.3 the number of quadratically integrable functions included for total spin $S = 1/2$ and for each L and π combination with $L \leq 4$, where we assume that the 1s orbital remains doubly occupied and a maximum of one electron is excited to one of the

Table 2.2 Orbital angular momenta ℓ_i of the scattered electron coupled to each of the target eigenstates defined by (2.16) for electron collisions with Be-like ions for $S = 1/2$ and for each L and π combination with $L \leq 4$. Also given in this table are the corresponding total number of coupled channels

L	0	1	2	3	4	0	1	2	3	4
π	$(-1)^L$					$(-1)^{L+1}$				
$1s^2 2s^2\ ^1S^e$	0	1	2	3	4	–	–	–	–	–
$1s^2 2s2p\ ^3P^o$	1	0,2	1,3	2,4	3,5	–	1	2	3	4
$1s^2 2s2p\ ^1P^o$	1	0,2	1,3	2,4	3,5	–	1	2	3	4
$1s^2 2p^2\ ^3P^e$	–	1	2	3	4	1	0,2	1,3	2,4	3,5
$1s^2 2p^2\ ^1D^e$	2	1,3	0,2,4	1,3,5	2,4,6	–	2	1,3	2,4	3,5
$1s^2 2p^2\ ^1S^e$	0	1	2	3	4	–	–	–	–	–
No. coupled channels	5	9	10	10	10	1	5	6	6	6

Table 2.3 Number of quadratically integrable functions corresponding to configurations that can be formed from the physical orbitals and pseudo-orbitals, given by (2.17), with a maximum of one electron in a pseudo-orbital, for electron collisions with Be-like ions for $S = 1/2$ and for each L and π combination with $L \leq 4$

L	0	1	2	3	4	0	1	2	3	4
π	$(-1)^L$					$(-1)^{L+1}$				
$1s^2 2s^2 2p$	–	1	–	–	–	–	–	–	–	–
$1s^2 2s 2p^2$	1	–	1	–	–	–	1	–	–	–
$1s^2 2p^3$	–	1	–	–	–	–	–	1	–	–
$1s^2 2s^2 \overline{3s}$	1	–	–	–	–	–	–	–	–	–
$1s^2 2s^2 \overline{3p}$	–	1	–	–	–	–	–	–	–	–
$1s^2 2s^2 \overline{3d}$	–	–	1	–	–	–	–	–	–	–
$1s^2 2s 2p \overline{3s}$	–	2	–	–	–	–	–	–	–	–
$1s^2 2s 2p \overline{3p}$	2	–	2	–	–	–	2	–	–	–
$1s^2 2s 2p \overline{3d}$	–	2	–	2	–	–	–	2	–	–
$1s^2 2p^2 \overline{3s}$	1	–	1	–	–	–	1	–	–	–
$1s^2 2p^2 \overline{3p}$	–	3	–	1	–	1	–	2	–	–
$1s^2 2p^2 \overline{3d}$	1	–	3	–	1	–	2	–	2	–
Total no. of functions	6	10	8	3	1	1	6	5	2	0

$\overline{3s}$, $\overline{3p}$ or $\overline{3d}$ pseudo-orbitals. These quadratically integrable functions are those that must be retained in expansion (2.57) to ensure that the orthogonality constraints defined by (2.62), which we assume are applied, do not lead to incompleteness in the target orbital basis. As an example of one entry in Table 2.3, we observe that the $1s^2 2p^2 \overline{3p}$ configuration gives rise to the following three quadratically integrable functions

$$1s^2 2p^2\ {}^3P^e\ \overline{3p}\ {}^2P^o, \quad 1s^2 2p^2\ {}^1D^e\ \overline{3p}\ {}^2P^o, \quad 1s^2 2p^2\ {}^1S^e\ \overline{3p}\ {}^2P^o, \tag{2.77}$$

which must be included in expansion (2.57) for $L = 1$, $S = 1/2$ and $\pi = -1$.

In our discussion of the target eigenstates in Sect. 2.2.1, we observed that in addition to zero-electron and one-electron excitation configurations we could also include two-electron excitation configurations which would improve the target eigenstates. However, in order to balance the correlation effects in the target and the collision wave functions we would also have to include two-electron excitation configurations in the collision wave function which would give rise to quadratically integrable functions with two electrons in pseudo-orbitals. While the inclusion of these additional configurations usually give improved collision results at low energies they will also give rise to unphysical pseudo-resonances at intermediate energies, close to and above the ionization threshold, which have to be energy

averaged to give reliable scattering amplitudes and cross sections. We will return to this question in Chap. 6 when we discuss electron collisions with multi-electron atoms and ions at intermediate energies.

Finally, we observe that the quadratically integrable configurations included in Table 2.3 do not contribute to L, S and π combinations with $L \geq 5$. This is an example of a general result that quadratically integrable configurations, which are defined in terms of target physical and pseudo-orbitals, only contribute to low L collisions. Hence the correlation potential $X^{\Gamma}_{ii'}(r, r')$ in (2.63) does not contribute at high L. Also, while the non-local exchange potential $W^{\Gamma}_{ii'}(r, r')$ in (2.63) is in principle non-zero for all L, its contribution to the scattering amplitude and cross section becomes negligible compared with the contribution from the local direct potential $V^{\Gamma}_{ii'}(r)$ for large L. This is because for large L the repulsive angular momentum term $-\ell_i(\ell_i + 1)/r^2$ in (2.63) ensures that the scattered electron does not appreciably penetrate the internal region, and hence it only experiences the long-range contribution from the direct potential on the right-hand side of (2.76). This result also has implications for methods of solution of the close coupling equations (2.63) for large L, where the repulsive angular momentum term causes the contribution from the direct potential to become small and hence the Born approximation for the scattering amplitude and cross section becomes applicable, as discussed in Sect. 2.4.

2.4 K-Matrix and Kohn Variational Principle

In this section we consider the asymptotic form of the solution of the close coupling equations (2.63) as $r \to \infty$. In this limit, we have seen that the local direct potential $V^{\Gamma}_{ii'}(r)$ has the asymptotic form given by (2.73) and the non-local exchange and correlation potentials $W^{\Gamma}_{ii'}(r, r')$ and $X^{\Gamma}_{ii'}(r, r')$ vanish exponentially so that (2.63) reduces to (2.76). We first generalize the expression for the K-matrix given in Sect. 1.1 for potential scattering to multichannel collisions considered in this and later chapters. We then show that the exact solution of (2.63) satisfies the Kohn variational principle [542] and we derive a Born series expansion for the K-matrix. Finally, we show that the Kohn variational principle enables a corrected K-matrix to be obtained from an approximate solution of (2.63) where this K-matrix is correct to second order in the error in the collision wave function.

We commence our discussion by ordering the target eigenstates and pseudostates retained in expansion (2.57), so that their energies e_i defined by (2.5) are in increasing order. It then follows from (2.64) and (2.65) that when the total energy E is real the square of the channel wave numbers k_i are real and satisfy

$$k_1^2 \geq k_2^2 \geq \cdots \geq k_n^2. \tag{2.78}$$

The equalities in this expression arise either because some of the target states included in expansion (2.57) are degenerate or because more than one channel function $\overline{\Phi}^{\Gamma}_i$ in expansion (2.57) corresponds to a given target state, as is the case when the target orbital angular momentum L_i in (2.59) is non-zero (see, for

example, Table 2.2). We now assume that at the total energy E of interest, the first n_a channels are open (i.e. have $k_i^2 \geq 0$) so that the corresponding reduced radial functions $F_{ij}^{\Gamma}(r)$ in (2.57) and (2.63) are oscillatory or linear as $r \to \infty$ and the last n_b channels are closed (i.e. have $k_i^2 < 0$) so that the corresponding reduced radial functions $F_{ij}^{\Gamma}(r)$ in (2.57) and (2.63) vanish as $r \to \infty$. Hence

$$n_a + n_b = n, \tag{2.79}$$

where the quantities n_a and n_b depend on the total energy E. We see that when E is greater than all the energies $\bar{e}_i^{\Gamma}$ defined by (2.65), the channels are all open so that $n_a = n$ and $n_b = 0$. On the other hand, when E is less than all the energies $\bar{e}_i^{\Gamma}$, the channels are all closed, so that $n_a = 0$ and $n_b = n$, corresponding to a bound state of the electron–atom or electron–ion system.

In order to define the asymptotic boundary conditions satisfied by the reduced radial wave functions $F_{ij}^{\Gamma}(r)$ we must consider the second index j on these functions. As we have already mentioned in Sect. 2.3.2, this second index labels the linearly independent solutions of the n close coupling equations (2.63) satisfied by the functions $F_{ij}^{\Gamma}(r)$. It follows from the general theory of linear coupled second-order differential equations that n coupled equations have in general $2n$ linearly independent solutions. However, the requirement that the total wave function must be normalizable near the origin implies that

$$F_{ij}^{\Gamma}(r) \underset{r\to 0}{\sim} n_{ij} r^{\ell_i+1}, \quad i = 1, \ldots, n, \quad \text{all } j, \tag{2.80}$$

where n_{ij} are normalization factors. Hence the reduced radial functions vanish at the origin. The n conditions (2.80) reduce the number of physical linearly independent solutions from $2n$ to n. We will see below that when some of the channels are closed, so that $n_b > 0$, the number of linearly independent solutions is further reduced to $n - n_b = n_a$. The second index j is thus required to label these n_a linearly independent solutions.

We consider first the situation where all channels are open, so that $n_a = n$. The asymptotic boundary conditions satisfied by the n linearly independent solutions of (2.63), which reduce to (2.76) asymptotically, can be written in analogy with (1.71) in potential scattering in the form

$$F_{ij}^{\Gamma}(r) \underset{r\to\infty}{\sim} k_i^{-1/2} \left[\sin\theta_i(r)\delta_{ij} + \cos\theta_i(r) K_{ij}^{\Gamma} \right], \quad i,\ j = 1, \ldots, n. \tag{2.81}$$

The quantity $\theta_i(r)$ in (2.81) is defined in analogy with (1.58) and (1.59) by

$$\theta_i(r) = k_i r - \frac{1}{2}\ell_i \pi - \eta_i \ln 2k_i r + \sigma_{\ell_i}, \quad i = 1, \ldots, n, \tag{2.82}$$

where

$$\eta_i = -\frac{Z - N}{k_i}, \quad i = 1, \ldots, n \tag{2.83}$$

and

$$\sigma_{\ell_i} = \arg \Gamma(\ell_i + 1 + \mathrm{i}\eta_i), \quad i = 1, \ldots, n, \tag{2.84}$$

for electron collisions with atoms or ions with N electrons and nuclear charge number Z. The factor $k_i^{-1/2}$ in (2.81), normalizes the ingoing spherical wave to unit flux which we will see below means that the $n \times n$-dimensional K-matrix K_{ij}^{Γ}, defined by the asymptotic boundary conditions (2.81), is symmetric.

When n_b channels are closed then the corresponding terms $\sin\theta_i(r)$ and $\cos\theta_i(r)$, $i = n_a + 1, \ldots, n$ in (2.81) diverge exponentially asymptotically. This follows from (2.64) since $k_i^2 < 0$, $i = n_a+1, \ldots, n$, and hence k_i is pure imaginary. Such divergent solutions are physically inadmissible since they are not normalizable. Hence they must be eliminated by combining together the n linearly independent solutions $F_{ij}^{\Gamma}(r)$, $j = 1, \ldots, n$ in (2.81). Since there are n_b divergent terms to be eliminated we are left with $n_a = n - n_b$ linearly independent physical solutions which are finite at infinity. We choose these n_a solutions of (2.63) to satisfy the asymptotic boundary conditions

$$\begin{aligned} F_{ij}^{\Gamma}(r) &\underset{r\to\infty}{\sim} k_i^{-1/2}\left[\sin\theta_i(r)\delta_{ij} + \cos\theta_i(r)K_{ij}^{\Gamma}\right], \quad i,\ j = 1, \ldots, n_a, \\ F_{ij}^{\Gamma}(r) &\underset{r\to\infty}{\sim} 0, \quad i = n_a + 1, \ldots, n, \quad j = 1, \ldots, n_a. \end{aligned} \tag{2.85}$$

Equations (2.85) define a reduced $n_a \times n_a$-dimensional K-matrix K_{ij}^{Γ} which connects the n_a open channels.

Also, since the potentials $V_{ii'}^{\Gamma}(r)$, $W_{ii'}^{\Gamma}(r, r')$ and $X_{ii'}^{\Gamma}(r, r')$ in the close coupling equations (2.63) are real and the normalization factors n_{ij} in (2.80) can be chosen to be real, then the solutions $F_{ij}^{\Gamma}(r)$ are real. It follows that all the quantities in the asymptotic boundary conditions (2.81) or (2.85) are real and hence the K-matrix must be real. We will show below that the $n_a \times n_a$-dimensional K-matrix is also symmetric.

We now derive the multichannel Kohn variational principle for the K-matrix satisfied by the solutions of (2.63). We consider the following integral taken over the space and spin coordinates of all $N + 1$ electrons

$$I_{jj'}^{\Gamma} = \int \Psi_{jE}^{\Gamma *}(\mathbf{X}_{N+1})(H_{N+1} - E)\Psi_{j'E}^{\Gamma}(\mathbf{X}_{N+1})\mathrm{d}\mathbf{X}_{N+1}, \tag{2.86}$$

where the solutions Ψ_{jE}^{Γ} and $\Psi_{j'E}^{\Gamma}$ are defined by (2.57). We find that

$$\begin{aligned} I_{jj'}^{\Gamma} = \int_0^{\infty} \sum_{i=1}^{n}\sum_{i'=1}^{n} F_{ij}^{\Gamma}(r) \Bigg\{ &-\frac{1}{2}\left(\frac{\mathrm{d}^2}{\mathrm{d}r^2} - \frac{\ell_i(\ell_i+1)}{r^2} + \frac{2(Z-N)}{r} + k_i^2\right) \\ &\times F_{ij'}^{\Gamma}(r)\delta_{ii'} + V_{ii'}^{\Gamma}(r)F_{i'j'}^{\Gamma}(r) \\ &+ \int_0^{\infty}\left[W_{ii'}^{\Gamma}(r, r') + X_{ii'}^{\Gamma}(r, r')\right]F_{i'j'}^{\Gamma}(r')\mathrm{d}r'\Bigg\}\mathrm{d}r, \quad j,\ j' = 1, \ldots, n_a, \end{aligned} \tag{2.87}$$

where we have used the same procedure that we adopted to reduce (2.60), (2.61), (2.62) and (2.63). In (2.87) the subscripts j and j' label the linearly independent solutions, and in the following discussion we assume there are n_a open channels so that the K-matrix has dimensions $n_a \times n_a$. Also in (2.87) the local direct potential $V^{\Gamma}_{ii'}(r)$ and the non-local exchange and correlation potentials $W^{\Gamma}_{ii'}(r, r')$ and $X^{\Gamma}_{ii'}(r, r')$ are defined by (2.66), (2.67) and (2.70), respectively. In (2.87), and in the following analysis, we find it convenient not to impose the orthogonality constraints, defined by (2.62). This means that the Lagrange multiplier terms in (2.63) and the additional quadratically integrable functions, which would otherwise need to be included in expansion (2.57) for completeness, are no longer required although the K-matrix, which is defined by the asymptotic form of the wave function, will be unaltered.

It is convenient to rewrite the integral, defined by (2.87), using Dirac bracket notation as follows:

$$\mathbf{I}^{\Gamma} = \langle \mathbf{F}^{\Gamma} | \mathbf{L}^{\Gamma} | \mathbf{F}^{\Gamma} \rangle, \tag{2.88}$$

so that the close coupling equations (2.63) can be written in the following matrix form

$$\mathbf{L}^{\Gamma} \mathbf{F}^{\Gamma}(r) = 0. \tag{2.89}$$

Hence $\mathbf{I}^{\Gamma} = 0$ when $\mathbf{F}^{\Gamma}(r)$ is an exact solution of (2.89). It follows that $\mathbf{I}^{\Gamma}$ is an $n_a \times n_a$-dimensional matrix, $\mathbf{L}^{\Gamma}$ is an $n \times n$-dimensional integrodifferential matrix operator and $\mathbf{F}^{\Gamma}(r)$ is an $n \times n_a$-dimensional solution matrix satisfying the boundary conditions

$$\begin{aligned} \mathbf{F}^{\Gamma}(r) &\underset{r\to 0}{\sim} 0, \\ \mathbf{F}^{\Gamma}(r) &\underset{r\to \infty}{\sim} \mathbf{k}^{-1/2} \left[\sin \boldsymbol{\theta}(r) + \cos \boldsymbol{\theta}(r) \mathbf{K}^{\Gamma} \right], \end{aligned} \tag{2.90}$$

corresponding to (2.80) and (2.85). Also in (2.90), we have only considered the non-vanishing asymptotic components of $\mathbf{F}^{\Gamma}(r)$ so that $\mathbf{k}$, $\boldsymbol{\theta}(r)$ and $\mathbf{K}^{\Gamma}$ are $n_a \times n_a$-dimensional matrices where both $\mathbf{k}$ and $\boldsymbol{\theta}(r)$ are diagonal.

We now consider variations in $\mathbf{I}^{\Gamma}$ due to arbitrary small variations $\delta\mathbf{F}^{\Gamma}(r)$ about the exact solution of (2.89) satisfying the boundary conditions (2.90) where the variations satisfy the boundary conditions

$$\begin{aligned} \delta\mathbf{F}^{\Gamma}(r) &\underset{r\to 0}{\sim} 0, \\ \delta\mathbf{F}^{\Gamma}(r) &\underset{r\to \infty}{\sim} \mathbf{k}^{-1/2} \cos \boldsymbol{\theta}(r) \delta\mathbf{K}^{\Gamma}. \end{aligned} \tag{2.91}$$

The corresponding first-order variation in $\mathbf{I}^{\Gamma}$ is then

$$\delta\mathbf{I}^{\Gamma} = \langle \delta\mathbf{F}^{\Gamma} | \mathbf{L}^{\Gamma} | \mathbf{F}^{\Gamma} \rangle + \langle \mathbf{F}^{\Gamma} | \mathbf{L}^{\Gamma} | \delta\mathbf{F}^{\Gamma} \rangle, \tag{2.92}$$

which after using (2.89) becomes

$$\delta \mathbf{I}^{\Gamma} = \langle \mathbf{F}^{\Gamma} | \mathbf{L}^{\Gamma} | \delta \mathbf{F}^{\Gamma} \rangle \, . \tag{2.93}$$

We can evaluate the right-hand side of (2.93) by rewriting $\mathbf{L}^{\Gamma}$ in the form

$$\mathbf{L}^{\Gamma} = \mathbf{D}^{\Gamma} + \mathbf{O}^{\Gamma}, \tag{2.94}$$

where $\mathbf{D}^{\Gamma}$ is the second-order differential operator term $-\frac{1}{2}\mathbf{I}d^2/dr^2$ in $\mathbf{L}^{\Gamma}$ and $\mathbf{O}^{\Gamma}$ represents the remaining terms in $\mathbf{L}^{\Gamma}$. It follows from the reality and symmetry relations (2.71) satisfied by the potentials, that $\mathbf{O}^{\Gamma}$ is real and symmetric so that

$$\langle \mathbf{F}^{\Gamma} | \mathbf{O}^{\Gamma} | \delta \mathbf{F}^{\Gamma} \rangle = \langle \mathbf{O}^{\Gamma} \mathbf{F}^{\Gamma} | \delta \mathbf{F}^{\Gamma} \rangle \, . \tag{2.95}$$

Hence using (2.89), (2.94) and (2.95), we find that (2.93) reduces to

$$\delta \mathbf{I}^{\Gamma} = \langle \mathbf{F}^{\Gamma} | \mathbf{D}^{\Gamma} | \delta \mathbf{F}^{\Gamma} \rangle - \langle \mathbf{D}^{\Gamma} \mathbf{F}^{\Gamma} | \delta \mathbf{F}^{\Gamma} \rangle \, . \tag{2.96}$$

Integrating the terms on the right-hand side of (2.96) by parts then yields

$$\delta \mathbf{I}^{\Gamma} = -\frac{1}{2} \left\{ \left[\mathbf{F}^{\Gamma}(r) \right]^{\mathrm{T}} \frac{\mathrm{d}}{\mathrm{d}r} \delta \mathbf{F}^{\Gamma}(r) - \left[\frac{\mathrm{d}}{\mathrm{d}r} \mathbf{F}^{\Gamma}(r) \right]^{\mathrm{T}} \delta \mathbf{F}^{\Gamma}(r) \right\}_{r=0}^{r=\infty}, \tag{2.97}$$

where the superscript T means transpose. The surface terms in (2.97) can be evaluated using the boundary conditions (2.90) and (2.91) satisfied by $\mathbf{F}^{\Gamma}(r)$ and $\delta \mathbf{F}^{\Gamma}(r)$ at $r = 0$ and ∞ giving

$$\delta \mathbf{I}^{\Gamma} = \frac{1}{2} \delta \mathbf{K}^{\Gamma}. \tag{2.98}$$

Hence we obtain the Kohn variational principle for the K-matrix [542]

$$\delta \left(\mathbf{I}^{\Gamma} - \frac{1}{2} \mathbf{K}^{\Gamma} \right) = 0, \tag{2.99}$$

which is satisfied by the exact solution of (2.89). This equation is the multichannel generalization of the result obtained in potential scattering given by (1.212).

It follows from the above analysis that since the potential operator $\mathbf{O}^{\Gamma}$ in (2.94) is real and symmetric then $\mathbf{K}^{\Gamma}$ is a real symmetric $n_a \times n_a$-dimensional matrix. The K-matrix thus depends on $n_a(n_a + 1)/2$ real parameters, where n_a is the number of open channels.

We can extend this result to obtain an integral expression for the K-matrix. We consider the variation of the solution $\delta \mathbf{F}^{\Gamma}(r)$ corresponding to a variation in the operator $\delta \mathbf{L}^{\Gamma}$. Equation (2.89) then becomes

$$\left(\mathbf{L}^{\Gamma} + \delta \mathbf{L}^{\Gamma} \right) \left[\mathbf{F}^{\Gamma}(r) + \delta \mathbf{F}^{\Gamma}(r) \right] = 0. \tag{2.100}$$

After using (2.89), (2.100) formally reduces to

$$\begin{aligned}\mathbf{L}^{\Gamma}\delta\mathbf{F}^{\Gamma}(r) &= -\delta\mathbf{L}^{\Gamma}\mathbf{F}^{\Gamma}(r) - \delta\mathbf{L}^{\Gamma}\delta\mathbf{F}^{\Gamma}(r) \\ &= -\delta\mathbf{L}^{\Gamma}\mathbf{F}^{\Gamma}(r) + \delta\mathbf{L}^{\Gamma}\frac{1}{\mathbf{L}^{\Gamma}+\delta\mathbf{L}^{\Gamma}}\delta\mathbf{L}^{\Gamma}\mathbf{F}^{\Gamma}(r) \\ &= \delta\mathbf{M}^{\Gamma}\mathbf{F}^{\Gamma}(r)\ , \end{aligned} \tag{2.101}$$

where $\delta\mathbf{M}^{\Gamma}$ is obtained by expanding $\left(\mathbf{L}^{\Gamma}+\delta\mathbf{L}^{\Gamma}\right)^{-1}$ yielding

$$\delta\mathbf{M}^{\Gamma} = -\delta\mathbf{L}^{\Gamma} + \delta\mathbf{L}^{\Gamma}\frac{1}{\mathbf{L}^{\Gamma}}\delta\mathbf{L}^{\Gamma} - \delta\mathbf{L}^{\Gamma}\frac{1}{\mathbf{L}^{\Gamma}}\delta\mathbf{L}^{\Gamma}\frac{1}{\mathbf{L}^{\Gamma}}\delta\mathbf{L}^{\Gamma} + \cdots\ . \tag{2.102}$$

Hence we obtain from (2.101)

$$\langle\mathbf{F}^{\Gamma}|\mathbf{L}^{\Gamma}|\delta\mathbf{F}^{\Gamma}\rangle = \langle\mathbf{F}^{\Gamma}|\delta\mathbf{M}^{\Gamma}|\mathbf{F}^{\Gamma}\rangle\ . \tag{2.103}$$

Substituting for the left-hand side of (2.103) from (2.93) and (2.98) we then obtain

$$\delta\mathbf{K}^{\Gamma} = 2\langle\mathbf{F}^{\Gamma}|\delta\mathbf{M}^{\Gamma}|\mathbf{F}^{\Gamma}\rangle. \tag{2.104}$$

It follows from (2.102) that (2.104) is an exact integral expression relating the variation $\delta\mathbf{K}^{\Gamma}$ in the K-matrix $\mathbf{K}^{\Gamma}$ to the variation $\delta\mathbf{L}^{\Gamma}$ in the integrodifferential operator $\mathbf{L}^{\Gamma}$.

We can choose the variation $\delta\mathbf{L}^{\Gamma}$ to correspond to the sum of the direct, exchange and correlation potentials in (2.63), that is

$$\delta\mathbf{L}^{\Gamma} = \mathbf{U}^{\Gamma} \equiv \mathbf{V}^{\Gamma} + \mathbf{W}^{\Gamma} + \mathbf{X}^{\Gamma}. \tag{2.105}$$

Equation (2.100) can then be rewritten as

$$\left(\mathbf{L}_0^{\Gamma} + \mathbf{U}^{\Gamma}\right)\left[\mathbf{F}_0^{\Gamma}(r) + \delta\mathbf{F}^{\Gamma}(r)\right] = 0, \tag{2.106}$$

where $\mathbf{L}_0^{\Gamma}$ is the diagonal differential operator on the left-hand side of (2.63) corresponding to pure Coulomb scattering in the absence of the potential $\mathbf{U}^{\Gamma}$, $\mathbf{F}_0^{\Gamma}(r)$ is the corresponding diagonal Coulomb solution defined by the boundary conditions (2.90) with $\mathbf{K}^{\Gamma} = 0$ and $\delta\mathbf{F}^{\Gamma}(r)$ is the variation in the solution caused by the potential $\mathbf{U}^{\Gamma}$. It follows from (2.104) that the K-matrix corresponding to the operator $(\mathbf{L}_0^{\Gamma} + \mathbf{U}^{\Gamma})$ is

$$\mathbf{K}^{\Gamma} = 2\langle\mathbf{F}_0^{\Gamma}|\mathbf{M}^{\Gamma}|\mathbf{F}_0^{\Gamma}\rangle\ , \tag{2.107}$$

where $\mathbf{M}^{\Gamma}$ is formally defined by the expression

$$\mathbf{M}^{\Gamma} = -\mathbf{U}^{\Gamma} + \mathbf{U}^{\Gamma}\frac{1}{\mathbf{L}_0^{\Gamma}}\mathbf{U}^{\Gamma} - \mathbf{U}^{\Gamma}\frac{1}{\mathbf{L}_0^{\Gamma}}\mathbf{U}^{\Gamma}\frac{1}{\mathbf{L}_0^{\Gamma}}\mathbf{U}^{\Gamma} + \cdots . \tag{2.108}$$

Equations (2.107) and (2.108) correspond to the Born series expansion of the K-matrix. This expansion converges if the incident electron is fast or if the potential interaction $\mathbf{U}^{\Gamma}$ is sufficiently weak, which occurs, for example, when the total orbital angular momentum L becomes sufficiently large. In these cases, the first-order Born term in the expansion of $\mathbf{M}^{\Gamma}$ often yields an accurate estimate for the K-matrix. However, when these conditions do not apply, higher order terms in the Born series must be included to obtain accurate results and, even if the Born series converges, these higher order terms are difficult to evaluate for electron collisions with multi-electron atoms and ions. It is then usually preferable to solve the close coupling equations (2.89) directly to obtain the K-matrix. We will consider an accurate solution of these equations using the R-matrix method in Chap. 5. We will also consider how the Born series approach can be combined with the R-matrix method to obtain accurate results at intermediate energies in Chap. 6. Further discussion of the convergence properties of the Born series expansion has been given by Goldberger and Watson [387] and by Joachain [503].

The Kohn variational principle can also be used to improve an approximate solution of (2.89). Thus if $\mathbf{F}_{\mathrm{t}}^{\Gamma}(r)$ is an approximate trial solution of (2.89) and $\mathbf{K}_{\mathrm{t}}^{\Gamma}$ is the corresponding approximate K-matrix, then it follows from (2.99) that an improved K-matrix, correct to second order in the error in the collision wave function, is given by the Kohn-corrected K-matrix

$$\mathbf{K}_{\mathrm{Kohn}}^{\Gamma} = \mathbf{K}_{\mathrm{t}}^{\Gamma} - 2\mathbf{I}_{\mathrm{t}}^{\Gamma}, \tag{2.109}$$

where $\mathbf{I}_{\mathrm{t}}^{\Gamma}$ is calculated from (2.88) using the trial solution $\mathbf{F}_{\mathrm{t}}^{\Gamma}(r)$. We note that if an accurate solution of (2.89) is obtained, for example, by using the R-matrix method, then the correction $\mathbf{I}_{\mathrm{t}}^{\Gamma}$ to the corresponding K-matrix, given by (2.109), vanishes.

The variational principle (2.99) clearly depends on the asymptotic boundary condition, defined by (2.90), chosen for the reduced radial functions $\mathbf{F}^{\Gamma}(r)$. However, this asymptotic form is not unique and as we have already shown in Sect. 1.5 different asymptotic forms can lead to different variational principles in potential scattering. In the present multichannel collision situation an infinity of different variational principles can be constructed by taking different linear combinations of the n_a linearly independent solutions defined by (2.90). As an example, in Sect. 2.5 we will form n_a solutions satisfying S-matrix asymptotic boundary conditions. The corresponding Kohn variational principle for the S-matrix has been applied to reactive scattering and electron–molecule collisions, for example, by Miller [651] and by McCurdy and Rescigno [614] where it has been shown to have computational advantages over the Kohn variational principle for the K-matrix. However, all of these variational principles are satisfied by an accurate solution of the close coupling equations (2.89).

2.5 S-Matrix, T-Matrix and Cross Sections

In this section we define the S-matrix and T-matrix in terms of the K-matrix and hence obtain expressions for the total and differential cross sections for electron–atom collisions. In order to determine the S-matrix it is necessary to express the asymptotic solutions of the close coupling equations (2.63) in terms of ingoing and outgoing waves rather than in terms of sine and cosine waves as in (2.85). When n_a channels are open the required solutions are defined by the asymptotic boundary conditions

$$\begin{aligned} G_{ij}^{\Gamma}(r) &\underset{r\to\infty}{\sim} k_i^{-1/2}\left\{\exp[-\mathrm{i}\theta_i(r)]\delta_{ij} - \exp[\mathrm{i}\theta_i(r)]S_{ij}^{\Gamma}\right\}, \quad i,\ j = 1,\ldots,n_a, \\ G_{ij}^{\Gamma}(r) &\underset{r\to\infty}{\sim} 0, \quad i = n_a+1,\ldots,n, \quad j = 1,\ldots,n_a, \end{aligned} \tag{2.110}$$

which are linear combinations of the solutions defined by (2.85). The relationship between these solutions is given by the matrix equation

$$\mathbf{F}^{\Gamma}(r) = -\frac{1}{2\mathrm{i}}\mathbf{G}^{\Gamma}(r)\left(\mathbf{I} - \mathrm{i}\mathbf{K}^{\Gamma}\right), \tag{2.111}$$

where $\mathbf{F}^{\Gamma}(r)$ satisfies the asymptotic boundary conditions (2.85) and $\mathbf{G}^{\Gamma}(r)$ satisfies the asymptotic boundary conditions (2.110). The $n_a \times n_a$-dimensional open channel S-matrix $\mathbf{S}^{\Gamma}$, defined by (2.110), is related to the $n_a \times n_a$-dimensional K-matrix $\mathbf{K}^{\Gamma}$, defined by (2.85), by the matrix equation

$$\mathbf{S}^{\Gamma} = \frac{\mathbf{I} + \mathrm{i}\mathbf{K}^{\Gamma}}{\mathbf{I} - \mathrm{i}\mathbf{K}^{\Gamma}}. \tag{2.112}$$

Since $\mathbf{K}^{\Gamma}$ is real and symmetric it follows from (2.112) that $\mathbf{S}^{\Gamma}$ is unitary and symmetric. Hence $\mathbf{S}^{\Gamma}$ can be diagonalized by the real orthogonal transformation which also diagonalizes $\mathbf{K}^{\Gamma}$. Hence we can write

$$(\mathbf{A}^{\Gamma})^{\mathrm{T}}\,\mathbf{S}^{\Gamma}\mathbf{A}^{\Gamma} = \exp(2\mathrm{i}\boldsymbol{\Delta}), \tag{2.113}$$

where $\mathbf{A}^{\Gamma}$ is a real orthogonal matrix and $(\mathbf{A}^{\Gamma})^{\mathrm{T}}$ is the transpose of $\mathbf{A}^{\Gamma}$. The diagonal matrix $\exp(2\mathrm{i}\boldsymbol{\Delta})$ can be written explicitly as

$$\exp(2\mathrm{i}\boldsymbol{\Delta}) = \begin{bmatrix} \exp(2\mathrm{i}\delta_1) & 0 & \ldots & 0 \\ 0 & \exp(2\mathrm{i}\delta_2) & & \vdots \\ \vdots & \vdots & \ddots & \\ 0 & 0 & \ldots & \exp(2\mathrm{i}\delta_{n_a}) \end{bmatrix}, \tag{2.114}$$

where $\delta_1,\ \delta_2, \ldots, \delta_{n_a}$ are n_a real eigenphases. In the situation when only one channel is open ($n_a = 1$), δ_1 can be identified with the potential scattering phase shift

defined by (1.9) and (1.71). However, when $n_a > 1$, a further $n_a(n_a-1)/2$ real mixing parameters are necessary to completely specify the S-matrix. These parameters define the real orthogonal matrix $\mathbf{A}^{\Gamma}$ in (2.113) and are related to the independent rotations possible in n_a dimensions (i.e. to the three Euler rotation angles discussed in Appendix B.5, when $n_a = 3$). Hence the S-matrix as well as the K-matrix corresponding to n_a open channels are specified by $n_a(n_a+1)/2$ real parameters.

As an example, when $n_a = 2$, $\exp(2i\mathbf{\Delta})$ is represented by two eigenphases δ_1 and δ_2 and the corresponding orthogonal matrix $\mathbf{A}^{\Gamma}$ can be expressed in terms of an additional mixing parameter as follows:

$$\mathbf{A}^{\Gamma} = \begin{bmatrix} \cos\epsilon & \sin\epsilon \\ -\sin\epsilon & \cos\epsilon \end{bmatrix}, \tag{2.115}$$

where ϵ is called the mixing angle. The corresponding S-matrix defined by (2.113) is then given by

$$\mathbf{S}^{\Gamma} = \begin{bmatrix} \cos^2\epsilon\exp(2i\delta_1) + \sin^2\epsilon\exp(2i\delta_2) & \cos\epsilon\sin\epsilon[\exp(2i\delta_1) - \exp(2i\delta_2)] \\ \cos\epsilon\sin\epsilon[\exp(2i\delta_1) - \exp(2i\delta_2)] & \sin^2\epsilon\exp(2i\delta_1) + \cos^2\epsilon\exp(2i\delta_2) \end{bmatrix}. \tag{2.116}$$

This equation expresses the S-matrix for two open channels explicitly in terms of the three real parameters δ_1, δ_2 and ϵ.

It is also useful to define solutions of (2.63) satisfying outgoing wave T-matrix asymptotic boundary conditions as follows

$$\begin{aligned} H_{ij}^{\Gamma+}(r) &\underset{r\to\infty}{\sim} k_i^{-1/2}\left\{\sin\theta_i(r)\delta_{ij} + (2i)^{-1}\exp[i\theta_i(r)]T_{ij}^{\Gamma}\right\}, \quad i,\ j = 1,\ldots,n_a, \\ H_{ij}^{\Gamma+}(r) &\underset{r\to\infty}{\sim} 0, \quad i = n_a+1,\ldots,n,\quad j = 1,\ldots,n_a. \end{aligned} \tag{2.117}$$

These solutions can be related to those satisfying S-matrix asymptotic boundary conditions given by (2.110) by the matrix equation

$$\mathbf{H}^{\Gamma+}(r) = -(2i)^{-1}\mathbf{G}^{\Gamma}(r). \tag{2.118}$$

It follows that the $n_a \times n_a$-dimensional T-matrix is related to the $n_a \times n_a$-dimensional S-matrix by the matrix equation

$$\mathbf{T}^{\Gamma} = \mathbf{S}^{\Gamma} - \mathbf{I}. \tag{2.119}$$

We will see that the T-matrix occurs in the expressions for the cross sections given below. Finally, we can define solutions of (2.63) satisfying ingoing wave asymptotic boundary conditions by

$$\begin{aligned} H_{ij}^{\Gamma-}(r) &\underset{r\to\infty}{\sim} k_i^{-1/2}\left\{\sin\theta_i(r)\delta_{ij} - (2i)^{-1}\exp[-i\theta_i(r)]T_{ij}^{\Gamma\star}\right\}, \ i,\ j = 1,\ldots,n_a, \\ H_{ij}^{\Gamma-}(r) &\underset{r\to\infty}{\sim} 0, \quad i = n_a+1,\ldots,n,\quad j = 1,\ldots,n_a, \end{aligned} \tag{2.120}$$

where $T_{ij}^{\Gamma\star}$ is the complex conjugate of T_{ij}^{Γ}. These solutions are related to those satisfying outgoing wave boundary conditions by

$$\mathbf{H}^{\Gamma+}(r) = \mathbf{H}^{\Gamma-\star}(r) \tag{2.121}$$

and are required in the calculation of transition amplitudes, for example, the atomic photoionization amplitude discussed in Sect. 8.1.

Having obtained expressions for the multichannel S-matrix and T-matrix we can now derive formulae for the total and differential cross sections for transitions between the target states retained in expansion (2.57). We consider first electron collisions with neutral atomic targets and we then generalize our results to electron collisions with atomic ions.

Our basic problem is to relate the scattering amplitude $f_{ji}(\theta, \phi)$, defined by (2.6), to the T-matrix T_{ij}^{Γ}, defined by (2.117). In order to derive this relation we first rewrite the wave function Ψ_i in (2.6) in terms of incident and scattered wave functions as

$$\Psi_i = \Psi_i^{\text{inc}} + \Psi_i^{\text{scatt}}. \tag{2.122}$$

After introducing the space and spin coordinates of the N target electrons $\mathbf{X}_N$ and the scattered electron $\mathbf{x}_{N+1}$ we can write the asymptotic forms of these wave functions for neutral atomic targets as

$$\Psi_i^{\text{inc}} \underset{r_{N+1}\to\infty}{\sim} \Phi_i(\mathbf{X}_N)\chi_{\frac{1}{2}m_i}(\sigma_{N+1})\exp(\mathrm{i}k_i z_{N+1}) \tag{2.123}$$

and

$$\Psi_i^{\text{scatt}} \underset{r_{N+1}\to\infty}{\sim} \sum_j \Phi_j(\mathbf{X}_N)\chi_{\frac{1}{2}m_j}(\sigma_{N+1}) f_{ji}(\theta_{N+1}, \phi_{N+1}) r_{N+1}^{-1}\exp(\mathrm{i}k_j r_{N+1}). \tag{2.124}$$

The scattering amplitude $f_{ji}(\theta_{N+1}, \phi_{N+1})$ in (2.124) thus describes a transition from the target state and incident electron spin state denoted by the quantum numbers $i \equiv \alpha_i L_i S_i M_{L_i} M_{S_i} \pi_i m_i$ to the target state and scattered electron spin state denoted by the quantum numbers $j \equiv \alpha_j L_j S_j M_{L_j} M_{S_j} \pi_j m_j$, where we have used the notation of (2.14) in describing the target states.

Following the procedure which we have used for potential scattering in Sect. 1.1, we expand the plane wave term in Ψ_i^{inc} in partial waves using (1.27). We also introduce the channel functions $\overline{\Phi}_i^{\Gamma}(\mathbf{X}_N; \hat{\mathbf{r}}_{N+1}\sigma_{N+1})$ which are defined in terms of the target states $\Phi_i(\mathbf{X}_N)$ by (2.59). After inverting (2.59), using the orthogonality conditions satisfied by the Clebsch–Gordan coefficients given in Appendix A.1, we obtain

$$\begin{aligned}\Psi_i^{\text{inc}} \underset{r_{N+1}\to\infty}{\sim} \sum_{LS\pi\ell_i} & \frac{\mathrm{i}\pi^{1/2}}{k_i}(L_i M_{L_i} \ell_i 0 | L M_L)(S_i M_{S_i} \tfrac{1}{2} m_i | S M_S)\mathrm{i}^{\ell_i}(2\ell_i + 1)^{1/2} \\ & \times \overline{\Phi}_i^{\Gamma}(\mathbf{X}_N; \hat{\mathbf{r}}_{N+1}\sigma_{N+1}) r_{N+1}^{-1} \\ & \times \{\exp[-\mathrm{i}\theta_i(r_{N+1})] - \exp[\mathrm{i}\theta_i(r_{N+1})]\},\end{aligned} \tag{2.125}$$

where $\theta_i(r_{N+1}) = k_i r_{N+1} - \frac{1}{2}\ell_i\pi$ for neutral atomic targets. We now carry out a partial wave decomposition of Ψ_i in (2.122) by writing

$$\Psi_i(\mathbf{X}_{N+1}) = \sum_{LS\pi} \Psi_i^{\Gamma}(\mathbf{X}_{N+1}) B_i^{\Gamma}(E), \tag{2.126}$$

where the functions $\Psi_i^{\Gamma}(\mathbf{X}_{N+1})$ have the asymptotic form

$$\Psi_i^{\Gamma}(\mathbf{X}_{N+1}) \underset{r_{N+1}\to\infty}{\sim} \sum_{j=1}^{n} \overline{\Phi}_j^{\Gamma}(\mathbf{X}_N; \hat{\mathbf{r}}_{N+1}\sigma_{N+1}) r_{N+1}^{-1} G_{ji}^{\Gamma}(r_{N+1}), \tag{2.127}$$

which follows from expansion (2.57) since the exchange terms and the quadratically integrable functions vanish in this limit. Also in (2.127) the reduced radial wave functions $G_{ji}^{\Gamma}(r)$ are chosen to satisfy the S-matrix asymptotic boundary conditions (2.110). The coefficients $B_i^{\Gamma}(E)$ in (2.126) are then chosen so that the ingoing wave terms in Ψ_i and Ψ_i^{inc} are the same. This yields

$$B_i^{\Gamma}(E) = \frac{\mathrm{i}\pi^{1/2}}{k_i^{1/2}} \mathrm{i}^{\ell_i}(2\ell_i+1)^{1/2}(L_i M_{L_i} \ell_i 0 | L M_L)(S_i M_{S_i} \tfrac{1}{2} m_i | S M_S). \tag{2.128}$$

Substituting this result into (2.126) and using (2.122) and (2.124) then gives

$$\begin{aligned}\Psi_i^{\text{scatt}} \underset{r_{N+1}\to\infty}{\sim} & - \sum_{LS\pi\ell_i\alpha_j L_j S_j \ell_j} \mathrm{i}\left(\frac{\pi}{k_i k_j}\right)^{1/2} (L_i M_{L_i} \ell_i 0 | L M_L)(S_i M_{S_i} \tfrac{1}{2} m_i | S M_S) \\ & \times \mathrm{i}^{\ell_i}(2\ell_i+1)^{1/2} \overline{\Phi}_i^{\Gamma}(\mathbf{X}_N; \hat{\mathbf{r}}_{N+1}\sigma_{N+1}) r_{N+1}^{-1} \\ & \times \exp(\mathrm{i}\theta_j)\left(S_{ji}^{\Gamma} - \delta_{ji}\right). \end{aligned} \tag{2.129}$$

The scattering amplitude is obtained by expanding the channel functions $\overline{\Phi}_i^{\Gamma}(\mathbf{X}_N; \hat{\mathbf{r}}_{N+1}\sigma_{N+1})$ in (2.129) in terms of the target states $\Phi_i(\mathbf{X}_N)$ using (2.59) and comparing with (2.124). This gives

$$\begin{aligned} f_{ji}(\theta,\phi) = & - \sum_{LS\pi\ell_i\ell_j} \mathrm{i}\left(\frac{\pi}{k_i k_j}\right)^{1/2} \mathrm{i}^{\ell_i - \ell_j}(2\ell_i+1)^{1/2}(L_i M_{L_i} \ell_i 0 | L M_L) \\ & \times (S_i M_{S_i} \tfrac{1}{2} m_i | S M_S)(L_j M_{L_j} \ell_j m_{\ell_j} | L M_L)(S_j M_{S_j} \tfrac{1}{2} m_j | S M_S) \\ & \times T_{ji}^{\Gamma}\, Y_{\ell_j m_{\ell_j}}(\theta,\phi), \end{aligned} \tag{2.130}$$

where the T-matrix elements T_{ji}^{Γ} in this equation are defined in terms of the S-matrix elements S_{ji}^{Γ} by (2.119).

The differential cross section for a transition from a state represented by the quantum numbers $\alpha_i L_i S_i \pi_i$ to a state represented by the quantum numbers $\alpha_j L_j S_j \pi_j$

is obtained by substituting (2.130) into (2.8) resulting in an expression for the differential cross section, given, for example, by Blatt and Biedenharn [116]. The total cross section is then obtained by averaging this expression for the differential cross section over the initial quantum numbers of the target atomic state and incident electron, summing over their final quantum numbers and integrating over the scattering angles of the outgoing electron. We obtain the following result for the total cross section:

$$\sigma^{\mathrm{Tot}}(i \to j) = \sum_{LS\pi} \sigma^{LS\pi}(i \to j), \tag{2.131}$$

where the partial wave cross sections $\sigma^{LS\pi}(i \to j)$ corresponding to the conserved quantum numbers $LS\pi$ are given in units of πa_0^2 by

$$\sigma^{LS\pi}(i \to j) = \frac{(2L+1)(2S+1)}{2k_i^2(2L_i+1)(2S_i+1)} \sum_{\ell_i \ell_j} |T_{ji}^{\Gamma}|^2. \tag{2.132}$$

We note that the slow convergence of expansion (2.132) for optically allowed transitions can be overcome by using a method proposed by Burke and Seaton [190] using the Burgess sum rule [149].

The expression for the differential cross section obtained by substituting (2.130) into (2.8) can be simplified using the angular momentum transfer formalism introduced by Fano and Dill [310]. We define the angular momentum transferred from the scattered electron to the target during the collision by $\boldsymbol{\ell}_t$ where

$$\boldsymbol{\ell}_t = \boldsymbol{\ell}_j - \boldsymbol{\ell}_i = \mathbf{L}_i - \mathbf{L}_j. \tag{2.133}$$

The relationship between these vectors and the total orbital angular momentum vector $\mathbf{L}$ is illustrated in Fig. 2.2. We now introduce a transformed T-matrix $\widetilde{T}_{ji}^{tS}$ by the equation

$$\widetilde{T}_{ji}^{tS} = \sum_{L\pi} (-1)^L (2L+1) W(\ell_i L_i \ell_j L_j; L\ell_t) T_{ji}^{\Gamma}, \tag{2.134}$$

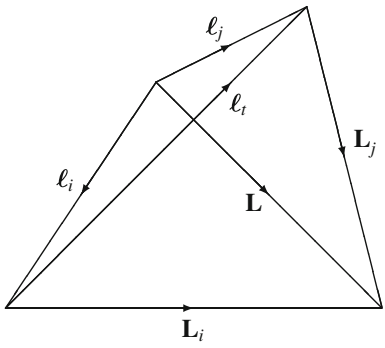

Fig. 2.2 Relationship between the angular momentum transfer vector $\boldsymbol{\ell}_t$ and the vectors $\mathbf{L}_i$, $\mathbf{L}_j$, $\boldsymbol{\ell}_i$, $\boldsymbol{\ell}_j$ and $\mathbf{L}$

where $W(abcd;ef)$ are Racah coefficients defined in Appendix A.2. We can then show that (2.130) for the scattering amplitude can be rewritten as

$$\begin{aligned} f_{ji}(\theta,\phi) = -\sum_{\ell_t S \ell_i \ell_j} \mathrm{i}\left(\frac{\pi}{k_i k_j}\right)^{1/2} \mathrm{i}^{\ell_i-\ell_j}(2\ell_i+1)^{1/2}(-1)^{L_i+L_j+\ell_i+\ell_j-\ell_t+M_{L_j}} \\ \times (S_i M_{S_i} \tfrac{1}{2} m_i | S M_S)(S_j M_{S_j} \tfrac{1}{2} m_j | S M_S) \\ \times (L_i M_{L_i} L_j - M_{L_j} | \ell_t M_{L_i} - M_{L_j}) \\ \times (\ell_i 0 \ell_j m_{\ell_j} | \ell_t M_{L_i} - M_{L_j}) \widetilde{T}^{tS}_{ji}\, Y_{\ell_j m_{\ell_j}}(\theta,\phi). \end{aligned} \tag{2.135}$$

The differential cross section, obtained by averaging (2.8) over the initial magnetic quantum numbers and summing over the final magnetic quantum numbers, can be written as

$$\frac{\mathrm{d}\sigma_{ji}}{\mathrm{d}\Omega} = \sum_{\lambda} A_\lambda(i \to j) P_\lambda(\cos\,\theta), \tag{2.136}$$

where

$$\begin{aligned} A_\lambda(i \to j) = \frac{(-1)^\lambda}{8k_i^2(2L_i+1)(2S_i+1)} \sum_{\ell_i \ell_{i'} \ell_j \ell_{j'}} \mathrm{i}^{\ell_i-\ell_j-\ell_{i'}+\ell_{j'}} \\ \times \left[(2\ell_i+1)(2\ell_{i'}+1)(2\ell_j+1)(2\ell_{j'}+1)\right]^{1/2} \\ \times (\ell_i 0 \ell_{i'} 0 | \lambda 0)(\ell_j 0 \ell_{j'} 0 | \lambda 0) \sum_{\ell_t} (-1)^{\ell_t}(2\ell_t+1) W(\ell_i \ell_j \ell_{i'} \ell_{j'}; \ell_t \lambda) \\ \times \sum_S (2S+1) \widetilde{T}^{tS}_{ji}\, \widetilde{T}^{tS}_{j'i'}. \end{aligned} \tag{2.137}$$

The subscripts i, j, i' and j' on $\widetilde{T}^{tS}_{ji}$ and $\widetilde{T}^{tS}_{j'i'}$ denote the channel quantum numbers $\alpha_i L_i S_i \ell_i \pi_i$, $\alpha_j L_j S_j \ell_j \pi_j$, $\alpha_i L_i S_i \ell_{i'} \pi_{i'}$ and $\alpha_j L_j S_j \ell_{j'} \pi_{j'}$, respectively.

The introduction of the angular momentum transfer ℓ_t in the expression for the differential cross section given by (2.136) and (2.137) replaces the double summation over L and L' in the earlier expression for the differential cross section given, for example, by Blatt and Biedenharn [116], by a single incoherent summation over ℓ_t. The corresponding evaluation of the summation is very much more efficient and has been incorporated into several computer programs (e.g. by Salvini [808]).

A second advantage of the angular momentum transfer formalism is that it enables simple qualitative features of the angular distribution to be readily described and understood. For example, it is useful to introduce the concept of parity-favoured and parity-unfavoured transitions by the equations

$$\begin{aligned} \ell_i + \ell_j + \ell_t &= \text{even}, \quad \text{parity favoured}, \\ \ell_i + \ell_j + \ell_t &= \text{odd}, \quad \text{parity unfavoured}. \end{aligned} \tag{2.138}$$

An example of a parity-favoured transition is

$$\mathrm{e}^- + \mathrm{He}(1\mathrm{s}^2\ {}^1\mathrm{S}^\mathrm{e}) \to \mathrm{e}^- + \mathrm{He}(1\mathrm{s}2\mathrm{p}\ {}^1\mathrm{P}^\mathrm{o}). \tag{2.139}$$

In this case $L_i = 0$ and $L_j = 1$ so from Fig. 2.2 we see that $\ell_t = 1$. On the other hand, from the conservation of total parity, $\ell_i - \ell_j$ must be odd. An example of a parity-unfavoured transition is

$$\mathrm{e}^- + \mathrm{N}(1\mathrm{s}^2 2\mathrm{s}^2 2\mathrm{p}^3\ {}^4\mathrm{S}^\mathrm{o}) \to \mathrm{e}^- + \mathrm{N}(1\mathrm{s}^2 2\mathrm{s}^2 2\mathrm{p}^3\ {}^2\mathrm{P}^\mathrm{o}). \tag{2.140}$$

In this case $L_i = 0$ and $L_j = 1$ so again $\ell_t = 1$. However, from conservation of total parity, $\ell_i - \ell_j$ is even.

One of the most interesting features of parity-unfavoured transitions is that the differential cross sections in the forward and backward directions vanish. This follows by considering the factor

$$(\ell_i 0 \ell_j m_{\ell_j} | \ell_t M_{L_i} - M_{L_j}) Y_{\ell_j m_{\ell_j}}(\theta, \phi) \tag{2.141}$$

in expression (2.135) for the scattering amplitude. The spherical harmonic $Y_{\ell_j m_{\ell_j}}(\theta, \phi)$ contains a factor $(\sin\theta)^{m_{\ell_j}}$ which causes the angular distribution to vanish at $\theta = 0$ and π when $m_{\ell_j} \neq 0$. However, when $m_{\ell_j} = 0$, the Clebsch–Gordan coefficient in (2.141) reduces to $(\ell_i 0 \ell_j 0 | \ell_t 0)$ which vanishes when $\ell_i + \ell_j + \ell_t$ is odd, which proves this result.

The preceding theory must be extended to describe electron collisions with ions. As before, we rewrite the wave function Ψ_i in (2.6) in terms of incident and scattered waves as in (2.122), which now has the following asymptotic form:

$$\begin{aligned}\Psi_i \underset{r\to\infty}{\sim}\ & \Phi_i \chi_{\frac{1}{2}m_i} \exp[\mathrm{i}(k_i z + \eta_i \ln k_i \zeta)] \\ & + \sum_j \Phi_j \chi_{\frac{1}{2}m_j} f_{ji}(\theta, \phi) \frac{\exp[\mathrm{i}(k_j r - \eta_j \ln 2k_j r)]}{r}.\end{aligned} \tag{2.142}$$

The incident Coulomb-distorted plane wave term in Ψ_i^{inc} can be decomposed into partial waves using (1.49) and (1.64). This gives

$$\begin{aligned}\exp[\mathrm{i}(kz + \eta \ln k\zeta)] \underset{r\to\infty}{\sim}\ & \sum_{\ell=0}^{\infty} (2\ell+1)\mathrm{i}^\ell \exp(\mathrm{i}\sigma_\ell)(kr)^{-1} F_\ell(\eta, kr) P_\ell(\cos\theta) \\ & - f_c(\theta) r^{-1} \exp[\mathrm{i}(kr - \eta \ln 2kr)],\end{aligned} \tag{2.143}$$

where $f_c(\theta)$ is the Coulomb scattering amplitude defined by (1.52), and where we note that (2.143) applies except when $\theta = 0$, since in this case $r \to \infty$ does not imply $|r - z| \to \infty$. After substituting (2.143) into (2.142) we then find that

$$\Psi_i^{\text{inc}} \underset{r_{N+1}\to\infty}{\sim} \sum_{LS\pi\ell_i} \Big\{ \mathrm{i}\pi^{1/2} k_i^{-1} (L_i M_{L_i} \ell_i 0 | L M_L) \times (S_i M_{S_i} \tfrac{1}{2} m_i | S M_S) \mathrm{i}^{\ell_i} (2\ell_i + 1)^{1/2} \exp(\mathrm{i}\sigma_{\ell_i}) \times \overline{\Phi}_i^{\Gamma}(\mathbf{X}_N; \hat{\mathbf{r}}_{N+1}\sigma_{N+1}) r_{N+1}^{-1} [\exp(-\mathrm{i}\theta_i) - \exp(\mathrm{i}\theta_i)] \Big\} - \Phi_i(\mathbf{X}_N) \chi_{\frac{1}{2}m_i}(\sigma_{N+1}) f_c(\theta_{N+1}) r_{N+1}^{-1} \times \exp[\mathrm{i}(k_i r_{N+1} - \eta_i \ln 2k_i r_{N+1})], \tag{2.144}$$

where

$$\theta_i = k_i r_{N+1} - \frac{1}{2}\ell_i \pi - \eta_i \ln 2k_i r_{N+1} + \sigma_{\ell_i}. \tag{2.145}$$

We then carry out a partial wave decomposition of Ψ_i using (2.126), where the coefficients $B_i^{\Gamma}(E)$ are now chosen so that the ingoing wave terms in (2.126) and (2.144) are the same. The scattered wave function Ψ_i^{scatt} is then

$$\Psi_i^{\text{scatt}} \underset{r_{N+1}\to\infty}{\sim} - \sum_{LS\pi\ell_i\alpha_j L_j S_j \ell_j} \Big\{ \mathrm{i}\pi^{1/2} (k_i k_j)^{-1/2} (L_i M_{L_i} \ell_i 0 | L M_L) \times (S_i M_{S_i} \tfrac{1}{2} m_i | S M_S) \mathrm{i}^{\ell_i} (2\ell_i + 1)^{1/2} \exp(\mathrm{i}\sigma_{\ell_i}) \times \overline{\Phi}_i^{\Gamma}(\mathbf{X}_N; \hat{\mathbf{r}}_{N+1}\sigma_{N+1}) r_{N+1}^{-1} \exp(\mathrm{i}\theta_j) \left(S_{ji}^{\Gamma} - \delta_{ji} \right) \Big\} - \Phi_i(\mathbf{X}_N) \chi_{\frac{1}{2}m_i}(\sigma_{N+1}) f_c(\theta_{N+1}) r_{N+1}^{-1} \times \exp[\mathrm{i}(k_i r_{N+1} - \eta_i \ln 2k_i r_{N+1})]. \tag{2.146}$$

The scattering amplitude for electron–ion collisions is obtained by expanding the channel functions $\overline{\Phi}_i^{\Gamma}(\mathbf{X}_N; \hat{\mathbf{r}}_{N+1}\sigma_{N+1})$ in (2.146) and comparing with (2.142). We obtain

$$f_{ji}(\theta, \phi) = f_c(\theta)\delta_{ji} + f_{ji}^S(\theta, \phi), \tag{2.147}$$

where, as in (1.75), $f_c(\theta)$ is the Coulomb scattering amplitude and $f_{ji}^S(\theta, \phi)$ is the scattering amplitude arising from the additional short-range potential. We find that

$$f_{ji}^S(\theta, \phi) = - \sum_{LS\pi\ell_i\ell_j} \mathrm{i}\pi^{1/2} (k_i k_j)^{-1/2} \mathrm{i}^{\ell_i - \ell_j} (2\ell_i + 1)^{1/2} \exp[\mathrm{i}(\sigma_{\ell_i} + \sigma_{\ell_j})] \times (L_i M_{L_i} \ell_i 0 | L M_L)(S_i M_{S_i} \tfrac{1}{2} m_i | S M_S)(L_j M_{L_j} \ell_j m_{\ell_j} | L M_L) \times (S_j M_{S_j} \tfrac{1}{2} m_j | S M_S) T_{ji}^{\Gamma} Y_{\ell_j m_{\ell_j}}(\theta, \phi) \tag{2.148}$$

where, as in (2.119), the T-matrix is defined by $T_{ji}^{\Gamma} = S_{ji}^{\Gamma} - \delta_{ji}$. Equation (2.148) describes a transition from a state defined by the quantum numbers

$i \equiv \alpha_i L_i S_i M_{L_i} M_{S_i} \pi_i m_i$ to a state defined by the quantum numbers $j \equiv \alpha_j L_j S_j M_{L_j} M_{S_j} \pi_j m_j$.

The differential cross section for a transition from a state denoted by the quantum numbers $\alpha_i L_i S_i \pi_i$ to a state represented by the quantum numbers $\alpha_j L_j S_j \pi_j$ is obtained by substituting (2.147) into the expression for the differential cross section, given by (2.8), averaging over the initial quantum numbers and summing over the final quantum numbers of the target state and scattered electron. The total cross section for inelastic collisions is then obtained by integrating over all scattering angles of the outgoing electron and summing over all $LS\pi$ values giving (2.131) and (2.132).

Finally, in applications involving electron–ion collisions it is often necessary to determine a quantity $\Omega(i, j)$, first introduced by Hebb and Menzel [447] and subsequently called the collision strength by Seaton [849, 850, 857]. It is defined in terms of the total cross section $\sigma^{\mathrm{Tot}}(i \rightarrow j)$ measured in units of πa_0^2 by

$$\Omega(i, j) = \omega_i k_i^2 \sigma^{\mathrm{Tot}}(i \rightarrow j), \tag{2.149}$$

where $\omega_i = (2L_i + 1)(2S_i + 1)$ is the statistical weight of the initial state, denoted by the quantum numbers $\alpha_i L_i S_i$. Since k_i has the dimensions of a reciprocal length, $\Omega(i, j)$ is dimensionless. It is also symmetric so that $\Omega(i, j) = \Omega(j, i)$. In an ionized plasma, we also need to consider the electron–ion collision cross section averaged over a Maxwell distribution of electron velocities. We introduce the collisional transition probability $q(i \rightarrow j)N_e$ where

$$q(i \rightarrow j) = \int_0^\infty \sigma^{\mathrm{Tot}}(i \rightarrow j) v_i f(v_i, T_e) \mathrm{d}v_i. \tag{2.150}$$

Here $f(v_i, T_e)$ is the Maxwell velocity distribution function, normalized according to

$$\int_0^\infty f(v_i, T_e) \mathrm{d}v_i = 1, \tag{2.151}$$

v_i is the velocity of the incident electron, N_e is the electron density and T_e is the electron temperature of the plasma. Expressing $\sigma^{\mathrm{Tot}}(i \rightarrow j)$ in terms of the collision strength we find that the probability of *de-excitation* is

$$q(j \rightarrow i) = \frac{8.63 \times 10^{-6} \Upsilon(j, i)}{\omega_j T_e^{1/2}}, \quad e_j \geq e_i, \tag{2.152}$$

in cubic centimetres per second, where T_e is in degrees Kelvin, ω_j is the statistical weight of the jth target state and e_i and e_j are the target energies defined by (2.5). The effective collision strength $\Upsilon(j, i)$ introduced in (2.152) is defined by

$$\Upsilon(j, i) = \int_0^\infty \Omega(j, i) \exp\left[-\frac{\epsilon_j}{kT_e}\right] \mathrm{d}\left[\frac{\epsilon_j}{kT_e}\right], \tag{2.153}$$

where ϵ_j is the energy of the scattered electron in the jth state in Rydbergs and $k = 6.339 \times 10^{-6}$ Rydbergs/°K is Boltzmann's constant. Clearly if $\Omega(j,i)$ is independent of energy, then $\Upsilon(j,i) = \Omega(j,i)$. Also we find that the probability of *excitation* is

$$q(i \to j) = \frac{\omega_j}{\omega_i} q(j \to i) \exp\left(-\frac{e_j - e_i}{kT_e}\right), \quad e_j \geq e_i. \tag{2.154}$$

We also note that in many applications in plasma physics and astrophysics it is sufficient to know the effective collision strength $\Upsilon(j,i)$ rather than the collision strength $\Omega(j,i)$ for the transitions of interest. This can be important since we will see when we discuss recent low-energy electron–ion collision calculations in Sect. 5.6 that in many cases of interest the collision strength is dominated by resonance structure requiring a very large number of energy values to fully resolve. However, the corresponding effective collision strength is usually a smoothly varying function of temperature that can be accurately represented by a few well-chosen parameters.

Chapter 3
Resonances and Threshold Behaviour

We consider in this chapter the theory of resonance reactions and the closely related behaviour of cross sections near threshold. Our treatment will concentrate on theoretical methods that have found wide applicability in atomic and molecular collision processes. For example, we will see in Chap. 5 that resonances play a crucial role in low-energy electron collisions with multi-electron atoms and atomic ions, where effective collision strengths can be increased by an order of magnitude or more at low temperatures by resonance processes. We will also see in later chapters that resonances are important in electron impact ionization, in single- and multiphoton ionization processes, in photorecombination and in electron–molecule collisions. Hence, understanding and interpreting resonances in collision processes are important goals for theory and their detailed and accurate prediction provides a challenge for computational methods.

A fundamental approach to the study of resonances and threshold behaviour is through an analysis of the analytic properties of the S-matrix or collision matrix introduced by Wheeler [961] and Heisenberg [452]. We have already defined the S-matrix in Chaps. 1 and 2 in terms of the asymptotic form of the radial wave function describing electron collisions with atoms and atomic ions. We have also considered in Sect. 1.3 the analytic properties of the single-channel S-matrix which arises in potential scattering. We found in that section that bound states and resonances are closely related to poles in the S-matrix in the complex momentum plane. In this chapter we extend our discussion of S-matrix theory to multichannel resonances and threshold behaviour.

We commence in Sect. 3.1 by generalizing our discussion of the analytic properties of the S-matrix in Sect. 1.3 by defining multichannel Jost functions in terms of the solutions of coupled second-order integrodifferential equations (2.63) which describe electron collisions with multi-electron atoms and atomic ions. By expressing the S-matrix in terms of Jost functions we can then relate the analytic properties of the S-matrix in the multi-Riemann-sheeted complex energy plane to the simpler analytic properties of the Jost functions. This provides the basis for discussing the distribution of bound-state and resonance poles in the S-matrix in the complex energy plane.

In Sect. 3.2 we derive explicit expressions for the K-matrix and S-matrix in the neighbourhood of an isolated resonance pole using a theoretical approach

P.G. Burke, *R-Matrix Theory of Atomic Collisions*, Springer Series on Atomic, Optical, and Plasma Physics 61, DOI 10.1007/978-3-642-15931-2_3,

introduced by Brenig and Haag [137] and Fano [301]. In this approach, a zero-order Hamiltonian is defined which can be solved exactly in terms of discrete and continuum states. The full Hamiltonian then mixes these states giving rise to resonances in the S-matrix and we obtain expressions for the individual eigenphases and the eigenphase sum in the neighbourhood of a resonance. We also discuss the time-delay matrix, first introduced by Smith [881], and we relate the trace of this matrix to the derivative of the eigenphase sum with respect to energy. We then show that this quantity can often provide an accurate procedure for analysing overlapping resonances. We also consider in this section, the projection operator approach of Feshbach [320, 321], which provides a powerful framework for describing resonance phenomena in a wide range of atomic, molecular and nuclear collision processes. Finally, we discuss the hyperspherical system of coordinates which has been important in the analysis of resonances and threshold behaviour of three-body systems, such as two electrons in a Coulomb field and three-nucleon molecules such as H_3^+, as well as in the general description of the three-body problem.

In Sect. 3.3, we consider the threshold behaviour of excitation and ionization cross sections. This behaviour was investigated in a fundamental paper by Wigner [970] who showed that the analytic behaviour of cross sections near threshold depends, apart from a constant, on the form of the long-range interaction between the particles. We consider first two-body collision processes where we use the analytic properties of the multichannel R-matrix, discussed in Chap. 5, to derive a multichannel effective range theory for short-range potentials, following the work of Ross and Shaw [798]. We then extend this theory to treat long-range dipole potentials considered by Gailitis and Damburg [359] and a Coulomb potential considered by Gailitis [357]. We also discuss multichannel quantum defect theory (MQDT) introduced, developed and reviewed by Seaton [859], and we summarize the extension of MQDT to molecular collision processes first considered by Fano [303]. Finally, we consider the threshold law of electron impact ionization of atoms and positive ions first derived by Wannier [954, 955]. In this analysis we adopt the hyperspherical system of coordinates, introduced in Sect. 3.2.6.

3.1 Analytic Properties of the S-Matrix

In this section we generalize our discussion of the analytic properties of the S-matrix in potential scattering given in Sect. 1.3 to multichannel collisions. As in Chap. 2 we illustrate this discussion by considering low-energy elastic and inelastic electron collisions with multi-electron atoms and atomic ions described by

$$e^- + A_i \rightarrow A_j + e^-, \tag{3.1}$$

where A_i and A_j are the initial and final bound states of the target. We consider the solution of the n coupled second-order integrodifferential equations (2.63), which describe these collisions for a given set of conserved quantum numbers. We rewrite

these equations using matrix notation as follows:

$$\left(\frac{\mathrm{d}^2}{\mathrm{d}r^2} - \frac{\boldsymbol{\ell}(\boldsymbol{\ell}+\mathbf{I})}{r^2} + \frac{2(Z-N)}{r} - \mathbf{U}(r) + \mathbf{k}^2\right)\mathbf{F}(r) = 0, \tag{3.2}$$

where Z is the nuclear charge number, N is the number of target electrons, $\mathbf{U}$ is an $n \times n$-dimensional matrix representing the sum of the local direct, non-local exchange and non-local correlation potentials $2(\mathbf{V}+\mathbf{W}+\mathbf{X})$ in (2.63), $\mathbf{I}$ is the $n \times n$-dimensional unit matrix and $\boldsymbol{\ell}$ and $\mathbf{k}^2$ are $n \times n$-dimensional diagonal matrices representing the channel orbital angular momenta and wave numbers squared, respectively. We note that in (3.2) we have not imposed the orthogonality constraints defined by (2.62). Hence the Lagrange multiplier terms in (2.63) and the additional quadratically integrable functions included in the original expansion (2.57) for completeness are not required. However, as pointed out following (2.87), the relaxation of these constraints does not affect the K-matrix, S-matrix and scattering amplitudes and hence the analytic properties of the S-matrix considered here.

We find it convenient, as in Sect. 2.4, to order the target eigenstates and pseudostates retained in expansion (2.57) so that their energies defined by (2.5) are in increasing order. It follows that the corresponding channel wave numbers squared k_i^2, defined by (2.7), satisfy (2.78) when the total energy E is real. Initially we limit our discussion to neutral atomic targets where the nuclear charge number Z equals the number of target electrons N. It then follows from (2.73) that the leading term in the long-range potential experienced by the scattered electron is $\sim r^{-2}$. Later in this chapter we will consider electron collisions with atomic ions where a long-range Coulomb potential is also present.

In analogy with our consideration of the analytic properties of the S-matrix in potential scattering, discussed in Sect. 1.3, we define, following Jost [515], two linearly independent matrix solutions $\mathbf{f}(\pm\mathbf{k}, r)$ of (3.2) by the asymptotic boundary conditions

$$\lim_{r\to\infty} \exp(\pm \mathrm{i}\mathbf{k}r)\mathbf{f}(\pm\mathbf{k}, r) = \mathbf{I}, \tag{3.3}$$

where the diagonal elements of $\mathbf{k}$ are defined by (2.7) and where the total energy E can now be complex. Also $\mathbf{f}(\pm\mathbf{k}, r)$ are diagonal $n \times n$-dimensional matrices in the limit $r \to \infty$ but, as shown below, are in general non-diagonal for finite values of r. For potentials which occur in electron–atom collisions, the boundary conditions (3.3) define $\mathbf{f}(\mathbf{k}, r)$ uniquely for $\mathrm{Im}\, k_i < 0$ and $\mathbf{f}(-\mathbf{k}, r)$ uniquely for $\mathrm{Im}\, k_i > 0$ for $i = 1, \ldots, n$. If we can impose stronger conditions on the potentials V_{ij}, W_{ij} and X_{ij} in (2.63) then the functions $\mathbf{f}(\pm\mathbf{k}, r)$ can be analytically continued outside of these regions, as discussed in Sect. 1.3 in the case of potential scattering.

The physical solutions of (3.2) which vanish at the origin can be expressed as linear combinations of the functions $\mathbf{f}(\pm\mathbf{k}, r)$. Let us normalize these physical solutions so that they satisfy the following boundary condition at the origin:

$$\lim_{r\to 0} r^{-\boldsymbol{\ell}-\mathbf{I}}\mathbf{F}(\mathbf{k}, r) = \mathbf{I}, \tag{3.4}$$

where $\boldsymbol{\ell}$ is the $n \times n$-dimensional diagonal matrix whose diagonal elements are ℓ_i, $i = 1, \ldots, n$ and where we have introduced the $n \times n$-dimensional solution matrix $\mathbf{F}(\mathbf{k}, r)$ which is diagonal in the limit $r \to 0$ but is in general non-diagonal for non-zero values of r. The second subscript k on this solution matrix F_{ik} runs from 1 to n and denotes the n linearly independent solutions of (3.2) which are defined by the boundary conditions (3.4). These solutions form a complete set of solutions which vanish at the origin. The boundary condition (3.4), which does not depend on $\mathbf{k}$, then ensures that, as in potential scattering, $\mathbf{F}(\mathbf{k}, r)$ is an entire function of $\mathbf{k}$. We then define the multichannel Jost function matrices $\tilde{\mathbf{f}}(\pm\mathbf{k})$ by the Wronskian

$$\tilde{\mathbf{f}}(\pm\mathbf{k}) = W[\mathbf{f}(\pm\mathbf{k}, r), \mathbf{F}(\mathbf{k}, r)], \tag{3.5}$$

where $\tilde{\mathbf{f}}(\pm\mathbf{k})$ are $n \times n$-dimensional matrices. Also in (3.5) we have defined the Wronskian of any two solution vectors $\mathbf{u}$ and $\mathbf{v}$ by

$$W[\mathbf{u}, \mathbf{v}] = \mathbf{u}^{\mathrm{T}}\mathbf{v}' - \mathbf{u}'^{\mathrm{T}}\mathbf{v}, \tag{3.6}$$

where $\mathbf{u}^{\mathrm{T}}$ is the transpose of $\mathbf{u}$ and the prime denotes the derivative with respect to r. It is straightforward to show that the Wronskian is independent of r.

We now use the relations

$$W[\mathbf{f}(\pm\mathbf{k}, r), \mathbf{f}(\mp\mathbf{k}, r)] = \pm 2\mathrm{i}\mathbf{k} \tag{3.7}$$

and

$$W[\mathbf{f}(\pm\mathbf{k}, r), \mathbf{f}(\pm\mathbf{k}, r)] = 0, \tag{3.8}$$

which follow from (3.3), to write $\mathbf{F}(\mathbf{k}, r)$ in the form

$$\mathbf{F}(\mathbf{k}, r) = (2\mathrm{i})^{-1}[\mathbf{f}(-\mathbf{k}, r)\mathbf{k}^{-1}\tilde{\mathbf{f}}(\mathbf{k}) - \mathbf{f}(\mathbf{k}, r)\mathbf{k}^{-1}\tilde{\mathbf{f}}(-\mathbf{k})]. \tag{3.9}$$

If we compare this equation with the asymptotic form (2.110), we find that the S-matrix can be defined in terms of the Jost functions by

$$\mathbf{S}_n(\mathbf{k}) = \exp\left(\tfrac{1}{2}\mathrm{i}\pi\boldsymbol{\ell}\right)\mathbf{k}^{-1/2}\tilde{\mathbf{f}}(\mathbf{k})\tilde{\mathbf{f}}^{-1}(-\mathbf{k})\mathbf{k}^{1/2}\exp\left(\tfrac{1}{2}\mathrm{i}\pi\boldsymbol{\ell}\right), \tag{3.10}$$

where the subscript n on $\mathbf{S}_n$ refers to the dimension of the S-matrix and where in the following discussion we assume that all channels are open so that the number of open channels $n_a = n$ in (2.110). This equation enables the analytic properties of the S-matrix to be related to the simpler analytic properties of the Jost functions.

In order to study the analytic properties of the Jost functions we return to (3.2) satisfied by $\mathbf{f}(\pm\mathbf{k}, r)$. We assume that $\mathbf{f}(-\mathbf{k}, r)$ satisfies the equation

$$\left(\frac{\mathrm{d}^2}{\mathrm{d}r^2} - \frac{\boldsymbol{\ell}(\boldsymbol{\ell} + \mathbf{I})}{r^2} + \frac{2(Z - N)}{r} - \mathbf{U}(r) + \mathbf{k}^2\right)\mathbf{f}(-\mathbf{k}, r) = 0. \tag{3.11}$$

We then take the complex conjugate of this equation yielding

$$\left(\frac{\mathrm{d}^2}{\mathrm{d}r^2} - \frac{\boldsymbol{\ell}(\boldsymbol{\ell}+\mathbf{I})}{r^2} + \frac{2(Z-N)}{r} - \mathbf{U}(r) + \mathbf{k}^{*2}\right)\mathbf{f}^*(-\mathbf{k}, r) = 0, \tag{3.12}$$

where we assume that r, $\boldsymbol{\ell}$, Z, N and $\mathbf{U}$ are real but $\mathbf{k}$, which is defined in terms of the total energy E by (2.7), can be complex. In addition it follows, by replacing $-\mathbf{k}$ by $\mathbf{k}^*$ in (3.11), that $\mathbf{f}(\mathbf{k}^*, r)$ is a solution of

$$\left(\frac{\mathrm{d}^2}{\mathrm{d}r^2} - \frac{\boldsymbol{\ell}(\boldsymbol{\ell}+\mathbf{I})}{r^2} + \frac{2(Z-N)}{r} - \mathbf{U}(r) + \mathbf{k}^{*2}\right)\mathbf{f}(\mathbf{k}^*, r) = 0. \tag{3.13}$$

Hence $\mathbf{f}^*(-\mathbf{k}, r)$ and $\mathbf{f}(\mathbf{k}^*, r)$ satisfy the same differential equation and from (3.3) they satisfy the same boundary condition. Hence

$$\mathbf{f}^*(-\mathbf{k}, r) = \mathbf{f}(\mathbf{k}^*, r) \tag{3.14}$$

is satisfied for all points in the upper half k-plane with $\operatorname{Im} k_i > 0,\ i = 1, \ldots, n$, and for all other points in the complex k-plane for which the potential admits an analytic continuation from the upper half k-plane.

In a similar way, we can show from (3.11) and the boundary condition (3.4) satisfied by $\mathbf{F}(\mathbf{k}, r)$ that

$$\mathbf{F}^*(\mathbf{k}, r) = \mathbf{F}(\mathbf{k}^*, r) \tag{3.15}$$

and

$$\mathbf{F}(\mathbf{k}, r) = \mathbf{F}(-\mathbf{k}, r). \tag{3.16}$$

Using (3.14), (3.15) and (3.16), we find from (3.5) that the Jost functions satisfy

$$\tilde{\mathbf{f}}^*(-\mathbf{k}) = \tilde{\mathbf{f}}(\mathbf{k}^*). \tag{3.17}$$

Hence we obtain from (3.10)

$$\mathbf{S}_n^*(\mathbf{k}^*) = \exp(-\tfrac{1}{2}\mathrm{i}\pi\boldsymbol{\ell})\mathbf{k}^{-1/2}\tilde{\mathbf{f}}(-\mathbf{k})\tilde{\mathbf{f}}^{-1}(\mathbf{k})\mathbf{k}^{1/2}\exp(-\tfrac{1}{2}\mathrm{i}\pi\boldsymbol{\ell}). \tag{3.18}$$

Combining this equation with (3.10) gives

$$\mathbf{S}_n(\mathbf{k})\mathbf{S}_n^*(\mathbf{k}^*) = \mathbf{I}. \tag{3.19}$$

Also, as we have shown in Sect. 2.4, the K-matrix is symmetric and hence from (2.112) the S-matrix is also symmetric so that

$$\mathbf{S}_n(\mathbf{k}) = \mathbf{S}_n^{\mathrm{T}}(\mathbf{k}), \tag{3.20}$$

where $\mathbf{S}_n^{\mathrm{T}}$ denotes the transpose of $\mathbf{S}_n$. Hence it follows from (3.19) and (3.20) that

$$\mathbf{S}_n(\mathbf{k})\mathbf{S}_n^{\dagger}(\mathbf{k}^*) = \mathbf{I}, \tag{3.21}$$

where $\mathbf{S}_n^{\dagger}$ denotes the hermitian conjugate of $\mathbf{S}_n$. This is the generalization of the unitarity relation given by (1.97) for potential scattering.

A further analytic property of the S-matrix can be obtained by considering $\mathbf{S}_n^*(-\mathbf{k}^*)$. From (3.10) and (3.17) we obtain

$$\mathbf{S}_n^*(-\mathbf{k}^*) = \exp\left(-\tfrac{1}{2}\mathrm{i}\pi\boldsymbol{\ell}\right)\mathbf{k}^{-1/2}\tilde{\mathbf{f}}(\mathbf{k})\tilde{\mathbf{f}}^{-1}(-\mathbf{k})\mathbf{k}^{1/2}\exp\left(-\tfrac{1}{2}\mathrm{i}\pi\boldsymbol{\ell}\right). \tag{3.22}$$

Combining this equation with (3.10) and (3.20) yields

$$\mathbf{S}_n(\mathbf{k}) = \exp(\mathrm{i}\pi\boldsymbol{\ell})\mathbf{S}_n^{\dagger}(-\mathbf{k}^*)\exp(\mathrm{i}\pi\boldsymbol{\ell}), \tag{3.23}$$

which is the generalization of the reflection relation given by (1.98) in potential scattering.

It is useful at this point to discuss the continuation paths in the complex energy plane implied by relations (3.21) and (3.23). Since the k_i occur in the definition of the Jost functions given by (3.3) and (3.5) and hence in the S-matrix given by (3.10), the value of $\mathbf{S}_n(\mathbf{k})$ is only defined uniquely in terms of the total energy E of the electron–atom system if the sign ambiguities

$$k_i = \pm[2(E - e_i)]^{1/2}, \quad i = 1, \ldots, n, \tag{3.24}$$

which follow from (2.7), are resolved. These signs can be chosen in 2^n different ways and consequently the S-matrix can only be made single valued, or uniformized, by introducing 2^n Riemann sheets in the complex E-plane. We define these sheets in Fig. 3.1, by introducing n branch points $e_i, i = 1, \ldots, n$, with their associated branch cuts chosen to run in each case from $E = e_i$ along the real energy axis to $E = +\infty$. The physical sheet, which we denote by P, is defined by the condition

$$\operatorname{Im} k_i > 0, \quad i = 1, \ldots, n, \tag{3.25}$$

and the physical scattering region, which is illustrated in Fig. 3.1 by arrows, lies on the real energy axis, along the upper edge of the n branch cuts.

Following Eden and Taylor [283], we let U_m denote the unphysical sheet reached from the physical sheet by crossing the branch cuts in Fig. 3.1 which originate from the branch points e_i, $i = 1, \ldots, m$, where $1 \leq m \leq n$. We then find using (3.24) that on U_m

$$\begin{aligned} &\operatorname{Im} k_i < 0, \quad i = 1, \ldots, m, \\ &\operatorname{Im} k_i > 0, \quad i = m+1, \ldots, n. \end{aligned} \tag{3.26}$$

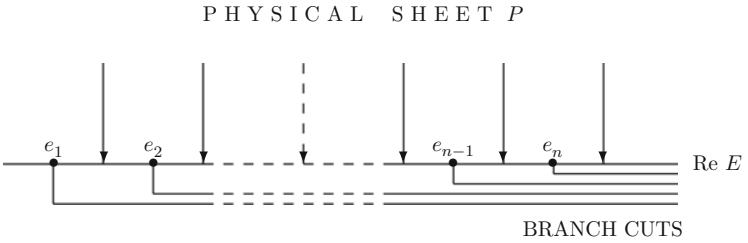

Fig. 3.1 The analytic properties of the multichannel S-matrix in the complex energy plane E, showing the branch points e_i, $i = 1, \ldots, n$, and the associated branch cuts starting from the branch points e_i (where the branch cuts are displaced from the real energy axis for clarity). Also shown is the physical sheet P and the paths, denoted by (*arrows*), from this sheet to reach the physical scattering region on the real energy axis

Furthermore, on the real energy axis between e_m and e_{m+1} k_i is real for $i = 1, \ldots, m$ and positive imaginary for $i = m + 1, \ldots, n$. Other unphysical sheets can be reached by following more complicated paths from the physical sheet so that all combinations of the signs of $\mathrm{Im}\, k_i$ can be achieved on these sheets.

As an example, when $n = 2$ there are $2^n = 4$ Riemann sheets, or three unphysical sheets in addition to the physical sheet. We show in Fig. 3.2 four continuation paths which enable E^* on the unphysical sheets and on the physical sheet to be reached from E on the physical sheet, where E^* denotes the complex conjugate of E. The path labelled (1) goes from E on P to E^* on U_1, the path labelled (2) goes from E on P to E^* on U_2, the path labelled (1,2) goes from E on P to E^* on $U_{1,2}$ and the path labelled (0) goes from E to E^* on the physical sheet P. It is clear from Fig. 3.2 that on $U_{1,2}$, $\mathrm{Im}\, k_1 > 0$ and $\mathrm{Im}\, k_2 < 0$. The signs of $\mathrm{Im}\, k_1$ and $\mathrm{Im}\, k_2$ for E^* on U_1 and U_2 are given by (3.26), while $\mathrm{Im}\, k_1 > 0$ and $\mathrm{Im}\, k_2 > 0$ on P.

Returning to the general case illustrated in Fig. 3.3 where there are n channels, we see that if the point represented by $\mathbf{k}$ in (3.21) and (3.23) lies on the physical sheet defined by (3.25) then the point represented by $\mathbf{k}^*$ lies on U_n defined by (3.26) with $m = n$. In addition, the point represented by $-\mathbf{k}^*$ lies on the physical sheet. Hence the unitarity relation (3.21) can be rewritten as

$$\mathbf{S}_n(E \text{ on } P)\mathbf{S}_n^\dagger(E^* \text{ on } U_n) = \mathbf{I}, \tag{3.27}$$

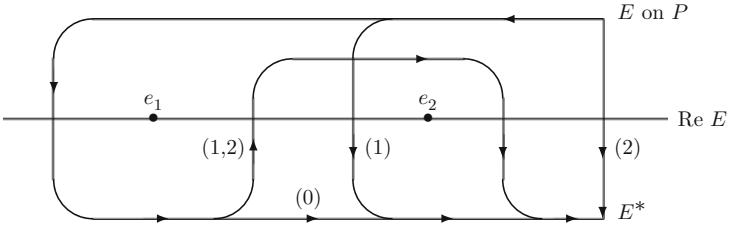

Fig. 3.2 The four continuation paths in the complex energy plane when $n = 2$ which enable E^* on the three unphysical sheets and on the physical sheet to be reached from E on the physical sheet denoted by P. The branch points are denoted by e_1 and e_2

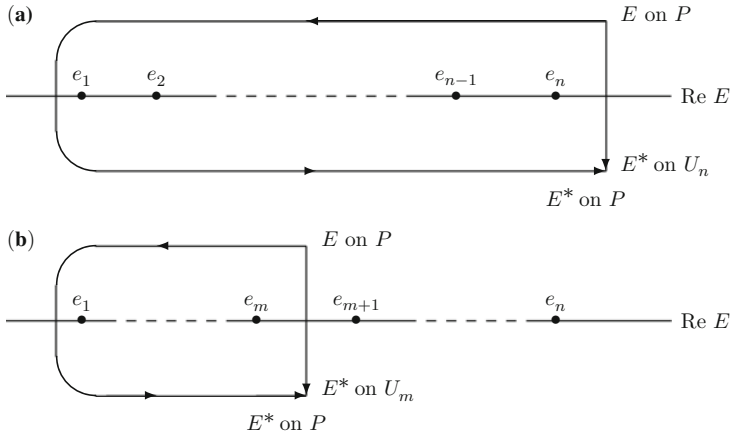

Fig. 3.3 Continuation paths in the complex energy plane when there are n non-degenerate channels, where P denotes the physical sheet and U_n and U_m denote unphysical sheets as explained in the text. The branch points are denoted by $e_i,\ i = 1, \ldots, n$

where E^* on U_n is reached by the path indicated in Fig. 3.3a. In a similar way, the reflection relation (3.23) can be rewritten as

$$\mathbf{S}_n(E \text{ on } P) = \exp(\mathrm{i}\pi\ell)\mathbf{S}_n^{\dagger}(E^* \text{ on } P)\exp(\mathrm{i}\pi\ell), \tag{3.28}$$

where E^* on P is reached by the path also indicated in Fig. 3.3a.

The above discussion can be generalized to determine the analytic properties of the S-matrix under the continuation paths indicated in Fig. 3.3b. Under the continuation from E on P to E^* on U_m we see from (3.26) that the k_i transform according to

$$\begin{aligned} k_i &\to k_i^*, \qquad i = 1, \ldots, m, \\ k_i &\to -k_i^*, \qquad i = m+1, \ldots, n. \end{aligned} \tag{3.29}$$

Hence (3.17) and (3.18) are no longer valid under this continuation and the unitarity relation (3.27) is not satisfied if U_n is replaced by U_m with $m < n$. However, we can show that the $m \times m$-dimensional leading submatrix of $\mathbf{S}_n$ which we call $\mathbf{S}_m$ does satisfy a generalized unitarity relation analogous to (3.27).

To prove this, we introduce an $n \times m$-dimensional solution matrix $\mathbf{G}(\mathbf{k}, r)$ of (3.11) by the equation

$$\mathbf{G}(\mathbf{k}, r) = \mathbf{F}(\mathbf{k}, r)\mathbf{A}(\mathbf{k}), \tag{3.30}$$

where $\mathbf{F}$ is the $n \times n$-dimensional solution matrix defined by (3.4) and $\mathbf{A}$ is an $n \times m$-dimensional matrix which is chosen so that $\mathbf{G}$ is real on the real energy axis in the range between e_m and e_{m+1} and so that in this energy range the exponentially increasing components in the last $n - m$ channels of $\mathbf{F}(\mathbf{k}, \mathbf{r})$ are eliminated. $\mathbf{G}(\mathbf{k}, r)$

thus corresponds to the physical solutions in the energy range $e_m \leq \mathrm{Re}E < e_{m+1}$, where m channels are open and $n-m$ channels are closed. It is then straightforward to show that (3.15), which can be rewritten as

$$\mathbf{F}(E \text{ on } P) = \mathbf{F}^*(E^* \text{ on } U_n), \tag{3.31}$$

is replaced by

$$\mathbf{G}(E \text{ on } P) = \mathbf{G}^*(E^* \text{ on } U_m). \tag{3.32}$$

We now introduce an $m \times m$-dimensional Jost function matrix by the equation

$$\tilde{\mathbf{f}}_m(\pm\mathbf{k}) = W[\mathbf{f}_m(\pm\mathbf{k}, r), \mathbf{G}(\mathbf{k}, r)], \tag{3.33}$$

where $\mathbf{f}_m(\pm\mathbf{k}, r)$ are the first m columns of the solutions defined by (3.3). Hence, in analogy with (3.9) we can write

$$\mathbf{G}(\mathbf{k}, r) = (2\mathrm{i})^{-1}[\mathbf{f}_m(-\mathbf{k}, r)\mathbf{k}_m^{-1}\tilde{\mathbf{f}}_m(\mathbf{k}) - \mathbf{f}_m(\mathbf{k}, r)\mathbf{k}_m^{-1}\tilde{\mathbf{f}}_m(-\mathbf{k})], \tag{3.34}$$

where $\mathbf{k}_m$ is an $m \times m$ diagonal matrix with diagonal elements $k_i, \quad i = 1, \ldots, m$. Comparing this equation with the asymptotic form (2.110) where $n_a = m$ gives immediately

$$\mathbf{S}_m(\mathbf{k}) = \exp\left(\tfrac{1}{2}\mathrm{i}\pi\boldsymbol{\ell}_m\right)\mathbf{k}_m^{-1/2}\tilde{\mathbf{f}}_m(\mathbf{k})\tilde{\mathbf{f}}_m^{-1}(-\mathbf{k})\mathbf{k}_m^{1/2}\exp\left(\tfrac{1}{2}\mathrm{i}\pi\boldsymbol{\ell}_m\right), \tag{3.35}$$

where $\boldsymbol{\ell}_m$ is the $m \times m$ diagonal matrix with diagonal elements $\ell_i, i = 1, \ldots, m$. We can then show from the analytic properties of $\mathbf{f}_m(\pm\mathbf{k}, r)$ and $\mathbf{G}(\pm\mathbf{k}, r)$ that

$$\mathbf{S}_m(E \text{ on } P)\mathbf{S}_m^\dagger(E^* \text{ on } U_m) = \mathbf{I}. \tag{3.36}$$

This is the generalization of the unitarity relation given by (3.27). Equation (3.36), together with the generalization of the reflection relation (3.28), which can be written as

$$\mathbf{S}_m(E \text{ on } P) = \exp(\mathrm{i}\pi\boldsymbol{\ell}_m)\mathbf{S}_m^\dagger(E^* \text{ on } P)\exp(\mathrm{i}\pi\boldsymbol{\ell}_m), \tag{3.37}$$

defines the analytic properties of the $m \times m$-dimensional submatrix $\mathbf{S}_m$.

3.2 Bound States and Resonances

In this section we commence our discussion of bound-state and resonance poles in the S-matrix for multichannel collisions by considering their distribution in the multi-Riemann-sheeted complex energy plane. We then derive an explicit

expression for the multichannel K-matrix and S-matrix in the neighbourhood of an isolated resonance pole using a theoretical approach introduced by Brenig and Haag [137] and Fano [301]. We also derive an expression for the behaviour of the eigenphases near this resonance. We then introduce the projection operator approach of Feshbach [320, 321], used initially to describe nuclear resonance reactions, which has provided a powerful framework for describing resonance phenomena in atomic and molecular collision processes. Finally, we mention that early applications of these theories in electron and photon collisions with atoms and molecules were reviewed by Burke [151, 153].

3.2.1 Bound-State and Resonance Poles in the S-Matrix

In order to discuss the distribution of bound-state and resonance poles in the complex energy plane we consider (3.9) and (3.10) which express, respectively, the physical solution and the S-matrix in terms of the Jost function matrices $\mathbf{f}(\pm\mathbf{k}, r)$ and $\tilde{\mathbf{f}}(\pm\mathbf{k})$. We first diagonalize the $n\times n$-dimensional matrix $\tilde{\mathbf{f}}(-\mathbf{k})$ by the similarity transformation

$$\mathbf{X}^{-1}\tilde{\mathbf{f}}(-\mathbf{k})\mathbf{X} = \mathbf{D}, \tag{3.38}$$

where $\mathbf{D}$ is a diagonal $n \times n$-dimensional matrix. Let us assume that one of the diagonal elements of $\mathbf{D}$, say the first $d_1(E)$, has a simple zero at some energy E_p. It follows that $\tilde{\mathbf{f}}^{-1}(-\mathbf{k})$ and, hence from (3.10), $\mathbf{S}_n(\mathbf{k})$ are both singular with simple poles at $E = E_p$. We substitute (3.38) into (3.9) and postmultiply by $\mathbf{X}$ yielding

$$\mathbf{F}\mathbf{X} = (2\mathrm{i})^{-1}[\mathbf{f}(-\mathbf{k}, r)\mathbf{k}^{-1}\tilde{\mathbf{f}}(\mathbf{k})\mathbf{X} - \mathbf{f}(\mathbf{k}, r)\mathbf{k}^{-1}\mathbf{X}\mathbf{D}]. \tag{3.39}$$

Since $d_1(E_p) = 0$, the first column of $\mathbf{f}(\mathbf{k}, r)\mathbf{k}^{-1}\mathbf{X}\mathbf{D}$ vanishes when $E = E_p$. Hence the corresponding solution can be written as

$$\mathbf{F}\mathbf{x}_1 = (2\mathrm{i})^{-1}\mathbf{f}(-\mathbf{k}, r)\mathbf{k}^{-1}\tilde{\mathbf{f}}(\mathbf{k})\mathbf{x}_1, \quad E = E_p, \tag{3.40}$$

where the vector $\mathbf{x}_1$ is the first column of $\mathbf{X}$. It follows from (3.3) that at a pole in the S-matrix

$$\mathbf{F}\mathbf{x}_1 \underset{r\to\infty}{\sim} \mathrm{e}^{\mathrm{i}\mathbf{k}r}\mathbf{N}, \quad E = E_p, \tag{3.41}$$

where the normalization vector $\mathbf{N} = (2\mathrm{i}\mathbf{k})^{-1}\tilde{\mathbf{f}}(\mathbf{k})\mathbf{x}_1$. This equation is the multichannel generalization of (1.100).

If the energy E_p lies on the physical sheet of the complex energy plane then conditions (3.25) are satisfied. Consequently, the physical solution (3.41) vanishes asymptotically and hence is normalizable. Since the Hamiltonian is Hermitian, all normalizable wave functions must belong to real energy eigenvalues. Hence poles in

the S-matrix on the physical sheet must lie on the real energy axis. If this real energy lies below the first threshold $E < e_1$, then it follows from (3.24) and (3.25) that

$$k_i = +\mathrm{i}\kappa_i = +\mathrm{i}[2(e_i - E)]^{1/2}, \quad i = 1, \ldots, n, \tag{3.42}$$

where the κ_i are real and positive. Hence the solution defined by (3.41) has the asymptotic form

$$\mathbf{F}\mathbf{x}_1 \underset{r\to\infty}{\sim} \mathrm{e}^{-\boldsymbol{\kappa} r}\mathbf{N}, \quad E = E_p, \tag{3.43}$$

where $\boldsymbol{\kappa}$ is an $n \times n$-dimensional diagonal matrix with diagonal elements κ_i, $i = 1, \ldots, n$. Since the solution corresponding to (3.43) is normalizable it clearly corresponds to a bound state. We illustrate the position of such bound-state poles by crosses in Fig. 3.4.

In certain circumstances poles in the S-matrix can lie on the real energy axis with $E > e_1$. Consider, for example, real energies in the range $e_m < E < e_{m+1}$. Poles can lie in this range of energies if the channels with threshold energies e_i, $i = 1, \ldots, m$, are not coupled to the channels with threshold energies e_i, $i = m+1, \ldots, n$. This occurs, for example, if these two sets of channels have a different conserved quantum number such as parity and hence are not coupled by the Hamiltonian. In this case the $n \times n$-dimensional S-matrix $\mathbf{S}_n$ can be partitioned into disconnected sub-matrices as follows:

$$\mathbf{S}_n = \begin{bmatrix} \mathbf{S}_m & 0 \\ 0 & \mathbf{S}_{n-m} \end{bmatrix}, \tag{3.44}$$

where $\mathbf{S}_m$ has dimension $m \times m$ and $\mathbf{S}_{n-m}$ has dimension $(n-m) \times (n-m)$. From the generalized unitarity relation (3.36), $\mathbf{S}_m$ must be unitary and hence non-singular in this range of energies. However, a pole can occur in $\mathbf{S}_{n-m}$. A pole of this type corresponds to a bound state lying in the continuum and is denoted by an open circle in Fig. 3.4.

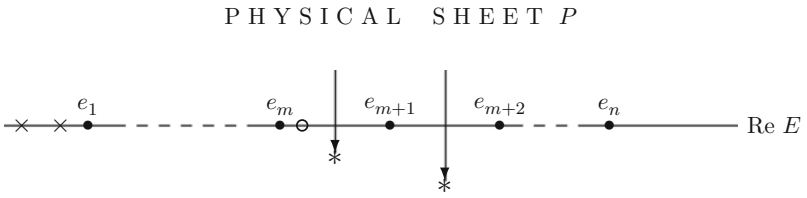

Fig. 3.4 Distribution of S-matrix poles in the complex energy plane. $\times$, bound-state poles lying on the physical sheet; $\circ$, bound-state pole lying in the continuum on the real energy axis; $*$, resonance poles lying on unphysical sheets U_m and U_{m+1}. The *arrows* denote the continuation paths from the physical sheet P to the resonance poles. The branch points are denoted by e_i, $i = 1, \ldots, n$

In the general case, when all n channels are coupled by the Hamiltonian, poles cannot occur in the S-matrix for real energies with $E > e_1$ corresponding to the physical scattering region, except in very exceptional circumstances. This is because the unitarity equation (3.36) would then be violated. However poles can occur on any of the unphysical sheets U_m since the sign of at least one $\mathrm{Im}\, k_i,\ i = 1, \ldots, n$, is then negative and hence from (3.41) the corresponding wave function is then not normalizable. If such poles lie close to the physical scattering region they give rise to observable effects and are called resonance poles and the corresponding wave functions, which satisfy outgoing wave boundary conditions, are often called Siegert states [876]. We define the real and imaginary parts of the energy of such a pole by

$$E_p = E_r - \frac{1}{2}\mathrm{i}\Gamma, \quad \text{on } U_m, \tag{3.45}$$

where E_r and Γ are both real and Γ is small and positive. Poles of this type are denoted by an asterisk in Fig. 3.4. We also denote by arrows in this figure the continuation paths from the physical sheet to these resonance poles. The generalized unitarity relation (3.36) shows that at the corresponding energies

$$E_p^* = E_r + \frac{1}{2}\mathrm{i}\Gamma, \quad \text{on } P, \tag{3.46}$$

one of the eigenvalues of $\mathbf{S}_m$ has a simple zero, that is the rank of $\mathbf{S}_m$ is $m - 1$. Eden and Taylor [283] have shown that the presence of a resonance pole on U_m usually also implies the presence of "shadow poles" on other Riemann sheets of the complex energy plane which are further removed from the physical scattering region. These shadow poles can play a role in a number of applications such as dissociative attachment and multiphoton ionization discussed in later chapters in this monograph.

Finally, we note that the preceding discussion was based on the assumption that bound-state and resonance poles in the S-matrix are simple. Although there is no general principle that guarantees that all such poles are simple, in practice this is usually the case. However, in atomic multiphoton processes, discussed in Chap. 9, laser induced degenerate states, or LIDS, corresponding to double poles in the S-matrix have been found in detailed calculations (see Sect. 9.2.3). If the S-matrix does contain a double pole in the complex energy plane then the main effects will be to distort the shape of the associated resonance profile from that considered in the next section and to produce a decay which deviates from the usual exponential behaviour. These effects have been considered by Goldberger and Watson [387], Newton [683] and Kylstra and Joachain [557].

3.2.2 Behaviour of the S-Matrix Near a Resonance

In this section we derive explicit expressions for the behaviour of the multichannel K-matrix and S-matrix in the physical scattering region near an isolated resonance pole lying on an adjacent unphysical sheet of the complex energy plane. We also

derive expressions for the behaviour of the eigenphases in the neighbourhood of a resonance. This was originally discussed by Brenig and Haag [137] and by Fano [301] and we consider here the configuration interaction theory of Fano.

Following Sect. 3.1, we consider low-energy elastic and inelastic electron collisions with multi-electron atoms and atomic ions containing N electrons and we analyse the interaction of one discrete state with n continuum states. We sub-divide configuration space into a zero-order discrete state, represented by a quadratically integrable function $\chi_0^0(\mathbf{X}_{N+1})$, which gives rise to the resonance, and n zero-order continuum states $\psi_{jE}^0(\mathbf{X}_{N+1})$, $j = 1, \ldots, n$, which do not have resonances or thresholds in the energy range of interest. We can expand these zero-order continuum states as

$$\begin{aligned}\psi_{jE}^0(\mathbf{X}_{N+1}) = \mathcal{A}\sum_{i=1}^{n}\overline{\Phi}_i(\mathbf{X}_N;\hat{\mathbf{r}}_{N+1}\sigma_{N+1})r_{N+1}^{-1}F_{ij}^0(r_{N+1}) \\ + \sum_{i=1}^{m}\chi_i^0(\mathbf{X}_{N+1})b_{ij}^0, \quad j = 1, \ldots, n,\end{aligned} \tag{3.47}$$

where we have adopted a notation analogous to expansion (2.57) and where the superscript Γ, which denotes the conserved quantum numbers, has been omitted for notational convenience. It is convenient in the following analysis to include only the n open channels in the first expansion in (3.47). The χ_i^0, $i = 1, \ldots, m$, in the second expansion are then zero-order quadratically integrable functions, which represent the effect of the closed channels whose thresholds lie above the energy range of interest.

We can now assume, without approximation, that these zero-order states satisfy the orthonormality relations

$$\begin{aligned}\langle\chi_0^0|\chi_0^0\rangle &= 1, \\ \langle\chi_0^0|\psi_{jE}^0\rangle &= 0, \quad j = 1, \ldots, n, \\ \langle\psi_{jE}^0|\psi_{j'E'}^0\rangle &= \delta_{jj'}\delta(E - E'), \quad j, j' = 1, \ldots, n.\end{aligned} \tag{3.48}$$

We also define the matrix elements of the $(N + 1)$-electron Hamiltonian H_{N+1} in this zero-order basis by the equations

$$\begin{aligned}\langle\chi_0^0|H_{N+1}|\chi_0^0\rangle &= E_0, \\ \langle\chi_0^0|H_{N+1}|\psi_{jE}^0\rangle &= V_j(E), \quad j = 1, \ldots, n, \\ \langle\psi_{jE}^0|H_{N+1}|\psi_{j'E'}^0\rangle &= E\delta_{jj'}\delta(E - E'), \quad j,\ j' = 1, \ldots, n,\end{aligned} \tag{3.49}$$

where we choose real asymptotic boundary conditions for the radial functions $F_{ij}^0(r)$ in (3.47) so that the $V_j(E)$ are real. The assumption made in the last of Eqs. (3.49), that the Hamiltonian is prediagonalized in the subspace spanned by the zero-order continuum states, is inessential and has been relaxed by Fano and Prats [309].

We introduce n new continuum basis states θ_{jE}, $j = 1, \ldots, n$, which are linear combinations of the basis ψ^0_{jE}, chosen so that only the first, θ_{1E}, interacts through the Hamiltonian with the discrete state χ^0_0. We define

$$\theta_{iE} = \sum_{j=1}^{n} \psi^0_{jE} U_{ji}(E), \quad i = 1, \ldots, n, \tag{3.50}$$

where $\mathbf{U}$ is an orthogonal matrix whose first column is defined by

$$U_{j1}(E) = V_j(E) \left[\sum_{i=1}^{n} V_i(E)^2 \right]^{-1/2}, \quad j = 1, \ldots, n, \tag{3.51}$$

while the remaining $n - 1$ columns are orthonormal and are orthogonal to the first column but are otherwise arbitrary. In terms of this new basis, Eqs.(3.49) are replaced by

$$\begin{aligned} \langle \chi^0_0 | H_{N+1} | \chi^0_0 \rangle &= E_0, \\ \langle \chi^0_0 | H_{N+1} | \theta_{jE} \rangle &= V(E)\delta_{j1}, \quad j = 1, \ldots, n, \\ \langle \theta_{jE} | H_{N+1} | \theta_{j'E'} \rangle &= E\delta_{jj'}\delta(E - E'), \quad j, j' = 1, \ldots, n, \end{aligned} \tag{3.52}$$

where we have introduced the real quantity

$$V(E) = \left[\sum_{i=1}^{n} V_i(E)^2 \right]^{1/2}, \tag{3.53}$$

which is a measure of the strength of the interaction of the discrete state with the continuum.

The eigensolutions of the Schrödinger equation which diagonalize the Hamiltonian can now be expanded in terms of these new zero-order states as follows:

$$\begin{aligned} \Psi_{1E} &= \int \theta_{1E'} a(E, E') \mathrm{d}E' + \chi^0_0 b(E), \\ \Psi_{jE} &= \theta_{jE}, \quad j = 2, \ldots, n, \end{aligned} \tag{3.54}$$

where the coefficients $a(E, E')$ and $b(E)$ are determined by projecting the Schrödinger equation

$$(H_{N+1} - E)\Psi_{1E} = 0 \tag{3.55}$$

onto the zero-order basis states θ_{1E} and χ^0_0. We obtain

$$\begin{aligned} \langle \theta_{1E'} | H_{N+1} - E | \Psi_{1E} \rangle &= 0, \\ \langle \chi^0_0 | H_{N+1} - E | \Psi_{1E} \rangle &= 0. \end{aligned} \tag{3.56}$$

Substituting for Ψ_{1E} from (3.54) into (3.56) and using (3.48) and (3.52), then gives

$$E'a(E,E') + V(E')b(E) = Ea(E,E'),$$
$$\int V(E')a(E,E')\mathrm{d}E' + E_0 b(E) = Eb(E). \tag{3.57}$$

The first equation in (3.57) can be formally solved for $a(E, E')$ yielding

$$a(E,E') = \left[\frac{\mathcal{P}}{E-E'} + z(E)\delta(E-E')\right]V(E')b(E), \tag{3.58}$$

where $\mathcal{P}$ is the principal value integral and $z(E)$ is then obtained by substituting (3.58) for $a(E, E')$ into the second equation in (3.57). We obtain

$$z(E) = \frac{E - E_0 - \Delta(E)}{V(E)^2}, \tag{3.59}$$

where we have introduced the quantity

$$\Delta(E) = \mathcal{P}\int \frac{V(E')^2}{E-E'}\mathrm{d}E', \tag{3.60}$$

which is called the resonance shift.

In order to determine the K-matrix and S-matrix for the interacting system, we assume that the zero-order reduced radial wave function matrix $\mathbf{F}^0$ in (3.47) satisfies the real K-matrix asymptotic boundary conditions

$$\mathbf{F}^0(r) \underset{r\to\infty}{\sim} \left(\frac{2}{\pi\mathbf{k}}\right)^{1/2}(\sin\boldsymbol{\theta} + \cos\boldsymbol{\theta}\mathbf{K}_0)(\mathbf{I}+\mathbf{K}_0^2)^{-1/2}. \tag{3.61}$$

In this equation $\mathbf{F}^0$ is an $n \times n$-dimensional matrix, $\mathbf{k}$ and $\boldsymbol{\theta}$ are diagonal matrices, where the diagonal elements of $\boldsymbol{\theta}$ are defined by (2.82), (2.83) and(2.84), and $\mathbf{K}_0$ is the multichannel zero-order $n \times n$-dimensional K-matrix obtained in the absence of the interaction between the zero-order discrete state and the continuum states. In analogy with our discussion in Sect. 1.1, see (1.21), the coefficient $(2/\pi\mathbf{k})^{1/2}$ and the factor $(1+\mathbf{K}_0^2)^{-1/2}$ in (3.61) are included so that the δ-function orthonormality relation in the last equation in (3.48) is satisfied. It follows from (3.47), (3.50) and (3.54) that Ψ_{jE} can be expanded as follows:

$$\Psi_{jE}(\mathbf{x}_1,\ldots,\mathbf{x}_{N+1}) = \mathcal{A}\sum_{i=1}^{n}\overline{\Phi}_i(\mathbf{x}_1,\ldots,\mathbf{x}_N;\hat{\mathbf{r}}_{N+1}\sigma_{N+1})r_{N+1}^{-1}G_{ij}(r_{N+1})$$
$$+\sum_{i=0}^{m}\chi_i(\mathbf{x}_1,\ldots,\mathbf{x}_N)c_{ij}, \quad j=1,\ldots,n, \tag{3.62}$$

where the reduced radial wave function matrix $\mathbf{G}$ in this equation is obtained by substituting (3.58) into (3.54), using (3.61) and carrying out the integration over E'.

We find that $\mathbf{G}$ satisfies the asymptotic boundary conditions

$$\begin{aligned}\mathbf{G}_1(r) &\underset{r\to\infty}{\sim} \left(\frac{2}{\pi\mathbf{k}}\right)^{1/2} \{\sin\boldsymbol{\theta}[z(E)+\pi\mathbf{K}_0]+\cos\boldsymbol{\theta}[-\pi+z(E)\mathbf{K}_0]\} \\ &\quad\times(1+\mathbf{K}_0^2)^{-1/2}\mathbf{U}_1, \\ \mathbf{G}_j(r) &\underset{r\to\infty}{\sim} \left(\frac{2}{\pi\mathbf{k}}\right)^{1/2} (\sin\boldsymbol{\theta}+\cos\boldsymbol{\theta}\mathbf{K}_0)(1+\mathbf{K}_0^2)^{-1/2}\mathbf{U}_j, \\ &\quad j=2,\ldots,n, \end{aligned} \tag{3.63}$$

where $\mathbf{G}_j$ and $\mathbf{U}_j$ are the jth columns of the $n\times n$-dimensional matrices $\mathbf{G}$ and $\mathbf{U}$, respectively. Also the quadratically integrable functions $\chi_i,\ i=0,\ldots,m$, in (3.62) are linear combinations of the zero-order discrete state represented by the quadratically integrable function χ_0^0 and the zero-order quadratically integrable functions $\chi_i^0,\ i=1,\ldots,m$, in (3.47).

Equations (3.63) can be written in a more convenient form by post-multiplying by $\mathbf{U}^{-1}$ and substituting for $z(E)$ from (3.59). This gives

$$\begin{aligned}\mathbf{G}(r)\mathbf{U}^{-1} \underset{r\to\infty}{\sim} \left(\frac{2}{\pi\mathbf{k}}\right)^{1/2} \Bigg[&\sin\boldsymbol{\theta}\left((1+\mathbf{K}_0^2)^{-1/2}+\mathbf{K}_0(1+\mathbf{K}_0^2)^{-1/2}\frac{1}{2}\Gamma\frac{\boldsymbol{\gamma}\times\boldsymbol{\gamma}}{E-E_r}\right) \\ &+\cos\boldsymbol{\theta}\left(\mathbf{K}_0(1+\mathbf{K}_0^2)^{-1/2}-(1+\mathbf{K}_0^2)^{-1/2}\frac{1}{2}\Gamma\frac{\boldsymbol{\gamma}\times\boldsymbol{\gamma}}{E-E_r}\right)\Bigg], \end{aligned} \tag{3.64}$$

where the partial width amplitudes γ_i are defined by

$$\gamma_i = V_i V^{-1}, \quad i=1,\ldots,n, \tag{3.65}$$

and the resonance energy E_r and total width Γ are defined by

$$\begin{aligned} E_r &= E_0+\Delta, \\ \Gamma &= 2\pi V^2. \end{aligned} \tag{3.66}$$

The quantity $\boldsymbol{\gamma}\times\boldsymbol{\gamma}$ in (3.64) is a real symmetric $n\times n$-dimensional matrix with matrix elements $\gamma_i\gamma_j$ where we note that the real K-matrix boundary condition (3.61) implies that $V_j(E),\ j=1,\ldots,n$, defined by (3.49), are real and hence the partial width amplitudes γ_i are real.

By taking linear combinations of the solutions defined by (3.64), we can choose the reduced radial wave functions to have the following asymptotic form analogous to that given by (3.61)

$$\mathbf{F}(r) \underset{r\to\infty}{\sim} \left(\frac{2}{\pi\mathbf{k}}\right)^{1/2} (\sin\boldsymbol{\theta}+\cos\boldsymbol{\theta}\mathbf{K})(\mathbf{I}+\mathbf{K}^2)^{-1/2}, \tag{3.67}$$

where the K-matrix is defined by

$$\mathbf{K} = \mathbf{K}_0 - \frac{1}{2}\Gamma \frac{(1+\mathbf{K}_0^2)^{1/2}\boldsymbol{\gamma} \times \boldsymbol{\gamma}(1+\mathbf{K}_0^2)^{1/2}}{E - E_r + \frac{1}{2}\Gamma \boldsymbol{\gamma}^{\mathrm{T}}\mathbf{K}_0\boldsymbol{\gamma}}. \tag{3.68}$$

The S-matrix, which is related to the K-matrix by (2.112), can then be written as

$$\mathbf{S} = \mathbf{S}_0 - \mathrm{i}\Gamma \frac{\mathbf{S}_0^{1/2}\boldsymbol{\gamma} \times \boldsymbol{\gamma}\mathbf{S}_0^{1/2}}{E - E_r + \frac{1}{2}\mathrm{i}\Gamma}, \tag{3.69}$$

where the zero-order S-matrix $\mathbf{S}_0$ is defined by

$$\mathbf{S}_0 = \frac{\mathbf{I} + \mathrm{i}\mathbf{K}_0}{\mathbf{I} - \mathrm{i}\mathbf{K}_0}. \tag{3.70}$$

Equations (3.68) and (3.69) are the basic expressions which describe the behaviour of the K-matrix and S-matrix in the neighbourhood of an isolated resonance. We see that all elements of the S-matrix are singular at the complex energy $E = E_r - \frac{1}{2}\mathrm{i}\Gamma$ while the K-matrix elements are singular at the shifted real energy $E = E_r - \frac{1}{2}\Gamma\boldsymbol{\gamma}^{\mathrm{T}}\mathbf{K}_0\boldsymbol{\gamma}$. Equation (3.68), which is discussed further by Burke [153], forms the basis of a computer program written by Bartschat and Burke [64] which enables the resonance position and its total and partial widths to be determined from K-matrix elements calculated at a few energy values in the neighbourhood of an isolated resonance.

Finally, using the definition of $V_j(E)$ given by (3.49) together with the definitions of γ_j and Γ given by (3.65) and (3.66), we find that

$$\gamma_j \Gamma^{1/2} = (2\pi)^{1/2}\langle \chi_0^0 | H_{N+1} | \psi_{jE}^0 \rangle, \tag{3.71}$$

where the reduced radial wave functions $F_{ij}^0(r)$ in ψ_{jE}^0 satisfy the real K-matrix boundary conditions (3.61). Squaring (3.71), summing over j and using (3.53) and (3.65) then yields

$$\Gamma = 2\pi \sum_{j=1}^{n} \left[\langle \chi_0^0 | H_{N+1} | \psi_{jE}^0 \rangle \right]^2. \tag{3.72}$$

This expression has often been used to calculate an approximate value for the total resonance width Γ given approximate representations for the zero-order discrete state χ_0^0 and the zero-order continuum states ψ_{jE}^0, $j = 1, \ldots, n$.

3.2.3 *Behaviour of Eigenphases Near a Resonance*

We have shown in Sect. 1.3 that in the case of potential scattering the phase shift increases by approximately π radians as the energy increases through the resonance

energy, as described by (1.105) and (1.106). In this section we show that the eigenphase sum

$$\delta_{\text{sum}} = \sum_{i=1}^{n} \delta_i, \tag{3.73}$$

where the eigenphases δ_i are defined by (2.113) and (2.114), satisfies a generalization of these equations. In addition, we will derive an equation satisfied by the individual eigenphases near a resonance. As in Sect. 3.2.2, we assume that n channels are open.

Following (2.113), we diagonalize the S-matrix defined by (3.69) giving

$$\begin{aligned} \mathbf{S} &= \mathbf{A} \exp(2\mathrm{i}\boldsymbol{\Delta})\mathbf{A}^{\mathrm{T}} \\ &= \mathbf{A}_0 \exp(\mathrm{i}\boldsymbol{\Delta}_0)\mathbf{A}_0^{\mathrm{T}} \left[1 - \mathrm{i}\Gamma \frac{\boldsymbol{\gamma} \times \boldsymbol{\gamma}}{E - E_r + \frac{1}{2}\mathrm{i}\Gamma} \right] \mathbf{A}_0 \exp(\mathrm{i}\boldsymbol{\Delta}_0)\mathbf{A}_0^{\mathrm{T}}, \end{aligned} \tag{3.74}$$

where $\mathbf{A}$ and $\mathbf{A}_0$ are the real orthogonal matrices which diagonalize $\mathbf{S}$ and $\mathbf{S}_0$, respectively, and $\boldsymbol{\Delta}$ and $\boldsymbol{\Delta}_0$ are diagonal matrices whose diagonal elements are the eigenphases $\delta_i, i = 1, \ldots, n$ and the zero-order non-resonant eigenphases $\delta_i^0, i = 1, \ldots, n$, respectively. We now take the determinant of both sides of (3.74) yielding

$$\exp\left(2\mathrm{i}\delta_{\text{sum}}\right) = \exp(2\mathrm{i}\delta_{\text{sum}}^0) \det \left[1 - \mathrm{i}\Gamma \frac{\boldsymbol{\gamma} \times \boldsymbol{\gamma}}{E - E_r + \frac{1}{2}\mathrm{i}\Gamma} \right], \tag{3.75}$$

where in analogy with (3.73) we have defined

$$\delta_{\text{sum}}^0 = \sum_{i=1}^{n} \delta_i^0. \tag{3.76}$$

We now observe from (3.53) and (3.65) that $\boldsymbol{\gamma}^{\mathrm{T}}\boldsymbol{\gamma} = 1$. Hence by diagonalizing the matrix in square brackets in (3.75) we find that

$$\det \left[1 - \mathrm{i}\Gamma \frac{\boldsymbol{\gamma} \times \boldsymbol{\gamma}}{E - E_r + \frac{1}{2}\mathrm{i}\Gamma} \right] = \exp \left[2\mathrm{i} \tan^{-1} \frac{\frac{1}{2}\Gamma}{E_r - E} \right]. \tag{3.77}$$

Combining (3.75) and (3.77) then yields the equation

$$\delta_{\text{sum}} = \delta_{\text{sum}}^0 + \tan^{-1} \frac{\frac{1}{2}\Gamma}{E_r - E}. \tag{3.78}$$

This equation, obtained by Hazi [446], is the multichannel generalization of (1.105) and (1.106) describing the behaviour of the phase shift near a resonance in potential

scattering. We see that the resonant part of $\delta_{\rm sum}$, given by the second term on the right-hand side of (3.78), increases by π radians as the energy increases through the resonance, while the non-resonant term $\delta^0_{\rm sum}$ is smoothly varying with energy. Equation (3.78) is often used to determine the position and width of a multichannel resonance from the calculated S-matrix (e.g. [918]). Also, Quigley et al. [761, 762] combined this equation with the analytic properties of the R-matrix to obtain an accurate "QB" procedure for analysing resonances.

In order to determine the behaviour of the individual eigenphases in the neighbourhood of a resonance we follow Macek [620] by diagonalizing the S-matrix defined by (3.69) in two stages. We first transform $\mathbf{S}$ by the real orthogonal matrix $\mathbf{A}_0$ which diagonalizes $\mathbf{S}_0$ giving

$$\mathbf{S}' = \mathbf{A}_0^{\rm T}\mathbf{S}\mathbf{A}_0 = \exp(2{\rm i}\boldsymbol{\Delta}) - {\rm i}\Gamma\frac{\exp({\rm i}\boldsymbol{\Delta}_0)\mathbf{y}\times\mathbf{y}\exp({\rm i}\boldsymbol{\Delta}_0)}{E-E_r+\frac{1}{2}{\rm i}\Gamma}, \tag{3.79}$$

where $\mathbf{y} = \mathbf{A}_0^{\rm T}\boldsymbol{\gamma}$ is a vector whose elements give the amplitudes for the decay of the resonance into the eigenchannels of $\mathbf{S}_0$. We then substitute (3.79) into the eigenvalue equation

$$\mathbf{S}'\mathbf{b}_j = \exp(2{\rm i}\delta_j)\mathbf{b}_j, \quad j = 1,\ldots,n, \tag{3.80}$$

where δ_j is the jth eigenphase of $\mathbf{S}$. We obtain

$$\exp(2{\rm i}\delta_j)\mathbf{b}_j = \exp(2{\rm i}\boldsymbol{\Delta}_0)\mathbf{b}_j - {\rm i}\Gamma\frac{\exp({\rm i}\boldsymbol{\Delta}_0)\mathbf{y}}{E-E_r+\frac{1}{2}{\rm i}\Gamma}a_j, \tag{3.81}$$

where a_j is defined by

$$a_j = \mathbf{y}^{\rm T}\exp({\rm i}\boldsymbol{\Delta}_0)\mathbf{b}_j. \tag{3.82}$$

Equation (3.81) defines the vector $\mathbf{b}_j$ in terms of the quantity a_j. Substituting this expression for $\mathbf{b}_j$ into (3.82) then yields the consistency relation

$$a_j = -\frac{{\rm i}\Gamma}{E-E_r+\frac{1}{2}{\rm i}\Gamma}\sum_{i=1}^{n} y_i^2\frac{\exp(2{\rm i}\delta_i^0)}{\exp(2{\rm i}\delta_j)-\exp(2{\rm i}\delta_i^0)}a_j, \quad j = 1,\ldots,n. \tag{3.83}$$

In order for (3.83) to have a non-trivial solution, the coefficients of a_j on both sides must be equal. Using the condition $\mathbf{y}^{\rm T}\mathbf{y} = \boldsymbol{\gamma}^{\rm T}\boldsymbol{\gamma} = 1$ we obtain the required relation

$$E - E_r = \frac{1}{2}\Gamma\sum_{i=1}^{n} y_i^2\cot(\delta_i^0-\delta_j), \quad j = 1,\ldots,n. \tag{3.84}$$

When $n = 1$ this equation reduces to

$$\delta = \delta^0 + \tan^{-1} \frac{\frac{1}{2}\Gamma}{E_r - E}, \tag{3.85}$$

which corresponds to (3.78) obtained earlier.

Equations (3.84) define the behaviour of the eigenphases δ_j as a function of E. For any given energy this equation has n solutions, each solution δ_j lying between adjacent values of the non-resonant eigenphases δ_i^0. As the energy increases from a value well below the resonance energy E_r to a value well above E_r, the corresponding eigenphases increase from close to and just above each non-resonant eigenphase δ_i^0 to close to and just below the next higher non-resonant eigenphase δ_{i+1}^0. Taking the derivative of (3.84) with respect to the energy E and assuming that the δ_i^0 are independent of energy we obtain

$$1 = \frac{1}{2}\Gamma \frac{\mathrm{d}\delta_j}{\mathrm{d}E} \sum_{i=1}^{n} y_i^2 \mathrm{cosec}^2(\delta_i^0 - \delta_j), \quad j = 1, \ldots, n, \tag{3.86}$$

which shows that each eigenphase δ_j increases monotonically with energy. It also follows from this equation that the eigenphases δ_j increase most rapidly near E_r.

As an illustration of (3.84), we show in Fig. 3.5 the calculated eigenphase sum δ_{sum} and the three eigenphases δ_1, δ_2 and δ_3 in radians for e^-–H collisions, plotted as a function of the incident electron energy in Rydbergs in the neighbourhood of the $^1S^e$ resonance lying between the $n = 2$ and 3 thresholds at ~ 0.862 Rydbergs. The

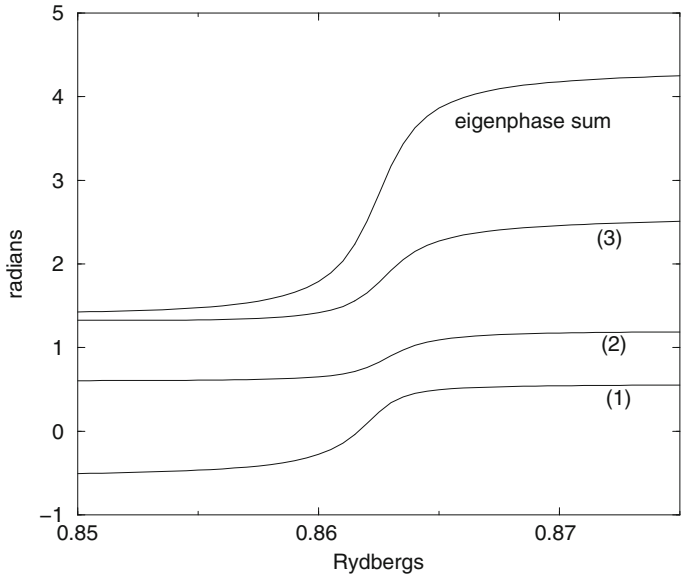

Fig. 3.5 The behaviour of the eigenphase sum δ_{sum} and the eigenphases δ_1, δ_2 and δ_3, labelled (*1*), (*2*) and (*3*), respectively, for e^-–H collisions in the neighbourhood of the $^1S^e$ resonance lying below the $n = 3$ thresholds at an incident electron energy ~ 0.862 Rydbergs

calculation, carried out using the R-matrix method discussed in Chap. 5, retained the six atomic hydrogen target states 1s, 2s, 2p, 3s, 3p and 3d in the close coupling expansion (2.57) for the conserved quantum numbers $L = 0$, $S = 0$ and $\pi =$ even. This results in six coupled channels in (2.63), where three channels, corresponding to the 1s, 2s and 2p states, are open and the three remaining channels, corresponding to the 3s, 3p and 3d states, are closed. Hence $n = 6$, $n_a = 3$ and $n_b = 3$ in (2.79) and the corresponding K- and S-matrices have dimensions 3×3. The eigenphase sum and the three eigenphases are seen to be continuous functions of energy through the resonance which was achieved by adding or subtracting the appropriate multiple of π radians at each calculated energy. As expected $\delta_{\rm sum}$, which is given by (3.78), increases by approximately π radians as the energy increases through the resonance. Also the individual eigenphases behave as described in the preceding paragraph. Further details of e^-–H collision calculations and the resonances that occur are given in Sect. 5.6.1 where we discuss the results of solving (2.63) using the R-matrix method.

3.2.4 Time-Delay Matrix

In the previous sections we have shown that the presence of poles in the S-matrix, lying on unphysical sheets of the complex energy plane close to the physical scattering region, gives rise to resonance effects in the corresponding eigenphases and scattering amplitudes. It was shown by Wigner [971] that a resonance not only gives a sharp peak or dip in the cross section but also gives rise to a time delay in the collision. In this section we consider the time delay caused by these resonances and, following the work of Smith [881], we introduce the time-delay matrix $\mathbf{Q}(E)$[1] on the real energy axis. We also relate the trace of this matrix to the derivative of the eigenphase sum with respect to energy and we show that this quantity often provides an accurate procedure for analysing overlapping resonances.

It was shown in early work by Eisenbud [288], Bohm [121] and Wigner [971], using wave-packet analyses, that the time delay Δt which arises in a single-channel collision can be described in terms of the derivative of the phase shift δ with respect to energy E by

$$\Delta t = 2\frac{\mathrm{d}\delta}{\mathrm{d}E}, \tag{3.87}$$

in atomic units. Remembering that the single-channel S-matrix is related to the phase shift δ by $S = \exp(2\mathrm{i}\delta)$ we find that

$$\Delta t = \mathrm{i}S\frac{\mathrm{d}S^*}{\mathrm{d}E} \quad = -\mathrm{i}\frac{\mathrm{d}S}{\mathrm{d}E}S^*, \tag{3.88}$$

where S^* is the complex conjugate of S.

[1] In the original work of Smith [881] $\mathbf{Q}(E)$ was called the lifetime matrix.

In the analysis of Smith [881], which was considered further by Celenza and Tobocman [206], the time delay was analysed using a steady-state wave function describing the collision. In this analysis, the lifetime is determined by considering the excess number of particles in an interaction region, after subtracting the number of particles that would have been present in the absence of the interaction. This excess number will remain finite even if the integration is taken to infinity, provided that the interaction vanishes rapidly enough at large distances. This excess, divided by the total flux in (or out) through a closed surface at large distances from the centre of the interaction region, gives the required lifetime. Using this independent analysis of the time delay yields the same results as the wave-packet analysis which leads to (3.88).

Smith [881] also generalized (3.88) to multichannel collisions by introducing a time-delay matrix $\mathbf{Q}$. In this analysis (3.88) becomes

$$\mathbf{Q} = \mathrm{i}\mathbf{S}\frac{\mathrm{d}\mathbf{S}^\dagger}{\mathrm{d}E} \quad = -\mathrm{i}\frac{\mathrm{d}\mathbf{S}}{\mathrm{d}E}\mathbf{S}^\dagger, \tag{3.89}$$

where $\mathbf{Q} = \mathbf{Q}^\dagger$ is hermitian and, like the S-matrix $\mathbf{S}$, has dimension $n \times n$, where n is the number of open channels at the energy E. Following Igarashi and Shimamura [486] we can relate the trace of the time-delay matrix $\mathbf{Q}$ to the eigenphase sum δ_{sum}, defined by (3.78). We first diagonalize the S-matrix by a real orthogonal transformation $\mathbf{A}$. Following (2.113) we write

$$\mathbf{A}^{\mathrm{T}}\mathbf{S}\mathbf{A} = \exp(2\mathrm{i}\boldsymbol{\Delta}) = \boldsymbol{\Lambda}, \tag{3.90}$$

where the diagonal elements of $\boldsymbol{\Lambda}$ can be expressed in terms of the eigenphases δ_i, as follows:

$$\Lambda_{ii} = \exp(2\mathrm{i}\delta_i), \quad i = 1, \ldots, n. \tag{3.91}$$

We find using (3.90) that

$$2\frac{\mathrm{d}\boldsymbol{\Delta}}{\mathrm{d}E} = \mathrm{i}\boldsymbol{\Lambda}\frac{\mathrm{d}\boldsymbol{\Lambda}^\dagger}{\mathrm{d}E}, \tag{3.92}$$

and

$$\frac{\mathrm{d}\boldsymbol{\Lambda}^\dagger}{\mathrm{d}E} = \mathbf{A}^{\mathrm{T}}\frac{\mathrm{d}\mathbf{S}^\dagger}{\mathrm{d}E}\mathbf{A} + \frac{\mathrm{d}\mathbf{A}^{\mathrm{T}}}{\mathrm{d}E}\mathbf{S}^\dagger\mathbf{A} + \mathbf{A}^{\mathrm{T}}\mathbf{S}^\dagger\frac{\mathrm{d}\mathbf{A}}{\mathrm{d}E}. \tag{3.93}$$

Substituting (3.93) into (3.92) and using (3.90) gives

$$2\frac{\mathrm{d}\boldsymbol{\Delta}}{\mathrm{d}E} = \mathrm{i}\left(\mathbf{A}^{\mathrm{T}}\mathbf{S}\frac{\mathrm{d}\mathbf{S}^\dagger}{\mathrm{d}E}\mathbf{A} + \mathbf{A}^{\mathrm{T}}\mathbf{S}\mathbf{A}\frac{\mathrm{d}\mathbf{A}^{\mathrm{T}}}{\mathrm{d}E}\mathbf{S}^\dagger\mathbf{A} + \mathbf{A}^{\mathrm{T}}\frac{\mathrm{d}\mathbf{A}}{\mathrm{d}E}\right). \tag{3.94}$$

Taking the trace of this equation then gives

$$\mathrm{Tr}\left(2\frac{\mathrm{d}\boldsymbol{\Delta}}{\mathrm{d}E}\right) = \mathrm{iTr}\left(\mathbf{S}\frac{\mathrm{d}\mathbf{S}^{\dagger}}{\mathrm{d}E}\right) + \mathrm{iTr}\left(\mathbf{A}\frac{\mathrm{d}\mathbf{A}^{\mathrm{T}}}{\mathrm{d}E} + \mathbf{A}^{\mathrm{T}}\frac{\mathrm{d}\mathbf{A}}{\mathrm{d}E}\right), \tag{3.95}$$

since the trace of a matrix is unaltered by an orthogonal transformation. It follows from (3.89) that the first term on the right-hand-side of (3.95) is Tr($\mathbf{Q}$) and the second term can be written as

$$\mathrm{iTr}\left(\mathbf{A}\frac{\mathrm{d}\mathbf{A}^{\mathrm{T}}}{\mathrm{d}E} + \mathbf{A}^{\mathrm{T}}\frac{\mathrm{d}\mathbf{A}}{\mathrm{d}E}\right) = \mathrm{iTr}\left(\frac{\mathrm{d}\left(\mathbf{A}^{\mathrm{T}}\mathbf{A}\right)}{\mathrm{d}E}\right) = 0. \tag{3.96}$$

Hence it follows from (3.95) that

$$\mathrm{Tr}\mathbf{Q} = 2\mathrm{Tr}\left(\frac{\mathrm{d}\boldsymbol{\Delta}}{\mathrm{d}E}\right). \tag{3.97}$$

Finally, we see from (3.90) and (3.91) that the diagonal elements of $\boldsymbol{\Delta}$ are the eigenphases δ_i and, therefore, using (3.73) we obtain

$$\mathrm{Tr}\mathbf{Q} = 2\frac{\mathrm{d}\delta_{\mathrm{sum}}}{\mathrm{d}E}. \tag{3.98}$$

This result generalizes the single-channel result given by (3.87) to multichannel collisions.

So far we have not made any assumption concerning the functional form of the S-matrix or the eigenphase sum. If we assume that δ_{sum} in (3.98) satisfies (3.78), then we find that (3.98) can be rewritten as

$$\mathrm{Tr}\mathbf{Q} = 2\frac{\mathrm{d}\delta_{\mathrm{sum}}}{\mathrm{d}E} = \frac{\Gamma}{(E-E_r)^2 + \left(\frac{1}{2}\Gamma\right)^2} + 2\frac{\mathrm{d}\delta^0_{\mathrm{sum}}}{\mathrm{d}E}. \tag{3.99}$$

In the case of N resonances, which may be overlapping, it follows immediately from (3.99) that

$$\frac{\mathrm{d}\delta_{\mathrm{sum}}}{\mathrm{d}E} = \sum_{i=1}^{N} \frac{\frac{1}{2}\Gamma_i}{(E-E_i)^2 + \left(\frac{1}{2}\Gamma_i\right)^2} + \frac{\mathrm{d}\delta^0_{\mathrm{sum}}}{\mathrm{d}E}, \tag{3.100}$$

where in this equation E_i are the resonance positions and Γ_i are the resonance widths.

Equation (3.100) has been used by a number of workers to determine the positions and widths of resonances. For example, this approach has been used by Stibbe and Tennyson [889] to analyse R-matrix calculations of resonances in e^-–H_2 and e^-–H_2^+ collisions, by Igarashi and Shimamura [486, 487] to analyse hyperspherical coordinate calculations of resonances in e^+–He^+ collisions, by Igarashi and Shimamura [488] and Shimamura et al. [873] to analyse hyperspherical coordinate calculations of resonances in e^-–Ps collisions and by Aiba et al. [5] to

analyse hyperspherical coordinate calculations of resonances in e^-–He and e^-–Ps collisions.

As an example of these calculations we consider results obtained by Aiba et al. [5] for overlapping resonances in electron–positronium atom collisions at energies below the $n = 5$ Ps threshold. In this case the scattered electron moves in a long-range dipole potential, discussed in Sect. 3.3.2, which gives rise to infinite series of overlapping resonances converging to the $n = 5$ and 6 thresholds. We show in Fig. 3.6 the results of calculations in a small energy region just below the $n = 5$ Ps threshold. We see in Fig. 3.6a that the $^1P^o$ eigenphase sum $\delta_{sum}(E)$ increases by about 3π in this energy region, suggesting that there may be three resonances. However, an appreciable change of slope in $\delta_{sum}(E)$ occurs only twice. Also, we see in Fig. 3.6b that Tr$\mathbf{Q}(E)$ exhibits only two peaks. However, by examining the individual eigenvalues $q_i(E)$ of the time-delay matrix in Fig. 3.6b we see that there is a strongly avoided crossing between the two largest eigenvalues and we observe a broad resonance peak corresponding to the third eigenvalue. This third

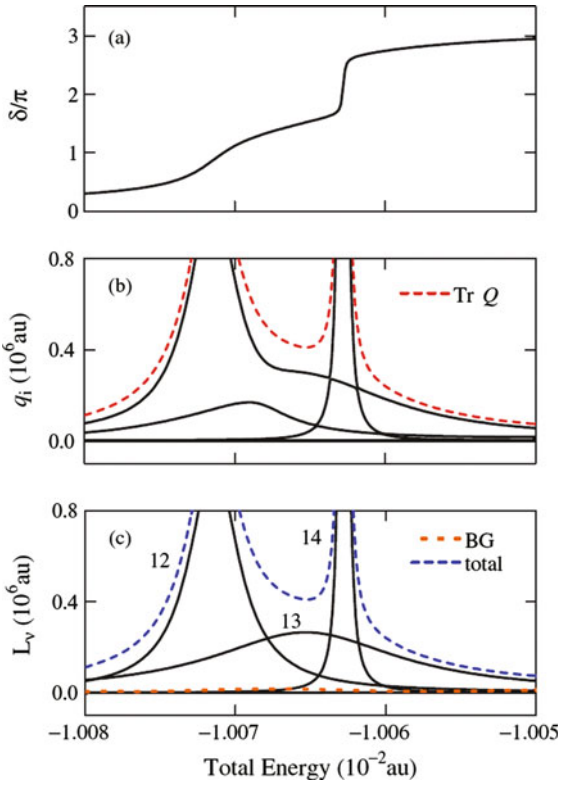

Fig. 3.6 A small energy region just below the Ps $n = 5$ threshold in electron–positronium atom collisions showing Ps^- ($^1P^o$) overlapping resonances. (**a**) The eigenphase sum $\delta_{sum}(E)$. (**b**) The eigenvalues $q_i(E)$ of the time-delay matrix and their sum Tr$\mathbf{Q}(E)$. (**c**) The three Lorentzians $L_i(E)$ representing the three resonances, the background $d\delta^0_{sum}/dE$ (BG) and their sum (Fig. 5 from [5])

resonance would be very difficult to find and analyse using a resonance analysis of the eigenphase sum $\delta_{\rm sum}(E)$ based on (3.78). Finally, in Fig. 3.6c we show the result of fitting the calculated result for $\mathrm{d}\delta_{\rm sum}/\mathrm{d}E$ on the left-hand side of (3.100) to three Lorentzians, defined by the first summation on the right-hand side of (3.100), together with a smoothly varying background term $\delta^0_{\rm sum}/\mathrm{d}E$. We see that this procedure clearly shows the existence of three resonances in the energy region with an almost negligible background and enables accurate positions and widths for these resonances to be determined.

In conclusion, resonance analyses based on the time-delay matrix provide an accurate procedure for resolving overlapping resonances in atomic, molecular and nuclear physics.

3.2.5 Feshbach Projection Operator Theory

In this section we discuss the widely used theory of resonance reactions introduced by Feshbach [320, 321]. This theory is based on a projection operator formalism in which Hilbert space spanned by the eigensolutions of the Schrödinger equation describing the collision process is sub-divided into two mutually orthogonal spaces by two projection operators P and Q. In this application bound states in Q-space, in the absence of coupling between P- and Q-spaces, evolve into resonances when the interaction with the open channels in P-space is included. This theory, which was first used to describe nuclear resonance reactions, has provided a powerful framework for describing resonance phenomena in atomic and molecular collision processes.

In Feshbach theory, the projection operators P and Q are chosen to satisfy the equations

$$\begin{aligned} P + Q &= 1, \\ P^2 = P,\ \ Q^2 &= Q, \\ PQ = QP &= 0. \end{aligned} \tag{3.101}$$

Using these definitions, the Schrödinger equation (2.2), describing multichannel collisions, can be formally rewritten as

$$P(H_{N+1} - E)(P + Q)\Psi = 0 \tag{3.102}$$

and

$$Q(H_{N+1} - E)(P + Q)\Psi = 0. \tag{3.103}$$

We can solve (3.103) for $Q\Psi$ yielding

$$Q\Psi = Q\frac{1}{Q(E - H_{N+1})Q}QH_{N+1}P\Psi. \tag{3.104}$$

Substituting this result for $Q\Psi$ into (3.102) then gives

$$P(H_{N+1} + V_{\text{opt}} - E)P\Psi = 0, \tag{3.105}$$

where V_{opt}, referred to as the "optical potential", is defined here as

$$V_{\text{opt}} = PH_{N+1}Q\frac{1}{Q(E - H_{N+1})Q}QH_{N+1}P. \tag{3.106}$$

We see that the optical potential describes collisions through the Hamiltonian H_{N+1} out of P-space into Q-space, propagation in Q-space and then collisions through the Hamiltonian back from Q-space into P-space. The optical potential contains all the complexity resulting from coupling Q-space to P-space. It is clear from the above derivation that the solution of (3.105) for $P\Psi$ yields identical results to that obtained by solving the original Schrödinger equation (2.2) for Ψ and then projecting this solution onto P-space.

Equations (3.105) and (3.106) hold for any projection operators P and Q satisfying (3.101). We now consider an explicit realization of these operators which has been particularly useful in studies of resonances in atomic and molecular collision processes. We choose P to project onto all the open channels at a particular value of the total energy E and Q to project onto the remaining closed channels at this energy. That is we assume that the wave function Ψ can be expanded in the form given by (2.45) where $P\Psi$ includes all the open channels in this expansion with the corresponding k_i^2 satisfying $k_i^2 \geq 0, \quad i = 1, \ldots, n$. We now introduce the eigenfunctions ξ_s of the operator $QH_{N+1}Q$ by the equation

$$QH_{N+1}Q\ \xi_s = \epsilon_s\ \xi_s, \tag{3.107}$$

where, since $Q = 1 - P$, this operator has a discrete spectrum in the energy range of interest below the lowest threshold in Q-space, plus a continuum spectrum starting from this threshold. The optical potential V_{opt} defined by (3.106) can be written as

$$V_{\text{opt}} = \sum_s \int \frac{PH_{N+1}Q|\xi_s\rangle\langle\xi_s|QH_{N+1}P}{E - \epsilon_s}\,\mathrm{d}\epsilon_s, \tag{3.108}$$

where the summation in this equation goes over the discrete spectrum and the integral over the continuum spectrum of $QH_{N+1}Q$. It is the discrete spectrum, which corresponds physically to an electron bound in the field of an excited atom or ion in Q-space, that gives rise to closed-channel resonance solutions of (3.105).

We now consider the solution of (3.105) for a given set of conserved quantum numbers, when the total energy E lies in the neighbourhood of an isolated eigenvalue ϵ_s of $QH_{N+1}Q$. We can then rewrite (3.105) as

$$P\left[H_{N+1}+\sum_{j\neq s}\int\frac{PH_{N+1}Q|\xi_j\rangle\langle\xi_j|QH_{N+1}P}{E-\epsilon_j}\,\mathrm{d}\epsilon_j-E\right]P\Psi$$
$$=-\frac{PH_{N+1}Q|\xi_s\rangle\langle\xi_s|QH_{N+1}P}{E-\epsilon_s}\,P\Psi, \tag{3.109}$$

where we have separated out on the right-hand side of this equation the rapidly varying pole term in the optical potential, corresponding to the isolated eigenvalue ϵ_s. In order to solve (3.109) we rewrite it as

$$(H'-E)P\Psi=-\frac{\mathcal{H}_{PQ}\xi_s\rangle\langle\xi_s\mathcal{H}_{QP}}{E-\epsilon_s}\,P\Psi, \tag{3.110}$$

where

$$\mathcal{H}_{PQ}=PH_{N+1}Q\quad\text{and}\quad\mathcal{H}_{QP}=QH_{N+1}P. \tag{3.111}$$

We also introduce a quantity Λ_s defined by

$$\Lambda_s=\frac{\langle\xi_s\mathcal{H}_{QP}\Psi\rangle}{E-\epsilon_s}. \tag{3.112}$$

Hence (3.110) can be rewritten as

$$(H'-E)P\Psi=-\Lambda_s\,\mathcal{H}_{PQ}\,\xi_s. \tag{3.113}$$

The solution of (3.113) can be obtained by introducing outgoing and ingoing wave solutions, Ψ_{iE}^{+} and Ψ_{iE}^{-}, of the equation

$$(H'-E)P\;\Psi_{iE}^{\pm}=0, \tag{3.114}$$

where the reduced radial wave functions corresponding to Ψ_{iE}^{+} and Ψ_{iE}^{-} satisfy the outgoing wave

$$\mathbf{F}^{+}(r)\underset{r\to\infty}{\sim}\frac{2}{\sqrt{\mathbf{k}}}\left(\sin\boldsymbol{\theta}+\frac{1}{2\mathrm{i}}\mathrm{e}^{\mathrm{i}\boldsymbol{\theta}}\mathbf{T}_0\right) \tag{3.115}$$

and ingoing wave

$$\mathbf{F}^{-}(r)\underset{r\to\infty}{\sim}\frac{2}{\sqrt{\mathbf{k}}}\left(\sin\boldsymbol{\theta}-\frac{1}{2\mathrm{i}}\mathrm{e}^{-\mathrm{i}\boldsymbol{\theta}}\mathbf{T}_0^{\dagger}\right), \tag{3.116}$$

boundary conditions, respectively. In analogy with our discussion in Sect. 1.1, see (1.21), $\Psi_{iE}^{\pm}$ in (3.114) then satisfy the δ-function orthonormality relation

$$\langle \Psi^{\pm}_{iE} | \Psi^{\pm}_{i'E'} \rangle = \delta_{ii'}\, \delta(E - E'), \tag{3.117}$$

where we remember from Sect. 2.5 that the T-matrix in (3.115) and (3.116) is related to the S-matrix by

$$\mathbf{T}_0 = \mathbf{S}_0 - \mathbf{I}. \tag{3.118}$$

We can then formally solve (3.113) yielding

$$P\Psi = \Psi^{+}_{iE} + \Lambda_s \frac{1}{E + \mathrm{i}\eta - H'} \mathcal{H}_{PQ}\, \xi_s, \tag{3.119}$$

where η is a positive infinitesimal quantity. Substituting (3.119) into (3.112) and collecting terms in Λ_s then gives

$$\Lambda_s = \frac{\langle \xi_s \mathcal{H}_{QP} \Psi^{+}_{iE} \rangle}{E - \epsilon_s - \langle \xi_s \mathcal{H}_{QP} (E + \mathrm{i}\eta - H')^{-1} \mathcal{H}_{PQ} \xi_s \rangle}. \tag{3.120}$$

Using this result for Λ_s, (3.119) becomes

$$P\Psi = \Psi^{+}_{iE} + \frac{1}{E + \mathrm{i}\eta - H'} \frac{\mathcal{H}_{PQ}\xi_s \langle \xi_s \mathcal{H}_{QP} \Psi^{+}_{iE} \rangle}{E - \epsilon_s - \langle \xi_s \mathcal{H}_{QP} (E + \mathrm{i}\eta - H')^{-1} \mathcal{H}_{PQ} \xi_s \rangle}. \tag{3.121}$$

In order to simplify (3.121) we consider the term appearing in the denominator on the right-hand side of this equation. We can write

$$\left\langle \xi_s \mathcal{H}_{QP} \frac{1}{E + \mathrm{i}\eta - H'} \mathcal{H}_{PQ} \xi_s \right\rangle = \sum_j \int \frac{|\langle \xi_s \mathcal{H}_{QP} \Psi^{+}_{jE'} \rangle|^2}{E - E' + \mathrm{i}\eta} \mathrm{d}E', \tag{3.122}$$

where we have expanded the inverse operator $(E + \mathrm{i}\eta - H')^{-1}$ in terms of the complete set of outgoing wave solutions of (3.114). The right-hand side of (3.122) can be written as a sum of its real and imaginary parts. The real part corresponds to the resonance shift Δ_s which is given by

$$\Delta_s = \sum_j \mathcal{P} \int \frac{|\langle \xi_s \mathcal{H}_{QP} \Psi^{+}_{jE'} \rangle|^2}{E - E'} \mathrm{d}E', \tag{3.123}$$

where $\mathcal{P}$ denotes the principal value integral. The imaginary part of (3.122) arises from the pole at $E = E'$ and is related to the resonance width Γ_s by the equation

$$\frac{1}{2} \mathrm{i} \Gamma_s = \mathrm{i}\pi \sum_j |\langle \xi_s \mathcal{H}_{QP} \Psi^{+}_{jE} \rangle|^2, \tag{3.124}$$

which gives

$$\Gamma_s = 2\pi \sum_j |\langle \xi_s \mathcal{H}_{QP} \Psi^+_{jE} \rangle|^2, \tag{3.125}$$

where the summation is taken over all final states. We see that this result for the resonance width has the same form as that given by (3.72) derived in Sect. 3.2.2.

Finally, we operate on the left-hand side of (3.121) by $(E + \mathrm{i}\eta - H')$, project onto the ingoing wave solution Ψ^-_{fE} of (3.114) and use the results for the resonance shift and width given by (3.123) and (3.125). The transition amplitude $\mathcal{T}_{fi}$ from an initial state i to a final state f is then given by

$$\mathcal{T}_{fi} = \mathcal{T}_{0fi} + \frac{\langle \Psi^-_{fE} \mathcal{H}_{PQ} \xi_s \rangle \langle \xi_s \mathcal{H}_{QP} \Psi^+_{iE} \rangle}{E - \epsilon_s - \Delta_s + \frac{1}{2}\mathrm{i}\Gamma_s}, \tag{3.126}$$

where $\mathcal{T}_{0fi}$ is the transition amplitude describing non-resonant scattering in P-space in the absence of the isolated eigenfunction ξ_s of $QH_{N+1}Q$. We see that (3.126) has the same general form as (3.69) describing the S-matrix in the neighbourhood of an isolated resonance.

The above theory has been extended by Feshbach [320, 321] to treat overlapping resonances. In this case $\mathcal{T}_{0fi}$ in (3.126) varies rapidly over the width of one of the resonances and the separation of the transition amplitude into two parts, given by (3.126), is no longer appropriate. If only a few closely spaced resonances are involved, such that the remaining background transition amplitude omitting these resonances is slowly varying, then the above theory can be straightforwardly extended to include these resonances. Equation (3.110) then becomes

$$(H' - E)P\Psi = -\sum_s \frac{\mathcal{H}_{PQ}\xi_s\rangle\langle\xi_s \mathcal{H}_{QP}}{E - \epsilon_s} P\Psi, \tag{3.127}$$

where H' is the Hamiltonian omitting these closely spaced resonances, and the subsequent equations are modified accordingly.

However, we also have to consider the situation in electron collisions with positive ions, where infinite series of resonances converging to each excited state threshold occur. In this case resonance series may overlap and it is then necessary to include the interaction between resonance series in the theory. This is achieved using multichannel effective range theory or multichannel quantum defect theory which we discuss in Sect. 3.3.

3.2.6 *Hyperspherical Coordinates*

We conclude this section by discussing the hyperspherical system of coordinates which has been important in the analysis of resonances and threshold behaviour

of three-body systems. For example, Fock [326] and Demkov and Ermolaev [260] used these coordinates in variational calculations of bound states of helium, Delves [257, 258] used them to describe the nuclear three-body problem and Smith [882, 883] has given a general discussion of the three-body problem in terms of these coordinates. They have also played an important role in the analysis of doubly excited resonance states of helium and other two-electron atoms, for example, by Macek [618, 619], Lin [598, 599], Greene [416] and Fano [307] as well as in positron collisions calculations, for example, by Igarashi et al. [485–487]. These coordinates have also been used in the calculation of weakly bound levels of triatomic molecules such as the helium trimer $^4He_3$ and isotopomers of the He_3^+ ion discussed by Kokoouline and Masnou-Seeuws [546]. Finally, we will use these coordinates in our derivation of the Wannier [954] threshold law of ionization in Sect. 3.3.5

Hyperspherical coordinates for two electrons moving in the field of an infinitely heavy nucleus at the origin of coordinates are defined in terms of the electronic spherical polar coordinates (r_1, θ_1, ϕ_1) and (r_2, θ_2, ϕ_2) by

$$R = (r_1^2 + r_2^2)^{1/2}, \quad \alpha = \tan^{-1}\frac{r_2}{r_1}, \quad 0 \le \alpha \le \frac{\pi}{2}, \tag{3.128}$$

while the four remaining coordinates are usually chosen to be $(\theta_1, \phi_1, \theta_2, \phi_2)$. The Schrödinger equation, defined by (2.2) and (2.3) with $N = 1$ and nuclear charge number Z can be expressed in terms of these coordinates as (e.g. [664])

$$\left(\frac{\mathrm{d}^2}{\mathrm{d}R^2} + \frac{5}{R}\frac{\mathrm{d}}{\mathrm{d}R} - \frac{\Lambda^2}{R^2} + \frac{C}{R} + 2E\right)\Psi = 0. \tag{3.129}$$

In this equation the potential function C is given in terms of the electron–electron and electron–nuclear potentials by

$$\begin{aligned} C(\alpha, \theta_{12}) &= R\left(\frac{2Z}{r_1} + \frac{2Z}{r_2} - \frac{2}{r_{12}}\right) \\ &= \frac{2Z}{\cos\alpha} + \frac{2Z}{\sin\alpha} - \frac{2}{(1 - \sin 2\alpha \cos\theta_{12})^{1/2}}, \end{aligned} \tag{3.130}$$

where θ_{12} is the angle between the radial vectors $\mathbf{r_1}$ and $\mathbf{r_2}$. Also the operator Λ^2 in (3.129) is defined by

$$\Lambda^2 = -\frac{1}{\sin^2\alpha\cos^2\alpha}\frac{\mathrm{d}}{\mathrm{d}\alpha}\left(\sin^2\alpha\cos^2\alpha\frac{\mathrm{d}}{\mathrm{d}\alpha}\right) + \frac{\boldsymbol{\ell}_1^2}{\cos^2\alpha} + \frac{\boldsymbol{\ell}_2^2}{\sin^2\alpha}, \tag{3.131}$$

where $\boldsymbol{\ell}_1^2$ and $\boldsymbol{\ell}_2^2$ are the squared orbital angular momentum operators for electrons 1 and 2, defined in Appendix B.3, with eigenfunctions $Y_{\ell_1 m_1}(\theta_1, \phi_1)$ and $Y_{\ell_2 m_2}(\theta_2, \phi_2)$ belonging to the eigenvalues $\ell_1(\ell_1 + 1)$ and $\ell_2(\ell_2 + 1)$, respectively. Λ^2 is thus the square of the grand angular momentum operator in six dimensions

and is the Casimir operator for the O(6) group. Its eigenvalues are $\lambda(\lambda+4)$ where λ is a non-negative integer. It commutes with $\mathbf{L}^2$, $\mathbf{S}^2$ and the parity as well as with $\boldsymbol{\ell}_1^2$ and $\boldsymbol{\ell}_2^2$ but it does not commute with C.

Returning to (3.129), we transform this equation to a more familiar form which removes the first derivative with respect to R by the transformation

$$\Psi = R^{-5/2}\psi. \tag{3.132}$$

Equation (3.129) then becomes

$$\left(\frac{\mathrm{d}^2}{\mathrm{d}R^2} - \frac{\Lambda^2 + \frac{15}{4}}{R^2} + \frac{C}{R} + 2E\right)\psi = 0, \tag{3.133}$$

which resembles the Schrödinger equation for the motion of a particle moving in the reduced potential $-C/R$ with centrifugal potential energy given by $(\Lambda^2 + 15/4)/R^2$. However, unlike the similar equation for the hydrogen atom C, which depends on the angular coordinates α and θ_{12}, does not commute with Λ^2. It follows from (3.133) that at large R the dynamics of the motion of two electrons moving in the field of the nucleus depends on the form of C as a function of α and θ_{12}. In Fig. 3.7 we give a three-dimensional plot of $-C(\alpha, \theta_{12})$ in the range $0 \le \alpha \le \pi/2$ and $0 \le \theta_{12} \le \pi$ for the case where the nuclear charge $Z = 1$ which was determined by Lin [598]. At $\alpha = 0$ and $\pi/2$ the potential surface tends to $-\infty$ corresponding to the electron–nuclear attraction singularity, while at $\alpha = \pi/4$ and

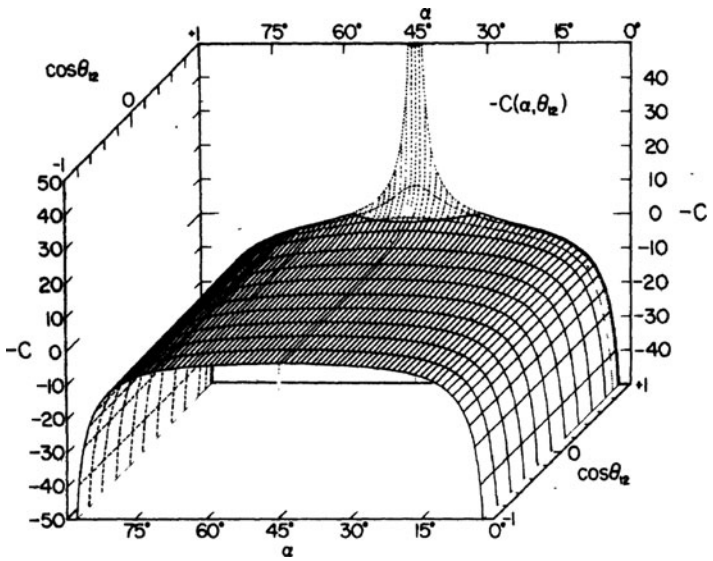

Fig. 3.7 Potential function $-C(\alpha, \theta_{12})$ as a function of α and $\cos\theta_{12}$ in Rydbergs for two electrons moving in the field of an H^+ ion (Fig. 1 from [598])

$\theta_{12} = 0$ there is a singularity corresponding to the electron–electron repulsion. The saddle point in the potential energy surface at $\alpha = \pi/4$ and $\theta_{12} = \pi$ corresponds to the situation where the two electrons are equidistant from and on opposite sides of the nucleus. We will see in Sect. 3.3.5 that it is this configuration of the outgoing electrons that Wannier [954] showed leads to the threshold behaviour of the electron impact ionization cross section.

In order to solve (3.133) it is convenient to introduce the eigenfunctions $U_K^\Gamma(\Omega)$ of the operator Λ^2. These hyperspherical harmonics, or K-harmonics, satisfy the equation

$$[\Lambda^2 - K(K+4)]U_K^\Gamma(\Omega) = 0, \tag{3.134}$$

where K is a non-negative integer which can be written as

$$K = \ell_1 + \ell_2 + 2m, \tag{3.135}$$

ℓ_1 and ℓ_2 being the usual orbital angular momentum quantum numbers and m a new non-negative integer quantum number associated with the motion in α. Also in (3.134), Ω specifies the angular variables

$$\Omega \equiv \alpha\ \theta_1\ \phi_1\ \theta_2\ \phi_2, \tag{3.136}$$

and Γ represents the conserved quantum numbers defined by (2.58).

We can eliminate the first derivative term in Λ^2 defined by (3.131) by introducing the eigenfunctions

$$\phi^\Gamma_{\ell_1\ell_2 m}(\Omega) = \sin\alpha\ \cos\alpha\ U_K^\Gamma(\Omega), \tag{3.137}$$

which satisfy the equation

$$\left[-\frac{\partial^2}{\partial\alpha^2} + \frac{\boldsymbol{\ell}_1^2}{\cos^2\alpha} + \frac{\boldsymbol{\ell}_2^2}{\sin^2\alpha} - (K+2)^2\right]\phi^\Gamma_{\ell_1\ell_2 m}(\Omega) = 0. \tag{3.138}$$

These eigenfunctions are given by

$$\phi^\Gamma_{\ell_1\ell_2 m}(\Omega) = \frac{1}{\sqrt{2}}\Big[f_{\ell_1\ell_2 m}(\alpha)Y_{\ell_1\ell_2 L M_L}(\hat{\mathbf{r}}_1,\hat{\mathbf{r}}_2) + (-1)^{\ell_1+\ell_2-L+S+m} \times\ f_{\ell_2\ell_1 m}(\alpha)Y_{\ell_2\ell_1 L M_L}(\hat{\mathbf{r}}_1,\hat{\mathbf{r}}_2)\Big], \quad \ell_1 \neq \ell_2 \tag{3.139}$$

and

$$\phi^\Gamma_{\ell_1\ell_2 m}(\Omega) = \frac{1}{\sqrt{2}}\left[1 + (-1)^{-L+S+m}\right] f_{\ell\ell m}(\alpha)Y_{\ell\ell L M_L}(\hat{\mathbf{r}}_1,\hat{\mathbf{r}}_2), \quad \ell_1 = \ell_2 = \ell, \tag{3.140}$$

where the functions $f_{\ell_1\ell_2 m}(\alpha)$ are defined in terms of Jacobi polynomials [618] and the functions $Y_{\ell_1\ell_2 LM_L}(\hat{\mathbf{r}}_1, \hat{\mathbf{r}}_2)$ are defined by (B.57).

The wave function ψ in (3.133) can now be expanded for each set of conserved quantum numbers Γ as

$$\psi^{\Gamma}(R; \Omega) = \sum_{i=1}^{n} \phi_i^{\Gamma}(\Omega) F_i^{\Gamma}(R), \tag{3.141}$$

where the subscript i represents the quantum numbers $\ell_1\ell_2 m$ and where the functions $F_i^{\Gamma}(R)$ depend only on R. Substituting this expansion into (3.133) and projecting onto the channel functions $\phi_i^{\Gamma}(\Omega)$ then gives after using (3.138)

$$\left(\frac{\mathrm{d}^2}{\mathrm{d}R^2} - \frac{(K_i+2)^2 - \frac{1}{4}}{R^2} + k^2\right) F_i^{\Gamma}(R) = -\frac{1}{R}\sum_{j=1}^{n} V_{ij}^{\Gamma} F_j^{\Gamma}(R), \quad i = 1, \ldots, n, \tag{3.142}$$

where $k^2 = 2E$. Also in (3.142) the potential matrix

$$V_{ij}^{\Gamma} = \langle \phi_i^{\Gamma}(\Omega) | C(\alpha, \theta_{12}) | \phi_j^{\Gamma}(\Omega) \rangle, \quad i,\ j = 1, \ldots, n, \tag{3.143}$$

where the integration which is over all angles Ω does not depend on R. We see that (3.142), unlike (2.63) which they replace for two electrons moving in the field of a nucleus, are a set of n coupled second-order differential equations rather than coupled second-order integrodifferential equations, where n is the number of terms retained in expansion (3.141). The Pauli exclusion principle is now represented by the form of the matrix V_{ij}^{Γ}, defined by (3.143), where the function C, defined by (3.130), satisfies the symmetry relation

$$C(\alpha, \theta_{12}) = C\left(\frac{\pi}{2} - \alpha, \theta_{12}\right), \quad 0 \le \alpha \le \frac{\pi}{2}, \tag{3.144}$$

as illustrated in Fig. 3.7. Equations (3.142) therefore partition into symmetric and antisymmetric sets corresponding to $S = 0$ and 1, respectively.

In spite of their formal simplicity, (3.142) are in principle still members of an infinite set of coupled second-order differential equations which have to be approximated in some way in practical applications. What makes the hyperspherical coordinate representation particularly useful is that in describing doubly excited resonance states of atoms, the motion in the variable R is approximately separable from the motion in other variables in a way which is analogous to the Born–Oppenheimer separation of the electronic and nuclear motion in the theory of molecular structure. This follows by examining the power series expansion of the solution $F_i^{\Gamma}(R)$ of (3.142) about $R = 0$, where we find that the leading term in the expansion does not depend on the coupling matrix V_{ij}^{Γ} on the right-hand side of (3.142) as discussed by Fano [307]. This leads us to introduce the adiabatic expansion

$$\psi^{\Gamma}(R;\Omega)=\sum_{i=1}^{n}\Phi_i^{\Gamma}(R;\Omega)G_i^{\Gamma}(R), \tag{3.145}$$

rather than expansion (3.141), where the functions $\Phi_i^{\Gamma}(R;\Omega)$ are chosen to diagonalize all the terms in (3.142) except $\mathrm{d}^2/\mathrm{d}R^2$ arising from the kinetic energy operator.

In order to determine the equations satisfied by $G_i^{\Gamma}(R)$ we introduce the symmetric matrix

$$X_{ij}^{\Gamma}(R)=\frac{(K_i+2)^2-\frac{1}{4}}{R^2}\delta_{ij}-\frac{1}{R}V_{ij}^{\Gamma},\quad i,\ j=1,\ldots,n, \tag{3.146}$$

which we diagonalize by an R-dependent orthogonal transformation as follows:

$$\left(\mathbf{A}^{\Gamma}\right)^{\mathrm{T}}\mathbf{X}^{\Gamma}\mathbf{A}^{\Gamma}=\mathbf{D}^{\Gamma}, \tag{3.147}$$

where $\mathbf{A}^{\Gamma}$ is an orthogonal matrix and $\mathbf{D}^{\Gamma}$ is a diagonal matrix, both of which are functions of R. Equations (3.142) can then be rewritten as

$$\left(\frac{\mathrm{d}^2}{\mathrm{d}R^2}-D_i^{\Gamma}(R)+k^2\right)G_i^{\Gamma}(R)=\sum_{j=1}^{n}W_{ij}^{\Gamma}(R)G_j^{\Gamma}(R),\quad i=1,\ldots,n, \tag{3.148}$$

where the functions Φ_i^{Γ} and G_i^{Γ} in (3.145) are defined in terms of the functions ϕ_i^{Γ} and F_i^{Γ} in (3.141) by the matrix equations

$$\boldsymbol{\Phi}^{\Gamma}(R;\Omega)=\left[\mathbf{A}^{\Gamma}(R)\right]^{\mathrm{T}}\boldsymbol{\phi}^{\Gamma}(\Omega) \tag{3.149}$$

and

$$\mathbf{G}^{\Gamma}(R)=\left[\mathbf{A}^{\Gamma}(R)\right]^{\mathrm{T}}\mathbf{F}^{\Gamma}(R). \tag{3.150}$$

Also the coupling potential matrix $\mathbf{W}^{\Gamma}$ on the right-hand side of (3.148) is defined by

$$\mathbf{W}^{\Gamma}(R)\mathbf{G}^{\Gamma}(R)=-2\left[\mathbf{A}^{\Gamma}(R)\right]^{\mathrm{T}}\frac{\mathrm{d}\mathbf{A}^{\Gamma}}{\mathrm{d}R}\frac{\mathrm{d}\mathbf{G}^{\Gamma}}{\mathrm{d}R}-\left[\mathbf{A}^{\Gamma}(R)\right]^{\mathrm{T}}\frac{\mathrm{d}^2\mathbf{A}^{\Gamma}}{\mathrm{d}R^2}\mathbf{G}^{\Gamma}(R). \tag{3.151}$$

The extreme adiabatic approximation is obtained by neglecting all coupling terms on the right-hand side of (3.148), while the adiabatic approximation is obtained by retaining in addition the diagonal terms $W_{ii}^{\Gamma}(R)$. If we retain all the terms in the coupling potential $W_{ij}^{\Gamma}(R)$ on the right-hand side of (3.148) then (3.142) and (3.148) give identical results.

3.3 Threshold Behaviour of Cross Sections

In this section we consider the behaviour of excitation and ionization cross sections in the neighbourhood of threshold. It was shown in a fundamental paper by Wigner [970] that the behaviour of cross sections near the threshold of a new reaction does not depend on the collision dynamics in the "reaction zone" where all the particles are close together and strongly interacting. Instead, Wigner showed that the threshold behaviour depends, apart from a constant multiple, only on the form of the potential between the reacting particles at large distances. This fundamental result is the basis of our treatment of both excitation and ionization scattering amplitudes and cross sections in the neighbourhood of threshold. We note that a review of collisions near threshold has been written by Sadeghpour et al. [804].

We commence our discussion of threshold behaviour by generalizing our treatment of effective range theory in potential scattering, to treat excitation processes involving many coupled two-body channels. In Sect. 3.3.1 we derive a multichannel effective range theory for the K-matrix and T-matrix for short-range potentials, following the work of Ross and Shaw [798], where in this derivation we make use of the analytic properties of the multichannel R-matrix introduced and discussed in Chap. 5 and later chapters. Then in Sect. 3.3.2, we extend this theory to treat excitation processes, where long-range dipole potentials are present, which was first considered by Gailitis and Damburg [359]. We conclude our treatment of threshold behaviour of excitation by considering in Sects. 3.3.3 and 3.3.4 the situation which arises in electron collisions with positive and negative ions where long-range Coulomb potentials between the interacting particles are present. We consider first in Sect. 3.3.3 an extension of multichannel effective range theory developed by Gailitis [357] using the analytic properties of the R-matrix. Then in Sect. 3.3.4 we discuss multichannel quantum defect theory (MQDT), introduced, developed and reviewed by Seaton [859] which has been widely used in the analysis of electron collisions with positive ions and photoionization processes in the neighbourhood of threshold. Also in this section we summarize extensions of MQDT to treat molecular collision processes. Finally, in Sect. 3.3.5 we consider the threshold behaviour of ionization with emphasis on single ionization of atoms and positive ions by electrons. The foundations of this subject were laid by Wannier [954, 955] and, in an introduction to this section, we summarize the threshold law of single ionization and the main theoretical and experimental developments that have been made since Wannier's fundamental analysis. We then derive the threshold law of single ionization adopting a classical analysis analogous to that used by Wannier, based on hyperspherical coordinates discussed in Sect. 3.2.6. Finally we mention some recent ab initio calculations of threshold behaviour of ionization which satisfy Wannier's threshold law.

3.3.1 Excitation: Short-Range Potentials

We commence our discussion of threshold behaviour by generalizing our treatment of effective range theory in potential scattering given in Sect. 1.4 to treat excitation

processes involving many coupled channels where the potential interactions are short range. In this way we derive a multichannel generalization of (1.120) which was first obtained by Ross and Shaw [798].

We consider the solution of n coupled second-order integrodifferential equations corresponding to electron collisions with neutral atoms, obtained by setting $N = Z$ in (3.2), which then becomes

$$\left(\frac{\mathrm{d}^2}{\mathrm{d}r^2} - \frac{\boldsymbol{\ell}(\boldsymbol{\ell}+\mathbf{I})}{r^2} - \mathbf{U}(r) + \mathbf{k}^2\right)\mathbf{F}(r) = 0, \tag{3.152}$$

where initially we assume that the potential $\mathbf{U}$ is short range satisfying

$$\mathbf{U}(r) = 0, \quad r \geq a, \tag{3.153}$$

for some finite radius $r = a$. This enables us to develop a multichannel effective range theory which forms the basis for later developments when long-range dipole and Coulomb potentials are present. In all of this work we assume that the target states are ordered so that (2.78) is satisfied.

In the energy region where all the channels are open, we showed in Sect. 2.4 that the matrix solution of (3.152), which vanishes at the origin, has the following asymptotic form:

$$\mathbf{F}(r) = \mathbf{k}^{-1/2}[\mathbf{s}_\ell(\mathbf{k}r) + \mathbf{c}_\ell(\mathbf{k}r)\mathbf{K}], \quad r \geq a, \tag{3.154}$$

where $\mathbf{K}$ is the $n \times n$-dimensional K-matrix. Also in (3.154), $\mathbf{s}_\ell(\mathbf{k}r)$ and $\mathbf{c}_\ell(\mathbf{k}r)$ are diagonal matrices which satisfy the following asymptotic boundary conditions

$$\mathbf{s}_\ell(\mathbf{k}r) = \mathbf{k}r j_\ell(\mathbf{k}r) = \left(\frac{\pi \mathbf{k}r}{2}\right)^{1/2} J_{\ell+\frac{1}{2}}(\mathbf{k}r) \underset{r\to\infty}{\sim} \sin\left(\mathbf{k}r - \tfrac{1}{2}\boldsymbol{\ell}\pi\right) \tag{3.155}$$

and

$$\mathbf{c}_\ell(\mathbf{k}r) = -\mathbf{k}r n_\ell(\mathbf{k}r) = (-1)^{\boldsymbol{\ell}}\left(\frac{\pi \mathbf{k}r}{2}\right)^{1/2} J_{-\boldsymbol{\ell}-\frac{1}{2}}(\mathbf{k}r) \underset{r\to\infty}{\sim} \cos\left(\mathbf{k}r - \tfrac{1}{2}\boldsymbol{\ell}\pi\right), \tag{3.156}$$

where the diagonal elements are expressed in terms of spherical Bessel functions of half-odd integer order defined in Appendix C.2. We previously encountered these functions in Sect. 1.1 where we observed that $\mathbf{c}_\ell(\mathbf{k}r)$ can also be expressed in terms of spherical Neumann functions.

In order to determine the analytic properties of the K-matrix we relate it to the analytic properties of the $n \times n$-dimensional R-matrix $\mathbf{R}(E)$, introduced in Sect. 5.1.2. In that section we show that the R-matrix, defined by (5.19), is a real meromorphic function of energy with simple poles only on the real energy axis. Hence the R-matrix does not contain threshold branch cuts, discussed in Sect. 3.1,

which arise from the solution of the coupled second-order integrodifferential equations (3.152) in the external and asymptotic regions.

The solution of (3.152) which vanishes at the origin $r = 0$ satisfies the following equation:

$$\mathbf{F}(a) = \mathbf{R}(E)\left(a\frac{\mathrm{d}\mathbf{F}}{\mathrm{d}r} - b\mathbf{F}\right)_{r=a}, \tag{3.157}$$

where b is an arbitrary constant and where we have chosen the boundary of the internal R-matrix region to be the range $r = a$ of the potential $\mathbf{U}(r)$. We then substitute the solution $\mathbf{F}(r)$, defined by (3.154), into (3.157) yielding

$$\mathbf{k}^{-1/2}(\mathbf{s}_\ell + \mathbf{c}_\ell\mathbf{K}) = \mathbf{R}(E)\mathbf{k}^{-1/2}[\boldsymbol{\rho}(\mathbf{s}'_\ell + \mathbf{c}'_\ell\mathbf{K}) - b(\mathbf{s}_\ell + \mathbf{c}_\ell\mathbf{K})], \tag{3.158}$$

where the diagonal matrix $\boldsymbol{\rho} = \mathbf{k}a$ and where the diagonal matrices $\mathbf{s}_\ell$, $\mathbf{c}_\ell$, $\mathbf{s}'_\ell$ and $\mathbf{c}'_\ell$ are defined by

$$\mathbf{s}_\ell = \mathbf{s}_\ell(\mathbf{k}a), \quad \mathbf{c}_\ell = \mathbf{c}_\ell(\mathbf{k}a), \quad \mathbf{s}'_\ell = \frac{1}{\mathbf{k}}\left.\frac{\mathrm{d}\mathbf{s}_\ell(\mathbf{k}r)}{\mathrm{d}r}\right|_{r=a}, \quad \mathbf{c}'_\ell = \frac{1}{\mathbf{k}}\left.\frac{\mathrm{d}\mathbf{c}_\ell(\mathbf{k}r)}{\mathrm{d}r}\right|_{r=a}. \tag{3.159}$$

Setting the arbitrary constant $b = 0$ in (3.157) and (3.158), using the Wronskian relation $\mathbf{s}'_\ell\mathbf{c}_\ell - \mathbf{c}'_\ell\mathbf{s}_\ell = \mathbf{I}$ and re-arranging the terms in (3.158), we obtain the following expression for the K-matrix in terms of the R-matrix evaluated at $r = a$:

$$\mathbf{K}^{-1} = -\frac{\mathbf{c}_\ell}{\mathbf{s}_\ell} + \frac{\mathbf{I}}{\mathbf{s}'_\ell\mathbf{s}_\ell} + \boldsymbol{\rho}^{-1/2}\mathbf{s}'^{-1}_\ell\left(\mathbf{R}(E) - \boldsymbol{\rho}^{-1}\frac{\mathbf{s}_\ell}{\mathbf{s}'_\ell}\right)^{-1}\mathbf{s}'^{-1}_\ell\boldsymbol{\rho}^{-1/2}. \tag{3.160}$$

The analytic behaviour of the K-matrix in the complex energy plane is therefore given in terms of the analytic properties of the matrices $\mathbf{s}_\ell$, $\mathbf{s}'_\ell$ and $\mathbf{c}_\ell$ together with that of the R-matrix $\mathbf{R}(E)$. We find, following our discussion in potential scattering which led to (1.117), that $\mathbf{k}^{-\ell-1}\mathbf{s}_\ell$, $\mathbf{k}^{-\ell}\mathbf{s}'_\ell$ and $\mathbf{k}^{\ell}\mathbf{c}_\ell$ are diagonal matrices whose elements are analytic functions of energy which do not contain threshold branch cuts. Hence, after substituting these results into (3.160) we find that $\mathbf{K}^{-1}$ can be written in the following form:

$$\mathbf{K}^{-1} = \mathbf{k}^{-\ell-\frac{1}{2}}\mathbf{M}(E)\mathbf{k}^{-\ell-\frac{1}{2}}, \tag{3.161}$$

where the $n \times n$-dimensional M-matrix $\mathbf{M}(E)$ is a real symmetric analytic function of energy E which does not contain threshold branch cuts.

We can also obtain an analogous expression for the T-matrix, introduced in Sect. 2.5, which is defined in terms of the K-matrix by

$$\mathbf{T} = \frac{2\mathrm{i}\mathbf{K}}{\mathbf{I} - \mathrm{i}\mathbf{K}}. \tag{3.162}$$

We find, after substituting (3.161) into (3.162), that

$$\mathbf{T} = \mathbf{k}^{\ell+\frac{1}{2}} \frac{2\mathrm{i}}{\mathbf{M}(E) - \mathrm{i}\mathbf{k}^{2\ell+1}} \mathbf{k}^{\ell+\frac{1}{2}}. \tag{3.163}$$

Equations (3.161) and (3.163) were first obtained by Ross and Shaw [798].

It follows from the above discussion that the M-matrix $\mathbf{M}(E)$ can be expanded as a power series in energy

$$\mathbf{M}(E) = \mathbf{M}_0 + \mathbf{M}_1 E + \mathbf{M}_2 E^2 + \cdots, \tag{3.164}$$

where $\mathbf{M}_0$, $\mathbf{M}_1$, $\mathbf{M}_2, \ldots$ are real symmetric energy-independent matrices. This expansion is valid through thresholds although the radius of convergence of the expansion will in general be finite. We see that (3.161), (3.163) and (3.164) reduce, when the number of channels $n = 1$, to (1.118), (1.119) and (1.120) which we obtained for potential scattering in Sect. 1.4.1.

The above effective range theory enables theoretical calculations or experimental measurements above and below thresholds to be related. For example, we have shown in Sect. 3.2.1 that bound states and resonances correspond to poles in the S-matrix and hence in the T-matrix. It follows from (3.163) that these poles occur when the denominator of this equation satisfies

$$\det\left[\mathbf{M}(E) - \mathrm{i}\mathbf{k}^{2\ell+1}\right] = 0. \tag{3.165}$$

Hence (3.161), (3.163) and (3.164) relate the scattering amplitudes and cross sections above threshold to the bound states and resonances below threshold through the analytic properties of the M-matrix.

We consider briefly an application of the above theory to two coupled channels. In this case we can relate the parameters of a resonance lying below the upper threshold to the two elastic scattering amplitudes, the inelastic scattering amplitude and the corresponding cross sections above this threshold. We see this most clearly if the elements of the M-matrix are slowly varying over this energy range so that we need to only consider the three independent elements of $\mathbf{M}_0$ in (3.164). These elements can be fitted to give the resonance position, resonance width and background phase shift which then enables the three scattering amplitudes and hence the cross sections to be determined over a limited energy range above this threshold. This relationship between resonances below threshold and cross sections above threshold in two-channel models has been considered by several workers. For example, Damburg and Peterkop [244] explored this relationship in a 1s–2s model e^-–H collision calculation, and Burke [151, 152] related the resonance parameters of the ^{2}S resonance at 19.37 eV, which lies below the $2\,^3$S threshold in e^-–He collisions, to the $1\,^1$S–$2\,^3$S excitation cross section in the ^{2}S state just above this threshold. Further discussions of resonances which arise in e^-–He collisions are given in Sect. 5.6.2.

Finally, we remark that, as in potential scattering, although the effective range expansion, defined by (3.161), (3.162), (3.163) and(3.164), has been derived for a finite range potential satisfying (3.153), it is also valid for potentials that fall off asymptotically as fast as or faster than an exponential, provided that the radius a is chosen so that these potentials are negligibly small for $r \geq a$.

3.3.2 Excitation: Dipole Potentials

In this section we extend our discussion of threshold behaviour of excitation to treat many coupled two-body channels where long-range dipole potentials are present. We obtain a multichannel effective range expression first derived by Gailitis and Damburg [358, 359] and we consider an application to electron–hydrogen atom collisions near the $n = 2$ threshold.

As in Sect. 3.3.1, we consider the solution of the n coupled second-order integro-differential equations (3.2) where we set $N = Z$ corresponding to electron collisions with neutral atoms. We have shown in Sect. 2.3.2 that we can choose a radius $r = a$ such that the local direct potential included in $\mathbf{U}(r)$ in (3.2) is represented by a sum of terms behaving as inverse powers of the radius r, while the non-local exchange and correlation potentials are negligibly small beyond this radius. It follows that for neutral atoms the leading term in the long-range potential has the form

$$\mathbf{U}(r) = \frac{\boldsymbol{\alpha}}{r^2}, \quad r \geq a, \tag{3.166}$$

where $\boldsymbol{\alpha}$ is a real symmetric matrix. Hence the coupled integrodifferential equations (3.2) corresponding to electron collisions with neutral atoms reduce to

$$\left(\frac{\mathrm{d}^2}{\mathrm{d}r^2} - \frac{\boldsymbol{\ell}(\boldsymbol{\ell}+\mathbf{I}) + \boldsymbol{\alpha}}{r^2} + \mathbf{k}^2\right)\mathbf{F}(r) = 0, \quad r \geq a, \tag{3.167}$$

where we have neglected higher order terms in the long-range potential. However, these terms can be included in the internal region, $r < a$, together with the non-local exchange and correlation potentials.

We now describe the modified multichannel effective range theory, developed by Gailitis and Damburg [358, 359], which is applicable to scattering by long-range potentials defined by (3.166). We will see that this theory describes the situation where the off-diagonal dipole terms retained in the calculation couple degenerate or almost degenerate channels. This includes the most important long-range potential terms in electron collisions with hydrogen atoms, where the degeneracy of the non-relativistic target states corresponding to principal quantum numbers $n \geq 2$ results in the target atom acquiring a non-zero dipole moment in the field of the scattered electron. This theory is also applicable to electron collisions with atoms in highly excited states which are almost degenerate and with polar molecules when the rotational splitting of the levels can be neglected.

We commence by introducing an r- and energy-independent orthogonal matrix $\mathbf{A}$ which diagonalizes the matrix coefficient of the r^{-2} term $\boldsymbol{\ell}(\boldsymbol{\ell}+\mathbf{I})+\boldsymbol{\alpha}$ in (3.167) giving

$$\mathbf{A}^{-1}[\boldsymbol{\ell}(\boldsymbol{\ell}+\mathbf{I})+\boldsymbol{\alpha}]\mathbf{A}=\boldsymbol{\lambda}(\boldsymbol{\lambda}+\mathbf{I}). \tag{3.168}$$

In accord with the above discussion, we only retain terms in $\boldsymbol{\alpha}$ which couple degenerate or almost degenerate channels. Hence $\boldsymbol{\ell}(\boldsymbol{\ell}+\mathbf{I})+\boldsymbol{\alpha}$ has block diagonal form, where each block corresponds to a set of degenerate channels. It follows that $\mathbf{A}$ has the same block diagonal form and consequently commutes with the diagonal matrix $\mathbf{k}^2$ in (3.167). We can therefore transform (3.167) to diagonal form by multiplying on the left by $\mathbf{A}^{-1}$ yielding

$$\left(\frac{\mathrm{d}^2}{\mathrm{d}r^2}-\frac{\boldsymbol{\lambda}(\boldsymbol{\lambda}+\mathbf{I})}{r^2}+\mathbf{k}^2\right)\mathbf{A}^{-1}\mathbf{F}(r)=0,\quad r\geq a. \tag{3.169}$$

We observe that while the elements of the diagonal matrix $\boldsymbol{\lambda}(\boldsymbol{\lambda}+\mathbf{I})$ are real the corresponding effective angular momentum components λ_i are non-integral and can become complex for sufficiently strong long-range dipole interactions represented by the matrix $\boldsymbol{\alpha}$. We will see below that this leads to new and anomalous threshold behaviour.

In order to determine the threshold behaviour we introduce a transformed K-matrix $\mathcal{K}$ in analogy with (3.154) by the asymptotic form

$$\mathbf{A}^{-1}\mathbf{F}(r)=\mathbf{k}^{-1/2}[\mathbf{s}_{\boldsymbol{\lambda}}(\mathbf{k}r)+\mathbf{c}_{\boldsymbol{\lambda}}(\mathbf{k}r)\mathcal{K}],\quad r\geq a, \tag{3.170}$$

where $\mathbf{s}_{\boldsymbol{\lambda}}(\mathbf{k}r)$ and $\mathbf{c}_{\boldsymbol{\lambda}}(\mathbf{k}r)$ are diagonal matrices which satisfy the following asymptotic boundary conditions

$$\mathbf{s}_{\boldsymbol{\lambda}}(\mathbf{k}r)=\mathbf{k}r\,j_{\boldsymbol{\lambda}}(\mathbf{k}r)=\left(\frac{\pi\mathbf{k}r}{2}\right)^{1/2}J_{\boldsymbol{\lambda}+\frac{1}{2}}(\mathbf{k}r)\underset{r\to\infty}{\sim}\sin\left(\mathbf{k}r-\tfrac{1}{2}\boldsymbol{\lambda}\pi\right) \tag{3.171}$$

and

$$\mathbf{c}_{\boldsymbol{\lambda}}(\mathbf{k}r)=-\mathbf{k}r\,n_{\boldsymbol{\lambda}}(\mathbf{k}r)=\left(\frac{\pi\mathbf{k}r}{2}\right)^{1/2}\frac{J_{-\boldsymbol{\lambda}-\frac{1}{2}}(\mathbf{k}r)}{\cos\boldsymbol{\lambda}\pi}\underset{r\to\infty}{\sim}\frac{\cos\left(\mathbf{k}r+\frac{1}{2}\boldsymbol{\lambda}\pi\right)}{\cos\boldsymbol{\lambda}\pi}. \tag{3.172}$$

These equations reduce to Eqs. (3.155) and (3.156) when the dipole potential matrix $\boldsymbol{\alpha}$ is zero and hence the diagonal elements of $\boldsymbol{\lambda}$ reduce to integer values given by $\boldsymbol{\ell}$. Also, as discussed in Appendix C.2, the spherical Bessel functions, defined by (3.171) and (3.172), have simple analytic properties in the complex energy plane for non-integral and complex values of $\boldsymbol{\lambda}$ which enables the development of the multichannel effective range theory described below.

The analytic properties of the transformed K-matrix $\boldsymbol{\mathcal{K}}$ can be determined by relating it to the analytic properties of the transformed R-matrix $\boldsymbol{\mathcal{R}}(E)$ corresponding to (3.169). In analogy with (3.157) the R-matrix is defined by

$$\mathbf{A}^{-1}\mathbf{F}(a) = \boldsymbol{\mathcal{R}}(E)\left(a\mathbf{A}^{-1}\frac{\mathrm{d}\mathbf{F}}{\mathrm{d}r} - b\mathbf{A}^{-1}\mathbf{F}\right)_{r=a}. \tag{3.173}$$

It follows from this definition that $\boldsymbol{\mathcal{R}}(E)$ is related to the R-matrix $\mathbf{R}(E)$, corresponding to the original coupled integrodifferential equations, defined by (3.152) and (3.167), by the transformation

$$\boldsymbol{\mathcal{R}}(E) = \mathbf{A}^{-1}\mathbf{R}(E)\mathbf{A}. \tag{3.174}$$

Since $\mathbf{R}(E)$ is an analytic function of energy with simple poles only on the real energy axis and since $\mathbf{A}$ does not depend on the energy, then $\boldsymbol{\mathcal{R}}(E)$ is also an analytic function of energy with poles only on the real energy axis. We set the arbitrary constant $b = 0$ in (3.173) and substitute the expression for $\mathbf{A}^{-1}\mathbf{F}(a)$ given by (3.170) into (3.173). After re-arranging the terms and using the Wronskian relation $\mathbf{s}'_{\boldsymbol{\lambda}}\mathbf{c}_{\boldsymbol{\lambda}} - \mathbf{c}'_{\boldsymbol{\lambda}}\mathbf{s}_{\boldsymbol{\lambda}} = \mathbf{I}$, we obtain

$$\boldsymbol{\mathcal{K}}^{-1} = -\frac{\mathbf{c}_{\boldsymbol{\lambda}}}{\mathbf{s}_{\boldsymbol{\lambda}}} + \frac{\mathbf{I}}{\mathbf{s}'_{\boldsymbol{\lambda}}\mathbf{s}_{\boldsymbol{\lambda}}} + \boldsymbol{\rho}^{-1/2}\mathbf{s}'^{-1}_{\boldsymbol{\lambda}}\left(\boldsymbol{\mathcal{R}}(E) - \boldsymbol{\rho}^{-1}\frac{\mathbf{s}_{\boldsymbol{\lambda}}}{\mathbf{s}'_{\boldsymbol{\lambda}}}\right)^{-1}\mathbf{s}'^{-1}_{\boldsymbol{\lambda}}\boldsymbol{\rho}^{-1/2}, \tag{3.175}$$

where $\boldsymbol{\rho} = \mathbf{k}a$ and $\mathbf{s}_{\boldsymbol{\lambda}}$, $\mathbf{s}'_{\boldsymbol{\lambda}}$, $\mathbf{c}_{\boldsymbol{\lambda}}$ and $\mathbf{c}'_{\boldsymbol{\lambda}}$ are defined by (3.159) with $\boldsymbol{\ell}$ replaced by $\boldsymbol{\lambda}$. We see that (3.175) has the same form as (3.160) where the diagonal elements of $\boldsymbol{\lambda}$ are replaced by integer values given by $\boldsymbol{\ell}$. The analytic behaviour of the K-matrix $\boldsymbol{\mathcal{K}}$ in the complex energy plane is then given in terms of the analytic properties of $\mathbf{s}_{\boldsymbol{\lambda}}$, $\mathbf{s}'_{\boldsymbol{\lambda}}$ and $\mathbf{c}_{\boldsymbol{\lambda}}$ together with those of the R-matrix $\boldsymbol{\mathcal{R}}(E)$.

Following our discussion which led to (3.161), we find that $\boldsymbol{\mathcal{K}}^{-1}$ can be written in the form

$$\boldsymbol{\mathcal{K}}^{-1} = \mathbf{k}^{-\boldsymbol{\lambda}-\frac{1}{2}}\boldsymbol{\mathcal{M}}(E)\mathbf{k}^{-\boldsymbol{\lambda}-\frac{1}{2}}, \tag{3.176}$$

where the M-matrix $\boldsymbol{\mathcal{M}}(E)$ is an analytic function of energy which does not contain threshold branch cuts. Also, it follows from (3.175) and (3.176) that $\boldsymbol{\mathcal{M}}(E)$ is symmetric and when all the elements of $\boldsymbol{\lambda}$ are real then $\boldsymbol{\mathcal{M}}(E)$ is also real. However, if some of the elements of $\boldsymbol{\lambda}$ are complex then $\boldsymbol{\mathcal{M}}(E)$ will also be complex. Hence $\boldsymbol{\mathcal{M}}(E)$ can be expanded as a power series in the energy

$$\boldsymbol{\mathcal{M}}(E) = \boldsymbol{\mathcal{M}}_0 + \boldsymbol{\mathcal{M}}_1 E + \boldsymbol{\mathcal{M}}_2 E^2 + \cdots, \tag{3.177}$$

where the coefficients $\boldsymbol{\mathcal{M}}_0$, $\boldsymbol{\mathcal{M}}_1$, $\boldsymbol{\mathcal{M}}_2, \ldots$ are in general complex symmetric energy-independent matrices.

In order to determine the corresponding multichannel effective range theory expressions for the S- and T-matrices we recombine the columns of (3.170) by multiplying on the right by a matrix $\mathbf{B}$ to give

$$\mathbf{A}^{-1}\mathbf{F}(r)\mathbf{B} = \mathbf{k}^{-1/2}\left\{\exp\left[-\mathrm{i}\left(\mathbf{k}r - \tfrac{1}{2}\boldsymbol{\lambda}\pi\right)\right] - \exp\left[\mathrm{i}\left(\mathbf{k}r - \tfrac{1}{2}\boldsymbol{\lambda}\pi\right)\right]\boldsymbol{\mathcal{S}}\right\}, \quad r \geq a, \tag{3.178}$$

where the transformed S-matrix $\boldsymbol{\mathcal{S}}$ is defined by

$$\boldsymbol{\mathcal{S}} = [\mathbf{I} + \mathrm{i}(\mathbf{I} + \mathrm{i}\tan\boldsymbol{\lambda}\pi)\boldsymbol{\mathcal{K}}]\,[\mathbf{I} - \mathrm{i}(\mathbf{I} - \mathrm{i}\tan\boldsymbol{\lambda}\pi)\boldsymbol{\mathcal{K}}]^{-1} \tag{3.179}$$

and $\mathbf{B}$ is defined by

$$\mathbf{B}^{-1} = -\frac{1}{2\mathrm{i}}\,[\mathbf{I} - \mathrm{i}(\mathbf{I} - \mathrm{i}\tan\boldsymbol{\lambda}\pi)\boldsymbol{\mathcal{K}}]\,. \tag{3.180}$$

We then transform (3.178) by multiplying this equation on the left by $\mathbf{A}$ and on the right by

$$\mathbf{C} = \exp\left(-\tfrac{1}{2}\mathrm{i}\boldsymbol{\lambda}\pi\right)\mathbf{A}^{-1}\exp\left(\tfrac{1}{2}\mathrm{i}\boldsymbol{\ell}\pi\right), \tag{3.181}$$

which yields

$$\mathbf{F}(r)\mathbf{B}\mathbf{C} = \mathbf{k}^{-1/2}\left\{\exp\left[-\mathrm{i}\left(\mathbf{k}r - \tfrac{1}{2}\boldsymbol{\ell}\pi\right)\right] - \exp\left[\mathrm{i}\left(\mathbf{k}r - \tfrac{1}{2}\boldsymbol{\ell}\pi\right)\right]\mathbf{S}\right\}, \quad r \geq a, \tag{3.182}$$

where the S-matrix $\mathbf{S}$ is defined by

$$\mathbf{S} = \exp\left(\tfrac{1}{2}\mathrm{i}\boldsymbol{\ell}\pi\right)\mathbf{A}\exp\left(-\tfrac{1}{2}\mathrm{i}\boldsymbol{\lambda}\pi\right)\boldsymbol{\mathcal{S}}\exp\left(-\tfrac{1}{2}\mathrm{i}\boldsymbol{\lambda}\pi\right)\mathbf{A}^{-1}\exp\left(\tfrac{1}{2}\mathrm{i}\boldsymbol{\ell}\pi\right). \tag{3.183}$$

Finally, we substitute for $\boldsymbol{\mathcal{S}}$ given by (3.179) into (3.183), where $\boldsymbol{\mathcal{K}}$ is written in terms of $\boldsymbol{\mathcal{M}}(E)$ using (3.176). We find that

$$\begin{aligned}\mathbf{T} = {} & \exp\left(\tfrac{1}{2}\mathrm{i}\boldsymbol{\ell}\pi\right)\mathbf{A}\exp\left(-\tfrac{1}{2}\mathrm{i}\boldsymbol{\lambda}\pi\right)\mathbf{k}^{\boldsymbol{\lambda}+\frac{1}{2}}\,\frac{2\mathrm{i}}{\boldsymbol{\mathcal{M}}(E) - \mathrm{i}(\mathbf{I} - \mathrm{i}\tan\boldsymbol{\lambda}\pi)\mathbf{k}^{2\boldsymbol{\lambda}+1}} \\ & \times \mathbf{k}^{\boldsymbol{\lambda}+\frac{1}{2}}\exp\left(-\tfrac{1}{2}\mathrm{i}\boldsymbol{\lambda}\pi\right)\mathbf{A}^{-1}\exp\left(\tfrac{1}{2}\mathrm{i}\boldsymbol{\ell}\pi\right) \\ & + \exp\left(\tfrac{1}{2}\mathrm{i}\boldsymbol{\ell}\pi\right)\mathbf{A}\exp(-\mathrm{i}\boldsymbol{\lambda}\pi)\mathbf{A}^{-1}\exp\left(\tfrac{1}{2}\mathrm{i}\boldsymbol{\ell}\pi\right) - \mathbf{I},\end{aligned} \tag{3.184}$$

which is the effective range expression for the T-matrix in the presence of long-range dipole potentials, where we remember that $\mathbf{T} = \mathbf{S} - \mathbf{I}$. We see that when the dipole potential matrix $\boldsymbol{\alpha}$ is zero then $\boldsymbol{\lambda} = \boldsymbol{\ell}$ and $\mathbf{A} = \mathbf{I}$ so that $\tan\boldsymbol{\lambda}\pi = 0$. Equation (3.184) then reduces to (3.163) valid for short-range potentials. It follows from (3.184) that the well-known symmetry of the S-matrix, and hence the T-matrix,

corresponds to the symmetry of the M-matrix $\boldsymbol{\mathcal{M}}(E)$ discussed above. In addition it should be noted that the unitarity of the S-matrix imposes further restrictions on $\boldsymbol{\mathcal{M}}(E)$.

We observe that, as in potential scattering discussed in Sect. 1.4.2, for a sufficiently strong long-range dipole potential $\mathbf{U}(r)$, defined by (3.166), individual components λ_i of the diagonal matrix $\boldsymbol{\lambda}$ defined by (3.168) can be complex and can be written as

$$\lambda_i = -\frac{1}{2} + \mathrm{i}\,\mathrm{Im}\,\lambda_i, \tag{3.185}$$

where $\mathrm{Im}\,\lambda_i$ can be positive or negative. It follows that the corresponding components of the factor $\mathbf{k}^{\lambda+\frac{1}{2}}$ in the T-matrix defined by (3.184) can be written as

$$k_i^{\lambda_i+\frac{1}{2}} = k_i^{\mathrm{i}\,\mathrm{Im}\lambda_i} = \exp(\mathrm{i}\,\mathrm{Im}\,\lambda_i \ln k_i), \tag{3.186}$$

which gives rise to an infinite number of oscillations in the cross section as the energy tends to threshold from above. Also, an infinite number of bound states or resonances converge to this threshold from below.

As an example of the above analysis we consider electron collisions with atomic hydrogen for total orbital angular momentum $L = 0$ near the $n = 2$ threshold. The coupled second-order integrodifferential equations coupling the 2s and 2p states then have the following form for $r \geq a$:

$$\begin{aligned}\left(\frac{\mathrm{d}^2}{\mathrm{d}r^2} + k_2^2\right) F_{2\mathrm{s}}(r) - \frac{6}{r^2} F_{2\mathrm{p}}(r) = 0,\\ \left(\frac{\mathrm{d}^2}{\mathrm{d}r^2} - \frac{2}{r^2} + k_2^2\right) F_{2\mathrm{p}}(r) - \frac{6}{r^2} F_{2\mathrm{s}}(r) = 0,\end{aligned} \tag{3.187}$$

where a is chosen such that non-local exchange and correlation potentials vanish for $r \geq a$ so that the following analysis applies for both singlet $S = 0$ and triplet $S = 1$ total spin states. Also in (3.187) we have neglected the diagonal r^{-3} potential in the 2p channel, since its presence does not significantly alter the following analysis. Comparing (3.187) with (3.167) we see that the coefficient of the r^{-2} term in (3.167) has the following matrix form

$$\boldsymbol{\ell}(\boldsymbol{\ell} + \mathbf{I}) + \boldsymbol{\alpha} = \begin{bmatrix} 0 & 6 \\ 6 & 2 \end{bmatrix}, \tag{3.188}$$

which can be diagonalized, as in (3.168), to yield the matrix

$$\boldsymbol{\lambda}(\boldsymbol{\lambda} + \mathbf{I}) = \begin{bmatrix} 1 + \sqrt{37} & 0 \\ 0 & 1 - \sqrt{37} \end{bmatrix}. \tag{3.189}$$

The corresponding diagonal elements of $\boldsymbol{\lambda}$ are then

$$\lambda_1 = -\frac{1}{2} \pm \left[\sqrt{37} + \frac{5}{4}\right]^{1/2},$$
$$\lambda_2 = -\frac{1}{2} \pm \mathrm{i}\left[\sqrt{37} - \frac{5}{4}\right]^{1/2}, \tag{3.190}$$

and the diagonalized form of (3.187) can be written as

$$\left(\frac{\mathrm{d}^2}{\mathrm{d}r^2} - \frac{\boldsymbol{\lambda}(\boldsymbol{\lambda}+\mathbf{I})}{r^2} + \mathbf{k}_2^2\right)\mathbf{A}^{-1}\mathbf{F}(r) = 0, \quad r \geq a, \tag{3.191}$$

where the orthogonal matrix $\mathbf{A}$ is defined by (3.168).

We now consider the zero-energy solution of (3.191) corresponding to the complex second eigenvalue λ_2, defined by (3.190). Writing $\mathbf{G} = \mathbf{A}^{-1}\mathbf{F}$ we see that the general solution of (3.191) corresponding to this eigenvalue can be written as

$$G_2(r) = d_1 r^{\lambda_2+1} + d_2 r^{-\lambda_2}, \quad r \geq a. \tag{3.192}$$

After substituting for λ_2 from (3.190) we can re-write (3.192) in the general form

$$G_2(r) = b r^{1/2} \sin(\mathrm{Im}\,\lambda_2 \ln r + \delta), \quad r \geq a. \tag{3.193}$$

where

$$\mathrm{Im}\,\lambda_2 = \left[\sqrt{37} - \frac{5}{4}\right]^{1/2} = 2.19835\ldots, \tag{3.194}$$

and where the coefficients b and δ in (3.193) are determined by fitting to the internal region solution of the coupled integrodifferential equations at $r = a$. We see that the solution $G_2(r)$, defined by (3.193), has an infinite number of oscillations in r in the range $a \leq r \leq \infty$, which corresponds to an infinite number of bound states supported by the angular momentum term in (3.191), which can be written in this case as

$$-\frac{\lambda_2(\lambda_2+1)}{r^2} = \frac{0.25 + (\mathrm{Im}\,\lambda_2)^2}{r^2}, \tag{3.195}$$

which is clearly attractive.

We next consider the solution of (3.191) for negative k_2^2. We first observe that an increase in the argument of the zero-energy solution (3.193) by π radians, corresponding to an additional node in the oscillation, occurs when the radius r increases by the ratio

$$\frac{r_2}{r_1} = \exp\left(\frac{\pi}{\mathrm{Im}\,\lambda_2}\right). \tag{3.196}$$

When k_2^2 is negative these oscillations are cut off for large r when the k_2^2 term in (3.191) dominates the angular momentum term. As the magnitude of k_2^2 decreases towards zero, additional oscillations are supported by the angular momentum term, each corresponding to an additional bound state. We then see from (3.191) and (3.196) that the ratio of the magnitudes of k_2^2 before and after the additional oscillation is supported is

$$R = \frac{(k_2^2)_{r=r_1}}{(k_2^2)_{r=r_2}} = \frac{r_2^2}{r_1^2} = \exp\left(\frac{2\pi}{\mathrm{Im}\,\lambda_2}\right). \tag{3.197}$$

In the present example we find, using (3.194), that the resonance spacing ratio

$$R = 17.429\ldots. \tag{3.198}$$

We note that (3.197) can be obtained directly from the multichannel effective range theory expansion for the T-matrix, given by (3.184), assuming the constancy of the M-matrix.

The infinite series of bound states predicted by this theory is reduced in practice to a finite number due to relativistic splitting of the $n = 2$ levels of atomic hydrogen, which removes the degeneracy of the levels with the same principal quantum number assumed in the above derivation. In addition, inclusion of coupling with the open 1s channel shifts the energies of the bound states into the complex energy plane where they give rise to a series of resonances, where the ratio of the widths of the neighbouring resonances also satisfies (3.197) and (3.198). The first resonance in this series with $^1S^e$ symmetry was found by Burke and Schey [160] at ~9.6 eV incident electron energy in a close coupling calculation including the 1s, 2s and 2p target states in expansion (2.57) and was first observed experimentally by Schulz [836].

The above analysis can be carried out for electron–hydrogen atom collisions for all total orbital angular momentum L and at all thresholds corresponding to principal quantum numbers $n \geq 2$, as discussed by Burke [151, 152] and Pathak et al. [720, 721]. We find that complex λ values leading to anomalous threshold behaviour are found at all thresholds with $n \geq 2$ for small L. We summarize the resonance spacing ratio R defined by (3.197) for $L \leq 6$ and for $n \leq 5$ in Table 3.1, where relativistic fine-structure splitting of the levels is neglected. We see that for some (L, n) values more than one resonance series occur. Also, as the principal quantum number n increases we find that resonance series occur for an increasing number of L values. We also find that for a given L, however large, resonance series will occur for sufficiently high n.

3.3.3 Excitation: Coulomb Potential

In this and the next section we extend our discussion of the threshold behaviour of excitation cross sections to treat many coupled two-body channels interacting through a Coulomb potential, corresponding to electron collisions with positive and

Table 3.1 Level spacing ratios R for electron–hydrogen atom resonances at thresholds corresponding to total orbital angular momentum $L \leq 6$ and principal quantum number $n \leq 5$ for both total spin angular momenta $S = 0$ and 1

n	$L=0$	$L=1$	$L=2$	$L=3$	$L=4$	$L=5$	$L=6$
2	17.429	29.334	4422.18	–	–	–	–
3	4.823	5.164	6.134	9.323	62.416	–	–
	–	16.752	80.552	–	–	–	–
4	2.982	3.047	3.197	3.485	4.070	5.608	16.698
	16.210	4.360	4.940	6.494	14.492	–	–
	–	27.299	18.777	8.516^{8}	–	–	–
	–	–	3226.6	–	–	–	–
5	2.312	2.334	2.382	2.463	2.594	2.812	3.213
	4.107	2.792	2.901	3.103	3.484	4.326	7.354
	–	4.224	4.091	4.892	7.396	59.907	–
	–	32.955	4.766	6.184	12.838	–	–
	–	–	9.577^{5}	25.479	–	–	–

The superscripts 5 and 8 are abbreviations for $\times 10^5$ and $\times 10^8$, respectively.

negative ions. In this section we obtain an effective range expression, first derived by Gailitis [357] using the analytic properties of the R-matrix, and we discuss the behaviour of the cross sections near threshold for an attractive Coulomb potential. Then in Sect. 3.3.4 we consider multichannel quantum defect theory (MQDT) introduced, developed and reviewed by Seaton [859], which is widely used in the analysis and calculation of electron collisions with positive ions and corresponding photoionization processes in the neighbourhood of threshold. Also, we summarize some of the most important extensions of MQDT to molecular collision processes.

3.3.3.1 Effective Range Theory

We consider the solution of n coupled second-order integrodifferential equations (3.2) describing the scattering of electrons by multi-electron positive or negative ions. We assume that the potential matrix $\mathbf{U}(r)$ in this equation, representing the local direct, non-local exchange and non-local correlation potentials, can be neglected for r greater than some radius a. Hence (3.2) then reduces to

$$\left(\frac{\mathrm{d}^2}{\mathrm{d}r^2} - \frac{\boldsymbol{\ell}(\boldsymbol{\ell}+\mathbf{I})}{r^2} + \frac{2(Z-N)}{r} + \mathbf{k}^2\right)\mathbf{F}(r) = 0, \quad r \geq a, \tag{3.199}$$

The general solution of (3.199) which vanishes at the origin has the following asymptotic form:

$$\mathbf{F}(r) = \mathbf{k}^{-1/2}\left[\mathbf{F}_{\boldsymbol{\ell}}(\boldsymbol{\eta}, \mathbf{k}r) + \mathbf{G}_{\boldsymbol{\ell}}(\boldsymbol{\eta}, \mathbf{k}r)\mathbf{K}\right], \quad r \geq a, \tag{3.200}$$

where $\mathbf{F}_\ell(\boldsymbol{\eta}, \mathbf{k}r)$ and $\mathbf{G}_\ell(\boldsymbol{\eta}, \mathbf{k}r)$ are diagonal matrices whose diagonal elements are the regular and irregular Coulomb wave functions, defined, respectively, by (1.58) and (1.59), where $\boldsymbol{\eta} = -(Z-N)/\mathbf{k}$ and $\mathbf{K}$ is the $n \times n$-dimensional K-matrix.

In order to determine the analytic properties of the K-matrix we proceed, as in our discussion of short-range potentials in Sect. 3.3.1, by relating the K-matrix to the analytic properties of the $n \times n$-dimensional R-matrix $\mathbf{R}(E)$, defined on the boundary $r = a$ by

$$\mathbf{F}(a) = \mathbf{R}(E)\left(a\frac{\mathrm{d}\mathbf{F}}{\mathrm{d}r} - b\mathbf{F}\right)_{r=a}, \tag{3.201}$$

We then set the arbitrary constant $b = 0$ in (3.201) and substitute the expression for $\mathbf{F}(a)$ given by (3.200) into (3.201). After re-arranging terms and using the Wronskian relation $\mathbf{F}'_\ell\mathbf{G}_\ell - \mathbf{G}'_\ell\mathbf{F}_\ell = \mathbf{I}$ we obtain

$$\mathbf{K}^{-1} = -\frac{\mathbf{G}_\ell}{\mathbf{F}_\ell} + \frac{\mathbf{I}}{\mathbf{F}'_\ell\mathbf{F}_\ell} + \boldsymbol{\rho}^{-1/2}\mathbf{F}'^{-1}_\ell\left(\mathbf{R}(E) - \boldsymbol{\rho}^{-1}\frac{\mathbf{F}_\ell}{\mathbf{F}'_\ell}\right)^{-1}\mathbf{F}'^{-1}_\ell\boldsymbol{\rho}^{-1/2}, \tag{3.202}$$

where the diagonal matrix $\boldsymbol{\rho} = \mathbf{k}a$ and the diagonal matrices $\mathbf{F}_\ell$, $\mathbf{F}'_\ell$, $\mathbf{G}_\ell$ and $\mathbf{G}'_\ell$ are defined by

$$\mathbf{F}_\ell = \mathbf{F}_\ell(\boldsymbol{\eta}, \mathbf{k}a), \quad \mathbf{G}_\ell = \mathbf{G}_\ell(\boldsymbol{\eta}, \mathbf{k}a), \quad \mathbf{F}'_\ell = \frac{1}{\mathbf{k}}\frac{\mathrm{d}\mathbf{F}_\ell}{\mathrm{d}r}\bigg|_{r=a}, \quad \mathbf{G}'_\ell = \frac{1}{\mathbf{k}}\frac{\mathrm{d}\mathbf{G}_\ell}{\mathrm{d}r}\bigg|_{r=a}. \tag{3.203}$$

We see that (3.202) has the same form as (3.160) obtained for short-range potentials and (3.175) obtained for dipole potentials. Hence, as in those cases, the analytic properties of the K-matrix in the complex energy plane can be obtained in terms of the analytic properties of the matrices $\mathbf{F}_\ell$, $\mathbf{F}'_\ell$ and $\mathbf{G}_\ell$ together with those of the R-matrix $\mathbf{R}(E)$.

The analytic properties of the Coulomb wave functions have been described in our development of an effective range expansion for potential scattering by a Coulomb potential in Sect. 1.4.3 and are given by (1.175) and the following equations. Using these results, we find that (3.202) yields the following multichannel effective range expression for the T-matrix:

$$\mathbf{T} = \mathbf{k}^{\ell+\frac{1}{2}}(2\boldsymbol{\ell}+\mathbf{I})!!\mathbf{C}_\ell(\boldsymbol{\eta})\frac{2\mathrm{i}}{\mathbf{M}(E) - \mathbf{k}^{2\ell+1}[(2\boldsymbol{\ell}+\mathbf{I})!!]^2\mathbf{p}_\ell(\boldsymbol{\eta})\boldsymbol{\tau}(2\boldsymbol{\ell}+\mathbf{I})^{-1}} \times \mathbf{C}_\ell(\boldsymbol{\eta})(2\boldsymbol{\ell}+\mathbf{I})!!\,\mathbf{k}^{\ell+\frac{1}{2}}, \tag{3.204}$$

where $\mathbf{C}_\ell(\boldsymbol{\eta})$, $\mathbf{p}_\ell(\boldsymbol{\eta})$ and $\boldsymbol{\tau}$ are diagonal matrices whose diagonal elements are defined by (1.60), (1.179) and (1.185), respectively. We can then show that the M-matrix in (3.204) is given by

$$\mathbf{M}(E) = \frac{(2\boldsymbol{\ell}+\mathbf{I})!!}{a^{\boldsymbol{\ell}+\frac{1}{2}}}\left\{-\frac{\boldsymbol{\Psi}_{\boldsymbol{\ell}}}{(2\boldsymbol{\ell}+\mathbf{I})\boldsymbol{\Phi}_{\boldsymbol{\ell}}} - \frac{\mathbf{k}^{2\boldsymbol{\ell}+1}\mathbf{p}_{\boldsymbol{\ell}}(\boldsymbol{\eta})a^{2\boldsymbol{\ell}+1}}{(2\boldsymbol{\ell}+\mathbf{I})}\right.$$
$$\times\left[\ln 2a + \frac{\mathbf{q}_{\boldsymbol{\ell}}(\boldsymbol{\eta})}{\mathbf{p}_{\boldsymbol{\ell}}(\boldsymbol{\eta})} - f(\boldsymbol{\eta})\right] + \frac{1}{\boldsymbol{\Phi}_{\boldsymbol{\ell}}\overline{\boldsymbol{\Phi}}_{\boldsymbol{\ell}}} - \frac{1}{\overline{\boldsymbol{\Phi}}_{\boldsymbol{\ell}}}\left[\frac{\boldsymbol{\Phi}_{\boldsymbol{\ell}}}{\overline{\boldsymbol{\Phi}}_{\boldsymbol{\ell}}} - \mathbf{R}(E)\right]\frac{1}{\overline{\boldsymbol{\Phi}}_{\boldsymbol{\ell}}}\Bigg\}$$
$$\times \frac{(2\boldsymbol{\ell}+\mathbf{I})!!}{a^{\boldsymbol{\ell}+\frac{1}{2}}}, \tag{3.205}$$

where

$$\overline{\boldsymbol{\Phi}}_{\boldsymbol{\ell}} = (\boldsymbol{\ell}+\mathbf{I})\boldsymbol{\Phi}_{\boldsymbol{\ell}} + a\frac{\mathrm{d}\boldsymbol{\Phi}_{\boldsymbol{\ell}}}{\mathrm{d}r}\bigg|_{r=a}. \tag{3.206}$$

Also in (3.205) we have written $\boldsymbol{\Phi}_{\boldsymbol{\ell}} \equiv \boldsymbol{\Phi}_{\boldsymbol{\ell}}(\boldsymbol{\eta}, \mathbf{k}a)$, $\boldsymbol{\Psi}_{\boldsymbol{\ell}} \equiv \boldsymbol{\Psi}_{\boldsymbol{\ell}}(\boldsymbol{\eta}, \mathbf{k}a)$ and $\overline{\boldsymbol{\Phi}}_{\boldsymbol{\ell}} \equiv \overline{\boldsymbol{\Phi}}_{\boldsymbol{\ell}}(\boldsymbol{\eta}, \mathbf{k}a)$, which are diagonal matrices whose diagonal elements Φ_ℓ, Ψ_ℓ and $\overline{\Phi}_\ell$ are entire functions of the energy. It follows from (3.205) that the M-matrix $\mathbf{M}(E)$ is a symmetric matrix which is real on the real energy axis and which is an analytic function of energy without threshold branch cuts. Hence $\mathbf{M}(E)$ can be expanded as a power series in energy

$$\mathbf{M}(E) = \mathbf{M}_0 + \mathbf{M}_1 E + \mathbf{M}_2 E^2 + \cdots, \tag{3.207}$$

where $\mathbf{M}_0, \mathbf{M}_1, \mathbf{M}_2, \ldots$ are real symmetric energy-independent matrices.

The multichannel effective range equation (3.204) was first derived by Gailitis [357]. We can show that it reduces to (1.187) for single-channel scattering by a Coulomb potential and to (3.163), obtained by Ross and Shaw [798], for multichannel scattering by short-range potentials. It follows that (3.204) enables the T-matrix to be extrapolated through thresholds, relating the cross sections above and below thresholds.

3.3.3.2 Cross Sections Near Threshold

We now obtain an equation relating the T-matrix and the cross sections above and below threshold for scattering by an attractive long-range Coulomb potential. We consider processes involving n coupled channels, corresponding to a given set of conserved quantum numbers, where the target states included are ordered in increasing energy so that (2.78) is satisfied. We determine the behaviour of the cross sections in the neighbourhood of the nth or highest threshold which we assume is non-degenerate.

We commence by observing that the M-matrix $\mathbf{M}(E)$ and the quantity $\mathbf{k}^{2\boldsymbol{\ell}+1}\mathbf{p}_{\boldsymbol{\ell}}(\boldsymbol{\eta})$ in (3.204) are analytic through the thresholds. We then obtain the following relation by evaluating (3.204) just above and just below the nth threshold

$$\left[\boldsymbol{\tau} + \mathrm{i}\mathbf{C}_0(\boldsymbol{\eta})\boldsymbol{\eta}^{-1/2}\mathbf{T}^{-1}\boldsymbol{\eta}^{-1/2}\mathbf{C}_0(\boldsymbol{\eta})\right]^a = \left[\boldsymbol{\tau} + \mathrm{i}\mathbf{C}_0(\boldsymbol{\eta})\boldsymbol{\eta}^{-1/2}\mathbf{T}^{-1}\boldsymbol{\eta}^{-1/2}\mathbf{C}_0(\boldsymbol{\eta})\right]^b. \tag{3.208}$$

The superscript a in (3.208) and later equations means that the quantity is evaluated in the limit $k_n^2 \to 0$ from above the nth threshold and the superscript b in this and later equations means that the quantity is evaluated in the limit $k_n^2 \to 0$ from below the nth threshold.

In order to relate $\mathbf{T}^a$ and $\mathbf{T}^b$ using (3.208) we consider the behaviour of the diagonal matrices $\mathbf{C}_0(\boldsymbol{\eta})\boldsymbol{\eta}^{-1/2}$ and $\boldsymbol{\tau}$ in the neighbourhood of the nth threshold. It follows from (1.61) that the first $(n-1)$ diagonal elements of $\mathbf{C}_0(\boldsymbol{\eta})\boldsymbol{\eta}^{-1/2}$ are continuous at the nth threshold. However, while the nth diagonal element is smoothly varying above this threshold, where the limit at threshold is

$$\left(\mathbf{C}_0^2(\boldsymbol{\eta})\boldsymbol{\eta}^{-1/2}\right)^a = -2\pi, \tag{3.209}$$

it is rapidly oscillating and discontinuous below this threshold. Also, it follows from (1.190) and (1.191) that while the first $(n-1)$ diagonal elements of the matrix $\boldsymbol{\tau}$ are continuous at the nth threshold, the nth diagonal element is discontinuous at this threshold. We find that

$$\tau_{jj}^a - \tau_{jj}^b = 0, \quad j = 1, \ldots, n-1 \tag{3.210}$$

and

$$\tau_{nn}^a - \tau_{nn}^b = -\mathrm{i}\pi - \pi \cot \frac{\pi z}{\kappa_n}. \tag{3.211}$$

Substituting these results into (3.208) and solving for the matrix $\mathbf{T}^b$, we find that the elements of the first $(n-1) \times (n-1)$ sub-matrix of $\mathbf{T}^b$ are given in terms of the $n \times n$ matrix $\mathbf{T}^a$ by

$$T_{jk}^b = \left[\left(\mathbf{T}^a\right)^{-1} - \boldsymbol{\Delta}\right]_{jk}^{-1}, \quad j,\ k = 1, \ldots, n-1, \tag{3.212}$$

where the only non-zero element of $\boldsymbol{\Delta}$ is

$$\Delta_{nn} = \frac{1}{2}\mathrm{i}\left(\cot \frac{\pi z}{\kappa_n} + \mathrm{i}\right) \equiv \frac{1}{2}\mathrm{i}(y + \mathrm{i}), \tag{3.213}$$

which defines y. On the right-hand side of (3.212), the inverse of the full $n \times n$ matrix $\left[(\mathbf{T}^a)^{-1} - \boldsymbol{\Delta}\right]$ is first determined, and then the $(n-1) \times (n-1)$ sub-matrix elements of this inverse matrix are equated to the $(n-1) \times (n-1)$ matrix elements on the left-hand side of (3.212). Owing to the special form of the matrix $\boldsymbol{\Delta}$, defined by (3.213), we can determine the inverse of $\left[(\mathbf{T}^a)^{-1} - \boldsymbol{\Delta}\right]$ explicitly in terms of the matrix elements of $\mathbf{T}^a$ and $\boldsymbol{\Delta}$. We find that (3.212) can be rewritten as

$$T_{jk}^b = T_{jk}^a - \frac{T_{jn}^a\, T_{kn}^a}{T_{nn}^a} + \frac{T_{jn}^a\, T_{kn}^a}{T_{nn}^a} \frac{2\mathrm{i}}{(y+\mathrm{i})\, T_{nn}^a + 2\mathrm{i}}, \quad j,\ k = 1, \ldots, n-1. \tag{3.214}$$

This equation expresses the T-matrix elements T^b_{jk} below threshold in terms of the slowly varying T-matrix elements T^a_{jk} above threshold, which can be taken to have their threshold values. We can see that the T-matrix elements below threshold are rapidly varying because of the factor $y = \cot(\pi z/\kappa_n)$, which has the same value at energies for which z/κ_n differs by an integer. By comparing (3.214) with (3.126) we see that the last term in (3.214) gives rise to a Rydberg series of resonances as $k_n^2 = -\kappa_n^2 \to 0$ from below the nth threshold. We can also show that the corresponding resonance widths Γ are related to the distances D between resonances by the expression

$$\frac{\Gamma}{D} = \frac{1}{2\pi}\left(2\mathrm{Re}\, T^a_{nn} - |T^a_{nn}|^2\right) = \frac{1}{2\pi}\sum_{j=1}^{n-1}|T^a_{jn}|^2, \tag{3.215}$$

which is constant for all resonances in the series.

We can also obtain a relation between the cross sections above and below the nth threshold. We observe that the resonances become very close together as we approach the nth threshold from below. Hence the quantity of interest just below the threshold is the partial wave cross section averaged over resonances, defined by

$$\overline{\sigma}(j \to k) = \frac{1}{D}\int_{E-D/2}^{E+D/2}\sigma(j \to k)\mathrm{d}E = \frac{1}{\pi}\int_{-\infty}^{\infty}\sigma(j \to k)\frac{\mathrm{d}y}{1+y^2}, \tag{3.216}$$

where the cross section is defined in terms of the T-matrix by (2.132) for non-relativistic collisions and by (5.129) for heavy ionic targets where relativistic effects become important. Using (3.214) and (3.216) we obtain the following expression relating the partial wave cross sections above and below the nth threshold:

$$\overline{\sigma}^b(j \to k) = \sigma^a(j \to k) + \frac{\sigma^a(j \to n)\,\sigma^a(n \to k)}{\sum_{k'=1}^{n-1}\sigma^a(n \to k')}, \quad j,\ k = 1, \ldots, n-1. \tag{3.217}$$

We see from this expression that the averaged cross sections below the nth threshold decrease abruptly at the threshold as the energy increases through this threshold. We also see that the total cross section, obtained by summing (3.217) over k, the open channels below the nth threshold, gives

$$\sum_{k=1}^{n-1}\overline{\sigma}^b(j \to k) = \sum_{k=1}^{n-1}\sigma^a(j \to k) + \sigma^a(j \to n), \quad j,\ k = 1, \ldots, n-1. \tag{3.218}$$

Hence, the total partial wave cross section is continuous across the nth threshold for all initial states. Also, the total cross section, obtained by summing over all conserved quantum numbers, is continuous across thresholds. The continuity of the

total cross section across a new threshold was first proved by Baz [83] and by Fonda and Newton [336, 337] by averaging the imaginary part of the scattering amplitude, which is related to the total cross section through the optical theorem.

The above theory has been generalized by Gailitis [357] to the situation where several degenerate channels open at the highest threshold. This occurs, for example, when several degenerate channels are coupled to a target state with non-zero angular momentum. When the cross sections for excitation of target states belonging to the highest threshold are small, corresponding to narrow resonances below this threshold, then the generalization of (3.217) can be written as follows:

$$\overline{\sigma}^b(j \to k) = \sigma^a(j \to k) + \sum_l \frac{\sigma^a(j \to l)\, \sigma^a(l \to k)}{\sum_{k'} \sigma^a(l \to k')}. \tag{3.219}$$

In this equation, j and k correspond to the channels which are open below the highest degenerate threshold, k' is summed over the open channels below this threshold and l is summed over the degenerate channels corresponding to the highest threshold. Hence, as in the case of one threshold channel, the averaged cross sections below the highest degenerate threshold decreases abruptly as the energy increases through this threshold. Also, we find by summing (3.219) over k, corresponding to the open channels below the highest degenerate threshold, that as in (3.218) the total cross section is continuous across this threshold. Again, this result can be obtained by averaging the imaginary part of the scattering amplitude.

Finally, the application of R-matrix theory in the analysis of the behaviour of electron–ion collision cross sections in the neighbourhood of thresholds has also been considered by Lane [565]. In this work the relationship with multichannel quantum defect theory, reviewed in the next section, was discussed.

3.3.4 Multichannel Quantum Defect Theory

In this section we conclude our discussion of the threshold behaviour of excitation cross sections by considering electron collisions with multi-electron positive ions using multichannel quantum defect theory (MQDT) introduced and developed by Seaton [851, 852, 854–856, 858] who also comprehensively reviewed this theory [859]. We then summarize some of the most important developments in the application of MQDT to molecular collision processes.

In our discussion of atomic MQDT it is convenient to introduce z-scaled radial and energy variables defined by

$$\rho = zr, \quad \epsilon = \frac{2E}{z^2}, \tag{3.220}$$

where $z = Z - N$ is the ionic charge, Z being the nuclear charge number and N the number of target electrons. Also, in (3.220), E is the energy of the colliding electron

in atomic units. It is also convenient to define the z-scaled wave number k and the quantity ν^2 by the equations

$$k^2 = \epsilon, \quad \epsilon \geq 0\,; \qquad \epsilon = -\frac{1}{\nu^2}, \quad \epsilon < 0. \tag{3.221}$$

The radial Schrödinger equation describing single-channel electron–ion collisions in the external region $r \geq a$, when the local direct, non-local exchange and non-local correlation potentials are negligible, then becomes

$$\left(\frac{\mathrm{d}^2}{\mathrm{d}\rho^2} - \frac{\ell(\ell+1)}{\rho^2} + \frac{2}{\rho} + \epsilon\right) G(\rho) = 0, \quad \rho \geq za. \tag{3.222}$$

It is clear that (3.199) reduces to (3.222) when only one channel is coupled, where we have written $F(r) \equiv G(\rho)$.

Functions f, g and h which are solutions of (3.222) have been defined by Ham [440] and Seaton [859]. The functions f and g are analytic functions of energy through threshold such that

$$f(\epsilon, \ell; \rho) = \sum_{n=0}^{\infty} \epsilon^n f_n(\ell; \rho), \quad g(\epsilon, \ell; \rho) = \sum_{n=0}^{\infty} \epsilon^n g_n(\ell; \rho). \tag{3.223}$$

Also the function h can be written as

$$h = -(g + \mathcal{G} f), \tag{3.224}$$

where $\mathcal{G}$ is defined by the asymptotic expansion

$$\mathcal{G}(\epsilon, \ell) = \frac{\epsilon A(\epsilon, \ell)}{\pi} \left[\sum_{p=0}^{\ell} \frac{p}{1 + p^2\epsilon} + \frac{1}{12}\left(1 + \frac{\epsilon}{10} + \frac{\epsilon^2}{21} + \frac{\epsilon^3}{20} + \cdots\right)\right], \tag{3.225}$$

with

$$A(\epsilon, \ell) = \prod_{p=0}^{\ell} (1 + p^2\epsilon). \tag{3.226}$$

For small ϵ, a good approximation for $\mathcal{G}$ is obtained by retaining a finite number of terms in the expansion in powers of ϵ. Hence $\mathcal{G}$ and thus h are "nearly analytic functions" of ϵ. The asymptotic forms of the functions f and h when $\epsilon \geq 0$ are given by

$$f(\epsilon, \ell; \rho) \underset{\rho \to \infty}{\sim} \left(\frac{2}{\pi k}\right)^{1/2} \left(\frac{1 - \exp(-2\pi/k)}{A(k^2, \ell)}\right)^{1/2} \sin\theta \tag{3.227}$$

and

$$h(\epsilon, \ell; \rho) \underset{\rho\to\infty}{\sim} \left(\frac{2}{\pi k}\right)^{1/2} \left(\frac{A(k^2, \ell)}{1 - \exp(-2\pi/k)}\right)^{1/2} \cos\theta, \tag{3.228}$$

where

$$\theta = k\rho - \frac{1}{2}\ell\pi + \frac{1}{k}\ln(2k\rho) + \arg\Gamma(\ell + 1 - \mathrm{i}/k). \tag{3.229}$$

The asymptotic forms of the functions f and h when $\epsilon < 0$ are given by

$$f(\epsilon, \ell; \rho) \underset{\rho\to\infty}{\sim} (-1)^\ell \nu^{\ell+1} \left(\frac{\sin(\pi\nu)\Gamma(\nu - \ell)}{\pi}\xi - \frac{\cos(\pi\nu)}{\Gamma(\nu + \ell + 1)}\theta\right) \tag{3.230}$$

and

$$h(\epsilon, \ell; \rho) \underset{\rho\to\infty}{\sim} (-1)^\ell \nu^{\ell+1} A(\epsilon, \ell) \left(\frac{\cos(\pi\nu)\Gamma(\nu - \ell)}{\pi}\xi + \frac{\sin(\pi\nu)}{\Gamma(\nu + \ell + 1)}\theta\right), \tag{3.231}$$

where

$$\xi(\epsilon, \rho) \underset{\rho\to\infty}{\sim} \left(\frac{2\rho}{\nu}\right)^{-\nu} \exp\left(\frac{\rho}{\nu}\right), \quad \theta(\epsilon, \rho) \underset{\rho\to\infty}{\sim} \left(\frac{2\rho}{\nu}\right)^{\nu} \exp\left(-\frac{\rho}{\nu}\right). \tag{3.232}$$

We now use the analytic properties of the functions f and h to derive MQDT equations relating the K-matrix and the S-matrix above and below thresholds. We first observe that the n coupled second-order integrodifferential equations (3.2) reduce to (3.199) when $r \geq a$. Also, we adopt the normalization defined by (3.200) for the solutions which vanish at the origin. When all the channels are open the general solution of (3.2), which defines the $n \times n$-dimensional K-matrix, can then be written as follows:

$$\mathbf{F}(r) = \left(\frac{\pi}{2z}\right)^{1/2} [\mathbf{f} + \mathbf{hK}], \quad r \geq a, \tag{3.233}$$

where $\mathbf{f}$ and $\mathbf{h}$ are diagonal $n \times n$-dimensional matrices, whose diagonal elements have the asymptotic forms defined by (3.227) and (3.228).

We now consider the solution of (3.2) when n_a channels are open and n_b channels are closed, where $n = n_a + n_b$. We can analytically continue the solution defined by (3.233) to this energy region yielding the solution

$$\boldsymbol{\mathcal{F}}(r) = \left(\frac{\pi}{2z}\right)^{1/2} [\mathbf{f} + \mathbf{h}\boldsymbol{\mathcal{K}}], \quad r \geq a, \tag{3.234}$$

where, in the n_b closed channels, the corresponding diagonal elements of $\mathbf{f}$ and $\mathbf{h}$ now have the asymptotic forms defined by (3.230) and (3.231), respectively. Also the $n \times n$-dimensional K-matrix $\mathcal{K}$ in (3.234) is the analytic continuation of the physical K-matrix, defined by (3.233). However, because the functions $\mathbf{f}$ and $\mathbf{h}$ in (3.234) now diverge exponentially in the closed channels, because of the ξ terms in (3.230) and (3.231), the corresponding solution, and hence the K-matrix $\mathcal{K}$, is non-physical.

In order to obtain physical solutions when n_a channels are open, we take linear combinations of the n solutions defined by (3.234), which eliminate the exponentially diverging terms in the closed channels. Hence we write

$$\mathcal{F}(r)\mathbf{C} = \left(\frac{\pi}{2z}\right)^{1/2} [\mathbf{f} + \mathbf{h}\mathcal{K}]\mathbf{C}, \quad r \geq a, \tag{3.235}$$

where $\mathbf{C}$ is an $n \times n_a$-dimensional matrix and where the matrices $\mathcal{F}$, $\mathcal{K}$ and $\mathbf{C}$ are partitioned into open- and closed-channel sub-matrices as follows:

$$\mathcal{F} \equiv \begin{bmatrix} \mathcal{F}_{oo} & \mathcal{F}_{oc} \\ \mathcal{F}_{co} & \mathcal{F}_{cc} \end{bmatrix}, \quad \mathcal{K} \equiv \begin{bmatrix} \mathcal{K}_{oo} & \mathcal{K}_{oc} \\ \mathcal{K}_{co} & \mathcal{K}_{cc} \end{bmatrix}, \quad \mathbf{C} \equiv \begin{bmatrix} \mathbf{C}_{oo} \\ \mathbf{C}_{co} \end{bmatrix}. \tag{3.236}$$

The $n_a \times n_a$-dimensional open-channel sub-matrix of $\mathcal{F}(r)\mathbf{C}$ is then

$$[\mathcal{F}(r)\mathbf{C}]_{oo} \equiv \left(\frac{\pi}{2z}\right)^{1/2} [(\mathbf{f}_o + \mathbf{h}_o\mathcal{K}_{oo})\mathbf{C}_{oo} + \mathbf{h}_o\mathcal{K}_{oc}\mathbf{C}_{co}], \tag{3.237}$$

and the $n_b \times n_a$-dimensional closed-channel sub-matrix of $\mathcal{F}(r)\mathbf{C}$ is

$$[\mathcal{F}(r)\mathbf{C}]_{co} \equiv \left(\frac{\pi}{2z}\right)^{1/2} [\mathbf{h}_c\mathcal{K}_{co}\mathbf{C}_{oo} + (\mathbf{f}_c + \mathbf{h}_c\mathcal{K}_{cc})\mathbf{C}_{co}], \tag{3.238}$$

where in these equations $\mathbf{f}_o$ and $\mathbf{h}_o$ are the diagonal open-channel components of $\mathbf{f}$ and $\mathbf{h}$, and $\mathbf{f}_c$ and $\mathbf{h}_c$ are the diagonal closed-channel components of $\mathbf{f}$ and $\mathbf{h}$, respectively. We then choose $\mathbf{C}_{oo} = \mathbf{I}_{oo}$, where $\mathbf{I}_{oo}$ is the $n_a \times n_a$-dimensional unit matrix, so that the matrix multiplying $\mathbf{f}_o$ in $[\mathcal{F}(r)\mathbf{C}]_{oo}$ is diagonal and we choose the $\mathbf{C}_{co}$ so that the divergent terms in $[\mathcal{F}(r)\mathbf{C}]_{co}$ involving ξ, which arise in $\mathbf{f}_c$ and $\mathbf{h}_c$ defined by (3.230) and (3.231), are eliminated. This last condition yields

$$\mathbf{A}\cos(\pi\nu_c)\mathcal{K}_{co}\mathbf{C}_{oo} + [\sin(\pi\nu_c) + \mathbf{A}\cos(\pi\nu_c)\mathcal{K}_{cc}]\,\mathbf{C}_{co} = 0. \tag{3.239}$$

After setting $\mathbf{A} = \mathbf{I}$, which we see from (3.226) is valid in the neighbourhood of threshold, we find that

$$\mathbf{C}_{co} = -\frac{1}{\mathcal{K}_{cc} + \tan(\pi\boldsymbol{\nu}_c)}\mathcal{K}_{co}, \tag{3.240}$$

where $\boldsymbol{\nu}_c$ is an $n_b \times n_b$-dimensional diagonal matrix in the closed channels, whose diagonal elements are defined by (3.221). It follows that we can write

$$[\boldsymbol{\mathcal{F}}(r)\mathbf{C}]_{oo} = \left(\frac{\pi}{2z}\right)^{1/2} [\mathbf{f}_o + \mathbf{h}_o \mathbf{K}_{oo}], \quad r \geq a, \tag{3.241}$$

where

$$\mathbf{K}_{oo} = \boldsymbol{\mathcal{K}}_{oo} - \boldsymbol{\mathcal{K}}_{oc} \frac{1}{\boldsymbol{\mathcal{K}}_{cc} + \tan(\pi \boldsymbol{\nu}_c)} \boldsymbol{\mathcal{K}}_{co}. \tag{3.242}$$

The $n_a \times n_a$-dimensional K-matrix $\mathbf{K}_{oo}$ defined by (3.242) is the physical K-matrix in the open channels, which can be used to determine the S-matrix, T-matrix and cross sections, as described in Sect. 2.5. We see that it is expressed in terms of the elements of the $n \times n$-dimensional non-physical K-matrix $\boldsymbol{\mathcal{K}}$ which can be analytically continued through thresholds.

We can obtain a similar expression for the $n_a \times n_a$-dimensional S-matrix $\mathbf{S}_{oo}$. When all channels are open the $n \times n$-dimensional physical S-matrix is defined in analogy with (3.233) by

$$\mathbf{G}(r) = \left(\frac{\pi}{2z}\right)^{1/2} [(\mathbf{h} - \mathrm{i}\mathbf{f}) - (\mathbf{h} + \mathrm{i}\mathbf{f})\mathbf{S}], \quad r \geq a, \tag{3.243}$$

where it follows from (3.227) and (3.228) that $(\mathbf{h} - \mathrm{i}\mathbf{f})$ and $(\mathbf{h} + \mathrm{i}\mathbf{f})$ are ingoing and outgoing waves, respectively. We now analytically continue the solution, defined by (3.243) to an energy region where n_a channels are open and n_b channels are closed, yielding in analogy with (3.234) the solution

$$\boldsymbol{\mathcal{G}}(r) = \left(\frac{\pi}{2z}\right)^{1/2} [(\mathbf{h} - \mathrm{i}\mathbf{f}) - (\mathbf{h} + \mathrm{i}\mathbf{f})\boldsymbol{\chi}], \quad r \geq a, \tag{3.244}$$

where the $n \times n$-dimensional unphysical S-matrix $\boldsymbol{\chi}$ is the analytic continuation of the physical S-matrix defined by (3.243). In order to obtain the physical solution when n_a channels are open, we take linear combinations of the n solutions defined by (3.244) which eliminate the exponentially diverging terms in the closed channels. Hence we write

$$\boldsymbol{\mathcal{G}}(r)\mathbf{D} = \left(\frac{\pi}{2z}\right)^{1/2} [(\mathbf{h} - \mathrm{i}\mathbf{f}) - (\mathbf{h} + \mathrm{i}\mathbf{f})\boldsymbol{\chi}]\,\mathbf{D}, \quad r \geq a, \tag{3.245}$$

where $\mathbf{D}$ is an $n \times n_a$-dimensional matrix. We then partition $\boldsymbol{\mathcal{G}}$, $\boldsymbol{\chi}$ and $\mathbf{D}$ into open- and closed-channel sub-matrices as follows:

$$\boldsymbol{\mathcal{G}} \equiv \begin{bmatrix} \boldsymbol{\mathcal{G}}_{oo} & \boldsymbol{\mathcal{G}}_{oc} \\ \boldsymbol{\mathcal{G}}_{co} & \boldsymbol{\mathcal{G}}_{cc} \end{bmatrix}, \quad \boldsymbol{\chi} \equiv \begin{bmatrix} \boldsymbol{\chi}_{oo} & \boldsymbol{\chi}_{oc} \\ \boldsymbol{\chi}_{co} & \boldsymbol{\chi}_{cc} \end{bmatrix}, \quad \mathbf{D} \equiv \begin{bmatrix} \mathbf{D}_{oo} \\ \mathbf{D}_{co} \end{bmatrix}. \tag{3.246}$$

The $n_a \times n_a$-dimensional open-channel sub-matrix of $\mathcal{G}(r)\mathbf{D}$ is then

$$[\mathcal{G}(r)\mathbf{D}]_{oo} \equiv \left(\frac{\pi}{2z}\right)^{1/2} \left\{\left[(\mathbf{h}_o - \mathrm{i}\mathbf{f}_o) - (\mathbf{h}_o + \mathrm{i}\mathbf{f}_o)\boldsymbol{\chi}_{oo}\right]\mathbf{D}_{oo} - \left[(\mathbf{h}_o + \mathrm{i}\mathbf{f}_o)\boldsymbol{\chi}_{oc}\right]\mathbf{D}_{co}\right\}, \tag{3.247}$$

and the $n_b \times n_a$-dimensional closed-channel sub-matrix of $\mathcal{G}(r)\mathbf{D}$ is

$$[\mathcal{G}(r)\mathbf{D}]_{co} \equiv \left(\frac{\pi}{2z}\right)^{1/2} \left\{-\left[(\mathbf{h}_c + \mathrm{i}\mathbf{f}_c)\boldsymbol{\chi}_{co}\right]\mathbf{D}_{oo} + [(\mathbf{h}_c - \mathrm{i}\mathbf{f}_c) - (\mathbf{h}_c + \mathrm{i}\mathbf{f}_c)\boldsymbol{\chi}_{cc}\right]\mathbf{D}_{co}\right\}. \tag{3.248}$$

We then choose $\mathbf{D}_{oo} = \mathbf{I}_{oo}$ so that the matrix multiplying $(\mathbf{h}_o - \mathrm{i}\mathbf{f}_o)$ in $[\mathcal{G}(r)\mathbf{D}]_{oo}$ is diagonal, and we choose $\mathbf{D}_{co}$ so that the divergent terms in $[\mathcal{G}(r)\mathbf{D}]_{co}$ involving ξ, defined by (3.232), are eliminated. This yields

$$\mathbf{D}_{co} = -\frac{1}{\boldsymbol{\chi}_{cc} - \exp(-2\pi\mathrm{i}\boldsymbol{\nu}_c)}\boldsymbol{\chi}_{co}. \tag{3.249}$$

It follows that we can write

$$[\mathcal{G}(r)\mathbf{D}]_{oo} = \left(\frac{\pi}{2z}\right)^{1/2} [(\mathbf{h} - \mathrm{i}\mathbf{f}) - (\mathbf{h} + \mathrm{i}\mathbf{f})\mathbf{S}_{oo}] \ , \quad r \geq a, \tag{3.250}$$

where

$$\mathbf{S}_{oo} = \boldsymbol{\chi}_{oo} - \boldsymbol{\chi}_{oc}\frac{1}{\boldsymbol{\chi}_{cc} - \exp(-2\pi\mathrm{i}\boldsymbol{\nu}_c)}\boldsymbol{\chi}_{co}. \tag{3.251}$$

The $n_a \times n_a$-dimensional matrix $\mathbf{S}_{oo}$ defined by (3.251) is the physical S-matrix in the open channels, which enables the cross sections to be determined, as described in Sect. 2.5. We see that it is expressed in terms of the elements of the non-physical S-matrix $\boldsymbol{\chi}$, which can be analytically continued through the thresholds.

Equation (3.251) can be obtained directly from the $n \times n$-dimensional non-physical K-matrix $\mathcal{K}$, defined by (3.234). In the energy region where n_a channels are open we define an $n \times n$-dimensional matrix $\boldsymbol{\mathcal{S}}$ by the equation

$$\boldsymbol{\mathcal{S}} = \frac{\mathrm{i}\mathbf{I} - \mathcal{K}}{\mathbf{t} + \mathcal{K}}, \tag{3.252}$$

where $\mathbf{t}$ is an $n \times n$-dimensional diagonal matrix with diagonal elements

$$\begin{aligned} t_{jj} &= \mathrm{i}, \quad \text{open channels} \quad j = 1, \ldots, n_a, \\ t_{jj} &= \tan\pi\nu_j, \quad \text{closed channels} \quad j = n_a + 1, \ldots, n. \end{aligned} \tag{3.253}$$

We then express the non-physical $n \times n$-dimensional K-matrix $\mathcal{K}$ in (3.252) in terms of the non-physical $n \times n$-dimensional S-matrix $\boldsymbol{\chi}$ using the equation

$$\boldsymbol{\chi} = \frac{\mathbf{I} + \mathrm{i}\mathcal{K}}{\mathbf{I} - \mathrm{i}\mathcal{K}}, \tag{3.254}$$

which is the analytic continuation of the usual expression relating the K-matrix to the S-matrix when all channels are open, discussed in Sect. 2.5. Substituting the expression for $\mathcal{K}$ in terms of $\boldsymbol{\chi}$ obtained from (3.254) into the right-hand side of (3.252) and separating out the $n_a \times n_a$-dimensional open-channel component of this equation yields

$$\mathcal{S}_{oo} = \boldsymbol{\chi}_{oo} - \boldsymbol{\chi}_{oc} \frac{1}{\boldsymbol{\chi}_{cc} - \exp(-2\pi \mathrm{i}\boldsymbol{\nu}_c)} \boldsymbol{\chi}_{co}. \tag{3.255}$$

We see that the right-hand sides of (3.251) and (3.255) are identical and hence the open-channel component of $\mathcal{S}$, defined by (3.252) and (3.253), corresponds to the physical S-matrix when n_a channels are open. It follows from this analysis that the open-channel K-matrix and S-matrix can be expressed in terms of matrices $\mathcal{K}$ and $\boldsymbol{\chi}$ which can be analytically continued through thresholds.

In concluding our discussion of atomic MQDT we observe that there have been many applications of this theory following its introduction and development by Seaton. These include a series of early applications to the following atomic collision processes: scattering of electrons by He^+ by Bely [89]; absorption of radiation by Ca atoms by Moores [657]; autoionizing and bound states of neutral beryllium atoms by Moores [658]; extrapolation along isoelectronic sequences by Doughty et al. [268]; resonances in the collision strengths for O^+ by Martins and Seaton [638]; complex quantum defects for the e^-–Be^+ system by Norcross and Seaton [695]; photoionization by Dubau and Wells [273] and complex quantum defects for the e^-–He^+ system by Dubau [272]. This series of papers together with many later papers have established MQDT as an essential component of the analysis of atomic resonance and threshold behaviour.

3.3.4.1 Molecular MQDT

Multichannel quantum defect theory has also been extended to describe resonance and threshold behaviour of electron collisions with positive molecular ions as well as near-threshold molecular photoionization and photoabsorption processes. In the remainder of this section we summarize some of the most important developments in this area.

In the pioneering work on molecular collision processes, Fano [303] extended and applied MQDT to the analysis of high-resolution photoabsorption spectra of H_2 near threshold reported by Herzberg [458] and in two Comments [305, 306] discussed the evolution of quantum defect methods. The work on H_2 was later extended by Jungen and Atabek [517], who developed and applied MQDT to ro-vibronic interactions in the photoabsorption spectrum of H_2 and D_2, and by Jungen

and Dill [518], who studied rotational and vibrational preionization channels of H_2 obtaining good agreement with photoionization data of Dehmer and Chupka [255]. Also, Giusti [376] extended molecular MQDT to describe dissociation into two atoms in electron collisions with molecular ions, and Giusti-Suzor and Jungen [377] adapted molecular MQDT to treat the simultaneous vibrational preionization and electronic predissociation in NO observed in the photoabsorption and photoionization spectra. Jungen [516] also developed a unified MQDT treatment of dissociation and ionization processes which was applied to preionized and predissociated resonances in the H_2 spectrum and Stephans and Greene [887] presented an MQDT procedure to calculate the broadening of preionization resonances due to competing predissociation in the ionization continuum of H_2. A review of the earlier developments and applications of molecular MQDT was written by Greene and Jungen [421]. In more recent work, a non-iterative eigenchannel R-matrix approach combined with MQDT was developed by Gao et al. [360] and applied to predissociation of H_2 and a unified MQDT treatment of both molecular ionization and dissociation was developed by Jungen and Ross [519].

We conclude this section by mentioning a major series of dissociative recombination studies of the triatomic ion H_3^+ which has been carried out by Kokoouline and Greene [543, 544] and by dos Santos et al. [267], and which has been extended by Kokoouline and Greene [544, 545] to dissociative recombination of the triatomic ions D_3^+, H_2D^+ and D_2H^+. We will also consider in Sect. 11.1.7.4 intermediate energy electron–H_3^+ collision calculations carried out using R-matrix theory. Dissociative recombination of H_3^+ ion is a fundamental process in diffuse interstellar clouds and, as the simplest triatomic ion, detailed theoretical studies can be seen as a prototype for the study of electron collisions with more complex polyatomic molecules and molecular ions. Also, in contrast to dissociative attachment/recombination in diatomic molecules and ions there is an additional three-body dissociative pathway for H_3^+ where the molecule dissociates into three hydrogen atoms. The theoretical approach developed by Kokoouline and Greene [543, 544] for treating this process combined MQDT to represent the closed channels, the hyperspherical coordinate approach, discussed in Sect. 3.2.6, to represent the motion of the nuclei and inclusion of outgoing wave Siegert [876] pseudostates to represent the vibrational continuum. These pseudostates, which are analogous to the pseudostates introduced in intermediate-energy collisions in Sects. 6.1 and 6.2, are included to let dissociative flux escape if it reaches the hyper-radial boundary. In the later work by dos Santos et al. [267], accurate vibrational wave functions were used and a large number of rotational states of the H_3^+ ground vibrational state were included in the calculation. This resulted in good agreement with dissociative recombination measurements using the Stockholm (CRYRING) and the Heidelberg (TSR) ion storage rings [734], showing the importance of Jahn–Teller coupling between the electronic and vibrational motion. In conclusion, this work has shown that recent state-of-the-art ab initio calculations on dissociative recombination of simple polyatomic molecules using MQDT and a hyperspherical coordinate representation of the collision process are now capable of accurately describing this complex process.

3.3.5 Threshold Behaviour of Ionization

In this section we consider the threshold behaviour of the single ionization process

$$e^- + A \rightarrow A^+ + e^- + e^-, \tag{3.256}$$

where an electron is incident on a neutral atom or positive ion target which we denote by A and an electron is ejected from the target. The foundations of this subject were laid by Wannier [954] who, using an elegant classical analysis, showed that the ionization cross section $\sigma_{\rm ion}$ satisfies the threshold law

$$\sigma_{\rm ion} = aE^m. \tag{3.257}$$

In this equation a is a constant, E is the sum of the kinetic energies of the two outgoing electrons in (3.256) which is zero at threshold and m is defined by

$$m = \frac{1}{4}\left[\left(\frac{100Z-9}{4Z-1}\right)^{1/2} - 1\right], \tag{3.258}$$

where in this case Z is the residual charge number of the ion denoted by A^+ in (3.256). When $Z = 1$, corresponding to ionization of a neutral atomic target, $m \approx 1.127$ and as the charge number of the ion $Z \rightarrow \infty$ we see from (3.258) that $m \rightarrow 1$. We note that in a later paper Wannier [955] extended the analysis to discuss the threshold law for multiple ionization.

Further developments in the classical theory of single ionization were made by Vinkalns and Gailitis [940], who investigated the dependence of the distribution of the ionization cross section on the angle θ_{12} between the final directions of the two outgoing electrons and found that this distribution has a sharp maximum at $\theta_{12} = \pi$ with a width which tends to zero as $E^{1/4}$ as the energy E tends to zero. The classical analysis was extended by Read [780] to small negative values of E and to study the energy partitioning of the two outgoing electrons in the ionization process using accurate trajectory calculations. Wannier's threshold law of ionization has also been derived using semiclassical theory by Peterkop [728–730] and Crothers [236, 237] and was shown by Rau [776] to follow from the two-electron Schrödinger equation. There have been many other important theoretical and computational investigations including studies by Fano [304], Rau [777], Klar and Schlecht [538], Klar [537], Greene and Rau [419, 420], Feagin [315], Altick [15], Kazansky and Ostrovsky [526], Macek and Ovchinnikov [622], Kato and Watanabe [522–524] and Bartlett and Stelbovics [59]. Experimentally, the validity of Wannier's threshold law was first clearly verified by Cvejanović and Read [239] and other early experiments confirming this law were carried out by Spence [884] and by Pichou et al. [735]. Finally, we mention earlier reviews of threshold behaviour of ionization written by Rau [778] and by Read [781] and a more recent review of collisions near threshold written by Sadeghpour et al. [804].

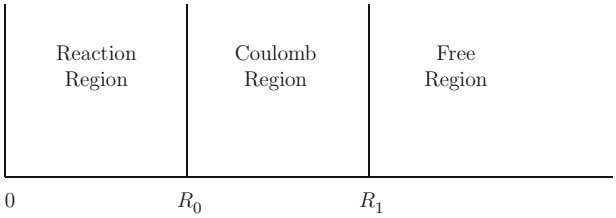

Fig. 3.8 Partitioning of configuration space into three regions in the Wannier theory of threshold ionization

Following Wannier [954], we now derive the threshold law of ionization using a classical analysis. We consider the process represented by (3.256), where the motion of the two electrons in the final state is described using hyperspherical coordinates discussed in Sect. 3.2.6 and defined by (3.128). In Wannier's analysis, configuration space is partitioned into three regions or zones, as illustrated in Fig. 3.8. These are an inner reaction region ($0 \leq R \leq R_0$), an intermediate Coulomb region ($R_0 \leq R \leq R_1$) and an outer free region ($R \geq R_1$). Following the fundamental paper by Wigner [970] on the behaviour of cross sections near threshold, Wannier observed that it is not necessary to know the detailed behaviour of the two electrons taking part in the ionization process in the reaction region. Instead, he assumed that the distribution in phase space of the two electrons is approximately uniform (i.e. quasi-ergodic) when they enter the Coulomb region. Wannier also assumed that for large enough R_0, the Coulomb potential varies sufficiently slowly for classical mechanics to be applicable in the Coulomb region, even when the total energy E of the two outgoing electrons in (3.256) tends to zero. This assumption can be seen to be valid since for a Coulomb potential the local de Broglie wavelength

$$\lambda(R) = \left(2E + \frac{2Z}{R}\right)^{-1/2} \tag{3.259}$$

is slowly varying for large R and the derivative $\mathrm{d}\lambda/\mathrm{d}R$ tends to zero as R tends to infinity. Finally, at very large R, where $R > R_1$, the magnitude of the Coulomb potential energy is less than the combined kinetic energies of the two outgoing electrons, so that these electrons move essentially freely. As $E \to 0$, then the radius $R_1 \to \infty$ and hence the Coulomb region extends to infinity. Hence the threshold behaviour of the ionization cross section is determined by the motion of the two electrons in the Coulomb region.

In order to determine the threshold behaviour of the ionization cross section, we consider the potential function $-C(\alpha, \theta_{12})$ defined by (3.130) and shown in Fig. 3.7. We have already observed that the valleys which occur at $\alpha = 0$ and $\pi/2$ correspond to the electron–nuclear attraction singularities. As a result, when $E \approx 0$ nearly all the classical trajectories end up in one or other of these valleys corresponding to single-electron escape. In order to consider the threshold behaviour of ionization we must consider the behaviour of the trajectories in the neighbourhood of the

saddle point at $\alpha = \pi/4$ and $\theta_{12} = \pi$. Near the saddle point the effective charge $\zeta(\alpha, \theta_{12}) = C(\alpha, \theta_{12})/2$ can be expanded as

$$\zeta(\alpha, \theta_{12}) = \zeta_0 + \frac{1}{2}\zeta_1 \left(\alpha - \frac{\pi}{4}\right)^2 + \frac{1}{8}\zeta_2(\theta_{12} - \pi)^2 + \cdots, \tag{3.260}$$

where

$$\zeta_0 = \frac{4Z - 1}{\sqrt{2}}, \quad \zeta_1 = \frac{12Z - 1}{\sqrt{2}}, \quad \zeta_2 = -\frac{1}{\sqrt{2}}. \tag{3.261}$$

It follows that the motion is stable in θ_{12} but unstable in α at constant R. Clearly, classical trajectories with $\alpha = \pi/4$ and $\theta_{12} = \pi$ lead to double-electron escape since as $R \to \infty$ both r_1 and r_2 tend to infinity.

Following Wannier, we consider the case where the total orbital angular momentum L of the two electrons is equal to zero which dominates the ionization cross section close to threshold. The motion of the electrons can then be described by three variables R, α and θ_{12}. The classical equations of motion then take the form

$$\frac{\mathrm{d}^2 R}{\mathrm{d}t^2} = R\left(\frac{\mathrm{d}\alpha}{\mathrm{d}t}\right)^2 + \frac{1}{4}R\sin^2 2\alpha \left(\frac{\mathrm{d}\theta_{12}}{\mathrm{d}t}\right)^2 - \frac{\zeta}{R^2}, \tag{3.262}$$

$$\frac{\mathrm{d}}{\mathrm{d}t}\left(R^2 \frac{\mathrm{d}\alpha}{\mathrm{d}t}\right) = \frac{1}{2}R^2 \sin 2\alpha \cos 2\alpha \left(\frac{\mathrm{d}\theta_{12}}{\mathrm{d}t}\right)^2 + \frac{1}{R}\frac{\partial \zeta}{\partial \alpha}, \tag{3.263}$$

$$\frac{\mathrm{d}}{\mathrm{d}t}\left(R^2 \sin^2 2\alpha \frac{\mathrm{d}\theta_{12}}{\mathrm{d}t}\right) = \frac{4}{R}\frac{\partial \zeta}{\partial \theta_{12}}, \tag{3.264}$$

and the energy of the system is given by

$$E = \frac{1}{2}\left(\frac{\mathrm{d}R}{\mathrm{d}t}\right)^2 + \frac{1}{2}R^2\left(\frac{\mathrm{d}\alpha}{\mathrm{d}t}\right)^2 + \frac{1}{8}R^2 \sin^2 2\alpha \left(\frac{\mathrm{d}\theta_{12}}{\mathrm{d}t}\right)^2 - \frac{\zeta}{R}. \tag{3.265}$$

We then write

$$\Delta\alpha = \alpha - \frac{\pi}{4} = u_1, \quad \Delta\theta_{12} = \theta_{12} - \pi = u_2, \tag{3.266}$$

and we assume that $\Delta\alpha$ and $\Delta\theta_{12}$ are small quantities. Retaining terms of the same order enables us to write (3.262)–(3.264) in the form

$$\frac{\mathrm{d}^2 R}{\mathrm{d}t^2} = -\frac{\zeta_0}{R} \tag{3.267}$$

and

$$\frac{\mathrm{d}}{\mathrm{d}t}\left(R^2\frac{\mathrm{d}u_i}{\mathrm{d}t}\right)=\frac{\zeta_i u_i}{R},\quad i=1,\ 2, \tag{3.268}$$

where we note that (3.268) are linear uncoupled equations for u_1 and u_2. It follows from (3.265) and (3.267) that the first integral for the velocity is given by

$$\frac{\mathrm{d}R}{\mathrm{d}t}=\left(2E+2\frac{\zeta_0}{R}\right)^{1/2}. \tag{3.269}$$

If we introduce the dimensionless variables

$$\rho=\frac{ER}{\zeta_0},\quad \tau=\frac{E^{3/2}t}{\zeta_0}, \tag{3.270}$$

then (3.268) and (3.269) can be written as

$$\frac{\mathrm{d}}{\mathrm{d}\tau}\left(\rho^2\frac{\mathrm{d}u_i}{\mathrm{d}\tau}\right)=\frac{\zeta_i/\zeta_0}{\rho}u_i,\quad i=1,\ 2 \tag{3.271}$$

and

$$\frac{\mathrm{d}\rho}{\mathrm{d}\tau}=\sqrt{2}\left(1+\frac{1}{\rho}\right)^{1/2}. \tag{3.272}$$

We remark that (3.270), (3.271) and (3.272) imply that the classical orbits are invariant under the transformation

$$R\to aR,\quad E\to a^{-1}E,\quad t\to a^{3/2}t,\quad u_i\to u_i, \tag{3.273}$$

which is sometimes referred to as the "similarity principle" [729, 954]. In particular we see that the quantities u_1 and u_2 depend on E only through the dimensionless variables ρ and τ. We note that the exact classical equations given by (3.262), (3.263) and (3.264) also satisfy this similarity principle.

Equation (3.272) can now be used to rewrite (3.271) in a form such that the independent variable is ρ instead of τ. We find that

$$2\rho(1-\rho)\frac{\mathrm{d}^2u_i}{\mathrm{d}\rho^2}+(3-4\rho)\frac{\mathrm{d}u_i}{\mathrm{d}\rho}=\frac{\zeta_i/\zeta_0}{\rho}u_i,\quad i=1,\ 2. \tag{3.274}$$

Since we are interested in the threshold behaviour $E\to 0$, the situation where $ER\ll\zeta_0$ (i.e. where $\rho\ll 1$) is of particular interest. Equations (3.274) then reduce to

$$\frac{\mathrm{d}^2 u_i}{\mathrm{d}\rho^2} + \frac{3}{2\rho}\frac{\mathrm{d}u_i}{\mathrm{d}\rho} = \frac{\zeta_i/\zeta_0}{2\rho^2} u_i, \quad i = 1,\ 2, \tag{3.275}$$

which have solutions of the form

$$u_1 = c_{11} R^{m_{11}} + c_{12} R^{m_{12}} \tag{3.276}$$

and

$$u_2 = c_{21} R^{m_{21}} + c_{22} R^{m_{22}}, \tag{3.277}$$

where we have reverted to the variable R and where c_{ij} are integration constants. The exponents m_{ij} in (3.276) and (3.277) are given by

$$m_{i1} = -\frac{1}{4} - \frac{1}{2}\mu_i, \quad m_{i2} = -\frac{1}{4} + \frac{1}{2}\mu_i, \quad i = 1,\ 2, \tag{3.278}$$

where

$$\mu_1 = \frac{1}{2}\left(\frac{100Z - 9}{4Z - 1}\right)^{1/2}, \quad \mu_2 = \frac{\mathrm{i}}{2}\left(\frac{9 - 4Z}{4Z - 1}\right)^{1/2}. \tag{3.279}$$

Since $Z \geq 1$ then μ_1 is real and $\geq 5/2$ and μ_2 is imaginary when $1 \leq Z < 9/4$ and is real and less than $1/2$ when $Z \geq 9/4$.

We consider first the dependence of u_2, defined by (3.277), on R and E, where we remember from (3.266) that $u_2 = \Delta\theta_{12}$. For sufficiently small values of E, (3.276) and (3.277) are valid at the inner boundary of the Coulomb region. Now from (3.278) and (3.279) we see that Re $m_{2i} < 0$ when $1/4 < Z < 9/4$ and m_{2i} is real and < 0 when $Z \geq 9/4$, for $i = 1, 2$. Hence when R increases, $\Delta\theta_{12}$ either oscillates with decreasing amplitude or falls off monotonically. This confirms that near threshold the two electrons escape in opposite directions where $\theta_{12} \approx \pi$.

The key equation that enables us to determine the threshold behaviour of ionization is (3.276), where we remember from (3.266) that $u_1 = \Delta\alpha$. We first observe that since μ_1 is real and $\geq 5/2$ when $Z > 1/4$, then m_{11} is real and < 0. Hence as R increases the term $c_{11} R^{m_{11}}$ in (3.276) will tend to zero. On the other hand, m_{12} is always positive and ≥ 1 and hence the term $c_{12} R^{m_{12}}$ will increase as R increases. Therefore, unless restrictions are placed on c_{12} this term will cause u_1 to increase and thus α to move away from the vicinity of $\pi/4$ and to fall into one of the potential wells at $\alpha = 0$ and $\pi/2$ in Fig. 3.7, corresponding to single-electron escape. Hence for ionizing trajectories the coefficient c_{12} must lie in a small interval, namely

$$|c_{12}| \leq c_{\max}, \tag{3.280}$$

where $c_{\max} \to 0$ as $E \to 0$. Moreover, according to the "similarity principle" defined by (3.273), u_1 can only depend on E through ER. We must therefore write

$$c_{12} = d_{12} E^{m_{12}}, \tag{3.281}$$

where d_{12} is a constant. Hence (3.276) becomes

$$u_1 = c_{11} R^{m_{11}} + d_{12} E^{m_{12}} R^{m_{12}}. \tag{3.282}$$

Since, in the neighbourhood of the boundary between the reaction region and the Coulomb region in Fig. 3.8 we have $E \ll Z/R$ we see that for variations of d_{12} of order unity, u_1 will remain small as R increases from R_0.

Wannier calculated the flux of phase space points which corresponds to double-electron escape for constant energy E and a given hyper-radius R. Making use of the quasi-ergodic hypothesis, he showed that this flux does not depend on the hyper-radius and that it varies with energy in the same way as $c_{\max}$. Since this flux is proportional to the total ionization cross section σ_{ion} it follows, using (3.280) and (3.281), that the Wannier threshold law of ionization is given by (3.257) where $m = m_{12}$ is defined by (3.278) and (3.279). Hence we find that m is given by (3.258).

As we pointed out in the introduction to this section, the Wannier threshold law of ionization has been confirmed using both semiclassical and quantum theory derivations. In addition, a number of detailed ab initio quantum theory calculations have been carried out which have provided strong support both for the threshold energy dependence of the ionization cross section and for its angular distribution predicted by Vinkalns and Gailitis [940]. These calculations include (i) an angle–Sturmian basis expansion of the wave function in hyperspherical coordinates by Macek and Ovchinnikov [622], (ii) the representation of hyperspherical channel functions using a smooth-variable-discretization method combined with an R-matrix propagator method by Kato and Watanabe [522–524], (iii) the application of the time-dependent close-coupling method by Colgan et al. [221, 225] and (iv) the use of a propagating exterior complex scaling (PECS) method by Bartlett and Stelbovics [59]. In this last calculation on electron–hydrogen atom ionizing collisions, Bartlett and Stelbovics found that for $L = 0$ singlet scattering $\sigma_{\text{ion}} \propto E^{1.122\pm0.015}$ and $(\pi - \theta_{12})_{\text{FWHM}} \approx 3.0 E^{1/4}$, and for $L = 1$ triplet scattering $\sigma_{\text{ion}} \propto E^{3.36\pm0.02}$, in excellent agreement with classical and semiclassical predictions. Further details of the PECS approach to electron–hydrogen atom collisions have been given by Bartlett [57, 58]. We will return to a discussion of electron impact ionization of atoms and atomic ions, including R-matrix calculations near threshold, when we consider intermediate-energy collisions in Chap. 6.

Part II
R-Matrix Theory and Applications

Chapter 4
Introduction to *R*-Matrix Theory: Potential Scattering

In this chapter we commence our discussion of *R*-matrix theory by introducing the fundamental concepts of this theory and its role in electron–atom collisions. We then consider its application in non-relativistic and relativistic potential scattering, providing an introduction to later chapters in this monograph.

R-matrix theory was introduced in 1946 and 1947 by Wigner [968, 969] and by Wigner and Eisenbud [972] in fundamental papers describing nuclear resonance reactions, and its extension to relativistic collisions described by the Dirac equation was first formulated in 1948 by Goertzel [385]. This early work was reviewed and further developments and applications of *R*-matrix theory in nuclear physics were made in the 1950s and 1960s, for example by Blatt and Weisskopf [117], Lane and Thomas [566], Breit [134], Lane and Robson [567–569, 795] and Mahaux and Weidenmüller [630].

The realization that *R*-matrix theory could be extended to describe atomic and molecular collision processes began to emerge in the 1960s when new resonance phenomena were observed using synchrotron radiation sources and high-resolution electron spectrometers. It became clear from this work, which was reviewed by Fano [301], Cooper et al. [230] and Burke [153], that processes such as resonant electron–atom collisions and photoionization could be understood and analysed using an atomic extension of nuclear *R*-matrix theory. As a result, in the early 1970s *R*-matrix theory was introduced by Burke et al. [178] and by Burke [155–157] as an ab initio method for treating electron–atom collisions, which was extended by Allison et al. [13, 14] and Robb [793] to treat atomic polarizabilities and van der Waal's coefficients, by Burke and Taylor [168] to treat atomic photoionization and by Schneider et al. [821, 822, 826] and Burke et al. [180] to treat electron–molecule collisions. *R*-matrix theory has since been developed and applied as an ab initio method for calculating a wide range of atomic, molecular and optical collision processes, stimulated by the need for a detailed understanding of these processes in many applications and a number of reviews have been written, for example by Barrett et al. [55], Aymar et al. [28] and Burke et al. [167, 170, 189].

The fundamental idea in *R*-matrix theory is to partition configuration space describing the collision process into two or more regions where the processes in each of these regions have distinctly different physical properties. A different representation of the wave function describing the process is then adopted in each region,

P.G. Burke, *R-Matrix Theory of Atomic Collisions*, Springer Series on Atomic, Optical, and Plasma Physics 61, DOI 10.1007/978-3-642-15931-2_4,

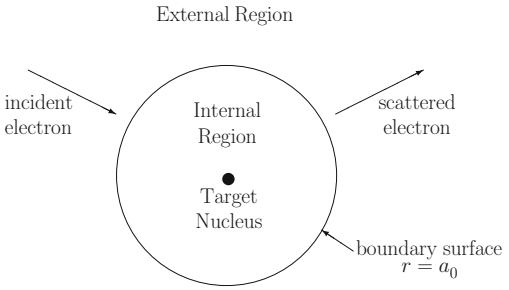

Fig. 4.1 Partitioning of configuration space into an internal and an external region by a boundary surface of radius $r = a_0$ in R-matrix theory of electron–atom collisions. An asymptotic region, where the wave function can be accurately represented by an asymptotic expansion, lies beyond the external region and is not shown in this figure

where these wave functions are connected by the R-matrix defined on the common boundaries. As an example we consider electron–atom collisions, illustrated in Fig. 4.1, where a sphere of radius $r = a_0$ separates an internal region from an external region, r being the radial distance of the incident or scattered electron from the target nucleus. The radius a_0 of the sphere is chosen so that the charge distributions of the target eigenstates of interest are essentially completely contained in the internal region. In the internal region, where electron exchange and correlation effects between the scattered electron and the target electrons are important, a configuration interaction basis expansion of the total wave function is adopted. The R-matrix expansion on the boundary $r = a_0$ of the internal region then has the general form

$$R_{ij}(E) = \frac{1}{2a_0} \sum_k \frac{w_{ik} w_{jk}}{E_k - E}, \tag{4.1}$$

which is a meromorphic function of energy E with poles only on the real energy axis. The eigenenergies E_k in (4.1) are obtained by diagonalizing the total Hamiltonian in the internal region in a configuration interaction basis, and the surface amplitudes w_{ik} are constructed from the wave function on the boundary $r = a_0$ in the ith channel, corresponding to the eigenenergies E_k. The R-matrix relates the reduced radial wave function $F_i(r)$, describing the radial motion of the scattered electron in the ith channel, to its derivative on the boundary $r = a_0$ by the equation

$$F_i(a_0) = \sum_j R_{ij}(E) a_0 \frac{\mathrm{d}F_j}{\mathrm{d}r}\bigg|_{r=a_0}. \tag{4.2}$$

In Wigner and Eisenbud's original theory, the terms in expansion (4.1) were identified with resonances at the energies E_k, where the w_{ik} were related to the partial decay width of the kth resonance in the ith channel. In the applications of R-matrix

theory in atomic, molecular and optical collisions, the terms in the summation in (4.1) represent both resonant and non-resonant collision processes and their mutual interference effects. Hence the R-matrix represents the full complexity of the multi-electron collision process in the internal region. In the external region, the scattered electron moves in the long-range local multipole potential of the target atom or ion in the eigenstates of interest. The R-matrix can then be propagated outwards in this potential from $r = a_0$ to the boundary with the asymptotic region $r = a_p$, where the corresponding wave function can be fitted to an asymptotic expansion yielding the K-matrix, S-matrix, scattering amplitudes and cross sections. Finally, other observables, such as effective collision strengths, f-values, photoionization cross sections, opacities and damping coefficients can be calculated using these results.

In this chapter we consider first in Sect. 4.1 the solution of the radial Schrödinger equation in potential scattering, using the approach first introduced by Wigner and Eisenbud in their treatment of nuclear resonance reactions. In this approach the collision wave function in the internal region is expanded in terms of a complete set of basis functions satisfying homogeneous boundary conditions on the surface of this region. The analytic properties of the R-matrix, defined by (4.1), then enables the analytic behaviour of the phase shift and scattering amplitude to be determined when the potential interaction in the external and asymptotic regions can be neglected except for the long-range Coulomb potential. Next, in Sect. 4.2, we generalize Wigner–Eisenbud theory to derive expressions for the collision wave function and the R-matrix in terms of basis functions satisfying arbitrary boundary conditions on the surface of the internal region, which are finding increasing use in recent calculations. In this generalized theory we introduce a surface or Bloch operator which when added to the Hamiltonian operator makes their sum hermitian over the internal region in the arbitrary boundary condition basis. In Sect. 4.3 we conclude our introduction to the basic concepts of R-matrix theory by discussing variational principles for the R-matrix in potential scattering using approaches first introduced by Kohn [542] and Jackson [495]. In Sect. 4.4 we turn to a discussion of approximation methods which have been used in practical R-matrix calculations, discussed in later chapters in this monograph. In Sect. 4.4.1 we review the homogeneous boundary condition method which has been widely used in R-matrix calculations of electron collisions with atoms, ions and molecules as well as multi-photon processes. Then in Sect. 4.4.2 we consider Buttle corrections to the R-matrix and to the wave function which are necessary when homogeneous boundary condition methods are used. Next, in Sect. 4.4.3, we present an overview of arbitrary boundary condition methods which are derivable from variational principles and, in Sect. 4.4.4, we describe a linear equations method for calculating the R-matrix, which avoids diagonalizing the Hamiltonian matrix and is efficient if the solution is required at only a few energies. We then consider four arbitrary boundary condition methods which have been used in multichannel collision calculations. These are eigenchannel methods discussed in Sect. 4.4.5, Lagrange mesh methods discussed in Sect. 4.4.6, B-spline basis methods discussed in Sect. 4.4.7 and a direct method for calculating resonance parameters discussed in Sect. 4.4.8. Next, in Sect. 4.5 we discuss R-matrix propagator methods which are appropriate when the wavelength

of the scattered particle is small compared with the range over which the potential interaction varies appreciably. This situation occurs in the external region where the scattered electron moves in the long-range potential of an atom or ion or in heavy particle collisions where the large mass of the interacting particles leads to short scattering wavelengths. Finally, in Sect. 4.6, we consider the extension of R-matrix theory to treat relativistic potential scattering described by the Dirac equation. This extension is necessary in order to accurately describe relativistic electron collision energies or electron collisions with heavy atoms and ions.

4.1 Wigner–Eisenbud Theory

We consider first the solution of the radial Schrödinger equation in potential scattering using the approach introduced by Wigner [968, 969] and Wigner and Eisenbud [972] in their treatment of nuclear resonance reactions. We discuss initially zero orbital angular momentum or s-wave scattering of a particle by a short-range spherically symmetric potential. The radial Schrödinger equation (1.8) satisfied by the reduced radial wave function $u_0(r)$ is then

$$\left(\frac{\mathrm{d}^2}{\mathrm{d}r^2} - U(r) + k^2\right) u_0(r) = 0, \tag{4.3}$$

where we assume that the potential

$$U(r) = 0, \quad r \geq a_0, \tag{4.4}$$

for some radius a_0 called the R-matrix radius. In this way we have divided the range of r into an "internal region" where $0 \leq r \leq a_0$ and an "external region" where $a_0 \leq r \leq \infty$.

Following (1.9) we look for the solution of (4.3) satisfying the boundary conditions

$$\begin{aligned} &u_0(0) = 0, \\ &u_0(r) = \sin(kr) + \cos(kr)\tan\delta_0(k), \quad r \geq a_0. \end{aligned} \tag{4.5}$$

The R-matrix, $R_0(E)$, is then defined in terms of the solution $u_0(a_0)$ and its derivative $[\mathrm{d}u_0(r)/\mathrm{d}r]_{r=a_0}$ on the boundary $r = a_0$ between the internal and external regions by the equation

$$u_0(a_0) = R_0(E)\left(a_0\frac{\mathrm{d}u_0}{\mathrm{d}r} - b_0 u_0\right)_{r=a_0}, \tag{4.6}$$

where b_0 is an arbitrary constant which is often set zero. When $b_0 = 0$ we see that $R_0(E)$ is equal to the reciprocal of a_0 times the logarithmic derivative of $u_0(r)$ at $r = a_0$.

Wigner–Eisenbud R-matrix theory is based on an expansion of the solution of (4.3) at any energy in the internal region in terms of a complete set of continuum basis orbitals. These basis orbitals $u_{0i}(r)$ are defined as eigensolutions of the original radial Schrödinger equation (4.3) given by

$$\left(\frac{\mathrm{d}^2}{\mathrm{d}r^2} - U(r) + k_i^2\right) u_{0i}(r) = 0, \quad 0 \le r \le a_0, \tag{4.7}$$

satisfying the homogeneous boundary conditions

$$\begin{aligned} u_{0i}(0) &= 0, \\ \frac{a_0}{u_{0i}(a_0)} \frac{\mathrm{d}u_{0i}}{\mathrm{d}r}\bigg|_{r=a_0} &= b_0, \end{aligned} \tag{4.8}$$

and the orthonormality condition

$$\int_0^{a_0} u_{0i}(r) u_{0j}(r) \mathrm{d}r = \delta_{ij}, \tag{4.9}$$

where b_0 in (4.8) is an arbitrary constant which we will see is the same as that appearing in (4.6). The solution $u_0(r)$ of (4.3) at any energy $E = \frac{1}{2}k^2$ is then expanded in terms of this basis as

$$u_0(r) = \sum_{i=1}^{\infty} u_{0i}(r) c_i, \quad 0 \le r < a_0. \tag{4.10}$$

This expansion converges uniformly except on the boundary $r = a_0$ for all values of b_0. However, on the boundary this expansion cannot represent the derivative of the solution $u_0(r)$ except at the eigenenergies $E_i = \frac{1}{2}k_i^2$ of (4.7) and (4.8).

This lack of uniform convergence of the expansion for the derivative of the wave function on the boundary $r = a_0$ can be understood by replacing the infinite summation on the right-hand side of (4.10) by a summation over its first n terms, which we write as

$$u_0^n(r) = \sum_{i=1}^{n} u_{0i}(r) c_i, \quad 0 \le r < a_0. \tag{4.11}$$

Taking the derivative of this equation term by term and letting $r \to a_0$ from below gives

$$\left.\frac{\mathrm{d}u_0^n}{\mathrm{d}r}\right|_{r=a_0} = \sum_{i=1}^{n} \left.\frac{\mathrm{d}u_{0i}}{\mathrm{d}r}\right|_{r=a_0} c_i\,. \tag{4.12}$$

We then substitute for $\mathrm{d}u_{0i}/\mathrm{d}r$ at $r = a_0$ from the boundary condition (4.8) into the right-hand side of (4.12), giving

$$\left.\frac{\mathrm{d}u_0^n}{\mathrm{d}r}\right|_{r=a_0} = \frac{b_0}{a_0} \sum_{i=1}^{n} u_{0i}(a_0) c_i\,. \tag{4.13}$$

Finally, substituting for the summation on the right-hand side of this equation from (4.11) yields, in the limit $r \to a_0$ from below,

$$\frac{a_0}{u_0^n(a_0)} \left.\frac{\mathrm{d}u_0^n}{\mathrm{d}r}\right|_{r=a_0} = b_0. \tag{4.14}$$

This equation is only satisfied by the exact solution of (4.3) at the eigenenergies $E_i = \frac{1}{2}k_i^2$ defined by (4.7) and (4.8), for all finite values of n, however large. For all other energies the exact solution of (4.3) does not satisfy (4.14), showing that the expansion for the derivative of the wave function is not uniformly convergent on the boundary $r = a_0$ at these energies. It is clear that this result arises because the original basis orbitals $u_{0i}(r)$ satisfy the homogeneous boundary conditions (4.8) at $r = a_0$. However, we will see in Sect. 4.2 when we consider basis orbitals satisfying arbitrary boundary conditions at $r = a_0$ that this difficulty does not arise.

In order to calculate the R-matrix defined by (4.6), which involves the derivative of the wave function on the boundary, an alternative approach must be used. We proceed by premultiplying (4.3) by $u_{0i}(r)$, premultiplying (4.7) by $u_0(r)$, integrating the resultant equations over the range from $r = 0$ to a_0 and subtracting these integrals. This gives

$$\int_0^{a_0} \left(u_{0i} \frac{\mathrm{d}^2 u_0}{\mathrm{d}r^2} - u_0 \frac{\mathrm{d}^2 u_{0i}}{\mathrm{d}r^2} \right) \mathrm{d}r = \left(k_i^2 - k^2\right) \int_0^{a_0} u_{0i} u_0 \mathrm{d}r. \tag{4.15}$$

Evaluating the left-hand side of this equation using Green's theorem and the boundary conditions at the origin given by (4.5) and (4.8) and using the orthonormality condition (4.9) and expansion (4.10) to simplify the right-hand side we then obtain

$$\left(u_{0i} \frac{\mathrm{d}u_0}{\mathrm{d}r} - u_0 \frac{\mathrm{d}u_{0i}}{\mathrm{d}r} \right)_{r=a_0} = \left(k_i^2 - k^2\right) c_i\,. \tag{4.16}$$

Dividing this equation through by $(k_i^2 - k^2)$ and using (4.8) then gives

$$c_i = \frac{1}{a_0} \frac{u_{0i}(a_0)}{k_i^2 - k^2} \left(a_0 \frac{\mathrm{d}u_0}{\mathrm{d}r} - b_0 u_0 \right)_{r=a_0}. \tag{4.17}$$

Substituting this result for c_i into (4.10) then yields the following expansion of the radial wave function $u_0(r)$ in terms of the basis orbitals $u_{0i}(r)$:

$$u_0(r) = \frac{1}{a_0} \sum_{i=1}^{\infty} \frac{u_{0i}(r) u_{0i}(a_0)}{k_i^2 - k^2} \left(a_0 \frac{\mathrm{d}u_0}{\mathrm{d}r} - b_0 u_0 \right)_{r=a_0}, \tag{4.18}$$

which is valid for all r in the range $0 \leq r < a_0$. However, when basis orbitals satisfying homogeneous boundary conditions corresponding to (4.8) are adopted care must be taken in the limit $r \to a_0$ from below, as discussed by Szmytkowski and Hinze [907]. We find that the limiting process $r \to a_0$ and the summation over i in (4.18) can be interchanged except when $b_0 = \pm\infty$, which we see from (4.8) corresponds to basis orbitals $u_{0i}(r)$ which vanish on the boundary $r = a_0$. Hence the expansion of the wave function in (4.18) converges when $r = a_0$ except when $b_0 = \pm\infty$. We then find, after setting $r = a_0$ in (4.18) and comparing with (4.6), the following convergent expansion of the R-matrix:

$$R_0(E) = \frac{1}{2a_0} \sum_{i=1}^{\infty} \frac{[u_{0i}(a_0)]^2}{E_i - E}, \tag{4.19}$$

where the energies E_i and E are defined in terms of k_i^2 and k^2 by (1.3). The R-matrix is seen to be a real meromorphic function of the energy with poles only on the real energy axis at the eigenenergies E_i. The residues of these poles are given in terms of the surface amplitudes $u_{0i}(a_0)$.

The relationship between the R-matrix and the phase shift is determined by substituting the solution in the external region defined by (4.5), evaluated at $r = a_0$, into (4.6) giving

$$\tan \delta_0(k) = \frac{-\sin(ka_0) + R_0(E)[ka_0 \cos(ka_0) - b_0 \sin(ka_0)]}{\cos(ka_0) + R_0(E)[ka_0 \sin(ka_0) + b_0 \cos(ka_0)]}, \tag{4.20}$$

where the phase shift $\delta_0(k)$ is related to the K-matrix by (1.15) and to the S-matrix by (1.14).

The extension of the above theory to non-zero orbital angular momenta ℓ is straightforward. The radial Schrödinger equation is then given by (1.8), namely

$$\left(\frac{\mathrm{d}^2}{\mathrm{d}r^2} - \frac{\ell(\ell+1)}{r^2} - U(r) + k^2 \right) u_\ell(r) = 0, \tag{4.21}$$

where we assume that the potential $U(r)$ is, as before, short range satisfying (4.4). We now look for solutions of (4.21) satisfying the boundary conditions

$$\begin{aligned} &u_\ell(0) = 0, \\ &u_\ell(r) = s_\ell(kr) + c_\ell(kr) \tan \delta_\ell(k), \quad r \geq a_0, \end{aligned} \tag{4.22}$$

where $s_\ell(kr)$ and $c_\ell(kr)$ are defined by (1.10) and (1.11), respectively.

As in the s-wave case, we expand the solution $u_\ell(r)$ in the internal region in terms of eigensolutions of the original radial Schrödinger equation (4.21) given by

$$\left(\frac{\mathrm{d}^2}{\mathrm{d}r^2} - \frac{\ell(\ell+1)}{r^2} - U(r) + k_i^2\right) u_{\ell i}(r) = 0, \tag{4.23}$$

satisfying the homogeneous boundary conditions (4.8) and the orthonormality condition (4.9), where b_0 can depend on the angular momentum. Defining the R-matrix in analogy with (4.6) as

$$u_\ell(a_0) = R_\ell(E)\left(a_0\frac{\mathrm{d}u_\ell}{\mathrm{d}r} - b_0 u_\ell\right)_{r=a_0}, \tag{4.24}$$

we then obtain the following expansion of the radial wave function in terms of the basis orbitals $u_{\ell i}(r)$

$$u_\ell(r) = \frac{1}{a_0}\sum_{i=1}^{\infty}\frac{u_{\ell i}(r)u_{\ell i}(a_0)}{k_i^2 - k^2}\left(a_0\frac{\mathrm{d}u_\ell}{\mathrm{d}r} - b_0 u_\ell\right)_{r=a_0}, \tag{4.25}$$

and the following expansion of the R-matrix

$$R_\ell(E) = \frac{1}{2a_0}\sum_{i=1}^{\infty}\frac{[u_{\ell i}(a_0)]^2}{E_i - E}, \tag{4.26}$$

where, as in (4.18), expansion (4.25) converges for all r satisfying $0 \le r \le a_0$ except when $b_0 = \pm\infty$ when it fails to converge at $r = a_0$. The relation between the R-matrix and the phase shift which replaces (4.20) is then

$$\tan\delta_\ell(k) = \frac{-s_\ell(ka_0) + R_\ell(E)[ka_0 s'_\ell(ka_0) - b_0 s_\ell(ka_0)]}{c_\ell(ka_0) - R_\ell(E)[ka_0 c'_\ell(ka_0) - b_0 c_\ell(ka_0)]}, \tag{4.27}$$

where $s'_\ell(kr)$ and $c'_\ell(kr)$ are the derivatives of $s_\ell(kr)$ and $c_\ell(kr)$ with respect to their arguments kr.

We see from (4.26) and (4.27) that a knowledge of the R-matrix enables the phase shift and hence the scattering amplitude and cross section to be determined as a function of energy. Also, as we have seen in Sect. 1.4, the analytic properties of the R-matrix as a function of energy enables the analytic properties of the phase shift and the scattering amplitude to be determined in the neighbourhood of threshold energy.

4.2 Generalized R-Matrix Theory

In this section we generalize Wigner–Eisenbud R-matrix theory to derive expressions for the collision wave function and the R-matrix in terms of basis orbitals satisfying arbitrary boundary conditions at $r = a_0$. This approach avoids the need for a Buttle correction [195] to the R-matrix, and in some applications to the wave function, which is required when basis orbitals satisfying homogeneous boundary conditions at $r = a_0$ are used, as discussed in Sects. 4.4.1 and 4.4.2. In practice analytic basis orbitals including Gaussian orbitals, Slater-type orbitals, Legendre functions and B-splines, which are linearly independent and complete in the internal region, have been used in the expansion of the radial wave function. We will discuss some of these methods later in Sect. 4.4.

We proceed by first introducing an operator L_ℓ which is defined by rewriting (4.21) in the form

$$L_\ell u_\ell(r) = 0, \tag{4.28}$$

where

$$L_\ell = \frac{\mathrm{d}^2}{\mathrm{d}r^2} - \frac{\ell(\ell+1)}{r^2} - U(r) + k^2, \tag{4.29}$$

and where the potential $U(r)$ may be non-zero for $r \geq a_0$. We observe that L_ℓ is not hermitian in the space of square-integrable functions which vanish at the origin and satisfy arbitrary boundary conditions on the surface $r = a_0$ of the internal region. To see this we consider the integral

$$\begin{aligned}\int_0^{a_0} (vL_\ell w - wL_\ell v)\mathrm{d}r &= \int_0^{a_0} \left(v\frac{\mathrm{d}^2 w}{\mathrm{d}r^2} - w\frac{\mathrm{d}^2 v}{\mathrm{d}r^2} \right) \mathrm{d}r \\ &= \left(v\frac{\mathrm{d}w}{\mathrm{d}r} - w\frac{\mathrm{d}v}{\mathrm{d}r} \right)_{r=a_0},\end{aligned} \tag{4.30}$$

where we have used Green's theorem and where $v(r)$ and $w(r)$ are arbitrary differentiable functions which are quadratically integrable over the internal region and are zero at the origin. If both $v(r)$ and $w(r)$ satisfy the homogeneous boundary conditions (4.8), then the surface term on the right-hand side of (4.30) is zero. However, if they satisfy arbitrary boundary conditions at $r = a_0$ then the surface term does not vanish and L_ℓ is then not hermitian in this basis.

This difficulty can be overcome using a procedure first introduced by Bloch [118]. We define a surface or Bloch operator $\mathcal{L}(a_0, b_0)$ by the equation

$$\mathcal{L}(a_0, b_0) = \delta(r - a_0) \left(\frac{\mathrm{d}}{\mathrm{d}r} - \frac{b_0}{r} \right), \tag{4.31}$$

where $\delta(r-a_0)$ is the Dirac delta function [263, 817] and b_0 is an arbitrary constant which can depend on ℓ and which we will identify with the constant b_0 in (4.6). We then consider the integral

$$\begin{aligned}&\int_0^{a_0}[v(L_\ell-\mathcal{L})w-w(L_\ell-\mathcal{L})v]\mathrm{d}r\\&=\left(v\frac{\mathrm{d}w}{\mathrm{d}r}-w\frac{\mathrm{d}v}{\mathrm{d}r}\right)_{r=a_0}-\left(v\frac{\mathrm{d}w}{\mathrm{d}r}-w\frac{\mathrm{d}v}{\mathrm{d}r}\right)_{r=a_0}\\&=0,\end{aligned}\tag{4.32}$$

where the terms in the first bracket on the right-hand side of this equation arise from the operator L_ℓ and the terms in the second bracket arise from the Bloch operator $\mathcal{L}$. In (4.32), and in later equations, the limit of the integral involving the Dirac delta function $\delta(r-a_0)$ is defined by the equation

$$\lim_{\epsilon\to 0+}\int^{a_0+\epsilon} f(r)\delta(r-a_0)\mathrm{d}r=f(a_0),\tag{4.33}$$

where $f(r)$ is some function of r, which is regular in the neighbourhood of a_0. It follows from (4.32) that the operator $L_\ell-\mathcal{L}$ is hermitian over the internal region in the space of functions satisfying arbitrary boundary conditions at $r=a_0$.

We can now solve (4.28) by rewriting it as

$$(L_\ell-\mathcal{L})u_\ell=-\mathcal{L}u_\ell,\tag{4.34}$$

which has the formal solution

$$u_\ell=-(L_\ell-\mathcal{L})^{-1}\mathcal{L}u_\ell.\tag{4.35}$$

A spectral representation of the Green's function $(L_\ell-\mathcal{L})^{-1}$ in this equation can be obtained by introducing a complete linearly independent set of square integrable continuum basis orbitals in the internal region

$$\phi_i(r),\quad i=1,\ldots,\infty,\quad 0\le r\le a_0,\tag{4.36}$$

which are chosen to be real and which are zero at the origin and satisfy arbitrary boundary conditions at $r=a_0$. We then define linear combinations of these basis orbitals by the equation

$$\chi_j(r)=\sum_{i=1}^{\infty}\phi_i(r)c_{ij},\quad j=1,\ldots,\infty,\quad 0\le r\le a_0,\tag{4.37}$$

where the expansion coefficients c_{ij} are determined by diagonalizing $L_\ell-\mathcal{L}$ in this basis so that

$$\int_0^{a_0} \chi_i(r)(L_\ell - \mathcal{L})\chi_j(r)\mathrm{d}r = 2(E - E_i)\delta_{ij}, \tag{4.38}$$

where the eigenenergies E_i are real since $(L_\ell - \mathcal{L})$ is hermitian. Hence, the required spectral representation of $(L_\ell - \mathcal{L})^{-1}$ is given by

$$-(L_\ell - \mathcal{L})^{-1} = \frac{1}{2}\sum_{i=1}^{\infty} \frac{\chi_i(r)\chi_i(r')}{E_i - E}, \quad 0 \le r \le a_0, \quad 0 \le r' \le a_0. \tag{4.39}$$

Substituting this result into (4.35) and using (4.31) gives

$$u_\ell(r) = \frac{1}{2a_0}\sum_{i=1}^{\infty} \frac{\chi_i(r)\chi_i(a_0)}{E_i - E}\left(a_0\frac{\mathrm{d}u_\ell}{\mathrm{d}r} - b_0 u_\ell\right)_{r=a_0}, \quad 0 \le r \le a_0. \tag{4.40}$$

Evaluating this equation on the boundary $r = a_0$ of the internal region then gives

$$u_\ell(a_0) = R_\ell(E)\left(a_0\frac{\mathrm{d}u_\ell}{\mathrm{d}r} - b_0 u_\ell\right)_{r=a_0}, \tag{4.41}$$

where we have written

$$R_\ell(E) = \frac{1}{2a_0}\sum_{i=1}^{\infty} \frac{[\chi_i(a_0)]^2}{E_i - E}. \tag{4.42}$$

Thus we recover (4.24) for the logarithmic derivative of the wave function on the boundary and (4.26) for the R-matrix.

The significance of this result is that the surface amplitudes $\chi_i(a_0)$ are now expressed through (4.36) and (4.37) in terms of an arbitrary set of basis orbitals $\phi_i(r)$ which are complete over $0 \le r \le a_0$ and which vanish at the origin, rather than in terms of eigensolutions of the original differential equation, defined by (4.7) or (4.23). In addition, (4.40) provides an expansion of the solution $u_\ell(r)$ in the internal region at any energy in terms of the basis orbitals $\chi_i(r)$, where the expansion coefficients involve $u_\ell(r)$ and its derivative on the boundary $r = a_0$. This expansion is important in situations such as photoionization, discussed in Chap. 8, where the wave function, as well as the phase shift and S-matrix, is required.

We observe that (4.41) relates the reduced radial wave function $u_\ell(r)$ to its derivative on the boundary $r = a_0$ between the internal and external regions. It is sometimes convenient to adopt an equivalent expression which relates the full radial wave function $w_\ell(r)$ to its derivative on the boundary, where

$$w_\ell(r) = r^{-1}u_\ell(r). \tag{4.43}$$

It follows immediately from this definition that

$$\left(a_0 \frac{\mathrm{d}u_\ell}{\mathrm{d}r} - b_0 u_\ell\right)_{r=a_0} = a_0^2 \left(\frac{\mathrm{d}w_\ell}{\mathrm{d}r} - \frac{b_0 - 1}{r} w_\ell\right)_{r=a_0}. \tag{4.44}$$

Hence (4.41) becomes

$$w_\ell(a_0) = \mathcal{R}_\ell(E) \left(\frac{\mathrm{d}w_\ell}{\mathrm{d}r} - \frac{b_0 - 1}{r} w_\ell\right)_{r=a_0}, \tag{4.45}$$

where the modified R-matrix $\mathcal{R}_\ell(E)$ is defined by

$$\mathcal{R}_\ell(E) = \frac{1}{2} \sum_{i=1}^{\infty} \frac{[\chi_i(a_0)]^2}{E_i - E}. \tag{4.46}$$

Finally, the partial wave phase shifts and hence the scattering amplitude and cross section can be determined by solving (4.28) in the external region $r \geq a_0$. The solution in this region can be written in the form

$$u_\ell(r) = f_\ell(kr) + g_\ell(kr) \tan \delta_\ell(k), \quad r \geq a_0, \tag{4.47}$$

where $f_\ell(kr)$ and $g_\ell(kr)$ are linearly independent solutions of (4.28) satisfying the asymptotic boundary conditions

$$f_\ell(kr) \underset{r\to\infty}{\sim} \sin\left(kr - \frac{1}{2}\ell\pi\right), \quad g_\ell(kr) \underset{r\to\infty}{\sim} \cos\left(kr - \frac{1}{2}\ell\pi\right), \tag{4.48}$$

and where we have assumed that the potential $U(r)$ vanishes faster than r^{-1} at large distances. The functions $f_\ell(kr)$ and $g_\ell(kr)$ can be determined by solving (4.28) in the external region, subject to the asymptotic boundary conditions defined by (4.48). The phase shift is then defined in terms of the R-matrix by an equation analogous to (4.27) given by

$$\tan \delta_\ell(k) = \frac{-f_\ell(ka_0) + R_\ell(E)[ka_0 f'_\ell(ka_0) - b_0 f_\ell(ka_0)]}{g_\ell(ka_0) - R_\ell(E)[ka_0 g'_\ell(ka_0) - b_0 g_\ell(ka_0)]}, \tag{4.49}$$

where $f'_\ell(kr)$ and $g'_\ell(kr)$ are the derivatives of $f_\ell(kr)$ and $g_\ell(kr)$ with respect to their arguments kr. The scattering amplitude and cross section can then be determined from the phase shifts, as described in Sect. 1.1. If the potential behaves as r^{-1} at large distances, corresponding to a long-range Coulomb potential, then the above analysis must be modified as described in Sect. 1.2.

4.3 Variational Principles for the R-Matrix

We conclude our introduction to the basic concepts of R-matrix theory in potential scattering by discussing in this section variational principles for the R-matrix first obtained by Kohn [542] and by Jackson [495]. Variational principles for the R-matrix have also been considered by Lane and Robson [568], Oberoi and Nesbet [701, 702], Schlessinger and Payne [820], Shimamura [872], Nesbet [678], Greene [417, 418] and Aymar et al. [28]. These principles, which we generalize to multichannel collisions in Sect. 5.2, provide the basis for approximation methods discussed in Sect. 4.4 and later chapters.

Kohn [542] considered the variational functional

$$F_\ell^{(1)}[u_\ell^t] = \frac{\int_0^{a_0} u_\ell^t(r)(-L_\ell + \mathcal{L})u_\ell^t(r)\mathrm{d}r}{[u_\ell^t(a_0)]^2}, \tag{4.50}$$

where L_ℓ is defined by (4.29), $\mathcal{L}$ is a Bloch operator defined by (4.31) and $u_\ell^t(r)$ is a trial function which is zero at the origin and satisfies arbitrary boundary conditions at $r = a_0$. It follows from (4.31) and (4.41) that when u_ℓ is an exact solution of (4.28) then

$$F_\ell^{(1)}[u_\ell] = [a_0 R_\ell(E)]^{-1}. \tag{4.51}$$

We define the first-order variation $\delta u_\ell(r)$ about the exact solution $u_\ell(r)$ by

$$\delta u_\ell(r) = u_\ell^t(r) - u_\ell(r), \tag{4.52}$$

where $\delta u_\ell(r)$ satisfies the boundary condition $\delta u_\ell(0) = 0$. The corresponding first-order variation $\delta F_\ell^{(1)}[u_\ell]$ of the functional $F_\ell^{(1)}[u_\ell]$ is

$$\delta F_\ell^{(1)}[u_\ell] = \frac{2\int_0^{a_0} \delta u_\ell(r)(-L_\ell + \mathcal{L})u_\ell(r)\mathrm{d}r}{[u_\ell(a_0)]^2} - \frac{2F_\ell^{(1)}[u_\ell]\delta u_\ell(a_0)}{u_\ell(a_0)}, \tag{4.53}$$

where in the first term on the right-hand side of this equation we have made use of the hermiticity of $L_\ell - \mathcal{L}$. Using (4.28) and (4.31) and substituting for $F_\ell^{(1)}[u_\ell]$ from (4.51) into the second term on the right-hand side of (4.53) gives immediately

$$\delta F_\ell^{(1)}[u_\ell] = 0. \tag{4.54}$$

Hence $F_\ell^{(1)}[u_\ell]$ is a variational functional which enables the R-matrix, which is given in terms of $F_\ell^{(1)}[u_\ell]$ by (4.51), to be determined from its stationary value.

Jackson [495] introduced a second variational functional defined as follows:

$$F_\ell^{(2)}[u_\ell^t] = \int_0^{a_0} u_\ell^t(r)(-L_\ell + \mathcal{L})u_\ell^t(r)\mathrm{d}r - 2a_0^{-1}u_\ell^t(a_0). \tag{4.55}$$

Unlike $F_\ell^{(1)}[u_\ell]$, the functional $F_\ell^{(2)}[u_\ell]$ depends on the normalization of the trial function. We therefore consider first-order variations $\delta F_\ell^{(2)}[u_\ell]$ of the functional $F_\ell^{(2)}[u_\ell]$ due to first-order variations $\delta u_\ell(r)$ about the exact solution $u_\ell(r)$ of (4.28), subject to the normalization condition

$$\left(a_0 \frac{\mathrm{d}u_\ell^t}{\mathrm{d}r} - b_0 u_\ell^t\right)_{r=a_0} = 1. \tag{4.56}$$

It follows from (4.55) that the first-order variation $\delta F_\ell^{(2)}[u_\ell]$ of the functional $F_\ell^{(2)}[u_\ell]$ is

$$\delta F_\ell^{(2)}[u_\ell] = 2\int_0^{a_0} \delta u_\ell(r)(-L_\ell + \mathcal{L})u_\ell(r)\mathrm{d}r - 2a_0^{-1}\delta u_\ell(a_0), \tag{4.57}$$

which, using (4.28) and (4.31), reduces to

$$\delta F^{(2)}[u_\ell] = 2a_0^{-1}\delta u_\ell(a_0)\left(a_0\frac{\mathrm{d}u_\ell}{\mathrm{d}r} - b_0 u_\ell\right)_{r=a_0} - 2a_0^{-1}\delta u_\ell(a_0). \tag{4.58}$$

Since the exact solution $u_\ell(r)$ satisfies (4.56) then (4.58) shows that

$$\delta F^{(2)}[u_\ell] = 0. \tag{4.59}$$

Also, when the exact solution $u_\ell(r)$ is substituted into (4.55), we obtain

$$\begin{aligned} F_\ell^{(2)}[u_\ell] &= u_\ell(a_0)\left(\frac{\mathrm{d}u_\ell}{\mathrm{d}r} - \frac{b_0}{a_0}u_\ell\right)_{r=a_0} - 2a_0^{-1}u_\ell(a_0) \\ &= a_0^{-1}u_\ell(a_0) - 2a_0^{-1}u_\ell(a_0) \\ &= -a_0^{-1}R_\ell(E), \end{aligned} \tag{4.60}$$

since from (4.24) and (4.56)

$$R_\ell(E) = u_\ell(a_0)\left(a_0\frac{\mathrm{d}u_\ell}{\mathrm{d}r} - b_0 u_\ell\right)^{-1}_{r=a_0} = u_\ell(a_0). \tag{4.61}$$

Hence $F_\ell^{(2)}[u_\ell]$ is also a variational functional which enables the R-matrix to be determined from its stationary value.

We apply these variational principles to the determination of the R-matrix using the arbitrary boundary condition method in Sect. 4.4.3 and later sections. These variational principles can be generalized in a straightforward way to multichannel collisions and we consider the generalization of the second variational principle, defined by (4.55), in Sect. 5.2.

4.4 R-Matrix Approximation Methods

In previous sections of this chapter we have introduced the basic concepts of R-matrix theory. In this section we discuss approximation methods that can be used in practical calculations. We consider first in Sect. 4.4.1, the method introduced by Wigner [968, 969] and Wigner and Eisenbud [972] in their treatment of nuclear resonance reactions, where the basis orbitals satisfy homogeneous boundary conditions on the outer boundary of the internal region. This method has had wide use in electron–atom and electron–molecule collision calculations discussed in later chapters. However, as first proposed by Buttle [195], a correction must be applied to the R-matrix, and in some applications to the wave function, in order to obtain accurate results. These corrections are discussed in Sect. 4.4.2. Then in Sect. 4.4.3 we present an overview of methods which can be derived from variational principles, discussed in Sect. 4.3, where the basis orbitals satisfy arbitrary boundary conditions on the outer boundary of the internal region. We consider next, in Sect. 4.4.4, a linear equations method which avoids diagonalizing the operator $L_\ell - \mathcal{L}$ in the set of basis orbitals, which is efficient when calculations at only a few energy values are required. In Sect. 4.4.5 we review iterative and non-iterative eigenchannel methods which ensure that the wave function and its derivative are continuous on the boundary of the internal region. In Sect. 4.4.6 we discuss Lagrange mesh methods which provide variational accuracy for calculations carried out on a mesh or grid of points. In Sect. 4.4.7 we describe B-spline methods which are finding increasing application in electron collisions and multiphoton ionization processes. Finally, in Sect. 4.4.8 we discuss a method which enables the position and width of Siegert resonance states to be calculated directly.

4.4.1 Homogeneous Boundary Condition Method

We consider the solution of the radial Schrödinger equation

$$\left(\frac{\mathrm{d}^2}{\mathrm{d}r^2} - \frac{\ell(\ell+1)}{r^2} - U(r) + k^2\right) u_\ell(r) = 0, \tag{4.62}$$

in the internal region $0 \le r \le a_0$, where $U(r)$ is a potential which may be non-zero for $r \ge a_0$. In order to solve (4.62) in the internal region we introduce a set of continuum basis orbitals $u^0_{\ell i}(r)$ which are eigensolutions of a zero-order differential equation which we write as follows:

$$\left(\frac{\mathrm{d}^2}{\mathrm{d}r^2} - \frac{\ell(\ell+1)}{r^2} - U_0(r) + k^2_{0i}\right) u^0_{\ell i}(r) = 0, \tag{4.63}$$

satisfying the homogeneous boundary conditions

$$u^0_{\ell i}(0) = 0,$$
$$\frac{a_0}{u^0_{\ell i}(a_0)} \frac{\mathrm{d}u^0_{\ell i}}{\mathrm{d}r}\bigg|_{r=a_0} = b_0, \tag{4.64}$$

and the orthonormality conditions

$$\int_0^{a_0} u^0_{\ell i}(r) u^0_{\ell j}(r) \mathrm{d}r = \delta_{ij}, \tag{4.65}$$

where b_0 in (4.64) is an arbitrary constant. The zero-order potential $U_0(r)$ in (4.63) is chosen so that (4.63) and (4.64) can be easily solved to yield the eigenenergies $E^0_i = \frac{1}{2}k^2_{0i}$ and the corresponding basis orbitals $u^0_{\ell i}(r)$, while at the same time representing the main features of the exact solutions of (4.62). These criteria are particularly important in the case of electron–atom and electron–ion collisions, which we will discuss in Sect. 5.3.1, where the original equations corresponding to (4.62) involve many coupled channels with non-local potentials and where a careful choice of the local zero-order potential $U_0(r)$ can greatly reduce the number of basis orbitals required to yield accurate results and hence the time taken to solve the relevant multichannel coupled integrodifferential equations in the internal region.

We now introduce linear combinations $u^n_{\ell j}(r)$ of n zero-order basis orbitals $u^0_{\ell i}(r)$, which are defined by

$$u^n_{\ell j}(r) = \sum_{i=1}^{n} u^0_{\ell i}(r) c^n_{ij}, \quad j = 1, \ldots, n, \quad 0 \le r \le a_0, \tag{4.66}$$

where the coefficients c^n_{ij} are obtained by diagonalizing $L_\ell - \mathcal{L}$ according to

$$\int_0^{a_0} u^n_{\ell i}(r)(L_\ell - \mathcal{L}) u^n_{\ell j}(r) \mathrm{d}r = 2(E - E^n_i)\delta_{ij}, \quad i,\ j = 1, \ldots, n, \tag{4.67}$$

where L_ℓ is the operator in (4.62) defined by (4.29) and $\mathcal{L}$ is the Bloch operator defined by (4.31). Following our discussion in Sect. 4.2 we can rewrite (4.62) as

$$(L_\ell - \mathcal{L}) u_\ell = -\mathcal{L} u_\ell, \tag{4.68}$$

which has the formal solution

$$u_\ell = -(L_\ell - \mathcal{L})^{-1} \mathcal{L} u_\ell. \tag{4.69}$$

A spectral representation of the Green's function $(L_\ell - \mathcal{L})^{-1}$ in (4.69) can then be obtained in terms of the basis functions $u^n_{\ell i}(r)$ defined by (4.66) and (4.67). Equation (4.69) can then be rewritten as

$$u_\ell^n(r) = \frac{1}{2a_0} \sum_{i=1}^{n} \frac{u_{\ell i}^n(r) u_{\ell i}^n(a_0)}{E_i^n - E} \left(a_0 \frac{\mathrm{d}u_\ell^n}{\mathrm{d}r} - b_0 u_\ell^n \right)_{r=a_0}, \quad 0 \le r \le a_0, \tag{4.70}$$

which is an approximate expression for the solution of the radial Schrödinger equation (4.62) in the internal region. Setting $r = a_0$ in (4.70) then yields

$$u_\ell^n(a_0) = R_\ell^n(E) \left(a_0 \frac{\mathrm{d}u_\ell^n}{\mathrm{d}r} - b_0 u_\ell^n \right)_{r=a_0}, \tag{4.71}$$

where the R-matrix $R_\ell^n(E)$ is defined in terms of the surface amplitudes $u_{\ell i}^n(a_0)$ and eigenenergies E_i^n by

$$R_\ell^n(E) = \frac{1}{2a_0} \sum_{i=1}^{n} \frac{\left[u_{\ell i}^n(a_0) \right]^2}{E_i^n - E}, \tag{4.72}$$

which provides a variational expression for the R-matrix. However, its usefulness depends on how fast the summation converges to the exact solution. We will show in Sect. 4.4.2 that in order to obtain accurate results for reasonably small values of n, a correction to the R-matrix, first proposed by Buttle [195], must be added to the summation in (4.72). In addition, we will see that in certain circumstances a correction to the wave function is also necessary.

Returning to the expression for the solution in the internal region given by (4.70), we see that its normalization is given by the term in brackets on the right-hand side of this equation, which is defined by the normalization of the solution of the radial Schrödinger equation (4.62) in the external region. For example, if the potential $U(r)$ in (4.62) vanishes for $r \ge a_0$ then the solution $u_\ell^n(r)$ is given up to an arbitrary normalization factor by (4.22) where $\tan \delta_\ell(k)$ can be determined in terms of the R-matrix by (4.27). All the terms on the right-hand side of (4.70) are then known and $u_\ell^n(r)$ can be determined corresponding to this normalization factor for $0 \le r \le a_0$. If the potential $U(r)$ is not zero for $r \ge a_0$, we can determine the terms in brackets in (4.70) by first solving (4.62) in the external region $a_0 \le r \le a_p$ using an analytic or numerical method subject to the boundary condition defined by (4.71) and (4.72) at $r = a_0$. For example, we can use one of the R-matrix propagator methods, discussed in Sect. 4.5 and Appendix E, for solving (4.62) in the external region $a_0 \le r \le a_p$. We can then fit the solution to an asymptotic expansion at $r = a_p$, discussed in Appendix F.1, with the asymptotic form

$$u_\ell^n(r) \underset{r \to \infty}{\sim} N \sin[kr - \tfrac{1}{2}\ell\pi + \delta_\ell^n(k)], \tag{4.73}$$

where N is an arbitrary normalization factor and $\delta_\ell^n(k)$ is the phase shift. Finally, we can determine the solution in the internal region, corresponding to this normalization factor, using (4.70).

4.4.2 Buttle Corrections to the R-Matrix and Wave Function

We now consider the convergence properties of expansion (4.72) for the R-matrix and expansion (4.70) for the wave function. As already noted in Sect. 4.4.1, (4.72) provides a variational expression for the R-matrix. However, its usefulness depends on how fast $R_\ell^n(E)$ converges to the exact R-matrix as $n \to \infty$. This depends on two factors:

i. The rapidity of convergence to their exact values of the individual surface amplitudes $u_{\ell i}^n(a_0)$, $i = 1, \ldots, n$, and the corresponding eigenenergies E_i^n as $n \to \infty$
ii. The rapidity of convergence of expansion (4.72) to its exact value as $n \to \infty$

In the homogeneous boundary condition method, discussed in Sect. 4.4.1, the second factor usually gives the largest error at low energies and a correction for the omitted terms in the expansion must be included in order for the resultant R-matrix to be accurate for reasonably small values of n.

The procedure that is most often used for correcting the R-matrix for the omission of high-lying pole terms in expansion (4.72) was first proposed by Buttle [195]. In this procedure, a corrected R-matrix $R_\ell^c(E)$ is defined as follows:

$$R_\ell^c(E) = R_\ell^n(E) + R_\ell^{(\mathrm{BC})}(E), \tag{4.74}$$

where the second term on the right-hand side of this equation, called the "Buttle correction", is approximated by

$$R_\ell^{(\mathrm{BC})}(E) = \frac{1}{2a_0} \sum_{i=n+1}^{\infty} \frac{\left[u_{\ell i}^0(a_0)\right]^2}{E_i^0 - E}. \tag{4.75}$$

This correction at the energy E of interest can be easily determined in terms of the solution $u_\ell^0(r)$ of the zero-order differential equation (4.63) at this energy, satisfying the boundary condition

$$u_\ell^0(0) = 0 \tag{4.76}$$

and the normalization condition

$$\int_0^{a_0} [u_\ell^0(r)]^2 \mathrm{d}r = 1. \tag{4.77}$$

The zero-order R-matrix is then given by the identity

$$R_\ell^0(E) = u_\ell^0(a_0) \left(a_0 \frac{\mathrm{d}u_\ell^0}{\mathrm{d}r} - b_0 u_\ell^0 \right)_{r=a_0}^{-1} = \frac{1}{2a_0} \sum_{i=1}^{\infty} \frac{\left[u_{\ell i}^0(a_0)\right]^2}{E_i^0 - E}, \tag{4.78}$$

which follows from (4.71) and (4.72) by replacing $u_\ell^n(a_0)$ and $u_{\ell i}^n(a_0)$ by the corresponding exact solutions of the zero-order differential equation (4.63). Hence the Buttle correction can be approximated by

$$R_\ell^{(\mathrm{BC})}(E) = u_\ell^0(a_0)\left(a_0\frac{\mathrm{d}u_\ell^0}{\mathrm{d}r} - b_0 u_\ell^0\right)^{-1}_{r=a_0} - \frac{1}{2a_0}\sum_{i=1}^{n}\frac{\left[u_{\ell i}^0(a_0)\right]^2}{E_i^0 - E}. \tag{4.79}$$

The first term on the right-hand side of (4.79) is determined by solving the zero-order differential equation (4.63) at the energy E of interest, subject to the boundary condition $u_{\ell i}^0(0) = 0$, while the second term is easily determined since the first n eigenenergies $E_i^0 = \frac{1}{2}k_{0i}^2,\ i = 1, \ldots, n$, and the corresponding eigensolutions $u_{\ell i}^0(r),\ i = 1, \ldots, n$, of (4.63) have already been calculated.

The Buttle correction is found to be important at all energies except very close to or at the R-matrix poles in $R_\ell^n(E)$ given by expansion (4.72). In the neighbourhood of these poles the Buttle correction can be neglected compared with the pole term since, as can be seen from (4.75), it is finite and smoothly varying at energies below the energy E_{n+1}^0 of the lowest pole included in the Buttle correction. It also follows from the absence of poles in the Buttle correction in the low- and intermediate-energy regions, that this correction can be calculated at a few energy values spanning this region and then interpolated. It is thus very quick to evaluate. This advantage becomes even more pronounced for electron–atom and electron–ion collisions, considered in Chap. 5, where diagonalizing $L_\ell - \mathcal{L}$ in (4.67) is by far the most time-consuming part of the calculation in the internal region.

In certain situations, for example, in the calculation of the radial integrals which arise in atomic photoionization, considered in Chap. 8, a Buttle-type correction to the wave function as well as to the R-matrix may be required to obtain highly accurate results. This can be seen by considering the expansion of the wave function given by (4.70). As discussed following (4.10) this expansion is not uniformly convergent on the boundary $r = a_0$ since the basis orbitals $u_{\ell i}^0(r),\ i = 1, \ldots, n$, satisfy homogeneous boundary conditions given by (4.64). Consequently (4.70) only provides an accurate representation of the wave function near the boundary $r = a_0$ when the energy E is at or very close to a pole E_i. It follows that a correction to the wave function $u_\ell(r)$ may be required for $r \lesssim a_0$ to allow for the omitted terms $i = n+1, \ldots, \infty$ in expansion (4.70) when highly accurate results which depend on the wave function are required. This correction was considered by Yu Yan and Seaton [987] in the case of the electron plus proton system where highly accurate results are available. They found that the error in the radial integrals may be reduced by an order of magnitude by including this correction, although the radial integrals obtained without this correction were found to be adequate for most applications.

In order to calculate the correction to the wave function we first normalize the wave function defined by (4.70). A convenient normalization condition is

$$\left(a_0\frac{\mathrm{d}u_\ell^n}{\mathrm{d}r} - b_0 u_\ell^n\right)_{r=a_0} = 1, \tag{4.80}$$

which can be applied except at energies at or very close to an R-matrix pole where the correction is negligible. Expansion (4.70) for the wave function then becomes

$$u_\ell^n(r) = \frac{1}{2a_0} \sum_{i=1}^{n} \frac{u_{\ell i}^n(r) u_{\ell i}^n(a_0)}{E_i^n - E}, \quad 0 \le r \le a_0. \tag{4.81}$$

A corrected wave function at the energy E can be defined, in analogy with the correction to the R-matrix given by (4.74), as follows:

$$u_\ell^c(r) = u_\ell^n(r) + u_\ell^{(\mathrm{BC})}(r), \quad 0 \le r \le a_0, \tag{4.82}$$

where the second term on the right-hand side of this equation is the correction, given by

$$u_\ell^{(\mathrm{BC})}(r) = \frac{1}{2a_0} \sum_{i=n+1}^{\infty} \frac{u_{\ell i}^0(r) u_{\ell i}^0(a_0)}{E_i^0 - E}, \quad 0 \le r \le a_0. \tag{4.83}$$

This correction can be calculated using the identity

$$u_\ell^0(r) = \frac{1}{2a_0} \sum_{i=1}^{\infty} \frac{u_{\ell i}^0(r) u_{\ell i}^0(a_0)}{E_i^0 - E}, \quad 0 \le r \le a_0, \tag{4.84}$$

which follows from (4.70) after letting $n \to \infty$ and replacing $u_\ell^n(r)$ by the solution of the zero-order differential equation (4.63), where the zero-order solution $u_\ell^0(r)$ is also normalized using (4.80). The correction to the wave function at the energy E is then given by

$$u_\ell^{(\mathrm{BC})}(r) = u_\ell^0(r) - \frac{1}{2a_0} \sum_{i=1}^{n} \frac{u_{\ell i}^0(r) u_{\ell i}^0(a_0)}{E_i^0 - E}, \quad 0 \le r \le a_0. \tag{4.85}$$

This correction can be calculated in a similar way to the Buttle correction to the R-matrix defined by (4.79). The first term on the right-hand side of (4.85) is calculated by solving the zero-order differential equation (4.63) at the given energy E of interest, while the second term is given in terms of the first n eigenenergies E_i^0 and the corresponding zero-order eigensolutions $u_{\ell i}^0(r)$, $i = 1, \ldots, n$, of (4.63). Having calculated the corrected wave function defined by (4.82) it can be renormalized to satisfy the relevant normalization condition for the process under consideration.

Finally, while we have observed that expansion (4.72) provides a variational expression for the R-matrix, the inclusion of the Buttle correction in (4.74), while essential to obtain high accuracy, means that the resultant expression for the R-matrix is no longer variational. This disadvantage is, however, outweighed by the much faster rate of convergence as $n \to \infty$ of the Buttle-corrected result.

4.4.3 Arbitrary Boundary Condition Methods

In this section we consider the solution of the radial Schrödinger equation (4.62) in the internal region $0 \leq r \leq a_0$ using basis orbitals which satisfy arbitrary boundary conditions at $r = a_0$. We will see that there is increasing interest in these methods which do not require a Buttle correction to the R-matrix or wave function. Also, following from our discussion in Sect. 4.3, we will show that the R-matrix obtained using these basis orbitals can be derived from a variational principle.

For each orbital angular momentum ℓ under consideration we introduce a linearly independent set of n basis orbitals in the internal region as follows:

$$\phi_i(r), \ i = 1, \ldots, n, \quad 0 \leq r \leq a_0, \tag{4.86}$$

which are chosen to be real, vanish at the origin and satisfy arbitrary boundary conditions at $r = a_0$. We choose this basis so that as $n \to \infty$ this basis tends to a complete set over $0 \leq r \leq a_0$ given by (4.36). Hence the scattering wave function $u_\ell(r)$ at any energy can be expanded in the internal region in this basis. We then introduce linear combinations of these basis orbitals defined by

$$\chi_j(r) = \sum_{i=1}^{n} \phi_i(r) c_{ij}, \quad j = 1, \ldots, n, \quad 0 \leq r \leq a_0, \tag{4.87}$$

where, for notational convenience, we omit the explicit dependence of $\chi_j(r)$, c_{ij} and related quantities on the number of terms n retained in the expansion in this and later equations. The expansion coefficients c_{ij} are then determined by diagonalizing $L_\ell - \mathcal{L}$ so that

$$\int_0^{a_0} \chi_i(r)(L_\ell - \mathcal{L})\chi_j(r)\mathrm{d}r = 2(E - E_i)\delta_{ij}, \quad i, \ j = 1, \ldots, n, \tag{4.88}$$

where L_ℓ is defined by (4.29) and $\mathcal{L}$ is the Bloch operator defined by (4.31). Equation (4.88) defines the eigenenergies E_i, which converge to the eigenenergies given by (4.37) and (4.38) as $n \to \infty$. Also, it follows from the Hylleraas–Undheim theorem [484] that the n eigenenergies E_i defined by (4.88) are upper bounds on the lowest n exact eigenenergies defined by (4.37) and (4.38).

We now expand the trial function $u_\ell^t(r)$ in expression (4.50) for the first Kohn variational functional $F_\ell^{(1)}[u_\ell^t]$, discussed in Sect. 4.3, in terms of the basis functions $\chi_i(r)$ as follows:

$$u_\ell^t(r) = \sum_{i=1}^{n} \chi_i(r) d_i, \quad 0 \leq r \leq a_0. \tag{4.89}$$

Substituting this expansion into (4.50) and using (4.88) gives

$$F_\ell^{(1)}[u_\ell^t] = \frac{2\sum_{i=1}^n (E_i - E)\, d_i^2}{\sum_{i=1}^n \sum_{j=1}^n \chi_i(a_0)\chi_j(a_0) d_i d_j}. \tag{4.90}$$

It is convenient to rewrite this expression in matrix form by introducing the diagonal matrix $\boldsymbol{\Gamma}$ and the symmetric matrix $\boldsymbol{\Lambda}$ with components

$$\Gamma_{ij} = 2\,(E_i - E)\,\delta_{ij}, \quad i,\ j = 1, \ldots, n \tag{4.91}$$

and

$$\Lambda_{ij} = \chi_i(a_0)\chi_j(a_0), \quad i,\ j = 1, \ldots, n. \tag{4.92}$$

We also introduce the column vector $\mathbf{d}$ with components d_i. Equation (4.90) can then be rewritten as

$$f_1 = \frac{\mathbf{d}^{\mathrm{T}} \boldsymbol{\Gamma} \mathbf{d}}{\mathbf{d}^{\mathrm{T}} \boldsymbol{\Lambda} \mathbf{d}}, \tag{4.93}$$

where for notational convenience we have written $f_1 = F_\ell^{(1)}[u_\ell^t]$. The functional f_1 is stationary with respect to small variations of the expansion coefficient vector $\mathbf{d}$ if

$$\frac{\partial f_1}{\partial \mathbf{d}} = \frac{2\boldsymbol{\Gamma}\mathbf{d}}{\mathbf{d}^{\mathrm{T}} \boldsymbol{\Lambda} \mathbf{d}} - \frac{\mathbf{d}^{\mathrm{T}} \boldsymbol{\Gamma} \mathbf{d}}{(\mathbf{d}^{\mathrm{T}} \boldsymbol{\Lambda} \mathbf{d})^2} 2\boldsymbol{\Lambda}\mathbf{d} = 0, \tag{4.94}$$

which reduces after using (4.93) to the generalized eigenvalue equation

$$\boldsymbol{\Gamma}\mathbf{d} = f_1 \boldsymbol{\Lambda}\mathbf{d}. \tag{4.95}$$

In order to solve (4.95) we diagonalize $\boldsymbol{\Lambda}$ by the transformation

$$\mathbf{O}\boldsymbol{\Lambda}\mathbf{O}^{\mathrm{T}} = \mathbf{D}, \tag{4.96}$$

where $\mathbf{O}$ is an orthogonal matrix. Because of the special form of $\boldsymbol{\Lambda}$, defined by (4.92), only one element of $\mathbf{D}$ is non-zero and the remaining elements are zero. It is convenient to choose the elements of the first row of $\mathbf{O}$ to be

$$O_{1i} = \frac{\chi_i(a_0)}{\left(\sum_{j=1}^n \left[\chi_j(a_0)\right]^2\right)^{1/2}}, \quad i = 1, \ldots, n, \tag{4.97}$$

and the remaining rows to be normalized to unity and to be orthogonal to the first row and to each other, but otherwise to be arbitrary. Hence

$$\mathbf{O}\mathbf{O}^{\mathrm{T}} = \mathbf{I}. \tag{4.98}$$

Substituting this definition of $\mathbf{O}$ into (4.96) then gives

$$D_{11} = \sum_{i=1}^{n} [\chi_i(a_0)]^2, \quad D_{ij} = 0, \quad i \text{ or } j \neq 1. \tag{4.99}$$

Using these definitions we find, after premultiplying (4.95) by $\mathbf{O}$ and using (4.98), that

$$\mathbf{O}\boldsymbol{\Gamma}\mathbf{d} = f_1 \mathbf{D}\mathbf{O}\mathbf{d}. \tag{4.100}$$

It then follows from (4.99) that only the first element of the vector $\mathbf{D}\mathbf{O}\mathbf{d}$ on the right-hand side of (4.100) is non-zero and hence only the first element of the vector $\mathbf{O}\boldsymbol{\Gamma}\mathbf{d}$ on the left-hand side of (4.100) is non-zero. Consequently the vector $\boldsymbol{\Gamma}\mathbf{d}$ is orthogonal to the last $n-1$ rows of $\mathbf{O}$ and is therefore proportional to the first row of $\mathbf{O}$. Hence, after substituting for $\boldsymbol{\Gamma}$ from (4.91) and for the first row of $\mathbf{O}$ from (4.97) we obtain

$$2(E_i - E)d_i = \alpha \chi_i(a_0), \quad i = 1, \ldots, n, \tag{4.101}$$

where α is a constant of proportionality. Hence

$$d_i = \alpha \frac{\chi_i(a_0)}{2(E_i - E)}, \quad i = 1, \ldots, n. \tag{4.102}$$

Substituting this result for d_i into the first element of the vectors on both sides of (4.100) we find, after cancelling the constant of proportionality α, that

$$1 = \frac{1}{2} f_1 \sum_{i=1}^{n} \frac{[\chi_i(a_0)]^2}{E_i - E}. \tag{4.103}$$

Since, from (4.51), the stationary value of the functional $f_1 = F_\ell^{(1)}[u_\ell] = [a_0 R_\ell(E)]^{-1}$ we then obtain the following variational expression for the R-matrix:

$$R_\ell(E) = \frac{1}{2a_0} \sum_{i=1}^{n} \frac{[\chi_i(a_0)]^2}{E_i - E}. \tag{4.104}$$

As the number n of basis orbitals $\phi_i(r)$ retained in expansion (4.87) is increased to completeness, both the surface amplitudes $\chi_i(a_0)$ and the R-matrix eigenenergies E_i converge to their exact values and the R-matrix given by (4.104) converges to the exact result given by (4.42).

We obtain the same result using expression (4.55) for the second Jackson variational functional $F_\ell^{(2)}[u_\ell^t]$, discussed in Sect. 4.3. Substituting expansion (4.89) into (4.55) and using (4.88) gives

$$F_\ell^{(2)}[u_\ell^t] = 2\sum_{i=1}^{n}(E_i - E)\,d_i^2 - 2a_0^{-1}\sum_{i=1}^{n}\chi_i(a_0)d_i. \tag{4.105}$$

This functional is stationary with respect to small variations in the expansion coefficients d_i if

$$\frac{\partial F_\ell^{(2)}}{\partial d_i} = 4\,(E_i - E)\,d_i - 2a_0^{-1}\chi_i(a_0) = 0, \quad i = 1, \ldots, n. \tag{4.106}$$

This equation gives

$$d_i = \frac{1}{2a_0}\frac{\chi_i(a_0)}{E_i - E}, \quad i = 1, \ldots, n. \tag{4.107}$$

The stationary value of the functional $F_\ell^{(2)}[u_\ell^t]$ is obtained by substituting (4.107) into (4.105) giving

$$F_\ell^{(2)}[u_\ell^t] = -\frac{1}{2a_0^2}\sum_{i=1}^{n}\frac{[\chi_i(a_0)]^2}{E_i - E}. \tag{4.108}$$

Remembering from (4.60) that the stationary value of the functional $F_\ell^{(2)}[u_\ell^t] = -a_0^{-1}R_\ell(E)$, we obtain the following variational expression for the R-matrix

$$R_\ell(E) = \frac{1}{2a_0}\sum_{i=1}^{n}\frac{[\chi_i(a_0)]^2}{E_i - E}, \tag{4.109}$$

which is the same as (4.104), obtained using the functional $F_\ell^{(1)}[u_\ell^t]$.

We can also obtain an expression for the solution of (4.62) in the internal region corresponding to the variational expression for the R-matrix given by (4.104) or (4.109). It follows from (4.40) that

$$u_\ell(r) = \frac{1}{2a_0}\sum_{i=1}^{n}\frac{\chi_i(r)\chi_i(a_0)}{E_i - E}\left(a_0\frac{\mathrm{d}u_\ell}{\mathrm{d}r} - b_0u_\ell\right)_{r=a_0}, \quad 0 \le r \le a_0, \tag{4.110}$$

where the term on the boundary $r = a_0$ of the internal region, in brackets in (4.110), is defined by the normalization of the solution of the Schrödinger equation (4.62) in the external region. The solution in the external region has been discussed in Sect. 4.4.1 and will not be considered further here.

4.4.4 Linear Equations Method

In both the homogeneous and arbitrary boundary condition methods for determining the R-matrix considered in Sects. 4.4.1 and 4.4.3, we have to diagonalize the operator $L_\ell - \mathcal{L}$ in (4.67) or (4.88) to form the bases $u^n_{\ell i}(r)$ or $\chi_i(r)$, respectively. The corresponding R-matrices, given by (4.72) or (4.104), are then expressed directly in terms of these basis functions, evaluated on the boundary of the internal region, and the corresponding eigenenergies E_i. It follows that the R-matrices are determined at all energies E by a single matrix diagonalization. This approach is efficient if the corresponding phase shifts and cross sections are required at many energies. However, we will see in later chapters that in many applications the matrices can become very large and their diagonalization can then often dominate the total computing time. This can occur, for example, in electron collisions with atoms and atomic ions considered in Chaps. 5 and 6. In this case methods that involve the diagonalization of large matrices become inefficient if the R-matrix is required at only a few energies, such as in non-resonant energy regions. It can also occur in time-dependent multiphoton processes, discussed in Chap. 10, where the R-matrix is required at a single energy $E = 2\mathrm{i}\Delta t^{-1}$ where Δt is the time interval used in the propagation.

It was shown by Glass et al. [380] in a study of atomic multiphoton processes that this inefficiency can be removed by replacing matrix diagonalization by the solution of a set of linear simultaneous equations. To illustrate the method we consider the homogeneous boundary condition method, discussed in Sect. 4.4.1, where the R-matrix is given by (4.72). We rewrite this equation in matrix form as

$$R(E) = (2a_0)^{-1}\mathbf{u}^{\mathrm{T}}(\mathbf{E} - E\mathbf{I})^{-1}\mathbf{u}, \tag{4.111}$$

where the R-matrix $R(E)$ is a scalar and we have introduced the column vector $\mathbf{u}$, with components $u^n_{\ell i}(a_0)$, $i = 1, \ldots, n$, the diagonal matrix $\mathbf{E}$, with diagonal components E^n_i, $i = 1, \ldots, n$, and the $n \times n$ unit matrix $\mathbf{I}$. We can also rewrite (4.66), evaluated at $r = a_0$, in matrix form as

$$\mathbf{u} = \mathbf{C}^{\mathrm{T}}\mathbf{u}^0, \tag{4.112}$$

where we have introduced the orthogonal matrix $\mathbf{C}$ with components c^n_{ij}, $i, j = 1, \ldots, n$, and the column vector $\mathbf{u}^0$ with components $u^0_{\ell i}(a_0)$, $i = 1, \ldots, n$. Substituting (4.112) into (4.111) then gives

$$R(E) = (2a_0)^{-1}\mathbf{u}^{0\mathrm{T}}\mathbf{C}(\mathbf{E} - E\mathbf{I})^{-1}\mathbf{C}^{\mathrm{T}}\mathbf{u}^0. \tag{4.113}$$

Using (4.112) we can then rewrite (4.67) in the following matrix form:

$$\mathbf{C}^{\mathrm{T}}(\mathbf{L}_\ell - \boldsymbol{\mathcal{L}})\mathbf{C} = 2(E\mathbf{I} - \mathbf{E}), \tag{4.114}$$

where $\mathbf{L}_\ell - \boldsymbol{\mathcal{L}}$ is an $n \times n$ matrix with matrix elements given by

$$(L_\ell - \mathcal{L})_{ij} = \int_0^{a_0} u_{\ell i}^0(r)(L_\ell - \mathcal{L})u_{\ell j}^0(r)\mathrm{d}r, \quad i,\ j = 1, \ldots, n. \tag{4.115}$$

Hence, using the orthogonality of the matrix $\mathbf{C}$, we can rewrite (4.114) as

$$(\mathbf{L}_\ell - \boldsymbol{\mathcal{L}})^{-1} = \frac{1}{2}\mathbf{C}(E\mathbf{I} - \mathbf{E})^{-1}\mathbf{C}^{\mathrm{T}}. \tag{4.116}$$

The right-hand side of (4.113) can now be calculated by solving the following set of n linear simultaneous equations:

$$(\mathbf{L}_\ell - \boldsymbol{\mathcal{L}})\mathbf{x} = \mathbf{u}^0, \tag{4.117}$$

to yield the vector $\mathbf{x}$. Combining (4.116) and (4.117) then gives

$$\mathbf{x} = (\mathbf{L}_\ell - \boldsymbol{\mathcal{L}})^{-1}\mathbf{u}^0 = \frac{1}{2}\mathbf{C}(E\mathbf{I} - \mathbf{E})^{-1}\mathbf{C}^{\mathrm{T}}\mathbf{u}^0. \tag{4.118}$$

After substituting this result into (4.113), we then obtain the following expression for the R-matrix at the energy E in terms of the vector $\mathbf{x}$:

$$R(E) = -a_0^{-1}\mathbf{u}^{0\mathrm{T}}\mathbf{x}. \tag{4.119}$$

Thus we have replaced the diagonalization of the $n \times n$-dimensional matrix $\mathbf{L}_\ell - \boldsymbol{\mathcal{L}}$ to determine all of its eigenvalues and eigenvectors by the solution of a set of n linear simultaneous equations (4.117) with one right-hand side. However, since $\mathbf{L}_\ell$ depends on the energy E, these simultaneous equations have to be solved for each energy of interest, so this approach is efficient if the R-matrix is required at only a few energies.

Finally, we remark that the Buttle correction to the R-matrix, which is required in the homogeneous boundary condition method, can be calculated and added to the R-matrix given by (4.119) as discussed in Sect. 4.4.2.

4.4.5 Eigenchannel Methods

Eigenchannel methods are based on an approximation scheme introduced by Danos and Greiner [249] in a study of nuclear reactions, and its early use in nuclear physics was reviewed by Barrett et al. [54]. These methods have now been developed and applied in atomic and molecular physics by many workers including Fano and Lee [311], Lee [585], Shimamura [872], O'Malley et al. [705], Greene [417, 418], Raşeev and Le Rouzo [774], Le Rouzo and Raşeev [586], Aymar et al. [28] and Greene and Kim [422].

We commence by considering an iterative approach adopted in electron–atom collisions and photoabsorption by Fano and Lee [311] and Lee [585], which follows

closely the approach of Danos and Greiner [249]. In this approach, a set of n radial functions $v_j(r)$ are introduced for the orbital angular momentum ℓ under consideration, which are expanded in the internal region $0 \le r \le a_0$ in terms of a set of m basis orbitals $\phi_i(r)$ $(m > n)$ as follows:

$$v_j(r) = \sum_{i=1}^{m} \phi_i(r) a_{ij}, \quad j = 1, \ldots, n, \quad 0 \le r \le a_0. \tag{4.120}$$

The basis orbitals $\phi_i(r)$ are quadratically integrable over the internal region $0 \le r \le a_0$, are zero at the origin and satisfy arbitrary boundary conditions at $r = a_0$. In the work of Fano and Lee [311] and Lee [585], the basis orbitals $\phi_i(r)$ were chosen to be Slater-type orbitals. The coefficients a_{ij} in (4.120) are then chosen so that $v_j(r)$ satisfy the homogeneous boundary conditions

$$\begin{aligned} v_j(0) &= 0, \\ a_0 \frac{\mathrm{d}v_j}{\mathrm{d}r}\bigg|_{r=a_0} &= b_0 v_j(a_0), \quad j = 1, \ldots, n, \end{aligned} \tag{4.121}$$

and the orthonormality conditions

$$\int_0^{a_0} v_i(r) v_j(r) \mathrm{d}r = \delta_{ij}, \quad i,\ j = 1, \ldots, n, \tag{4.122}$$

where b_0 is an arbitrary constant discussed below. In addition, the functions $v_i(r)$ are orthogonalized to the reduced radial bound orbitals of the target atom, $P_i(r)$, $i = 1, \ldots, p$, corresponding to the orbital angular momentum under consideration, yielding the constraints

$$\int_0^{a_0} P_i(r) v_j(r) \mathrm{d}r = 0, \quad i = 1, \ldots, p, \quad j = 1, \ldots, n. \tag{4.123}$$

Equations (4.121), (4.122) and (4.123) enable the coefficients a_{ij} in (4.120) to be determined for each orbital angular momentum using, for example, a Schmidt orthogonalization procedure. It follows that n, the number of functions $v_j(r)$, is related to m, the number of basis orbitals $\phi_i(r)$, by

$$n = m - p - 1. \tag{4.124}$$

Hence in the case of potential scattering, where $p = 0$, the inclusion of $n + 1$ basis orbitals $\phi_i(r)$ yields n functions $v_j(r)$ satisfying (4.121) and (4.122).

We now consider the solution of the radial Schrödinger equation (4.62) in the internal region $0 \le r \le a_0$ using the iterative eigenchannel method. We introduce linear combinations of the n functions $v_j(r)$, by the equation

$$u_j(r) = \sum_{i=1}^{n} v_i(r) c_{ij}, \quad j = 1, \ldots, n, \quad 0 \le r \le a_0, \tag{4.125}$$

where the coefficients c_{ij} are obtained by diagonalizing the operator $L_\ell - \mathcal{L}$ in this basis giving

$$\int_0^{a_0} u_i(r)(L_\ell - \mathcal{L}) u_j(r) \mathrm{d}r = 2(E - E_i)\delta_{ij}, \quad i, \ j = 1, \ldots, n. \tag{4.126}$$

In this equation L_ℓ is the operator defined by (4.29) and $\mathcal{L}$ is the Bloch operator defined by (4.31). This procedure gives a set of n eigenenergies E_i and the corresponding eigensolutions $u_i(r)$ both of which depend on the value chosen for b_0 in (4.121). If the solution is required at a particular energy E, the value of b_0 can be varied and the above process repeated iteratively until one of the eigenvalues E_i in (4.126), which are functions of b_0, satisfies the equation

$$E_i(b_0) = E, \tag{4.127}$$

where E is the energy of interest. The wave function in the internal region is then given by the corresponding eigensolution $u_i(r)$, defined by (4.125) and (4.126) to within a normalization factor. It follows from (4.72) that the corresponding R-matrix at the energy E is singular and hence the corresponding solution in the external region satisfies the boundary condition

$$a_0 \frac{\mathrm{d}u_i}{\mathrm{d}r}\bigg|_{r=a_0} = b_0 u_i(a_0). \tag{4.128}$$

This shows that both the wave function and its derivative are continuous on the boundary. Also, since the R-matrix is singular at the energy E_i, a Buttle correction which is finite is not required. We also note that although an iterative procedure is in principle required to satisfy (4.127), as described above, this process can in practice be speeded up by plotting the eigenvalues $E_i(b_0)$ against b_0 and interpolating to determine the solution of (4.127).

Finally, the calculation of the phase shift is straightforward using the eigenchannel method since the R-matrix is singular at the energy E_i. If the interaction potential vanishes for $r \ge a_0$ then it follows from (4.27) that

$$\tan \delta_\ell(k) = \frac{ka_0 s'_\ell(ka_0) - b_0 s_\ell(ka_0)}{-ka_0 c'_\ell(ka_0) + b_0 c_\ell(ka_0)}. \tag{4.129}$$

Once the phase shifts have been calculated for all relevant angular momenta, then the scattering amplitude and cross sections can be determined using (1.29), (1.30) and (1.31).

A disadvantage of the eigenchannel method discussed so far is that an iterative procedure is necessary in order to obtain the eigenvalue at a particular energy defined by (4.127). Although, as we have observed, this procedure can be speeded up using an interpolation technique, this method still suffers from the disadvantage that the Hamiltonian matrix must be diagonalized several times in order to determine the required eigenvalue. This disadvantage was overcome by Greene [417, 418] who introduced a non-iterative eigenchannel method, based on the Kohn variational principle for the R-matrix, discussed in Sect. 4.3, which avoids repeated diagonalization of the Hamiltonian matrix.

In the non-iterative eigenchannel method we commence, as in the arbitrary boundary condition methods considered in Sect. 4.4.3, by introducing a linearly independent set of real basis orbitals in the internal region as follows:

$$\phi_i(r), \quad i = 1, \ldots, n, \quad 0 \leq r \leq a_0, \tag{4.130}$$

which vanish at the origin and satisfy arbitrary boundary conditions at $r = a_0$. We now expand the trial function $u_\ell^t(r)$ directly in terms of this basis as follows:

$$u_\ell^t(r) = \sum_{i=1}^{n} \phi_i(r) c_i, \quad 0 \leq r \leq a_0. \tag{4.131}$$

Substituting this expansion into the Kohn variational functional given by (4.50) then gives

$$F_\ell^{(1)}[u_\ell^t] = \frac{\sum_{i=1}^n \sum_{j=1}^n c_i A_{ij} c_j}{\sum_{i=1}^n \sum_{j=1}^n c_i \phi_i(a_0) \phi_j(a_0) c_j}, \tag{4.132}$$

where

$$A_{ij} = \int_0^{a_0} \phi_i(r)(-L_\ell + \mathcal{L})\phi_j(r) \mathrm{d}r, \quad i, \ j = 1, \ldots, n. \tag{4.133}$$

Since $-L_\ell + \mathcal{L}$ is hermitian and the basis orbitals $\phi_i(r)$ are real then the matrix A_{ij} is real and symmetric. We also introduce the real symmetric matrix $\mathbf{B}$ with matrix elements

$$B_{ij} = \phi_i(a_0)\phi_j(a_0), \quad i, \ j = 1, \ldots, n. \tag{4.134}$$

We can then rewrite (4.132) in matrix form as

$$f_1 = \frac{\mathbf{c}^{\mathrm{T}} \mathbf{A} \mathbf{c}}{\mathbf{c}^{\mathrm{T}} \mathbf{B} \mathbf{c}}, \tag{4.135}$$

where $f_1 = F_\ell^{(1)}[u_\ell^t]$. It then follows from the Kohn variational principle that the functional f_1 is stationary with respect to small variations of the expansion coefficients c_i. Hence

$$\frac{\partial f_1}{\partial \mathbf{c}} = \frac{2\mathbf{Ac}}{\mathbf{c}^{\mathrm{T}}\mathbf{Bc}} - \frac{\mathbf{c}^{\mathrm{T}}\mathbf{Ac}}{(\mathbf{c}^{\mathrm{T}}\mathbf{Bc})^2} 2\mathbf{Bc} = 0, \tag{4.136}$$

which, after using (4.135), reduces to the generalized eigenvalue equation

$$\mathbf{Ac} = f_1 \mathbf{Bc}. \tag{4.137}$$

Following the procedure adopted in Sect. 4.4.3, we solve (4.137) by diagonalizing **B** by an orthogonal transformation **O** so that

$$\mathbf{OBO}^{\mathrm{T}} = \mathbf{D}, \tag{4.138}$$

where the elements of the first row of **O** are defined by

$$O_{1i} = \frac{\phi_i(a_0)}{\left(\sum_{j=1}^n \left[\phi_j(a_0)\right]^2\right)^{1/2}}, \quad i = 1, \ldots, n, \tag{4.139}$$

and the remaining rows of **O** are normalized to unity and orthogonal to the first row and to each other, but otherwise arbitrary, so that

$$\mathbf{OO}^{\mathrm{T}} = \mathbf{I}. \tag{4.140}$$

Hence we can rewrite (4.137) as

$$\mathbf{Mx} = f_1 \mathbf{Dx}, \tag{4.141}$$

where

$$\mathbf{M} = \mathbf{OAO}^{\mathrm{T}} \text{ and } \mathbf{x} = \mathbf{Oc}, \tag{4.142}$$

and where the elements of the matrix **D** are given by

$$D_{11} = \sum_{i=1}^{n} [\phi_i(a_0)]^2, \quad D_{ij} = 0, \quad i \text{ or } j \neq 1. \tag{4.143}$$

It follows that only the first element of the vector $f_1\mathbf{Dx}$ on the right-hand side of (4.141) is non-zero. Hence (4.141) can be rewritten as

$$\mathbf{M}'\mathbf{x} = 0, \tag{4.144}$$

where the elements of the matrix $\mathbf{M}'$ are defined in terms of the elements of the matrix $\mathbf{M}$ by

$$M'_{11} = M_{11} - g, \quad M'_{ij} = M_{ij}, \quad i \text{ or } j \neq 1, \tag{4.145}$$

and where

$$g = f_1 \sum_{i=1}^{n} [\phi_i(a_0)]^2 . \tag{4.146}$$

We now observe that (4.144) only has a non-trivial solution when

$$\det \mathbf{M}' = 0, \tag{4.147}$$

which is a linear equation in f_1 of the form

$$\alpha - \beta f_1 = 0, \tag{4.148}$$

where α and β can be obtained using a standard procedure for reducing the n linear simultaneous equations defined by (4.144) to a single equation. Remembering that $f_1 = F_\ell^{(1)}[u_\ell^t]$ it then follows from (4.51) that the stationary value of the R-matrix is given in terms of α and β by

$$R_\ell(E) = \frac{\beta}{a_0 \alpha}, \tag{4.149}$$

which yields the R-matrix at the energy $E = 2k^2$ corresponding to the operator L_ℓ in the Kohn variational functional given by (4.50). This procedure for determining α and β and hence $R_\ell(E)$ can be repeated for each energy of interest. Hence we see that for each energy the R-matrix is obtained by reducing a set of linear simultaneous equations defined by (4.147), rather than by an iterative procedure involving repeated diagonalization of the Hamiltonian matrix.

4.4.6 Lagrange Mesh Methods

We consider in this section Lagrange mesh methods which provide variational accuracy for bound state and collision problems calculated on a mesh or grid of points. The main principles of mesh calculations were discussed by Harris et al. [441] in which they proposed a mesh representation in which the potential terms are diagonal so that the Hamiltonian matrix generation is fast. In addition, these methods need fewer mesh points than finite differences or finite element methods and higher accuracy may be obtained [81]. They are also related to Gauss quadrature methods [261] and to discrete variable representations (DVR) in quantum theory

[596, 597]. The methods have had applications in several fields including nuclear, atomic and molecular physics and Lagrange mesh R-matrix calculations in potential scattering have been carried out by a number of authors including Layton [582], Layton and Stade [583], Malegat [631] and Baye et al. [82]. In this section we discuss the background to Lagrange mesh methods and consider their application in potential scattering.

A Lagrange basis is defined as a set of n Lagrange functions satisfying definite properties at n associated mesh points on an interval which we will take to be [0, 1]. The indefinitely differential Lagrange functions $f_i(x)$ satisfy the Lagrange conditions

$$f_i(x_j) = \lambda_i^{-1/2}\delta_{ij}, \quad i,\ j = 1, \ldots, n, \tag{4.150}$$

which means that each function $f_i(x_j)$ vanishes at all mesh points x_j, $j = 1, \ldots, n$, except x_i. These functions also satisfy the orthonormality relations

$$\int_0^1 f_i(x) f_j(x) \mathrm{d}x = \delta_{ij}, \quad i,\ j = 1, \ldots, n. \tag{4.151}$$

An integration over an indefinitely differential function $g(x)$ is then given by the following Gauss quadrature approximation associated with the mesh

$$\int_0^1 g(x) \mathrm{d}x \approx \sum_{i=1}^{n} \lambda_i g(x_i), \tag{4.152}$$

where the weights λ_i are generalized Christoffel numbers [900]. With this approximate quadrature, the overlap of two Lagrange functions is given by

$$\int_0^1 f_i(x) f_j(x) \mathrm{d}x \approx \sum_{k=1}^{n} \lambda_k f_i(x_k) f_j(x_k) = \delta_{ij}, \quad i,\ j = 1, \ldots, n, \tag{4.153}$$

where we have used the Gauss quadrature approximation defined by (4.152) and the Lagrange conditions defined by (4.150) in evaluating this integral.

As an example, the n-dimensional Lagrange mesh associated with Legendre polynomials of degree n, shifted from $[-1, +1]$ to [0, 1], has been used by Malegat [631] in a model study of scattering by an exponential potential. The corresponding orthonormal Lagrange basis functions are

$$f_i(x) = (-1)^i [x_i(1 - x_i)]^{1/2} \frac{P_n(2x - 1)}{x - x_i}, \quad i = 1, \ldots, n, \quad 0 \le x \le 1, \tag{4.154}$$

where the mesh points are the zeros of the shifted Legendre polynomials, discussed in Appendix B.1, which are defined by

$$P_n(2x_j - 1) = 0, \quad j = 1, \ldots, n. \tag{4.155}$$

It follows that $f_i(x)$ is zero at all the mesh points x_j, $j = 1, \ldots, n$, except when $j = i$ where the zero in $P_n(2x - 1)$ at $x = x_i$ is cancelled by the zero in $x - x_i$ in (4.154). The shifted Legendre polynomials then yield a Gauss–Legendre quadrature defined by (4.152), where the weights are

$$\lambda_i = \left\{ x_i(1 - x_i) \left[P_n'(2x_i - 1) \right]^2 \right\}^{-1}, \quad i = 1, \ldots, n. \tag{4.156}$$

Other Lagrange meshes that have been considered include those based on Jacobi, Hermite and Laguerre polynomials [81, 82]. In addition a generalized Lagrange basis, introduced by Baye [80], has been defined as

$$\hat{f}_i(x) = x_i^{-1} x f_i(x), \quad i = 1, \ldots, n. \tag{4.157}$$

These functions satisfy the Lagrange conditions given by (4.150) and, while they are not strictly orthogonal, they satisfy the Gauss orthogonality condition defined by (4.153) which depends on the validity of (4.150). Also, in place of (4.151), they satisfy

$$\int_0^1 \hat{f}_i(x) x^{-2} \hat{f}_j(x) \mathrm{d}x = x_i^{-2} \delta_{ij}, \tag{4.158}$$

which is important in the accurate treatment of the singular centrifugal term in the Schrödinger equation. A regularization technique which allows Lagrange mesh methods to retain their accuracy and simplicity when the Hamiltonian is singular at a finite distance has also been developed by Vincke et al. [939].

As a further example we consider the solution of the radial Schrödinger equation

$$\left(\frac{\mathrm{d}^2}{\mathrm{d}r^2} - \frac{\ell(\ell + 1)}{r^2} - U(r) + k^2 \right) u_\ell(r) = 0, \tag{4.159}$$

in an internal region $0 \leq r \leq a_0$, using the Lagrange mesh method. In order to express the solution in terms of generalized Lagrange functions it is convenient to transform the internal region from $0 \leq r \leq a_0$ to $0 \leq x \leq 1$ by writing $r = a_0 x$. Equation (4.159) then becomes

$$L_\ell v_\ell(x) = \left(\frac{\mathrm{d}^2}{\mathrm{d}x^2} - \frac{\ell(\ell + 1)}{x^2} - V(x) + p^2 \right) v_\ell(x) = 0, \quad 0 \leq x \leq 1, \tag{4.160}$$

which defines the operator L_ℓ and where we have written

$$V(x) = a_0^2 U(r), \quad p^2 = a_0^2 k^2, \quad v_\ell(x) = u_\ell(r). \tag{4.161}$$

We now solve (4.160) in the internal region, discussed in Sect. 4.2, by introducing the Bloch operator

$$\mathcal{L} = \delta(x-1)\left(\frac{\mathrm{d}}{\mathrm{d}x} - b_0\right), \tag{4.162}$$

where b_0 is an arbitrary constant. Equation (4.160) then has the formal solution

$$v_\ell = -(L_\ell - \mathcal{L})^{-1}\mathcal{L}v_\ell. \tag{4.163}$$

where the operator $L_\ell - \mathcal{L}$ is hermitian in the space of the generalized Lagrange basis functions which satisfy arbitrary boundary conditions at $x = 1$. A spectral representation of Green's function $(L_\ell - \mathcal{L})^{-1}$ in (4.163) can be obtained by introducing a new basis

$$\chi_j(x) = \sum_{i=1}^{n} \hat{f}_i(x) c_{ij}, \quad j = 1, \ldots, n, \tag{4.164}$$

where the expansion coefficients c_{ij} are determined by diagonalizing the $n \times n$-dimensional matrix

$$A_{ij} = \int_0^1 \hat{f}_i(x)(L_\ell - \mathcal{L})\hat{f}_j(x)\mathrm{d}x, \quad i,\ j = 1, \ldots, n. \tag{4.165}$$

The matrix elements in this equation, corresponding to the kinetic energy, orbital angular momentum and potential energy terms in $L_\ell - \mathcal{L}$, can be written in compact form using the Gauss quadrature approximation. In particular, the potential is diagonal in this approximation so that

$$\int_0^1 \hat{f}_i(x) V(x) \hat{f}_j(x)\mathrm{d}x \approx V(x_i)\delta_{ij}, \quad i,\ j = 1, \ldots, n. \tag{4.166}$$

We can then write

$$\int_0^1 \chi_j(x)(L_\ell - \mathcal{L})\chi_{j'}(x)\mathrm{d}x = 2(e - e_j)\delta_{jj'}, \quad j,\ j' = 1, \ldots, n, \tag{4.167}$$

and hence, after substituting this result into (4.163) we obtain

$$v_\ell(x) = \frac{1}{2}\sum_{i=1}^{n} \frac{\chi_i(x)\chi_i(1)}{e_i - e}\left(\frac{\mathrm{d}v_\ell}{\mathrm{d}x} - b_0 v_\ell\right)_{x=1}, \tag{4.168}$$

where the energy $e = 2p^2$. Evaluating (4.168) on the boundary $x = 1$ of the internal region then gives

$$v_\ell(x) = \mathcal{R}_\ell(e)\left(\frac{\mathrm{d}v_\ell}{\mathrm{d}x} - b_0 v_\ell\right)_{x=1}, \tag{4.169}$$

where the R-matrix

$$\mathcal{R}_\ell(e) = \frac{1}{2}\sum_{i=1}^{n}\frac{[\chi_i(1)]^2}{e_i - e}. \tag{4.170}$$

We can rewrite (4.169) in standard form, in terms of the reduced radial functions $u_\ell(r)$, which satisfy (4.159), as follows:

$$u_\ell(r) = R_\ell(E)\left(a_0\frac{\mathrm{d}u_\ell}{\mathrm{d}r} - b_0 u_\ell\right)_{r=a_0}, \tag{4.171}$$

where the R-matrix $R_\ell(E)$ at the energy E is defined in terms of the R-matrix $\mathcal{R}_\ell(e)$ at the transformed energy e by the equation

$$R_\ell(E) = \mathcal{R}_\ell(e), \quad e = a_0^2 E. \tag{4.172}$$

It follows that the R-matrix $\mathcal{R}_\ell(e)$ at $x = 1$, obtained by solving (4.160) using the Lagrange mesh method, yields the R-matrix $R_\ell(E)$ at $r = a_0$, where $E = a_0^{-2}e$. The R-matrix $R_\ell(E)$ then provides the boundary condition at $r = a_0$ for solving (4.159) in the external region.

Since the generalized Lagrange functions $\hat{f}_i(x)$ satisfy arbitrary boundary conditions at $x = 1$, there is no need to add a Buttle correction to the R-matrix $\mathcal{R}_\ell(e)$, defined by (4.170), and hence to the R-matrix $R_\ell(E)$, defined by (4.172). Also, following our discussion in Sects. 4.3 and 4.4.3, the R-matrix can be derived from a variational principle using this method.

Finally, we remark that a Lagrange mesh method for determining continuum orbitals has been incorporated by Plummer and Noble [743] into the general R-matrix electron–atom and electron–ion collision program RMATRXII discussed in Sect. 5.1.1.

4.4.7 B-Spline Methods

B-splines were first introduced by Schoenberg [831] in 1946, but it was not until the publication of the monograph by de Boor [254] that they started to be used in atomic physics studies. Since then they have been widely applied in both atomic and molecular physics calculations, and their many applications have been reviewed by Bachau et al. [29]. In this section we summarize the basic properties of B-splines and their application in representing bound and continuum orbitals in electron–atom and electron–ion R-matrix collision calculations and in multiphoton R-matrix calculations.

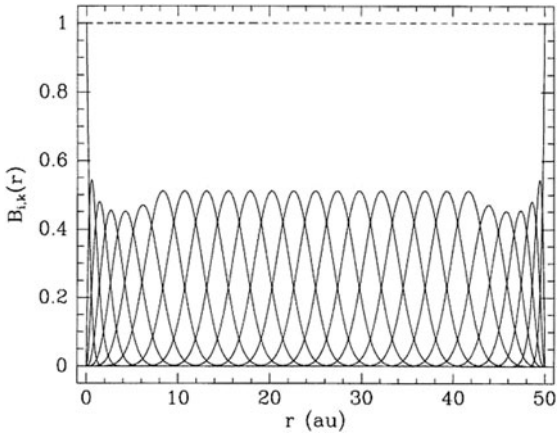

Fig. 4.2 An example of a B-spline basis using a linear distribution of knot points in a region $0 \leq r \leq 50$ a.u. The *dashed line* corresponds to the sum over all B-splines which equals 1. The first and last six B-splines differ in shape due to multiple knots on the boundaries (Fig. 1 from [930])

We show in Fig. 4.2 an example of a B-spline basis, given by van der Hart [930], which spans the range $0 \leq r \leq 50$ a.u., which corresponds to the internal region in an R-matrix calculation. In this example the full range is sub-divided into 25 equal intervals each of length 2 a.u. by a set of 26 equally spaced knots, discussed below. In general, the intervals need not be of equal length. For example, in atomic physics applications the intervals are usually chosen to be smaller near the nucleus in order to accurately represent the rapid oscillations of the electronic wave functions in this region.

Each B-spline $B_i(r)$ is defined by an order $k > 0$ and a set of $k + 1$ values of r or knots $t_i \leq t_{i+1} \leq \cdots \leq t_{i+k}$ where in certain circumstances two or more knots can coincide, that is, have multiplicity higher than 1. This higher multiplicity usually occurs at the beginning and end of the full range of r under consideration and results in the first and last B-splines being non-zero on the boundaries of the range, as seen in Fig. 4.2. This is important in R-matrix theory where the value of the B-spline on the outer boundary of the internal region is used in the construction of the R-matrix. Another important property of B-splines is their strong linear independence. We see from Fig. 4.2 that the individual B-splines are positive definite and only overlap with near neighbours. This means that the overlap matrix is sparse which leads to matrices which are easier to diagonalize. We now mention some other properties of B-splines:

- $B_i(r)$ is represented by different polynomials of degree $k - 1$ over each interval $t_j < r \leq t_{j+1}, \quad j = i, \ldots, \ i + k - 1$.
- $B_i(r) > 0, \quad t_i < r < t_{i+k}$.
- $B_i(r) = 0, \ r \leq t_i$ and $r \geq t_{i+k}$.
- $B_i(r)$ is continuous together with its first $k - 2$ derivatives at interior knots t_j, $j = i + 1, \ldots, \ i + k - 1$ of unit multiplicity.

- The summation $\sum_i B_i(r) = 1$, where the summation goes over all non-zero splines at the position r.

B-splines can be generated by a recursion relation. We define the B-spline of order 1 by

$$B_i^1(r) = \begin{cases} 1, & t_i \le r < t_{i+1}, \\ 0, & \text{otherwise}, \end{cases} \tag{4.173}$$

then

$$B_i^k(r) = \frac{r - t_i}{t_{i+k-1} - t_i} B_i^{k-1}(r) + \frac{t_{i+k} - r}{t_{i+k} - t_{i+1}} B_{i+1}^{k-1}(r), \quad k = 2,\ 3, \ldots . \tag{4.174}$$

In the case of knot points with multiplicity larger than 1, these definitions must be modified slightly. Using the above properties of B-splines we find, by way of illustration, that the B-spline of order 3 corresponding to four equally spaced knots $t_i = 0$, $t_{i+1} = 1$, $t_{i+2} = 2$ and $t_{i+3} = 3$ is represented by the following polynomials

$$B_i(r) = \begin{cases} \frac{1}{2}r^2 & 0 \le r < 1 \\ -r^2 + 3r - \frac{3}{2} & 1 \le r < 2 \\ \frac{1}{2}r^2 - 3r + \frac{9}{2} & 2 \le r < 3 \end{cases}, \tag{4.175}$$

and is zero otherwise. In general, B-splines can be calculated for arbitrary order and arbitrary knot distributions using Fortran programs published by de Boor [254].

We now consider the application of B-splines in representing bound and continuum orbitals in electron–atom and electron–ion R-matrix collision calculations. We introduce a B-spline basis for a given orbital angular momentum symmetry as follows:

$$B_i(r), \quad i = 1, \ldots, n, \tag{4.176}$$

where we assume that the order k and the location and number of knots are chosen so that this basis provides an accurate representation of the corresponding bound and continuum orbitals over the R-matrix internal region $0 \le r \le a_0$ for the energy range under consideration. We assume that there are $p \ll n$ bound orbitals, which may include pseudo-orbitals,

$$P_i(r), \quad i = 1, \ldots, p, \tag{4.177}$$

corresponding to the given orbital angular momentum. We also assume that these orbitals have been determined from previous bound state calculations and are orthonormal over the internal region, satisfying

$$\langle P_i | P_j \rangle = \delta_{ij}, \quad i,\ j = 1, \ldots, p, \tag{4.178}$$

where in this and later equations in this section the Dirac bracket notation corresponds to integration over the range $0 \le r \le a_0$.

We wish to represent these bound orbitals by the B-spline basis and also to generate a set of $n-p$ orthonormal continuum orbitals which are also represented by this basis. A convenient procedure is to introduce a zero-order differential operator analogous to that used in the homogeneous boundary condition method discussed in Sect. 4.4.1, which we write here as

$$H_0 = \left[\frac{\mathrm{d}^2}{\mathrm{d}r^2} - \frac{\ell(\ell+1)}{r^2} - U_0(r) \right], \tag{4.179}$$

where $U_0(r)$ is a zero-order potential. We then look for solutions of the equation

$$(H_0 + \mathcal{L} - k^2) u(r) = 0, \tag{4.180}$$

which are orthonormal in the internal region $0 \le r \le a_0$, where $\mathcal{L}$ is the Bloch operator defined by (4.31) which ensures that $H_0 + \mathcal{L}$ is hermitian in the internal region for arbitrary b_0. In order to solve (4.180) we expand $u(r)$ in the B-spline basis as follows:

$$u(r) = \sum_{j=1}^{n} B_j(r) c_j. \tag{4.181}$$

We now consider the functional

$$I = \langle u | H_0 + \mathcal{L} - k^2 | u \rangle = \sum_{i=1}^{n} \sum_{j=1}^{n} \langle B_i | H_0 + \mathcal{L} - k^2 | B_j \rangle c_i c_j. \tag{4.182}$$

Variational solutions of (4.180) are then obtained by minimizing the functional I which gives

$$\frac{\partial I}{\partial c_i} = \sum_{j=1}^{n} \langle B_i | H_0 + \mathcal{L} - k^2 | B_j \rangle c_j = 0, \quad i = 1, \ldots, n, \tag{4.183}$$

which we can rewrite in matrix form as

$$\mathbf{Hc} = k^2 \mathbf{Bc}, \tag{4.184}$$

where the matrix elements of $\mathbf{H}$ are

$$H_{ij} = \langle B_i | H_0 + \mathcal{L} | B_j \rangle, \quad i,\ j = 1, \ldots, n \tag{4.185}$$

and those of $\mathbf{B}$ are

$$B_{ij} = \langle B_i | B_j \rangle, \quad i,\ j = 1, \ldots, n. \tag{4.186}$$

The generalized eigenvalue equation (4.184) can be solved by introducing an orthogonal matrix $\mathbf{O}$ which diagonalizes the real positive definite symmetric matrix $\mathbf{B}$ so that

$$\mathbf{O}^{\mathrm{T}}\mathbf{B}\mathbf{O} = \mathbf{D}, \tag{4.187}$$

where the diagonal elements of $\mathbf{D}$ are real and positive. We then introduce a new basis

$$\boldsymbol{\phi} = \mathbf{D}^{-1/2}\mathbf{O}^{\mathrm{T}}\mathbf{b}, \tag{4.188}$$

where $\boldsymbol{\phi}$ is a column vector with n elements $\phi_i(r),\ i = 1, \ldots, n$, and $\mathbf{b}$ is a column vector with n elements $B_i(r),\ i = 1, \ldots, n$. Equation (4.184) then reduces to the standard eigenvalue equation

$$\mathbf{H}'\mathbf{d} = k^2\mathbf{d}, \tag{4.189}$$

where the matrix elements of $\mathbf{H}'$ are defined by

$$H'_{ij} = \langle \phi_i | H_0 + \mathcal{L} | \phi_j \rangle, \quad i,\ j = 1, \ldots, n \tag{4.190}$$

and

$$\mathbf{d} = \mathbf{D}^{1/2}\mathbf{O}^{\mathrm{T}}\mathbf{c}. \tag{4.191}$$

It follows that the new basis $\boldsymbol{\phi}$ is orthonormal since

$$\langle \boldsymbol{\phi} | \boldsymbol{\phi}^{\mathrm{T}} \rangle = \mathbf{D}^{-1/2}\mathbf{O}^{\mathrm{T}} \langle \mathbf{b} | \mathbf{b}^{\mathrm{T}} \rangle \mathbf{O}\mathbf{D}^{-1/2} = \mathbf{D}^{-1/2}\mathbf{O}^{\mathrm{T}}\mathbf{B}\mathbf{O}\mathbf{D}^{-1/2} = \mathbf{I}, \tag{4.192}$$

where we have used (4.187) and (4.188).

Having determined the orthonormal basis $\phi_i(r),\ i = 1, \ldots, n$, we can express the bound orbitals in terms of this basis. We write

$$P_j(r) = \sum_{i=1}^{n} \phi_i(r) a_{ij}, \quad j = 1, \ldots, p, \tag{4.193}$$

where the expansion coefficients a_{ij} are given by

$$a_{ij} = \langle \phi_i | P_j \rangle, \quad i = 1, \ldots, n, \quad j = 1, \ldots, p, \tag{4.194}$$

and where it follows from (4.178) and (4.192) that

$$\sum_{i=1}^{n} a_{ij}^2 = 1, \quad j = 1, \ldots, p. \tag{4.195}$$

We also have to determine $n - p$ continuum orbitals which are expressed in the B-spline basis and which are mutually orthogonal and also orthogonal to the bound orbitals. We can achieve this using a procedure for introducing orthogonality constraints into basis set calculations, described by Landtman et al. [564] and Bentley [90].

We consider a modified matrix eigenvalue equation in which we introduce projection operators in the n-dimensional space spanned by the orthonormal basis $\phi_i(r)$, $i = 1, \ldots, n$, defined by (4.188). The projection operators $\mathbf{P}$ and $\mathbf{Q}$ are defined by

$$\mathbf{P} = \mathbf{A}\mathbf{A}^{\mathrm{T}}, \quad \mathbf{Q} = \mathbf{I} - \mathbf{P}, \tag{4.196}$$

where $\mathbf{A}$ is an $n \times p$-dimensional matrix formed by the expansion coefficients a_{ij}, defined by (4.194) and (4.195). It follows that $\mathbf{P}$ projects onto the p-dimensional space spanned by the functions $P_j(r)$, $j = 1, \ldots, p$, and $\mathbf{Q}$ projects onto the $(n-p)$-dimensional space orthogonal to $\mathbf{P}$. Hence $\mathbf{P} + \mathbf{Q}$ projects onto the n-dimensional space spanned by the B-spline basis $B_i(r)$ or, equivalently, by the orthonormal basis $\phi_i(r)$. It follows from (4.196) that

$$\mathbf{P}^2 = \mathbf{P}, \quad \mathbf{Q}^2 = \mathbf{Q}, \quad \mathbf{P}\mathbf{Q} = \mathbf{Q}\mathbf{P} = \mathbf{I}. \tag{4.197}$$

We now look for solutions satisfying the matrix eigenvalue equation

$$(\mathbf{I} - \mathbf{P})\mathbf{H}'(\mathbf{I} - \mathbf{P})\mathbf{a} = k^2\mathbf{a}, \tag{4.198}$$

where the $n \times n$-dimensional matrix operator on the left-hand side of this equation is constructed from $\mathbf{H}'$ and $\mathbf{P}$, defined by (4.190), (4.194) and (4.196). We see immediately that the p vectors defined by (4.194) and (4.195) are eigenvectors of (4.198) belonging to the eigenvalue $k^2 = 0$, since $(\mathbf{I} - \mathbf{P})$ operating on each of these eigenvectors gives zero. The remaining $n - p$ eigenvectors of (4.198) will in general belong to non-zero and non-degenerate eigenvalues and hence will be orthogonal to each other and to the eigenvectors spanning P-space. Hence they provide an orthonormal representation of the $n - p$ continuum orbitals in terms of the basis $\phi_i(r)$.

It is interesting to note that the first step in the above procedure, where we expand the bound orbitals in B-splines using an orthonormal basis ϕ_i defined by (4.188), can be modified. Instead, the bound orbitals can be expanded directly in terms of the original B-spline basis using a least-squares fitting procedure. The projection operator method, which has been extended by Bentley [90] to allow for the possibility of using non-orthogonal orbitals, can then be used to determine the continuum orbitals directly in terms of the B-spline basis. However, since this modified approach

commences from the same B-spline basis and fits to the same bound orbitals as the procedure described in this section, then the **P** and **Q** operators project onto the same bound and continuum spaces. Hence both procedures will yield the same results.

Finally, we mention that recent electron–atom and electron–ion collision calculations and time-dependent multiphoton calculations, discussed in Sects. 5.6 and 10.2, respectively, have been carried out using a general B-spline R-matrix computer program BSR written by Zatsarinny [992]. In this program, discussed further in Sect. 5.1.1, the orthogonality constraint between orbitals in the R-matrix calculation is relaxed and target state-dependent non-orthogonal bound orbitals and continuum orbitals are represented by B-spline bases. This added flexibility reduces the need for the inclusion of pseudo-orbitals to represent the target states, discussed in Sect. 2.2, at the expense of greater complexity in the calculation of the target and collision Hamiltonian matrices. B-spline orbital bases have also been implemented by van der Hart in the R-matrix computer program RMATRXII, discussed in Sect. 5.1.1, which has been used in R-matrix–Floquet and time-dependent multiphoton calculations discussed in Chaps. 9 and 10.

4.4.8 Direct Calculation of Siegert State Parameters

We consider in this section solutions of the radial Schrödinger equation (4.62) which are zero at the origin and satisfy the outgoing wave boundary condition

$$u_\ell(r) \underset{r\to\infty}{\sim} N\mathrm{e}^{\mathrm{i}kr}, \tag{4.199}$$

where N is a normalization factor and k lies in the lower half complex k-plane. We showed in Sect. 1.3 that these solutions correspond to resonance states when k lies close to the real k-axis, which is illustrated in Fig. 1.1 where resonance states, which we showed correspond to poles in the S-matrix, are denoted by open circles. We also showed in Sect. 1.3 that the partial wave cross section at real energies in the neighbourhood of an isolated pole is described by the Breit–Wigner one-level resonance formula, given by (1.107), if the background phase shift is zero. Following the work of Siegert [876], the solutions of (4.62) satisfying outgoing wave boundary conditions are often called Siegert states.

In many applications it is necessary to determine the resonance position E_r and the resonance width Γ which appear in the partial wave cross section defined by (1.107). These resonance parameters can be determined by calculating the phase shift $\delta_\ell(k)$ at a number of real energies in the neighbourhood of E_r, using one of the methods described earlier in this section, and then fitting to the analytic expression for the phase shift given by (1.105) and (1.106). However, Schneider [824] showed that the position of the resonance pole in the complex k-plane can be calculated directly using a modified R-matrix method which uses real basis orbitals and involves the diagonalization of a complex non-hermitian matrix for a few values of the complex momentum k in the neighbourhood of the resonance pole. The

resonance position and width are then given directly in terms of the real and imaginary parts of the pole position using (1.103).

In order to solve (4.62) subject to the outgoing wave boundary condition (4.199) we proceed as in Sect. 4.4.3 by introducing a linearly independent set of n real basis orbitals in the internal region defined by

$$\phi_i(r), \quad i = 1, \ldots, n, \quad 0 \leq r \leq a_0, \tag{4.200}$$

which vanish at the origin and satisfy arbitrary boundary conditions at $r = a_0$. We then expand the trial function in this basis as follows:

$$u_\ell^t(r) = \sum_{i=1}^{n} \phi_i(r) c_i, \quad 0 \leq r \leq a_0, \tag{4.201}$$

where the expansion coefficients c_i will in general be complex since $u_\ell^t(r)$ represents a resonant state satisfying complex asymptotic boundary conditions. The coefficients c_i in (4.201) are determined by diagonalizing the matrix

$$H_{ij}(k, b_0) = \int_0^{a_0} \phi_i(r)[L_\ell(k) - \mathcal{L}(a_0, b_0)]\phi_j(r)\mathrm{d}r, \quad i, \ j = 1, \ldots, n, \tag{4.202}$$

where $L_\ell(k)$ is defined by (4.29) with its dependence on the momentum k shown explicitly, and $\mathcal{L}(a_0, b_0)$ is a Bloch operator defined by (4.31). We see that $L_\ell(k)$, and hence $H_{ij}(k, b_0)$, is complex since the momentum k, which corresponds to the outgoing wave boundary condition (4.199), is complex. Also b_0 in $\mathcal{L}(a_0, b_0)$ is obtained by choosing an initial value of the complex momentum k and integrating (4.62) inwards from the asymptotic region to $r = a_0$ subject to the asymptotic boundary condition defined by (4.199). This can be accomplished using a standard method, such as an R-matrix propagator method discussed in Sect. 4.5. The quantity b_0 in (4.202) is then given in terms of the solution at $r = a_0$ by

$$b_0(k) = \frac{a_0}{u_\ell(a_0)} \left.\frac{\mathrm{d}u_\ell}{\mathrm{d}r}\right|_{r=a_0}. \tag{4.203}$$

After diagonalizing $\mathbf{H}$, defined by (4.202), we can write

$$\mathbf{HC} = \mathbf{CD}, \tag{4.204}$$

where $\mathbf{D}$ is a diagonal matrix whose elements are the eigenvalues of $\mathbf{H}$ and the columns of $\mathbf{C}$ are the corresponding eigenvectors which define the eigenstates by (4.201).

The Siegert states will then correspond to the eigenvalues of $\mathbf{H}$ which lie closest to the real k-axis. However, the corresponding value of the complex momentum k will in general differ from the value of k input in (4.202) and in the definition of

b_0 in (4.203). As a result, an iterative procedure must be adopted so that the value of the complex momentum k obtained from diagonalizing the matrix $\mathbf{H}$ corresponds to the input value of k used in the definition of $b_0(k)$. In practice Schneider [824] found that by diagonalizing the Hamiltonian matrix $\mathbf{H}$ for a few values of the complex momentum k, it is possible to locate the resonant eigenvalue and to fit it to a simple power series. The Newton–Raphson iterative method [143, 444] may then be used to find the precise location of the resonance eigenvalue in the complex k-plane. In this way the position and width of the resonance can be determined in a few iterations if the original complex momentum k is chosen appropriately.

In comparing this direct approach for calculating the Siegert state parameters with the method mentioned above of fitting the phase shift on the real energy axis to an analytic expression, given by (1.105) and (1.106), we observe that the latter approach is usually only accurate if the resonance width is relatively small compared with the range of energies over which the background phase shift varies appreciably. If the background phase shift is rapidly varying, which occurs, for example, when there are several resonances in close proximity, then the direct calculation of the resonance parameters discussed in this section is to be preferred. Other examples where it is necessary to calculate the resonance parameters directly are in the calculation of the spectra of atoms in fields discussed in Sect. 8.4, in R-matrix–Floquet theory of multiphoton processes discussed in Sect. 9.1 and in the example of laser-induced degenerate states discussed in Sect. 9.2.3. In this last case the resonance width Γ corresponds to the total ionization rate of the target atom or ion in an intense laser field. As the intensity and frequency of the laser is changed the complex energies of these "dressed states" describe trajectories in the complex energy plane which interact with each other in a way that can only be accurately calculated using a direct approach.

4.5 Propagator Methods

When the wavelength of the scattered particle is small compared with the range over which the potential interaction is important, it is no longer feasible to represent accurately the wave function of this particle in terms of a single expansion basis. This situation occurs, for example, in electron–atom collisions in the external region where the electron lies outside the charge distribution of the target atom but still experiences the long-range, slowly varying polarization and multipole potentials of the residual atom. It also occurs in heavy particle collisions, such as H–He collisions, where the wavelength of the motion of the heavy particles is short compared with the range of the interaction even for low-energy collisions.

In order to solve the coupled second-order differential equations that arise in these collision processes, R-matrix propagator methods have been introduced by Light and Walker [594] and log-derivative propagator methods have been introduced by Gordon [402] and Johnson [506]. In these methods the region of interest $a_0 \leq r \leq a_p$ is divided into a number of sub-regions, as illustrated in Fig. 4.3, where in practice the sub-regions may be of unequal length. Equations are then derived in

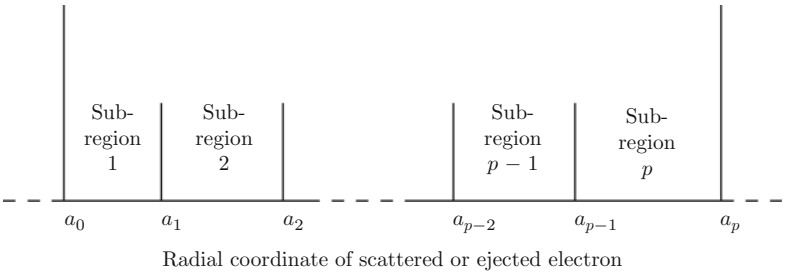

Fig. 4.3 Partitioning of configuration space into p sub-regions in R-matrix and log-derivative propagator methods

each sub-region which enable, the R-matrix, or the log-derivative matrix, as well as the wave function to be propagated across the sub-regions from $r = a_0$ to a_p. In this section we illustrate this approach in potential scattering by describing two commonly used R-matrix propagator methods, where the generalization of these and other propagator methods to multichannel collisions is considered in Appendix E.

4.5.1 Light–Walker Propagator

We consider first the solution of the radial Schrödinger equation (4.62) using the R-matrix propagator method introduced by Light and Walker [594]. We write this equation in the form

$$\left(\frac{\mathrm{d}^2}{\mathrm{d}r^2} + V(r) + k^2\right) u(r) = 0, \tag{4.205}$$

where $V(r)$ includes the angular momentum term as well as the potential $U(r)$.

The basic assumption made in the Light–Walker propagator method is that the potential $V(r)$ is a slowly varying function of r so that it can be accurately represented by a constant in each sub-region in Fig. 4.3 without the number of sub-regions p becoming excessively large. Hence in the sth sub-region we assume that we can write

$$\lambda_s^2 \approx V(r) + k^2, \quad a_{s-1} \le r \le a_s, \tag{4.206}$$

so that (4.205) becomes

$$L_s u(r) \equiv \left(\frac{\mathrm{d}^2}{\mathrm{d}r^2} + \lambda_s^2\right) u(r) = 0, \quad a_{s-1} \le r \le a_s. \tag{4.207}$$

In order to solve (4.207) in the sth sub-region we introduce the Bloch operator

$$\mathcal{L}_s = \left(\delta(r - a_s) \frac{\mathrm{d}}{\mathrm{d}r} - \delta(r - a_{s-1}) \frac{\mathrm{d}}{\mathrm{d}r} \right). \tag{4.208}$$

In analogy with (4.32) we find that

$$\int_{a_{s-1}}^{a_s} [v(L_s - \mathcal{L}_s)w - w(L_s - \mathcal{L}_s)v] \, \mathrm{d}r = 0, \tag{4.209}$$

where $v(r)$ and $w(r)$ are quadratically integrable functions over $a_{s-1} \leq r \leq a_s$ satisfying arbitrary boundary conditions at $r = a_{s-1}$ and a_s. Hence the operator $L_s - \mathcal{L}_s$ is hermitian in the sth sub-region in this function basis. We then rewrite (4.207) as

$$(L_s - \mathcal{L}_s)\, u = -\mathcal{L}_s u, \quad a_{s-1} \leq r \leq a_s, \tag{4.210}$$

which has the formal solution

$$u = -\,(L_s - \mathcal{L}_s)^{-1}\, \mathcal{L}_s u, \quad a_{s-1} \leq r \leq a_s, \tag{4.211}$$

where the Green's function $-\,(L_s - \mathcal{L}_s)^{-1}$ in (4.211) is a solution of the equation

$$(L_s - \mathcal{L}_s)\, G_s(r, r') = -\delta(r - r'). \tag{4.212}$$

By integrating (4.212) across the singularities at $r = a_{s-1}$ and a_s we find that $G_s(r, r')$ satisfies the boundary conditions

$$\left. \frac{\mathrm{d}G_s(r, r')}{\mathrm{d}r} \right|_{r=a_{s-1}} = \left. \frac{\mathrm{d}G_s(r, r')}{\mathrm{d}r} \right|_{r=a_s} = 0, \quad a_{s-1} < r' < a_s, \tag{4.213}$$

which are imposed by the Bloch operator defined by (4.208). Also, by integrating (4.212) across the singularity at $r = r'$ we obtain

$$\lim_{\epsilon \to 0+} \left(\left. \frac{\mathrm{d}G_s(r, r')}{\mathrm{d}r} \right|_{r=r'+\epsilon} - \left. \frac{\mathrm{d}G_s(r, r')}{\mathrm{d}r} \right|_{r=r'-\epsilon} \right) = -1, \tag{4.214}$$

It follows from (4.212), (4.213) and (4.214) that when $\lambda^2 \geq 0$ the Green's function is defined by

$$G_s(r, r') = -\frac{\cos \lambda_s (r' - a_s) \cos \lambda_s (r - a_{s-1})}{\lambda_s \sin \lambda_s (a_s - a_{s-1})}, \quad a_{s-1} \leq r \leq r', \tag{4.215}$$

and

$$G_s(r, r') = -\frac{\cos \lambda_s (r - a_s) \cos \lambda_s (r' - a_{s-1})}{\lambda_s \sin \lambda_s (a_s - a_{s-1})}, \quad r' \leq r \leq a_s. \tag{4.216}$$

Also, when $\lambda^2 < 0$ the Green's function is defined by

$$G_s(r, r') = -\frac{\cosh \mu_s(r' - a_s) \cosh \mu_s(r - a_{s-1})}{\mu_s \sinh \mu_s(a_s - a_{s-1})}, \quad a_{s-1} \le r \le r' \tag{4.217}$$

and

$$G_s(r, r') = -\frac{\cosh \mu_s(r - a_s) \cosh \mu_s(r' - a_{s-1})}{\mu_s \sinh \mu_s(a_s - a_{s-1})}, \quad r' \le r \le a_s, \tag{4.218}$$

where in (4.217) and (4.218) we have written $\mu^2 = -\lambda^2$.

We can now rewrite (4.210) explicitly in terms of the Green's function $G_s(r, r')$ as follows:

$$u(r) = \int_{a_{s-1}}^{a_s} G_s(r, r') \mathcal{L}_s u(r') \mathrm{d}r', \quad a_{s-1} \le r \le a_s. \tag{4.219}$$

Evaluating this equation at $r = a_{s-1}$ and a_s and using (4.208) for the Bloch operator $\mathcal{L}_s$ then yields the equations

$$u(a_{s-1}) = G_s(a_{s-1}, a_s) \left.\frac{\mathrm{d}u}{\mathrm{d}r}\right|_{r=a_s} - G_s(a_{s-1}, a_{s-1}) \left.\frac{\mathrm{d}u}{\mathrm{d}r}\right|_{r=a_{s-1}} \tag{4.220}$$

and

$$u(a_s) = G_s(a_s, a_s) \left.\frac{\mathrm{d}u}{\mathrm{d}r}\right|_{r=a_s} - G_s(a_s, a_{s-1}) \left.\frac{\mathrm{d}u}{\mathrm{d}r}\right|_{r=a_{s-1}}. \tag{4.221}$$

After defining the R-matrix at $r = a_{s-1}$ and a_s by the equations

$$u(a_{s-1}) = R_{s-1} a_{s-1} \left.\frac{\mathrm{d}u}{\mathrm{d}r}\right|_{r=a_{s-1}} \tag{4.222}$$

and

$$u(a_s) = R_s a_s \left.\frac{\mathrm{d}u}{\mathrm{d}r}\right|_{r=a_s}, \tag{4.223}$$

we then find that (4.220) and (4.221) yield the following equations for outward and inward propagation of the R-matrix

$$\begin{aligned} a_s R_s = {} & G_s(a_s, a_s) - G_s(a_s, a_{s-1}) \left[G_s(a_{s-1}, a_{s-1}) + a_{s-1} R_{s-1}\right]^{-1} \\ & \times G_s(a_{s-1}, a_s) \end{aligned} \tag{4.224}$$

and

$$a_{s-1}R_{s-1} = -G_s(a_{s-1}, a_{s-1}) + G_s(a_{s-1}, a_s)\,[G_s(a_s, a_s) - a_s R_s]^{-1} \times G_s(a_s, a_{s-1}). \tag{4.225}$$

Equation (4.224) enables the R-matrix R_0 at $r = a_0$ to be propagated outwards across the p sub-regions to yield the R-matrix R_p at $r = a_p$. In a similar way (4.225) enables the R-matrix R_p at $r = a_p$ to be propagated inwards across the p sub-regions to yield the R-matrix R_0 at $r = a_0$.

Having determined the R-matrix on the boundaries $r = a_s$ of the p sub-regions we can propagate the wave function $u(a_s)$ across these sub-regions using (4.220) and (4.221). We obtain the following equations for outward and inward propagation of the wave function

$$u(a_s) = a_s R_s\,[G_s(a_s, a_s) - a_s R_s]^{-1}\, G_s(a_s, a_{s-1}) a_{s-1}^{-1} R_{s-1}^{-1} u(a_{s-1}) \tag{4.226}$$

and

$$u(a_{s-1}) = a_{s-1}R_{s-1}\left[G_s(a_{s-1}, a_{s-1}) + a_{s-1}R_{s-1}\right]^{-1} G_s(a_{s-1}, a_s) \times a_s^{-1} R_s^{-1} u(a_s). \tag{4.227}$$

The wave function in the region $a_0 \le r \le a_p$ is often required in the calculation of matrix elements of various operators as, for example, in the R-matrix theory of photoionization discussed in Chap. 8.

4.5.2 BBM Propagator

We now consider the BBM propagator method introduced by Baluja et al. [47]. We again commence from (4.205) which we rewrite in the sth sub-region $a_{s-1} \le r \le a_s$ as

$$(D - \mathcal{L}_s + k^2)u(r) = -\mathcal{L}_s u(r), \quad a_{s-1} \le r \le a_s, \tag{4.228}$$

where

$$D = \frac{\mathrm{d}^2}{\mathrm{d}r^2} + V(r), \tag{4.229}$$

and where the Bloch operator $\mathcal{L}_s$ is defined by (4.208). It follows from our previous discussion that the operator $D - \mathcal{L}_s$ is hermitian in the sth sub-region in the space of quadratically integrable functions over $a_{s-1} \le r \le a_s$ satisfying arbitrary boundary conditions at $r = a_{s-1}$ and a_s. Equation (4.228) then has the formal solution

$$u = -(D - \mathcal{L}_s + k^2)^{-1}\mathcal{L}_s u, \quad a_{s-1} \le r \le a_s. \tag{4.230}$$

A spectral representation of the Green's function $(D - \mathcal{L}_s + k^2)^{-1}$ can be obtained by introducing an orthonormal set of basis functions $\phi_j^s(r)$, $j = 1, \ldots, m$, defined in the sth sub-region, which satisfy arbitrary boundary conditions at $r = a_{s-1}$ and a_s. We define linear combinations of these basis functions by the equation

$$\chi_i^s(r) = \sum_{j=1}^{m} \phi_j^s(r) a_{ji}^s, \quad a_{s-1} \le r \le a_s, \quad i = 1, \ldots, m, \tag{4.231}$$

where the expansion coefficients a_{ji}^s are obtained by diagonalizing $D - \mathcal{L}_s$ in the sth sub-region so that

$$\int_{a_{s-1}}^{a_s} \chi_i^s(r)(D - \mathcal{L}_s + k^2)\chi_{i'}^s(r)\mathrm{d}r = 2(E - E_i^s)\delta_{ii'}, \quad i,\ i' = 1, \ldots, m, \tag{4.232}$$

and where $k^2 = 2E$. Substituting this result into (4.230) then gives

$$u(r) = \int_{a_{s-1}}^{a_s} G_s(r, r')\mathcal{L}_s u(r')\mathrm{d}r', \quad a_{s-1} \le r \le a_s, \tag{4.233}$$

where the Green's function $G_s(r, r')$ is defined by

$$G_s(r, r') = \frac{1}{2} \sum_{i=1}^{m} \frac{\chi_i^s(r)\chi_i^s(r')}{E_i - E}. \tag{4.234}$$

Evaluating (4.233) at $r = a_{s-1}$ and a_s and using (4.208) for the Bloch operator, then yields (4.220) and (4.221), obtained using the Light–Walker propagator method. After defining the R-matrices at $r = a_{s-1}$ and a_s by (4.222) and (4.223), the outward and inward propagation equations for the R-matrix are again given by (4.224) and (4.225), respectively, and the outward and inward propagation equations for the wave function are again given by (4.226) and (4.227).

We observe that in the BBM propagator method, the operator $D - \mathcal{L}_s$ is diagonalized once in each sub-region to yield the eigenvalues E_i^s and eigenfunctions χ_i^s. After this initial diagonalization, the Green's function, defined by (4.234) and the corresponding propagation equations for the R-matrix and wave function, can be rapidly applied to all required scattering energies.

In comparing the Light–Walker and the BBM propagator methods we observe that no diagonalization is required in the former case. However, the approximation made in the Light–Walker method of replacing $V(r) + k^2$ in each sub-region by a constant λ_s^2, given by (4.206), means that typically the sub-region $a_s - a_{s-1}$ must be small to yield high accuracy unless the potential is very slowly varying. Therefore, in practice, many more sub-regions are required in the Light–Walker method and hence the BBM method is usually preferred in resonance regions where the calculation must be carried out at many scattered energy values to accurately resolve the

resonances. On the other hand, when the scattering amplitude is smoothly varying with energy, which usually occurs at higher energies or in heavy particle collisions, the Light–Walker method is to be preferred. The relative merits of these and other propagator methods are discussed further in Appendix E where multichannel collisions are considered.

4.6 Dirac R-Matrix Theory

We conclude this chapter by extending R-matrix theory to treat relativistic potential scattering described by the Dirac equation, which we introduced in Sect. 1.6. We will see in Sect. 5.5 that this extension is necessary in order to accurately describe electron collisions with heavy atoms and atomic ions where the nuclear charge number Z is large and where consequently relativistic effects are important even at low incident electron energies. This section thus provides an introduction to R-matrix theory of electron collisions with heavy atoms and atomic ions using the Dirac Hamiltonian.

In this section we follow our discussion of non-relativistic potential theory in Sects. 4.1 and 4.2, by considering the solution in an internal and an external region, where $r = a_0$ is the R-matrix radius separating these regions. We consider first the solution in the internal region where relativistic effects are most important. The radial Dirac equations, introduced in Sect. 1.6, must then be solved to yield the R-matrix on the boundary of this region. We then consider the convergence properties of the solution on the boundary of the internal region and compare these properties with non-relativistic R-matrix theory. Finally, we consider the solution of the Dirac equation or the equivalent Schrödinger equation in the external region to yield the scattering matrix and cross sections.

We have shown in Sect. 1.6 that the Dirac equation reduces to two coupled first-order differential equations (1.254) and (1.255) which can be written for each κ as

$$\left(\frac{\mathrm{d}}{\mathrm{d}r} + \frac{\kappa}{r}\right) p(r) - \frac{1}{\mathrm{c}}\left[2\mathrm{c}^2 + E - V(r)\right] q(r) = 0 \tag{4.235}$$

and

$$\left(\frac{\mathrm{d}}{\mathrm{d}r} - \frac{\kappa}{r}\right) q(r) + \frac{1}{\mathrm{c}}\left[E - V(r)\right] p(r) = 0, \tag{4.236}$$

where for notational convenience we have omitted the subscript κ on $p(r)$ and $q(r)$, and we remember that the energy E in this equation does not include the electron rest mass and hence reduces in the non-relativistic limit to the energy E in (1.1). Also, the relationship of κ in (4.235) and (4.236) to the usual spectroscopic notation ℓ and j is given in Table 1.1. We can rewrite these equations in matrix form as follows:

$$H^{\mathrm{D}}\theta = E\theta, \tag{4.237}$$

where the Dirac Hamiltonian matrix H^{D} is defined by

$$H^{\mathrm{D}} = \begin{pmatrix} V(r) & -\mathrm{c}\left(\frac{\mathrm{d}}{\mathrm{d}r} - \frac{\kappa}{r}\right) \\ \mathrm{c}\left(\frac{\mathrm{d}}{\mathrm{d}r} + \frac{\kappa}{r}\right) & -2\mathrm{c}^2 + V(r) \end{pmatrix} \tag{4.238}$$

and the solution matrix $\theta(r)$ is defined by

$$\theta(r) = \begin{pmatrix} p(r) \\ q(r) \end{pmatrix}. \tag{4.239}$$

We consider first the solution of (4.237) in the internal region $0 \leq r \leq a_0$. As in non-relativistic R-matrix theory we observe that the Hamiltonian matrix H^{D} in (4.237) is not hermitian in the internal region in the space of functions satisfying arbitrary boundary conditions at $r = a_0$ because of the derivative terms $\mathrm{d}/\mathrm{d}r$ occurring in its off-diagonal elements. To explore this further we consider the integral

$$\int_0^{a_0} v(r)\frac{\mathrm{d}w}{\mathrm{d}r}\mathrm{d}r = [v(r)w(r)]_{r=a_0} - \int_0^{a_0} \frac{\mathrm{d}v}{\mathrm{d}r}w(r)\mathrm{d}r, \tag{4.240}$$

where $v(r)$ and $w(r)$ are real square-integrable functions which are chosen to vanish at the origin and to satisfy arbitrary boundary conditions at $r = a_0$. The presence of the surface term on the right-hand side of (4.240), which arises from the integration by parts of the integral on the left-hand side, gives rise to the non-hermiticity. As in Sect. 4.2, this non-hermiticity can be eliminated by introducing a Bloch operator. Thus we rewrite (4.240) in the form

$$\int_0^{a_0} v(r)\left(\frac{\mathrm{d}}{\mathrm{d}r} - \frac{1}{2}\delta(r-a_0)\right)w(r)\mathrm{d}r = \int_0^{a_0}\left[\left(-\frac{\mathrm{d}}{\mathrm{d}r} + \frac{1}{2}\delta(r-a_0)\right)v(r)\right] \times w(r)\mathrm{d}r. \tag{4.241}$$

It follows that if we introduce the matrix Bloch operator

$$\mathcal{L}^{\mathrm{D}} = \frac{1}{2}\mathrm{c}\begin{pmatrix} 0 & 1 \\ -1 & 0 \end{pmatrix}\delta(r-a_0), \tag{4.242}$$

then we find that

$$\int_0^{a_0} \theta_1^{\mathrm{T}}(r)\left(H^{\mathrm{D}} + \mathcal{L}^{\mathrm{D}}\right)\theta_2(r)\mathrm{d}r = \int_0^{a_0}\left[\left(H^{\mathrm{D}} + \mathcal{L}^{\mathrm{D}}\right)\theta_1(r)\right]^{\mathrm{T}}\theta_2(r)\mathrm{d}r, \tag{4.243}$$

for real square-integrable two-dimensional vector functions $\theta_1(r)$ and $\theta_2(r)$ which vanish at the origin and which satisfy arbitrary boundary conditions at $r = a_0$, where T represents matrix transpose. Hence $H^{\mathrm{D}} + \mathcal{L}^{\mathrm{D}}$ is a real hermitian matrix operator over the internal region in this basis.

The matrix Bloch operator $\mathcal{L}^{\mathrm{D}}$, defined by (4.242), is not the most general operator which, when added to H^{D}, yields a real hermitian matrix operator. The most general matrix operator can be obtained by adding an arbitrary real symmetric matrix to (4.242) giving

$$\mathcal{L}^{\mathrm{D}} = \frac{1}{2}\mathrm{c}\begin{pmatrix} a & d+1 \\ d-1 & b \end{pmatrix}\delta(r-a_0), \tag{4.244}$$

where a, b and d are real numbers which we determine below.

Using this matrix Bloch operator we can now solve the radial Dirac equation (4.237) in the internal region by rewriting it as

$$(H^{\mathrm{D}} + \mathcal{L}^{\mathrm{D}} - E)\theta = \mathcal{L}^{\mathrm{D}}\theta. \tag{4.245}$$

The formal solution of (4.245) is then

$$\theta = (H^{\mathrm{D}} + \mathcal{L}^{\mathrm{D}} - E)^{-1}\mathcal{L}^{\mathrm{D}}\theta. \tag{4.246}$$

An explicit representation for the Green's function $(H^{\mathrm{D}} + \mathcal{L}^{\mathrm{D}} - E)^{-1}$ in (4.246) can be obtained by introducing the following real orthonormal vector basis functions

$$\theta_i^0(r) = \begin{pmatrix} p_i^0(r) \\ q_i^0(r) \end{pmatrix}, \quad i = 1, \ldots, n, \tag{4.247}$$

defined over the internal region $0 \leq r \leq a_0$, where $p_i^0(r)$ and $q_i^0(r)$ are the corresponding continuum basis orbitals. Following our discussion of the non-relativistic homogeneous boundary condition method in Sect. 4.4.1, we consider an analogous approach which has been adopted in many applications of Dirac R-matrix theory. We choose the basis functions $\theta_i^0(r)$ to be eigensolutions of the following coupled first-order differential equations

$$(H_0^{\mathrm{D}} - E_i^0)\theta_i^0(r) = 0, \tag{4.248}$$

satisfying homogeneous boundary conditions at $r = 0$ and a_0 given, respectively, by

$$\theta_i^0(0) = \begin{pmatrix} p_i^0(0) \\ q_i^0(0) \end{pmatrix} = 0 \tag{4.249}$$

and

$$\mathcal{L}^{\mathrm{D}}\theta_i^0 = 0, \tag{4.250}$$

and the orthonormality conditions

$$\int_0^{a_0} \theta_i^{0\mathrm{T}}(r)\theta_j^0(r)\mathrm{d}r = \int_0^{a_0} \left[p_i^0(r)p_j^0(r) + q_i^0(r)q_j^0(r)\right]\mathrm{d}r = \delta_{ij}. \tag{4.251}$$

Also, as in Sect. 4.4.1, the Dirac Hamiltonian matrix H_0^{D} in (4.248) is defined by (4.238) with $V(r)$ replaced by a zero-order potential $V_0(r)$, which is chosen so that (4.248), (4.249) and (4.250) can be easily solved. This is important when we consider Dirac R-matrix theory of electron collisions with atoms and ions in Sect. 5.5, where the original equations corresponding to (4.235) and (4.236) involve many coupled channels. Writing (4.250) explicitly using (4.244) yields

$$\begin{pmatrix} a & d+1 \\ d-1 & b \end{pmatrix} \begin{pmatrix} p_i^0(a_0) \\ q_i^0(a_0) \end{pmatrix} = 0. \tag{4.252}$$

This equation has a non-trivial solution only if the determinant of the matrix is zero. Hence we require

$$ab = d^2 - 1. \tag{4.253}$$

A further relationship between a, b and d can be obtained by requiring that the boundary condition at $r = a_0$ goes over in the non-relativistic limit to that given by (4.64). As discussed in Sect. 1.6, the non-relativistic limit of the coupled differential equations (4.235) and (4.236) is obtained by neglecting $|E - V(r)|$ compared with $2\mathrm{c}^2$. The first differential equation in (4.248), corresponding to (4.235), can then be rewritten following (1.257) as

$$2\mathrm{c}q_i^0(r) = \frac{\mathrm{d}p_i^0}{\mathrm{d}r} + \frac{\kappa}{r}p_i^0(r), \quad i = 1, \ldots, n. \tag{4.254}$$

In order to obtain a simple relation between the boundary condition at $r = a_0$ satisfied by $p_i^0(r)$ and $q_i^0(r)$ and the non-relativistic boundary condition at $r = a_0$ satisfied by the functions $u_{\ell i}^0(r)$ defined by (4.64), we introduce a quantity b_r defined by

$$q_i^0(a_0) = \frac{b_r}{2a_0\mathrm{c}}p_i^0(a_0), \quad i = 1, \ldots, n. \tag{4.255}$$

We then set $r = a_0$ in (4.254) and substitute for $q_i^0(a_0)$ from (4.255) yielding

$$\frac{a_0}{p_i^0(a_0)}\frac{\mathrm{d}p_i^0}{\mathrm{d}r}\bigg|_{r=a_0} = b_r - \kappa, \quad i = 1, \ldots, n. \tag{4.256}$$

Hence by comparing this result with (4.64) we find that in the non-relativistic limit

$$b_r = b_0 + \kappa. \tag{4.257}$$

It follows that if we introduce the quantity b' defined by

$$b' = \frac{b_r}{2a_0\mathrm{c}}, \tag{4.258}$$

then (4.252), (4.253) and (4.255) give

$$\frac{a}{d+1} = \frac{d-1}{b} = -b'. \tag{4.259}$$

Finally, we set $d = 0$ which we will see ensures that our theory yields the usual formula for the R-matrix in the non-relativistic limit. Substituting these results into (4.244), we find that the matrix Bloch operator can be written as

$$\mathcal{L}^{\mathrm{D}} = \frac{1}{2}\mathrm{c}\begin{pmatrix} -b' & 1 \\ -1 & b'^{-1} \end{pmatrix}\delta(r - a_0), \tag{4.260}$$

which depends only on a single parameter b'. We now determine the basis functions $\theta_i^0(r)$, $0 \le r \le a_0$, by solving (4.248) subject to the boundary conditions defined by (4.249) and (4.250) where $\mathcal{L}^{\mathrm{D}}$ is defined by (4.260).

Having determined the basis functions $\theta_i^0(r)$ we introduce a linear combination of these functions, defined by

$$\theta_j^n(r) = \sum_{i=1}^{n} \theta_i^0(r) c_{ij}^n, \quad j = 1, \ldots, n, \tag{4.261}$$

where the coefficients c_{ij}^n are determined by diagonalizing $H^{\mathrm{D}} + \mathcal{L}^{\mathrm{D}}$ as follows:

$$\int_0^{a_0} \theta_i^{n\mathrm{T}}(r)\left(H^{\mathrm{D}} + \mathcal{L}^{\mathrm{D}}\right)\theta_{i'}^n(r)\mathrm{d}r = E_i^n \delta_{ii'}, \quad i,\ i' = 1, \ldots, n. \tag{4.262}$$

We can expand the formal solution of the radial Dirac equation (4.246) in the internal region in terms of the functions $\theta_i^n(r)$ as follows:

$$\theta^n(r) = \sum_{i=1}^{n} \theta_i^n(r) \frac{1}{E_i^n - E} \langle \theta_i^n(r) | \mathcal{L}^{\mathrm{D}} | \theta^n(r) \rangle. \tag{4.263}$$

Substituting for the matrix Bloch operator $\mathcal{L}^{\mathrm{D}}$ defined by (4.260) into (4.263) yields

$$\theta^n(r) = \frac{1}{2a_0} \sum_{i=1}^{n} \frac{\theta_i^n(r)\theta_i^{n\mathrm{T}}(a_0)}{E_i^n - E} B\theta^n(a_0), \quad 0 \le r < a_0, \tag{4.264}$$

where the matrix B is defined by

$$B = a_0 \mathrm{c} \begin{pmatrix} -b' & 1 \\ -1 & b'^{-1} \end{pmatrix}. \tag{4.265}$$

The function $\theta^n(r)$ defined by (4.264) is an approximate solution of (4.237) in the internal region $0 \leq r < a_0$ which depends on the choice of the zero-order basis functions $\theta_i^0(r)$, defined by (4.248), (4.249), (4.250) and (4.251), and on the number n of these basis functions retained in expansion (4.261).

We next consider the convergence of (4.264) in the limit as $r \to a_0$ from below. We rewrite (4.264) in this limit in the following form as

$$\theta^n(a_0) = R^n(E) B \theta^n(a_0), \tag{4.266}$$

where the R-matrix $R^n(E)$ is defined by

$$R^n(E) = \frac{1}{2a_0} \sum_{i=1}^{n} \frac{\theta_i^n(a_0) \theta_i^{n\mathrm{T}}(a_0)}{E_i^n - E}, \tag{4.267}$$

and where the $\theta_i^n(a_0)$ are the surface amplitudes. Equations (4.266) and (4.267) correspond to (4.71) and (4.72) obtained in our derivation of non-relativistic R-matrix theory in Sect. 4.4.1. However, as already mentioned in Sect. 4.1, where we considered non-relativistic Wigner–Eisenbud R-matrix theory of potential scattering, care must be taken in proceeding to the limit $r \to a_0$ when the solution is expanded in terms of basis functions $\theta_i^0(r)$ satisfying homogeneous boundary conditions (4.255) at $r = a_0$, an aspect of the solution considered by Szmytkowski and Hinze [907].

In order to explore the limit $r \to a_0$ from below we rewrite (4.264) in terms of its matrix elements as follows:

$$\begin{pmatrix} p^n(r) \\ q^n(r) \end{pmatrix} = \frac{1}{2a_0} \sum_{i=1}^{n} \begin{pmatrix} p_i^n(r) \\ q_i^n(r) \end{pmatrix} \frac{1}{E_i^n - E} A_i, \quad 0 \leq r < a_0, \tag{4.268}$$

where the scalar

$$A_i = \theta_i^{n\mathrm{T}}(a_0) B \theta^n(a_0). \tag{4.269}$$

We can now rewrite A_i defined by (4.269) using the homogeneous boundary conditions at $r = a_0$ satisfied by the orbitals $p_i^n(r)$ and $q_i^n(r)$

$$q_i^n(a_0) = b' p_i^n(a_0), \quad i = 1, \ldots, n, \tag{4.270}$$

which follows from (4.255) and (4.261), where b' is defined by (4.258). We then obtain

$$A_i = p_i^n(a_0)\left[2a_0 c q^n(a_0) - b_r p^n(a_0)\right], \quad i = 1, \ldots, n. \tag{4.271}$$

Substituting (4.271) into (4.268) then yields the following two equations:

$$p^n(r) = \frac{1}{2a_0}\sum_{i=1}^{n} \frac{p_i^n(r)p_i^n(a_0)}{E_i^n - E}\left[2a_0 c q^n(a_0) - b_r p^n(a_0)\right], \quad 0 \le r < a_0 \tag{4.272}$$

and

$$q^n(r) = \frac{1}{2a_0}\sum_{i=1}^{n} \frac{q_i^n(r)p_i^n(a_0)}{E_i^n - E}\left[2a_0 c q^n(a_0) - b_r p^n(a_0)\right], \quad 0 \le r < a_0. \tag{4.273}$$

We now consider the limit of (4.272) and (4.273) when $r \to a_0$ from below. We obtain after using (4.270) the following equations:

$$p^n(a_0) = \mathcal{R}^n(E)\left[2a_0 c q^n(a_0) - b_r p^n(a_0)\right] \tag{4.274}$$

and

$$q^n(a_0) = b'\mathcal{R}^n(E)\left[2a_0 c q^n(a_0) - b_r p^n(a_0)\right], \tag{4.275}$$

where $\mathcal{R}^n(E)$ is the (1,1) element of the R-matrix defined by (4.267), which is defined by

$$\mathcal{R}^n(E) = \frac{1}{2a_0}\sum_{i=1}^{n} \frac{\left[p_i^n(a_0)\right]^2}{E_i^n - E}. \tag{4.276}$$

We then rewrite (4.274) and (4.275) in matrix form as

$$\begin{pmatrix} 1 + b_r\mathcal{R}^n(E) & -2a_0 c\mathcal{R}^n(E) \\ \left(b_r^2/2a_0 c\right)\mathcal{R}^n(E) & 1 - b_r\mathcal{R}^n(E) \end{pmatrix}\begin{pmatrix} p^n(a_0) \\ q^n(a_0) \end{pmatrix} = 0. \tag{4.277}$$

We see that the determinant of the 2×2 matrix in (4.277) equals 1 for all finite values of $\mathcal{R}^n(E)$. Hence for finite values of $\mathcal{R}^n(E)$, (4.277) only has the trivial solution $p^n(a_0) = q^n(a_0) = 0$. On the other hand, at the poles E_i^n in $\mathcal{R}^n(E)$, (4.277) yields the non-trivial solution

$$2a_0 c q^n(a_0) = b_r p^n(a_0), \tag{4.278}$$

which corresponds to the homogeneous boundary condition (4.255) satisfied by the basis orbitals $p_i^0(r)$ and $q_i^0(r)$.

In order to examine this result further, we consider first the non-relativistic limit of (4.274). It follows from (1.256) and (1.257) that in this limit $q(r)$ can be written in terms of $p(r)$ as follows:

$$q(r) = \frac{1}{2c}\left(\frac{d}{dr} + \frac{\kappa}{r}\right) p(r). \tag{4.279}$$

Substituting this result into (4.274) and using (4.257) then gives

$$p^n(a_0) = \mathcal{R}^n(E)\left(a_0 \frac{dp^n}{dr} - b_0 p^n\right)_{r=a_0}. \tag{4.280}$$

Hence in the non-relativistic limit, (4.274) reduces to (4.280) which is the usual equation relating the reduced radial wave function to its derivative on the boundary of the internal region given by (4.71). Also in Sect. 1.6, we showed that the radial Dirac equations (4.235) and (4.236) reduce in the non-relativistic limit to the equivalent radial Schrödinger equation

$$\left(\frac{d^2}{dr^2} - \frac{\ell(\ell+1)}{r^2} - U(r) + k^2\right) p(r) = 0, \tag{4.281}$$

where $U(r) = 2V(r)$. It follows that, after a Buttle correction to the R-matrix has been included, (4.274) reduces in the non-relativistic limit to the usual boundary condition at $r = a_0$ for integrating the non-relativistic Schrödinger equation outwards to the asymptotic region to yield the phase shift and partial wave cross section.

We consider next the non-relativistic limit of (4.275). It follows from our discussion of (4.277) that since (4.274) has a non-trivial solution at all energies, then (4.275) can only be satisfied at the poles of the R-matrix $\mathcal{R}^n(E)$. Hence since $q(r)$ in (4.273) is related through the first Dirac equation (4.235) to the derivative dp/dr, then it follows that the expansion of the derivative given by (4.273) is not uniformly convergent on the boundary $r = a_0$ except at these poles. This result corresponds to that obtained in non-relativistic R-matrix theory described in Sect. 4.1, see (4.11), (4.12), (4.13) and (4.14), where we show that when the wave function is expanded in terms of basis functions satisfying homogeneous boundary conditions at $r = a_0$ then the expansion of the derivative of the wave function in terms of the derivative of these basis functions is not uniformly convergent on the boundary $r = a_0$ of the internal region except at the poles of the R-matrix.

It follows from the above discussion that (4.274) provides the boundary condition at $r = a_0$ for integrating the coupled differential equations (4.235) and (4.236) outwards from $r = a_0$ in the external region, where the R-matrix in (4.274) must include a Buttle correction as discussed below. The corresponding boundary condition for electron collisions with a general atom are discussed in Sect. 5.5.2.

The final step in determining the solution of (4.237) in the internal region is the calculation of the Buttle correction to the R-matrix $\mathcal{R}^n(E)$, defined by (4.276), which is required in order to obtain accurate results when basis functions satisfying homogeneous boundary conditions, defined by (4.249) and (4.250), are adopted. In order to calculate the Buttle correction to the R-matrix we proceed as in our discussion of the non-relativistic homogeneous boundary condition method, discussed

in Sect. 4.4.1. We determine the solution of the zero-order Dirac equations (4.248) which we rewrite as follows:

$$\left(\frac{\mathrm{d}}{\mathrm{d}r}+\frac{\kappa}{r}\right)p^0(r)-\frac{1}{\mathrm{c}}\left[2\mathrm{c}^2+E-V_0(r)\right]q^0(r)=0 \tag{4.282}$$

and

$$\left(\frac{\mathrm{d}}{\mathrm{d}r}-\frac{\kappa}{r}\right)q^0(r)+\frac{1}{\mathrm{c}}\left[E-V_0(r)\right]p^0(r)=0, \tag{4.283}$$

at the energy E of interest, subject to the boundary condition

$$\theta^0(0)=\begin{pmatrix}p^0(0)\\ q^0(0)\end{pmatrix}=0. \tag{4.284}$$

Following our discussion in Sect. 4.4.2, the R-matrix $\mathcal{R}^n(E)$ defined by (4.276) is corrected in analogy with (4.74) and (4.75) as follows:

$$\mathcal{R}^{\mathrm{c}}(E)=\mathcal{R}^n(E)+\mathcal{R}^{(\mathrm{BC})}(E), \tag{4.285}$$

where the Buttle correction on the right-hand side of this equation is approximated by

$$\mathcal{R}^{(\mathrm{BC})}(E)=\frac{1}{2a_0}\sum_{i=n+1}^{\infty}\frac{\left[p_i^0(a_0)\right]^2}{E_i^0-E}. \tag{4.286}$$

This correction can be determined in terms of the solution of the zero-order equations (4.282) and (4.283) at the energy E subject to the boundary condition (4.284). We obtain

$$\mathcal{R}^0(E)=p^0(a_0)\left[2a_0\mathrm{c}q^0(a_0)-b_rp^0(a_0)\right]^{-1}, \tag{4.287}$$

where we have used (4.274) with $n=0$ to express the zero-order R-matrix in terms of the solution of the zero-order Dirac equations (4.282) and (4.283) on the boundary $r=a_0$. Hence, it follows from (4.285), (4.286) and (4.287) that the Buttle correction at the energy E is given in analogy with (4.79) by

$$\mathcal{R}^{(\mathrm{BC})}(E)=p^0(a_0)\left[2a_0\mathrm{c}q^0(a_0)-b_rp^0(a_0)\right]^{-1}-\frac{1}{2a_0}\sum_{i=1}^{n}\frac{\left[p_i^0(a_0)\right]^2}{E_i^0-E}. \tag{4.288}$$

The first term on the right-hand side of (4.288) is determined by solving the zero-order equations (4.282) and (4.283) at the energy E of interest subject to the boundary condition (4.284). The second term on the right-hand side of (4.288) is given

in terms of the first n eigenenergies E_i^0 and the corresponding eigensolutions $p_i^0(r)$ which we obtained by solving the zero-order equations defined by (4.248), (4.249), (4.250) and (4.251). It follows that all the terms on the right-hand side of (4.288) can be easily calculated and hence the Buttle correction to the R-matrix determined. As in non-relativistic theory, the Buttle correction is a smoothly varying function of energy in the low- and intermediate-energy regions and hence can be calculated at a few energy values, spanning the energy range of interest, and interpolated at the required energies.

Having determined the corrected R-matrix on the boundary $r = a_0$ of the internal region, the coupled Dirac equations (4.235) and (4.236) have to be solved in the external region $a_0 \le r \le a_p$. It follows from the above discussion that (4.274), with $\mathcal{R}^n(E)$ replaced by $\mathcal{R}^c(E)$, provides the boundary condition at $r = a_0$ for integrating the coupled Dirac equations outwards from $r = a_0$ to a_p. However, for low-energy electron collisions with atoms and atomic ions, where $|E - V(r)| \ll c^2$ in the external region, we have shown in Sect. 1.6 that the coupled Dirac equations can be reduced to the equivalent radial Schrödinger equation (4.281). This equation can then be integrated outwards from $r = a_0$ to a_p, subject to the boundary condition (4.280), using an R-matrix propagator method discussed in Sect. 4.5 and Appendix E where, if basis functions satisfying homogeneous boundary conditions defined by (4.249) and (4.250) are adopted, a Buttle correction defined by (4.288) must be added to the R-matrix $\mathcal{R}^n(E)$.

We note, however, that for electron collisions with heavy ions, where the residual charge on the ion $Z - N$ is large, the procedure for reducing the equations is more complicated. As shown in Sect. 1.6, the coupled first-order Dirac equations can be reduced to the following second-order differential equation with first-order derivative term:

$$\frac{\mathrm{d}^2 p}{\mathrm{d}r^2} - \frac{A'(r)}{A(r)}\frac{\mathrm{d}p}{\mathrm{d}r} + \left(A(r)B(r) - \frac{A'(r)}{A(r)}\frac{\kappa}{r} - \frac{\kappa(\kappa+1)}{r^2}\right)p(r) = 0, \qquad (4.289)$$

where $A(r)$, $A'(r)$ and $B(r)$ are defined by (1.263). Equation (4.289) is now in a form that can be solved in the external region using the propagator method discussed in Appendix E.5, where the inhomogeneous term $\theta(r)$ is zero. The quantity $P(r) = -A'(r)/A(r)$ in (E.94), which is zero in the non-relativistic limit, is a slowly varying function of r which can be accurately represented by its value at the mid-point of each sub-region in Fig. E.1 and the R-matrix at the start of the external region propagation $r = a_0$ is given by

$$R_0(E) = a_0^{-1} p(a_0)\left(\frac{\mathrm{d}p}{\mathrm{d}r} + \frac{1}{2}P(r)p(r)\right)^{-1}_{r=a_0}, \qquad (4.290)$$

which follows from (E.105). The quantities $p(r)$ and $\mathrm{d}p/\mathrm{d}r$ at $r = a_0$ in (4.290) can be obtained from the solution in the internal region, described earlier in this section where, if basis functions satisfying homogeneous boundary conditions are

adopted in the internal region, Buttle corrections to $p(a_0)$ and $\mathrm{d}p/\mathrm{d}r|_{r=a_0}$, analogous to that discussed in Sect. 4.4.2, will be necessary to obtain accurate results. The R-matrix and, if necessary, the wave function can then be propagated outwards from $r = a_0$ to a_p using (E.106) and (E.110), where either the Light–Walker or the BBM propagator method, discussed in Sects. 4.5.1 and 4.5.2, respectively can be used to calculate the Green's functions.

We also remember from our analysis in Sect. 1.6 that the second-order differential equation (4.289) can be further reduced to Schrödinger form by making the substitution

$$p(r) = [A(r)]^{1/2}\,\tilde{p}(r), \tag{4.291}$$

which we see from (1.265) gives the following equation for $\tilde{p}(r)$:

$$\left(\frac{\mathrm{d}^2}{\mathrm{d}r^2} - \frac{\kappa(\kappa+1)}{r^2} - U_\kappa(r) + k_r^2\right)\tilde{p}(r) = 0, \tag{4.292}$$

where k_r^2 and $U_\kappa(r)$ are defined by (1.266) and (1.267), respectively. In principle (4.292) can be solved using one of the standard propagator methods discussed in Sect. 4.5 and Appendix E. However, the complexity of the calculation of the potential $U_\kappa(r)$ makes this approach less attractive, and the R-matrix propagation solution of (4.289) discussed above and the direct solution of the original Dirac equations (4.235) and (4.236) using a standard approach for solving first-order differential equations (see, for example, [573]) are to be preferred.

Finally, having integrated either the equivalent Schrödinger equation or the coupled Dirac equations outwards from $r = a_0$ to a_p, the solution is then fitted to the asymptotic boundary conditions discussed in Sect. 1.6. The scattering amplitudes and cross sections can then be obtained as described in that section.

Chapter 5
Electron Collisions with Atoms and Ions

In this chapter we commence our discussion of multichannel R-matrix theory by considering its application in the study of low-energy electron collisions with atoms and atomic ions. As well as describing an important application of the theory, this chapter provides an introduction to the basic concepts of multichannel R-matrix theory which will be applied in later chapters to a wide range of other atomic, molecular and optical collision processes. We restrict our consideration in this chapter to low-energy electron collisions, where only elastic scattering and excitation processes are energetically allowed or play a significant role in the collision process. We consider electron collisions with atoms and atomic ions at intermediate energies, which range from close to the ionization threshold to several times this threshold, in Chap. 6.

We introduce multichannel R-matrix theory in Sect. 5.1 by considering first electron collisions with light multi-electron atoms and atomic ions where an accurate representation of the collision process can be obtained by solving the time-independent non-relativistic Schrödinger equation. We commence in Sect. 5.1.1 with a general introduction to R-matrix theory describing the partitioning of configuration space adopted in this theory. We then give a brief overview of the computer programs that have been developed to implement this theory, where we mention further developments of these programs to include relativistic effects which can be described using the Breit–Pauli Hamiltonian. In the rest of this section we describe in detail the solution of the Schrödinger equation, first in an internal region in Sect. 5.1.2, then in an external region in Sect. 5.1.3 and finally in an asymptotic region in Sect. 5.1.4, yielding the K-matrix and S-matrix from which the collision cross sections can be determined.

In Sect. 5.2, we derive a variational principle for the R-matrix defined on the boundary of the internal region. We consider explicitly low-energy electron collisions with atoms and atomic ions although the variational principle that we obtain will be applicable for any multichannel collision process which can be described in the internal region by coupled second-order integrodifferential equations. In Sect. 5.3 we consider methods for determining zero-order radial continuum basis orbitals which represent the scattered electron in the expansion of the total wave function in the internal region. We also discuss methods for calculating corrections

P.G. Burke, *R-Matrix Theory of Atomic Collisions*, Springer Series on Atomic, Optical, and Plasma Physics 61, DOI 10.1007/978-3-642-15931-2_5,

to the R-matrix and wave function. We consider first in Sect. 5.3.1 an approach using basis orbitals which satisfy homogeneous boundary conditions on the surface of the internal region. We then show in Sect. 5.3.2 that when the radial continuum basis orbitals satisfy homogeneous boundary conditions a Buttle correction to the R-matrix must be included to obtain accurate results. We also discuss how a Buttle-type correction to the wave function near the boundary of the internal region can be calculated, which may be required in some applications. In Sect. 5.3.3, we summarize methods for determining analytic continuum basis orbitals which satisfy arbitrary boundary conditions on the surface of the internal region, where these methods have been reviewed in Sect. 4.4. In recent years these basis orbitals have found increasing use in many applications of R-matrix theory, ranging from electron collisions with atoms and molecules to photoionization and multiphoton ionization processes. Then, in Sect. 5.3.4 we describe a partitioned R-matrix method where the calculation of the R-matrix is sub-divided into two parts: a low-energy part which is accurately determined and a high-energy part for which an approximation is derived which enables much larger problems to be treated.

Next, in Sect. 5.4 we consider electron collisions with atoms and ions with higher nuclear charge number Z where relativistic effects must be included in the calculation. Initially as Z increases these effects are small and in this case the collision calculation can first be carried out in $LS\pi$-coupling, using the non-relativistic Hamiltonian. The K-matrices, obtained from this calculation, are then recoupled to give K-matrices, cross sections and collision strengths including relativistic effects. We consider this approach in Sect. 5.4.1. Then as the nuclear charge number Z increases further, relativistic effects must be included in both the target wave function and the collision wave function. Provided Z is not too large, this can be achieved by replacing the non-relativistic Hamiltonian in these calculations by the Breit–Pauli Hamiltonian. We consider this approach in Sect. 5.4.2. Next, in Sect. 5.4.3, we consider a frame-transformation theory approach where relativistic effects are omitted, or only partly included, in the internal region with considerable saving in computational effort. However, for the heaviest atomic targets it is necessary to treat both the target and the collision wave functions using the Dirac Hamiltonian. We consider this approach in Sect. 5.5 where we follow our analysis of non-relativistic collisions, in Sect. 5.1, by considering the solution in internal, external and asymptotic regions in turn, enabling the K-matrix, S-matrix and cross sections to be determined.

Finally, in Sect. 5.6 we describe the results of some representative low-energy electron–atom and electron–ion collision calculations.

5.1 Multichannel R-Matrix Theory

In this section we introduce R-matrix theory by considering low-energy electron collisions with multi-electron atoms and ions which are accurately described by the non-relativistic Schrödinger equation.

5.1.1 Introduction and Computer Programs

We consider the following low-energy electron collision process:

$$\mathrm{e}^- + A_i \rightarrow A_j + \mathrm{e}^-, \tag{5.1}$$

where A_i and A_j are the initial and final bound states of the target atom or ion which we assume contains N electrons and has nuclear charge number Z. For light atoms and ions this process can be accurately described by the time-independent Schrödinger equation

$$H_{N+1}\Psi = E\Psi, \tag{5.2}$$

where Ψ is the collision wave function and H_{N+1} is the non-relativistic Hamiltonian defined in atomic units by

$$H_{N+1} = \sum_{i=1}^{N+1}\left(-\frac{1}{2}\nabla_i^2 - \frac{Z}{r_i}\right) + \sum_{i>j=1}^{N+1}\frac{1}{r_{ij}}. \tag{5.3}$$

In this equation we have taken the origin of coordinates to be the target nucleus, which we assume has infinite mass, and we have written $r_{ij} = \left|\mathbf{r}_i - \mathbf{r}_j\right|$ where $\mathbf{r}_i$ and $\mathbf{r}_j$ are the vector coordinates of the ith and jth electrons.

In order to solve (5.2), and the corresponding equations in relativistic R-matrix theory discussed in Sects. 5.4 and 5.5, the theory commences, as briefly discussed in our introduction to Chap. 4, by partitioning configuration space into an internal region, an external region and an asymptotic region as shown in Fig. 5.1. The three regions are separated, as shown in this figure, by spheres of radius $r = a_0$ and a_p which are centered on the target nucleus where r is the radial coordinate of the scattered electron. We now consider the calculation of the solutions in each of these regions in turn.

In the internal region $0 \leq r \leq a_0$, where r is the radial coordinate of the scattered electron relative to the target nucleus, electron exchange and electron–electron

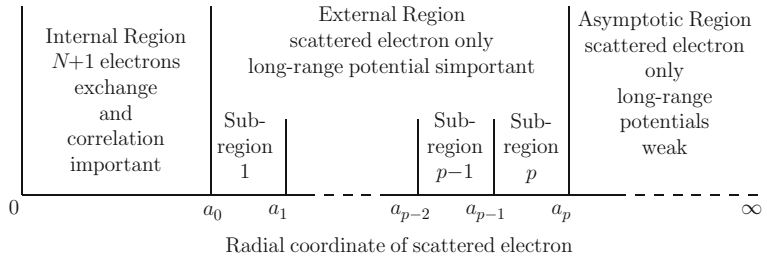

Fig. 5.1 Partitioning of configuration space in R-matrix theory of electron–atom and electron–ion collisions

correlation effects between the scattered electron and the N electrons in the target are important and the $(N+1)$-electron collision complex behaves in a similar way to a bound state. Consequently, a configuration interaction expansion of this complex, similar to that used in Sect. 2.2 for target eigenstates and pseudostates, is adopted. We discuss the solution in this region in Sect. 5.1.2 and we consider the continuum basis orbitals which are used to represent the scattered electron in this region in Sect. 5.3.

In the external region $a_0 \leq r \leq a_p$, electron exchange and correlation effects between the scattered electron and the target are negligible if the radius a_0 of the sphere is chosen, as discussed in Sect. 2.3.2, so that the charge distributions of the target eigenstates and pseudostates retained in the configuration interaction expansion in the internal region are negligible for $r \geq a_0$. This is achieved if we choose the radius a_0 so that

$$P_{n\ell}(r) \approx 0, \quad r \geq a_0, \tag{5.4}$$

where the $P_{n\ell}(r)$ are the reduced radial physical and pseudo-orbitals used to construct the target eigenstates and pseudostates. With this definition, the scattered electron then moves in the external region in the long-range multipole potential of the target, defined by (2.73) and (2.74), and the corresponding reduced radial wave functions describing the motion of this electron satisfy the coupled second-order differential equations (2.76). The solution in this region can be obtained by sub-dividing it into p sub-regions, as illustrated in Fig. 5.1, and using a standard method for solving ordinary coupled second-order differential equations. We discuss the solution in the external region in Sect. 5.1.3 and we consider R-matrix and log-derivative methods for propagating the solution of these equations across the p sub-regions in Appendix E.

Finally, in the asymptotic region $r \geq a_p$, the solution is represented by an asymptotic expansion where a_p is chosen large enough that the expansion yields accurate results on this boundary. We show how the solution can be fitted to this expansion at $r = a_p$ in Sect. 5.1.4, yielding the K-matrix, S-matrix and cross sections and we consider asymptotic expansion methods in Appendix F.1.

Hence we see that by a suitable choice of radii a_0 and a_p, the wave function in the internal, external and asymptotic regions have very different properties and thus it is appropriate both from a physical and from a computational point of view to obtain the solutions in these regions independently and then to link these solutions by the R-matrix on their common boundaries. It is also important to appreciate that this sub-division of configuration space is appropriate even in the presence of long-range Coulomb potentials, since electron exchange and correlation effects are confined to a volume defined by the range of the target states and pseudostates included in the calculation which decay exponentially at large distances.

To conclude this introductory section we briefly summarize in Fig. 5.2 the computer programs developed to obtain accurate target states and electron–atom and electron–ion phase shifts and collision cross sections, when relativistic effects are either not important or can be accurately described using the Breit–Pauli

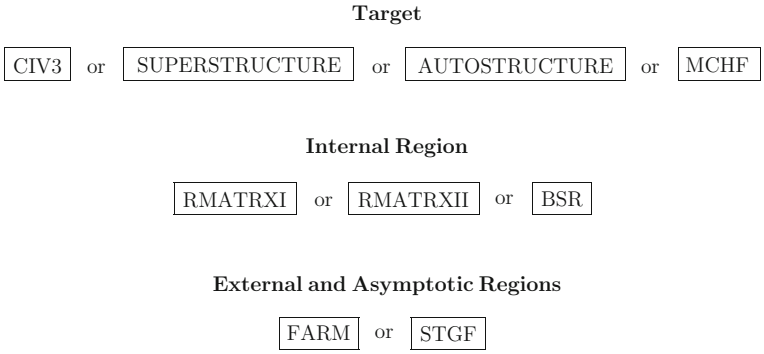

Fig. 5.2 Computer programs which have been developed and used in R-matrix electron–atom and electron–ion collision calculations classified into three stages corresponding to (i) target state calculations; (ii) internal region calculations yielding the R-matrix on the boundary $r = a_0$; (iii) external and asymptotic region calculations yielding the K-matrix, S-matrix and collision cross sections

Hamiltonian, discussed in Sect. 5.4.2. We will briefly summarize the corresponding computer programs used when the solution of the Dirac equation is appropriate in Sect. 5.5.1.

In the first stage of the calculation shown in Fig. 5.2 we mention four programs that have been written to obtain accurate target state energies and wave functions, which are used in the following stages of the R-matrix calculations. These are

i. CIV3 written by Hibbert [464] and extended by Glass and Hibbert [381, 383]
ii. SUPERSTRUCTURE written by Eissner et al. [290]
iii. AUTOSTRUCTURE written by Badnell [30, 31], which incorporates SUPERSTRUCTURE
iv. MCHF written by Froese Fischer et al. [344–350].

An important component of these atomic structure calculations are general programs to calculate angular integrals written by Hibbert and Froese Fischer [463, 466].

In the second stage of the calculation shown in Fig. 5.2 we mention three programs written to solve the electron–atom collision problem in the R-matrix internal region shown in Fig. 5.1. These are

i. RMATRXI written by Berrington et al. [95, 98] and extended to include relativistic effects using the Breit–Pauli Hamiltonian by Scott and Burke [843], Scott and Taylor [844] and Berrington et al. [102]. A parallel version of RMATRXI has been developed by Mitnik et al. [654, 655] which is summarized by Ballance and Griffin [43], and a no-exchange program RMATRX NX has been developed by V.M. Burke et al. [192], which enables R-matrix calculations at higher energies and for higher angular momenta to be carried out efficiently.
ii. RMATRXII written by Burke et al. [185], which extended the procedure adopted in RMATRXI for evaluating the angular integrals. Relativistic effects

are not included in RMATRXII. Instead, an extra stage FINE, transforms the non-relativistic R-matrix surface amplitudes calculated on the internal region boundary $r = a_0$ to include relativistic fine-structure effects, ready for the inclusion of these effects in the external region calculation.

iii. BSR written by Zatsarinny [992], which includes relativistic effects using the Breit–Pauli Hamiltonian. It describes the target states using non-orthogonal term-dependent orbitals and represents the bound and continuum orbitals by expansions in B-splines, discussed in Sect. 4.4.7.

In the third stage of the calculation shown in Fig. 5.2 we mention two programs that have been written to solve the electron–atom collision problem in the R-matrix external and asymptotic regions shown in Fig. 5.1. These are

i. FARM, written by V.M. Burke and Noble [191], which uses R-matrix propagator methods, discussed in Appendices E.1 and E.3. A parallel version of FARM (PFARM) has been developed by Sunderland et al. [896] as part of the electron–atom and electron–ion collision program PRMAT which combines PFARM with the internal region program RMATRXII.

ii. STGF, written by Seaton [860], which calculates solutions which are correct to second order in the long-range potentials. A parallel version PSTGF which runs on massively parallel computers has been developed by Mitnik et al. [654].

These programs enable the K-matrix, S-matrix and hence collision cross sections to be determined.

5.1.2 Internal Region Solution

We consider first the solution of the non-relativistic Schrödinger equation (5.2) in the internal region defined in Fig. 5.1 for each set of conserved quantum numbers Γ defined by (2.58). The R-matrix expansion of the collision wave function Ψ in this region at a total energy E takes the form

$$\Psi_{jE}^{\Gamma}(\mathbf{X}_{N+1}) = \sum_{k=1}^{n_t} \psi_k^{\Gamma}(\mathbf{X}_{N+1}) A_{kj}^{\Gamma}(E), \tag{5.5}$$

where j labels the linearly independent solutions of (5.2), ψ_k^{Γ} are energy-independent basis functions and $A_{kj}^{\Gamma}(E)$ are energy-dependent expansion coefficients, which depend on the asymptotic boundary conditions satisfied by the wave function Ψ_{jE}^{Γ} at the energy E. Following our discussion in Sect. 2.3, we expand the basis functions ψ_k^{Γ} in an R-matrix expansion, which has the same general form as the close coupling with pseudostates expansion (2.57), which we write here as

$$\psi_k^{\Gamma}(\mathbf{X}_{N+1}) = \mathcal{A}\sum_{i=1}^{n}\sum_{j=1}^{n_c}\overline{\Phi}_i^{\Gamma}(\mathbf{X}_N;\hat{\mathbf{r}}_{N+1}\sigma_{N+1})r_{N+1}^{-1}u_{ij}^0(r_{N+1})a_{ijk}^{\Gamma}$$
$$+\sum_{i=1}^{m}\chi_i^{\Gamma}(\mathbf{X}_{N+1})b_{ik}^{\Gamma}, \quad k=1,\ldots,n_t, \tag{5.6}$$

where n is the number of channels retained in the expansion, n_c is the number of radial continuum basis orbitals retained in each channel, m is the number of quadratically integrable functions and $n_t = nn_c + m$ is the total number of linearly independent basis functions in this expansion. The channel functions $\overline{\Phi}_i^{\Gamma}$ and the quadratically integrable functions χ_i^{Γ} in (5.6) are defined following (2.57) and do not need to be discussed further here except to note that condition (5.4) satisfied by the physical and pseudo-orbitals implies that these functions are negligible by the boundary $r = a_0$ of the internal region. However, the radial continuum basis orbitals $u_{ij}^0(r)$, $j = 1,\ldots,n_c$ in (5.6), which replace the reduced radial functions $F_{ij}^{\Gamma}(r)$ in (2.57), are now defined only over the range $0 \le r \le a_0$. They represent the radial motion of the scattered electron in the internal region and are chosen to vanish at the origin and are in general non-zero on the boundary $r = a_0$ of the internal region, thus providing a link between the solutions in the internal and external regions. We will consider their explicit form in Sect. 5.3. Also we note that the coefficients b_{ik}^{Γ} multiplying the quadratically integrable functions in (5.6) are related to the corresponding coefficients in (2.57) through the expansion of the collision wave function Ψ_{jE}^{Γ} in terms of the basis functions ψ_k^{Γ} given by (5.5). Finally we determine the coefficients a_{ijk}^{Γ} and b_{ik}^{Γ} in (5.6) by diagonalizing $H_{N+1} + \mathcal{L}_{N+1}$ in this basis as follows:

$$\langle\psi_k^{\Gamma}|H_{N+1} + \mathcal{L}_{N+1}|\psi_{k'}^{\Gamma}\rangle_{\text{int}} = E_k^{\Gamma}\delta_{kk'}, \quad k,\ k' = 1,\ldots,n_t, \tag{5.7}$$

where $\mathcal{L}_{N+1}$ is a Bloch operator [118], discussed below, and where the integration in this equation is carried out over the space and spin coordinates of all $N+1$ electrons and where the radial integrals are confined to the internal region.

The Bloch operator $\mathcal{L}_{N+1}$ in (5.7) has been introduced, following our discussion in potential scattering in Sect. 4.2, since the kinetic energy operators $-\frac{1}{2}\nabla_i^2$, $i = 1,\ldots,N+1$, in H_{N+1} are not hermitian over the internal region in the space of functions satisfying arbitrary boundary conditions on the surface of the sphere of radius $r = a_0$ enveloping this region. The appropriate Bloch operator which ensures that $H_{N+1} + \mathcal{L}_{N+1}$ is hermitian is defined by the equation

$$\mathcal{L}_{N+1} = \frac{1}{2}\sum_{i=1}^{N+1}\delta(r_i - a_0)\left(\frac{\mathrm{d}}{\mathrm{d}r_i} - \frac{b_0 - 1}{r_i}\right), \tag{5.8}$$

where, as in potential scattering, b_0 is an arbitrary constant which can depend on the channel of the scattered electron and which is set zero in most applications. We

can prove that $H_{N+1} + \mathcal{L}_{N+1}$ is hermitian in the internal region by showing that the following integral is zero:

$$\langle \psi^{(1)} | H_{N+1} + \mathcal{L}_{N+1} | \psi^{(2)} \rangle_{\text{int}} - \langle \psi^{(2)} | H_{N+1} + \mathcal{L}_{N+1} | \psi^{(1)} \rangle_{\text{int}} = 0, \tag{5.9}$$

where $\psi^{(1)}$ and $\psi^{(2)}$, which are defined over the internal region, are arbitrary quadratically integrable functions of the space and spin coordinates $\mathbf{x}_1, \ldots, \mathbf{x}_{N+1}$ of the $N + 1$ interacting electrons which vanish at the origin and satisfy arbitrary boundary conditions on the surface $r = a_0$ of the internal region. Also in (5.9) the integrations are carried out over all $N + 1$ electronic space and spin coordinates, where the integration over radial coordinates r_i of the electrons is restricted to the internal region so that

$$0 \le r_i \le a_0, \quad i = 1, \ldots, N + 1. \tag{5.10}$$

In the evaluation of (5.9) we have to consider radial integrals of the form

$$I = \int_0^{a_0} \left\{ r^{-1} v(r) \left[-\frac{1}{2r^2} \frac{\mathrm{d}}{\mathrm{d}r} r^2 \frac{\mathrm{d}}{\mathrm{d}r} + \frac{1}{2} \delta(r - a_0) \left(\frac{\mathrm{d}}{\mathrm{d}r} - \frac{b_0 - 1}{r} \right) \right] r^{-1} w(r) \right\} \times r^2 \mathrm{d}r, \tag{5.11}$$

where $v(r)$ and $w(r)$ are arbitrary differentiable functions of r, which are quadratically integrable over the internal region and which vanish at the origin and satisfy arbitrary boundary conditions at $r = a_0$. Also the first term in the square brackets in (5.11) is the radial part of the kinetic energy operator $-\frac{1}{2}\nabla^2$. It is straightforward to show that (5.11) reduces to

$$I = \int_0^{a_0} v(r) \left[-\frac{1}{2} \frac{\mathrm{d}^2}{\mathrm{d}r^2} + \frac{1}{2} \delta(r - a_0) \left(\frac{\mathrm{d}}{\mathrm{d}r} - \frac{b_0}{r} \right) \right] w(r) \mathrm{d}r. \tag{5.12}$$

It then follows that, as in potential scattering, see (4.32), the operator in square brackets in (5.12) is hermitian over the internal region for arbitrary b_0 and hence the integral I in (5.11) can be rewritten as

$$I = \int_0^{a_0} \left\{ r^{-1} w(r) \left[-\frac{1}{2r^2} \frac{\mathrm{d}}{\mathrm{d}r} r^2 \frac{\mathrm{d}}{\mathrm{d}r} + \frac{1}{2} \delta(r - a_0) \left(\frac{\mathrm{d}}{\mathrm{d}r} - \frac{b_0 - 1}{r} \right) \right] r^{-1} v(r) \right\} \times r^2 \mathrm{d}r. \tag{5.13}$$

This shows that the operator in the square brackets in (5.11) and (5.13) is hermitian over the internal region and hence, from (5.9), that the operator

$$H_{N+1} + \mathcal{L}_{N+1} \tag{5.14}$$

is hermitian over the internal region.

We can now solve (5.2) in the internal region, for each set of conserved quantum numbers Γ and for each linearly independent solution labelled by j, by including the Bloch operator term $\mathcal{L}_{N+1}\Psi$ on both sides of this equation giving

$$(H_{N+1} + \mathcal{L}_{N+1} - E)\,\Psi_{jE}^{\Gamma} = \mathcal{L}_{N+1}\Psi_{jE}^{\Gamma}, \tag{5.15}$$

where the solution Ψ_{jE}^{Γ} corresponds to (5.5), (5.6) and (5.7). Equation (5.15) then has the formal solution in the internal region

$$\Psi_{jE}^{\Gamma} = (H_{N+1} + \mathcal{L}_{N+1} - E)^{-1}\,\mathcal{L}_{N+1}\Psi_{jE}^{\Gamma}. \tag{5.16}$$

The spectral representation of the Green's function $(H_{N+1} + \mathcal{L}_{N+1} - E)^{-1}$ in (5.16) can be obtained in terms of the R-matrix basis functions ψ_k^{Γ} defined by (5.6) and (5.7). Equation (5.16) then becomes

$$|\Psi_{jE}^{\Gamma}\rangle = \sum_{k=1}^{n_t} |\psi_k^{\Gamma}\rangle \frac{1}{E_k^{\Gamma} - E} \langle\psi_k^{\Gamma}|\mathcal{L}_{N+1}|\Psi_{jE}^{\Gamma}\rangle. \tag{5.17}$$

We then project (5.17) onto the n channel functions $\overline{\Phi}_i^{\Gamma}(\mathbf{X}_N; \hat{\mathbf{r}}_{N+1}\sigma_{N+1})$ and evaluate it on the boundary $r_{N+1} = a_0$ of the internal region. We find using (5.5) and (5.6) that the reduced radial wave functions $F_{ij}^{\Gamma}(r)$ describing the motion of the scattered electron in the ith channel at the energy E satisfy the equation

$$F_{ij}^{\Gamma}(a_0) = \sum_{i'=1}^{n} R_{ii'}^{\Gamma}(E) \left(a_0 \frac{\mathrm{d}F_{i'j}^{\Gamma}}{\mathrm{d}r} - b_0 F_{i'j}^{\Gamma} \right)_{r=a_0}, \quad i = 1, \ldots, n, \tag{5.18}$$

where the elements of the R-matrix $R_{ii'}^{\Gamma}(E)$ are defined by

$$R_{ii'}^{\Gamma}(E) = \frac{1}{2a_0} \sum_{k=1}^{n_t} \frac{w_{ik}^{\Gamma} w_{i'k}^{\Gamma}}{E_k^{\Gamma} - E}, \quad i, i' = 1, \ldots, n, \tag{5.19}$$

the functions $F_{ij}^{\Gamma}(r)$ are defined by

$$F_{ij}^{\Gamma}(r_{N+1}) = \langle r_{N+1}^{-1} \overline{\Phi}_i^{\Gamma} | \Psi_{jE}^{\Gamma} \rangle', \quad i = 1, \ldots, n \tag{5.20}$$

and the surface amplitudes w_{ik}^{Γ} are defined by

$$\begin{aligned} w_{ik}^{\Gamma} &= \langle r_{N+1}^{-1} \overline{\Phi}_i^{\Gamma} | \psi_k^{\Gamma} \rangle'_{r_{N+1}=a_0} \\ &= \sum_{j=1}^{n_c} u_{ij}^0(a_0) a_{ijk}^{\Gamma}, \quad i = 1, \ldots, n, \quad k = 1, \ldots, n_t. \end{aligned} \tag{5.21}$$

We can also write down an alternative expression for the reduced radial wave functions $F_{ij}^{\Gamma}(r)$ in the internal region by substituting for Ψ_{jE}^{Γ} from (5.5) into (5.20) giving

$$F_{ij}^{\Gamma}(r_{N+1}) = \sum_{k=1}^{n_t} \langle r_{N+1}^{-1} \overline{\Phi}_i^{\Gamma} | \psi_k^{\Gamma} \rangle' A_{kj}^{\Gamma}(E), \quad i = 1, \ldots, n. \tag{5.22}$$

The primes on the Dirac brackets in (5.20), (5.21) and (5.22) mean that the integrations are carried out over the space and spin coordinates of all $N + 1$ electrons in the internal region, except the radial coordinate r_{N+1} of the scattered electron, where the r_{N+1}^{-1} factors in these and later integrands correspond to the r_{N+1}^{-1} factor on the right-hand side of (5.6). Also the number of linearly independent solutions, denoted by the subscript j in (5.18), (5.20) and (5.22), is discussed below.

Equations (5.18) and (5.19) are the basic equations describing electron collisions with atoms and atomic ions in the internal region. The R-matrix, defined by (5.19), is determined at all energies by a single diagonalization of $H_{N+1} + \mathcal{L}_{N+1}$ in (5.7) in the basis defined by (5.6) for each set of conserved quantum numbers Γ, which yields the surface amplitudes w_{ik}^{Γ} and the corresponding eigenenergies E_k^{Γ}. The logarithmic derivatives of the reduced radial wave functions $F_{ij}^{\Gamma}(r)$ on the boundary of the internal region are then given by (5.18). This equation provides the boundary condition for the solution of the electron–atom collision problem in the external region considered in the next section.

We consider next the determination of the reduced radial wave functions $F_{ij}^{\Gamma}(r)$, defined in the internal region by (5.20) and (5.22), and the full collision wave function $\Psi_{jE}^{\Gamma}(\mathbf{X}_{N+1})$, defined in the internal region by (5.5), which we will see are required in many applications. We first observe that while (5.20) defines $F_{ij}^{\Gamma}(r)$ for all r, it is only when the exchange and quadratically integrable functions in (5.6) are negligible, that $F_{ij}^{\Gamma}(r)$ has a simple form. This occurs in the external and asymptotic regions, discussed in Sects. 5.1.3 and 5.1.4, respectively, and near the boundary $r = a_0$ in the internal region. It follows from (5.5), (5.6) and (5.22) that near the boundary $r = a_0$ in the internal region, the expression for $F_{ij}^{\Gamma}(r)$ reduces to the following simple form:

$$F_{ij}^{\Gamma}(r) = \sum_{k=1}^{n_t} w_{ik}^{\Gamma}(r) A_{kj}^{\Gamma}(E), \quad i = 1, \ldots, n, \quad r \lesssim a_0, \tag{5.23}$$

where the functions $w_{ik}^{\Gamma}(r)$ can be expanded in terms of the continuum basis orbitals $u_{ik}^0(r)$ in (5.6) by

$$w_{ik}^{\Gamma}(r) = \sum_{j=1}^{n_c} u_{ij}^0(r) a_{ijk}^{\Gamma}, \quad i = 1, \ldots, n, \quad k = 1, \ldots, n_t. \tag{5.24}$$

Comparing this result with (5.21) we see that $w_{ik}^{\Gamma} = w_{ik}^{\Gamma}(a_0)$. It follows that in order to determine $F_{ij}^{\Gamma}(r)$ near the boundary $r = a_0$ in the internal region and the full collision wave function $\Psi_{jE}^{\Gamma}(\mathbf{X}_{N+1})$ in the internal region, we have to determine the expansion coefficients $A_{kj}^{\Gamma}(E)$ in (5.5). This can be achieved by comparing (5.17) with (5.5) giving

$$A_{kj}^{\Gamma}(E) = \frac{1}{E_k^{\Gamma} - E} \langle \psi_k^{\Gamma} | \mathcal{L}_{N+1} | \Psi_{jE}^{\Gamma} \rangle, \qquad k = 1, \ldots, n_t. \tag{5.25}$$

We then substitute in this equation for ψ_k^{Γ} from (5.6) and for the Bloch operator $\mathcal{L}_{N+1}$ from (5.8). We also use the result

$$\Psi_{jE}^{\Gamma}(\mathbf{X}_{N+1}) = \sum_{i=1}^{n} \overline{\Phi}_i^{\Gamma}(\mathbf{X}_N; \hat{\mathbf{r}}_{N+1}\sigma_{N+1}) r_{N+1}^{-1} F_{ij}^{\Gamma}(r_{N+1}), \quad r_{N+1} = a_0, \tag{5.26}$$

which follows from (5.20). Equation (5.25) then reduces to

$$A_{kj}^{\Gamma}(E) = \frac{1}{2a_0(E_k^{\Gamma} - E)} \sum_{i=1}^{n} w_{ik}^{\Gamma} \left(a_0 \frac{\mathrm{d}F_{ij}^{\Gamma}}{\mathrm{d}r} - b_0 F_{ij}^{\Gamma} \right)_{r=a_0}, \quad k = 1, \ldots, n_t. \tag{5.27}$$

We see from this equation that in order to determine the expansion coefficients $A_{kj}^{\Gamma}(E)$ we have to determine $\mathrm{d}F_{ij}^{\Gamma}/\mathrm{d}r$ and $F_{ij}^{\Gamma}(r)$ on the boundary $r = a_0$ of the internal region. This is achieved by solving the relevant coupled second-order differential equations in the external and asymptotic regions, as discussed in Sects. 5.1.3 and 5.1.4, respectively, subject to the R-matrix boundary condition at $r = a_0$ defined by (5.18) and (5.19). These solutions can be combined to yield the relevant asymptotic boundary conditions, enabling $A_{kj}^{\Gamma}(E)$ to be determined. We will see that the number of linearly independent solutions labelled by j depends on these asymptotic boundary conditions and will usually correspond to the number of open channels n_a at the energy E considered. In this way we can determine the reduced radial wave functions $F_{ij}^{\Gamma}(r)$ in the external and asymptotic regions. We also show in Sect. 5.3.2 that when the radial continuum basis orbitals $u_{ij}^0(r)$, retained in expansion (5.6), satisfy homogeneous boundary conditions a Buttle correction to the reduced radial wave function is required near the boundary $r = a_0$ in the internal region. Hence we can determine the full collision wave function $\Psi_{jE}^{\Gamma}(\mathbf{X}_{N+1})$, defined by (5.5) in the internal region, which is important in applications such as photoionization, discussed in Chap. 8, where the collision wave function in the internal region as well as the R-matrix is required.

We conclude this section by remarking that the R-matrix, defined by (5.18) and (5.19), together with the basis functions ψ_k^{Γ}, defined by (5.6), and the expansion coefficients $A_{kj}^{\Gamma}(E)$, defined by (5.27), provide a complete description of the collision process in the internal region. Furthermore, it follows from (5.19) that the

R-matrix is a real symmetric analytic function of energy with simple poles only on the real energy axis. This property has been used as the basis of the development of multichannel effective range theories in Sect. 3.3 which enable the analytic properties of the K-matrix and T-matrix to be determined in the neighbourhood of thresholds.

5.1.3 External Region Solution

We now consider the solution of the Schrödinger equation (5.2) in the external region, corresponding to $a_0 \leq r \leq a_p$ in Fig. 5.1, for each required energy E. We have seen that a_0 is chosen so that electron exchange and correlation effects between the scattered electron and the target atom or atomic ion can be neglected in this region. The close coupling expansion (2.57) of the total wave function at energy E for each set of conserved quantum numbers Γ then reduces to

$$\Psi^{\Gamma}_{jE}(\mathbf{X}_{N+1}) = \sum_{i=1}^{n} \overline{\Phi}^{\Gamma}_{i}(\mathbf{X}_N; \hat{\mathbf{r}}_{N+1}\sigma_{N+1}) r^{-1}_{N+1} F^{\Gamma}_{ij}(r_{N+1}), \quad r_{N+1} \geq a_0, \tag{5.28}$$

where j labels the linearly independent solutions. Also the channel functions $\overline{\Phi}^{\Gamma}_{i}$ retained in this expansion are the same as those retained in the internal region expansion (5.6) and $F^{\Gamma}_{ij}(r)$ are energy-dependent reduced radial wave functions, defined by (5.20). In comparing (5.28) with (5.5) and (5.6), we see that we no longer include the antisymmetrization operator $\mathcal{A}$ in (5.28), since the scattered and target electrons occupy different regions of space and hence exchange effects are negligible, enabling more efficient algorithms to be used in solving the coupled equations in this region, as discussed in Appendix E. In addition, the quadratically integrable functions χ^{Γ}_{i}, which are included in expansion (5.6), vanish in the external region since the boundary a_0 is chosen so that the target physical and pseudo-orbitals $P_{n\ell}(r)$, used to construct these functions, satisfy (5.4).

The coupled second-order differential equations, satisfied by the reduced radial wave functions $F^{\Gamma}_{ij}(r)$ in (5.28), are obtained by substituting (5.28) into the Schrödinger equation (5.2) and projecting onto the channel functions $\overline{\Phi}^{\Gamma}_{i}$. We then find that the functions $F^{\Gamma}_{ij}(r)$ satisfy the following set of coupled equations:

$$\left(\frac{\mathrm{d}^2}{\mathrm{d}r^2} - \frac{\ell_i(\ell_i+1)}{r^2} + \frac{2(Z-N)}{r} + k_i^2\right) F^{\Gamma}_{ij}(r) = 2\sum_{i'=1}^{n} V^{\Gamma}_{ii'}(r) F^{\Gamma}_{i'j}(r), \quad i = 1, \ldots, n, \; r \geq a_0, \tag{5.29}$$

where ℓ_i is the orbital angular momentum of the scattered electron, Z is the nuclear charge number, N is the number of target electrons and k_i^2 is the square of the wave number of the scattered electron defined by (2.64) and (2.65). Also the potential matrix $V^{\Gamma}_{ii'}(r)$, which is defined by (2.66), can be written as a summation over inverse powers of r given by (2.73), that is by

$$V_{ii'}^{\Gamma}(r) = \sum_{\lambda=1}^{\lambda_{\max}} \alpha_{ii'\lambda}^{\Gamma} r^{-\lambda-1}, \quad r \geq a_0, \quad i,\ i' = 1, \ldots, n. \tag{5.30}$$

The long-range potential coefficients $\alpha_{ii'\lambda}^{\Gamma}$ in (5.30) are defined by (2.74) and a general expression for them is derived in Appendix D.1. We see that the coupled second-order differential equations (5.29) can be obtained from (2.63) by setting the non-local exchange potential $W_{ii'}^{\Gamma}$ and the non-local correlation potential $X_{ii'}^{\Gamma}$ zero, and omitting the Lagrange multiplier terms which vanish in the external region.

The solution of (5.29) in the external region for each required energy E can be obtained by sub-dividing this region into p sub-regions, as illustrated in Fig. 5.1. In Appendices E.1, E.2 and E.3 we describe methods for propagating the R-matrix, or the log-derivative matrix, and the reduced radial wave functions across this region, where the R-matrix at $r = a_0$ is usually defined by setting the arbitrary constant $b_0 = 0$ in (5.18) which, as pointed out following (5.8), is the value adopted in most applications.

However, if b_0 is not set equal to zero in the internal region calculation, we can relate the corresponding R-matrix to that obtained by setting $b_0 = 0$. To obtain this relation we rewrite (5.18), where b_0 is non-zero, in matrix form as follows:

$$\mathbf{F}(a_0) = \mathbf{R}_{b_0}(E) \left(a_0 \frac{\mathrm{d}\mathbf{F}}{\mathrm{d}r} - b_0 \mathbf{F} \right)_{r=a_0}, \tag{5.31}$$

where we have shown explicitly in this equation the dependence of the R-matrix $\mathbf{R}_{b_0}(E)$ on the value of b_0. The boundary condition corresponding to setting $b_0 = 0$ in (5.31) is then

$$\mathbf{F}(a_0) = \mathbf{R}_0(E)\ a_0 \left. \frac{\mathrm{d}\mathbf{F}}{\mathrm{d}r} \right|_{r=a_0}. \tag{5.32}$$

Eliminating $\mathbf{F}(a_0)/(\mathrm{d}\mathbf{F}/\mathrm{d}r)_{r=a_0}$ between (5.31) and (5.32) then yields the following relation between the R-matrices

$$\mathbf{R}_0(E) = \frac{\mathbf{R}_{b_0}(E)}{\mathbf{I} + b_0 \mathbf{R}_{b_0}(E)}, \tag{5.33}$$

which can be inverted giving

$$\mathbf{R}_{b_0}(E) = \frac{\mathbf{R}_0(E)}{\mathbf{I} - b_0 \mathbf{R}_0(E)}. \tag{5.34}$$

Equations (5.33) and (5.34) are the required relations between the R-matrix $\mathbf{R}_{b_0}(E)$, defined when b_0 is non-zero, and the R-matrix $\mathbf{R}_0(E)$, defined when b_0 is zero. It is interesting to note that this transformation shifts the pole positions in the R-matrix, where the poles of $\mathbf{R}_{b_0}(E)$ now occur where

$$\det\left[\mathbf{I} - b_0 \mathbf{R}_0(E)\right] = 0. \tag{5.35}$$

This can be useful in situations where calculations close to a pole in the R-matrix lead to inaccuracies. In the present context we set the arbitrary constant $b_0 = 0$ in the rest of Sect. 5.1, as well as in Appendix E.

Finally, we observe that since the expression for the long-range potential coefficients $\alpha^{\Gamma}_{ii'\lambda}$, derived in Appendix D.1, is diagonal in the target spin quantum number S_i for non-relativistic collisions and the non-local exchange and correlation potentials vanish in the external region, it follows that the coupled second-order differential equations (5.29) sub-divide into two uncoupled sets of equations depending on whether the target spin $S_i = S - 1/2$ or $S_i = S + 1/2$. This enables more efficient R-matrix propagator methods to be used, as discussed in Appendix E.6. Using one of these methods, the R-matrix at $r = a_0$ can be propagated from $r = a_0$ to a_p to yield the R-matrix at $r = a_p$, thus providing the boundary condition satisfied by the solution in the asymptotic region $r \geq a_p$.

5.1.4 Asymptotic Region Solution

The final step in solving the Schrödinger equation (5.2) is to determine the solution in the asymptotic region, corresponding to $r \geq a_p$ in Fig. 5.1, and hence to calculate the K-matrix, S-matrix and cross sections for each required energy E. In this region the close coupling expansion again reduces to (5.28) where the reduced radial wave functions $F^{\Gamma}_{ij}(r)$ satisfy the coupled second-order differential equations (5.29). We will assume that the radius a_p is chosen large enough that one of the asymptotic expansion methods discussed in Appendix F.1 gives an accurate solution of (5.29) for r satisfying $a_p \leq r \leq \infty$.

Following our discussion in Appendix F.1 we assume that the channels are ordered so that

$$k_1^2 \geq k_2^2 \geq \cdots \geq k_n^2, \tag{5.36}$$

where, at the energy E of interest, the first n_a channels are open with $k_i^2 \geq 0$ and the last n_b channels are closed with $k_i^2 < 0$, where $n_a + n_b = n$. We show in Appendix F.1 that we can determine $n + n_a$ linearly independent asymptotic solutions of (5.29) which are regular as $r \to \infty$. In this section we find it convenient to define these $n + n_a$ solutions to satisfy the following asymptotic boundary conditions:

$$\begin{aligned} s_{ij}(r) &\underset{r\to\infty}{\sim} k_i^{-1/2} \sin\theta_i \delta_{ij}, \quad i = 1, \ldots, n, \quad j = 1, \ldots, n_a, \\ c_{ij}(r) &\underset{r\to\infty}{\sim} k_i^{-1/2} \cos\theta_i \delta_{ij}, \quad i = 1, \ldots, n, \quad j = 1, \ldots, n_a, \\ c_{ij}(r) &\underset{r\to\infty}{\sim} \exp(-\phi_i)\delta_{ij}, \quad i = 1, \ldots, n, \quad j = n_a + 1, \ldots, n, \end{aligned} \tag{5.37}$$

where

$$\theta_i = k_i r - \frac{1}{2}\ell_i \pi - \eta_i \ln 2k_i r + \sigma_{\ell_i}, \quad i = 1, \ldots, n_a, \tag{5.38}$$

with

$$\eta_i = -\frac{Z-N}{k_i}, \quad i = 1, \ldots, n_a \tag{5.39}$$

and

$$\sigma_{\ell_i} = \arg(\ell_i + 1 + \mathrm{i}\eta_i), \quad i = 1, \ldots, n_a, \tag{5.40}$$

and where

$$\phi_i = |k_i|r - \frac{Z-N}{|k_i|}\ln(2|k_i|r), \quad i = n_a + 1, \ldots, n. \tag{5.41}$$

When n_a channels are open we showed in Sect. 2.4 that there are n_a linearly independent physical solutions which vanish at the origin and are finite at infinity. These physical solutions, defined by (2.85), can be written in terms of the $n + n_a$ asymptotic solutions defined by (5.37) as follows:

$$\mathbf{F}^{\Gamma}(r) = \mathbf{s}(r) + \mathbf{c}(r)\mathbf{N}^{\Gamma}, \quad r \geq a_p, \tag{5.42}$$

where $\mathbf{F}^{\Gamma}(r)$ has dimension $n \times n_a$, $\mathbf{s}(r)$ has dimension $n \times n_a$, $\mathbf{c}(r)$ has dimension $n \times n$ and $\mathbf{N}^{\Gamma}$ has dimension $n \times n_a$. The matrix $\mathbf{N}^{\Gamma}$ can be written in the form

$$\mathbf{N}^{\Gamma} = \begin{bmatrix} \mathbf{K}^{\Gamma} \\ \mathbf{L}^{\Gamma} \end{bmatrix}, \tag{5.43}$$

where $\mathbf{K}^{\Gamma}$ is the usual $n_a \times n_a$-dimensional K-matrix defined by (2.85) and $\mathbf{L}^{\Gamma}$ is a subsidiary $n_b \times n_a$-dimensional matrix which multiplies the decaying solutions $\mathbf{c}(r)$ defined by the last equation in (5.37). We see from (5.42) that $\mathbf{K}^{\Gamma}$ postmultiplies the first n_a columns of the matrix $\mathbf{c}(r)$ while $\mathbf{L}^{\Gamma}$ postmultiplies the last n_b columns of the matrix $\mathbf{c}(r)$.

We can now express the $n_a \times n_a$-dimensional K-matrix $\mathbf{K}^{\Gamma}$ in terms of the $n \times n$-dimensional R-matrix $\mathbf{R}_p^{\Gamma}(E)$ at $r = a_p$. Since we have set the arbitrary constant $b_0 = 0$ then these matrices are related by the equation

$$\mathbf{F}^{\Gamma}(a_p) = \mathbf{R}_p^{\Gamma}(E)a_p\dot{\mathbf{F}}^{\Gamma}(a_p), \tag{5.44}$$

where $\dot{\mathbf{F}}^{\Gamma}(r)$ is the derivative of $\mathbf{F}^{\Gamma}(r)$, which from (5.42) can be written as

$$\dot{\mathbf{F}}^{\Gamma}(r) = \frac{\mathrm{d}\mathbf{F}^{\Gamma}}{\mathrm{d}r} = \dot{\mathbf{s}}(r) + \dot{\mathbf{c}}(r)\mathbf{N}^{\Gamma}, \quad r \geq a_p. \tag{5.45}$$

We then substitute the expressions for $\mathbf{F}^{\Gamma}(a_p)$ and $\dot{\mathbf{F}}^{\Gamma}(a_p)$, given respectively by (5.42) and (5.45), into (5.44). After rearranging the terms we obtain

$$\left[\mathbf{c}(a_p) - a_p \mathbf{R}_p^{\Gamma}(E)\dot{\mathbf{c}}(a_p)\right]\mathbf{N}^{\Gamma} = -\mathbf{s}(a_p) + a_p \mathbf{R}_p^{\Gamma}(E)\dot{\mathbf{s}}(a_p), \tag{5.46}$$

which is a set of n linear simultaneous equations with n_a right-hand sides. The solution of these equations for each required energy E yields the $n \times n_a$-dimensional matrix $\mathbf{N}^{\Gamma}$, from which the $n_a \times n_a$-dimensional K-matrix $\mathbf{K}^{\Gamma}$ can be determined from (5.43). It follows from (5.37) and (5.42) that the required physical solution matrix $\mathbf{F}^{\Gamma}(r)$ satisfies the asymptotic boundary conditions

$$\mathbf{F}^{\Gamma}(r) \underset{r\to\infty}{\sim} \mathbf{k}^{-1/2}\left[\sin\boldsymbol{\theta} + \cos\boldsymbol{\theta}\mathbf{K}^{\Gamma}\right] \tag{5.47}$$

in the open channels, since the decaying solutions in (5.37) vanish asymptotically.

We also find it convenient to define a solution matrix satisfying the asymptotic boundary conditions

$$\mathbf{G}^{\Gamma}(r) \underset{r\to\infty}{\sim} \mathbf{k}^{-1/2}\left[\exp(-\mathrm{i}\boldsymbol{\theta}) - \exp(\mathrm{i}\boldsymbol{\theta})\mathbf{S}^{\Gamma}\right], \tag{5.48}$$

which is obtained by taking linear combinations of the solutions defined by (5.47). The $n_a \times n_a$-dimensional S-matrix $\mathbf{S}^{\Gamma}$ in (5.48) is defined in terms of the $n_a \times n_a$-dimensional K-matrix by the matrix equation

$$\mathbf{S}^{\Gamma} = \frac{\mathbf{I} + \mathrm{i}\mathbf{K}^{\Gamma}}{\mathbf{I} - \mathrm{i}\mathbf{K}^{\Gamma}}. \tag{5.49}$$

The T-matrix and cross sections can then be determined using the procedure described in Sect. 2.5. The solutions in the internal, external and asymptotic regions can be determined in a similar way for all relevant $LS\pi$ values enabling the corresponding total cross sections, angular distributions and rate coefficients to be calculated, as described in Sect. 2.5.

5.2 Variational Principle for the R-Matrix

In this section we derive a variational principle for the multichannel R-matrix defined on the boundary $r = a_0$ of the internal region. We consider explicitly low-energy electron collisions with atoms and atomic ions. However, the variational principle that we obtain will be applicable for any multichannel collision process which can be described in an internal region by coupled second-order integro-differential equations with the form defined by (2.63). Variational principles for the R-matrix have been considered by many workers, as discussed in Sect. 4.3. Our approach is a generalization of the variational principles derived by Kohn [542] and Jackson [495], which we considered in Sect. 4.3 in the special case of potential scattering.

Following our treatment of multichannel collisions in Sects. 2.3 and 5.1.2, we expand the wave function describing the collision of an electron with an N-electron atom or atomic ion in the internal R-matrix region as follows:

$$\Psi_{jE}^{\Gamma}(\mathbf{X}_{N+1}) = \mathcal{A}\sum_{i=1}^{n}\overline{\Phi}_i^{\Gamma}(\mathbf{X}_N;\hat{\mathbf{r}}_{N+1}\sigma_{N+1})r_{N+1}^{-1}F_{ij}^{\Gamma}(r_{N+1}) + \sum_{i=1}^{m}\chi_i^{\Gamma}(\mathbf{X}_{N+1})c_{ij}^{\Gamma}, \quad j=1,\ldots,n. \tag{5.50}$$

In this equation we have adopted the same notation for the channel functions $\overline{\Phi}_i^{\Gamma}$ and the quadratically integrable functions χ_i^{Γ} as in (2.57) and (5.6) and we observe that the coefficients c_{ij}^{Γ} in (5.50) can be written in terms of the coefficients b_{ik}^{Γ} in (5.6) and the coefficients $A_{kj}^{\Gamma}(E)$ in (5.5) by the equation

$$c_{ij}^{\Gamma} = \sum_{k=1}^{n_t} b_{ik}^{\Gamma}A_{kj}^{\Gamma}(E), \quad i=1,\ldots,m, \quad j=1,\ldots,n. \tag{5.51}$$

Also the subscript j in (5.50) labels the complete set of n linearly independent solutions of the corresponding coupled second-order integrodifferential equations (2.63), where the reduced radial functions $F_{ij}^{\Gamma}(r)$ vanish at the origin $r=0$. Since we are considering a variational principle for the $n\times n$-dimensional R-matrix on the surface $r=a_0$ of the internal region, we are not restricted in this analysis to the n_a solutions which are regular at infinity as in Sect. 5.1.4. We now derive a variational principle for the solutions of (2.63) in the internal region $0\le r\le a_0$, where a_0 is such that electron exchange and correlation effects between the scattered electron and the target atom or ion can be neglected for $r\ge a_0$.

We commence by defining the integral

$$I_{jj'} = \langle\Psi_j|H_{N+1}+\mathcal{L}_{N+1}-E|\Psi_{j'}\rangle_{\text{int}}, \quad j,\ j'=1,\ldots,n, \tag{5.52}$$

where we have omitted the superscript Γ and the subscript E on the wave functions Ψ_{jE}^{Γ} and $\Psi_{j'E}^{\Gamma}$ for notational convenience, where Γ represents the conserved quantum numbers and E is the total energy being considered. The integrations in (5.52) are carried out over the space and spin coordinates of all $N+1$ electrons, where the radial integrations are confined to the internal region. Also $\mathcal{L}_{N+1}$ is the Bloch operator, defined by (5.8), which ensures that $H_{N+1}+\mathcal{L}_{N+1}$ is hermitian in the internal region for functions satisfying arbitrary boundary conditions on the surface $r=a_0$ of the internal region. The first-order variations of $\delta I_{jj'}$ in $I_{jj'}$ corresponding to first-order variations $\delta\Psi_j$ in Ψ_j and $\delta\Psi_{j'}$ in $\Psi_{j'}$ about the exact solutions of the coupled second-order integrodifferential equations (2.63) in the internal region are then given by

$$\delta I_{jj'} = \langle\Psi_j|H_{N+1}+\mathcal{L}_{N+1}-E|\delta\Psi_{j'}\rangle_{\text{int}} + \langle\delta\Psi_j|H_{N+1}+\mathcal{L}_{N+1}-E|\Psi_{j'}\rangle_{\text{int}}. \tag{5.53}$$

Using the hermiticity of $H_{N+1}+\mathcal{L}_{N+1}$, (5.53) can be written as

$$\delta I_{jj'} = \langle \delta\Psi_{j'} | H_{N+1} + \mathcal{L}_{N+1} - E | \Psi_j \rangle_{\rm int} + \langle \delta\Psi_j | H_{N+1} + \mathcal{L}_{N+1} - E | \Psi_{j'} \rangle_{\rm int}. \quad (5.54)$$

On the boundary $r = a_0$ of the internal region the exchange terms and the quadratically integrable functions in (5.50) vanish and hence this equation reduces to

$$\Psi_j(\mathbf{X}_{N+1}) = \sum_{i=1}^{n} \overline{\Phi}_i(\mathbf{X}_N; \hat{\mathbf{r}}_{N+1}\sigma_{N+1}) r_{N+1}^{-1} F_{ij}(r_{N+1}), \quad j = 1, \ldots, n. \quad (5.55)$$

Substituting (5.55) into (5.54) and remembering that $F_{ij}(r)$ and $F_{ij'}(r)$ are both exact solutions of (2.63) in the internal region, we obtain

$$\delta I_{jj'} = \frac{1}{2} \sum_{i=1}^{n} \left[\delta F_{ij'}(a_0) \left(\frac{\mathrm{d}F_{ij}}{\mathrm{d}r} - \frac{b_0}{a_0} F_{ij} \right)_{r=a_0} + \delta F_{ij}(a_0) \left(\frac{\mathrm{d}F_{ij'}}{\mathrm{d}r} - \frac{b_0}{a_0} F_{ij'} \right)_{r=a_0} \right], \quad (5.56)$$

where we have used definition (5.8) for the Bloch operator.

Following our discussion of the variational principle introduced by Jackson [495] in Sect. 4.3, we now consider the variational functional

$$\mathcal{F}\left[\Psi_j^t, \Psi_{j'}^t\right] = \langle\, \Psi_j^t | H_{N+1} + \mathcal{L}_{N+1} - E\, | \Psi_{j'}^t \rangle_{\rm int} - \frac{1}{2a_0} \left[F_{jj'}^t(a_0) + F_{j'j}^t(a_0) \right], \quad (5.57)$$

where Ψ_j^t is a trial function and $F_{j'j}^t(r)$ is the corresponding reduced radial wave function. We consider first-order variations $\delta\Psi_j$ in Ψ_j and $\delta\Psi_{j'}$ in $\Psi_{j'}$ about the exact solutions of (2.63) in the internal region, subject to the boundary conditions

$$\left(a_0 \frac{\mathrm{d}F_{ij}^t}{\mathrm{d}r} - b_0 F_{ij}^t \right)_{r=a_0} = \delta_{ij}, \quad i, j = 1, \ldots, n. \quad (5.58)$$

It follows from (5.52) and (5.56) that this functional is stationary for first-order variations about the exact solutions so that

$$\delta\mathcal{F}\left[\Psi_j, \Psi_{j'}\right] = 0, \quad (5.59)$$

where we note that the boundary condition (5.58) defines n particular linear combinations of the n linearly independent solutions of (2.63) which vanish at the origin. We see that (5.57), (5.58) and (5.59) are the multichannel generalization of the variational principle for potential scattering given by (4.55), (4.56) and (4.59), respectively.

When the exact solutions of (2.63) are substituted into (5.57) we find that

$$\mathcal{F}\left[\Psi_j, \Psi_{j'}\right] = \frac{1}{2}\left[\langle\Psi_j|\mathcal{L}_{N+1}|\Psi_{j'}\rangle + \langle\Psi_{j'}|\mathcal{L}_{N+1}|\Psi_j\rangle\right] - \frac{1}{2a_0}\left[F_{jj'}(a_0) + F_{j'j}(a_0)\right]. \tag{5.60}$$

Substituting for the Bloch operator and using the boundary condition (5.58) then yields

$$\mathcal{F}\left[\Psi_j, \Psi_{j'}\right] = -\frac{1}{4a_0}\left[F_{jj'}(a_0) + F_{j'j}(a_0)\right]. \tag{5.61}$$

However, the R-matrix on the boundary $r = a_0$ of the internal region is defined by (5.18) which, when combined with the boundary condition (5.58), reduces to

$$F_{ij}(a_0) = R_{ij}(E). \tag{5.62}$$

Hence, it follows from (5.61) and (5.62) and the symmetry of the R-matrix that

$$\mathcal{F}\left[\Psi_j, \Psi_{j'}\right] = -\frac{1}{2a_0}R_{jj'}(E). \tag{5.63}$$

This shows that the R-matrix can be determined from the stationary value of the functional $\mathcal{F}\left[\Psi_j, \Psi_{j'}\right]$.

We now demonstrate that this variational principle provides a variational procedure for calculating the R-matrix. Following (5.6), we introduce a basis in the internal region defined by

$$\psi_k(\mathbf{X}_{N+1}) = \mathcal{A}\sum_{i=1}^{n}\sum_{j=1}^{n_c}\overline{\Phi}_i(\mathbf{X}_N; \hat{\mathbf{r}}_{N+1}\sigma_{N+1})r_{N+1}^{-1}u_{ij}^0(r_{N+1})a_{ijk} + \sum_{i=1}^{m}\chi_i(\mathbf{X}_{N+1})b_{ik}, \quad k = 1, \ldots, n_t, \tag{5.64}$$

where, as in (5.6), $n_t = nn_c + m$ is the number of linearly independent basis functions. Also in (5.64) $u_{ij}^0(r)$ are radial continuum basis orbitals defined over the internal region $0 \le r \le a_0$ and the functions $\overline{\Phi}_i$ and χ_i are defined as in (2.57) and (5.6). The coefficients a_{ijk} and b_{ik} are obtained by diagonalizing $H_{N+1} + \mathcal{L}_{N+1}$ in this basis as follows:

$$\langle\psi_k|H_{N+1} + \mathcal{L}_{N+1}|\psi_{k'}\rangle_{\text{int}} = E_k\delta_{kk'}, \quad k,\ k' = 1, \ldots, n_t, \tag{5.65}$$

where, as in (5.52), the integration is carried out over the internal region. Following (5.5) we now expand the wave functions Ψ_j^t and $\Psi_{j'}^t$ in the functional $\mathcal{F}\left[\Psi_j^t, \Psi_{j'}^t\right]$ in this basis giving

$$\Psi_j^t(\mathbf{X}_{N+1}) = \sum_{k=1}^{n_t} \psi_k(\mathbf{X}_{N+1}) A_{kj}(E), \quad j = 1, \ldots, n,$$
$$\Psi_{j'}^t(\mathbf{X}_{N+1}) = \sum_{k=1}^{n_t} \psi_k(\mathbf{X}_{N+1}) A_{kj'}(E), \quad j' = 1, \ldots, n, \tag{5.66}$$

where $A_{kj}(E)$ and $A_{kj'}(E)$ are variational coefficients which depend on the total energy E of interest. Substituting these expansions into (5.57) then gives the following equation for this functional

$$\mathcal{F}\left[\Psi_j^t, \Psi_{j'}^t\right] = \sum_{kk'} (E_k - E) A_{kj}(E) A_{k'j'}(E) \delta_{kk'} - \frac{1}{2a_0} \sum_k \left[w_{jk} A_{kj'}(E) + w_{j'k} A_{kj}(E) \right], \tag{5.67}$$

where the surface amplitudes w_{jk} are defined by

$$w_{jk} = \sum_{i=1}^{n_c} u_{ji}^0(a_0) a_{jik}, \quad j = 1, \ldots, n, \quad k = 1, \ldots, n_t. \tag{5.68}$$

Writing $\mathcal{F}_{jj'} \equiv \mathcal{F}\left[\Psi_j^t, \Psi_{j'}^t\right]$, for notational convenience, and using the stationary property of this functional with respect to variations in the wave functions Ψ_j^t and $\Psi_{j'}^t$ we obtain

$$\frac{\partial \mathcal{F}_{jj'}}{\partial A_{kj}} = (E_k - E) A_{kj'}(E) - \frac{1}{2a_0} w_{j'k} = 0 \tag{5.69}$$

and

$$\frac{\partial \mathcal{F}_{jj'}}{\partial A_{kj'}} = (E_k - E) A_{kj}(E) - \frac{1}{2a_0} w_{jk} = 0. \tag{5.70}$$

Both these equations give the following result:

$$A_{kj}(E) = \frac{1}{2a_0} \frac{w_{jk}}{E_k - E}, \quad j = 1, \ldots, n, \quad k = 1, \ldots, n_t. \tag{5.71}$$

The stationary value of the functional $\mathcal{F}_{jj'}$ is obtained by substituting (5.71) into (5.67) yielding

$$\mathcal{F}_{jj'} = \frac{1}{4a_0^2}\sum_{k=1}^{n_t}\frac{w_{jk}w_{j'k}}{E_k - E} - \frac{1}{2a_0^2}\sum_{k=1}^{n_t}\frac{w_{jk}w_{j'k}}{E_k - E}$$
$$= -\frac{1}{4a_0^2}\sum_{k=1}^{n_t}\frac{w_{jk}w_{j'k}}{E_k - E}, \quad j,\ j' = 1, \ldots, n. \tag{5.72}$$

We then combine this result with (5.63), which relates the stationary value of the functional $\mathcal{F}_{jj'} \equiv \mathcal{F}\left[\Psi_j^t, \Psi_{j'}^t\right]$ to the R-matrix, to give the following variational expression for the R-matrix:

$$R_{jj'}(E) = \frac{1}{2a_0}\sum_{k=1}^{n_t}\frac{w_{jk}w_{j'k}}{E_k - E}, \quad j, j' = 1, \ldots, n. \tag{5.73}$$

We see that this equation for the R-matrix is identical to (5.19) showing that our procedure for calculating the R-matrix described in Sect. 5.1.2 yields a variational result.

We can also obtain a variational expression for the wave function Ψ_j by substituting the expansion for $A_{kj}(E)$ given by (5.71) into (5.66). This gives

$$\Psi_j(\mathbf{X}_{N+1}) = \frac{1}{2a_0}\sum_{k=1}^{n_t}\psi_k(\mathbf{X}_{N+1})\frac{w_{jk}}{E_k - E}, \quad j = 1, \ldots, n, \tag{5.74}$$

where the reduced wave functions $F_{ij}(r)$ in expansion (5.50) of Ψ_j satisfy the boundary condition (5.58) at $r = a_0$. This result corresponds to the expression for the full collision wave function given by (5.5) and (5.27) when we impose the boundary conditions (5.58). As pointed out in Sect. 5.1.2, where we determined the solution in the internal region, this result is important in applications such as photoionization, discussed in Chap. 8, where the wave function as well as the R-matrix is required.

5.3 Continuum Basis Orbitals and Correction Methods

In this section we consider methods for determining the zero-order radial continuum basis orbitals $u_{ij}^0(r)$ in (5.6) which represent the radial motion of the scattered electron in the expansion of the wave function in the internal region $0 \le r \le a_0$. We also consider methods for calculating and correcting the R-matrix. In principle, as discussed in the case of potential scattering in Sect. 4.4, members of any linearly independent set of orbitals which vanish at the origin and are complete over the range $0 \le r \le a_0$ can be used. However, a careful choice of basis orbitals will enable the convergence of expansion (5.6) to be made more rapid. We consider first in Sect. 5.3.1 an approach using radial continuum basis orbitals which satisfy homogeneous boundary conditions on the surface of the internal region. We then show in Sect. 5.3.2 that a Buttle correction to the R-matrix must be included to

obtain accurate results. We also consider in this section how a Buttle-type correction to the wave function can be determined. We will see later that this approach has been widely used in calculations of electron collisions with atoms, ions and molecules. Then in Sect. 5.3.3 we summarize methods where the radial continuum basis orbitals satisfy arbitrary boundary conditions on the surface of the internal region. Some of these methods have been reviewed in Sect. 4.4, where we showed that in general they avoid the need for a Buttle correction to the R-matrix and to the wave function and, as a consequence, the resultant solution can be derived from a variational principle. However, it is found that for electron collisions with multi-electron atomic targets the number of continuum orbitals required to obtain converged results can often be larger than when homogeneous boundary conditions are used with a Buttle correction. Finally, in Sect. 5.3.4 we consider a method for partitioning the R-matrix into a part which can be accurately determined and a part which is approximated, enabling accurate results to be efficiently obtained when the Hamiltonian matrix becomes large.

5.3.1 Homogeneous Boundary Condition Method

We consider first a procedure for calculating the radial continuum basis orbitals $u^0_{ij}(r)$ in (5.6) in the R-matrix internal region, which was described by Robb [791] and adopted by Burke et al. [155, 178] in their study of low-energy electron collisions with multi-electron atoms and atomic ions.

In this method, the radial continuum basis orbitals $u^0_{ij}(r)$ in (5.6) are chosen to be solutions of the following zero-order differential equation for each continuum orbital angular momentum ℓ_i

$$\left(\frac{\mathrm{d}^2}{\mathrm{d}r^2} - \frac{\ell_i(\ell_i+1)}{r^2} - U_0(r) + k^2_{ij}\right) u^0_{ij}(r) = \sum_{n_b=\ell_i+1}^{\ell_i+n_{\ell_i}} \lambda_{ijn_b} P_{n_b\ell_i}(r), \quad i = 1,\ldots,n, \quad j = 1,\ldots,n_c, \tag{5.75}$$

satisfying the homogeneous boundary conditions

$$u^0_{ij}(0) = 0, \quad i = 1,\ldots,n, \quad j = 1,\ldots,n_c \tag{5.76}$$

and

$$\frac{a_0}{u^0_{ij}(a_0)} \frac{\mathrm{d}u^0_{ij}}{\mathrm{d}r}\bigg|_{r=a_0} = b_0, \quad i = 1,\ldots,n, \quad j = 1,\ldots,n_c, \tag{5.77}$$

where b_0 is an arbitrary constant which can depend on the orbital angular momentum ℓ_i, although in most applications b_0 is set equal to zero. Also in (5.75), the summation n_b goes over the n_{ℓ_i} reduced radial physical bound orbitals $P_{n_b\ell_i}(r)$,

which are included in the representation of the atomic target states for each ℓ_i. However, any pseudo-orbitals retained in the configuration interaction representation of the target states are not included in this summation, since their inclusion would slow the convergence of the expansion over the radial continuum basis orbitals, as described below. Finally, the λ_{ijn_b} in (5.75) are Lagrange multipliers which are chosen so that the continuum basis orbitals are orthogonal to the physical bound orbitals with the same orbital angular momentum symmetry, so that

$$\int_0^{a_0} u_{ij}^0(r) P_{n_b\ell_i}(r) \mathrm{d}r = 0, \quad j = 1, \ldots, n_c, \quad n_b = \ell_i + 1, \ldots, \ell_i + n_{\ell_i} \tag{5.78}$$

are satisfied for each ℓ_i. It follows that the continuum basis orbitals, generated in this way for each ℓ_i, are mutually orthogonal and in addition can be normalized so that

$$\int_0^{a_0} u_{ij}^0(r) u_{ij'}^0(r) \mathrm{d}r = \delta_{jj'}, \quad j,\ j' = 1, \ldots, n_c. \tag{5.79}$$

It also follows that for each ℓ_i the reduced radial orbitals

$$P_{n_b\ell_i}(r), \quad n_b = \ell_i + 1, \ldots, \ell_i + n_{\ell_i}\ ; \quad u_{ij}^0(r), \quad j = 1, \ldots, n_b \tag{5.80}$$

form a complete set over the range $0 \le r < a_0$ in the limit $n_c \to \infty$ for any b_0 and zero-order potential $U_0(r)$ in (5.75).

In order to obtain rapid convergence of the R-matrix expansion (5.19), including the Buttle correction discussed below, the zero-order potential $U_0(r)$ in (5.75) should provide a good representation of the charge distribution of the target atom or ion. In many applications the simple form

$$U_0(r) = -\frac{2N}{r} \exp(-Z^{1/3} r) - \frac{2(Z-N)}{r} \tag{5.81}$$

suggested by the Thomas–Fermi statistical model of the atom (see, for example, [817]) has proved suitable, in that it has the correct form near the nucleus and asymptotically and a reasonably accurate charge distribution radius. A more sophisticated potential which also satisfies these criteria is the static potential of the target atom or ion in its ground state with possibly the addition of a local polarization potential. Such a form becomes increasingly appropriate for high Z atoms and ions. It is important to note that in practical electron–atom and electron–ion collision calculations, the solution of (5.75), (5.76), (5.77), (5.78) and (5.79) to generate the radial continuum basis orbitals takes a very small part of the overall computer time. Hence the use of a more sophisticated zero-order potential is fully justified if it increases the rate of convergence of the R-matrix expansion.

The inclusion of Lagrange multiplier terms on the right-hand side of (5.75) is related to the inclusion of Lagrange multiplier terms in (2.63) which ensure that the orthogonality constraints (2.62) are satisfied. In the present situation the inclusion

of these terms in (5.75) has the following further justification. It is well known that in the static exchange approximation in electron–atom collisions, the difference between the phase shift at zero energy and at infinite energy for each orbital angular momentum satisfies the equation

$$\delta(0) - \delta(\infty) = (n_{bs} + n_p)\pi, \tag{5.82}$$

which is a generalization of Levinson's theorem [587] first studied by Swan [899]. In (5.82), n_{bs} is the number of bound states of the electron–atom system and n_p is the number of states excluded by the Pauli principle corresponding to the orbital angular momentum symmetry being considered. For example, in the case of electron collisions with Ne which has the Hartree–Fock ground-state configuration $1s^2 2s^2 2p^6\ {}^1S^e$ and where $n_{bs} = 0$, we have $n_p = 2$ for s-wave scattering, since the scattered electron is excluded from the fully occupied $1s$ and $2s$ shells, and $n_p = 1$ for p-wave scattering, since the scattered electron is excluded from the fully occupied 2p shell. The effect of including the 1s and 2s orbitals on the right-hand side of (5.75) for s-wave scattering, and the 2p orbital for p-wave scattering and using a suitable zero-order potential $U_0(r)$ ensures that the zero-order solution also satisfies (5.82). We see therefore that the inhomogeneous term on the right-hand side of (5.75) plays the role of an exchange potential, while at the same time ensuring that the continuum basis orbitals are orthogonal to the physical orbitals. Hence the inclusion of the Lagrange multiplier terms on the right-hand side of (5.75) in the generation of the zero-order radial continuum basis orbitals usually means that the R-matrix expansion over these orbitals will converge rapidly. We note that an inhomogeneous term of this type was used by Lippmann and Schey [601] in their model study of elastic e^-–H collisions. Finally, as observed in our discussion following (2.57), the imposition of orthogonality constraints on the radial continuum basis orbitals means that additional quadratically integrable functions must be included in the second expansion in (5.6) to ensure completeness of the collision wave function.

5.3.2 Buttle Correction to the R-Matrix and Wave Function

Since the radial continuum basis orbitals $u_{ij}^0(r)$, retained in expansion (5.6) in the homogeneous boundary condition method, satisfy the zero-order differential equation (5.75) subject to homogeneous boundary conditions (5.76) and (5.77) it is necessary to add a Buttle correction to the R-matrix to obtain accurate results. This procedure, first introduced by Buttle [195] and discussed in the case of potential scattering in Sect. 4.4.2, corrects for the omission of high-lying pole terms in expansion (5.19) of the R-matrix $R_{ij}^{\Gamma}(E)$. In our discussion here, which is a straightforward generalization of potential scattering theory given in Sect. 4.4.2 to multichannel collisions, we consider in turn the Buttle correction to the R-matrix and to the wave function.

5.3.2.1 Buttle Correction to the *R*-Matrix

An important simplification which arises in applying the Buttle correction to the multichannel R-matrix expansion (5.19) is that usually only the diagonal elements of the R-matrix need to be corrected. This can be seen by examining the elements of the Hamiltonian matrix which is diagonalized to yield the basis functions ψ_k^Γ in (5.7). If the zero-order differential equation (5.75) provides a good representation of the electron–atom or electron–ion collision process at high energies, then the Hamiltonian matrix corresponding to the high-lying zero-order radial continuum basis orbitals $u_{ij}^0(r)$ will be dominated by the diagonal elements. In this case we can augment the internal region expansion (5.6) of the basis functions ψ_k^Γ by the following zero-order basis functions:

$$B_k^\Gamma(\mathbf{X}_{N+1}) = \mathcal{A}\overline{\Phi}_i^\Gamma(\mathbf{X}_N; \hat{\mathbf{r}}_{N+1}\sigma_{N+1}) r_{N+1}^{-1} u_{ij}^0(r_{N+1}), \quad i = 1, \ldots, n, \\ j = n_c + 1, \ldots, \infty, \quad k = n_t + 1, \ldots, \infty, \tag{5.83}$$

where the integers i, j and k are related by

$$k = n_t + i + (j - n_c - 1)n. \tag{5.84}$$

Hence, in each channel $i = 1, \ldots, n$, an infinite number of zero-order basis functions $j = n_c + 1, \ldots, \infty$ are included in the internal region expansion, where n_c is the number of radial continuum basis orbitals retained in expansion (5.6) for each channel.

The Buttle correction to the diagonal elements of the R-matrix defined by (5.19) corresponding to the inclusion of the additional zero-order basis functions (5.83) is then given by

$$R_{ii}^{\Gamma(\mathrm{BC})}(E) = \frac{1}{2a_0} \sum_{j=n_c+1}^{\infty} \frac{[u_{ij}^0(a_0)]^2}{E_{ij}^0 - E}, \quad i = 1, \ldots, n, \tag{5.85}$$

where the summation over j goes over the zero-order continuum basis orbitals included in (5.83) for each channel i, and the zero-order energies E_{ij}^0 are obtained from the corresponding zero-order eigenvalues k_{ij}^2 in (5.75) which, using (2.7), gives

$$E_{ij}^0 = e_i + \frac{1}{2}k_{ij}^2. \tag{5.86}$$

As in potential scattering, see (4.79), this correction can be rewritten as

$$R_{ii}^{\Gamma(\mathrm{BC})}(E) = u_i^0(a_0) \left(a_0 \frac{\mathrm{d}u_i^0}{\mathrm{d}r} - b_0 u_i^0 \right)_{r=a_0}^{-1} - \frac{1}{2a_0} \sum_{j=1}^{n_c} \frac{[u_{ij}^0(a_0)]^2}{E_{ij}^0 - E}, \\ i = 1, \ldots, n, \tag{5.87}$$

where the first term on the right-hand side of this equation is obtained by solving the zero-order equation (5.75), subject to the boundary condition (5.76) and the orthogonality constraint (5.78) at the given energy E of interest, while the second term is obtained from the zero-order continuum basis orbitals included in expansion (5.6). Both terms can be rapidly calculated and the correction added to the diagonal elements of the R-matrix given by (5.19). Indeed, since the Buttle correction is smoothly varying without poles in the low-energy region of interest, it can usually be calculated at a few energies in this region and interpolated to give the correction at any required energy.

5.3.2.2 Buttle Correction to the Wave Function

We now discuss how a Buttle correction to the wave function near the boundary in the internal region can be determined. We have already remarked in our discussion of potential scattering that such a correction may be required to obtain accurate results in, for example, atomic photoionization calculations where the accuracy of the wave function near the boundary $r = a_0$ of the internal region may be important. In order to derive a correction to the wave function in multichannel collisions, we commence from (5.17) which we rewrite here as

$$|\Psi_{jE}^{\Gamma}\rangle = \sum_{k=1}^{n_t} |\psi_k^{\Gamma}\rangle \frac{1}{E_k^{\Gamma} - E} \langle \psi_k^{\Gamma} | \mathcal{L}_{N+1} | \Psi_{jE}^{\Gamma} \rangle, \quad j = 1, \ldots, n, \tag{5.88}$$

where the subscript j on the functions Ψ_{jE}^{Γ} now labels the n linearly independent solutions that can be formed in the internal region. We project this equation onto the n channel functions $\overline{\Phi}_i^{\Gamma}(\mathbf{x}_1, \ldots, \mathbf{x}_N; \hat{\mathbf{r}}_{N+1}\sigma_{N+1})$ yielding the following expression for the reduced radial wave functions $F_{ij}^{\Gamma}(r)$ near the boundary $r = a_0$ of the internal region

$$F_{ij}^{\Gamma}(r) = \frac{1}{2a_0} \sum_{k=1}^{n_t} \sum_{i'=1}^{n} \frac{w_{ik}^{\Gamma}(r) w_{i'k}^{\Gamma}(a_0)}{E_k^{\Gamma} - E} \left(a_0 \frac{\mathrm{d}F_{i'j}^{\Gamma}}{\mathrm{d}r} - b_0 F_{i'j}^{\Gamma} \right)_{r=a_0}, \quad i, \ j = 1, \ldots, n, \tag{5.89}$$

where the amplitudes $w_{ik}^{\Gamma}(r)$ are defined by (5.24). It is convenient to choose these n solutions to satisfy the boundary condition

$$\left(a_0 \frac{\mathrm{d}F_{ij}^{\Gamma}}{\mathrm{d}r} - b_0 F_{ij}^{\Gamma} \right)_{r=a_0} = \delta_{ij}, \quad i, \ j = 1, \ldots, n, \tag{5.90}$$

where we note that any other linearly independent set of solutions in the internal region can be expressed as a linear combination of these solutions. Substituting this boundary condition into (5.89) then yields the following expression for the reduced radial wave function near the boundary of the internal region:

$$F_{ij}^{\Gamma}(r) = \frac{1}{2a_0} \sum_{k=1}^{n_t} \frac{w_{ik}^{\Gamma}(r) w_{jk}^{\Gamma}(a_0)}{E_k^{\Gamma} - E}, \quad i, \quad j = 1, \ldots, n. \tag{5.91}$$

In determining the correction to the reduced radial wave function defined by (5.91) we observe that the simplification adopted in our derivation of the Buttle correction to the R-matrix, that only the diagonal elements need correcting, also applies in the present case. Hence the correction to the wave function (5.91) can be written, in analogy with the correction to the R-matrix (5.85), as

$$F_{ii}^{\Gamma(\mathrm{BC})}(r) = \frac{1}{2a_0} \sum_{j=n_c+1}^{\infty} \frac{u_{ij}^0(r) u_{ij}^0(a_0)}{E_{ij}^0 - E}, \quad i = 1, \ldots, n, \tag{5.92}$$

where the summation j goes over the additional zero-order continuum basis orbitals included in (5.83) and the zero-order energies E_{ij}^0 are again given by (5.86). Equation (5.92) can then be rewritten as

$$F_{ii}^{\Gamma(\mathrm{BC})}(r) = \frac{1}{2a_0} \sum_{j=1}^{\infty} \frac{u_{ij}^0(r) u_{ij}^0(a_0)}{E_{ij}^0 - E} - \frac{1}{2a_0} \sum_{j=1}^{n_c} \frac{u_{ij}^0(r) u_{ij}^0(a_0)}{E_{ij}^0 - E}, \quad i = 1, \ldots, n, \tag{5.93}$$

where the first term on the right-hand side of this equation can be written in terms of the solution of the zero-order equation (5.75) as

$$\frac{1}{2a_0} \sum_{j=1}^{\infty} \frac{u_{ij}^0(r) u_{ij}^0(a_0)}{E_{ij}^0 - E} = u_i^0(r) \left(a_0 \frac{\mathrm{d}u_i^0}{\mathrm{d}r} - b_0 u_i^0 \right)_{r=a_0}^{-1}, \quad i = 1, \ldots, n, \tag{5.94}$$

which follows from (5.89) by replacing $F_{ij}^{\Gamma}(r)$ with the solution of the zero-order equation (5.75) at the energy E. Hence the correction to the wave function near the boundary of the internal region is given by

$$F_{ii}^{\Gamma(\mathrm{BC})}(r) = u_i^0(r) \left(a_0 \frac{\mathrm{d}u_i^0}{\mathrm{d}r} - b_0 u_i^0 \right)_{r=a_0}^{-1} - \frac{1}{2a_0} \sum_{j=1}^{n_c} \frac{u_{ij}^0(r) u_{ij}^0(a_0)}{E_{ij}^0 - E}, \quad i = 1, \ldots, n. \tag{5.95}$$

Both terms on the right-hand side of this equation can be rapidly calculated in terms of the solutions of (5.75).

In the above derivation we have seen that with our special choice of boundary condition defined by (5.90) only the diagonal elements of the reduced radial wave function near the boundary $r = a_0$ need correcting. However, the general solution of the Schrödinger equation, defined by (5.89), is a linear combination of the solutions satisfying (5.90). Hence each element of the general solution will be corrected.

We conclude this section by remarking that including a Buttle correction to the R-matrix and the wave function, obtained using the homogeneous boundary condition method, means that these quantities are no longer derivable from the variational principle discussed in Sect. 5.2. However, this does not mean that the resultant R-matrix and wave function are less accurate than the R-matrix and wave function which are derived from a variational principle. Indeed in many practical situations the inclusion of a Buttle correction enables accurate results to be obtained using fewer terms in the R-matrix expansion.

5.3.3 Arbitrary Boundary Condition Methods

In this section we summarize methods where the radial continuum basis orbitals $u_{ij}^0(r)$ in the R-matrix expansion (5.6) are represented by functions which satisfy arbitrary boundary conditions at $r = a_0$. The application of some of these methods in potential scattering has been reviewed in Sect. 4.4.

In recent years R-matrix calculations using arbitrary boundary condition bases have found increasing application in the study of electron collisions with atoms and molecules as well as photoionization and multiphoton ionization processes. Non-orthogonal continuum basis orbitals satisfying arbitrary boundary conditions have also been found to give rapid convergence in studies of atomic vibrations in self-consistent field models of condensed matter by Liberman and Bennett [593] and in studies of electron transport in semiconductor devices discussed in Sect. 12.2.

The use of orbitals satisfying arbitrary boundary conditions removes the need to include a Buttle correction to the R-matrix, as well as to the wave function, as discussed in Sect. 5.3.2. In addition, the resultant solution can be derived from the multichannel variational principle for the R-matrix, as discussed in Sect. 5.2. Although homogeneous boundary condition methods with an appropriate choice of the zero-order differential equation (5.75) can often give fast convergence, for example, for electron collisions with atoms and atomic ions with many open and closed channels at low and intermediate energies, the use of arbitrary boundary condition basis orbitals is required to obtain accurate results in some applications. This is particularly true for time-dependent R-matrix theory of multiphoton processes discussed in Chap. 10, where the time evolution operator requires an accurate representation of the wave function on and near the boundary of the internal region.

A wide variety of basis orbitals satisfying arbitrary boundary conditions have been used in R-matrix calculations including Gaussian-type orbitals, Slater-type orbitals, Legendre functions, Lagrange meshes and B-splines. In early work on electron collisions with diatomic molecules, discussed further in Sect. 11.1, Schneider [821, 822] and Schneider and Hay [826] expanded the continuum orbitals in terms of Gaussian orbitals, yielding low-energy static-exchange cross sections for electron collisions with H_2 and F_2. Also, the convergence properties of Slater-type orbital bases were explored by Noble et al. [690] for electron collisions with H_2 and N_2, where it was found that accurate results can be efficiently obtained at low electron impact energies, but because of linear dependence problems numerical continuum

basis functions satisfying homogeneous boundary conditions were to be preferred at higher energies. A procedure for generating these continuum orbitals for electron–molecule collisions, analogous to that used in Sect. 5.3.1, was later developed by Tennyson et al. [922]. More recently, a considerable body of work has been carried out using Gaussian-type orbitals to represent both the bound and continuum orbitals in electron collisions with polyatomic molecules, in particular by Nestmann and Peyerimhoff [680], Pfingst et al. [732, 733], Nestmann et al. [682], Morgan et al. [661, 662] and Faure et al. [313]. This work showed that Gaussian-type orbitals can give accurate phase shifts and cross sections at low electron impact energies with relatively small bases.

Legendre basis functions have also been used in R-matrix collision calculations. For example, shifted Legendre polynomials have been used by Baluja et al. [47] and Sunderland et al. [896] in their implementation of the BBM propagator method for solving the coupled differential equations (5.29) in the external R-matrix region, discussed in Appendix E.3. These basis functions were also used in time-dependent R-matrix theory calculations of multiphoton processes in potential scattering by Burke and Burke [172]. Lagrange mesh methods have also been used in R-matrix calculations and work using these methods is reviewed in Sect. 4.4.6.

Recently, B-spline methods, which are reviewed in Sect. 4.4.7, have been increasingly used in R-matrix calculations. For example, van der Hart [930] used B-spline bases in R-matrix calculations for two-electron processes, obtaining accurate results for low-energy electron collisions with atomic hydrogen. This work was later extended by van der Hart [931] to electron impact excitation and ionization of He^+, by van der Hart and Feng [318, 319, 935] to study double-electron ionization of He and by McKenna and van der Hart [623] to study single- and two-photon ionization of Ca. B-spline bases have also been used in time-dependent multiphoton ionization calculations by van der Hart et al. [937, 938] and by Lysaght et al. [603–606], which are discussed in Chap. 10.

Also, Zatsarinny [991] and Zatsarinny and Froese Fischer [993] have developed a general computer program for calculating matrix elements in atomic structure with non-orthogonal orbitals, which has been extended by Zatsarinny and Froese Fischer [994] to enable B-splines to be used in R-matrix calculations, with an application to Li photoionization. This program, which has been further extended to enable a wide range of atomic continuum processes to be calculated using non-orthogonal orbitals represented by B-splines, has been published by Zatsarinny [992]. This has enabled accurate calculations to be carried out for a number of collision processes including investigations by Zatsarinny et al. on photodetachment of He^- [1002], by Zatsarinny and Tayal on low-energy electron collisions with atomic oxygen [995] and sulphur [996, 997] and by Zatsarinny and Bartschat on electron collisions with neon [998], argon [999], zinc [1000] and Fe^+ [1001]. Finally we mention the use of B-spline bases in time-dependent multiphoton ionization calculations by Guan et al. [429, 431, 432] which are discussed in Chap. 10.

In conclusion, we will present results from R-matrix calculations using both homogeneous and arbitrary boundary condition methods in Sect. 5.6 and in later chapters.

5.3.4 Partitioned R-Matrix Method

We have seen in Sect 5.1 that in order to calculate the R-matrix, defined by (5.19), which determines the boundary condition (5.18) satisfied by the external region solution at $r = a_0$, it is necessary to diagonalize the Hamiltonian matrix H_{N+1} plus Bloch operator $\mathcal{L}_{N+1}$ in a set of basis functions ψ_k^Γ yielding the eigenenergies E_k^Γ, defined by (5.7), and surface amplitudes w_{ik}^Γ defined by (5.21). We will see when we discuss recent low-energy electron collision calculations in Sect. 5.6 that the dimension of the Hamiltonian matrix can become very large and hence the time taken to diagonalize this matrix may dominate the total computation time. For example, in our discussion of electron collisions with Fe II in Sect. 5.6.5, we will see that the number of coupled channels can exceed many thousands and hence the dimension of the corresponding Hamiltonian matrix will be many tens of thousands. Also, in electron–molecule collisions the number of coupled channels can become very large. In this section we consider a partitioned R-matrix method, introduced for electron–atom and electron–ion collisions by Berrington and Ballance [94] which alleviates this difficulty. In this method, the eigenvalues and eigenvectors of the Hamiltonian matrix are partitioned into two groups, the first consisting of those with low eigenvalues which are accurately determined and the remainder with higher eigenvalues for which an approximation is derived. This enables accurate results to be obtained more efficiently, particularly when the Hamiltonian becomes large.

The partitioned R-matrix method commences from (5.6), which we rewrite using matrix notation as

$$\boldsymbol{\psi} = \boldsymbol{\phi}\mathbf{X}, \tag{5.96}$$

where we have defined the quantities in this equation as follows:

$\boldsymbol{\psi}$ – row vector with dimension n_t, corresponding to ψ_k^Γ in (5.6);
$\boldsymbol{\phi}$ – row vector with dimension n_t, corresponding to $\overline{\Phi}_i^\Gamma r_{N+1}^{-1} u_{ij}^0$ and χ_i^Γ in (5.6);
$\mathbf{X}$ – matrix with dimensions $n_t \times n_t$, corresponding to the coefficients a_{ijk}^Γ and b_{ik}^Γ in (5.6).

The coefficient matrix $\mathbf{X}$ is determined by diagonalizing the Hamiltonian matrix H_{N+1} plus Bloch operator $\mathcal{L}_{N+1}$ in the basis $\boldsymbol{\phi}$ where we define

$$H_{ij} = \langle \phi_i | H_{N+1} + \mathcal{L}_{N+1} | \phi_j \rangle_{\text{int}}, \quad i,\ j = 1, \ldots, n_t. \tag{5.97}$$

It then follows from (5.96) that (5.7) can be rewritten as

$$\mathbf{X}^{\mathrm{T}}\mathbf{H}\mathbf{X} = \mathbf{E}, \tag{5.98}$$

where $\mathbf{E}$ is a diagonal $n_t \times n_t$-dimensional matrix with diagonal elements E_k, $k = 1, \ldots, n_t$. Also, since $\mathbf{H}$ defined by (5.97) is a real symmetric matrix, then $\mathbf{X}$ is a real orthogonal matrix.

The partitioned R-matrix method assumes that we have accurately determined only the l lowest eigenvalues E_j and the corresponding eigenvectors of the matrix $\mathbf{H}$. It follows from (5.98) that

$$\sum_{k=1}^{n_t} H_{ik} X_{kj} = X_{ij} E_j, \quad i = 1, \ldots, n_t, \quad j = 1, \ldots, l. \tag{5.99}$$

The remaining eigenvalues are then approximated by a single degenerate energy E_0 such that

$$\sum_{k=1}^{n_t} H_{ik} X_{kj} \approx X_{ij} E_0, \quad i = 1, \ldots, n_t, \quad j = l+1, \ldots, n_t, \tag{5.100}$$

where the combined $n_t \times n_t$-dimensional eigenvector matrix $\mathbf{X}$ is still real and orthogonal satisfying

$$\mathbf{X}^{\mathrm{T}} \mathbf{X} = \mathbf{X} \mathbf{X}^{\mathrm{T}} = \mathbf{I}. \tag{5.101}$$

In order to determine E_0 we minimize the following functional formed from (5.100)

$$\mathcal{X}(E_0) = \sum_{i=1}^{n_t} \sum_{j=l+1}^{n_t} \left(X_{ij} E_0 - \sum_{k=1}^{n_t} H_{ik} X_{kj} \right)^2, \tag{5.102}$$

which gives

$$\frac{\partial \mathcal{X}}{\partial E_0} = 2 \sum_{i=1}^{n_t} \sum_{j=l+1}^{n_t} X_{ij} \left(X_{ij} E_0 - \sum_{k=1}^{n_t} H_{ik} X_{kj} \right). \tag{5.103}$$

After using (5.101) we obtain

$$\frac{\partial \mathcal{X}}{\partial E_0} = 2 \left(\sum_{j=l+1}^{n_t} E_0 - \sum_{i=1}^{n_t} \sum_{j=l+1}^{n_t} \sum_{k=1}^{n_t} H_{ik} X_{ij} X_{kj} \right). \tag{5.104}$$

Then, setting $\partial \mathcal{X} / \partial E_0 = 0$ and using (5.101) gives

$$E_0 = \frac{\left(\mathrm{Tr}\mathbf{H} - \sum_{i=1}^{l} E_i \right)}{(n_t - l)}, \tag{5.105}$$

where

$$\mathrm{Tr}\mathbf{H} = \sum_{i=1}^{n_t} H_{ii}. \tag{5.106}$$

The partitioned R-matrix which replaces $R_{ij}^{\Gamma}(E)$ in (5.19) is then given by

$$R_{ij}^{\mathrm{p}}(E) = \sum_{k=1}^{l} \frac{w_{ik}w_{jk}}{E_k - E} + \frac{1}{E_0 - E} \sum_{k=l+1}^{n_t} w_{ik}w_{jk}, \quad i,\ j = 1, \ldots, n, \tag{5.107}$$

which can be rewritten as

$$R_{ij}^{\mathrm{p}}(E) = \sum_{k=1}^{l} \frac{w_{ik}w_{jk}}{E_k - E} - \frac{1}{E_0 - E} \sum_{k=1}^{l} w_{ik}w_{jk} + \frac{1}{E_0 - E} \sum_{k=1}^{n_t} w_{ik}w_{jk}, \quad i,\ j = 1, \ldots, n. \tag{5.108}$$

The first two terms on the right-hand side of (5.108) can be calculated since we know the surface amplitudes $w_{ik},\ i = 1, \ldots, n_t,\ k \le l$ from the solution of (5.99). The last term on the right-hand side of (5.108) can be calculated using expansion (5.21) for the surface amplitudes w_{ik}. We obtain

$$\sum_{k=1}^{n_t} w_{ik}w_{jk} = \sum_{k'=1}^{n_c} \sum_{k''=1}^{n_c} u_{ik'}^{0}(a_0) u_{jk''}^{0}(a_0) \sum_{k=1}^{n_t} a_{ik'k}a_{jk''k}. \tag{5.109}$$

It then follows from the orthogonality relation (5.101) that the following summation in (5.109) is given by

$$\sum_{k=1}^{n_t} a_{ik'k}a_{jk''k} = \delta_{ij}\delta_{k'k''}, \tag{5.110}$$

and hence

$$\sum_{k=1}^{n_t} w_{ik}w_{jk} = \sum_{k=1}^{n_c} \left[u_{ik}^{0}(a_0)\right]^2 \delta_{ij} = S_i\delta_{ij}, \tag{5.111}$$

which defines S_i. Substituting this result into (5.108) gives the following expression for the partitioned R-matrix

$$R_{ij}^{\mathrm{p}}(E) = \sum_{k=1}^{l} w_{ik} \left(\epsilon_k^{-1} - \epsilon_0^{-1}\right) w_{jk} + \left[S_i\epsilon_0^{-1} + R_i^{c}(E)\right]\delta_{ij}, \tag{5.112}$$

where we have written

$$\epsilon_k = E_k - E, \quad k = 0, \ldots, l, \tag{5.113}$$

and where $R_i^c(E)$ is an estimate of the partitioning error. It follows from (5.19) and (5.107) that this error is given by

$$R_{ij}^c(E) = \sum_{k=l+1}^{n_t} w_{ik} w_{jk} \left(\frac{1}{E_k - E} - \frac{1}{E_0 - E} \right). \tag{5.114}$$

We can obtain an estimate for this error by replacing the surface amplitudes w_{ik} in (5.114) by the corresponding zero-order radial continuum basis orbitals $u_{ij}^0(a_0)$ in (5.21) obtained by neglecting the off-diagonal terms in diagonalizing $H_{N+1} + \mathcal{L}_{N+1}$ in the internal region. This is analogous to our choice of radial continuum basis orbitals used in the Buttle correction described in Sect. 5.3.2. With this approximation (5.114) yields the following estimate of the partitioning error:

$$R_i^c(E) = \sum_{j=N_i+1}^{n_c} \left[u_{ij}^0(a_0) \right]^2 \left(\frac{1}{E_{ij} - E} - \frac{1}{E_0 - E} \right), \tag{5.115}$$

where E_{ij} is the energy of the radial continuum basis orbital and N_i is such that the radial continuum basis orbitals in the ith channel above N_i lie above the highest eigenvalue explicitly included in (5.108).

The above theory has been extended to electron–molecule collisions by Tennyson [916]. In this case several modifications of the above theory were found to be necessary, which also apply to a lesser extent in electron–atom collisions. The first modification arises from the procedure used to generate the continuum orbitals for the electron–molecule collision problem. The need to orthogonalize the continuum orbitals to the bound orbitals used to represent the target [662, 922] means that the energies of the resultant continuum orbitals are not well defined, which requires a modification to the energies E_{ij} of the radial continuum basis orbitals in (5.115). The second and more important modification concerns the definition of E_0 in (5.105). This definition averages over all diagonal elements of the Hamiltonian matrix regardless of whether the configuration involved makes any contribution to the boundary amplitude. This means that many high-lying L^2 configurations included in the second expansion on the right-hand side of (5.6), which make no contribution to the boundary amplitude, contribute to the value of E_0. As a result, a systematic improvement in the configuration interaction representation of the target and the consequent increase in the number of L^2 configurations included in the expansion leads to an undesirable increase in E_0, even if all the other parameters of the calculation remain the same. It is therefore preferable to define E_0 using only those configurations which contribute directly to the boundary amplitude and hence to the R-matrix; a procedure for achieving this is given by Tennyson [916]. A final problem arises from the error correction procedure leading to (5.115). The use of

the entire boundary amplitude of the higher lying radial continuum basis orbitals $\left[u_{ij}^0(a_0)\right]^2$ in the error correction will lead to an over correction if these orbitals contribute to any significant extent to the lower l surface amplitudes retained explicitly in the first summation in (5.112). It is straightforward to estimate the contribution of these orbitals to the surface amplitudes not explicitly included in the summation in (5.112) and to make a corresponding modification to the error correction formula (5.114).

Finally, we observe that, if the radial continuum basis orbitals $u_{ij}^0(r)$ retained in expansion (5.6) satisfy homogeneous boundary conditions (5.76) and (5.77), as discussed in Sect. 5.3.1, then it is necessary to add a Buttle correction to the partitioned R-matrix defined by (5.112). However, if these orbitals satisfy arbitrary boundary conditions, as discussed in Sect. 5.3.3, then this correction will usually not be required although it will still be appropriate to include the partitioning error correction defined by (5.115).

5.4 Inclusion of Relativistic Effects

As the charge number Z on the atomic nucleus increases, relativistic effects become progressively more important in the collision process. In this section and in Sect. 5.5 we consider how these effects can be accurately represented in low-energy electron collisions with heavy atoms and atomic ions. There are two main ways in which relativistic effects play a role in low-energy electron collisions. First, there is a direct effect which is due to the relativistic distortion of the wave function of the scattered electron induced by the strong nuclear potential, when this electron is in the neighbourhood of the nucleus. Second, there is an indirect effect caused by the change in the charge distribution of the target electrons due to relativity which in turn affects the motion of the scattered electron. Our objective in this section and the next is to show how these two effects can be included in multichannel R-matrix theory, in addition to electron exchange and electron–electron correlation effects which we considered earlier in this chapter.

There are several procedures for including relativistic effects in low-energy electron collisions with atoms and atomic ions. For relatively light targets, these effects are small so that the energy intervals between the fine-structure levels of the target are small compared both with the energy intervals between the $LS\pi$-coupled energy levels of the target and with the energy of the scattered electron. In this case the collision calculation can first be carried out in $LS\pi$-coupling using the non-relativistic Hamiltonian, as described earlier in this chapter. The K-matrices obtained from this calculation are then recoupled to give the K-matrices, and hence the corresponding cross sections, for transitions between the fine-structure levels of the target. This approach was introduced by Saraph [810, 811] and extended by Griffin et al. [426] and Badnell and Griffin [34] using multichannel quantum defect theory. We discuss this approach in Sect. 5.4.1.

As the nuclear charge number Z increases, relativistic effects must be included both in the calculation of the N-electron wave function describing the target and

in the calculation of the $(N + 1)$-electron wave function describing the collision process. Provided Z is not too large, this can be achieved by replacing the non-relativistic Hamiltonian, defined by (5.3), by the Breit–Pauli Hamiltonian discussed, for example, by Bethe and Salpeter [105], Akhiezer and Berestetsky [7] and Glass and Hibbert [382]. The conserved quantum numbers are now J the total angular momentum of the electron target atom collision wave function, M_J its z-component and π the total parity rather than L, S, M_L, M_S and π defined following (2.58). This leads to many more coupled channels which have to be included in the expansion of the collision wave function and to many more coupled integrodifferential equations which have to be solved. We consider in detail the extension of R-matrix collision theory to include the relativistic Breit–Pauli terms in the Hamiltonian in Sect. 5.4.2, having summarized the computer programs which implement this approach in Sect. 5.1.1. Then in Sect. 5.4.3 we consider a frame-transformation theory extension of this approach where the relativistic terms in the Breit–Pauli Hamiltonian are omitted in the high-energy spectrum in the internal R-matrix region but are included in the low-energy spectrum in the internal region and also in the external and asymptotic regions, with considerable saving in computational effort.

Finally, we observe that the above approaches for including relativistic effects using the Breit–Pauli Hamiltonian have been used with considerable success to treat electron collisions with a wide range of low and intermediate Z atoms and ions. However, in order to obtain accurate results for electron collisions with the heaviest atomic targets it is necessary to treat both the target and the collision wave function using the Dirac Hamiltonian. We present a detailed discussion of Dirac R-matrix theory of electron collisions with heavy atoms and ions in Sect. 5.5.

5.4.1 Transformation of the K- and S-Matrices

This approach is appropriate for light atomic or ionic targets where relativistic effects are small and hence the energy intervals between the fine-structure levels of the target are small compared with the energy intervals between the $LS\pi$-coupled energy levels of the target and the energy of the scattered electron. K-matrices are first calculated, omitting all relativistic terms in the Hamiltonian, as described in Sect. 5.1. These K-matrices are then transformed to full intermediate coupling to yield cross sections corresponding to transitions between fine-structure levels of the target. This is the basis of a widely used computer program JAJOM, written by Saraph [810, 811] for electron–ion collisions. We also consider an extension of this approach using multichannel quantum defect theory by Griffin et al. [426] and Badnell and Griffin [34], which yields accurate transformed K- and S-matrices when some channels are closed.

For the situation where relativistic effects are not large, it is convenient to adopt the pair-coupling scheme defined by the equations

$$\mathbf{L}_i + \mathbf{S}_i = \mathbf{J}_i, \quad \mathbf{J}_i + \boldsymbol{\ell}_i = \mathbf{K}_i, \quad \mathbf{K}_i + \mathbf{s}_i = \mathbf{J}, \tag{5.116}$$

where $\mathbf{L}_i$, $\mathbf{S}_i$ and $\mathbf{J}_i$ are the orbital, spin and total angular momentum operators of the target atom or ion, $\boldsymbol{\ell}_i$ and $\mathbf{s}_i$ are the orbital and spin angular momentum operators of the scattered electron, $\mathbf{K}_i$ is an intermediate angular momentum operator and $\mathbf{J}$ is the total angular momentum operator of the electron plus target atom or ion system which is conserved in the collision. This pair-coupling scheme can be related to the $LS\pi$-coupling scheme adopted in Sect. 5.1 which is defined by the equations

$$\mathbf{L}_i + \boldsymbol{\ell}_i = \mathbf{L}, \quad \mathbf{S}_i + \mathbf{s}_i = \mathbf{S}, \quad \mathbf{L} + \mathbf{S} = \mathbf{J}. \tag{5.117}$$

The recoupling coefficient between these schemes can be simply expressed in terms of Racah coefficients, defined in Appendix A.2, as follows:

$$\begin{aligned}&\langle[(L_i S_i)J_i, \ell_i]K_i \tfrac{1}{2}; J M_J|(L_i \ell_i)L, (S_i \tfrac{1}{2})S; J M_J\rangle \\ &= [(2L+1)(2S+1)(2J_i+1)(2K_i+1)]^{1/2} W(L\ell_i S_i J_i; L_i K_i) \\ &\quad \times W(L J S_i \tfrac{1}{2}; S K_i).\end{aligned} \tag{5.118}$$

We can then express the K-matrix $K^{J\pi}_{\alpha\beta}(E)$, defined in the pair-coupling scheme, in terms of the K-matrix $K^{\Gamma}_{ij}(E)$, determined in the $LS\pi$-coupling scheme by the equation

$$\begin{aligned}K^{J\pi}_{\alpha\beta}(E) = \sum_{LS} &\langle[(L_i S_i)J_i, \ell_i]K_i \tfrac{1}{2}; J M_J|(L_i \ell_i)L, (S_i \tfrac{1}{2})S; J M_J\rangle K^{\Gamma}_{ij}(E) \\ &\times \langle(L_j \ell_j)L, (S_j \tfrac{1}{2})S; J M_J|[(L_j S_j)J_j, \ell_j]K_j \tfrac{1}{2}; J M_J\rangle,\end{aligned} \tag{5.119}$$

where the summation goes over all LS values which contribute to the J value considered. Also the channel subscripts α and β on the K-matrix elements $K^{J\pi}_{\alpha\beta}(E)$ in (5.119) represent the quantum numbers

$$\alpha \equiv \alpha_i \; L_i \; S_i \; J_i \; \ell_i \; K_i \; \tfrac{1}{2}, \quad \beta \equiv \alpha_j \; L_j \; S_j \; J_j \; \ell_j \; K_j \; \tfrac{1}{2}. \tag{5.120}$$

It follows that the K-matrix must first be determined in $LS\pi$-coupling for all significant $LS\pi$ values when relativistic terms in the Hamiltonian are omitted. Equation (5.119) is then used to transform the K-matrix from the $LS\pi$-coupling scheme to the pair-coupling scheme for all relevant $J\pi$ values.

For atoms and ions where the term splitting[1] in the target due to relativistic effects is small compared with the term separation, the transformation involving the angular momentum variables given by (5.119) provides an accurate representation of the collision. However, with increasing nuclear charge number Z, relativistic effects increase in importance and the target Hamiltonian can no longer be treated as diagonal with respect to the target quantum numbers L_i and S_i. If relativistic effects are

[1] In this discussion a term corresponds to a target state belonging to the quantum numbers $\alpha_i L_i S_i \pi_i$ in the absence of relativistic effects (see, for example, [232]).

not large, it is appropriate to represent these effects by expanding the resultant target states in terms of the target states retained in the original $LS\pi$-coupled expansion defined by (5.5) and (5.6) omitting relativistic effects. We first recouple the original $LS\pi$-coupled target states as follows:

$$\Phi_i(\alpha_i L_i S_i J_i M_{J_i} \pi_i | \mathbf{X}_N) = \sum_{M_{L_i} M_{S_i}} (L_i M_{L_i} S_i M_{S_i} | J_i M_{J_i}) \times \Phi_i(\alpha_i L_i S_i M_{L_i} M_{S_i} \pi_i | \mathbf{X}_N), \tag{5.121}$$

where $(L_i M_{L_i} S_i M_{S_i} | J_i M_{J_i})$ are Clebsch–Gordan coefficients defined in Appendix A.1 and where we have explicitly denoted the dependence of the target states on the angular momentum quantum numbers, as in (2.14). We then expand the target states including relativistic effects in terms of these recoupled states according to

$$\Phi_i(\Delta_i J_i M_{J_i} \pi_i | \mathbf{X}_N) = \sum_{\alpha_i L_i S_i} f(\Delta_i J_i \pi_i; \alpha_i L_i S_i \pi_i) \Phi_i(\alpha_i L_i S_i J_i M_{J_i} \pi_i | \mathbf{X}_N), \tag{5.122}$$

where the summation goes over all the target states retained in the original $LS\pi$-coupled expansion defined by (5.6) which can couple to $J_i M_{J_i} \pi_i$ and where we have introduced a parameter Δ_i which replaces α_i and which serves to distinguish different target states with the same total angular momentum and parity. The term-coupling coefficients $f(\Delta_i J_i \pi_i; \alpha_i L_i S_i \pi_i)$, defined by (5.122) [509, 510], can be obtained by diagonalizing the Breit–Pauli target Hamiltonian H_N^{BP}, which includes relativistic terms as described in Sect. 5.4.2, in this new basis for each $J_i \pi_i$ as follows:

$$\langle \Phi_i(\Delta_i J_i M_{J_i} \pi_i | \mathbf{X}_N) | H_N^{\mathrm{BP}} | \Phi_j(\Delta_j J_j M_{J_j} \pi_j | \mathbf{X}_N) \rangle = e_i^{J_i \pi_i} \delta_{ij}, \quad i, j = 1, \ldots, n_i, \tag{5.123}$$

where n_i is the number of target states with $J_i \pi_i$ symmetry represented by the parameters Δ_i and Δ_j. The K-matrix $K_{\mu\nu}^{J\pi}(E)$ in this "full intermediate coupling" representation is then given in terms of the original K-matrix $K_{\alpha\beta}^{J\pi}(E)$, defined by (5.119), by

$$K_{\mu\nu}^{J\pi}(E) = \sum_{\alpha_i L_i S_i} \sum_{\alpha_j L_j S_j} f(\Delta_i J_i \pi_i; \alpha_i L_i S_i \pi_i) K_{\alpha\beta}^{J\pi}(E) f(\Delta_j J_j \pi_j; \alpha_j L_j S_j \pi_j), \tag{5.124}$$

where the channel subscripts μ and ν on the K-matrix elements $K_{\mu\nu}^{J\pi}(E)$ in this equation represent the following quantum numbers:

$$\mu \equiv \Delta_i \; J_i \; \ell_i \; K_i \; \tfrac{1}{2}, \quad \nu \equiv \Delta_j \; J_j \; \ell_j \; K_j \; \tfrac{1}{2}. \tag{5.125}$$

The multichannel S-matrix and hence the T-matrix in the pair-coupling scheme are then obtained in terms of the K-matrices defined by (5.119) and (5.124) using

the procedure described in Sect. 2.5. The S-matrix is defined in terms of the K-matrix, in analogy with (2.112), by the matrix equation

$$\mathbf{S}^{J\pi} = \frac{\mathbf{I} + \mathrm{i}\mathbf{K}^{J\pi}}{\mathbf{I} - \mathrm{i}\mathbf{K}^{J\pi}}, \tag{5.126}$$

and the corresponding T-matrix is defined in analogy with (2.119) by

$$\mathbf{T}^{J\pi} = \mathbf{S}^{J\pi} - \mathbf{I}. \tag{5.127}$$

The cross sections and collision strengths for transitions between the fine-structure levels of the target can be obtained in this new coupling scheme, as described in Sect. 2.5. We obtain the following result for the total cross section

$$\sigma^{\mathrm{Tot}}(i \to j) = \sum_{J\pi} \sigma^{J\pi}(i \to j), \tag{5.128}$$

where the partial wave cross sections

$$\sigma^{J\pi}(i \to j) = \frac{(2J+1)}{2k_i^2(2J_i+1)} \sum_{\ell_i \ell_j K_i K_j} |T_{ji}^{J\pi}|^2 \tag{5.129}$$

are given in units of πa_0^2.

The transformation procedure using (5.119) and (5.124) is appropriate when all the channels included in (5.5) and (5.6) are open. However, a difficulty arises at low electron impact energies where some of these channels are closed. In this energy region, some of the terms included in the term coupling expansion (5.122) correspond to open channels and others correspond to closed channels. Consequently, the transformation of the K-matrix to full intermediate coupling, defined by (5.119) and (5.124), breaks down since the K-matrix, which has dimension $n_a \times n_a$, only includes the n_a open channels. The procedure usually adopted for dealing with this situation, using the Saraph computer program [810, 811], has been to set all the energy levels corresponding to a given term equal and to include after renormalization only those components of the term-coupling coefficients corresponding to open channels in the calculation. However, this procedure can lead to poor threshold energies, incorrect resonance structure and anomalous threshold effects in the cross sections as new terms are included in the calculation when the energy increases through the term thresholds.

In more recent electron–positive ion collision calculations by Griffin et al. [426] and Badnell and Griffin [34], the inconsistencies discussed in the previous paragraph have been removed using multichannel quantum defect theory (MQDT), discussed in Sect. 3.3.4. In this intermediate coupling frame transformation (ICFT) method, the unphysical K-matrices ($\mathcal{K}$) and S-matrices (χ), defined in Sect. 3.3.4, are first calculated on a coarse mesh in $LS\pi$-coupling, neglecting relativistic effects.

These unphysical matrices are analytic functions of energy, which do not contain the threshold branch cuts, and have the dimension $n \times n$ at all energies, where n is the number of coupled channels. Hence they can be interpolated onto a fine energy mesh. The resultant unphysical matrices can then be transformed to full intermediate coupling using (5.119) and (5.124) for all required energies both above and below the thresholds. The physical K- and S-matrices in the open channels are then shown in Sect. 3.3.4 to be related to the unphysical K- and S-matrices as follows:

$$\mathbf{K}_{oo}^{J\pi} = \mathcal{K}_{oo}^{J\pi} - \mathcal{K}_{oc}^{J\pi} \frac{1}{\mathcal{K}_{cc}^{J\pi} + \tan(\pi \boldsymbol{\nu}_c)} \mathcal{K}_{co}^{J\pi} \tag{5.130}$$

and

$$\mathbf{S}_{oo}^{J\pi} = \boldsymbol{\chi}_{oo}^{J\pi} - \boldsymbol{\chi}_{oc}^{J\pi} \frac{1}{\boldsymbol{\chi}_{cc}^{J\pi} - \exp(-2\pi \mathrm{i} \boldsymbol{\nu}_c)} \boldsymbol{\chi}_{co}^{J\pi}, \tag{5.131}$$

where $\boldsymbol{\nu}_c$ is a diagonal matrix in the closed channels whose diagonal elements are defined by

$$\nu_i^2 = -\frac{(Z-N)^2}{k_i^2}, \quad i = n_a + 1, \ldots, n, \tag{5.132}$$

where n_a is the number of open channels at the energy under consideration.

The T-matrix and cross sections for transitions between the fine-structure levels corresponding to the open channels are then given in terms of the open channel physical S-matrix $\mathbf{S}_{oo}^{J\pi}$ by (5.127), (5.128) and (5.129). Since the unphysical K- and S-matrices are smooth functions of energy, the fine-structure splitting of the energy levels of the target can be accurately included in the calculation. Also resonance structures which converge to all excited thresholds are included through the inverse terms in (5.130) and (5.131). In conclusion, this application of MQDT enables relativistic effects and resonance structures to be accurately included in electron–positive ion collisions for relatively light targets, by solving the time-independent Schrödinger equation in $LS\pi$-coupling on a coarse mesh of energies using the non-relativistic R-matrix method, discussed in Sect. 5.1.

5.4.2 Breit–Pauli Hamiltonian

As the nuclear charge number Z increases relativistic effects must be included in the Hamiltonian used to determine both the target atom or ion wave function and the electron–target atom or ion collision wave function. This can be achieved, provided Z is not too large, by using the Breit–Pauli Hamiltonian (e.g. [7, 105, 382]).

The $(N+1)$-electron Breit–Pauli Hamiltonian can be written as

$$H_{N+1}^{\mathrm{BP}} = H_{N+1}^{\mathrm{NR}} + H_{N+1}^{\mathrm{REL}}, \tag{5.133}$$

where $H_{N+1}^{\rm NR}$, the non-relativistic Hamiltonian, is defined by (5.3) and $H_{N+1}^{\rm REL}$ consists of one- and two-body relativistic terms resulting from the reduction of the Dirac equation and the Breit interaction to Pauli form.

The one-body terms are defined by

$$H_{N+1}^{\rm MC} = -\frac{1}{8}\alpha^2 \sum_{i=1}^{N+1} \nabla_i^4, \quad \text{relativistic mass-correction,} \tag{5.134}$$

$$H_{N+1}^{\rm D_1} = -\frac{1}{8}\alpha^2 Z \sum_{i=1}^{N+1} \nabla_i^2 \left(\frac{1}{r_i}\right), \quad \text{one-body Darwin,} \tag{5.135}$$

$$H_{N+1}^{\rm SO} = \frac{1}{2}\alpha^2 Z \sum_{i=1}^{N+1} r_i^{-3}(\boldsymbol{\ell}_i \cdot \mathbf{s}_i), \quad \text{spin–orbit,} \tag{5.136}$$

and the two-body terms are defined by

$$H_{N+1}^{\rm SOO} = -\frac{1}{2}\alpha^2 \sum_{i\neq j=1}^{N+1} \left(\frac{\mathbf{r}_{ij}}{r_{ij}^3} \times \mathbf{p}_i\right) \cdot (\mathbf{s}_i + 2\mathbf{s}_j), \quad \text{spin–other orbit,} \tag{5.137}$$

$$H_{N+1}^{\rm OO} = -\frac{1}{2}\alpha^2 \sum_{i<j=1}^{N+1} \left(\frac{\mathbf{p}_i \cdot \mathbf{p}_j}{r_{ij}} + \frac{\mathbf{r}_{ij}(\mathbf{r}_{ij} \cdot \mathbf{p}_i) \cdot \mathbf{p}_j}{r_{ij}^3}\right), \quad \text{orbit–orbit,} \tag{5.138}$$

$$H_{N+1}^{\rm SS} = \alpha^2 \sum_{i<j=1}^{N+1} \frac{1}{r_{ij}^3} \left(\mathbf{s}_i \cdot \mathbf{s}_j - \frac{3(\mathbf{s}_i \cdot \mathbf{r}_{ij})(\mathbf{s}_j \cdot \mathbf{r}_{ij})}{r_{ij}^2}\right), \quad \text{spin–spin,} \tag{5.139}$$

$$H_{N+1}^{\rm D_2} = \frac{1}{4}\alpha^2 \sum_{i<j=1}^{N+1} \nabla_i^2 \left(\frac{1}{r_{ij}}\right), \quad \text{two-body Darwin,} \tag{5.140}$$

$$H_{N+1}^{\rm SSC} = -\frac{8\pi\alpha^2}{3} \sum_{i<j=1}^{N+1} (\mathbf{s}_i \cdot \mathbf{s}_j)\delta(\mathbf{r}_i \cdot \mathbf{r}_j), \quad \text{spin–spin contact.} \tag{5.141}$$

The Breit–Pauli Hamiltonian can then be rewritten as

$$H_{N+1}^{\rm BP} = H_{N+1}^{\rm NR} + H_{N+1}^{\rm FS} + H_{N+1}^{\rm NFS}, \tag{5.142}$$

where $H_{N+1}^{\rm FS}$ are fine-structure terms defined by

$$H_{N+1}^{\rm FS} = H_{N+1}^{\rm SO} + H_{N+1}^{\rm SOO} + H_{N+1}^{\rm SS}, \tag{5.143}$$

while $H_{N+1}^{\rm NFS}$ are non-fine-structure terms defined by

$$H_{N+1}^{\rm NFS} = H_{N+1}^{\rm MC} + H_{N+1}^{\rm D_1} + H_{N+1}^{\rm OO} + H_{N+1}^{\rm D_2} + H_{N+1}^{\rm SSC}. \tag{5.144}$$

The non-fine-structure terms commute with the operators $\mathbf{L}^2$, $\mathbf{S}^2$, L_z, S_z and π while the fine-structure terms only commute with the operators $\mathbf{J}^2$, J_z and π. Thus it is necessary to use a representation which is diagonal in $\mathbf{J}^2$, J_z and π. In practice, for electron collision calculations, the one-body terms defined by (5.134), (5.135) and (5.136) are found to be the most important and often only these terms in addition to $H_{N+1}^{\rm NR}$ are retained in calculations using the Breit–Pauli Hamiltonian $H_{N+1}^{\rm BP}$. However, other terms, including in particular the spin–other orbit term (5.137), can also play a significant role and have been included in some recent R-matrix calculations.

We now consider the solution of the time-independent Breit–Pauli equation

$$H_{N+1}^{\rm BP}\Psi = E\Psi. \tag{5.145}$$

As in non-relativistic R-matrix theory of electron collisions with atoms and atomic ions, we partition configuration space into three regions as illustrated in Fig. 5.1. We now discuss the solution in each of these regions in turn.

5.4.2.1 Internal Region Solution

In the internal region, corresponding to $0 \le r \le a_0$ in Fig. 5.1, the collision wave function can be written in analogy with (5.5) as

$$\Psi_{jE}^{J M_J \pi}(\mathbf{X}_{N+1}) = \sum_k \psi_k^{J M_J \pi}(\mathbf{X}_{N+1}) A_{kj}^{J M_J \pi}(E), \tag{5.146}$$

for each set of conserved quantum numbers J, M_J and π, where J is the total angular momentum quantum number, M_J is the corresponding magnetic quantum number and π is the parity. Also in (5.146) j labels the linearly independent solutions of (5.145), $\psi_k^{J M_J \pi}$ are energy-independent basis functions and $A_{kj}^{J M_J \pi}(E)$ are energy-dependent expansion coefficients which depend on the asymptotic boundary conditions satisfied by the wave function $\Psi_{jE}^{J M_J \pi}$ at the energy E. In analogy with (5.6) we expand the basis functions $\psi_k^{J M_J \pi}$ as follows:

$$\begin{aligned}\psi_k^{J M_J \pi}(\mathbf{X}_{N+1}) = \mathcal{A} \sum_{i=1}^{n} \sum_{j=1}^{n_c} \overline{\Phi}_i^{J M_J \pi}(\mathbf{X}_N; \hat{\mathbf{r}}_{N+1}\sigma_{N+1}) r_{N+1}^{-1} u_{ij}^0(r_{N+1}) a_{ijk}^{J\pi} \\ + \sum_{i=1}^{m} \chi_i^{J M_J \pi}(\mathbf{X}_{N+1}) b_{ik}^{J\pi}, \quad k = 1, \ldots, n_t,\end{aligned} \tag{5.147}$$

where n is the number of channel functions, n_c is the number of continuum orbitals retained in each channel, m is the number of quadratically integrable functions and $n_t = n n_c + m$ is the total number of linearly independent basis functions retained in this expansion. As noted earlier, the values of n, n_c, m and n_t are now considerably larger than the values corresponding to equivalent calculations using the non-relativistic expansion (5.6).

In order to determine the channel functions $\overline{\Phi}_i^{J M_J \pi}$ in (5.147) we commence with the target states $\Phi_i(\alpha_i L_i S_i M_{L_i} M_{S_i} \pi_i | \mathbf{X}_N)$ which diagonalize the non-relativistic target Hamiltonian $H_N^{\rm NR}$ as described in Sect. 2.2. We then recouple these states as in (5.121) to yield target states $\Phi_i(\alpha_i L_i S_i J_i M_{J_i} \pi_i | \mathbf{X}_N)$ belonging to the quantum numbers $L_i S_i J_i M_{J_i} \pi_i$. If relativistic effects in the target are not important then the channel functions are determined in the pair-coupling scheme defined by (5.116) as follows:

$$\begin{aligned}
&\overline{\Phi}_i^{J M_J \pi}(\mathbf{X}_N; \hat{\mathbf{r}}_{N+1} \sigma_{N+1}) \\
&= \sum_{M_{J_i} m_{\ell_i} M_{K_i} m_i} \sum (J_i M_{J_i} \ell_i m_{\ell_i} | K_i M_{K_i}) (K_i M_{K_i} \tfrac{1}{2} m_i | J M_J) \\
&\quad \times \Phi_i(\alpha_i L_i S_i J_i M_{J_i} \pi_i | \mathbf{X}_N) Y_{\ell_i m_{\ell_i}}(\theta_{N+1}, \phi_{N+1}) \chi_{\frac{1}{2} m_i}(\sigma_{N+1}). \qquad (5.148)
\end{aligned}$$

However, with increasing nuclear charge number Z the channel functions $\overline{\Phi}_i^{J M_J \pi}$ can no longer be accurately represented by eigenstates of the total orbital and spin angular momentum operators $\mathbf{L}_i^2$ and $\mathbf{S}_i^2$, as assumed in (5.121) and (5.148). If the relativistic effects are not too large, then the target states can be represented by an expansion over the target states defined by (5.121) for each $J_i M_{J_i} \pi_i$ symmetry. Following our discussion in Sect. 5.4.1 we write

$$\Phi_i(\Delta_i J_i M_{J_i} \pi_i | \mathbf{X}_N) = \sum_{\alpha_i L_i S_i} f(\Delta_i J_i \pi_i; \alpha_i L_i S_i \pi_i) \Phi_i(\alpha_i L_i S_i J_i M_{J_i} \pi_i | \mathbf{X}_N), \qquad (5.149)$$

where the summation in this equation goes over all target states retained in the original R-matrix expansion in (5.147) with the given $J_i \pi_i$ symmetry, and where we have introduced a level parameter Δ_i in this equation to distinguish different target states with the same $J_i M_{J_i} \pi_i$ symmetry. The term-coupling coefficients $f(\Delta_i J_i \pi_i; \alpha_i L_i S_i \pi_i)$ in (5.149) are determined by diagonalizing the target Breit–Pauli Hamiltonian $H_N^{\rm BP}$ in the basis $\Phi_i(\alpha_i L_i S_i J_i M_{J_i} \pi_i | \mathbf{X}_N)$ for each $J_i \pi_i$ symmetry as in (5.123) yielding the target energies $e_i^{J_i \pi_i}$. Equation (5.148), defining the channel functions, is then replaced by

$$\begin{aligned}
&\overline{\Phi}_i^{J M_J \pi}(\mathbf{X}_N; \hat{\mathbf{r}}_{N+1} \sigma_{N+1}) \\
&= \sum_{M_{J_i} m_{\ell_i} M_{K_i} m_i} \sum (J_i M_{J_i} \ell_i m_{\ell_i} | K_i M_{K_i}) (K_i M_{K_i} \tfrac{1}{2} m_i | J M_J) \\
&\quad \times \Phi_i(\Delta_i J_i M_{J_i} \pi_i | \mathbf{X}_N) Y_{\ell_i m_{\ell_i}}(\theta_{N+1}, \phi_{N+1}) \chi_{\frac{1}{2} m_i}(\sigma_{N+1}). \qquad (5.150)
\end{aligned}$$

Next the quadratically integrable functions $\chi_i^{J M_J \pi}$ in (5.147) can be obtained by recoupling the quadratically integrable functions χ_i^{Γ} retained in (5.6) in the absence of relativistic effects. In analogy with (5.121) we write

$$\chi_i^{J M_J \pi}(\alpha L S J M_J \pi | \mathbf{X}_{N+1}) = \sum_{M_L M_S} (L M_L S M_S | J M_J) \chi_i^{\Gamma}(\alpha L S M_L M_S \pi | \mathbf{X}_{N+1}). \tag{5.151}$$

Finally, the continuum basis orbitals $u_{ij}^0(r)$ in (5.147) can be determined using a similar approach to that described in Sect. 5.3.

Having defined the channel functions, quadratically integrable functions and continuum basis orbitals in (5.147), we can determine the coefficients $a_{ijk}^{J\pi}$ and $b_{ik}^{J\pi}$ by diagonalizing $H_{N+1}^{\mathrm{BP}} + \mathcal{L}_{N+1}$ in this basis as follows:

$$\langle \psi_k^{J M_J \pi} | H_{N+1}^{\mathrm{BP}} + \mathcal{L}_{N+1} | \psi_{k'}^{J M_J \pi} \rangle_{\mathrm{int}} = E_k^{J\pi} \delta_{kk'}, \quad k,\ k' = 1, \ldots, n_t, \tag{5.152}$$

where the Bloch operator $\mathcal{L}_{N+1}$ in this equation ensures that $H_{N+1}^{\mathrm{BP}} + \mathcal{L}_{N+1}$ is hermitian in the space of functions satisfying arbitrary boundary conditions on the surface of the sphere of radius $r = a_0$ enveloping the internal region. It is defined by (5.8) since we will see that the relativistic terms in the Breit–Pauli Hamiltonian do not modify the form of the coupled second-order differential equations, given by (5.159), which are satisfied by the scattered electron on the boundary $r = a_0$ of the internal region, for the intermediate values of Z of interest in this section.

We then proceed using a straightforward extension of the approach adopted in non-relativistic electron collisions with atoms and atomic ions, described in Sect. 5.1.2. The reduced radial wave functions $F_{ij}^{J\pi}(r)$, describing the motion of the scattered electron in the ith channel, satisfy the equation

$$F_{ij}^{J\pi}(a_0) = \sum_{i'=1}^{n} R_{ii'}^{J\pi}(E) \left(a_0 \frac{\mathrm{d}F_{i'j}^{J\pi}}{\mathrm{d}r} - b_0 F_{i'j}^{J\pi} \right)_{r=a_0}, \quad i = 1, \ldots, n, \tag{5.153}$$

where the elements of the R-matrix $R_{ii'}^{J\pi}(E)$ are defined by

$$R_{ii'}^{J\pi}(E) = \frac{1}{2a_0} \sum_{k=1}^{n_t} \frac{w_{ik}^{J\pi} w_{i'k}^{J\pi}}{E_k^{J\pi} - E}, \quad i,\ i' = 1, \ldots, n, \tag{5.154}$$

the functions $F_{ij}^{J\pi}(r)$ are defined by

$$F_{ij}^{J\pi}(r_{N+1}) = \langle r_{N+1}^{-1} \overline{\Phi}_i^{J M_J \pi} | \Psi_{jE}^{J M_J \pi} \rangle', \quad i = 1, \ldots, n \tag{5.155}$$

and the surface amplitudes $w_{ik}^{J\pi}$ are defined by

$$w_{ik}^{J\pi} = \langle r_{N+1}^{-1} \overline{\Phi}_i^{JM_J\pi} | \psi_k^{JM_J\pi} \rangle'_{r_{N+1}=a_0}$$
$$= \sum_{j=1}^{n_c} u_{ij}^0(a_0) a_{ijk}^{J\pi}, \quad i = 1, \ldots, n, \quad k = 1, \ldots, n_t. \tag{5.156}$$

A Buttle correction to the R-matrix and wave function can be included as discussed for non-relativistic electron collisions in Sect. 5.3.2. We can also write down an alternative expression for the reduced radial wave functions $F_{ij}^{J\pi}(r)$ by substituting for $\Psi_{jE}^{JM_J\pi}$ from (5.146) into (5.155) giving

$$F_{ij}^{J\pi}(r_{N+1}) = \sum_{k=1}^{n_t} \langle r_{N+1}^{-1} \overline{\Phi}_i^{JM_J\pi} | \psi_k^{JM_J\pi} \rangle' A_{kj}^{JM_J\pi}(E), \quad i = 1, \ldots, n. \tag{5.157}$$

As in (5.20), (5.21) and (5.22), the primes on the Dirac brackets in (5.155), (5.156) and (5.157) mean that the integrations are carried out over the space and spin coordinates of all $N + 1$ electrons in the internal region, except the radial coordinate r_{N+1} of the scattered electron, where the resulting integral is independent of the magnetic quantum number M_J. Finally, we note that (5.153) provides the boundary condition for the solution of the electron–atom collision problem in the external region.

5.4.2.2 External Region Solution

In the external region, corresponding to $a_0 \le r \le a_p$ in Fig. 5.1, electron exchange and correlation effects between the scattered electron and the target atom or atomic ion can be neglected and (5.147) reduces to

$$\Psi_{jE}^{JM_J\pi}(\mathbf{X}_{N+1}) = \sum_{i=1}^{n} \overline{\Phi}_i^{JM_J\pi}(\mathbf{X}_N; \hat{\mathbf{r}}_{N+1}\sigma_{N+1}) r_{N+1}^{-1} F_{ij}^{J\pi}(r_{N+1}), \quad r_{N+1} \ge a_0, \tag{5.158}$$

where j labels the linearly independent solutions. Also, the channel functions $\overline{\Phi}_i^{JM_J\pi}$ in (5.158) are defined by either (5.148) or (5.150), depending on the importance of relativistic effects in the target, and $F_{ij}^{J\pi}(r)$ are energy-dependent reduced radial wave functions, defined by (5.155). Following our discussion of non-relativistic collisions given in Sect. 5.1.3, the coupled equations satisfied by the reduced radial functions $F_{ij}^{J\pi}(r)$ in (5.158) are obtained by substituting (5.158) into the Breit–Pauli equation (5.145) and projecting onto the channel functions $\overline{\Phi}_i^{JM_J\pi}$. We find that the functions $F_{ij}^{J\pi}(r)$ satisfy the following set of coupled second-order differential equations:

$$\left(\frac{\mathrm{d}^2}{\mathrm{d}r^2} - \frac{\ell_i(\ell_i+1)}{r^2} + \frac{2(Z-N)}{r} + k_i^2 \right) F_{ij}^{J\pi}(r) = 2 \sum_{i'=1}^{n} V_{ii'}^{J\pi}(r) F_{i'j}^{J\pi}(r),$$
$$i = 1, \ldots, n, \quad r \ge a_0, \tag{5.159}$$

where ℓ_i is the orbital angular momentum of the scattered electron, k_i^2 is the square of the wave number of the scattered electron defined by

$$k_i^2 = 2\left(E - e_i^{J_i\pi_i}\right), \quad i = 1, \ldots, n \tag{5.160}$$

and the potential matrix $V_{ii'}^{J\pi}(r)$ is defined by

$$V_{ii'}^{J\pi}(r_{N+1}) = \langle r_{N+1}^{-1}\overline{\Phi}_i^{JM_J\pi}(\mathbf{X}_N; \hat{\mathbf{r}}_{N+1}\sigma_{N+1}) \left| \sum_{k=1}^{N} \frac{1}{r_{kN+1}} - \frac{N}{r_{N+1}} \right| \times r_{N+1}^{-1}\overline{\Phi}_{i'}^{JM_J\pi}(\mathbf{X}_N; \hat{\mathbf{r}}_{N+1}\sigma_{N+1})\rangle', \quad i,\ i' = 1, \ldots, n, \tag{5.161}$$

which replaces (2.66) when relativistic terms are retained in the Hamiltonian. Following our discussion in Sect. 2.3, this potential matrix can be written as a summation over inverse powers of r as follows:

$$V_{ii'}^{J\pi}(r) = \sum_{\lambda=1}^{\lambda_{\max}} \alpha_{ii'\lambda}^{J\pi} r^{-\lambda-1}, \quad r \geq a_0, \quad i,\ i' = 1, \ldots, n, \tag{5.162}$$

where the long-range potential coefficients $\alpha_{ii'\lambda}^{J\pi}$ are defined, in analogy with (2.74), by the equation

$$\alpha_{ii'\lambda}^{J\pi} = \langle r_{N+1}^{-1}\overline{\Phi}_i^{JM_J\pi}(\mathbf{X}_N; \hat{\mathbf{r}}_{N+1}\sigma_{N+1}) \left| \sum_{k=1}^{N} r_k^{\lambda} P_\lambda(\cos\theta_{kN+1}) \right| \times r_{N+1}^{-1}\overline{\Phi}_{i'}^{JM_J\pi}(\mathbf{X}_N; \hat{\mathbf{r}}_{N+1}\sigma_{N+1})\rangle', \quad i,\ i' = 1, \ldots, n, \quad \lambda = 1, \ldots, \lambda_{\max}. \tag{5.163}$$

We derive explicit expressions for these coefficients in Appendix D.1; see (D.25) and (D.26).

The solution of (5.159) can be obtained by sub-dividing the external region into p sub-regions, as illustrated in Fig. 5.1, and propagating the R-matrix for each required energy from $r = a_0$ to a_p as described in Appendix E. Since the expression for the long-range potential coefficients, defined by (D.25) and (D.26), is diagonal in the quantum number K_i, defined following (5.116), then the set of second-order differential equations (5.159) sub-divide into two uncoupled sets of equations depending on whether $K_i = J - \frac{1}{2}$ or $K_i = J + \frac{1}{2}$. This enables more efficient R-matrix propagator methods to be used with considerable saving in computational effort, as discussed in Appendix E.6. This is analogous to the situation in non-relativistic collisions of electrons with atoms and atomic ions, discussed in Sect. 5.1.3, where the corresponding second-order differential equations sub-divide into two uncoupled sets of equations depending on whether the target spin $S_i = S - \frac{1}{2}$ or $S_i = S + \frac{1}{2}$.

5.4.2.3 Asymptotic Region Solution

The solution of the time-independent Breit–Pauli equation (5.145) in the asymptotic region, corresponding to $a_p \le r \le \infty$ proceeds as in non-relativistic electron collisions described in Sect. 5.1.4. In this region (5.147) again reduces to (5.158), where the reduced radial wave functions $F_{ij}^{J\pi}(r)$ satisfy the coupled second-order differential equations (5.159). As in Sect. 5.1.4 we assume that the radius a_p is chosen large enough that one of the asymptotic expansion methods discussed in Appendix F.1 gives an accurate solution of (5.159) in this region. We are then able to use these solutions to relate the $n_a \times n_a$-dimensional K-matrix $\mathbf{K}^{J\pi}(E)$ to the $n \times n$-dimensional R-matrix $\mathbf{R}^{J\pi}(E)$ at $r = a_p$, where n_a is the number of open channels at the energy under consideration. Finally, having determined the K-matrix we can determine the S-matrix and hence the T-matrix, as described in Sect. 5.1.4.

The total and partial wave cross sections for transitions between fine-structure levels of the target are then given by (5.128) and (5.129). We see that the definition of the cross section is formally the same as that given in Sect. 5.4.1, where the transformed K-matrices, defined by (5.119) and (5.124), are used to calculate the S- and T-matrices. However, using the Breit–Pauli Hamiltonian correctly accounts for the kinematics of the scattered electron and gives a consistent treatment of the collision above and below thresholds.

5.4.3 Frame-Transformation Theory

One computational difficulty, which arises as a result of using the Breit–Pauli Hamiltonian (5.133) rather than the non-relativistic Hamiltonian (5.3), is that the number of coupled channels included in the internal region expansion (5.147) is greatly increased for the same set of target states included in the non-relativistic expansion (5.6). This results in a corresponding increase in the size of the Hamiltonian matrices in (5.152) that must be diagonalized. For example in e^-–Fe II collisions, considered in Sect. 5.6.5, if all $LS\pi$-coupled target states corresponding to the five target configurations

$$3d^6 4s,\ 3d^7,\ 3d^6 4p,\ 3d^5 4s^2,\ 3d^5 4s4p \tag{5.164}$$

are included in the expansion of the total wave function then, when relativistic effects are omitted, a maximum of 818 coupled channels are obtained for total spin state $S = 1$ and a maximum of 354 coupled channels are obtained for total spin state $S = 2$. On the other hand, if relativistic Breit–Pauli terms are included in the Hamiltonian then the calculation must be carried out in $J\pi$-coupling which results in a maximum of 5,076 coupled channels. However, it is pointed out in Sect. 5.6.5 that converged results at low energies may require target states from additional configurations to be included in the R-matrix expansion. For example, we see from Table 5.2 that if target states from the 10 configurations, illustrated in Fig. 5.10, are included in the expansion then the maximum number of coupled channels increases

to 2,575 in $LS\pi$-coupling and to 15,576 in $J\pi$-coupling. In both the 5 and 10 target configuration cases, including relativistic terms in the Hamiltonian increases the time required to diagonalize the Hamiltonian matrices by more than two orders of magnitude, making the calculations much more demanding.

In order to address this computational difficulty we observe that for many low-energy electron–atom and electron–ion collision calculations, where relativistic effects play an important role, it is often appropriate to omit or partly omit the relativistic terms in the Hamiltonian in the internal region, although these terms must still be included in the external and asymptotic regions in order to obtain accurate threshold energies and hence accurate scattering amplitudes and cross sections. Also, we will see in Chap. 6, where we consider electron collisions at intermediate energies, that it is often necessary to include a large number of pseudostates to allow for inelastic effects above the ionization threshold. In this case, it is not necessary to include relativistic effects involving these pseudostates although these effects can still be important for the physical states included in the R-matrix expansion. In a similar way, it is not necessary to include relativistic effects in the higher continuum basis orbitals represented by the expansion over j in (5.147) which are included to give a converged R-matrix expansion.

In the frame-transformation theory (FTT) method, the relativistic Breit–Pauli terms in the Hamiltonian are omitted in the internal region in the high-energy spectrum, where they are dominated by the electron kinetic energy contribution to the total energy. However, they can be included in the internal region in the low-energy spectrum. These terms are then fully included in the external and asymptotic regions, where they give rise to the relativistic term splitting of the channels which plays an important role, particularly for low-energy electron collisions with atoms and near neutral ions. The corresponding partitioning of configuration space is illustrated in Fig. 5.3, which can be compared with Fig. 5.1 applicable when the FTT method is not used.

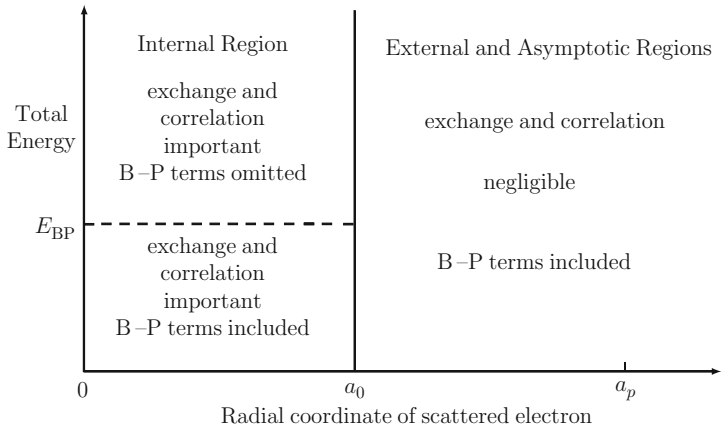

Fig. 5.3 Partitioning of configuration space in the FTT method showing the procedure for including relativistic Breit–Pauli (B–P) terms in the internal, external and asymptotic regions

In the FTT method the calculation is carried out in the following four steps:

(i) The non-relativistic Hamiltonian H_{N+1} defined by (5.3) is first diagonalized in the internal region in the basis (5.6) for all $LS\pi$ values of importance. The R-matrices $\mathbf{R}^{\Gamma}(E)$ on the boundary $r = a_0$ of the internal region defined by (5.19) are calculated in the usual way, as described in Sect. 5.1.2. If required, this step of the calculation can be made more efficient by using the partitioned R-matrix method discussed in Sect. 5.3.4.

(ii) The R-matrices $\mathbf{R}^{\Gamma}(E)$ at $r = a_0$ calculated in step (i) are transformed from the $LS\pi$-coupling scheme to the pair-coupling scheme by transformation (5.119). Also, if relativistic effects in the target are important, a further transformation (5.124) of the R-matrices to full intermediate coupling is made using term-coupling coefficients, yielding the R-matrices $\mathbf{R}^{J\pi}(E)$ for each $J\pi$. This can be achieved using the computer program FINE discussed in Sect. 5.1.1.

(iii) The R-matrices calculated in step (ii) are partitioned for each $J\pi$ into two sub-matrices $\mathbf{R}_A^{J\pi}(E)$ and $\mathbf{R}_B^{J\pi}(E)$ as follows:

$$\mathbf{R}^{J\pi}(E) = \mathbf{R}_A^{J\pi}(E) + \mathbf{R}_B^{J\pi}(E). \tag{5.165}$$

The sub-matrix $\mathbf{R}_A^{J\pi}(E)$ corresponds to the terms in the R-matrix expansion where the energies of the R-matrix poles E_k^{Γ} satisfy $E_k^{\Gamma} > E_{\mathrm{BP}}$ and the sub-matrix $\mathbf{R}_B^{J\pi}(E)$ corresponds to the remaining terms in the R-matrix expansion where the energies of the R-matrix poles E_k satisfy $E_k^{\Gamma} \leq E_{\mathrm{BP}}$, where the energy E_{BP} shown in Fig. 5.3 separates the high-energy spectrum from the low-energy spectrum in the internal region. The Breit–Pauli Hamiltonian H_{N+1}^{BP}, defined in (5.133), is then diagonalized in the internal region in the basis defined by the sub-matrix $\mathbf{R}_B^{J\pi}(E)$ for each $J\pi$, and the corresponding R-matrix $\boldsymbol{\mathcal{R}}_B^{J\pi}(E)$ calculated. The R-matrix replacing (5.165) is then given by

$$\mathbf{R}_{\mathrm{FTT}}^{J\pi}(E) = \mathbf{R}_A^{J\pi}(E) + \boldsymbol{\mathcal{R}}_B^{J\pi}(E). \tag{5.166}$$

In some situations involving electron collisions with intermediate Z atoms and ions it is appropriate to choose E_{BP} so that $E_k^{\Gamma} > E_{\mathrm{BP}}$ for all k. Hence, in this case step (iii) is omitted and

$$\mathbf{R}_{\mathrm{FTT}}^{J\pi}(E) = \mathbf{R}_A^{J\pi}(E). \tag{5.167}$$

This approach has been used by Cassidy et al. [204] who carried out low-energy electron collision calculations for Ni II. In this calculation the non-relativistic program RMATRXII was used to determine the surface amplitudes for the R-matrix $\mathbf{R}^{\Gamma}(E)$ on the boundary $r = a_0$ of the internal region. The program FINE, discussed in Sect. 5.1.1, was then used to transform these surface amplitudes to full intermediate coupling yielding the R-matrix $\mathbf{R}_{\mathrm{FTT}}^{J\pi}(E)$ on the boundary $r = a_0$.

(iv) Finally, the R-matrix $\mathbf{R}^{J\pi}_{\mathrm{FTT}}(E)$ at $r = a_0$ provides the boundary condition at $r = a_0$ for determining the solution in the external and asymptotic regions using the Breit–Pauli Hamiltonian, as discussed in Sect. 5.4.2. As shown in Sect. 5.4.2 the corresponding coupled second-order differential equations subdivide into two uncoupled sets of equations depending on whether the quantum number $K_i = J - \frac{1}{2}$ or $J + \frac{1}{2}$ with considerable saving in computational effort. Finally, the K-matrix, S-matrix and T-matrix are determined for each energy E and $J\pi$, as described in Sect. 5.4.2, and the cross sections determined. We see in this way that the FTT method correctly accounts for the kinematics of the scattered electron giving a consistent treatment of the collision above and below thresholds.

In conclusion, we observe that the ICFT method, discussed in Sect. 5.4.1, can be regarded as a further approximation to the FTT method. In the ICFT method the R-matrices $\mathbf{R}^{\Gamma}(E)$ at $r = a_0$ resulting from step (i) are propagated outwards across the external region in $LS\pi$-coupling, neglecting the relativistic terms in the Hamiltonian in this region. The transformation to full intermediate coupling is then carried out on the K-matrices in the asymptotic region, rather than on the R-matrices on the internal region boundary in the FTT method. Hence the FTT method includes the relativistic terms in the Hamiltonian fully in the external region. This can be important for neutral targets where the ICFT method, which uses multichannel quantum defect theory, is not applicable and for low-energy electron collisions with targets where the relativistic term splitting is large. However, both methods reduce the size of the very large Hamiltonian matrices which arise when relativistic terms in the Breit–Pauli Hamiltonian are fully included in the internal region and are therefore much less demanding computationally.

5.5 Dirac R-Matrix Theory

In this section we extend R-matrix theory to treat electron collisions with heavy atoms and atomic ions where the nuclear charge number Z is large and as a result relativistic effects must be included using the Dirac Hamiltonian. We commence in Sect. 5.5.1 by introducing the Dirac Hamiltonian describing electron collisions with an N-electron target atom or ion. We then summarize the historical background of work in this area commencing with the first introduction of Dirac R-matrix theory in nuclear physics and its first application in the study of electron–atom collisions. We conclude this section by summarizing recent theoretical developments and computer programs. Then in Sect. 5.5.2 we commence our detailed analysis of Dirac R-matrix theory by considering the solution of the time-independent Dirac equation in an internal region yielding the R-matrix on the boundary of this region. This analysis takes advantage of our discussion of the solution of the Dirac equation in potential scattering in Sect. 1.6 and our discussion of Dirac R-matrix theory in potential scattering in Sect. 4.6. We also consider the convergence of the

solution on the boundary of the internal region when radial continuum basis orbitals satisfying homogeneous boundary conditions are used; a problem which we also considered in non-relativistic potential scattering in Sect. 4.1. Having determined the R-matrix on the boundary of the internal region, we then consider the solution of the Dirac equation, or the equivalent Schrödinger equation, in the external region in Sect. 5.5.3 and in the asymptotic region in Sect. 5.5.4 which yields the K-matrix, S-matrix and collision cross sections. Finally, in Sect. 5.5.5 we consider the procedure usually adopted for calculating the radial continuum basis orbitals in the expansion of the wave function in the internal region. Since in many applications these orbitals satisfy homogeneous boundary conditions, similar to those adopted in many non-relativistic calculations, we conclude our analysis in Sect. 5.5.6 by describing the procedure for calculating a Buttle correction to the R-matrix which is required in this case.

5.5.1 Introduction and Computer Programs

The Dirac Hamiltonian describing electron collisions with N-electron target atoms or ions with nuclear charge number Z is given in atomic units by

$$H^{\mathrm{D}}_{N+1} = \sum_{i=1}^{N+1} \left(\mathrm{c}\boldsymbol{\alpha}.\mathbf{p}_i + \beta' \mathrm{c}^2 - \frac{Z}{r_i} \right) + \sum_{i>j=1}^{N+1} \frac{1}{r_{ij}}, \tag{5.168}$$

where, adopting the notation introduced in potential scattering in Sect. 1.6, $\boldsymbol{\alpha}$ and $\beta' = \beta - I_4$ are 4×4-dimensional Dirac matrices defined by (1.233) and (1.234). The solution of the time-independent Dirac equation

$$H^{\mathrm{D}}_{N+1} \Psi = E \Psi \tag{5.169}$$

is then required for each set of conserved quantum numbers J, M_J and π, where J is the total angular momentum quantum number, M_J is the corresponding magnetic quantum number in some preferred direction and π is the total parity.

Dirac R-matrix theory was first introduced by Goertzel [385] who extended Wigner [968, 969] and Wigner and Eisenbud [972] R-matrix theory of nuclear reactions using the Dirac equation and a theory of electron–hydrogen atom collisions using the Dirac Hamiltonian was developed by Carse and Walker [203]. Dirac R-matrix theory of atomic collisions was first formulated by Chang [211–213] who wrote a computer program which he used to study electron collisions with Ne II and Ne photoionization. Later, Thumm and Norcross [926, 927] carried out low-energy electron–Cs collision calculations and Szmytkowski and Hinze [903–908] analysed the application of Dirac R-matrix theory in electron–atom collisions with emphasis on the convergence of the R-matrix expansion.

Recent work using Dirac R-matrix theory to study electron–atom collisions is based on the development of the general-purpose relativistic atomic structure program GRASP by Grant et al. [279, 408–410, 413–415, 514, 625, 718, 719]. As well

as calculating the target states used in electron–atom collision calculations described below, GRASP enables oscillator strengths and radiative decay rates for high Z atoms and ions to be determined. It also includes the facility for calculating corrections to the electron–electron interaction considered by Breit [131–133], as well as other quantum electrodynamic (QED) corrections.

Following the development of the relativistic atomic structure program GRASP, Norrrington and Grant [696, 697] initiated the development of a general electron–atom Dirac atomic R-matrix collision program DARC which they used to study electron collisions with Ne II, Fe VII and Fe XXIII. Later further calculations were carried out by Wijesundera et al. [973–975], Ait-Tahar et al. [6] and other workers to study electron collisions with a wide range of heavy atoms and atomic ions and a detailed description of the program has been written by Norrington and Grant [698]. The theory and the DARC program have been further developed by Badnell [32] to treat electron collisions with atoms and atomic ions at intermediate energy, extending the analysis presented in Chap. 6, and recent developments of the theory have been discussed by Grant [411, 412].

5.5.2 Internal Region Solution

Following our discussion of non-relativistic R-matrix theory of electron–atom collisions in Sect. 5.1 we partition configuration space into an internal region, an external region and an asymptotic region, as shown in Fig. 5.1. We consider first the solution of the Dirac equation (5.169) in the internal region $0 \le r \le a_0$ for each set of conserved quantum numbers J, M_J and π. The first step is to determine the target states and pseudostates included in the expansion of the collision wave function. These states are defined in terms of four-component spinor basis functions $\phi_i(\mathbf{x})$ which can be written following (1.244) as

$$\phi_i(\mathbf{x}) = \frac{1}{r}\begin{pmatrix} P_i^a(r)\eta_{\kappa_i m_i}(\hat{\mathbf{r}},\sigma) \\ \mathrm{i}Q_i^a(r)\eta_{-\kappa_i m_i}(\hat{\mathbf{r}},\sigma)\end{pmatrix}, \tag{5.170}$$

where the two-component spinors $\eta_{\kappa m}(\hat{\mathbf{r}},\sigma)$ are defined by (1.245). Also in (5.170) the reduced radial orbitals $P_i^a(r)$ and $Q_i^a(r)$ are usually chosen to satisfy the orthonormality relations

$$\int_0^\infty [P_i^a(r)P_j^a(r) + Q_i^a(r)Q_j^a(r)]\mathrm{d}r = \delta_{ij}, \quad \text{all } i \text{ and } j, \tag{5.171}$$

for each κ defined by (1.250) and Table 1.1. The radius a_0 of the internal region in Dirac R-matrix theory is then chosen so that the reduced radial orbitals $P_i^a(r)$ and $Q_i^a(r)$ satisfy

$$P_i^a(r) \approx 0, \quad Q_i^a(r) \approx 0, \quad r \ge a_0, \quad \text{all } i, \tag{5.172}$$

which ensures that electron exchange and correlation effects between the scattered electron and the target atom are negligible in the external and asymptotic regions, discussed below. The target states and pseudostates $\Phi_i^{J_i M_{J_i} \pi_i}(\mathbf{X}_N)$, which are constructed from these orbitals are then chosen to diagonalize the target Hamiltonian H_N^{D} as follows:

$$\langle \Phi_i^{J_i M_{J_i} \pi_i} | H_N^{\mathrm{D}} | \Phi_j^{J_j M_{J_j} \pi_j} \rangle = e_i^{J_i \pi_i} \delta_{ij}, \tag{5.173}$$

for each $J_i M_{J_i} \pi_i$, where J_i is the total target angular momentum quantum number, M_{J_i} is the corresponding target magnetic quantum number, π_i is the target parity and $e_i^{J_i \pi_i}$ is the target energy.

Having determined the target states and pseudostates the collision wave function $\Psi_{jE}^{J M_J \pi}(\mathbf{X}_{N+1})$ at a total energy E can be expanded in analogy with (5.5) as follows:

$$\Psi_{jE}^{J M_J \pi}(\mathbf{X}_{N+1}) = \sum_k \psi_k^{J M_J \pi}(\mathbf{X}_{N+1}) A_{kj}^{J\pi}(E), \tag{5.174}$$

where j labels the linearly independent solutions of (5.169), $\psi_k^{J M_J \pi}$ are energy-independent basis functions and $A_{kj}^{J\pi}(E)$ are energy-dependent expansion coefficients, which depend on the asymptotic boundary conditions satisfied by the wave function $\Psi_{jE}^{J M_J \pi}$ at the energy E. We then expand the basis functions $\psi_k^{J M_J \pi}$ in (5.174) for each $J M_J \pi$ in analogy with (5.6) as follows:

$$\begin{aligned} \psi_k^{J M_J \pi}(\mathbf{X}_{N+1}) = \mathcal{A} \sum_{i=1}^{n} \sum_{j=1}^{n_c} \overline{\Phi}_i^{J M_J \pi}(\mathbf{X}_N; \hat{\mathbf{r}}_{N+1} \sigma_{N+1}) r_{N+1}^{-1} u_{ij}^0(r_{N+1}) a_{ijk}^{J\pi} \\ + \sum_{i=1}^{m} \chi_i^{J M_J \pi}(\mathbf{X}_{N+1}) b_{ik}^{J\pi}, \quad k = 1, \ldots, n_t, \end{aligned} \tag{5.175}$$

where n is the number of channels retained in the expansion, n_c is the number of continuum basis functions retained in each channel, m is the number of quadratically integrable functions and $n_t = n n_c + m$ is the total number of linearly independent basis functions in this expansion. The channel functions $\overline{\Phi}_i^{J M_J \pi}$ are defined by coupling the target states and pseudostates $\Phi_i^{J_i M_i \pi_i}(\mathbf{X}_N)$ with the relativistic spin–angle functions describing the scattered electron, as follows:

$$\begin{aligned} &\overline{\Phi}_i^{J M_J \pi}(\mathbf{X}_N; \hat{\mathbf{r}}_{N+1} \sigma_{N+1}) \\ &= \sum_{M_i m_i} (J_i M_i j_i m_i | J M_J) \Phi_i^{J_i M_i \pi_i}(\mathbf{X}_N) \phi_i^{j_i m_i}(\hat{\mathbf{r}}_{N+1}, \sigma_{N+1}), \end{aligned} \tag{5.176}$$

where the four-component spin–angle functions $\phi_i^{j_i m_i}(\hat{\mathbf{r}}, \sigma)$ describing the scattered electron are defined by

$$\phi_i^{j_i m_i}(\hat{\mathbf{r}}, \sigma) = \begin{pmatrix} \eta_{\kappa_i m_i}(\hat{\mathbf{r}}, \sigma) \\ \mathrm{i}\eta_{-\kappa_i m_i}(\hat{\mathbf{r}}, \sigma) \end{pmatrix}. \tag{5.177}$$

As in (5.170), the spin–angle functions $\eta_{\kappa_i m_i}(\hat{\mathbf{r}}, \sigma)$ in this equation are two-component spinors defined by (1.245), where the angular momentum quantum number j_i is given in terms of the eigenvalue κ_i by (1.250). Finally, the radial motion of the scattered electron in the internal region is described by the two-component reduced radial continuum basis functions $u_{ij}^0(r)$ in (5.175) which are defined by

$$u_{ij}^0(r) = \begin{pmatrix} p_{ij}^0(r) \\ q_{ij}^0(r) \end{pmatrix}, \quad i = 1, \ldots, n, \quad 0 \le r \le a_0, \tag{5.178}$$

where $p_{ij}^0(r)$ and $q_{ij}^0(r)$ are reduced radial continuum basis orbitals. Hence, in analogy with (1.244), we can rewrite (5.177) and (5.178) as a four-component spinor

$$r^{-1} u_{ij}^0(r) \phi_i^{j_i m_i}(\hat{\mathbf{r}}, \sigma) \equiv \frac{1}{r} \begin{pmatrix} p_{ij}^0(r) \eta_{\kappa_i m_i}(\hat{\mathbf{r}}, \sigma) \\ \mathrm{i} q_{ij}^0(r) \eta_{-\kappa_i m_i}(\hat{\mathbf{r}}, \sigma) \end{pmatrix}, \quad i = 1, \ldots, n, \quad 0 \le r \le a_0. \tag{5.179}$$

Following our discussion of Dirac R-matrix theory in potential scattering in Sect. 4.6, the reduced radial continuum basis orbitals $p_{ij}^0(r)$ and $q_{ij}^0(r)$ in (5.178) are chosen to vanish at the origin and to be non-zero on the boundary $r = a_0$ of the internal region. We describe a procedure in Sect. 5.5.5 which is often adopted for calculating these orbitals when they satisfy homogeneous boundary conditions at $r = a_0$.

Returning to (5.175), $\mathcal{A}$ is the usual antisymmetrization operator defined by (2.46) which ensures that each term in the first expansion is antisymmetric with respect to interchange of the space and spin coordinates of any pair of the $N + 1$ electrons. Also, the functions $\chi_i^{J M_J \pi}(\mathbf{X}_{N+1})$ are quadratically integrable functions which are constructed from the bound spinor basis functions $\phi_i(\mathbf{x})$ defined by (5.170) which are negligible by the boundary $r = a_0$ of the internal region. As in the non-relativistic expansion (5.6), these quadratically integrable functions are included in the expansion of the wave function for two reasons. First, for computational convenience the radial continuum basis orbitals $p_{ij}^0(r)$ and $q_{ij}^0(r)$ are usually constrained to be orthogonal to the physical orbitals used to construct the target states included in (5.175). Appropriate quadratically integrable functions constructed from these orbitals must therefore be included in the second expansion for completeness. The second reason for including the quadratically integrable functions is to represent short-range electron–electron correlation effects which are difficult to accurately represent by including a finite number of target states and pseudostates in the first expansion in (5.175).

We can determine the coefficients $a_{ijk}^{J\pi}$ and $b_{ik}^{J\pi}$ in (5.175) by diagonalizing the operator $H_{N+1}^{\mathrm{D}} + \mathcal{L}_{N+1}^{\mathrm{D}}$ as follows:

$$\langle \psi_k^{J M_J \pi} | H_{N+1}^{\mathrm{D}} + \mathcal{L}_{N+1}^{\mathrm{D}} | \psi_{k'}^{J M_J \pi} \rangle_{\mathrm{int}} = E_k^{J\pi} \delta_{kk'}, \quad k, k' = 1, \ldots, n_t, \tag{5.180}$$

where $\mathcal{L}_{N+1}^{\mathrm{D}}$ is a matrix Bloch operator, discussed below, and where the integrations in this equation are carried out over the space and spin coordinates of all $N+1$ electrons, the radial integrals being confined to the internal region. It follows from the rotational symmetry of the Hamiltonian and the Bloch operator that the coefficients $a_{ijk}^{J\pi}$ and $b_{ik}^{J\pi}$ and the energy $E_k^{J\pi}$ depend on J and π but are independent of the magnetic quantum number M_J.

The matrix Bloch operator $\mathcal{L}_{N+1}^{\mathrm{D}}$ in (5.180), which operates only on the two-component space part of the scattered electron wave function, is introduced, as in (5.7), so that $H_{N+1}^{\mathrm{D}} + \mathcal{L}_{N+1}^{\mathrm{D}}$ is hermitian in the space of quadratically integrable functions $\psi^{(1)}$ and $\psi^{(2)}$ which vanish at the origin and satisfy arbitrary boundary conditions on the surface $r = a_0$ of the internal region. Hence, in analogy with (5.9), it follows that

$$\langle \psi^{(1)} | H_{N+1}^{\mathrm{D}} + \mathcal{L}_{N+1}^{\mathrm{D}} | \psi^{(2)} \rangle_{\mathrm{int}} - \langle \psi^{(2)} | H_{N+1}^{\mathrm{D}} + \mathcal{L}_{N+1}^{\mathrm{D}} | \psi^{(1)} \rangle_{\mathrm{int}} = 0, \tag{5.181}$$

where the integration is carried out over all $N+1$ electronic space and spin coordinates which are confined to the internal region. Following our discussion of Dirac R-matrix theory in potential scattering given in Sect. 4.6, the required matrix Bloch operator, which is a generalization of (4.260), is given by

$$\mathcal{L}_{N+1}^{\mathrm{D}} = \frac{1}{2}\mathrm{c} \sum_{i=1}^{N+1} \begin{pmatrix} -b' & 1 \\ -1 & b'^{-1} \end{pmatrix} \delta(r_i - a_0), \tag{5.182}$$

where b' is an arbitrary constant. In the non-relativistic limit b' and hence b_{r}, introduced in Sect. 4.6, are related to the arbitrary constant b_0 in (5.8) by (4.257) and (4.258) which give

$$b' = \frac{b_r}{2a_0\mathrm{c}} = \frac{1}{2a_0\mathrm{c}}(b_0 + \kappa), \tag{5.183}$$

where κ is defined in terms of the orbital and total scattered electron angular momentum quantum numbers ℓ and j by (1.250) and Table 1.1. Hence b' and b_r will depend on the corresponding quantum numbers of the scattered electron in each channel.

We can now solve (5.169) in the internal region for each linearly independent solution defined by (5.174). In analogy with the procedure adopted in non-relativistic R-matrix theory in Sect. 5.1.2, we first include the Bloch operator term $\mathcal{L}_{N+1}^{\mathrm{D}} \Psi$ on both sides of (5.169) giving

$$\left(H_{N+1}^{\mathrm{D}} + \mathcal{L}_{N+1}^{\mathrm{D}} - E\right) \Psi_{jE}^{J M_J \pi} = \mathcal{L}_{N+1}^{\mathrm{D}} \Psi_{jE}^{J M_J \pi}. \tag{5.184}$$

Equation (5.184) then has the formal solution in the internal region given by

$$\Psi_{jE}^{J M_J \pi} = \left(H_{N+1}^{\mathrm{D}} + \mathcal{L}_{N+1}^{\mathrm{D}} - E\right)^{-1} \mathcal{L}_{N+1}^{\mathrm{D}} \Psi_{jE}^{J M_J \pi}. \tag{5.185}$$

The spectral representation of the Green's function $\left(H_{N+1}^{\mathrm{D}} + \mathcal{L}_{N+1}^{\mathrm{D}} - E\right)^{-1}$ in (5.185) can be obtained in terms of the R-matrix basis functions $\psi_k^{JM_J\pi}$ defined by (5.175) and (5.180) giving

$$|\Psi_{jE}^{JM_J\pi}\rangle = \sum_{k=1}^{n_t} |\psi_k^{JM_J\pi}\rangle \frac{1}{E_k^{J\pi} - E} \langle \psi_k^{JM_J\pi} | \mathcal{L}_{N+1}^{\mathrm{D}} | \Psi_{jE}^{JM_J\pi}\rangle. \tag{5.186}$$

We then project (5.186) onto the n channel functions $\overline{\Phi}_i^{JM_J\pi}(\mathbf{X}_N; \hat{\mathbf{r}}_{N+1}\sigma_{N+1})$, defined by (5.176), and substitute for the matrix Bloch operator $\mathcal{L}_{N+1}^{\mathrm{D}}$ defined by (5.182). We find using (5.174) and (5.175) that

$$\begin{aligned} F_{ij}^{J\pi}(r) = \frac{1}{2a_0} \sum_{i'=1}^{n} \sum_{k=1}^{n_t} \frac{v_{ik}^{J\pi}(r)\, [v_{i'k}^{J\pi}(a_0)]^{\mathrm{T}}}{E_k^{J\pi} - E} B_{i'}\; F_{i'j}^{J\pi}(a_0), \\ i = 1, \ldots, n, \quad 0 \le r < a_0, \end{aligned} \tag{5.187}$$

where the two-component reduced radial wave functions $F_{ij}^{J\pi}(r)$ are defined by

$$F_{ij}^{J\pi}(r_{N+1}) = \langle r_{N+1}^{-1} \overline{\Phi}_i^{JM_J\pi} | \Psi_{jE}^{JM_J\pi}\rangle', \quad i = 1, \ldots, n, \tag{5.188}$$

and where the two-component functions $v_{ik}^{J\pi}(r)$ are defined by

$$v_{ik}^{J\pi}(r_{N+1}) = \langle r_{N+1}^{-1} \overline{\Phi}_i^{JM_J\pi} | \psi_k^{JM_J\pi}\rangle', \quad i = 1, \ldots, n, \quad k = 1, \ldots, n_t. \tag{5.189}$$

As in (5.20) and (5.21), the primes on the Dirac brackets in (5.188) and (5.189) mean that the integrations and summations are carried out over the space and spin coordinates of all $N+1$ electrons in the internal region, except the radial coordinate r_{N+1} of the scattered electron. Also, as in (5.20) and (5.21), the contributions from the exchange terms and quadratically integrable functions in (5.175) to the integrals in (5.188) and (5.189) become negligibly small near the boundary $r = a_0$ of the internal region. Hence near the boundary $r = a_0$ the expression for $F_{ij}^{J\pi}(r)$ reduces to

$$F_{ij}^{J\pi}(r) = \sum_{k=1}^{n_t} v_{ik}^{J\pi}(r) A_{kj}^{J\pi}(E), \quad i = 1, \ldots, n, \quad r \lesssim a_0, \tag{5.190}$$

where the functions $v_{ik}^{J\pi}(r)$ can be expanded in terms of the radial continuum basis functions $u_{ij}^0(r)$ in (5.178) as follows:

$$v_{ik}^{J\pi}(r) = \sum_{j=1}^{n_c} u_{ij}^0(r) a_{ijk}^{J\pi}, \quad i = 1, \ldots, n, \quad k = 1, \ldots, n_t, \quad 0 \le r \le a_0. \tag{5.191}$$

Finally in (5.187), the B_i, which arise from the Bloch operator $\mathcal{L}_{N+1}^{\mathrm{D}}$ defined by (5.182), are 2×2 matrices given by

$$B_i = a_0 \mathrm{c} \begin{pmatrix} -b_i' & 1 \\ -1 & b_i'^{-1} \end{pmatrix}, \quad i = 1, \ldots, n, \tag{5.192}$$

where the elements b_i' in this matrix are defined in terms of the orbital and total scattered electron angular momentum quantum numbers in the ith channel by (5.183) and (1.250). Also in the above equations, $F_{ij}^{J\pi}(r)$, $v_{ik}^{J\pi}(r)$ and $u_{ij}^{0}(r)$ are two-component functions, where the radial continuum basis functions $u_{ij}^{0}(r)$ are defined by (5.178). We observe that when the number of channels $n = 1$, (5.187) reduces to (4.264) obtained in our discussion of Dirac R-matrix theory in potential scattering.

Following our discussion of Dirac R-matrix theory in potential scattering in Sect. 4.6, we now consider the convergence of expansion (5.187) as $r \to a_0$ from below when the continuum basis orbitals $p_{ij}^{0}(r)$ and $q_{ij}^{0}(r)$ satisfy homogeneous boundary conditions at $r = a_0$. We first rewrite the reduced radial wave functions $F_{ij}^{J\pi}(r)$ and the functions $v_{ik}^{J\pi}(r)$ in terms of their components as follows:

$$F_{ij}^{J\pi}(r) = \begin{pmatrix} P_{ij}^{J\pi}(r) \\ Q_{ij}^{J\pi}(r) \end{pmatrix}, \quad i = 1, \ldots, n \tag{5.193}$$

and

$$v_{ik}^{J\pi}(r) = \begin{pmatrix} w_{ik}^{J\pi}(r) \\ y_{ik}^{J\pi}(r) \end{pmatrix} = \sum_{i'=1}^{n_c} \begin{pmatrix} p_{ii'}^{0}(r) \\ q_{ii'}^{0}(r) \end{pmatrix} a_{ii'k}^{J\pi}, \quad i = 1, \ldots, n, \quad k = 1, \ldots, n_t. \tag{5.194}$$

Substituting these equations into (5.187) then yields the coupled equations

$$P_{ij}^{J\pi}(r) = \frac{1}{2a_0} \sum_{i'=1}^{n} \sum_{k=1}^{n_t} \frac{w_{ik}^{J\pi}(r)}{E_k^{J\pi} - E} C_{i'kj}, \quad i = 1, \ldots, n, \quad 0 \le r < a_0 \tag{5.195}$$

and

$$Q_{ij}^{J\pi}(r) = \frac{1}{2a_0} \sum_{i'=1}^{n} \sum_{k=1}^{n_t} \frac{y_{ik}^{J\pi}(r)}{E_k^{J\pi} - E} C_{i'kj}, \quad i = 1, \ldots, n, \quad 0 \le r < a_0, \tag{5.196}$$

where

$$C_{ikj} = a_0 \mathrm{c} \left[\, w_{ik}^{J\pi}(a_0) \;\; y_{ik}^{J\pi}(a_0) \, \right] \begin{pmatrix} -b_i' & 1 \\ -1 & b_i'^{-1} \end{pmatrix} \begin{pmatrix} P_{ij}^{J\pi}(a_0) \\ Q_{ij}^{J\pi}(a_0) \end{pmatrix}. \tag{5.197}$$

We now assume that the radial continuum basis orbitals $p_{ij}^{0}(r)$ and $q_{ij}^{0}(r)$ satisfy homogeneous boundary conditions at $r = a_0$ defined by

$$q_{ij}^{0}(a_0) = b_i' p_{ij}^{0}(a_0), \quad i = 1, \ldots, n, \quad j = 1, \ldots, n_c, \tag{5.198}$$

which corresponds to the boundary condition procedure often adopted in calculating these orbitals, described in Sect. 5.5.5. Hence it follows from (5.194) that

$$y_{ik}^{J\pi}(a_0) = b_i' w_{ik}^{J\pi}(a_0), \quad i = 1, \ldots, n, \quad k = 1, \ldots, n_t. \tag{5.199}$$

Substituting this result into (5.197) we find that (5.195) and (5.196) become

$$P_{ij}^{J\pi}(r) = \frac{1}{2a_0} \sum_{i'=1}^{n} \sum_{k=1}^{n_t} \frac{w_{ik}^{J\pi}(r) w_{i'k}^{J\pi}(a_0)}{E_k^{J\pi} - E} \left[2a_0 \mathrm{c} Q_{i'j}^{J\pi}(a_0) - b_{ri'} P_{i'j}^{J\pi}(a_0) \right], \quad i = 1, \ldots, n, \quad 0 \le r < a_0 \tag{5.200}$$

and

$$Q_{ij}^{J\pi}(r) = \frac{1}{2a_0} \sum_{i'=1}^{n} \sum_{k=1}^{n_t} \frac{y_{ik}^{J\pi}(r) w_{i'k}^{J\pi}(a_0)}{E_k^{J\pi} - E} \left[2a_0 \mathrm{c} Q_{i'j}^{J\pi}(a_0) - b_{ri'} P_{i'j}^{J\pi}(a_0) \right], \quad i = 1, \ldots, n, \quad 0 \le r < a_0, \tag{5.201}$$

where using (5.183) we have written

$$b_{ri} = b_0 + \kappa_i = 2a_0 \mathrm{c} b_i', \quad i = 1, \ldots, n. \tag{5.202}$$

We see that when the number of channels $n = 1$ then (5.200), (5.201) and (5.202) reduce to (4.272), (4.273) and (4.258) which we obtained in Dirac R-matrix theory in potential scattering, where we remember that n_t in (5.200) and (5.201) is the total number of basis functions retained in expansion (5.175), which corresponds to n in (4.272) and (4.273).

The limit of (5.200) and (5.201) when $r \to a_0$ from below is then given by

$$P_{ij}^{J\pi}(a_0) = \sum_{i'=1}^{n} \mathcal{R}_{ii'}^{J\pi}(E) \left[2a_0 \mathrm{c} Q_{i'j}^{J\pi}(a_0) - b_{ri'} P_{i'j}^{J\pi}(a_0) \right], \quad i = 1, \ldots, n \tag{5.203}$$

and

$$Q_{ij}^{J\pi}(a_0) = b_i' \sum_{i'=1}^{n} \mathcal{R}_{ii'}^{J\pi}(E) \left[2a_0 \mathrm{c} Q_{i'j}^{J\pi}(a_0) - b_{ri'} P_{i'j}^{J\pi}(a_0) \right], \quad i = 1, \ldots, n, \tag{5.204}$$

where the $n \times n$-dimensional R-matrix $\mathcal{R}_{ij}^{J\pi}(E)$ is defined by

$$\mathcal{R}_{ij}^{J\pi}(E) = \frac{1}{2a_0} \sum_{k=1}^{n_t} \frac{w_{ik}^{J\pi}(a_0) w_{jk}^{J\pi}(a_0)}{E_k^{J\pi} - E}, \quad i, j = 1, \ldots, n \tag{5.205}$$

and where the surface amplitudes $w_{ik}^{J\pi}(a_0)$ are defined by (5.194). As in Dirac R-matrix theory in potential scattering considered in Sect. 4.6, see (4.274), (4.275),

and (4.276) and the following discussion, we can only find a trivial solution of both (5.203) and (5.204) given by

$$P_{ij}^{J\pi}(a_0) = Q_{ij}^{J\pi}(a_0) = 0, \quad i = 1, \ldots, n, \tag{5.206}$$

when the R-matrix $\mathcal{R}_{ij}^{J\pi}(E)$ is non-singular. To see this we substitute for the summation on the right-hand side of (5.204) from (5.203) showing, after using (5.202), that the terms $[2a_0 \mathrm{c} Q_{ij}^{J\pi}(a_0) - b_{ri} P_{ij}^{J\pi}(a_0)]$ in both (5.203) and (5.204) are zero. However, at the poles of the R-matrix $\mathcal{R}_{ij}^{J\pi}(E)$ we obtain, after using (5.202), the non-trivial solution of (5.203) and (5.204) given by

$$Q_{ij}^{J\pi}(a_0) = b_i' P_{ij}^{J\pi}(a_0), \quad i = 1, \ldots, n, \tag{5.207}$$

which corresponds to the homogeneous boundary condition (5.198) satisfied by the radial continuum basis orbitals.

We can understand this result by considering the non-relativistic limit of (5.203) and (5.204) as $r \to a_0$ from below. In analogy with our discussion of Dirac R-matrix theory in potential scattering following (4.274), we see that (5.203) reduces in the non-relativistic limit to the usual equation relating the reduced radial wave function to its derivative on the boundary $r = a_0$ of the internal region. On the other hand, (5.204) reduces in this limit to an expansion of the derivative of the wave function on the boundary of the internal region. However, when radial continuum basis orbitals satisfying homogeneous boundary conditions are adopted in the analysis, this expansion only converges to the exact solution at the poles of the R-matrix when (5.207) is satisfied. Hence, in this case, expansion (5.201) is not uniformly convergent on the boundary $r = a_0$ except at the poles of the R-matrix. A detailed analysis of the structure of the two-point boundary value problem for the Dirac operator by Grant [412] confirms that (5.203), where the R-matrix is defined by (5.205), provides the boundary condition at $r = a_0$ for integrating the coupled differential equations in the external region outwards from $r = a_0$, as discussed in Sect. 5.5.3.

Finally, we note that, as in non-relativistic collisions, in order to obtain accurate results when radial continuum basis orbitals satisfying homogeneous boundary conditions are adopted, a Buttle correction to the R-matrix must be included. We consider a procedure for calculating these continuum basis orbitals in Sect. 5.5.5 and for calculating a Buttle correction to the R-matrix in Sect. 5.5.6.

5.5.3 External Region Solution

We consider in this section the solution of the Dirac equation (5.169) in the external region, corresponding to $a_0 \leq r \leq a_p$ in Fig. 5.1. As in non-relativistic electron collisions, the radius a_0 is chosen so that the charge distribution of the target eigenstates and pseudostates retained in expansion (5.175) are negligible for $r \geq a_0$ and

hence electron exchange and correlation effects between the scattered electron and the target atom or atomic ion are negligible in this region. The expansion of the total wave function $\Psi_{jE}^{J M_J \pi}(\mathbf{X}_{N+1})$ defined by (5.174) and (5.175) then reduces to

$$\Psi_{jE}^{J M_J \pi}(\mathbf{X}_{N+1}) = \sum_{i=1}^{n} \overline{\Phi}_i^{J M_J \pi}(\mathbf{X}_N; \hat{\mathbf{r}}_{N+1} \sigma_{N+1}) r_{N+1}^{-1} F_{ij}^{J\pi}(r_{N+1}), \tag{5.208}$$

where j labels the linearly independent solutions. Also, the channel functions $\overline{\Phi}_i^{J M_J \pi}$ retained in expansion (5.208) are the same as those retained in the internal region expansion (5.175) and defined by (5.176). Finally, the reduced radial functions $F_{ij}^{J\pi}(r)$ in (5.208) can be written as energy-dependent two-component functions defined in terms of the reduced radial continuum orbitals $P_{ij}^{J\pi}(r)$ and $Q_{ij}^{J\pi}(r)$ by (5.193).

We obtain coupled first-order differential equations satisfied by the reduced radial continuum orbitals $P_{ij}^{J\pi}(r)$ and $Q_{ij}^{J\pi}(r)$ in the external region by substituting (5.208) into (5.169) and projecting onto the channel functions $\overline{\Phi}_i^{J M_J \pi}(\mathbf{X}_N; \hat{\mathbf{r}}_{N+1} \sigma_{N+1})$. This gives the following coupled first-order differential equations

$$\left(\frac{\mathrm{d}}{\mathrm{d}r} + \frac{\kappa_i}{r}\right) P_{ij}^{J\pi}(r) - \frac{1}{\mathrm{c}} \left(2\mathrm{c}^2 + \epsilon_i + \frac{z}{r}\right) Q_{ij}^{J\pi}(r) = -\frac{1}{\mathrm{c}} \sum_{i'=1}^{n} V_{ii'}^{J\pi}(r) Q_{i'j}^{J\pi}(r),$$
$$i = 1, \ldots, n \tag{5.209}$$

and

$$\left(\frac{\mathrm{d}}{\mathrm{d}r} - \frac{\kappa_i}{r}\right) Q_{ij}^{J\pi}(r) + \frac{1}{\mathrm{c}} \left(\epsilon_i + \frac{z}{r}\right) P_{ij}^{J\pi}(r) = \frac{1}{\mathrm{c}} \sum_{i'=1}^{n} V_{ii'}^{J\pi}(r) P_{i'j}^{J\pi}(r),$$
$$i = 1, \ldots, n, \tag{5.210}$$

where $r \geq a_0$. Also in (5.209) and (5.210) $z = Z - N$, ϵ_i are the channel energies in atomic units and the potential matrix $V_{ii'}^{J\pi}(r)$, which has a similar form to (2.66) in non-relativistic electron collisions with atoms and atomic ions, is defined by

$$V_{ii'}^{J\pi}(r_{N+1}) = \langle r_{N+1}^{-1} \overline{\Phi}_i^{J M_J \pi}(\mathbf{X}_N; \hat{\mathbf{r}}_{N+1} \sigma_{N+1}) \left| \sum_{k=1}^{N} \frac{1}{r_{kN+1}} - \frac{N}{r_{N+1}} \right|$$
$$\times r_{N+1}^{-1} \overline{\Phi}_{i'}^{J M_J \pi}(\mathbf{X}_N; \hat{\mathbf{r}}_{N+1} \sigma_{N+1}) \rangle', \quad i,\ i' = 1, \ldots, n, \tag{5.211}$$

where the prime on the Dirac bracket in (5.211) and later equations means that the integration is carried out over the space and spin coordinates of all $N + 1$ electrons except the radial coordinate r_{N+1} of the scattered electron. Also, the inclusion of the term $-N/r_{N+1}$ in the definition of $V_{ii'}^{J\pi}(r)$ means that the long-range Coulomb

potential experienced by the scattered electron is completely included on the left-hand side of (5.209) and (5.210). Also, as in non-relativistic electron collisions, the potential terms on the right-hand side of (5.209) and (5.210) can be simplified using (2.72). We obtain

$$V_{ii'}^{J\pi}(r) = \sum_{\lambda=1}^{\lambda_{\max}} \alpha_{ii'\lambda}^{J\pi} r^{-\lambda-1}, \quad r \geq a_0, \quad i,\ i' = 1, \ldots, n, \tag{5.212}$$

where the long-range potential coefficients $\alpha_{ii'\lambda}^{\Gamma}$ are defined, in analogy with (2.74) in non-relativistic collisions, by

$$\begin{aligned} \alpha_{ii'\lambda}^{J\pi} = \langle r_{N+1}^{-1} \overline{\Phi}_i^{JM_J\pi}(\mathbf{X}_N; \hat{\mathbf{r}}_{N+1}\sigma_{N+1}) \left| \sum_{k=1}^{N} r_k^{\lambda} P_\lambda(\cos\theta_{kN+1}) \right| \\ \times r_{N+1}^{-1} \overline{\Phi}_{i'}^{JM_J\pi}(\mathbf{X}_N; \hat{\mathbf{r}}_{N+1}\sigma_{N+1}) \rangle', \quad i,\ i' = 1, \ldots, n, \\ \lambda = 1, \ldots, \lambda_{\max}, \end{aligned} \tag{5.213}$$

and where the upper limit $\lambda_{\max}$ in the summation over λ in (5.212) results from the triangular relations satisfied by the angular momentum quantum numbers which arise in the integral in (5.213).

For low-energy electron collisions with atoms and atomic ions, where the ionic interaction potential $(Z-N)/r$ in the external region and the channel energies are both small compared with c^2 then the coupled differential equations (5.209) and (5.210) can be reduced to non-relativistic limiting form. Following our discussion of the Dirac equation in potential scattering, given in Sect. 1.6, these equations can be transformed to the non-relativistic limiting form given by

$$\begin{aligned} \left(\frac{\mathrm{d}^2}{\mathrm{d}r^2} - \frac{\kappa_i(\kappa_i+1)}{r^2} + \frac{2(Z-N)}{r} + k_i^2 \right) P_{ij}^{J\pi}(r) = 2 \sum_{i'=1}^{n} V_{ii'}^{J\pi}(r) P_{i'j}^{J\pi}(r), \\ i = 1, \ldots, n, \ r \geq a_0, \end{aligned} \tag{5.214}$$

where $k_i^2 = 2\epsilon_i$. In addition in the non-relativistic limit (5.203) reduces to

$$P_{ij}^{J\pi}(a_0) = \sum_{i'=1}^{n} \mathcal{R}_{ii'}^{J\pi}(E) \left(a_0 \frac{\mathrm{d}P_{i'j}^{J\pi}}{\mathrm{d}r} - b_0 P_{i'j}^{J\pi} \right)_{r=a_0}, \quad i = 1, \ldots, n, \tag{5.215}$$

where we have used (5.183) and (5.202) to relate b_{ri} in (5.203) to b_0 in (5.215). Equations (5.214) and (5.215) are in standard non-relativistic form as discussed in Sect. 5.1.3. Hence, after the Buttle correction, discussed in Sect. 5.5.6, has been added to the diagonal elements of the R-matrix $\mathcal{R}_{ij}^{J\pi}(E)$, defined by (5.205), (5.214)

can be integrated outwards from $r = a_0$, subject to the boundary condition at $r = a_0$, defined by (5.215), to $r = a_p$ and fitted to an asymptotic expansion to yield the K-matrix and S-matrix, using the procedure discussed in Sects. 5.1.3 and 5.1.4.

However, for electron collisions with highly ionized ions, where $Z-N$ and hence the excitation energies are large, the use of (5.214) in the external and asymptotic regions can lead to error. For example, for electron collisions with the He-like ion Fe XXV, which has a residual charge of 24, an incident electron energy of $\sim$ 500 Rydbergs is required to excite the target from the ground state [985]. For these incident electron energies the velocity v of the electron is approximately 0.16 c. Hence for ionic targets with high values of the effective charge $Z - N$, one possibility is to transform the coupled first-order differential equations (5.209) and (5.210) to coupled second-order differential equations with a first-order derivative term, analogous to (4.289) in potential scattering. The R-matrix can then be propagated outwards from $r = a_0$ to a_p, using the propagator method discussed in Appendix E.5. Alternatively, the original coupled first-order differential equations (5.209) and (5.210) can be integrated outwards from $r = a_0$ to a_p, using a standard approach for solving these equations (see, for example, [573]). In both cases a Buttle correction, discussed in Sect. 5.5.6, has to be added to the R-matrix $\mathcal{R}_{ij}^{J\pi}(E)$ defined by (5.205) if continuum basis orbitals satisfying homogeneous boundary conditions at $r = a_0$ are used in the internal region.

5.5.4 Asymptotic Region Solution

We now consider the solution of (5.209) and (5.210) in the asymptotic region, corresponding to $r \geq a_p$ in Fig. 5.1. We have seen in our discussion of the external region solution in Sect. 5.5.3 that for low-energy collisions, when the interaction potential $(Z - N)/r$ and the channel energies are small compared with c^2, (5.209) and (5.210) can be reduced to non-relativistic form. In this case we can solve the resultant equations in the asymptotic region as discussed in Sect. 5.1.4 yielding the S-matrix, T-matrix and cross sections. However, for electron collisions with highly ionized ions it is necessary to determine the asymptotic region solution of (5.209) and (5.210) directly. In this analysis we assume that the channels are ordered so that the channel energies ϵ_i in (5.209) and (5.210) satisfy

$$\epsilon_1 \geq \epsilon_2 \geq \cdots \geq \epsilon_n, \tag{5.216}$$

where the first n_a channels are open with $\epsilon_i \geq 0$ and the last n_b channels are closed with $\epsilon_i < 0$, where $n_a + n_b = n$. As in non-relativistic collisions, considered in Sect. 5.1.4, we define, in analogy with (5.37), $n + n_a$ linearly independent solutions of (5.209) and (5.210) satisfying the following asymptotic boundary conditions:

$$
\begin{aligned}
p_{ij}(r) &\underset{r\to\infty}{\sim} g_i \sin\theta_i \delta_{ij}, \quad q_{ij}(r) \underset{r\to\infty}{\sim} \frac{\epsilon_i}{k_i \mathrm{c}} g_i \cos\theta_i \delta_{ij}, \\
&\qquad\qquad i = 1, \ldots, n, \quad j = 1, \ldots, n_a, \\
p_{ij}(r) &\underset{r\to\infty}{\sim} g_i \cos\theta_i \delta_{ij}, \quad q_{ij}(r) \underset{r\to\infty}{\sim} -\frac{\epsilon_i}{k_i \mathrm{c}} g_i \sin\theta_i \delta_{ij}, \\
&\qquad\qquad i = 1, \ldots, n, \quad j = 1, \ldots, n_a, \\
p_{ij}(r) &\underset{r\to\infty}{\sim} \overline{g}_i \exp(-\phi_i)\delta_{ij}, \quad q_{ij}(r) \underset{r\to\infty}{\sim} \frac{\epsilon_i}{|k_i|\mathrm{c}} \overline{g}_i \exp(-\phi_i)\delta_{ij}, \\
&\qquad\qquad i = 1, \ldots, n, \quad j = n_a + 1, \ldots, n, \qquad (5.217)
\end{aligned}
$$

where

$$
g_i = \left[\frac{1}{k_i}\left(1 + \frac{\epsilon_i}{2\mathrm{c}^2}\right)\right]^{1/2}, \quad k_i = \left[\frac{\epsilon_i}{\mathrm{c}}\left(\frac{\epsilon_i}{\mathrm{c}} + 2\mathrm{c}\right)\right]^{1/2}, \quad \overline{g}_i = \left[\frac{1}{|k_i|}\left(1 + \frac{\epsilon_i}{2\mathrm{c}^2}\right)\right]^{1/2}. \qquad (5.218)
$$

Also in (5.217),

$$
\theta_i = k_i r - \frac{1}{2}(\gamma_i - 1)\pi + y_i \ln 2k_i r + \psi_i - \arg\Gamma(\gamma_i + \mathrm{i}y_i), \quad i = 1, \ldots, n_a, \qquad (5.219)
$$

where

$$
\gamma_i = \left(\kappa_i^2 - \frac{z^2}{\mathrm{c}^2}\right)^{1/2}, \quad y_i = \frac{z}{k_i}\left(1 + \frac{\epsilon_i}{\mathrm{c}^2}\right), \quad \psi_i = \frac{1}{2\mathrm{i}} \ln\left(\frac{\mathrm{i}z/k_i - \kappa_i}{\gamma_i - \mathrm{i}y_i}\right) \qquad (5.220)
$$

and

$$
\phi_i = |k_i| r - y_i \ln 2k_i r. \qquad (5.221)
$$

These asymptotic boundary conditions are discussed by Young and Norrington [985] who obtained asymptotic expansions for these solutions, analogous to the non-relativistic asymptotic expansions considered in Appendix F.1 [160, 356].

Following our discussion in Sect. 5.1.4, we can find n_a linearly independent solutions of the coupled differential equations (5.209) and (5.210) that vanish at the origin and are finite at infinity. The $n_a \times n_a$-dimensional K-matrix is then defined in terms of the large components in the n_a open channels as follows:

$$
\mathbf{P}^{J\pi}(r) \underset{r\to\infty}{\sim} \left[\frac{1}{\mathbf{k}}\left(\mathbf{I} + \frac{\boldsymbol{\epsilon}}{2\mathrm{c}^2}\right)\right]^{1/2} \left[\sin\boldsymbol{\theta} + \cos\boldsymbol{\theta}\mathbf{K}^{J\pi}\right], \qquad (5.222)
$$

where the corresponding components in the n_b closed channels vanish asymptotically. By taking linear combinations of these solutions we can define a solution matrix $\mathbf{G}^{J\pi}(r)$ satisfying the asymptotic boundary conditions

$$\mathbf{G}^{J\pi}(r) \underset{r\to\infty}{\sim} \left[\frac{1}{\mathbf{k}}\left(\mathbf{I}+\frac{\boldsymbol{\epsilon}}{2c^2}\right)\right]^{1/2} [\exp(-\mathrm{i}\boldsymbol{\theta}) - \exp(\mathrm{i}\boldsymbol{\theta})\mathbf{S}^{J\pi}], \tag{5.223}$$

where the S-matrix, defined by this equation, and the corresponding T-matrix can be expressed in terms of the K-matrix by the usual matrix equations

$$\mathbf{S}^{J\pi} = \frac{\mathbf{I}+\mathrm{i}\mathbf{K}^{J\pi}}{\mathbf{I}-\mathrm{i}\mathbf{K}^{J\pi}}, \quad \mathbf{T}^{J\pi} = \mathbf{S}^{J\pi} - \mathbf{I}. \tag{5.224}$$

The cross sections can then be determined using the procedure described in Sect. 2.5. The partial cross section for a transition from an initial state $i \equiv \alpha_i J_i j_i$ to a final state $f \equiv \alpha_f J_f j_f$ corresponding to the conserved quantum numbers $J\pi$ is given by

$$\sigma^{J\pi}(i \to f) = \frac{2J+1}{2k_i^2(2J_i+1)} \sum_{j_i j_f} |T_{fi}^{J\pi}|^2, \tag{5.225}$$

where α_i and α_f distinguish target states with the same total angular momentum J_i and J_f, and where j_i and j_f are the initial and final angular momenta of the scattered electron. The total cross section is then defined by

$$\sigma^{\mathrm{Tot}}(i \to f) = \sum_{J\pi} \sigma^{J\pi}(i \to f), \tag{5.226}$$

in units of πa_0^2.

5.5.5 *Continuum Basis Orbitals*

We now consider the procedure usually adopted for calculating the reduced radial continuum basis orbitals $p_{ij}^0(r)$ and $q_{ij}^0(r)$ which are used in definition (5.178) of $u_{ij}^0(r)$ in the internal region. In most applications these orbitals have been chosen to satisfy homogeneous boundary conditions similar to those adopted in non-relativistic electron collisions, described in Sect. 5.3.1 and, as a result, a Buttle correction to the R-matrix, considered in Sect. 5.5.6, is required. However, as in non-relativistic electron–atom collisions and multiphoton ionization, arbitrary boundary condition methods, considered in Sect. 5.3.3, can also be used to determine the continuum basis orbitals.

In analogy with the coupled first-order differential equations (4.248), which arise in Dirac R-matrix theory in potential scattering, we consider here orbitals $p_{ij}^0(r)$ and $q_{ij}^0(r)$ which satisfy the following coupled first-order differential equations for each κ_i

$$\left(\frac{\mathrm{d}}{\mathrm{d}r}+\frac{\kappa_i}{r}\right)p^0_{ij}(r)-\frac{1}{\mathrm{c}}[2\mathrm{c}^2+\epsilon_i-V_0(r)]q^0_{ij}(r)=-\frac{1}{\mathrm{c}}\sum_k\lambda_{ijk}Q^a_k(r),$$
$$i=1,\ldots,n,\quad j=1,\ldots,n_c \qquad (5.227)$$

and

$$\left(\frac{\mathrm{d}}{\mathrm{d}r}-\frac{\kappa_i}{r}\right)q^0_{ij}(r)+\frac{1}{\mathrm{c}}[\epsilon_i-V_0(r)]p^0_{ij}(r)=\frac{1}{\mathrm{c}}\sum_k\lambda_{ijk}P^a_k(r),$$
$$i=1,\ldots,n,\quad j=1,\ldots,n_c, \qquad (5.228)$$

subject to the homogeneous boundary conditions, defined in analogy with (4.249) and (4.250), which can be written here as

$$\begin{pmatrix}p^0_{ij}(0)\\ q^0_{ij}(0)\end{pmatrix}=0,\quad i=1,\ldots,n,\quad j=1,\ldots,n_c \qquad (5.229)$$

and

$$q^0_{ij}(a_0)=b'_i p^0_{ij}(a_0),\quad i=1,\ldots,n,\quad j=1,\ldots,n_c. \qquad (5.230)$$

Also in (5.227), (5.228), (5.229) and (5.230), n is the number of channels retained in the R-matrix expansion and n_c is the number of continuum basis functions retained in each channel. In the non-relativistic limit we have seen that b'_i in (5.230) is related to b_0 and κ_i by (5.183). Also the summations over k on the right-hand sides of (5.227) and (5.228) go over the reduced radial physical bound orbitals $P^a_k(r)$ and $Q^a_k(r)$ used to construct the target states retained in expansion (5.175) corresponding to the κ_i under consideration and the λ_{ijk} are Lagrange multipliers which are chosen so that the following orthogonality constraints

$$\int_0^{a_0}[p^0_{ij}(r)P^a_k(r)+q^0_{ij}(r)Q^a_k(r)]\mathrm{d}r=0,\quad i=1,\ldots,n \qquad (5.231)$$

are satisfied for all j and k, for each κ_i. It follows that the reduced radial continuum basis orbitals $p^0_{ij}(r)$ and $q^0_{ij}(r)$ generated in this way are orthogonal and can be normalized so that

$$\int_0^{a_0}[p^0_{ij}(r)p^0_{ij'}(r)+q^0_{ij}(r)q^0_{ij'}(r)]\mathrm{d}r=\delta_{jj'},\quad i=1,\ldots,n \qquad (5.232)$$

for all j and j'. For each κ_i, the reduced radial physical bound orbitals $P^a_k(r)$ and $Q^a_k(r)$, retained on the right-hand side of (5.227) and (5.228), together with the corresponding reduced radial continuum orbitals $p^0_{ij}(r)$ and $q^0_{ij}(r)$, generated by solving (5.227), (5.228), (5.229) and (5.230) subject to the orthonormality constraints

given by (5.231) and (5.232), form a complete set over the range $0 \le r < a_0$ in the limit $n_c \to \infty$, for any value of b_r in (5.183) and zero-order potential $V_0(r)$.

In order to obtain rapid convergence of the R-matrix expansion (5.205), including the Buttle correction discussed below, the zero-order potential $V_0(r)$ in (5.227) and (5.228) should provide a good representation of the charge distribution of the target atom or ion. In practice, the static potential of the target atom or ion in its ground state is often adopted. Also, as in non-relativistic collisions, the inhomogeneous terms on the right-hand sides of (5.227) and (5.228) play the role of an exchange potential while at the same time ensuring that the continuum basis orbitals are orthogonal to the physical orbitals used to construct the target states.

5.5.6 Buttle Correction

When the reduced radial continuum basis orbitals $p_{ij}^0(r)$ and $q_{ij}^0(r)$ in definition (5.178) of $u_{ij}^0(r)$ satisfy the zero-order coupled differential equations (5.227) and (5.228) subject to homogeneous boundary conditions (5.229) and (5.230), then it is necessary to add a "Buttle correction" to the R-matrix to obtain accurate results. Our procedure, which is analogous to that adopted in non-relativistic collisions discussed in Sect. 5.3.2, corrects for the omission of the high-lying pole terms in expansion (5.205) of the R-matrix $\mathcal{R}_{ij}^{J\pi}(E)$. Also, as in non-relativistic electron collisions with atoms and ions, only the diagonal elements of the R-matrix usually need to be corrected.

The diagonal elements of the R-matrix $\mathcal{R}_{ij}^{J\pi}(E)$ are determined in terms of the solution of the coupled zero-order differential equations (5.227) and (5.228) used to calculate the reduced radial continuum basis orbitals $p_{ij}^0(r)$ and $q_{ij}^0(r)$. The diagonal elements of the zero-order R-matrix $\mathcal{R}_{ij}^0(E)$ at an arbitrary energy E are given, following (4.287), by

$$\mathcal{R}_{ii}^0(E) = p_i^0(a_0)\left[2a_0 c q_i^0(a_0) - b_{ri}\, p_i^0(a_0)\right]^{-1}, \quad i = 1, \ldots, n, \tag{5.233}$$

where $p_i^0(r)$ and $q_i^0(r)$ are solutions of (5.227) and (5.228) at the energy E, subject to the boundary condition (5.229) at the origin and to the orthogonality constraints (5.231). The diagonal elements of the zero-order R-matrix can also be written in terms of the infinite set of eigensolutions $p_{ij}^0(r)$ of (5.227) and (5.228), subject to the boundary conditions (5.229) and (5.230) and the orthogonality and normalization constraints (5.231) and (5.232). We obtain

$$\mathcal{R}_{ii}^0(E) = \frac{1}{2a_0} \sum_{k=1}^{\infty} \frac{\left[p_{ik}^0(a_0)\right]^2}{E_k^0 - E}, \quad i = 1, \ldots, n. \tag{5.234}$$

Finally, the Buttle correction to the diagonal elements of the R-matrix $\mathcal{R}_{ij}^{J\pi}(E)$, defined by (5.205), can be written as

$$\mathcal{R}_{ii}^{J\pi(\mathrm{BC})}(E) = \frac{1}{2a_0} \sum_{k=n_t+1}^{\infty} \frac{\left[p_{ik}^0(a_0)\right]^2}{E_k^0 - E}, \quad i = 1, \ldots, n. \tag{5.235}$$

Using (5.233) and (5.234) we then find that

$$\mathcal{R}_{ii}^{J\pi(\mathrm{BC})}(E) = p_i^0(a_0)\left[2a_0 \mathrm{c} q_i^0(a_0) - b_{ri}\, p_i^0(a_0)\right]^{-1} - \frac{1}{2a_0} \sum_{k=1}^{n_t} \frac{\left[p_{ik}^0(a_0)\right]^2}{E_k^0 - E}, \quad i = 1, \ldots, n. \tag{5.236}$$

The first term on the right-hand side of (5.236) is obtained by solving the coupled differential equations (5.227) and (5.228) at the energy E of interest and the second term is given in terms of the reduced radial continuum basis orbitals evaluated on the boundary $r = a_0$ of the internal region together with the corresponding eigenenergies. As in non-relativistic collisions, both terms in (5.236) can be rapidly calculated at a few energies and since the Buttle correction is smoothly varying in the low-energy region of interest it can be interpolated to give the correction at the required energies.

5.6 Low-Energy Electron Collision Calculations

Over the last 40 years a vast number of electron–atom and electron–ion collision calculations have been carried out using R-matrix computer programs which have implemented the theory reviewed in this chapter. These calculations have been undertaken both in support of experiment and also to provide data required in the analysis of applications, for example, in plasma physics, laser physics and astrophysics. In this section we consider low-energy electron–atom and electron–ion collision calculations where only elastic scattering and excitation processes are energetically allowed or are important, reserving a discussion of electron collisions at intermediate energies, where ionizing collisions are important, to Chap. 6. The examples that we present illustrate both the criteria necessary to obtain reliable cross sections and the accuracy now obtainable for low-energy electron collisions with atoms and atomic ions. However, we will see that difficulties are still experienced for heavier open d- and f-shell targets involving many coupled channels.

5.6.1 Electron Collisions with H

We begin by considering electron collisions with atomic hydrogen, the lightest one-electron target atom. This simplifies the collision calculation since the non-relativistic hydrogen atom wave functions are known exactly and hence we are not concerned with electron–electron correlation effects among the target electrons

which arise in more complex atomic targets. However, the Schrödinger equation for the electron–hydrogen atom system describes a three-body problem and is therefore not solvable exactly. The importance of obtaining accurate numerical solutions for this system is not only because of its intrinsic importance arising from the fact that atomic hydrogen is the most abundant atom in the universe, but also because these solutions illustrate features, such as resonances and threshold effects, which are common to multi-electron atomic targets. Hence calculations carried out for electron–hydrogen atom collisions provide a test of methods, such as the R-matrix method, which are applicable to general multi-electron targets.

We have pointed out in Sects. 2.2 and 2.3 that in order to obtain accurate low-energy electron–atom collision cross sections it is necessary to include target pseudostates in the expansion of the collision wave function to represent the long-range polarization of the target in the field of the scattered electron. In early calculations by Burke et al. [177] and Fon et al. [328] full account of the long-range polarization potential was taken by including the $\overline{2p}$ pseudostate defined by (2.23) as well as the 1s target eigenstate in the "close coupling with pseudostates" expansion (2.55). Differential cross sections for elastic scattering were calculated from 1 to 200 eV by Fon et al. [328] which compared well with absolute angular distribution measurements by Williams [977–979]. However, the $\overline{2p}$ state has an unphysical threshold at ∼11.4 eV and the omission of physical excited states in the expansion meant that resonance and threshold effects in the 9–13.6 eV range were not accurately represented.

In order to obtain accurate elastic and inelastic e^-–H collision cross sections at low energies, including resonance and threshold effects, Bartschat et al. [72] carried out benchmark calculations using two independent R-matrix methods and also using the convergent close-coupling (CCC) method developed by Bray and Stelbovics [126, 127] and reviewed by Bray et al. [129, 130]. The two R-matrix methods, the R-matrix with pseudostates (RMPS) method and the intermediate energy R-matrix (IERM) method, which are described in detail in Chap. 6, are designed to obtain accurate collision cross sections close to and above the ionization threshold. However, both methods give convergent results at low energies. In the RMPS calculation eight S-states, eight P-states and three D-states were included in expansion (5.6), where the lowest six states corresponded to the exact $n = 1,\ 2$ and 3 non-relativistic H atom eigenstates, while the remaining 13 states were pseudostates, allowing for long-range polarization and short-range correlation effects. The corresponding IERM calculation also included the six $n = 1,\ 2$ and 3 H atom eigenstates as well as orbitals representing long-range polarization and short-range correlation effects. We show the results of these three calculations for the total elastic and 1s–2s and 1s–2p excitation cross sections between the $n = 2$ and 3 thresholds compared with the experimental data of Williams [980] in Fig. 5.4. We see that the agreement between theory and experiment is excellent, with theory accurately reproducing the resonance structure converging to the $n = 3$ threshold at 0.8889 Rydbergs and the $^1P^o$ resonance just above the $n = 2$ threshold, which had been analysed in detail by Macek and Burke [621]. We note that the $^1S^e$ resonance at ∼0.862 Rydbergs has been discussed in Sect. 3.2.3 (see Fig. 3.5).

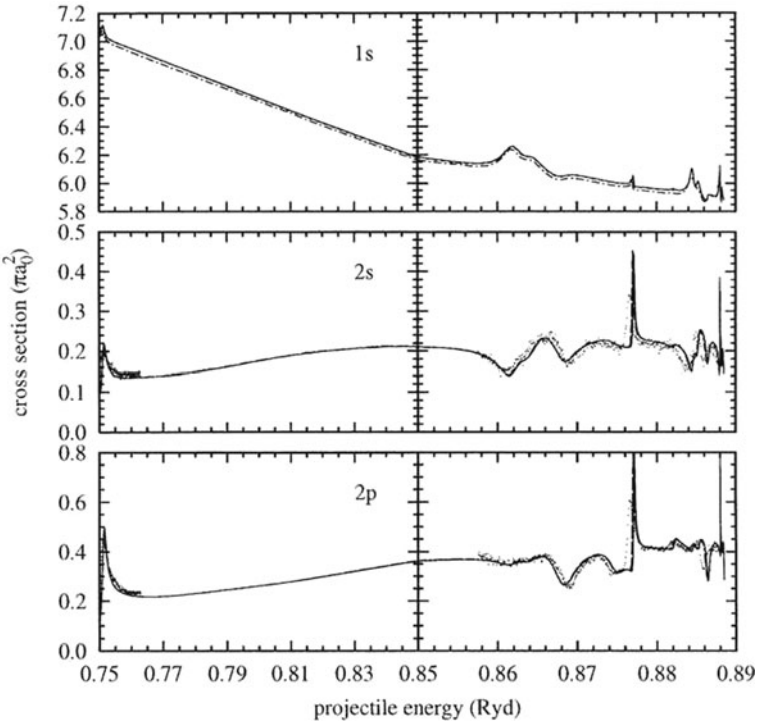

Fig. 5.4 Total electron–hydrogen atom 1s–1s elastic cross section and 1s–2s and 1s–2p excitation cross sections for collision energies between the $n = 2$ and 3 thresholds. *Full curve*, RMPS; *broken curve*, IERM; *chain curve*, CCC. The *dots* represent the experimental data of Williams [980] (Fig. 4 from [72])

In conclusion, low-energy scattering amplitudes and cross sections for e^-–H collisions can be accurately calculated using the R-matrix method for low n states. However, there are still major computational problems remaining in order to obtain accurate low-energy excitation cross sections for high n states of atomic hydrogen which, for example, are of importance in some diffuse hydrogen clouds in the cold interstellar medium. This computational difficulty is due to the many coupled channels involved and the large extent of the corresponding target atom wave functions. We will return to this difficulty when we discuss electron collisions with hydrogen atoms at intermediate energies in Chap. 6.

5.6.2 Electron Collisions with He

Results from electron–helium atom collision calculations have many applications. Helium is relatively easy to study in the laboratory, so many experiments have been performed providing stringent tests for theory. In astronomy, helium is the second

most abundant element in the universe, after atomic hydrogen, and helium lines associated with the excited $n = 2$, $n = 3$ and higher states are ubiquitous in spectra from many types of astronomical objects (see [709]). Since most emission line spectra observed in astronomy are produced by electron impact excitation or by radiative capture, followed by radiative decay of excited states, it is clear that there is a demand for high-quality atomic data to interpret these lines.

Also, helium is the simplest multi-electron atom and electron–helium collision calculations exhibit many features of calculations for more complex atomic targets. The most obvious difference from electron–hydrogen atom collisions is that the helium target wave function cannot be represented exactly; the system of nucleus plus two electrons being a three-body problem. Approximate target wave functions have to be used, usually employing configuration interaction expansions. Another difference is that the helium target can be in either a singlet or a triplet spin state rather than in just a doublet state as in the case of atomic hydrogen, which doubles the number of excited states for each principal quantum number n. Both of these differences result in increasing complexity in the corresponding collision calculations.

5.6.2.1 Elastic Scattering

The first low-energy e^-–He elastic scattering R-matrix calculations were carried out by Robb [792] using a static-exchange approximation where the target was represented by a configuration interaction expansion. These calculations were later extended by O'Malley et al. [705] who used an R-matrix eigenchannel method, discussed in Sect. 4.4.5. In this latter work, O'Malley et al. adopted a multiconfigurational helium ground-state wave function together with ^{1}P and ^{1}D pseudostates, constructed from the Hartree–Fock ground state 1s orbital and 2s–4f pseudo-orbitals. These pseudo-orbitals were optimized to simultaneously minimize the ground-state energy and maximize the dipole and quadrupole polarizabilities of the target, as discussed by Vo Ky Lan et al. [941]. In this way they obtained 98% of the ground-state correlation energy as well as 99.8% of the dipole polarizability and approximately the correct quadrupole polarizability. The estimated error in the calculated total cross section below 8 eV was about 1% and this was born out by the excellent agreement with experiments by Kennerly and Bonham [530]. Both the total and momentum transfer cross sections were also in good agreement with variational calculations by Nesbet [677].

5.6.2.2 Inelastic Collisions

A series of R-matrix calculations have been carried out to determine the convergence of low-energy e^-–He excitation cross sections and resonance structure. In these calculations He target eigenstates were included in expansion (5.6) with progressively higher principal quantum number n. These were 5-state calculations by Berrington et al. [96] which included all eigenstates with $n \leq 2$, 11-state calculations by Freitus et al. [341] and Berrington et al. [99] which included all

eigenstates with $n \leq 3$, 19-state calculations by Berrington and Kingston [93] and Fon et al. [332] which included all eigenstates with $n \leq 4$, and 29-state calculations by Sawey et al. [815] and Fon et al. [333–335] which included all eigenstates with $n \leq 5$. The main conclusion from these calculations was that as the number of target eigenstates retained in the calculation increased, the cross sections converged at the lowest energies. However, the calculated cross sections were in error above the threshold of the highest eigenstate retained in the R-matrix expansion. That is the 5-state calculation had not converged above the $n = 2$ thresholds, the 11-state calculation had not converged above the $n = 3$ thresholds and so on. We will show in Chap. 6, when we discuss intermediate-energy collisions, that it is necessary to include pseudostates representing highly excited states and the ionization continuum in the R-matrix expansion, in order to obtain converged results close to and above the ionization threshold. We have also observed in Sect. 2.2.2 that, in order to obtain highly accurate results at low energies, it is necessary to include pseudostates in this expansion which represent long-range polarization effects and other virtual transitions via high-lying excited states and the continuum.

Recently, close to converged inelastic e^-–He R-matrix collision cross section calculations have been carried out and compared with experiment by Stepanović et al. [886] and by Lange et al. [570]. In the work of Stepanović et al. cross sections for exciting the 3^3S and 3^1S states of helium near threshold were studied. In the work of Lange et al. cross sections for exciting both the $n = 2$ and 3 states of helium were studied and were also compared with accurate calculations by Fursa and Bray [355] using the convergent close coupling method. We illustrate this work by showing in Fig. 5.5 the angle-integrated cross sections for excitation of helium to the 3^3S and 3^1S states. The calculations were carried out using the B-spline R-matrix (BSR) computer program written by Zatsarinny [992], discussed in Sect. 5.1.1. The collision model adopted included 69 target states with S, P, D and F symmetries consisting of all target eigenstates with these symmetries up to $n = 5$, together with 42 pseudostates representing higher bound and continuum states. The experimental cross sections were obtained using a high-resolution electron impact spectrometer, in a crossed beam geometry, described in detail by Cvejanović et al. [240]. The experimental data were normalized to the theory, including a cascade contribution, at 23.20 eV for both the 3^3S and 3^1S states since the cross sections exhibit a smooth energy dependence in the neighbourhood of this energy and hence the experimental energy resolution does not play a significant role. The cascade contribution was found to be important only for the 3^3S excitation, whereas it was negligible for the 3^1S state. Overall the experimental cross sections shown in Fig. 5.5 are in good agreement with the optical excitation functions published by Heddle et al. [448]. The convoluted theoretical cross sections also exhibit remarkably good agreement with experiment although there are some discrepancies in the near-threshold region for excitation of the 3^3S state where theory predicts somewhat higher values for the resonance structure than observed experimentally. This may be due to the higher model sensitivity of the predicted resonance structure very close to threshold. A detailed analysis of this resonance structure is given by Lange et al. [570].

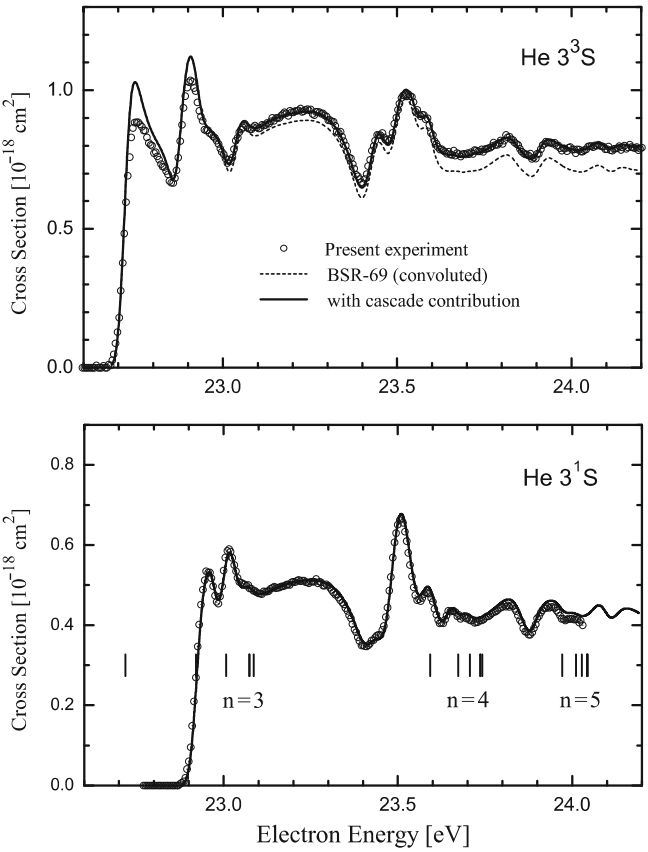

Fig. 5.5 Angle-integrated cross sections for electron impact excitation of the 3^3S and 3^1S states of helium. The experimental results are represented by *circles*. The theoretical *R*-matrix results without (*dashed line*) and with (*solid line*) cascade contributions were convoluted with a Gaussian of 37 meV (FWHM). The *vertical bars* in the *lower panel* represent the thresholds for the helium target states (Fig. 2 from [886])

Finally, we note that the results presented in both Figs. 5.4 and 5.5 show the important role that resonances play in determining low-energy electron–atom collision cross sections. In earlier work on He it was shown [175, 176] that two pronounced peaks which dominate the 1^1S–2^3S collision strength close to threshold were due to $^2P^o$ and $^2D^e$ shape resonances, in agreement with angular distribution measurements by Ehrhardt and William [285] and Ehrhardt et al. [287]. Detailed elastic collision calculations below the 2^3S threshold also revealed the presence of a $^2S^e$ resonance at ∼19.31 eV, which was first observed by Schulz [835] and which has been discussed more recently by Hudson et al. [478]. We will see when we discuss further examples in this section that resonances are a common feature of all low-energy electron–atom and electron–ion collision cross sections.

5.6.3 Electron Collisions with Ne

We consider next low-energy electron collisions with neon atoms which are important both in fundamental studies and for their many applications. The latter include modelling applications in the lighting and lasing industry, in plasma processing and in the interpretation of astrophysical observations.

Elastic electron collisions with inert gases have been studied both experimentally and theoretically for many years. In particular, elastic scattering R-matrix calculations have been carried out by Fon and co-workers on He [329], Ne [327], Ar [330] and Kr [331], in which the ground state of the target together with a $^1P^o$ polarized pseudostate, representing the full dipole polarizability of the target, were included in the R-matrix expansion. In addition, elastic electron–neon collision calculations have been carried out by many other workers including McEachran and Stauffer [617], Dasgupta and Bhatia [250] and Saha [805], where in all these calculations good agreement with experiment was obtained. However, until recently the situation for inelastic collisions has been less satisfactory where, as shown by Khakoo et al. [533], none of the theoretical methods discussed in their paper were able to consistently reproduce the experimental data for angle-differential cross sections for excitation of the $2p^5 3s$ states, or their ratios.

However, more recent calculations carried out by Zatsarinny and Bartschat [998], using the B-spline R-matrix computer program BSR, have obtained very good agreement with experiments by Buckman et al. [146], which measured the cross section for exciting the $2p^5 3s\ ^3P^o_{0,2}$ states of neon from threshold to just above the $3p^5 3p$ thresholds. The sum of these two excitation cross sections had been used by Brunt et al. [141, 142] and Buckman et al. [146] to analyse the details of the resonance structure seen in these cross sections, discussed in the review of atomic negative ion resonances by Buckman and Clark [145].

Also, in later studies by Bömmels et al. [122] and Allan et al. [12], excellent agreement was obtained between R-matrix calculations and experiment for excitation of the $2p^5 3s$ states from threshold to above the $3p^5 3p$ thresholds. As an example, we show in Fig. 5.6 a comparison of calculated and experimental cross sections for excitation of the Ne $2p^5 3s\ ^3P_2$, $^3P_1$, $^3P_0$ and $^1P_1$ states reported by Allan et al. [12]. The experimental results were obtained using an electron scattering apparatus involving two-stage hemispherical analysers with an energy resolution (FWHM) of 9 meV [11]. Absolute cross sections reliable to $\pm 15\%$ were obtained by normalization to helium results. The R-matrix calculations were obtained including the $2p^6\ ^1S_0$ ground state of neon together with the $2p^5 3s$ and $2p^5 3p$ excited states in the R-matrix internal region expansion. This figure illustrates prominent resonance features just above the $2p^5 3s$ thresholds and a Wigner cusp together with a group of narrow resonances associated with the higher lying $2p^5 3p$ thresholds. The lower resonances can be assigned as core-excited shape resonances with the dominant configuration $2p^5 3s3p$ as discussed by Bömmels et al. [122], while further work is required to fully identify the resonances at the higher thresholds. Overall the excellent agreement between theory and experiment indicates that the main features of this collision process are accurately reproduced by the R-matrix calculation. Finally,

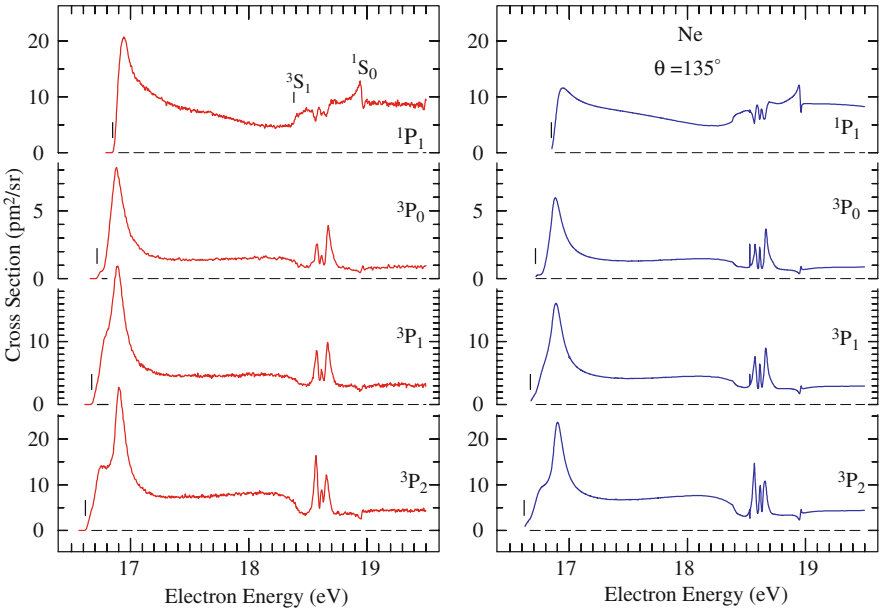

Fig. 5.6 Absolute cross sections (experiment in the *left panels* and *R*-matrix calculations in the *right panels*) for electron impact excitation of the $2p^5 3s$ states of Ne at a scattering angle $\theta = 135°$. The *vertical bars* indicate the excitation thresholds including those of the $2p^5 3p\ ^3S_1$ and $^1S_0$ states of Ne (Fig. 2 from [12])

we note that the B-spline *R*-matrix computer program has been used to study a number of other electron–atom collision processes including low-energy electron collisions with argon [999], zinc [1000] and oxygen [1003].

5.6.4 Electron Collisions with Si III

As our next example we consider electron collisions with Si III (Si^{2+}). There is considerable demand for excitation rates for this ion, particularly in the study of laboratory plamas and in the analysis of solar spectra where, for example, the intensity ratio of Si III lines have been used to determine the electron densities of quiet and active regions of the sun (e.g. [228]). Absorption lines of Si III have also been found in quasi-stellar objects [41]. Of particular importance is the following excitation process

$$\begin{array}{ccccc} e^- + \mathrm{Si\,III}\,(3s^2\ ^1S) & \rightarrow & \mathrm{Si\,III}\,(3s3p\ ^3P^o) + e^- \\ \searrow & & \nearrow \\ & \mathrm{Si\,II}\,(3s3p\ ^1P^o\, n\ell) & \end{array} \tag{5.237}$$

which is dominated close to threshold by a Rydberg series of Feshbach resonances. These resonances are caused by capture of the incident electron into a bound

Rydberg state in the field of Si III in the excited $3s3p\ ^1P^o$ state, which decays leaving the target ion in its $3s3p\ ^3P^o$ first excited state. *R*-matrix calculations for this process have been carried out by Baluja et al. [46] and Griffin et al. [425], where the latter authors also studied transitions in the isoelectronic ion Ar VII (Ar^{6+}). In these calculations the 12 lowest target eigenstates of Si III were included in expansion (5.6), where each eigenstate was represented by a configuration interaction expansion. We present in Fig. 5.7 the collision strength for the $3s^2\ ^1S \rightarrow 3s3p\ ^3P^o$ transition calculated by Baluja et al. [46], compared with distorted wave results calculated by Blaha (quoted by Nicolas [684]). We see that at these low energies, the collision strength is dominated by resonance structure while the distorted wave results, which omit the intermediate resonance states in the collision, represent the much smaller non-resonant background. The importance of resonances for this transition is demonstrated in Table 5.1 where we compare the effective collision strength,

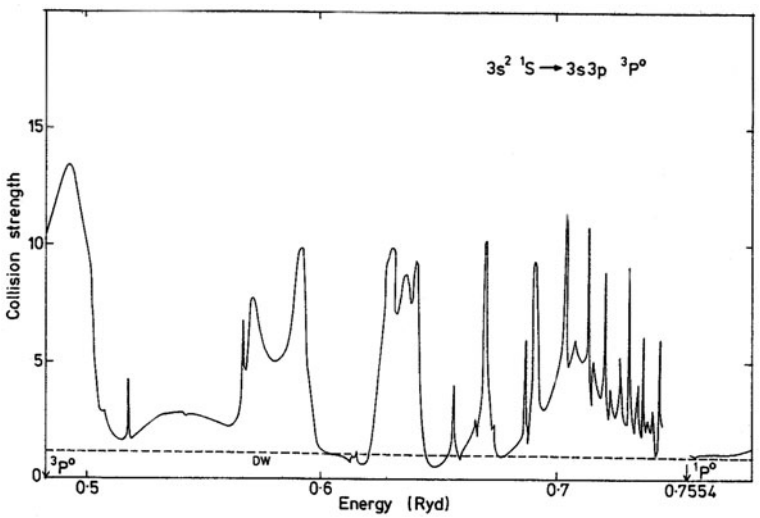

Fig. 5.7 Collision strength for the transition $3s^2\ ^1S \rightarrow 3s3p\ ^3P^o$ in Si III. *Full line*, *R*-matrix calculation [46]; *dashed line*, distorted wave calculation [684] (Fig. 1 from [46])

Table 5.1 Effective collision strength for the transition $3s^2\ ^1S \rightarrow 3s3p\ ^3P^o$ in Si III as a function of electron temperature for *R*-matrix and distorted wave calculations

Electron temp 10^4 K	*R*-matrix	Distorted wave
0.50	6.898	1.120
0.75	5.961	1.111
1.00	5.428	1.101
2.00	4.407	1.065
5.00	3.188	0.969
10.00	2.292	0.842
20.00	1.529	0.667

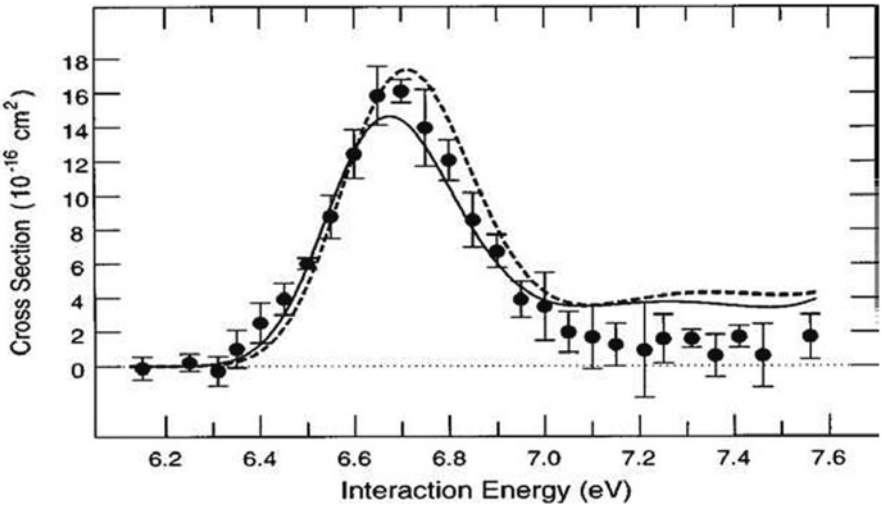

Fig. 5.8 Cross section for $3s^2\ ^1S \rightarrow 3s3p\ ^3P^o$ electron impact in Si III. *Points* represent average experimental values and *bars* give relative uncertainties at 90% confidence level. *Dashed curve*, *R*-matrix calculation [46]; *solid curve*, *R*-matrix calculation [425], both calculations convoluted with a Gaussian width 0.24 eV (Fig. 3 from [946])

defined by (2.153), for these two calculations for a range of electron temperatures. At 5,000 K the *R*-matrix result is larger by a factor of about 6 and even at 2×10^5 K it is still more than a factor of 2 higher.

More recently, absolute excitation cross sections for the $3s^2\ ^1S \rightarrow 3s3p\ ^3P^o$ and $^1P^o$ transitions in Si III were measured close to threshold by Wallbank et al. [946] using a merged electron–ion beams energy-loss technique. We show in Fig. 5.8 the measured cross section for the $3s^2\ ^1S \rightarrow 3s3p\ ^3P^o$ transition compared with the *R*-matrix calculation by Baluja et al. [46] and Griffin et al. [425]. The resonance peak close to the threshold seen in the *R*-matrix calculations is confirmed by experiment which is also in good agreement with its predicted magnitude. However, the agreement between the *R*-matrix calculations and experiment is less good at energies more than 1 eV above threshold, which Wallbank et al. believe may be due to the omission of backscatter electrons in the experiment.

In conclusion, the important experiment by Wallbank et al. [946] has shown that *R*-matrix theory can accurately predict low-energy cross sections for relatively light multi-electron ions. This work again demonstrates the crucial role that resonances play in enhancing low-energy electron–atom and electron–ion collision cross sections.

5.6.5 Electron Collisions with Fe II

Electron impact excitation cross sections and the related effective collision strengths for all ionization stages of iron peak elements are of crucial importance in the

quantitative analysis of many astronomical spectra, see, for example, [79]. As a result, for nearly two decades there has been a major effort as part of the international Iron Project [482] to calculate electron impact excitation data for all ionization stages of iron peak elements using R-matrix computer programs, and around 70 papers describing the results have been published in *Astronomy and Astrophysics*. Of particular importance is singly ionized iron where its high cosmic abundance, its relatively low ionization potential and its complex open d-shell atomic structure ensure that a very large number of electron impact excited lines are observed in objects as diverse as gaseous nebulae, active galactic nuclei, quasars, Seyfert galaxies and supernovae remnants. In addition, collisional data are required in the analysis of many laboratory plasmas which occur, for example, in laser plasma interactions and controlled thermonuclear fusion devices.

In the absence at present of experimental data for electron impact excitation cross sections for Fe II, this requirement for accurate collisional data can only be met by detailed and accurate calculations. However, there are a number of reasons why the calculation of collision cross sections for this and similar iron peak elements is difficult. First, the complexity of the open d-shell target means that large configuration interaction expansions, discussed in Sect. 2.2.1, are required to obtain accurate target wave functions and energies. Second, a very large number of coupled channels are required to accurately represent the collision wave function even for low-energy electron collisions. Third, the complex resonance structure which dominates the low-energy cross sections requires a very fine energy mesh to accurately resolve.

In order to illustrate the complexity of this problem we show in Fig. 5.9 the energy level diagram of Fe II below 30,000 cm^{-1} ($\sim$3.72 eV), taken from the tables of Johansson [505] and Corliss and Sugar [232], with some forbidden infra-red and optical transitions observed in gaseous nebulae indicated. In this low-energy region there are 16 LS-coupled states of Fe II resulting in 46 fine-structure levels, where particular interest in earlier work has focused on transitions between the four lowest LS-coupled states, corresponding to the $3d^6 4s\ a\,^6D$ ground state and the $3d^7\ a\,^4F$, $3d^6 4s\ a\,^4D$ and $3d^7\ a\,^4P$ excited states. In order to obtain accurate excitation cross sections involving these states it is important to represent them by accurate configuration interaction expansions, as discussed in Sect. 2.2.1, and to adequately represent higher states that play an important role in the transitions as virtual states. In particular, these higher states give rise to resonances that lie in the energy range of interest which we will see below dominate the low-energy cross sections. We present in Fig. 5.10 an energy level diagram of Fe II which shows the range of energies of the LS-coupled states which could play an important role in low-energy electron collisions. As an indication of the size of the computation involved in including in the R-matrix expansion (5.6) all target states corresponding to the 10 lowest lying configurations $3d^6 4s$, $3d^7$, $3d^5 4s^2$, $3d^6 4p$, $3d^5 4s4p$, $3d^6 5s$, $3d^6 4d$, $3d^6 5p$, $3d^6 4f$ and $3d^5 4p^2$, we give in Table 5.2 the maximum number of channels that can occur both in $LS\pi$-coupling and in $J\pi$-coupling including relativistic effects as an increasing number of these configurations are included in the calculation.

Over more than 25 years, a number of increasingly sophisticated e^-–Fe II collision calculations have been carried out. We summarize here some of the most

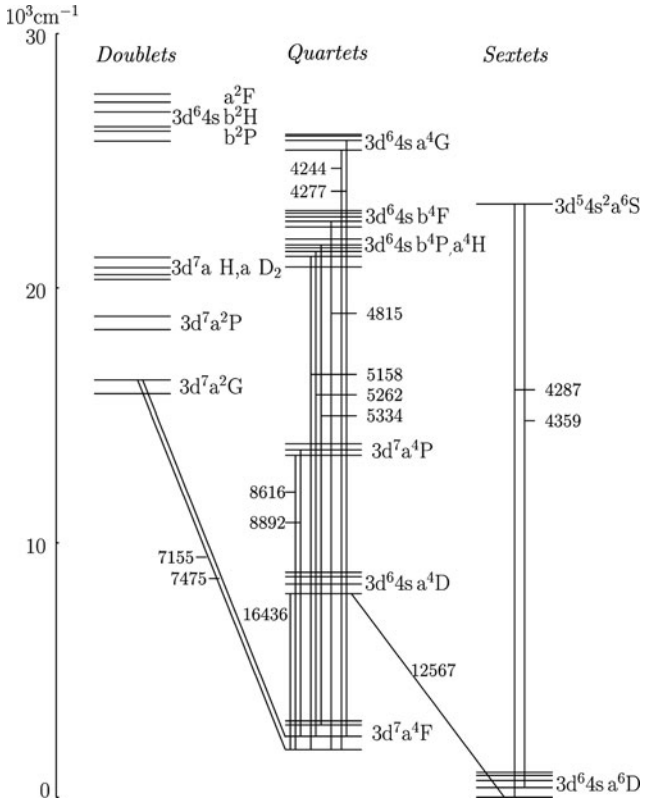

Fig. 5.9 The 16 *LS*-coupled states of Fe II below 30,000 cm^{-1} showing the corresponding 46 fine-structure levels and some forbidden infra-red and optical transitions observed in gaseous nebulae, with their wavelengths given in Angstrom (Fig. 2 from [188])

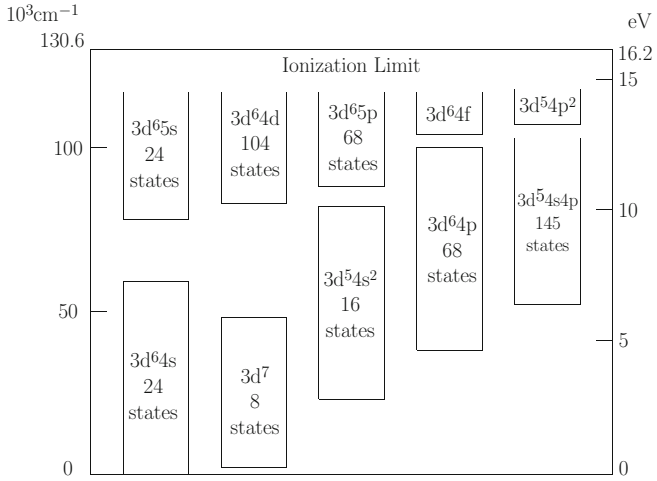

Fig. 5.10 Energy level diagram of Fe II showing the range of energies of the *LS*-coupled target states corresponding to the 10 lowest lying target configurations

Table 5.2 Maximum number of LS-coupled target states and coupled channels and the corresponding maximum number of fine-structure target states and coupled channels in an R-matrix expansion for e^-–Fe II collisions, where the numbers correspond to retaining in the calculation an increasing number of the target configurations illustrated in Fig. 5.10

	$LS\pi$		$J\pi$	
No. of configs	States	Channels	States	Channels
1	24	73	63	420
2	32	98	82	540
3	48	148	119	792
4	116	366	299	2,052
5	261	818	716	5,076
6	285	891	779	5,496
7	389	1,254	1,055	7,596
8	457	1,472	1,235	8,856
9	585	1,980	1,581	11,796
10	770	2,575	2,094	15,576

significant studies. The first detailed calculations were made by Nussbaumer and Storey [699], who included in their expansion of the collision wave function the four lowest LS-coupled states of Fe II shown in Fig. 5.9. However, these calculations were only carried out for three energies above all thresholds and hence no resonance structure was found. Later, Baluja et al. [48] extended this earlier work by adopting configuration interaction wave functions for the target and carrying out an R-matrix calculation including the four lowest LS-coupled states of Fe II using a finer energy mesh, which also included the resonance region below the highest threshold. It was found that even in the non-resonant region the excitation cross sections differed by a factor of 2 from the earlier results [699]. This work was further extended by Berrington et al. [101] who included relativistic terms from the Breit–Pauli Hamiltonian, discussed in Sect. 5.4.2, in the calculation of both the target and the collision wave functions, yielding effective collision strengths for transitions between the 16 fine-structure levels corresponding to the 4 lowest LS-coupled states of Fe II. The collision strengths obtained from this calculation were subsequently used by Keenan et al. [527] to obtain electron density-sensitive relative populations for the $3d^64s$ a ^{6}D fine-structure levels down to a temperature of 100 K and densities $N_e = 10^2$–10^6 cm^{-3} applicable to astrophysical plasmas, which were found to be a factor of 2 different from previous calculations.

With the rapid increase in computer power, Pradhan and Berrington [755] were able to carry out more sophisticated R-matrix calculations, which included all 38 quartet and sextet LS-coupled target states belonging to the $3d^64s$, $3d^7$ and $3d^64p$ configurations. It was found that the additional states belonging to the $3d^64p$ configuration, omitted in previous calculations, played an important role due to strong coupling with the $3d^64s$ states. Later, Zhang and Pradhan [1007] and Bautista and Pradhan [78] extended this LS-coupled calculation to yield collision strengths and effective collision strengths between the corresponding fine-structure levels, by recoupling the K-matrix elements using the pair-coupling scheme defined by (5.119). The rate coefficients for the transitions among the lowest 16 fine-structure levels were found to be substantially different from those predicted by Keenan

et al. [527] and by Nussbaumer and Storey [699], indicating that further work was required to obtain reliable rate coefficients.

In a series of more recent R-matrix calculations by Ramsbottom et al. [770–772] and by Zatsarinny and Bartschat [1001] all 113 quartet and sextet LS-coupled target states belonging to the lowest five configurations, $3d^64s$, $3d^7$, $3d^54s^2$, $3d^64p$ and $3d^54s4p$ in Fig. 5.10, were included in the expansion of the total wave function. This gave rise to a maximum of 354 channels for the total spin state $S = 2$ coupling the quartet and sextet target states. These calculations, carried out using two independent R-matrix computer programs RMATRXII and BSR, discussed in Sect. 5.1.1, were generally in good agreement although there were some differences in the low-energy region dominated by resonances caused by different representations of configuration interaction effects.

In order to calculate collision strengths and effective collision strengths for low-lying fine-structure forbidden transitions required in many astrophysical applications, Ramsbottom et al. [769, 773] also carried out Breit–Pauli R-matrix calculations including all fine-structure levels corresponding to the $3d^64s$, $3d^7$ and $3d^64p$ target configurations. It follows from Table 5.2 that this calculation included 262 coupled target states and a maximum of 1,800 coupled channels. We note that the target states and channels corresponding to the $3d^54s^2$ and $3d^54s4p$ configurations, which we see from Fig. 5.10 lie in the same energy range as the $3d^64p$ configuration, were not included in this calculation since their effect on the low-energy transitions of interest was expected to be small. We illustrate the results obtained in this calculation by showing in Fig. 5.11 the collision strength between the $3d^64s\ a\ ^6D^e_{9/2}$ and the

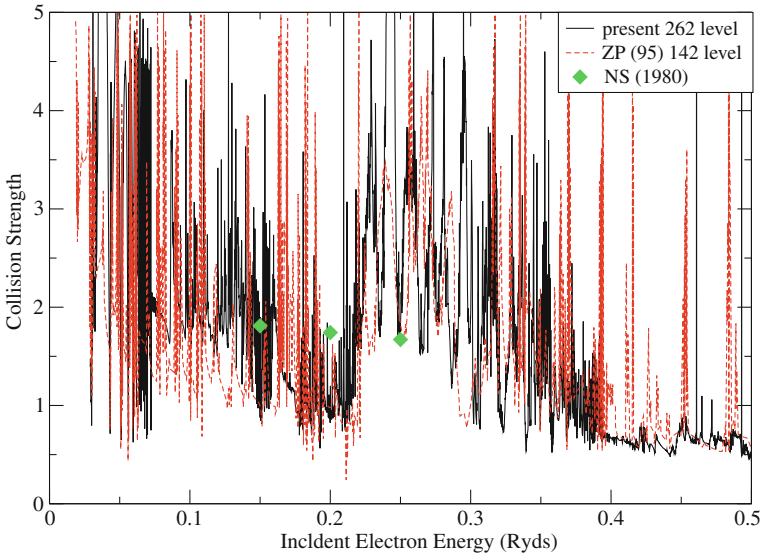

Fig. 5.11 Collision strengths for the $3d^64s\ a\ ^6D^e_{9/2} \rightarrow 3d^7\ a\ ^4F^e_{9/2}$ fine-structure transition in e^-–Fe II collisions. *Solid line*: Ramsbottom et al. 262-state calculation [773]; *dashed line*: Zhang and Pradhan 142-state calculation [1007]; *diamonds*: Nussbaumer and Storey calculation [699] (Fig. 3 from [773])

$3d^7\ a\,^4F^e_{9/2}$ fine-structure levels, which are compared with the earlier calculations by Zhang and Pradhan [1007] and by Nussbaumer and Storey [699]. We see that the collision strength is dominated by resonances, which required the evaluation at 16,200 distinct energy values to accurately delineate, 16,000 being in the resonance region and 200 above this region. We also note that the agreement between the calculations by Ramsbottom et al. [773] and by Zhang and Pradhan [1007] is quite good, although the non-resonant background collision strength of the latter calculation appears lower at incident electron energies around 0.1 Rydbergs. The corresponding effective collision strength for this transition is shown in Fig. 5.12 for the temperature range from 30 to 100,000 K, which incorporates temperatures important in astrophysical and plasma applications. We see that the effective collision strengths predicted by Zhang and Pradhan [1007] lie between 10 and 15% higher than the Ramsbottom et al. [773] values. However, the single temperature value of Bautista and Pradhan [78] lies a factor of 3 lower than the Ramsbottom et al. [773] results. For this transition the early prediction of Berrington et al. [101] is in reasonably good agreement with the most recent results but the results of Keenan et al. [527] differ significantly from the most recent work [773]. It is thus clear from this figure that more work needs to be carried out to confirm the result for even this low-lying transition. Since there are no experimental measurements to compare these calculations with, accurate results can only be confirmed by systematically

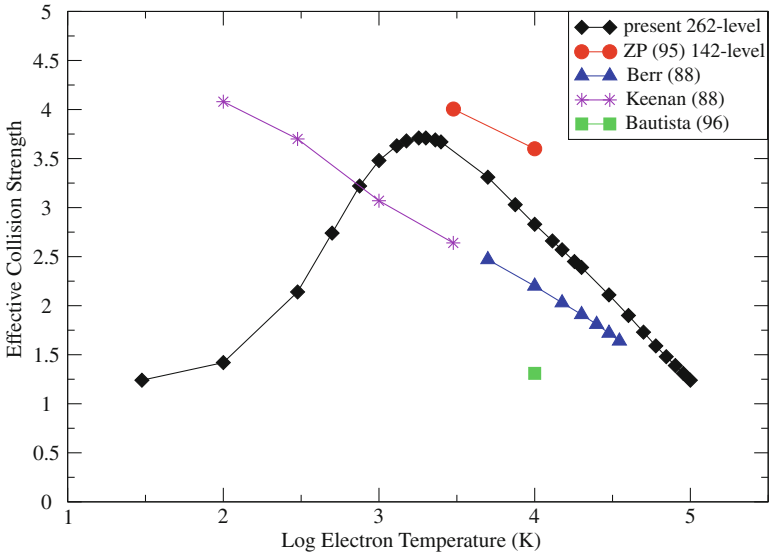

Fig. 5.12 Effective collision strengths as a function of log electron temperature in kelvin for the $3d^6 4s\ a\,^6D^e_{9/2} \rightarrow 3d^7\ a\,^4F^e_{9/2}$ fine-structure transition in e^-–Fe II collisions. *Diamonds*: Ramsbottom et al. 262-state calculation [773]; *circles*: Zhang and Pradhan 142-state calculation [1007]; *triangles*: Berrington et al. [101]; *stars*: Keenan et al. [527]; *square*: Bautista and Pradhan [78] (Fig. 4 from [773])

increasing the number of configurations included in the target and in the collision wave functions until convergence is obtained.

In conclusion, we see by examining Fig. 5.10 that, in addition to configurations included in the recent calculations, target states belonging to higher and omitted configurations are expected to play an important role, particularly for transitions involving higher states of interest in applications. The role of the continuum, which could be represented by pseudostates discussed in Chap. 6, may also be important. We see from Table 5.2 that the inclusion of these additional target states greatly increases the number of coupled channels, particularly when collision strengths for transitions between fine-structure levels of the target are required. However, with the development of parallel R-matrix collision programs and the implementation of efficient methods for including relativistic terms in the calculation, discussed in Sects. 5.4 and 5.5, these objectives, while presenting a computational grand challenge [188], should be achievable in the near future.

5.6.6 Electron Collisions with Fe XV

We have observed in our discussion of electron collisions with Fe II in Sect. 5.6.5 that accurate calculations of collision strengths for many transitions of importance in the analysis of astronomical spectra will require the inclusion of relativistic effects in the Hamiltonian. We have also seen in Sects. 5.4 and 5.5 that there are several procedures for including these effects, whose accuracy depends on the nuclear charge number Z of the atomic nucleus, ranging from transforming the non-relativistic K-matrix for relatively small Z targets to solving the Dirac equation for large Z targets. An important question that arises is when can accurate results be obtained using the Breit–Pauli Hamiltonian, discussed in Sect. 5.4.2, and when is it necessary to use the Dirac Hamiltonian, discussed in Sect. 5.5. In this section we consider detailed R-matrix collision strength calculations for Mg-like Fe XV which addressed this question.

There have been a number of R-matrix calculations of electron impact excitation of Fe XV. These include Breit–Pauli R-matrix calculations by Eissner et al. [291] and Griffin et al. [427] and Dirac R-matrix calculations by Aggarwal et al. [3]. In this last work it was found that there were significant differences between the Breit–Pauli and the Dirac calculations and it was therefore suggested that a fully relativistic Dirac calculation is necessary in order to obtain accurate results for a 14 times ionized $Z = 26$ target.

In order to explain whether the differences in the calculations were due to the different treatment of the relativistic effects or to the approximations made in solving the resultant equations, Berrington et al. [103] carried out detailed calculations for electron collisions with Fe XV using both the Breit–Pauli computer program RMATRXI, discussed in Sect. 5.1.1, and the Dirac computer program DARC, discussed in Sect. 5.5.1, removing as far as possible any variation in algorithmic features, such as the energy mesh and the target states included in the expansion. In

both calculations 45 $J\pi$ target states were retained in the R-matrix expansion corresponding to the 9 configurations $3s^2$, 3s3p, 3s3d, 3s4s, 3s4p, 3s4d, $3p^2$, 3p3d and $3d^2$. In addition, the configuration interaction representation of these target states was expanded in terms of the same set of configurations. In this way the possibility of pseudoresonances was avoided. Finally, in both calculations a fine energy mesh was adopted in order to fully resolve the resonance structure. As an example of the results obtained, the effective collision strengths for two double-electron transitions are shown in Fig. 5.13. We see that the Breit–Pauli and Dirac R-matrix results are in close agreement, with the variations between the calculations at lower temperatures being primarily attributed to the differences in the resonance positions determined by the Breit–Pauli and the Dirac target orbitals.

In conclusion, it was found that the average difference between the Breit–Pauli and Dirac R-matrix effective collision strengths for the 990 transitions considered between the 45 target states was only 6.14%. Furthermore, there is evidence from this work that the small differences that persist between the two calculations are due

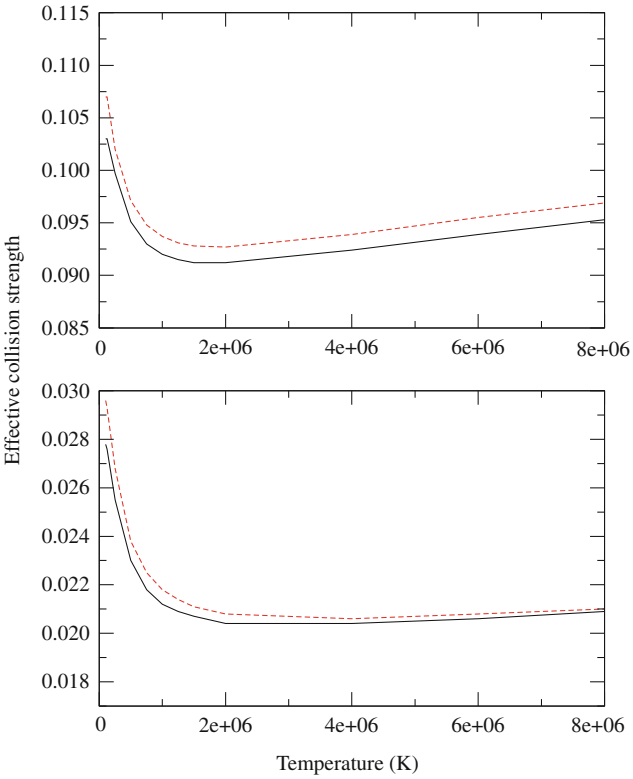

Fig. 5.13 Electron collisions with Fe XV. Effective collision strengths for the $3s^2\ {}^1S_0 \rightarrow 3p^2\ {}^1D_2$ (*upper graph*) and $3s^2\ {}^1S_0 \rightarrow 3p^2\ {}^3P_2$ (*lower graph*) transitions. Breit–Pauli R-matrix results are represented by *solid lines* and the Dirac R-matrix results are represented by *dashed lines* (Fig. 2 from [103])

primarily to variations in the target states rather than due to differences in collision theories. Consequently, this work shows that the Breit–Pauli Hamiltonian can be used with confidence in calculating transitions between the relatively low-Z iron peak elements.

5.6.7 Electron Collisions with Xe XXVII

As our last example in this chapter we consider Dirac R-matrix calculations of electron collisions with Ni-like Xe XXVII (Xe^{26+}) ions by Badnell et al. [37]. The spectra arising from electron impact excitation of heavier ions, such as ions

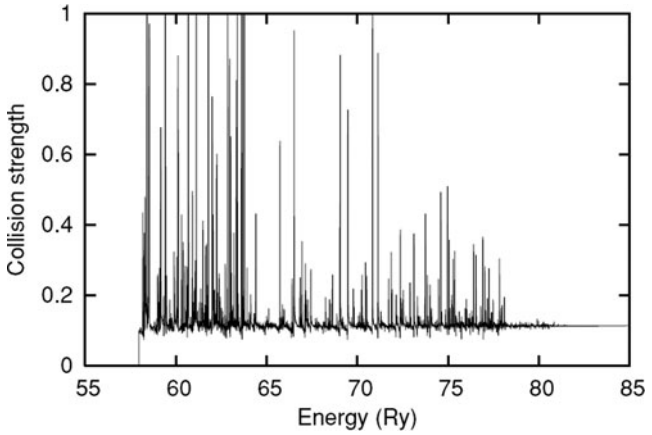

Fig. 5.14 Electron collisions with Xe^{26+}. Collision strength for the 129-state Dirac R-matrix $J = 0$–0 $3d^{10}\ {}^1S_0$–$3d^9 4d\ {}^1S_0$ transition (Fig. 2 from [37])

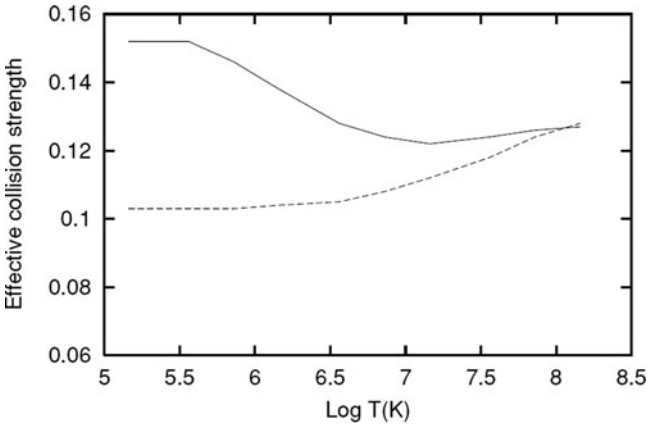

Fig. 5.15 Electron collisions with Xe^{26+}. Effective collision strength for the 129-state Dirac R-matrix $J = 0$–0 $3d^{10}\ {}^1S_0$–$3d^9 4d\ {}^1S_0$ transition. *Solid curve*: 129-state Dirac R-matrix calculation; *dashed curve*: plane wave Born approximation (Fig. 3 from [37])

of Xe, are important in many applications such as found in ITER (International Thermonuclear Experimental Reactor) and in the context of microlithographic light sources required to provide the next generation of etching for the semiconductor industry. In this work results for "feature photon emissivity coefficients", which are important in these applications, were obtained for Xe^{26+} from the calculated collision strengths.

In order to obtain accurate results for this relatively heavy ion the Dirac R-matrix program DARC, discussed in Sect. 5.5.1, was used in the internal R-matrix region which was interfaced with an extended and parallelized version of the external region program, originally developed for the Opacity Project [100, 860], discussed in Sect. 8.3. The calculation included 129 states of Xe^{26+} arising from the configurations $3d^{10}$ and $3d^9n\ell$ for $n = 4$ and 5 and $\ell = 0$ to $n - 1$, which yield a maximum of 821 coupled channels. Also, 21 continuum basis orbitals were retained in each channel for $2J = 1$–43 and 16 continuum basis orbitals were retained for $2J = 44$–71, resulting in Hamiltonian matrices of rank 17,356 and 13,136, respectively. The contribution to the cross sections from $2J > 71$ ("top-up") was obtained for dipole-allowed transitions using the sum rule proposed by Burgess [149] and for non-dipole transitions by assuming a geometric series in energy.

As an example of this study we show in Fig. 5.14 the results of the 129-state calculation of the strong $J = 0$–0 collision strength for the $3d^{10}\ {}^1S_0$–$3d^9 4d\ {}^1S_0$ transition, which populates the upper level of the lasing transition $3d^9 4d\ {}^1S_0$–$3d^9 4p\ {}^1P_1$ in Xe^{26+}. We see that over most of this energy range the collision strength is dominated by resonance structure which has to be included to obtain accurate results. To see this we compare the Maxwellian-averaged effective collision strength for this transition with plane wave Born approximation calculations in Fig. 5.15. We see that the Dirac R-matrix calculation is ∼18% larger than the Born result at $\log T(K) = 6.8$, which corresponds to the temperature of peak fractional abundance for Xe^{26+} over a wide range of electron densities. We also see that at lower temperatures this discrepancy becomes even larger.

In conclusion, these calculations show that the Dirac R-matrix calculations give significantly different effective collision strengths from the Born approximation in the temperature range of interest. In addition, the resonance enhancement of the effective collision strength plays a crucial role in obtaining accurate results. In general, the Dirac R-matrix method will play an essential role in obtaining accurate electron collision strengths for the heaviest atomic targets at energies and temperatures of importance in many applications.

Chapter 6
Intermediate-Energy Collisions

In this chapter we consider electron collisions with atoms and atomic ions at intermediate energies which are defined to range from close to the ionization threshold to several times this threshold. In this energy range the target can be ionized as well as excited and, since the energy is not high, strong coupling effects can exist between the channels leading to excitation and to ionization, which can involve intermediate resonances. Hence, theoretical methods that give reliable results for excitation and ionization cross sections at intermediate energies must accurately represent these effects.

We commence our discussion of intermediate-energy collisions in Sect. 6.1 by considering examples that illustrate the complexity of the processes that can occur at these energies. We then give a brief overview of methods that have been developed to enable accurate electron scattering amplitudes and cross sections to be calculated at intermediate energies. This provides an introduction to our description of the R-matrix with pseudostates (RMPS) method in Sect. 6.2, which in recent years has enabled accurate electron collision and photoionization cross sections to be calculated at low and intermediate energies for multi-electron atoms, ions and molecules. In Sect. 6.3 we describe the intermediate-energy R-matrix (IERM) method where the emphasis is to enable accurate electron impact excitation and ionization cross sections involving highly excited states to be calculated close to the ionization threshold. In Sect. 6.4 we analyse the analytic behaviour of the scattering amplitude and cross sections at intermediate energies using these methods. We show that the scattering amplitude exhibits non-physical resonances which must be eliminated by energy averaging the corresponding T-matrices in order to obtain accurate scattering amplitudes and cross sections. Then in Sect. 6.5 we describe distorted wave and Born series R-matrix methods for electron impact ionization. In the distorted wave method, the faster ionizing electron is represented by a distorted wave and a slower ejected electron and resultant residual ion are represented by an R-matrix expansion. This enables processes, such as excitation–autoionization discussed below, to be accurately calculated when the incident ionizing electron energy is well above the ionization threshold. Finally, in Sect. 6.6 we present results from some recent electron–atom and electron–ion collision R-matrix calculations at intermediate energies.

P.G. Burke, *R-Matrix Theory of Atomic Collisions*, Springer Series on Atomic, Optical, and Plasma Physics 61, DOI 10.1007/978-3-642-15931-2_6,

6.1 Overview of Intermediate-Energy Methods

The complexity of the processes that can occur at intermediate energies is illustrated below for electron collisions with C IV (C^{3+}), which has been the subject of experiments [235, 669] as well as detailed R-matrix calculations [653, 842]. In addition to excitation and to the direct ionization (DI) process, which we write as

$$e^- + C^{3+}(1s^2 2s) \rightarrow C^{4+}(1s^2) + 2e^-, \tag{6.1}$$

three important indirect ionization processes can occur. These are as follows:

i. Excitation–autoionization (EA), where the target is excited to an intermediate doubly excited resonance state which autoionizes with the emission of an electron

$$\begin{aligned} e^- + C^{3+}(1s^2 2s) \rightarrow\ & C^{3+**}(1sn'\ell' n''\ell'') + e^- \\ & \downarrow \\ & C^{4+}(1sn\ell) + e^-. \end{aligned} \tag{6.2}$$

ii. Resonant excitation–double-autoionization (REDA), where the incident electron is captured into an intermediate triply excited resonance state which decays with the sequential emission of two electrons

$$\begin{aligned} e^- + C^{3+}(1s^2 2s) \rightarrow\ & C^{2+***}(1sn'\ell' n''\ell'' n'''\ell''') \\ & \downarrow \\ & C^{3+**}(1sn''''\ell'''' n''''\ell'''') + e^- \\ & \downarrow \\ & C^{4+}(1sn\ell) + e^-. \end{aligned} \tag{6.3}$$

iii. Resonant excitation–auto-double-ionization (READI), where the incident electron is captured into an intermediate triply excited resonance state which decays with the simultaneous emission of two electrons

$$\begin{aligned} e^- + C^{3+}(1s^2 2s) \rightarrow\ & C^{2+***}(1sn'\ell' n''\ell'' n'''\ell''') \\ & \downarrow \\ & C^{4+}(1sn\ell) + 2e^-. \end{aligned} \tag{6.4}$$

The intermediate resonance states in (6.2), (6.3) and (6.4) are indicated by asterisks and the excited electron orbitals in these states are marked by primes. In all three processes C^{4+} can be left in its ground state or in an excited state. In addition to these processes, the scattered electron can be captured into an intermediate resonance state which can decay with the emission of a photon giving rise to dielectronic recombination. This radiative decay process becomes particularly important

for Rydberg resonances involving highly charged ions, which we will discuss in Sect. 8.2.

Many approaches have been developed to enable accurate electron impact excitation and ionization cross sections of atoms and ions to be calculated at intermediate energies. These include optical potential methods (e.g. [612, 613]), Born series methods (e.g. [503, 948]) and distorted wave methods (e.g. [512, 513, 629]), where Born series and distorted wave methods are perturbative approaches which are appropriate when the coupling between the initial and final states is not strong.

Considerable progress has also been made in recent years in extracting accurate continuum information from expansions in square (L^2) integrable functions, which are applicable when the coupling between the bound and continuum states becomes strong. In these L^2 integrable methods the usual specification of the asymptotic form of the wave function is avoided by expanding it in terms of functions which vanish asymptotically. Diagonalization of the Hamiltonian in an L^2 integrable basis then yields a discretization of the continuum spectrum from which electron scattering or photoionization information can be extracted. A number of procedures for extracting this information have been developed. These include T-matrix extrapolation from complex energies [266, 616, 818, 819], Fredholm analytic continuation [787] and Stieltjes imaging and moment T-matrix methods [571, 572, 981, 982]. These L^2 approaches, which have been reviewed by Reinhardt [785, 786], have been particularly successful in the calculation of resonance positions and widths and in the study of photoionization cross sections.

More recently, an exterior complex scaling (ECS) method, proposed by Simon [877] and developed further by Rescigno et al. [789], has been used with considerable success by Rescigno et al. [790], Baertschy et al. [39, 40] and McCurdy et al. [615] to obtain accurate electron–hydrogen atom ionization cross sections at intermediate energies. In this method, the time-independent Schrödinger equation is solved numerically on a two-dimensional grid where the radial coordinates are rotated into the complex plane at a radius R_0, using the transformation

$$z(r) = \begin{cases} r & r < R_0 \\ R_0 + (r - R_0)e^{i\eta} & r \geq R_0 \end{cases} . \tag{6.5}$$

The transformation defines a box of side R_0 such that in the box the radial coordinates are real and outside the box one or both the radial coordinates are complex. Inside the box the Schrödinger equation can be solved using standard numerical procedures and outside the box the ECS procedure transforms any outgoing wave into a function that falls off exponentially. Also, a propagating exterior complex scaling (PECS) method has been developed by Bartlett and Stelbovics [59, 60], Bartlett et al. [61] and Bartlett [57, 58] which has been used to obtain accurate electron impact differential ionization cross sections for hydrogenic targets with $Z \leq 4$ and which gave strong support for the Wannier threshold behaviour of the electron–hydrogen atom ionization cross section discussed in Sect. 3.3.5. It has also been shown that

this approach has the potential to treat electron collisions with multi-electron atoms and ions at intermediate energies.

In the next section we consider R-matrix methods based on the "close coupling with pseudostates" expansion introduced in Sect. 2.3.1. These methods have some aspects of similarity to the L^2 integrable methods mentioned above, in that the close coupling expansion is carried out in terms of basis functions confined to an internal region and the summation over target bound states is augmented by a summation over suitably chosen L^2 integrable pseudostates, representing the highly excited and continuum eigenstates of the target Hamiltonian. In this method, coupling between bound states and continuum states is treated to all orders at the expense of a considerable increase in the number of coupled second-order integrodifferential equations that have to be solved. We will see that this close coupling with pseudostates expansion is the basis of recent applications of R-matrix theory which have yielded accurate cross sections at intermediate energies for electron impact excitation and ionization, as well as for photoionization, of multi-electron atoms and ions. We will also consider the extension of this method to electron–molecule collisions at intermediate energies in Chap. 11.

The importance of strong coupling effects between bound and continuum states of the target in electron–atom collisions has long been recognized and many workers have considered including pseudostates in the close coupling expansion in order to represent the continuum states of the target. Early work, carried out by Burke and Schey [160], suggested that pseudostates should be retained in their low-energy electron–atomic hydrogen close coupling calculations, which included the 1s, 2s and 2p target eigenstates, in order to remove certain inadequacies in their results. At the same time Rotenberg [799] introduced a Sturmian basis in positron–hydrogen atom elastic scattering, where this basis was discrete and non-orthogonal and where the first member was the hydrogen atom ground state and the remaining members were pseudostates. Also, as we have already mentioned in Sect. 2.2.2, the observation by Castillejo et al. [205], that 18.6% of the polarizability of atomic hydrogen in its ground state comes from the continuum terms in the expansion of the polarizability, led Damburg and Karule [245] to point out that the full polarizability in electron scattering by atomic hydrogen can be obtained by including a single $\overline{2p}$ polarized pseudostate in the close coupling expansion. This polarized pseudostate was incorporated in close coupling with pseudostates calculations for elastic electron–hydrogen atom collisions by Burke et al. [177] and Fon et al. [328], giving improved convergence over calculations including only target eigenstates. Also, Geltman and Burke [368] and Burke and Webb [163] extended this work by including several pseudostates in the electron–hydrogen atom close coupling expansion used to study the excitation of the 2s and 2p states, with improved agreement with experiment. Later, polarized pseudostates were incorporated into elastic electron–helium, neon and argon collision calculations by Fon et al. [327, 329, 330].

In the applications of pseudostate methods that we have discussed so far, there has been no systematic attempt to explore the convergence of the pseudostate expansion. In order to address this question, we compare in Fig. 6.1 the exact spectrum of a typical target atom or ion with its approximate representation by a close coupling

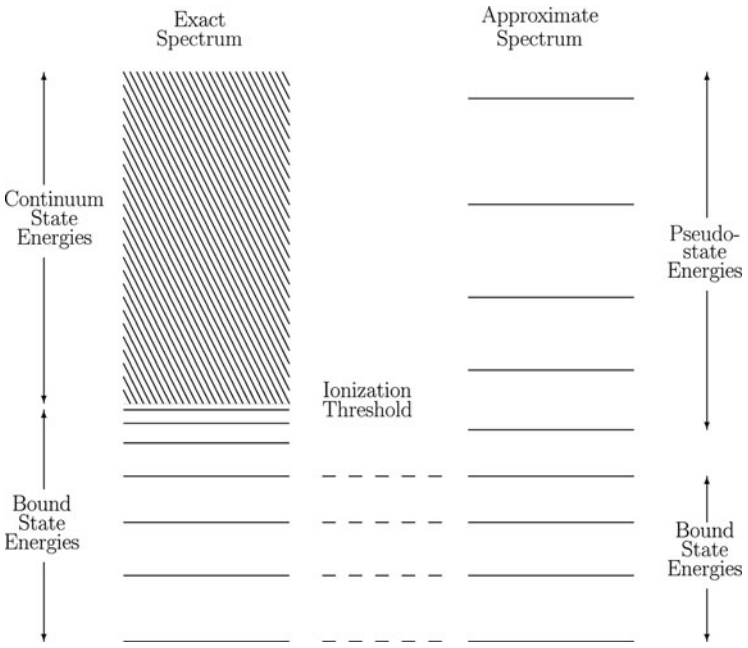

Fig. 6.1 Exact spectrum of a target atom or ion and its approximate representation by a bound with pseudostates spectrum at low and intermediate energies

with pseudostates expansion corresponding to expansion (2.55). We see that the lowest bound target eigenstates are accurately represented by the close coupling with pseudostates expansion. However, the infinite number of high-lying Rydberg state energies and the continuum spectrum of the target are represented by a discrete spectrum so that ionization is approximated by an appropriate summation over excitations of pseudostates lying at higher energies in the continuum. It is thus clear that, in order to obtain an accurate representation of both excitation and ionization at intermediate energies, the continuum must be spanned by a sufficiently dense pseudostate basis.

An early study of the convergence of the close coupling with pseudostates expansion was made by Burke and Mitchell [165] for electron collisions with hydrogen atoms. They included the 1s and 2s eigenstates and up to three s-wave pseudostates in this expansion and found that the 1s–2s excitation cross section converged rapidly at intermediate energies to a result significantly smaller than that obtained omitting the pseudostates. However, the resultant cross sections exhibited non-physical resonances associated with the pseudostate thresholds which had to be averaged over to obtain physically meaningful results, as we will discuss in Sect. 6.4. These calculations were extended by Oza and Callaway [711] and by Oza [710], who included further s-wave eigenstates and pseudostates in the expansion of the wave function, giving results in good agreement with accurate results obtained by Poet [747, 748] for this s-wave model. In more elaborate studies of e^-–H collisions at intermediate

energies, Callaway and Wooten [198, 199] and Callaway [197] included 1s, 2s, 2p and 3d target eigenstates together with seven pseudostates in this expansion. They found that the 1s–2s and 1s–2p excitation cross sections at intermediate energies were lower than the cross sections obtained including 1s, 2s and 2p eigenstates alone, with substantially better agreement with experiment. Later, as greater computing resources became available, Callaway and Unnikrishnan [200] extended these calculations to study excitation of the $n = 3$ states of atomic hydrogen at intermediate energies where they retained seven target eigenstates and ten pseudostates in the close coupling with pseudostates expansion.

Finally, in important more recent developments we mention the "convergent close coupling" (CCC) method, introduced by Bray and Stelbovics [126–128], in which the radial basis of the target eigenstates and pseudostates is expanded in members of a complete Laguerre basis, and the scattering amplitude is obtained by solving the resultant coupled integrodifferential equations in momentum space. Using this method the cross sections have been shown to be rapidly convergent as the Laguerre basis is expanded towards completeness. The CCC method has been successfully applied to both electron impact excitation of atoms and ions with one active electron as well as photoionization of atoms and the method and results have been reviewed by Bray and Stelbovics [129] and Bray et al. [130]. We also mention the time-dependent close coupling method which was first applied to calculate total cross sections for electron impact ionization of H by Pindzola et al. [736, 737] and photon double ionization of He by Pindzola and Robicheaux [738]. In this method, the time-dependent close coupled second-order partial differential equations are solved using a wave packet approach on a two-dimensional numerical lattice for total and differential cross sections and on a three-dimensional numerical lattice for electron impact ionization of atoms and ions. Applications of this method, which now include electron and photon collisions with few-electron atoms, ions and molecules, have been reviewed by Pindzola et al. [740].

6.2 *R*-Matrix with Pseudostates Method

In this section we describe the *R*-matrix with pseudostates (RMPS) method, introduced by Bartschat et al. [70, 71] and further developed by Badnell and Gorczyca [33], Gorczyca and Badnell [394] and Marchalant and Bartschat [633, 634]. The RMPS method has enabled accurate electron collision cross sections to be calculated at low and intermediate energies for arbitrary multi-electron atoms and ions. It has also been used to determine accurate atomic photoionization cross sections and electron–molecule collision cross sections at low and intermediate energies, as discussed in Chaps. 8 and 11, respectively.

The RMPS method commences, as in standard *R*-matrix theory described in Sect. 5.1, by partitioning configuration space into an internal region, an external region and an asymptotic region as illustrated in Fig. 5.1. The time-independent

Schrödinger equation (5.2) is then solved by expanding the total wave function using (5.5) and (5.6) in the internal region and using (5.28) in the external and asymptotic regions. The new feature of the RMPS method arises in the choice of the target eigenstates and pseudostates representing the exact spectrum in Fig. 6.1. These are chosen to diagonalize the N-electron target Hamiltonian H_N as follows:

$$\langle \Phi_i | H_N | \Phi_j \rangle = e_i \delta_{ij}, \tag{6.6}$$

where for notational convenience both the target eigenstates and pseudostates are denoted by Φ_i. Hence, in accord with our discussion of Fig. 6.1, it follows that the lowest energies e_i in (6.6) provide an accurate representation of the lowest bound-state eigenenergies of the target, while the higher energies e_i provide a discrete representation of the high-lying bound and continuum spectrum of the target. As in Sect. 2.2, we expand both the target eigenstates and pseudostates as a summation over an orthonormal set of target configurations ϕ_i in the form

$$\Phi_j(\mathbf{X}_N) = \sum_i \phi_i(\mathbf{X}_N) c_{ij}, \tag{6.7}$$

where the ϕ_i are constructed from both physical and pseudo-orbitals and where the coefficients c_{ij} are obtained by diagonalizing the target Hamiltonian in (6.6).

We consider first the choice of the physical and pseudo-orbitals used to construct the target eigenstates and pseudostates included in expansion (6.7). We consider a procedure analogous to that used by Bartschat et al. [70] in their RMPS study of electron–hydrogen atom collisions at low and intermediate energies. For illustrative purposes, we assume that the following orbitals are retained in the calculation:

$$\begin{array}{rrrrr} 1\mathrm{s} & 2\mathrm{s} & \overline{3\mathrm{s}} & \overline{4\mathrm{s}} & \ldots \ \overline{n_{\max}\mathrm{s}} \\ 2\mathrm{p} & \overline{3\mathrm{p}} & \overline{4\mathrm{p}} & \ldots & \overline{n_{\max}\mathrm{p}} \\ & \overline{3\mathrm{d}} & \overline{4\mathrm{d}} & \ldots & \overline{n_{\max}\mathrm{d}}, \end{array} \tag{6.8}$$

where 1s, 2s, 2p are physical orbitals and $\overline{3\mathrm{s}}$, $\overline{3\mathrm{p}}$, $\overline{3\mathrm{d}}$, …, $\overline{n_{\max}\mathrm{s}}$, $\overline{n_{\max}\mathrm{p}}$, $\overline{n_{\max}\mathrm{d}}$, which are denoted here and below by a bar, are pseudo-orbitals. In the case of atomic hydrogen the 1s, 2s and 2p physical orbitals are the exact non-relativistic orbitals of the hydrogen atom and in the case of general multi-electron atoms and ions, such as Be-like ions considered in Sect. 2.2.1, the physical orbitals are usually chosen to be the Hartree–Fock orbitals of the target ground state and low-lying excited states.

The choice of the pseudo-orbitals in (6.8) can be made in many different ways subject to the condition that as $n_{\max} \to \infty$ the orbital basis is complete for each orbital angular momentum ℓ. A convenient choice is to expand the radial component of the pseudo-orbitals in a Sturmian-type basis as follows:

$$\overline{P_{n\ell}}(r) = \sum_{i=\ell+1}^{n} a_{i\ell}^{n} r^i \mathrm{e}^{-\alpha r}, \quad n = n_{\min}, \ldots, n_{\max}, \tag{6.9}$$

where $n_{\min}$ is the minimum value of n, which is 3 in the example defined by (6.8) and $n_{\max}$ is the maximum value of n. The coefficients $a_{i\ell}^{n}$ in (6.9) are then determined so that, for each orbital angular momentum ℓ, the pseudo-orbitals are orthogonal to the corresponding physical orbitals and are orthonormal so that

$$\int_0^{a_0} P_{n\ell}(r)\overline{P_{n'\ell}}(r) = 0, \quad \int_0^{a_0} \overline{P_{n\ell}}(r)\overline{P_{n'\ell}}(r) = \delta_{nn'}, \quad \text{all } n \text{ and } n'. \tag{6.10}$$

In this analysis we have assumed that the radius a_0 of the internal region is chosen so that both the physical and pseudo-orbitals are effectively zero for $r \geq a_0$. Owing to the completeness of the Sturmian-type basis, the choice of the range parameter α in (6.9) is in principle arbitrary. However, its choice will affect the convergence properties of the pseudostate expansion, with different choices of α being required to obtain the most rapid convergence in different energy regions and for different transitions. Also, by adopting a pseudostate expansion, we see from Fig. 6.1 that we have replaced the continuum spectrum of the atom by a discrete spectrum, thus introducing non-physical pseudostate thresholds into the calculation. By varying α or the value of $n_{\max}$ in (6.9) we can move the non-physical thresholds, associated with pseudo-resonances, away from the energy range of interest. We will return to this question again in Sect. 6.4 where we consider a T-matrix energy-averaging procedure for eliminating the non-physical thresholds and pseudo-resonances.

We now consider the relationship between the physical and pseudo-orbitals, determined as discussed above, and the continuum basis orbitals u_{ij}^{0} in (5.6), which we assume are generated by solving (5.75) subject to the boundary conditions (5.76) and (5.77) and the orthonormality conditions (5.78) and (5.79), which ensures that the continuum orbitals are orthogonal to the physical bound orbitals with the same orbital angular momentum symmetry. We assume that for a given orbital angular momentum ℓ we have defined the following basis orbitals:

$$\begin{aligned} \text{physical orbitals,} \quad & P_i(r), \quad i = 1, \ldots, q, \\ \text{pseudo-orbitals,} \quad & \overline{P}_i(r), \quad i = 1, \ldots, p, \\ \text{continuum orbitals,} \quad & u_i(r), \quad i = 1, \ldots, n_{\mathrm{c}}. \end{aligned} \tag{6.11}$$

We have seen that while the physical orbitals are orthogonal to both the pseudo-orbitals and the continuum orbitals, the pseudo-orbitals defined by (6.9) and (6.10) are only orthogonal to the physical orbitals. Hence the normalization and overlap integrals involving the pseudo-orbitals and the continuum orbitals can be summarized by the three matrix equations

$$\langle \overline{\mathbf{P}}\,\overline{\mathbf{P}}^{\mathrm{T}} \rangle = \mathbf{I}, \quad \langle \mathbf{U}\mathbf{U}^{\mathrm{T}} \rangle = \mathbf{I}, \quad \langle \mathbf{U}\overline{\mathbf{P}}^{\mathrm{T}} \rangle = \mathbf{M}, \tag{6.12}$$

where we have used Dirac bracket notation to represent the integration over the range $0 \leq r \leq a_0$ and where $\overline{\mathbf{P}}$ and $\mathbf{U}$ are vectors with components $\overline{P}_i(r)$ and $u_i(r)$, respectively.

While non-orthogonal B-spline orbitals have been used with considerable success in a number of R-matrix applications, for example, by Zatsarinny and Froese Fischer [994], Zatsarinny and Tayal [995–997], Zatsarinny and Bartschat [998–1001] and van der Hart et al. [930, 937, 938], the evaluation of the Hamiltonian matrix elements in (5.7) is simplified if the continuum orbitals are orthogonalized to the pseudo-orbitals. This can be achieved by introducing a new vector $\mathbf{V}$ with components

$$v_i(r), \quad i = 1, \ldots, p + n_c. \tag{6.13}$$

We then express this new basis in terms of $\overline{\mathbf{P}}$ and $\mathbf{U}$ by the following matrix equation:

$$\mathbf{V} = \begin{bmatrix} \overline{\mathbf{P}} \\ \mathbf{A}\overline{\mathbf{P}} + \mathbf{B}\mathbf{U} \end{bmatrix}, \tag{6.14}$$

where $\mathbf{A}$ has dimensions $n_c \times p$ and $\mathbf{B}$ has dimensions $n_c \times n_c$. We require that this new basis is orthonormal so that

$$\langle \mathbf{V}\mathbf{V}^{\mathrm{T}} \rangle = \mathbf{I}, \quad \langle (\mathbf{A}\overline{\mathbf{P}} + \mathbf{B}\mathbf{U})\overline{\mathbf{P}}^{\mathrm{T}} \rangle = 0. \tag{6.15}$$

This yields the following equations:

$$\mathbf{A}\mathbf{A}^{\mathrm{T}} + \mathbf{B}\mathbf{B}^{\mathrm{T}} + \mathbf{A}\mathbf{M}^{\mathrm{T}}\mathbf{B}^{\mathrm{T}} + \mathbf{B}\mathbf{M}\mathbf{A}^{\mathrm{T}} = \mathbf{I} \tag{6.16}$$

and

$$\mathbf{A} = -\mathbf{B}\mathbf{M}, \tag{6.17}$$

where we have used (6.12) in simplifying these equations. After substituting for $\mathbf{A}$ from (6.17) into (6.16) we obtain

$$\mathbf{B}(\mathbf{I} - \mathbf{M}\mathbf{M}^{\mathrm{T}})\mathbf{B}^{\mathrm{T}} = \mathbf{I}. \tag{6.18}$$

A solution of these equations yielding an orthonormal basis can be obtained using the Schmidt orthogonalization procedure [976]. For example, in the approach adopted by Burke and Robb [167] and Bartschat et al. [70], the last n_c elements in $\mathbf{V}$ defined by (6.14) are written in the form

$$v_{i+p}(r) = \sum_{j=1}^{p} a_{ij}\overline{P}_j(r) + \sum_{j=1}^{i} b_{ij}u_j(r), \quad i = 1, \ldots, n_c, \tag{6.19}$$

which can be solved recursively in the order $i = 1, 2, \ldots, n_c$. At each step the $p + i$ coefficients a_{ij}, $j = 1, \ldots, p$, and b_{ij}, $j = 1, \ldots, i$, are determined by imposing the following p orthogonality conditions

$$\langle \overline{P}_j \; v_{i+p} \rangle = 0, \quad j = 1, \ldots, p, \tag{6.20}$$

and i orthonormality conditions

$$\langle v_{j+p} \; v_{i+p} \rangle = \delta_{ij}, \quad j = 1, \ldots, i. \tag{6.21}$$

In this way the matrices **A** and **B** in (6.16) are determined, where the matrix **B** has zero elements in the upper triangle, so that

$$b_{ij} = 0, \quad j > i, \;\; i, \; j = 1, \ldots, n_c. \tag{6.22}$$

This approach has been widely used and has proved to be satisfactory provided that the number of pseudo-orbitals does not exceed 2 or 3 for each orbital angular momentum. However, as $p \to \infty$ the Gram–Schmidt procedure becomes unstable since the pseudo-orbital basis and the continuum orbital basis become linearly dependent in this limit. This follows since the continuum orbital basis is complete in the limit $n_c \to \infty$ in the space orthogonal to the physical orbitals over the range $0 \le r < a_0$. Hence we can expand the pseudo-orbitals in this basis as follows:

$$\overline{P}_i(r) = \sum_{j=1}^{\infty} c_{ij} u_j(r), \quad 0 \le r < a_0, \;\; i = 1, \ldots, p, \tag{6.23}$$

which is uniformly convergent except in the neighbourhood of the boundary $r = a_0$. This does not cause difficulties for low-energy electron collisions where only a few pseudo-orbitals of each angular symmetry are required and where the convergence of the R-matrix expansion is fast. However, errors due to linear dependence can arise at higher energies where n_c is larger and where many pseudo-orbitals may be required for each orbital angular momentum to represent ionization.

To explore this problem in more detail we assume that, for n_c values which accurately describe intermediate-energy collisions, $p \ll n_c$ and we can write to a high degree of accuracy

$$\overline{P}_i(r) = \sum_{j=1}^{n_c} c_{ij} u_j(r), \quad 0 \le r < a_0, \;\; i = 1, \ldots, p. \tag{6.24}$$

It follows, using the notation of (6.12), that

$$\mathbf{I} = \langle \overline{\mathbf{P}} \, \overline{\mathbf{P}}^{\mathrm{T}} \rangle = \mathbf{C} \langle \mathbf{U} \, \mathbf{U}^{\mathrm{T}} \rangle \mathbf{C}^{\mathrm{T}} = \mathbf{C}\mathbf{C}^{\mathrm{T}}, \tag{6.25}$$

where **C** is the $p \times n_c$ matrix with matrix elements c_{ij}. Also

$$\mathbf{M} = \langle \mathbf{U} \, \overline{\mathbf{P}}^{\mathrm{T}} \rangle = \langle \mathbf{U} \, \mathbf{U}^{\mathrm{T}} \rangle \mathbf{C}^{\mathrm{T}} = \mathbf{C}^{\mathrm{T}}, \tag{6.26}$$

so that the $n_c \times n_c$-dimensional matrix $\mathbf{M}\mathbf{M}^{\mathrm{T}}$ in (6.18) can be written as

$$\mathbf{M}\mathbf{M}^{\mathrm{T}} = \mathbf{C}^{\mathrm{T}}\mathbf{C}. \tag{6.27}$$

We now construct $n_c - p$ additional orthonormal vectors which are orthogonal to the p rows of the matrix $\mathbf{C}$ but which are otherwise arbitrary. These $n_c - p$ vectors together with the p rows of $\mathbf{C}$ then span an n_c-dimensional space. We call the matrix whose rows correspond to these $n_c - p$ vectors $\mathbf{D}$. It follows that

$$\mathbf{C}\mathbf{D}^{\mathrm{T}} = 0, \quad \mathbf{D}\mathbf{D}^{\mathrm{T}} = \mathbf{I}. \tag{6.28}$$

We then define the $n_c \times n_c$ matrix $\mathbf{B}$ in (6.18) in terms of $\mathbf{C}$ and $\mathbf{D}$ as follows:

$$\mathbf{B} = \begin{bmatrix} \mathbf{C} \\ \mathbf{D} \end{bmatrix}. \tag{6.29}$$

Then

$$\mathbf{B}\mathbf{B}^{\mathrm{T}} = \begin{bmatrix} \mathbf{C} \\ \mathbf{D} \end{bmatrix} [\mathbf{C}^{\mathrm{T}}\ \mathbf{D}^{\mathrm{T}}] = \begin{bmatrix} \mathbf{C}\mathbf{C}^{\mathrm{T}} & \mathbf{C}\mathbf{D}^{\mathrm{T}} \\ \mathbf{D}\mathbf{C}^{\mathrm{T}} & \mathbf{D}\mathbf{D}^{\mathrm{T}} \end{bmatrix} = \mathbf{I}, \tag{6.30}$$

where we have used (6.25) and (6.28). Hence $\mathbf{B}$ is an orthogonal matrix. We now consider

$$\mathbf{B}\mathbf{M}\mathbf{M}^{\mathrm{T}}\mathbf{B}^{\mathrm{T}} = \mathbf{B}\mathbf{C}^{\mathrm{T}}\mathbf{C}\mathbf{B}^{\mathrm{T}} = \begin{bmatrix} \mathbf{I} & \mathbf{O} \\ \mathbf{O} & \mathbf{O} \end{bmatrix}. \tag{6.31}$$

Hence the orthogonal matrix $\mathbf{B}$ diagonalizes the matrix $\mathbf{M}\mathbf{M}^{\mathrm{T}}$ where the first p diagonal elements are unity and the last $n_c - p$ diagonal elements are zero. Also it follows that the matrix $\mathbf{I} - \mathbf{M}\mathbf{M}^{\mathrm{T}}$ which arises in (6.18) is also diagonalized by $\mathbf{B}$ giving

$$\mathbf{B}(\mathbf{I} - \mathbf{M}\mathbf{M}^{\mathrm{T}})\mathbf{B}^{\mathrm{T}} = \begin{bmatrix} \mathbf{O} & \mathbf{O} \\ \mathbf{O} & \mathbf{I} \end{bmatrix}, \tag{6.32}$$

where now the first p diagonal elements are zero and the last $n_c - p$ diagonal elements are unity. We see from this result that the p eigenvalues of $\mathbf{I} - \mathbf{M}\mathbf{M}^{\mathrm{T}}$, which are zero, correspond to the p pseudo-orbitals, which can be accurately represented in terms of the continuum orbitals by expansion (6.24) and which give rise to the linear dependence problem discussed above.

In practice, the matrix obtained by diagonalizing $\mathbf{I} - \mathbf{M}\mathbf{M}^{\mathrm{T}}$ is only approximated by the form given by (6.32) since expansion (6.24) is not exact. However, the eigenvalues of $\mathbf{I} - \mathbf{M}\mathbf{M}^{\mathrm{T}}$, which are close to zero, correspond to eigenvectors which are accurately represented by the pseudo-orbitals and hence can be omitted from the expansion without appreciable error. This is the basis of the method proposed by

Gorczyca and Badnell [394], who omitted from the expansion those eigenvectors corresponding to eigenvalues below a certain threshold, which they took to be 10^{-4}. Hence they included in their expansion the physical orbitals and pseudo-orbitals defined in (6.11) and a reduced set of continuum orbitals $v_i(r)$, defined by (6.14), corresponding to eigenvalues of $\mathbf{I}-\mathbf{M}\mathbf{M}^{\mathrm{T}}$ larger than the threshold. In this way they avoided the errors due to linear dependence discussed above.

An extension to the procedure for calculating the Buttle correction, described in Sect. 5.3.2, is required if pseudostates are retained in (5.5) and (5.6). If the Gram–Schmidt orthonormalization method discussed above is used then additional high-energy R-matrix poles arising from these additional pseudostates occur in the R-matrix expansion (5.19). These additional pole terms, which duplicate part of the Buttle correction, can lead to significant error and have to be discarded before the Buttle correction is included.

On the other hand, if the procedure adopted by Gorczyca and Badnell [394] for omitting eigenvectors corresponding to eigenvalues of $\mathbf{I}-\mathbf{M}\mathbf{M}^{\mathrm{T}}$ close to zero is used, then these additional high-energy R-matrix poles do not arise. However, the second term on the right-hand side of (5.87) defining the Buttle correction must be replaced by

$$\mathbf{R}_{\mathrm{corr}} = \frac{1}{2a_0}\,\mathbf{V}(a_0)\,\frac{1}{H_0-E}\,\mathbf{V}^{\mathrm{T}}(a_0), \tag{6.33}$$

where $\mathbf{V}(a_0)$ is the vector of transformed continuum orbitals obtained after omitting those corresponding to eigenvalues of $\mathbf{I}-\mathbf{M}\mathbf{M}^{\mathrm{T}}$ below a certain threshold and H_0 is the zero-order Hamiltonian defined by (5.75). Due to the admixture in $\mathbf{V}(a_0)$ of the pseudo-orbitals $\mathbf{R}_{\mathrm{corr}}$ is not in general diagonal although all the eigenvalues and surface eigenvectors of (5.75) are recovered.

Having determined the R-matrix at $r = a_0$, corresponding to the target eigenstates and pseudostates retained in (5.5) and (5.6), we can then solve the Schrödinger equation in the external and asymptotic regions, as described in Sects. 5.1.3 and 5.1.4. The K-matrix, S-matrix and cross sections for transitions between the target eigenstates and pseudostates can then be calculated for each set of conserved quantum numbers L, S and π and the ionization cross section is then defined as the sum of the excitation cross sections to the pseudostates whose energies lie above the ionization threshold in Fig. 6.1.

6.3 Intermediate-Energy *R*-Matrix Method

In this section we describe the intermediate-energy R-matrix (IERM) method introduced by Burke et al. [182] and developed by a number of workers including LeDourneuf et al. [584], Scholz [832], Dunseath et al. [277] and Heggarty et al. [449, 450]. A two-dimensional R-matrix propagator computer program 2DRMP has been written by Scott et al. [845], which implements this method for electron

collisions with H-like atoms and ions and uses a modified version of the program FARM [193] discussed in Sect. 5.1.1.

In the IERM method we consider the following electron impact excitation and ionization processes:

$$\mathrm{e}^- + A_i \rightarrow A_j^+ + 2\mathrm{e}^- \begin{array}{l} \nearrow A_k^* + \mathrm{e}^- \\ \searrow A_l^+ + 2\mathrm{e}^-, \end{array} \tag{6.34}$$

where A_i is an atom or atomic ion. In the intermediate state in (6.34) both the electron ejected from the target and the scattered electron are in orbitals which can extend out to distances much greater than those of the electrons in the residual ion A_j^+, and in the final state one of these outer electrons can be captured into the ground or excited state A_k^* of the target or can result in an ionized state A_l^+ of the target. This method enables excitation cross sections to highly excited Rydberg states and ionization cross sections to be accurately calculated close to threshold, whereas the RMPS method, discussed in Sect. 6.2, which yields accurate excitation and ionization cross sections over a wide energy range, requires an excessive number of long-range pseudostates to obtain similar accuracy close to the ionization threshold. We also observe that this method has the potential for application in time-dependent R-matrix theory of multiphoton processes, discussed in Chap. 10, enabling double ionization via the recollision mechanism to be accurately calculated. In this mechanism a single electron is first ejected from the target atom or ion near the peak of the laser field which then returns to the target, as the field changes sign, with sufficient energy to ionize a second electron, as described by Corkum [231] and Schafer et al. [816].

6.3.1 General Procedure

We now describe the general procedure for carrying out calculations using the IERM method, reserving a detailed discussion of electron collisions with atoms and ions containing one active electron until Sect. 6.3.2. We consider electron collisions with an $(N + 1)$-electron atom or atomic ion, described by the time-independent Schrödinger equation

$$H_{N+2}\Psi = E\Psi, \tag{6.35}$$

where the non-relativistic Hamiltonian H_{N+2} is defined in atomic units by

$$H_{N+2} = \sum_{i=1}^{N+2} \left(-\frac{1}{2}\nabla_i^2 - \frac{Z}{r_i} \right) + \sum_{i>j=1}^{N+2} \frac{1}{r_{ij}}. \tag{6.36}$$

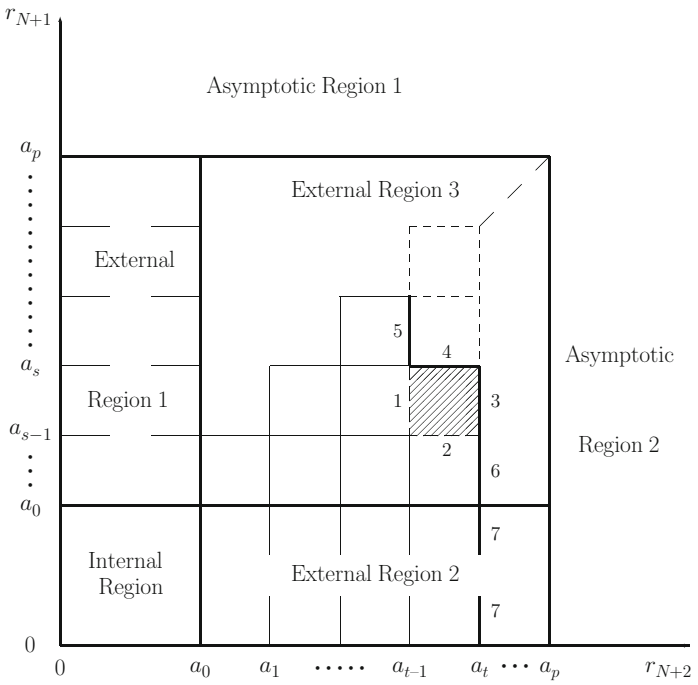

Fig. 6.2 Partitioning of the two-dimensional plane into sub-regions in the IERM method as follows: an internal region containing $N + 2$ strongly interacting electrons; two external regions labelled 1 and 2 containing one electron moving in the potential field of the remaining strongly interacting $N + 1$ electrons; an external region labelled 3 containing two interacting electrons moving in the potential field of the remaining strongly interacting N electrons and two asymptotic regions labelled 1 and 2 containing one electron moving in the long-range potential field of the remaining $N + 1$ electrons

It follows that in the processes defined by (6.34), the initial state A_i and the final state A_k^* each contain $N + 1$ electrons and the final ionized state A_l^+ contains N electrons. We introduce a two-dimensional plane, illustrated in Fig. 6.2, where the radial coordinates of the two continuum electrons in ionization are denoted by r_{N+1} and r_{N+2} which label the axes. This plane is sub-divided into a number of sub-regions, as follows. First, an internal region of radius a_0, where the $N + 2$ electrons are strongly interacting and exchange and correlation effects, involving all these electrons, are important. Second, two external regions labelled 1 and 2, where the radial coordinate of one of the electrons, either r_{N+1} or r_{N+2}, lies in the range $a_0 \leq r \leq a_p$ and where the remaining $N + 1$ electrons lie in the internal region. These external regions, which are related by symmetry, are sub-divided into p sub-regions. Third, an external region labelled 3, where the radial coordinates of two electrons, r_{N+1} and r_{N+2}, lie in the range $a_0 \leq r \leq a_p$ and the remaining N electrons lie in the internal region. This external region is sub-divided into sub-regions, where the symmetry of the Hamiltonian means that only the diagonal sub-

regions and the off-diagonal sub-regions where $r_{N+2} > r_{N+1}$ need to be considered, as shown in Fig. 6.2. We discuss in Sect. 6.3.2 a procedure which enables the R-matrix, describing the motion of these two electrons in the field of the remaining N electrons, to be propagated across external regions 2 and 3. Finally, two asymptotic regions labelled 1 and 2 where the radial coordinate of one of the electrons, either r_{N+1} or r_{N+2}, lies in the range $r \geq a_p$ and where the remaining $N+1$ electrons lie in the internal and external regions. The R-matrix describing the motion of this outer electron in the potential field of the remaining $N+1$ electrons can then be propagated outwards in asymptotic region 2 and the solution fitted to an asymptotic expansion yielding the K-matrix, S-matrix and cross sections.

We now consider the form of the $(N+2)$-electron wave functions in each of the regions illustrated in Fig. 6.2.

6.3.1.1 Internal Region

In this region we replace the $(N+1)$-electron basis (5.6), adopted in low-energy electron collisions with atoms and atomic ions, by the following $(N+2)$-electron basis

$$\psi_k^{\Gamma}(\mathbf{X}_{N+2}) = \mathcal{A} \sum_{ijl} \overline{\overline{\Phi}}_i^{\Gamma}(\mathbf{X}_N; \hat{r}_{N+1}\sigma_{N+1}\hat{r}_{N+2}\sigma_{N+2}) r_{N+1}^{-1} u_j^0(r_{N+1}) \times r_{N+2}^{-1} u_l^0(r_{N+2}) a_{ijlk}^{\Gamma} + \sum_i \chi_i^{\Gamma}(\mathbf{X}_{N+2}) b_{ik}^{\Gamma}. \tag{6.37}$$

The channel functions $\overline{\overline{\Phi}}_i^{\Gamma}$ in this equation are obtained by coupling the N-electron wave function $\Phi_i(\mathbf{X}_N)$ representing the residual ion A_j^+ in (6.34) with the spin–angle functions of the two continuum electrons to form eigenstates belonging to the conserved quantum numbers denoted by Γ, defined by (2.58). The basis orbitals $u_j^0(r_{N+1})$ and $u_l^0(r_{N+2})$ represent the radial motion of the two continuum electrons in the internal region, which are non-zero on the boundaries $r_{N+1} = a_0$ and $r_{N+2} = a_0$ of this region. Also in (6.37), $\chi_i^{\Gamma}(\mathbf{X}_{N+2})$ are quadratically integrable functions which vanish by the boundaries $r_{N+1} = a_0$ and $r_{N+2} = a_0$ of the internal region and are included for completeness and to represent additional electron–electron correlation effects, as discussed following (2.57). Finally, the coefficients a_{ijlk}^{Γ} and b_{ik}^{Γ} are determined by diagonalizing the operator $H_{N+2}+\mathcal{L}_{N+2}$ in the basis $\psi_k^{\Gamma}(\mathbf{X}_{N+2})$ defined by (6.37), where H_{N+2} is the $(N+2)$-electron Hamiltonian, defined by (6.36) and $\mathcal{L}_{N+2}$ is a Bloch operator which is included to ensure that $H_{N+2}+\mathcal{L}_{N+2}$ is hermitian in the internal region in this basis which does not vanish on the boundaries $r_{N+1} = a_0$ and $r_{N+2} = a_0$.

6.3.1.2 External Region 2

In external region 2 in Fig. 6.2, where the electron with radial coordinate r_{N+2} lies in the sub-range $a_{t-1} \leq r_{N+2} \leq a_t$ and the remaining $N+1$ electrons lie in the internal region, we expand the wave function in the following $(N+2)$-electron basis:

$$\psi_k^{\Gamma}(\mathbf{X}_{N+2}) = \sum_{ij} \overline{\Theta}_i^{\Gamma}(\mathbf{X}_{N+1}; \hat{r}_{N+2}\sigma_{N+2}) r_{N+2}^{-1} u_j^t(r_{N+2}) c_{ijk}^{\Gamma}. \tag{6.38}$$

The channel functions $\overline{\Theta}_i^{\Gamma}$ in this equation are obtained by summing over the $(N+1)$ -electron wave functions $\Theta_i^{\gamma}(\mathbf{X}_{N+1})$, describing the $N+1$ electrons in the internal region, which are coupled with the spin–angle function of the $(N+2)$th electron and the basis orbitals $u_j^t(r_{N+2})$ represent the radial motion of the continuum electron in the sub-range $a_{t-1} \le r_{N+2} \le a_t$. The functions $\Theta_i^{\gamma}(\mathbf{X}_{N+1})$ are in turn expanded as follows:

$$\begin{aligned}\Theta_i^{\gamma}(\mathbf{X}_{N+1}) = \mathcal{A} \sum_{jl} \overline{\Phi}_j^{\gamma}(\mathbf{X}_N; \hat{r}_{N+1}\sigma_{N+1}) r_{N+1}^{-1} u_l^0(r_{N+1}) a_{jli}^{\gamma} \\ + \sum_j \eta_j^{\gamma}(\mathbf{X}_{N+1}) b_{ji}^{\gamma},\end{aligned} \tag{6.39}$$

where the channel functions $\overline{\Phi}_j^{\gamma}$ in this equation are obtained by coupling the N-electron wave function $\Phi_j(\mathbf{X}_N)$, representing the residual ion A_j^+ in (6.34), with the spin–angle functions of the $(N+1)$th electron remaining in the internal region to form eigenstates belonging to the conserved quantum numbers denoted by γ. Also in (6.39), $\eta_j^{\gamma}(\mathbf{X}_{N+1})$ are quadratically integrable functions included for completeness and to represent additional electron–electron correlation effects. The coefficients c_{ijk}^{Γ} in (6.38) are obtained by diagonalizing the operator $H_{N+2} + \mathcal{L}_{N+2}$ in the basis (6.38) and the coefficients a_{jli}^{γ} and b_{ji}^{γ} in (6.39) are obtained by diagonalizing the operator $H_{N+1} + \mathcal{L}_{N+1}$ in the basis (6.39), where $\mathcal{L}_{N+1}$ and $\mathcal{L}_{N+2}$ are the appropriate Bloch operators.

6.3.1.3 External Region 3

In the shaded external sub-region in Fig. 6.2, where the electron with radial coordinate r_{N+1} lies in the sub-range $a_{s-1} \le r_{N+1} \le a_s$, the electron with radial coordinate r_{N+2} lies in the sub-range $a_{t-1} \le r_{N+2} \le a_t$ and the remaining N electrons lie in the internal region, we expand the wave function in the following $(N+2)$-electron basis:

$$\begin{aligned}\psi_k^{\Gamma}(\mathbf{X}_{N+2}) = \sum_{ijl} \overline{\overline{\Phi}}_i^{\Gamma}(\mathbf{X}_N; \hat{r}_{N+1}\sigma_{N+1}\hat{r}_{N+2}\sigma_{N+2}) r_{N+1}^{-1} u_j^s(r_{N+1}) \\ \times r_{N+2}^{-1} u_l^t(r_{N+2}) a_{ijlk}^{\Gamma}.\end{aligned} \tag{6.40}$$

As in (6.37) the channel functions $\overline{\overline{\Phi}}_i^{\Gamma}$ in this equation are obtained by coupling the N-electron wave function $\Phi_i(\mathbf{X}_N)$, representing the residual ion A_j^+ in (6.34), with the spin–angle functions of the two continuum electrons to form eigenstates belonging to the conserved quantum numbers denoted by Γ. Also, the basis orbitals

$u_j^s(r_{N+1})$ and $u_l^t(r_{N+2})$ represent the radial motion of the two continuum electrons in sub-ranges $a_{s-1} \le r_{N+1} \le a_s$ and $a_{t-1} \le r_{N+2} \le a_t$ respectively. The coefficients a_{ijlk}^{Γ} in (6.40) are obtained by diagonalizing the operator $H_{N+2} + \mathcal{L}_{N+2}$ in the basis (6.40), where $\mathcal{L}_{N+2}$ is the appropriate Bloch operator which ensures that $H_{N+2} + \mathcal{L}_{N+2}$ is hermitian in this sub-region.

6.3.1.4 Asymptotic Region 2

Finally, we consider the solution of the Schrödinger equation (6.35) in asymptotic region 2 in Fig. 6.2, where the radial coordinate $r_{N+2} \ge a_p$ and the remaining $N+1$ electrons lie in the internal and external regions. The $(N+2)$-electron wave function in this region is expanded as follows:

$$\Psi_{jE}^{\Gamma}(\mathbf{X}_{N+2}) = \sum_i \overline{\Phi}_i^{\Gamma}(\mathbf{X}_{N+1}; \hat{r}_{N+2}\sigma_{N+2}) r_{N+2}^{-1} F_{ij}^{\Gamma}(r_{N+2}), \tag{6.41}$$

which is analogous to (5.28) adopted in the external and asymptotic regions in low-energy electron–atom collisions. The channel functions $\overline{\Phi}_i^{\Gamma}$ in (6.41) are obtained by coupling the $(N+1)$-electron wave function $\Phi_i(\mathbf{X}_{N+1})$ representing the residual ion, which can be in a bound or continuum state, with the spin–angle functions of the $(N+2)$th electron. A detailed description of the form of the wave function representing the residual atom or ion is given in Sect. 6.3.2 where we discuss the two-electron example. We can then derive a set of coupled second-order differential equations satisfied by the reduced radial wave functions $F_{ij}^{\Gamma}(r_{N+2})$, by substituting expansion (6.41) into the Schrödinger equation (6.35) and projecting onto the channel functions $\overline{\Phi}_i^{\Gamma}$ in (6.41). The solution of these coupled differential equations, which have a form analogous to (5.29), is then fitted on the boundary $r_{N+2} = a_p$ to the R-matrix obtained from the solutions in the internal and external regions in Fig. 6.2. The solution of these coupled differential equations can, if necessary, be first integrated outwards from $r_{N+2} = a_p$, using one of the R-matrix propagator methods discussed in Appendix E, and then fitted to an asymptotic expansion. However, in most applications the value of a_p is such that the R-matrix can be fitted directly to an asymptotic expansion at $r_{N+2} = a_p$. The K-matrix and S-matrix can be determined as discussed in Sect. 5.1.4 and the corresponding scattering amplitudes and cross sections for transitions between bound and continuum states in (6.34) calculated.

6.3.2 Two-Electron Example

In order to illustrate the new features of the IERM method in greater detail, we consider electron collisions with atoms and atomic ions containing one active electron, such as atomic hydrogen or alkali-like metal atoms and ions with a closed-shell

core. The time-independent Schrödinger equation describing this collision can be written in the form of (6.35) with $N = 0$ as follows:

$$H_2\Psi = E\Psi, \tag{6.42}$$

where the two-electron Hamiltonian H_2 is defined in atomic units by

$$H_2 = \sum_{i=1}^{2}\left(-\frac{1}{2}\nabla_i^2 + V(r_i)\right) + \frac{1}{r_{12}}, \tag{6.43}$$

and where the interaction of the active target electron and the scattered electron with the nucleus and with the remaining core electrons is represented by a model potential $V(r)$. This model potential represents electron exchange and correlation effects with the closed-shell core in the internal region and the long-range potential seen by the ejected and scattered electrons in the external and asymptotic regions. It follows that in this two-electron example, the wave function takes a similar form in the internal region and in the external regions in Fig. 6.2 with only the boundary conditions where $r_1 = 0$ and where $r_2 = 0$ distinguishing the internal region and external regions 1 and 2 from external region 3. Therefore, in the following analysis we will consider the solution in the internal and external regions together.

The two-electron time-independent Schrödinger equation (6.42) is first solved in the internal region and external regions 2 and 3 in Fig. 6.2 where we note the symmetry of the Hamiltonian means that we do not need to consider the solution in external region 1. Also, since $N = 0$ in this two-electron example, the radial coordinates r_1 and r_2 now label the axes. External regions 2 and 3 are divided into a number of sub-regions, where again the symmetry of the Hamiltonian means that we need to only consider the solution in the internal region and in the diagonal external sub-regions and off-diagonal external sub-regions where $r_2 > r_1$. The solution is obtained by diagonalizing the Hamiltonian in a basis in the internal region and in each of the external sub-regions and the R-matrix propagated across the internal and external sub-regions using a two-dimensional extension of propagator methods discussed in Appendix E. This yields the R-matrix on the boundary $0 \le r_1 \le a_p$, $r_2 = a_p$ of external regions 2 and 3 with the asymptotic region. In the asymptotic region, where $r_2 \ge a_p$, the reduced radial wave function describing the motion of the scattered electron satisfies a set of coupled second-order differential equations. These equations can, if necessary, be integrated outwards using a standard procedure, as discussed in Sect. 5.1.3, and the solution then fitted to an asymptotic expansion, as discussed in Sect. 5.1.4. This yields the K-matrix and S-matrix and hence the cross sections for elastic scattering and exciting bound and continuum states of the target. We now consider the solutions in the internal, external and asymptotic regions in greater detail.

6.3.2.1 Internal and External Regions Solution

We consider first the solution of the time-independent Schrödinger equation (6.42) in a general (s, t) sub-region, illustrated by shading in Fig. 6.2, where the

two-electron Hamiltonian H_2 is defined by (6.43). The space part of the collision wave function can be expanded in this (s,t) sub-region, in analogy with (5.5) as follows:

$$\Psi^{\Gamma}_{stj}(\mathbf{r}_1,\mathbf{r}_2) = \sum_k \psi^{\Gamma}_{stk}(\mathbf{r}_1,\mathbf{r}_2) A^{\Gamma}_{stkj}(E), \tag{6.44}$$

for each set of conserved quantum numbers Γ defined by (2.58). Also in (6.44), j labels the linearly independent solutions of (6.42) at the energy E, ψ^{Γ}_{stk} are energy-independent basis functions and $A^{\Gamma}_{stkj}(E)$ are energy-dependent expansion coefficients, which depend on the asymptotic boundary conditions satisfied by the wave function Ψ^{Γ}_{stj}. We now expand the basis functions ψ^{Γ}_{stk}, in analogy with (5.6), as follows:

$$\psi^{\Gamma}_{stk}(\mathbf{r}_1,\mathbf{r}_2) = \sum_{n_1\ell_1}\sum_{n_2\ell_2} \Phi^{\Gamma}_{n_1\ell_1 n_2\ell_2}(\mathbf{r}_1,\mathbf{r}_2) a^{\Gamma}_{n_1\ell_1 n_2\ell_2 k}. \tag{6.45}$$

In the diagonal sub-regions in Fig. 6.2 where $s = t$, the normalized two-electron functions $\Phi^{\Gamma}_{n_1\ell_1 n_2\ell_2}(\mathbf{r}_1,\mathbf{r}_2)$ are defined by

$$\begin{aligned}\Phi^{\Gamma}_{n_1\ell_1 n_2\ell_2}(\mathbf{r}_1,\mathbf{r}_2) = {} & \frac{1}{\sqrt{2}}\left(1 + (-1)^S P_{12}\right) r_1^{-1} u^t_{n_1\ell_1}(r_1) r_2^{-1} u^t_{n_2\ell_2}(r_2) \\ & \times Y_{\ell_1\ell_2 L M_L}(\hat{\mathbf{r}}_1,\hat{\mathbf{r}}_2),\end{aligned} \tag{6.46}$$

and in the off-diagonal sub-regions where $s < t$, the functions $\Phi^{\Gamma}_{n_1\ell_1 n_2\ell_2}(\mathbf{r}_1,\mathbf{r}_2)$ are defined by

$$\Phi^{\Gamma}_{n_1\ell_1 n_2\ell_2}(\mathbf{r}_1,\mathbf{r}_2) = r_1^{-1} u^s_{n_1\ell_1}(r_1) r_2^{-1} u^t_{n_2\ell_2}(r_2) Y_{\ell_1\ell_2 L M_L}(\hat{\mathbf{r}}_1,\hat{\mathbf{r}}_2). \tag{6.47}$$

In (6.46) and (6.47), $u^s_{n\ell}(r_1)$ are orthonormal one-electron radial basis orbitals, defined over $a_{s-1} \le r_1 \le a_s$, $u^t_{n\ell}(r_2)$ are orthonormal one-electron radial basis orbitals, defined over $a_{t-1} \le r_2 \le a_t$, which are determined as described below, and $Y_{\ell_1\ell_2 L M_L}(\hat{\mathbf{r}}_1,\hat{\mathbf{r}}_2)$ are two-electron angular functions, defined by (B.57). The operator P_{12} in (6.46) exchanges the space coordinates of electrons labelled 1 and 2 so that the space part of the two-electron wave functions in the internal and external diagonal sub-regions are symmetric for singlet spin states ($S = 0$) and antisymmetric for triplet spin states ($S = 1$), in accordance with the Pauli exclusion principle. The summations over n_1, ℓ_1, n_2 and ℓ_2 in (6.45) are restricted in the internal and external diagonal sub-regions to include only linearly independent 2-electron functions. The angular momenta ℓ_1, ℓ_2 and L in (6.46) and (6.47) are also restricted by the triangular relations imposed by the Clebsch–Gordan coefficient in the definition of $Y_{\ell_1\ell_2 L M_L}(\hat{\mathbf{r}}_1,\hat{\mathbf{r}}_2)$. In addition, the range of summations over n_1 and n_2 in (6.45) has some given maximum $n_{\max}$ and the range of summations over ℓ_1 and ℓ_2 has some given maximum $\ell_{\max}$. Finally, we observe that the Pauli exclusion principle is not applicable in the off-diagonal external sub-regions since the two electrons then occupy different regions of space. However, the wave functions in sub-regions

which are reflections of each other in the line $r_1 = r_2$ in Fig. 6.2 must satisfy the symmetry relation

$$\psi_k^{\Gamma}(\mathbf{r}_1, \mathbf{r}_2) = (-1)^S \psi_k^{\Gamma}(\mathbf{r}_2, \mathbf{r}_1). \tag{6.48}$$

Consequently the calculations need only be carried out for the internal region and for external diagonal sub-regions and external sub-regions where $r_2 > r_1$ shown in Fig. 6.2.

We consider next the choice of the one-electron radial basis orbitals $u_{n\ell}^s(r)$ and $u_{n\ell}^t(r)$ in (6.46) and (6.47) in each (s, t) sub-region. In the case of electron collisions with a general atomic target, the radius a_0 of the internal region in Fig. 6.2 is chosen so that the reduced radial orbitals $P_{n\ell}(r)$ of the closed-shell residual ion A_j^+ in (6.34) satisfy the condition

$$P_{n\ell}(r) = 0, \quad r \geq a_0. \tag{6.49}$$

With this choice, only the wave functions of the scattered and active target electrons extend beyond $r = a_0$. In addition, it follows that the model potential $V(r)$ in (6.43) achieves its asymptotic form for $r \geq a_0$ where it is given by

$$V(r) = \frac{2(Z - N + 1)}{r}, \quad r \geq a_0, \tag{6.50}$$

where Z is the nuclear charge number and $N - 1$ is the number of electrons in the closed-shell core. In principle, a potential behaving asymptotically as r^{-4}, $r \geq a_0$, caused by polarization of the closed-shell core electrons by the two outer electrons, can be added to $V(r)$ in (6.50) without essential modification of the following discussion. The one-electron radial continuum basis orbitals in the internal region can then be chosen using a procedure analogous to that adopted in Sect. 5.3.1. That is, the orbitals are defined to be eigensolutions of the following zero-order differential equation:

$$\left(\frac{\mathrm{d}^2}{\mathrm{d}r^2} - \frac{\ell(\ell+1)}{r^2} + V(r) + k_{n\ell}^2\right) u_{n\ell}^0(r) = \sum_{n'} \lambda_{nn'\ell} P_{n'\ell}(r),$$
$$n = 1, \ldots, n_{\max}, \quad \ell = 0, \ldots, \ell_{\max}, \quad 0 \leq r \leq a_0, \tag{6.51}$$

satisfying the homogeneous boundary conditions

$$u_{n\ell}^0(0) = 0$$
$$\frac{a_0}{u_{n\ell}^0(a_0)} \frac{\mathrm{d}u_{n\ell}^0}{\mathrm{d}r}\bigg|_{r = a_0} = b_0, \tag{6.52}$$

where b_0 is an arbitrary constant, which is usually taken to be zero. Also the Lagrange multipliers $\lambda_{nn'\ell}$ are chosen so that the eigensolutions $u_{n\ell}^0(r)$ satisfy the orthogonality constraints

$$\int_0^{a_0} u^0_{n\ell}(r) P_{n'\ell}(r) \mathrm{d}r = 0, \tag{6.53}$$

for all closed-shell orbitals $P_{n'\ell}(r)$ of the residual ion. Finally, the basis orbitals, which are orthogonal, are chosen to be normalized so that

$$\int_0^{a_0} u^0_{n\ell}(r) u^0_{n'\ell}(r) \mathrm{d}r = \delta_{nn'}, \quad n,\ n' = 1, \ldots, n_{\max},\ \ell = 0, \ldots, \ell_{\max}. \tag{6.54}$$

With this choice of orbitals a Buttle correction must be added to the R-matrix at $r = a_0$ to obtain accurate results, as discussed in Sect. 5.3.2.

For all other sub-ranges $a_{s-1} \le r_1 \le a_s$, $s = 1, \ldots, p$, and $a_{t-1} \le r_2 \le a_t$, $t = 1, \ldots, p$, the basis orbitals $u^s_{n\ell}(r_1)$ and $u^t_{n\ell}(r_2)$ can be represented by members of any linearly independent complete basis. For example, in a number of recent calculations, the basis orbitals have been represented by shifted Legendre polynomials as in the BBM propagator method described in Appendix E.3. In this case the basis orbitals satisfy arbitrary boundary conditions at $r_1 = a_{s-1}$ and $r_1 = a_s$ and at $r_2 = a_{t-1}$ and $r_2 = a_t$, respectively, and hence a Buttle correction is not required.

The final step in our determination of the R-matrix basis functions ψ^Γ_{stk} defined by (6.45) is to diagonalize the Hamiltonian H_2 in the internal region and in each external (s, t) sub-region in the corresponding basis. Let us consider the (s, t) sub-region in Fig. 6.2 with edges labelled 1, 2, 3 and 4 where r_1 and r_2 satisfy the inequalities

$$a_{s-1} \le r_1 \le a_s, \quad a_{t-1} \le r_2 \le a_t, \tag{6.55}$$

and where we assume initially that, as in Fig. 6.2, the sub-region is neither diagonal where $s = t$ nor bounded by the r_2-axis. We introduce the Bloch operator $\mathcal{L}_{st}$ in this (s, t) sub-region, defined by

$$\begin{aligned}\mathcal{L}_{st} = \frac{1}{2}\Bigg[&\delta(r_2 - a_t)\left(\frac{\mathrm{d}}{\mathrm{d}r_2} - \frac{b_3 - 1}{r_2}\right) - \delta(r_2 - a_{t-1})\left(\frac{\mathrm{d}}{\mathrm{d}r_2} - \frac{b_1 - 1}{r_2}\right) \\ &+ \delta(r_1 - a_s)\left(\frac{\mathrm{d}}{\mathrm{d}r_1} - \frac{b_4 - 1}{r_1}\right) - \delta(r_1 - a_{s-1})\left(\frac{\mathrm{d}}{\mathrm{d}r_1} - \frac{b_2 - 1}{r_1}\right)\Bigg],\end{aligned} \tag{6.56}$$

which ensures that $H_2 + \mathcal{L}_{st}$ is hermitian in the space of functions satisfying arbitrary boundary conditions on the four edges of the (s, t) sub-region, for arbitrary values of the constants b_1, b_2, b_3 and b_4, which are usually taken to be zero. The coefficients $a^\Gamma_{n_1\ell_1 n_2\ell_2 k}$ in (6.45) are then determined by diagonalizing the operator $H_2 + \mathcal{L}_{st}$ in the R-matrix basis in the (s, t) sub-region as follows:

$$\langle \psi^\Gamma_{stk} | H_2 + \mathcal{L}_{st} | \psi^\Gamma_{stk'} \rangle = E^\Gamma_{stk} \delta_{kk'}, \quad k,\ k' = 1, \ldots n_{st}. \tag{6.57}$$

The integrations in this equation are carried out over all space variables where the radial variables satisfy inequalities (6.55) and where n_{st} is the number of linearly independent basis functions retained in the (s,t) sub-region.

The Schrödinger equation (6.42) can be rewritten in the (s,t) sub-region as

$$(H_2 + \mathcal{L}_{st} - E)\Psi_{st}^{\Gamma} = \mathcal{L}_{st}\Psi_{st}^{\Gamma}, \tag{6.58}$$

which has the formal solution

$$\Psi_{st}^{\Gamma} = (H_2 + \mathcal{L}_{st} - E)^{-1}\mathcal{L}_{st}\Psi_{st}^{\Gamma}. \tag{6.59}$$

The spectral representation of the Green's function $(H_2 + \mathcal{L}_{st} - E)^{-1}$ in the (s,t) sub-region can be obtained in terms of the R-matrix basis functions ψ_{stk}^{Γ} defined by (6.45) and (6.57). Equation (6.59) then becomes

$$|\Psi_{st}^{\Gamma}\rangle = \sum_{k=1}^{n_{st}} |\psi_{stk}^{\Gamma}\rangle \frac{1}{E_{stk}^{\Gamma} - E} \langle\psi_{stk}^{\Gamma}|\mathcal{L}_{st}|\Psi_{st}^{\Gamma}\rangle. \tag{6.60}$$

The required R-matrix equations in the (s,t) sub-region are obtained by projecting (6.60) onto the channel functions

$$\phi_{\mu}^{1}(\mathbf{r}_1, \hat{\mathbf{r}}_2) = r_1^{-1} u_{n\ell_1}^{t}(r_1) Y_{\ell_1\ell_2 L M_L}(\hat{\mathbf{r}}_1, \hat{\mathbf{r}}_2), \tag{6.61}$$

and evaluating the result at the edges $r_2 = a_{t-1}$ and a_t, and by projecting (6.60) onto the channel functions

$$\phi_{\mu}^{2}(\hat{\mathbf{r}}_1, \mathbf{r}_2) = r_2^{-1} u_{n\ell_2}^{s}(r_2) Y_{\ell_1\ell_2 L M_L}(\hat{\mathbf{r}}_1, \hat{\mathbf{r}}_2), \tag{6.62}$$

and evaluating the result at the edges $r_1 = a_{s-1}$ and a_s, where the channel index μ in these equations is defined by

$$\mu = n\ell_1\ell_2. \tag{6.63}$$

This yields the following matrix equations:

$$\mathcal{F}_i = \sum_{j=1}^{4} \mathbf{R}_{ij}\eta_j \mathcal{D}_j, \quad i = 1, \ldots, 4, \tag{6.64}$$

where the generalized radial wave functions on the edges of the (s,t) sub-region are given by

$$\begin{aligned}
\mathcal{F}_{1\mu} &= \langle \phi^1_\mu(\mathbf{r}_1, \hat{\mathbf{r}}_2)|\Psi\rangle_{r_2 = a_{t-1}}, \\
\mathcal{F}_{2\mu} &= \langle \phi^2_\mu(\hat{\mathbf{r}}_1, \mathbf{r}_2)|\Psi\rangle_{r_1 = a_{s-1}}, \\
\mathcal{F}_{3\mu} &= \langle \phi^1_\mu(\mathbf{r}_1, \hat{\mathbf{r}}_2)|\Psi\rangle_{r_2 = a_t}, \\
\mathcal{F}_{4\mu} &= \langle \phi^2_\mu(\hat{\mathbf{r}}_1, \mathbf{r}_2)|\Psi\rangle_{r_1 = a_s},
\end{aligned} \tag{6.65}$$

and the corresponding generalized derivatives are given by

$$\begin{aligned}
\mathcal{D}_{1\mu} &= \langle \phi^1_\mu(\mathbf{r}_1, \hat{\mathbf{r}}_2) \left| \left(\frac{\mathrm{d}}{\mathrm{d}r_2} - \frac{b_1 - 1}{r_2} \right) \right| \Psi\rangle_{r_2 = a_{t-1}}, \\
\mathcal{D}_{2\mu} &= \langle \phi^2_\mu(\hat{\mathbf{r}}_1, \mathbf{r}_2) \left| \left(\frac{\mathrm{d}}{\mathrm{d}r_1} - \frac{b_2 - 1}{r_1} \right) \right| \Psi\rangle_{r_1 = a_{s-1}}, \\
\mathcal{D}_{3\mu} &= \langle \phi^1_\mu(\mathbf{r}_1, \hat{\mathbf{r}}_2) \left| \left(\frac{\mathrm{d}}{\mathrm{d}r_2} - \frac{b_3 - 1}{r_2} \right) \right| \Psi\rangle_{r_2 = a_t}, \\
\mathcal{D}_{4\mu} &= \langle \phi^2_\mu(\hat{\mathbf{r}}_1, \mathbf{r}_2) \left| \left(\frac{\mathrm{d}}{\mathrm{d}r_1} - \frac{b_4 - 1}{r_1} \right) \right| \Psi\rangle_{r_1 = a_s},
\end{aligned} \tag{6.66}$$

where in these equations and in the following equations we have omitted the conserved quantum numbers Γ and the (s, t) sub-region indices for notational convenience. The R-matrix $\mathbf{R}_{ij}$ in (6.64) is then defined by

$$(R_{ij})_{\mu\mu'} = \frac{1}{2} \sum_k \frac{w_{i\mu k} w_{j\mu' k}}{E_k - E}, \quad i,\ j = 1, \ldots, 4, \tag{6.67}$$

where the surface amplitudes are given by

$$\begin{aligned}
w_{1\mu k} &= \langle \phi^1_\mu(\mathbf{r}_1, \hat{\mathbf{r}}_2)|\psi_k\rangle_{r_2 = a_{t-1}}, \\
w_{2\mu k} &= \langle \phi^2_\mu(\hat{\mathbf{r}}_1, \mathbf{r}_2)|\psi_k\rangle_{r_1 = a_{s-1}}, \\
w_{3\mu k} &= \langle \phi^1_\mu(\mathbf{r}_1, \hat{\mathbf{r}}_2)|\psi_k\rangle_{r_2 = a_t}, \\
w_{4\mu k} &= \langle \phi^2_\mu(\hat{\mathbf{r}}_1, \mathbf{r}_2)|\psi_k\rangle_{r_1 = a_s},
\end{aligned} \tag{6.68}$$

and where $\eta_1 = \eta_2 = -1$ and $\eta_3 = \eta_4 = +1$ in (6.64). We observe that the R-matrix defined by (6.67) and (6.68) relates the full radial wave functions to their derivatives in (6.64), in analogy with (4.45) in Sect. 4.2.

In order to propagate the R-matrix across the (s, t) sub-region defined in Fig. 6.2, it is convenient to rewrite (6.64) in the following block matrix form:

$$\begin{pmatrix} \mathbf{f}_\mathrm{I} \\ \mathbf{f}_\mathrm{O} \end{pmatrix} = \begin{pmatrix} -\mathbf{r}_\mathrm{II} & \mathbf{r}_\mathrm{IO} \\ -\mathbf{r}_\mathrm{OI} & \mathbf{r}_\mathrm{OO} \end{pmatrix} \begin{pmatrix} \mathbf{d}_\mathrm{I} \\ \mathbf{d}_\mathrm{O} \end{pmatrix}, \tag{6.69}$$

where the subscript I represents the input edges 1 and 2 and the subscript O represents the output edges 3 and 4 of the (s, t) sub-region. Thus we have written

$$\mathbf{r}_{\mathrm{II}} = \begin{pmatrix} \mathbf{R}_{11} & \mathbf{R}_{12} \\ \mathbf{R}_{21} & \mathbf{R}_{22} \end{pmatrix}, \quad \mathbf{r}_{\mathrm{IO}} = \begin{pmatrix} \mathbf{R}_{13} & \mathbf{R}_{14} \\ \mathbf{R}_{23} & \mathbf{R}_{24} \end{pmatrix},$$
$$\mathbf{r}_{\mathrm{OI}} = \begin{pmatrix} \mathbf{R}_{31} & \mathbf{R}_{32} \\ \mathbf{R}_{41} & \mathbf{R}_{42} \end{pmatrix}, \quad \mathbf{r}_{\mathrm{OO}} = \begin{pmatrix} \mathbf{R}_{33} & \mathbf{R}_{34} \\ \mathbf{R}_{43} & \mathbf{R}_{44} \end{pmatrix}. \tag{6.70}$$

We then introduce a global input R-matrix $\mathcal{R}^{\mathrm{I}}$ associated with the input edges 5, 1, 2, 6, 7 in Fig. 6.2 and a global output R-matrix $\mathcal{R}^{\mathrm{O}}$ associated with the output edges 5, 4, 3, 6, 7 in Fig. 6.2, where we refer to the common edges 5, 6 and 7 by the subscript X. We can then write the global input R-matrix as

$$\mathcal{R}^{\mathrm{I}} = \begin{pmatrix} \mathcal{R}^{\mathrm{I}}_{\mathrm{II}} & \mathcal{R}^{\mathrm{I}}_{\mathrm{I}X} \\ \mathcal{R}^{\mathrm{I}}_{X\mathrm{I}} & \mathcal{R}^{\mathrm{I}}_{XX} \end{pmatrix}, \tag{6.71}$$

and the global output R-matrix as

$$\mathcal{R}^{\mathrm{O}} = \begin{pmatrix} \mathcal{R}^{\mathrm{O}}_{\mathrm{OO}} & \mathcal{R}^{\mathrm{O}}_{\mathrm{O}X} \\ \mathcal{R}^{\mathrm{O}}_{X\mathrm{O}} & \mathcal{R}^{\mathrm{O}}_{XX} \end{pmatrix}, \tag{6.72}$$

where the corresponding generalized functions and derivatives satisfy the equations

$$\begin{pmatrix} \mathbf{f}_{\mathrm{I}} \\ \mathbf{f}_X \end{pmatrix} = \begin{pmatrix} \mathcal{R}^{\mathrm{I}}_{\mathrm{II}} & \mathcal{R}^{\mathrm{I}}_{\mathrm{I}X} \\ \mathcal{R}^{\mathrm{I}}_{X\mathrm{I}} & \mathcal{R}^{\mathrm{I}}_{XX} \end{pmatrix} \begin{pmatrix} \mathbf{d}_{\mathrm{I}} \\ \mathbf{d}_X \end{pmatrix} \tag{6.73}$$

and

$$\begin{pmatrix} \mathbf{f}_{\mathrm{O}} \\ \mathbf{f}_X \end{pmatrix} = \begin{pmatrix} \mathcal{R}^{\mathrm{O}}_{\mathrm{OO}} & \mathcal{R}^{\mathrm{O}}_{\mathrm{O}X} \\ \mathcal{R}^{\mathrm{O}}_{X\mathrm{O}} & \mathcal{R}^{\mathrm{O}}_{XX} \end{pmatrix} \begin{pmatrix} \mathbf{d}_{\mathrm{O}} \\ \mathbf{d}_X \end{pmatrix}. \tag{6.74}$$

Finally, we eliminate $\mathbf{f}_{\mathrm{I}}$ and $\mathbf{d}_{\mathrm{I}}$ from (6.69) and (6.73) to obtain the following expressions relating the sub-matrices of $\mathcal{R}^{\mathrm{O}}$ to the sub-matrices of $\mathcal{R}^{\mathrm{I}}$ and the matrices $\mathbf{r}_{\mathrm{II}}$, $\mathbf{r}_{\mathrm{IO}}$, $\mathbf{r}_{\mathrm{OI}}$ and $\mathbf{r}_{\mathrm{OO}}$,

$$\begin{aligned} \mathcal{R}^{\mathrm{O}}_{\mathrm{OO}} &= \mathbf{r}_{\mathrm{OO}} - \mathbf{r}_{\mathrm{OI}}(\mathcal{R}^{\mathrm{I}}_{\mathrm{II}} + \mathbf{r}_{\mathrm{II}})^{-1}\mathbf{r}_{\mathrm{IO}}, \\ \mathcal{R}^{\mathrm{O}}_{\mathrm{O}X} &= \mathbf{r}_{\mathrm{OI}}(\mathcal{R}^{\mathrm{I}}_{\mathrm{II}} + \mathbf{r}_{\mathrm{II}})^{-1}\mathcal{R}^{\mathrm{I}}_{\mathrm{I}X}, \\ \mathcal{R}^{\mathrm{O}}_{X\mathrm{O}} &= \mathcal{R}^{\mathrm{I}}_{X\mathrm{I}}(\mathcal{R}^{\mathrm{I}}_{\mathrm{II}} + \mathbf{r}_{\mathrm{II}})^{-1}\mathbf{r}_{\mathrm{IO}}, \\ \mathcal{R}^{\mathrm{O}}_{XX} &= \mathcal{R}^{\mathrm{I}}_{XX} - \mathcal{R}^{\mathrm{I}}_{X\mathrm{I}}(\mathcal{R}^{\mathrm{I}}_{\mathrm{II}} + \mathbf{r}_{\mathrm{II}})^{-1}\mathcal{R}^{\mathrm{I}}_{\mathrm{I}X}. \end{aligned} \tag{6.75}$$

Equations (6.75) express the global output R-matrix $\mathcal{R}^{\mathrm{O}}$ obtained by propagating the global input R-matrix $\mathcal{R}^{\mathrm{I}}$ across the (s, t) sub-region. Repeated use of these equations enables the global R-matrix to be propagated outwards across the sub-regions in the lower triangular plane shown in Fig. 6.2 to the outer boundary $0 \leq r_1 \leq a_p, r_2 = a_p$.

It is clear from the above discussion that the procedure that we can adopt for propagating the global R-matrix is not unique. One commonly used procedure, adopted by Heggarty et al. [450], and incorporated in the computer program 2DRMP written by Scott et al. [845], is to propagate the global R-matrix in successive vertical strips of sub-regions (s, t), as follows:

$$(0,0),\ (0,1),\ (1,1),\ (0,2),\ (1,2),\ (2,2),\ \ldots,\ (p,p), \tag{6.76}$$

commencing with the $(0, 0)$ internal region and finishing with the (p, p) external sub-region in Fig. 6.2. In this way we can determine the global R-matrix on the outer boundary $0 \le r_1 \le a_p, r_2 = a_p$ of external regions 2 and 3.

While (6.75) can be applied across an arbitrary sub-region, two special cases should be noted. First, propagation across the internal or diagonal external sub-regions where $s = t$ and second, propagation across an external sub-region bounded by the r_2-axis at the beginning of a new vertical strip. In the case of the internal or diagonal external sub-regions, the symmetry or antisymmetry of the wave function under exchange of the space coordinates of the scattered target electrons means that (6.69) simplifies to

$$\begin{pmatrix} \mathbf{f}_{\mathrm{I}} \\ \mathbf{f}_{\mathrm{O}} \end{pmatrix} = \begin{pmatrix} -2\mathbf{R}_{22} & 2\mathbf{R}_{23} \\ -2\mathbf{R}_{32} & 2\mathbf{R}_{33} \end{pmatrix} \begin{pmatrix} \mathbf{d}_{\mathrm{I}} \\ \mathbf{d}_{\mathrm{O}} \end{pmatrix}, \tag{6.77}$$

where the input and output edges are labelled 2 and 3, respectively, in Fig. 6.2. Hence we obtain

$$\mathbf{r}_{\mathrm{II}} = 2\mathbf{R}_{22}, \quad \mathbf{r}_{\mathrm{IO}} = 2\mathbf{R}_{23}, \quad \mathbf{r}_{\mathrm{OI}} = 2\mathbf{R}_{32}, \quad \mathbf{r}_{\mathrm{OO}} = 2\mathbf{R}_{33}, \tag{6.78}$$

and (6.75) can be applied as in the propagation across an arbitrary sub-region. In the case of an external sub-region bounded by the r_2-axis at the beginning of a new vertical strip we observe that the input boundary consists of only one input edge labelled 1 in Fig. 6.2, reducing the size of the matrices in (6.75). In addition, when propagating across the first (0, 1) sub-region in external region 2, there are no common edges X so that only the first equation in (6.75) needs to be solved.

6.3.2.2 Asymptotic Region Solution

In order to calculate accurate elastic scattering, excitation and ionization cross sections we must determine the solution in asymptotic region 2, in Fig. 6.2, given the R-matrix on the boundary $r_2 = a_p$. In most applications the value of a_p is such that the solution in the asymptotic region can be accurately determined by fitting the external region solution directly to an asymptotic expansion. However, we will also discuss the possibility that the value of a_p is such that it is first necessary, in order to obtain accurate results, to propagate the R-matrix out to a larger radius before fitting to an asymptotic expansion. We commence by assuming that the boundary a_p is large enough so that exchange effects between the scattered and the active

target electron are negligible outside of this boundary. The solution can then be described by the R-matrix procedure, considered in Sects. 5.1.3 and 5.1.4.

We expand the total wave function in asymptotic region 2, in analogy with (5.28), in a close coupling expansion as follows:

$$\Psi^{\Gamma}(\mathbf{r}_1, \mathbf{r}_2) = \sum_{n\ell_1\ell_2} r_1^{-1} v_{n\ell_1}(r_1) Y_{\ell_1\ell_2 L M_L}(\hat{\mathbf{r}}_1, \hat{\mathbf{r}}_2) r_2^{-1} F^{\Gamma}_{n\ell_1\ell_2}(r_2),$$
$$0 \le r_1 \le a_p, \quad r_2 \ge a_p. \tag{6.79}$$

The reduced radial target orbitals and pseudo-orbitals $v_{n\ell_1}(r_1)$ in (6.79) can be chosen to be eigensolutions of the following differential equation:

$$\left(\frac{\mathrm{d}^2}{\mathrm{d}r^2} - \frac{\ell_i(\ell_i+1)}{r^2} + V(r) + {k'_{n\ell}}^2\right) v_{n\ell}(r) = \sum_{n'} \lambda'_{nn'\ell} P_{n'\ell}(r),$$
$$n = 1, \ldots, n'_{\max}, \quad \ell = 0, \ldots, \ell_{\max}, \; 0 \le r \le a_p, \tag{6.80}$$

satisfying the homogeneous boundary conditions

$$v_{n\ell}(0) = 0$$
$$\frac{a_p}{v_{n\ell}(a_p)} \frac{\mathrm{d}v_{n\ell}}{\mathrm{d}r}\bigg|_{r=a_p} = b_0, \tag{6.81}$$

where $V(r)$ is the model potential adopted in the two-electron Hamiltonian H_2 defined by (6.43) and ${k'_{n\ell}}^2$ are the corresponding eigenvalues. The range of angular momenta $\ell = 0$ to $\ell_{\max}$ in (6.80) is the same as that used in the definition of the basis functions in the internal region and b_0 is an arbitrary constant, which is usually taken to be zero. Also, the Lagrange multipliers $\lambda'_{nn'\ell}$ are chosen so that the orbitals $v_{n\ell}(r)$ satisfy the orthogonality constraints

$$\int_0^{a_p} v_{n\ell}(r) P_{n'\ell}(r) \mathrm{d}r = 0, \tag{6.82}$$

where the $P_{n'\ell}(r)$ are bound orbitals corresponding to the residual closed-shell ion in electron collisions with alkali-like atoms and ions. Finally, the orbitals $v_{n\ell}(r)$ are normalized so that

$$\int_0^{a_p} v_{n\ell}(r) v_{n'\ell}(r) \mathrm{d}r = \delta_{nn'}, \quad n, \; n' = 1, \ldots, n'_{\max}, \; \ell = 0, \ldots, \ell_{\max}. \tag{6.83}$$

We observe that the reduced radial target orbitals and pseudo-orbitals $v_{n\ell}(r)$, defined by (6.80), (6.81), (6.82) and (6.83), satisfy equations similar to those satisfied by the one-electron basis orbitals $u^0_{n\ell}(r)$, defined by (6.51), (6.52), (6.53) and (6.54). The essential difference is that the orbitals $v_{n\ell}(r)$ are defined over the larger range $0 \le r \le a_p$ whereas $u^0_{n\ell}(r)$ are defined only over $0 \le r \le a_0$. This means that the

orbitals $v_{n\ell}(r)$ will accurately represent higher energy bound states of the target and provide a denser spectrum of pseudostates representing the continuum. It follows that propagating the global R-matrix across the sub-regions in Fig. 6.2 to larger values of a_p will provide an increasingly accurate representation of the exact bound and continuum spectrum in Fig. 6.1 close to the ionization threshold.

We can derive coupled second-order differential equations satisfied by the reduced radial functions $F^{\Gamma}_{n\ell_1\ell_2}(r_2)$ by substituting expansion (6.79) into the Schrödinger equation (6.42) and projecting onto the channel functions $r_1^{-1} v_{n\ell_1}(r_1)$ $Y_{\ell_1\ell_2 LM_L}(\hat{\mathbf{r}}_1, \hat{\mathbf{r}}_2)$. We find that the functions $F^{\Gamma}_{n\ell_1\ell_2}(r_2)$ satisfy coupled second-order differential equations analogous to (5.29) for $r_2 \geq a_p$. On the boundary $r_2 = a_p$, the R-matrix $\mathbf{R}$ in the close coupling basis defined by (6.79) is obtained from the global R-matrix $\boldsymbol{\mathcal{R}}$ in the two-dimensional propagation basis at $r_2 = a_p$, by an orthogonal transformation

$$\mathbf{R} = \mathbf{O}^{\mathrm{T}} \boldsymbol{\mathcal{R}} \mathbf{O}, \tag{6.84}$$

where the elements of the orthogonal matrix $\mathbf{O}$ are the projections of the one-electron R-matrix reduced radial basis orbitals $u^s_{n\ell}(r_1)$, in each sub-region $a_{s-1} \leq r_1 \leq a_s$, onto the reduced radial target orbitals and pseudo-orbitals $v_{n\ell}(r_1)$ giving

$$\mathbf{O}^s_{n\ell n'\ell} = \langle u^s_{n\ell} | v_{n'\ell} \rangle = \int_{a_{s-1}}^{a_s} u^s_{n\ell}(r_1) v_{n'\ell}(r_1) \mathrm{d}r_1. \tag{6.85}$$

The resultant R-matrix can then be propagated outwards from $r_2 = a_p$, using one of the R-matrix propagator methods discussed in Appendix E, to a value of r_2 where the solution can be accurately fitted to an asymptotic expansion, as in Sect. 5.1.4. In this way, the K-matrix and hence the S-matrix and cross sections for transitions between the target physical and pseudostates can be calculated for each set of conserved quantum numbers Γ.

In conclusion, since the boundary radius a_p in Fig. 6.2 using the IERM method can be made much larger than the internal region boundary $r = a_0$ in the RMPS method, the IERM method will enable excitation cross sections to considerably higher Rydberg states to be accurately calculated. Also, as the value of the radius a_p becomes larger the density of continuum pseudostates increases. Since the ionization cross section is defined as the sum of excitation cross sections to pseudostates lying in the continuum, as illustrated in Fig. 6.1, increasing the value of a_p will enable the ionization cross section to be determined with greater accuracy, particularly close to threshold.

6.4 T-Matrix Energy Averaging

In this section we consider the analytic properties of the T-matrix and the scattering amplitude in the complex energy plane for electron–atom and electron–ion

collisions where we represent the total wave function by a close coupling with pseudostates expansion defined by (2.57) or equivalently by an R-matrix expansion defined by (5.5) and (5.6). In both cases the exact spectrum of the target is approximated by the bound with pseudostates spectrum, illustrated in Fig. 6.1, and the T-matrix and scattering amplitude will, as a result, exhibit unphysical structures due to the presence of pseudothresholds and pseudoresonances.

As an example of the unphysical structures that can occur at intermediate energies, we show in Fig. 6.3 the total collision strength for the $2s^2\ {}^1S^e$–$2s2p\ {}^3P^o$ transition in e^-–C^{2+} collisions calculated using the R-matrix method [97, 181]. In this calculation six target eigenstates, defined by (2.16), were included in the first expansion in (5.6), where $\overline{3}s$, $\overline{3}p$, $\overline{3}d$ and $\overline{4}f$ pseudo-orbitals were optimized to improve the energies of these states. Also quadratically integrable functions constructed from the physical and pseudo-orbitals were included in the second expansion in (5.6). We see that the calculated collision strength, denoted by the full curve in Fig. 6.3, exhibits pseudoresonance structure for electron collision energies above about 2 Rydbergs. This pseudoresonance structure is caused by the capture of the incident electron into these quadratically integrable functions which partially represent the discrete and continuum channels not explicitly included in the R-matrix expansion. Later in this section we will show how to extract physically meaningful cross sections from

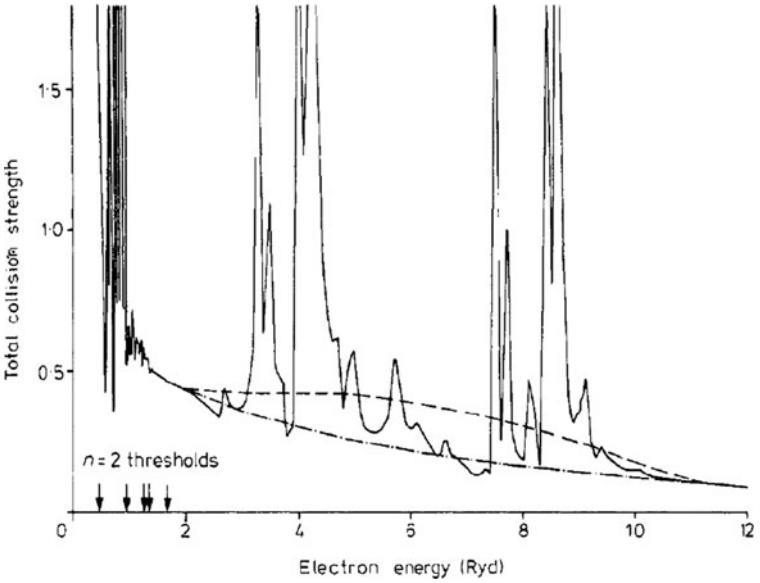

Fig. 6.3 Total collision strength defined by (2.149) for the $2s^2\ {}^1S^e$–$2s2p\ {}^3P^o$ transition in e^-–C^{2+} collisions. *Full curve*: calculated collision strength using the R-matrix method; *chain curve*: collision strength obtained by averaging the T-matrix over pseudoresonances; *broken curve*: collision strength obtained by averaging the calculated collision strength over pseudoresonances (Fig. 6 from [181])

this pseudoresonance structure, where we will also consider the significance of the chain curve and the broken curve in this figure.

The R-matrix calculation [97, 181] did not include pseudostates in the R-matrix expansion. However, the pseudoresonances are not all removed by their inclusion, as pointed out in our discussion of the close coupling with pseudostates expansion following (2.71). For example, detailed e^-–H scattering calculations were carried out by Callaway [197] and by Callaway and Unnikrishnan [200], which included seven and ten pseudostates, respectively, in the close coupling with pseudostates expansions. In order to obtain physically meaningful results at intermediate energies, these workers used the T-matrix energy-averaging procedure, discussed below, to remove the strong energy-dependent structures due to pseudoresonances, which they found near the pseudostate thresholds. The presence of pseudoresonances in close coupling with pseudostate calculations is an indication that the wave function and hence the T-matrix and cross sections have not fully converged.

A procedure for energy averaging the T-matrix over the pseudoresonance structure, to obtain physically meaningful scattering amplitudes and cross sections, was developed by Burke et al. [181] and by Slim and Stelbovics [878, 879]. We commence our consideration of this procedure by examining the analytic structure in the complex energy plane of the T-matrix, defined by (2.117) and (2.119). Following our discussion of the behaviour of the S-matrix near a resonance in Sect. 3.2.2, we show schematically in Fig. 6.4 the analytic structure of the T-matrix corresponding to the close coupling with pseudostates expansion of the wave function given by (5.6), compared with the analytic structure of the exact T-matrix. By comparing

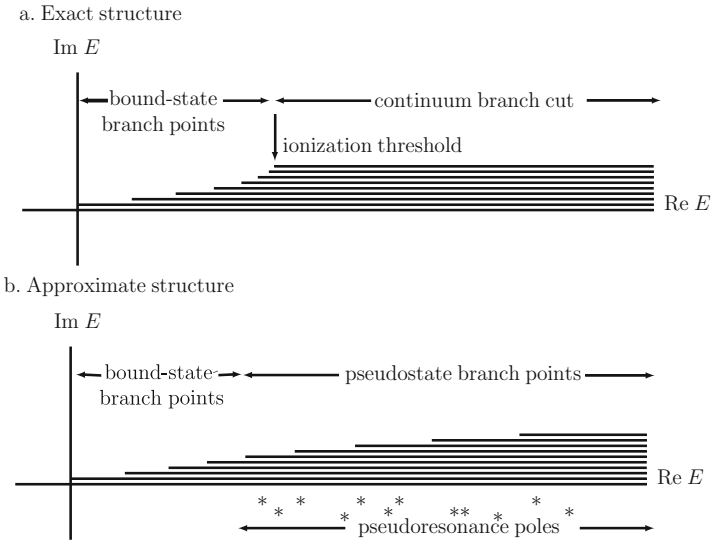

Fig. 6.4 Analytic structure of the T-matrix in the complex energy plane where the branch cuts are shown displaced from the real energy axis for clarity: (**a**) the exact structure; (**b**) for comparison, the approximate structure. The pseudoresonance poles represented by *asterisks* lie in the complex energy plane close to and below the real energy axis

this figure with Fig. 6.1, we see that the exact T-matrix in Fig. 6.4a has an infinite number of threshold branch points and corresponding branch cuts converging onto the ionization threshold of the target, together with a continuum branch cut commencing at this threshold. On the other hand, the approximate T-matrix in Fig. 6.4b has a finite number of physical and pseudostate branch points and corresponding physical and pseudostate branch cuts, which arise from the first expansion in (5.6), together with the pseudoresonance poles which arise from the quadratically integrable functions included in the second expansion in (5.6). We see that only the four lowest branch points and branch cuts in Fig. 6.4b provide an accurate representation of the exact branch points and branch cuts in Fig. 6.4a. We remember from our discussion following (2.71) that the quadratically integrable functions, which give rise to the majority of these poles and hence pseudoresonances in the T-matrix, are included in the second expansion to represent electron–electron correlation effects in the wave function which are not included in the first expansion rather than to remove the orthogonality constraints imposed on the scattered electron radial wave functions, as discussed following (2.57).

The physical ideas underlying the T-matrix averaging procedure that we consider below were introduced in the development of the optical potential model in nuclear reactions, discussed, for example, by Friedman and Weisskopf [342], Feshbach et al. [320, 322] and Brown [140]. This work suggested that the physical T-matrix element corresponding to a transition between target states retained in the first expansion in (5.6) can be defined by

$$T(E) = \lim_{n\to\infty} \langle T^n_{\text{approx}}(E)\rangle_{\text{Av}}. \tag{6.86}$$

In this equation $\langle T^n_{\text{approx}}(E)\rangle_{\text{Av}}$ is an appropriate energy average of the T-matrix element calculated retaining n quadratically integrable functions in the second expansion in (5.6), where the energy interval over which the average is taken is large compared with the distance between pseudoresonances but small compared with the range over which the background T-matrix varies appreciably.

Following Brown [140], Burke et al. [181] adopted the following averaging function:

$$\rho(E - E') = \frac{I}{\pi}\,\frac{1}{(E - E')^2 + I^2}, \tag{6.87}$$

where I is the energy-averaging interval. The energy-averaged T-matrix element at a real energy E is then related to the calculated T-matrix element at the real energies E' by

$$\langle T(E)\rangle_{\text{Av}} = \int_{-\infty}^{\infty} \rho(E - E')T(E')\mathrm{d}E' = T(E + \mathrm{i}I), \tag{6.88}$$

which is valid for functions like the T-matrix that have poles only in the lower half energy plane. In the limit when the number of quadratically integrable functions

$n \to \infty$, the width and separation of the pseudoresonances tend to zero and hence we can let the energy-averaging interval $I \to 0$. In complementary work, Slim and Stelbovics [878, 879] adopted the definition of the energy average proposed by Friedman and Weisskopf [342] given by

$$\langle T(E)\rangle_{\mathrm{Av}} = \frac{1}{E_b - E_a}\int_{E_a}^{E_b} T(E')\mathrm{d}E', \quad E_a \le E \le E_b, \tag{6.89}$$

where the energy interval $E_b - E_a \to 0$ as the number of quadratically integrable functions $n \to \infty$. These workers also considered an averaging procedure which consisted of fitting a low-degree polynomial in the energy variable.

In order to examine the validity of the T-matrix energy-averaging procedure, Burke et al. [181] applied it to a two-coupled channel S-wave model represented by the following coupled second-order differential equations:

$$\begin{aligned}\left(\frac{\mathrm{d}^2}{\mathrm{d}r^2} - V_{11}(r) + k_1^2\right) F_1(r) &= V_{12}(r)F_2(r),\\ \left(\frac{\mathrm{d}^2}{\mathrm{d}r^2} - V_{22}(r) + k_2^2\right) F_2(r) &= V_{21}(r)F_1(r).\end{aligned} \tag{6.90}$$

A series of calculations were carried out with the potentials

$$\begin{aligned}V_{11}(r) = V_{22}(r) &= -1.5\frac{\exp(-r)}{r},\\ V_{12}(r) = V_{21}(r) &= -0.5\exp(-r),\end{aligned} \tag{6.91}$$

where the excitation energy was 0.1 Rydbergs so that

$$k_2^2 = k_1^2 - 0.1. \tag{6.92}$$

The coupled equations (6.90) were first solved, using an accurate numerical procedure, to yield the coupled channel elastic scattering T-matrix and cross section. The first differential equation in (6.90) was then solved, omitting the coupling with the second inelastic equation, yielding the single-channel elastic scattering T-matrix and cross section. Finally, the solution in the second inelastic equation in (6.90) was represented by an expansion in quadratically integrable basis functions given by

$$u_i(r) = r^i \exp(-\alpha r), \quad i = 1, \ldots, n, \tag{6.93}$$

with $\alpha = 0.5$ and $n = 10$. The elastic T-matrix containing resonance structures, due to these basis functions, was then calculated and energy averaged using (6.88) and the energy-averaged elastic scattering cross section determined. We present the results of these calculations in Fig. 6.5 . We see that there is good agreement between the elastic scattering cross section obtained by solving the coupled channel problem

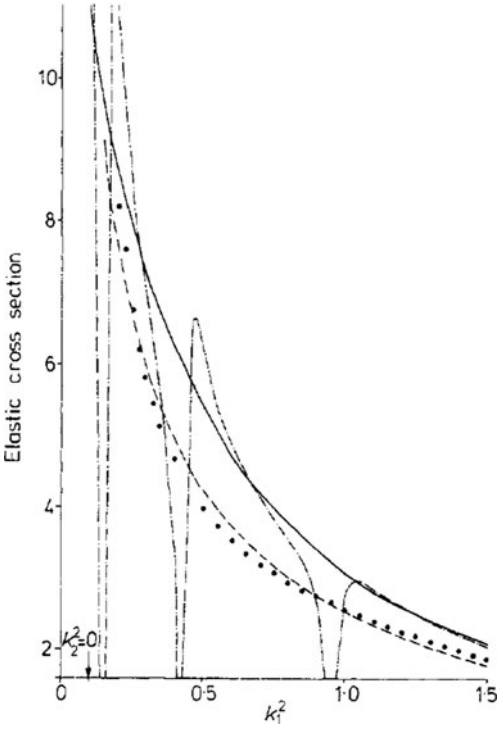

Fig. 6.5 Elastic cross section calculated in four approximations. *Broken curve*: accurate coupled channel calculation; *full curve*: accurate single-channel calculation; *chain curve*: inelastic channel represented by quadratically integrable basis functions; *dotted curve*: T-matrix energy-averaged calculation (Fig. 4 from [181])

exactly and the result obtained by representing the inelastic channel by quadratically integrable functions and energy averaging the resultant elastic T-matrix over the pseudoresonances. In the limit when the number of basis functions retained in (6.93) $n \to \infty$, the elastic scattering cross section obtained by energy averaging the T-matrix tends to the exact solution of (6.90).

In the work of Slim and Stelbovics [878, 879], both two- and three-channel S-wave models with separable potentials were considered, where the inelastic channel wave functions were expanded in Laguerre bases. This had the advantage that the resultant equations were amenable to analytic solution. In the two-channel model, it was shown analytically that averaging the amplitude using (6.89), where the energy interval becomes infinitesimal, converged to the exact amplitude, while the moments obtained by fitting to a low-degree polynomial also converged to the exact moments. In the three-channel case, the moments of a polynomial fit of degree 2 were also found to converge to the exact result using a numerical procedure.

In general, as emphasized by Scholz [832], we observe that the T-matrix energy-averaging procedure removes flux from the channels included explicitly in the first

expansion in (5.6) into the channels represented by the quadratically integrable functions included in the second expansion in (5.6). It follows that the corresponding energy-averaged S-matrix $\langle \mathbf{S}(E) \rangle_{\mathrm{Av}}$, coupling the channels included in the first expansion in (5.6), and defined in terms of the energy-averaged T-matrix $\langle \mathbf{T}(E) \rangle_{\mathrm{Av}}$, by

$$\langle \mathbf{S}(E) \rangle_{\mathrm{Av}} = \langle \mathbf{T}(E) \rangle_{\mathrm{Av}} + \mathbf{I} \tag{6.94}$$

is not unitary. On the other hand, the S-matrix $\mathbf{S}(E)$ obtained before energy averaging, which is defined in terms of the T-matrix $\mathbf{T}(E)$ by (2.119), is unitary at each energy since it is calculated by solving a set of coupled second-order differential equations with real symmetric potentials. Hence the energy-averaged cross section, which is proportional to $\langle |\mathbf{T}(E)|^2 \rangle_{\mathrm{Av}}$, is different from the cross section obtained from the energy-averaged T-matrix, which is proportional to $|\langle \mathbf{T}(E) \rangle_{\mathrm{Av}}|^2$. This difference has already been observed in Fig. 6.3 where the broken curve, which corresponds to the energy-averaged cross section, is very different from the chain curve, which corresponds to the energy-averaged T-matrix. Our discussion in this section has shown that the dotted curve in Fig. 6.5 is obtained using the correct T-matrix energy-averaging procedure for extracting physically meaningful cross sections at intermediate energies from this calculation and that spurious results can be obtained by energy averaging the cross section.

In conclusion, we observe that in general, as the number of pseudostates included in the expansion of the collision wave function is increased, so that the representation of the continuum spectrum by pseudostates in Fig. 6.1 is expanded towards completeness, then the role of the quadratically integrable functions, which give rise to pseudoresonances, decreases. We find that the inclusion of pseudostates in the R-matrix expansion, together with T-matrix energy averaging over pseudoresonances where necessary, enables accurate scattering amplitudes and cross sections to be determined at intermediate energies.

6.5 Distorted Wave and Second-Born Methods

The intermediate-energy R-matrix methods discussed in Sects. 6.3 and 6.4 have been applied to a wide range of electron–atom and electron–ion collisions, yielding accurate excitation and ionization cross sections at intermediate energies. These methods have also been extended to enable accurate positron–atom collision cross sections, atomic photoionization cross sections and electron–molecule collision cross sections, considered in later chapters in this monograph, to be calculated at intermediate energies. However, as the incident or ejected electron energy increases the number of pseudostates that need to be included in expansions (5.6) and (5.28) to yield reliable results at intermediate energies also increases. Since the resultant computing requirement increases as the cube of the number of target eigenstates and pseudostates included in these expansions, these requirements quickly become excessive.

However, if the energies of the incident and scattered electrons are well above the ionization threshold, then, in the absence of resonant capture, the interaction time of the electron with the target is short. In this case, the interaction of this electron with the target can often be reliably treated using distorted waves or a second-Born expansion, rather than by the non-perturbative approach of expanding in pseudostates. As an example, we consider the excitation–autoionization process illustrated by (6.2). If the energies of the incident and scattered electrons are well above the energy necessary to excite the intermediate autoionizing state $C^{3+**}(1sn'\ell'n''\ell'')$ then their motion can often be accurately described by a distorted wave or Born series approximation. On the other hand, the slower electron emitted in the decay of the autoionizing state will usually be strongly coupled to the residual state $C^{4+}(1sn\ell)$, and hence this interaction will need to be treated non-perturbatively using a close coupling or R-matrix expansion, possibly including pseudostates. This is the basis of the distorted wave R-matrix (DWRM) method, introduced by Bartschat and Burke [65], which extended the Coulomb–Born exchange and distorted wave exchange approximations using close coupling wave functions developed by Jacubowicz and Moores [497]. In the following discussion we will describe the DWRM method and we will then mention further developments which have been made to extend its range of validity.

We consider the electron–atom or electron–ion excitation–ionization process

$$e^-(\mathbf{k}_0) + A_j^{q+} \rightarrow e^-(\mathbf{k}_1) + \left[A_f^{(q+1)+} + e^-(\mathbf{k}_2)\right], \tag{6.95}$$

where we make the following assumptions:

i. The incident and scattered electrons $e^-(\mathbf{k}_0)$ and $e^-(\mathbf{k}_1)$ with momenta $\mathbf{k}_0$ and $\mathbf{k}_1$ are both fast and can therefore be described by distorted waves.
ii. The initial bound state of the target A_j^{q+} and the final continuum state of the target $\left[A_f^{(q+1)+} + e^-(\mathbf{k}_2)\right]$, which we assume contain $N+1$ electrons, can both be accurately described by R-matrix expansions analogous to (5.5) and (5.6) in the internal region and (5.28) in the external region.
iii. Only the direct Coulomb interactions between the fast incident and scattered electrons and the $N+1$ target electrons are retained in the calculation.
iv. The exchange interactions between the fast incident and scattered electrons and the $N+1$ target electrons can be neglected.
v. Relativistic effects are neglected in the following analysis, although their inclusion using the Breit–Pauli or the Dirac Hamiltonian, discussed in Sects. 5.4 and 5.5, respectively, would be straightforward.

The scattering amplitude describing the ionization process (6.95) is then given in the distorted wave approximation [123, 628, 666] by

$$f(\mathbf{k}_0, \mathbf{k}_1, \mathbf{k}_2) = -(2\pi)^{-5/2} \langle \Psi_{fE}^-(\mathbf{k}_2; \mathbf{X}_{N+1}) \phi_1^-(\mathbf{k}_1; \mathbf{x}_{N+2}) \, |V(\mathbf{X}_{N+1}, \mathbf{x}_{N+2})| \times \Psi_j(\mathbf{X}_{N+1}) \phi_0^+(\mathbf{k}_0; \mathbf{x}_{N+2}) \rangle, \tag{6.96}$$

where $\mathbf{x}_{N+2}$ denotes the space and spin coordinates of the incident and scattered electrons, $\mathbf{X}_{N+1}$ denotes the space and spin coordinates of the $N+1$ target electrons and $V(\mathbf{X}_{N+1}, \mathbf{x}_{N+2})$ is the Coulomb interaction between the incident and scattered electrons and the $N+1$ target electrons which is defined by

$$V(\mathbf{X}_{N+1}, \mathbf{x}_{N+2}) = \sum_{i=1}^{N+1} \frac{1}{|\mathbf{r}_i - \mathbf{r}_{N+2}|}. \tag{6.97}$$

Finally, the integration in the matrix element, which appears on the right-hand side of (6.96), goes over the space and spin coordinates of all $N+2$ electrons.

We now consider the approximations made for the initial and final state wave functions in (6.96). The distorted waves describing the incident and scattered electrons in this equation are expanded in partial waves as follows:

$$\phi_0^+(\mathbf{k}_0; \mathbf{x}) = \frac{4\pi}{k_0^{1/2} r} \sum_{\ell m_\ell} \mathrm{i}^\ell \exp(\mathrm{i}\delta_\ell) Y_{\ell m_\ell}^*(\theta_{k_0}, \phi_{k_0}) Y_{\ell m_\ell}(\theta, \phi) \times P_{k_0 \ell}(r) \chi_{\frac{1}{2} m_0}(\sigma) \tag{6.98}$$

and

$$\phi_1^-(\mathbf{k}_1; \mathbf{x}) = \frac{4\pi}{k_1^{1/2} r} \sum_{\ell m_\ell} \mathrm{i}^\ell \exp(-\mathrm{i}\delta_\ell) Y_{\ell m_\ell}^*(\theta_{k_1}, \phi_{k_1}) Y_{\ell m_\ell}(\theta, \phi) \times P_{k_1 \ell}(r) \chi_{\frac{1}{2} m_1}(\sigma), \tag{6.99}$$

where $\chi_{\frac{1}{2} m_0}(\sigma)$ and $\chi_{\frac{1}{2} m_1}(\sigma)$ are the spin functions of the incident and scattered electrons, respectively, and $Y_{\ell m_\ell}(\theta, \phi)$ are spherical harmonics defined in Appendix B.3. The reduced radial functions $P_{k\ell}(r)$ in (6.98) and (6.99) are usually taken to satisfy a radial Schrödinger equation with the general form

$$\left(\frac{\mathrm{d}^2}{\mathrm{d}r^2} - \frac{\ell(\ell+1)}{r^2} + 2U(r) + k^2 \right) P_{k\ell}(r) = 0, \tag{6.100}$$

satisfying the boundary conditions

$$P_{k\ell}(0) = 0, \quad P_{k\ell}(r) \underset{r \to \infty}{\sim} k^{1/2} \sin(kr - \tfrac{1}{2}\ell\pi + \delta_{k\ell}), \tag{6.101}$$

where we have assumed that the target is neutral. If it is ionic then the usual Coulomb phase and logarithmic terms would have to be included in (6.98), (6.99) and (6.101),

as discussed in Sect. 2.5. Finally, $U(r)$ in (6.100) is a suitably chosen model potential which represents the charge distribution of the target atom or ion.

We consider next the calculation of the initial bound state $\Psi_j(\mathbf{X}_{N+1})$ and the final continuum state $\Psi^-_{fE}(\mathbf{k}_2; \mathbf{X}_{N+1})$ in (6.96). Both of these states can be determined in the R-matrix internal region using expansions (5.5) and (5.6), where the coefficients $A^{\Gamma}_{kj}(E)$ are defined by (5.27) as described in Sect. 5.1.2. In (5.27), $F^{\Gamma}_{ij}(r)$ is the ith component of the reduced radial wave function describing the motion of the $(N+1)$th electron in the external and asymptotic regions defined in Fig. 5.1. We can determine $F^{\Gamma}_{ij}(r)$ and $\mathrm{d}F^{\Gamma}_{ij}/\mathrm{d}r$ at $r = a_0$, the radius of the internal region, by integrating the coupled second-order differential equations (5.29), satisfied by these functions, from $r = a_0$ to a_p using a propagator method discussed in Appendix E. In the case of the initial bound state Ψ_j we then fit the solution on the boundary $r = a_p$ to a decaying wave asymptotic boundary condition

$$F^{\Gamma}_{ij}(r) \underset{r\to\infty}{\sim} N_{ij} \exp(-\kappa_{ij} r), \quad \text{all } i. \tag{6.102}$$

Since all the channels are closed, the wave number k_{ij} of the $(N+1)$th electron in the ith channel satisfies $k^2_{ij} = -\kappa^2_{ij}$ so that $k_{ij} = \mathrm{i}\kappa_{ij}$. Also in (6.102) N_{ij} are normalization factors. The boundary condition given by (6.102) is achieved by iteratively varying the total energy E_j of the initial bound state and re-solving the coupled second-order differential equations (5.29) in the external and asymptotic regions until the asymptotic boundary condition (6.102) is satisfied. In the case of an atomic target, an infinite number of solutions can be obtained, corresponding to the ground and excited Rydberg states, where in most experiments the target A^{q+}_j in (6.95) will be in its ground state corresponding to the lowest energy solution. The wave function $\Psi_j(\mathbf{X}_{N+1})$ in (6.96) is then obtained by normalizing the total wave function in the internal, external and asymptotic regions to unity so that

$$\langle \Psi_j, \Psi_{j'} \rangle = \delta_{jj'}, \tag{6.103}$$

which yields the normalization factor N_{ij} in (6.102).

Finally, we consider the calculation of the continuum state $\Psi^-_{fE}(\mathbf{k}_2; \mathbf{X}_{N+1})$ in (6.96). In this case we expand the wave function in the internal region using (5.5) and (5.6) for each required continuum-state energy and for all total orbital angular momenta L and parities π which give a significant contribution to the scattering amplitude defined by (6.96). We note that for relatively light targets there is no summation over the total spin angular momenta S since this quantity is conserved in non-relativistic theory considered here. The expansion coefficients in (5.5), which we denote here by $A^{\Gamma-}_{kf}(E)$, are again determined using (5.27) which can be written here as

$$A^{\Gamma-}_{kf}(E) = \frac{1}{2a_0(E^{\Gamma}_k - E)} \sum_{i=1}^{n} w^{\Gamma}_{ik} \left(a_0 \frac{\mathrm{d}F^{\Gamma-}_{if}}{\mathrm{d}r} - b_0 F^{\Gamma-}_{if}(r) \right)_{r=a_0}, \tag{6.104}$$

for each L and π. We can determine $F_{if}^{\Gamma-}(r)$ and $\mathrm{d}F_{if}^{\Gamma-}/\mathrm{d}r$ at $r = a_0$, by integrating (5.29) from $r = a_0$ to a_p and fitting to an asymptotic expansion, as discussed in Appendix F.1. In this case the leading term in the asymptotic expansion can be written in matrix notation as

$$\mathbf{F}^{\Gamma-}(r) \underset{r\to\infty}{\sim} \left(\frac{2}{\pi \mathbf{k}}\right)^{1/2} (\sin\boldsymbol{\theta} + \cos\boldsymbol{\theta}\mathbf{K})(\mathbf{I} + \mathrm{i}\mathbf{K})^{-1}, \tag{6.105}$$

where $\mathbf{K}$ is the usual K-matrix and the elements of the diagonal matrix $\boldsymbol{\theta}$ are defined by (5.38). The total wave function then satisfies the normalization condition

$$\langle \Psi_{fE}^{-} | \Psi_{f'E'}^{-} \rangle = \delta_{ff'}\delta(E - E'), \tag{6.106}$$

and the ingoing wave boundary condition

$$\Psi_{fE}^{-} \underset{r_{N+1}\to\infty}{\sim} \Psi_{fE}^{\mathrm{inc}} + \Psi_{fE}^{\mathrm{ing}}, \tag{6.107}$$

required by definition (6.96) of the scattering amplitude, where (6.107) corresponds to a Coulomb modified plane wave plus ingoing waves in all channels.

An R-matrix computer program package RMATRX-ION, which implements the above theory for electrons incident on a general atom or atomic ion, was developed by Bartschat [62], based on the electron–atom collision program RMATRXI, discussed in Sect. 5.1.1, although the relativistic options were not implemented. This program has been used to calculate electron impact ionization cross sections at intermediate energies for a number of atoms and ions including He, Ne^{6+}, Ar, Ar^{9+} and Cr [65, 66, 69, 560, 561, 768, 782]. RMATRX-ION was later extended by Bartschat [63] enabling positron collisions with noble gases to be calculated at intermediate energies.

The computer program RMATRX-ION was also extended by Schweinhorst et al. [840] to enable double-differential cross sections (DDCS) and triple-differential cross sections (TDCS) to be calculated. They then used this program to calculate DDCS and TDCS for helium which they compared with experiment. The experimental data for DDCS were well reproduced by the theory at incident electron energies of 200 and 300 eV. However, a more detailed comparison with TDCS data showed that higher order effects should be included to further improve the theoretical model. This conclusion is consistent with TDCS studies of helium ionization by Byron et al. [196] and other workers that have demonstrated the necessity of including second-Born approximation terms in the scattering amplitude to account for details of the observations. In order to explore this possibility further, Reid et al. [783, 784] included second-order effects in the DWRM method by replacing the potential $V(\mathbf{X}_{N+1}, \mathbf{x}_{N+2})$ in (6.96) by

$$V + V \lim_{\eta\to 0+} (E - H_0 + \mathrm{i}\eta)^{-1} V, \tag{6.108}$$

where $H_0 + V(\mathbf{X}_{N+1}, \mathbf{x}_{N+2})$ is the Hamiltonian for the $(N + 2)$-electron system. In order to calculate the contribution from the second-order term in (6.108) several approximations were made, including restricting the evaluation of the additional matrix elements to the internal region. The inclusion of second-order effects in this way improved the overall agreement between the experimental data for helium and the theoretical predictions. However, the results for the TDCS were found to be sensitive to the representation of the initial state.

A further important extension of the theory was made by Fang and Bartschat [298–300] who replaced the distorted waves used by Reid et al. [783, 784] by plane waves in a second-Born R-matrix with pseudostates (RMPS) theory. This enabled analytical simplifications to be made in the theory and, as a result, it was not only possible to perform calculations at higher incident electron energies, where the partial wave expansion converges more slowly, but it also enabled a larger number of coupled target eigenstates to be included in the expansion. Some results of this work are shown in Sect. 6.6.3.

Finally, we mention more recent work by Bartschat and Grum-Grzhimailo [68], in which simultaneous electron impact excitation–ionization has been reformulated in terms of irreducible tensors, and benchmark calculations carried out for e^-–He collisions, where the decay photon from $He^+(2p\ ^2P^o)$ is observed in triple coincidence with the two outgoing electrons. Also Andersen and Bartschat [17] have considered the dipole polarization of a coherently excited Stark manifold for the simplest case of excitation–ionization of the $He^+(2s, 2p)$ manifold in e^-–He collisions. It is thus clear, from this and other work reported in this section, that the distorted wave R-matrix method and the associated second-Born RMPS method have opened up important new areas of electron–atom and electron–ion collision calculations at intermediate energies.

6.6 Intermediate-Energy Electron Collision Calculations

In this section we present results from some recent electron–atom and electron–ion collision calculations and experiments at intermediate energies. In Sect. 11.1.7 we present results for an electron–H_3^+ collision calculation at intermediate energies using a molecular extension of the RMPS method.

6.6.1 Electron Collisions with H

As our first example of electron collisions with atoms and ions at intermediate energies, we consider RMPS and convergent close coupling (CCC) calculations for electron impact ionization of the 1s state of atomic hydrogen, carried out by Bartschat and Bray [67]. We present in Fig. 6.6 results obtained using the RMPS method and the CCC method (discussed in Sect. 6.1) for the total ionization cross section $\sigma_{\rm I}$ and for the ionization spin asymmetry $A_{\rm I}$ of atomic hydrogen compared

with experiment over the energy range from the ionization threshold at 13.6–100 eV. The total ionization cross section measurements σ_I were made by Shah et al. [869] and the ionization spin asymmetry measurements A_I were made by Fletcher et al. [324] and by Crowe et al. [238], where A_I is defined by

$$A_I = \frac{1}{P_e P_A} \frac{N_a - N_p}{N_a + N_p} = \frac{\sigma_I^s - \sigma_I^t}{\sigma_I^s + \sigma_I^t}. \tag{6.109}$$

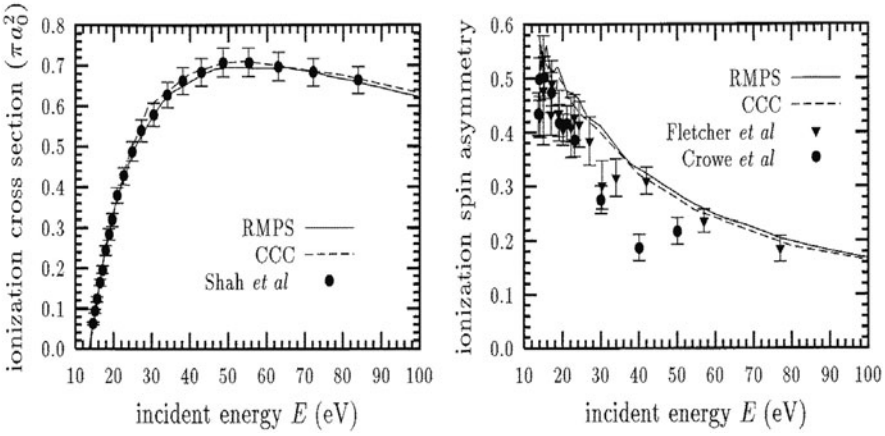

Fig. 6.6 Total ionization cross section σ_I (*left*) and ionization spin asymmetry A_I (*right*) for electron impact ionization of atomic hydrogen using the RMPS and CCC methods compared with experiment (Fig. 1 from [67])

In this equation N_a and N_p are the count rates for ionization with antiparallel and parallel scattered electron (P_e) and target (P_A) spin polarizations, respectively, while σ_I^s and σ_I^t are the singlet and triplet contributions to the total ionization cross section, respectively. The agreement between the results from the two independent calculations is very good for both σ_I and A_I. Also, the agreement between theory and experiment for σ_I is excellent and, while there are some discrepancies between these calculations and experiments for A_I, we observe that there is also some scattering in the corresponding experimental data. This comparison between theory and experiment shows that both the RMPS and CCC methods, which include pseudostates in the expansion, can yield reliable cross sections over a wide energy range for atomic hydrogen. More recent work by Mouret et al. [667] has shown that the IERM approach, discussed in Sect. 6.3, also gives accurate total ionization cross sections and spin asymmetries for electron–hydrogen atom collisions.

The RMPS method has also been applied by Anderson et al. [18] to obtain electron impact excitation cross sections and effective collision strengths for transitions in atomic hydrogen between target states up to principal quantum number $n = 5$. In these calculations, the 15 $n = 1, 2, 3, 4$ and 5 target eigenstates together with 24

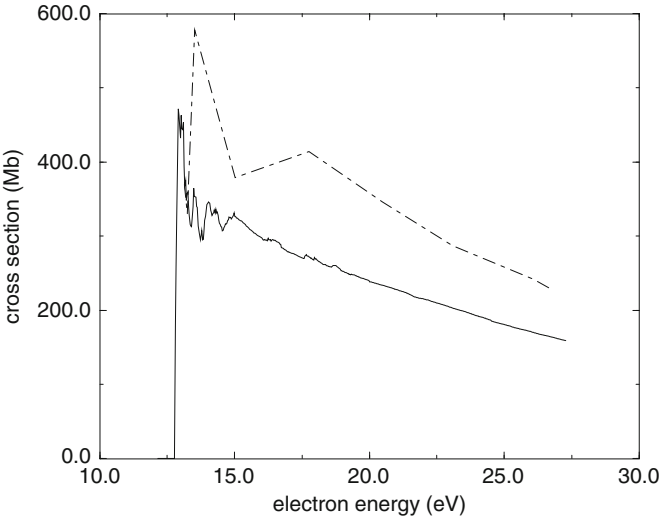

Fig. 6.7 Electron impact excitation cross section for the 3d–4d transition in atomic hydrogen. *Solid curve*: 15 target states plus 24 pseudostates calculation [18]. *Dashed curve*: 15 target states calculation with no pseudostates [2] (Fig. 3 from [18])

target pseudostates were included in the R-matrix expansion (5.6) giving reliable effective collision strengths up to a temperature of 25 eV. As an example of these calculations, we show in Fig. 6.7 the excitation cross section for the 3d–4d transition obtained by Anderson et al. compared with an R-matrix calculation by Aggarwal et al. [2] who included the first 15 target eigenstates up to $n = 5$ in their calculation but did not include any pseudostates. We see that the two calculations are in good agreement at low energies but above about 14 eV the discrepancies are in excess of 30%. This pattern is continued but the discrepancy is even larger for transitions between the $n = 4$ and 5 target states. This result is in accord with the results of electron–helium atom collision calculations discussed in Sect. 5.6.2, where it was found that in the absence of pseudostates in the R-matrix expansion, the cross sections were in error above the threshold of the highest eigenstate retained in the R-matrix expansion.

The results for electron–hydrogen atom collisions obtained by Anderson et al. [18], which are of importance for diagnostic applications in fusion plasmas, have now been extended by Ballance et al. [45] to the hydrogen-like ions He^{+}, Li^{2+}, Be^{3+}, B^{4+}, C^{5+}, O^{7+} and Ne^{9+}.

Finally, we remark that extending these calculations to target states with higher principal quantum numbers $n \lesssim 10$, of astrophysical interest, would prove expensive using the RMPS approach because of the very large number of target states and pseudostates that would have to be included in the expansion and also because of their range which behaves as n^2. In this situation, calculations using the IERM method would have some advantages, as discussed in Sect. 6.3.

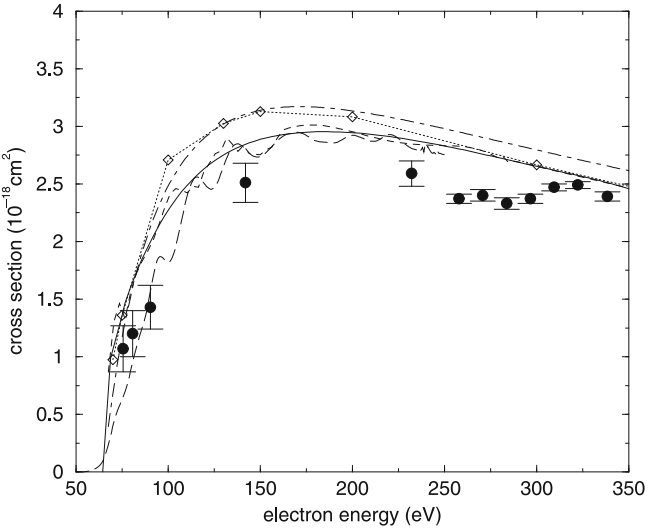

Fig. 6.8 Electron impact ionization of C^{3+}. *Full curve*: RMPS calculation smoothed [842]; *short-broken curve*: RMPS calculation unsmoothed [842]; *long-broken curve*: RMPS calculation unsmoothed [653]; *dotted curve with diamonds*: CCC calculation [125]; *chain curve*: distorted wave calculation [986]; *full circles*: experiment [235] (Fig. 1 from [842])

6.6.2 Electron Collisions with C IV

As a further example of electron collisions at intermediate energies, we present in Fig. 6.8 independent RMPS calculations by Mitnik et al. [653] and Scott et al. [842] for electron impact ionization of C IV (C^{3+}) given by

$$e^- + C^{3+}(1s^2 2s) \rightarrow C^{4+}(1s^2) + 2e^-, \tag{6.110}$$

compared with a CCC calculation by Bray [125], a distorted wave calculation by Younger [986] and with experiments by Crandall et al. [235]. In the RMPS calculation [842], the five lowest target eigenstates of C^{3+}, $1s^2 2s\ ^2S^e$, $1s^2 2p\ ^2P^o$, $1s^2 3s\ ^2S^e$, $1s^2 3p\ ^2P^o$ and $1s^2 3d\ ^2D^e$, together with 21 pseudostates with the form $1s^2\overline{n\ell}$ up to $\overline{9s}$, $\overline{9p}$, $\overline{7d}$, $\overline{6f}$ and $\overline{6g}$ were included in expansion (5.6) in the internal region and in expansion (5.28) in the external and asymptotic regions. The small oscillations in the cross section before smoothing resulted from the representation of the continuum by a discrete pseudostate basis and are damped as this basis is increased. We see from this figure that there is good overall agreement between the RMPS and CCC calculations (discussed in Sect. 6.1) and experiment and there is also good agreement between the distorted wave calculation and experiment, indicating that intermediate states are not playing a major role in this case.

In addition to the direct ionization process considered above, we have seen that there are three important indirect processes, defined by (6.2), (6.3) and (6.4). An RMPS calculation of the indirect processes that arise in electron impact ionization

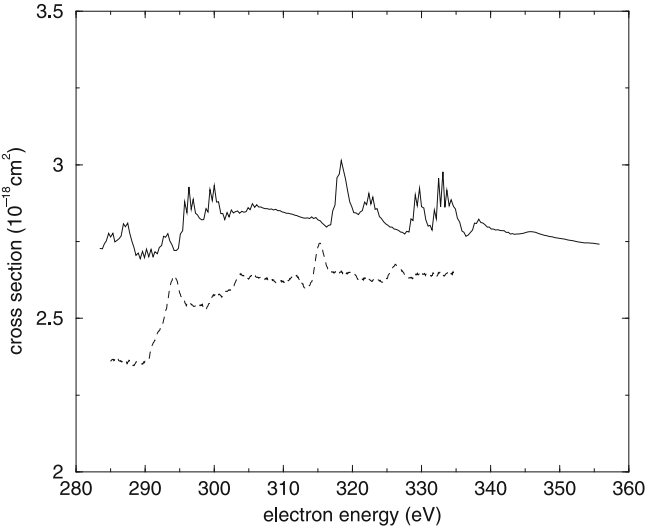

Fig. 6.9 Electron impact inner-shell ionization of C^{3+} showing autoionizing resonance features. *Full curve*: convoluted RMPS results [842]; *dashed curve*: experimental measurements [669] (Fig. 4 from [842])

of C^{3+} was also made by Scott et al. [842] by augmenting the 5 eigenstates and 21 pseudostates retained in expansions (5.6) and (5.28), discussed above, with an additional 16 autoionizing states, where only one electron was retained in the 1s orbital. In this way intermediate states in (6.2), (6.3) and (6.4) were represented in the calculation. We compare their calculated ionization cross section in the energy range from 284 to 356 eV with the experimental data of Müller et al. [669] in Fig. 6.9, where the calculated cross section was convoluted with a 2.0 eV full width at half maximum Gaussian to simulate the experimental energy resolution. The RMPS calculation reproduces a number of resonance features observed in the experiment. However, the calculated non-resonant background is about 10% higher than experiment and there is an energy shift of the calculated resonance peaks by about 2 eV from their observed positions. This shift indicates that more pseudostates should be included in the calculation to give convergence, while the discrepancy in normalization between theory and experiment is larger than that shown for direct ionization in Fig. 6.8, indicating that part of this discrepancy could be attributed to experiment. However, in view of the complexity of these indirect processes and the difficulty of the experiment, the overall agreement is encouraging.

6.6.3 Electron Impact Excitation–Ionization of He

Although the previous example shows that the RMPS method can accurately describe ionizing collisions at incident electron energies well above the ionization

threshold, the number of coupled channels required to obtain accurate results can often become very large. In this case, as discussed in Sect. 6.5, in the absence of resonant capture of the incident or scattered electron by the target, accurate results can be obtained by treating this electron by a distorted wave or Born series expansion.

As an example, we present the results of calculations by Fang and Bartschat [298] who considered the following simultaneous electron impact excitation–ionization process in He:

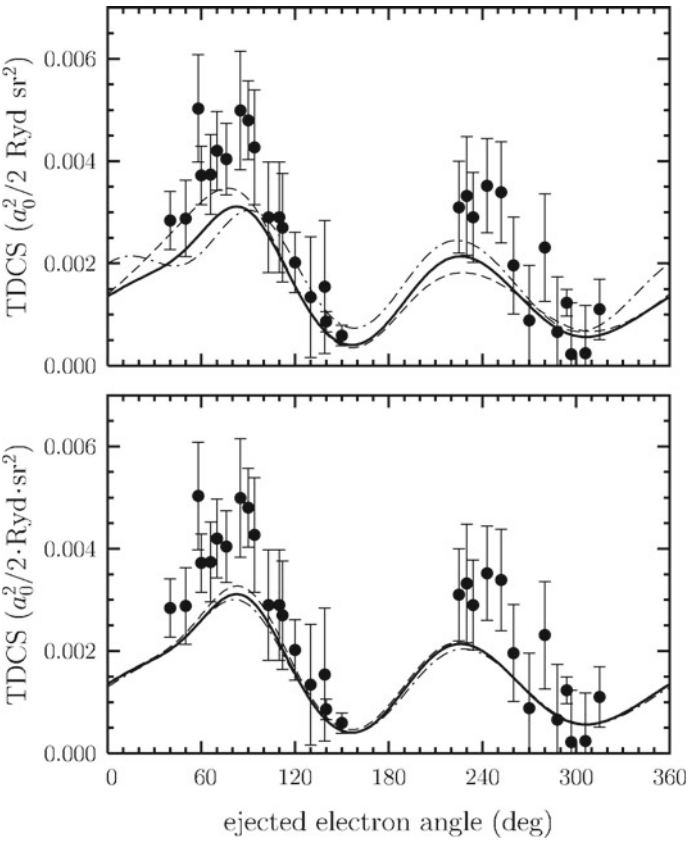

Fig. 6.10 Electron impact excitation–ionization of He showing in-plane angular distribution of the ejected electron for excitation–ionization to the He^+ $n = 2$ states. The experimental data of Avaldi et al. [27] for an incident electron energy of 1,585 eV, final electron energies of 1,500 and 20 eV and a detection angle of 4° for the fast electron are compared with the results obtained from several models. *Top*, second-order results: *full curve*, 23-state RMPS model; *broken curve*, 12-state RMPS model; *chain curve*, 6-state eigenstate model. *Bottom*, second-order 23-state RMPS model for intermediate-state energies of the fast electron: *full curve* 1,543 eV; *chain curve* 1,521 eV; *broken curve* 1,565 eV. The energies in the *bottom curves* correspond to the geometric mean of the initial and final energies as well as one value closer to each one of these energies (Fig. 2 from [298])

$$e^- + He(1s^2\ ^1S) \rightarrow He^+(2s, 2p) + 2e^-, \tag{6.111}$$

where the He^+ ion in the final state is left in a 2s or 2p excited state. As noted by Marchalant et al. [635–637], who carried out first- and second-Born (e, 2e) calculations of this process, the inclusion of second-order effects clearly improves the agreement between theory and experiment in the shape of the angular distribution and to a lesser extent in the magnitude. In the calculations by Fang and Bartschat the incident and scattered electrons were described using the second-Born approximation, while the initial He bound state and the final He^+ excited state plus the ejected electron were described by a 23-state RMPS expansion, which included the first six 1s, 2s, 2p, 3s, 3p and 3d He^+ eigenstates, together with up to 17 He^+ pseudostates. We compare these calculations with experiments by Avaldi et al. [27] in Fig. 6.10 for an incident electron energy of 1,585 eV. We see from the top results presented in this figure that the 23-state and 12-state second-Born RMPS results are in good agreement with experiment. However, the 6-state second-Born results, which only included the lowest 6 He^+ eigenstates in the R-matrix expansion, show a deviation at small ejected angles indicating a lack of convergence in the representation of the intermediate $He^+ + e^-$ state. It should also be noted from the bottom results presented in Fig. 6.10 that these results are, as expected, insensitive to changing the average energy of the fast electron in the intermediate state.

Overall there is qualitative agreement between the results of Fang and Bartschat and those of Marchalant et al. regarding the effect of the second-order correction on the results. However, the results differ quantitatively. While part of the deviation may be due to the different treatment of the fast incident and scattered electrons it is probable that the most important reason for the difference is the more accurate R-matrix expansion treatment of the interaction between the ejected electron and the residual ion in the former calculation [298]. Thus it is found that the 6-state results are closer to those of Marchalant et al. than the 12-state and 23-state predictions, which appear close to convergence. In general, the convergence of the Fang and Bartschat results with respect to the number of pseudostates included in the R-matrix expansion indicate that the treatment of this aspect of the model has converged to a few percent.

In conclusion, the treatment of electron impact excitation–ionization of atoms and ions by fast electrons, where the incident and scattered electrons are treated using a second-Born approximation and the ejected electron and residual ion are treated using an R-matrix with pseudostates expansion, can yield close to converged results.

Chapter 7
Positron Collisions with Atoms and Ions

In this chapter we extend our discussion of multichannel R-matrix theory of electron collisions with atoms and atomic ions given in Chaps. 5 and 6 to consider positron collisions with these targets. Since the positron is distinguishable from the target electrons, we no longer have to antisymmetrize the total wave function with respect to interchange of the positron coordinates with those of the target electrons. However, this simplification is balanced by the additional channels that have to be included where the incident positron combines with one of the target electrons to form a bound state of the positron–electron system, called positronium (Ps). In this respect, positron collisions with atoms and ions have similarities to electron–molecule collisions which we will consider in Chap. 11 where rearrangement processes corresponding to dissociation and dissociative attachment can occur. A further process that can occur in positron collisions with atoms and ions is where the incident positron annihilates with one of the target electrons with the emission of γ-rays providing a further important test of collision theory. Also processes where positronium atoms are incident on atomic targets are of increasing interest both experimentally and theoretically.

The processes involved in positron and positronium collisions with atoms and ions clearly provide new challenges for both experiment and theory. This has stimulated new developments in the measurement of positron and positronium collision cross sections and in the theory and calculation of positron– and positronium–atom collision cross sections, where applications of R-matrix theory by Walters et al. [949–953] have been particularly successful. Reviews of these developments and applications have been written by Armour and Humbertson [23], Laricchia [576] and Surko et al. [898]. They have also been discussed in the proceedings of conferences edited by Surko and Gianturco [897] and by Gribakin and Walters [423].

We commence in Sect. 7.1 with a general discussion of the processes that can occur in positron and positronium collisions with atoms and atomic ions. We then consider the new extensions to multichannel R-matrix theory of electron collisions with atoms and ions, considered in Chaps. 5 and 6, to enable the channels corresponding to positronium collisions to be included in the theory. Finally, in Sect. 7.2 we present the results of some recent positron and positronium collision calculations using R-matrix theory.

P.G. Burke, *R-Matrix Theory of Atomic Collisions*, Springer Series on Atomic, Optical, and Plasma Physics 61, DOI 10.1007/978-3-642-15931-2_7,

7.1 Multichannel *R*-Matrix Theory

In this section we introduce *R*-matrix theory of positron and positronium collisions with atoms and atomic ions by summarizing in Sect. 7.1.1 the various processes that can occur and we compare and contrast these processes with those that occur in electron collisions with atoms and atomic ions discussed in Chap. 5. We also consider the form of the Schrödinger equation which describes positron or positronium collisions with an atom or atomic ion and we discuss the partitioning of configuration space into internal, external and asymptotic regions. We then consider in turn the solution in the internal region in Sect. 7.1.2, in the external region in Sect. 7.1.3 and in the asymptotic region in Sect. 7.1.4 yielding the K-matrix, S-matrix and cross sections for positron and positronium collisions with atoms and ions.

7.1.1 Introduction

In collisions of positrons with atoms and atomic ions the following processes can occur:

$$\begin{aligned}
\mathrm{e}^+ + A_i &\rightarrow A_i + \mathrm{e}^+ && \text{elastic scattering,}\\
&\rightarrow A_j + \mathrm{e}^+ && \text{excitation,}\\
&\rightarrow A_j^+ + \mathrm{e}^- + \mathrm{e}^+ && \text{ionization,}\\
&\rightarrow A_j^+ + \mathrm{Ps} && \text{Ps formation,}\\
&\rightarrow A_j^{2+} + \mathrm{Ps}^- && \mathrm{Ps}^- \text{ formation,}\\
&\rightarrow A_j^{2+} + \mathrm{Ps} + \mathrm{e}^- && \text{transfer ionization with Ps formation,}\\
&\rightarrow A_j^{3+} + \mathrm{Ps}^- + \mathrm{e}^- && \text{transfer ionization with } \mathrm{Ps}^- \text{ formation,}\\
&\rightarrow A_j^+ + \gamma \text{ rays} && \text{annihilation.}
\end{aligned} \tag{7.1}$$

The positronium atom (Ps) in (7.1), which can be formed in an excited state, consists of a bound state of the positron and a target electron and is formally the same as the hydrogen atom but with a reduced mass of 0.5 a.u. rather than 1 a.u. Consequently, Ps bound states are classified in the same way as those of atomic hydrogen but with half the energy of the corresponding states, i.e. $E_{n\ell m} = -0.25\ n^{-2}$ a.u., where n is the principal quantum number. Positronium can be formed in two spin states, referred to as "ortho" where the positron and electron spins are in the triplet state and as "para" where the two spins are in the singlet state. An interesting discussion of the electron–positron system has been given by Jauch and Rohrlich [499] and recent detailed quantum electrodynamic calculations of Ps lifetimes have been discussed by Kniehl and Penin [539]. In the work of Kniehl and Penin it was shown that the para-positronium 1s state decays predominantly into two photons with a lifetime of 0.125 ns and the ortho-positronium 1s state decays predominantly into three photons with a lifetime of 142 ns. As a result of the relatively long lifetime of ortho-positronium, monoenergetic energy-tunable beams of ortho-positronium

have been developed and the following elastic, inelastic and positronium ionization (fragmentation) collision processes have been studied:

$$\begin{aligned} \mathrm{Ps} + A_i &\rightarrow A_i + \mathrm{Ps} && \text{elastic scattering,} \\ &\rightarrow A_j + \mathrm{Ps} && \text{atomic excitation,} \\ &\rightarrow A_j^+ + \mathrm{e}^- + \mathrm{Ps} && \text{atomic ionization,} \\ &\rightarrow A_i + \mathrm{Ps}^* && \text{positronium excitation,} \\ &\rightarrow A_i + \mathrm{e}^- + \mathrm{e}^+ && \text{positronium ionization.} \end{aligned} \tag{7.2}$$

Returning to (7.1), we have also included the process where a positronium negative ion Ps^- is formed which can also occur in positronium collisions. Wheeler [962] showed that Ps could bind an electron to form a negative ion Ps^-, which is the analogue of H^-, and recent values of its binding energy and lifetime are 0.3267 eV and 0.477 ns, respectively [351]. Finally, we observe that the last process listed in (7.1), where the incident positron is annihilated with the emission of γ-rays, is sufficiently weak that it can be ignored in calculating cross sections for the previous positron collision processes listed in (7.1). However, the annihilation rate, which is proportional to the probability of finding the positron and an atomic electron at the same position in space, provides a further important test of the validity of the approximations made in collision theory and calculations.

We observe that the essential distinction between electron and positron collisions with atoms and ions is that in the former case the Pauli exclusion principle means that the wave function must be antisymmetrized with respect to the colliding electron and the target electrons, whereas in the latter case the strong attractive interaction between the positron and the target electrons causes the target atom to be strongly distorted at low incident energies. It follows that short-range correlation effects are more important in low-energy positron collisions than in low-energy electron collisions. As a result the additional complexity of using antisymmetrized wave functions in electron collisions is replaced by the greater importance of correlation effects in positron collisions. While these effects can be represented by including additional terms in the expansion of the collision wave function at energies below the positronium formation threshold, they are most appropriately represented by including positronium formation channels in the expansion of the collision wave function, even if results are only required for positron–atom collision channels.

We consider next the form of the Schrödinger equation which describes positron or positronium collisions with an atom or atomic ion with nuclear charge number Z. For light atomic targets, where relativistic effects can be neglected, we must solve the time-independent Schrödinger equation

$$H_{N+\mathrm{p}}\Psi = E\Psi, \tag{7.3}$$

where $H_{N+\mathrm{p}}$ is the non-relativistic Hamiltonian corresponding to a positron moving in the field of an N-electron atom or a positronium atom moving in the field of an $(N-1)$-electron ion. In order to determine explicit expressions for $H_{N+\mathrm{p}}$ and Ψ

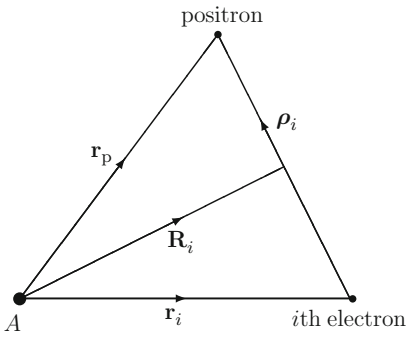

Fig. 7.1 Jacobi coordinates for positron–atom and positronium–ion collisions, where the ith target atom electron is captured to form positronium

in (7.3) we introduce a Jacobi system of coordinates illustrated in Fig. 7.1, where in this figure $\mathbf{r}_\mathrm{p}$ and $\mathbf{r}_i$ are the vector coordinates of the positron and the ith electron in the atom with respect to the atomic nucleus labelled A which is assumed to be infinitely heavy and which is chosen as the origin of coordinates. Also, $\boldsymbol{\rho}_i$ and $\mathbf{R}_i$ in Fig. 7.1 are defined by

$$\boldsymbol{\rho}_i = \mathbf{r}_\mathrm{p} - \mathbf{r}_i, \quad \mathbf{R}_i = \frac{1}{2}(\mathbf{r}_\mathrm{p} + \mathbf{r}_i). \tag{7.4}$$

We can write $H_{N+\mathrm{p}}$ in two distinct forms, the first corresponding to positron–atom collisions and the second corresponding to positronium–ion collisions. In the first form

$$H_{N+\mathrm{p}} = H_N - \frac{1}{2}\nabla_\mathrm{p}^2 + \frac{Z}{r_\mathrm{p}} - \sum_{i=1}^{N}\frac{1}{\rho_i}, \tag{7.5}$$

where H_N is the non-relativistic atomic Hamiltonian defined by (5.3) with $N+1$ replaced by N, $-\frac{1}{2}\nabla_\mathrm{p}^2$ is the positron kinetic energy operator and the remaining two terms on the right-hand side of (7.5) are the potential interaction of the positron with the atomic nucleus, with charge number Z, and with the N target electrons, respectively.

In the second form corresponding to positronium–ion collisions, one of the N target atom electrons is captured to form positronium. When the ith electron is captured, the Hamiltonian can be written as

$$H_{N+\mathrm{p}} = H_{N-i} + H_{\mathrm{p}i} - \frac{1}{4}\nabla_{R_i}^2 + V_{N-i\,\mathrm{p}i}. \tag{7.6}$$

In this equation, H_{N-i} is the residual $(N-1)$-electron ion Hamiltonian which is defined by

$$H_{N-i} = \sum_{\substack{j=1 \\ j\neq i}}^{N} \left(-\frac{1}{2}\nabla_j^2 - \frac{Z}{r_j} \right) + \sum_{\substack{j>j'=1 \\ j,j'\neq i}}^{N} \frac{1}{|\mathbf{r}_j - \mathbf{r}_{j'}|}, \tag{7.7}$$

$H_{\mathrm{p}i}$ is the positronium atom Hamiltonium, formed by the positron and the ith captured electron, which is defined by

$$H_{\mathrm{p}i} = \nabla_{\rho_i}^2 - \frac{1}{\rho_i}, \tag{7.8}$$

$-\frac{1}{4}\nabla_{R_i}^2$ is the positronium atom kinetic energy operator defined relative to the atomic nucleus and $V_{N-i\ \mathrm{p}i}$ is the potential interaction between the residual $(N-1)$-electron ion and the positronium atom, which is defined by

$$V_{N-i\ \mathrm{p}i} = -\frac{Z}{r_i} + \frac{Z}{r_\mathrm{p}} + \sum_{\substack{j=1 \\ j\neq i}}^{N} \frac{1}{|\mathbf{r}_j - \mathbf{r}_i|} - \sum_{\substack{j=1 \\ j\neq i}}^{N} \frac{1}{\rho_j}, \tag{7.9}$$

where in the above equations p refers to the positron and i to the ith electron captured by the positron to form the positronium atom. It follows from the indistinguishability of the N atomic electrons that the Hamiltonian defined by (7.6) is invariant with respect to interchange of any pair of the N electrons.

In order to solve (7.3) using multichannel R-matrix theory we partition configuration space into internal, external and asymptotic regions, as illustrated in Fig. 7.2, which we will see is analogous to the partitioning of configuration space in non-adiabatic electron–molecule collision theory shown in Fig. 11.4. The positron–atom complex in the internal region where all the particles are strongly interacting, defined by $0 \le r_\mathrm{p} \le a_0$ and $0 \le R_i \le A_0, i = 1, \ldots, N$, can dissociate into both positron–atom collision channels and positronium–ion collision channels. The radius a_0 is chosen so that the amplitudes of the target atom states of interest are negligible for $r_\mathrm{p} \ge a_0$ and the radius A_0 is chosen so that the amplitudes of the positronium atom and the target ion states of interest have negligible overlap for $R_i \ge A_0, i = 1, \ldots, N$. We discuss the solution in the internal region in Sect. 7.1.2. In the external region, corresponding to positron–atom collisions where $a_0 \le r_\mathrm{p} \le a_p$ and positronium–ion collisions where $A_0 \le R_N \le A_q$, the scattered positron and positronium atom move in the long-range multipole potentials of the residual atom or ion, where from symmetry we need to only consider the motion of the positronium atom formed by the positron and the Nth target atom electron. In this region the potential interaction between the scattered particles and the residual atom or ion is strong and must be treated by solving the resultant differential equations using accurate numerical propagation methods, as discussed in Sect. 7.1.3. Finally, in the asymptotic region where for positron–atom collisions $r_\mathrm{p} \ge a_p$ and for positronium–ion collisions $R_N \ge A_q$, the solutions can be obtained using asymptotic expansions in each of these regions which enable the K-matrix and S-matrix

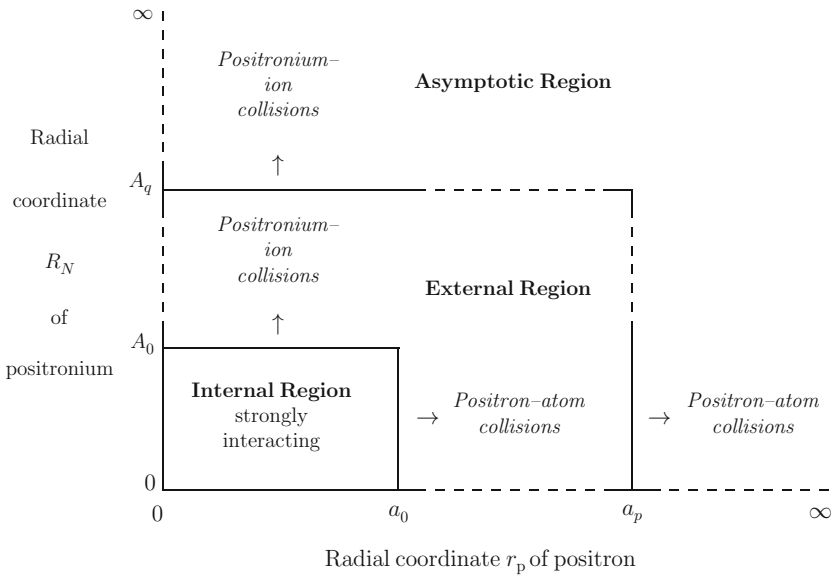

Fig. 7.2 Partitioning of configuration space in R-matrix theory of positron–atom and positronium–ion collisions, where the Nth target atom electron is captured to form positronium

to be determined, as discussed in Sect. 7.1.4. We now consider the solution in the internal, external and asymptotic regions in turn.

7.1.2 Internal Region Solution

We consider first the solution of the non-relativistic Schrödinger equation (7.3) in the internal region in Fig. 7.2 for each set of conserved quantum numbers Λ defined below. In analogy with expansions (5.5) and (5.6) adopted in electron–atom collisions we expand the positron–atom collision wave function as follows:

$$\Psi_{jE}^{\Lambda}(\mathbf{X}_N; \mathbf{x}_\mathrm{p}) = \sum_k \psi_k^{\Lambda}(\mathbf{X}_N; \mathbf{x}_\mathrm{p}) A_{kj}^{\Lambda}(E)\,. \tag{7.10}$$

In this equation

$$\mathbf{X}_N \equiv \mathbf{x}_1, \mathbf{x}_2, \ldots, \mathbf{x}_N\,, \tag{7.11}$$

where $\mathbf{x}_i \equiv \mathbf{r}_i\sigma_i$ represents the space and spin coordinates of the ith electron, $\mathbf{x}_\mathrm{p} \equiv \mathbf{r}_\mathrm{p}\sigma_\mathrm{p}$ represents the space and spin coordinates of the positron, j labels the linearly independent solutions of (7.3), ψ_k^{Λ} are energy-independent basis functions and $A_{kj}^{\Lambda}(E)$ are energy-dependent expansion coefficients which depend on the asymptotic boundary conditions satisfied by the wave function Ψ_{jE}^{Λ} at the energy E. Also

in (7.10), Λ represents the conserved quantum numbers in the collision defined by

$$\Lambda \equiv \alpha\ L\ S\ M_L\ M_S\ m_{\rm p}\ \pi, \tag{7.12}$$

where L and M_L are the total orbital angular momentum quantum numbers of the positron–atom and positronium–ion collision processes, S and M_S are the total electron spin angular momentum quantum numbers of the target atom and $m_{\rm p}$ is the spin magnetic quantum number of the positron, which are separately conserved, π is the total parity and α represents any further quantum numbers which are conserved in the collision. Unlike the conserved quantum numbers Γ in electron–atom collisions, defined by (2.58), we have not coupled the spin of the positron to that of the target atom since the positron is distinguishable from the target electrons and hence, in the absence of relativistic spin–orbit interactions, M_S and $m_{\rm p}$ are separately conserved in the positron–atom collision. It follows that the collision wave function Ψ_{jE}^{Λ} and the basis functions ψ_k^{Λ} in (7.10) are antisymmetric with respect to interchange of any pair of the space and spin coordinates $\mathbf{x}_i \equiv \mathbf{r}_i\sigma_i,\ i = 1, \ldots, N$, of the target electrons, but are not antisymmetrized with respect to interchange of the space and spin coordinates $\mathbf{x}_{\rm p} \equiv \mathbf{r}_{\rm p}\sigma_{\rm p}$ of the positron with those of the target electrons.

We now expand the basis functions ψ_k^{Λ} in (7.10) in the form

$$\begin{aligned}\psi_k^{\Lambda}(\mathbf{X}_N; \mathbf{x}_{\rm p}) = &\sum_{i=1}^{n}\sum_{j=1}^{n_c} \overline{\Phi}_i^{\Lambda}(\mathbf{X}_N; \hat{\mathbf{r}}_{\rm p}\sigma_{\rm p}) r^{-1} u_{ij}^0(r_{\rm p}) a_{ijk}^{\Lambda} \\ &+ \mathcal{A}_N \sum_{i=1}^{m}\sum_{j=1}^{m_c} \overline{\Theta}_i^{\Lambda}(\mathbf{X}_{N-1}; \boldsymbol{\rho}_N\sigma_N\sigma_{\rm p}; \hat{\mathbf{R}}_N) \\ &\times R_N^{-1} v_{ij}^0(R_N) b_{ijk}^{\Lambda} \\ &+ \sum_{i=1}^{b} \chi_i^{\Lambda}(\mathbf{X}_N; \mathbf{x}_{\rm p}) c_{ik}^{\Lambda}, \quad k = 1, \ldots, n_t, \end{aligned} \tag{7.13}$$

where $n_t = nn_c + mm_c + b$ is the number of linearly independent basis functions included in these expansions. The first expansion on the right-hand side of (7.13) corresponds to positron–atom collisions, the second expansion corresponds to positronium–ion collisions, where the Nth electron is captured to form positronium leaving the remaining $N - 1$ electrons in the residual ion and the third expansion is over quadratically integrable functions which are included for completeness and to represent correlation effects. Also in (7.13), $\overline{\Phi}_i^{\Lambda}$ and u_{ij}^0 are the channel functions and radial continuum basis orbitals corresponding to positron–atom collisions and $\overline{\Theta}_i^{\Lambda}$ and v_{ij}^0 are the channel functions and radial continuum basis orbitals corresponding to positronium–ion collisions, which are discussed below. Finally, in (7.13) $\mathcal{A}_N$ is the antisymmetrization operator which ensures that each term in the second expansion is antisymmetric with respect to interchange of the space and spin

coordinates of any pair of the N electrons taking part in the collision. In analogy with (2.46) $\mathcal{A}_N$ is defined by

$$\mathcal{A}_N = N^{-1/2}\left(1 - \sum_{i=1}^{N-1} P_{iN}\right), \tag{7.14}$$

where P_{iN} is the operator which interchanges the space and spin coordinates of electrons labelled i and N.

We observe that the expansions over the channel functions $\overline{\Phi}_i^{\Lambda}$ and $\overline{\Theta}_i^{\Lambda}$ in (7.13) may both include pseudostates representing the continuum in positron–atom collisions and positronium–ion collisions, respectively. We have seen in Chaps. 2, 5 and 6 that the inclusion of pseudostates is required both to accurately represent the polarizability of the target by the incident particle at low energies and to allow for ionization at intermediate energies. As a result, in principle, the two expansions span the same configuration space, which could lead to instability in the solution if close to complete sets of target basis functions are included in each expansion. However, in practical calculations both expansions are truncated to a finite number of basis functions and hence any difficulty due to over completeness usually does not arise. Retaining both expansions together with the expansion over quadratically integrable functions χ_i^{Λ} in (7.13) then gives faster convergence and enables positron collision and positronium formation cross sections to be defined and accurately calculated at low and intermediate energies.

The channel functions $\overline{\Phi}_i^{\Lambda}$ in (7.13) corresponding to positron–atom collisions are constructed by coupling the orbital angular momentum of the antisymmetrized N-electron target atom wave functions Φ_i^N with the orbital angular momentum of the scattered positron as follows:

$$\overline{\Phi}_i^{\Lambda}(\mathbf{X}_N; \hat{\mathbf{r}}_{\rm p}\sigma_{\rm p}) = \sum_{M_i m_i} (L_i M_i \ell_i m_i | L M_L) \Phi_i^N(\mathbf{X}_N) Y_{\ell_i m_i}(\theta_{\rm p}, \phi_{\rm p}) \chi_{\frac{1}{2} m_{\rm p}}(\sigma_{\rm p}),$$
$$i = 1, \ldots, n, \tag{7.15}$$

where the boundary radius a_0 of the internal region in Fig. 7.2 is chosen so that the target atom wave functions $\Phi_i^N(\mathbf{X}_N)$ are negligible for $r_i \geq a_0,\ i = 1, \ldots, N$.

The channel functions $\overline{\Theta}_i^{\Lambda}$ in (7.13) corresponding to positronium–ion collisions are constructed by coupling the orbital and spin angular momenta of the antisymmetrized residual atomic ion wave function $\Phi_i^{N-1}(\mathbf{X}_{N-1})$ with the orbital and spin angular momenta of the positronium atom wave function, where we assume that the Nth atomic electron and the positron form the positronium atom. We now introduce the following wave function describing the positron and the Nth atomic electron:

$$\xi_i(\boldsymbol{\rho}_N; \sigma_N \sigma_{\rm p}) = \phi_i(\boldsymbol{\rho}_N) \chi_{\frac{1}{2} m_N}(\sigma_N) \chi_{\frac{1}{2} m_p}(\sigma_{\rm p}), \tag{7.16}$$

where $\phi_i(\boldsymbol{\rho}_N)$ is the space part of the positronium atom wave function, $\chi_{\frac{1}{2}m_N}(\sigma_N)$ is the Nth atomic electron spin function and $\chi_{\frac{1}{2}m_p}(\sigma_\mathrm{p})$ is the positron spin function. Using (A.20), we can rewrite (7.16) as a linear combination of singlet and triplet positronium atom spin functions $\chi_{s_i m_s}(\sigma_N\sigma_\mathrm{p})$ as follows:

$$\xi_i(\boldsymbol{\rho}_N;\sigma_N\sigma_\mathrm{p}) = \sum_{s_i}\left(\tfrac{1}{2}m_N\tfrac{1}{2}m_p|s_i m_s\right)\phi_i(\boldsymbol{\rho}_N)\chi_{s_i m_s}(\sigma_N\sigma_\mathrm{p}), \tag{7.17}$$

where the Clebsch–Gordan coefficients in this equation are defined in Sect. A.1. The channel functions $\overline{\Theta}_i^{\Lambda}$ in (7.13) are then defined by

$$\begin{aligned}
&\overline{\Theta}_i^{\Lambda}(\mathbf{X}_{N-1};\boldsymbol{\rho}_N\sigma_N\sigma_\mathrm{p};\hat{\mathbf{R}}_N)\\
&= \sum_{M'_L m'_\ell}\sum_{M_K m_j}\sum_{M'_S m_S}(L'_i M'_L \ell'_i m'_\ell|K_i M_K)(K_i M_K j_i m_j|L M_L)\\
&\quad\times(S'_i M'_S s_i m_s|S M_S)\Phi_i^{N-1}(\mathbf{X}_{N-1})\phi_i(\boldsymbol{\rho}_N)\\
&\quad\times\chi_{s_i m_s}(\sigma_N\sigma_\mathrm{p})Y_{j_i m_j}(\theta_N,\phi_N),\quad i=1,\ldots,m,
\end{aligned}\tag{7.18}$$

where the boundary radius A_0 of the internal region in Fig. 7.2 is chosen so that the overlap of the residual atomic ion wave functions $\Phi_i^{N-1}(\mathbf{X}_{N-1})$ and the positronium wave function $\phi_i(\boldsymbol{\rho}_N)$ is negligible for $R_N \geq A_0$.

The angular momentum coupling scheme that we have adopted in (7.18), in defining the channel functions $\overline{\Theta}_i^{\Lambda}$ in (7.13), is summarized in Fig. 7.3. The orbital and spin angular momentum quantum numbers of the residual atomic ion are L'_i, M'_L, S'_i, M'_S, the orbital angular momentum quantum numbers of the positronium atom are ℓ'_i, m'_ℓ and the spin magnetic quantum numbers of the captured Nth electron and the positron are m_N and m_p, respectively. Then K_i and M_K are intermediate angular momentum quantum numbers obtained by coupling the orbital angular momenta of the residual ion denoted by L'_i and M'_L with the orbital angular

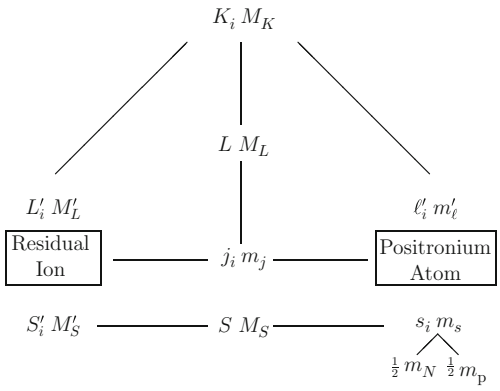

Fig. 7.3 Positronium–ion orbital and spin angular momentum coupling scheme defining the positronium wave function ξ_i in (7.17) and the channel functions $\overline{\Theta}_i^{\Lambda}$ in (7.18)

momenta of the positronium atom denoted by ℓ_i' and m_ℓ', j_i and m_j are the orbital angular momentum quantum numbers describing the orbital motion of the positronium atom relative to the residual ion and L and M_L are the total conserved orbital angular momentum quantum numbers of the positronium atom and the residual ion. Also S and M_S are the total conserved electron spin angular momentum quantum numbers of the positronium atom and the residual ion obtained by coupling the electron spin angular momentum of the residual ion denoted by S_i' and M_S' with the spin angular momentum of the positronium atom denoted by s_i and m_s. We also remember from (7.16) and (7.17) that electron and positron spins are coupled to yield the positronium atom spin quantum numbers s_i and m_s. Finally, we observe that the total parity π in (7.12), defined by

$$\pi = \pi_i(-1)^{\ell_i} = \pi_i'(-1)^{\ell_i'+j_i}, \tag{7.19}$$

is conserved in the collision where π_i is the parity of the N-electron target atom and π_i' is the parity of the residual atomic ion.

The zero-order radial continuum basis orbitals $u_{ij}^0(r_\mathrm{p})$ and $v_{ij}^0(R_N)$ in (7.13) are defined over the ranges $0 \le r_\mathrm{p} \le a_0$ and $0 \le R_N \le A_0$, respectively, in the internal region defined in Fig. 7.2. In practice the continuum basis orbitals can be calculated using a homogeneous boundary condition method similar to that described in Sect. 5.3.1 for electron–atom collisions (e.g. [531]). However, since the positron is distinguishable from the electrons in the target atom or residual ion, the Lagrange orthogonalization procedure adopted for electron–atom collisions is not required. Hence, the continuum basis orbitals in (7.13) can be obtained by solving equations analogous to (5.75) with the right-hand side set zero. In the case of $u_{ij}^0(r_\mathrm{p})$, corresponding to the positron–atom collision channels, the potential $U_0(r)$ in (5.75) can be taken to be the repulsive static potential of the target atom ground state. In the case of $v_{ij}^0(R_N)$, corresponding to the positronium–ion collision channels, the potential $U_0(r)$ in (5.75) can be taken to be zero. This is justified for positron collisions with alkali metal atoms since the diagonal elements of the potential corresponding to positronium collisions with the resultant closed-shell ion are zero.

The final step in the definition of the quantities in (7.13) is to determine the coefficients a_{ijk}^Λ, b_{ijk}^Λ and c_{ik}^Λ. This is achieved by diagonalizing the operator $H_{N+\mathrm{p}}+\mathcal{L}_r+\mathcal{L}_R$ in the basis ψ_k^Λ defined by (7.13) where the integral is taken over the internal region in Fig. 7.2 as follows:

$$\langle\psi_k^\Lambda|H_{N+\mathrm{p}}+\mathcal{L}_r+\mathcal{L}_R|\psi_{k'}^\Lambda\rangle_\mathrm{int} = E_k^\Lambda\delta_{kk'}, \quad k,\ k' = 1,\ldots,n_t. \tag{7.20}$$

In this equation we have introduced the Bloch operator for positron–atom collision channels in (7.13) defined by

$$\mathcal{L}_r = \frac{1}{2}\delta(r_\mathrm{p}-a_0)\left(\frac{\mathrm{d}}{\mathrm{d}r_\mathrm{p}} - \frac{b_0-1}{r_\mathrm{p}}\right), \tag{7.21}$$

which corresponds to the form of the Hamiltonian defined by (7.5), and the Bloch operator for positronium–ion collision channels in (7.13) defined by

$$\mathcal{L}_R = \frac{1}{4}\sum_{i=1}^{N}\delta(R_i - A_0)\left(\frac{\mathrm{d}}{\mathrm{d}R_i} - \frac{B_0 - 1}{R_i}\right), \tag{7.22}$$

which corresponds to the form of the Hamiltonian defined by (7.6), where b_0 in (7.21) and B_0 in (7.22) are arbitrary constants. It follows that $H_{N+\mathrm{p}} + \mathcal{L}_r + \mathcal{L}_R$ is hermitian in the basis of quadratically integrable functions (7.13), satisfying arbitrary boundary conditions on the surface of the internal region in Fig. 7.2 where $r_\mathrm{p} = a_0$ and $R_i = A_0,\ i = 1, \ldots, N$.

The solution of (7.3) in the internal region for each set of conserved quantum numbers Λ defined by (7.12) can be obtained by rewriting (7.3) as follows:

$$(H_{N+\mathrm{p}} + \mathcal{L}_r + \mathcal{L}_R - E)\Psi^\Lambda = (\mathcal{L}_r + \mathcal{L}_R)\Psi^\Lambda, \tag{7.23}$$

which has the formal solution

$$\Psi^\Lambda = (H_{N+\mathrm{p}} + \mathcal{L}_r + \mathcal{L}_R - E)^{-1}(\mathcal{L}_r + \mathcal{L}_R)\Psi^\Lambda. \tag{7.24}$$

The spectral representation of the Green's function in this equation can be written in terms of the basis functions ψ_k^Λ defined by (7.13) and (7.20). We obtain

$$|\Psi^\Lambda\rangle = \sum_{k=1}^{n_t}|\psi_k^\Lambda\rangle\frac{1}{E_k^\Lambda - E}\langle\psi_k^\Lambda|\mathcal{L}_r + \mathcal{L}_R|\Psi^\Lambda\rangle. \tag{7.25}$$

We then project (7.25) onto the n channel functions $\overline{\Phi}_i^\Lambda,\ i = 1, \ldots, n$, defined by (7.15) and evaluate it on the boundary $r_\mathrm{p} = a_0$ and project (7.25) onto the m channel functions $\overline{\Theta}_i^\Lambda,\ i = 1, \ldots, m$, defined by (7.18) and evaluate it on the boundary $R_N = A_0$. We obtain, after using (7.21) and (7.22)

$$\begin{aligned} F_i^\Lambda(a_0) = &\sum_{j=1}^{n} R_{ij}^\Lambda(E)\left(a_0\frac{\mathrm{d}F_j^\Lambda}{\mathrm{d}r_\mathrm{p}} - b_0 F_j^\Lambda\right)_{r_\mathrm{p}=a_0} \\ &+\sum_{j=1}^{m} R_{ij+n}^\Lambda(E)\left(A_0\frac{\mathrm{d}G_j^\Lambda}{\mathrm{d}R_N} - B_0 G_j^\Lambda\right)_{R_N=A_0},\ i = 1, \ldots, n \end{aligned} \tag{7.26}$$

and

$$G_i^{\Lambda}(A_0) = \sum_{j=1}^{n} R_{i+n\ j}^{\Lambda}(E) \left(a_0 \frac{\mathrm{d}F_j^{\Lambda}}{\mathrm{d}r_\mathrm{p}} - b_0 F_j^{\Lambda} \right)_{r_\mathrm{p}=a_0}$$

$$+ \sum_{j=1}^{m} R_{i+n\ j+n}^{\Lambda}(E) \left(A_0 \frac{\mathrm{d}G_j^{\Lambda}}{\mathrm{d}R_N} - B_0 G_j^{\Lambda} \right)_{R_N=A_0}, \quad i = 1, \ldots, m\,. \tag{7.27}$$

In (7.26) and (7.27), the reduced radial functions $F_i^{\Lambda}(r_\mathrm{p})$, which correspond to positron–atom collisions, are obtained by projecting the total wave function Ψ^{Λ} onto the channel functions $\overline{\Phi}_i^{\Lambda}$ defined by (7.15) as follows:

$$F_i^{\Lambda}(r_\mathrm{p}) = \langle r_\mathrm{p}^{-1} \overline{\Phi}_i^{\Lambda} | \Psi^{\Lambda} \rangle', \quad i = 1, \ldots, n, \tag{7.28}$$

and the reduced radial functions $G_i^{\Lambda}(R_N)$, which correspond to positronium–ion collisions, are obtained by projecting the total wave function Ψ^{Λ} onto the channel functions $\overline{\Theta}_i^{\Lambda}$ defined by (7.18) as follows:

$$G_i^{\Lambda}(R_N) = \langle R_N^{-1} \overline{\Theta}_i^{\Lambda} | \Psi^{\Lambda} \rangle', \quad i = 1, \ldots, m. \tag{7.29}$$

The R-matrices in (7.26) and (7.27) are then combined into a generalized R-matrix defined by

$$R_{ij}^{\Lambda}(E) = \frac{1}{2a_0} \sum_{k=1}^{n_t} \frac{w_{ik}^{\Lambda} w_{jk}^{\Lambda}}{E_k^{\Lambda} - E}, \quad i = 1, \ldots, n+m, \quad j = 1, \ldots, n \tag{7.30}$$

and

$$R_{ij}^{\Lambda}(E) = \frac{1}{4A_0} \sum_{k=1}^{n_t} \frac{w_{ik}^{\Lambda} w_{jk}^{\Lambda}}{E_k^{\Lambda} - E}, \quad i = 1, \ldots, n+m, \quad j = n+1, \ldots, n+m\,, \tag{7.31}$$

where the surface amplitudes in these equations are defined by

$$w_{ik}^{\Lambda} = \langle r_\mathrm{p}^{-1} \overline{\Phi}_i^{\Lambda} | \psi_k^{\Lambda} \rangle'_{r_\mathrm{p}=a_0}$$

$$= \sum_{j=1}^{n_t} u_{ij}^{0}(a_0) a_{ijk}^{\Lambda}, \quad i = 1, \ldots, n, \quad k = 1, \ldots, n_t \tag{7.32}$$

and

$$w^{\Lambda}_{i+n\,k} = \langle R_N^{-1}\,\overline{\Theta}^{\Lambda}_i | \psi^{\Lambda}_k \rangle'_{R_N=A_0}$$
$$= \sum_{j=1}^{m_c} v^0_{ij}(A_0) b^{\Lambda}_{ijk}, \quad i = 1, \ldots, m, \quad k = 1, \ldots, n_t, \tag{7.33}$$

which follow from (7.13). The primes on the Dirac brackets in the above equations mean that the integrations are carried out over all coordinates except the radial coordinate $r_{\rm p}$ in (7.28) and (7.32) and except the radial coordinate R_N in (7.29) and (7.33).

Equations (7.26) and (7.27) are the basic equations which result from the solution of the Schrödinger equation (7.3) describing positron–atom collisions and positronium–ion collisions in the internal region. The R-matrix defined by (7.30) and (7.31) is determined at all energies by diagonalizing $H_{N+{\rm p}} + \mathcal{L}_r + \mathcal{L}_R$ in the basis defined by (7.13) to yield the eigenenergies E^{Λ}_k in (7.20) for each set of conserved quantum numbers Λ. If the zero-order radial continuum basis orbitals $u^0_{ij}(r_{\rm p})$ and $v^0_{ij}(R_N)$ in (7.13) are calculated using the homogeneous boundary condition method then a Buttle correction to the diagonal elements of the R-matrix must be applied as described in Sect. 5.3.2. Having determined the R-matrix, (7.26) and (7.27) then provide the boundary conditions satisfied by the solution of the equations describing positron–atom collisions and positronium–ion collisions in the external region described in the next section.

7.1.3 External Region Solution

The external region, defined in Fig. 7.2, is divided into two sub-regions corresponding to positron–atom collision channels and positronium–ion collision channels. We assume that the corresponding radii a_0 and A_0 are chosen large enough so that for the channels of interest the corresponding wave functions in these two external sub-regions have negligible overlap and can therefore be treated independently.

In the external sub-region corresponding to positron–atom collisions, we expand the total wave function in terms of channel functions $\overline{\Phi}^{\Lambda}_i$ defined by (7.15) as follows:

$$\Psi^{\Lambda}_{jE}(\mathbf{X}_N; \mathbf{r}_{\rm p}\sigma_{\rm p}) = \sum_{i=1}^{n} \overline{\Phi}^{\Lambda}_i(\mathbf{X}_N; \hat{\mathbf{r}}_{\rm p}\sigma_{\rm p}) r_{\rm p}^{-1} F^{\Lambda}_{ij}(r_{\rm p})\,, \tag{7.34}$$

where j labels the linearly independent solutions. We then substitute this expansion into the Schrödinger equation (7.3), where the Hamiltonian $H_{N+{\rm p}}$ is defined by (7.5), and project this equation onto the channel functions $\overline{\Phi}^{\Lambda}_i$. We then find that

the reduced radial functions $F_{ij}^{\Lambda}(r_\mathrm{p})$ in (7.34) satisfy the following set of coupled second-order differential equations:

$$\left(\frac{\mathrm{d}^2}{\mathrm{d}r_\mathrm{p}^2} - \frac{\ell_i(\ell_i+1)}{r_\mathrm{p}^2} - \frac{2(Z-N)}{r_\mathrm{p}} + k_i^2\right) F_{ij}^{\Lambda}(r_\mathrm{p}) = 2\sum_{i'=1}^{n} V_{ii'}^{\Lambda}(r_\mathrm{p}) F_{i'j}^{\Lambda}(r_\mathrm{p}),$$
$$i = 1, \ldots, n, \;\; r_\mathrm{p} \geq a_0, \quad (7.35)$$

where ℓ_i is the orbital angular momentum of the scattered positron, Z is the nuclear charge number, N is the number of target electrons and k_i^2 is the square of the wave number of the scattered positron defined by

$$k_i^2 = 2\left(E - \bar{e}_i^{\Lambda}\right), \quad i = 1, \ldots, n, \quad (7.36)$$

where

$$\bar{e}_i^{\Lambda} = \langle r_\mathrm{p}^{-1}\overline{\Phi}_i^{\Lambda}(\mathbf{X}_N; \hat{\mathbf{r}}_\mathrm{p}\sigma_\mathrm{p}) | H_N | r_\mathrm{p}^{-1}\overline{\Phi}_i^{\Lambda}(\mathbf{X}_N; \hat{\mathbf{r}}_\mathrm{p}\sigma_\mathrm{p})\rangle, \quad i = 1, \ldots, n. \quad (7.37)$$

Finally in (7.35), $V_{ii'}^{\Lambda}(r_\mathrm{p})$ is the potential matrix defined in analogy with (2.66) by

$$V_{ii'}^{\Lambda}(r_\mathrm{p}) = \langle r_\mathrm{p}^{-1}\overline{\Phi}_i^{\Lambda}(\mathbf{X}_N; \hat{\mathbf{r}}_\mathrm{p}\sigma_\mathrm{p}) \left| -\sum_{k=1}^{N}\frac{1}{\rho_k} + \frac{N}{r_\mathrm{p}} \right| r_\mathrm{p}^{-1}\overline{\Phi}_{i'}^{\Lambda}(\mathbf{X}_N; \hat{\mathbf{r}}_\mathrm{p}\sigma_\mathrm{p})\rangle',$$
$$i, \; i' = 1, \ldots, n. \quad (7.38)$$

We see that (7.35) has the same general form as the coupled second-order differential equations (5.29) describing electron–atom collisions in the external region. This is because the electron exchange terms in electron–atom collisions are confined to the internal region and hence the potential in (5.29) only describes the long-range interaction between the electron and the atom. The differences between (7.35) and (5.29) then arise because the positron has positive charge and the electron negative charge. This results in the change in sign in the long-range Coulomb potential $-2(Z-N)/r_\mathrm{p}$ and in the sign of the potential matrix $V_{ii'}^{\Lambda}(r_\mathrm{p})$. It follows that

$$V_{ii'}^{\Lambda}(r_\mathrm{p}) = -V_{ii'}^{\Gamma}(r), \quad r_\mathrm{p} = r, \quad i, \; i' = 1, \ldots, n, \quad (7.39)$$

where in the external region the conserved quantum numbers in positron–atom collisions represented by Λ are the same as the conserved quantum numbers in electron–atom collisions represented by Γ. Hence we find that the potential matrix $V_{ii'}^{\Lambda}(r_\mathrm{p})$ in (7.35) can be written as a summation over inverse powers of r_p where the coefficients in the expansion have the opposite sign to those given in (5.30).

In the external sub-region in Fig. 7.2 corresponding to positronium–ion collisions, we expand the total wave function in terms of channel functions $\overline{\Theta}_i^{\Lambda}$ defined by (7.18) as follows:

$$\Psi_{jE}^{\Lambda}(\mathbf{X}_{N-1};\boldsymbol{\rho}_N\sigma_N\sigma_{\rm p};\mathbf{R}_N)=\sum_{i=1}^{m}\overline{\Theta}_i^{\Lambda}(\mathbf{X}_{N-1};\boldsymbol{\rho}_N\sigma_N\sigma_{\rm p};\hat{\mathbf{R}}_N)R_N^{-1}G_{ij}^{\Lambda}(R_N), \tag{7.40}$$

where j, which has the same meaning as in (7.34), labels the linearly independent solutions. We then substitute this expansion into the Schrödinger equation (7.3), where the Hamiltonian $H_{N+{\rm p}}$ is now defined by (7.6) and where, as in Fig. 7.2, we assume that the Nth target atom electron has been captured to form positronium. After projecting (7.3) onto the channel functions $\overline{\Theta}_i^{\Lambda}$ we then find that the reduced radial functions $G_{ij}^{\Lambda}(\mathbf{R}_N)$ in (7.40) satisfy the following coupled second-order differential equations:

$$\left(\frac{{\rm d}^2}{{\rm d}R_N^2}-\frac{j_i(j_i+1)}{R_N^2}+K_i^2\right)G_{ij}^{\Lambda}(R_N)=4\sum_{i'=1}^{m}U_{ii'}^{\Lambda}(R_N)G_{i'j}^{\Lambda}(R_N),$$
$$i=1,\ldots,m,\ \ R_N\geq A_0\,. \tag{7.41}$$

In this equation j_i, defined in Fig. 7.3, is the angular momentum quantum number in the ith channel corresponding to the orbital motion of the positronium atom relative to the residual ion. Also in (7.41) K_i^2 is the square of the wave number K_i of the positronium atom in the ith channel defined by

$$K_i^2=4\left[E-(E_{N-1})_i-(E_{{\rm p}N})_i\right], \tag{7.42}$$

where $(E_{N-1})_i$ is the energy of the residual $(N-1)$-electron ion in the ith channel defined by

$$(E_{N-1})_i=\langle\Phi_i^{N-1}(\mathbf{X}_{N-1})|H_{N-1}|\Phi_i^{N-1}(\mathbf{X}_{N-1})\rangle,\quad i=1,\ldots,m\,, \tag{7.43}$$

and $(E_{{\rm p}N})_i$ is the energy of the positronium atom in the ith channel defined by

$$(E_{{\rm p}N})_i=\langle\phi_i(\boldsymbol{\rho}_N)\chi_{s_im_s}(\sigma_N\sigma_{\rm p})|H_{{\rm p}N}|\phi_i(\boldsymbol{\rho}_N)\chi_{s_im_s}(\sigma_N\sigma_{\rm p})\rangle,\quad i=1,\ldots,m\,, \tag{7.44}$$

where H_{N-1} and $H_{{\rm p}N}$ are defined by (7.7) and (7.8), respectively, with i replaced by N. Finally in (7.41), $U_{ii'}^{\Lambda}(R_N)$ is the potential matrix defined by

$$U_{ii'}^{\Lambda}(R_N)=\langle R_N^{-1}\overline{\Theta}_i^{\Lambda}(\mathbf{X}_{N-1};\boldsymbol{\rho}_N\sigma_N\sigma_{\rm p};\hat{\mathbf{R}}_N)|V_{N-1\,{\rm p}N}|$$
$$\times R_N^{-1}\overline{\Theta}_{i'}^{\Lambda}(\mathbf{X}_{N-1};\boldsymbol{\rho}_N\sigma_N\sigma_{\rm p};\hat{\mathbf{R}}_N)\rangle,\quad i,\ i'=1,\ldots,m, \tag{7.45}$$

where $V_{N-1\,{\rm p}N}$ is the potential interaction between the residual ion and the positronium atom defined by (7.9), with i replaced by N.

Having determined the coupled second-order differential equations (7.35) and (7.41), satisfied by the functions $F_{ij}^{\Lambda}(r_{\rm p})$ and $G_{ij}^{\Lambda}(R_N)$, respectively, the generalized $(n+m)\times(n+m)$-dimensional R-matrix $\mathbf{R}^{\Lambda}$ defined by (7.30) and (7.31) can then be propagated outwards from the boundaries $r_{\rm p}=a_0$ and $R_N=A_0$ to the outer boundaries $r_{\rm p}=a_p$ and $R_N=A_q$ in Fig. 7.2 using the procedure described in Appendix E.6. The R-matrix at the outer boundaries then provides the boundary condition for the solution in the asymptotic region, discussed in Sect. 7.1.4.

7.1.4 Asymptotic Region Solution

The solution of (7.3) in the asymptotic region, where $r_{\rm p}\geq a_p$ and $R_N\geq A_q$ in Fig. 7.2, proceeds using an extension of the method adopted in the asymptotic region in electron–atom collisions, discussed in Sect. 5.1.4. First, we assume that we have chosen the radii a_p and A_q in Fig. 7.2 large enough that the asymptotic expansion methods discussed in Appendix F.1 can be used to obtain accurate linearly independent solutions of (7.35) when $r_{\rm p}\geq a_p$ and of (7.41) when $R_N\geq A_q$. Following our discussion in Sect. 5.1.4, we then assume that the n positron–atom collision channels corresponding to (7.35), which we distinguish by a bar, are ordered so that

$$\overline{k}_1^2\geq\overline{k}_2^2\geq\cdots\geq\overline{k}_n^2, \tag{7.46}$$

where at the energy E of interest the first n_a channels are open with $\overline{k}_i^2\geq 0$ and the last n_b channels are closed with $\overline{k}_i^2<0$, where $n_a+n_b=n$. We then determine $n+n_a$ linearly independent asymptotic solutions of (7.35), which are regular as $r_{\rm p}\rightarrow\infty$ and which satisfy the following asymptotic boundary conditions:

$$\begin{aligned}
&\overline{s}_{ij}(r_{\rm p})\underset{r_{\rm p}\rightarrow\infty}{\sim}\overline{k}_i^{-1/2}\sin\overline{\theta}_i\delta_{ij},\quad i=1,\ldots,n,\quad j=1,\ldots,n_a,\\
&\overline{c}_{ij}(r_{\rm p})\underset{r_{\rm p}\rightarrow\infty}{\sim}\overline{k}_i^{-1/2}\cos\overline{\theta}_i\delta_{ij},\quad i=1,\ldots,n,\quad j=1,\ldots,n_a,\\
&\overline{c}_{ij}(r_{\rm p})\underset{r_{\rm p}\rightarrow\infty}{\sim}\exp(-\overline{\phi}_i)\delta_{ij},\quad i=1,\ldots,n,\quad j=n_a+1,\ldots,n,
\end{aligned} \tag{7.47}$$

where $\overline{\theta}_i$ and $\overline{\phi}_i$ are defined by equations analogous to (5.38), (5.39), (5.40) and (5.41). Also, we assume that the m positronium–ion collision channels corresponding to (7.41), which we distinguish by a tilde, are ordered so that

$$\widetilde{k}_1^2\geq\widetilde{k}_2^2\geq\cdots\geq\widetilde{k}_m^2, \tag{7.48}$$

where at the energy E of interest the first m_a channels are open with $\widetilde{k}_i^2\geq 0$ and the last m_b channels are closed with $\widetilde{k}_i^2<0$, where $m_a+m_b=m$. We then determine

$m + m_a$ linearly independent asymptotic solutions of (7.41), which are regular as $R_N \to \infty$ and which satisfy the following asymptotic boundary conditions:

$$\begin{aligned}
\widetilde{s}_{ij}(R_N) &\underset{R_N\to\infty}{\sim} \widetilde{k}_i^{-1/2} \sin\widetilde{\theta}_i \delta_{ij}, \quad i = 1,\ldots,m, \quad j = 1,\ldots,m_a,\\
\widetilde{c}_{ij}(R_N) &\underset{R_N\to\infty}{\sim} \widetilde{k}_i^{-1/2} \cos\widetilde{\theta}_i \delta_{ij}, \quad i = 1,\ldots,m, \quad j = 1,\ldots,m_a,\\
\widetilde{c}_{ij}(R_N) &\underset{R_N\to\infty}{\sim} \exp(-\widetilde{\phi}_i)\delta_{ij}, \quad i = 1,\ldots,m, \quad j = m_a+1,\ldots,m\,, \qquad (7.49)
\end{aligned}$$

where $\widetilde{\theta}_i$ and $\widetilde{\phi}_i$ are also defined by equations analogous to (5.38), (5.39), (5.40) and (5.41).

We observe that at an energy E where n_a channels of (7.35) and m_a channels of (7.41) are open, we can determine $n_a + m_a$ linearly independent physical solutions of the combined internal and external region equations which vanish at the origin and which are finite at infinity. In analogy with (5.42), these solutions can be written in terms of the $n + n_a$ asymptotic solutions defined by (7.47) and the $m + m_a$ asymptotic solutions defined by (7.49) as follows

$$\boldsymbol{\mathcal{F}}^{\Lambda}(\rho) = \mathbf{s}(\rho) + \mathbf{c}(\rho)\mathbf{N}^{\Lambda}, \quad r_{\mathrm{p}} \geq a_p, \quad R_N \geq A_q, \qquad (7.50)$$

where we have written $\mathbf{s}(\rho)$ to represent $\overline{\mathbf{s}}(r)$ or $\widetilde{\mathbf{s}}(R_N)$ and $\mathbf{c}(\rho)$ to represent $\overline{\mathbf{c}}(r)$ or $\widetilde{\mathbf{c}}(R_N)$ and where the variable ρ represents r_{p} in the channels corresponding to (7.35) and R_N in the channels corresponding to (7.41). It follows that in (7.50)

$$\begin{aligned}
\boldsymbol{\mathcal{F}}^{\Lambda}(\rho) &\text{ has dimension } (n+m)\times(n_a+m_a),\\
\mathbf{s}(\rho) &\text{ has dimension } (n+m)\times(n_a+m_a),\\
\mathbf{c}(\rho) &\text{ has dimension } (n+m)\times(n+m),\\
\mathbf{N}^{\Lambda} &\text{ has dimension } (n+m)\times(n_a+m_a). \qquad (7.51)
\end{aligned}$$

Also, so that the ordering of open and closed channels in (7.50) is the same as in (5.42), we have re-ordered the channels in (7.50) so that the first $n_a + m_a$ channels are open and the last $n_b + m_b$ channels are closed. Hence the ordering of open and closed channels in (7.50) is as follows:

$$\begin{aligned}
\text{channels } 1 \text{ to } n_a &\equiv n_a \text{ open channels in (7.35)},\\
\text{channels } n_a+1 \text{ to } n_a+m_a &\equiv m_a \text{ open channels in (7.41)},\\
\text{channels } n_a+m_a+1 \text{ to } n+m_a &\equiv n_b \text{ closed channels in (7.35)},\\
\text{channels } n+m_a+1 \text{ to } n+m &\equiv m_b \text{ closed channels in (7.41)}. \qquad (7.52)
\end{aligned}$$

In analogy with (5.43), the matrix $\mathbf{N}^{\Lambda}$ in (7.50) can then be rewritten in the form

$$\mathbf{N}^{\Lambda} = \begin{bmatrix} \mathbf{K}^{\Lambda} \\ \mathbf{L}^{\Lambda} \end{bmatrix}, \qquad (7.53)$$

where $\mathbf{K}^{\Lambda}$ is the $(n_a + m_a) \times (n_a + m_a)$-dimensional K-matrix which couples the $n_a + m_a$ open channels in (7.35) and (7.41) and $\mathbf{L}^{\Lambda}$ is a subsidiary $(n_b+m_b) \times (n_a+m_a)$-dimensional matrix which couples the solutions in (7.47) and (7.49) which vanish asymptotically. We see that $\mathbf{K}^{\Lambda}$ postmultiplies the first n_a+m_a columns in the matrix $\mathbf{c}(\rho)$ in (7.50) and $\mathbf{L}^{\Lambda}$ postmultiplies the last n_b+m_b columns of $\mathbf{c}(\rho)$.

Following our discussion in Sect. 5.1.4, we now express the $(n_a + m_a) \times (n_a + m_a)$-dimensional K-matrix coupling the open channels in (7.35) and (7.41) in terms of the $(n + m) \times (n + m)$-dimensional R-matrix $\mathbf{R}^{\Lambda}$, defined on the outer boundaries of the external region $r_{\mathrm{p}} = a_p$ and $R_N = A_q$ in Fig. 7.2, obtained using the propagator method described in Appendix E.6, or an equivalent procedure. The R-matrix on the boundary $r_{\mathrm{p}} = a_p$ and $R_N = A_q$ is then defined in analogy with (E.116) and (E.117) as follows:

$$\begin{aligned}\mathbf{F}^{\Lambda}(a_p, A_q) &= \mathbf{R}^{\Lambda}_{11}(a_p, A_q) a_p \mathbf{F}^{\Lambda'}(a_p, A_q) + \mathbf{R}^{\Lambda}_{12}(a_p, A_q) A_q \mathbf{G}^{\Lambda'}(a_p, A_q),\\ \mathbf{G}^{\Lambda}(a_p, A_q) &= \mathbf{R}^{\Lambda}_{21}(a_p, A_q) a_p \mathbf{F}^{\Lambda'}(a_p, A_q) + \mathbf{R}^{\Lambda}_{22}(a_p, A_q) A_q \mathbf{F}^{\Lambda'}(a_p, A_q),\end{aligned} \tag{7.54}$$

where $\mathbf{F}^{\Lambda'}$ and $\mathbf{G}^{\Lambda'}$ are the derivatives $\mathrm{d}\mathbf{F}^{\Lambda}/\mathrm{d}r_{\mathrm{p}}$ and $\mathrm{d}\mathbf{G}^{\Lambda}/\mathrm{d}R_N$, respectively.

We now observe that the components of the asymptotic solution $\boldsymbol{\mathcal{F}}^{\Lambda}$, defined by (7.50), and their derivatives, defined by

$$\boldsymbol{\mathcal{F}}^{\Lambda'}(\rho) = \mathbf{s}'(\rho) + \mathbf{c}'(\rho)\mathbf{N}^{\Lambda}, \quad r_{\mathrm{p}} \geq a_p, \quad R_N \geq A_q, \tag{7.55}$$

correspond on the boundary $r_{\mathrm{p}} = a_p$ and $R_N = A_q$ to solutions (7.54), after appropriate re-ordering corresponding to (7.52). Hence, following our analysis in Sect. 5.1.4, we can substitute the appropriate re-ordered asymptotic solutions $\boldsymbol{\mathcal{F}}^{\Lambda}$ and $\boldsymbol{\mathcal{F}}^{\Lambda'}$ defined by (7.50) and (7.55) on the boundary $r_{\mathrm{p}} = a_p$ and $R_N = A_q$ of the external region for the functions $\mathbf{F}^{\Lambda}$ and $\mathbf{G}^{\Lambda}$ and the derivatives $\mathbf{F}^{\Lambda'}$ and $\mathbf{G}^{\Lambda'}$ in (7.54). This yields a set of $n+m$ linear simultaneous equations with n_a+n_b right-hand sides, which are analogous to (5.46). The solution of these equations then yields the elements of the $(n+m) \times (n_a+m_a)$-dimensional matrix $\mathbf{N}^{\Lambda}$ and hence from (7.53) the $(n_a+m_a) \times (n_a+m_a)$-dimensional K-matrix $\mathbf{K}^{\Lambda}$.

It follows from (7.50) that the required physical solution matrix $\boldsymbol{\mathcal{F}}^{\Lambda}(\rho)$ satisfies the asymptotic boundary condition

$$\boldsymbol{\mathcal{F}}^{\Lambda}(\rho) \underset{\substack{r_{\mathrm{p}}\to\infty \\ R_N\to\infty}}{\sim} \mathbf{s}(\rho) + \mathbf{c}(\rho)\mathbf{K}^{\Lambda}, \tag{7.56}$$

where we remember from (7.52) that the first n_a channels in (7.56) correspond to open positron–atom channels, and the next m_a channels in (7.56) correspond to open positronium–ion channels. Hence the K-matrix $\mathbf{K}^{\Lambda}$ couples the n_a open

positron–atom channels and the m_a open positronium–ion channels. The $(n_a + m_a) \times (n_a + m_a)$-dimensional S-matrix $\mathbf{S}^{\Lambda}$ is then defined in terms of the K-matrix $\mathbf{K}^{\Lambda}$ in the usual way by the matrix equation

$$\mathbf{S}^{\Lambda} = \frac{\mathbf{I} + \mathrm{i}\mathbf{K}^{\Lambda}}{\mathbf{I} - \mathrm{i}\mathbf{K}^{\Lambda}}. \tag{7.57}$$

The corresponding T-matrix and cross sections describing transitions between the open positron–atom channels and the open positronium–ion channels can then be determined using the procedure described in Sect. 2.5. The solutions in the internal, external and asymptotic regions in Fig. 7.2 can be determined in a similar way for all relevant conserved quantum numbers Λ defined by (7.12) enabling the corresponding cross sections for transitions between the open positron–atom and positronium–ion channels to be determined.

7.2 Positron and Positronium Collision Calculations

In recent years detailed positron– and positronium–atom collision calculations have been carried out using R-matrix computer programs, where a major motivation for these theoretical and computational advances has been new developments in experiments. In addition to R-matrix calculations for positron collisions with atomic hydrogen carried out by Higgins et al. [467, 468, 470] and Kernoghan et al. [531, 532] detailed R-matrix calculations have been carried out for positron collisions with "one-electron" alkali metal atoms Li, Na, K, Rb and Cs by McAlinden et al. [607–611], Campbell et al. [202] and Walters et al. [950, 951] and with "two-electron" atoms He, Mg, Ca and Zn by Campbell et al. [202]. Also in recent years there has been a rapid increase in the experimental capability to produce monoenergetic, energy-tunable beams of the longer life ortho-positronium which are used in collision experiments, for example, by Laricchia et al. [574, 575, 577–580], Charlton et al. [215, 216], Zafar et al. [988–990], Garner et al. [362–364], Gilbert et al. [372], Armitage et al. [20] and Brawley et al. [124]. These developments have stimulated considerable interest in the calculation of positronium collisions with atoms and detailed R-matrix calculations have been carried out for positronium collisions with H by Campbell et al. [201] and Blackwood et al. [112–114] and with He, Na, Ar, Kr and Xe by Blackwood et al. [111, 113]. We will discuss examples of these collision calculations in the following sections.

7.2.1 Positron Collisions with H

As our first example we consider R-matrix calculations of positron collisions with atomic hydrogen at low and intermediate energies carried out by Kernoghan et al. [531, 532]. In this work they considered the following processes:

$$\begin{aligned} e^+ + H(1s) &\rightarrow H(1s) + e^+ && \text{elastic scattering,} \\ &\rightarrow H(2s, 2p) + e^+ && \text{excitation,} \\ &\rightarrow H^+ + e^- + e^+ && \text{ionization,} \\ &\rightarrow H^+ + Ps(1s, 2s, 2p) && \text{Ps formation,} \end{aligned} \tag{7.58}$$

where they compared their results with experimental measurements by Jones et al. [508] and Zhou et al. [1010].

The R-matrix calculations were carried out in the energy range 0–110 eV using a 33-state approximation which included in expansion (7.13) the 1s, 2s and 2p eigenstates of both positronium and atomic hydrogen with 27 atomic hydrogen pseudostates, which represented the hydrogen atom ionization continuum. The results presented in Fig. 7.4 show excellent agreement between the calculations and experiment for the total positronium formation cross section, the ionization cross section and the total cross section over the full range of energies considered, showing that the 33-state calculation can accurately describe the main features of the cross section for positron collisions with the ground state of atomic hydrogen. In particular, the inclusion of pseudostates in this calculation gives an accurate representation of the ionization continuum at intermediate energies.

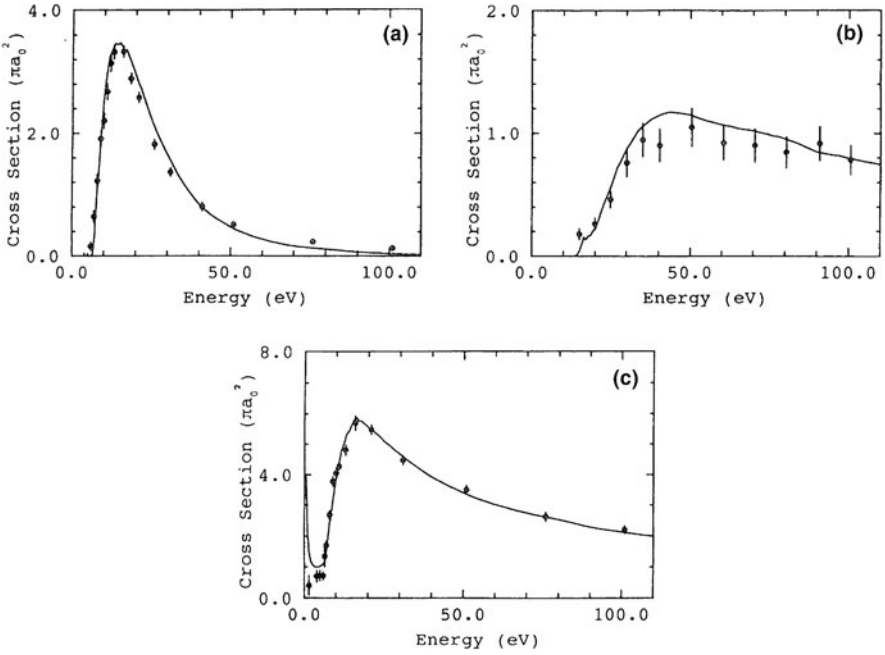

Fig. 7.4 Positron collisions with atomic hydrogen: (**a**) total positronium formation cross section, (**b**) ionization cross section, (**c**) total cross section. *Solid curve*: 33-state calculation [532]; *points*: experimental data from [508, 1010] (Fig. 1 from [953])

7.2.2 Positronium Collisions with He

We consider next R-matrix calculations of positronium collisions with helium atoms where initially the target helium atom is restricted to its $^1S^e$ ground state. This "frozen-target" approximation has been successfully applied by Blackwood et al. [111] to describe elastic scattering, positronium excitation and positronium ionization in the energy range 0–40 eV. However, this work also highlighted significant discrepancies between theory and experiment for low-energy positronium–helium atom collisions. Hence in Sect. 7.2.3 we consider calculations for positronium collisions with helium and hydrogen atoms by Walters et al. [952] which, by including virtual transitions in the target, show the importance of target polarization in low-energy collisions.

7.2.2.1 Frozen-Target Approximation

We consider first R-matrix calculations for positronium collisions with helium atoms carried out by Blackwood et al. [111] who studied the following collision processes:

$$\begin{aligned} \mathrm{Ps} + \mathrm{He} &\rightarrow \mathrm{He} + \mathrm{Ps} && \text{elastic scattering,} \\ &\rightarrow \mathrm{He} + \mathrm{Ps}(n=2) && \text{positronium excitation,} \\ &\rightarrow \mathrm{He} + \mathrm{e}^- + \mathrm{e}^+ && \text{positronium ionization.} \end{aligned} \tag{7.59}$$

In this work results from three levels of approximation were reported, where in each case the frozen-target approximation is adopted where only the $^1S^e$ ground state of He was retained in the second expansion in (7.13). In the first static exchange approximation, only the Ps(1s) state and the He($^1S^e$) state were retained in (7.13). In the second nine-state approximation (9ST), the 1s, 2s and 2p eigenstates of Ps together with $\overline{3}$s, $\overline{3}$p, $\overline{3}$d, $\overline{4}$s, $\overline{4}$p, $\overline{4}$d pseudostates were retained in (7.13). Finally, in the third 22-state approximation (22ST), the 1s, 2s and 2p eigenstates of Ps as well as $\overline{3}$s–$\overline{7}$s, $\overline{3}$p–$\overline{7}$p, $\overline{3}$d–$\overline{7}$d and $\overline{4}$f–$\overline{7}$f pseudostates were retained in (7.13). In all of these calculations we note that since the target helium atom is restricted to the $^1S^e$ ground state, an ortho-positronium projectile cannot be converted into a para-positronium projectile or vice versa. Hence in this approximation the collision cross sections for ortho-positronium and para-positronium collisions are the same.

We show in Fig. 7.5 the total cross section for the 22ST approximation and its principal components, i.e. the elastic cross section, the positronium ionization (fragmentation) cross section and the positronium excitation cross section to the 2s and 2p states, calculated by Blackwood et al. [111]. The ionization cross section was extracted from the calculation [532, 611] by taking

$$\sigma_{\mathrm{ion}}(\mathrm{Ps}) = \sum_j f_j \sigma_j(\mathrm{Ps}), \tag{7.60}$$

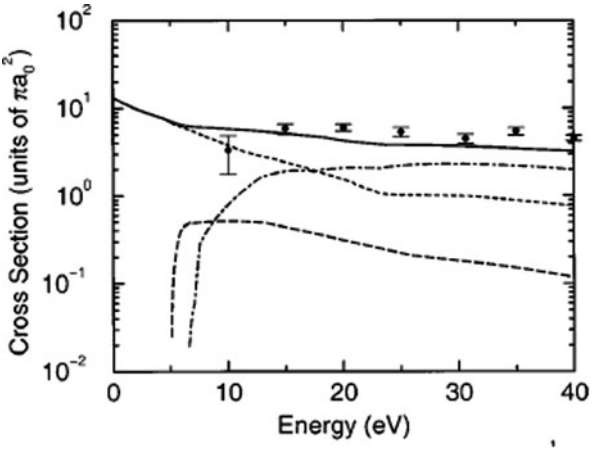

Fig. 7.5 Cross sections for positronium collisions with helium atoms calculated in the 22ST R-matrix approximation by Blackwood et al. [111]. *Solid curve*: total cross section; *short dashed curve*: elastic scattering cross section; *dash-dot curve*: Ps ionization (fragmentation) cross section; *long-dashed curve*: Ps($n = 2$) excitation cross section; *solid circles*: total cross section measurements by Garner et al. [362, 363] (Fig. 2 from [111])

where σ_j(Ps) is the cross section for exciting the jth positronium pseudostate and f_j is the fraction of this state overlapping the positronium continuum. We see from this figure that the calculated total cross section is in good agreement with the measurements of Garner et al. [362, 363].

We also compare the calculated positronium ionization cross section with later measurements by Armitage et al. [20] and with Born approximation calculations by Biswas and Adhikari [109] in Fig. 7.6. We see from this figure that including pseudostates in the R-matrix calculation gives a good representation of the ionization

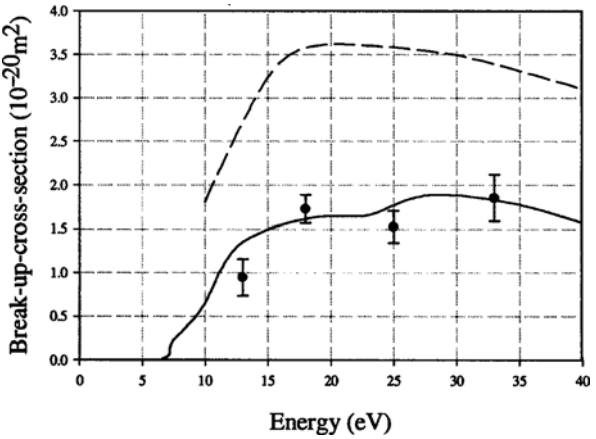

Fig. 7.6 Positronium ionization cross section for positronium collisions with helium atoms. *Solid curve*: R-matrix calculation by Blackwood et al. [111]; *dashed curve*: Born approximation calculation by Biswas and Adhikari [109]; *solid circles*: experimental measurements by Armitage et al. [20] (Fig. 2. from [20])

cross section in this energy range. However, it is also clear from this figure that the Born approximation is, as expected, not accurate at these relatively low energies.

7.2.3 Target Polarization in Positronium Collisions

In order to study the effect of target polarization on low-energy collision cross sections, Walters et al. [952] carried out a series of calculations for positronium collisions with helium and atomic hydrogen targets including excited states and pseudostates in both the expansions of the positronium and target states.

In the case of S-wave positronium collisions with helium, 1s, 2s and 2p eigenstates and $\overline{3s}$, $\overline{3p}$, $\overline{3d}$, $\overline{4s}$, $\overline{4p}$, $\overline{4d}$ pseudostates of Ps together with 1 $^1S^e$, 2 $^1S^e$, 2 $^1P^o$ eigenstates and 3 $\overline{^1S^e}$, 3 $\overline{^1P^o}$, 3 $\overline{^1D^e}$, 4 $\overline{^1S^e}$, 4 $\overline{^1P^o}$, 4 $\overline{^1D^e}$ pseudostates of helium were retained in expansion (7.13) giving a 9Ps9He calculation. In the case of P-wave positronium collisions with helium some numerical instabilities were encountered

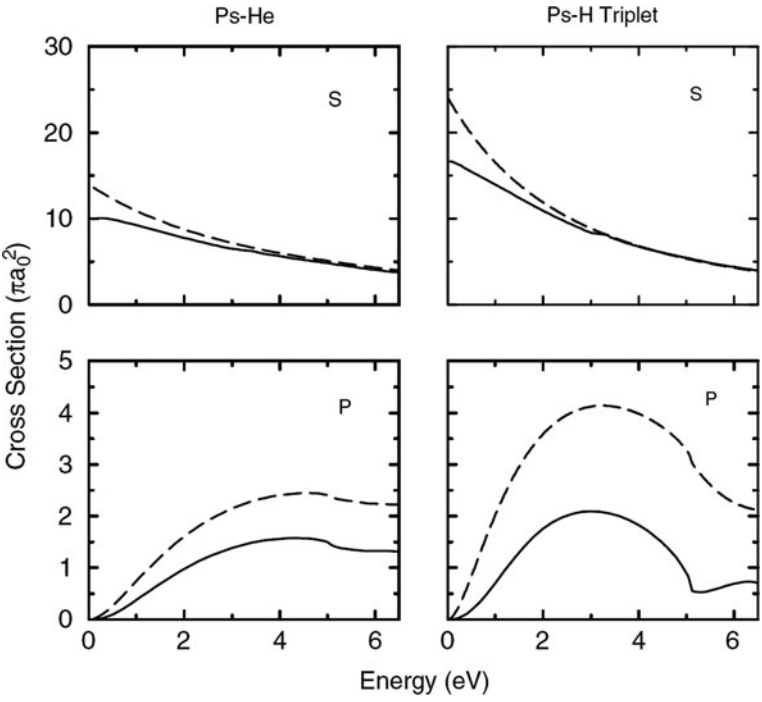

Fig. 7.7 S-wave and P-wave cross sections for Ps(1s) elastic scattering by He(1 $^1S^e$) and H(1s). The Ps–H cross sections are for collisions in the electron spin triplet state. For He: *solid curve*, 9Ps9He approximation for S-wave and 7Ps7He approximation for P-wave; *dashed curve*, 9Ps1He approximation for S-wave and 7Ps1He approximation for P-wave. For H: *solid curves*, 9Ps9H approximation; *dashed curves*, 9Ps1H approximation for S-wave and for P-wave (Fig. 5 from [952])

so a reduced 7Ps7He calculation was adopted in which the positronium and helium D-wave pseudostates were omitted. We compare in Fig. 7.7 the corresponding S- and P-wave Ps–He elastic scattering cross sections with results obtained using frozen He target approximations corresponding to 9Ps1He for S-wave and 7Ps1He for P-wave scattering. Also shown in Fig. 7.7 are corresponding results for positronium collisions with atomic hydrogen in the triplet electronic spin state. We see from this figure that the results for both atomic hydrogen and helium targets are similar with a significant reduction in the cross section occurring at low energies when virtual transitions in the target are included in the calculation. Also we observe that the reduction is more significant for atomic hydrogen, probably because of the higher excitation energies for the He target.

In conclusion, these calculations show that target polarization plays an important role in low-energy positronium–atom collisions and that virtual transitions of the target must be included to obtain accurate low-energy collision cross sections.

Chapter 8
Photoionization, Photorecombination and Atoms in Fields

In recent years there has been a considerable growth of interest in atomic photoionization and photorecombination processes stimulated, for example, by the need to analyse increasingly sophisticated experiments using synchrotron radiation sources and to calculate atomic data required in many applications. In this chapter we consider the development of R-matrix theory to treat atomic photoionization and photorecombination processes, where we restrict our consideration to single photon processes, reserving a treatment of multiphoton processes to Chaps. 9 and 10. We also consider an extension of R-matrix theory to describe the spectra of atoms in external fields.

We commence our analysis of atomic photoionization processes in Sect. 8.1 by deriving a general expression for the differential cross section for photoionization of an unpolarized atom or atomic ion by a polarized beam of photons. The differential photoionization cross section is then written in a general form consisting of an integrated cross section and an asymmetry parameter, which follows from invariance arguments discussed by Yang [983]. We then extend multichannel R-matrix theory, introduced in Chap. 5, to enable atomic photoionization cross sections to be calculated using an approach developed by Burke and Taylor [168]. This section includes a discussion of R-matrix methods for calculating both the initial bound state of the target atom and the final continuum state. We also consider methods for carrying out calculations in the neighbourhood of R-matrix poles using an approach introduced by Burke and Seaton [169].

In Sect. 8.2 we consider photorecombination and radiation damping in electron collisions with positive ions. In photorecombination a free electron is accelerated by the ion and as a result emits a photon of sufficient energy that the electron is captured into a bound state. This process can proceed non-resonantly or, alternatively, resonantly through intermediate doubly excited states which is called dielectronic recombination. Also, for electron collisions with highly ionized ions, the scattering amplitude must be modified to include radiation damping, where the lifetimes of intermediate resonance states can be strongly affected by the interaction between the radiation field and the scattered and target electrons. After a general introduction to photorecombination and radiation damping and a summary of recent work, we describe a generalization of R-matrix theory for electron–ion collisions in the presence of a radiation field. In this theory we extend the usual Schrödinger

P.G. Burke, *R-Matrix Theory of Atomic Collisions*, Springer Series on Atomic, Optical, and Plasma Physics 61, DOI 10.1007/978-3-642-15931-2_8,

equation describing electron–ion collisions by the addition of a "radiation damping potential". By solving this modified Schrödinger equation in internal, external and asymptotic regions, as discussed in Chap. 5, we show how photorecombination and free–free scattering cross sections, modified by radiation damping, can be calculated.

In Sect. 8.3 we summarize the objectives and achievements of the international Opacity Project, initiated and led by Seaton [861, 863], which is an important application of the processes discussed earlier in this chapter. A knowledge of the opacity of stellar material is of importance in studies of stellar structure and evolution, of stellar atmospheres and of solar element abundancies. After discussing the relationship between the cross sections for absorption or scattering of radiation and the Rosseland-mean opacity a brief summary of the calculations carried out is given and the R-matrix computer programs used in these calculations are briefly reviewed.

In Sect. 8.4 we describe a computational approach, introduced and developed by Halley et al. [438, 439] and Seipp and Taylor [867], which describes the spectra of atoms in external fields. This approach combines the complex coordinate rotation method with a new external region R-matrix method. We commence by describing the complex coordinate rotation method which has played an important role in the study of atoms, ions and molecules in external fields. We then show how this method can be combined with a new external region R-matrix method, introduced by O'Mahony and Taylor [703], to accurately describe the spectra of atoms in laboratory strength electric and magnetic fields.

Finally, in Sect. 8.5 we present illustrative results of atomic photoionization, photorecombination and radiation damping calculations. We also consider a calculation of the photoionization spectrum of an atom in an external magnetic field.

8.1 Atomic Photoionization

In this section we commence by giving a general introduction to the theory of atomic photoionization and we derive expressions for the integrated and differential photoionization cross sections. We then describe how these cross sections can be calculated using multichannel R-matrix theory.

8.1.1 Introduction and General Theory

We consider the following process where an atom is ionized by a photon of frequency ν

$$\mathrm{h}\nu + A_i \rightarrow A_j^+ + \mathrm{e}^- \tag{8.1}$$

where A_i is the atom in state i and A_j^+ is the residual positive ion in state j. Both A_i and A_j^+ can be in their ground states or either or both can be in excited states. We also consider the analogous photoionization process for positive ions defined by

$$\mathrm{h}\nu + A_i^{n+} \rightarrow A_j^{(n+1)+} + \mathrm{e}^-, \tag{8.2}$$

and for negative ions defined by

$$\mathrm{h}\nu + A_i^- \rightarrow A_j + \mathrm{e}^-, \tag{8.3}$$

where the latter process is called photodetachment.

We assume that a beam of photons, linearly polarized in the z-direction denoted by the unit vector $\hat{\boldsymbol{\epsilon}}$, is incident in the x-direction on an atom or ion at the origin of coordinates, as illustrated in Fig. 8.1. The photoelectron is then ejected at polar angles (θ_k, ϕ_k) with respect to a right-handed Cartesian frame of reference (x, y, z). The differential photoionization cross section for a transition from an atomic or ionic state i to state j is defined by

$$\frac{\mathrm{d}\sigma_{ij}}{\mathrm{d}\Omega} = \frac{1}{f} W_{ji}, \tag{8.4}$$

where W_{ji} is the transition probability per unit time from state i to state j at an energy E and f is the incident photon flux. From first-order time-dependent perturbation theory, which is valid for the weak photon fields considered in this section, we obtain in atomic units

$$W_{ji} = 2\pi \left| T_{ji} \right|^2 \rho_j, \tag{8.5}$$

where the transition amplitude

$$T_{ji} = \langle \Psi_{jE}^- | H' | \Psi_{iB} \rangle, \tag{8.6}$$

and ρ_j is the density of final states. In (8.6) Ψ_{iB} is the initial bound-state wave function of the target atom, which is normalized to unity according to

$$\langle \Psi_{iB} | \Psi_{iB} \rangle = 1, \tag{8.7}$$

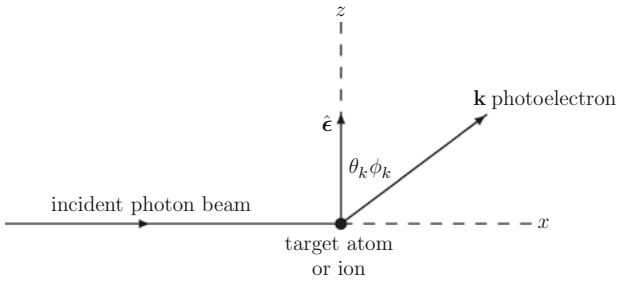

Fig. 8.1 Basic atomic photoionization process where the incident photon beam is linearly polarized in the z-direction denoted by the unit vector $\hat{\boldsymbol{\epsilon}}$

and Ψ^-_{jE} is the final ingoing wave continuum-state wave function belonging to the energy E describing the residual ion and the ejected photoelectron, which we assume is normalized according to

$$\langle \Psi^-_{jE} | \Psi^-_{j'E'} \rangle = \delta_{jj'} \delta(E - E'), \tag{8.8}$$

corresponding to the density of states $\rho_j = 1$ in (8.5). We will consider the ingoing wave boundary condition satisfied by Ψ^-_{jE} below.

We can express the interaction term H' in the Hamiltonian appearing in the transition amplitude T_{ji} in (8.6), in terms of the vector potential $\mathbf{A}(\mathbf{r}, t)$ by

$$H' = -\frac{\mathrm{i}}{\mathrm{c}} \sum_{i=1}^{N+1} \mathbf{A}(\mathbf{r}_i, t) \cdot \nabla_i, \tag{8.9}$$

where we assume that the atomic system in the initial state consists of an atom or ion with $N + 1$ electrons with coordinates $\mathbf{r}_i$, $i = 1, \ldots, N + 1$. Also, we have adopted the Coulomb gauge such that the vector potential $\mathbf{A}$ satisfies div $\mathbf{A} = 0$ and the scalar potential $\phi = 0$. The vector potential corresponding to a beam of photons linearly polarized in the z-direction, defined in Fig. 8.1, is given by

$$\begin{aligned} \mathbf{A}(\mathbf{r}, t) &= \hat{\boldsymbol{\epsilon}} A_0 \cos(\boldsymbol{\kappa} \cdot \mathbf{r} - \omega t) \\ &= \hat{\boldsymbol{\epsilon}} \frac{1}{2} A_0 \exp[\mathrm{i}(\boldsymbol{\kappa} \cdot \mathbf{r} - \omega t)] + \hat{\boldsymbol{\epsilon}} \frac{1}{2} A_0 \exp[-\mathrm{i}(\boldsymbol{\kappa} \cdot \mathbf{r} - \omega t)], \end{aligned} \tag{8.10}$$

where $\omega = \kappa \mathrm{c}$ is the angular frequency and $\boldsymbol{\kappa}$ is the direction of the incident photon beam x in Fig. 8.1. Also in (8.10), the first term corresponds to photon absorption and the second term corresponds to photon emission. The incident photon flux f can be expressed in terms of the Poynting vector $\mathbf{P}$ defined by (e.g. [817])

$$\mathbf{P} = \frac{\mathrm{c}}{4\pi} \mathbf{E} \times \mathbf{H}, \tag{8.11}$$

where the electric and magnetic field strengths $\mathbf{E}$ and $\mathbf{H}$ are given by

$$\mathbf{E} = -\frac{1}{\mathrm{c}} \frac{\partial \mathbf{A}}{\partial t} = -\kappa \hat{\boldsymbol{\epsilon}} A_0 \sin(\boldsymbol{\kappa} \cdot \mathbf{r} - \omega t) \tag{8.12}$$

and

$$\mathbf{H} = \mathrm{curl} \mathbf{A} = -\boldsymbol{\kappa} \times \hat{\boldsymbol{\epsilon}} A_0 \sin(\boldsymbol{\kappa} \cdot \mathbf{r} - \omega t). \tag{8.13}$$

The Poynting vector is thus in the direction $\boldsymbol{\kappa}$ and its magnitude, averaged over a period of the oscillation $2\pi/\omega$, is

$$P_{\mathrm{Av}} = \frac{\omega^2}{8\pi \mathrm{c}} A_0^2. \tag{8.14}$$

It follows that the photon flux given by the number of photons passing through unit area in unit time is

$$f = \frac{1}{\omega} P_{\mathrm{Av}} = \frac{\nu}{4\mathrm{c}} A_0^2, \tag{8.15}$$

where the frequency $\nu = \omega/2\pi$. Combining these results and assuming that the dipole approximation is valid (i.e. the wavelength of the photon field is large compared with the size of the atomic target so that $\exp(\mathrm{i}\boldsymbol{\kappa} \cdot \mathbf{r})$ in (8.10) can be replaced by unity) we obtain the dipole velocity form of the differential photoionization cross section

$$\frac{\mathrm{d}\sigma_{ij}^{V}}{\mathrm{d}\Omega} = \frac{2\pi}{\mathrm{c}\nu} \left| \langle \Psi_{jE}^{-} | \hat{\boldsymbol{\epsilon}} \cdot \mathbf{D}_V | \Psi_{iB} \rangle \right|^2, \tag{8.16}$$

where the dipole velocity operator

$$\mathbf{D}_V = \sum_{i=1}^{N+1} \boldsymbol{\nabla}_i. \tag{8.17}$$

We can also obtain the dipole length form of the differential photoionization cross section using the operator identity

$$\mathbf{p} = \frac{\mathrm{d}\mathbf{r}}{\mathrm{d}t} = -\mathrm{i}[\mathbf{r}, H], \tag{8.18}$$

which yields

$$\frac{\mathrm{d}\sigma_{ij}^{L}}{\mathrm{d}\Omega} = \frac{8\pi^3 \nu}{\mathrm{c}} \left| \langle \Psi_{jE}^{-} | \hat{\boldsymbol{\epsilon}} \cdot \mathbf{D}_L | \Psi_{iB} \rangle \right|^2, \tag{8.19}$$

where the dipole length operator

$$\mathbf{D}_L = \sum_{i=1}^{N+1} \mathbf{r}_i. \tag{8.20}$$

The velocity form of the differential photoionization cross section can then be written as

$$\frac{\mathrm{d}\sigma_{ij}^{V}}{\mathrm{d}\Omega_k} = \frac{4\pi^2 \alpha \mathrm{a}_0^2}{\omega} \left| \langle \Psi_{jE}^{-}(\hat{\mathbf{k}}) | \hat{\boldsymbol{\epsilon}} \cdot \mathbf{D}_V | \Psi_{iB} \rangle \right|^2, \tag{8.21}$$

and the length form of this cross section as

$$\frac{\mathrm{d}\sigma_{ij}^{L}}{\mathrm{d}\Omega_k} = 4\pi^2 \alpha \mathrm{a}_0^2 \omega \left| \langle \Psi_{jE}^{-}(\hat{\mathbf{k}}) | \hat{\boldsymbol{\epsilon}} \cdot \mathbf{D}_L | \Psi_{iB} \rangle \right|^2, \tag{8.22}$$

where in these equations α is the fine-structure constant and ω is the incident photon energy expressed in atomic units.

If exact wave functions are used for the initial and final states, the dipole velocity and the dipole length forms of the cross sections give identical results. However, agreement between the dipole velocity and length cross sections is a necessary but not a sufficient condition for the accuracy of the wave functions. Also, in addition to the above two forms of the cross sections, Chandrasekhar [209] defined a further cross section which uses the acceleration form of the dipole operator. This emphasizes the wave function close to the nucleus and usually gives poorer results than the other two forms when approximate wave functions are used, although we will see in Sect. 9.1.6 that using the acceleration frame in the asymptotic region in the treatment of multiphoton processes can simplify the analysis.

We now derive explicit expressions for the differential photoionization cross sections defined by (8.21) and (8.22) in terms of the bound- and continuum-state wave functions Ψ_{iB} and $\Psi^-_{jE}(\hat{\mathbf{k}})$, where we confine our attention to targets where relativistic effects can be neglected. We consider first the continuum-state wave function $\Psi^-_{jE}(\hat{\mathbf{k}})$ which has the following asymptotic form:

$$\Psi^-_{jE}(\hat{\mathbf{k}}) \sim \Psi^{\rm inc}_{jE}(\hat{\mathbf{k}}) + \Psi^{\rm ing}_{jE}(\hat{\mathbf{k}}), \tag{8.23}$$

where $\Psi^{\rm inc}_{jE}(\hat{\mathbf{k}})$ is a Coulomb-modified plane wave incident in direction $\hat{\mathbf{k}}$ on the residual ion and $\Psi^{\rm ing}_{jE}(\hat{\mathbf{k}})$ is the corresponding ingoing wave which has components in all channels coupled to $\Psi^{\rm inc}_{jE}(\hat{\mathbf{k}})$ by the interaction. These ingoing wave boundary conditions have been discussed by many authors, see, for example, [136, 387, 454, 665].

The Coulomb-modified incident plane wave in (8.23) can be written as

$$\Psi^{\rm inc}_{jE}(\mathbf{X}_{N+1}) = \mathcal{A}\left[\left(\frac{k_j}{(2\pi)^3}\right)^{1/2} \Phi_j(\mathbf{X}_N)\chi_{\frac{1}{2}m_j}(\sigma_{N+1})\psi^-_{cj}(\mathbf{r}_{N+1})\right], \tag{8.24}$$

where we have adopted the notation introduced in Sect. 2.3, describing an electron labelled $N+1$ interacting with an N-electron atom or ion. Thus $\mathcal{A}$ is the usual antisymmetrization operator, Φ_j is the residual atom or ion wave function, $\chi_{\frac{1}{2}m_j}$ is the ejected electron spin function and ψ^-_{cj} is a Coulomb wave function representing the ejected electron in the jth channel. We can expand ψ^-_{cj} as follows:

$$\psi^-_{cj}(\mathbf{r}) = \sum_{\ell=0}^{\infty}(2\ell+1)\mathrm{i}^\ell \exp(-\mathrm{i}\sigma_\ell)(k_j r)^{-1} F_\ell(\eta_j, k_j r) P_\ell(\cos\theta), \tag{8.25}$$

which is obtained from (1.64) by replacing $\exp(\mathrm{i}\sigma_\ell)$ by $\exp(-\mathrm{i}\sigma_\ell)$ so that $\exp(-\mathrm{i}\sigma_\ell)F_\ell(\eta, kr)$ has the following asymptotic form

$$\exp(-\mathrm{i}\sigma_\ell)F_\ell(\eta, kr) \underset{r\to\infty}{\sim} (2\mathrm{i})^{-1}\left[\exp(\mathrm{i}\theta^c_\ell) - \exp(-\mathrm{i}\theta^c_\ell)S^c_\ell(k)\right], \tag{8.26}$$

corresponding to a Coulomb-modified plane wave plus an ingoing Coulomb scattered wave. Also, θ in (8.25) is the angle between the ejected electron vector $\mathbf{r}$ and the vector $\hat{\boldsymbol{\epsilon}}$ in Fig. 8.1. Finally, the factor $\left[k_j/(2\pi)^3\right]^{1/2}$ in (8.24) ensures that $\Psi_{jE}^{\rm inc}$ and hence Ψ_{jE}^{-} satisfy the normalization condition (8.8). We now substitute (8.25) for $\psi_{cj}^{-}(\mathbf{r})$ into (8.24) and expand $P_\ell(\cos\theta)$ in terms of spherical harmonics using (B.48), giving

$$\Psi_{jE}^{\rm inc}(\mathbf{X}_{N+1}) = \mathcal{A}\sum_{\ell_j m_{\ell_j}} \Phi_j(\mathbf{X}_N)\chi_{\frac{1}{2}m_j}(\sigma_{N+1})\mathrm{i}^{\ell_j}\exp(-\mathrm{i}\sigma_{\ell_j})Y^*_{\ell_j m_{\ell_j}}(\theta_k,\phi_k)$$
$$\times\, Y_{\ell_j m_{\ell_j}}(\theta_{N+1},\phi_{N+1})r_{N+1}^{-1}u_j^0(r_{N+1}), \tag{8.27}$$

where (θ_k,ϕ_k) and $(\theta_{N+1},\phi_{N+1})$ are the spherical polar coordinates of $\mathbf{k}$ and $\mathbf{r}_{N+1}$ with respect to the (x,y,z) Cartesian coordinate frame of reference in Fig. 8.1 and

$$u_j^0(r) = \frac{2}{(2\pi k_j)^{1/2}}F_{\ell_j}(\eta_j,k_j r)\underset{r\to\infty}{\sim}\frac{\mathrm{i}}{(2\pi k_j)^{1/2}}\left[\exp(-\mathrm{i}\theta_j^c)-\exp(\mathrm{i}\theta_j^c)\right]. \tag{8.28}$$

where θ_j^c is defined by (2.82), (2.83) and (2.84). The final step in our determination of $\Psi_{jE}^{\rm inc}$ is to rewrite (8.27) as an expansion in terms of channel functions $\overline{\Phi}_j^{\Gamma'}$, introduced in Sect. 2.3.2. It follows by inverting (2.59) that we can write

$$\Phi_j(\mathbf{X}_N)Y_{\ell'_j m_{\ell'_j}}(\theta_{N+1},\phi_{N+1})\chi_{\frac{1}{2}m'_j}(\sigma_{N+1})$$
$$=\sum_{L'S'}(L'_jM_{L'_j}\ell'_jm_{\ell'_j}|L'M_{L'})(S'_jM_{S'_j}\tfrac{1}{2}m'_j|S'M_{S'})$$
$$\times\,\overline{\Phi}_j^{\Gamma'}(\mathbf{X}_N;\hat{\mathbf{r}}_{N+1}\sigma_{N+1}), \tag{8.29}$$

where $\Gamma' \equiv \alpha' L' S' M_{L'} M_{S'} \pi'$ are the conserved quantum numbers for the final continuum state.[1]

We now substitute (8.29) into (8.27) and include, as in (8.23), the contribution from the incident channels in the ingoing wave channels allowed by the conserved quantum numbers. The continuum wave function Ψ_{jE}^{-} then has the asymptotic form

$$\Psi_{jE}^{-}\sim\mathcal{A}\sum_{\ell'_jm_{\ell'_j}}\sum_{L'S'}\sum_{\alpha'_iL'_iS'_i\ell'_i}(L'_jM_{L'_j}\ell'_jm_{\ell'_j}|L'M_{L'})(S'_jM_{S'_j}\tfrac{1}{2}m'_j|S'M_{S'})$$
$$\times\,\mathrm{i}^{\ell'_j}\exp(-\mathrm{i}\sigma_{\ell'_j})Y^*_{\ell'_jm_{\ell'_j}}(\theta_k,\phi_k)\overline{\Phi}_i^{\Gamma'}(\mathbf{X}_N;\hat{\mathbf{r}}_{N+1}\sigma_{N+1})$$
$$\times\,r_{N+1}^{-1}u_{ij}^{\Gamma'-}(r_{N+1}), \tag{8.30}$$

[1] We note that in (8.29), and in subsequent equations, we have used primes to denote the quantum numbers corresponding to the final continuum state, while the quantum numbers of the initial bound state are left unprimed.

where, using matrix notation, the reduced radial wave functions $u_{ij}^{\Gamma'-}(r)$ satisfy the asymptotic ingoing wave boundary conditions

$$\mathbf{u}^{\Gamma'-}(r) \underset{r\to\infty}{\sim} -\mathrm{i}(2\pi\mathbf{k})^{-1/2}\left[\exp(\mathrm{i}\boldsymbol{\theta}) - \exp(-\mathrm{i}\boldsymbol{\theta})\mathbf{S}^{\Gamma'*}\right]. \tag{8.31}$$

The quantity $\mathbf{S}^{\Gamma'*}$ is the complex conjugate of the usual S-matrix, where the matrix elements $S_{ij}^{\Gamma'}$ describe the scattering between channels denoted by the quantum numbers $i \equiv \alpha_i' L_i' S_i' \ell_i'$ and $j \equiv \alpha_j' L_j' S_j' \ell_j'$ corresponding to the final continuum state for each Γ'. The quantum numbers $\alpha_i' L_i' S_i'$ and $\alpha_j' L_j' S_j'$ define the states of the residual atom or ion, as discussed in Sect. 2.2, and ℓ_i' and ℓ_j' are the orbital angular momentum quantum numbers of the ejected photoelectron. We note that $\mathbf{u}^{\Gamma'-} = (2/\pi)^{1/2}\mathbf{H}^{\Gamma'-}$, where $\mathbf{H}^{\Gamma'-}$ is the solution satisfying ingoing wave asymptotic boundary conditions, defined by (2.120).

In practical calculations it is usually convenient to use K-matrix boundary conditions rather than the ingoing wave boundary conditions defined by (8.31). To achieve this we rewrite (8.31) in the equivalent form

$$\mathbf{u}^{\Gamma'-}(r) \underset{r\to\infty}{\sim} \left(\frac{2}{\pi\mathbf{k}}\right)^{1/2}\left(\sin\boldsymbol{\theta} + \cos\boldsymbol{\theta}\mathbf{K}^{\Gamma'}\right)\left(\mathbf{I} + \mathrm{i}\mathbf{K}^{\Gamma'}\right)^{-1}, \tag{8.32}$$

where, as in Sect. 2.5, we have defined the open-channel S-matrix $\mathbf{S}^{\Gamma'}$ in terms of the K-matrix $\mathbf{K}^{\Gamma'}$, by

$$\mathbf{S}^{\Gamma'} = \frac{\mathbf{I} + \mathrm{i}\mathbf{K}^{\Gamma'}}{\mathbf{I} - \mathrm{i}\mathbf{K}^{\Gamma'}}. \tag{8.33}$$

Also in these calculations it is convenient to express Ψ_{jE}^{-} in terms of functions which can be determined using the R-matrix method. To achieve this we rewrite (8.30) in the form

$$\begin{aligned}\Psi_{jE}^{-} = \sum_{\ell_j' m_{\ell_j'}} \sum_{L'S'} (L_j' M_{L_j'} \ell_j' m_{\ell_j'} | L' M_{L'}) \left(S_j' M_{S_j'} \tfrac{1}{2} m_j' | S' M_{S'}\right) \\ \times \mathrm{i}^{\ell_j'} \exp(-\mathrm{i}\sigma_{\ell_j'}) Y^*_{\ell_j' m_{\ell_j'}}(\theta_k, \phi_k) \Psi_{jE}^{\Gamma'-},\end{aligned} \tag{8.34}$$

where $\Psi_{jE}^{\Gamma'-}$ is defined in analogy with (2.57) by the expansion

$$\begin{aligned}\Psi_{jE}^{\Gamma'-}(\mathbf{X}_{N+1}) = \mathcal{A}\sum_i \overline{\Phi}_i^{\Gamma'}(\mathbf{X}_N; \hat{\mathbf{r}}_{N+1}\sigma_{N+1}) r_{N+1}^{-1} u_{ij}^{\Gamma'-}(r_{N+1}) \\ + \sum_k \chi_k^{\Gamma'}(\mathbf{X}_{N+1}) b_{kj}^{\Gamma'-}.\end{aligned} \tag{8.35}$$

The second summation in (8.35) over quadratically integrable functions $\chi_k^{\Gamma'}$ vanishes when any electron radial coordinate $r_i \geq a_0, \quad i = 1, \ldots, N+1$, where

a_0 is the radius of the internal R-matrix region. Hence in the asymptotic limit (8.34) goes over to the asymptotic form defined by (8.30) and (8.31). We will show in Sect. 8.1.2.1 that the functions $\Psi_{jE}^{\Gamma'-}$ can be determined by solving the non-relativistic time-independent Schrödinger equation (5.2) using the R-matrix method for all Γ' coupled to the initial state Ψ_{iB} by the electric dipole operators in (8.21) and (8.22).

We also need to consider the initial bound-state wave function Ψ_{iB} in (8.21) and (8.22). This wave function can be represented by a similar expansion to that adopted for $\Psi_{jE}^{\Gamma'-}$ in (8.35). Thus we can write

$$\Psi_{iB}^{\Gamma}(\mathbf{X}_{N+1}) = \mathcal{A}\sum_j \overline{\Phi}_i^{\Gamma}(\mathbf{X}_N;\hat{\mathbf{r}}_{N+1}\sigma_{N+1})r_{N+1}^{-1}v_{ji}^{\Gamma}(r_{N+1}) + \sum_k \chi_k^{\Gamma}(\mathbf{X}_{N+1})b_{ki}^{\Gamma}, \tag{8.36}$$

where $\Gamma \equiv \alpha L S M_l M_S \pi$ represents the conserved quantum numbers for the initial bound state and the radial basis functions v_{ji}^{Γ} satisfy the asymptotic boundary conditions corresponding to a bound state given by

$$v_{ji}^{\Gamma}(r) \underset{r\to\infty}{\sim} 0. \tag{8.37}$$

Since the second expansion in (8.36), as in (8.35), is over quadratically integrable functions the wave function Ψ_{iB}^{Γ} vanishes asymptotically and is normalizable. We will show in Sect. 8.1.2.2 that the function Ψ_{iB}^{Γ} can also be determined by solving (5.2) using the R-matrix method.

Having obtained explicit expressions for both the continuum-state and bound-state wave functions $\Psi_{jE}^{\Gamma'-}$ and Ψ_{iB}^{Γ}, we can now derive expressions for the matrix elements of the dipole operators which arise in (8.21) and (8.22) and hence for the differential photoionization cross section. We use the Wigner–Eckart theorem, discussed in Appendix D.1, see (D.8), to write the dipole matrix elements $\langle\Psi_{jE}^{\Gamma'-}|D_\mu|\Psi_{iB}^{\Gamma}\rangle$ appearing in (8.21) and (8.22) in terms of the reduced matrix elements $\langle\alpha'_j L'_j S'_j \ell'_j L' S'||D||\alpha_i L S\rangle$ defined by the following equation:

$$\langle\Psi_{jE}^{\Gamma'-}|D_\mu|\Psi_{iB}^{\Gamma}\rangle = (2L'+1)^{-1/2}(LM_L 1\mu|L'M_{L'}) \times\langle\alpha'_j L'_j S'_j \ell'_j L' S'||D_\mu||\alpha_i L S\rangle\delta_{SS'}\delta_{M_S M_{S'}}. \tag{8.38}$$

In this equation, D_μ are the spherical components of either the dipole velocity or dipole length operators in (8.21) or (8.22), respectively, which are defined in terms of their Cartesian components by

$$\begin{aligned} D_1 &= -\frac{1}{\sqrt{2}}(D_x + \mathrm{i}D_y),\\ D_0 &= D_z,\\ D_{-1} &= \frac{1}{\sqrt{2}}(D_x - \mathrm{i}D_y). \end{aligned} \tag{8.39}$$

It follows from (8.34) and (8.38) that the matrix elements which arise in (8.21) and (8.22) can be written as

$$\begin{aligned}\langle\Psi_{jE}^{-}|D_\mu|\Psi_{iB}\rangle = &\sum_{\ell'_j m_{\ell'_j}}\sum_{L'S'}(L'_j M_{L'_j}\ell'_j m_{\ell'_j}|L'M_{L'})\left(S'_j M_{S'_j}\tfrac{1}{2}m'_j|S'M_{S'}\right)\\ &\times (LM_L 1\mu|L'M_{L'})(2L'+1)^{-1/2}(-\mathrm{i})^{\ell'_j}\exp(\mathrm{i}\sigma_{\ell'_j})Y_{\ell'_j m_{\ell'_j}}(\theta_k,\phi_k)\\ &\times \langle\alpha'_j L'_j S'_j \ell'_j L'S'||D||\alpha_i LS\rangle\delta_{SS'}\delta_{M_S M_{S'}}. \end{aligned}\tag{8.40}$$

We now substitute this expression into the equations for the differential cross section for photoionization of an unpolarized atom or ion by a polarized photon beam. These equations are obtained from (8.21) and (8.22) by averaging over the initial magnetic quantum numbers and summing over the final magnetic quantum numbers yielding

$$\frac{\mathrm{d}\sigma_{ij}^{V,L}}{\mathrm{d}\Omega} = \frac{A_{V,L}}{(2L+1)(2S+1)}\sum_{M_L M_S}\sum_{M_{L'}M_{S'}}\sum_{m'_j}\left|\langle\Psi_{jE}^{-}|D_\mu|\Psi_{iB}\rangle\right|^2, \tag{8.41}$$

where the coefficients A_V and A_L are defined by

$$A_V = \frac{4\pi^2\alpha a_0^2}{\omega}, \quad A_L = 4\pi^2\alpha a_0^2\omega. \tag{8.42}$$

Finally, we substitute (8.40) into (8.41) and carry out the summations over the magnetic quantum numbers using angular momentum algebra techniques discussed in Appendix D.4. We obtain

$$\frac{\mathrm{d}\sigma_{ij}^{V,L}}{\mathrm{d}\Omega} = \frac{A_{V,L}}{4\pi(2L+1)}\sum_{\ell}A_\ell(\mu)P_\ell(\cos\theta_k), \tag{8.43}$$

where

$$\begin{aligned}A_\ell(\mu) = &\sum_{L'L''\ell'_j\ell''_j}(-1)^{L+L'_j+\mu}\exp(-\mathrm{i}\sigma_{\ell'_j}+\mathrm{i}\sigma_{\ell''_j})\left[(2\ell'_j+1)(2\ell''_j+1)\right]^{1/2}\\ &\times\left[(2L'+1)(2L''+1)\right]^{1/2}(1{-}\mu1\mu|\ell0)(\ell'_j0\ell''_j0|\ell0)\\ &\times W(L'\ell'_jL''\ell''_j;L'_j\ell)W(1L'1L'';L\ell)\\ &\times\langle\alpha'_jL'_jS'_j\ell'_jL'S||D||\alpha_iLS\rangle^*\langle\alpha'_jL'_jS'_j\ell''_jL''S||D||\alpha_iLS\rangle. \end{aligned}\tag{8.44}$$

For incident photons linearly polarized in the z-direction in Fig. 8.1, it follows from (8.39) that $\mu = 0$. The Clebsch–Gordan coefficient $(1{-}\mu1\mu|\ell0)$ in (8.44) then has

only two values, $(1010|\ell 0) = 1$ when $\ell = 0$ or 2 and $(1010|\ell 0) = 0$ when $\ell = 1$. It follows that we can write the differential photoionization cross section as

$$\frac{\mathrm{d}\sigma_{ij}^{V,L}}{\mathrm{d}\Omega} = \frac{\sigma_{ij}^{V,L}}{4\pi}\left(1 + \beta_{ij}^{V,L} P_2(\cos\theta_k)\right), \tag{8.45}$$

where $\sigma_{ij}^{V,L}$ is the integrated, or total, photoionization cross section and $\beta_{ij}^{V,L}$ is called the asymmetry parameter. From (8.43) and (8.45) we obtain the following expression for the total cross section:

$$\sigma_{ij}^{V,L} = \frac{A_{V,L}}{(2L+1)} A_0(0). \tag{8.46}$$

After substituting the values of the Clebsch–Gordan and Racah coefficients, defined in Appendices A.1 and A.2, respectively, into (8.44) we find that

$$\sigma_{ij}^{V,L} = \frac{A_{V,L}}{3(2L+1)} \sum_{\ell'_j L'} \left|\langle \alpha'_j L'_j S'_j \ell'_j L' S || D || \alpha_i L S\rangle\right|^2. \tag{8.47}$$

Also, from (8.45), the asymmetry parameter is given by

$$\sigma_{ij}^{V,L}\beta_{ij}^{V,L} = \frac{A_{V,L}}{(2L+1)} A_2(0). \tag{8.48}$$

Again substituting for $A_2(0)$ from (8.44) gives

$$\begin{aligned}\sigma_{ij}^{V,L}\beta_{ij}^{V,L} = \frac{A_{V,L}}{(2L+1)}\left(\frac{2}{3}\right)^{1/2} & \sum_{L' L'' \ell'_j \ell''_j} (-1)^{L+L'_j} \exp(-\mathrm{i}\sigma_{\ell'_j} + \mathrm{i}\sigma_{\ell''_j}) \\ & \times \left[(2\ell'_j+1)(2\ell''_j+1)(2L'+1)(2L''+1)\right]^{1/2} \\ & \times (\ell'_j 0 \ell''_j 0 | 20) W(L' \ell'_j L'' \ell''_j; L'_j 2) W(1L'1L''; L2) \\ & \times \langle \alpha'_j L'_j S'_j \ell'_j L' S || D || \alpha_i L S\rangle^* \langle \alpha'_j L'_j S'_j \ell''_j L'' S || D || \alpha_i L S\rangle. \end{aligned} \tag{8.49}$$

The general form of (8.45) follows from invariance arguments discussed by Yang [983]. These are first that only one direction in space is defined by the photon polarization direction, second it follows from parity conservation that only final states of one parity are present, and hence interference effects between even and odd parities do not occur, and finally since photon absorption takes place through an electric dipole operator the summation over ℓ in (8.43) is restricted to two values, 0 and 2.

If the photons are unpolarized we can obtain the resultant angular distribution from (8.45) by assuming that the incident beam is composed of an incoherent mixture of two beams linearly polarized at right angles. In this case we obtain

$$\left[\frac{\mathrm{d}\sigma_{ij}^{V,L}}{\mathrm{d}\Omega}\right]_{\mathrm{unpol}} = \frac{\sigma_{ij}^{V,L}}{4\pi}\left(1 - \frac{1}{2}\beta_{ij}^{V,L} P_2(\cos\theta)\right), \tag{8.50}$$

where θ is the azimuthal angle defined relative to the incident photon beam direction x in Fig. 8.1, and $\sigma_{ij}^{V,L}$ and $\beta_{ij}^{V,L}$ are given as before by (8.47) and (8.49), respectively.

The requirement that both differential photoionization cross sections given by (8.45) and (8.50) are positive or zero at all angles implies that the asymmetry parameter satisfies

$$-1 \leq \beta_{ij}^{V,L} \leq 2. \tag{8.51}$$

Further, for photoionization of an atom or ion in an s-state $\beta_{ij}^{V,L} = 2$ at all energies. It follows that the differential photoionization cross section given by (8.50) vanishes in the incident photon propagation direction, a result which follows from angular momentum conservation considerations.

8.1.2 R-Matrix Theory

In this section we extend multichannel R-matrix theory, introduced in Chap. 5, to calculate atomic photoionization cross sections using the approach first developed by Burke and Taylor [168]. In the previous section we showed that the integrated photoionization cross section and the asymmetry parameter, defined by (8.47) and (8.49), respectively, can both be expressed in terms of reduced matrix elements which contain all the information on the detailed structure of the target atom or ion. These reduced matrix elements depend on the initial bound-state and final continuum-state wave functions Ψ_{iB}^{Γ} and $\Psi_{jE}^{\Gamma'-}$ through (8.38). Our objective in this section is to show how R-matrix theory can be used to accurately calculate these wave functions and hence to calculate the reduced matrix elements, asymmetry parameter and cross sections.

8.1.2.1 Final Continuum-State Wave Function

Both the initial bound-state wave function Ψ_{iB}^{Γ}, defined by (8.36), and the final continuum-state wave function $\Psi_{jE}^{\Gamma'-}$, defined by (8.35), are solutions of the time-independent Schrödinger equation

$$H_{N+1}\Psi = E\Psi, \tag{8.52}$$

where H_{N+1} is the $(N+1)$-electron non-relativistic Hamiltonian in the absence of the photon field, defined by (5.3).

We consider first the calculation of the final continuum-state wave function $\Psi_{jE}^{\Gamma'-}$ for all Γ' coupled to the initial state Ψ_{iB}^{Γ} by the electric dipole operator in (8.21) or (8.22). Following our discussion in Sect. 5.1 we consider in turn the calculation of this wave function in the internal, external and asymptotic regions illustrated in Fig. 5.1, where for notational simplicity we do not give explicitly the ranges of the variables in this section.

In the internal region, $0 \le r \le a_0$, the final continuum-state wave function is expanded, following (5.5), as

$$\Psi_{jE}^{\Gamma'-}(\mathbf{X}_{N+1}) = \sum_k \psi_k^{\Gamma'}(\mathbf{X}_{N+1}) A_{kj}^{\Gamma'-}(E), \tag{8.53}$$

where the R-matrix basis functions $\psi_k^{\Gamma'}$ are defined by (5.6) and (5.7) with Γ replaced by Γ'. Following our discussion in Sect. 5.1.2, the Schrödinger equation (8.52) can be rewritten for each Γ' as

$$(H_{N+1} + \mathcal{L}_{N+1} - E)\, \Psi_{jE}^{\Gamma'-} = \mathcal{L}_{N+1} \Psi_{jE}^{\Gamma'-}, \tag{8.54}$$

where $\mathcal{L}_{N+1}$ is the Bloch operator defined by (5.8) which ensures that $H_{N+1} + \mathcal{L}_{N+1}$ is hermitian in the internal region. Equation (8.54) has the formal solution

$$\Psi_{jE}^{\Gamma'-} = (H_{N+1} + \mathcal{L}_{N+1} - E)^{-1}\, \mathcal{L}_{N+1} \Psi_{jE}^{\Gamma'-}, \tag{8.55}$$

where the Green's function $(H_{N+1} + \mathcal{L}_{N+1} - E)^{-1}$ in this equation can be expanded in terms of the R-matrix basis functions $\psi_k^{\Gamma'}$. Following (5.17), we find that the final continuum-state wave function can be expanded in the internal region as follows:

$$|\Psi_{jE}^{\Gamma'-}\rangle = \sum_k |\psi_k^{\Gamma'}\rangle \frac{1}{E_k^{\Gamma'} - E} \langle \psi_k^{\Gamma'} | \mathcal{L}_{N+1} | \Psi_{jE}^{\Gamma'-} \rangle. \tag{8.56}$$

Projecting (8.56) onto the channel functions $\overline{\Phi}_i^{\Gamma'}(\mathbf{X}_N; \hat{\mathbf{r}}_{N+1}\sigma_{N+1})$ defined by (2.59), which we assume are n' in number, and evaluating it on the boundary $r_{N+1} = a_0$ of the internal region give

$$u_{ij}^{\Gamma'-}(a_0) = \sum_{i'} R_{ii'}^{\Gamma'}(E) \left(a_0 \frac{\mathrm{d}u_{i'j}^{\Gamma'-}}{\mathrm{d}r} - b_0 u_{i'j}^{\Gamma'-} \right)_{r=a_0}, \tag{8.57}$$

where the elements of the R-matrix $R_{ii'}^{\Gamma'}(E)$ at $r = a_0$ are defined by

$$R_{ii'}^{\Gamma'}(E) = \frac{1}{2a_0} \sum_k \frac{w_{ik}^{\Gamma'} w_{i'k}^{\Gamma'}}{E_k^{\Gamma'} - E}, \tag{8.58}$$

and where, if necessary, a Buttle correction is added to the R-matrix as discussed in Sect. 5.3.2. The reduced radial wave functions $u_{ij}^{\Gamma'-}(r)$, which we introduced in (8.35), are then defined on the boundary of the internal region by

$$u_{ij}^{\Gamma'-}(a_0) = \langle r_{N+1}^{-1} \overline{\Phi}_i^{\Gamma'} | \Psi_{jE}^{\Gamma'-} \rangle'_{r_{N+1}=a_0} = \sum_{i'k} u_{ii'}^0(a_0) a_{ii'k}^{\Gamma'} A_{kj}^{\Gamma'-}(E), \tag{8.59}$$

and the surface amplitudes $w_{ik}^{\Gamma'}$ are defined by

$$w_{ik}^{\Gamma'} = \langle r_{N+1}^{-1} \overline{\Phi}_i^{\Gamma'} | \psi_k^{\Gamma'} \rangle'_{r_{N+1}=a_0} = \sum_{i'} u_{ii'}^0(a_0) a_{ii'k}^{\Gamma'}. \tag{8.60}$$

Also, the coefficients $a_{ii'k}^{\Gamma'}$ in (8.59) and (8.60) are determined by diagonalizing the operator $H_{N+1} + \mathcal{L}_{N+1}$ in the basis $\psi_k^{\Gamma'}$ defined by (5.6) where, as in (5.20) and (5.21), the primes on the Dirac brackets in (8.59) and (8.60) mean that the integrations are carried out over all the electronic space and spin coordinates of the $N + 1$ electrons, except the radial coordinate r_{N+1} of the ejected electron, which is set equal to the radius a_0 of the internal region. We can determine the final continuum-state wave function in the internal region, defined by (8.53), by comparing this equation with (8.56) which yields the following expression for the expansion coefficients $A_{kj}^{\Gamma'-}(E)$ in (8.53):

$$A_{kj}^{\Gamma'-}(E) = \frac{1}{E_k^{\Gamma'} - E} \langle \psi_k^{\Gamma'} | \mathcal{L}_{N+1} | \Psi_{jE}^{\Gamma'-} \rangle. \tag{8.61}$$

Substituting the definition of $\psi_k^{\Gamma'}$ given by (5.6) and the explicit form of the Bloch operator $\mathcal{L}_{N+1}$ given by (5.8) into (8.61), then yields

$$A_{kj}^{\Gamma'-}(E) = \frac{1}{2a_0(E_k^{\Gamma'} - E)} \sum_i w_{ik}^{\Gamma'} \left(a_0 \frac{\mathrm{d}u_{ij}^{\Gamma'-}}{\mathrm{d}r} - b_0 u_{ij}^{\Gamma'-}(r) \right)_{r=a_0}. \tag{8.62}$$

It follows from (8.62) that in order to determine the expansion coefficients $A_{kj}^{\Gamma'-}$, and hence the final continuum-state wave function $\Psi_{jE}^{\Gamma'-}$ in the internal region, defined by (8.53), we need to know the values of the reduced radial wave functions $u_{ij}^{\Gamma'-}$ and their derivatives on the boundary $r = a_0$ of the internal region. These quantities are determined by solving the Schrödinger equation (8.52) in the external and asymptotic regions.

We choose the radius a_0 of the internal region, as in Sect. 5.1.3, so that electron exchange and correlation effects between the ejected photoelectron and the residual atom or ion can be neglected for $r \geq a_0$. Hence in the external and asymptotic regions the expansion of the final continuum-state wave function defined by (8.35) reduces to

$$\Psi_{jE}^{\Gamma'-}(\mathbf{X}_{N+1}) = \sum_i \overline{\Phi}_i^{\Gamma'}(\mathbf{X}_N; \hat{\mathbf{r}}_{N+1}\sigma_{N+1}) r_{N+1}^{-1} u_{ij}^{\Gamma'-}(r_{N+1}), \quad r_{N+1} \geq a_0. \tag{8.63}$$

Following our discussion in Sect. 5.1.3 we then find that the reduced radial wave functions $u_{ij}^{\Gamma'-}(r)$ satisfy the coupled second-order differential equations

$$\left(\frac{\mathrm{d}^2}{\mathrm{d}r^2} - \frac{\ell_i(\ell_i+1)}{r^2} + \frac{2(Z-N)}{r} + k_i^2\right) u_{ij}(r) = 2\sum_{i'} V_{ii'}(r) u_{i'j}(r), \quad r \geq a_0. \tag{8.64}$$

The potential matrix $V_{ii'}(r)$ in this equation can be written as a summation in inverse powers of r given by (5.30). We also note that in (8.64) and in our later analysis we have omitted the superscripts on $u_{ij}(r)$ and $V_{ii'}(r)$ for notational convenience.

In order to solve (8.64) to obtain the continuum-state wave function for $r \geq a_0$ we can proceed, as discussed in Sects. 5.1.3 and 5.1.4, by first propagating the R-matrix, defined at $r = a_0$ by (8.58), outwards from $r = a_0$ to a_p, using one of the propagator methods discussed in Appendix E. For example, if the Light–Walker propagator method is used then we would propagate the R-matrix using (E.27). We then determine $n' + n'_a$ solutions $\mathbf{s}(r)$ and $\mathbf{c}(r)$ in the asymptotic region $a_p \leq r < \infty$ satisfying the boundary conditions (5.37), as discussed in Appendix F.1, where n'_a is the number of channels above threshold at the energy under consideration. By taking linear combinations of these $n' + n'_a$ solutions we obtain an $n' \times n'_a$-dimensional solution matrix satisfying the boundary conditions (8.32), which we can rewrite in terms of $\mathbf{s}(r)$ and $\mathbf{c}(r)$ as follows:

$$\mathbf{u}(r) = \left(\frac{2}{\pi}\right)^{1/2} [\mathbf{s}(r) + \mathbf{c}(r)\mathbf{N}] (\mathbf{I} + \mathrm{i}\mathbf{K})^{-1}, \quad r \geq a_p, \tag{8.65}$$

where the $n' \times n'_a$-dimensional matrix $\mathbf{N}$, which is defined in terms of the K-matrix and the subsidiary L-matrix by (5.43), is determined by fitting this solution matrix to the R-matrix boundary conditions (8.57) at $r = a_p$. Finally, in order to determine the solution matrix satisfying the asymptotic boundary conditions (8.65) in the region $a_0 \leq r \leq a_p$, we propagate the solution inwards from $r = a_p$ to a_0 using one of the propagators discussed in Appendix E. For example, if the Light–Walker propagator method is used then we would propagate the solution using (E.30).

Having calculated the solution matrix $\mathbf{u}(r)$ and hence its derivative at $r = a_0$, we can determine the expansion coefficients $A_{kj}^{\Gamma'-}(E)$ given by (8.62), and the final

continuum-state wave function in the internal region $\Psi_{jE}^{\Gamma'-}$ given by (8.53). Hence we have shown how the final continuum-state wave function $\Psi_{jE}^{\Gamma'-}$ can be accurately calculated in the internal, external and asymptotic regions.

8.1.2.2 Initial Bound-State Wave Function

We now consider the calculation of the initial bound-state wave function Ψ_{iB}^{Γ} defined by (8.36). This wave function is also a solution of the time-independent Schrödinger equation (8.52) belonging to the bound-state eigenenergy E_{iB}^{Γ}. It follows that as well as calculating this wave function we must also determine the corresponding eigenenergy. The approach described here for calculating bound-state wave functions and eigenenergies using the R-matrix method differs from that used by Seaton [860] and Berrington and Seaton [92] in that a propagator method is used to determine the solution in the external region rather than a perturbation method.

In the internal region, $0 \leq r \leq a_0$ the initial bound-state wave function is expanded, following (5.5), as

$$\Psi_{iB}^{\Gamma}(\mathbf{X}_{N+1}) = \sum_k \psi_k^{\Gamma}(\mathbf{X}_{N+1}) A_{ki}^{\Gamma}(E_{iB}), \tag{8.66}$$

where the R-matrix basis functions ψ_k^{Γ} are defined by (5.6) and (5.7) and where E_{iB}^{Γ}, the initial bound-state eigenenergy, is determined by an iterative procedure discussed below. Following our procedure for determining the final continuum-state wave function, we rewrite the Schrödinger equation describing the bound state in the same form as (8.54), that is, as

$$\left(H_{N+1} + \mathcal{L}_{N+1} - E_{iB}^{\Gamma}\right) \Psi_{iB}^{\Gamma} = \mathcal{L}_{N+1} \Psi_{iB}^{\Gamma}. \tag{8.67}$$

We then observe that (8.67) has a formal solution analogous to (8.55), where the Green's function $\left(H_{N+1} + \mathcal{L}_{N+1} - E_{iB}^{\Gamma}\right)^{-1}$ is expanded in terms of the R-matrix basis functions ψ_k^{Γ}. Hence we find that the initial bound-state wave function can be expanded in the internal region as follows:

$$|\Psi_{iB}^{\Gamma}\rangle = \sum_k |\psi_k^{\Gamma}\rangle \frac{1}{E_k^{\Gamma} - E_{iB}^{\Gamma}} \langle \psi_k^{\Gamma} | \mathcal{L}_{N+1} | \Psi_{iB}^{\Gamma} \rangle. \tag{8.68}$$

Projecting (8.68) onto the channel functions $\overline{\Phi}_j^{\Gamma}(\mathbf{X}_N; \hat{\mathbf{r}}_{N+1}\sigma_{N+1})$ defined by (2.59), which we assume are n in number, and evaluating it on the boundary $r_{N+1} = a_0$ of the internal region then gives

$$v_{ji}^{\Gamma}(a_0) = \sum_{j'} R_{jj'}^{\Gamma}(E) \left(a_0 \frac{\mathrm{d}v_{j'i}^{\Gamma}}{\mathrm{d}r} - b_0 v_{j'i}^{\Gamma} \right)_{r=a_0}, \tag{8.69}$$

where the elements of the R-matrix $R^{\Gamma}_{jj'}(E)$ at $r = a_0$ are defined by

$$R^{\Gamma}_{jj'}(E) = \frac{1}{2a_0} \sum_k \frac{w^{\Gamma}_{jk} w^{\Gamma}_{j'k}}{E^{\Gamma}_k - E}, \tag{8.70}$$

and where, if necessary, a Buttle correction is added to the R-matrix, as discussed in Sect. 5.3.2. The reduced radial wave functions $v^{\Gamma}_{ji}(r)$, which we introduced in (8.36), are then defined on the boundary $r = a_0$ of the internal region by

$$v^{\Gamma}_{ji}(a_0) = \left\langle r^{-1}_{N+1} \overline{\Phi}^{\Gamma}_j \,|\Psi^{\Gamma}_{iB}\right\rangle_{r_{N+1}=a_0} = \sum_{i'k} u^0_{ji'}(a_0) a^{\Gamma}_{ji'k} A^{\Gamma}_{ki}(E^{\Gamma}_{iB}), \tag{8.71}$$

and the surface amplitudes w^{Γ}_{jk} are defined by

$$w^{\Gamma}_{jk} = \left\langle r^{-1}_{N+1} \overline{\Phi}^{\Gamma}_j \,|\psi^{\Gamma}_k\right\rangle'_{r_{N+1}=a_0} = \sum_i u^0_{ji}(a_0) a^{\Gamma}_{jik}. \tag{8.72}$$

We can determine the initial bound-state wave function Ψ^{Γ}_{iB} in the internal region, defined by (8.66), by comparing this equation with (8.68) which yields the following expression for the expansion coefficients $A^{\Gamma}_{ki}(E^{\Gamma}_{iB})$:

$$A^{\Gamma}_{ki}(E^{\Gamma}_{iB}) = \frac{1}{2a_0(E^{\Gamma}_k - E^{\Gamma}_{iB})} \sum_j w^{\Gamma}_{jk} \left(a_0 \frac{\mathrm{d}v^{\Gamma}_{ji}}{\mathrm{d}r} - b_0 v^{\Gamma}_{ji} \right)_{r=a_0}. \tag{8.73}$$

It follows from (8.73) that in order to determine the expansion coefficients $A^{\Gamma}_{ki}(E^{\Gamma}_{iB})$, and hence the initial bound-state wave function Ψ^{Γ}_{iB} in the internal region, we need to know the reduced radial wave functions v^{Γ}_{ji} and their derivatives on the boundary $r = a_0$ of the internal region. These quantities are determined by solving the Schrödinger equation (8.52) in the external and asymptotic regions.

In the external region $a_0 \le r \le a_p$ the reduced radial wave functions v^{Γ}_{ji} satisfy the coupled second-order differential equations (8.64) corresponding to the conserved quantum numbers Γ. The solutions of these coupled equations are obtained by propagating the R-matrix, defined at $r = a_0$ by (8.70), outwards from $r = a_0$ to a_p across the p sub-regions in the external region, defined in Fig. 5.1, using one of the propagators discussed in Appendix E. This yields the R-matrix $\mathbf{R}^{\Gamma}_p$ at $r = a_p$.

In the asymptotic region $r \ge a_p$, the reduced radial wave functions v^{Γ}_{ji} satisfy the asymptotic boundary conditions given by (8.37). Hence the number of linearly independent asymptotic solutions of (8.64) in this region is n since the number of open channels $n_a = 0$. These solutions can be determined as described in Appendix F.1 for $a_p \le r \le \infty$. We define these solutions here by asymptotic boundary conditions which vanish exponentially at infinity according to

$$e_{ij}(r) \underset{r\to\infty}{\sim} \exp(-\phi_i)\delta_{ij}, \quad i,\ j = 1,\ldots,n, \tag{8.74}$$

where ϕ_i is defined by (F.19). Hence the required bound-state solution of (8.64) can be written as a linear combination of these n linearly independent solutions as follows:

$$v_j^{\Gamma}(r) = \sum_{k=1}^{n} e_{jk}(r)c_k, \quad j = 1,\ldots,n, \quad a_p \le r \le \infty. \tag{8.75}$$

In order to determine the expansion coefficients $c_k,\ k = 1,\ldots,n$, we substitute (8.75) into the equation defining the R-matrix at $r = a_p$ yielding

$$\mathbf{e}(a_p)\,\mathbf{c} = a_p \mathbf{R}_p^{\Gamma} \mathbf{e}'(a_p)\,\mathbf{c}, \tag{8.76}$$

where $\mathbf{e}'(a_p) = (\mathrm{d}\mathbf{e}/\mathrm{d}r)_{r=a_p}$ and where we have set the arbitrary constant b_0 in the definition of the R-matrix to zero. Also in (8.76), $\mathbf{e}(a_p)$, $\mathbf{e}'(a_p)$ and $\mathbf{R}_p^{\Gamma}$ are $n \times n$-dimensional matrices and $\mathbf{c}$ is an n-dimensional vector with components c_k. Equation (8.76) corresponds to a set of n homogeneous coupled linear simultaneous equations for the n unknown expansion coefficients $c_k,\ k = 1,\ldots,n$. In general these equations will only have a non-trivial solution when the energy E_{iB}^{Γ} adopted corresponds to a bound-state eigenenergy of the original Schrödinger equation. Hence finding non-trivial solutions of (8.76) provides a procedure for calculating the bound-state eigenenergies and the corresponding eigensolutions of the Schrödinger equation.

In order to show how (8.76) may be used to determine the bound-state eigenenergies, we rewrite this equation in the form

$$\sum_{j=1}^{n} a_{ij}(E)c_j = 0, \quad i = 1,\ldots,n, \tag{8.77}$$

where the coefficients $a_{ij}(E)$ are functions of a trial energy E assumed for E_{iB}^{Γ}. As discussed above, these coefficients are determined by solving the problem in the internal, external and asymptotic regions for the trial energy E. We now set one of the c_j, say c_1, in (8.77) equal to 1 and rewrite the last $n-1$ equations as follows:

$$\sum_{j=2}^{n} a_{ij}(E)c_j = -a_{i1}, \quad i = 2,\ldots,n. \tag{8.78}$$

These are $n-1$ linear simultaneous equations in $n-1$ unknowns which can be solved for the coefficients $c_j,\ j = 2,\ldots,n$. We then rewrite the discrepancy of the first equation in (8.77) as

$$d(E) = \sum_{j=2}^{n} a_{1j}(E) c_j + a_{11}(E). \tag{8.79}$$

When $d(E) = 0$, then it is clear that (8.77) has a non-trivial solution and the corresponding energy E is a bound-state eigenenergy E_{iB}^{Γ} of the Schrödinger equation. The problem of determining the eigenenergies E_{iB}^{Γ} thus reduces to finding the zeros of the discrepancy function $d(E)$. This can be achieved by solving the coupled differential equations (8.64) in the external and asymptotic regions as described above for a series of values of the energy E, and determining the zeros of the discrepancy function $d(E)$ using a standard method, such as the Newton–Raphson method [143, 757]. It is important to note that in this iterative procedure, the solution in the internal region does not have to be repeated for each energy, since the R-matrix defined by (8.70) on the boundary $r = a_0$ is obtained at all the required energies E by a single diagonalization of the Hamiltonian in the internal region.

Having obtained the bound-state eigenenergies E_{iB}^{Γ} of interest and the coefficients c_k, $k = 1, \ldots, n$, then the corresponding eigensolutions can be calculated in the asymptotic region using (8.75). In order to calculate the eigensolution in the external region, we propagate the solution inwards from $r = a_p$ to a_0 across the p sub-regions using one of the propagators discussed in Appendix E. The expansion coefficients $A_{ki}^{\Gamma}(E_{iB}^{\Gamma})$ defined by (8.73) can then be calculated given the eigensolution and its derivative at $r = a_0$. Hence the eigensolution in the internal region can be determined using (8.66). The initial bound-state wave function Ψ_{iB}^{Γ} has thus been calculated in the internal, external and asymptotic regions up to an overall normalization factor. This factor can be determined by requiring that the bound-state wave function satisfies (8.7). Having determined both the initial bound-state wave function and the final continuum-state wave function, the dipole velocity and dipole length reduced matrix elements, defined by (8.38), can then be calculated. The photoionization cross section and asymmetry parameter are then obtained immediately from (8.47) and (8.49), respectively.

If we are considering photoionization from the target ground state or from a low-lying excited state, then the above procedure can often be simplified due to the short-range nature of this state. The charge distribution of the initial bound state is then usually contained within the internal region radius a_0, which has been chosen, as discussed in Sect. 5.1, to contain the charge distribution of the residual ion states retained in expansions (8.35) and (8.36). In this case there is no contribution to the reduced matrix elements coming from the integral over the wave functions in the external and asymptotic regions. The calculation of the initial bound-state and the final continuum-state wave functions in the external and asymptotic regions is then not required. However, the continuum-state wave function will still have to satisfy the ingoing wave asymptotic boundary condition defined by (8.32) and (8.65), which will require propagating the corresponding

R-matrix out to the boundary $r = a_p$ and fitting to the appropriate asymptotic expansion.

On the other hand, if the initial bound state is a highly excited Rydberg state or a weakly bound negative ion state then a substantial contribution to the reduced matrix elements comes from the integral over the bound-state and continuum-state wave functions in the external and asymptotic regions. The above general theory which describes the calculation of these wave functions in the external and asymptotic regions is then required.

8.1.2.3 Calculations Near an R-Matrix Pole

In certain circumstances, the energy of interest can lie near to the energy E_k^{Γ} of an R-matrix pole. This can occur when the photoionization or electron collision calculations are carried out at a very fine energy mesh in order to resolve resonance structure in the cross sections. We have seen that this happens in the collision of electrons with Fe II which has been discussed in Sect. 5.6.5. There is then a high probability that one of these energies will lie very near to an R-matrix pole. Another example of a near coincidence occurs when bound-state eigenenergies and wave functions are calculated which we have discussed earlier in this section. In particular, for highly excited Rydberg states the energy of separation between adjacent bound-state energies for a given symmetry is proportional to n^{-3}, where n is the principal quantum number. As $n \to \infty$ this separation tends to zero and again there is a high probability of a near coincidence.

In both of these examples, expressions for quantities such as the K-matrix and S-matrix in electron–ion collision calculations and for bound-state eigenenergies and wave functions in bound-state calculations become indeterminate at energies which are equal to the R-matrix pole energy E_k^{Γ}. In this section we will show that determinate expressions can be obtained using a diagonalization procedure introduced by Burke and Seaton [169]. An alternative procedure for calculating physical quantities at energies near poles in the R-matrix has been described by Mil'nikov and Nakamura [652].

We consider the R-matrix defined by (5.19), which is determined on the boundary $r = a_0$ of the internal region. We write this equation in matrix notation as

$$\mathbf{R}(E) = \sum_k \frac{\boldsymbol{\gamma}_k \boldsymbol{\gamma}_k^{\mathrm{T}}}{E_k - E}, \tag{8.80}$$

where we assume there are n coupled channels, so that $\mathbf{R}(E)$ is an $n \times n$-dimensional matrix and where in this equation and later equations in this section we have omitted the superscript Γ for notational convenience. Also in (8.80), $\boldsymbol{\gamma}_k$ is an n-dimensional column vector whose elements are given in terms of the surface amplitudes w_{ik} by

$$\gamma_{ki} = \left(\frac{1}{2a_0}\right)^{1/2} w_{ik}, \tag{8.81}$$

where the w_{ik} are defined by (5.21). The reduced radial wave function is then related to its derivative on the boundary $r = a_0$ by (5.18) which we rewrite here in matrix notation as

$$\mathbf{F}(a_0) = \mathbf{R}(E)\mathbf{F}'(a_0), \tag{8.82}$$

where

$$\mathbf{F}'(a_0) = \left(a_0 \frac{\mathrm{d}\mathbf{F}}{\mathrm{d}r} - b_0\mathbf{F}\right)_{r=a_0}. \tag{8.83}$$

We now consider energies E close to an isolated R-matrix pole which we can assume without loss of generality to be E_1. Equation (8.80) can then be rewritten as

$$\mathbf{R}(E) = \frac{\mathbf{P}}{E_1 - E} + \mathbf{Q}(E), \tag{8.84}$$

where

$$\mathbf{P} = \boldsymbol{\gamma}_1 \boldsymbol{\gamma}_1^{\mathrm{T}} \tag{8.85}$$

and

$$\mathbf{Q}(E) = \sum_{k=2}^{\infty} \frac{\boldsymbol{\gamma}_k \boldsymbol{\gamma}_k^{\mathrm{T}}}{E_k - E}. \tag{8.86}$$

It follows that $\mathbf{Q}(E)$ is regular in the neighbourhood of $E = E_1$.

As an example of the difficulty that arises when E is near E_1, we consider first the calculation of the K-matrix described in Sect. 5.1.4. For illustrative purposes, we assume that there are n_a open channels for energies in the neighbourhood of E_1 and hence it follows from (5.37) that there are $n + n_a$ linearly independent asymptotic solutions. Also we assume that these solutions can be accurately determined on the boundary $r = a_0$ of the internal region and can thus be substituted directly into (8.82). We now proceed using the approach adopted in Sect. 5.1.4 which led to (5.46). We remember that the solution matrix

$$\mathbf{F}(r) = \mathbf{s}(r) + \mathbf{c}(r)\mathbf{N}, \quad r \geq a_0, \tag{8.87}$$

where $\mathbf{s}(r)$ and $\mathbf{c}(r)$ are linearly independent solutions of the coupled second-order differential equations (5.29) satisfying the asymptotic boundary conditions (5.37) and where $\mathbf{N}$ is an $n \times n_a$-dimensional matrix, defined by (5.43), which involves the open-channel K-matrix. We then find after substituting (8.87) into (8.82) that on the boundary $r = a_0$

$$\left[\mathbf{c}(a_0) - \mathbf{R}(E)\mathbf{c}'(a_0)\right]\mathbf{N} = -\mathbf{s}(a_0) + \mathbf{R}(E)\mathbf{s}'(a_0), \tag{8.88}$$

where, following (8.83), we have defined

$$\mathbf{s}'(a_0) = \left(a_0 \frac{\mathrm{d}\mathbf{s}}{\mathrm{d}r} - b_0 \mathbf{s}\right)_{r=a_0} \tag{8.89}$$

and

$$\mathbf{c}'(a_0) = \left(a_0 \frac{\mathrm{d}\mathbf{c}}{\mathrm{d}r} - b_0 \mathbf{c}\right)_{r=a_0}. \tag{8.90}$$

Substituting for $\mathbf{R}(E)$ from (8.84) into (8.88) then yields

$$\begin{aligned}\mathbf{N} = &\left[\mathbf{c}(a_0) - \mathbf{Q}(E)\mathbf{c}'(a_0) - (E_1 - E)^{-1}\mathbf{P}\mathbf{c}'(a_0)\right]^{-1} \\ &\times \left[-\mathbf{s}(a_0) + \mathbf{Q}(E)\mathbf{s}'(a_0) + (E_1 - E)^{-1}\mathbf{P}\mathbf{s}'(a_0)\right].\end{aligned} \tag{8.91}$$

Since in general $\mathbf{c}(a_0)$, $\mathbf{s}(a_0)$, $\mathbf{c}'(a_0)$ and $\mathbf{s}'(a_0)$ are regular functions of E in the neighbourhood of E_1, then if $|E_1 - E|$ is very small (8.91) reduces to

$$\mathbf{N} \approx -\left[\mathbf{P}\mathbf{c}'(a_0)\right]^{-1}\left[\mathbf{P}\mathbf{s}'(a_0)\right]. \tag{8.92}$$

It follows from (8.85) that $\det \mathbf{P} = 0$ and hence $[\mathbf{P}\mathbf{c}'(a_0)]^{-1}$ in (8.92) is singular. Consequently expression (8.91) for $\mathbf{N}$ and hence for the K-matrix becomes indeterminate as $E \to E_1$. Our problem is therefore to define $\mathbf{N}$ at $E = E_1$ and hence to obtain an accurate and stable method for computing the K-matrix when $|E_1 - E|$ is small.

We solve this problem by introducing a real orthogonal $n \times n$-dimensional matrix $\mathbf{U}$ which diagonalizes $\mathbf{P}$ according to

$$\mathbf{U}^{\mathrm{T}}\mathbf{P}\mathbf{U} = \mathbf{D}, \tag{8.93}$$

where $\mathbf{D}$ is a diagonal matrix. However, (8.93) does not define $\mathbf{U}$ uniquely. We therefore proceed as follows. We choose the first column of $\mathbf{U}$ to be a unit vector proportional to the vector $\boldsymbol{\gamma}_1$ so that

$$U_{i1} = \gamma_{i1}\Gamma^{-1}, \tag{8.94}$$

where

$$\Gamma = \left(\sum_{i=1}^{n} \gamma_{i1}^2\right)^{1/2}. \tag{8.95}$$

We then choose the remaining $n - 1$ columns of $\mathbf{U}$ to span the $(n - 1)$-dimensional space orthogonal to $\boldsymbol{\gamma}_1$, and to be mutually orthonormal so that $\mathbf{U}$ is orthogonal and

satisfies

$$\sum_{i=1}^{n} U_{ij}U_{ik} = \delta_{jk}, \quad j,\ k = 1, \ldots, n. \tag{8.96}$$

It follows that the matrix elements of $\mathbf{D}$ are

$$D_{ij} = \Gamma^2 \delta_{i1}\delta_{j1}, \quad i,\ j = 1, \ldots, n. \tag{8.97}$$

We note that any orthonormal choice of vectors for the last $n-1$ columns of $\mathbf{U}$ spanning the $(n-1)$-dimensional space orthogonal to $\boldsymbol{\gamma}_1$ would yield (8.97). However, the following discussion does not depend on this choice.

We now define

$$x = E_1 - E, \tag{8.98}$$

and we use (8.84) to rewrite (8.88) as

$$\left[\mathbf{c}(a_0) - \mathbf{Q}(E)\mathbf{c}'(a_0) - x^{-1}\mathbf{P}\mathbf{c}'(a_0)\right]\mathbf{N} = -\mathbf{s}(a_0) + \mathbf{Q}(E)\mathbf{s}'(a_0) + x^{-1}\mathbf{P}\mathbf{s}'(a_0). \tag{8.99}$$

We then premultiply (8.99) by $\mathbf{U}^{\mathrm{T}}$ and use (8.93) to give

$$(\mathbf{a} - x^{-1}\mathbf{D}\mathbf{b})\mathbf{N} = \mathbf{p} + x^{-1}\mathbf{D}\mathbf{q}, \tag{8.100}$$

where we have defined

$$\begin{aligned}
\mathbf{a} &= \mathbf{U}^{\mathrm{T}}\left[\mathbf{c}(a_0) - \mathbf{Q}(E)\mathbf{c}'(a_0)\right], \\
\mathbf{b} &= \mathbf{U}^{\mathrm{T}}\mathbf{c}'(a_0), \\
\mathbf{p} &= \mathbf{U}^{\mathrm{T}}\left[-\mathbf{s}(a_0) + \mathbf{Q}(E)\mathbf{s}'(a_0)\right], \\
\mathbf{q} &= \mathbf{U}^{\mathrm{T}}\mathbf{s}'(a_0).
\end{aligned} \tag{8.101}$$

Multiplying (8.100) by x and writing this equation explicitly in terms of its matrix elements gives, after using (8.97),

$$\sum_{j=1}^{n}\left(xa_{ij} - \Gamma^2\sum_{i'=1}^{n}\delta_{i1}\delta_{i'1}b_{i'j}\right)N_{jk} = xp_{ik} + \Gamma^2\sum_{i'=1}^{n}\delta_{i1}\delta_{i'1}q_{i'k}, \quad i = 1, \ldots, n. \tag{8.102}$$

We see that the term involving Γ^2 on both sides of (8.102) only occurs in the first equation where $i = 1$. We can therefore rewrite these equations as

$$\sum_{j=1}^{n}\left(xa_{1j}-\Gamma^2 b_{1j}\right)N_{jk}=xp_{1k}+\Gamma^2 q_{1k},\quad i=1,$$

$$\sum_{j=1}^{n}a_{ij}N_{jk}=p_{ik},\quad i=2,\ldots,n. \tag{8.103}$$

Equations (8.103) give a unique solution for $\mathbf{N}$, and hence from (5.43) for the K-matrix, for all values of x including the limiting case where $x \to 0$.

This diagonalization procedure can also be extended to obtain determinate results for bound-state eigenenergies and wave functions, where the bound-state eigenenergy E_B lies at or near an R-matrix pole. This can occur when calculating the initial bound-state wave function in photoionization discussed earlier in this section. In this case we have to solve the matching equation (8.76). We rewrite this equation here using the notation defined by (8.83) as

$$\mathbf{e}(a_0)\mathbf{c}=\mathbf{R}(E)\mathbf{e}'(a_0)\mathbf{c}, \tag{8.104}$$

where the functions $\mathbf{e}(r)$ decay exponentially at infinity and where we again assume that the matching can be carried out on the boundary $r = a_0$ of the internal region. Equation (8.104) gives an eigenvalue problem for determining the bound-state eigenenergy. As before, we assume that the energy E is close to an isolated R-matrix pole E_1, so that the R-matrix can be written in the form given by (8.84). Substituting this result into (8.104) and putting $x = E_1 - E$ yields

$$\left[\mathbf{e}(a_0)-\mathbf{Q}(E)\mathbf{e}'(a_0)-x^{-1}\mathbf{P}\mathbf{e}'(a_0)\right]\mathbf{c}=0. \tag{8.105}$$

We then premultiply (8.105) by $\mathbf{U}^{\mathrm{T}}$, defined by (8.93), to give

$$(\mathbf{a}-x^{-1}\mathbf{D}\mathbf{b})\mathbf{c}=0, \tag{8.106}$$

where

$$\begin{aligned}\mathbf{a}&=\mathbf{U}^{\mathrm{T}}\left[\mathbf{e}(a_0)-\mathbf{Q}(E)\mathbf{e}'(a_0)\right],\\ \mathbf{b}&=\mathbf{U}^{\mathrm{T}}\mathbf{e}'(a_0).\end{aligned} \tag{8.107}$$

Multiplying (8.106) by x and writing it explicitly in terms of its matrix elements gives, after using (8.97), the following set of n coupled homogeneous equations for the coefficients c_j, $j = 1, \ldots, n$,

$$\sum_{j=1}^{n} \left(x a_{1j} - \Gamma^2 b_{1j} \right) c_j = 0, \quad i = 1,$$

$$\sum_{j=1}^{n} a_{ij} c_j = 0, \quad i = 2, \ldots, n. \tag{8.108}$$

These equations are well behaved for all values of x, including the limiting case where $x \to 0$. They can be solved using an iterative procedure to yield the bound-state eigenenergy E_B and the coefficients c_j, $j = 1, \ldots, n$, as described earlier in our solution of (8.77).

We now consider the calculation of the bound-state wave function, which is defined in the internal region up to an overall normalization factor by (8.66). Clearly when $x = E_1 - E_B = 0$, where E_B is the bound-state eigenenergy determined as described above, then the expansion coefficient A_{1i} defined by (8.73) is singular. We can remove this singularity by introducing new expansion coefficients B_{ki} which are defined in terms of the A_{ki} by

$$B_{ki} = (E_1 - E_B) A_{ki}. \tag{8.109}$$

The new bound-state wave function, which is defined by

$$\Psi_{iB} = \sum_k \psi_k B_{ki}, \tag{8.110}$$

is then related to the wave function defined by (8.66) by the overall normalization factor $x = E_1 - E_B$ and is well behaved for all values of x, including the limiting case where $x \to 0$. Having obtained a well-behaved bound-state wave function, the final step is to normalize this wave function to unity so that it satisfies (8.7).

We have assumed in the above analysis that the asymptotic region solutions, defined by (5.37), can be matched to the R-matrix on the boundary $r = a_0$ of the internal region. However, if these solutions have not achieved their asymptotic form on this boundary, we would have to solve the coupled second-order differential equations (8.64) corresponding to the initial bound state or the final continuum state to determine the solutions in the external region. This would enable the solutions at $r = a_0$ to be related to the corresponding asymptotic region solutions at $r = a_p$. One way of achieving this is by propagating the R-matrix from $r = a_0$ to a_p across the external region, as discussed in Appendix E. In this case, as well as singularities arising in the matching equations at the R-matrix poles, singularities can also arise in the R-matrix propagation equations. Again, the resultant expression can be made determinate by a modification of the above diagonalization procedure, which transforms the singular term into one of the diagonal elements of the corresponding propagation equations.

In conclusion, we have shown in this section that determinate results can be obtained for the K-matrix, S-matrix and bound-state eigenenergies and wave func-

tions for energies at or near R-matrix poles. However, we observe that this problem has rarely given rise to difficulties in practical calculations. This is because the underlying stability of the matching equations, discussed in this section, implies that the energy of interest can lie very close to an R-matrix pole without significantly affecting the accuracy of the results.

8.2 Photorecombination and Radiation Damping

In this section we commence with a general introduction to the theory of photorecombination and radiation damping in which we summarize early developments and recent advances. We then describe a generalization of R-matrix theory of electron–ion collisions in the presence of a radiation field, which enables photorecombination and radiation damping processes to be calculated.

8.2.1 Introduction

We commence with an introductory survey of photorecombination and radiation damping in electron collisions with highly charged ions. In photorecombination a free electron is accelerated by a charged atomic ion and, as a result, emits a photon of sufficient energy that the electron is captured into an atomic or ionic bound state by the attractive Coulomb field of the ion. This is an important cooling mechanism in hot plasmas and is also used as a plasma diagnostic [895]. In the absence of radiation damping, which we discuss below, the cross section for photorecombination $\sigma_{\rm PR}$ is related to the cross section for photoionization $\sigma_{\rm PI}$ through detailed balance given by the Milne relation (e.g. [709])

$$\sigma_{\rm PR} = \sigma_{\rm PI} \frac{g_i}{g_j} \frac{\alpha^2 E_{\rm ph}^2}{4(E_{\rm ph} - I)}, \tag{8.111}$$

in atomic units. In this equation g_i and g_j are the statistical weights of the initial and residual ions respectively, $E_{\rm ph}$ and I are the photon energy and ionization potential of the final ionic state, respectively, and α is the fine-structure constant.

Photorecombination can proceed non-resonantly through the electron–ion continuum as follows:

$$\mathrm{e}^- + A_i^{n+} \begin{array}{l} \nearrow \; A_j^{n+} + \mathrm{e}^- \\ \searrow \; A_k^{(n-1)+} + \mathrm{h}\nu, \end{array} \tag{8.112}$$

which is called radiative recombination (RR). It can also proceed resonantly through intermediate doubly excited states as follows:

$$\mathrm{e}^- + A_i^{n+} \rightarrow \left(A_l^{(n-1)+}\right)^{**} \begin{array}{l} \nearrow A_j^{n+} + \mathrm{e}^- \\ \searrow A_k^{(n-1)+} + \mathrm{h}\nu, \end{array} \tag{8.113}$$

which is called dielectronic recombination (DR) since two electrons are actively involved in the excitation and decay processes. In both cases, photorecombination occurs in competition with electron–ion scattering, as indicated in (8.112) and (8.113). In addition, the emitted photon can be recaptured by the ion, giving rise to a modification of the electron–ion collision cross section called radiation damping. We also mention that a photon can be emitted leaving behind an electron–ion collision state as follows:

$$\mathrm{e}^- + A_i^{n+} \rightarrow A_j^{n+} + \mathrm{e}^- + \mathrm{h}\nu, \tag{8.114}$$

which again can occur resonantly or non-resonantly. This process is known as free–free scattering or bremsstrahlung.

The DR process was discussed in early work by Massey and Bates [644] and Bates and Massey [74], who were concerned with recombination in plasmas at fairly low temperatures such as occur in the Earth's ionosphere, and this process was investigated further by Bates [73], Bates and Dalgarno [76], Seaton [853] and Burgess and Seaton [150]. Also, Burgess [147, 148] showed that the DR process can be one to two orders of magnitude larger than the RR process at higher temperatures where complete Rydberg series of resonances converging to excited states of the ion contribute to recombination. This work proved to be of crucial importance in resolving a problem concerning the temperature of the solar corona; namely, the temperature deduced from studies of the ionization equilibrium was significantly lower than that deduced from the density gradient of the corona and from the Doppler widths of the spectral lines. A very interesting summary of the historical background to this work, as well as a general review of DR, has been written by Seaton and Storey [864].

It was shown by Davies and Seaton [251] that in order to determine accurate electron–ion collision cross sections, as well as photoionization and photorecombination cross sections, for highly ionized atomic targets, the scattering amplitudes must be modified to include radiation damping where the lifetimes of intermediate resonance states can be strongly affected by the interaction between the radiation field and the scattered and target electrons. In their work on radiation damping, Davies and Seaton adopted an approach analogous to that used by Weisskopf and Wigner [958, 959] who were concerned with radiative transitions between bound states. An R-matrix theory of free–free scattering was also developed by Bell et al. [87]. Later, a general theory of dielectronic recombination including radiative channels and using quantum defect theory was developed by Bell and Seaton [88]. This enabled Rydberg series of resonances converging to excited states of the ion to be treated and was applied by Pradhan and Seaton [754] to determine the effects of radiative decays on collision strengths for electron impact excitation of positive ions.

Also, Sakimoto et al. [806] showed the importance of radiation damping on bound–continuum transitions involving highly ionized ions in the energy range corresponding to low-lying resonances, where they used R-matrix computer programs to solve the resultant electron–ion close coupling equations. R-matrix programs were also used in studies of photorecombination, for example, by Terao and Burke [923] and Nahar and Pradhan [671,672,673].

More recently, Robicheaux et al. [794] developed a non-perturbative approach for including radiation damping in the close coupling equations describing electron–ion collisions, which they showed could be implemented using R-matrix theory and computer programs. Using this approach many detailed photorecombination and radiation damping calculations have been carried out for highly charged ions using extensions of the R-matrix computer program RMATRXI, discussed in Sect. 5.1.1, where relativistic effects were included using the Breit–Pauli Hamiltonian. These calculations included detailed studies by Gorczyca et al. [397, 399, 400], Gorczyca and Badnell [392, 393], Badnell et al. [36] and Whiteford et al. [963], where we note that Gorczyca et al. [400] found that fundamental difficulties arose in the calculation of DR which overestimated the rate near the series limit. Also, independent R-matrix calculations of photorecombination and radiation damping have been carried out by Zhang et al. [1006, 1008, 1009] and by Pradhan and Zhang [756], again using an extension of the computer program RMATRXI where relativistic effects were included using the Breit–Pauli Hamiltonian. Finally, we mention radiation damping calculations, carried out by Ballance and Griffin [44] and by Griffin and Ballance [424], where relativistic effects were included using an extension of the Dirac R-matrix program DARC, discussed in Sect. 5.5.1. We consider two examples of radiation damping calculations in Sects. 8.5.4 and 8.5.5.

We conclude this introductory survey by mentioning treatments of photorecombination using Feshbach projection operator methods by LaGattuta [558, 559], Haan and Jacobs [434] and Jacobs and Behar [496]. Reviews of this work on photorecombination and related resonance processes have also been written by Hahn [435, 436] and Hahn and LaGattuta [437].

8.2.2 R-Matrix Theory

In this section we extend multichannel R-matrix theory to treat photorecombination and radiation damping in low-energy electron collisions with an N-electron ion with nuclear charge number Z. These processes are described by the time-dependent Schrödinger equation

$$\left[H_{N+1}^{\rm BP} + H_{\rm rad}(t)\right] \widetilde{\Psi}(\mathbf{X}_{N+1}, t) = {\rm i}\frac{\partial}{\partial t}\widetilde{\Psi}(\mathbf{X}_{N+1}, t), \tag{8.115}$$

where we adopt the convention used in Chap. 9 that the tilde on $\widetilde{\Psi}(\mathbf{X}_{N+1}, t)$ indicates that the wave function is time dependent. In (8.115), $H_{N+1}^{\rm BP}$ is the $(N+1)$-electron Breit–Pauli Hamiltonian, defined by (5.133), which accurately describes

many higher Z ionic targets of importance in applications. Also, $H_{\rm rad}(t)$ describes the interaction of the radiation field with the electron–ion system. This interaction Hamiltonian can be written in the length gauge as

$$H_{\rm rad}(t) = \sum_{\mu} \int_0^{\infty} \left(\frac{2\omega^3\alpha^3}{3\pi}\right)^{1/2} \left[R_\mu \exp(-{\rm i}\omega t) + R_\mu^* \exp({\rm i}\omega t)\right] {\rm d}\omega, \qquad (8.116)$$

in atomic units (e.g. [88]), where the first term in square brackets in (8.116) corresponds to absorption (annihilation) of a photon with angular frequency ω and polarization μ and the second term corresponds to emission (creation) of a photon with angular frequency ω and polarization μ. Also in (8.116)

$$R_\mu = \sum_{i=1}^{N+1} r_{i\mu}, \quad \mu = -1,\ 0,\ +1, \qquad (8.117)$$

where $r_{i\mu}$ are the spherical tensor components of the radial coordinate r_i of the ith electron which are defined by

$$r_{i\,-1} = \frac{1}{\sqrt{2}}(x_i - {\rm i}y_i), \quad r_{i\,0} = z_i, \quad r_{i\,+1} = -\frac{1}{\sqrt{2}}(x_i + {\rm i}y_i), \qquad (8.118)$$

so that

$$R_\mu = \left(\frac{4\pi}{3}\right)^{1/2} \sum_{i=1}^{N+1} r_i Y_{1\mu}(\theta_i, \phi_i), \quad \mu = -1,\ 0,\ +1, \qquad (8.119)$$

where $Y_{1\mu}(\theta, \phi)$ are spherical harmonics defined in Appendix B.3.

We now consider the interaction of an element $V_\mu(t)$ of the radiation field with the electron–ion system, where

$$V_\mu(t) = D_\mu \exp(-{\rm i}\omega t) + D_\mu^* \exp({\rm i}\omega t), \qquad (8.120)$$

with

$$D_\mu = \left(\frac{2\omega^3\alpha^3}{3\pi}\right)^{1/2} R_\mu, \quad \mu = -1,\ 0,\ +1. \qquad (8.121)$$

We expand the time-dependent wave function $\widetilde{\Psi}(\mathbf{X}_{N+1}, t)$ in (8.115) as follows:

$$\widetilde{\Psi}(\mathbf{X}_{N+1}, t) = \exp(-{\rm i}Et) \sum_{n=-\infty}^{\infty} \exp(-{\rm i}n\omega t)\Psi_n(\mathbf{X}_{N+1}), \qquad (8.122)$$

which is analogous to the Floquet–Fourier expansion (9.8) adopted in R-matrix Floquet theory, considered in Sect. 9.1. Substituting expansion (8.122) into (8.115) with

$H_{\rm rad}(t)$ set equal to $V_\mu(t)$ and equating the coefficients of $\exp[-{\rm i}(E+n\omega)t]$ to zero yields the following set of coupled time-independent equations

$$D_\mu(\omega)\Psi_{n-1} + (H^{\rm BP}_{N+1} - E - n\omega)\Psi_n + D^*_\mu(\omega)\Psi_{n+1} = 0, \quad n = -\infty, \ldots, +\infty. \tag{8.123}$$

The initial state in (8.112), (8.113) and (8.114), corresponding to electron–ion collisions in the absence of photons, is Ψ_0 in (8.123) while the final state in these equations, with one emitted photon, is Ψ_{-1} in (8.123). Hence the equations coupling these states correspond to taking $n = -1$ and 0 in (8.123) which, when written out explicitly, are

$$(H^{\rm BP}_{N+1} - E + \omega)\Psi_{-1} + D^*_\mu(\omega)\Psi_0 = 0 \tag{8.124}$$

and

$$D_\mu(\omega)\Psi_{-1} + (H^{\rm BP}_{N+1} - E)\Psi_0 = 0, \tag{8.125}$$

where we have omitted Ψ_{-2} in (8.124) and Ψ_1 in (8.125), which correspond, respectively, to emission of two photons and absorption of one photon from the field, both of which will not be important in the process under consideration here.

When the interaction with the radiation field is weak, corresponding to electron collisions with ions with small ionic charge $Z - N$, we can neglect the $D_\mu(\omega)$ term in (8.125), which corresponds to re-absorption of the emitted photon, and solve the resulting equations (8.124) and (8.125) using first-order perturbation theory. This leads to the Milne relation (8.111). However, as the ionic charge increases, higher order effects become important and we must retain the $D_\mu(\omega)$ term and solve the resultant coupled equations (8.124) and (8.125) accurately.

We now consider the solution of (8.124) and (8.125) when Ψ_{-1} is a bound state of the electron–ion system, corresponding to the photorecombination processes depicted by (8.112) and (8.113). In this case the formal solution of (8.124) can be written as

$$\Psi_{-1} = -(H^{\rm BP}_{N+1} - E + \omega)^{-1} D^*_\mu(\omega)\Psi_0. \tag{8.126}$$

Substituting this result into (8.125) yields

$$\left(H^{\rm BP}_{N+1} + \frac{D_\mu(\omega)|\Psi_b\rangle\langle\Psi_b|D^*_\mu(\omega)}{E - E_b - \omega} - E\right)\Psi_0 = 0, \tag{8.127}$$

where we have relabelled the bound state as Ψ_b and

$$E_b = \langle\Psi_b|H^{\rm BP}_{N+1}|\Psi_b\rangle. \tag{8.128}$$

Equation (8.127) describes electron–ion collisions with the emission and subsequent absorption of a photon of energy ω and polarization μ. In order to determine the full

interaction of the radiation field, defined by (8.116), with the electron–ion collision system we must integrate the interaction term in (8.127) over the photon energy ω, sum over the photon polarization directions μ and over the bound states Ψ_b which are coupled by the radiation field. This yields the equation

$$\left(H_{N+1}^{\mathrm{BP}} + \lim_{\delta \to 0} \sum_{\mu b} \int \frac{D_\mu(\omega) |\Psi_b\rangle\langle\Psi_b| D_\mu^*(\omega)}{E - E_b - \omega \pm \mathrm{i}\delta} \mathrm{d}\omega - E \right) \Psi_0 = 0, \tag{8.129}$$

where the $\pm \mathrm{i}\delta$ term in the denominator of this equation defines the contour of integration past the singularity at $\omega = E = E_b$. We will show later that the summation over intermediate bound states in (8.129) can be extended in a straightforward way to include continuum states corresponding to free–free scattering depicted by (8.114).

The real part of the integral over ω in the second term in (8.129) diverges. However, after mass renormalization using quantum electrodynamics (e.g. [499]), this yields an energy shift, analogous to the Lamb shift, which is small for most systems of interest. We will therefore not consider this shift further. The remaining imaginary part of the integral corresponds to radiation damping in the electron–ion collision process. Hence we obtain an additional potential contribution arising from this term given by

$$V_{\mathrm{rad}} = -\mathrm{i}\pi \sum_{\mu b} D_\mu(\omega_b) |\Psi_b\rangle\langle\Psi_b| D_\mu^*(\omega_b), \tag{8.130}$$

where

$$\omega_b = E - E_b \tag{8.131}$$

is the energy difference between the electron–ion collision state and the bound state. The sign chosen for the "radiation damping potential" V_{rad}, defined by (8.130), is such that it is antihermitian and corresponds to absorption. It gives rise to loss of flux from the electron–ion scattering channels into the photorecombination channels. We also observe from (8.130) that we must sum over the photon polarization directions μ and over the bound states Ψ_b to obtain the full radiation damping potential. We note that the form of the radiation damping potential given by (8.130) was derived from a different viewpoint by Robichaux et al. [794].

We now consider the solution of (8.129) describing electron–ion collisions in the presence of the radiation field using R-matrix theory. We partition configuration space into three regions as illustrated in Fig. 5.1. In the internal region $0 \le r \le a_0$ in Fig. 5.1 we expand Ψ_0 in analogy with (5.146) as

$$\Psi_{jE}^{J M_J \pi}(\mathbf{X}_{N+1}) = \sum_k \psi_k^{J M_J \pi}(\mathbf{X}_{N+1}) A_{kj}^{J M_J \pi}(E), \tag{8.132}$$

for each set of conserved quantum numbers J, M_J and π, where J is the total angular momentum quantum number, M_J is the corresponding magnetic quantum number and π is the parity. Also in (8.132), j labels the linearly independent solutions of

(8.129), $\psi_k^{J M_J \pi}$ are energy-independent basis functions and $A_{kj}^{J M_J \pi}(E)$ are energy-dependent expansion coefficients which depend on the asymptotic boundary conditions satisfied by the wave function $\Psi_{jE}^{J M_J \pi}$ at the energy E. In analogy with (5.147), the basis functions $\psi_k^{J M_J \pi}$ in (8.132) can be expanded in the internal region as

$$\psi_k^{J M_J \pi}(\mathbf{X}_{N+1}) = \mathcal{A} \sum_{i=1}^{n} \sum_{j=1}^{n_c} \overline{\Phi}_i^{J M_J \pi}(\mathbf{X}_N; \hat{\mathbf{r}}_{N+1} \sigma_{N+1}) r_{N+1}^{-1} u_{ij}^0(r_{N+1}) a_{ijk}^{J\pi} + \sum_{i=1}^{m} \chi_i^{J M_J \pi}(\mathbf{X}_{N+1}) b_{ik}^{J\pi}, \quad k = 1, \ldots, n_t, \tag{8.133}$$

which we rewrite as

$$\psi_k^{J M_J \pi}(\mathbf{X}_{N+1}) = \sum_{k'=1}^{n_t} \theta_{k'}^{J M_J \pi}(\mathbf{X}_{N+1}) O_{k'k}^{J\pi}, \quad k = 1, \ldots n_t, \tag{8.134}$$

where $\theta_{k'}^{J M_J \pi}$ represents the $n_t = n n_c + m$ linearly independent basis functions in (8.133) and $O_{k'k}^{J\pi}$ represents the coefficients $a_{ijk}^{J\pi}$ and $b_{ik}^{J\pi}$ in (8.133).

In order to determine the solution of (8.129) in the internal region we rewrite this equation using (8.130) as

$$(H_{N+1}^{\mathrm{BP}} + V_{\mathrm{rad}} + \mathcal{L}_{N+1} - E) \Psi_{jE}^{J M_J \pi} = \mathcal{L}_{N+1} \Psi_{jE}^{J M_J \pi}, \tag{8.135}$$

where $\mathcal{L}_{N+1}$ is the usual Bloch operator defined so that $H_{N+1}^{\mathrm{BP}} + \mathcal{L}_{N+1}$ is hermitian in the internal region. Equation (8.129) then has the formal solution in the internal region given by

$$\Psi_{jE}^{J M_J \pi} = (H_{N+1}^{\mathrm{BP}} + V_{\mathrm{rad}} + \mathcal{L}_{N+1} - E)^{-1} \mathcal{L}_{N+1} \Psi_{jE}^{J M_J \pi}. \tag{8.136}$$

We then introduce matrices $\mathbf{H}$ and $\mathbf{D}$ whose matrix elements are defined by the following integrals over the internal region

$$H_{kk'} = \langle \theta_k | H_{N+1}^{\mathrm{BP}} + \mathcal{L}_{N+1} - E | \theta_{k'} \rangle_{\mathrm{int}}, \quad k, \; k' = 1, \ldots, n_t \tag{8.137}$$

and

$$D_{kj} = \langle \theta_k | D_\mu(\omega_b) | \Psi_b \rangle_{\mathrm{int}}, \quad k = 1, \ldots, n_t, \quad j = 1, \ldots, n_v, \tag{8.138}$$

where in (8.138) the index j goes over the combination of the polarization index μ and the bound state index b in (8.130), which we define to be n_v in number. Also in (8.137) and (8.138) and in later equations we omit the conserved quantum number superscripts J, M_j and π for notational convenience. It thus follows from (8.130), (8.137) and (8.138) that

$$\langle\theta_k|H_{N+1}^{\rm BP}+V_{\rm rad}+\mathcal{L}_{N+1}-E|\theta_{k'}\rangle_{\rm int}=(\mathbf{H}-{\rm i}\pi\mathbf{D}\mathbf{D}^\dagger)_{kk'},\quad k,\ k'=1,\ldots,n_t, \tag{8.139}$$

where the matrix $\mathbf{D}^\dagger$ is the hermitian conjugate of $\mathbf{D}$ and hence $-{\rm i}\pi\mathbf{D}\mathbf{D}^\dagger$ is an $n_t\times n_t$-dimensional antihermitian matrix. Also $H_{N+1}^{\rm BP}+\mathcal{L}_{N+1}$ is hermitian in the internal region and with the usual choice of phase $\mathbf{H}$, defined by (8.137), is real and symmetric. We then choose the matrix $\mathbf{O}$ in (8.134) to be orthogonal and to diagonalize $\mathbf{H}$ as follows:

$$\mathbf{O}^{\rm T}\mathbf{H}\mathbf{O}=\mathbf{E}-E\mathbf{I}, \tag{8.140}$$

where $\mathbf{E}$ is a diagonal $n_t\times n_t$-dimensional matrix with diagonal elements E_k and $\mathbf{I}$ is the unit matrix. It follows that

$$\langle\psi_k|H_{N+1}^{\rm BP}+\mathcal{L}_{N+1}-E|\psi_{k'}\rangle_{\rm int}=(E_k-E)\delta_{kk'},\quad k,\ k'=1,\ldots,n_t, \tag{8.141}$$

where the basis functions ψ_k are defined by (8.134). We see that (8.141) corresponds to (5.152) which arises in the absence of radiation damping.

In determining the matrix elements of $\mathbf{H}-{\rm i}\pi\mathbf{D}\mathbf{D}^\dagger$ in (8.139), we have to carry out a summation over the intermediate states that arise in the matrix multiplication in $\mathbf{D}\mathbf{D}^\dagger$, where $\mathbf{D}$ is defined by (8.138). This can be achieved by solving the collision problem in the internal region, corresponding to the conserved quantum numbers J', $M_{J'}$ and π', which are coupled by the radiation field to the collision state corresponding to J, M_J and π. In analogy with (8.133) the required basis functions can be expanded in the internal region as

$$\begin{aligned}\psi_k^{J'M_{J'}\pi'}(\mathbf{X}_{N+1})=\mathcal{A}\sum_{i=1}^{n'}\sum_{j=1}^{n'_c}\overline{\Phi}_i^{J'M_{J'}\pi'}(\mathbf{X}_N;\hat{\mathbf{r}}_{N+1}\sigma_{N+1})r_{N+1}^{-1}u_{ij}^0(r_{N+1})a_{ijk}^{J'\pi'}\\+\sum_{i=1}^{m'}\chi_i^{J'M_{J'}\pi'}(\mathbf{X}_{N+1})b_{ik}^{J'\pi'},\quad k=1,\ldots,n'_t,\end{aligned} \tag{8.142}$$

where the coefficients $a_{ijk}^{J'\pi'}$ and $b_{ik}^{J'\pi'}$ are determined by diagonalizing $H_{N+1}^{\rm BP}+\mathcal{L}_{N+1}$ as follows:

$$\langle\psi_k^{J'M_{J'}\pi'}|H_{N+1}^{\rm BP}+\mathcal{L}_{N+1}|\psi_{k'}^{J'M_{J'}\pi'}\rangle_{\rm int}=E_k^{J'\pi'}\delta_{kk'}. \tag{8.143}$$

The summation over intermediate states in $\mathbf{D}\mathbf{D}^\dagger$ can then be replaced by a summation over the basis functions $\psi_k^{J'M_{J'}\pi'}$ for each intermediate symmetry. Also, the inclusion of the continuum in the summation over intermediate states in $\mathbf{D}\mathbf{D}^\dagger$ can be achieved by including quadratically integrable pseudostates in expansion (8.142). This procedure is analogous to that used in the representation of the continuum in intermediate-energy electron–atom collisions, discussed in Chap. 6, and its contribution will often be necessary to obtain accurate radiation damping results.

We now use these results to obtain an explicit form for the solution of (8.136) in the internal region. We rewrite this equation as

$$|\Psi_{jE}\rangle = \sum_{k=1}^{n_t}\sum_{k'=1}^{n_t} |\psi_k\rangle\langle\psi_k|(H_{N+1}^{\mathrm{BP}} + V_{\mathrm{rad}} + \mathcal{L}_{N+1} - E)^{-1}|\psi_{k'}\rangle_{\mathrm{int}} \times \langle\psi_{k'}|\mathcal{L}_{N+1}|\Psi_{jE}\rangle. \tag{8.144}$$

We then consider the following matrix element in this equation:

$$\begin{aligned}&\langle\psi_k|(H_{N+1}^{\mathrm{BP}} + V_{\mathrm{rad}} + \mathcal{L}_{N+1} - E)^{-1}|\psi_{k'}\rangle_{\mathrm{int}} \\ &= \sum_{j=1}^{n_t}\sum_{j'=1}^{n_t} O_{jk}\langle\theta_j|(H_{N+1}^{\mathrm{BP}} + V_{\mathrm{rad}} + \mathcal{L}_{N+1} - E)^{-1}|\theta_{j'}\rangle_{\mathrm{int}} O_{j'k'} \\ &= \left[\mathbf{O}^{\mathrm{T}}(\mathbf{H} - \mathrm{i}\pi\mathbf{D}\mathbf{D}^{\dagger})^{-1}\mathbf{O}\right]_{kk'},\end{aligned} \tag{8.145}$$

where we have used (8.134) and (8.139). Using (8.140) we can then show that

$$\mathbf{O}^{\mathrm{T}}(\mathbf{H} - \mathrm{i}\pi\mathbf{D}\mathbf{D}^{\dagger})^{-1}\mathbf{O} = (\mathbf{E} - E\mathbf{I})^{-1} - (\mathbf{E} - E\mathbf{I})^{-1}\mathbf{O}^{\mathrm{T}}\mathbf{D}\mathbf{C}^{-1} \times \mathbf{D}^{\dagger}\mathbf{O}(\mathbf{E} - E\mathbf{I})^{-1}, \tag{8.146}$$

where

$$\mathbf{C} = \mathbf{J}^{-1} + \mathbf{D}^{\dagger}\mathbf{O}(\mathbf{E} - E\mathbf{I})^{-1}\mathbf{O}^{\mathrm{T}}\mathbf{D}, \tag{8.147}$$

and where $\mathbf{J}$ is defined in terms of the $n_v \times n_v$-dimensional unit matrix $\mathbf{I}_v$ by

$$\mathbf{J} = -\mathrm{i}\pi\mathbf{I}_v. \tag{8.148}$$

Substituting this result into (8.144) then yields

$$|\Psi_{jE}\rangle = \sum_{k=1}^{n_t}\sum_{k'=1}^{n_t} |\psi_k\rangle[(\mathbf{E} - E\mathbf{I})^{-1} - (\mathbf{E} - E\mathbf{I})^{-1}\widetilde{\mathbf{D}}\mathbf{C}^{-1}\widetilde{\mathbf{D}}^{\dagger}(\mathbf{E} - E\mathbf{I})^{-1}]_{kk'} \times \langle\psi_{k'}|\mathcal{L}_{N+1}|\Psi_{jE}\rangle, \tag{8.149}$$

where $\widetilde{\mathbf{D}} = \mathbf{O}^{\mathrm{T}}\mathbf{D}$ has the matrix elements

$$\widetilde{D}_{kj} = \langle\psi_k|D_{\mu}(\omega_b)|\Psi_b\rangle_{\mathrm{int}}, \quad k = 1, \ldots, n_t, \quad j = 1, \ldots, n_v, \tag{8.150}$$

which follows from (8.134) and (8.138).

We now proceed as in standard R-matrix theory in the absence of radiation damping, discussed in Sect. 5.4.2. We project (8.149) onto the n channel functions $\overline{\Phi}_i$ retained in expansion (8.133) and evaluate it on the boundary $r_{N+1} = a_0$ of the internal region. We obtain

$$F_{ij}(a_0) = \sum_{i'=1}^{n} \widetilde{R}_{ii'}(E) \left(a_0 \frac{\mathrm{d}F_{i'j}}{\mathrm{d}r} - b_0 F_{i'j} \right)_{r=a_0}, \quad i = 1, \ldots, n, \tag{8.151}$$

where the elements of the R-matrix $\widetilde{R}_{ii'}(E)$ are defined by

$$\widetilde{R}_{ii'}(E) = \frac{1}{2a_0} \sum_{k,k'=1}^{n_t} w_{ik} \left[(\mathbf{E} - E\mathbf{I})^{-1} - (\mathbf{E} - E\mathbf{I})^{-1} \widetilde{\mathbf{D}} \mathbf{C}^{-1} \widetilde{\mathbf{D}}^{\dagger} (\mathbf{E} - E\mathbf{I})^{-1} \right]_{kk'} \times w_{i'k'}, \quad i,\ i' = 1, \ldots, n, \tag{8.152}$$

the reduced radial wave functions $F_{ij}(r)$ are defined by

$$F_{ij}(r_{N+1}) = \langle r_{N+1}^{-1} \overline{\Phi}_i | \Psi_j \rangle', \quad i = 1, \ldots, n \tag{8.153}$$

and the surface amplitudes w_{ik} are defined by

$$\begin{aligned} w_{ik} &= \langle r_{N+1}^{-1} \overline{\Phi}_i | \psi_k \rangle'_{r_{N+1}=a_0} \\ &= \sum_{j=1}^{n_c} u_{ij}^0(a_0) a_{ijk}, \quad i = 1, \ldots, n, \quad k = 1, \ldots, n_t. \end{aligned} \tag{8.154}$$

The primes on the Dirac brackets in (8.153) and (8.154) mean that the integrations are carried out over the space and spin coordinates of all $N + 1$ electrons in the internal region, except the radial coordinate r_{N+1} of the scattered electron.

It is important to note that the second term in square brackets in (8.152), which corresponds to radiation damping, means that the R-matrix is no longer real nor hermitian. In addition, since the matrix $\mathbf{C}$, defined by (8.147), depends on the energy E a matrix inversion has to be carried out for each scattering energy of interest. This must be compared with the situation in the absence of radiation damping when a single matrix diagonalization to obtain the surface amplitudes w_{ik} and eigenenergies E_k yields the R-matrix at all energies. However, the dimension $n_v \times n_v$ of the matrix $\mathbf{C}$ to be inverted is much less than the dimension $n_t \times n_t$ of the matrix to be diagonalized in standard R-matrix theory, so the additional computational effort is usually not excessive.

Having determined the R-matrix on the boundary $r = a_0$ of the internal region, we can then propagate it outwards across the external region from $r = a_0$ to a_p, using one of the methods discussed in Appendix E, where the radiation damping term can be included in the external region if necessary. Finally, we fit the solution on the outer boundary $r = a_p$ of the external region to an asymptotic expansion which yields the K-matrix and S-matrix. Since the R-matrix is no longer real and symmetric, the K-matrix will no longer be real and symmetric and hence the S-matrix will no longer be unitary and symmetric.

As a result of the non-unitarity of the S-matrix, flux is lost from the electron–ion scattering channels into photorecombination and free–free scattering channels.

Hence the partial wave cross sections $\sigma^{J\pi}(i \rightarrow j)$ for each $J\pi$ combination, given by (5.129), are modified corresponding to radiation damping, and the partial wave cross sections for photorecombination including free–free scattering are given by

$$\sigma_{\mathrm{PR}}^{J\pi} = \frac{2J+1}{2k_i^2(2J_i+1)} \sum_{i=1}^{n_i} \left[1 - \sum_{j=1}^{n_a} S_{ji}^* S_{ji} \right], \tag{8.155}$$

in units of πa_0^2, where n_a is the number of open channels, n_i is the number of channels coupled to the target state and J_i is the angular momentum of the target state.

In conclusion we mention that a related optical potential R-matrix approach, combined with multichannel quantum defect theory, has been introduced by Gorczyca and Robicheaux [395] to treat photoionization in the vicinity of the $2p^{-1}ns(nd)$ photoexcited resonance states in argon. In this approach the infinite number of Auger decay channels are correctly treated by the optical potential, which is based on similar ideas to the radiation damping potential (8.130). In addition to argon, other applications of this approach include inner-shell photoexcited resonances in neon by Gorczyca [391] and in atomic oxygen by Gorczyca and McLaughlin [396]. This optical potential approach has also been applied to post-collision recapture in K-shell photodetachment of Li^- by Gorczyca et al. [401], while in later work discussed in Sect. 9.1.2 two-photon detachment of K-shell electrons in Li^- has been calculated by van der Hart [932].

8.3 The Opacity Project

An important application of the processes discussed earlier in this chapter has been the calculations carried out by the international Opacity Project (OP). In this section we briefly describe the objectives and achievements of this project. The OP, which was initiated in 1983 and led by Seaton [861, 863], has involved research workers from many countries in Europe and North and South America who have collaborated in the calculation of stellar opacities. Knowledge of the opacity of stellar material is of importance in all studies of stellar structure and evolution and of stellar atmospheres. The opacities are determined by a very large number of atomic processes (radiative bound–bound, bound–free and free–free transitions) and in cooler stars by molecular processes. Calculations of the necessary atomic parameters have spanned more than 20 years, using R-matrix computer programs which are summarized below, where the earlier work has been republished in two volumes by the "Opacity Project Team" [706, 707].

More recently, as a result of detailed comparisons with work carried out by an independent study of stellar opacities, called OPAL, at the Lawrence Livermore National Laboratory, see, for example, Iglesias et al. [489, 490], the importance of the contribution of inner-shell transitions to the opacity has been realized. In a major

new initiative the contribution to stellar opacities from these transitions has been calculated by Badnell and Seaton [35], Seaton and Badnell [865] and Badnell et al. [38], using an extension of the atomic structure configuration interaction computer program AUTOSTRUCTURE [30, 31], discussed in Sect. 5.1.1.

We now outline the theory connecting the Rosseland-mean opacity used by astronomers with the cross sections for absorption or scattering of radiation, calculated by atomic structure and collision programs. In a stellar interior an atom of an element, denoted by k, can exist in a number of ionization stages, denoted by i, and energy levels, denoted by j. We then define the cross section for absorption or scattering of radiation by a level, denoted by (i, j, k) as $\sigma_{ijk}(u)$, where the frequency variable $u = \mathrm{h}\nu/k_{\mathrm{B}}T$, k_{B} being Boltzmann's constant, and where the correction factor for stimulated emission $[1 - \exp(-u)]$ is not included in the definition of $\sigma_{ijk}(u)$.[2] The monochromatic opacity cross section for element k is then defined by

$$\sigma_k(u) = \sum_{ij} p_{ijk}\sigma_{ijk}(u). \tag{8.156}$$

The mean cross section for a mixture of elements is then

$$\sigma(u) = \sum_k f_k\sigma_k(u), \tag{8.157}$$

where f_k is the fractional abundance of the element which is normalized to unity as follows:

$$\sum_k f_k = 1. \tag{8.158}$$

The Rosseland-mean cross section σ_{R} is then given by

$$\frac{1}{\sigma_{\mathrm{R}}} = \int_0^\infty \frac{F(u)}{\sigma(u)[1 - \exp(-u)]}\mathrm{d}u, \tag{8.159}$$

where

$$F(u) = \frac{15}{4\pi^4}u^4\frac{\exp(-u)}{[1 - \exp(-u)]^2}. \tag{8.160}$$

Finally, the Rosseland-mean opacity per unit mass is

$$\kappa_{\mathrm{R}} = \frac{\sigma_{\mathrm{R}}}{\mu}, \tag{8.161}$$

where μ is the mean atomic weight.

[2] We consider here the quantity actually tabulated in the OP archives [863].

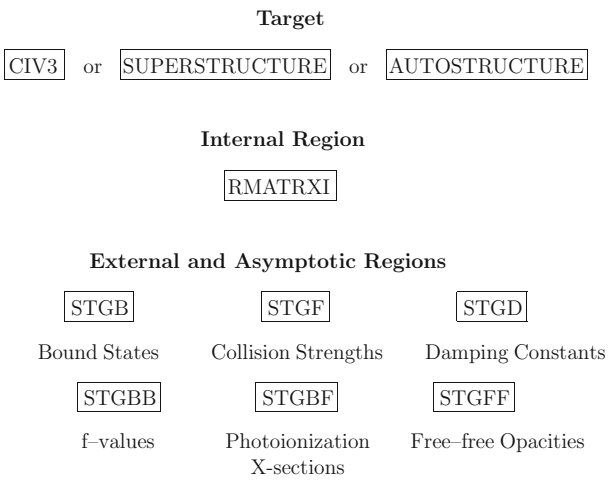

Fig. 8.2 The Opacity Project computer programs

The first results from the Opacity Project were reviewed by Seaton et al. [866] and involved detailed calculations of atomic energy levels, oscillator strengths, collision strengths, photoionization cross sections and electron line broadening and damping constants for a wide range of atomic ions of high stellar abundance. These calculations were carried out using the R-matrix method together with a range of new computer programs for calculating external and asymptotic region solutions and dipole integrals, which were described by Berrington et al. [100]. We conclude this section by summarizing in Fig. 8.2 the computer programs used in these calculations. We have already briefly reviewed the atomic structure programs CIV3, SUPERSTRUCTURE and AUTOSTRUCTURE, the R-matrix internal region program RMATRXI and the external and asymptotic region program STGF in our discussion of computer programs used in electron–atom collision calculations in Sect. 5.1.1. In addition, a number of new programs were developed specifically for the OP. These were STGB to calculate bound-state wave functions and energies; STGD to calculate damping constants; STGBB to calculate bound–bound oscillator strengths; STGBF to calculate bound–free photoionization cross sections and STGFF to calculate free–free opacities.

8.4 Spectra of Atoms in Fields

In this section we describe a computational approach which enables the spectra of atoms in laboratory strength electric and magnetic fields to be accurately calculated. This approach, which combines a new external region R-matrix method with the complex coordinate rotation method, was introduced by Halley et al. [438, 439] and Seipp and Taylor [867].

The complex coordinate rotation method, which has been reviewed, for example, by Reinhardt [786] and Junker [520], has played an important role in the study of the properties of atoms and ions in external electric and magnetic fields. In this method, the radial variable r is rotated into the complex plane by the transformation $r \rightarrow r\exp(\mathrm{i}\theta)$ where θ is a real positive rotation angle. Similarly, the momentum variable p is rotated in the opposite direction by the transformation $p \rightarrow p\exp(-\mathrm{i}\theta)$ which preserves the canonical commutation relations. When all the radial and momentum variables are scaled in this way the Hamiltonian H is transformed to a new rotated Hamiltonian $H(\theta)$ which is a non-hermitian operator whose spectrum is complex. In addition, if $H(\theta)$ is represented by real basis functions the resultant matrix is complex and symmetric.

Following our discussion of the analytic properties of the S-matrix in the complex energy plane in Sects. 3.1 and 3.2.1, see, for example, Figs. 3.1 and 3.4, we show in Fig. 8.3 how the bound and resonance states of $H(\theta)$ behave as a result of the rotation θ. In Fig. 8.3a we show the distribution of bound-state and resonance S-matrix poles, branch points and branch cuts of the Hamiltonian H in the absence of the rotation. We note that, unlike Fig. 3.1, the branch cuts which start from the branch points e_i, $i = 1, \ldots, 4$, are not shown displaced from the real energy axis but lie on top of each other along this axis. Following Fig. 3.4, we also show the continuation paths from the physical sheet to the resonance poles, corresponding to Siegert states, which lie on unphysical sheets in the complex energy plane. Then in Fig. 8.3b we show the distribution of bound-state and resonance S-matrix poles, branch points and branch cuts of the Hamiltonian $H(\theta)$ corresponding to the rotation θ. An important aspect of the transformation is that the bound states of H remain real isolated eigenstates of $H(\theta)$, while the resonance states of H lying in the lower complex energy plane are now revealed by the rotation of the threshold branch cuts through 2θ. These states are now square-integrable (L^2) eigenstates of $H(\theta)$ corresponding to complex eigenvalues. Thus diagonalizing the non-hermitian Hamiltonian $H(\theta)$ with real L^2 basis functions gives a description of both the discrete and continuum spectra of the Hamiltonian H including the positions and widths of the resonances revealed by the rotation.

The development and application of the external region R-matrix method in a study of atoms in magnetic fields were first made by O'Mahony and Taylor [703] who considered the quadratic Zeeman effect in Sr and Ba atoms. Following an observation by Clark and Taylor [219], they pointed out that for magnetic fields of laboratory strength (5–50 kG or $\beta = 10^{-6}$–10^{-5} a.u.) the quadratic Zeeman potential $\frac{1}{2}\beta r^2 \sin^2\theta$ can be ignored compared with the atomic electron–nucleus and electron–electron potentials in an internal region extending out to several hundred atomic units from the nucleus. Hence, in order to represent the effects of the magnetic field, O'Mahony and Taylor expanded the wave function in a basis set in the external region rather than in the internal region, as in standard R-matrix theory. The external R-matrix theory expansion was then combined with the complex coordinate rotation method by Halley et al. [438, 439] and Seipp and Taylor [867]. In this

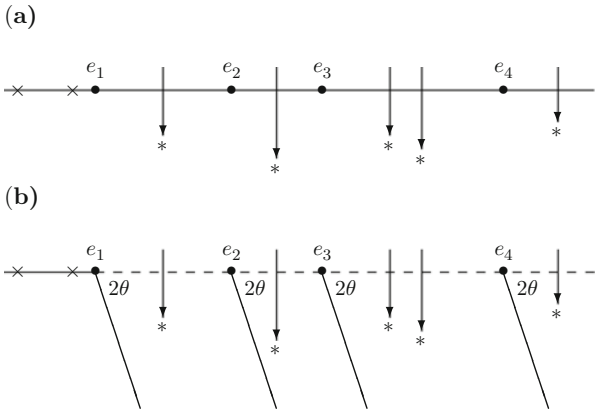

Fig. 8.3 Distribution of S-matrix poles in the complex energy plane and the corresponding branch points and associated branch cuts. (**a**) Poles of H when the rotation angle $\theta = 0$. (**b**) Poles of $H(\theta)$ when the rotation angle θ is non-zero. $\times$, bound-state poles lying on the physical sheet; $*$, resonance poles which lie on unphysical sheets when $\theta = 0$ and which are revealed by the rotation of the branch cuts by 2θ. The branch points are denoted by e_i, $i = 1, \ldots, 4$, and the *arrows* denote the continuation paths from the physical sheet to the resonance poles

combined method the atomic wave function in the internal region must accurately describe the ejected electron on the boundary $r = a_0$ of this region, where this electron may be in a highly excited or continuum state. Following Halley et al. [439] we illustrate this method by considering a one-channel problem where the highly excited or continuum electron moves in the external region in the Coulomb potential of the residual ion and an external field.

In the internal region the solution on the boundary $r = a_0$ of this region can be accurately described using quantum defect theory, discussed in Sect. 3.3.4, as follows:

$$F_\ell(a_0) = s_\ell(a_0) + \tan(\mu_\ell \pi) c_\ell(a_0). \tag{8.162}$$

In this equation $s_\ell(r)$ and $c_\ell(r)$ are energy-normalized regular and irregular Coulomb wave functions and μ_ℓ is the quantum defect corresponding to the orbital angular momentum ℓ. The quantum defect can be obtained by accurate measurement or calculation of the field-free target atom in the internal region.

We now consider the bound-state solutions in the external region where $a_0 \leq r \leq \infty$ using R-matrix theory, commencing with the solution when there is no complex coordinate rotation. In this case the Schrödinger equation satisfied by the reduced radial wave function $F_\ell(r)$ describing the highly excited electron moving in the potential $U(r)$ is

$$\left(\frac{\mathrm{d}^2}{\mathrm{d}r^2} - \frac{\ell(\ell+1)}{r^2} - U(r) + k^2\right) F_\ell(r) = 0, \quad a_0 \le r \le \infty, \tag{8.163}$$

subject to the asymptotic boundary condition

$$\lim_{r\to\infty} F_\ell(r) = 0, \tag{8.164}$$

where $U(r)$ represents the interaction of the electron with the external field and with the residual ion. In order to solve (8.163) in the external region we first write this equation in the form

$$L_\ell F_\ell(r) = 0, \quad a_0 \le r \le \infty, \tag{8.165}$$

and we introduce a Bloch operator $\mathcal{L}(a_0, b_0)$ on the boundary $r = a_0$ defined by

$$\mathcal{L}(a_0, b_0) = \delta(r - a_0)\left(\frac{\mathrm{d}}{\mathrm{d}r} - \frac{b_0}{r}\right), \tag{8.166}$$

where b_0 is an arbitrary constant. Following our discussion in Sect. 4.2, we find that

$$\int_{a_0}^{\infty} [v(r)\,(L_\ell + \mathcal{L})\,w(r) - w(r)(L_\ell + \mathcal{L})v(r)]\mathrm{d}r = 0, \tag{8.167}$$

for L^2 integrable functions $v(r)$ and $w(r)$ which satisfy arbitrary boundary conditions at $r = a_0$ and vanish asymptotically as $r \to \infty$. It follows that $L_\ell + \mathcal{L}$ is hermitian over the external region in the space of these functions.

We then solve (8.163) in the external region by introducing a complete linearly independent set of real L^2 integrable basis functions

$$\phi_i(r), \quad i = 1, \ldots, \infty, \quad a_0 \le r \le \infty, \tag{8.168}$$

which satisfy the above boundary conditions at $r = a_0$ and $r \to \infty$. In practice, a set of Sturmian functions has been used in detailed calculations by Halley et al. [438, 439]. We then form a linear combination of these basis functions

$$\chi_j(r) = \sum_{i=1}^{\infty} \phi_i(r) c_{ij}, \quad j = 1, \ldots, \infty, \quad a_0 \le r \le \infty, \tag{8.169}$$

where the expansion coefficients c_{ij} are determined by diagonalizing $L_\ell + \mathcal{L}$ in this basis so that

$$\int_{a_0}^{\infty} \chi_i(r)(L_\ell + \mathcal{L})\chi_j(r)\mathrm{d}r = 2(E - E_i)\delta_{ij}, \tag{8.170}$$

where the energy $E = k^2/2$ and where the eigenenergies E_i are real since $L_\ell + \mathcal{L}$ is hermitian. We can now solve (8.165) by rewriting this equation as

$$(L_\ell + \mathcal{L})\, F_\ell(r) = \mathcal{L} F_\ell(r), \tag{8.171}$$

which has the formal solution

$$F_\ell(r) = (L_\ell + \mathcal{L})^{-1}\, \mathcal{L} F_\ell(r), \tag{8.172}$$

where the spectral representation of the Green's function $(L_\ell + \mathcal{L})^{-1}$ is given by

$$(L_\ell + \mathcal{L})^{-1} = \frac{1}{2} \sum_{i=1}^{\infty} \frac{\chi_i(r)\chi_i(r')}{E - E_i}, \quad a_0 \le r \le \infty, \quad a_0 \le r' \le \infty. \tag{8.173}$$

Hence it follows from (8.166) and (8.172) that

$$F_\ell(a_0) = R(E) \left(a_0 \frac{\mathrm{d}F_\ell}{\mathrm{d}r} - b_0 F_\ell \right)_{r=a_0}, \tag{8.174}$$

where the R-matrix

$$R(E) = \frac{1}{2a_0} \sum_{i=1}^{\infty} \frac{[\chi_i(a_0)]^2}{E - E_i}. \tag{8.175}$$

In conclusion, we see from (8.169), (8.170) and (8.175) that the calculation of the R-matrix at $r = a_0$ involves the diagonalization of the Hamiltonian in an external region basis. On the other hand, the function $F_\ell(a_0)$ and the derivative $(\mathrm{d}F_\ell/\mathrm{d}r)_{r=a_0}$ are given by the solution defined by (8.162) in the internal region. Hence (8.162) and (8.174) can only be simultaneously satisfied at negative real eigenenergies which can be determined by an iterative procedure. The corresponding eigensolutions will then correspond to bound states defined over the full range $0 \le r \le \infty$.

We now briefly review the corresponding analysis when the complex coordinate rotation method is used in the external region. In this case r in (8.163) is replaced by $r \exp(\mathrm{i}\theta)$, where θ is a fixed positive rotation angle, and we again include a potential $U(r)$ representing the interaction of the electron with the residual ion and with the field in the external region. Equation (8.163) then becomes

$$\left(\mathrm{e}^{-2\mathrm{i}\theta} \frac{\mathrm{d}^2}{\mathrm{d}r^2} - \mathrm{e}^{-2\mathrm{i}\theta} \frac{\ell(\ell+1)}{r^2} - U\left(r\mathrm{e}^{\mathrm{i}\theta}\right) + k^2 \right) F_\ell\left(r\mathrm{e}^{\mathrm{i}\theta}\right) = 0, \quad a_0 \le r \le \infty, \tag{8.176}$$

where r is a real variable. We then look for L^2 integrable solutions of this equation which vanish asymptotically and which correspond to bound states and to resonance states which are revealed by the rotation, as in Fig. 8.3b. Following our analysis of the solution in the external region when the rotation angle $\theta = 0$, we determine

a basis $\chi_i(r \exp \mathrm{i}\theta)$ by diagonalizing $L_\ell(\theta) + \mathcal{L}(\theta)$ in a set of real L^2 integrable functions analogous to (8.168), where $L_\ell(\theta)$ is the operator in brackets on the left-hand side of (8.176) and $\mathcal{L}(\theta)$ is the corresponding Bloch operator defined by

$$\mathcal{L}(\theta) = \mathrm{e}^{-2\mathrm{i}\theta}\delta(r - a_0)\frac{\mathrm{d}}{\mathrm{d}r}, \tag{8.177}$$

where we have set the arbitrary constant b_0, which we included in (8.166), equal to zero. We then obtain

$$\int_{a_0}^{\infty} \chi_i\left(r\mathrm{e}^{\mathrm{i}\theta}\right)\left[L_\ell(\theta) + \mathcal{L}(\theta)\right]\chi_j\left(r\mathrm{e}^{\mathrm{i}\theta}\right)\mathrm{d}r = 2(E - E_i)\delta_{ij}, \tag{8.178}$$

where the energy $E = k^2/2$ can now be complex since θ is non-zero. We then find in analogy with (8.174) and (8.175) that

$$F_\ell\left(r\mathrm{e}^{\mathrm{i}\theta}\right) = R(E,\theta)\, a_0 \frac{\mathrm{d}F_\ell\left(r\mathrm{e}^{\mathrm{i}\theta}\right)}{\mathrm{d}\left(r\mathrm{e}^{\mathrm{i}\theta}\right)}\bigg|_{r=a_0}, \tag{8.179}$$

where the R-matrix at $r = a_0$ is given by

$$R(E,\theta) = \frac{\mathrm{e}^{-\mathrm{i}\theta}}{2a_0}\sum_{i=1}^{\infty}\frac{\left[\chi_i\left(a_0\mathrm{e}^{\mathrm{i}\theta}\right)\right]^2}{E - E_i}, \tag{8.180}$$

which we see is a function of the complex energy E and the rotation angle θ.

Having calculated the R-matrix at $r = a_0$ we can now match the solution in the external region to the solution in the internal region at $r = a_0$ defined by (8.162). Unlike the situation discussed earlier in the absence of the complex coordinate rotation, the energy E that is varied in the matching can now be complex, corresponding to resonances which are revealed by the rotation, which increases the computational effort required in the search for a match. In practice it was found [438, 439] that this effort could be reduced using the procedure introduced by Schneider [824], discussed in Sect. 4.4.8, where information from the inner region solution is built into the calculation before the diagonalization of $L_\ell(\theta) + \mathcal{L}(\theta)$ in (8.178) is performed.

Following Delande et al. [256] the photoionization cross section $\sigma(\omega)$ from an initial state ψ_0 with energy E_0 in an external field is given by

$$\sigma(\omega) = \frac{4\pi\omega}{\mathrm{c}}\mathrm{Im}\,\langle\psi_0\left|T\frac{1}{H - \omega - E_0 - \mathrm{i}\epsilon}T\right|\psi_0\rangle, \tag{8.181}$$

where $T = \hat{\boldsymbol{\epsilon}}\cdot\mathbf{r}$ is the dipole operator for polarization in the direction of the unit vector $\hat{\boldsymbol{\epsilon}}$. The matrix element in (8.181) can be rewritten by introducing the complex

rotation angle θ and by writing $|\psi\rangle$ as the complex rotation transform of $T|\psi_0\rangle$. After expressing $|\psi\rangle$ as a linear combination of the eigenvectors of $H(\theta)$ with complex coefficients $c_i(\theta)$, we then obtain

$$\sigma(\omega) = \frac{4\pi\omega}{\mathrm{c}} \mathrm{Im} \sum_i \frac{c_i^2(\theta)}{E_i(\theta) - \omega - E_0}. \tag{8.182}$$

For a given resonance which is uncovered by the rotation angle θ, neither E_i nor c_i depends on θ. On the other hand, there is a θ-dependence for the continuum states. However, the sum over all eigenstates of the rotated Hamiltonian in (8.182) is θ-independent.

Finally, we summarize a number of calculations that have been carried out using the external region R-matrix with complex coordinate rotation method. In the initial work by Halley et al. [438], discussed in Sect. 8.5.6, detailed calculations were carried out for the diamagnetic spectrum of Li obtaining almost perfect agreement with the high-resolution experiments by Iu et al. [494]. This work was extended by Halley et al. [439] who calculated the diamagnetic spectrum of Ba and Sr obtaining excellent agreement with the experimental results of Lu et al. [602]. Later, Seipp and Taylor [867] applied the method to the Stark and Stark diamagnetic Rydberg spectra of Na. The results obtained for the spectrum in an electric field were in satisfactory agreement with experiment and with theoretical results obtained using a different theoretical approach and new results were obtained for the spectrum in combined electric and magnetic fields. Atomic resonance effects in parallel electric and magnetic fields for H and Na atoms were also obtained using the combined R-matrix and complex coordinate approach by Seipp et al. [868]. Also, precision measurements on lithium atoms in electric fields were compared by Stevens et al. [888] with calculations using the R-matrix with complex coordinate method and with two other theories showing that the R-matrix approach was the most accurate. Finally, we mention related work by Rao and Taylor [775] which used the external region R-matrix method with an unrotated coordinate system which enabled the photoabsorption spectrum of Ba in crossed electric and magnetic fields to be accurately calculated. This last study shows the importance of the external region R-matrix method without rotation in the study of the bound-state spectra of atoms in external electric and magnetic fields.

8.5 Illustrative Examples

In this section we present illustrative examples of atomic photoionization, photorecombination and radiation damping calculations. We also consider a calculation of the photoionization spectrum of an atom in an external magnetic field.

8.5.1 Photoionization of Li

In recent years, many R-matrix calculations have been carried out in support of atomic photoionization experiments at synchrotron radiation facilities. As our first example we discuss photoionization measurements of hollow-atom–hollow-ion decay paths of triply excited lithium, carried out at the Advanced Light Source at Berkeley, by Diehl et al. [262]. Understanding the many-electron behaviour of hollow lithium atoms, in which all three electrons are in excited states, provides a formidable challenge to both experimentalists and theorists. Hollow-atom dynamics are also of considerable interest, for example, in the interpretation of ion–surface collision processes [138].

In the experiment by Diehl et al. the following resonant two-step decay process was observed for photon energies in excess of 151.7 eV:

$$\begin{aligned} \mathrm{h}\nu + \mathrm{Li}(1\mathrm{s}^2 2\mathrm{s}\ {}^2\mathrm{S}) \rightarrow\ & \mathrm{Li}^{***}(n\ell n'\ell' n''\ell'') \\ & \downarrow \\ & \mathrm{Li}^{+**}(n'''\ell'''n''''\ell'''') + \mathrm{e}^- \\ & \downarrow \\ & \mathrm{Li}^{2+}(1\mathrm{s}) + \mathrm{e}^-. \end{aligned} \tag{8.183}$$

We illustrate this process schematically in Fig. 8.4. The incident photon first excites the lithium atom to a triply excited hollow-atom state Li^{***}. This state then decays with the emission of an electron to a doubly excited state Li^{+**} which in turn decays with the emission of a further electron to the $\mathrm{Li}^{2+}(1\mathrm{s})$ ground state. Observing the secondary Li^+ Auger decays in (8.183) as a function of the incident photon energy in the experiment was found to be a valuable technique for the detection of new triply excited hollow-atom resonances of the parent lithium ion.

In the R-matrix calculation, 29 Li^+ ground and singly excited states and 10 Li^+ doubly excited states were included in the internal region expansion (8.53) and the external region expansion (8.63) of both the final $\mathrm{e}^- + \mathrm{Li}^+$ collision wave function and in the corresponding initial Li bound-state wave function. In this way triply excited resonance states of Li^{***} in (8.183) and their contribution to the photoionization cross section were calculated.

We compare in Fig. 8.5 the relative experimental partial photoionization cross section measurements for Li atoms when the Li^+ ion is left in the $2\mathrm{s}^2\ {}^1\mathrm{S}^\mathrm{e}$, $2\mathrm{s}2\mathrm{p}\ {}^3\mathrm{P}^\mathrm{o}$ and $2\mathrm{s}2\mathrm{p}\ {}^1\mathrm{P}^\mathrm{o}$ state together with their sum, with the corresponding ab initio R-matrix calculation for incident photons in the energy range from 160.1 to 163.6 eV. The R-matrix resonance predictions show a small systematic energy shift from the experimental values. However, the number and relative magnitudes of the resonances and even small spectral features are well reproduced by the theory. Overall, the good agreement between theory and experiment has enabled a clear understanding of the excitation and decay mechanisms of the hollow-atom states summarized in (8.183) to be obtained.

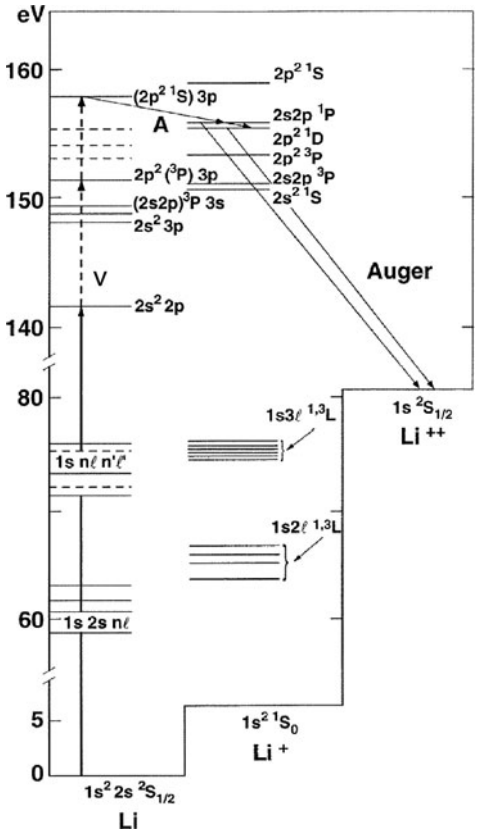

Fig. 8.4 Schematic energy level diagram for neutral lithium, Li^+ and Li^{2+} in the energy region corresponding to the production of hollow Li and hollow Li^+ states using a synchrotron radiation source. A selection of the hollow-atom and hollow-ion levels are shown to illustrate the excitation, indicated by the *upward pointing arrows*, and the decay paths, indicated by *arrows* labelled *A* and Auger (Fig. 1 from [262])

8.5.2 Photoionization of Fe VII

As our second example of photoionization calculations we present results from one of many calculations carried out as part of the Opacity Project, reviewed in Sect. 8.3. We consider the work of Saraph et al. [812] who carried out detailed R-matrix calculations for radiative transitions in Fe VII and Fe VIII. We show in Fig. 8.6 their results for two transitions in Fe VII. The transitions shown in Fig. 8.6 are

$$\begin{aligned} &h\nu + \text{Fe VII}\,(3p^6 3d4p\ {}^1P^o) \rightarrow \text{Fe VIII} + e^-, \\ &h\nu + \text{Fe VII}\,(3p^5({}^2P^o)\,3d^3({}^2D_b)\ {}^1P^o) \rightarrow \text{Fe VIII} + e^-, \end{aligned} \tag{8.184}$$

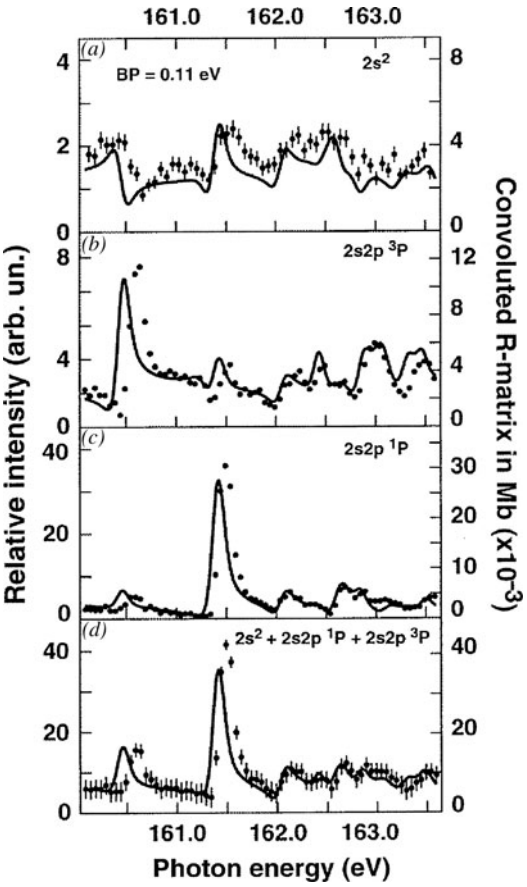

Fig. 8.5 Partial cross sections for photoionizing lithium atoms to (**a**) $2s^2\ {}^1S^e$, (**b**) $2s2p\ {}^3P^o$, (**c**) $2s2p\ {}^1P^o$ and (**d**) their sum for incident photons in the energy range 160.1–163.6 eV. *Full curves*: *R*-matrix calculation convoluted with an experimental bandpass of 0.11 eV. *Dots*: experimental measurements. The *vertical scales* on the right-hand side give the theoretical cross section in MBarn ($\times 10^{-3}$). The *vertical scales* on the left-hand side provide relative experimental values (Fig. 3 from [262])

where 31 states of Fe VIII with configurations $3p^63d$, $3p^53d^2$, $3s3p^63d^2$, $3p^64s$, $3p^64p$, $3p^64d$ and $3p^64f$, were retained in the internal region expansion (8.53) and the external region expansion (8.63) representing both the initial bound and final continuum states of Fe VII. The cross section in Fig. 8.6a for photoionization of the $3p^63d4p\ {}^1P^o$ state was found to be strongly enhanced by PEC (photoexcitation of the core) resonances corresponding to intermediate autoionizing states with configurations $3p^53d^24p$ and $3p^64p^2$. In general, the photoionization cross sections of these and similar ions are found to be dominated by resonances at low energies, which must be accurately determined in order to obtain reliable opacities.

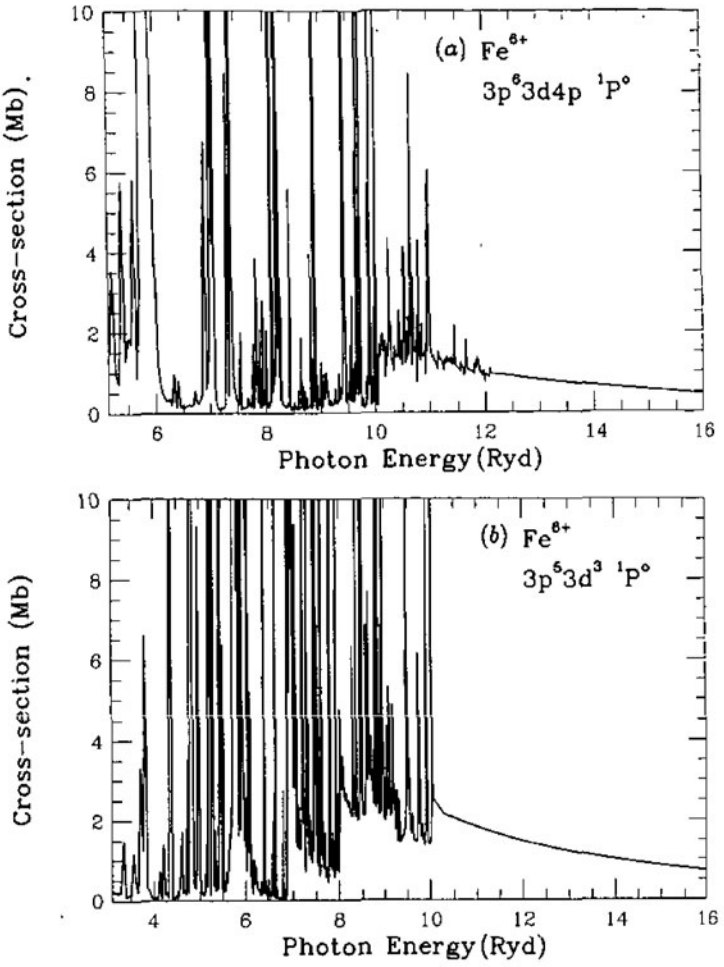

Fig. 8.6 Calculated photoionization cross sections in Mb from (**a**) $3p^6 3d4p\ {}^1P^o$ valence electron state of Fe VII and (**b**) $3p^5({}^2P^o)\ 3d^3({}^2D_b)\ {}^1P^o$ open core state of Fe VII (Fig. 4 from [812])

8.5.3 Photorecombination in Electron Collisions with O VIII

In this example we consider electron–ion photorecombination calculations including the effect of radiation damping which were carried out by Zhang et al. [1008]. Results were obtained for C V, C VI, O VIII and Fe XXV, using both non-relativistic and relativistic versions of the RMATRXI program, discussed in Sect. 5.1.1, where the latter calculations included one-body terms from the Breit–Pauli Hamiltonian, discussed in Sect. 5.4.2. In these calculations all target states up to and including $n = 3$ were included in the R-matrix expansion. We illustrate this work by showing in Fig. 8.7 recombination cross sections for the H-like ion O VIII (O^{7+}), where

the non-resonant and resonant contributions, corresponding to (8.112) and (8.113), respectively, were obtained as part of the same R-matrix calculation. The resonant contribution to the cross section, corresponding to (8.113), proceeds through doubly excited states of O VII (O^{6+}) as follows:

$$e^- + O^{7+}(1s) \rightarrow \left[O^{6+}(2\ell, n'\ell')\right]^{**} \begin{array}{l} \nearrow\ O^{7+}(1s) + e^- \\ \searrow\ O^{6+}(1s, n''\ell'') + h\nu. \end{array} \tag{8.185}$$

We see that in this process the electron incident on the H-like O VIII ion is captured in a doubly excited state of O VII, where one electron is in an excited 2s or 2p orbital and the second electron is in an excited $n'\ell'$ orbital, where resonances corresponding to $n' = 2, 3, 4, \ldots$ are shown in Fig. 8.7. These doubly excited states then decay leaving either O VIII in its ground state plus an emitted electron or leaving O VII in its ground state plus an emitted photon. We see by comparing Figs. 8.7a and b that inclusion of relativistic effects introduces additional fine-structure resonances

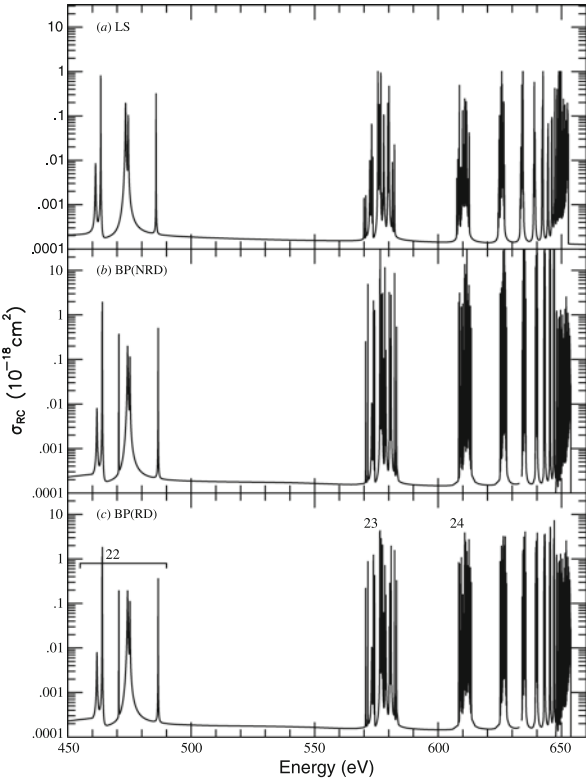

Fig. 8.7 Photorecombination cross sections for $e^- + O\ VIII \rightarrow O\ VII + h\nu$; (**a**) non-relativistic LS-coupling calculations, (**b**) relativistic Breit–Pauli calculations without radiation damping, (**c**) relativistic Breit–Pauli calculations with radiation damping (Fig. 5 from [1008])

and modifies the cross sections. Also, by comparing Figs. 8.7b and c, we see that the effect of including radiation damping is to significantly reduce the photorecombination cross sections. Finally, we observe that the resultant photorecombination cross section was found to be in good agreement with experimental results reported by Kilgus et al. [534] obtained using the heavy-ion Test Storage Ring in Heidelberg.

8.5.4 Radiation Damping in Electron Collisions with Fe XXVI

As an example of the effect of radiation damping on electron collisions, we consider electron impact excitation of the $n = 2$ states of the hydrogen-like ion Fe XXVI. Calculations carried out by Gorczyca and Badnell [392] used the RMATRXI program, discussed in Sect. 5.1.1, which included the one-body terms from the Breit–Pauli Hamiltonian, discussed in Sect. 5.4.2, and which was extended to include the radiation damping potential defined by (8.130). In these calculations all nine fine-structure target states up to $n = 3$ were retained in the R-matrix expansion and excitation cross sections from the $1s_{1/2}$ ground state to the $2s_{1/2}$, $2p_{1/2}$ and $2p_{3/2}$ excited states were calculated, both including and omitting radiation damping. The resultant cross sections are given in Fig. 8.8 where 10,000 energy points were retained in the energy range shown. We see from this figure the important role that radiation damping plays in these cross sections. Thus the KLn resonances, primarily the $2pn\ell$ ($n \geq 20$) resonances just above the $2s_{1/2}$ and $2p_{1/2}$ thresholds, are completely damped, as are the KMn resonances for $n \geq 6$ ($E \geq 590$ Rydbergs). Also we see that even the KMM resonances at $E \sim 535$ Rydbergs show approximately 10% damping. These results show the importance of including radiation damping in calculations for highly ionized ions even for relatively low-lying resonances.

8.5.5 Radiation Damping in Electron Collisions with W XLVII

In this example we consider the effect of radiation damping on electron impact excitation of Ni-like tungsten, W^{46+}, obtained using relativistic Dirac R-matrix calculations by Ballance and Griffin [44]. Accurate atomic collision data are needed in many applications involving tungsten. For example, plans for the International Thermonuclear Experimental Reactor (ITER) include the use of tungsten for certain facing components in the diverter region. Tungsten will also be used for diagnostics of the erosion of heavy species into the plasma. In addition there have been numerous experiments using tungsten within existing tokamaks generating a demand for theoretical electron impact ionization, recombination and excitation data for tungsten and its ions. Of particular importance in this work is the need for electron impact excitation data for Ni-like tungsten since it emits some of the most intense spectral lines resulting from the ionization stages of tungsten.

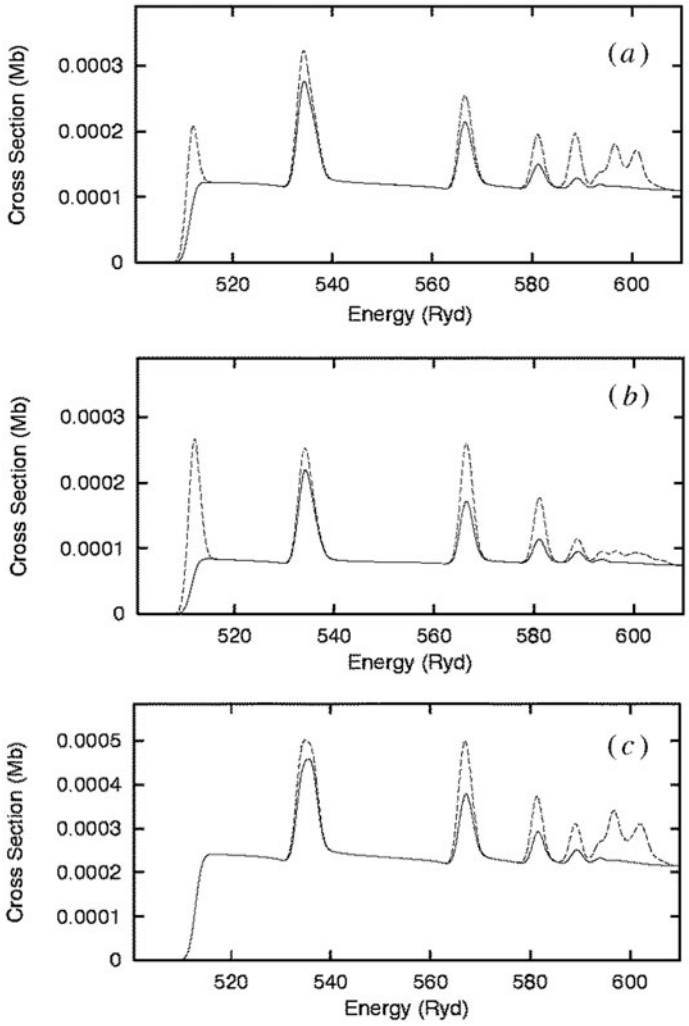

Fig. 8.8 *R*-matrix calculation for electron impact excitation of Fe XXVI from the ground state to the (**a**) $2s_{1/2}$ (**b**) $2p_{1/2}$ and (**c**) $2p_{3/2}$ states, convoluted in each case with a 2.5 Rydberg FWHM Gaussian. *Dotted line*: undamped; *full line*: damped (Fig. 1 from [392])

In these *R*-matrix calculations the target orbitals, energy levels and radiative rates were obtained using the relativistic Dirac–Fock atomic structure program GRASP, and the electron–atom collision calculations were carried out using the Dirac atomic *R*-matrix collision program DARC, discussed in Sect. 5.5.1. The Dirac programs were augmented by sections from the parallel Breit–Pauli RMATRXI package and PSTGF, discussed in Sect. 5.1.1, which had been extended to include radiation damping by Gorczyca et al. [36, 392, 397].

In the W^{46+} calculation 115 target levels were retained in the R-matrix expansion and in the configuration interaction expansion of the target. These levels arose from the 13 configurations $3d^{10}$, $3d^9 4s$, $3d^9 4p$, $3d^9 4d$, $3d^9 4f$, $3d^9 5s$, $3d^9 5p$, $3p^5 3d^{10} 4s$, $3p^5 3d^{10} 4p$, $3p^5 3d^{10} 4d$, $3p^5 3d^{10} 4f$, $3s3p^6 3d^{10} 4s$ and $3s3p^6 3d^{10} 4p$. Also 25 basis orbitals were included for each continuum-electron angular momentum using an R-matrix boundary of 2.0 a.u. All partial waves from $J = 0.5$ to 35.5 were included in the $J\pi$ partial wave expansions and the contribution from the higher partial waves was estimated using a top-up procedure.

As an example of these calculations we compare in Fig. 8.9 the results for the effective collision strength, which is defined in terms of the collision strength by (2.153), for two transitions from the $3p^6 3d^{10}\ ^1S_0$ ground state to (**a**) the $3d^9 4p$

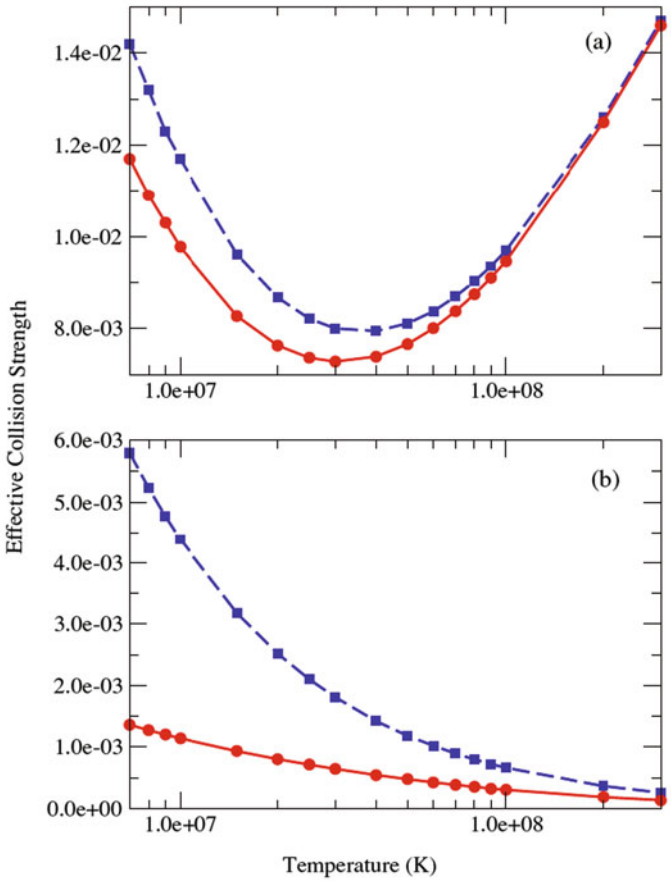

Fig. 8.9 Effective collision strengths for electron impact excitation of Ni-like tungsten (W^{46+}) from the $3p^6 3d^{10}\ ^1S_0$ ground state to (**a**) the $3d^9 4p$ $(5/2,3/2)_1$ level and (**b**) the $3d^9 4d$ $(3/2,3/2)_1$ level. The *long dashed curves with solid squares* are the results with no radiation damping and the *solid curves with solid circles* are with radiation damping (Fig. 4 from [44])

$(5/2,3/2)_1$ and (**b**) the $3d^9 4d\ (3/2,3/2)_1$ levels, where a jj designation is employed since the excited states are highly mixed in LS-coupling. The first transition is an electric dipole-allowed excitation while the second is a much weaker dipole-forbidden transition. However, in both cases the original cross sections have large low-energy resonance contributions. It can be seen from this figure that radiation damping causes a pronounced change in the effective collision strength resulting from its influence on the original cross sections.

In analysing the results it was found that the damping involves the transition of a core electron, leaving the Rydberg electron unchanged. This corresponds to the transitions $3p^6 3d^9 4\ell n\ell' \rightarrow 3p^6 3d^{10} n\ell'$ and $3p^5 3d^{10} 4\ell n\ell' \rightarrow 3p^6 3d^{10} n\ell'$ which are referred to as type I damping. In conclusion we observe that while the damping effects are not as large as might be expected for a 46 times ionized species, due to the closed-shell nature of the Ni-like ground state, they are sufficiently significant that they should be included in collisional–radiative modelling of this ion.

8.5.6 Photoionization Spectrum of Li in a Magnetic Field

As our last example we consider R-matrix calculations of the photoionization spectrum of Li in a magnetic field by Halley et al. [438], using a combination of the external region R-matrix method and the complex coordinate rotation method, discussed in Sect. 8.4. In Fig. 8.10 we compare the calculated spectrum obtained

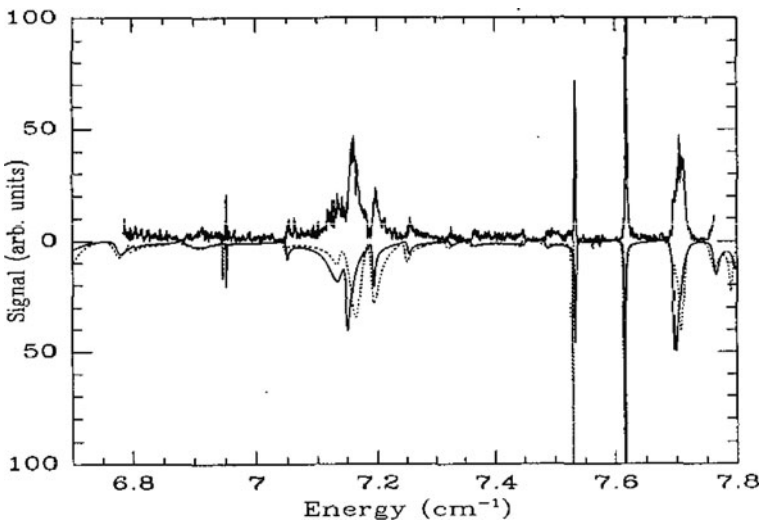

Fig. 8.10 Comparison of an above-threshold experimental spectrum for Li (*full line above*) with the calculated spectrum (*full line below*) and with a previously calculated spectrum for H atoms (*broken line below*). The experimental spectrum was obtained by photoionizing the 3s state of Li in a measured magnetic field of 6.1131 ± 0.001 T. The calculations were carried out for the 3s state in a field of 6.1143 T and convoluting the cross section with a Gaussian window with a 1×10^{-3} cm^{-1} line width equal to the experimental resolution (Fig. 2 from [438])

by Halley et al. [438] for photoionization of Li, from the 3s state to an $m = 0$ odd parity final state, in a magnetic field of strength 6.1143 T over an energy range of 6.7–7.8 cm^{-1}, with previously calculated results for H atoms, obtained by Iu et al. [494] using a complex coordinate approach, and with high-resolution experimental measurements by Iu et al. [493, 494]. The Li calculation by Halley et al. [438] involved the inclusion of 62,500 basis functions in the R-matrix expansion.

The following comments can be made about the calculated results for Li: (i) the absolute values of experimental and theoretical energies of the peaks are in almost perfect agreement where the order of magnitude of the discrepancy is 10^{-3} cm^{-1} which is within the experimental accuracy. This is in contrast to the H-atom spectrum calculated by Iu et al. [494], which did not use the external region R-matrix method, where the discrepancy was of the order 3×10^{-3} cm^{-1}; (ii) the calculated results for Li give a more accurate representation of the peaks around 7.15 cm^{-1}; (iii) some peaks in the H-atom calculation are shifted to higher energies and some to lower energies compared with the Li calculation.

In conclusion, this calculation has shown that the combination of the external region R-matrix method and the complex coordinate rotation method yields accurate results for the spectrum of Li. Calculations using this method for other atoms in electric and magnetic fields, discussed in Sect. 8.4, have also yielded very satisfactory results.

Chapter 9
Multiphoton Processes: Floquet Theory

The study of the interaction of intense laser fields with atoms and molecules has attracted considerable attention in recent years. In particular, the availability of increasingly intense lasers has made possible the observation of a wide variety of multiphoton processes, including multiphoton ionization, laser-assisted electron–atom collisions and harmonic generation. Also, in the case of molecules, the loss of spherical symmetry and the degrees of freedom associated with the nuclear motion give rise to additional computational difficulties and new effects including multiphoton dissociation. Many reviews of these processes have been written and we mention here comprehensive overviews by Gavrila [365], Burnett et al. [194], Mason [639], Protopapas et al. [759] and Joachain et al. [504] where the emphasis is on atomic multiphoton processes, and by Bandrauk et al. [50, 51], Giusti-Suzor et al. [378] and Posthumus [751], where the emphasis is on molecular multiphoton processes. In our discussion of these processes we observe that the atomic unit of electric field strength experienced by an electron in the ground state of atomic hydrogen $\epsilon_a \approx 5.1 \times 10^9$ V/cm corresponds to a laser intensity $I_a \approx 3.5 \times 10^{16}$ W/cm^2. Lasers delivering pulses with intensities much larger than this are now available using the "chirped pulse amplification" (CPA) scheme, in which the laser pulses are stretched, amplified and then compressed [891]. Consequently, many new processes have been observed as a result of exposing atoms and molecules to intense laser fields which require a fully non-perturbative approach for their analysis going beyond the first-order perturbation theory treatment of photoionization considered in Chap. 8. Finally, we mention the fourth-generation light sources which are now coming online which will address new fundamental scientific challenges through their ultra-fast and ultra-bright nature [338].

We commence our discussion of multiphoton processes by considering in this chapter atomic R-matrix–Floquet (RMF) theory and applications, reserving a discussion of time-dependent R-matrix theory, necessary to treat the interaction of ultra-short laser pulses with atoms and ions, until Chap. 10 and R-matrix–Floquet theory of molecular multiphoton processes until Chap. 11. In Sect. 9.1 we consider atomic RMF theory, based on the Floquet–Fourier ansatz [218, 325, 632, 874], which was first formulated by Burke et al. [183, 184] and by Dörr et al. [264] and has since been applied to a wide range of atomic multiphoton processes,

P.G. Burke, *R-Matrix Theory of Atomic Collisions*, Springer Series on Atomic, Optical, and Plasma Physics 61, DOI 10.1007/978-3-642-15931-2_9,

including multiphoton ionization, laser-assisted electron–atom collisions and harmonic generation. This is an ab initio theory, which is fully non-perturbative and is applicable to arbitrary multi-electron atoms and atomic ions, allowing an accurate description of electron–electron correlation effects. In principle this theory is confined to treating laser pulses involving many cycles of the field, typically exceeding tens of femtoseconds (10^{-15} s) and we will discuss applications of this theory to multiphoton ionization, laser-assisted electron–atom collisions and to harmonic generation. We also discuss an extension of this theory using multistate non-hermitian Floquet dynamics [253, 473, 746], which has enabled detailed calculations to be carried out for shorter laser pulse interactions which are in good agreement with fully time-dependent calculations.

Finally, in Sect. 9.2 we present the results of some recent R-matrix–Floquet calculations of multiphoton processes which illustrate the theory presented earlier in this chapter.

9.1 *R*-Matrix–Floquet Theory

In this section we describe an ab initio R-matrix–Floquet theory of atomic multiphoton processes where we consider the interaction of an intense laser field with an atom or atomic ion, which we assume has $N+1$ electrons and nuclear charge number Z.

9.1.1 Introduction

We consider the following three processes: first, multiphoton ionization

$$n\mathrm{h}\nu + A_i \rightarrow A_j^+ + \mathrm{e}^-, \tag{9.1}$$

where the target atom or ion A_i and the residual ion A_j^+ may be in their ground or excited states; second, laser-assisted electron–atom collisions

$$n\mathrm{h}\nu + \mathrm{e}^- + A_i \rightarrow A_j + \mathrm{e}^-, \tag{9.2}$$

where again the target atom or ion A_i and the final atom or ion A_j may be in their ground or excited states; and third, harmonic generation

$$n\mathrm{h}\nu + A_i \rightarrow A_i + \mathrm{h}\nu', \tag{9.3}$$

where A_i may be an atom or an ion and the frequencies ν and ν' are related by $\nu' = n\nu$. We mainly consider processes where there is at most one ejected or scattered electron. However, as in Chap. 6, two electrons in the continuum can be treated by including pseudostates in the R-matrix expansion.

In R-matrix–Floquet theory the laser field, which is treated classically, is usually assumed to be monochromatic, monomode, linearly polarized and spatially homogeneous, and its wavelength is assumed to be large compared with the size of the target atom. The corresponding electric field vector can then be written as

$$\boldsymbol{\mathcal{E}}(t) = -\frac{1}{\mathrm{c}}\frac{\mathrm{d}}{\mathrm{d}t}\mathbf{A}(t) = \hat{\boldsymbol{\epsilon}}\mathcal{E}_0 \cos\omega t, \tag{9.4}$$

where $\hat{\boldsymbol{\epsilon}}$ is a unit vector along the laser polarization direction as in Fig. 8.1, $\mathcal{E}_0$ is the electric field strength and ω is the angular frequency. The corresponding vector potential $\mathbf{A}(t)$ is then given by

$$\mathbf{A}(t) = \hat{\boldsymbol{\epsilon}} A_0 \sin\omega t, \tag{9.5}$$

where $A_0 = -\mathrm{c}\mathcal{E}_0/\omega$ and where we have adopted the Coulomb gauge such that $\mathrm{div}\mathbf{A} = 0$. Neglecting relativistic effects, the atomic system in the presence of the external laser field is described by the time-dependent Schrödinger equation

$$\left[H_{N+1} + \frac{1}{\mathrm{c}}\mathbf{A}(t)\cdot\mathbf{P}_{N+1} + \frac{N+1}{2\mathrm{c}^2}\mathbf{A}^2(t)\right]\widetilde{\Psi}(\mathbf{X}_{N+1}, t) = \mathrm{i}\frac{\partial}{\partial t}\widetilde{\Psi}(\mathbf{X}_{N+1}, t), \tag{9.6}$$

where H_{N+1} is the non-relativistic Hamiltonian of the $(N+1)$-electron atomic system in the absence of the laser field defined by (5.3) and

$$\mathbf{P}_{N+1} = \sum_{i=1}^{N+1} \mathbf{p}_i \tag{9.7}$$

is the total electron momentum operator. Also in (9.6) and later equations in this chapter, the tilde on the time-dependent wave function $\widetilde{\Psi}$ distinguishes it from time-independent wave functions Ψ which we consider later in our analysis.

In accordance with multichannel R-matrix theory of electron–atom collisions discussed in Chap. 5 we partition configuration space into three regions as illustrated in Fig. 9.1. We see that the same partitioning is used as in electron–atom collisions, illustrated in Fig. 5.1. Also the same physical criteria for defining the boundaries a_0 and a_p between the three regions, described in Sect. 5.1, are adopted. Having divided configuration space into three regions, we must solve the time-dependent Schrödinger equation (9.6) in each region. Since the laser field, defined by (9.4), has constant amplitude $\mathcal{E}_0$ and angular frequency ω, we can represent the wave function $\widetilde{\Psi}(\mathbf{X}_{N+1}, t)$ in each of the three regions by a Floquet–Fourier expansion [218, 325, 632, 874] in terms of time-independent wave functions $\Psi_n(\mathbf{X}_{N+1})$ as follows:

$$\widetilde{\Psi}(\mathbf{X}_{N+1}, t) = \exp(-\mathrm{i}Et)\sum_{n=-\infty}^{\infty}\exp(-\mathrm{i}n\omega t)\Psi_n(\mathbf{X}_{N+1}). \tag{9.8}$$

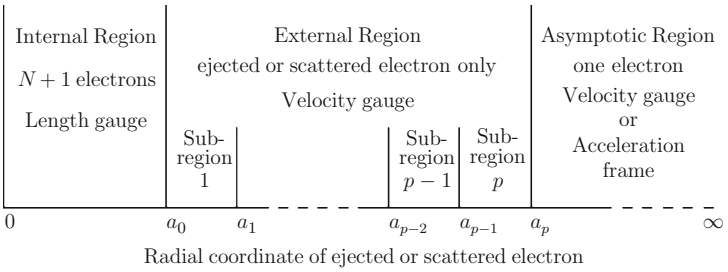

Fig. 9.1 Partitioning of configuration space in R-matrix–Floquet theory

After substituting (9.8) into (9.6) and equating the coefficients of $\exp[-\mathrm{i}(E+n\omega)t]$ to zero, we obtain an infinite set of coupled time-independent equations for the functions Ψ_n, where in practical calculations a finite number of positive and negative terms are retained in the expansion over n in (9.8). The solutions of these equations in each region are then matched on the boundaries a_0 and a_p between the regions using the R-matrix.

In the internal region it is convenient and appropriate to use the length gauge since in this gauge the laser–atom interaction tends to zero at the origin and hence the Floquet–Fourier expansion (9.8) converges more rapidly. However, at larger distances the interaction in the length gauge diverges and hence we use the velocity gauge to describe the ejected or scattered electron in the external region. Finally, in the asymptotic region we derive an asymptotic expansion where the ejected or scattered electron is described in the velocity gauge. We also consider an asymptotic expansion where the ejected or scattered electron is described in the acceleration frame of reference [453, 547] which enables the asymptotic boundary conditions to be expressed in a simple way.

9.1.2 Internal Region Solution

In the internal region in Fig. 9.1 we transform the time-dependent Schrödinger equation (9.6) to the dipole length gauge defined by the unitary gauge transformation

$$\widetilde{\Psi}(\mathbf{X}_{N+1},t)=\exp\left[-\frac{\mathrm{i}}{\mathrm{c}}\mathbf{A}(t)\cdot\mathbf{R}_{N+1}\right]\widetilde{\Psi}^{\mathbf{L}}(\mathbf{X}_{N+1},t), \tag{9.9}$$

where

$$\mathbf{R}_{N+1}=\sum_{i=1}^{N+1}\mathbf{r}_i, \tag{9.10}$$

and the boldface superscript $\mathbf{L}$ in (9.9) and later equations indicates that the $N+1$ electrons are described in the dipole length gauge. Substituting (9.9) into (9.6) we

find that the wave function $\widetilde{\Psi}^{\mathbf{L}}$ satisfies the time-dependent Schrödinger equation

$$(H_{N+1} + \boldsymbol{\mathcal{E}}(t) \cdot \mathbf{R}_{N+1})\, \widetilde{\Psi}^{\mathbf{L}}(\mathbf{X}_{N+1}, t) = \mathrm{i}\frac{\partial}{\partial t}\widetilde{\Psi}^{\mathbf{L}}(\mathbf{X}_{N+1}, t). \tag{9.11}$$

In order to solve this equation we introduce the Floquet–Fourier expansion defined by (9.8) which in this region can be written as

$$\widetilde{\Psi}^{\mathbf{L}}(\mathbf{X}_{N+1}, t) = \exp(-\mathrm{i}Et) \sum_{n=-\infty}^{\infty} \exp(-\mathrm{i}n\omega t)\Psi_n^{\mathbf{L}}(\mathbf{X}_{N+1}), \tag{9.12}$$

where E is the quasi-energy of the corresponding stationary state. Substituting (9.12) into (9.11) and equating the coefficient of $\exp[-\mathrm{i}(E + n\omega)t]$ to zero yields the infinite set of coupled time-independent equations

$$(H_{N+1} - E - n\omega)\Psi_n^{\mathbf{L}} + D_{N+1}(\Psi_{n-1}^{\mathbf{L}} + \Psi_{n+1}^{\mathbf{L}}) = 0, \tag{9.13}$$

where the dipole length operator

$$D_{N+1} = \frac{1}{2}\mathcal{E}_0\hat{\boldsymbol{\epsilon}} \cdot \mathbf{R}_{N+1}. \tag{9.14}$$

If we regard the functions $\Psi_n^{\mathbf{L}}$ as the components of a vector $\boldsymbol{\Psi}^{\mathbf{L}}$ in photon space, then (9.13) can be written as a matrix equation in this space as

$$\left(\mathbf{H}_{\mathrm{F}}^{\mathbf{L}} - E\mathbf{I}\right)\boldsymbol{\Psi}^{\mathbf{L}} = 0, \tag{9.15}$$

where the Floquet–Fourier Hamiltonian $\mathbf{H}_{\mathrm{F}}^{\mathbf{L}}$ is an infinite-dimensional tridiagonal matrix operator in photon space with components

$$\mathbf{H}_{\mathrm{F}}^{\mathbf{L}} = \begin{bmatrix} \ddots & & & & & 0 \\ & H_{N+1} - (n-1)\omega & D_{N+1} & & & \\ & D_{N+1} & H_{N+1} - n\omega & D_{N+1} & & \\ & & D_{N+1} & H_{N+1} - (n+1)\omega & & \\ 0 & & & & & \ddots \end{bmatrix}. \tag{9.16}$$

Also in (9.15), $\boldsymbol{\Psi}^{\mathbf{L}}$ is a solution vector with components $\ldots, \Psi_{n-1}^{\mathbf{L}}, \Psi_n^{\mathbf{L}}, \Psi_{n+1}^{\mathbf{L}}, \ldots$ and $\mathbf{I}$ is a unit matrix operator.

In order to solve (9.15) in the internal region we expand the solution vector $\boldsymbol{\Psi}^{\mathbf{L}}$, in analogy with (5.5), as follows:

$$\boldsymbol{\Psi}_{jE}^{\mathbf{L}\gamma}(\mathbf{X}_{N+1}) = \sum_k \boldsymbol{\psi}_k^{\mathbf{L}\gamma}(\mathbf{X}_{N+1})A_{kj}^{\mathbf{L}\gamma}(E). \tag{9.17}$$

In this equation, and in the following equations, we introduce a superscript γ which represents the quantum numbers which are conserved in the laser–atom interaction process discussed below. Also in (9.17), j labels the linearly independent solutions of (9.15), $\boldsymbol{\psi}_k^{\mathbf{L}\gamma}$ are energy-independent vector basis functions with Floquet–Fourier components $\psi_{nk}^{\mathbf{L}\gamma}$ defined by (9.20) and $A_{kj}^{\mathbf{L}\gamma}(E)$ are energy-dependent expansion coefficients which depend on the asymptotic boundary conditions satisfied by the solution $\boldsymbol{\Psi}_{jE}^{\mathbf{L}\gamma}$.

The conserved quantum numbers γ depend on the symmetry of the atomic target state and the polarization of the laser field. One example of considerable experimental and theoretical interest is the interaction of linearly polarized laser light with a closed-shell atom such as neon or argon initially in its $^1\mathrm{S}_0^\mathrm{e}$ ground state. We show in Fig. 9.2 the allowed transitions from the $^1\mathrm{S}_0^\mathrm{e}$ $M_L = 0$ state as linearly polarized photons are absorbed or emitted. In this case the conserved quantum numbers represented by γ are given by

$$\gamma \equiv \alpha \; S \; M_S \; M_L \; \pi', \tag{9.18}$$

where S is the total spin angular momentum, M_S and M_L are the total spin and orbital magnetic quantum numbers in the laser polarization direction, π' is defined in terms of the parity π of the target atom by

$$\pi' = (-1)^n \pi \tag{9.19}$$

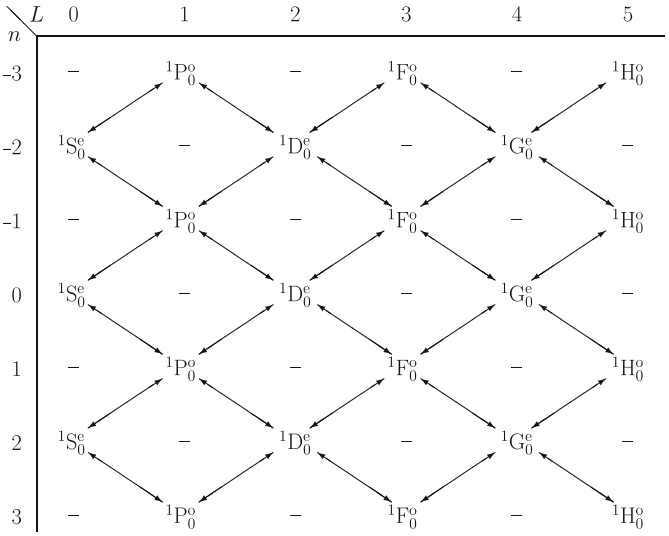

Fig. 9.2 Allowed transitions for linearly polarized laser light incident on an atom in a $^1\mathrm{S}_0^\mathrm{e}$ state. L is the total orbital angular momentum of the atom and n is the number of photons absorbed, or emitted, corresponding to the Floquet–Fourier expansion index in (9.12). The *arrowed lines* show the transitions allowed by the laser field

and α represents any other quantum numbers which are conserved in the collision. Unlike the conserved quantum numbers Γ in non-relativistic electron–atom collisions, defined by (2.58), we see that the total orbital angular momentum L of the target atom or ion is not conserved. Also, since the total orbital magnetic quantum numbers of the target atom and the linearly polarized laser light are zero, see (B.55), it follows from the parity selection rule (A.27), satisfied by the Clebsch–Gordan coefficients, that dipole transitions such as ${}^1\mathrm{P}^{\mathrm{e}}_0 \rightarrow {}^1\mathrm{P}^{\mathrm{o}}_0$, ${}^1\mathrm{D}^{\mathrm{e}}_0 \rightarrow {}^1\mathrm{D}^{\mathrm{o}}_0$ are forbidden. This limits the number of $LS\pi$ states that are coupled to one-half the maximum number, as illustrated in Fig. 9.2, and results in the conservation of π' defined by (9.19). However, π' would not be conserved for linearly polarized laser light incident on target atoms where $M_L \neq 0$ nor for circularly polarized laser light incident on an arbitrary atom. As a second example, we show in Fig. 9.3 the allowed transitions from the ${}^1\mathrm{S}^{\mathrm{e}}_0$ $M_L = 0$ state as circularly polarized photons are absorbed or emitted, where the subscript on the target states in this figure is the M_L value, which is now not conserved in the transitions.

Following (5.6) we expand each Floquet–Fourier component of the vector basis functions $\boldsymbol{\psi}_k^{\mathbf{L}\gamma}(\mathbf{X}_{N+1})$ in (9.17) in a close coupling with pseudostates expansion given by

$$\begin{aligned}\psi_{nk}^{\mathbf{L}\gamma}(\mathbf{X}_{N+1}) = \mathcal{A}\sum_{Lij}\overline{\Phi}^{\gamma}_{nLi}(\mathbf{X}_N;\hat{\mathbf{r}}_{N+1}\sigma_{N+1})r_{N+1}^{-1}u^0_{nLij}(r_{N+1})a^{\mathbf{L}\gamma}_{nLijk}\\ + \sum_{Li}\chi^{\gamma}_{nLi}(\mathbf{X}_{N+1})b^{\mathbf{L}\gamma}_{nLik},\\ k = 1,\ldots,n_t,\end{aligned} \tag{9.20}$$

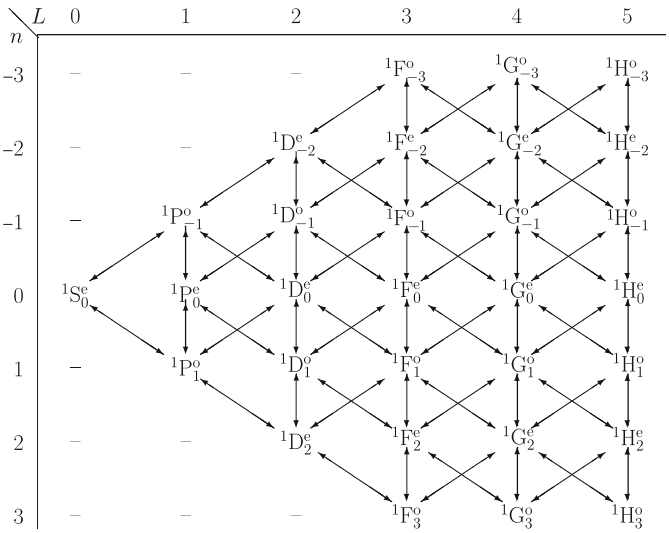

Fig. 9.3 Allowed transitions for circularly polarized laser light incident on an atom in a ${}^1\mathrm{S}^{\mathrm{e}}_0$ state. L is the total orbital angular momentum of the atom and n is the number of photons absorbed, or emitted, corresponding to the Floquet–Fourier expansion index in (9.12). The *arrowed lines* show the transitions allowed by the laser field

where $\overline{\Phi}^{\gamma}_{nLi}$ are channel functions obtained by coupling the residual atom or ion states in the case of multiphoton ionization (or target atom or ion states in the case of laser-assisted electron–atom collisions) and possibly pseudostates with the spin – angle functions of the ejected or scattered electron, u^{0}_{nLij} are radial continuum basis orbitals, χ^{γ}_{nLi} are quadratically integrable functions and n_t is the total number of terms retained in the expansion. By reference to Figs. 9.2 and 9.3, we see that, in addition to the usual expansion (5.6) for each $LS\pi$ combination which appear in these figures, a summation must also be carried out over the number of photons n absorbed or emitted and over the number of total orbital angular momenta L retained in the expansion of $\boldsymbol{\psi}^{\mathbf{L}\gamma}_{k}$ in (9.17). Hence the value of n_t will be very much larger than that arising in electron–atom collisions in the absence of the laser field, defined following (5.6). The coefficients $a^{\mathbf{L}\gamma}_{nLijk}$ and $b^{\mathbf{L}\gamma}_{nLik}$ in (9.20) are determined by diagonalizing the matrix operator $\mathbf{H}^{\mathbf{L}}_{\mathrm{F}} + \boldsymbol{\mathcal{L}}_{N+1}$ in the basis functions $\boldsymbol{\psi}^{\mathbf{L}\gamma}_{k}$ as follows:

$$\langle \Psi^{\mathbf{L}\gamma}_{k} | \mathbf{H}^{\mathbf{L}}_{\mathrm{F}} + \boldsymbol{\mathcal{L}}_{N+1} | \Psi^{\mathbf{L}\gamma}_{k'} \rangle_{\mathrm{int}} = \mathbf{E}^{\mathbf{L}\gamma}_{k} \delta_{kk'}, \quad k,\ k' = 1, \ldots, n_t, \tag{9.21}$$

where $\mathbf{H}^{\mathbf{L}}_{\mathrm{F}}$ is the Floquet Hamiltonian matrix defined by (9.16) and $\boldsymbol{\mathcal{L}}_{N+1}$ is a Bloch matrix operator which has the following form:

$$\boldsymbol{\mathcal{L}}_{N+1} = \sum_{i=1}^{N+1} \frac{1}{2} \delta(r_i - a_0) \left(\frac{\mathrm{d}}{\mathrm{d}r_i} - \frac{b_0 - 1}{r_i} \right) \mathbf{I}, \tag{9.22}$$

where $\mathbf{I}$ is a unit matrix in photon space. It follows from our analysis in Sect. 5.1.2 that $\mathbf{H}^{\mathrm{L}}_{\mathrm{F}} + \boldsymbol{\mathcal{L}}_{N+1}$ is hermitian in the internal region in the basis of quadratically integrable vector functions in photon space satisfying arbitrary boundary conditions at $r = a_0$.

We can now solve (9.15) in the internal region to determine $\boldsymbol{\Psi}^{\mathbf{L}\gamma}_{jE}$, defined by (9.17). We rewrite (9.15) as

$$\left(\mathbf{H}^{\mathbf{L}}_{\mathrm{F}} + \boldsymbol{\mathcal{L}}_{N+1} - E\mathbf{I} \right) \boldsymbol{\Psi}^{\mathbf{L}\gamma}_{jE} = \boldsymbol{\mathcal{L}}_{N+1} \boldsymbol{\Psi}^{\mathbf{L}\gamma}_{jE}, \tag{9.23}$$

which has the formal solution

$$\boldsymbol{\Psi}^{\mathbf{L}\gamma}_{jE} = \left(\mathbf{H}^{\mathbf{L}}_{\mathrm{F}} + \boldsymbol{\mathcal{L}}_{N+1} - E\mathbf{I} \right)^{-1} \boldsymbol{\mathcal{L}}_{N+1} \boldsymbol{\Psi}^{\mathbf{L}\gamma}_{jE}. \tag{9.24}$$

Using the spectral representation of $\mathbf{H}^{\mathbf{L}}_{\mathrm{F}} + \boldsymbol{\mathcal{L}}_{N+1}$ given by (9.21), we can rewrite (9.24) as

$$|\boldsymbol{\Psi}^{\mathbf{L}\gamma}_{jE}\rangle = \sum_{k} |\Psi^{\mathbf{L}\gamma}_{k}\rangle \frac{1}{\mathbf{E}^{\mathbf{L}\gamma}_{k} - E\mathbf{I}} \langle \Psi^{\mathbf{L}\gamma}_{k} | \boldsymbol{\mathcal{L}}_{N+1} | \boldsymbol{\Psi}^{\mathbf{L}\gamma}_{jE} \rangle. \tag{9.25}$$

We then project this equation onto the nth component in photon space and onto the channel functions $\overline{\Phi}^{\gamma}_{nLi}$ included in expansion (9.20). We obtain after setting $r_{N+1} = a_0$

$$F^{\mathbf{L}\gamma}_{nLij}(a_0) = \sum_{n'L'i'} R^{\mathbf{L}\gamma}_{nLin'L'i'}(E) \left(a_0 \frac{\mathrm{d}F^{\mathbf{L}\gamma}_{n'L'i'j}}{\mathrm{d}r} - b_0 F^{\mathbf{L}\gamma}_{n'L'i'j} \right)_{r=a_0}, \tag{9.26}$$

where we have introduced the R-matrix $R^{\mathbf{L}\gamma}_{nLin'L'i'}(E)$ in the length gauge by

$$R^{\mathbf{L}\gamma}_{nLin'L'i'}(E) = \frac{1}{2a_0} \sum_{k=1}^{n_t} \frac{w^{\mathbf{L}\gamma}_{nLik} w^{\mathbf{L}\gamma}_{n'L'i'k}}{E^{\gamma}_k - E}, \tag{9.27}$$

the reduced radial wave functions $F^{\mathbf{L}\gamma}_{nLij}(r)$ defined by

$$F^{\mathbf{L}\gamma}_{nLij}(r_{N+1}) = \langle r^{-1}_{N+1} \overline{\Phi}^{\gamma}_{nLi} | \Psi^{\mathbf{L}\gamma}_{njE} \rangle' \tag{9.28}$$

and the surface amplitudes $w^{\mathbf{L}\gamma}_{nLik}$ by

$$w^{\mathbf{L}\gamma}_{nLik} = \langle r^{-1}_{N+1} \overline{\Phi}^{\gamma}_{nLi} | \psi^{\mathbf{L}\gamma}_{nk} \rangle'_{r_{N+1}=a_0} = \sum_j u^0_{nLij}(a_0) a^{\mathbf{L}\gamma}_{nLijk}. \tag{9.29}$$

As in (5.20) and (5.21), the primes on the Dirac brackets in (9.28) and (9.29) mean that the integrations are carried out over the space and spin coordinates of all $N + 1$ electrons in the internal region except the radial coordinate r_{N+1} of the ejected or scattered electron. Also, $\Psi^{\mathbf{L}\gamma}_{njE}$ in (9.28) are the Floquet–Fourier components of the solution vector $\boldsymbol{\Psi}^{\mathbf{L}\gamma}_{jE}$ defined by (9.17). We note that if the radial continuum basis orbitals $u^0_{nLij}(r)$, retained in expansion (9.20), satisfy homogeneous boundary conditions at $r = a_0$, then a Buttle correction must be added to the R-matrix defined by (9.27), as discussed in Sect. 5.3.2.

Equations (9.26) and (9.27) are the basic equations describing the solution of (9.6) in the internal region, where (9.26) provides the boundary condition at $r = a_0$ for solving (9.6) in the external region considered in the next section.

9.1.3 External Region Solution

In the external region, shown in Fig. 9.1, the ejected or scattered electron with radial coordinate $a_0 \leq r_{N+1} \leq a_p$ is described using the velocity gauge, while the remaining N electrons with radial coordinates $r_i \leq a_0, i = 1, \ldots, N$, are described using the length gauge. This is possible since the outer electron and the N inner electrons occupy different regions of space and are distinguishable. Hence

their wave functions can be transformed independently. The corresponding unitary transformation of the time-dependent Schrödinger equation (9.6) is given by

$$\widetilde{\Psi}(\mathbf{X}_{N+1},t)=\exp\left[-\frac{\mathrm{i}}{\mathrm{c}}\mathbf{A}(t)\cdot\mathbf{R}_N-\frac{\mathrm{i}}{2\mathrm{c}^2}\int^t\mathbf{A}^2(t')\mathrm{d}t'\right]\widetilde{\Psi}^{\mathbf{V}}(\mathbf{X}_{N+1},t),\tag{9.30}$$

where

$$r_i\le a_0,\quad i=1,\ldots,N,\quad r_{N+1}\ge a_0,\tag{9.31}$$

and where $\mathbf{R}_N$ is defined by (9.10) with $N+1$ replaced by N. Substituting (9.30) into (9.6) then yields the following time-dependent Schrödinger equation satisfied by $\widetilde{\Psi}^{\mathbf{V}}(\mathbf{X}_{N+1},t)$:

$$\left(H_{N+1}+\boldsymbol{\mathcal{E}}(t)\cdot\mathbf{R}_N+\frac{1}{\mathrm{c}}\mathbf{A}(t)\cdot\mathbf{p}_{N+1}\right)\widetilde{\Psi}^{\mathbf{V}}(\mathbf{X}_{N+1},t)=\mathrm{i}\frac{\partial}{\partial t}\widetilde{\Psi}^{\mathbf{V}}(\mathbf{X}_{N+1},t),\tag{9.32}$$

where the boldface superscript $\mathbf{V}$ in (9.30) and (9.32) and later equations indicates that the ejected or scattered electron is described in the velocity gauge.

Following our discussion of the internal region solution we now make a Floquet – Fourier expansion of the wave function $\widetilde{\Psi}^{\mathbf{V}}$ as follows:

$$\widetilde{\Psi}^{\mathbf{V}}(\mathbf{X}_{N+1},t)=\exp(-\mathrm{i}E^{\mathbf{V}}t)\sum_{n=-\infty}^{\infty}\exp(-\mathrm{i}n\omega t)\Psi_n^{\mathbf{V}}(\mathbf{X}_{N+1}),\tag{9.33}$$

where $E^{\mathbf{V}}$ is the quasi-energy in the velocity gauge. The quasi-energy $E^{\mathbf{V}}$ has a negative imaginary part for multiphoton ionization and harmonic generation, corresponding to Siegert [876] outgoing wave boundary conditions, discussed in Sect. 1.3, and is real for laser-assisted electron–atom collisions. The relationship between $E^{\mathbf{V}}$ and the quasi-energy E in (9.12) is given by (9.48) and (9.52). Substituting (9.33) into (9.32) and equating the coefficient of $\exp[-\mathrm{i}(E^{\mathbf{V}}+n\omega)t]$ to zero yields the following infinite set of coupled time-independent equations:

$$\left(H_{N+1}-E^{\mathbf{V}}-n\omega\right)\Psi_n^{\mathbf{V}}+D_N\left(\Psi_{n-1}^{\mathbf{V}}+\Psi_{n+1}^{\mathbf{V}}\right)+P_{N+1}\left(\Psi_{n-1}^{\mathbf{V}}-\Psi_{n+1}^{\mathbf{V}}\right)=0,\tag{9.34}$$

where the dipole length operator D_N is defined by (9.10) and (9.14) with $N+1$ replaced by N and the dipole velocity operator P_{N+1} is defined by

$$P_{N+1}=\mathrm{i}\frac{A_0}{2\mathrm{c}}\hat{\boldsymbol{\epsilon}}\cdot\mathbf{p}_{N+1}.\tag{9.35}$$

In analogy with (9.15) the functions $\Psi_n^{\mathbf{V}}$ can be regarded as components of a vector $\boldsymbol{\Psi}^{\mathbf{V}}$ in photon space and hence (9.34) can be written as a matrix equation in this space as

$$\left(\mathbf{H}_{\mathrm{F}}^{\mathbf{V}} - E^{\mathbf{V}}\mathbf{I}\right)\boldsymbol{\Psi}^{\mathbf{V}} = 0, \tag{9.36}$$

where the Floquet Hamiltonian $\mathbf{H}_{\mathrm{F}}^{\mathbf{V}}$ is an infinite-dimensional tridiagonal matrix operator in photon space.

9.1.3.1 Derivation of Coupled Differential Equations

In order to solve (9.36) in the external region we adopt the following close coupling expansion of the components $\Psi_n^{\mathbf{V}\gamma}$ of the total wave function at energy E, for each set of conserved quantum numbers denoted by γ,

$$\Psi_{njE}^{\mathbf{V}\gamma}(\mathbf{X}_{N+1}) = \sum_{Li} \overline{\Phi}_{nLi}^{\gamma}(\mathbf{X}_N; \hat{\mathbf{r}}_{N+1}\sigma_{N+1}) r_{N+1}^{-1} F_{nLij}^{\mathbf{V}\gamma}(r_{N+1}), \quad r_{N+1} \geq a_0, \tag{9.37}$$

where the channel functions $\overline{\Phi}_{nLi}^{\gamma}$ retained in this expansion are the same as those retained in the internal region expansion (9.20). Also in (9.37), $F_{nLij}^{\mathbf{V}\gamma}(r)$ are the reduced radial wave functions in the velocity gauge corresponding to $F_{nLij}^{\mathbf{L}\gamma}(r)$ in the length gauge defined by (9.28) and j labels the linearly independent solutions of (9.15) and (9.36). We note that (9.37) is not antisymmetrized with respect to the $(N+1)$th electron since, as pointed out above, this electron now occupies a different region of space than the remaining N electrons and hence is distinguishable. Also, the quadratically integrable functions in (9.20), which are confined to the internal region, are not included in (9.37).

After substituting (9.37) into (9.36) and projecting onto the channel functions $\overline{\Phi}_{nLi}^{\gamma}$ we obtain the following coupled second-order differential equations, satisfied by the reduced radial functions $F_{nLij}^{\mathbf{V}\gamma}(r)$:

$$\begin{aligned}\left(\frac{\mathrm{d}^2}{\mathrm{d}r^2} - \frac{\ell_i(\ell_i+1)}{r^2} + \frac{2(Z-N)}{r} + k_{ni}^2\right) F_{nLij}^{\mathbf{V}\gamma}(r) \\ = 2\sum_{n'L'i'} W_{nLin'L'i'}^{\mathbf{V}\gamma}(r) F_{n'L'i'j}^{\mathbf{V}\gamma}(r), \quad r \geq a_0,\end{aligned} \tag{9.38}$$

where ℓ_i is the orbital angular momentum of the ejected or scattered electron and k_{ni}^2 can be expressed in terms of the channel energies $\overline{e}_i$ of the residual N-electron ion by the equation

$$k_{ni}^2 = 2\left(E^{\mathbf{V}} - f_{ni}\right), \tag{9.39}$$

where

$$f_{ni} = \overline{e}_i + n\omega. \tag{9.40}$$

Also in (9.38), $W^{\mathbf{V}\gamma}_{nLin'L'i'}(r)$ is the long-range potential matrix coupling the channels which can be written in matrix notation as[1]

$$\mathbf{W}^{\mathbf{V}\gamma} = \mathbf{V}^{E\gamma} + \mathbf{V}^{D\gamma} + \mathbf{V}^{P\gamma}, \tag{9.41}$$

where $\mathbf{V}^{E\gamma}$, $\mathbf{V}^{D\gamma}$ and $\mathbf{V}^{P\gamma}$ arise, respectively, from H_{N+1}, D_N and P_{N+1} and are defined by the following matrix elements:

$$V^{E\gamma}_{nLin'L'i'} = \langle r^{-1}_{N+1}\overline{\Phi}^{\gamma}_{nLi}(\mathbf{X}_N;\hat{\mathbf{r}}_{N+1}\sigma_{N+1})\left|\sum_{j=1}^{N}\frac{1}{r_{jN+1}} - \frac{N}{r_{N+1}}\right| \times r^{-1}_{N+1}\overline{\Phi}^{\gamma}_{n'L'i'}(\mathbf{X}_N;\hat{\mathbf{r}}_{N+1}\sigma_{N+1})\rangle'\delta_{nn'}, \tag{9.42}$$

$$V^{D\gamma}_{nLin'L'i'} = \langle r^{-1}_{N+1}\overline{\Phi}^{\gamma}_{nLi}(\mathbf{X}_N;\hat{\mathbf{r}}_{N+1}\sigma_{N+1})\,|D_N|\,r^{-1}_{N+1} \times \overline{\Phi}^{\gamma}_{n'L'i'}(\mathbf{X}_N;\hat{\mathbf{r}}_{N+1}\sigma_{N+1})\rangle'\left(\delta_{nn'-1} + \delta_{nn'+1}\right) \tag{9.43}$$

and

$$V^{P\gamma}_{nLin'L'i'} = \langle r^{-1}_{N+1}\overline{\Phi}^{\gamma}_{nLi}(\mathbf{X}_N;\hat{\mathbf{r}}_{N+1}\sigma_{N+1})\left|\mathrm{i}\frac{A_0}{2c}\hat{\boldsymbol{\epsilon}}\cdot\mathbf{p}_{N+1}\right| r^{-1}_{N+1} \times \overline{\Phi}^{\gamma}_{n'L'i'}(\mathbf{X}_N;\hat{\mathbf{r}}_{N+1}\sigma_{N+1})\rangle'\left(\delta_{nn'+1} - \delta_{nn'-1}\right). \tag{9.44}$$

The integrals in these matrix elements are carried out over all $N+1$ electron space and spin coordinates except the radial coordinate of the $(N+1)$th electron.

9.1.3.2 Boundary Condition at $r = a_0$

The boundary condition at $r = a_0$ satisfied by the reduced radial functions $F^{\mathbf{V}\gamma}_{nLij}(r)$ in (9.38) can be determined by expressing these functions in terms of the functions $F^{\mathbf{L}\gamma}_{nLij}(r)$ in (9.26) at $r = a_0$. The relationship between $F^{\mathbf{V}\gamma}_{nLij}(a_0)$ and $F^{\mathbf{L}\gamma}_{nLij}(a_0)$ can be obtained from (9.9) and (9.30) which gives

$$\widetilde{\Psi}^{\mathbf{V}}(\mathbf{X}_{N+1},t) = \exp\left[\frac{\mathrm{i}}{2c^2}\int^t \mathbf{A}^2(t')\mathrm{d}t' - \frac{\mathrm{i}}{c}\mathbf{A}(t)\cdot\mathbf{r}_{N+1}\right]\widetilde{\Psi}^{\mathbf{L}}(\mathbf{X}_{N+1},t), \tag{9.45}$$

where

$$r_i \le a_0, \quad i = 1,\ldots,N, \quad r_{N+1} = a_0. \tag{9.46}$$

[1] Explicit expressions for the potential matrices $\mathbf{V}^{E\gamma}$, $\mathbf{V}^{D\gamma}$ and $\mathbf{V}^{P\gamma}$ in (9.41) are derived in Appendix D.2.

We make use of the explicit form of the vector potential $\mathbf{A}(t)$, given by (9.5), to rewrite (9.45) as

$$\widetilde{\Psi}^{\mathbf{V}}(\mathbf{X}_{N+1}, t) = \exp\left(\frac{\mathrm{i}A_0^2}{4\mathrm{c}^2}t\right)\exp\left[-\frac{\mathrm{i}A_0^2}{8\omega\mathrm{c}^2}\sin(2\omega t) - \frac{\mathrm{i}A_0}{\mathrm{c}}\hat{\boldsymbol{\epsilon}}\cdot\mathbf{r}_{N+1}\sin(\omega t)\right] \times \widetilde{\Psi}^{\mathbf{L}}(\mathbf{X}_{N+1}, t), \tag{9.47}$$

where we have taken the lower limit of integration in (9.45) to be zero. The first exponential on the right-hand side of (9.47) has the form $\exp(\mathrm{i}E_{\mathrm{p}}t)$, where

$$E_{\mathrm{p}} = \frac{A_0^2}{4\mathrm{c}^2} = \frac{\mathcal{E}_0^2}{4\omega^2} \tag{9.48}$$

is the ponderomotive energy of the ejected or scattered electron. This energy is the average kinetic energy of a free electron oscillating in a laser field corresponding to the vector potential defined by (9.5) and the electric field vector defined by (9.4). The second exponential in (9.47) can be expanded in a Fourier series using the equation

$$\exp(\mathrm{i}z\sin\theta) = \sum_{n=-\infty}^{\infty} J_n(z)\exp(\mathrm{i}n\theta), \tag{9.49}$$

which follows from (C.9) by writing $t = \exp(\mathrm{i}\theta)$, where the $J_n(z)$ are Bessel functions of the first kind. Substituting the Floquet–Fourier expansions for $\widetilde{\Psi}^{\mathbf{L}}$ and $\widetilde{\Psi}^{\mathbf{V}}$, given by (9.12) and (9.33), respectively, into (9.47) then gives

$$\begin{aligned}\exp(-\mathrm{i}E^{\mathbf{V}}t)&\sum_{n=-\infty}^{\infty}\exp(-\mathrm{i}n\omega t)\Psi_n^{\mathbf{V}}(\mathbf{X}_{N+1})\\ &= \exp[-\mathrm{i}(E-E_{\mathrm{p}})t]\sum_{\ell=-\infty}^{\infty} f_\ell(A_0, \hat{\boldsymbol{\epsilon}}\cdot\mathbf{r}_{N+1})\exp(-\mathrm{i}\ell\omega t)\\ &\times\sum_{n'=-\infty}^{\infty}\exp(-\mathrm{i}n'\omega t)\Psi_{n'}^{\mathbf{L}}(\mathbf{X}_{N+1}),\end{aligned} \tag{9.50}$$

where

$$f_\ell(A_0, \hat{\boldsymbol{\epsilon}}\cdot\mathbf{r}_{N+1}) = \sum_{\ell'=-\infty}^{\infty} J_{\ell'}\left(\frac{A_0^2}{8\omega\mathrm{c}^2}\right)J_{\ell-2\ell'}\left(\frac{A_0}{\mathrm{c}}\hat{\boldsymbol{\epsilon}}\cdot\mathbf{r}_{N+1}\right). \tag{9.51}$$

From (9.50) we deduce that the quasi-energies E and $E^{\mathbf{V}}$ are related by

$$E^{\mathbf{V}} = E - E_{\mathrm{p}} \tag{9.52}$$

and that

$$\Psi_n^{\mathbf{V}}(\mathbf{X}_{N+1}) = \sum_{n'=-\infty}^{\infty} f_{n-n'}(A_0, \hat{\boldsymbol{\epsilon}} \cdot \mathbf{r}_{N+1}) \Psi_{n'}^{\mathbf{L}}(\mathbf{X}_{N+1}). \tag{9.53}$$

Projecting (9.53) onto the channel functions $\overline{\Phi}_{nLi}^{\gamma}$ retained in the internal and external regions in expansions (9.20) and (9.37), evaluating the result on the boundary $r_{N+1} = a_0$ and remembering that $F_{nLij}^{\mathbf{L}\gamma}$ and $F_{nLij}^{\mathbf{V}\gamma}$ are defined by (9.28) and (9.37), respectively, we obtain

$$F_{nLij}^{\mathbf{V}\gamma}(a_0) = \sum_{n'L'i'} C_{nLin'L'i'}^{\gamma} F_{n'L'i'j}^{\mathbf{L}\gamma}(a_0), \tag{9.54}$$

where we have introduced the matrix elements

$$\begin{aligned} C_{nLin'L'i'}^{\gamma} = {} & \langle r_{N+1}^{-1} \overline{\Phi}_{nLi}^{\gamma}(\mathbf{X}_N; \hat{\mathbf{r}}_{N+1}\sigma_{N+1}) | f_{n-n'}(A_0, \hat{\boldsymbol{\epsilon}} \cdot \mathbf{r}_{N+1}) | \\ & \times r_{N+1}^{-1} \overline{\Phi}_{n'L'i'}^{\gamma}(\mathbf{X}_N; \hat{\mathbf{r}}_{N+1}\sigma_{N+1}) \rangle', \quad r_{N+1} = a_0. \end{aligned} \tag{9.55}$$

For notational convenience we rewrite (9.54) in matrix notation as

$$\mathbf{F}_j^{\mathbf{V}\gamma}(a_0) = \mathbf{C}\mathbf{F}_j^{\mathbf{L}\gamma}(a_0), \tag{9.56}$$

where $\mathbf{F}_j^{\mathbf{V}\gamma}(a_0)$ and $\mathbf{F}_j^{\mathbf{L}\gamma}(a_0)$ are column vectors, for each linearly independent solution j, whose dimensions are the number of coupled channels, and $\mathbf{C}$ is an orthogonal matrix.

We can determine the required relation between $\mathbf{F}_j^{\mathbf{V}\gamma}$ and $\mathrm{d}\mathbf{F}_j^{\mathbf{V}\gamma}/\mathrm{d}r$ on the boundary $r = a_0$ by first rewriting (9.26) in matrix notation as

$$\mathbf{F}_j^{\mathbf{L}\gamma}(a_0) = \mathbf{R}^{\mathbf{L}\gamma}(E) a_0 \left. \frac{\mathrm{d}\mathbf{F}_j^{\mathbf{L}\gamma}}{\mathrm{d}r} \right|_{r=a_0}, \tag{9.57}$$

where we have set the arbitrary constant $b_0 = 0$. Taking the derivative of both sides of (9.56) with respect to r and using (9.57) gives

$$\frac{\mathrm{d}\mathbf{F}_j^{\mathbf{V}\gamma}}{\mathrm{d}r} = \left\{ \frac{\mathrm{d}\mathbf{C}}{\mathrm{d}r} + a_0^{-1} \mathbf{C} \left[\mathbf{R}^{\mathbf{L}\gamma}(E) \right]^{-1} \right\} \mathbf{C}^{-1} \mathbf{F}_j^{\mathbf{V}\gamma}, \quad r = a_0. \tag{9.58}$$

This equation can be rewritten as

$$\mathbf{F}_j^{\mathbf{V}\gamma}(a_0) = \mathbf{R}^{\mathbf{V}\gamma}(E) a_0 \left. \frac{\mathrm{d}\mathbf{F}_j^{\mathbf{V}\gamma}}{\mathrm{d}r} \right|_{r=a_0}, \tag{9.59}$$

where

$$\mathbf{R}^{\mathbf{V}\gamma}(E) = a_0^{-1}\mathbf{C}\left\{\frac{\mathrm{d}\mathbf{C}}{\mathrm{d}r} + a_0^{-1}\mathbf{C}\left[\mathbf{R}^{\mathbf{L}\gamma}(E)\right]^{-1}\right\}^{-1}. \tag{9.60}$$

Equation (9.60) enables the R-matrix $\mathbf{R}^{\mathbf{V}\gamma}(E)$ in the velocity gauge at $r = a_0$ to be determined in terms of the R-matrix $\mathbf{R}^{\mathbf{L}\gamma}(E)$ in the length gauge at $r = a_0$, and hence provides the boundary condition at $r = a_0$ satisfied by the solution of (9.38) in the external region.

9.1.3.3 Solution of Coupled Differential Equations

In order to solve the coupled second-order differential equations (9.38) in the external region we rewrite these equations in matrix form as follows:

$$\left(\frac{\mathrm{d}^2}{\mathrm{d}r^2} + \mathbf{P}\frac{\mathrm{d}}{\mathrm{d}r} + \mathbf{Q}\frac{1}{r} + \mathbf{V}(r) + \mathbf{D} + \mathbf{k}^2\right)\mathbf{F}^{\mathbf{V}}(r) = 0, \tag{9.61}$$

where the $\mathbf{P}$ and $\mathbf{Q}$ terms arise from the $\mathbf{V}^{P\gamma}$ term in (9.41), the $\mathbf{D}$ term arises from the $\mathbf{V}^{D\gamma}$ term in (9.41) and the $\mathbf{V}(r)$ term arises from the $\mathbf{V}^{E\gamma}$ term in (9.41) together with the orbital angular momentum and Coulomb terms on the left-hand side of (9.38), as discussed in Sect. D.2. For notational convenience, we omit the superscripts $\mathbf{V}$ and γ on the quantities in this and later equations except for the superscript $\mathbf{V}$ on $\mathbf{F}^{\mathbf{V}}(r)$ and related functions and on $E^{\mathbf{V}}$. For example, $\mathbf{R}^{\mathbf{V}\gamma}(E)$, defined by (9.60), is written as $\mathbf{R}(E)$. Also in (9.61), the diagonal matrix $\mathbf{k}^2$, defined by (9.39), is written as

$$\mathbf{k}^2 = 2E^{\mathbf{V}}\mathbf{I} - 2\mathbf{f}, \tag{9.62}$$

where $\mathbf{I}$ is the unit matrix, the diagonal matrix $\mathbf{f}$ is real and the quasi-energy $E^{\mathbf{V}}$ is complex for multiphoton ionization and real for laser-assisted electron–atom collisions. The matrices $\mathbf{P}$, $\mathbf{Q}$, $\mathbf{V}(r)$ and $\mathbf{D}$ are shown in Appendix D.2 to have the following properties using the Fano–Racah phase convention:

$\mathbf{P}$ — pure imaginary, symmetric, antihermitian, r-independent
$\mathbf{Q}$ — pure imaginary, antisymmetric, hermitian, r-independent
$\mathbf{V}$ — real, symmetric, hermitian, r-dependent
$\mathbf{D}$ — pure imaginary, antisymmetric, hermitian, r-independent.

We consider first the solution of (9.61) in the external region using the R-matrix propagator method described in Appendix E.5, or an equivalent method, where the first derivative term is non-zero. In order to reduce (9.61) to standard form, we first diagonalize the r-independent terms $\mathbf{D}+\mathbf{k}^2$. Since $\mathbf{D}$ is hermitian and independent of energy and the quasi-energy E-dependent part of $\mathbf{k}^2$, defined by (9.39), is a multiple

of the unit matrix, then $\mathbf{D} + \mathbf{k}^2$ can be diagonalized by a unitary, r- and energy-independent matrix $\mathbf{U}_1$ giving

$$\mathbf{U}_1^\dagger \left(\mathbf{D} + \mathbf{k}^2\right) \mathbf{U}_1 = \mathcal{K}^2. \tag{9.63}$$

Equations (9.61) can then be rewritten as

$$\left(\frac{\mathrm{d}^2}{\mathrm{d}r^2} + \mathcal{P}\frac{\mathrm{d}}{\mathrm{d}r} + \mathcal{V}(r) + \mathcal{K}^2\right) \mathcal{F}^{\mathbf{V}}(r) = 0, \tag{9.64}$$

where

$$\begin{aligned} \mathcal{P} &= \mathbf{U}_1^\dagger \mathbf{P} \mathbf{U}_1, \\ \mathcal{V}(r) &= \mathbf{U}_1^\dagger \left[\mathbf{Q}\frac{1}{r} + \mathbf{V}(r)\right] \mathbf{U}_1, \\ \mathcal{F}^{\mathbf{V}}(r) &= \mathbf{U}_1^\dagger \mathbf{F}^{\mathbf{V}}(r). \end{aligned} \tag{9.65}$$

The unitary transformation (9.63) defines a new target basis which is a linear combination of the original basis and corresponds to target states which are "dressed" by the laser field. The elements of the diagonal matrix $\mathcal{K}^2$ are the modified kinetic energies of the ejected or scattered electron corresponding to these dressed states and hence the corresponding wave numbers given by the diagonal elements of $\mathcal{K}$ are shifted by the laser field from their original values given by $\mathbf{k}$. In practice only a finite number of terms can be retained in the original Floquet–Fourier expansion (9.8). It is then found that while the shifts in the channel wave numbers given by $\mathcal{K}$ corresponding to small n in this expansion are small, the shifts become larger as n tends to the upper and lower limits of n retained in expansion (9.8). In some calculations this shift has been neglected. However, it was shown by Day et al. [252], in a model potential study, that while the results obtained neglecting this shift tend to the same limit as those obtained including this shift as the number of terms retained in the Floquet–Fourier expansion (9.33) tends to infinity, convergence is faster for calculations which use the shifted wave numbers. In the remainder of our analysis we will therefore assume that shifted wave numbers are used.

Equation (9.64) is now in a form that can be solved in the external region using the R-matrix propagator method described in Appendix E.5 where the inhomogeneous term is omitted. In this case, the R-matrix is defined by (E.104) where $\mathbf{T}(a_{s-1})$ is omitted and $s = 1$, corresponding to $r = a_0$. Hence we can write

$$\mathcal{F}^{\mathbf{V}}(a_0) = \mathcal{R}_0(E) a_0 \left(\frac{\mathrm{d}\mathcal{F}^{\mathbf{V}}}{\mathrm{d}r} + \frac{1}{2}\mathcal{P}\mathcal{F}^{\mathbf{V}}\right)_{r=a_0}, \tag{9.66}$$

where $\mathcal{F}^{\mathbf{V}}$ and $\mathcal{P}$ are defined by (9.65). In order to determine the R-matrix $\mathcal{R}_0(E)$ defined by (9.66) at $r = a_0$, we observe that the boundary condition satisfied by

$\mathbf{F}^{\mathbf{V}}(r)$ at $r = a_0$ is given by (9.59), where the R-matrix $\mathbf{R}(E)$ in the velocity gauge at $r = a_0$ is defined in terms of the R-matrix in the length gauge at $r = a_0$ by (9.60). We now substitute for $\boldsymbol{\mathcal{F}}^{\mathbf{V}}(a_0)$ and $(\mathrm{d}\boldsymbol{\mathcal{F}}^{\mathbf{V}}/\mathrm{d}r)_{r=a_0}$ from (9.65) into (9.66) giving

$$\mathbf{U}_1^{\dagger}\mathbf{F}^{\mathbf{V}}(a_0) = \boldsymbol{\mathcal{R}}_0(E)a_0\left(\mathbf{U}_1^{\dagger}\frac{\mathrm{d}\mathbf{F}^{\mathbf{V}}}{\mathrm{d}r} + \frac{1}{2}\boldsymbol{\mathcal{P}}\mathbf{U}_1^{\dagger}\mathbf{F}^{\mathbf{V}}\right)_{r=a_0}. \tag{9.67}$$

After substituting for $(\mathrm{d}\mathbf{F}^{\mathbf{V}}/\mathrm{d}r)_{r=a_0}$ from (9.59) into (9.67) and re-arranging terms we obtain

$$\boldsymbol{\mathcal{R}}_0(E) = \left(\mathbf{U}_1^{\dagger}\left[\mathbf{R}(E)\right]^{-1}\mathbf{U}_1 + \frac{1}{2}a_0\boldsymbol{\mathcal{P}}\right)^{-1}, \tag{9.68}$$

which defines the R-matrix $\boldsymbol{\mathcal{R}}_0(E)$ at $r = a_0$ in terms of the R-matrix $\mathbf{R}(E)$ at $r = a_0$, obtained from the solution in the internal region using (9.60). $\boldsymbol{\mathcal{R}}_0(E)$ can then be propagated outwards from $r = a_0$ to a_p, using the propagator method described in Appendix E.5, yielding the R-matrix $\boldsymbol{\mathcal{R}}_p(E)$ at $r = a_p$ which satisfies the equation

$$\boldsymbol{\mathcal{F}}^{\mathbf{V}}(a_p) = \boldsymbol{\mathcal{R}}_p(E)a_p\left(\frac{\mathrm{d}\boldsymbol{\mathcal{F}}^{\mathbf{V}}}{\mathrm{d}r} + \frac{1}{2}\boldsymbol{\mathcal{P}}\boldsymbol{\mathcal{F}}^{\mathbf{V}}\right)_{r=a_p}. \tag{9.69}$$

Alternatively, we can eliminate the first derivative term in (9.64) and propagate the resultant R-matrix using the R-matrix propagator method described in Appendix E.1 or an equivalent method. Since $\mathbf{P}$ in (9.61) is antihermitian and $\mathbf{U}_1$ is unitary, it follows from (9.65) that $\boldsymbol{\mathcal{P}}$ is also antihermitian and hence can be diagonalized by a unitary r-independent matrix $\mathbf{U}_2$ as follows:

$$\mathbf{U}_2^{\dagger}\boldsymbol{\mathcal{P}}\mathbf{U}_2 = 2\mathrm{i}\mathbf{d}, \tag{9.70}$$

where $\mathbf{d}$ is a real, diagonal r-independent matrix. We now introduce a new radial function $\overline{\boldsymbol{\mathcal{F}}}^{\mathbf{V}}(r)$ defined in terms of $\boldsymbol{\mathcal{F}}^{\mathbf{V}}(r)$ by the equation

$$\overline{\boldsymbol{\mathcal{F}}}^{\mathbf{V}}(r) = \exp(\mathrm{i}\mathbf{d}r)\mathbf{U}_2^{\dagger}\boldsymbol{\mathcal{F}}^{\mathbf{V}}(r). \tag{9.71}$$

Substituting this expression for $\boldsymbol{\mathcal{F}}^{\mathbf{V}}(r)$ into (9.64) then yields the following second-order differential equation without first derivative satisfied by $\overline{\boldsymbol{\mathcal{F}}}^{\mathbf{V}}(r)$:

$$\left(\frac{\mathrm{d}^2}{\mathrm{d}r^2} + \boldsymbol{\mathcal{W}}(r) + \mathbf{d}^2\right)\overline{\boldsymbol{\mathcal{F}}}^{\mathbf{V}}(r) = 0, \tag{9.72}$$

where the potential matrix $\mathcal{W}(r)$ is defined in terms of $\mathcal{V}(r)$ and $\mathcal{K}^2$ by

$$\mathcal{W}(r) = \exp(\mathrm{i}\mathbf{d}r)\mathbf{U}_2^\dagger \left(\mathcal{V}(r) + \mathcal{K}^2\right) \mathbf{U}_2 \exp(-\mathrm{i}\mathbf{d}r). \tag{9.73}$$

The final step is to determine the boundary condition satisfied by the function $\overline{\mathcal{F}}^{\mathbf{V}}(r)$ at $r = a_0$ in terms of the boundary condition satisfied by $\mathbf{F}^{\mathbf{V}}(r)$ defined by (9.59). It follows from (9.65) and (9.71) that

$$\mathbf{F}^{\mathbf{V}}(r) = \mathbf{U}_1\mathbf{U}_2 \exp(-\mathrm{i}\mathbf{d}r)\overline{\mathcal{F}}^{\mathbf{V}}(r), \tag{9.74}$$

and taking the derivative of this equation gives

$$\frac{\mathrm{d}\mathbf{F}^{\mathbf{V}}}{\mathrm{d}r} = \mathbf{U}_1\mathbf{U}_2 \exp(-\mathrm{i}\mathbf{d}r) \left(\frac{\mathrm{d}\overline{\mathcal{F}}^{\mathbf{V}}}{\mathrm{d}r} - \mathrm{i}\mathbf{d}\overline{\mathcal{F}}^{\mathbf{V}} \right). \tag{9.75}$$

We now substitute for $\mathbf{F}^{\mathbf{V}}(r)$ and $\mathrm{d}\mathbf{F}^{\mathbf{V}}/\mathrm{d}r$ at $r = a_0$ into (9.59) yielding the following boundary condition satisfied by $\overline{\mathcal{F}}^{\mathbf{V}}(r)$:

$$\overline{\mathcal{F}}^{\mathbf{V}}(a_0) = \overline{\mathcal{R}}(E)a_0 \left. \frac{\mathrm{d}\overline{\mathcal{F}}^{\mathbf{V}}}{\mathrm{d}r} \right|_{r=a_0}, \tag{9.76}$$

where the R-matrix $\overline{\mathcal{R}}(E)$ at $r = a_0$ is defined by

$$\overline{\mathcal{R}}(E) = \left(\mathbf{I} + \mathrm{i}a_0\overline{\overline{\mathcal{R}}}(E)\mathbf{d}\right)^{-1} \overline{\overline{\mathcal{R}}}(E), \tag{9.77}$$

and the intermediate matrix $\overline{\overline{\mathcal{R}}}(E)$ is defined by

$$\overline{\overline{\mathcal{R}}}(E) = \exp(\mathrm{i}\mathbf{d}a_0)\mathbf{U}_2^\dagger\mathbf{U}_1^\dagger\mathbf{R}(E)\mathbf{U}_1\mathbf{U}_2 \exp(-\mathrm{i}\mathbf{d}a_0). \tag{9.78}$$

Equation (9.76) defines the boundary condition at $r = a_0$ satisfied by the solution $\overline{\mathcal{F}}^{\mathbf{V}}(r)$ of (9.72), where the R-matrix $\overline{\mathcal{R}}(E)$ is defined in terms of $\mathbf{R}(E)$ by (9.77) and (9.78). The R-matrix $\mathbf{R}(E)$ at $r = a_0$, defined by (9.60), is determined by the solution in the internal region.

Since the potential $\mathcal{W}(r)$, defined by (9.73), is energy dependent the use of the BBM propagator method, discussed in Appendix E.3, is not appropriate. However, the Light–Walker propagator, discussed in Appendix E.1, or any equivalent method of solving coupled second-order differential equations without first derivative, can be used to propagate the R-matrix from $r = a_0$ to a_p.

9.1.4 Asymptotic Region Solution in the Velocity Gauge

In the asymptotic region, shown in Fig. 9.1, the ejected or scattered electron with radial coordinate $r_{N+1} \geq a_p$ can be described either in the velocity gauge or in the acceleration frame of reference while the remaining N electrons, with radial coordinates $r_i \leq a_0,\ i = 1, \ldots, N$, are described in the length gauge. We consider first in this section the asymptotic solution in the velocity gauge which involves modifying the asymptotic expansion used in field-free transitions. We then consider in Sects. 9.1.5 and 9.1.6 two approaches when the solution in the asymptotic region is treated in the acceleration frame of reference. In Sect. 9.1.5 the transformation to the acceleration frame of reference is carried out at a relatively small radius a_p and involves a detailed discussion of the transformation from the velocity gauge to the acceleration frame. In Sect. 9.1.6 the transformation is carried out at a much larger radius a_p which simplifies the analysis. In both cases the wave function describing the ejected or scattered electron is described in a frame of reference where the target states are dressed by the laser field, as described in our discussion following (9.63).

We consider the solution of the coupled second-order differential equations (9.64) when the velocity gauge is adopted. It is convenient first to transform these equations by the r-independent unitary matrix $\mathbf{U}_2$, defined by (9.70), yielding the coupled second-order differential equations

$$\left(\frac{\mathrm{d}^2}{\mathrm{d}r^2} + 2\mathrm{i}\mathbf{d}\frac{\mathrm{d}}{\mathrm{d}r} + \mathbf{W}(r)\right)\mathbf{G}^{\mathbf{V}}(r) = 0, \tag{9.79}$$

where we have introduced the reduced radial solution matrix

$$\mathbf{G}^{\mathbf{V}}(r) = \mathbf{U}_2^{\dagger}\boldsymbol{\mathcal{F}}^{\mathbf{V}}(r) \tag{9.80}$$

and the potential matrix

$$\mathbf{W}(r) = \mathbf{U}_2^{\dagger}\left(\boldsymbol{\mathcal{V}}(r) + \boldsymbol{\mathcal{K}}^2\right)\mathbf{U}_2. \tag{9.81}$$

Also $\boldsymbol{\mathcal{V}}(r)$ and $\boldsymbol{\mathcal{K}}^2$ in (9.81) are defined by (9.65) and (9.63), respectively. It follows that we can expand $\mathbf{W}(r)$ as

$$\mathbf{W}(r) = \sum_{\lambda=0}^{\lambda_{\max}} \mathbf{W}_\lambda r^{-\lambda}, \tag{9.82}$$

where $\lambda_{\max}$ is determined by the angular momentum triangular relations satisfied by the potential $\mathbf{V}(r)$ in (9.61). Also it follows from (9.63), (9.81) and (9.82) that

$$\mathbf{W}_0 = \mathbf{U}_2^{\dagger}\mathbf{U}_1^{\dagger}(\mathbf{D} + \mathbf{k}^2)\mathbf{U}_1\mathbf{U}_2, \tag{9.83}$$

where $\mathbf{k}^2$ is defined by (9.62). Hence $\mathbf{W}_0$ is non-hermitian if $E^{\mathbf{V}}$ in (9.62) is complex, corresponding to multiphoton ionization, and $\mathbf{W}_0$ is hermitian if $E^{\mathbf{V}}$ is real, corresponding to laser-assisted electron–atom collisions. Also the $\mathbf{W}_\lambda$ in (9.82) when $\lambda \geq 1$ do not depend on $E^{\mathbf{V}}$ and are hermitian.

In Appendix F.2 we derive a complete set of asymptotic solutions of the coupled second-order differential equations (9.79), which we assume here are n_t in number. We obtain $2n_t$ solutions with the following asymptotic form:

$$\mathbf{G}_j^{\mathbf{V}}(r) = \sum_{s=0}^{\infty} r^{-s} \exp\left(\mathrm{i}p_j r + \mathrm{i}\frac{Z_j}{p_j} \ln 2p_j r\right) \mathbf{A}_j^s, \quad j = 1, \ldots, 2n_t. \tag{9.84}$$

Physical solutions corresponding to multiphoton ionization or laser-assisted electron–atom collisions are obtained by taking linear combinations of these solutions which satisfy R-matrix boundary conditions at $r = a_p$ and the appropriate asymptotic boundary conditions as $r \to \infty$.

We also show in Appendix F.2 that the effective momenta p_j and the corresponding vector coefficients $\mathbf{A}_j^0$ in (9.84) are determined by solving the $2n_t$ coupled equations

$$\left(\mathbf{I}p_j^2 + 2\mathbf{d}p_j - \mathbf{W}_0\right)\mathbf{A}_j^0 = 0, \quad j = 1, \ldots, 2n_t, \tag{9.85}$$

where $\mathbf{I}$ is the unit matrix and $\mathbf{W}_0$ is defined by (9.83). These equations have non-trivial solutions when

$$\det\left(\mathbf{I}p_j^2 + 2\mathbf{d}p_j - \mathbf{W}_0\right) = 0. \tag{9.86}$$

Expanding this determinant yields a set of algebraic equations of order $2n_t$ which has $2n_t$ solutions

$$p_j, \quad j = 1, \ldots, 2n_t. \tag{9.87}$$

Substituting for each p_j into (9.85) then gives a set of n_t linear simultaneous equations which enable the n_t components of the vector $\mathbf{A}_j^0$ to be determined up to an overall normalization factor. Finally, the effective charges Z_j, $j = 1, \ldots, 2n_t$, and the vectors $\mathbf{A}_j^s$, $j = 1, \ldots, 2n_t$, for $s \geq 1$ in (9.84) are determined from the recurrence relations derived in Appendix F.2.

We consider first the solution of (9.79) corresponding to multiphoton ionization. In this case we have to find the solutions of (9.86) when $\mathbf{W}_0$ is non-hermitian. We observe that in the limit when the laser field strength is zero then (9.86) reduces to

$$\det\left(\mathbf{I}p_j^2 - \mathbf{k}^2\right) = 0, \tag{9.88}$$

which follows from (9.83) since the unitary matrices $\mathbf{U}_1$ and $\mathbf{U}_2$ are both equal to the unit matrix and $\mathbf{D} = 0$. It then follows that if an element k_j^2 of the diagonal matrix $\mathbf{k}^2$ satisfies $k_j^2 \geq 0$ then the corresponding effective momentum $p_j = \pm k_j$. On the other hand, if an element k_j^2 satisfies $k_j^2 < 0$ then the corresponding effective momentum $p_j = \pm \mathrm{i}|k_j|$. Hence, the solutions of (9.88) either appear in pairs on the real momentum axis or they appear in pairs in the complex momentum plane where one is the complex conjugate of the other. We can then show that when the laser field is switched on the two solutions corresponding to $k_j^2 \geq 0$ move off the real momentum axis, one into the upper half complex momentum plane and the other into the lower half complex momentum plane. Also, the two solutions corresponding to $k_j^2 < 0$ move in the complex momentum plane but are no longer complex conjugates of each other. Hence, when the laser field is non-zero we find an equal number of solutions of (9.86) in the upper and lower halves of the complex momentum plane. The $2n_t$ solutions of (9.86) can therefore be written as

$$\begin{aligned} p_j &= a_j + \mathrm{i}b_j, \quad j = 1, \ldots, n_t, \\ p_j &= c_j - \mathrm{i}d_j, \quad j = n_t + 1, \ldots, 2n_t, \end{aligned} \tag{9.89}$$

where a_j, b_j, c_j and d_j are all real and where b_j and d_j are both positive. The general solution of (9.79) can then be written as a linear combination of the following $2n_t$ solutions defined by (9.89) with the asymptotic form

$$\begin{aligned} G_{ij}^{\mathbf{V}}(r) \underset{r\to\infty}{\sim} \exp\left(\mathrm{i}p_j r + \mathrm{i}\frac{Z_j}{p_j}\ln 2p_j r\right) A_{ij}^0 + O(r^{-1}), \\ i = 1, \ldots, n_t, \ \ j = 1, \ldots, 2n_t, \end{aligned} \tag{9.90}$$

where it is convenient to normalize the solutions by requiring that

$$\sum_{i=1}^{n_t} |A_{ij}^0|^2 = 1, \quad j = 1, \ldots, 2n_t. \tag{9.91}$$

It follows from (9.89) that the first n_t solutions $G_{ij}^{\mathbf{V}}(r)$, $j = 1, \ldots, n_t$, correspond to ingoing waves and the last n_t solutions $G_{ij}^{\mathbf{V}}(r)$, $j = n_t + 1, \ldots, 2n_t$, correspond to outgoing wave solutions. The required solution $G_i^{\mathrm{MI}}(r)$ corresponding to multiphoton ionization is then a linear combination of the outgoing wave solutions

$$G_i^{\mathrm{MI}}(r) = \sum_{j=n_t+1}^{2n_t} G_{ij}^{\mathbf{V}}(r) c_j, \quad i = 1, \ldots, n_t. \tag{9.92}$$

In order to determine the coefficients c_j, $j = n_t + 1, \ldots, 2n_t$, in (9.92) we substitute $G_i^{\mathrm{MI}}(r)$ into the equation obtained by propagating the R-matrix in the velocity gauge, defined at $r = a_0$ by (9.66), from $r = a_0$ to a_p, as described in

Appendix E.5. We then find, after using (9.70) and (9.80), that $G_i^{\rm MI}(r)$ satisfies the equation

$$\mathbf{G}^{\rm MI}(a_p) = \widetilde{\boldsymbol{\mathcal{R}}}_p(E) a_p \left(\frac{\mathrm{d}\mathbf{G}^{\rm MI}}{\mathrm{d}r} + \mathrm{i}\mathbf{G}^{\rm MI} \right)_{r=a_p}, \tag{9.93}$$

where $\widetilde{\boldsymbol{\mathcal{R}}}_p(E)$ in this equation is related to $\boldsymbol{\mathcal{R}}_p(E)$ resulting from propagating the R-matrix from $r = a_0$ to a_p by

$$\widetilde{\boldsymbol{\mathcal{R}}}_p(E) = \mathbf{U}_2^{\dagger} \boldsymbol{\mathcal{R}}_p(E) \mathbf{U}_2. \tag{9.94}$$

Substituting for $\mathbf{G}^{\rm MI}(a_p)$, given by (9.92), into (9.93) then yields a set of n_t linear homogeneous simultaneous equations satisfied by the coefficients c_j, $j = n_t + 1, \ldots, 2n_t$, which will only have a non-trivial solution when the complex quasi-energy $E^{\mathbf{V}}$ in (9.62) corresponds to a Siegert [876] outgoing wave solution of (9.79). In order to determine this solution, an iterative procedure can be adopted analogous to that used in determining the initial bound-state energy in photoionization, described in Sect. 8.1.2. The complex quasi-energy $E^{\mathbf{V}}$, corresponding to the solution of (9.93), can then be written as

$$E^{\mathbf{V}} = E_0 + \Delta - \frac{1}{2}\mathrm{i}\Gamma, \tag{9.95}$$

where E_0 is the field-free energy of the target atom, Δ is the dynamic Stark shift and Γ is the total multiphoton ionization rate. The corresponding Siegert outgoing wave solution defined by (9.90) and (9.92) then has the asymptotic form

$$G_i^{\rm MI}(r) \underset{r\to\infty}{\sim} \sum_{j=n_t+1}^{2n_t} \exp\left(\mathrm{i}p_j r + \mathrm{i}\frac{Z_j}{p_j} \ln 2p_j r \right) A_{ij}^0 c_j + O(r^{-1}), \quad i = 1, \ldots, n_t, \tag{9.96}$$

where p_j and Z_j depend on the quasi-energy $E^{\mathbf{V}}$. The branching ratios of the ejected electron can then be obtained from the coefficients A_{ij}^0 and c_j. Finally, we note that our discussion leading to (9.96) also defines the asymptotic form of the wave function in harmonic generation which we will consider in Sect. 9.1.7.

We consider next the solution of (9.79) corresponding to laser-assisted electron–atom collisions. In this case $\mathbf{W}_0$ is hermitian and hence if the effective momentum p_j is a solution of (9.85) then the complex conjugate p_j^* is also a solution. It follows that the solutions of (9.85) are either real or occur in $n_t - n_a$ complex conjugate pairs. We can, therefore, write the effective momenta as follows:

$$p_j = -a_j, \quad j = 1, \ldots, n_a, \tag{9.97}$$

$$p_j = c_j - \mathrm{i}d_j, \quad j = n_a + 1, \ldots, n_t, \tag{9.98}$$

$$p_{n_t+j} = b_j, \quad j = 1, \ldots, n_a, \tag{9.99}$$

$$p_{n_t+j} = c_j + \mathrm{i}d_j, \quad j = n_a + 1, \ldots, n_t, \tag{9.100}$$

where a_j, b_j, c_j and d_j are all real and where a_j, b_j and d_j are positive. We note that this division between real and complex and also between positive and negative solutions follows from the solutions of (9.88) when the laser field is switched on.

We can now write the general solution of (9.79) as a linear combination of the $n_t + n_a$ solutions defined by (9.97), (9.99) and (9.100) where the solutions corresponding to (9.98) are excluded since they diverge asymptotically and hence are non-physical. We can therefore define n_a ingoing wave solutions

$$G^{\mathrm{I}}_{ij}(r) = (-p_j)^{-1/2} G^{\mathbf{V}}_{ij}(r), \quad i = 1, \ldots, n_t, \ j = 1, \ldots, n_a, \tag{9.101}$$

n_a outgoing wave solutions

$$G^{\mathrm{O}}_{ij}(r) = (p_{n_t+j})^{-1/2} G^{\mathbf{V}}_{in_t+j}(r), \quad i = 1, \ldots, n_t, \ j = 1, \ldots, n_a, \tag{9.102}$$

and $n_b = n_t - n_a$ decaying wave solutions

$$G^{\mathrm{O}}_{ij}(r) = G^{\mathbf{V}}_{in_t+j}(r), \quad i = 1, \ldots, n_t, \ j = n_a + 1, \ldots, n_t. \tag{9.103}$$

In (9.101) and (9.102) we have normalized the solutions to unit ingoing and outgoing wave fluxes, respectively. The general solution of (9.79) corresponding to laser-assisted electron–atom collisions can then be written in terms of these solutions in analogy with our discussion of electron–atom collisions in Sect. 5.1.4. We obtain

$$\mathbf{G}^{\mathrm{C}}(r) = \mathbf{G}^{\mathrm{I}}(r) - \mathbf{G}^{\mathrm{O}}(r)\mathbf{H}, \tag{9.104}$$

where $\mathbf{G}^{\mathrm{I}}(r)$ has dimension $n_t \times n_a$, $\mathbf{G}^{\mathrm{O}}(r)$ has dimension $n_t \times n_t$ and $\mathbf{H}$ has dimension $n_t \times n_a$. Also, $\mathbf{H}$ is defined by

$$\mathbf{H} = \begin{bmatrix} \mathbf{S} \\ \mathbf{M} \end{bmatrix}, \tag{9.105}$$

where $\mathbf{S}$ is the $n_a \times n_a$-dimensional S-matrix which multiplies the outgoing wave solutions $G^{\mathrm{O}}_{ij}(r)$, defined by (9.102), and $\mathbf{M}$ is the $n_b \times n_a$-dimensional subsidiary matrix which multiplies the decaying wave solutions $G^{\mathrm{O}}_{ij}(r)$, defined by (9.103). Hence (9.104) reduces asymptotically to

$$\mathbf{G}^{\mathrm{C}}(r) \underset{r\to\infty}{\sim} \mathbf{G}^{\mathrm{I}}(r) - \mathbf{G}^{\mathrm{O}}(r)\mathbf{S}, \tag{9.106}$$

where $\mathbf{G}^{\mathrm{I}}(r)$ and $\mathbf{G}^{\mathrm{O}}(r)$ are the $n_t \times n_a$ asymptotic solution matrices defined by (9.101) and (9.102), respectively. This equation is analogous to (5.48) which defines the S-matrix in electron collisions with atoms and ions.

The final step in determining the S-matrix in (9.106) follows our analysis in multiphoton ionization leading to (9.93). The R-matrix in the velocity gauge is propagated from $r = a_0$ to a_p. The solution $\mathbf{G}^{\mathrm{C}}(r)$, defined by (9.104), then satisfies the equation

$$\mathbf{G}^{\mathrm{C}}(a_p) = \widetilde{\boldsymbol{\mathcal{R}}}_p(E) a_p \left(\frac{\mathrm{d}\mathbf{G}^{\mathrm{C}}}{\mathrm{d}r} + \mathrm{i}\mathbf{d}\mathbf{G}^{\mathrm{C}} \right)_{r=a_p}, \tag{9.107}$$

where $\widetilde{\boldsymbol{\mathcal{R}}}_p(E)$ is defined by (9.94). We can then determine the S-matrix in (9.106) by substituting (9.104), evaluated at $r = a_p$, into (9.107) which yields a set of n_t coupled linear simultaneous equations with n_a right-hand sides. The matrix $\mathbf{H}$, and hence the S-matrix, is then determined from the solution of these equations, and the solution of (9.79) corresponding to laser-assisted electron–atom collisions is then given by (9.104).

9.1.5 Asymptotic Region Solution in the Acceleration Frame

The transformation of the wave function describing the ejected or scattered electron from the velocity gauge, adopted in the external region in Sect. 9.1.3, to the acceleration frame of reference is accomplished using the following Kramers–Henneberger transformation [453, 547]:

$$\widetilde{\Psi}^{\mathbf{V}}(\mathbf{X}_{N+1}, t) = \exp\left[-\frac{\mathrm{i}}{\mathrm{c}} \mathbf{p}_{N+1} \cdot \int^t \mathbf{A}(t')\mathrm{d}t' \right] \widetilde{\Psi}^{\mathbf{A}}(\mathbf{X}_{N+1}, t), \tag{9.108}$$

where

$$r_i \leq a_0, \quad i = 1, \ldots, N, \quad r_{N+1} \geq a_p. \tag{9.109}$$

The boldface superscript $\mathbf{A}$ in (9.108) and later equations indicates that the functions describing the ejected or scattered electron are defined in the acceleration frame of reference. We now substitute (9.108) into the time-dependent Schrödinger equation (9.32) satisfied by the solution in the external region, and multiply this equation on the left by $\exp[\mathrm{i}\boldsymbol{\alpha}(t) \cdot \mathbf{p}_{N+1}]$. After using the operator identity

$$\exp[\mathrm{i}\boldsymbol{\alpha}(t) \cdot \mathbf{p}][f(\mathbf{r})g(\mathbf{r})] = f[\mathbf{r} + \boldsymbol{\alpha}(t)] \exp[\mathrm{i}\boldsymbol{\alpha}(t) \cdot \mathbf{p}] g(\mathbf{r}), \tag{9.110}$$

where $f(\mathbf{r})$ and $g(\mathbf{r})$ are analytic functions of $\mathbf{r}$, we obtain the following time-dependent Schrödinger equation satisfied by the wave function $\widetilde{\Psi}^{\mathbf{A}}(\mathbf{X}_{N+1}, t)$:

$$\left[\widetilde{H}^{\mathbf{A}}_{N+1}(t) + \boldsymbol{\mathcal{E}}(t) \cdot \mathbf{R}_N \right] \widetilde{\Psi}^{\mathbf{A}}(\mathbf{X}_{N+1}, t) = \mathrm{i} \frac{\partial}{\partial t} \widetilde{\Psi}^{\mathbf{A}}(\mathbf{X}_{N+1}, t). \tag{9.111}$$

The time-dependent Hamiltonian $\widetilde{H}^{\mathbf{A}}_{N+1}(t)$ in (9.111) is defined by

$$\widetilde{H}^{\mathbf{A}}_{N+1}(t) = H_N - \frac{1}{2}\nabla^2_{N+1} - \frac{Z}{|\mathbf{r}_{N+1} + \boldsymbol{\alpha}(t)|} + \sum_{i=1}^{N} \frac{1}{|\mathbf{r}_{N+1} + \boldsymbol{\alpha}(t) - \mathbf{r}_i|}, \quad (9.112)$$

where the tilde on $\widetilde{H}^{\mathbf{A}}_{N+1}(t)$ indicates that it is time dependent. Also in (9.111) and (9.112) $\boldsymbol{\mathcal{E}}(t)$ is defined by (9.4) and

$$\boldsymbol{\alpha}(t) = \frac{1}{\mathrm{c}} \int^t \mathbf{A}(t')\mathrm{d}t' = \hat{\boldsymbol{\epsilon}}\alpha(t) = \hat{\boldsymbol{\epsilon}}\alpha_0 \cos\omega t, \quad (9.113)$$

where $\alpha_0 = \mathcal{E}_0\omega^{-2}$. By expanding the last two terms in (9.112) in powers of $\alpha(t)$ we can write this equation as [184]

$$\widetilde{H}^{\mathbf{A}}_{N+1}(t) = H_{N+1} + \widetilde{A}_{N+1}(t), \quad (9.114)$$

where

$$\begin{aligned}\widetilde{A}_{N+1}(t) = \alpha(t) \Bigg[& \frac{Z-N}{r^2_{N+1}} \cos\theta_{N+1} + \frac{1}{r^3_{N+1}} \sum_{i=1}^{N} r_i \cos\theta_i \\ & - \frac{3}{r^3_{N+1}} \cos\theta_{N+1} \sum_{i=1}^{N} r_i \cos\phi_i + O\left(r^{-4}_{N+1}\right) \Bigg] \\ & + O\left[\alpha(t)^2 r^{-3}_{N+1}\right], \end{aligned} \quad (9.115)$$

and where

$$\cos\theta_i = \hat{\mathbf{r}}_i \cdot \hat{\boldsymbol{\epsilon}}, \quad i = 1, \ldots, N+1 \quad (9.116)$$

and

$$\cos\phi_i = \hat{\mathbf{r}}_i \cdot \hat{\mathbf{r}}_{N+1}, \quad i = 1, \ldots, N. \quad (9.117)$$

In practice, all terms in $\widetilde{A}_{N+1}(t)$, except the leading term behaving as $\alpha(t)r^{-2}_{N+1}$, can often be neglected. In Sect. 9.1.6 we consider a simplified analysis in the acceleration frame where the propagation in the velocity gauge is carried out to a sufficiently large radius $r = a_p$ so that the leading term $\alpha(t)r^{-2}_{N+1}$ can also be neglected.

Following the above analysis, (9.111) can be written as

$$\left[H_{N+1} + \boldsymbol{\mathcal{E}}(t) \cdot \mathbf{R}_N + \widetilde{A}_{N+1}(t)\right] \widetilde{\Psi}^{\mathbf{A}}(\mathbf{X}_{N+1}, t) = \mathrm{i}\frac{\partial}{\partial t} \widetilde{\Psi}^{\mathbf{A}}(\mathbf{X}_{N+1}, t), \quad (9.118)$$

which describes the motion of the ejected or scattered electron in a frame of reference in which this electron is oscillating in the laser field, while the remaining

N target electrons, which are bound to the nucleus, are described in the length gauge. This representation has the advantage that the time-dependent Hamiltonian $\widetilde{H}^{\mathbf{A}}_{N+1}(t)$, defined by (9.114), (9.115), (9.116) and (9.117), reduces to the field-free Hamiltonian H_{N+1} when the radial coordinate r_{N+1} of the ejected or scattered electron tends to infinity, enabling simple asymptotic boundary conditions for this electron to be introduced.

In order to solve (9.118) in the asymptotic region we proceed as in Sect. 9.1.3 by introducing the Floquet–Fourier expansion

$$\widetilde{\Psi}^{\mathbf{A}}(\mathbf{X}_{N+1}, t) = \exp\left(-\mathrm{i}E^{\mathbf{A}}t\right) \sum_{n=-\infty}^{\infty} \exp(-\mathrm{i}n\omega t)\Psi_n^{\mathbf{A}}(\mathbf{X}_{N+1}), \tag{9.119}$$

where $E^{\mathbf{A}}$ is the quasi-energy in the acceleration frame. Substituting (9.119) into (9.118) and equating the coefficient of $\exp[-\mathrm{i}(E^{\mathbf{A}}+n\omega)t]$ to zero yields the infinite set of time-independent equations

$$\left(H_{N+1} - E^{\mathbf{A}} - n\omega\right)\Psi_n^{\mathbf{A}} + D_N\left(\Psi_{n-1}^{\mathbf{A}} + \Psi_{n+1}^{\mathbf{A}}\right) + A_{N+1}\left(\Psi_{n-1}^{\mathbf{A}} + \Psi_{n+1}^{\mathbf{A}}\right) = 0, \tag{9.120}$$

where the acceleration term

$$A_{N+1} = \frac{1}{2}\alpha_0\left[\frac{Z-N}{r_{N+1}^2}\cos\theta_{N+1} + \frac{1}{r_{N+1}^3}\sum_{i=1}^{N} r_i\cos\theta_i - \frac{3}{r_{N+1}^3}\cos\theta_{N+1}\sum_{i=1}^{N} r_i\cos\phi_i + O(r_{N+1}^{-4})\right], \tag{9.121}$$

and we have omitted terms of $O[\alpha(t)^2 r_{N+1}^{-3}]$ in (9.115) which only contribute at high laser intensities. Also in (9.120) D_N is defined by (9.10) and (9.14) with $N+1$ replaced by N. We see that (9.120) has the same general form as the corresponding equation (9.34) obtained using the velocity gauge in the external region except that the last term in (9.34), involving the dipole velocity operator P_{N+1}, is now replaced by the last term in (9.120), involving the acceleration term A_{N+1}. We then rewrite (9.120) as a matrix equation in photon space as follows:

$$\left(\mathbf{H}_{\mathrm{F}}^{\mathbf{A}} - E^{\mathbf{A}}\mathbf{I}\right)\boldsymbol{\Psi}^{\mathbf{A}} = 0, \tag{9.122}$$

where the Floquet Hamiltonian $\mathbf{H}_{\mathrm{F}}^{\mathbf{A}}$ is an infinite-dimensional matrix in this space. Also we introduce the following close coupling expansion for the components $\Psi_n^{\mathbf{A}\gamma}$ of the total wave function at energy E for each set of conserved quantum numbers denoted by γ

$$\Psi^{\mathbf{A}\gamma}_{njE}(\mathbf{X}_{N+1}) = \sum_{Li} \overline{\Phi}^{\gamma}_{nLi}(\mathbf{X}_N; \hat{\mathbf{r}}_{N+1}\sigma_{N+1}) r^{-1}_{N+1} F^{\mathbf{A}\gamma}_{nLij}(r_{N+1}), \quad r_{N+1} \geq a_p, \tag{9.123}$$

where the channel functions $\overline{\Phi}^{\gamma}_{nLi}$ retained in this expansion are the same as those retained in the internal and external region expansions (9.20) and (9.37) and where j labels the linearly independent solutions. After substituting (9.123) into (9.122) and projecting onto the channel functions $\overline{\Phi}^{\gamma}_{nLi}$ we obtain the following coupled second-order differential equations satisfied by the reduced radial wave functions $F^{\mathbf{A}\gamma}_{nLij}(r)$:

$$\left(\frac{\mathrm{d}^2}{\mathrm{d}r^2} - \frac{\ell_i(\ell_i+1)}{r^2} + \frac{2(Z-N)}{r} + k^2_{ni}\right) F^{\mathbf{A}\gamma}_{nLij}(r) = 2 \sum_{n'L'i'} W^{\mathbf{A}\gamma}_{nLin'L'i'}(r) F^{\mathbf{A}\gamma}_{n'L'i'j}(r), \quad r \geq a_p, \tag{9.124}$$

where

$$k^2_{ni} = 2\left(E^{\mathbf{A}} - f_{ni}\right), \tag{9.125}$$

and where f_{ni} is defined by (9.40). Also in (9.124), $W^{\mathbf{A}\gamma}_{nLin'L'i'}(r)$ is the potential matrix coupling the channels which can be written in matrix notation as

$$\mathbf{W}^{\mathbf{A}\gamma} = \mathbf{V}^{E\gamma} + \mathbf{V}^{D\gamma} + \mathbf{V}^{A\gamma}. \tag{9.126}$$

The $\mathbf{V}^{E\gamma}$ and $\mathbf{V}^{D\gamma}$ terms arise, respectively, from the H_{N+1} and D_N terms in (9.120), which are the same as those found in the velocity gauge in (9.41), and the $\mathbf{V}^{A\gamma}$ term arises from the acceleration term A_{N+1} in (9.120) and is defined by the matrix elements

$$V^{A\gamma}_{nLin'L'i'} = \langle r^{-1}_{N+1} \overline{\Phi}^{\gamma}_{nLi}(\mathbf{X}_N; \hat{\mathbf{r}}_{N+1}\sigma_{N+1}) \,|A_{N+1}|\, r^{-1}_{N+1} \times \overline{\Phi}^{\gamma}_{n'L'i'}(\mathbf{X}_N; \hat{\mathbf{r}}_{N+1}\sigma_{N+1})\rangle'(\delta_{nn'-1} + \delta_{nn'+1}). \tag{9.127}$$

Finally, we note that the integrals in (9.127) are carried out over the space and spin coordinates of all $N+1$ electrons except the radial coordinate of the $(N+1)$th electron.

9.1.5.1 Boundary Condition at $r = a_p$

In order to solve (9.124) in the asymptotic region we must determine the boundary condition satisfied by the solution $F^{\mathbf{A}\gamma}_{nLij}(r)$ at $r = a_p$. This boundary condition can be determined by matching the solution of (9.38) in the velocity gauge with the solution of (9.124) in the acceleration frame at $r = a_p$. This can be achieved by substituting the Floquet–Fourier expansions for $\widetilde{\Psi}^{\mathbf{V}}(\mathbf{X}_{N+1}, t)$ and $\widetilde{\Psi}^{\mathbf{A}}(\mathbf{X}_{N+1}, t)$ given

by (9.33) and (9.119), respectively, into the Kramers–Henneberger transformation (9.108). We obtain

$$\exp\left(-\mathrm{i}E^{\mathbf{A}}t\right)\sum_{n=-\infty}^{\infty}\exp(-\mathrm{i}n\omega t)\Psi_n^{\mathbf{A}}(\mathbf{X}_{N+1})$$
$$=\exp\left\{-\mathrm{i}\left[E^{\mathbf{V}}t-\boldsymbol{\alpha}(t)\cdot\mathbf{p}_{N+1}\right]\right\}\sum_{n'=-\infty}^{\infty}\exp\left(-\mathrm{i}n'\omega t\right)\Psi_{n'}^{\mathbf{V}}(\mathbf{X}_{N+1}),\quad(9.128)$$

where we have used (9.113) to rewrite the integral in the exponent on the right-hand side of (9.108). We then substitute the close coupling expansions (9.37) and (9.123) for $\Psi_{njE}^{\mathbf{V}\gamma}$ and $\Psi_{njE}^{\mathbf{A}\gamma}$, respectively, into (9.128) giving

$$\exp\left(-\mathrm{i}E^{\mathbf{A}}t\right)\sum_{nLi}\exp(-\mathrm{i}n\omega t)\overline{\Phi}_{nLi}^{\gamma}(\mathbf{X}_N;\hat{\mathbf{r}}_{N+1}\sigma_{N+1})r_{N+1}^{-1}F_{nLij}^{\mathbf{A}\gamma}(r_{N+1})$$
$$=\exp\left\{-\mathrm{i}\left[E^{\mathbf{V}}t-\boldsymbol{\alpha}(t)\cdot\mathbf{p}_{N+1}\right]\right\}\sum_{n'L'i'}\exp\left(-\mathrm{i}n'\omega t\right)\overline{\Phi}_{n'L'i'}^{\gamma}(\mathbf{X}_N;\hat{\mathbf{r}}_{N+1}\sigma_{N+1})$$
$$\times\, r_{N+1}^{-1}F_{n'L'i'j}^{\mathbf{V}\gamma}(r_{N+1}).\quad(9.129)$$

In order to analyse (9.129), we consider the following expression that appears on the right-hand side of this equation:

$$I=\exp[\mathrm{i}\boldsymbol{\alpha}(t)\cdot\mathbf{p}_{N+1}]\overline{\Phi}_{n'L'i'}^{\gamma}(\mathbf{X}_N;\hat{\mathbf{r}}_{N+1}\sigma_{N+1})r_{N+1}^{-1}F_{n'L'i'j}^{\mathbf{V}\gamma}(r_{N+1}).\quad(9.130)$$

We expand the channel function in (9.130) as follows:

$$\overline{\Phi}_{n'L'i'}^{\gamma}(\mathbf{X}_N;\hat{\mathbf{r}}_{N+1}\sigma_{N+1})$$
$$=\sum_{M_{L_{i'}}m_{\ell_{i'}}}(L_{i'}M_{L_{i'}}\ell_{i'}m_{\ell_{i'}}|L'M_{L'})\,\overline{\Theta}_{n'L_{i'}M_{L_{i'}}i'}^{\gamma}(\mathbf{X}_N;\sigma_{N+1})$$
$$\times\, Y_{\ell_{i'}m_{\ell_{i'}}}(\theta_{N+1},\phi_{N+1}),\quad(9.131)$$

where $\overline{\Theta}_{n'L'M_{L_{i'}}i'}^{\gamma}(\mathbf{X}_N;\sigma_{N+1})$ are reduced channel functions in which the N-electron state is coupled to the spin state but not to the orbital angular momentum state of the scattered or ejected electron. Equation (9.130) then becomes

$$I=\exp[\mathrm{i}\boldsymbol{\alpha}(t)\cdot\mathbf{p}_{N+1}]\sum_{M_{L_{i'}}m_{\ell_{i'}}}(L_{i'}M_{L_{i'}}\ell_{i'}m_{\ell_{i'}}|L'M_{L'})\overline{\Theta}_{n'L_{i'}M_{L_{i'}}i'}^{\gamma}(\mathbf{X}_N;\sigma_{N+1})$$
$$\times\, Y_{\ell_{i'}m_{\ell_{i'}}}(\theta_{N+1},\phi_{N+1})r_{N+1}^{-1}F_{n'L'i'j}^{\mathbf{V}\gamma}(r_{N+1}).\quad(9.132)$$

We can evaluate this expression for I using the operator identity

$$\exp[\mathrm{i}\boldsymbol{\alpha}(t)\cdot\mathbf{p}]f(\mathbf{r})=f[\mathbf{r}+\boldsymbol{\alpha}(t)]\equiv f(\mathbf{r}_\alpha),\quad(9.133)$$

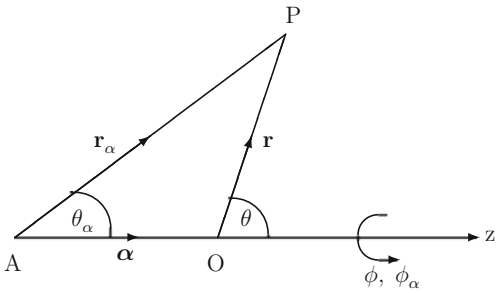

Fig. 9.4 Coordinate system representing the action of the operator $\exp(\mathrm{i}\boldsymbol{\alpha}\cdot\mathbf{p})$

which follows from (9.110) by setting $g(\mathbf{r})$ equal to unity. Hence the action of the operator $\exp[\mathrm{i}\boldsymbol{\alpha}(t)\cdot\mathbf{p}]$ on $f(\mathbf{r})$ is to yield the function $f[\mathbf{r}+\boldsymbol{\alpha}(t)]$ centred on a new origin. This is illustrated in Fig. 9.4 where we have chosen the z-axis to lie along the laser polarization direction $\boldsymbol{\alpha}$ and where we have defined $\mathbf{r}_\alpha(t)=\mathbf{r}+\boldsymbol{\alpha}(t)$. The displaced origin in this figure is denoted by A and the original origin is denoted by O. The two coordinate systems are thus related by the following equations:

$$\begin{aligned} r_\alpha^2 &= \alpha^2 + r^2 + 2\alpha r\cos\theta, \quad r_\alpha\sin\theta_\alpha = r\sin\theta, \\ r_\alpha\cos\theta_\alpha &= r\cos\theta+\alpha, \quad \phi_\alpha=\phi, \end{aligned} \tag{9.134}$$

where in this equation and the following equations we observe that α, r_α and θ_α are functions of time t.

In order to evaluate the expression I, defined by (9.132), we follow a procedure similar to that adopted by Harris and Michels [442], who determined an expansion for molecular orbitals on a displaced centre expanded about the original centre. We consider an orbital $u_{n\ell m}(\mathbf{r}_\alpha)$ centred on A which we wish to expand about O in Fig. 9.4. We assume that this orbital can be written in terms of spherical harmonics, defined in Appendix B.3, as follows:

$$u_{n\ell m}(\mathbf{r}_\alpha) = u_{n\ell}(r_\alpha)Y_{\ell m}(\theta_\alpha,\phi_\alpha), \tag{9.135}$$

where n represents all the quantum numbers except ℓ and m necessary to define the orbital. We then expand $u_{n\ell m}(\mathbf{r}_\alpha)$ about O in Fig. 9.4 as follows:

$$u_{n\ell m}(\mathbf{r}_\alpha) = \sum_{\ell'=m}^{\infty} v_{n\ell m\ell'}(\alpha,r)Y_{\ell' m}(\theta,\phi), \tag{9.136}$$

which can be inverted, after substituting for $u_{n\ell m}$ from (9.135), giving

$$v_{n\ell m\ell'}(\alpha,r) = \int_0^{2\pi}\int_0^{\pi} Y^*_{\ell' m}(\theta,\phi)u_{n\ell}(r_\alpha)Y_{\ell m}(\theta_\alpha,\phi_\alpha)\sin\theta\,\mathrm{d}\theta\mathrm{d}\phi. \tag{9.137}$$

The integration over ϕ can be carried out immediately, giving 2π, and the integration over θ can be carried out numerically remembering, after using (9.134), that

$$u_{n\ell}(r_\alpha) = u_{n\ell}\left[\left(\alpha^2 + r^2 + 2\alpha r\cos\theta\right)^{1/2}\right] \tag{9.138}$$

and

$$\cos\theta_\alpha = \frac{r\cos\theta + \alpha}{(\alpha^2 + r^2 + 2\alpha r\cos\theta)^{1/2}}. \tag{9.139}$$

Hence the radial functions $v_{n\ell m\ell'}(\alpha, r)$ in (9.136) can be calculated for all required values of ℓ', α and r. If α is much smaller than r then the rate of convergence in (9.136) will be very rapid.

It follows from the above analysis that the following operation in (9.132) can be written as

$$\begin{aligned}\exp(\mathrm{i}\boldsymbol{\alpha}\cdot\mathbf{p}_{N+1})\left[r_{N+1}^{-1}F^{\mathbf{V}\gamma}_{n'L'i'j}(r_{N+1})Y_{\ell_{i'}m_{\ell_{i'}}}(\theta_{N+1},\phi_{N+1})\right]\\ = r_\alpha^{-1}F^{\mathbf{V}\gamma}_{n'L'i'j}(r_\alpha)Y_{\ell_{i'}m_{\ell_{i'}}}(\theta_\alpha,\phi).\end{aligned} \tag{9.140}$$

The function on the right-hand side of this equation can be expanded about O in Fig. 9.4 in analogy with (9.136) as follows:

$$\begin{aligned}r_\alpha^{-1}F^{\mathbf{V}\gamma}_{n'L'i'j}(r_\alpha)Y_{\ell_{i'}m_{\ell_{i'}}}(\theta_\alpha,\phi) = \sum_{\ell=m_{\ell_{i'}}}^{\infty} r_{N+1}^{-1}u^{\mathbf{V}\gamma}_{n'L'i'\ell_{i'}m_{\ell_{i'}}\ell j}(\alpha, r_{N+1})\\ \times\, Y_{\ell m_{\ell_{i'}}}(\theta_{N+1},\phi_{N+1}).\end{aligned} \tag{9.141}$$

Then, in analogy with (9.137), we can invert (9.141) giving

$$\begin{aligned}&r_{N+1}^{-1}u^{\mathbf{V}\gamma}_{n'L'i'\ell_{i'}m_{\ell_{i'}}\ell j}(\alpha, r_{N+1})\\ &\quad= \int_0^{2\pi}\int_0^{\pi} Y^*_{\ell m_{\ell_{i'}}}(\theta_{N+1},\phi_{N+1})r_\alpha^{-1}F^{\mathbf{V}\gamma}_{n'L'i'j}(r_\alpha)Y_{\ell_{i'}m_{\ell_{i'}}}(\theta_\alpha,\phi_{N+1})\\ &\qquad\times\, \sin\theta_{N+1}\mathrm{d}\theta_{N+1}\mathrm{d}\phi_{N+1}.\end{aligned} \tag{9.142}$$

As in (9.137) the integration over ϕ_{N+1} can be carried out immediately and the integration over θ_{N+1} can be carried out numerically enabling $u^{\mathbf{V}\gamma}_{n'L'i'\ell_{i'}m_{\ell_{i'}}\ell j}(\alpha, r)$ to be determined for all ℓ, α and r values of importance.

We now substitute (9.140) into (9.132) and use (9.141). We then obtain

$$\begin{aligned}I = \sum_{M_{L_{i'}}m_{\ell_{i'}}} (L_{i'}M_{L_{i'}}\ell_{i'}m_{\ell_{i'}}|L'M_{L'})\overline{\Theta}^{\gamma}_{n'L_{i'}M_{L_{i'}}i'}(\mathbf{X}_N;\sigma_{N+1})\\ \times \sum_{\ell=m_{\ell_{i'}}}^{\infty} r_{N+1}^{-1}u^{\mathbf{V}\gamma}_{n'L'i'\ell_{i'}m_{\ell_{i'}}\ell j}(\alpha, r_{N+1})Y_{\ell m_{\ell_{i'}}}(\theta_{N+1},\phi_{N+1}).\end{aligned} \tag{9.143}$$

We next express the reduced channel functions $\overline{\Theta}^{\gamma}_{n'L_{i'}M_{L_{i'}}i'}(\mathbf{X}_N;\sigma_{N+1})$ in (9.143) in terms of the original channel functions $\overline{\Phi}^{\gamma}_{n'L'i'}(\mathbf{X}_N;\hat{\mathbf{r}}_{N+1}\sigma_{N+1})$ in (9.130) by the equation

$$\begin{aligned}&\overline{\Theta}^{\gamma}_{n'L_{i'}M_{L_{i'}}i'}(\mathbf{X}_N;\sigma_{N+1})Y_{\ell m_{\ell_{i'}}}(\theta_{N+1},\phi_{N+1})\\&\quad=\sum_{L''}(L_{i'}M_{L_{i'}}\ell m_{\ell_{i'}}|L''M_{L'})\overline{\Phi}^{\gamma}_{n'L''i'}(\mathbf{X}_N;\hat{\mathbf{r}}_{N+1}\sigma_{N+1}).\end{aligned}\tag{9.144}$$

Substituting this result into (9.143) gives

$$\begin{aligned}I=&\sum_{M_{L_{i'}}m_{\ell_{i'}}}\sum_{\ell=m_{\ell_{i'}}}^{\infty}\sum_{L''}(L_{i'}M_{L_{i'}}\ell_{i'}m_{\ell_{i'}}|L'M_{L'})(L_{i'}M_{L_{i'}}\ell m_{\ell_{i'}}|L''M_{L'})\\&\times\overline{\Phi}^{\gamma}_{n'L''i'}(\mathbf{X}_N;\hat{\mathbf{r}}_{N+1}\sigma_{N+1})r_{N+1}^{-1}u^{\mathbf{V}\gamma}_{n'L'i'\ell_{i'}m_{\ell_{i'}}\ell j}(\alpha,r_{N+1}).\end{aligned}\tag{9.145}$$

In order to evaluate I we expand the function $u^{\mathbf{V}\gamma}_{n'L'i'\ell_{i'}m_{\ell_{i'}}\ell j}(\alpha,r_{N+1})$ as follows:

$$u^{\mathbf{V}\gamma}_{n'L'i'\ell_{i'}m_{\ell_{i'}}\ell j}(\alpha,r_{N+1})=\sum_{s=-\infty}^{\infty}\exp(-\mathrm{i}s\omega t)u^{\mathbf{V}\gamma}_{n'L'i'\ell_{i'}m_{\ell_{i'}}\ell sj}(r_{N+1}),\tag{9.146}$$

where we remember that α is a function of t, defined by (9.113). After substituting this result into I, defined by (9.145), we find that (9.129) can be rewritten as

$$\begin{aligned}&\exp(-\mathrm{i}E^{\mathbf{A}}t)\sum_{nLi}\exp(-\mathrm{i}n\omega t)\overline{\Phi}^{\gamma}_{nLi}(\mathbf{X}_N;\hat{\mathbf{r}}_{N+1}\sigma_{N+1})r_{N+1}^{-1}F^{\mathbf{A}\gamma}_{nLij}(r_{N+1})\\&=\exp(-\mathrm{i}E^{\mathbf{V}}t)\sum_{n'L'i's}\exp[-\mathrm{i}(n'+s)\omega t]\sum_{M_{L_{i'}}m_{\ell_{i'}}}\sum_{\ell=m_{\ell_{i'}}}^{\infty}\sum_{L''}(L_{i'}M_{L_{i'}}\ell_{i'}m_{\ell_{i'}}|L'M_{L'})\\&\quad\times(L_{i'}M_{L_{i'}}\ell m_{\ell_{i'}}|L''M_{L'})\overline{\Phi}^{\gamma}_{n'L''i'}(\mathbf{X}_N;\hat{\mathbf{r}}_{N+1}\sigma_{N+1})r_{N+1}^{-1}\\&\quad\times u^{\mathbf{V}\gamma}_{n'L'i'\ell_{i'}m_{\ell_{i'}}\ell sj}(r_{N+1}).\end{aligned}\tag{9.147}$$

From the requirement that the time dependence on both sides of (9.147) is the same then

$$E^{\mathbf{A}}=E^{\mathbf{V}}\tag{9.148}$$

and

$$n=n'+s.\tag{9.149}$$

Hence, the summations over n' and s on the right-hand side of (9.147) can be replaced by a single summation over n'. Our final step is to project (9.147) onto the channel functions $\overline{\Phi}^{\gamma}_{nLi}$ which gives

$$F^{\mathbf{A}\gamma}_{nLij}(r) = \sum_{n'L'\ell} \sum_{M_{L_i} m_{\ell_i}} (L_i M_{L_i} \ell_i m_{\ell_i} | L' M_L)(L_i M_{L_i} \ell m_{\ell_i} | L M_L) \times u^{\mathbf{V}\gamma}_{n'L'i\ell_i m_{\ell_i} \ell s j}(r), \tag{9.150}$$

where $s = n - n'$ here and below. This equation, together with (9.142) and (9.146), relates the reduced radial wave function $F^{\mathbf{A}\gamma}_{nLij}(r)$ in the acceleration frame to the reduced radial wave function $F^{\mathbf{V}\gamma}_{nLij}(r)$ in the velocity gauge.

We can now determine the R-matrix $\mathbf{R}^{\mathbf{A}\gamma}(E)$ in the acceleration frame of reference at $r = a_p$. We define this R-matrix, in analogy with (9.26), in terms of the reduced radial wave function $F^{\mathbf{A}\gamma}_{nLij}(r)$ by

$$F^{\mathbf{A}\gamma}_{nLij}(a_p) = \sum_{n'L'i'} R^{\mathbf{A}\gamma}_{nLin'L'i'}(E)\, a_p \left. \frac{\mathrm{d}F^{\mathbf{A}\gamma}_{n'L'i'j}}{\mathrm{d}r} \right|_{r=a_p}, \tag{9.151}$$

where for notational convenience we have set the arbitrary constant $b_0 = 0$. The function $F^{\mathbf{A}\gamma}_{nLij}(a_p)$ in (9.151) is given by (9.150) and

$$\left. \frac{\mathrm{d}F^{\mathbf{A}\gamma}_{nLij}}{\mathrm{d}r} \right|_{r=a_p} = \sum_{n'L'\ell} \sum_{M_{L_i} m_{\ell_i}} (L_i M_{L_i} \ell_i m_{\ell_i} | L' M_L)(L_i M_{L_i} \ell m_{\ell_i} | L M_L) \times \left\{ \frac{\mathrm{d}}{\mathrm{d}r} \left[u^{\mathbf{V}\gamma}_{n'L'i\ell_i m_{\ell_i} \ell s j}(r) \right] \right\}_{r=a_p}, \tag{9.152}$$

which follows by taking the derivative of (9.150). Also, by inverting (9.146) we find that

$$\left\{ \frac{\mathrm{d}}{\mathrm{d}r} \left[u^{\mathbf{V}\gamma}_{n'L'i'\ell_{i'} m_{\ell_{i'}} \ell s j}(r) \right] \right\}_{r=a_p} = \frac{\omega}{2\pi} \int_0^{2\pi/\omega} \exp[\mathrm{i}s\omega t] \left\{ \frac{\mathrm{d}}{\mathrm{d}r} \left[u^{\mathbf{V}\gamma}_{n'L'i'\ell_{i'} m_{\ell_{i'}} \ell j}(\alpha, r) \right] \right\}_{r=a_p} \mathrm{d}t, \tag{9.153}$$

where the derivative term on the right-hand side of this equation can be obtained by differentiating (9.142) numerically. Thus both $F^{\mathbf{A}\gamma}_{nLij}(a_p)$ and $\left[\mathrm{d}F^{\mathbf{A}\gamma}_{nLij}/\mathrm{d}r\right]_{r=a_p}$ in (9.151) can be calculated and hence the R-matrix $\mathbf{R}^{\mathbf{A}\gamma}(E)$ at $r = a_p$, which

provides the boundary condition for the solution of the coupled differential equations (9.124) in the asymptotic region, can be determined.

Finally, we consider the solution of the coupled second-order differential equations (9.124) in the asymptotic region. We rewrite these equations in matrix form as

$$\left(\frac{\mathrm{d}^2}{\mathrm{d}r^2} + \mathbf{V}(r) + \mathbf{V}^A(r) + \mathbf{D} + \mathbf{k}^2\right)\mathbf{F}^{\mathbf{A}}(r) = 0, \tag{9.154}$$

where $\mathbf{V}(r)$ and $\mathbf{D}$ are the same as in (9.61) and $\mathbf{V}^A(r)$ is the long-range acceleration potential term, defined by (9.121) and (9.127) and where, for notational convenience, we have omitted the superscript γ representing the conserved quantum numbers. It follows that $\mathbf{V}(r)$ and $\mathbf{V}^A(r)$ are real and symmetric and can be expanded as summations in inverse powers of r. On the other hand, $\mathbf{D}$ is hermitian and r-independent. We therefore follow the procedure adopted in the velocity gauge by diagonalizing $\mathbf{D}+\mathbf{k}^2$ by a unitary, r- and energy-independent matrix $\mathbf{U}_1$, defined by (9.63). Equation (9.154) can then be rewritten as

$$\left(\frac{\mathrm{d}^2}{\mathrm{d}r^2} + \boldsymbol{\mathcal{V}}(r) + \mathcal{K}^2\right)\boldsymbol{\mathcal{F}}^{\mathbf{A}}(r) = 0, \tag{9.155}$$

where

$$\begin{aligned}\boldsymbol{\mathcal{V}}(r) &= \mathbf{U}_1^\dagger\left[\mathbf{V}(r) + \mathbf{V}^A(r)\right]\mathbf{U}_1,\\ \boldsymbol{\mathcal{F}}^{\mathbf{A}}(r) &= \mathbf{U}_1^\dagger\mathbf{F}^{\mathbf{A}}(r).\end{aligned} \tag{9.156}$$

It follows that the potential $\boldsymbol{\mathcal{V}}(r)$ can be expanded in inverse powers of r as follows:

$$\boldsymbol{\mathcal{V}}(r) = \frac{2(Z-N)}{r}\mathbf{I} + 2\sum_{\lambda=1}^{\infty}\mathbf{c}_\lambda r^{-\lambda-1}, \tag{9.157}$$

where we note that, as in (9.64), the unitary transformation (9.156) defines a new target basis corresponding to target states which are "dressed" by the laser field.

Equation (9.155) is now in a form that can be solved in the asymptotic region, using one of the asymptotic expansion methods described in Appendix F.1. In the case of laser-assisted electron–atom collisions we follow the procedure used to describe electron collisions with atoms and ions, discussed in Sect. 5.1.4, yielding a solution matrix $\boldsymbol{\mathcal{F}}^{\mathbf{A}}(r)$ satisfying the asymptotic boundary condition

$$\boldsymbol{\mathcal{F}}^{\mathbf{A}}(r) \underset{r\to\infty}{\sim} \mathcal{K}^{-1/2}\left[\sin\boldsymbol{\theta} + \cos\boldsymbol{\theta}\mathbf{K}\right], \tag{9.158}$$

in the open channels, where $\mathbf{K}$ is the K-matrix. We also define a solution matrix satisfying the asymptotic boundary conditions

$$\boldsymbol{\mathcal{G}}^{\mathbf{A}}(r) \underset{r\to\infty}{\sim} \mathcal{K}^{-1/2}\left[\exp(-\mathrm{i}\boldsymbol{\theta}) - \exp(\mathrm{i}\boldsymbol{\theta})\mathbf{S}\right], \tag{9.159}$$

which is obtained by taking linear combinations of the solutions defined by (9.158), where $\mathbf{S}$ is the S-matrix which is defined in terms of the K-matrix by (5.49). The T-matrix and cross sections can then be determined using the procedure described in Sect. 2.5.

In the case of atomic multiphoton ionization we must determine a solution of (9.155) satisfying Siegert outgoing wave boundary conditions [876] defined by

$$\mathcal{H}^{\mathbf{A}}(r) \underset{r\to\infty}{\sim} \mathbf{N}\exp(\mathrm{i}\mathcal{K}r), \tag{9.160}$$

where $\mathbf{N}$ is a normalization vector. It follows from our discussion in Sect. 3.2.1 that this solution corresponds to a pole in the S-matrix lying on an unphysical sheet in the complex energy plane, as illustrated in Fig. 3.4. The corresponding quasi-energy $E^{\mathbf{A}}$ can then be rewritten as

$$E^{\mathbf{A}} = E_0 + \Delta - \frac{1}{2}\mathrm{i}\Gamma, \tag{9.161}$$

where E_0 is the field-free energy of the target state, Δ is the dynamic Stark shift and Γ is the total multiphoton ionization rate. In order to determine the position of this pole, the energy $E^{\mathbf{A}}$ defined by (9.161) is varied iteratively and the solution in the asymptotic region re-calculated until the Siegert outgoing wave boundary condition (9.160) is satisfied. This iterative procedure is analogous to that used to calculate the initial bound state wave function in photoionization, discussed in Sect. 8.1.2, and to that used in determining the asymptotic solution in the velocity gauge, discussed in Sect. 9.1.4.

9.1.6 Asymptotic Region Solution: Simplified Analysis

In this section we consider a simplified analysis of the solution in the asymptotic region in the acceleration frame, where the transformation from the velocity gauge to the acceleration frame is carried out at such a large radius $r = a_p$ that the term $\widetilde{A}_{N+1}(t)$ on the right-hand side of (9.114) can be neglected. This approach, which was first considered by Charlo et al. [214], was analysed in detail by Terao-Dunseath and Dunseath [924] and has been developed and applied to a number of laser-assisted electron–atom collision calculations [275, 276, 278, 925].

In this approach the time-dependent Schrödinger equation (9.118) in the acceleration frame reduces to

$$(H_{N+1} + \boldsymbol{\mathcal{E}}(t)\cdot\mathbf{R}_N)\,\widetilde{\Psi}^{\mathbf{A}}(\mathbf{X}_{N+1}, t) = \mathrm{i}\frac{\partial}{\partial t}\widetilde{\Psi}^{\mathbf{A}}(\mathbf{X}_{N+1}, t), \tag{9.162}$$

which corresponds to a free electron moving in the field of the atom or ion where the N target electrons, which are bound to the nucleus, are described in the length gauge. In order to solve (9.162) we follow our discussion in Sect. 9.1.5 leading to

(9.124). We first introduce the following Floquet–Fourier expansion in the acceleration frame:

$$\widetilde{\Psi}^{\mathbf{A}}(\mathbf{X}_{N+1}, t) = \exp\left(-\mathrm{i}E^{\mathbf{A}}t\right) \sum_{n=-\infty}^{\infty} \exp(-\mathrm{i}n\omega t)\Psi_n^{\mathbf{A}}(\mathbf{X}_{N+1}), \tag{9.163}$$

where $E^{\mathbf{A}}$ is the quasi-energy in this frame. Substituting (9.163) into (9.162) and equating the coefficient of $\exp[-\mathrm{i}(E^{\mathbf{A}} + n\omega)t]$ to zero yields the infinite set of time-independent equations

$$\left(H_{N+1} - E^{\mathbf{A}} - n\omega\right)\Psi_n^{\mathbf{A}} + D_N\left(\Psi_{n-1}^{\mathbf{A}} + \Psi_{n+1}^{\mathbf{A}}\right) = 0, \tag{9.164}$$

where D_N is defined by (9.10) and (9.14) with $N + 1$ replaced by N. We then introduce the following close coupling expansion

$$\Psi_{njE}^{\mathbf{A}\gamma}(\mathbf{X}_{N+1}) = \sum_{Li} \overline{\Phi}_{nLi}^{\gamma}(\mathbf{X}_N; \hat{\mathbf{r}}_{N+1}\sigma_{N+1}) r_{N+1}^{-1} F_{nLij}^{\mathbf{A}\gamma}(r_{N+1}), \quad r_{N+1} \geq a_p, \tag{9.165}$$

using the same notation as (9.123). Substituting (9.165) into (9.164) and projecting onto the channel functions $\overline{\Phi}_{nLi}^{\gamma}$ then yields the following coupled second-order differential equations:

$$\left(\frac{\mathrm{d}^2}{\mathrm{d}r^2} - \frac{\ell_i(\ell_i+1)}{r^2} + \frac{2(Z-N)}{r} + k_{ni}^2\right) F_{nLij}^{\mathbf{A}\gamma}(r) = 2\sum_{n'L'i'} W_{nLin'L'i'}^{\mathbf{A}\gamma}(r) F_{n'L'i'j}^{\mathbf{A}\gamma}(r), \quad r \geq a_p, \tag{9.166}$$

where

$$k_{ni}^2 = 2\left(E^{\mathbf{A}} - f_{ni}\right), \tag{9.167}$$

and f_{ni} is defined by (9.40). We see that (9.166) has the same form as (9.124). However, the potential $W_{nLin'L'i'}^{\mathbf{A}\gamma}(r)$ can now be written in matrix notation as

$$\mathbf{W}^{\mathbf{A}\gamma} = \mathbf{V}^{E\gamma} + \mathbf{V}^{D\gamma}, \tag{9.168}$$

where $\mathbf{V}^{E\gamma}$ and $\mathbf{V}^{D\gamma}$ are the same as arose in (9.126) and in the velocity gauge in (9.41), but the acceleration term $\mathbf{V}^{A\gamma}$ is now absent.

In order to determine the solution of (9.166) we follow our discussion in Sect. 9.1.3 and rewrite this equation in matrix form as follows:

$$\left(\frac{\mathrm{d}^2}{\mathrm{d}r^2} + \mathbf{V}(r) + \mathbf{D} + \mathbf{k}^2\right)\mathbf{F}^{\mathbf{A}}(r) = 0, \tag{9.169}$$

where for notational convenience we have omitted the superscript γ representing the conserved quantum numbers. Following our discussion of (9.61) describing the corresponding equation in the velocity gauge, we transform (9.169) by the unitary r- and energy-independent matrix $\mathbf{U}_1$, defined by (9.63). Equation (9.169) can then be rewritten as

$$\left(\frac{\mathrm{d}^2}{\mathrm{d}r^2} + \boldsymbol{\mathcal{V}}(r) + \boldsymbol{\mathcal{K}}^2\right) \boldsymbol{\mathcal{F}}^{\mathbf{A}}(r) = 0, \tag{9.170}$$

where

$$\boldsymbol{\mathcal{V}}(r) = \mathbf{U}_1^{\dagger} \mathbf{V}(r) \mathbf{U}_1 \tag{9.171}$$

and

$$\boldsymbol{\mathcal{F}}^{\mathbf{A}}(r) = \mathbf{U}_1^{\dagger} \mathbf{F}^{\mathbf{A}}(r). \tag{9.172}$$

Also we order the channels in (9.170) so that

$$\mathcal{K}_1^2 \geq \mathcal{K}_2^2 \geq \cdots \geq \mathcal{K}_{n_t}^2 \tag{9.173}$$

where n_t is the total number of coupled channels, where the first n_a channels are open with $\mathcal{K}_i^2 \geq 0$ and the last n_b channels are closed with $\mathcal{K}_i^2 < 0$ and where $n_a + n_b = n_t$. Following our discussion of electron–atom collisions in Sect. 5.1.4 we define $n_t + n_a$ linearly independent solutions of (9.170) satisfying the asymptotic boundary conditions

$$\begin{aligned}
h_{ij}^{\mathbf{A}}(r) &\underset{r\to\infty}{\sim} \mathcal{K}_i^{-1/2} \exp(-\mathrm{i}\theta_i)\delta_{ij}, \quad i = 1, \ldots, n_t, \quad j = 1, \ldots, n_a, \\
h_{ij}^{\mathbf{A}}(r) &\underset{r\to\infty}{\sim} \mathcal{K}_i^{-1/2} \exp(\mathrm{i}\theta_i)\delta_{ij}, \quad i = 1, \ldots, n_t, \quad j = n_a + 1, \ldots, 2n_a, \\
h_{ij}^{\mathbf{A}}(r) &\underset{r\to\infty}{\sim} \exp(-\phi_i)\delta_{ij-n_a}, \quad i = 1, \ldots, n_t, \quad j = 2n_a + 1, \ldots, n_t + n_a,
\end{aligned} \tag{9.174}$$

where for neutral atomic targets

$$\begin{aligned}
\theta_i &= \mathcal{K}_i r - \frac{1}{2}\ell_i \pi, \quad i = 1, \ldots, n_a, \\
\phi_i &= |\mathcal{K}_i| r, \quad i = n_a + 1, \ldots, n_t,
\end{aligned} \tag{9.175}$$

with modifications defined by (5.38), (5.39), (5.40) and (5.41) for ionic targets.

In order to determine the S-matrix we transform these $n_t + n_a$ solutions from the acceleration frame to the velocity gauge and we then match these solutions at $r = a_p$ to the R-matrix $\boldsymbol{\mathcal{R}}_p(E)$ obtained by propagating $\boldsymbol{\mathcal{R}}_0(E)$, defined by (9.66), from $r = a_0$ to a_p as described following (9.68). We commence by rewriting the Kramers–Henneberger transformation (9.108) in the form

$$\widetilde{\Psi}^{\mathbf{V}}(\mathbf{X}_{N+1}, t) = \exp\left[-\mathrm{i}\boldsymbol{\alpha}(t)\cdot\mathbf{p}_{N+1}\right]\widetilde{\Psi}^{\mathbf{A}}(\mathbf{X}_{N+1}, t), \tag{9.176}$$

where

$$\boldsymbol{\alpha}(t) = \frac{1}{\mathrm{c}}\int^{t}\mathbf{A}(t')\mathrm{d}t' = \hat{\boldsymbol{\epsilon}}\alpha_0\cos\omega t. \tag{9.177}$$

We then substitute for $\widetilde{\Psi}^{\mathbf{A}}(\mathbf{X}_{N+1}, t)$, given by (9.163) and (9.165), into the right-hand side of (9.176) giving

$$\begin{aligned}\widetilde{\Psi}_j^{\mathbf{V}}(\mathbf{X}_{N+1}, t) = \exp\left[-\mathrm{i}\boldsymbol{\alpha}(t)\cdot\mathbf{p}_{n+1}\right]\sum_n \exp(-\mathrm{i}n\omega t)\sum_{Li}\overline{\Phi}^{\gamma}_{nLi}(\mathbf{X}_N; \hat{\mathbf{r}}_{N+1}\sigma_{N+1})\\ \times r_{N+1}^{-1}\sum_k(\mathbf{U}_1)_{nLik}\mathcal{F}^{\mathbf{A}}_{kj}(r_{N+1}), \quad r_{N+1}\geq a_p,\end{aligned} \tag{9.178}$$

where we have used (9.172). Also we observe, following our discussion of (9.147), that the time-dependent term $\exp(-\mathrm{i}E^{\mathbf{A}}t)$, which appeared on the right-hand side of (9.178), has cancelled the term $\exp(-\mathrm{i}E^{\mathbf{V}}t)$ which appeared on the left-hand side of this equation.

We now consider the action of the operator $\exp[-\mathrm{i}\boldsymbol{\alpha}(t)\cdot\mathbf{p}_{n+1}]$ on the function on the right-hand side of (9.178). Following our discussion of (9.133) and Fig. 9.4 we find that

$$\exp(-\mathrm{i}\boldsymbol{\alpha}\cdot\mathbf{p})f(\mathbf{r}) = f(\mathbf{r}-\boldsymbol{\alpha}) \equiv f(\mathbf{r}_\alpha), \tag{9.179}$$

which yields in analogy with (9.134)

$$\begin{aligned}r_\alpha^2 = \alpha^2 + r^2 - 2\alpha r\cos\theta, \quad r_\alpha\sin\theta_\alpha = r\sin\theta,\\ r_\alpha\cos\theta_\alpha = r\cos\theta - \alpha, \quad \phi_\alpha = \phi.\end{aligned} \tag{9.180}$$

Hence in the limit r, and hence r_α, tends to ∞

$$\begin{aligned}r_\alpha &= r - \alpha_0\cos\omega t\cos\theta + O(r^{-1}),\\ r_\alpha^{-1} &= r^{-1} + O(r^{-2}),\\ \theta_\alpha &= \theta + O(r^{-1}),\\ \phi_\alpha &= \phi,\end{aligned} \tag{9.181}$$

where, as in Fig. 9.4, the z-axis is chosen along the laser polarization direction $\boldsymbol{\alpha}$. It follows that in this limit, the operator $\exp[-\mathrm{i}\boldsymbol{\alpha}(t)\cdot\mathbf{p}_{n+1}]$ in (9.178) modifies the asymptotic forms of the functions $\mathcal{F}^{\mathbf{A}}_{kj}(r_{N+1})$ while leaving the channel functions $\overline{\Phi}^{\gamma}_{nLi}(\mathbf{X}_N; \hat{\mathbf{r}}_{N+1}\sigma_{N+1})$ unmodified to first order. Therefore, we need to only consider the effect of the operator $\exp[-\mathrm{i}\boldsymbol{\alpha}(t)\cdot\mathbf{p}_{n+1}]$ on the asymptotic form of the $n_t + n_a$ functions defined by (9.174). That is we introduce the $n_t + n_a$ functions

$$H_{ij}^{\mathbf{V}}(r) = \exp[-\mathrm{i}\boldsymbol{\alpha}(t)\cdot\mathbf{p}]h_{ij}^{\mathbf{A}}(r), \quad i = 1,\ldots,n_t, \quad j = 1,\ldots,n_t+n_a, \quad (9.182)$$

which in the case of neutral targets satisfy the asymptotic boundary conditions

$$\begin{aligned}
H_{ij}^{\mathbf{V}}(r) &\underset{r\to\infty}{\sim} \mathcal{K}_i^{-1/2}\exp\left[-\mathrm{i}\left(\mathcal{K}_i r - \frac{1}{2}\ell_i\pi\right)\right]\exp\left(\mathrm{i}\mathcal{K}_i\alpha_0\cos\omega t\cos\theta\right), \\
&\qquad i = 1,\ldots,n_t, \quad j = 1,\ldots,n_a, \\
H_{ij}^{\mathbf{V}}(r) &\underset{r\to\infty}{\sim} \mathcal{K}_i^{-1/2}\exp\left[\mathrm{i}\left(\mathcal{K}_i r - \frac{1}{2}\ell_i\pi\right)\right]\exp\left(-\mathrm{i}\mathcal{K}_i\alpha_0\cos\omega t\cos\theta\right), \\
&\qquad i = 1,\ldots,n_t, \quad j = n_a+1,\ldots,2n_a, \\
H_{ij}^{\mathbf{V}}(r)| &\underset{r\to\infty}{\sim} \exp\left(-|\mathcal{K}_i|\,r\right)\exp\left(|\mathcal{K}_i|\,\alpha_0\cos\omega t\cos\theta\right), \\
&\qquad i = 1,\ldots,n_t, \quad j = 2n_a+1,\ldots,n_t+n_a, \qquad (9.183)
\end{aligned}$$

with appropriate modifications in the case of ionic targets. In (9.183) it is convenient to expand the following exponentials:

$$\exp\left(\pm\mathrm{i}\mathcal{K}_i\alpha_0\cos\omega t\cos\theta\right) = 1 \pm \frac{1}{2}\mathrm{i}\mathcal{K}_i\alpha_0[\exp(\mathrm{i}\omega t)+\exp(-\mathrm{i}\omega t)]\cos\theta + O(\alpha_0^2) \quad (9.184)$$

and

$$\exp\left(|\mathcal{K}_i|\,\alpha_0\cos\omega t\cos\theta\right) = 1 + \frac{1}{2}|\mathcal{K}_i|\,\alpha_0[\exp(\mathrm{i}\omega t)+\exp(-\mathrm{i}\omega t)]\cos\theta + O(\alpha_0^2), \quad (9.185)$$

where in most applications it is only necessary to retain the first-order terms in α_0, although the higher order terms in α_0 can be retained for high laser intensities.

It follows from the above analysis that we can determine $n_t + n_a$ linearly independent asymptotic solutions in the velocity gauge by substituting $H_{kj}^{\mathbf{V}}$ defined by (9.182) and (9.183) for $\exp[-\mathrm{i}\boldsymbol{\alpha}(t)\cdot\mathbf{p}_{N+1}]\mathcal{F}_{kj}^{\mathbf{A}}(r_{N+1})$ in (9.178). We obtain

$$\begin{aligned}
\widetilde{\Psi}_j^{\mathbf{V}}(\mathbf{X}_{N+1},t) &= \sum_n \exp(-\mathrm{i}n\omega t)\sum_{Li}\overline{\Phi}_{nLi}^{\gamma}(\mathbf{X}_N;\hat{\mathbf{r}}_{N+1}\sigma_{N+1}) \\
&\quad\times r_{N+1}^{-1}\sum_k(\mathbf{U}_1)_{nLik}H_{kj}^{\mathbf{V}}(r_{N+1},\theta_{N+1},t), \\
&\quad j = 1,\ldots,n_t+n_a, \qquad (9.186)
\end{aligned}$$

where we observe from the definitions of $H_{kj}^{\mathbf{V}}$ that these functions depend on r_{N+1}, θ_{N+1} and t. We now rewrite (9.186) in standard form as

$$\widetilde{\Psi}_j^{\mathbf{V}}(\mathbf{X}_{N+1}, t) = \sum_n \exp(-\mathrm{i}n\omega t) \sum_{Li} \overline{\Phi}_{nLi}^{\gamma}(\mathbf{X}_N; \hat{\mathbf{r}}_{N+1}\sigma_{N+1}) \times r_{N+1}^{-1} \sum_k (\mathbf{U}_1)_{nLik} \mathcal{F}_{kj}^{\mathbf{V}}(r_{N+1}), \quad j = 1, \ldots, n_t + n_a, \tag{9.187}$$

where $\mathcal{F}_{kj}^{\mathbf{V}}(r)$ is defined by the last of equations (9.65). It follows, after expressing the functions $H_{kj}^{\mathbf{V}}$ in (9.186) in terms of the functions $h_{ij}^{\mathbf{A}}(r)$ using (9.182) and (9.183) and then projecting (9.186) and (9.187) onto the channel functions $\overline{\Phi}_{nLi}^{\gamma}(\mathbf{X}_N; \hat{\mathbf{r}}_{N+1}\sigma_{N+1})$ and onto the Floquet–Fourier expansion component denoted by n, that we can determine a linear relation between the functions $h_{ij}^{\mathbf{A}}(r)$ in (9.186) and the functions $\mathcal{F}_{kj}^{\mathbf{V}}(r)$ in (9.187). In principle this relation is exact only if an infinite number of channel functions and Floquet–Fourier components are retained in the expansion. However, rapid convergence in the number of terms retained in these expansions will occur for laser field strengths of most interest. It follows that we can write

$$\mathcal{F}_{kj}^{\mathbf{V}}(r) = \sum_{i=1}^{n_t} C_{ki} h_{ij}^{\mathbf{A}}(r), \quad k = 1. \ldots, n_t + n_a, \tag{9.188}$$

where the matrix C_{ki} is the required linear transformation which is independent of r and the solution index j.

We now consider the determination of the S-matrix and hence the scattering amplitudes and cross sections. This is achieved by returning to the solution of (9.170) in the acceleration frame. The required solution has the asymptotic form

$$\begin{aligned} \boldsymbol{\mathcal{F}}^{\mathbf{A}}(r) &\underset{r\to\infty}{\sim} \boldsymbol{\mathcal{K}}^{-1/2} \left[\exp(-\mathrm{i}\theta) - \exp(\mathrm{i}\theta)\mathbf{S}\right], \quad \text{open channels}, \\ \boldsymbol{\mathcal{F}}^{\mathbf{A}}(r) &\underset{r\to\infty}{\sim} 0, \quad \text{closed channels}, \end{aligned} \tag{9.189}$$

where $\mathbf{S}$ is the usual $n_a \times n_a$-dimensional S-matrix. In order to determine the S-matrix we rewrite (9.189) as

$$\boldsymbol{\mathcal{F}}^{\mathbf{A}} = \mathbf{I}^{\mathbf{A}}(r) - \mathbf{O}^{\mathbf{A}}(r)\mathbf{M}^{\mathbf{A}}, \tag{9.190}$$

where $\mathbf{I}^{\mathbf{A}}(r)$ and $\mathbf{O}^{\mathbf{A}}(r)$ are ingoing and outgoing waves whose matrix elements can be expressed in terms of the $n_t + n_a$ linearly independent solutions $h_{ij}^{\mathbf{A}}(r)$ defined by (9.174). We find that

$$\begin{aligned} I_{ij}^{\mathbf{A}}(r) &= h_{ij}^{\mathbf{A}}(r), \quad i = 1, \ldots, n_t, \quad j = 1, \ldots, n_a, \\ O_{ij}^{\mathbf{A}}(r) &= h_{ij+n_a}^{\mathbf{A}}(r), \quad i = 1, \ldots, n_t, \quad j = 1, \ldots, n_a, \\ O_{ij}^{\mathbf{A}}(r) &= h_{ij+n_a}^{\mathbf{A}}(r), \quad i = 1, \ldots, n_t, \quad j = n_a + 1, \ldots, n. \end{aligned} \tag{9.191}$$

Also, the matrix $\mathbf{M}^{\mathbf{A}}$ can be written in the form

$$\mathbf{M}^{\mathbf{A}} = \begin{bmatrix} \mathbf{S}^{\mathbf{A}} \\ \mathbf{N}^{\mathbf{A}} \end{bmatrix}, \tag{9.192}$$

where $\mathbf{S}^{\mathbf{A}}$ is the $n_a \times n_a$-dimensional S-matrix in (9.189) and $\mathbf{N}^{\mathbf{A}}$ is a subsidiary matrix, with dimensions $(n_t - n_a) \times n_a$, which multiplies decaying wave solutions in the closed channels in (9.189).

We can now determine the S-matrix $\mathbf{S}^{\mathbf{A}}$ by matching the solution in the velocity gauge to the $n_t \times n_t$-dimensional R-matrix $\mathcal{R}_p(E)$ in the velocity gauge determined at $r = a_p$, as described in Sect. 9.1.3 where we showed that the required solution satisfies (9.69). We now remember that $\boldsymbol{\mathcal{F}}^{\mathbf{V}}$ is related to $\mathbf{h}^{\mathbf{A}}$ and hence to $\mathbf{I}^{\mathbf{A}}$ and $\mathbf{O}^{\mathbf{A}}$ by the linear transformation (9.188) which we can rewrite as

$$\mathbf{h}^{\mathbf{A}}(r) = \mathbf{C}^{-1}\boldsymbol{\mathcal{F}}^{\mathbf{V}}(r), \tag{9.193}$$

where $\mathbf{C}^{-1}$ is the inverse of $\mathbf{C}$ defined by (9.188). We then multiply (9.69) on the left by $\mathbf{C}^{-1}$ and substitute for $\boldsymbol{\mathcal{F}}^{\mathbf{A}}$ in terms of $\mathbf{I}^{\mathbf{A}}$ and $\mathbf{O}^{\mathbf{A}}$ using (9.190) and (9.191). After re-arranging the terms we obtain the following coupled equations:

$$\begin{aligned} &\left[\mathbf{O}^{\mathbf{A}}(a_p) - a_p \mathbf{C}^{-1}\boldsymbol{\mathcal{R}}_p(E)\mathbf{C}\frac{\mathrm{d}\mathbf{O}^{\mathbf{A}}}{\mathrm{d}r}\bigg|_{r=a_p} - \frac{1}{2}\mathbf{C}^{-1}\boldsymbol{\mathcal{P}}\mathbf{C}\mathbf{O}^{\mathbf{A}}(a_p) \right] \mathbf{M}^{\mathbf{A}} \\ &= \mathbf{I}^{\mathbf{A}}(a_p) - a_p \mathbf{C}^{-1}\boldsymbol{\mathcal{R}}_p(E)\mathbf{C}\,\frac{\mathrm{d}\mathbf{I}^{\mathbf{A}}}{\mathrm{d}r}\bigg|_{r=a_p} - \frac{1}{2}\mathbf{C}^{-1}\boldsymbol{\mathcal{P}}\mathbf{C}\mathbf{I}^{\mathbf{A}}(a_p), \end{aligned} \tag{9.194}$$

where the derivatives of $\mathbf{I}^{\mathbf{A}}$ and $\mathbf{O}^{\mathbf{A}}$, evaluated at $r = a_p$, can be determined from the solution of (9.170) subject to the boundary conditions (9.190) and (9.191). Equations (9.194) are a set of n_t linear simultaneous equations with n_a right-hand sides which can be solved to yield the $n_t \times n_a$-dimensional matrix $\mathbf{M}^{\mathbf{A}}$. The $n_a \times n_a$-dimensional S-matrix is then determined from (9.192) and hence the corresponding scattering amplitude and cross section for laser-assisted electron–atom collisions determined using the procedure described in Sect. 2.5.

Finally, in order to calculate the atomic multiphoton ionization rate, we must determine a solution satisfying Siegert outgoing wave boundary conditions [876] corresponding to a pole in the S-matrix. This is achieved by an iterative process, as discussed in Sect. 9.1.4, yielding (9.95), and in Sect. 9.1.5, yielding (9.161). In this way we obtain the complex quasi-energy $E^{\mathbf{A}}$ given by

$$E^{\mathbf{A}} = E_0 + \Delta - \frac{1}{2}\mathrm{i}\Gamma, \tag{9.195}$$

where E_0 is the field-free energy of the target atom, Δ is the dynamic Stark shift and Γ is the total multiphoton ionization rate.

9.1.7 Harmonic Generation

Atoms interacting with an intense laser field can emit radiation at multiples, or harmonics, of the pump laser frequency, as illustrated in (9.3). For an initial target state with a given parity, the harmonic frequency ν' in (9.3) is an odd multiple of the laser frequency ν, i.e. $\nu' = n\nu$ where $n = 3, 5, 7, \ldots$. This process, called harmonic generation, has attracted considerable interest in recent years with the availability of intense lasers making it possible to observe high harmonics [590–592, 626, 627, 758]. For example, L'Huillier and Balcou [590] observed the emission spectra of various inert gases using a "pump" laser of wavelength $\lambda = 1053$ nm and found harmonic frequencies ν' with $n = 133$ in neon at an intensity $I = 1.5 \times 10^{15}$ W/cm^2. In these observations the harmonic spectrum exhibited characteristic behaviour of a rapid decrease for the first few harmonic yields, followed by a plateau and an abrupt cut-off at high harmonics.

The theoretical treatment of harmonic generation by an intense laser field interacting with a gaseous medium has two aspects, discussed by L'Huillier et al. [591] and Burnett et al. [194]. First, the microscopic, single-atom response to the laser field must be analysed, where the harmonic spectrum emitted by a single atom is calculated by solving the appropriate Schrödinger equation. Second, the single-atom response must then be combined to obtain the macroscopic harmonic fields generated from the coherent emission of all the atoms in the laser focus. This is achieved by using the single-atom response as source terms in Maxwell's equations [591]. In this section we will be concerned with the single-atom aspect of harmonic generation, which we will treat by solving the time-dependent Schrödinger equation using R-matrix–Floquet theory.

There have been many contributions to the study of harmonic generation by direct numerical solution of the time-dependent Schrödinger equation. For example, this method has been used to study harmonic generation by one-dimensional model atoms [280, 281], by model atoms with three-dimensional delta-function potentials [85, 86] and by realistic three-dimensional atoms in the single active electron approximation [548, 549, 552–554, 589]. In particular, the time-dependent calculations of Krause et al. [548] showed that for low laser frequencies the maximum cut-off energy at the end of the plateau mentioned above is approximated by $I_p + 3E_\mathrm{p}$ where I_p is the ionization potential of the atom and E_p is the ponderomotive energy of an electron in the laser field defined by (9.48). This simple result can be understood using a semi-classical model proposed by Kulander et al. [555] and Corkum [231], in which the electron first tunnels through the potential barrier formed by the atomic potential and the oscillating laser field. After escaping from the atom, some electrons driven by the oscillating laser field return to the residual ion and emit harmonics by recombining into the atomic ground state. The cut-off energy for the harmonics predicted by this rescattering model is given by $I_p + 3.2E_\mathrm{p}$ which is in good agreement with the time-dependent calculations of Krause et al. [548]. Detailed calculations of harmonic generation rates have also been carried out using the Floquet–Fourier ansatz by Potvliege and Shakeshaft [753], who expanded the harmonic components for atomic hydrogen in terms of Sturmian basis functions.

In this work they calculated non-perturbative harmonic generation rates in a linearly polarized laser field, where the intensity ranged from 10^{12} to 3×10^{13} W/cm^2 and the wavelength ranged from 265 to 1064 nm. However, the extension of this approach to multi-electron atoms becomes computationally very demanding.

More recently, a major programme of work going beyond the single active electron approximation has been undertaken by Parker et al. [713] and in later publications. In this work, the time-dependent Schrödinger equation for helium is solved making full allowance for two-electron correlation effects. This work has yielded accurate multiphoton double-electron ionization cross sections and harmonic generation spectra for helium. However, the extension of this work to more than two strongly interacting electrons presents a major computational challenge which we will return to in Sect. 10.1.5 where we discuss time-dependent R-matrix theory.

9.1.7.1 R-Matrix–Floquet Theory

We now consider R-matrix–Floquet theory of harmonic generation which is non-perturbative and includes electron–electron correlation effects in multi-electron targets. This theory, which is an extension of R-matrix–Floquet theory of multiphoton ionization and laser-assisted electron–atom collisions, discussed in earlier sections in this chapter, was developed by Gębarowski et al. [366] and has been applied to multi-electron atomic targets by Gębarowski et al. [367] and by Plummer and Noble [744, 745].

We consider an $(N+1)$-electron atomic system A_i in (9.3) in a laser field which is treated classically and which is assumed to be monochromatic, monomode, linearly polarized and spatially homogeneous, where the electric field vector is defined by (9.4) and the corresponding vector potential is defined by (9.5). The rate of spontaneous emission of photons of frequency $\Omega = n\omega$ with a specific polarization $\hat{\boldsymbol{\epsilon}}$ in a direction $\hat{\mathbf{n}}$ is then given by [753]

$$\frac{\mathrm{d}R(\Omega, \hat{\boldsymbol{\epsilon}})}{\mathrm{d}\hat{\mathbf{n}}} = \frac{\Omega^3}{8\pi \mathrm{c}^3} \left| \hat{\boldsymbol{\epsilon}}^* \cdot \mathbf{D} \right|^2, \tag{9.196}$$

corresponding to an electric dipole moment $\mathrm{Re}\,[\mathbf{D} \exp(-\mathrm{i}\Omega t)]$ oscillating at a frequency Ω, where the quantity $\mathbf{D}$ can be related to the oscillating electric dipole moment $\mathbf{d}(t)$ of the atom induced by the laser field which is given by

$$\mathbf{d}(t) = -\langle \widetilde{\Psi}_{\mathrm{T}}(\mathbf{X}_{N+1}, t) \, |\mathbf{R}_{N+1}| \, \widetilde{\Psi}(\mathbf{X}_{N+1}, t) \rangle. \tag{9.197}$$

In (9.197) $\widetilde{\Psi}(\mathbf{X}_{N+1}, t)$ satisfies the time-dependent Schrödinger equation (9.6), $\mathbf{R}_{N+1}$ is defined by (9.10) and $\widetilde{\Psi}_{\mathrm{T}}(\mathbf{X}_{N+1}, t)$ is the time-reversed wave function corresponding to $\widetilde{\Psi}(\mathbf{X}_{N+1}, t)$, which we discuss below. The wave function $\widetilde{\Psi}(\mathbf{X}_{N+1}, t)$ is expressed as a Floquet–Fourier expansion (9.8), where the functions $\Psi_n(\mathbf{X}_{N+1})$ in this equation are the time-independent harmonic components of the wave function

and the quasi-energy E, which corresponds to Siegert [876] outgoing wave boundary conditions, can be written as

$$E = E_0 + \Delta - \frac{1}{2}\mathrm{i}\Gamma. \tag{9.198}$$

In this equation E_0 is the field-free energy of the target atom, Δ is the dynamic Stark shift and Γ is the total multiphoton ionization rate of the atom.

The reason for using the time-reversed wave function $\widetilde{\Psi}_{\mathrm{T}}(\mathbf{X}_{N+1}, t)$ in (9.197) has been discussed by a number of authors including Potvliege and Shakeshaft [753], Piraux and Shakeshaft [741] and Plummer and McCann [742]. If we adopt a wave function satisfying the Floquet–Fourier ansatz with Siegert outgoing wave boundary conditions, then the norm of the wave function satisfies

$$\langle\widetilde{\Psi}(\mathbf{X}_{N+1}, t)|\widetilde{\Psi}(\mathbf{X}_{N+1}, t)\rangle \approx \chi(0)\exp(-\Gamma t), \tag{9.199}$$

where $\chi(0)$ is constant in time. However, the norm of the exact wave function satisfies

$$\langle\widetilde{\Psi}(\mathbf{X}_{N+1}, t)|\widetilde{\Psi}(\mathbf{X}_{N+1}, t)\rangle = C, \tag{9.200}$$

where C is a constant and the integral is taken over an expanding region of space where the wave function is non-zero. The reason for this anomaly is that when we make the Floquet–Fourier ansatz, we treat the atom as having a definite complex energy defined by (9.198) whereas, in fact, the atom has a distribution of energies with a width Γ and should be represented by a localized wave packet which is initially the bound state of the atom. The factor $-\frac{1}{2}\mathrm{i}\Gamma$ in (9.198) then describes the electron loss from the bound state into the continuum, which is correctly treated by the Floquet–Fourier ansatz because the Floquet state vector describes an electron which is not localized.

In order to resolve these contrasting views, Piraux and Shakeshaft [741] observed that if a fixed region of space, rather than an expanding region of space, is adopted in (9.200) then flux will leave this region as the atom expands in the laser field and the norm will decrease. However, they showed that it is possible to define a new norm corresponding to a fixed finite region of space which remains constant in time. This is achieved by introducing the time-reversed wave function $\widetilde{\Psi}_{\mathrm{T}}(\mathbf{X}_{N+1}, t)$ and defining a new norm by

$$\langle\widetilde{\Psi}_{\mathrm{T}}(\mathbf{X}_{N+1}, t)|\widetilde{\Psi}(\mathbf{X}_{N+1}, t)\rangle_F = N, \tag{9.201}$$

where the integral is taken over the fixed finite region of space denoted by F. In this case N is a constant, because in the time-reversed state flux enters the fixed finite region of space and compensates for the flux leaving this region in the original state.

Returning to (9.197) we represent the wave functions for the induced dipole moment in this expression by the Floquet–Fourier expansion (9.8) giving

$$\mathbf{d}(t) = -\sum_{m=-\infty}^{\infty}\sum_{n=-\infty}^{\infty}\langle\Psi_m(\mathbf{X}_{N+1})\,|\mathbf{R}_{N+1}|\,\Psi_n(\mathbf{X}_{N+1})\rangle\exp[-\mathrm{i}(n-m)\omega t]. \quad (9.202)$$

Writing $q = n - m$ and defining the dipole moments

$$\mathbf{d}_{qn} = -\langle\Psi_{n-q}(\mathbf{X}_{N+1})\,|\mathbf{R}_{N+1}|\,\Psi_n(\mathbf{X}_{N+1})\rangle \quad (9.203)$$

and

$$\mathbf{d}_q = \sum_{n=-\infty}^{\infty}\mathbf{d}_{qn}, \quad (9.204)$$

we then find that (9.202) becomes

$$\mathbf{d}(t) = \mathbf{d}_0 + \sum_{q=1}^{\infty}[\mathbf{d}_q\exp(-\mathrm{i}q\omega t) + \mathrm{CC}], \quad (9.205)$$

where CC is the complex conjugate term. Since $\mathbf{d}_q = \mathbf{d}^*_{-q}$ we can write (9.205) in the form

$$\mathbf{d}(t) = \mathbf{d}_0 + 2\sum_{q=1}^{\infty}\mathrm{Re}\,[\mathbf{d}_q\exp(-\mathrm{i}q\omega t)], \quad (9.206)$$

By comparing (9.196) and (9.206) it follows that the rate for generating photons of frequency $\Omega = q\omega$ and polarization $\hat{\boldsymbol{\epsilon}}$ is obtained by putting $\mathbf{D} = 2\mathbf{d}_q$ in (9.196). Hence we obtain

$$\frac{\mathrm{d}R(\Omega,\hat{\boldsymbol{\epsilon}})}{\mathrm{d}\hat{\mathbf{n}}} = \frac{\Omega^3}{2\pi\,\mathrm{c}^2}\left|\hat{\boldsymbol{\epsilon}}^*\cdot\mathbf{d}_q\right|^2. \quad (9.207)$$

The rate of emission of photons into a given solid angle $\mathrm{d}\hat{\mathbf{n}}$ is obtained by summing over polarizations of the emitted radiation. Finally, the total emission rate is obtained by integrating over all directions $\hat{\mathbf{n}}$.

In order to calculate the quantities $\mathbf{d}_q$ in (9.207), required to determine the harmonic generation emission rates, we proceed following our treatment of multiphoton ionization and laser-assisted electron–atom collisions discussed earlier in this chapter. We partition configuration space into three regions, as illustrated in Fig. 9.1. We then solve the time-dependent Schrödinger equation (9.6) by introducing Floquet–Fourier expansions of the wave function in each region, as discussed in Sects. 9.1.2, 9.1.3 and 9.1.4. In the internal region, where the radial coordinate of all $N+1$ electrons satisfy $r_i \le a_0$, we describe all $N+1$ electrons in the length gauge. In the external and asymptotic regions, where the radial coordinate of the ejected electron $r_{N+1} \ge a_0$ and the radial coordinate of the remaining N electrons satisfy

$r_i \leq a_0, \ i = 1, \ldots, N$, we adopt the velocity gauge for the ejected electron and the length gauge for the remaining N inner electrons. Having obtained the solution of (9.6) in each of these three regions, we then fit the radial asymptotic form of the ejected electron to outgoing wave Siegert [876] boundary conditions corresponding to (9.95) or (9.198). This is achieved, as described in Sect. 9.1.4, using an iterative procedure analogous to that used in determining the initial bound state energy in photoionization, described in Sect. 8.1.2. In this way we determine the complex quasi-energy $E^{\mathbf{V}}$ defined by (9.95), and the corresponding outgoing reduced radial wave solution (9.96) satisfied by the ejected electron up to an overall normalization factor. The Floquet–Fourier expansion of the total wave function describing the $N + 1$ electrons, defined by (9.8), is then obtained in all three regions in Fig. 9.1 up to an overall normalization factor.

Finally, in order to calculate the dipole moments $\mathbf{d}_{qn}$, defined by (9.203), the integrals must be confined to a finite region of space corresponding to (9.201). In most applications the range of integration can be confined to the internal region in Fig. 9.1 since, as pointed out by L'Huillier et al. [592], the main contribution to the dipole matrix elements comes from the region near the nucleus. In this case the wave function is defined by expansion (9.17). However, if necessary, the integration can be extended to part or all of the external region in Fig. 9.1 where the wave function is defined by expansion (9.37). In both cases, the wave function must be normalized to unity in the region included in the evaluation of the matrix elements and the Siegert outgoing wave boundary conditions (9.96) imposed on the wave function in the asymptotic region, to ensure the solution has the correct asymptotic form.

9.1.8 Non-hermitian Floquet Dynamics

In this section we consider atomic multiphoton ionization in short-pulse laser fields that cannot be accurately described by the Floquet–Fourier ansatz considered in earlier sections of this chapter. As pointed out by Potvliege and Shakeshaft [752], the Floquet–Fourier expansion (9.8) corresponding to a laser field defined by (9.4) and (9.5) contains no information about the way the field is turned on and is only valid if the initial state of the atom is not significantly depopulated during the rise time of the field. In addition, the laser pulse at constant amplitude must be sufficiently long that the multiphoton ionization rate corresponding to this amplitude is accurately defined.

In order to accurately describe atoms in short-pulse laser fields, we consider a coupled dressed state formalism, proposed by Ho and Chu [473] and generalized by Day et al. [253] to non-hermitian outgoing wave Siegert states. This procedure has been applied to multiphoton ionization of atomic hydrogen by Day et al. [253] and to multiphoton ionization of argon, using an R-matrix approach, by Plummer and Noble [746] and yields accurate results when the laser pulse is not so short that the direct R-matrix method for solving the time-dependent Schrödinger equation, considered in Chap. 10, must be used.

The non-hermitian Floquet approach to multiphoton ionization commences from solutions of the time-dependent Schrödinger equation (9.6) given by the following Fourier–Floquet expansion (9.8), which we write here as

$$\widetilde{\Psi}_j(\mathbf{X}_{N+1}, t) = \exp(-\mathrm{i}E_j t) \sum_{n=-\infty}^{\infty} \exp(-\mathrm{i}n\omega t)\Psi_{nj}(\mathbf{X}_{N+1}), \tag{9.208}$$

corresponding to Siegert outgoing wave boundary conditions defined by (9.160) and (9.161). In (9.208) the energies E_j are given by

$$E_j = E_{0j} + \Delta_j - \frac{1}{2}\mathrm{i}\Gamma_j, \tag{9.209}$$

where E_{0j} are the field-free energies of the target states included in the analysis, Δ_j are the dynamic Stark shifts of these states and Γ_j are the total multiphoton ionization rates of these states corresponding to the vector potential field strength A_0 in (9.5). We described earlier in this chapter how these quantities can be determined using R-matrix–Floquet theory. We now rewrite (9.208) as follows:

$$\widetilde{\Psi}_j(\mathbf{X}_{N+1}, t) = \exp(-\mathrm{i}E_j t)\widetilde{\psi}_j(\mathbf{X}_{N+1}, t). \tag{9.210}$$

We then assume that the wave function describing the atom or ion in a short-pulse laser field can be described, to a good approximation, by a finite superposition of Floquet wave functions of decaying dressed bound states defined by (9.210) given by

$$\widetilde{\Psi}(\mathbf{X}_{N+1}, t) = \sum_{j=1}^{n} a_j(t)\widetilde{\psi}_j(\mathbf{X}_{N+1}, t), \tag{9.211}$$

where $a_j(t)$ are time-dependent coefficients. In order to determine these coefficients we introduce the adjoint or time-reversed state corresponding to $\widetilde{\Psi}_j(\mathbf{X}_{N+1}, t)$, defined by

$$\widetilde{\Psi}_j^{\dagger}(\mathbf{X}_{N+1}, t) = \exp(-\mathrm{i}E_j^* t)\widetilde{\psi}_j^{\dagger}(\mathbf{X}_{N+1}, t), \tag{9.212}$$

which satisfies ingoing wave boundary conditions. It therefore follows that both $\widetilde{\Psi}_j(\mathbf{X}_{N+1}, t)$ and $\widetilde{\Psi}_j^{\dagger}(\mathbf{X}_{N+1}, t)$ are periodic functions of time with period $T = 2\pi/\omega$, where ω is the angular frequency of the field, and reduce to the field-free wave functions in the limit $A_0 \to 0$. Also, pairs of these Floquet wave functions are bi-orthogonal in the sense that for fixed A_0

$$\langle\langle \widetilde{\psi}_j^{\dagger} | \widetilde{\psi}_k \rangle\rangle \equiv \frac{1}{T}\int_0^T \langle \widetilde{\psi}_j^{\dagger} | \widetilde{\psi}_k \rangle \mathrm{d}t = \delta_{jk}, \tag{9.213}$$

where we have imposed the normalization condition $\langle\langle\widetilde{\psi}_j^{\dagger}|\widetilde{\psi}_j\rangle\rangle = 1$ on the wave function. Using this result and the time-dependent Schrödinger equation satisfied by $\widetilde{\Psi}(\mathbf{X}_{N+1}, t)$, Day et al. [253] show that the coefficients $a_j(t)$ in (9.211) satisfy the following coupled differential equations:

$$\mathrm{i}\frac{\mathrm{d}a_j}{\mathrm{d}t} = E_j a_j(t) - \mathrm{i}\frac{\mathrm{d}A_0}{\mathrm{d}t}\sum_{k=1}^{n}\langle\langle\widetilde{\psi}_j^{\dagger}|\widetilde{\psi}_k'\rangle\rangle a_k(t), \quad j = 1, \ldots, n, \tag{9.214}$$

where the laser field is treated as stationary when performing the cycle-averaging time integration of the matrix elements. Also in (9.214), $\widetilde{\psi}_k'$ denotes the derivative of $\widetilde{\psi}_k$ with respect to A_0. The coefficients $a_j(t)$ in (9.211) then represent the atomic state probability amplitudes at the beginning and end of the laser pulse.

As an example of this approach, we show in Fig. 9.5 non-hermitian Floquet calculations for multiphoton transitions between the 1s and 3p states in atomic hydrogen compared with results obtained by Day et al. [253] for the direct solution of the time-dependent equations. The laser pulses used in these calculations have a finite duration, with a temporal envelope $A_0(t) = A_{00}\sin^2\Omega t$ and are linearly polarized. The results presented in this figure show that there is a small but non-negligible transition from the 1s ground state to the 3p excited state, where the probability is marked by "Stückelberg oscillations" [892] caused by a Stark-shift-induced three-photon resonance between the 1s and 3p states dressed by the laser field. We see that there is excellent agreement between the non-hermitian Floquet results and accurate fully time-dependent calculations except for ultra-short laser pulses, less than a few cycles of the field, showing the accuracy of the non-hermitian Floquet results for all but the shortest laser pulses.

Finally, we note that the non-hermitian R-matrix–Floquet calculation carried out by Plummer and Noble [746] for argon has shown how the laser pulse length and shape can be used, together with a knowledge of the Floquet states, to control the atomic populations both during and at the end of each pulse. Future work comparing

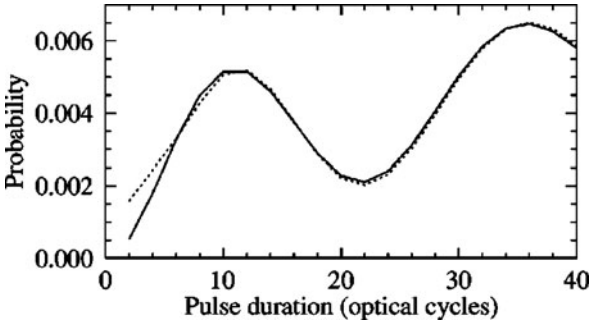

Fig. 9.5 Probability that a hydrogen atom, initially in the 1s state before a laser pulse, is in the 3p state at the end of a laser pulse of 300 nm wavelength and 8×10^{13} W/cm^2 peak intensity plotted against the duration of the pulse. *Solid line*, two-state (1s, 3p) non-hermitian Floquet results; *dotted line*, full time-dependent results (Fig. 1 from [253])

this and similar calculations for other atoms and ions with results obtained using the direct R-matrix solution of the time-dependent Schrödinger equation considered in Chap. 10 would be of considerable interest.

9.2 Illustrative Examples

In this section we present the results of some recent R-matrix–Floquet calculations of multiphoton processes which illustrate the theory presented in this chapter.

9.2.1 Resonances in Multiphoton Ionization

In the presence of an intense laser field, the ionization threshold energy of an atom and the energies of the associated Rydberg states are increased by approximately the ponderomotive energy $E_{\rm p}$ defined by (9.48). If the electric field strength $\mathcal{E}_0$ of the laser is sufficiently high then this will result in channel closing which occurs when

$$E_{\rm g} + n\mathrm{h}\nu - E_{\rm p} < 0, \tag{9.215}$$

where $E_{\rm g}$ is the energy of the ground state and n is the number of photons required to ionize the atom at low laser intensities. This effect is responsible for peak suppression in above-threshold ionization (ATI) and for resonance-enhanced multiphoton ionization (REMPI).

To illustrate the role of the ponderomotive energy in REMPI we consider the following multiphoton ionization process in helium:

$$\begin{array}{ccccc} n\mathrm{h}\nu + \mathrm{He}(1\mathrm{s}^2\ {}^1\mathrm{S}) & \rightarrow & \mathrm{He}^+(1\mathrm{s}\ {}^2\mathrm{S}) & + & \mathrm{e}^-. \\ \searrow & & \nearrow & & \\ \mathrm{h}\nu + \mathrm{He}^*(1\mathrm{s}n\ell) & & & & \end{array} \tag{9.216}$$

We illustrate this process in Fig. 9.6 which shows the energy level diagram of helium with the ionizing transitions that occur in the field of a KrF laser with wavelength 248 nm and for an intensity close to zero and for an intensity of 5×10^{14} W/cm^2. When the intensity of the KrF laser is close to zero we see in Fig. 9.6 that five photons are required to ionize helium from its ground state, but that four photons are insufficient to reach the lowest excited state and so no intermediate resonance occurs. As the laser intensity is increased the effective ionization threshold and the energies of the excited states are increased by the ponderomotive energy $E_{\rm p}$ with the result that six photons are then required to ionize the atom. Also, the excited state energies $1\mathrm{s}n\ell$ in (9.216) come into resonance, one at a time as the intensity is increased, with the energy of five photons giving rise to a series of resonances in the six-photon ionization rate. In Fig. 9.6 we see that at a laser intensity of 5×10^{14} W/cm^2 the five-photon energy corresponds closely to the energy of the $1\mathrm{s}2\mathrm{p}\ {}^1\mathrm{P}^{\rm o}$ excited state of helium giving rise to a REMPI enhancement in the six-photon ionization rate.

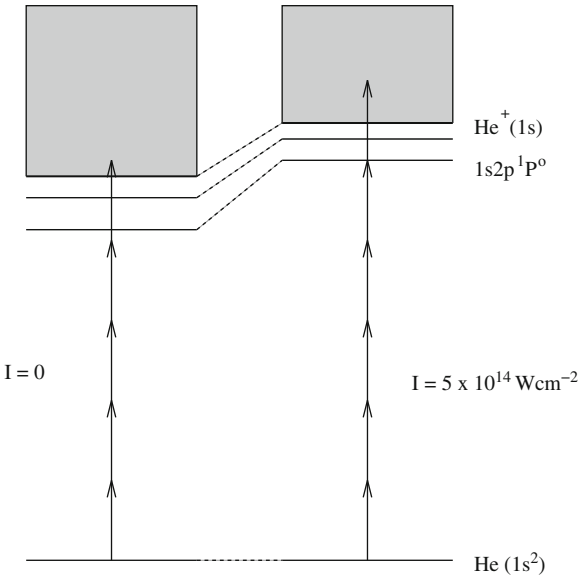

Fig. 9.6 Energy levels of He in a KrF laser field with intensity I close to zero and with intensity 5×10^{14} W/cm^2, showing multiphoton ionization in each case. The *shaded areas* represent the continuum spectrum of He and the *horizontal lines* represent the ground state and two excited states of He (Fig. 1 from [379])

To explore this situation in greater detail, Glass and Burke [379] carried out R-matrix–Floquet (RMF) calculations for helium multiphoton ionization corresponding to (9.216). In these calculations two approximations were considered. In the first, only the 1s ^{2}S ground state of He^+ was included in the RMF expansions (9.20) and (9.37), corresponding to the internal and external regions, respectively. In the second, $\overline{2s}$ and $\overline{2p}$ pseudostates representing electron–electron correlation effects were also included, where these pseudostates spanned the same range as the 1s ^{2}S ground state. Also, in order to obtain converged results at the higher laser intensities, up to 18 Floquet blocks (including 15 for absorption) and 10 angular momenta were retained in the RMF expansions.

The results of these calculations, which are presented in Fig. 9.7, illustrate the features mentioned above. At low intensities, five-photon ionization can occur and the behaviour is close to that predicted by the perturbative power law for the dependence of the ionization rate on intensity. Channel closing occurs at an intensity of 6.7×10^{13} W/cm^2 while at higher intensities six-photon ionization is the dominant process and the influence of REMPI on the total ionization rate now becomes apparent. Just above the intensity at which channel closing takes place five-photon resonances occur between the ground state and highly excited bound states with odd parity and, as the intensity increases further, the fifth photon sweeps through Rydberg series of these resonances. We note that for intensities close to the channel-closing intensity (6.7×10^{13} W/cm^2) the calculation became more difficult due to the large radial extent of the intermediate high-energy Rydberg states, requiring large propagation distances $r = a_p$ in the external region in Fig. 9.1, so results are not given in this region.

Multiphoton ionization rates for He have also been calculated by van der Hart et al. [936] for the frequency-doubled Ti:Sapphire laser wavelength of 390 nm

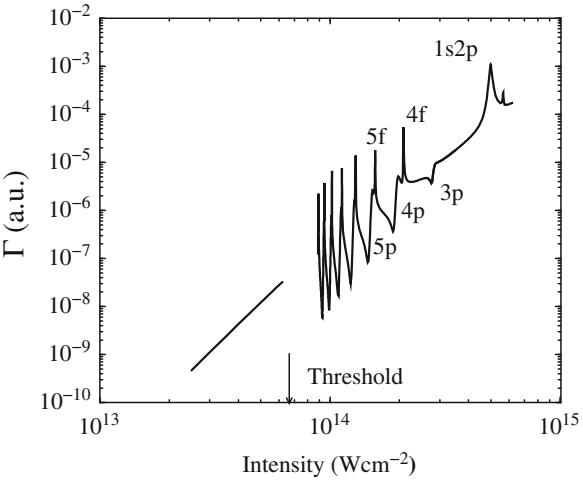

Fig. 9.7 Total ionization rate for He in a 248 nm KrF laser field as a function of laser intensity. The *arrow* marks the intensity where channel closing takes place. Below this intensity five-photon ionization occurs, while at higher intensities at least six photons are required for ionization (Fig. 2 from [379])

using both RMF theory and also by solving the time-dependent Schrödinger equation using direct numerical integration. The two calculations were found to be in excellent agreement for intensities between 1×10^{14} and 2.5×10^{14} W/cm^2 where the ionization rate is strongly enhanced by resonances. RMF multiphoton ionization calculations have also been carried out for Ar by Plummer and Noble [744], for Ne and Ar by McKenna and van der Hart [624] and by van der Hart [933] and for Ca by McKenna and van der Hart [623]. In the work on Ar by van der Hart [933], wavelengths between 248.6 and 390 nm were considered, where for the frequency-doubled Ti:Sapphire laser wavelength of 390 nm the ionization rates for Ne and Ar were investigated up to 2.5×10^{14} W/cm^2. We show in Fig. 9.8 the resonance-enhanced multiphoton ionization rate for Ar subjected to 390 nm laser light as a function of laser intensity using RMF theory compared with ADK

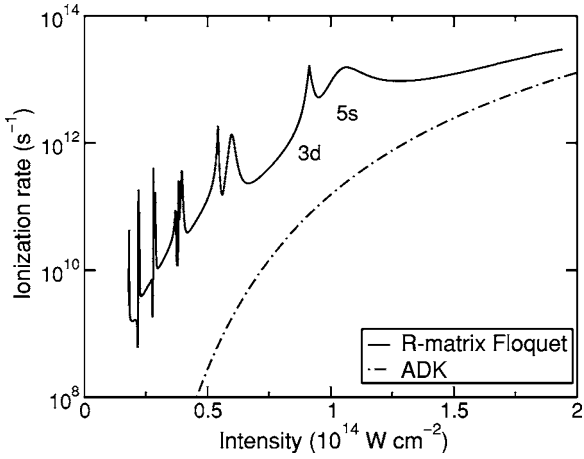

Fig. 9.8 Ionization rate for Ar subjected to 390 nm laser light as a function of laser intensity. RMF calculations (*solid line*) are compared with ADK calculations (*dashed-dotted line*). The label 5s indicates the $3s^2 3p^5 5s\ ^1P^o$ resonance and the label 3d indicates the $3s^2 3p^5 3d\ ^1P^o$ resonance (Fig. 5 from [933])

calculations. The RMF calculation included the $3s^2 3p^5\ ^2P^o$ Ar^+ ground state and retained 21 Floquet blocks (15 absorption and 5 emission) and angular momenta up to $L = 10$ in the RMF expansion. In the intensity region shown, between 1.8×10^{13} and 2×10^{14} W/cm^2, a minimum of six photons need to be absorbed to achieve ionization. Including the $3s3p^6\ ^2S^e$ Ar^+ excited state in the RMF expansion modifies the off-resonance ionization rates by ∼2% and the resonance peaks then occur at 1% higher intensity. The ionization rate increases rapidly with laser intensity from $\sim 1.6 \times 10^9$ s^{-1} at an intensity of 2×10^{13} W/cm^2 to 2.7×10^{13} s^{-1} at an intensity of 1.9×10^{14} W/cm^2. However, this is considerably less than the power law I^6 would yield. Also, the results are more than two orders of magnitude greater than the ADK tunnelling model [16, 727] at the lower laser intensities due to the exponential decay of the ADK rate compared with the I^6 behaviour of the RMF rate.

Recently, there has been increasing interest in resonance effects in multiphoton ionization of negative ions. We conclude this section by discussing R-matrix–Floquet calculations of two-photon detachment of Li^- by van der Hart [932]. We note that Li^- has also been the subject of R-matrix photoionization studies by Gorczyca et al. [401], mentioned in Sect. 8.2.2.

While most multiphoton detachment studies of negative ions have focused on outer-shell electrons, there is currently increasing interest in inner-shell processes. The simplest negative ion for which a distinction can be made between outer and inner electrons is Li^- which has a $1s^2 2s^2\ ^1S^e$ ground state configuration. In the work of van der Hart the following two-photon detachment process was considered:

$$2h\nu + Li^-(1s^2 2s^2\ ^1S^e) \rightarrow Li(1s\,2s^2\ ^2S^e) + e^-, \tag{9.217}$$

followed by

$$Li(1s\,2s^2\ ^2S^e) \rightarrow Li^+(1s^2\ ^1S^e) + e^-. \tag{9.218}$$

We see that an inner-shell 1s electron is first detached leaving the Li atom in a $1s\,2s^2\ ^2S^e$ doubly excited state which subsequently autoionizes leaving the Li^+ ion in its $1s^2\ ^1S^e$ ground state.

In the R-matrix–Floquet calculations by van der Hart 20 Li states were included in the internal region expansion. These consisted of eight physical states where two electrons were retained in the 1s orbital, six pseudostates where two electrons were retained in the 1s orbital and six physical states where only one electron was retained in the 1s orbital. In order to obtain convergence at the laser intensity 10^{12} W/cm^2 considered, five Floquet blocks were included in the calculation where three corresponded to absorption and one corresponded to emission. This gave 142 coupled channels where 66 channels described detachment. Finally, an internal region radius of 35 a.u. was adopted and the R-matrix then propagated out to 40 a.u. where it was matched to an asymptotic expansion.

Detachment of an inner-shell electron following absorption of two photons becomes possible for photon energies above 28.53 eV, the threshold photon energy

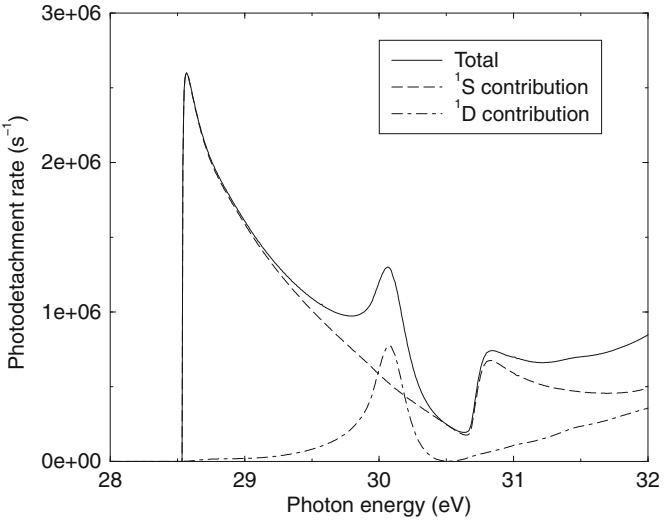

Fig. 9.9 Two-photon 1s-electron detachment rates for Li^- in a laser field of 10^{12} W/cm^2 as a function of photon energy leaving the residual Li atom in the excited $1s\,2s^2\,{}^2S^e$ state. The total rate (*solid line*) has been separated into the contribution from the emission of an s-electron (*dashed line*) and a d-electron (*dot-dashed line*) (Fig. 1 from [932])

for the $1s\,2s^2\,{}^2S^e$ state of Li in (9.217) and (9.218). We show in Fig. 9.9 the results of the calculation for the two-photon detachment rate of ground state Li^- leaving the Li atom in the excited $1s\,2s^2\,{}^2S^e$ state. We see that the photodetachment rate rises quickly from the threshold at 28.53 eV to a maximum of 2.6×10^6 s^{-1} and then drops rapidly before rising again due to two shape resonances. The first is identified as a $1s\,2s\,2p^2\,{}^1D^e$ shape resonance which occurs just above the $1s\,(2s\,2p\,{}^3P^o)\,{}^2P^o$ threshold and the second is identified as a $1s\,2s\,2p^2\,{}^1S^e$ shape resonance which occurs just above the $1s\,(2s\,2p\,{}^1P^o)\,{}^2P^o$ threshold.

We see from Fig. 9.9 that the $^1D^e$ channel contributes significantly less than the $^1S^e$ channel apart from the contribution from the $1s\,2s\,2p^2\,{}^1D^e$ shape resonance. This can be understood by observing that near the nucleus the d-orbital experiences significant repulsion due to the centrifugal potential barrier while the s-orbital experiences no repulsion. Hence two-photon absorption to the $^1D^e$ continuum only becomes important at higher continuum energies.

In conclusion, this R-matrix calculation has shown the importance of shape resonances in multiphoton ionization of inner-shell electrons in negative ions. It provides a challenge for future calculations and experiments in this field.

9.2.2 Harmonic Generation

A further example of the importance of resonances in multiphoton processes is their role in harmonic generation. This is illustrated by RMF calculations by Plummer

and Noble [745], who considered resonance-enhanced harmonic generation in argon at the KrF fundamental laser wavelength of 248 nm. In this work they considered the following process:

$$3h\nu + Ar(3p^6\ {}^1S^e) \rightarrow Ar^*(3p^5 4d\ {}^1P^o) \rightarrow Ar(3p^6\ {}^1S^e) + h\nu', \tag{9.219}$$

as well as the process where a further n photons are absorbed by the intermediate excited state of argon

$$nh\nu + Ar^*(3p^5 4d\ {}^1P^o) \rightarrow Ar^{**}(3p^5 k\ell\ {}^1P^o) \rightarrow Ar(3p^6\ {}^1S^e) + h\nu'', \tag{9.220}$$

where $\nu' = 3\nu$ and $\nu'' = (n+3)\nu$, with n even. At the KrF laser wavelength and low intensities, $\sim 7.5 \times 10^{12}$ W/cm^2, there is a three-photon resonance between the $3p^6\ {}^1S^e$ ground state and the $3p^5 4d\ {}^1P^o$ excited state of argon. If three photons with this intensity are absorbed by argon in its ground state, then the $3p^5 4d\ {}^1P^o$ state is excited which can decay back to the ground state with the emission of a photon with frequency $\nu' = 3\nu$, as indicated in (9.219). Alternatively, before decaying, the $3p^5 4d\ {}^1P^o$ excited state can absorb a further n photons as indicated in (9.220). The energy of the resultant argon atom then lies in the continuum and a laser-induced continuum structure (LICS) state[2], denoted by $Ar^{**}(3p^5 k\ell\ {}^1P^o)$ in (9.220), is formed. If the total number of photons n absorbed in (9.219) and (9.220) is odd and the spin and angular symmetry of the LICS state is $^1P^o$, then this state can decay back to the ground state with the emission of a photon with frequency $\nu'' = (n+3)\nu$.

In the RMF calculations by Plummer and Noble, both the $3s^2 3p^5\ {}^2P^o$ ground state and the $3s3p^6\ {}^2S^e$ first excited state of Ar^+ were included in the RMF expansions (9.20) and (9.37). In addition, between 8 and 10 Floquet blocks corresponding to absorption and between 3 and 5 Floquet blocks corresponding to emission were retained in the expansion. We show in Figs. 9.10 and 9.11 the third and fifth harmonic generation rates as a function of laser intensity. We see that there is a strong resonant enhancement of the rates at a laser intensity of 7.5×10^{12} W/cm^2 caused by the relative ponderomotive shifts of the $^1S^e$ ground state and the $^1P^o$ excited state. Also we see that there is a factor of about 600 in the relative heights of the peak rates between these two harmonics. The seventh harmonic, not shown, also has significant enhancement at this laser intensity, although the peak rate is now only $\sim 10^{-9}$ of the peak rate of the third harmonic.

The resonant enhancement of harmonic generation that we have described is a general feature of harmonic generation and similar results are expected for other atoms and ions. For example, RMF calculations by Gębarowski et al. [367] have shown strong enhancement of the third harmonic generation in Mg, corresponding

[2] See Sect. 9.2.3 for a further discussion of LICS states.

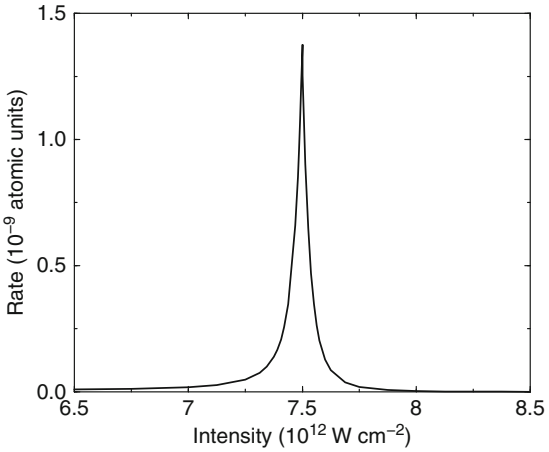

Fig. 9.10 Third harmonic generation rate in Ar as a function of laser intensity for the KrF laser wavelength 248 nm (Fig. 2 from [745])

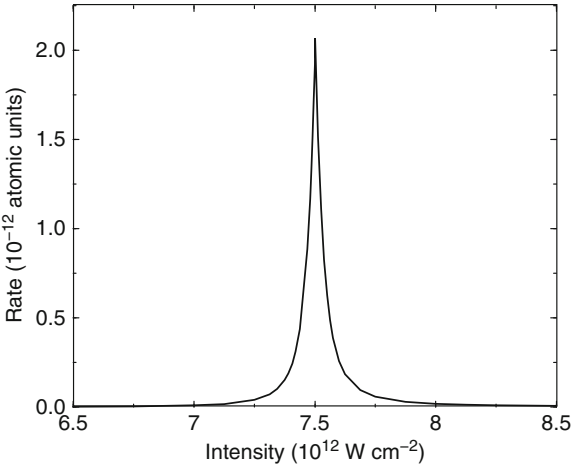

Fig. 9.11 Fifth harmonic generation rate in Ar as a function of laser intensity for the KrF laser wavelength 248 nm (Fig. 3 from [745])

to resonant excitation of the 3s3p ^{1}P^o autoionizing state and seven-photon resonances are predicted by Plummer and Noble [745] for neon in a frequency-doubled Ti:Sapphire laser field. Also for neon, there is predicted to be a resonance-enhanced boost to the 13th harmonic in a fundamental Ti:Sapphire laser field. Given the stability of the inert gases and the important role played by resonances, we expect inert gases to be stable sources for generating harmonics.

9.2.3 Laser-Induced Degenerate States

"Laser-induced degenerate states" (LIDS) arise when an autoionizing state in electron–ion collisions and a state lying in the continuum corresponding to an atom dressed by the laser field become degenerate at certain laser intensities and frequencies. To illustrate the LIDS mechanism we consider the following processes:

$$\begin{matrix} \mathrm{e}^- + A^+ \rightarrow A_1^{**} \\ n\mathrm{h}\nu + A \rightarrow A_2^{**} \end{matrix} \searrow \nearrow \; A^+ + \mathrm{e}^-. \tag{9.221}$$

The upper process in (9.221) corresponds to an electron–ion collision, which proceeds through an intermediate autoionizing state A_1^{**} lying in the continuum with a complex energy E_1. The lower process in (9.221) corresponds to multiphoton ionization from the ground state A which proceeds through a "Laser-induced continuum structure" (LICS) state A_2^{**} (discussed by Knight et al. [540, 541]) which also lies in the continuum with a complex energy E_2. This is illustrated in Fig. 9.12 where the LICS state A_2^{**}, formed by four-photon absorption from the ground state, lies close in energy to the autoionizing state A_1^{**}. By varying both the laser intensity and frequency, the real and imaginary parts of the energies E_1 and E_2 in the complex energy plane can be made to coincide, giving rise to a LIDS state corresponding to a double pole in the laser-assisted electron–ion collision S-matrix.

Latinne et al. [581] and Cyr et al. [241] first observed LIDS in RMF calculations of multiphoton ionization of argon. In these calculations, the $3s^2 3p^5\ {}^2P^o$ ground state and the $3s3p^6\ {}^2S^e$ first excited state of Ar^+ were included in the RMF

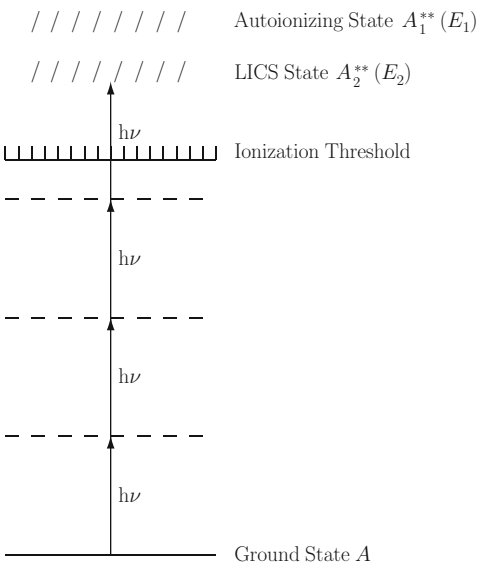

Fig. 9.12 Doubly excited autoionizing state A_1^{**}, with complex energy E_1, and laser-induced continuum structure (LICS) state A_2^{**}, with complex energy E_2, which gives rise to a laser-induced degenerate state (LIDS)

expansions (9.20) and (9.37). In this way the $3s3p^6 4p\ ^1P^o$ autoionizing state, corresponding to A_1^{**} in (9.221), and the $3s^2 3p^6\ ^1S^e$ ground state dressed by the laser field, corresponding to A_2^{**} in (9.221) were both included in the calculations. The RMF equations were solved in the internal, external and asymptotic regions and the solution fitted to Siegert outgoing wave boundary conditions [876], yielding the complex energy defined by (9.95), (9.161) or (9.195).

We now consider for illustrative purposes the results obtained by Latinne et al. [581] when $n = 1$ in (9.221) corresponding to one-photon absorption. We show in Fig. 9.13 the resultant trajectories in the complex energy plane of the Floquet energies E_1 and E_2 in Fig. 9.12 as the laser intensity is varied for fixed values of the angular frequency ω. Also for illustrative purposes, the Floquet energies E_1 and E_2 are both shifted down by the laser angular frequency ω. The zero-field position of the Ar ground state lies on the real axis at $E_g = -0.57816$ a.u., while the zero-field positions of the autoionizing state (denoted by circles in Fig. 9.13) lie at a complex energy of $0.40936 - 0.00119\mathrm{i} - \omega$ a.u., where the zero-field resonance width $\Gamma_a = 2 \times 0.00119$ a.u. For each angular frequency there are two trajectories, one originating at the zero-field position of the ground state and the other originating at the shifted zero-field position of the autoionizing state. We see by inspecting Fig. 9.13 that there are two complex energies where the trajectory originating from the ground state and the trajectory originating from the autoionizing state exchange their roles, corresponding to two LIDS. This occurs for laser angular frequencies $\omega \approx 0.98555$ and 0.98945. At large positive or negative detunings

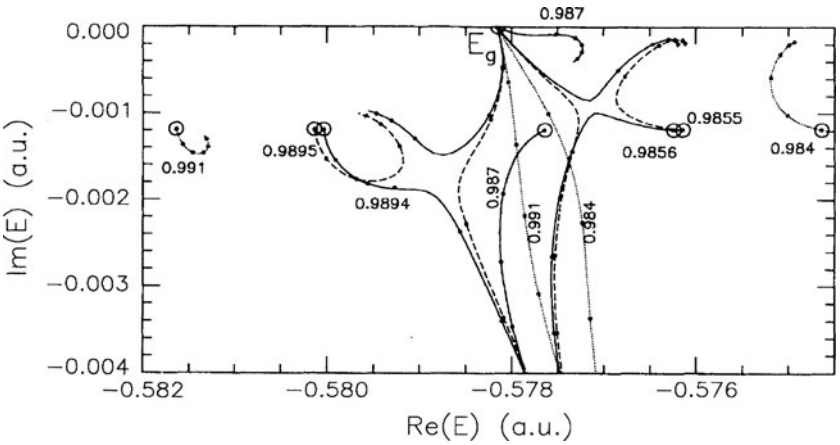

Fig. 9.13 Trajectories in the complex energy plane as a function of laser intensity for Ar showing two LIDS. The trajectories correspond to the Floquet energies for the $3s3p^6 4p\ ^1P^o$ autoionizing state of Ar and the $3s^2 3p^6\ ^1S^e$ ground state of Ar dressed by one photon (each shifted down by the laser angular frequency ω), for laser intensities varying from 0 to 5×10^{13} W/cm^2. The corresponding value of the laser angular frequency is indicated on the trajectories and the *dots* on the trajectories give the increase in the laser intensity in steps of 9×10^{12} W/cm^2 (Fig. 1 from [581])

from these angular frequencies, the autoionizing state does not move appreciably from its zero-field position, while the width of the ground state increases rapidly from zero with increasing intensity. On the other hand, at intermediate detunings (e.g. $\omega \approx 0.987$) the opposite occurs, with the width of the trajectory connected to the shifted autoionizing state increasing rapidly with intensity, while the ground state trajectory remains "trapped" close to the real energy axis. Finally, we observe that at these critical laser angular frequencies and intensities the two complex energies are degenerate. The corresponding LIDS therefore each results in a double pole in the S-matrix.

It has been known for many years that multiple poles in the S-matrix give rise to new phenomena, including a modification of the exponential decay law and the Breit–Wigner resonance profile (e.g. [387, 683]). Also, the physical implications of LIDS have been discussed by Kylstra and Joachain [557]. However, while LIDS occur quite generally in multiphoton processes and have been demonstrated for a number of targets including Ar, He and H^-, more work needs to be carried out both theoretically and experimentally to reveal the full implications of this interesting phenomenon in atomic and molecular multiphoton collision processes.

9.2.4 Laser-Assisted Electron–Atom Collisions

In recent years increasing attention has been given to laser-assisted electron–atom collisions defined by (9.2). This process is of fundamental interest as an aspect of laser–atom interactions and is of importance, for example, in the laser heating of plasmas and high-power gas lasers. One of the most interesting features of this process is the possibility of exciting the target atom at electron collision energies below the field-free threshold via the simultaneous absorption of one or more photons. The first experimental investigations of simultaneous electron–photon excitation (SEPE) of atoms were performed by Mason and Newell [640, 641] on helium in the field of a CW CO_2 laser (photon energy 0.117 eV, wavelength 10.6 μm) at intensities from 10^4 to 10^5 W/cm^2. This was followed by studies up to 10^8 W/cm^2 using a pulsed CO_2 laser by Wallbank et al. [945–947] and further experiments were carried out by Wallbank and Holmes [942–944] in which angular distributions were measured yielding cross sections which were much larger than those predicted by the low-frequency theory of Kroll and Watson [550]. An extensive review of early work in this field has been given by Mason [639].

In this section we discuss the results of laser-assisted electron–atom collision calculations carried out by Terao-Dunseath et al. [925] using the simplified R-matrix–Floquet analysis in the asymptotic region discussed in Sect. 9.1.6. In this work, the SEPE of helium atoms for exciting the $2\,^3S$ and $2\,^3P$ states near threshold was investigated in a linearly polarized Nd-YAG laser (photon energy 1.17 eV) with an intensity of $I = 10^{10}$ W/cm^2, where it was assumed that the colliding electron was incident along the polarization direction of the field. Also in these calculations, the first five target states $1\,^1S$, $2\,^3S$, $2\,^1S$, $2\,^3P^o$ and $2\,^1P^o$ of helium were included in

the R-matrix expansion, together with eight Floquet components with $-3 \leq n \leq 4$. This was sufficient to ensure convergence for the laser intensity and energy range considered. This approximation also gives good agreement, in the absence of the laser field, with the positions and widths of the resonances obtained in electron–helium atom collision calculations and experiments, discussed in Sect. 5.6.2.

We present in Fig. 9.14 cross sections for SEPE of the $2\,^3S$ state of He from the ground state together with the field-free excitation cross section. Also we note that although in this laser field there is AC Stark mixing between states (e.g. the $1s2s\,^3S^e$ and $1s2p\,^3P^o$ states), for simplicity of notation we denote the field-dressed states by the quantum numbers of their dominant component. A prominent feature in Fig. 9.14 is the pronounced isolated resonance in the excitation cross section corresponding to the absorption of one photon. This occurs below the $2\,^3S$ threshold at an energy corresponding to the $1s2s^2\,^2S^e$ He^- resonance in the field-free elastic cross section, first observed by Schulz [835]. It corresponds to the process where the incoming electron is first captured in the $1s2s^2\,^2S^e$ He^- resonance state. This state

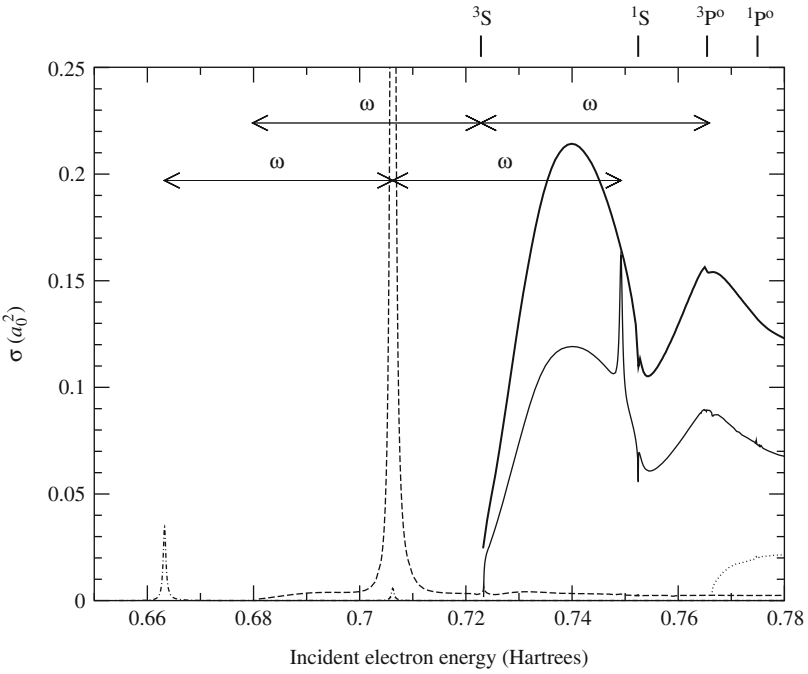

Fig. 9.14 Cross sections for electron impact excitation of the helium ground state into the $He(2\,^3S)$ excited state in the presence of a laser field with angular frequency ω. *Light solid line*: excitation with no exchange of photons; *dashed line*: excitation with absorption of one photon; *dash-dotted line*: excitation with absorption of two photons; *dotted line*: excitation with emission of one photon; *heavy solid line*: field-free cross section for exciting $He(2\,^3S)$. The field-free excitation thresholds are indicated by *vertical bars* above the figure (Fig. 2 from [925])

is then ionized by absorbing a laser photon leaving the helium atom in its $1s2s\ ^3S^e$ excited state, giving rise to the peak in the corresponding excitation cross section.

The cross section for exciting the $2\ ^3S$ state with no net exchange of photons in Fig. 9.14 is similar in shape to the field-free cross section but is about 40% lower in magnitude. A narrow resonance feature is obtained at an incident electron energy of 0.7492 Hartrees, which corresponds to the position of the $1s2s^2\ ^2S^e$ resonance shifted up by one photon energy. The origin of this resonance feature corresponds to the process where the electron–helium atom system emits one photon and the electron is temporarily captured in the $1s2s^2\ ^2S^e$ resonance state. It then absorbs one photon leading to excitation with no net exchange of photons. This explanation is supported by the fact that the width of this feature is only slightly larger than the one-photon absorption feature discussed above.

We also observe in Fig. 9.14 a small peak in the cross section for excitation of the $2\ ^3S$ state with the absorption of two photons. This corresponds to the process where the incoming electron together with a photon is captured in the $1s2s^2\ ^2S^e$ He^- resonance state. This state is then ionized by absorbing a second laser photon leaving the helium atom in its $1s2s\ ^3S^e$ excited state. In this case the resultant peak is much reduced in size since, as well as resulting from a two-photon process, the initial state of the electron plus helium atom is non-resonant. Similar results have also been reported by Terao-Dunseath et al. [925] for laser-assisted excitation of the helium ground state to the $1s2p\ ^3P^o$ excited state.

In conclusion we note that the calculations on helium have been extended to CO_2 laser fields and to very low-energy collisions by Dunseath and Terao-Dunseath [275, 276]. Also, general selection rules for differential cross sections for laser-assisted electron–atom collisions have been derived for the geometry in which a linearly polarized laser field is perpendicular to the scattering plane and results presented for electron–helium atom collisions in CO_2 and in Nd-YAG laser fields by Dunseatha et al. [278]. There is currently considerable interest in extending this work to other atoms and ions and to other laser intensities and frequencies.

Chapter 10
Multiphoton Processes: Time-Dependent Theory

In this chapter we consider the interaction of ultra-short laser pulses with atoms and atomic ions, where the laser pulses may involve only a few cycles of the field. In recent years there has been increasing interest in the production and application of these femtosecond (10^{-15} s) and attosecond (10^{-18} s) laser pulses which have opened up the possibility of time-resolved studies of unprecedented resolution, enabling the electronic motion in atoms, ions, molecules, plasmas and solids to be resolved for the first time. Examples of this work include the measurement of the response of an atomic system to a sub-femtosecond soft X-ray pulse by Hentschel et al. [456], the observation of a train of attosecond pulses from high harmonic generation by Paul et al. [722], the observation of the relaxation of core-excited atoms using a few-femtosecond visible light pulse with a sub-femtosecond soft X-ray pulse by Drescher et al. [269] and the observation of multiple ionization of Ne and Ar atoms by 25- and 7-femtosecond laser pulses by Rudenko et al. [801]. Of particular interest is the role that the re-collision mechanism plays in multiphoton ionization. This mechanism, which was discussed by Schafer et al. [816], was shown by Corkum [231] to lead with significant probability to the ejection of a second electron corresponding to double-electron multiphoton ionization. More recently, extreme ultraviolet (XUV) single-cycle isolated attosecond pulses with stable and tuneable carrier phases have been reported by Sansone et al. [809] and attosecond pulses have, for example, allowed the profiling of the electric field of few-femtosecond laser pulses by Goulielmakis et al. [407] and have enabled the stroboscopic study of single ionization events in Ar by Mauritsson et al. [647]. Recent reviews of few-femtosecond and attosecond laser science have been written by Agostini and DiMauro [4], Pfeifer et al. [731] and Scrinzi et al. [847], and an overview of recent developments in theoretical femtosecond physics has been written by Grossman [428].

The interaction of intense ultra-short laser pulses with atomic targets cannot be accurately treated by R-matrix–Floquet theory or by using multistate non-hermitian Floquet dynamics, considered in Chap. 9. Instead the full time-dependent Schrödinger equation describing the laser–atom interaction must be solved. Several groups have developed time-dependent approaches for He and other He-like two-electron atoms, including Parker et al. [713, 714, 716, 717], Scrinzi and Piraux [846]

P.G. Burke, *R-Matrix Theory of Atomic Collisions*, Springer Series on Atomic, Optical, and Plasma Physics 61, DOI 10.1007/978-3-642-15931-2_10,

and Lagmago et al. [562], and a time-dependent R-matrix theory that can be applied to arbitrary many-electron atoms was described by Burke and Burke [172]. More recently R-matrix methods and computer programs have been developed by van der Hart et al. [937, 938], Lysaght et al. [603–606] and Guan et al. [429, 431, 432] which have been applied to describe the full dynamics of general multi-electron atoms and ions in intense ultra-short laser pulses.

As well as providing a unique way of studying ultra-short laser pulse interactions with atomic targets, time-dependent theory complements Floquet theory by emphasizing the time domain instead of the energy domain of the process, as discussed in the case of helium by Parker et al. [715]. The time-dependent approach can accurately model laser–atom interactions with arbitrary laser pulse profiles and is the natural description of atomic processes in the intense field limit when ionization may occur in the order of a few field periods. However, new phenomena may be difficult to interpret using time-dependent theory, while the Floquet approach provides a framework for achieving this by describing the behaviour in terms of atomic states dressed by the laser field. The energies of dressed states are directly calculated in the Floquet approach, and in a wide range of multiphoton processes the dynamics can be understood very simply in terms of just a few dressed states. Thus, for longer laser pulses where both theories are applicable, they provide two ways of looking at the same problem which can lead to a deeper understanding of the physics involved.

In Sect. 10.1 we describe ab initio non-perturbative time-dependent R-matrix theories of atomic multiphoton processes which enable the interaction of few-femtosecond and attosecond laser pulses with arbitrary multi-electron atoms and atomic ions to be calculated. We commence with a derivation and analysis of the basic equations which enable the atomic wave function in the presence of the laser field to be propagated forward in time in internal and external R-matrix regions. Computational methods for solving these equations are then discussed and an analysis of the application of theoretical and computational methods to single- and double-electron multiphoton ionization is given. Finally, in Sect. 10.2 we describe results of recent calculations of ultra-short laser pulse interactions with neon and argon atoms using R-matrix computer programs developed in the last few years.

10.1 Time-Dependent *R*-Matrix Theory

In this section we describe ab initio time-dependent R-matrix theories of multiphoton ionization of atoms and atomic ions by intense ultra-short laser pulses, where we assume that the target atom or ion contains $N + 1$ electrons and has nuclear charge number Z.

10.1.1 Introduction

Following our discussion of R-matrix–Floquet theory in Chap. 9, we assume that the laser field, which is treated classically using the dipole approximation, is lin-

early polarized, spatially homogeneous and is described by the vector potential $\mathbf{A}(t)$. Neglecting relativistic effects, the atomic system in the presence of the laser field is then described by the time-dependent Schrödinger equation (9.6), which we rewrite here as

$$\left[H_{N+1} + \frac{1}{\mathrm{c}}\mathbf{A}(t)\cdot\mathbf{P}_{N+1} + \frac{N+1}{2\mathrm{c}^2}\mathbf{A}^2(t)\right]\Psi(\mathbf{X}_{N+1},t) = \mathrm{i}\frac{\partial}{\partial t}\Psi(\mathbf{X}_{N+1},t). \quad (10.1)$$

In this equation H_{N+1} is the non-relativistic Hamiltonian of the $(N+1)$-electron atom or ion in the absence of the laser field defined by (5.3) and $\mathbf{P}_{N+1}$ is the total electron momentum operator defined by (9.7). As discussed in the introduction to this chapter, the R-matrix–Floquet approach for solving (10.1) adopted in Chap. 9 is not applicable for ultra-short laser pulses and we must therefore solve (10.1) directly using time-dependent theory. Also, as in R-matrix–Floquet theory, double-electron multiphoton ionization could be treated by including pseudostates in the expansion of the wave function, as discussed in Sect. 6.2 and analysed in Sect. 10.1.5, or by using the IERM method discussed in Sect. 6.3. We now consider the direct solution of the time-dependent equation (10.1) by partitioning configuration space into internal and external regions.

In R-matrix–Floquet theory, discussed in Chap. 9, we found it convenient and appropriate to describe all $N+1$ interacting electrons in the internal region in the dipole length gauge and to describe the ejected or scattered electron in the dipole velocity gauge or the acceleration frame in the external and asymptotic regions. This asymmetry between the ejected or scattered electron and the remaining N electrons is not possible in the internal region where all $N+1$ electrons occupy the same region of space, since they are then strongly interacting and indistinguishable, and hence are described by an antisymmetrized wave function. It follows that the transformation from the length gauge to the velocity gauge for the ejected or scattered electron is carried out on the boundary between the internal and external regions in R-matrix–Floquet theory.

However, in time-dependent R-matrix theory it was found in a one-dimensional potential model calculation [172] that, in order to avoid build-up of errors in the time propagation algorithm due to the gauge transformation, the same gauge should be used to describe the ejected or scattered electron in both the internal and external regions. Hence, since in the multi-electron atom all $N+1$ electrons must be described in the same gauge in the internal region, the scattered or ejected electron has been described in the same gauge in the external region. In time-dependent calculations for He and other He-like two-electron systems, the dipole velocity gauge has been used throughout. However, the use of the dipole velocity gauge in the internal region for multi-electron atoms or ions emphasizes short-range electron–electron correlations near the nucleus and hence requires a much better description of the atomic structure than required using the length gauge. It has therefore so far not proved appropriate to adopt the velocity gauge in the internal region in the multi-electron calculations discussed in Sect. 10.2 and the length gauge has been used throughout. However, as pointed out in Sect. 9.1.1, this raises a problem in the

external region if the integration needs to be taken out to large distances since the dipole length gauge then diverges. Further work is therefore needed to avoid build-up of errors in the gauge transformation. In this chapter we consider the solution of the time-dependent Schrödinger equation using the dipole velocity gauge in both regions and we also consider modifications to the theory that are necessary when the dipole length gauge is adopted throughout.

In order to solve the time-dependent Schrödinger equation in the dipole velocity gauge we transform (10.1) using the unitary gauge transformation

$$\Psi(\mathbf{X}_{N+1}, t) = \exp\left[-\mathrm{i}\frac{N+1}{2\mathrm{c}^2}\int^t \mathbf{A}^2(t')\mathrm{d}t'\right]\Psi^{\mathbf{V}}(\mathbf{X}_{N+1}, t), \tag{10.2}$$

to eliminate the $\mathbf{A}^2(t)$ term in (10.1). Substituting (10.2) into (10.1) yields the following time-dependent equation:

$$\left[H_{N+1} + \frac{1}{\mathrm{c}}\mathbf{A}(t)\cdot\mathbf{P}_{N+1}\right]\Psi^{\mathbf{V}}(\mathbf{X}_{N+1}, t) = \mathrm{i}\frac{\partial}{\partial t}\Psi^{\mathbf{V}}(\mathbf{X}_{N+1}, t). \tag{10.3}$$

Alternatively, in order to solve the time-dependent Schrödinger equation in the dipole length gauge, we follow our discussion in Sect. 9.1.2 by transforming (10.1) using the unitary gauge transformation

$$\Psi(\mathbf{X}_{N+1}, t) = \exp\left[-\frac{\mathrm{i}}{\mathrm{c}}\mathbf{A}(t)\cdot\mathbf{R}_{N+1}\right]\Psi^{\mathbf{L}}(\mathbf{X}_{N+1}, t), \tag{10.4}$$

which yields the following time-dependent equation:

$$\left[H_{N+1} + \boldsymbol{\mathcal{E}}(t)\cdot\mathbf{R}_{N+1}\right]\Psi^{\mathbf{L}}(\mathbf{X}_{N+1}, t) = \mathrm{i}\frac{\partial}{\partial t}\Psi^{\mathbf{L}}(\mathbf{X}_{N+1}, t), \tag{10.5}$$

where $\boldsymbol{\mathcal{E}}(t)$ is defined by (9.4) and $\mathbf{R}_{N+1}$ is defined by (9.10). The boldface superscripts $\mathbf{V}$ and $\mathbf{L}$ in (10.3) and (10.5), respectively, indicate that the interacting electrons are described in the dipole velocity and in the dipole length gauges, respectively.

We now rewrite both (10.3) and (10.5) in the form

$$H(t)\Psi(\mathbf{X}_{N+1}, t) = \mathrm{i}\frac{\partial}{\partial t}\Psi(\mathbf{X}_{N+1}, t), \tag{10.6}$$

where

$$H(t) = H_{N+1} + \frac{1}{\mathrm{c}}\sum_{i=1}^{N+1}\mathbf{A}(t)\cdot\mathbf{p}_i \tag{10.7}$$

in the dipole velocity gauge corresponding to (10.3) and

$$H(t) = H_{N+1} + \sum_{i=1}^{N+1} \boldsymbol{\mathcal{E}}(t) \cdot \mathbf{r}_i \tag{10.8}$$

in the dipole length gauge corresponding to (10.5). In order to solve (10.6) we introduce a discrete mesh in time defined by

$$t_m = m\Delta t, \quad m = 0, 1, 2, \ldots, \tag{10.9}$$

where Δt is the time interval.

In the procedure adopted by van der Hart et al. [937, 938] and Lysaght et al. [603–606] and used in an earlier one-dimensional potential calculation by Burke and Burke [172], the solution of (10.6) at $t = t_{m+1}$ is expressed in terms of the solution at $t = t_m$ using the Cayley form of the time propagation operator $\exp[-\mathrm{i}tH(t)]$ discussed by Goldberg et al. [386]. This gives

$$\Psi(\mathbf{X}_{N+1}, t_{m+1}) = \frac{1 - \frac{1}{2}\mathrm{i}\Delta t H(t_{m+\frac{1}{2}})}{1 + \frac{1}{2}\mathrm{i}\Delta t H(t_{m+\frac{1}{2}})} \Psi(\mathbf{X}_{N+1}, t_m) + O(\Delta t^3), \tag{10.10}$$

where

$$t_{m+\frac{1}{2}} = t_m + \frac{1}{2}\Delta t. \tag{10.11}$$

This operator, as well as being unitary, has the further desirable property of being correct to $O(\Delta t^2)$. If we neglect terms of $O(\Delta t^3)$ then (10.10) can be rewritten as

$$\left[H(t_{m+\frac{1}{2}}) - E\right] \Psi(\mathbf{X}_{N+1}, t_{m+1}) = \Theta(\mathbf{X}_{N+1}, t_m), \tag{10.12}$$

where

$$\Theta(\mathbf{X}_{N+1}, t_m) = -\left[H(t_{m+\frac{1}{2}}) + E\right] \Psi(\mathbf{X}_{N+1}, t_m) \tag{10.13}$$

and the energy

$$E = 2\mathrm{i}\Delta t^{-1} \tag{10.14}$$

is imaginary. In the calculations carried out by van der Hart et al. and by Lysaght et al. the dipole length gauge, given by (10.8), is used for the interaction with the laser field. Using an L^2 basis expansion for the wave function in an internal region and a close coupling expansion in an external region, (10.12) then enables the wave function to be propagated forward in time, as discussed in Sects. 10.1.2 and 10.1.3.

In the procedure adopted by Guan et al. [429, 431, 432] the Arnoldi–Lanczos time propagator method [25, 563, 712] is used, where a general discussion and error analysis of the method has been given by Saad [803] and a computer program ALTDSE which implements this method has been written by Guan et al. [433]. The time-dependent Schrödinger equation (10.6), using the dipole length gauge for the interaction with the laser field, is rewritten by expanding the wave function in an L^2 n_t-dimensional basis in an internal region as follows:

$$\mathbf{H}(t)\mathbf{C}(t) = \mathrm{i}\frac{\partial}{\partial t}\mathbf{C}(t). \tag{10.15}$$

In this equation the Hamiltonian matrix $\mathbf{H}(t) = \mathbf{H}_0 + \mathcal{E}(t)\mathbf{D}$ where $\mathbf{H}_0$ and $\mathbf{D}$ are time independent and $\mathcal{E}(t) = \mathcal{E}_0 \cos \omega t$. In the Arnoldi–Lanczos time propagator method a reduced Krylov space is constructed at time $t_{m+1} = t_m + \Delta t$ of dimension p which is defined by the basis

$$\mathbf{u}_1 = \mathbf{v}_m, \quad \mathbf{u}_2 = \mathbf{H}(t_m)\mathbf{v}_m, \quad \ldots, \quad \mathbf{u}_p = [\mathbf{H}(t_m)]^{p-1}\mathbf{v}_m. \tag{10.16}$$

In this equation the vector $\mathbf{v}_m$ describes the previously computed solution at time t_m and the vectors $\mathbf{u}_i$ are generated by repeatedly operating on $\mathbf{v}_m$ with the Hamiltonian $\mathbf{H}(t_m)$. The value of p is defined such that for larger values of p the basis $\mathbf{u}_i$ will be linearly dependent. The vectors $\mathbf{u}_i$ are not used directly in the calculation, but are orthonormalized using the Lanczos recursion relation

$$\beta_{n+1}\mathbf{w}_{n+1} = (\mathbf{H} - \alpha_n)\,\mathbf{w}_n - \beta_n \mathbf{w}_{n-1}, \tag{10.17}$$

to transform the Hamiltonian matrix to tridiagonal form [803] as long as the original matrix is hermitian. The elements α_n and β_n of the tridiagonal matrix may be computed during the recursion process using simple scalar products. The resultant tridiagonal matrix is then diagonalized using a standard method (e.g. [976]). The result of the above procedure is an $n_\mathrm{t} \times p$-dimensional matrix $\mathbf{Q}$ which transforms the matrix $\mathbf{H}$ with rank n_t to a matrix $\mathbf{h}$ with rank p. The time evolution from $t = t_m$ to $t = t_m + \Delta t$ is then achieved through the relation

$$\mathbf{C}(t_m + \Delta t) = \mathbf{Q}\exp(-\mathrm{i}h\Delta t)\mathbf{Q}^\dagger \mathbf{C}(t_m). \tag{10.18}$$

At each time step m of the process, a convergence test can be applied. As long as the rank p of the process is substantially less than the original matrix size n_t the process can be very effective. Finally, we note that the Arnoldi–Lanczos algorithm outlined above conserves the norm, $|\mathbf{C}(t_m + \Delta t)|^2 = |\mathbf{C}(t_m)|^2$.

We now consider the partitioning of configuration space used in propagating the wave function in time. In the calculations by van der Hart et al. [937] and by Guan et al. [429, 431, 432] a single extended internal region was adopted, whereas in the calculations by Lysaght et al. [603–605] an external region was also included in the calculation. This enabled the internal region to be restricted to where exchange and

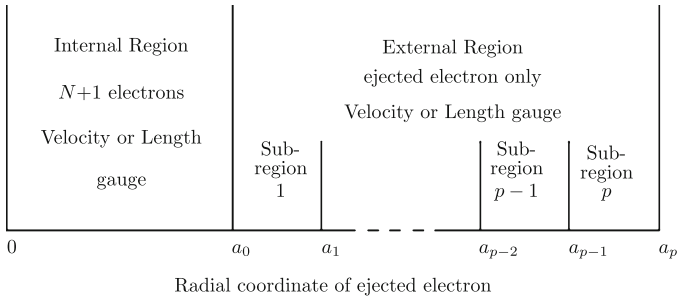

Fig. 10.1 Partitioning of configuration space in time-dependent R-matrix theory

correlation effects between the ejected electron and the residual ion are important thus allowing a much smaller internal region, and hence a much smaller internal region basis, to be adopted. In the following discussion we will assume that two regions, illustrated in Fig. 10.1, are retained in the calculation.

We note that the partitioning of configuration space into two regions in Fig. 10.1 differs from that adopted in electron–atom collisions and in R-matrix–Floquet theory, given by Figs. 5.1 and 9.1, respectively, in that the asymptotic region is now omitted. However, the conditions used to define the boundary $r = a_0$ between the internal and external regions are the same as in R-matrix–Floquet theory. That is, in the internal region electron exchange and electron–electron correlation effects between the ejected electron and the remaining N electrons are important, while in the external region electron exchange and correlation effects between the ejected electron and the remaining N electrons are negligible and hence this electron moves in the local long-range multipole potential of the residual N-electron atom or atomic ion together with the laser field. In many calculations of interest the radius a_p of the outer boundary of the external region can be chosen so large that the ejected electron does not reach this boundary in the length of time of the laser pulse under consideration. If this is not the case an absorbing mask function can be retained in the calculation near the outer boundary so that the ejected electron is not reflected.

In the rest of Sect. 10.1 we describe in detail a procedure which enables the wave function to be propagated forward in time using (10.12), commencing from an initial bound state of the atom or ion before the laser pulse is switched on. In Sects. 10.1.2 and 10.1.3 we describe an R-matrix approach for propagating the wave function in the internal and external regions, respectively, and in Sect. 10.1.4 we summarize the computational methods adopted. Finally, in Sect. 10.1.5 we analyse how the theoretical and computational methods can be applied to calculate single- and double-electron ionization of neutral and singly ionized neon and argon atoms.

10.1.2 Internal Region Solution

We consider first the propagation of the solution of the time-dependent Schrödinger equation (10.6) in the internal region, defined in Fig. 10.1, using the Cayley time

propagator (10.12). In this region we expand the wave function $\Psi(\mathbf{X}_{N+1}, t_{m+1})$ in (10.12) in a completely antisymmetric R-matrix basis $\psi_k(\mathbf{X}_{N+1}, t_{m+\frac{1}{2}})$ in analogy with (5.5) as follows:

$$\Psi_j^\gamma(\mathbf{X}_{N+1}, t_{m+1}) = \sum_k \psi_k^\gamma(\mathbf{X}_{N+1}, t_{m+\frac{1}{2}}) A_{kj}^\gamma(t_{m+\frac{1}{2}}). \tag{10.19}$$

In this equation, j labels the solution of (10.12) which corresponds to the initial bound state of the atom or ion before the laser is switched on and $A_{kj}^\gamma(t_{m+\frac{1}{2}})$ are the time-dependent expansion coefficients, which depend on the boundary conditions satisfied by the wave function Ψ_j^γ at the initial time $t = 0$. Also, we have introduced the superscript γ representing the conserved quantum numbers which depend on the symmetry of the atomic state and the polarization of the laser photons. As an example of the conserved quantum numbers represented by γ, we consider linearly polarized photons incident on an atom or ion in a $^1\mathrm{S}^\mathrm{e}$ state, where relativistic effects can be neglected. In this case we showed in Sect. 9.1.2 that

$$\gamma \equiv \alpha\ S\ M_S\ M_L\ \pi', \tag{10.20}$$

where S is the total spin angular momentum quantum number, M_S and M_L are the total spin and orbital magnetic quantum numbers in the laser polarization direction, π' is the product of the parities of the target state and the absorbed or emitted photons and α represents any other quantum numbers which are conserved in the collision.

Following (5.6) and (9.20) we then expand the basis functions ψ_k^γ in (10.19) in a close coupling with pseudostates expansion given by

$$\begin{aligned}\psi_k^\gamma(\mathbf{X}_{N+1}, t_{m+\frac{1}{2}}) = \mathcal{A} \sum_{pl} \overline{\Phi}_p^\gamma(\mathbf{X}_N; \hat{\mathbf{r}}_{N+1}\sigma_{N+1}) r_{N+1}^{-1} u_{pl}^0(r_{N+1}) a_{plk}^\gamma(t_{m+\frac{1}{2}}) \\ + \sum_p \chi_p^\gamma(\mathbf{X}_{N+1}) b_{pk}^\gamma(t_{m+\frac{1}{2}}), \quad k = 1, \ldots, n_t. \end{aligned} \tag{10.21}$$

As in (9.20), the channel functions $\overline{\Phi}_p^\gamma$ in (10.21) are obtained by coupling the residual atom or ion states, and possibly pseudostates, with the spin–angle function of the ejected electron, u_{pl}^0 are radial continuum basis functions describing the ejected electron and χ_p^γ are quadratically integrable functions. Also, the summation over the subscript p in (10.21) corresponds to the summation over the subscripts L and i in (9.20) but, unlike (9.20), there is no longer a dependence on the Floquet–Fourier index. We also assume in (10.21), and in later equations, that n channel functions $\overline{\Phi}_p^\gamma$ are retained in the first expansion, n_c radial continuum basis functions u_{pl}^0 are retained in each channel and n_b quadratically integrable functions χ_p^γ are retained in the second expansion. Finally, the expansion coefficients $a_{plk}^\gamma(t_{m+\frac{1}{2}})$ and $b_{pk}^\gamma(t_{m+\frac{1}{2}})$

in (10.21) are time dependent. We then find it convenient to rewrite (10.21) in the concise form

$$\psi_k^\gamma(\mathbf{X}_{N+1}, t_{m+\frac{1}{2}}) = \sum_{k'=1}^{n_t} \xi_{k'}^\gamma(\mathbf{X}_{N+1}) c_{k'k}^\gamma(t_{m+\frac{1}{2}}), \quad k = 1, \ldots, n_t, \tag{10.22}$$

where $n_t = nn_c + n_b$ is the total number of linearly independent basis functions $\xi_{k'}^\gamma(\mathbf{X}_{N+1})$ retained in (10.21) and $c_{k'k}^\gamma(t_{m+\frac{1}{2}})$ represents the time-dependent coefficients $a_{plk}^\gamma(t_{m+\frac{1}{2}})$ and $b_{pk}^\gamma(t_{m+\frac{1}{2}})$ in (10.21).

We now consider the solution of (10.12) in the internal region to yield the wave function $\Psi_j^\gamma(\mathbf{X}_{N+1}, t_{m+1})$ at the end of the time step $t = t_{m+1}$, given the inhomogeneous term $\Theta_j^\gamma(\mathbf{X}_{N+1}, t_m)$ which is defined in terms of the wave function $\Psi_j^\gamma(\mathbf{X}_{N+1}, t_m)$ at the end of the previous time step $t = t_m$ by (10.13). We consider first the solution of (10.12) using the dipole velocity gauge, where the Hamiltonian $H(t_{m+\frac{1}{2}})$ in (10.12) is defined by (10.7). We then briefly consider the modifications to this analysis which must be made when the dipole length gauge is adopted.

In order to solve (10.12) in the internal region we observe that the Hamiltonian $H(t_{m+\frac{1}{2}})$, defined by (10.7), is not hermitian in this region in the space of functions satisfying arbitrary boundary conditions at $r = a_0$, owing to the presence of the kinetic energy operator terms $-\frac{1}{2}\nabla_i^2$, $i = 1, \ldots, N+1$ and the laser interaction terms $\mathrm{c}^{-1}\mathbf{A}(t_{m+\frac{1}{2}}) \cdot \mathbf{p}_i$, $i = 1, \ldots, N+1$, in $H(t_{m+\frac{1}{2}})$. Hence we introduce the Bloch operator

$$\mathcal{L}_1 = \frac{1}{2} \sum_{i=1}^{N+1} \delta(r_i - a_0) \left(\frac{\mathrm{d}}{\mathrm{d}r_i} - \frac{b_0 - 1}{r_i} \right), \tag{10.23}$$

which is such that $H_{N+1} + \mathcal{L}_1$ is hermitian in the internal region for any value of the arbitrary constant b_0, which in later equations we take to be zero. Also we introduce the Bloch operator

$$\mathcal{L}_2(t_{m+\frac{1}{2}}) = \frac{\mathrm{i}}{2\mathrm{c}} A(t_{m+\frac{1}{2}}) \sum_{i=1}^{N+1} \delta(r_i - a_0) \cos\theta_i, \tag{10.24}$$

which is such that $\mathrm{c}^{-1} \sum_{i=1}^{N+1} \mathbf{A}(t_{m+\frac{1}{2}}) \cdot \mathbf{p_i} + \mathcal{L}_2(t_{m+\frac{1}{2}})$ is hermitian in the internal region, where we have chosen the z-axis to lie along the laser polarization direction $\hat{\boldsymbol{\epsilon}}$ so that

$$\frac{1}{\mathrm{c}} \sum_{i=1}^{N+1} \mathbf{A}(t_{m+\frac{1}{2}}) \cdot \mathbf{p}_i = -\frac{\mathrm{i}}{\mathrm{c}} A(t_{m+\frac{1}{2}}) \sum_{i=1}^{N+1} \left(\cos\theta_i \frac{\partial}{\partial r_i} - \frac{\sin\theta_i}{r} \frac{\partial}{\partial \theta_i} \right). \tag{10.25}$$

It follows that $H(t_{m+\frac{1}{2}}) + \mathcal{L}_1 + \mathcal{L}_2(t_{m+\frac{1}{2}})$ is hermitian in the internal region.

Using these results, we can solve (10.12) in the internal region for each set of conserved quantum numbers γ by including the Bloch operators $\mathcal{L}_1$ and $\mathcal{L}_2(t_{m+\frac{1}{2}})$ on both sides of this equation giving

$$\left[H(t_{m+\frac{1}{2}}) + \mathcal{L}_1 + \mathcal{L}_2(t_{m+\frac{1}{2}}) - E\right]\Psi_j^\gamma = \left(\mathcal{L}_1 + \mathcal{L}_2(t_{m+\frac{1}{2}})\right)\Psi_j^\gamma + \Theta_j^\gamma, \quad (10.26)$$

which has the formal solution in the internal region

$$\Psi_j^\gamma = \left[H(t_{m+\frac{1}{2}}) + \mathcal{L}_1 + \mathcal{L}_2(t_{m+\frac{1}{2}}) - E\right]^{-1}\left[\left(\mathcal{L}_1 + \mathcal{L}_2(t_{m+\frac{1}{2}})\right)\Psi_j^\gamma + \Theta_j^\gamma\right]. \quad (10.27)$$

The spectral representation of the Green's function in (10.27) can be obtained in terms of the R-matrix basis functions ψ_k^γ defined by (10.22), where the coefficients $c_{k'k}^\gamma(t_{m+\frac{1}{2}})$ in this equation are determined by diagonalizing the operator $H(t_{m+\frac{1}{2}}) + \mathcal{L}_1 + \mathcal{L}_2(t_{m+\frac{1}{2}})$ in this basis as follows:

$$\left\langle \psi_k^\gamma | H(t_{m+\frac{1}{2}}) + \mathcal{L}_1 + \mathcal{L}_2(t_{m+\frac{1}{2}}) | \psi_{k'}^\gamma \right\rangle_{\text{int}} = E_k^\gamma(t_{m+\frac{1}{2}})\delta_{kk'}, \quad k, k' = 1, \ldots, n_t, \quad (10.28)$$

where the integration in this equation is taken over the space and spin coordinates of all $N+1$ electrons and where the radial integrals are confined to the internal region. Equation (10.27) then becomes

$$|\Psi_j^\gamma\rangle = \sum_{k=1}^{n_t} |\psi_k^\gamma\rangle \frac{1}{E_k^\gamma - E}\langle\psi_k^\gamma|\left[(\mathcal{L}_1 + \mathcal{L}_2)|\Psi_j^\gamma\rangle + |\Theta_j^\gamma\rangle\right], \quad (10.29)$$

which can be written as

$$\Psi_j^\gamma(\mathbf{X}_{N+1}, t_{m+1}) = \sum_{k=1}^{n_t} \psi_k^\gamma(\mathbf{X}_{N+1}, t_{m+\frac{1}{2}}) B_{kj}^\gamma(E, t_{m+1}). \quad (10.30)$$

Our objective is to determine the coefficients $B_{kj}^\gamma(E, t_{m+1})$, which express the wave function $\Psi_j^\gamma(\mathbf{X}_{N+1}, t_{m+1})$ in the internal region in terms of the R-matrix basis functions $\psi_k^\gamma(\mathbf{X}_{N+1}, t_{m+\frac{1}{2}})$ defined by (10.22) and (10.28).

Before considering how to obtain the coefficients $B_{kj}^\gamma(E, t_{m+1})$ in (10.30) by diagonalizing the operator in (10.28), we briefly discuss how the required internal region solution Ψ_j^γ can also be obtained by solving a set of linear simultaneous equations. To achieve this we expand Ψ_j^γ in terms of the original basis ξ_k^γ retained in (10.21) and (10.22) as follows:

$$\Psi_j^{\gamma}(\mathbf{X}_{N+1}, t_{m+1}) = \sum_{k=1}^{n_t} \xi_k^{\gamma}(\mathbf{X}_{N+1}) a_{kj}^{\gamma}(t_{m+\frac{1}{2}}). \tag{10.31}$$

Substituting expansion (10.31) into (10.12) and projecting onto the basis functions ξ_i^{γ} yield the following set of linear simultaneous equations satisfied by the coefficients $a_{kj}^{\gamma}(t_{m+\frac{1}{2}})$:

$$\sum_{k=1}^{n_t} A_{ik}^{\gamma}(E) a_{kj}^{\gamma} = C_{ij}, \quad i = 1, \ldots, n_t, \tag{10.32}$$

where

$$A_{ik}^{\gamma}(E) = \langle \xi_i^{\gamma} | H(t_{m+\frac{1}{2}}) - E | \xi_k^{\gamma} \rangle_{\text{int}} \tag{10.33}$$

and

$$C_{ij} = \langle \xi_i^{\gamma} | \Theta_j^{\gamma} \rangle_{\text{int}}, \tag{10.34}$$

and where the integrals in (10.33) and (10.34) are taken over the internal region. Equation (10.32) can be solved using a standard linear simultaneous equations method [757, 976]. Also, by retaining the Bloch operators $\mathcal{L}_1$ and $\mathcal{L}_2(t_{m+\frac{1}{2}})$ on both sides of (10.32), as in (10.26), the R-matrix on the boundary $r = a_0$ of the internal region can be determined at the energy E using a multichannel generalization of the linear equations method discussed in Sect. 4.4.4.

We now consider in detail the procedure for determining the coefficients $B_{kj}^{\gamma}(E, t_{m+1})$ using (10.29). In order to achieve this objective we project (10.29) onto the n channel functions $r_{N+1}^{-1}\overline{\Phi}_p^{\gamma}$ and evaluate the result on the boundary $r_{N+1} = a_0$ of the internal region. We obtain

$$F_{pj}^{\gamma}(a_0) = \sum_{p'=1}^{n} R_{pp'}^{\gamma}(E) a_0 \overline{F}_{p'j}^{\gamma}(a_0) + T_{pj}^{\gamma}(a_0), \quad p = 1, \ldots, n, \tag{10.35}$$

where, for notational convenience, we have omitted the time dependence of $F_{pj}^{\gamma}(r_{N+1})$, $R_{pp'}^{\gamma}(E)$, $\overline{F}_{p'j}^{\gamma}(r_{N+1})$ and $T_{pj}^{\gamma}(a_0)$ in (10.35) and later equations and where the quantities in this equation are defined in turn as follows. The reduced radial wave functions $F_{pj}^{\gamma}(a_0)$ are defined by

$$F_{pj}^{\gamma}(a_0) = \langle r_{N+1}^{-1}\overline{\Phi}_p^{\gamma}(\mathbf{X}_N; \hat{\mathbf{r}}_{N+1}\sigma_{N+1}) | \Psi_j^{\gamma} \rangle'_{r_{N+1}=a_0}, \quad p = 1, \ldots, n, \tag{10.36}$$

where the prime on the matrix element in (10.36) and later matrix elements means that the integral is carried out over the space and spin coordinates of all $N + 1$ electrons except the radial coordinate r_{N+1} of the ejected electron. The R-matrix

elements $R^{\gamma}_{pp'}(E)$ in (10.35) are defined by

$$R^{\gamma}_{pp'}(E) = \frac{1}{2a_0} \sum_{k=1}^{n_t} \frac{w^{\gamma}_{pk} w^{\gamma}_{p'k}}{E^{\gamma}_k - E}, \quad p, p' = 1, \ldots, n, \tag{10.37}$$

where the surface amplitudes w_{pk} are defined by

$$w^{\gamma}_{pk} = \langle r^{-1}_{N+1} \overline{\Phi}^{\gamma}_p(\mathbf{X}_N; \hat{\mathbf{r}}_{N+1}\sigma_{N+1}) | \psi^{\gamma}_k \rangle'_{r_{N+1}=a_0}, \quad p = 1, \ldots, n, \quad k = 1, \ldots, n_t, \tag{10.38}$$

which becomes, after substituting for ψ^{γ}_k from (10.21),

$$w^{\gamma}_{pk} = \sum_{l=1}^{n_c} u^0_{pl}(a_0) a^{\gamma}_{plk}, \quad p = 1, \ldots, n, \quad k = 1, \ldots, n_t. \tag{10.39}$$

Also, the modified derivative functions $\overline{F}^{\gamma}_{pj}(a_0)$ in (10.35) are defined by

$$\overline{F}^{\gamma}_{pj}(a_0) = \left. \frac{\mathrm{d}F^{\gamma}_{pj}}{\mathrm{d}r} \right|_{r=a_0} + \frac{1}{2} \sum_{p'=1}^{n} P^{\gamma}_{pp'} F^{\gamma}_{p'j}(a_0), \quad p = 1, \ldots, n, \tag{10.40}$$

where the first term on the right-hand side of this equation arises from the Bloch operator $\mathcal{L}_1$ defined by (10.23) with b_0 set zero and the second term arises from the Bloch operator $\mathcal{L}_2$ defined by (10.24). It follows that the $n \times n$-dimensional matrix $\mathbf{P}^{\gamma}$ is defined by

$$\begin{aligned} P^{\gamma}_{pp'} = {} & \frac{2\mathrm{i}}{\mathrm{c}} A(t_{m+\frac{1}{2}}) \langle r^{-1}_{N+1} \overline{\Phi}^{\gamma}_p(\mathbf{X}_N; \hat{\mathbf{r}}_{N+1}\sigma_{N+1}) | \cos\theta_{N+1} | \\ & \times r^{-1}_{N+1} \overline{\Phi}^{\gamma}_{p'}(\mathbf{X}_N; \hat{\mathbf{r}}_{N+1}\sigma_{N+1}) \rangle'_{r_{N+1}=a_0}, \quad p, \ p' = 1, \ldots, n. \end{aligned} \tag{10.41}$$

The matrix $\mathbf{P}^{\gamma}$ also appears in the external region solution, see (10.55), and its matrix elements are determined in Appendix D.3. Finally, the inhomogeneous vector $T^{\gamma}_{pj}(a_0)$ in (10.35) is obtained by projecting the inhomogeneous term on the right-hand side of (10.29) onto the n channel functions, where the radial integrals are confined to the internal region. This gives after setting $r_{N+1} = a_0$

$$T^{\gamma}_{pj}(a_0) = \sum_{k=1}^{n_t} w^{\gamma}_{pk} (E^{\gamma}_k - E)^{-1} S^{\gamma}_{kj}, \quad p = 1, \ldots, n, \tag{10.42}$$

where it follows from (10.13) that

$$\begin{aligned} S_{kj}^{\gamma} &= \langle \psi_k^{\gamma} | \Theta_j^{\gamma} \rangle_{\text{int}} \\ &= -\left\langle \psi_k^{\gamma}(\mathbf{X}_{N+1}, t_{m+\frac{1}{2}}) | H(t_{m+\frac{1}{2}}) + E | \Psi_j^{\gamma}(\mathbf{X}_{N+1}, t_m) \right\rangle_{\text{int}}, \\ & \qquad k = 1, \ldots, n_t. \end{aligned} \tag{10.43}$$

The wave function $\Psi_j^{\gamma}(\mathbf{X}_{N+1}, t_m)$ in (10.43) has been determined at the end of the previous time step $t = t_m$ and is thus known. Hence the vector S_{kj}^{γ} and all the other quantities on the right-hand side of (10.42) can be calculated and the inhomogeneous vector $T_{pj}^{\gamma}(a_0)$ determined.

Returning to (10.30), the coefficients $B_{kj}^{\gamma}(E, t_{m+1})$ can now be written as

$$B_{kj}^{\gamma}(E, t_{m+1}) = \frac{1}{E_k^{\gamma} - E} \left[\frac{1}{2} \sum_{p=1}^{n} w_{pk}^{\gamma} \overline{F}_{pj}^{\gamma}(a_0) + S_{kj}^{\gamma} \right], \quad k = 1, \ldots, n_t, \tag{10.44}$$

where w_{pk}^{γ}, $\overline{F}_{pj}^{\gamma}(a_0)$ and S_{kj}^{γ} are defined by (10.38), (10.40) and (10.43), respectively. The only unknown quantity in the definition of $B_{kj}^{\gamma}(E, t_{m+1})$ is $\overline{F}_{pj}^{\gamma}(a_0)$ which we will see, in Sect. 10.1.4.3, can be determined from the result of the propagation in the external region. Hence $B_{kj}^{\gamma}(E, t_{m+1})$ can be calculated and the wave function $\Psi_j^{\gamma}(\mathbf{X}_{N+1}, t_{m+1})$, which provides the starting point for the calculation in the next time step, can be determined from (10.30).

In concluding our analysis of the solution using the dipole velocity gauge in the internal region, it is convenient to rewrite the solution on the boundary $r = a_0$ of the internal region, given by (10.35), in matrix notation as

$$\mathbf{F}_j^{\gamma}(a_0) = \mathbf{R}^{\gamma}(E) a_0 \overline{\mathbf{F}}_j^{\gamma}(a_0) + \mathbf{T}_j^{\gamma}(a_0), \tag{10.45}$$

where it follows from (10.40) that

$$\overline{\mathbf{F}}_j^{\gamma}(a_0) = \left(\frac{\mathrm{d}\mathbf{F}_j^{\gamma}}{\mathrm{d}r} + \frac{1}{2} \mathbf{P}^{\gamma} \mathbf{F}_j^{\gamma} \right)_{r=a_0}. \tag{10.46}$$

The R-matrix $\mathbf{R}^{\gamma}$ and the inhomogeneous vector $\mathbf{T}_j^{\gamma}$ at $r = a_0$ in (10.45) are defined by (10.37) and (10.42), respectively. These equations then provide the boundary condition for propagating $\mathbf{R}^{\gamma}$ and $\mathbf{T}_j^{\gamma}$ in the external region, as described in Sect. 10.1.3 and Appendix E.4.

In the above analysis we obtained the solution of (10.12) in the internal region when the dipole velocity gauge was adopted. We now briefly consider the modification of the above analysis that must be made when the dipole length gauge is adopted. In the dipole length gauge the Hamiltonian $H(t_{m+\frac{1}{2}})$ in (10.12) is defined by (10.8) instead of (10.7) used in the above analysis. We see from (10.8) that

$H(t_{m+\frac{1}{2}})$ is also not hermitian in the internal region. However, this is now due only to the kinetic energy operator terms $-\frac{1}{2}\nabla_i^2$, $i = 1, \ldots, N+1$, in the non-relativistic atomic Hamiltonian H_{N+1}, defined in the absence of the laser field by (5.3). The laser interaction term $\sum_{i=1}^{N+1} \boldsymbol{\mathcal{E}}(t) \cdot \mathbf{r}_i$ in (10.8), unlike the corresponding term $\mathrm{c}^{-1} \sum_{i=1}^{N+1} \mathbf{A}(t) \cdot \mathbf{p}_i$ in (10.7), is hermitian. Hence, only the Bloch operator $\mathcal{L}_1$ defined by (10.23) is required to ensure $H(t_{m+\frac{1}{2}}) + \mathcal{L}_1$ is hermitian in the internal region. It follows that (10.12) can now be written in the internal region as follows:

$$\left[H(t_{m+\frac{1}{2}}) + \mathcal{L}_1 - E\right] \Psi_j^\gamma = \mathcal{L}_1 \Psi_j^\gamma + \Theta_j^\gamma, \tag{10.47}$$

which has the formal solution

$$\Psi_j^\gamma = \left[H(t_{m+\frac{1}{2}}) + \mathcal{L}_1 - E\right]^{-1} \left(\mathcal{L}_1 \Psi_j^\gamma + \Theta_j^\gamma\right), \tag{10.48}$$

instead of (10.26) and (10.27). The spectral representation of the Green's function in (10.48) then proceeds as in the analysis following (10.27) except for the omission of the Bloch operator term $\mathcal{L}_2(t_{m+\frac{1}{2}})$. Hence the second term on the right-hand side of (10.40) involving the matrix $\mathbf{P}$ no longer appears in this analysis.

In concluding our discussion of the solution using the dipole length gauge in the internal region we find that, instead of (10.45), this solution satisfies the following boundary condition at $r = a_0$:

$$\mathbf{F}_j^\gamma(a_0) = \mathbf{R}^\gamma(E) a_0 \left.\frac{\mathrm{d}\mathbf{F}_j^\gamma}{\mathrm{d}r}\right|_{r=a_0} + \mathbf{T}_j^\gamma(a_0), \tag{10.49}$$

where in the calculation of $\mathbf{R}^\gamma(E)$ and $\mathbf{T}_j^\gamma(a_0)$ the dipole length operator $\sum_{i=1}^{N+1} \boldsymbol{\mathcal{E}}(t) \cdot \mathbf{r}_i$ is included in the Hamiltonian instead of the dipole velocity operator $\mathrm{c}^{-1} \sum_{i=1}^{N+1} \mathbf{A}(t) \cdot \mathbf{p}_i$ used in the calculation of $\mathbf{R}^\gamma(E)$ and $\mathbf{T}_j^\gamma(a_0)$ in (10.45).

10.1.3 External Region Solution

In this section we consider the solution of (10.12) in the external region defined in Fig. 10.1. In this region we expand the wave function as follows:

$$\Psi_j^\gamma(\mathbf{X}_{N+1}, t_{m+1}) = \sum_{p=1}^{n} \overline{\Phi}_p^\gamma(\mathbf{X}_N; \hat{\mathbf{r}}_{N+1}\sigma_{N+1}) r_{N+1}^{-1} F_{pj}^\gamma(r_{N+1}),$$
$$a_0 \le r_{N+1} \le a_p, \tag{10.50}$$

where, as in the internal region, we have omitted the time dependence of $F^{\gamma}_{pj}(r_{N+1})$ for notational convenience. Also the reduced radial functions $F^{\gamma}_{pj}(r_{N+1})$ in (10.50) correspond to the functions which are defined by (10.36) on the boundary $r = a_0$ of the internal region. We see that expansion (10.50) is not antisymmetrized with respect to the $(N+1)$th electron, since this electron, which has been ejected from the target atom or ion, now occupies a different region of space from the remaining N electrons and hence is distinguishable. Also, the quadratically integrable functions χ^{γ}_{p} in (10.21) are not included in (10.50) since they are confined to the internal region where electron–electron correlation effects are important.

Coupled inhomogeneous second-order differential equations satisfied by the reduced radial wave functions $F^{\gamma}_{pj}(r)$, which represent the motion of the ejected electron in the pth channel, are obtained by substituting (10.50) into (10.12) and projecting onto the channel functions $\overline{\Phi}^{\gamma}_{p}$ yielding

$$\left(\frac{\mathrm{d}^2}{\mathrm{d}r^2} - \frac{\ell_p(\ell_p+1)}{r^2} + \frac{2(Z-N)}{r} + k_p^2\right) F^{\gamma}_{pj}(r) - 2\sum_{p'=1}^{n} W^{\gamma}_{pp'}(r) F^{\gamma}_{p'j}(r)$$
$$= M^{\gamma}_{pj}(r), \quad p = 1, \ldots, n, \quad a_0 \le r \le a_p. \tag{10.51}$$

In this equation ℓ_p is the orbital angular momentum of the ejected electron and k_p^2 can be expressed in terms of the energy e_i of the ith residual N-electron atom or ion and the time interval Δt, by the equation

$$k_p^2 = 2(2\mathrm{i}\Delta t^{-1} - e_i), \tag{10.52}$$

where we have used (2.5) and (10.14) and where we remember from our discussion following (10.21) that the pth channel is related to a specific residual atom or ion state denoted by the subscript i. Also, $W^{\gamma}_{pp'}(r)$ in (10.51) is the long-range potential coupling the channels, which depends on whether the dipole velocity gauge or the dipole length gauge is used to describe the interaction of the ejected or scattered electron with the laser field. In the following discussion we assume that the dipole velocity gauge is used to describe this interaction, which corresponds to our treatment of this interaction in R-matrix–Floquet theory given in Sect. 9.1.3. However, as discussed in our treatment of the solution in the internal region in Sect. 10.1.2, the modifications required in the analysis to adopt the dipole length gauge are straightforward.

Following our discussion in Sect. 9.1.3, the long-range potential $W^{\gamma}_{pp'}(r)$ in (10.51) can be rewritten in matrix notation as[1]

$$\mathbf{W}^{\gamma} = \mathbf{V}^{E\gamma} + \mathbf{V}^{D\gamma} + \mathbf{V}^{P\gamma}. \tag{10.53}$$

[1] Explicit expressions for the potential matrices $\mathbf{V}^{E\gamma}$, $\mathbf{V}^{D\gamma}$ and $\mathbf{V}^{P\gamma}$ in (10.53) and for the potential matrices $\mathbf{P}$, $\mathbf{Q}$, $\mathbf{V}(r)$ and $\mathbf{D}$ in (10.55) are derived in Appendix D.3.

Here $\mathbf{V}^{E\gamma}$ arises from the electron–electron and electron–nuclear potential terms in the Hamiltonian $H(t_{m+\frac{1}{2}})$, while $\mathbf{V}^{D\gamma}$ and $\mathbf{V}^{P\gamma}$ arise, respectively, from the interaction of the laser field with the residual N-electron atom or ion and from the interaction of the laser field with the ejected electron.

Finally, the inhomogeneous term $M^{\gamma}_{pj}(r)$ in (10.51) is defined by

$$M^{\gamma}_{pj}(r_{N+1}) = -2\langle r^{-1}_{N+1}\overline{\Phi}^{\gamma}_{p}(\mathbf{X}_N; \hat{\mathbf{r}}_{N+1}\sigma_{N+1})|\Theta^{\gamma}_{j}(\mathbf{X}_{N+1}, t_m)\rangle', \tag{10.54}$$

where for notational convenience we have omitted the time variable in the inhomogeneous term $M^{\gamma}_{pj}(r_{N+1})$ and in the potential terms $W^{\gamma}_{pp'}(r)$ in (10.51).

In order to solve the coupled inhomogeneous second-order differential equations (10.51) we follow our discussion of equations (9.38), which were rewritten in matrix form as (9.61), to rewrite (10.51) in matrix form as follows:

$$\left(\frac{\mathrm{d}^2}{\mathrm{d}r^2} + \mathbf{P}\frac{\mathrm{d}}{\mathrm{d}r} + \mathbf{Q}\frac{1}{r} + \mathbf{V}(r) + \mathbf{D} + \mathbf{k}^2\right)\mathbf{F}(r) = \mathbf{M}(r). \tag{10.55}$$

We show in Appendix D.3 that when using the Fano–Racah phase convention these matrices have the following properties:

$\mathbf{P}$ — real, antisymmetric, antihermitian, r-independent
$\mathbf{Q}$ — real, symmetric, hermitian, r-independent
$\mathbf{V}$ — real, symmetric, hermitian, r-dependent
$\mathbf{D}$ — real, symmetric, hermitian, r-independent.

Since $\mathbf{D}$ is real and symmetric and the imaginary part of $\mathbf{k}^2$, defined by (10.52), is a multiple of the unit matrix, then $\mathbf{D} + \mathbf{k}^2$ can be diagonalized by a real orthogonal transformation as follows:

$$\mathbf{A}^{\mathrm{T}}(\mathbf{D} + \mathbf{k}^2)\mathbf{A} = \mathbf{K}^2. \tag{10.56}$$

As discussed following (9.63), this orthogonal transformation defines a new target basis which is a linear combination of the original target basis and corresponds to target states "dressed" by the laser field.

Following the procedure adopted in solving (9.61) we can solve (10.55) by eliminating the first derivative term, reducing this equation to standard form. We use the operator identity

$$\exp\left(\frac{1}{2}\mathbf{P}r\right)\left(\frac{\mathrm{d}^2}{\mathrm{d}r^2} + \mathbf{P}\frac{\mathrm{d}}{\mathrm{d}r}\right)\exp\left(-\frac{1}{2}\mathbf{P}r\right) = \left(\frac{\mathrm{d}^2}{\mathrm{d}r^2} - \frac{1}{4}\mathbf{P}^2\right) \tag{10.57}$$

and (10.52) to write (10.55) as

$$\left(\frac{\mathrm{d}^2}{\mathrm{d}r^2} - \frac{1}{4}\mathbf{P}^2 + \boldsymbol{\mathcal{V}}(r) + \frac{4\mathrm{i}}{\Delta t}\right)\boldsymbol{\mathcal{F}}(r) = \boldsymbol{\mathcal{M}}(r), \tag{10.58}$$

where in (10.58) the potential

$$\boldsymbol{\mathcal{V}}(r) = \exp\left(\frac{1}{2}\mathbf{P}r\right)\left(\mathbf{Q}\frac{1}{r} + \mathbf{V}(r) + \mathbf{D} - 2\mathbf{e}\right)\exp\left(-\frac{1}{2}\mathbf{P}r\right), \tag{10.59}$$

the function

$$\boldsymbol{\mathcal{F}}(r) = \exp\left(\frac{1}{2}\mathbf{P}r\right)\mathbf{F}(r) \tag{10.60}$$

and the inhomogeneous term

$$\boldsymbol{\mathcal{M}}(r) = \exp\left(\frac{1}{2}\mathbf{P}r\right)\mathbf{M}(r). \tag{10.61}$$

Finally, $\mathbf{e}$ in (10.59) is a diagonal matrix with diagonal elements e_i. Since $\mathbf{P}$ is anti-hermitian then the matrix $\exp(\frac{1}{2}\mathbf{P}r)$ is unitary, and hence the potential matrix $\boldsymbol{\mathcal{V}}(r)$ is hermitian.

Equation (10.58) can be further reduced by diagonalizing the real symmetric matrix $\mathbf{P}^2$ as follows:

$$\mathbf{O}^{\mathrm{T}}\mathbf{P}^2\mathbf{O} = -4\mathbf{d}^2, \tag{10.62}$$

where $\mathbf{O}$ is a real r-independent orthogonal matrix and the diagonal elements of $\mathbf{d}^2$ are real and greater than or equal to zero. Transforming (10.58) using this matrix then yields the coupled inhomogeneous second-order differential equations

$$\left(\frac{\mathrm{d}^2}{\mathrm{d}r^2} + \mathbf{U}(r) + \mathbf{g}^2\right)\mathbf{Y}(r) = \boldsymbol{\phi}(r), \tag{10.63}$$

where

$$\mathbf{U}(r) = \mathbf{O}^{\mathrm{T}}\boldsymbol{\mathcal{V}}(r)\mathbf{O}, \tag{10.64}$$

$$\mathbf{Y}(r) = \mathbf{O}^{\mathrm{T}}\boldsymbol{\mathcal{F}}(r), \tag{10.65}$$

$$\boldsymbol{\phi}(r) = \mathbf{O}^{\mathrm{T}}\boldsymbol{\mathcal{M}}(r), \tag{10.66}$$

and the diagonal matrix $\mathbf{g}^2$ is defined by

$$\mathbf{g}^2 = \mathbf{d}^2 + \frac{4\mathrm{i}}{\Delta t}\mathbf{I}. \tag{10.67}$$

Equation (10.63) is now in standard form.

We also need to determine the boundary condition at $r = a_0$ satisfied by the function $\mathbf{Y}(r)$ in (10.63). This is achieved by transforming the R-matrix obtained from the internal region solution. It follows from (10.60) and (10.65) that

$$\mathbf{F}(r) = \exp\left(-\frac{1}{2}\mathbf{P}r\right)\mathbf{O}\mathbf{Y}(r). \tag{10.68}$$

Also, by differentiating this equation it follows that since both $\mathbf{P}$ and $\mathbf{O}$ are r-independent

$$\frac{\mathrm{d}\mathbf{F}}{\mathrm{d}r} = \exp\left(-\frac{1}{2}\mathbf{P}r\right)\left(\mathbf{O}\frac{\mathrm{d}\mathbf{Y}}{\mathrm{d}r} - \frac{1}{2}\mathbf{P}\mathbf{O}\mathbf{Y}\right). \tag{10.69}$$

Substituting these results for $\mathbf{F}(r)$ and $\mathrm{d}\mathbf{F}/\mathrm{d}r$ into (10.45) gives

$$\mathbf{Y}(a_0) = \mathbf{R}_0 a_0 \left.\frac{\mathrm{d}\mathbf{Y}}{\mathrm{d}r}\right|_{r=a_0} + \mathbf{Z}(a_0), \tag{10.70}$$

where the R-matrix $\mathbf{R}_0$ at $r = a_0$ is defined in terms of the R-matrix $\mathbf{R}$ obtained from the internal region solution at $r = a_0$ by

$$\mathbf{R}_0 = \mathbf{O}^{\mathrm{T}} \exp\left(\frac{1}{2}\mathbf{P}a_0\right)\mathbf{R}\exp\left(-\frac{1}{2}\mathbf{P}a_0\right)\mathbf{O}, \tag{10.71}$$

and the transformed inhomogeneous term $\mathbf{Z}(a_0)$ is defined in terms of the inhomogeneous term $\mathbf{T}(a_0)$ in (10.45) by

$$\mathbf{Z}(a_0) = \mathbf{O}^{\mathrm{T}} \exp\left(\frac{1}{2}\mathbf{P}a_0\right)\mathbf{T}(a_0). \tag{10.72}$$

Finally, we observe that if the dipole length gauge had been used to describe the interaction of the laser field with the atomic system in the external region, then the coupled second-order differential equations describing the motion of the ejected electron would reduce directly to (10.63) without the intermediate analysis which eliminated the first derivative term in (10.55).

In Appendix E.4 we describe an R-matrix propagator method which enables (10.63) to be solved in the external region in Fig. 10.1 to yield the R-matrix and wave function on the boundaries of the sub-regions $r = a_s,\ s = 0, \ldots, p$. Also in Appendix E.5 we show that the coupled inhomogeneous second-order differential equations (10.55) can be solved directly without eliminating the first derivative term. Alternatively, a finite-difference propagation method for solving these equations in the external region has been proposed by Nikolopoulos et al. [685].

10.1.4 Computational Methods

In this section we describe computational methods for propagating the wave function of an atomic target in an ultra-short laser pulse forward in time. These methods are based on the analysis presented in Sects. 10.1.2 and 10.1.3 corresponding to the solutions in the internal and external regions defined in Fig. 10.1.

10.1.4.1 Target State Computation

Before the laser pulse is switched on we assume that the target is initially in an eigenstate of the target Hamiltonian H_{N+1} defined by (5.3). This eigenstate will usually be the ground state but can be an excited bound state or a continuum state if we are considering laser-assisted electron–atom collisions. In this section we restrict our consideration to the situation where the initial state is a bound eigenstate.

The initial bound state of the target $\Psi(\mathbf{X}_{N+1}, t)$ satisfies either the time-dependent Schrödinger equation (10.3) or (10.5) with $\mathbf{A}(t)$ or $\mathcal{E}(t)$ set zero.[2] We can then separate out the time dependence in the usual way by writing

$$\Psi(\mathbf{X}_{N+1}, t) = \Psi_{\text{in}}(\mathbf{X}_{N+1})\mathrm{e}^{-\mathrm{i}Et}, \tag{10.73}$$

where $\Psi_{\text{in}}(\mathbf{X}_{N+1})$ is the time-independent bound state wave function in the initial state. Substituting (10.73) into (10.3) or (10.5) then yields the time-independent Schrödinger equation

$$H_{N+1}\Psi_{\text{in}} = E\Psi_{\text{in}}. \tag{10.74}$$

The R-matrix method for solving (10.74) for bound-state calculations has been described in Sect. 8.1.2.2 where we determined the initial bound-state wave function in photoionization calculations. We will therefore not discuss this method further here except to note that in the internal region, defined in Fig. 10.1, the wave function Ψ_{in} is expanded, in analogy with (8.66), as follows:

$$\Psi_{\text{in}}(\mathbf{X}_{N+1}) = \sum_{k=1}^{n_t} \psi_k(\mathbf{X}_{N+1}) B_k(E), \tag{10.75}$$

where the basis functions ψ_k are defined by (10.21) and the coefficients $B_k(E)$ and the eigenenergy E are obtained by matching to a decaying wave solution of (10.74) in the external region using an iterative procedure. If the initial state is the ground state of the target then the internal region radius $r = a_0$ is taken to be large enough that the wave function is effectively zero for $r \geq a_0$. Alternatively, if initially one

[2] For notational convenience we will not include the usual subscripts and superscripts on the functions and operators in this section.

target electron is in a Rydberg orbital then a_0 is chosen so that the wave function of the residual N-electron atom or ion is effectively zero for $r \geq a_0$ while that of the outer Rydberg electron is zero for $r \geq a_p$. This is discussed in the external region computation section below.

10.1.4.2 Internal Region Computation

We assume that in this region the time-dependent wave function $\Psi(\mathbf{X}_{N+1}, t_m)$, required to compute the function S_k in (10.43) and hence $T_p(a_0)$ in (10.42), has been determined either by solving (10.74) before the laser pulse is switched on or by determining the wave function from the previous time step in the external region computation as described below. The R-matrix $\mathbf{R}$ defined by (10.37) can be determined by diagonalizing the operator $H + \mathcal{L}_1 + \mathcal{L}_2$ in (10.28) which yields the R-matrix basis functions ψ_k and the eigenenergies E_k, and hence the surface amplitudes w_{pk} defined by (10.38) and (10.39). Alternatively, the R-matrix can be determined by solving the linear simultaneous equations (10.32) including the Bloch operator terms, as discussed in Sect. 4.4.4. Finally, we determine the potential $\mathbf{P}$ defined by (10.41) using the analysis described in Appendix D.3.

We note that the computational steps involving the calculation of the angular and radial integrals for complex atomic targets occurring in the matrix elements in (10.28) and (10.43) are independent of the time step and hence need to be carried out only once using one of the standard procedures adopted in electron–atom collisions. Hence, most of the computing time in the internal region for each time step is taken in the diagonalization of the Hamiltonian matrix operator $H + \mathcal{L}_1 + \mathcal{L}_2$ in (10.28) or by solving the equivalent linear simultaneous equations. We describe an efficient procedure for diagonalizing the Hamiltonian matrix below.

10.1.4.3 External Region Computation

In this region we consider the solution of the coupled inhomogeneous second-order differential equations (10.63) using the propagator method described in Appendix E.4, where (10.63) corresponds to (E.74). In order to use the outward propagation equations (E.87) and (E.88) we first need to determine the R-matrix $\mathbf{R}_0$ on the boundary of the internal region, which is given by (10.71), and the inhomogeneous term $\mathbf{Z}(a_0)$ on the boundary of the internal region, which is given by (10.72). We also need to determine the vector $\mathbf{J}(r)$, defined by (E.82), for $r = a_s$, $s = 0, \ldots, p$. Equations (E.87) and (E.88) can then be propagated outwards across the p sub-regions from $r = a_0$ to a_p, as described in Appendix E.4, yielding the R-matrix $\mathbf{R}_i$ and the inhomogeneous term $\mathbf{Z}(a_i)$, for all values $i = 0, \ldots, p$.

We now assume that the outer radius $r = a_p$ is chosen large enough that the reduced radial wave function $\mathbf{F}(r)$ in (E.74), i.e. $\mathbf{Y}(r)$ in (10.63), describing the ejected electron or the electron in a Rydberg orbital, vanishes by $r = a_p$. Taking the boundary condition $\mathbf{Y}(a_p) = 0$, we can then propagate the wave function $\mathbf{Y}(r)$ inwards from $r = a_p$ to a_0 using (E.92), where the R-matrix $\mathbf{R}_i$ and the inhomogeneous term $\mathbf{Z}(a_i)$ are those determined in the outward propagation described above.

This yields the reduced radial wave function $\mathbf{F}(r)$ on the internal region boundary $r = a_0$.

Finally, it is necessary to determine the wave function $\Psi(\mathbf{X}_{N+1}, t_{m+1})$ ready to proceed to the internal region computation for the next time step, as discussed in Sect. 10.1. We observe that, having determined $\mathbf{Y}(r)$ in (10.63) at $r = a_0$, as described above, we can then determine $\mathcal{F}(a_0)$ using (10.65) and hence $\mathbf{F}(a_0)$ using (10.60). We can then determine $\overline{\mathbf{F}}(a_0)$ from (10.45), which is a set of n linear simultaneous equations which can be solved for the components of $\overline{\mathbf{F}}(a_0)$. We can then calculate the expansion coefficients $B_k(E, t_{m+1})$, $k = 1, \ldots, n_t$, using (10.44). Hence the wave function $\Psi(\mathbf{X}_{N+1}, t_{m+1})$ can be determined in the internal region using (10.30) and the computation for the next time step initiated.

For ultra-short laser pulses it is possible to choose the outer radius $r = a_p$ of the external region large enough so that during the time of the pulse the ejected electron does not reach this boundary. The boundary condition $\mathbf{Y}(a_p) = 0$ that we then impose accurately represents the physical situation. For example, for a typical atom we might choose $a_0 \approx 20$ a.u., which is large enough to contain the charge distributions of the initial ground state of the target and the residual ion, and $a_p \approx$ several hundred to a few thousand atomic units, which will contain the ejected electron wave function for attosecond or few-femtosecond laser pulses of moderate intensities. However, for longer laser pulses, where the ejected electron can reach this boundary during the pulse, this boundary condition leads to an unphysical reflected wave which can give rise to spurious results. To overcome this an absorbing mask function can be introduced near the outer boundary, similar to that used by Krause et al. [549] which proved successful in R-matrix potential scattering calculations [172].

We conclude this section by remarking that in the above analysis we considered the solution of the coupled inhomogeneous second-order differential equations (10.63) using the propagator method described in Appendix E.4. Instead we could have solved the original coupled inhomogeneous equations (10.55) without eliminating the first derivative term using the propagator method described in Appendix E.5.

10.1.4.4 Diagonalization of the Hamiltonian Matrix

In order to determine the R-matrix $\mathbf{R}$ and the inhomogeneous vector $\mathbf{T}$ in (10.45), we consider a procedure where the Hamiltonian matrix operator $H + \mathcal{L}_1 + \mathcal{L}_2$ in (10.28) is diagonalized at each time step where, for illustrative purposes, we consider the calculation when the dipole velocity gauge is adopted. In this section we consider an iterative procedure which enables this part of the calculation to be carried out efficiently.

We first remember that before the laser pulse has been switched on we have to determine the initial bound state of the target by solving the time-independent Schrödinger equation (10.74), which is achieved using an iterative procedure as described in Sect. 8.1.2.2. In this calculation the conserved quantum numbers Γ, defined by (2.58), correspond only to the initial bound state. Hence the number of

coupled channels will be relatively small. It follows that this stage of the calculation will be rapid.

However, when the laser pulse is switched on many more channels will be coupled and hence the corresponding Hamiltonian matrix will be much larger. Remembering that the R-matrix basis functions $\psi_k(\mathbf{X}_{N+1}, t_{m+\frac{1}{2}})$ in (10.28) are expanded in terms of the time-independent basis functions $\xi_k(\mathbf{X}_{N+1})$ according to (10.22), we then have to diagonalize the following $n_t \times n_t$-dimensional matrix at each time step:

$$H_{kk'}(t_{m+\frac{1}{2}}) = \left\langle \xi_k | H(t_{m+\frac{1}{2}}) + \mathcal{L}_1 + \mathcal{L}_2(t_{m+\frac{1}{2}}) | \xi_{k'} \right\rangle_{\text{int}}, \quad k, k' = 1, \ldots, n_t. \tag{10.76}$$

It follows that before the laser pulse is switched on the matrix $H_{kk'}(t_{m+\frac{1}{2}})$ is block diagonal with only one diagonal block, corresponding to the quantum numbers Γ of the initial target state, being non-zero. After the laser pulse has been switched on the matrix will be non-zero with each block corresponding to different sets of the quantum numbers Γ coupled by the laser field.

We now describe an iterative procedure which enables $H_{kk'}(t_{m+\frac{1}{2}})$ to be efficiently diagonalized by taking advantage of the small change which occurs in this matrix between time steps. Using (10.7), we can rewrite (10.76) as

$$\mathbf{H}(t_{m+\frac{1}{2}}) = \mathbf{H}_0 + A(t_{m+\frac{1}{2}})\mathbf{H}_1, \tag{10.77}$$

where the matrix elements of $\mathbf{H}_0$ and $\mathbf{H}_1$ are defined by

$$(H_0)_{kk'} = \langle \xi_k | H_{N+1} + \mathcal{L}_1 | \xi_{k'} \rangle_{\text{int}}, \quad k,\ k' = 1, \ldots, n_t \tag{10.78}$$

and

$$(H_1)_{kk'} = \langle \xi_k | D_{N+1} + \mathcal{L}_2' | \xi_{k'} \rangle_{\text{int}}, \quad k,\ k' = 1, \ldots, n_t. \tag{10.79}$$

Also, it follows from (10.25) that the time-independent operator D_{N+1} in (10.79) is defined by

$$D_{N+1} = -\frac{\mathrm{i}}{\mathrm{c}} \sum_{i=1}^{N+1} \left(\cos\theta_i \frac{\partial}{\partial r_i} - \frac{\sin\theta_i}{r} \frac{\partial}{\partial \theta_i} \right), \tag{10.80}$$

and using (10.24), the time-independent operator $\mathcal{L}_2'$ in (10.79) is defined by

$$\mathcal{L}_2' = \frac{\mathrm{i}}{2\mathrm{c}} \sum_{i=1}^{N+1} \delta(r_i - a_0) \cos\theta_i, \tag{10.81}$$

so that $\mathcal{L}_2 = A(t_{m+\frac{1}{2}})\mathcal{L}_2'$. Hence the matrices $\mathbf{H}_0$ and $\mathbf{H}_1$ are both time independent and the only time dependence in (10.77) comes from the strength of the laser vector potential $A(t_{m+\frac{1}{2}})$.

Let us assume that we have diagonalized $\mathbf{H}(t_{m-\frac{1}{2}})$ corresponding to the previous time step $t = t_{m-1}$ to t_m so that

$$\mathbf{C}^{\mathrm{T}}(t_{m-\frac{1}{2}})\mathbf{H}(t_{m-\frac{1}{2}})\mathbf{C}(t_{m-\frac{1}{2}}) = \mathbf{E}(t_{m-\frac{1}{2}}), \tag{10.82}$$

where $\mathbf{C}(t_{m-\frac{1}{2}})$ is an orthogonal matrix with elements $c_{kk'}(t_{m-\frac{1}{2}})$ defined by (10.22) and (10.28), and $\mathbf{E}(t_{m-\frac{1}{2}})$ is a real diagonal matrix with diagonal elements $E_k(t_{m-\frac{1}{2}})$. We now consider the diagonalization of $\mathbf{H}(t_{m+\frac{1}{2}})$ corresponding to the current time step $t = t_m$ to t_{m+1}. It follows from (10.77) that we can write

$$\mathbf{H}(t_{m+\frac{1}{2}}) = \mathbf{H}(t_{m-\frac{1}{2}}) + \Delta A(t_m)\mathbf{H}_1, \tag{10.83}$$

where

$$\Delta A(t_m) = A(t_{m+\frac{1}{2}}) - A(t_{m-\frac{1}{2}}). \tag{10.84}$$

Since the time interval $\Delta t = t_{m+1} - t_m = t_{m+\frac{1}{2}} - t_{m-\frac{1}{2}}$ used in the propagation of the wave function is taken to be so small that the term $O(\Delta t^3)$ in (10.10) is negligible, then $\Delta A(t_m)\mathbf{H}_1$ in (10.83) is much smaller than $\mathbf{H}(t_{m-\frac{1}{2}})$. In order to diagonalize $\mathbf{H}(t_{m+\frac{1}{2}})$ we consider the matrix

$$\boldsymbol{\mathcal{H}}(t_{m+\frac{1}{2}}) = \mathbf{C}^{\mathrm{T}}(t_{m-\frac{1}{2}})\mathbf{H}(t_{m+\frac{1}{2}})\mathbf{C}(t_{m-\frac{1}{2}}). \tag{10.85}$$

It follows from (10.82) and (10.83) that

$$\boldsymbol{\mathcal{H}}(t_{m+\frac{1}{2}}) = \mathbf{E}(t_{m-\frac{1}{2}}) + \Delta A(t_m)\mathbf{C}^{\mathrm{T}}(t_{m-\frac{1}{2}})\mathbf{H}_1\mathbf{C}(t_{m-\frac{1}{2}}). \tag{10.86}$$

Hence $\boldsymbol{\mathcal{H}}(t_{m+\frac{1}{2}})$ is a symmetric matrix whose off-diagonal elements are much smaller than its diagonal elements.

We now have to diagonalize $\boldsymbol{\mathcal{H}}(t_{m+\frac{1}{2}})$. There are several efficient procedures for diagonalizing matrices which are diagonally dominant. For example, the parallel Jacobi procedure described by Golub and Van Loan [389] will converge quadratically and only one or two "sweeps" will be required. An analysis of the convergence properties of the Jacobi method is given by Wilkinson [976]. If $\mathbf{D}(t_{m+\frac{1}{2}})$ is the resultant orthogonal matrix that diagonalizes $\boldsymbol{\mathcal{H}}(t_{m+\frac{1}{2}})$ so that

$$\mathbf{D}^{\mathrm{T}}(t_{m+\frac{1}{2}})\boldsymbol{\mathcal{H}}(t_{m+\frac{1}{2}})\mathbf{D}(t_{m+\frac{1}{2}}) = \mathbf{E}(t_{m+\frac{1}{2}}), \tag{10.87}$$

then it follows from (10.85) that the orthogonal matrix $\mathbf{C}(t_{m+\frac{1}{2}})$ that diagonalizes $\mathbf{H}(t_{m+\frac{1}{2}})$ is given by

$$\mathbf{C}(t_{m+\frac{1}{2}}) = \mathbf{C}(t_{m-\frac{1}{2}})\mathbf{D}(t_{m+\frac{1}{2}}). \tag{10.88}$$

We have thus determined the eigenvalues and eigenvectors of $H(t_{m+\frac{1}{2}}) + \mathcal{L}_1 + \mathcal{L}_2(t_{m+\frac{1}{2}})$ enabling the internal region calculation for the present time step to be carried out as described in Sect. 10.1.4.2.

Finally, we observe that this iterative procedure for diagonalizing the Hamiltonian matrix can also be used if the dipole length gauge instead of the dipole velocity gauge is adopted in the calculations. This procedure can also be used to diagonalize matrices which arise in the external region propagation in time-dependent R-matrix theory of atomic multiphoton processes discussed in Sects. E.4 and E.5.

10.1.5 Analysis of Applications

In this section we analyse the application of the theoretical and computational methods described in the previous sections to the calculation of atomic multiphoton processes in ultra-short laser pulses. We consider applications to single-electron multiphoton ionization of neutral and singly ionized neon and argon atoms and double-electron multiphoton ionization of neon atoms. This provides an introduction to the illustrative examples considered in Sect. 10.2. We also show that an accurate treatment of double-electron multiphoton ionization of multi-electron atoms and atomic ions by ultra-short laser pulses, which includes the re-collision mechanism, will result in substantial calculations.

10.1.5.1 Single-Electron Multiphoton Ionization of Ne and Ar

We consider first multiphoton ionization of neutral neon and argon atoms where a single electron is ejected from the target. This is the dominant process below the non-sequential double ionization regime which commences in the intensity range $\sim 10^{14}$–10^{15} W/cm^2 as discussed by Becker and Faisal [84]. In the following analysis we assume that the electron is ejected from the outer s- and p-shells of neon and argon as follows:

$$n\mathrm{h}\nu + \mathrm{Ne}\,(1\mathrm{s}^2 2\mathrm{s}^2 2\mathrm{p}^6\ {}^1\mathrm{S}^\mathrm{e}) \begin{cases} \nearrow \mathrm{Ne}^+\,(1\mathrm{s}^2 2\mathrm{s}^2 2\mathrm{p}^5\ {}^2\mathrm{P}^\mathrm{o}) + \mathrm{e}^- \\ \searrow \mathrm{Ne}^+\,(1\mathrm{s}^2 2\mathrm{s}2\mathrm{p}^6\ {}^2\mathrm{S}^\mathrm{e}) + \mathrm{e}^- \end{cases} \tag{10.89}$$

and

$$n\mathrm{h}\nu + \mathrm{Ar}\,(1\mathrm{s}^2 2\mathrm{s}^2 2\mathrm{p}^6 3\mathrm{s}^2 3\mathrm{p}^6\ {}^1\mathrm{S}^\mathrm{e}) \begin{cases} \nearrow\ \mathrm{Ar}^+\,(1\mathrm{s}^2 2\mathrm{s}^2 2\mathrm{p}^6 3\mathrm{s}^2 3\mathrm{p}^5\ {}^2\mathrm{P}^\mathrm{o}) + \mathrm{e}^- \\ \searrow\ \mathrm{Ar}^+\,(1\mathrm{s}^2 2\mathrm{s}^2 2\mathrm{p}^6 3\mathrm{s} 3\mathrm{p}^6\ {}^2\mathrm{S}^\mathrm{e}) + \mathrm{e}^-. \end{cases} \tag{10.90}$$

In many cases of interest there is expected to be strong coupling between channels where the electron is ejected from the outer p-shell and channels where the electron is ejected from the outer s-shell. Hence in our discussion both these possibilities will be retained in the analysis. However, we note that the ejection of an electron from an inner shell has lower probability and is weakly coupled to the above channels at the laser intensities considered here and hence will not be considered.

In general the $LS\pi$ states of the target neon or argon atoms which are coupled by the laser field are given in Fig. 10.2 where we have truncated the infinite series at total orbital angular momentum $L = 6$. Also in Fig. 10.2, the absorption or emission of a photon is indicated by a horizontal or a vertical line. In this analysis we consider the emission and absorption of linearly polarized laser photons. Hence, if the neon or argon atoms are initially in their ${}^1\mathrm{S}^\mathrm{e}$ ground state where $M_L = 0$, as in (10.89) and (10.90), then they will remain in a state with $M_L = 0$. The corresponding Clebsch–Gordan coefficient $(LM_L 10|L'M_L)$, which occurs in the transition matrix element, see (D.63) and (D.69) in Appendix D.3, is then zero unless $L' = L \pm 1$. It follows that in this case transitions between states in the upper line and in the lower line in Fig. 10.2 where $L = L'$ are forbidden. However, if $M_L = \pm 1$, then the Clebsch–Gordan coefficient $(LM_L 10|L'M_L)$ is non-zero for $L = L'$ and these transitions are allowed. The coupled channels for each $LS\pi$ state of neon or argon are obtained by coupling the spin and orbital angular momenta of the ejected electron with the spin and orbital angular momenta of the residual ion state in (10.89) and (10.90), respectively. The orbital angular momenta of the ejected electron coupled to each residual ion state for each target state in the upper line of Fig. 10.2 are given in Table 10.1 together with the corresponding number of coupled channels. We see that 20 channels are coupled if the total orbital angular momentum is restricted to $L \leq 6$. It follows that if 20 radial continuum basis functions u^0_{pl} are retained in each channel in expansion (10.21), then the corresponding dimension of the Hamiltonian matrix defined by (10.76) that has to be diagonalized at each time step is ∼400. This, together with the propagation of the corresponding coupled differential equations in the external region, can be accomplished very rapidly using the procedure described in Sect. 10.1.4.3.

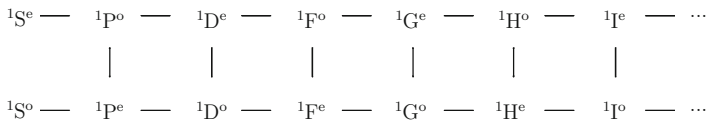

Fig. 10.2 $LS\pi$ states of neutral Ne or Ar coupled by the laser field

Table 10.1 Ejected electron orbital angular momenta and number of coupled channels for multiphoton ionization of neutral neon or argon atoms by linearly polarized photons

Ion state	Atom state							No. coupled channels
	$^1S^e$	$^1P^o$	$^1D^e$	$^1F^o$	$^1G^e$	$^1H^o$	$^1I^e$	
$^2P^o$	1	0,2	1,3	2,4	3,5	4,6	5,7	13
$^2S^e$	0	1	2	3	4	5	6	7

10.1.5.2 Single-Electron Multiphoton Ionization of Ne^+ and Ar^+

We consider next multiphoton ionization of Ne^+ and Ar^+ where again a single electron is ejected. The processes which then replace (10.89) and (10.90) are

$$n\mathrm{h}\nu + \mathrm{Ne}^+ (1s^2 2s^2 2p^5\ ^2P^o) \begin{cases} \nearrow \mathrm{Ne}^{2+} (1s^2 2s^2 2p^4\ ^3P^e, {}^1D^e, {}^1S^e) + e^- \\ \searrow \mathrm{Ne}^{2+} (1s^2 2s 2p^5\ ^3P^o,\ {}^1P^o) + e^-, \end{cases} \tag{10.91}$$

and analogous processes for Ar^+, where again we only consider the dominant processes where the electron is ejected from the outer s- or p-shells. The $LS\pi$ states of Ne^+ and Ar^+ which are coupled by the laser field are given in Fig. 10.3 where again we have truncated the infinite series at total orbital angular momentum $L = 6$. In this case, if the Ne^+ or Ar^+ ion is in its $^2P^o$ ground state then the corresponding value of $M_L = 0$ or ± 1. If $M_L = 0$ then, as in the case of neutral neon and argon targets, transitions between states in the upper and lower lines in Fig. 10.3 are forbidden for laser photons which are linearly polarized along the z-direction. However, if $M_L = \pm 1$, then the Clebsch–Gordan coefficient $(LM_L 10|L'M_L)$ is non-zero for $L = L'$ and these transitions are allowed.

The orbital angular momenta of the ejected electron coupled to each residual ion state for each target state in Fig. 10.3 are given in Tables 10.2 and 10.3 together with the corresponding number of coupled channels, where Table 10.2 refers to the target states in the upper line in Fig. 10.3 and Table 10.3 refers to target states in the lower line in Fig. 10.3. We see from Table 10.2 that 57 channels are coupled if the total orbital angular momentum is restricted to $L \leq 6$ and $M_L = 0$. Also it follows from Table 10.3 that a further 35 channels are coupled if $M_L = \pm 1$ making a total of 88 coupled channels, since both the $^2S^e$ and the $^2S^o$ target states cannot be coupled in this case. Assuming that we retain 20 radial continuum basis functions u^0_{pl} in each channel in expansion (10.21), then the corresponding dimension of the Hamiltonian matrix that has to be diagonalized at each time step when $M_L = \pm 1$ is ~1,800. While the computer time required to carry out this diagonalization together with

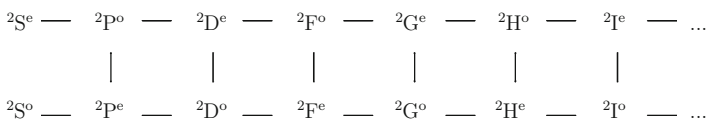

Fig. 10.3 $LS\pi$ states of Ne^+ or Ar^+ ions coupled by the laser field

Table 10.2 Ejected electron orbital angular momenta and number of coupled channels for multiphoton ionization of Ne^+ and Ar^+ by linearly polarized photons when $M_L = 0$

Final ion state	Initial ion state							No. coupled channels
	$^2S^e$	$^2P^o$	$^2D^e$	$^2F^o$	$^2G^e$	$^2H^o$	$^2I^e$	
$^3P^e$	–	1	2	3	4	5	6	6
$^1D^e$	2	1,3	0,2,4	1,3,5	2,4,6	3,5,7	4,6,8	18
$^1S^e$	0	1	2	3	4	5	6	7
$^3P^o$	1	0,2	1,3	2,4	3,5	4,6	5,7	13
$^1P^o$	1	0,2	1,3	2,4	3,5	4,6	5,7	13

Table 10.3 Additional ejected electron orbital angular momenta and number of coupled channels for multiphoton ionization of Ne^+ and Ar^+ by linearly polarized photons when $M_L = \pm 1$

Final ion state	Initial ion state							No. coupled channels
	$^2S^o$	$^2P^e$	$^2D^o$	$^2F^e$	$^2G^o$	$^2H^e$	$^2I^o$	
$^3P^e$	–	0,2	1,3	2,4	3,5	4,6	5,7	12
$^1D^e$	–	2	1,3	2,4	3,5	4,6	5,7	11
$^1S^e$	–	–	–	–	–	–	–	–
$^3P^o$	–	1	2	3	4	5	6	6
$^1P^o$	–	1	2	3	4	5	6	6

the propagation of the corresponding coupled differential equations in the external region, as described in Sect. 10.1.4.3, is considerably more than that required for neutral neon and argon atoms, due to the open shell nature of the target ions, the calculation is still easily accomplishable using present-day high-performance computing facilities.

10.1.5.3 Double-Electron Multiphoton Ionization of Ne

In recent years the development of laser technology has enabled atoms to be routinely subjected to laser light approaching or exceeding the atomic unit of intensity $I_a \approx 3.5 \times 10^{16}$ W/cm^2. At these intensities the laser field becomes comparable in magnitude to the Coulomb field in an atom and double-electron multiphoton ionization shows a dramatic increase, as discussed by van der Hart and Burnett [934]. Of particular interest and importance is the re-collision mechanism considered by Corkum [231], which plays a significant role in this process. In this mechanism, the first ejected electron wave packet moves in the laser field and, within the first laser period after ionization, there is a significant probability that this electron will return to the vicinity of the residual ion and excite or ionize a second electron. This re-collision mechanism has, for example, been observed by Mauritssen et al. [647] who used a combination of an intense attosecond XUV laser pulse which ionized the target atom, together with a femtosecond IR laser which was sufficiently strong to reverse the initial direction of the ejected electronic motion, causing it to rescatter from the parent ion. In concluding this introduction we mention that double-electron multiphoton ionization of He has been studied by many workers, including calculations by van der Hart and Feng [318, 319, 935] using B-spline

bases in R-matrix–Floquet theory, by Parker et al. [717], Feist et al. [317] and Guan et al. [430] who solved the full-dimensional time-dependent Schrödinger equation numerically. Also, Guan et al. [432] developed a time-dependent B-spline R-matrix approach for a general atom which they used to study double-electron multiphoton ionization of He. Finally, we note that double-electron two-photon ionization of neon has recently been studied experimentally by Kurka et al. [556].

In this section we consider double-electron multiphoton ionization of neon atoms, both directly and via the re-collision mechanism, by the inclusion of pseudostates in the R-matrix expansion. We note that these processes could also be studied using the IERM method discussed in Sect. 6.3. In direct double-electron multiphoton ionization we consider the following processes

$$n\mathrm{h}\nu + \mathrm{Ne}\,(1\mathrm{s}^2 2\mathrm{s}^2 2\mathrm{p}^6) \rightarrow \begin{cases} \mathrm{Ne}^{2+}\,(1\mathrm{s}^2 2\mathrm{s}^2 2\mathrm{p}^4) + 2\mathrm{e}^- \\ \mathrm{Ne}^{2+}\,(1\mathrm{s}^2 2\mathrm{s}2\mathrm{p}^5) + 2\mathrm{e}^- \\ \mathrm{Ne}^{2+}\,(1\mathrm{s}^2 2\mathrm{p}^6) + 2\mathrm{e}^- \end{cases}, \tag{10.92}$$

where we assume that double-electron multiphoton ionization can occur from both the 2s and 2p shells. In the re-collision mechanism we consider the following processes:

$$n\mathrm{h}\nu + \mathrm{Ne}\,(1\mathrm{s}^2 2\mathrm{s}^2 2\mathrm{p}^6) \begin{cases} \mathrm{Ne}^{+}\,(1\mathrm{s}^2 2\mathrm{s}^2 2\mathrm{p}^5) + \mathrm{e}^- \\ \mathrm{Ne}^{+}\,(1\mathrm{s}^2 2\mathrm{s}2\mathrm{p}^6) + \mathrm{e}^-, \end{cases} \tag{10.93}$$

where the ejected electron then returns under the influence of the laser field and ionizes a second electron from the Ne^+ ion as follows:

$$\mathrm{e}^- + \mathrm{Ne}^{+}\,(1\mathrm{s}^2 2\mathrm{s}^2 2\mathrm{p}^5) \begin{cases} \mathrm{Ne}^{2+}\,(1\mathrm{s}^2 2\mathrm{s}^2 2\mathrm{p}^4) + 2\mathrm{e}^- \\ \mathrm{Ne}^{2+}\,(1\mathrm{s}^2 2\mathrm{s}\,2\mathrm{p}^5) + 2\mathrm{e}^- \end{cases} \tag{10.94}$$

or

$$\mathrm{e}^- + \mathrm{Ne}^{+}\,(1\mathrm{s}^2 2\mathrm{s}\,2\mathrm{p}^6) \begin{cases} \mathrm{Ne}^{2+}\,(1\mathrm{s}^2 2\mathrm{s}\,2\mathrm{p}^5) + 2\mathrm{e}^- \\ \mathrm{Ne}^{2+}\,(1\mathrm{s}^2 2\mathrm{p}^6) + 2\mathrm{e}^-, \end{cases} \tag{10.95}$$

where again we assume that double-electron ionization can occur from both the 2s and 2p shells.

In order to describe the above processes we commence by defining the following Ne^{2+} target atom basis

$$\begin{aligned}
&\mathrm{Ne}^{2+}\ (1s^2 2s^2 2p^4\ {}^3\mathrm{P}^e,\ {}^1\mathrm{D}^e,\ {}^1\mathrm{S}^e),\\
&\mathrm{Ne}^{2+}\ (1s^2 2s 2p^5\ {}^3\mathrm{P}^o,\ {}^1\mathrm{P}^o),\\
&\mathrm{Ne}^{2+}\ (1s^2 2p^6\ {}^1\mathrm{S}^e),
\end{aligned} \tag{10.96}$$

which allows double-electron multiphoton ionization from both the 2s and 2p shells. These basis states can be determined using standard atomic structure programs, as discussed in Sect. 2.2.1.

The next step is to determine an Ne^+ target basis which should include the Ne^+ $(1s^2 2s^2 2p^5\ {}^2\mathrm{P}^o)$ and Ne^+ $(1s^2 2s 2p^6\ {}^1\mathrm{S}^e)$ states together with further excited states and pseudostates representing the higher excited states and continuum states of Ne^+. This can be achieved by introducing a set of pseudo-orbitals, for example, $\overline{3s}$, $\overline{3p}$, $\overline{3d}$, $\overline{4f}$ and higher pseudo-orbitals in addition to the 1s, 2s and 2p orbitals used in constructing the Ne^{2+} target basis (10.96). The Ne^+ target Hamiltonian is then diagonalized in the following basis:

$$\begin{aligned}
&\mathrm{Ne}^{+}\ (1s^2 2s^2 2p^4\ {}^3\mathrm{P}^e,\ {}^1\mathrm{D}^e,\ {}^1\mathrm{S}^e\ \overline{n\ell}),\\
&\mathrm{Ne}^{+}\ (1s^2 2s 2p^5\ {}^3\mathrm{P}^o,\ {}^1\mathrm{P}^o\ \overline{n\ell}),\\
&\mathrm{Ne}^{+}\ (1s^2 2p^6\ {}^1\mathrm{S}^e\ \overline{n\ell}),
\end{aligned} \tag{10.97}$$

where $\overline{n\ell}$ represents the 2s and 2p physical orbitals which correspond to the ground and excited states of Ne^+, and additional pseudo-orbitals including $\overline{3s}$, $\overline{3p}$, $\overline{3d}$ and $\overline{4f}$ which correspond to highly excited and continuum states of Ne^+.

In Table 10.4 we give the $LS\pi$ symmetries of the Ne^+ pseudostates which can be constructed from the Ne^{2+} basis states given in (10.96) and $\overline{3s}$, $\overline{3p}$, $\overline{3d}$ and $\overline{4f}$ pseudo-orbitals. Only doublet pseudostates are given in this table since spin conservation in non-relativistic theory means that quartet pseudostates cannot be excited from the singlet ground state of the target atom in (10.93). We see from this table that 52 Ne^+ pseudostates can be formed from the $\overline{3s}$, $\overline{3p}$, $\overline{3d}$ and $\overline{4f}$ pseudo-orbitals, where

Table 10.4 $LS\pi$ symmetries of the pseudostates of Ne^+ ions and number of pseudostates which can be constructed from the Ne^{2+} basis states given in (10.96) and $\overline{3s}$, $\overline{3p}$, $\overline{3d}$ and $\overline{4f}$ pseudo-orbitals

Ne^{2+} state	Pseudo-orbital				No. of Ne^+ pseudostates
	$\overline{3s}$	$\overline{3p}$	$\overline{3d}$	$\overline{4f}$	
${}^3\mathrm{P}^e$	${}^2\mathrm{P}^e$	${}^2\mathrm{S}^o, {}^2\mathrm{P}^o, {}^2\mathrm{D}^o$	${}^2\mathrm{P}^e, {}^2\mathrm{D}^e, {}^2\mathrm{F}^e$	${}^2\mathrm{D}^o, {}^2\mathrm{F}^o, {}^2\mathrm{G}^o$	10
${}^1\mathrm{D}^e$	${}^2\mathrm{D}^e$	${}^2\mathrm{P}^o, {}^2\mathrm{D}^o, {}^2\mathrm{F}^o$	${}^2\mathrm{S}^e, {}^2\mathrm{P}^e, {}^2\mathrm{D}^e$ ${}^2\mathrm{F}^e, {}^2\mathrm{G}^e$	${}^2\mathrm{P}^o, {}^2\mathrm{D}^o, {}^2\mathrm{F}^o$ ${}^2\mathrm{G}^o, {}^2\mathrm{H}^o$	14
$2 \times {}^1\mathrm{S}^e$	${}^2\mathrm{S}^e$	${}^2\mathrm{P}^o$	${}^2\mathrm{D}^e$	${}^2\mathrm{F}^o$	2×4
${}^3\mathrm{P}^o$	${}^2\mathrm{P}^o$	${}^2\mathrm{S}^e, {}^2\mathrm{P}^e, {}^2\mathrm{D}^e$	${}^2\mathrm{P}^o, {}^2\mathrm{D}^o, {}^2\mathrm{F}^o$	${}^2\mathrm{D}^e, {}^2\mathrm{F}^e, {}^2\mathrm{G}^e$	10
${}^1\mathrm{P}^o$	${}^2\mathrm{P}^o$	${}^2\mathrm{S}^e, {}^2\mathrm{P}^e, {}^2\mathrm{D}^e$	${}^2\mathrm{P}^o, {}^2\mathrm{D}^o, {}^2\mathrm{F}^o$	${}^2\mathrm{D}^e, {}^2\mathrm{F}^e, {}^2\mathrm{G}^e$	10

we observe from (10.97) that there are two Ne^{2+} doubly ionized states with $^1S^e$ symmetry, corresponding to the configurations $1s^2 2s^2 2p^4$ and $1s^2 2p^6$.

Having determined the bound and pseudostates basis of Ne^+ we can then proceed as in Sects. 10.1.2 and 10.1.3 to include these as target states in the internal region expansion (10.21) and in the external region expansion (10.50). As discussed in Sect. 10.1.4, the initial Ne ($1s^2 2s^2 2p^6\ ^1S^e$) target state in (10.93) is determined as a bound state of Ne^+ and the remaining electron as in photoionization calculations, described in Sect. 8.1.2. We then propagate the wave function forward in time as described in Sect. 10.1.4.

We now consider the number of channels which can be coupled in the internal and external region calculations corresponding to the Ne^+ target states and pseudostates discussed above. The orbital angular momenta of the first ejected electron coupled to the residual Ne^+ ion pseudostates for each symmetry are given in Table 10.5 for each symmetry of the target neon atom. We note that parity and orbital angular momentum conservation forbids any channels coupled to the $^2S^o$ pseudostate. If the laser intensity is not high so that the energy region where double-electron multiphoton ionization is important is restricted to low energies, then we can limit the orbital angular momentum of the pseudo-orbitals. We assume in this discussion that only target pseudo-orbitals with $\ell \leq 3$ are included. We also assume that we can restrict the total orbital angular momentum L of the target atom to $L \leq 5$. In this case we see from Table 10.5 that including the $\overline{3s}$, $\overline{3p}$, $\overline{3d}$ and $\overline{4f}$ pseudo-orbitals in the calculation yields 626 coupled channels. In order to obtain accurate results, it would probably be necessary to include ~10 pseudo-orbitals for each angular symmetry in the calculation which would then yield $10 \times 626 = 6,260$ coupled pseudo-channels in addition to the 20 coupled physical channels, given in Table 10.1, representing single-electron multiphoton ionization. Hence, if 20 radial

Table 10.5 Orbital angular momenta of the first ejected electron and number of channels coupled to the residual Ne^+ ion pseudostates for double-electron multiphoton ionization of neutral neon atoms by linearly polarized photons

Pseudostates		Sym. of collision state						No. coupled channels
Symmetry	No.	$^1S^e$	$^1P^o$	$^1D^e$	$^1F^o$	$^1G^e$	$^1H^o$	
$^2S^e$	5	0	1	2	3	4	5	30
$^2S^o$	1	–	–	–	–	–	–	0
$^2P^e$	5	–	1	2	3	4	5	25
$^2P^o$	9	1	0,2	1,3	2,4	3,5	4,6	99
$^2D^e$	9	2	1,3	0,2,4	1,3,5	2,4,6	3,5,7	135
$^2D^o$	6	–	2	1,3	2,4	3,5	4,6	54
$^2F^e$	4	–	3	2,4	1,3,5	2,4,6	3,5,7	48
$^2F^o$	7	3	2,4	1,3,5	0,2,4,6	1,3,5,7	2,4,6,8	126
$^2G^e$	3	4	3,5	2,4,6	1,3,5,7	0,2,4,6,8	1,3,5,7,9	60
$^2G^o$	2	–	4	3,5	2,4,6	1,3,5,7	2,4,6,8	28
$^2H^o$	1	5	4,6	3,5,7	2,4,6,8	1,3,5,7,9	0,2,4,6,8,10	21
Totals	52							626

continuum basis orbitals are retained in each channel to obtain convergence then the total dimension of the Hamiltonian matrix will be more than 100,000. The internal region calculation involving a matrix of this size, as well as the propagation of the corresponding coupled differential equations in the external region at each time step, as described in Sect. 10.1.4.3, will clearly result in a substantial calculation.

We observe that if the re-collision mechanism is being considered then the time over which the calculation must be carried out will be lengthened by the need to follow the motion of the wave packet representing the first ejected electron until it returns to excite or ionize the residual Ne^+ ion, as in (10.94) and (10.95). One computational simplification that is possible is to omit the coupling to the Ne^+ higher bound and continuum pseudostates in the internal and external region calculations at early times since the role of these pseudostates is mainly to represent excitation and ionization of the second electron at later times. However, these higher bound and continuum pseudostates will need to be included in the calculation at later times in order to accurately represent the excitation and ionization process caused by the re-collision mechanism. Finally, a further simplification in early work would be to omit multiphoton ionization and re-collision ionization from the inner 2s shell with considerable reduction in computational effort.

In concluding this section, we have shown that accurate time-dependent calculations of single-electron multiphoton ionization of neon and argon atoms by intense laser pulses can be carried out very rapidly, as discussed in the illustrative examples in Sect. 10.2. Also, accurate time-dependent calculations of single-electron multiphoton ionization of Ne^+ and Ar^+ ions, while more lengthy because of the open-shell nature of the target, are also relatively easily accomplishable. However, while we have shown that accurate calculations of double-electron multiphoton ionization of neon atoms, and hence of argon atoms, which arise either directly or via the re-collision mechanism are substantial, they are now being considered by workers in this field.

10.2 Illustrative Examples

We summarized in the introduction to this chapter the increasing experimental and theoretical interest in recent years in the interaction of ultra-short laser pulses with atoms and atomic ions. Until quite recently the most advanced theoretical advances had been restricted to two-active electron systems, such as He-like atoms and ions. However, in the last few years considerable effort has been given by van der Hart et al. [937, 938], Lysaght et al. [603–606] and Guan et al. [429, 431, 432] to developing R-matrix computer programs which have enabled the interaction of ultra-short laser pulses with general multi-electron atoms and ions to be accurately calculated. In this section we describe some illustrative results for ultra-short laser pulse interactions with neon and argon atoms using these programs that have opened up a new era of experimental and theoretical collaboration.

10.2.1 Multiphoton Ionization of Ne

In this section we describe the results of two independent time-dependent R-matrix calculations of ultra-short laser pulse interactions with neon atoms obtained by Guan et al. [429] and by Lysaght et al. [603].

In the work of Guan et al. [429], the calculations were carried out using an extension of the B-spline R-matrix BSR computer program [992], discussed in Sect. 5.1.1, which used the Arnoldi–Lanczos method of time propagation, outlined in Sect. 10.1.1. A linearly polarized laser field was adopted using the length form of the dipole operator and the $1s^2 2s^2 2p^5\ ^2P^o$ ground state of Ne^+ was retained in expansion (10.21). Also, an extended internal region with a boundary radius of 100 a.u. and an absorbing potential, to avoid artificial reflections from this boundary, was used in the calculations.

Calculations were carried out for the response of the neon atom in its $1s^2 2s^2 2p^6\ ^1S^e$ ground state to the effect of laser pulses with a $\sin^2$ envelope. As an example we show in Fig. 10.4 the form of a 10-cycle laser pulse, where the laser frequency $\omega = 0.825$ a.u. In Fig. 10.5 we show the response of the neon atom in its $1s^2 2s^2 2p^6\ ^1S^e$ ground state to the effect of 10-cycle laser pulses with peak intensity of 3.5×10^{14} W/cm^2 and laser frequencies $\omega = 0.425$ and 0.27 a.u., where two and three photons, respectively, need to be absorbed in order to ionize the atom. It was found that in order to obtain converged results, symmetries up to total angular momentum $L = 6$ needed to be retained in the expansion. We see from these results that for $\omega = 0.27$ a.u. excitation rather than ionization is the dominating mechanism. On the other hand, for the higher laser frequency $\omega = 0.425$ ionization is the dominant process.

Finally, we mention that as a check on this work, Guan et al. [429] made a comparison at a few energies with the R-matrix–Floquet (RMF) predictions of McKenna and van der Hart [624]. Satisfactory agreement was obtained at energies away from the first resonance structure, corresponding to the intermediate $1s^2 2s^2 2p^5 3s\ ^1P^o$ state, where the resonance was found to be broader and shifted from the RMF

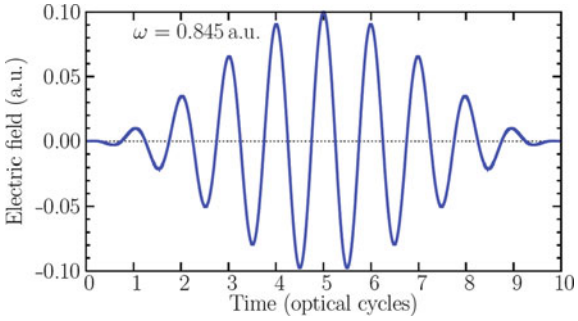

Fig. 10.4 Form of laser pulse with a $\sin^2$ envelope used in neon multiphoton ionization calculations by Guan et al. [429] corresponding in this example to a 10-cycle pulse with a laser frequency $\omega = 0.825$ a.u. (Fig. 1a from [429])

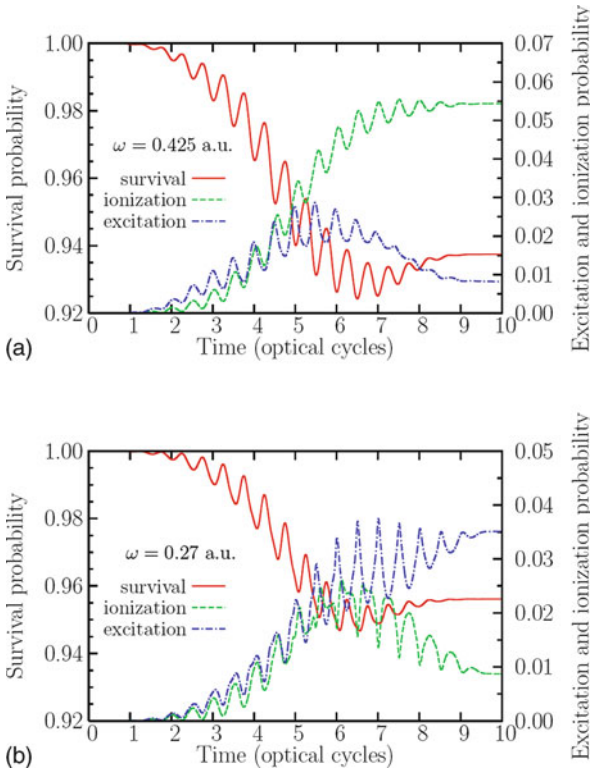

Fig. 10.5 Neon ground state survival probability (*left scale*) and total excitation and ionization probabilities (*right scale*) for laser frequencies of $\omega = 0.425$ and 0.27 a.u. and for a peak laser intensity of 3.5×10^{14} W/cm^2 (Fig. 2 from [429])

position. The broadening was due to the frequency width of the time-dependent laser pulse, while the shift in the position was due to the different structure models used in the two calculations.

We now turn to a discussion of R-matrix calculations of ultra-short laser pulse interactions with neon atoms carried out by Lysaght et al. [603], where the laser field was assumed to be linearly polarized and spatially homogeneous and the Cayley method of time propagation, outlined in Sect. 10.1.1, was used. In the internal region the calculation used an extension of the R-matrix RMATRXII computer program for electron impact collisions with atoms and ions [185], discussed in Sect. 5.1.1, which represented the continuum orbitals by expansions in B-spline functions discussed in Sect. 4.4.7. The laser field was described using the dipole length gauge form of the dipole operator and the linear equations method was used to solve (10.32) in the internal region at each time step. This yielded the R-matrix $\mathbf{R}$ and the inhomogeneous vector $\mathbf{T}$ in (10.35) on the boundary $r = a_0$ of the internal region, where $a_0 = 20$ a.u. In the external region, which was partitioned as in Fig. 10.1, the R-matrix and T-vector were propagated at each time step out to typically 400 a.u.

using a modification of the method described in Appendix E.4. Again a B-spline basis was used to represent the Green's function in the BBM propagator and a linear equations method used to solve the equations in each sub-region. Finally, both the $1s^2 2s^2 2p^5\ {}^2P^o$ ground state and the $1s^2 2s 2p^6\ {}^2S^e$ first excited state of Ne^+ together with channels up to total orbital angular momentum $L = 9$ were included in the internal and external region expansions (10.21) and (10.50).

Calculations were carried out corresponding to a proposed ultra-fast pump-probe experiment illustrated in Fig. 10.6. In this experiment neon in its ground state is irradiated with a 17 eV few-cycle free-electron-laser (FEL) pulse that is resonant with the $1s^2 2s^2 2p^5 3s\ {}^1P^o$ excited bound state, as shown in the figure. During this FEL pulse, population is transferred from the $1s^2 2s^2 2p^6\ {}^1S^e$ ground state to the $1s^2 2s^2 2p^5 3s\ {}^1P^o$ excited state. During this few-cycle pulse, neon is irradiated with an XUV ultra-short laser pulse that has a high enough frequency to transfer population from the $1s^2 2s^2 2p^5 3s\ {}^1P^o$ state to the continuum coupled to the Ne^+ $1s^2 2s 2p^6\ {}^2S^e$ ionic state. By varying the time delay $\Delta\tau$ between the FEL pulse and the XUV ultra-short laser pulse it is possible to study the time-dependent transfer of population between the ground state and the resonant excited state by investigating how the population in the channels coupled to the $1s^2 2s 2p^6\ {}^2S^e$ ionic state varies as a function of $\Delta\tau$.

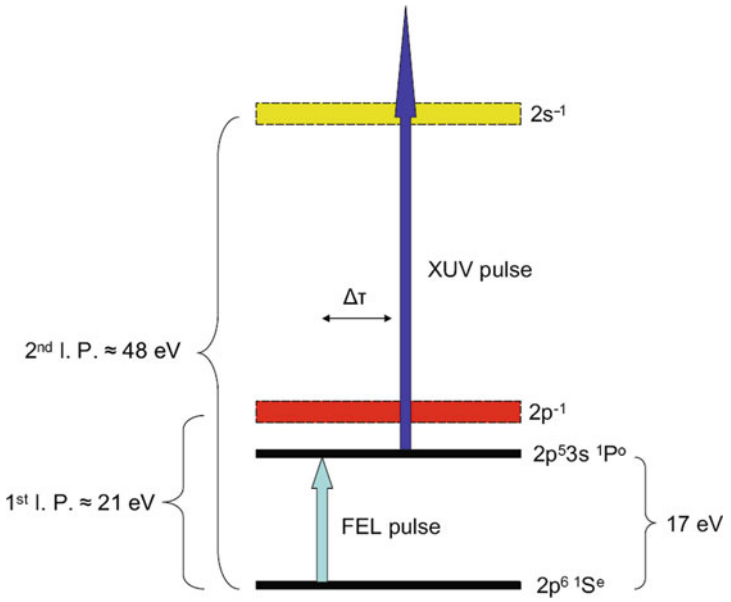

Fig. 10.6 Schematic diagram of a proposed ultra-fast pump-probe experiment in which neon in its $1s^2 2s^2 2p^6\ {}^1S^e$ ground state is irradiated with a 17 eV few-cycle FEL pulse and with an XUV ultra-short laser pulse leaving the atom in a continuum state coupled to the Ne^+ $1s^2 2s 2p^6\ {}^2S^e$ ionic state (Fig. 1 from [603])

In these calculations the 17 eV FEL pulse has a three-cycle electric field $\sin^2$ turn-on, 14 cycles at constant peak amplitude followed by a three-cycle $\sin^2$ turn-off. The XUV ultra-short laser pulse consists of a combination of the 15th, 17th, 19th and 21st harmonics of 780 nm radiation with a Gaussian time envelope. The profile of the electric field is given in the top half of Fig. 10.7 where the position of the XUV ultra-short laser pulse is shown for two time delays $\Delta\tau = \pm 1.5$ fs relative to the FEL pulse. The FEL pulse has peak intensity of 5×10^{13} W/cm^2 and the XUV ultra-short laser pulse has peak intensity of 1.72×10^{12} W/cm^2.

In the bottom half of Fig. 10.7, the population in the continuum channels coupled to the $1s^2 2s 2p^6\ ^2S^e$ ionic state of Ne^+ are shown as a function of time corresponding to the two different values of $\Delta\tau$ shown in the top half of Fig. 10.7. The population is determined by calculating the norm of the wave function beyond 50 a.u. The population in the continuum channels coupled to the $^2S^e$ ionic state after both pulses is greater for $\Delta\tau = +1.5$ fs than for $\Delta\tau = -1.5$ fs, as more population has been transferred from the ground state to the $1s^2 2s^2 2p^5 3s\ ^1P^o$ state at this late stage in the evolution of the FEL pulse. The delayed increase in the population of the continuum channels after the end of the laser pulse, in Fig. 10.7, is due to the time taken for the outgoing wave packets to reach the spatial region beyond 50 a.u. where the population is calculated. The Rabi oscillation of the population for $\Delta\tau = -1.5$ fs can be explained by the large difference between the FEL 17 eV photon energy and the transition energy difference of $\approx$27 eV between the $^2S^e$ ionic state and the $1s^2 2s^2 2p^5\ ^2P^o$ ground state of Ne^+. This leads to rapid population and depopulation of channels coupled to the $^2S^e$ ionic state with a Rabi period of $\approx$0.8 fs.

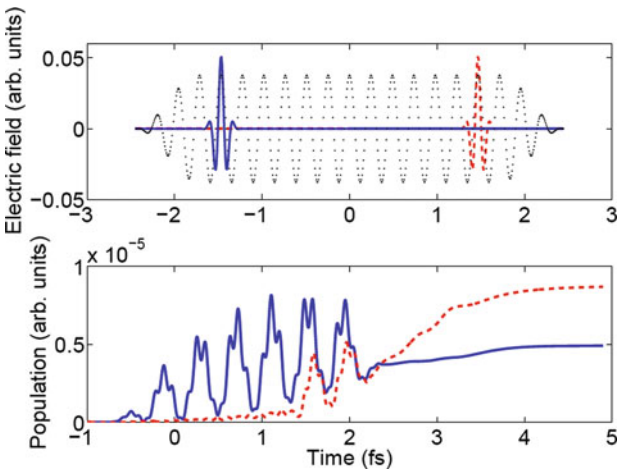

Fig. 10.7 *Top Half*: Electric field strength in arbitrary units. The FEL field is shown as *black dots*. The XUV ultra-short laser pulse is shown as a *solid line* ($\Delta\tau = -1.5$ fs) and as *heavy dots* ($\Delta\tau = +1.5$ fs). *Bottom half*: Population in the continuum channels coupled to the Ne^+ $1s^2 2s 2p^6\ ^2S^e$ ionic state are shown as a function of time for the two different time delays between the FEL pulse and the XUV ultra-short laser pulse. The *solid line* results are for $\Delta\tau = -1.5$ fs and the *dotted line* results are for $\Delta\tau = +1.5$ fs (Fig. 2 from [603])

In conclusion, this work has shown the importance of core excitation in multiphoton processes involving ultra-short laser pulses. An understanding of these ultra-fast, inner-shell processes will become of increasing interest as a result of the present rapid development of experimental techniques to attain higher photon energies, shorter pulse duration and increasing stability.

10.2.2 Multiphoton Ionization of Ar

In this section we describe the results of two independent time-dependent R-matrix calculations of ultra-short laser pulse interactions with argon atoms obtained by van der Hart et al. [937] and by Guan et al. [431].

In the work of van der Hart et al. [937] on argon, the calculations were carried out using the R-matrix computer program described in our earlier discussion in Sect. 10.2.1 of time-dependent R-matrix calculations for neon by Lysaght et al. [603]. The laser field was described using the length form of the dipole operator in an extended internal region with a radius of 100 a.u. and an outer absorbing boundary potential. The linear equations R-matrix method was used to solve the time-propagation equations (10.32) at each time step. For most of the results reported only the $1s^2 2s^2 2p^6 3s^2 3p^5\ ^2P^o$ ground state of Ar^+ was retained in expansion (10.21). Ionization rates were then calculated for frequency-doubled Ti:Sapphire laser light with a wavelength of 390 nm enabling the results to be compared with earlier accurate R-matrix–Floquet calculations by van der Hart [933]. The results also showed how detailed atomic structure can affect the atomic response in the time domain.

To demonstrate the accuracy of the time-dependent calculation, the time-dependent results were compared with R-matrix–Floquet calculations reported in Sect. 9.2.1. The Ti:Sapphire laser pulse shape adopted had a three-cycle $\sin^2$ turn-on of the electric field, followed by typically between 0 and 14 cycles of the oscillating field with constant amplitude, followed by a three-cycle $\sin^2$ turn-off. Also typically 2,000 time steps per cycle were used. This enabled the ionization rates at a constant intensity to be determined allowing comparisons with other work to be made. The ionization rates were determined in two different ways: first by calculating the survival probability as a function of the number of cycles during which a constant field intensity is maintained and second by calculating the decrease in the norm of the wave function during the pulse.

We show in Fig. 10.8 how the norm of the total wave function and the population of the field-free ground state wave function change as a function of the time dependence of the laser pulse, which is maintained at constant peak intensity for 12 optical cycles. The calculation extends beyond the end of the pulse to demonstrate that it takes time for the emitted electron to be absorbed by the absorbing boundary. The ground state population shows the expected rapid depopulation and repopulation during the laser pulse (see, for example, [739]). Also, the intensity was chosen such that the Ar ground state energy in the laser field is almost resonant with intermediate $3s^2 3p^5 3d\ ^1P^o$ and $^1F^o$ states [933]. The slow oscillation in the maximum population in the ground state as a function of time is due to resonant

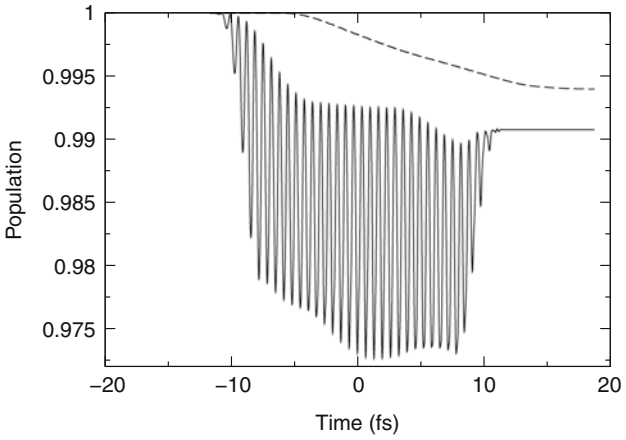

Fig. 10.8 Time dependence of the norm of the wave function (*dashed line*) and the population of the field-free ground state (*solid line*) for argon subjected to 390 nm laser light with a peak intensity of 0.7×10^{14} W/cm^2. The pulse has a three-cycle $\sin^2$ turn-on, a constant amplitude oscillating field for 12 cycles and a three-cycle $\sin^2$ turn-off. The time-dependent Schrödinger equation is solved for a further six cycles of the field at the end of the pulse (Fig. 2 from [937])

transfer of population into these excited states and back into the ground state. The norm of the wave function shows an exponential decay (with a small oscillation due to the influence of an excited state) and the ionization rate can be estimated from this decay curve.

Next, in Fig. 10.9 we compare the intensity dependence of the ionization rate for argon obtained using time-dependent R-matrix theory calculations with R-matrix–Floquet (RMF) calculations by van der Hart [933] and ADK tunnelling model calculations [16, 727], where the RMF and ADK calculations were previously compared in Fig. 9.8. The agreement between the time-dependent R-matrix and the R-matrix–Floquet calculations is excellent, being typically much better than 10%. Also, while it was found to be difficult to extend the R-matrix–Floquet calculation to intensities above 2.0×10^{14} W/cm^2, due to channel closing occurring at this intensity, the time-dependent calculation allows the rates to be determined to much higher intensities, as evidenced by the ionization rates plotted at $I = 2.5 \times 10^{14}$ W/cm^2 and 3.0×10^{14} W/cm^2 in Fig. 10.9.

Finally, we consider R-matrix calculations of ultra-short laser pulse interactions with argon atoms carried out by Guan et al. [431], which use the procedure outlined in our earlier discussion in Sect. 10.2.1 of time-dependent R-matrix calculations on neon carried out by Guan et al. [429]. In the work on argon the $3s^2 3p^5\ ^2P^o$ ground state and the $3s 3p^6\ ^2S^e$ and $3s^2 3p^4 3d\ ^2S^e$ excited states of Ar^+ were retained in the R-matrix expansion and an internal region radius of 500 a.u. was adopted, which avoided the need for an absorbing potential, which was used in the previous work on neon. Also in these calculations, channels up to total orbital angular momentum $L = 5$ were included in the case of two-photon ionization and up to $L = 9$ were included for five-photon ionization.

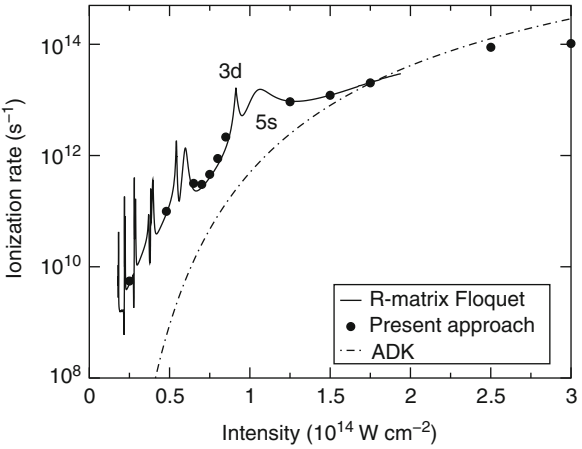

Fig. 10.9 Comparison of the ionization rates for argon irradiated with 390 nm laser light as a function of laser intensity. The rates using time-dependent R-matrix calculations (*solid circles*) are compared with those using the RMF approach (*solid line*) and the ADK approach (*dashed line*). The label 5s indicates the $3s^2 3p^5 5s\ ^1P^o$ resonance and the label 3d indicates the $3s^2 3p^5 3d\ ^1P^o$ resonance (Fig. 4 from [937])

We show in Fig. 10.10 time-dependent results for two-photon ionization of argon in the photon energy range from 8 to 14 eV compared with R-matrix–Floquet (RMF) calculations by McKenna and van der Hart [624]. The laser pulse had a peak intensity of 10^{12} W/cm^2 and a duration of 30 cycles including a linear ramp on and ramp off over five cycles. The results exhibit three resonances in this intensity range with peaks around photon energies of 12.0, 12.75 and 13.9 eV which we see also occur in

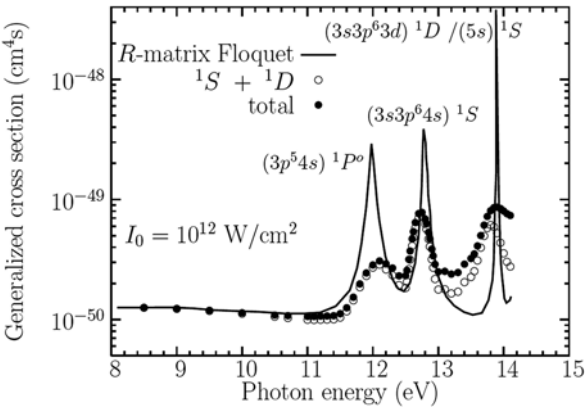

Fig. 10.10 Comparison of ionization rates for time-dependent two-photon ionization of argon atoms with a laser intensity of 10^{12} W/cm^2 obtained by Guan et al. [431] compared with RMF calculations by McKenna and van der Hart [624]. The *filled circles* represent the total time-dependent ionization yield, the *open circles* are the results obtained by summing the ionization yield from individual channels and the *solid line* shows the RMF results (Fig. 1 from [431])

the R-matrix–Floquet calculations, which corresponded to an infinitely long pulse and hence a sharply defined photon energy.

We note in Fig. 10.10 that there are two results for the ionization yield at the end of the pulse, namely the total yield and the sum of the partial ionization yields in the individual channels. For the dominant two-photon process described in this calculation, the latter yield corresponds to the $^1S^e$ and $^1D^e$ final continuum states. We see from Fig. 10.10 that there are no significant differences between these yields for photon energies below about 13 eV. However, when the photon energy approaches the threshold for one-photon ionization we see that the cross section extracted from the total ionization yield is noticeably larger than that obtained from the two-photon $^1S^e$ and $^1D^e$ contributions. In this case the total ionization cross section contains contributions from the $^1P^o$ symmetry corresponding to the single-photon ionization probability.

We also consider results obtained by Guan et al. [431] for processes requiring more than two photons to ionize the argon atoms. In Fig. 10.11 we show cross sections for time-dependent five-photon ionization of argon in the wavelength range between 330 and 390 nm obtained by Guan et al. [431] compared with R-matrix–Floquet calculations by van der Hart [933]. We see that the two calculations are in good agreement, bearing in mind the broadening of the features in the time-dependent calculation caused by the finite duration of the laser pulse and the difference in the atomic structure models.

In conclusion, the results presented in this section, obtained with two independent time-dependent R-matrix computer programs, have enabled for the first time accurate calculations of ultra-short laser pulse interactions with general multi-electron atoms and atomic ions to be carried out.

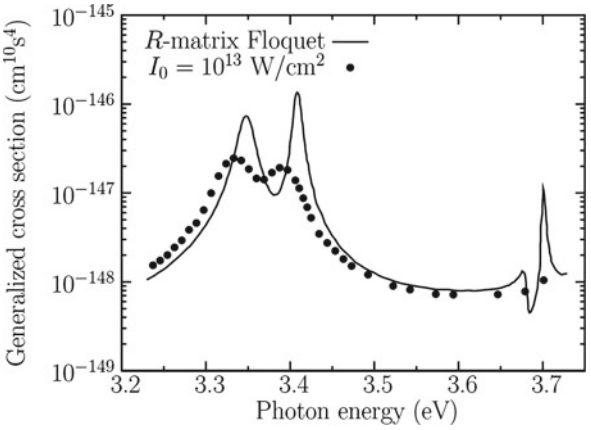

Fig. 10.11 Generalized cross sections for time-dependent five-photon ionization of argon atoms as a function of photon energy from a 30-cycle laser pulse of peak intensity 10^{13} W/cm^2 calculated by Guan et al. [431] compared with RMF calculations by van der Hart [933] (Fig. 6 from [431])

Chapter 11
Collisions with Molecules

So far in this monograph we have considered the collisions of electrons, positrons and photons with atoms and atomic ions. In this chapter we extend R-matrix theory to treat electron and positron collisions with molecules and we also consider an extension of R-matrix theory to treat molecular multiphoton processes. The processes that occur in electron–, positron– and photon–molecule collisions are considerably more varied and challenging than those that arise in electron collisions with atoms and atomic ions, partly because of the loss of spherical symmetry and partly because of the possibility of exciting degrees of freedom associated with the motion of the nuclei in the molecule. In this chapter we consider developments of both collision theory and R-matrix theory which enable these additional aspects of collision processes to be accurately treated.

We commence our discussion of electron–molecule collisions in Sect. 11.1.1 by reviewing the processes that occur in these collisions which, as well as excitation and ionization, considered in Chaps. 5 and 6, now include rotational and vibrational excitation, dissociative attachment and recombination, and dissociation including dissociative ionization. In Sect. 11.1.2 we introduce R-matrix theory of electron–molecule collisions by giving a detailed discussion of the fixed-nuclei approximation, where the electronic degrees of freedom are calculated in the molecular or body-fixed frame of reference. In Sect. 11.1.3 we consider methods for including molecular rotation, vibration and dissociation in the theory. First we consider the adiabatic-nuclei approximation, which is valid when the electron collision time is short compared with the rotation and vibration times, enabling scattering amplitudes for these transitions to be obtained from fixed-nuclei approximation results. This procedure owes its validity to the large ratio of the nuclear to the electronic mass, which is the basis of the Born–Oppenheimer separation of the electronic and nuclear motion made in molecular structure calculations. We then consider calculations carried out in the laboratory frame of reference, which involve solving the many coupled second-order integrodifferential equations describing rotational, vibrational and electronic motion. Finally we briefly review the frame-transformation theory of Chang and Fano [210], which takes advantage of the qualitative different features of the electron–target interaction as their relative distance changes and which has been influential in electron–atom as well as in electron–molecule collisions.

P.G. Burke, *R-Matrix Theory of Atomic Collisions*, Springer Series on Atomic, Optical, and Plasma Physics 61, DOI 10.1007/978-3-642-15931-2_11,

Also in this section, we compare the partitioning of configuration space in frame-transformation theory with that adopted in R-matrix theory. Then in Sect. 11.1.4 we describe non-adiabatic R-matrix theory of electron–molecule collisions, introduced by Schneider et al. [829], which enables dissociative processes as well as vibrational and electronic processes to be described in a unified theory. Next, in Sect. 11.1.5 we briefly describe a semi-phenomenological resonant R-matrix theory of electron–molecule collisions introduced by Fabrikant [293, 294]. We then conclude our discussion of electron–molecule collision theory in Sect. 11.1.6 by deriving expressions for electron–molecule scattering amplitudes and cross sections for diatomic and linear polyatomic molecules, which extend the corresponding derivations for electron collisions with atoms and ions given in Sect. 2.5. Finally, in Sect. 11.1.7 we present illustrative examples of electron–molecule collision calculations using non-adiabatic R-matrix theory and computer programs.

In Sect. 11.2 we extend our discussion of electron–molecule collisions to consider collisions of positrons with molecules. We observe that as well as processes which occur in the collision of electrons with molecules, we now have the possibility of positronium formation which we first considered in Chap. 7, where we discussed positron collisions with atoms and atomic ions. Hence, the additional complexity of using antisymmetrized wave functions in electron–molecule collisions is now replaced by the importance of correlation or polarization effects in the collision due to the strong attraction between the positron and the target electrons which gives rise to positronium formation. In Sect. 11.2.1 we consider the implications of these differences between electron– and positron–molecule collisions by discussing the most significant processes that can occur in positron–molecule collisions. We then summarize the advances that have been made in recent years in positron–molecule collision calculations commencing with simple studies of positron collisions with molecular hydrogen and nitrogen to recent studies of collisions with polyatomic molecules. Finally, in Sect. 11.2.2 we present illustrative examples of recent positron–molecule collision calculations which show the importance of polarization effects in low-energy positron collisions with non-polar molecules and we consider how these effects can be accurately included in future calculations.

In Sect. 11.3 we briefly consider an extension of our discussion of atomic multiphoton processes, considered in Chap. 9, to the interaction of intense laser fields with molecules using R-matrix–Floquet theory. As well as the additional complications due to loss of spherical symmetry and exciting degrees of freedom associated with the nuclear motion mentioned above, the laser field gives rise to new effects, for example, the modification of the nuclear potential energy curves by the laser field which gives rise to bond softening or hardening and the alignment of the molecular axis by the laser field which can play an important role in the dynamics of multiphoton processes. In Sect. 11.3.1 we describe developments made by Colgan et al. [187, 222–224] which extend R-matrix–Floquet theory to treat these processes. These developments have enabled the study of the interaction of intense laser fields with diatomic molecules using the fixed-nuclei approximation to be undertaken, providing an important first step to a full understanding of molecular multiphoton processes. Finally, in Sect. 11.3.2 we illustrate this theory by considering its

application to multiphoton ionization of H_2 in the fixed-nuclei approximation. Extensions of R-matrix theory and computer programs to include the nuclear motion using non-adiabatic R-matrix theory and to treat the interaction of ultra-short laser pulses with molecules, using an extension of time-dependent R-matrix theory discussed in Chap. 10, are now under active consideration.

11.1 Electron Collisions with Molecules

In this section we extend our treatment of electron collisions with atoms and atomic ions, considered in early chapters of this monograph, to electron collisions with molecules.

11.1.1 Introduction

We commence by briefly reviewing the processes that occur in electron–molecule collisions. As well as electronic excitation and ionization, which also occur in electron–atom collisions, additional processes that can now take place include rovibrational excitation

$$\mathrm{e}^- + AB_{jv} \rightarrow AB_{j'v'} + \mathrm{e}^-, \tag{11.1}$$

dissociative attachment and dissociative recombination

$$\mathrm{e}^- + AB_{jv} \rightarrow A + B^-, \tag{11.2}$$

$$\mathrm{e}^- + AB^+_{jv} \rightarrow A + B, \tag{11.3}$$

and dissociation and dissociative ionization

$$\mathrm{e}^- + AB_{jv} \rightarrow A + B + \mathrm{e}^-, \tag{11.4}$$

$$\mathrm{e}^- + AB_{jv} \rightarrow A + B^+ + 2\mathrm{e}^-. \tag{11.5}$$

In these equations AB_{jv} means that the molecule AB is in the jth rotational state and the vth vibrational state, where for notational simplicity we restrict our attention to diatomic molecules, although these processes will occur in electron collisions with polyatomic molecules.

A further complexity that arises in electron–molecule collisions is the multicentre and non-spherical nature of the collision process resulting in the need to solve much larger sets of coupled integrodifferential equations. The multicentre integrals that arise in the evaluation of the Hamiltonian matrix elements are also more difficult to calculate than the single-centre integrals that occur in electron–atom collisions.

There are two other distinctive features of electron–molecule collisions. The first is the crucial role that resonances play in vibrational excitation and in dissociative attachment and recombination. This is because when the scattered electron energy is near a resonance, this electron has a high probability of being captured into a resonant state where it can spend sufficient time in the neighbourhood of the molecule to transfer energy to the nuclear motion. The important role that resonances play in vibrational excitation was first examined theoretically by Herzenberg and Mandl [461] and experimentally by Schulz [834, 837], and early work was reviewed by Herzenberg [460] and more recent work by Hotop et al. [476]. The second feature is the distinctive nature of the long-range interaction potential between the scattered electron and the molecule. Thus for a linear neutral molecule, this potential has the asymptotic form

$$V(\mathbf{r}, \hat{\mathbf{R}}) = -\frac{\mu}{r^2} P_1(\cos\theta) - \frac{Q}{r^3} P_2(\cos\theta) - \frac{\alpha_0}{2r^4} - \frac{\alpha_2}{2r^4} P_2(\cos\theta), \tag{11.6}$$

plus higher order terms, where $\hat{\mathbf{R}}$ is the unit vector along the internuclear axis, $\mathbf{r}$ is the vector coordinate of the scattered electron referred to the centre of gravity of the molecule and θ is the angle between $\mathbf{r}$ and $\hat{\mathbf{R}}$. Also in (11.6) μ is the dipole moment, Q is the quadrupole moment and α_0 and α_2 are the polarizabilities of the molecule, which are given in terms of the polarizabilities $\alpha_\parallel$ and $\alpha_\perp$ along and perpendicular to the molecular axis by

$$\alpha_0 = \frac{1}{3}(\alpha_\parallel + 2\alpha_\perp), \quad \alpha_2 = \frac{2}{3}(\alpha_\parallel - \alpha_\perp). \tag{11.7}$$

For polar molecules, where μ is non-zero, the corresponding term in $V(\mathbf{r}, \hat{\mathbf{R}})$ dominates the differential cross section in the forward direction. Also, if μ is sufficiently large, as is the case for hydrogen halides, then this term in $V(\mathbf{r}, \hat{\mathbf{R}})$ gives rise to bound and virtual states in the electron–molecule system that lead to threshold peaks in the cross section first observed by Rohr and Linder [796]. Furthermore, the long-range nature of the quadrupole moment term Q and the polarization terms α_0 and α_2 in $V(\mathbf{r}, \hat{\mathbf{R}})$ often give rise to enhanced resonance effects at low incident electron energies. We conclude this section by noting that a review of these resonance and threshold effects in electron–molecule collisions has been written by Domcke [265].

11.1.2 Fixed-Nuclei R-Matrix Theory

The fixed-nuclei approximation was first used to describe low-energy electron collisions with diatomic molecules by Stier [890], Fisk [323] and Massey and Ridley [645]. In recent years it has been widely used as the basis of ab initio computational

methods that yield accurate cross sections for electron collisions with diatomic and polyatomic molecules. These methods include the complex Kohn variational method (Rescigno et al. [788]), the Schwinger variational method (Huo [483]) and the R-matrix method (e.g. Gillan et al. [373, 375], Tennyson and Morgan [920], Pfingst et al. [732, 733], Schneider [825], Burke and Tennyson [173] and Tennyson [917]).

The R-matrix method, first introduced to describe electron collisions with atoms and ions discussed in Chap. 5, was extended to treat electron collisions with diatomic molecules by Schneider [821, 822], Schneider and Hay [826] and Burke et al. [180]. In order to formulate the electron–molecule collision process in the fixed-nuclei approximation we adopt a frame of reference which is rigidly attached to the molecule, where the centre of gravity of the molecule is chosen as the origin of coordinates. In the case of diatomic molecules, which we will use as an example of the general case in the following discussion, we introduce a molecular fixed frame of reference where the z-axis is chosen to lie along the internuclear axis, as illustrated in Fig. 11.1. Also in this figure G is the centre of gravity of the two nuclei labelled A and B, which are fixed in space, $R = R_A + R_B$ is the distance between the nuclei and the vector distances between A, B and G and the ith electron are $\mathbf{r}_{Ai}$, $\mathbf{r}_{Bi}$ and $\mathbf{r}_i$, respectively. Finally, we assume the target molecule has N electrons and the nuclear charge numbers corresponding to A and B are Z_A and Z_B, respectively.

We consider first the collision process represented by the equation

$$\mathrm{e}^- + AB_i \rightarrow AB_j + \mathrm{e}^-, \tag{11.8}$$

where AB_i and AB_j are the initial and final electronic bound states of the target molecule. We assume that the target nuclei are light so that relativistic effects can be neglected for low-energy electron collisions. The collision process is then described by the time-independent Schrödinger equation

$$H_{N+1}\Psi = E\Psi, \tag{11.9}$$

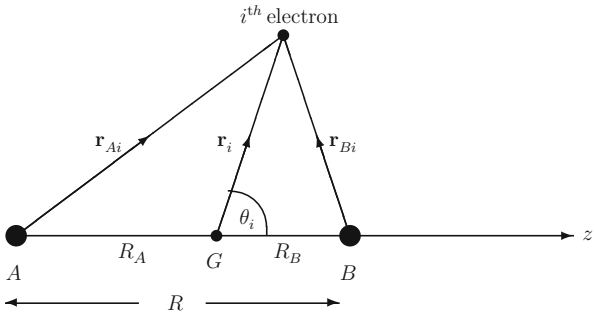

Fig. 11.1 Molecular frame of reference for electron collisions with diatomic molecules where the nuclei at A and B have nuclear charge numbers Z_A and Z_B, respectively, and G is the centre of gravity

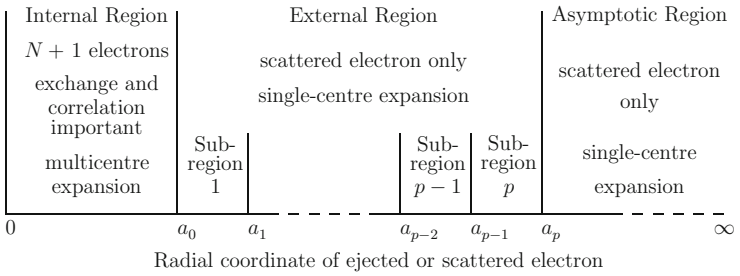

Fig. 11.2 Partitioning of configuration space in fixed-nuclei R-matrix theory of electron–molecule collisions

where H_{N+1} is the non-relativistic fixed-nuclei Hamiltonian defined in atomic units by

$$H_{N+1} = \sum_{i=1}^{N+1} \left(-\frac{1}{2}\nabla_i^2 - \frac{Z_A}{r_{Ai}} - \frac{Z_B}{r_{Bi}} \right) + \sum_{i>j=1}^{N+1} \frac{1}{r_{ij}} + \frac{Z_A Z_B}{R}. \tag{11.10}$$

In order to solve (11.9) using R-matrix theory we proceed, as in electron–atom collisions discussed in Chap. 5, by partitioning configuration space into an internal region, an external region and an asymptotic region as illustrated in Fig. 11.2. We now consider the solution in each of these regions in turn.

11.1.2.1 Internal Region Solution

In the internal region $0 \leq r \leq a_0$, where r is the radial coordinate of the scattered electron relative to the centre of gravity G of the target nuclei, electron exchange and electron–electron correlation effects between the scattered electron and the N target electrons are important and the $(N+1)$-electron collision complex behaves in a similar way to a bound state. Consequently a configuration interaction multicentre expansion of this complex, similar to that used for molecular bound-state calculations, is used for each internuclear separation R. In the case of diatomic molecules, a computer program using prolate spheroidal coordinates and Gaussian-type orbital (GTO) basis functions was first developed and used by Schneider [821, 822] and by Schneider and Hay [826]. Also, in more recent work a diatomic molecular computer program based on Slater-type orbitals (STOs) was developed and used by Buckley et al. [144], Kendrick and Buckley [528], Noble et al. [690], Gillan et al. [373, 375] and Morgan [660], and polyatomic computer programs using GTOs were developed and used by Nestmann and Peyerimhoff [680], Nestmann et al. [681, 682], Pfingst et al. [732, 733], Morgan et al. [661, 662], Tennyson and Morgan [920] and Faure et al. [313]. In this more recent work these orbitals are centred on the nuclei and are combined with continuum basis functions centred on the centre of gravity as discussed below. Finally, we note that a number of these computer programs have

been extended to enable electron–molecule collision calculations to be carried out using non-adiabatic R-matrix theory discussed in Sect. 11.1.4.

The solution of (11.9) in the internal region, which is analogous to that used to describe electron–atom collisions in Sect. 5.1.2, takes the following form:

$$\Psi_{jE}^{\Delta}(\mathbf{X}_{N+1};\, R) = \sum_{k} \psi_{k}^{\Delta}(\mathbf{X}_{N+1};\, R) A_{kj}^{\Delta}(E), \tag{11.11}$$

where, as in (5.5), j labels the linearly independent solutions of (11.9) at the energy E, ψ_k^{Δ} are energy-independent basis functions and $A_{kj}^{\Delta}(E)$ are energy-dependent expansion coefficients, which depend on the asymptotic boundary conditions satisfied by the wave function Ψ_{jE}^{Δ} at the energy E, as well as parametrically on R. As in Sect. 5.1.2 we expand the basis functions ψ_k^{Δ} as follows:

$$\begin{aligned}\psi_{k}^{\Delta}(\mathbf{X}_{N+1};\, R) = \mathcal{A} \sum_{i=1}^{n} \sum_{j=1}^{n_c} \overline{\Phi}_{i}^{\Delta}(\mathbf{X}_{N};\, \hat{\mathbf{r}}_{N+1}\sigma_{N+1}) r_{N+1}^{-1} u_{ij}^{0}(r_{N+1}) a_{ijk}^{\Delta} \\ + \sum_{i=1}^{m} \chi_{i}^{\Delta}(\mathbf{X}_{N+1}) b_{ik}^{\Delta}, \quad k = 1, \ldots, n_t,\end{aligned} \tag{11.12}$$

for each fixed internuclear separation R, where $n_t = nn_c + m$ is the number of linearly independent basis functions. The channel functions $\overline{\Phi}_i^{\Delta}$, the continuum orbitals u_{ij}^0 and the quadratically integrable functions χ_i^{Δ} depend parametrically on R and have the same meaning as the corresponding functions in expansion (5.6) in electron–atom collisions. Also Δ, which is discussed further when we consider scattering amplitudes and cross sections in Sect. 11.1.6, represents the quantum numbers which are conserved in the collision. Adopting this representation reduces to a minimum the number of coupled equations which have to be solved to obtain accurate results, and hence the complexity of the collision problem.

The channel functions $\overline{\Phi}_i^{\Delta}$ in (11.12) are formed by coupling the target physical states and possibly pseudostates Φ_i, including polarized pseudostates, to the angular and spin functions of the scattered electron, and the quadratically integrable functions χ_i^{Δ} are constructed from STOs or GTOs centred on the nuclei and possibly on the centre of gravity G. The radius a_0 is chosen so that these orbitals vanish by the boundary of the internal region $r = a_0$.

On the other hand the continuum basis orbitals u_{ij}^0 in (11.12), which represent the scattered electron, are non-vanishing on the boundary of the internal region $r = a_0$ and are used to construct the R-matrix linking the internal and external regions. In early work by Kendrick and Buckley [528] using the diatomic molecule program, these orbitals were formed from STOs centred on the centre of gravity G. However, difficulties have been experienced at higher incident electron energies due to linear dependence of these orbitals (Noble et al. [690]). Hence they are more

usually generated numerically as solutions of a zero-order second-order differential equation similar to that adopted in electron–atom collisions considered in Sect. 5.3.1 (Tennyson et al. [922]). In the case of the polyatomic molecule programs, representation of the continuum basis orbitals by GTOs centred on G has proved to be appropriate (e.g. Nestmann and Peyerimhoff [680] and Tennyson and Morgan [920]).

Finally, the coefficients a_{ijk}^{Δ} and b_{ik}^{Δ} in (11.12) are obtained by diagonalizing the operator $H_{N+1} + \mathcal{L}_{N+1}$ for fixed internuclear separation R in the basis ψ_k^{Δ} over the internal region as follows:

$$\langle \psi_k^{\Delta} | H_{N+1} + \mathcal{L}_{N+1} | \psi_{k'}^{\Delta} \rangle_{\text{int}} = E_k^{\Delta} \delta_{kk'}, \quad k,\ k' = 1, \ldots, n_t, \tag{11.13}$$

where $\mathcal{L}_{N+1}$ is the Bloch operator

$$\mathcal{L}_{N+1} = \sum_{i=1}^{N+1} \frac{1}{2} \delta(r_i - a_0) \left(\frac{\mathrm{d}}{\mathrm{d}r_i} - \frac{b_0 - 1}{r_i} \right), \tag{11.14}$$

where b_0 is an arbitrary constant. We can then show that $H_{N+1} + \mathcal{L}_{N+1}$ is hermitian in the basis of quadratically integrable functions satisfying arbitrary boundary conditions at $r = a_0$. We note that $\mathcal{L}_{N+1}$ has the same single-centre form as (5.8) used in electron–atom collisions since the only components of ψ_k^{Δ} which are non-zero on the boundary $r = a_0$ are the continuum basis orbitals centred on G. The Hamiltonian matrix elements in (11.13) involve the product of the number of target configurations multiplied by the number of continuum basis orbitals summed over the target states, which can present a major computational challenge when accurate results are required. To meet this challenge, an efficient algorithm has been developed by Tennyson [915], which has been incorporated into the UK molecular R-matrix computer programs and leads to a large reduction in both the number of integrals and matrix elements which need to be explicitly constructed and evaluated.

Equation (11.9) is solved in the internal region for each fixed internuclear separation R and for each set of conserved quantum numbers denoted by Δ, by rewriting it as follows:

$$(H_{N+1} + \mathcal{L}_{N+1} - E)\, \Psi_{jE}^{\Delta} = \mathcal{L}_{N+1} \Psi_{jE}^{\Delta}, \tag{11.15}$$

which has the formal solution

$$\Psi_{jE}^{\Delta} = (H_{N+1} + \mathcal{L}_{N+1} - E)^{-1}\, \mathcal{L}_{N+1} \Psi_{jE}^{\Delta}. \tag{11.16}$$

We expand the inverse operator in this equation in terms of the basis defined by (11.12) and (11.13), project this equation onto the channel functions $\overline{\Phi}_i^{\Delta}(\mathbf{X}_N; \hat{\mathbf{r}}_{N+1}\sigma_{N+1})$ and evaluate the result on the boundary of the internal region $r_{N+1} = a_0$. We then obtain

$$F_{ij}^{\Delta}(a_0) = \sum_{i'=1}^{n} R_{ii'}^{\Delta}(E) \left(a_0 \frac{\mathrm{d}F_{i'j}^{\Delta}}{\mathrm{d}r} - b_0 F_{i'j}^{\Delta} \right)_{r=a_0}, \quad i = 1, \ldots, n, \tag{11.17}$$

where the elements of the R-matrix $R_{ii'}^{\Delta}(E)$ at $r = a_0$ are defined by

$$R_{ii'}^{\Delta}(E) = \frac{1}{2a_0} \sum_{k=1}^{n_t} \frac{w_{ik}^{\Delta} w_{i'k}^{\Delta}}{E_k^{\Delta} - E}, \quad i,\ i' = 1, \ldots, n. \tag{11.18}$$

The reduced radial wave functions $F_{ij}^{\Delta}(r)$ in (11.17) are defined by

$$F_{ij}^{\Delta}(r_{N+1}) = \langle r_{N+1}^{-1} \overline{\Phi}_i^{\Delta} | \Psi_j^{\Delta} \rangle', \quad i = 1, \ldots, n, \tag{11.19}$$

and the surface amplitudes w_{ik}^{Δ} in (11.18) are defined by

$$\begin{aligned} w_{ik}^{\Delta} &= \langle r_{N+1}^{-1} \overline{\Phi}_i^{\Delta} | \psi_k^{\Delta} \rangle'_{r_{N+1}=a_0} \\ &= \sum_{j=1}^{n_c} u_{ij}^0(a_0) a_{ijk}^{\Delta}, \quad i = 1, \ldots, n, \quad k = 1, \ldots, n_t. \end{aligned} \tag{11.20}$$

The primes on the Dirac brackets in (11.19), (11.20) and later equations mean that the integrations are carried out over all $N+1$ electronic space and spin coordinates in the internal region except the radial coordinate r_{N+1} of the scattered electron. Equations (11.17), (11.18), (11.19) and (11.20) are identical in form to those obtained in Sect. 5.1.2 describing electron–atom collisions in the internal region. They are the basic equations which describe the collision of electrons with molecules in the internal region for fixed internuclear separation.

In concluding our discussion of the internal region solution we note that, as mentioned above in the case of diatomic molecules, the continuum basis orbitals u_{ij}^0 in (11.12) are often generated numerically as solutions of second-order differential equations subject to homogeneous boundary conditions at $r = 0$ and $r = a_0$. The fixed boundary condition at $r = a_0$ then results in slow convergence in the R-matrix expansion given by (11.18). Consequently we then have to add a Buttle correction

to the diagonal elements of the R-matrix and possibly to the wave function to obtain accurate results, as discussed in the case of electron collisions with atoms and ions in Sect. 5.3.2.

11.1.2.2 External Region Solution

In the external region, defined in Fig. 11.2, a_0 is chosen, as in electron–atom collisions discussed in Sect. 5.1.3, so that electron exchange and electron–electron correlation effects between the scattered electron and the target electrons can be neglected. The total wave function can then be expanded in the form

$$\Psi^{\Delta}_{jE}(\mathbf{X}_{N+1};\, R) = \sum_{i=1}^{n} \overline{\Phi}^{\Delta}_{i}(\mathbf{X}_N;\, \hat{\mathbf{r}}_{N+1}\sigma_{N+1}) r^{-1}_{N+1} F^{\Delta}_{ij}(r_{N+1}), \quad r_{N+1} \geq a_0. \tag{11.21}$$

In this expansion the multicentre channel functions $\overline{\Phi}^{\Delta}_{i}$ are the same as those retained in the internal region expansion (11.12). However we no longer include the antisymmetrization operator, since the scattered electron and the target electrons occupy different regions of space. Also, the multicentre quadratically integrable functions χ^{Δ}_{i} vanish in the external region and the scattered electron is represented by the single-centre reduced radial functions $F^{\Delta}_{ij}(r)$.

Substituting (11.21) into the Schrödinger equation (11.9) and projecting onto the channel functions $\overline{\Phi}^{\Delta}_{i}$ then yields the following set of coupled second-order differential equations satisfied by the reduced radial functions:

$$\left(\frac{\mathrm{d}^2}{\mathrm{d}r^2} - \frac{\ell_i(\ell_i+1)}{r^2} + \frac{2(Z_A + Z_B - N)}{r} + k_i^2\right) F^{\Delta}_{ij}(r)$$

$$= 2\sum_{i'=1}^{n} V^{\Delta}_{ii'}(r) F^{\Delta}_{i'j}(r), \quad i = 1, \ldots, n, \quad r \geq a_0. \tag{11.22}$$

In these equations ℓ_i is the orbital angular momentum of the scattered electron in the ith channel and

$$k_i^2 = 2(E - \overline{e}_i), \quad i = 1, \ldots, n, \tag{11.23}$$

where the channel energies $\overline{e}_i$ are defined by

$$\overline{e}_i = \langle r^{-1}_{N+1} \overline{\Phi}^{\Delta}_{i}(\mathbf{X}_N;\, \hat{\mathbf{r}}_{N+1}\sigma_{N+1}) | H_N | r^{-1}_{N+1} \overline{\Phi}^{\Delta}_{i}(\mathbf{X}_N;\, \hat{\mathbf{r}}_{N+1}\sigma_{N+1}) \rangle, \quad i = 1, \ldots, n, \tag{11.24}$$

H_N being the target molecule Hamiltonian. Also the potential matrix $V^{\Delta}_{ii'}$ in (11.22) is defined by

$$V_{ii'}^{\Delta}(r_{N+1}) = \Bigg\langle r_{N+1}^{-1}\overline{\Phi}_i^{\Delta}(\mathbf{X}_N;\hat{\mathbf{r}}_{N+1}\sigma_{N+1}) \times \left|\sum_{k=1}^{N}\frac{1}{r_{kN+1}} - \frac{Z_A}{r_{AN+1}} - \frac{Z_B}{r_{BN+1}} + \frac{Z_A+Z_B-N}{r_{N+1}}\right| \times r_{N+1}^{-1}\overline{\Phi}_{i'}^{\Delta}(\mathbf{X}_N;\hat{\mathbf{r}}_{N+1}\sigma_{N+1})\Bigg\rangle', \quad i,\ i' = 1,\ldots,n. \tag{11.25}$$

As in electron–atom collisions $V_{ii'}^{\Delta}(r)$ can be written as a summation over inverse powers of r as follows:

$$V_{ii'}^{\Delta}(r) = \sum_{\lambda=1}^{\infty}\alpha_{ii'\lambda}^{\Delta}r^{-\lambda-1}, \quad i,\ i' = 1,\ldots,n, \quad r \geq a_0, \tag{11.26}$$

where the long-range potential coefficients $\alpha_{ii'\lambda}^{\Delta}$ can be determined by carrying out the multicentre integrals in (11.25) and where, in general, only the first few terms in the expansion over λ play a significant role in the collision in the external and asymptotic regions.

The long-range interaction potentials in (11.6) are defined in terms of the coefficients $\alpha_{ii'\lambda}^{\Delta}$ in (11.26). Thus the dipole moment μ and the quadrupole moment Q are defined in terms of the diagonal elements α_{ii1}^{Δ} and α_{ii2}^{Δ}, respectively, while the polarization terms α_0 and α_2 are given by a second-order summation over intermediate states involving the dipole terms $\alpha_{ii'1}^{\Delta}$. The inclusion of polarized pseudostates in expansions (11.12) and (11.21), which represent the target continuum, is usually necessary in order to obtain an accurate representation of the polarizability. Alternatively, a procedure for including the effect of polarization in the external region, suggested by Nesbet et al. [679], can be used, where the long-range polarization and quadrupole moment terms in (11.6) are explicitly included in the external region propagation. The importance of the continuum contribution to the polarizability was first discussed by Castillejo et al. [205] in the case of electron collisions with atomic hydrogen and is considered in Sects. 2.2.2 and 6.2.

The solution of (11.22) can be obtained, as in electron–atom collisions, by propagating the R-matrix across the p sub-regions illustrated in Fig. 11.2 using one of the propagator methods discussed in Appendix E. Given the R-matrix at $r = a_0$ defined by (11.18), the R-matrix at $r = a_p$ can be obtained, providing the boundary condition for the solution in the asymptotic region.

11.1.2.3 Asymptotic Region Solution

The solution in the asymptotic region, defined in Fig. 11.2, proceeds as in electron–atom collisions considered in Sect. 5.1.4, using an asymptotic expansion solution of (11.22) as discussed in Appendix F.1. A solution matrix, satisfying the asymptotic boundary conditions

$$\mathbf{F}^{\Delta}(r) \underset{r\to\infty}{\sim} \mathbf{k}^{-1/2}\left[\sin\boldsymbol{\theta} + \cos\boldsymbol{\theta}\mathbf{K}^{\Delta}\right], \tag{11.27}$$

is obtained in the open channels ($k_i^2 \geq 0$), where $\boldsymbol{\theta}$ is a diagonal matrix with diagonal elements

$$\theta_i = k_i r - \frac{1}{2}\ell_i\pi - \eta_i \ln 2k_i r + \sigma_{\ell_i}, \tag{11.28}$$

with

$$\eta_i = -\frac{Z_A + Z_B - N}{k_i} \tag{11.29}$$

and

$$\sigma_{\ell_i} = \arg\Gamma(\ell_i + 1 + \mathrm{i}\eta_i). \tag{11.30}$$

In this way the $n_a \times n_a$-dimensional K-matrix $\mathbf{K}^{\Delta}$ is determined in terms of the $n \times n$-dimensional R-matrix at $r = a_p$, where n_a is the number of open channels at the incident electron energy under consideration.

In our discussion of the scattering amplitude and cross section in Sect. 11.1.6, we also find it convenient to define a solution matrix satisfying the asymptotic boundary conditions

$$\mathbf{G}^{\Delta}(r) \underset{r\to\infty}{\sim} \mathbf{k}^{-1/2}\left[\exp(-\mathrm{i}\boldsymbol{\theta}) - \exp(\mathrm{i}\boldsymbol{\theta})\mathbf{S}^{\Delta}\right], \tag{11.31}$$

which can be obtained by taking linear combinations of the solutions defined by (11.27). The $n_a \times n_a$-dimensional S-matrix $\mathbf{S}^{\Delta}$ in (11.31) is defined in terms of the K-matrix by the matrix equation

$$\mathbf{S}^{\Delta} = \frac{\mathbf{I} + \mathrm{i}\mathbf{K}^{\Delta}}{\mathbf{I} - \mathrm{i}\mathbf{K}^{\Delta}}. \tag{11.32}$$

The cross section in the molecular fixed frame can be expressed in terms of the S-matrix as described in Sect. 11.1.6.

11.1.3 Inclusion of Nuclear Motion

In this and the following section we review the theory of electron–molecule collision processes which involve the nuclear motion. In particular, we are interested in rotational and vibrational excitation and dissociative processes, defined by (11.1), (11.2), (11.3), (11.4) and (11.5). In this section we present a brief overview of these theoretical methods including a discussion of frame-transformation theory,

reserving a detailed discussion of non-adiabatic R-matrix theory of nuclear motion to Sect. 11.1.4.

11.1.3.1 Adiabatic-Nuclei Approximation

One of the most widely used approaches for including the nuclear motion is the adiabatic-nuclei approximation which was introduced by Drozdov [270, 271] and Chase [217] in studies of neutron scattering by nuclei. In the case of diatomic molecules in a $^1\Sigma$ state the scattering amplitude for a transition between electronic, vibrational and rotational states defined by the quantum numbers $ivjm_j$ and $i'v'j'm_{j'}$ is given by

$$f_{i'v'j'm_{j'},ivjm_j}(\mathbf{k}\cdot\hat{\mathbf{r}}) = \langle \eta_{i'v'}(R)Y_{j'm_{j'}}(\theta_R,\phi_R)|f_{i'i}(\theta,\phi)| \times \eta_{iv}(R)Y_{jm_j}(\theta_R,\phi_R)\rangle, \tag{11.33}$$

where $f_{i'i}(\theta,\phi)$ is the fixed-nuclei scattering amplitude for an electronic transition from state i to state i', calculated in the laboratory frame as described in Sect. 11.1.2, which depends parametrically on the inter-nuclear coordinate R, and η_{iv} and Y_{jm_j} are the molecular vibrational and rotational eigenfunctions, respectively. This approximation is valid provided that the collision time is short compared with the vibration and rotation times. Hence it can be accurately applied in non-resonant regions or at higher energies which are not close to threshold.

11.1.3.2 Laboratory Frame of Reference

The adiabatic-nuclei approximation breaks down in the neighbourhood of narrow resonances or close to thresholds (e.g. Morrison [663]). This is because, as pointed out in Sect. 11.1.1, the scattered electron then spends an appreciable time in the neighbourhood of the molecule increasing the probability of its transferring energy to the nuclear motion. One procedure for overcoming this difficulty is to carry out the calculation in the laboratory frame of reference including the nuclear motion explicitly. The time-independent Schrödinger equation (11.9) is then replaced by

$$(H_{N+1} + T_{\mathbf{R}})\Psi(\mathbf{X}_{N+1};\mathbf{R}) = E\Psi(\mathbf{X}_{N+1};\mathbf{R}), \tag{11.34}$$

where H_{N+1} is the fixed-nuclei Hamiltonian, $T_{\mathbf{R}}$ is the kinetic energy operator of nuclear motion, which includes both rotational and vibrational terms, and $\mathbf{R}$ represents the radial and angular coordinates of the internuclear motion of the target molecule.

We now briefly review the derivation of the coupled second-order differential equations corresponding to (11.34) which yield scattering amplitudes and cross sections for transitions between rotational and vibrational states as well as electronic states of the target molecule. Following our discussion of the derivation of the close

coupling equations describing electron–atom collisions in Sect. 2.3.2, we expand the total wave function satisfying (11.34) as follows:

$$\Psi^{\Upsilon}_{jE}(\mathbf{X}_{N+1};\mathbf{R}) = \mathcal{A}\sum_{p=1}^{s}\overline{\Theta}^{\Upsilon}_{p}(\mathbf{X}_{N+1};\hat{\mathbf{r}}_{N+1}\sigma_{N+1};\mathbf{R})r^{-1}_{N+1}F^{\Upsilon}_{pj}(r_{N+1}) + \sum_{p=1}^{t}\eta^{\Upsilon}_{p}(\mathbf{X}_{N+1};\mathbf{R})b^{\Upsilon}_{pj}, \tag{11.35}$$

where j labels the linearly independent solutions of (11.34) at the energy E. Also, the channel functions $\overline{\Theta}^{\Upsilon}_{p}$ and the quadratically integrable functions η^{Υ}_{p} in (11.35) are formed by coupling the corresponding electronic wave functions in the fixed-nuclei expansion (11.12) to the rotational and vibrational states of the target molecule to yield functions which belong to the generalized conserved quantum numbers represented by Υ. It follows that the summation p in (11.35) now goes over the rotational and vibrational states of the molecule as well as over the electronic states.

We obtain coupled second-order integrodifferential equations satisfied by the reduced radial wave functions F^{Υ}_{pj} describing the radial motion of the scattered electron in expansion (11.35), by substituting this expansion into (11.34) and projecting onto the channel functions $\overline{\Theta}^{\Upsilon}_{p}$ and onto the quadratically integrable functions η^{Υ}_{p}. After eliminating the coefficients b^{Υ}_{pj} these equations take the general form

$$\left(\frac{\mathrm{d}^2}{\mathrm{d}r^2}+k^2_p\right)F^{\Upsilon}_{pj}(r) = 2\sum_{q=1}^{s}\left(V^{\Upsilon}_{pq}+W^{\Upsilon}_{pq}+X^{\Upsilon}_{pq}\right)F^{\Upsilon}_{qj}(r), \quad p=1,\ldots,s, \tag{11.36}$$

where V^{Υ}_{pq}, W^{Υ}_{pq} and X^{Υ}_{pq} are local, non-local exchange and non-local correlation potentials, respectively, and where we have included the diagonal angular momentum and nuclear Coulomb terms in V^{Υ}_{pq} for notational simplicity. We see that these equations are similar in form to the close coupling equations (2.63) describing electron–atom collisions although, of course, the inclusion of the summations over the ro-vibrational quantum numbers greatly increases the number of coupled channels.

Coupled equations of this type have been studied by many workers. For example, Arthurs and Dalgarno [26] first obtained coupled equations describing the scattering of an electron by a rigid rotator which have been widely applied. Also, Chandra and Temkin [207, 208] used a hybrid theory in a study of electron collisions with N_2 molecules in the neighbourhood of the low-energy $^2\Pi_g$ resonance, which included a summation over vibrational states in (11.35) but which treated the rotational motion adiabatically. However, in general, the number of channels that have to be included in (11.35) using this approach becomes prohibitively large for polyatomic molecules

when ro-vibrational as well as electronic channels are included in the expansion of the wave function.

11.1.3.3 Frame-Transformation Theory

We now briefly review the frame-transformation theory of Chang and Fano [210] and we consider its relation to R-matrix theory. Frame-transformation theory, which has clarified the role of nuclear motion effects in electron–molecule collisions, has also been influential in the theory of electron–atom collisions. Following early work by Fano [303], who considered the extension of the quantum defect theory of Seaton [859] to molecular photoabsorption discussed in Sect. 3.3.4, Chang and Fano pointed out that the electron–molecule interaction exhibits qualitatively different physical features when the radial distance r of the scattered electron from the centre of gravity of the molecule lies in different regions. This enables different analytic and computational procedures to be adopted in these different regions, in analogy with the different computational procedures adopted in different regions of configuration space in R-matrix theory.

We illustrate the main features adopted in the partitioning of configuration space in frame-transformation theory in Fig. 11.3a where we compare it with the partitioning of configuration space adopted in R-matrix theory in Fig. 11.3b. We see in Fig. 11.3a that if the vibrational motion of the nuclei is not considered in frame-transformation theory, configuration space is sub-divided into two regions A and B. In region A, where $r \leq b_2$, the molecular frame of reference can be used to describe the collision and the $(N + 1)$-electron collision complex can be described as in molecular bound-state calculations. At larger distances in region B, where $r > b_2$, the coupling of the scattered electron to the molecular axis no longer dominates and the laboratory frame of reference should be used. However, if the vibrational motion is considered, region A must be partitioned into two sub-regions Aa and Ab. In sub-region Aa, where $r \leq b_1$, the scattered electron spends only a short time compared with the vibration time so that the Born–Oppenheimer approximation separation of the nuclear and electronic motion is appropriate and the problem can be solved as a function of the internuclear separation. On the other hand in region Ab where $b_1 \leq r < b_2$, the vibrational motion must be included non-adiabatically, particularly in the description of collisions at energies in the neighbourhood of narrow resonances or close to thresholds.

We now consider the partitioning of configuration space adopted in R-matrix theory shown in Fig. 11.3b and also in more detail in Fig. 11.2. We see that in R-matrix theory partitioning of configuration space is determined by the need to include electron–electron exchange and correlation effects in the internal region $r \leq a_0$, where the scattered electron penetrates the electronic cloud corresponding to the molecular target states of interest. An antisymmetrized multicentre configuration interaction expansion of the total electron–molecule wave function in the molecular frame of reference is adopted in this region. However, when $r > a_0$, the scattered electron lies outside the target electronic cloud and moves in the long-range multipole potential of the residual molecule including polarization terms which can be

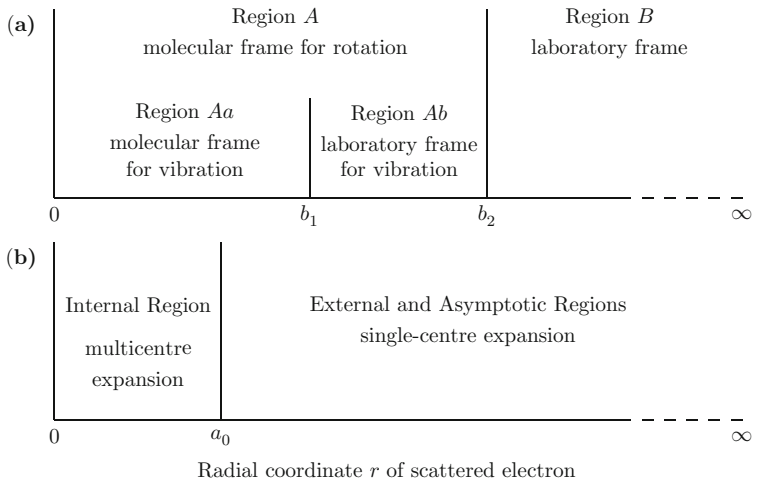

Fig. 11.3 Partitioning of configuration space in electron–molecule collisions as a function of the radial coordinate r of the scattered electron: (**a**) in frame-transformation theory, (**b**) in R-matrix theory

conveniently represented by a single-centre expansion. If rotational and vibrational motion of the molecule is being considered, then a transformation from the molecular frame of reference to the laboratory frame of reference is applied to the single-centre wave function at $r = a_0$, as required in frame-transformation theory discussed above. However, although a_0 is shown to be less than b_1 in Fig. 11.3 this may not be the case when electron collisions with excited molecular states are considered. In this case a_0 may need to be greater than b_1 in order to include electron exchange and correlation effects arising from the long-range tail of the excited state wave functions. In this case, since the representation of electron exchange by the usual antisymmetrized wave function requires that the whole of the internal region is treated uniformly, then the vibrational motion must be included explicitly in the whole of the internal region $r \leq a_0$, as discussed in our treatment of non-adiabatic R-matrix theory in Sect. 11.1.4.

Finally we note that frame-transformation theory must be extended to enable dissociative processes as well as rotational, vibrational and electronic processes to be calculated. In this case, as well as including the dependence on the radial coordinate r of the scattered electron it is also necessary to consider the dependence on the internuclear coordinate of the dissociating atoms. We consider this additional degree of freedom when we describe non-adiabatic R-matrix theory of electron–molecule collisions in Sect. 11.1.4.

11.1.4 Non-adiabatic R-Matrix Theory

In this section we describe non-adiabatic R-matrix theory of electron–molecule collisions, introduced by Schneider et al. [829] and generalized by Gillan et al. [373],

which enables dissociative processes as well as vibrational and electronic excitation processes to be calculated. In the case of diatomic molecules or molecular ions this theory enables the following processes to be studied:

$$\begin{aligned} \mathrm{e}^- + AB_{iv} &\rightarrow AB_{iv} + \mathrm{e}^- && \text{elastic scattering} \\ &\rightarrow AB_{i'v'} + \mathrm{e}^- && \text{vibrational and electronic excitation} \\ &\rightarrow A_{i'} + B_{i'}^- && \text{dissociative attachment/recombination} \\ &\rightarrow A_{i''} + B_{i''} + \mathrm{e}^- && \text{dissociation,} \end{aligned} \tag{11.37}$$

where i, i' and i'' label the electronic states of the molecule and dissociating atoms or ions and v and v' label the vibrational states of the molecule. We have not included the rotational quantum number j in (11.37) since rotational transitions can usually be included adiabatically as discussed in Sect. 11.1.3.

In non-adiabatic R-matrix theory we solve the following time-independent Schrödinger equation:

$$(H_{N+1} + T_R)\Psi(\mathbf{X}_{N+1}; R) = E\Psi(\mathbf{X}_{N+1}; R), \tag{11.38}$$

where the molecular frame of reference adopted for electron collisions with diatomic molecules is illustrated in Fig. 11.1. In (11.38), $\Psi(\mathbf{X}_{N+1}; R)$ is the total wave function describing the processes defined by (11.37), H_{N+1} is the fixed-nuclei Hamiltonian defined by (11.10) and T_R is the nuclear kinetic energy operator which is approximated by

$$T_R = -\frac{1}{2\mu}\frac{\mathrm{d}^2}{\mathrm{d}R^2}, \tag{11.39}$$

where μ is the reduced mass of the two nuclei and R is the internuclear separation. Also, the z-axis is chosen to lie along the internuclear axis, or along an axis of symmetry in the case of polyatomic molecules, where we assume that the molecule does not rotate appreciably during the collision.

In order to solve the Schrödinger equation (11.38) we partition configuration space into internal, external and asymptotic regions as illustrated in Fig. 11.4, which we see is analogous to the partitioning of configuration space in positron–atom collisions including positronium formation, given in Fig. 7.2.

In the internal region in Fig. 11.4 where $0 \leq r \leq a_0$ and $A_{\mathrm{in}} \leq R \leq A_0$ all the particles are strongly interacting. The electron–molecule complex can then dissociate either into electron–molecule collision channels, where the molecule can be vibrationally or electronically excited, or into an atom and a negative ion or into two atoms, corresponding to dissociative attachment/recombination or dissociation channels. The radius $r = a_0$ is chosen so that the electronic states of the target molecule of interest have negligible amplitudes for $r \geq a_0$. The inner radius $R = A_{\mathrm{in}}$ is chosen to exclude the nuclear Coulomb repulsion singularity at $R = 0$,

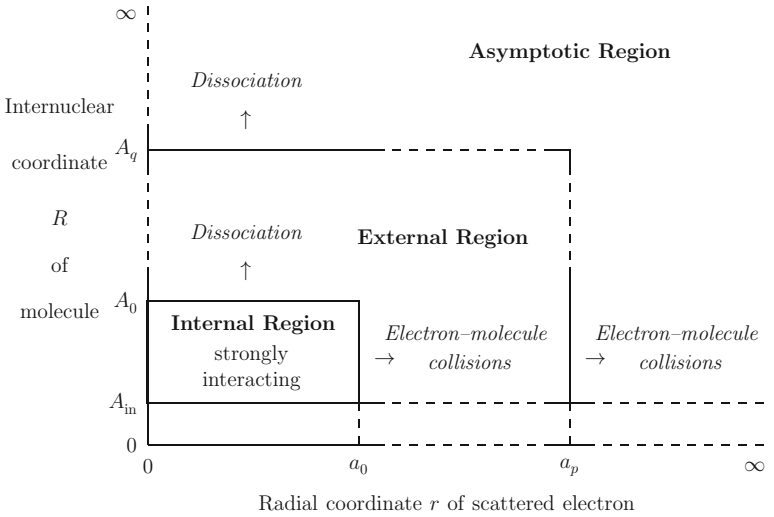

Fig. 11.4 Partitioning of configuration space in non-adiabatic R-matrix theory of electron–molecule collisions leading to molecular vibrational and electronic excitation and to dissociative attachment or dissociative recombination

where the wave function describing the molecular nuclear motion is negligible. Finally, the radius $R = A_0$ is chosen so that the target vibrational states of interest have negligible amplitude for $R \geq A_0$. In the external region corresponding to electron–molecule collisions, where $a_0 \leq r \leq a_p$, the scattered electron moves in the long-range potential of the residual molecule, and in the external region corresponding to dissociation, where $A_0 \leq R \leq A_q$, the dissociating atoms or ions move in the long-range multipole potential interaction between them. In these regions the potential interactions between the scattered particles are strong and must be treated by solving the resultant differential equations using accurate numerical propagation methods. Finally, in the asymptotic regions where for electron–molecule collisions $r \geq a_p$ and for atom–atom or atom–ion collisions $R \geq A_q$, the solutions can be obtained using asymptotic expansions which enable the K-matrix and S-matrix to be determined. We now consider the solutions in the internal, external and asymptotic regions in turn.

11.1.4.1 Internal Region Solution

The solution of (11.38) in the internal region in Fig. 11.4 can be written in analogy with (11.11) as follows:

$$\Psi_{jE}^{\Delta}(\mathbf{X}_{N+1}; R) = \sum_k \Theta_k^{\Delta}(\mathbf{X}_{N+1}; R) A_{kj}^{\Delta}(E), \tag{11.40}$$

where j labels the linearly independent solutions of (11.38) at the energy E, Θ_k^{Δ} are energy-independent basis functions and $A_{kj}^{\Delta}(E)$ are energy-dependent expansion coefficients, which depend on the asymptotic boundary conditions satisfied by the wave function Ψ_{jE}^{Δ} at the energy E. We now expand the basis functions in the internal region as follows:

$$\Theta_k^{\Delta}(\mathbf{X}_{N+1};\, R) = \sum_{is} \psi_i^{\Delta}(\mathbf{X}_{N+1};\, R)\zeta_s(R)c_{isk}^{\Delta}, \tag{11.41}$$

where the ψ_i^{Δ} are the fixed-nuclei R-matrix electronic basis functions defined by (11.12) and (11.13), which are solved over a mesh of fixed internuclear separations R spanning the range $A_{\text{in}} \leq R \leq A_0$ in Fig. 11.4, and the $\zeta_s(R)$ are linearly independent basis functions representing the nuclear motion, which are members of a complete set over this range. In practice shifted Legendre polynomials are often used to represent this basis.

The next step in determining the solution of (11.38) in the internal region is to diagonalize the operator $H_{N+1} + T_R + \mathcal{L}_{N+1} + \mathcal{L}_R$ in the basis (11.41), where the Bloch operators $\mathcal{L}_{N+1}$ and $\mathcal{L}_R$ are introduced so that $H_{N+1} + T_R + \mathcal{L}_{N+1} + \mathcal{L}_R$ is hermitian in a basis of quadratically integrable functions defined over the internal region and satisfying arbitrary boundary conditions on the boundaries of this region. We have already defined $\mathcal{L}_{N+1}$ by (11.14) such that $H_{N+1} + \mathcal{L}_{N+1}$ is hermitian for fixed internuclear separation R. The Bloch operator $\mathcal{L}_R$, which is defined by

$$\mathcal{L}_R = \frac{1}{2\mu}\left[\delta(R - A_0)\left(\frac{\mathrm{d}}{\mathrm{d}R} - \frac{B_0}{R}\right) - \delta(R - A_{\text{in}})\left(\frac{\mathrm{d}}{\mathrm{d}R} - \frac{B_{\text{in}}}{R}\right)\right], \tag{11.42}$$

where B_0 and B_{in} are arbitrary constants, is such that $T_R + \mathcal{L}_R$ is hermitian over the range $A_{\text{in}} \leq R \leq A_0$. It follows that $H_{N+1} + T_R + \mathcal{L}_{N+1} + \mathcal{L}_R$ satisfies the required hermitian property.

In diagonalizing the operator $H_{N+1} + T_R + \mathcal{L}_{N+1} + \mathcal{L}_R$ in the basis (11.41) we assume, in accordance with the Born–Oppenheimer (BO) approximation, that the contributions from the nuclear kinetic energy operator T_R acting on the electronic basis functions ψ_i^{Δ} are small and can be neglected. This assumption can be understood, following the discussion by Schneider [823], by observing that while the adiabatic-nuclei approximation breaks down for low-energy electron collisions, which led to the hybrid theory of Chandra and Temkin [207, 208] discussed in Sect. 11.1.3.2, the electronic and vibrational degrees of freedom of the compound $(N+1)$-electron system can still be separated as in the BO approximation. The appropriate expansion of the total wave function for the BO approximation to be valid is thus given in terms of electronic states of the compound $(N + 1)$-electron system. In R-matrix theory these compound states are the fixed-nuclei $(N + 1)$-electronic basis functions ψ_i^{Δ} in expansion (11.41). Hence, using the BO approximation we can write

$$\begin{aligned}
&\langle \Theta_k^{\Delta} | H_{N+1} + T_R + \mathcal{L}_{N+1} + \mathcal{L}_R | \Theta_{k'}^{\Delta} \rangle_{\text{int}} \\
&= \sum_{is} \sum_{i's'} \langle \psi_i^{\Delta} \zeta_s | H_{N+1} + T_R + \mathcal{L}_{N+1} + \mathcal{L}_R | \psi_{i'}^{\Delta} \zeta_{s'} \rangle_{\text{int}} \, c_{isk}^{\Delta} \, c_{i's'k'}^{\Delta} \\
&= \langle \xi_{it}^{\Delta} | T_R + E_i^{\Delta}(R) + \mathcal{L}_R | \xi_{i't'}^{\Delta} \rangle_{\text{int}} \, \delta_{ii'} \\
&= \epsilon_{it}^{\Delta} \, \delta_{ii'} \, \delta_{tt'}, \qquad (11.43)
\end{aligned}$$

where we have used (11.13), remembering that the energy E_k^{Δ} in (11.13) is now a function of the internuclear separation R. Also in (11.43) we have introduced the vibrational functions ξ_{it}^{Δ}, representing the nuclear motion in the ith electronic state ψ_i^{Δ}, which are determined by diagonalizing the operator $T_R + E_i^{\Delta}(R) + \mathcal{L}_R$ for each ith electronic state in the zero-order basis ζ_s. Hence we have written

$$\xi_{it}^{\Delta}(R) = \sum_s \zeta_s(R) c_{isk}^{\Delta}, \qquad (11.44)$$

where the subscript t goes over the range 1 to n_v for each i, where n_v is the number of zero-order basis functions ζ_s retained in expansion (11.41). Hence for a given i, the subscripts t and k in (11.44) are related by

$$t = k - (i-1) n_v. \qquad (11.45)$$

Equation (11.38) can now be solved in the internal region for each set of conserved quantum numbers Δ by rewriting it as follows:

$$(H_{N+1} + T_R + \mathcal{L}_{N+1} + \mathcal{L}_R - E) \Psi_{jE}^{\Delta} = (\mathcal{L}_{N+1} + \mathcal{L}_R) \Psi_{jE}^{\Delta}, \qquad (11.46)$$

which has the formal solution

$$\Psi_{jE}^{\Delta} = (H_{N+1} + T_R + \mathcal{L}_{N+1} + \mathcal{L}_R - E)^{-1} (\mathcal{L}_{N+1} + \mathcal{L}_R) \Psi_{jE}^{\Delta}, \qquad (11.47)$$

where, using (11.41) and (11.43), the inverse operator in (11.47) can be written as

$$(H_{N+1} + T_R + \mathcal{L}_{N+1} + \mathcal{L}_R - E)^{-1} = \sum_{it} \frac{|\psi_i^{\Delta} \, \xi_{it}^{\Delta}\rangle \langle \psi_i^{\Delta} \, \xi_{it}^{\Delta}|}{\epsilon_{it}^{\Delta} - E}. \qquad (11.48)$$

Also we introduce the channel functions θ_{iv}^{Δ} corresponding to vibrational and electronic excitation in (11.37) defined by

$$\theta_{iv}^{\Delta}(\mathbf{X}_N; \hat{\mathbf{r}}_{N+1} \sigma_{N+1}; R) = \overline{\Phi}_i^{\Delta}(\mathbf{X}_N; \hat{\mathbf{r}}_{N+1} \sigma_{N+1}) \eta_{iv}(R) \qquad (11.49)$$

and the channel functions corresponding to dissociative attachment and dissociative recombination in (11.37) defined by

$$\phi_i^{\Delta}(\mathbf{X}_{N+1}) = \left[\psi_{A_{i'}}(\mathbf{X}_A) \otimes \psi_{B_{i''}}(\mathbf{X}_B)\right]_i^{\Delta}. \tag{11.50}$$

In (11.49) $\overline{\Phi}_i^{\Delta}$ are the fixed-nuclei channel functions introduced in (11.12), which depend parametrically on the internuclear separation R, and η_{iv} are vibrational wave functions for the molecule in the ith electronic state. Also in (11.50), $\psi_{A_{i'}}$ and $\psi_{B_{i''}}$ are wave functions of the dissociating atoms or ions A and B, with electronic space and spin coordinates denoted by $\mathbf{X}_A$ and $\mathbf{X}_B$, respectively, which are coupled to give eigenstates labelled i, belonging to the conserved quantum numbers Δ. Dissociation in (11.37) can be represented in this theory by including additional pseudostate channel functions θ_{iv}^{Δ}, defined by (11.49), representing the vibrational continuum spectrum of AB_{iv}, in analogy with our treatment of ionization in Sect. 6.2.

We can then determine the R-matrix on the boundaries of the internal region in Fig. 11.4 by substituting the representation for $(H_{N+1} + T_R + \mathcal{L}_{N+1} + \mathcal{L}_R - E)^{-1}$ given by (11.48) into (11.47), projecting onto the channel functions θ_{iv}^{Δ} and ϕ_i^{Δ} and evaluating the projected equations at $r = a_0$ and $R = A_0$. We obtain

$$\begin{aligned} F_{ivj}^{\Delta}(a_0) = &\sum_{i'v'} R_{ivi'v'}^{\Delta}(E) \left(a_0 \frac{\mathrm{d}F_{i'v'j}^{\Delta}}{\mathrm{d}r} - b_0 F_{i'v'j}^{\Delta} \right)_{r=a_0} \\ &+ \sum_{i'} R_{ivi'}^{\Delta}(E) \left(A_0 \frac{\mathrm{d}G_{i'j}^{\Delta}}{\mathrm{d}R} - B_0 G_{i'j}^{\Delta} \right)_{R=A_0} \end{aligned} \tag{11.51}$$

and

$$\begin{aligned} G_{ij}^{\Delta}(A_0) = &\sum_{i'v'} R_{ii'v'}^{\Delta}(E) \left(a_0 \frac{\mathrm{d}F_{i'v'j}^{\Delta}}{\mathrm{d}r} - b_0 F_{i'v'j}^{\Delta} \right)_{r=a_0} \\ &+ \sum_{i'} R_{ii'}^{\Delta}(E) \left(A_0 \frac{\mathrm{d}G_{i'j}^{\Delta}}{\mathrm{d}R} - B_0 G_{i'j}^{\Delta} \right)_{R=A_0}, \end{aligned} \tag{11.52}$$

where the second term in the Bloch operator $\mathcal{L}_R$ defined by (11.42) does not contribute since A_{in} is chosen so that the wave functions describing the vibrational motion of the nuclei and their derivatives are negligibly small for $R \leq A_{\mathrm{in}}$.

The reduced radial wave functions $F_{ivj}^{\Delta}(r)$ in (11.51) and (11.52) are obtained by projecting the total wave function $\Psi_{jE}^{\Delta}(\mathbf{X}_{N+1}; R)$ onto the channel functions defined by (11.49) as follows:

$$F_{ivj}^{\Delta}(r_{N+1}) = \langle r_{N+1}^{-1} \theta_{iv}^{\Delta}(\mathbf{X}_N; \hat{\mathbf{r}}_{N+1}\sigma_{N+1}; R) | \Psi_{jE}^{\Delta}(\mathbf{X}_{N+1}; R) \rangle', \tag{11.53}$$

and the radial wave functions $G_{ij}^{\Delta}(R)$ in (11.51) and (11.52) are obtained by projecting the total wave function $\Psi_{jE}^{\Delta}(\mathbf{X}_{N+1}; R)$ onto the channel functions defined by (11.50) as follows:

$$G_{ij}^{\Delta}(R) = \langle \phi_i^{\Delta}(\mathbf{X}_{N+1}) | \Psi_{jE}^{\Delta}(\mathbf{X}_{N+1};\, R) \rangle', \tag{11.54}$$

where the primes on the Dirac brackets in these equations mean that the integrations are carried out over all coordinates except r_{N+1} in (11.53) and except R in (11.54). Also the R-matrices in (11.51) and (11.52) are defined by

$$R_{ivi'v'}^{\Delta}(E) = \frac{1}{2a_0} \sum_{kt} \frac{w_{ivkt}^{\Delta} w_{i'v'kt}^{\Delta}}{\epsilon_{kt} - E}, \tag{11.55}$$

$$R_{ivi'}^{\Delta}(E) = \frac{1}{2\mu A_0} \sum_{kt} \frac{w_{ivkt}^{\Delta} w_{i'kt}^{\Delta}}{\epsilon_{kt} - E}, \tag{11.56}$$

$$R_{ii'v'}^{\Delta}(E) = \frac{1}{2a_0} \sum_{kt} \frac{w_{ikt}^{\Delta} w_{i'v'kt}^{\Delta}}{\epsilon_{kt} - E}, \tag{11.57}$$

$$R_{ii'}^{\Delta}(E) = \frac{1}{2\mu A_0} \sum_{kt} \frac{w_{ikt}^{\Delta} w_{i'kt}^{\Delta}}{\epsilon_{kt} - E}, \tag{11.58}$$

where the surface amplitudes in (11.55), (11.56), (11.57) and (11.58) are defined by

$$w_{ivkt}^{\Delta} = \langle r_{N+1}^{-1} \theta_{iv}^{\Delta}(\mathbf{X}_N;\, \hat{\mathbf{r}}_{N+1}\sigma_{N+1};\, R) | \psi_k^{\Delta}(\mathbf{X}_{N+1};\, R) \xi_{kt}(R) \rangle'_{r_{N+1}=a_0}, \tag{11.59}$$

$$w_{ikt}^{\Delta} = \langle \phi_i^{\Delta}(\mathbf{X}_{N+1}) | \psi_k^{\Delta}(\mathbf{X}_{N+1};\, R) \xi_{kt}(R) \rangle'_{R=A_0}. \tag{11.60}$$

Substituting the expressions for the R-matrices given by (11.55), (11.56), (11.57) and (11.58) into (11.51) and (11.52) provides the boundary conditions satisfied by the solutions of (11.38) in the external region considered below.

The above procedure for calculating the R-matrices has proved to be satisfactory in most applications. However, Gillan et al. [373] pointed out that this procedure must be modified in situations where there are strongly avoided crossings between the eigenvalues E_k^{Δ} in (11.13) as a function of the internuclear separation R. In this situation the Born–Oppenheimer approximation separation of the electronic and nuclear motion is not valid in the neighbourhood of these avoided crossings and, as a result, the effect of the nuclear kinetic energy operator T_R, acting on the electronic basis functions ψ_k^{Δ} in (11.43), is no longer negligible. In principle this effect, which couples the electronic states involved in the avoided crossings, can be calculated. However, an alternative procedure, which is straightforward to apply, was proposed by Gillan et al. They replaced the expansion basis defined by (11.41) by a modified expansion given by

$$\Theta_k^{\Delta}(\mathbf{X}_{N+1};\, R) = \sum_{is} \psi_i^{\Delta}(\mathbf{X}_{N+1};\, R_0) \zeta_s(R) \gamma_{isk}^{\Delta}, \tag{11.61}$$

where the electronic basis functions ψ_i^{Δ} in this expansion are defined for a given *fixed* internuclear separation R_0 and are thus independent of R. The diagonalization of the Hamiltonian $H_{N+1} + T_R + \mathcal{L}_{N+1} + \mathcal{L}_R$ is then more difficult to apply than that given by (11.43) since the electronic basis functions no longer diagonalize the electronic part of the Hamiltonian except at $R = R_0$. However, a practical procedure for treating this problem was described by Gillan et al. which was used in a study of electron collisions with nitrogen molecules. This work has been extended to molecular ions where Rydberg series of resonances occur and to study dissociative recombination (Sarpal et al. [813]) and vibrational excitation (Rabadán and Tennyson [763]).

11.1.4.2 External Region Solution

The external region, defined in Fig. 11.4, can be divided into two sub-regions, corresponding to electron–molecule collisions and to dissociation. In the following discussion we assume that the corresponding radii a_0 and A_0 are chosen large enough so that for the channels of interest the corresponding wave functions in these external sub-regions have negligible overlap.

In the external sub-region corresponding to electron–molecule collisions, we expand the total wave function in terms of the channel functions θ_{iv}^{Δ}, defined by (11.49) as follows:

$$\Psi_{jE}^{\Delta}(\mathbf{X}_{N+1};\, R) = \sum_{iv} \theta_{iv}^{\Delta}(\mathbf{X}_N;\, \hat{\mathbf{r}}_{N+1}\sigma_{N+1};\, R) r_{N+1}^{-1} F_{ivj}^{\Delta}(r_{N+1}). \tag{11.62}$$

We substitute this expansion into the Schrödinger equation (11.38) and project it onto the channel functions θ_{iv}^{Δ}. This yields the following set of $p = nn_v$ coupled second-order differential equations satisfied by the reduced radial functions $F_{ivj}^{\Delta}(r)$:

$$\left(\frac{\mathrm{d}^2}{\mathrm{d}r^2} - \frac{\ell_i(\ell_i+1)}{r^2} + \frac{2(Z_A + Z_B - N)}{r} + k_{iv}^2\right) F_{ivj}^{\Delta}(r)$$
$$= 2\sum_{i'=1}^{n}\sum_{v'=1}^{n_v} V_{ivi'v'}^{\Delta}(r) F_{i'v'j}^{\Delta}(r),\ i = 1, \ldots, n,\ v = 1, \ldots, n_v,\ r \geq a_0, \tag{11.63}$$

where we assume that n electronic channels each with n_v vibrational states have been retained in expansion (11.62). Also in (11.63)

$$k_{iv}^2 = 2(E - E_{iv}), \quad i = 1, \ldots, n, \quad v = 1, \ldots, n_v, \tag{11.64}$$

where E_{iv} is the energy of the vth vibrational state in the ith electronic channel which is defined by

$$E_{iv} = \langle \eta_{iv}(R) | \overline{e}_i | \eta_{iv}(R) \rangle, \quad i = 1, \ldots, n, \quad v = 1, \ldots, n_v. \tag{11.65}$$

The energies $\overline{e}_i$ in (11.65), which are functions of the internuclear separation R, are defined by (11.24) in the fixed-nuclei approximation. Finally, the potential matrix $V^{\Delta}_{ivi'v'}(r)$ in (11.63) is defined by

$$V^{\Delta}_{ivi'v'}(r) = \langle \eta_{iv}(R) | V^{\Delta}_{ii'}(r) | \eta_{i'v'}(R) \rangle, \tag{11.66}$$

which can be written as a summation over inverse powers of r as follows:

$$V^{\Delta}_{ivi'v'}(r) = \sum_{\lambda=1}^{\infty} a^{\Delta}_{ivi'v'\lambda} r^{-\lambda-1}, \quad i,\ i' = 1, \ldots, n, \\ v,\ v' = 1, \ldots, n_v, \quad r \geq a_0, \tag{11.67}$$

where the potential matrix $V^{\Delta}_{ii'}(r)$ in (11.66), which is a function of the internuclear separation R, is defined by (11.25) in the fixed-nuclei approximation.

In the external sub-region corresponding to dissociative attachment or dissociative recombination, we expand the total wave function in terms of the channel functions defined by (11.50) as follows:

$$\Psi^{\Delta}_{jE}(\mathbf{X}_{N+1}; R) = \sum_i \phi^{\Delta}_i(\mathbf{X}_{N+1}) G^{\Delta}_{ij}(R). \tag{11.68}$$

In order to derive coupled second-order differential equations satisfied by the radial functions $G^{\Delta}_{ij}(R)$, we rewrite the Hamiltonian H_{N+1} in (11.38) in the following alternative form:

$$H_{N+1} = H_A + H_B + U_{AB}, \tag{11.69}$$

where H_A and H_B are the Hamiltonian operators corresponding to the dissociating atoms or ions in (11.37), which we assume contain N_A and N_B electrons, respectively, and U_{AB} is the long-range multipole potential interaction between these atoms or ions. We now substitute expansion (11.68) into the Schrödinger equation (11.38) and project it onto the channel functions ϕ^{Δ}_i. This yields the following set of m coupled second-order differential equations satisfied by the radial functions $G^{\Delta}_{ij}(r)$:

$$\left(\frac{\mathrm{d}^2}{\mathrm{d}R^2} - \frac{2\mu(Z_A - N_A)(Z_B - N_B)}{R} + k_i^2 \right) G^{\Delta}_{ij}(R) \\ = 2\mu \sum_{i'=1}^{m} U^{\Delta}_{ii'}(R) G^{\Delta}_{i'j}(R), \quad i = 1, \ldots, m, \quad R \geq A_0, \tag{11.70}$$

where we assume that m dissociation channels have been retained in expansion (11.68). Also in (11.70) we have defined

$$k_i^2 = 2\mu(E - E_{A_i} - E_{B_i}), \tag{11.71}$$

where E_{A_i} and E_{B_i} are the energies of the atomic states defined by

$$\langle \psi_{A_i}(\mathbf{X}_A)|H_A|\psi_{A_{i'}}(\mathbf{X}_A)\rangle = E_{A_i}\delta_{ii'} \tag{11.72}$$

and

$$\langle \psi_{B_i}(\mathbf{X}_B)|H_B|\psi_{B_{i'}}(\mathbf{X}_B)\rangle = E_{B_i}\delta_{ii'}. \tag{11.73}$$

Finally, the potential matrix $U^{\Delta}_{ii'}(R)$ in (11.70) is defined in terms of the Coulomb interaction term U_{AB} in (11.69) by

$$U^{\Delta}_{ii'}(R) = \left\langle \phi^{\Delta}_i(\mathbf{X}_{N+1}) \left| U_{AB}(\mathbf{X}_{N+1}; R) - \frac{(Z_A - N_A)(Z_B - N_B)}{R} \right| \right. \\ \left. \times \phi^{\Delta}_{i'}(\mathbf{X}_{N+1}) \right\rangle, \tag{11.74}$$

where the integrals in this equation are carried out over the space and spin coordinates of all $N+1$ electrons. We then find that $U^{\Delta}_{ii'}(R)$ can be written as a summation over inverse powers of R as follows:

$$U^{\Delta}_{ii'}(R) = \sum_{\lambda=1}^{\infty} A^{\Delta}_{ii'\lambda} R^{-\lambda-1}, \quad i,\ i' = 1, \ldots, m, \quad R \geq A_0, \tag{11.75}$$

where $A^{\Delta}_{ii'\lambda}$ are long-range potential coefficients.

The generalized $(p+m) \times (p+m)$-dimensional R-matrix, defined by (11.55), (11.56), (11.57) and (11.58), can be propagated outwards from the boundaries of the internal region $r = a_0$ and $R = A_0$ to $r = a_p$ and $R = A_q$ in Fig. 11.4 by solving the two sets of coupled second-order differential equations (11.63) and (11.70) where channels in different sets are not coupled, using the procedure described in Appendix E.6. The R-matrix at $r = a_p$ and $R = A_q$ then provides the boundary condition for the solution in the asymptotic region.

11.1.4.3 Asymptotic Region Solution

The solution in the asymptotic region, where $r \geq a_p$ and $R \geq A_q$ in Fig. 11.4, can be obtained by a procedure analogous to our treatment of the asymptotic region solution in positron collisions with atoms and ions given in Sect. 7.1.4. We assume that we have chosen the radii a_p and A_q in Fig. 11.4 large enough that asymptotic expansion methods discussed in Appendix F.1 can be used to obtain accurate linearly independent solutions of (11.63) where $r \geq a_p$ and of (11.70) where $R \geq A_q$.

We consider first the linearly independent solutions of (11.63) corresponding to electron–molecule collisions. We re-order the $p = nn_v$ coupled channels to be in

increasing energy order and we introduce the quantities $\overline{k}_i^2$, $i = 1, \ldots, p$, distinguished by a bar, corresponding to the re-ordered k_{iv}^2 in (11.64) so that

$$\overline{k}_1^2 \geq \overline{k}_2^2 \geq \cdots \geq \overline{k}_p^2. \tag{11.76}$$

We then assume that at the energy E of interest the first p_a of the re-ordered channels are open with $\overline{k}_i^2 \geq 0$ and the last p_b channels are closed with $\overline{k}_i^2 < 0$, where $p_a + p_b = p$. Using the asymptotic expansion methods discussed in Appendix F.1, we then determine $n + n_a$ linearly independent solutions of the re-ordered equations (11.63), which are regular as the radial coordinate of the scattered electron $r \to \infty$ and which satisfy the asymptotic boundary conditions

$$\begin{aligned}
\overline{s}_{ij}(r) &\underset{r\to\infty}{\sim} \overline{k}_i^{-1/2} \sin\overline{\theta}_i \delta_{ij}, \quad i = 1, \ldots, p, \quad j = 1, \ldots, p_a, \\
\overline{c}_{ij}(r) &\underset{r\to\infty}{\sim} \overline{k}_i^{-1/2} \cos\overline{\theta}_i \delta_{ij}, \quad i = 1, \ldots, p, \quad j = 1, \ldots, p_a, \\
\overline{c}_{ij}(r) &\underset{r\to\infty}{\sim} \exp(-\overline{\phi}_i)\delta_{ij}, \quad i = 1, \ldots, p, \quad j = p_a + 1, \ldots, p,
\end{aligned} \tag{11.77}$$

where $\overline{\theta}_i$ and $\overline{\phi}_i$ are defined by equations analogous to (5.38), (5.39), (5.40) and (5.41).

We consider next the linearly independent solutions of (11.70) corresponding to dissociative attachment or dissociative recombination. We assume that the m coupled channels, which we distinguish by a tilde, are ordered so that

$$\widetilde{k}_1^2 \geq \widetilde{k}_2^2 \geq \cdots \geq \widetilde{k}_m^2, \tag{11.78}$$

where the $\widetilde{k}_i^2$ correspond to the re-ordered quantities k_i^2 defined by (11.71). We now assume that at the energy E of interest the first m_a channels are open with $\widetilde{k}_i^2 \geq 0$ and the last m_b channels are closed with $\widetilde{k}_i^2 < 0$, where $m_a + m_b = m$. Using the asymptotic expansion methods discussed in Appendix F.1, we then determine $m + m_a$ linearly independent solutions of (11.70), which are regular as the internuclear separation $R \to \infty$ and which satisfy the asymptotic boundary conditions

$$\begin{aligned}
\widetilde{s}_{ij}(R) &\underset{R\to\infty}{\sim} \widetilde{k}_i^{-1/2} \sin\widetilde{\theta}_i \delta_{ij}, \quad i = 1, \ldots, m, \quad j = 1, \ldots, m_a, \\
\widetilde{c}_{ij}(R) &\underset{R\to\infty}{\sim} \widetilde{k}_i^{-1/2} \cos\widetilde{\theta}_i \delta_{ij}, \quad i = 1, \ldots, m, \quad j = 1, \ldots, m_a, \\
\widetilde{c}_{ij}(R) &\underset{R\to\infty}{\sim} \exp(-\widetilde{\phi}_i)\delta_{ij}, \quad i = 1, \ldots, m, \quad j = m_a + 1, \ldots, m,
\end{aligned} \tag{11.79}$$

where $\widetilde{\theta}_i$ and $\widetilde{\phi}_i$ are again defined by equations analogous to (5.38), (5.39), (5.40) and (5.41).

We now observe that at an energy E where p_a channels of (11.63) are open and m_a channels of (11.70) are open, we can determine $p_a + m_a$ linearly independent physical solutions of the combined internal and external region equations, which vanish at the origin and which are finite at infinity. In analogy with (7.50), these

solutions can be rewritten in terms of the $p + p_a$ asymptotic solutions defined by (11.77) and the $m + m_a$ asymptotic solutions defined by (11.79) as follows:

$$\mathcal{F}^{\Delta}(\rho) = \mathbf{s}(\rho) + \mathbf{c}(\rho)\mathbf{N}^{\Delta}, \quad r \geq a_p, \quad R \geq A_q, \tag{11.80}$$

where we have written $\mathbf{s}(\rho)$ to represent $\bar{\mathbf{s}}(r)$ and $\widetilde{\mathbf{s}}(R)$ and $\mathbf{c}(\rho)$ to represent $\bar{\mathbf{c}}(r)$ and $\widetilde{\mathbf{c}}(R)$ and where the variable ρ represents r in the channels corresponding to (11.63) and R in the channels corresponding to (11.70). It then follows using our analysis in Sect. 7.1.4 that the matrix $\mathbf{N}^{\Delta}$ has dimension $(p + m) \times (p_a + m_a)$ and can be written as

$$\mathbf{N}^{\Delta} = \begin{bmatrix} \mathbf{K}^{\Delta} \\ \mathbf{L}^{\Delta} \end{bmatrix}, \tag{11.81}$$

where $\mathbf{K}^{\Delta}$ is the $(p_a + m_a) \times (p_a + m_a)$-dimensional K-matrix which couples the open channels in (11.63) and (11.70) and $\mathbf{L}^{\Delta}$ is a subsidiary $(p_b + m_b) \times (p_a + m_a)$-dimensional matrix which couples the solutions in (11.77) and (11.79) which vanish asymptotically.

It then follows from our analysis in Sect. 7.1.4 that the $(p_a + m_a) \times (p_a + m_a)$-dimensional K-matrix $\mathbf{K}^{\Delta}$ in (11.81) corresponding to the open channels in (11.63) and (11.70) can be determined in terms of the $(p + m) \times (p + m)$-dimensional R-matrix obtained on the boundaries $r = a_p$ and $R = A_q$ of the external region by solving a set of linear simultaneous equations analogous to (7.54). Also it follows from (11.80) that the required physical solutions satisfy the asymptotic boundary condition

$$\mathcal{F}^{\Delta}(\rho) \underset{\rho \to \infty}{\sim} \mathbf{s}(\rho) + \mathbf{c}(\rho)\mathbf{K}^{\Delta} \tag{11.82}$$

in the open channels where, following our discussion in Sect. 7.1.4, the first p_a channels in (11.82) correspond to open electron–molecule collision channels, and the last m_a channels in (11.82) correspond to open dissociation channels. Hence the $(p_a + m_a) \times (p_a + m_a)$-dimensional K-matrix $\mathbf{K}^{\Delta}$ couples the p_a open electron–molecule channels and the m_a open dissociation channels. Finally, the $(p_a + m_a) \times (p_a + m_a)$-dimensional S-matrix $\mathbf{S}^{\Delta}$ is defined in terms of the K-matrix $\mathbf{K}^{\Delta}$ by the matrix equation

$$\mathbf{S}^{\Delta} = \frac{\mathbf{I} + \mathrm{i}\mathbf{K}^{\Delta}}{\mathbf{I} - \mathrm{i}\mathbf{K}^{\Delta}}. \tag{11.83}$$

The corresponding T-matrix and cross sections for electron–molecule collisions including dissociative attachment and dissociative recombination in (11.37) can then be determined. We obtain expressions for the scattering amplitude and cross sections for electron collisions with diatomic and linear polyatomic molecules in Sect. 11.1.6.

11.1.5 Resonant R-Matrix Theory

We conclude our discussion of R-matrix theory of electron–molecule collisions by briefly describing a semi-phenomenological resonant R-matrix theory, introduced and developed by Fabrikant [292–295], which has enabled low-energy resonant electron impact vibrational excitation and dissociative processes to be calculated for both diatomic and polyatomic molecules.

The fundamental assumption made in electron–molecule resonant R-matrix theory is that at low incident electron energies, vibrational excitation and dissociation cross sections are caused by a single discrete low-energy resonance state. This theory, which we illustrate by considering a single electronic channel, commences from the following resonant expression for the R-matrix in the fixed-nuclei approximation on the boundary $r = a_0$ of the internal region

$$R(\rho) = \frac{\gamma^2(\rho)}{E_1(\rho) - E_e} + R_r, \tag{11.84}$$

where r is the radial coordinate of the scattered electron relative to the centre-of-gravity of the molecule. Also in (11.84), ρ is the internuclear distance, E_e is the incident electron energy, $\gamma(\rho)$ and $E_1(\rho)$ are the usual resonance parameters and R_r is a background term which is weakly dependent on ρ and E_e. The vibrational dynamics is then included, as in non-adiabatic R-matrix theory, by the R-matrix

$$\mathbf{R}(\rho) = \boldsymbol{\gamma}(\rho)\,[\mathbf{H}_I(\rho) - E_t\mathbf{I}]^{-1}\,\boldsymbol{\gamma}^{\mathrm{T}}(\rho) + \mathbf{R}_r, \tag{11.85}$$

which couples the vibrational channels including the continuum, where the Hamiltonian

$$\mathbf{H}_I(\rho) = \mathbf{T} + \mathbf{U}(\rho), \tag{11.86}$$

with

$$\mathbf{U}(\rho) = \mathbf{V}_0(\rho) + \mathbf{E}_1(\rho). \tag{11.87}$$

In these equations $\mathbf{T}$ is the kinetic energy operator for nuclear motion, $\mathbf{V}_0(\rho)$ is the potential energy function describing the nuclear motion and E_t is the total energy.

In the external and asymptotic regions, where the radial coordinate of the scattered electron $r \geq a_0$, the solution is given in terms of the vibrational wave functions of the target molecule which involve a summation over the discrete vibrational states and an integration over the vibrational continuum states corresponding to dissociation. The reduced radial wave function $\mathbf{u}(r)$, with vibrational components $u_v(r)$, can then be written asymptotically in terms of ingoing and outgoing wave functions as follows:

$$\mathbf{u}(r) \underset{r\to\infty}{\sim} \mathbf{k}^{-1/2}\left[\exp(-\mathrm{i}\boldsymbol{\theta}) - \exp(\mathrm{i}\boldsymbol{\theta})\mathbf{S}\right], \tag{11.88}$$

where $\mathbf{k}$ and $\boldsymbol{\theta}$ are diagonal matrices and $\mathbf{S}$ is the S-matrix. This matrix, and hence the scattering amplitudes and cross sections, is determined by substituting the solution $\mathbf{u}(r)$ at $r = a_0$ into the R-matrix equation

$$\mathbf{u}(a_0) = \mathbf{R}(\rho) \left. \frac{\mathrm{d}\mathbf{u}}{\mathrm{d}r} \right|_{r=a_0} . \tag{11.89}$$

In practice, $\mathbf{u}(r)$ is often determined for $a_0 \leq r \leq \infty$ by retaining the main components of the long-range interaction potential between the scattered electron and the molecule in the calculation, given by (11.6).

In comparing this analysis with that adopted in non-adiabatic R-matrix theory, discussed in Sect. 11.1.4, we can make several observations. First, it follows from (11.84) and (11.85) that the electronic motion is represented by a single pole term in the R-matrix which describes low-energy resonant vibrational excitation and dissociative attachment, whereas in non-adiabatic R-matrix theory the R-matrix is described by many pole terms, providing an ab initio description of both resonant and non-resonant collisions over a wide energy range. Also, the internal region boundary $r = a_0$ is usually larger in non-adiabatic R-matrix theory in order to fully include electron exchange effects between the scattered electron and the target molecule. Finally, in non-adiabatic theory the long-range potential between the scattered electron and the target is fully retained in the external and asymptotic regions. As a result, non-adiabatic R-matrix calculations are much larger than those arising in resonant R-matrix theory discussed in this section. However, the relative simplicity of electron–molecule resonant R-matrix theory, and of the corresponding calculations, enables the role of resonances in low-energy electron–molecule collisions to be rapidly determined and evaluated, which can be a valuable guide to experiment and to more detailed theoretical studies using, for example, non-adiabatic R-matrix theory.

Finally, we mention a number of applications of electron–molecule resonant R-matrix theory that have been carried out. They include electron impact vibrational excitation of HCl by Fabrikant [292, 295], vibrational resonance and threshold effects in inelastic electron collisions with methyl iodide molecules by Schramm et al. [833], dissociative electron attachment to CH_3I by Fabrikant and Hartop [297] and electron attachment to van der Waal's clusters by Fabrikant [296].

11.1.6 Scattering Amplitudes and Cross Sections

In this section we derive expressions for the electron–molecule scattering amplitudes and cross sections, which extend our analysis given in Sect. 2.5 where we considered electron collisions with atoms and atomic ions. We limit our discussion to diatomic and linear polyatomic molecules. However, the analysis has been extended to electron collisions with non-linear polyatomic molecules by Burke et al. [179] and by Gianturco and Jain [369].

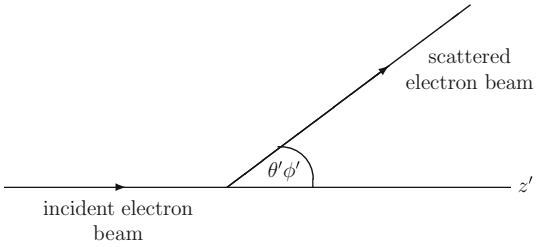

Fig. 11.5 Laboratory frame for electron–molecule collisions

We consider first the scattering amplitude and cross section in the fixed-nuclei approximation discussed in Sect. 11.1.2. We commence by introducing the laboratory frame of reference, illustrated in Fig. 11.5, where the z'-axis is taken to lie along the incident electron beam direction and the scattered beam is in the direction (θ', ϕ') relative to this direction. In this frame of reference the molecular frame of reference, illustrated in Fig. 11.1, is oriented in a direction defined by the Euler angles α, β, γ, discussed in Appendix B.5, which take the laboratory frame of reference into the molecular frame of reference.

The asymptotic form of the solution of the time-independent Schrödinger equation (11.9) can be written in the laboratory frame of reference as

$$\Psi_i = \Psi_i^{\text{inc}} + \Psi_i^{\text{scatt}}, \tag{11.90}$$

where the incident plane wave

$$\Psi_i^{\text{inc}} \underset{r'_{N+1}\to\infty}{\sim} \Phi_i(\mathbf{X}_N)\chi_{\frac{1}{2}m_i}(\sigma_{N+1})\exp(\mathrm{i}k_i z'_{N+1}), \tag{11.91}$$

and the outgoing scattered wave

$$\Psi_i^{\text{scatt}} \underset{r'_{N+1}\to\infty}{\sim} \sum_j \Phi_j(\mathbf{X}_N)\chi_{\frac{1}{2}m_j}(\sigma_{N+1}) f_{ji}(\theta'_{N+1}, \phi'_{N+1}) \frac{\exp(\mathrm{i}k_j r'_{N+1})}{r'_{N+1}}, \tag{11.92}$$

where we assume that the molecule is neutral. In (11.91) and (11.92) Φ_i and Φ_j are the physical and possibly pseudostates retained in expansions (11.12) and (11.21), $\chi_{\frac{1}{2}m_i}$ and $\chi_{\frac{1}{2}m_j}$ are the spin functions of the incident and scattered electron, f_{ji} is the scattering amplitude and k_i and k_j are the wave numbers of the incident and scattered electron defined by (11.23). The differential cross section for a transition from an initial target state Φ_i to a final target state Φ_j with the spin magnetic quantum numbers m_i and m_j is then given by

$$\frac{\mathrm{d}\sigma_{ji}}{\mathrm{d}\Omega} = \frac{k_j}{k_i}|f_{ji}(\theta', \phi')|^2, \tag{11.93}$$

in units of a_0^2/steradian. We see that the above equations are analogous to those considered in Sect. 2.5 in our discussion of electron–atom collisions.

For light diatomic or linear polyatomic molecular targets, where relativistic effects can be neglected, the conserved quantum numbers represented by Δ in (11.12) and in subsequent equations are given by

$$\Delta \equiv \alpha \ \Lambda \ S \ M_S \ \pi, \tag{11.94}$$

where $\Lambda = \lambda_i + m_{\ell_i}$ is the component of the total orbital angular momentum of the electron–molecule system along the internuclear axis, λ_i and m_{ℓ_i} being, respectively, the corresponding components of the orbital angular momenta of the target and scattered electron, and S and M_S are the total spin angular momentum and its component in some preferred direction, respectively. Also, in the case of a homonuclear diatomic molecule, or a linear polyatomic molecule, where the Hamiltonian is symmetric about its centre of gravity, the parity quantum number π is also conserved. Finally, α represents any further quantum numbers which are conserved in the collision.

The channel functions $\overline{\Phi}_i^{\Delta}(\mathbf{X}_N; \hat{\mathbf{r}}_{N+1}\sigma_{N+1})$ in (11.12) and (11.21) can then be written as

$$\overline{\Phi}_i^{\Delta}(\mathbf{X}_N; \hat{\mathbf{r}}_{N+1}\sigma_{N+1}) \equiv \overline{\Phi}_i^{SM_S}(\mathbf{X}_N; \sigma_{N+1}) \ Y_{\ell_i m_{\ell_i}}(\theta_{N+1}, \phi_{N+1}), \tag{11.95}$$

where the functions $\overline{\Phi}_i^{SM_S}$ are obtained by coupling the spin of the target with the spin of the scattered electron as follows:

$$\overline{\Phi}_i^{SM_S}(\mathbf{X}_N; \sigma_{N+1}) = \sum_{M_{S_i} m_i} \Phi_i(\mathbf{X}_N) \chi_{\frac{1}{2}m_i}(\sigma_{N+1}) (S_i M_{S_i} \tfrac{1}{2} m_i | S M_S), \tag{11.96}$$

which can be inverted giving

$$\Phi_i(\mathbf{X}_N) \chi_{\frac{1}{2}m_i}(\sigma_{N+1}) = \sum_{S} \overline{\Phi}_i^{SM_S}(\mathbf{X}_N; \sigma_{N+1}) (S_i M_{S_i} \tfrac{1}{2} m_i | S M_S). \tag{11.97}$$

Also $Y_{\ell_i m_{\ell_i}}(\theta_{N+1}, \phi_{N+1})$ in (11.95) is a spherical harmonic defined in Appendix B.3 and $(S_i M_{S_i} \frac{1}{2} m_i | S M_S)$ in (11.96) and (11.97) are Clebsch–Gordan coefficients defined in Appendix A.1. The summation over i in (11.12) and (11.21) thus involves both a summation over the functions $\overline{\Phi}_i^{SM_S}$ and also over the spherical harmonics $Y_{\ell_i m_{\ell_i}}$ subject to conservation of the quantum numbers represented by Δ. The incident plane wave, defined by (11.91), can then be written in terms of these channel functions using (11.97) and (B.53). We obtain

$$\Psi_i^{\text{inc}} \underset{r'_{N+1}\to\infty}{\sim} \frac{\mathrm{i}\pi^{1/2}}{k_i r'_{N+1}} \sum_{S\ell_i} \mathrm{i}^{\ell_i} (2\ell_i + 1)^{1/2} \, \overline{\Phi}_i^{SM_S}(\mathbf{X}_N; \sigma_{N+1}) (S_i M_{S_i} \tfrac{1}{2} m_i | S M_S)$$
$$\times \left[\exp(-\mathrm{i}\theta'_i) - \exp(\mathrm{i}\theta'_i)\right] Y_{\ell_i 0}(\theta'_{N+1}, 0), \tag{11.98}$$

where $\theta_i' = k_i r'_{N+1} - \frac{1}{2}\ell_i\pi$ for neutral molecular targets.

We now expand the solution Ψ_i, defined by (11.90), in terms of solutions obtained by solving the Schrödinger equation in the fixed-nuclei approximation as described in Sect. 11.1.2. Using the channel functions defined by (11.95), the solutions defined by (11.21) can be written as

$$\Psi_i^{\Delta}(\mathbf{X}_{N+1}; R) = \sum_{j=1}^{n} \overline{\Phi}_j^{SM_S}(\mathbf{X}_N; \sigma_{N+1}) Y_{\ell_j m_{\ell_j}}(\theta_{N+1}, \phi_{N+1}) r_{N+1}^{-1} G_{ji}^{\Delta}(r_{N+1}), \tag{11.99}$$

where we have introduced the reduced radial wave functions $G_{ji}^{\Delta}(r)$ which satisfy S-matrix boundary conditions defined by (11.31). We then expand Ψ_i in terms of these solutions as follows:

$$\Psi_i(\mathbf{X}_{N+1}; R) = \sum_{\Lambda S\pi} \Psi_i^{\Delta}(\mathbf{X}_{N+1}; R) A_i^{\Delta}, \tag{11.100}$$

where this equation applies for each value of M_S which is conserved in the collision. The coefficients A_i^{Δ} are obtained by comparing the ingoing wave terms on the right-hand side of (11.100) with the ingoing wave term in Ψ_i^{inc}, defined by (11.98). In making this comparison we remember that Ψ_i^{inc} is referred to the laboratory frame of reference, while Ψ_i^{Δ} in (11.100) is referred to the molecular frame of reference. Hence we must use the following equation:

$$Y_{\ell m}(\theta', \phi') = \sum_{m'} D_{mm'}^{\ell *}(\alpha, \beta, \gamma) Y_{\ell m'}(\theta, \phi), \tag{11.101}$$

which relates the spherical harmonics in these frames of reference, where $D_{mm'}^{\ell}(\alpha, \beta, \gamma)$ are Wigner rotation matrices, which are defined in Appendix B.5 and α, β and γ are Euler angles which transform the laboratory frame of reference into the molecular frame of reference, as discussed following Fig. 11.5. Substituting (11.101) into (11.98) and comparing the ingoing wave term with (11.100) then gives

$$A_i^{\Delta} = \frac{\mathrm{i}\pi^{1/2}}{k_i^{1/2}} \mathrm{i}^{\ell_i} (2\ell_i + 1)^{1/2} (S_i M_{S_i} \tfrac{1}{2} m_i | S M_S)\ D_{0 m_{\ell_i}}^{\ell_i *}(\alpha, \beta, \gamma). \tag{11.102}$$

After substituting this expression for A_i^{Δ} into (11.100) and using (11.90) and (11.92) we obtain the following result for the scattering amplitude:

$$f_{ji}(\theta', \phi') = -\mathrm{i}\left(\frac{\pi}{k_i k_j}\right)^{1/2} \sum_{\Lambda S \pi} \sum_{\ell_i m_{\ell_i} \ell_j m_{\ell_j} m_{\ell_{j'}}} \mathrm{i}^{\ell_i - \ell_j} (2\ell_i + 1)^{1/2}$$

$$\times (S_i M_{S_i} \tfrac{1}{2} m_i | S M_S)(S_j M_{S_j} \tfrac{1}{2} m_j | S M_S) T_{ji}^{\Delta}$$

$$\times D^{\ell_i *}_{0 m_{\ell_i}}(\alpha, \beta, \gamma) D^{\ell_j}_{m_{\ell_{j'}} m_{\ell_j}}(\alpha, \beta, \gamma) Y_{\ell_j m_{\ell_{j'}}}(\theta', \phi'), \quad (11.103)$$

where the T-matrix in this equation is defined in terms of the S-matrix by the usual matrix equation

$$\mathbf{T}^{\Delta} = \mathbf{S}^{\Delta} - \mathbf{I}, \quad (11.104)$$

for each Λ, S and π. Substituting (11.103) for the scattering amplitude into (11.93) gives an expression for the differential cross section for electrons with spin component m_i incident on a molecule in state i with spin component M_{S_i} and orientation defined by the Euler angles (α, β, γ), leading to a scattered electron with spin component m_j and a molecule in state j with spin component M_{S_j}.

If the initial state is unpolarized and we do not observe the spins in the final state then we must average over initial spin components and sum over final spin components. Also, if the electrons are scattered from a molecular gas then we must average over all molecular orientations defined by the Euler angles (α, β, γ), to obtain the observed differential cross section. The resultant averaged cross section is given by

$$\left[\frac{\mathrm{d}\sigma_{ji}}{\mathrm{d}\Omega}\right]_{\mathrm{av}} = \frac{1}{8\pi^2} \int_0^{2\pi} \mathrm{d}\alpha \int_0^{\pi} \sin\beta \mathrm{d}\beta \int_0^{2\pi} \mathrm{d}\gamma \left[\frac{\mathrm{d}\sigma_{ji}}{\mathrm{d}\Omega}\right]_{\text{spin av}}. \quad (11.105)$$

The summation over the spin magnetic quantum numbers can be carried out using the orthogonality relations satisfied by the Clebsch–Gordan coefficients. The integrals over the Euler angles in (11.105) can be carried out using the orthogonality relations satisfied by the Wigner rotation matrices.

Finally, the total cross section for a transition from a molecular state represented by the quantum numbers $\alpha_i \lambda_i S_i \pi_i$ to a state represented by the quantum numbers $\alpha_j \lambda_j S_j \pi_j$ is obtained by integrating the resultant differential cross section over the scattering angles (θ', ϕ') defined in Fig. 11.5. We obtain

$$\sigma^{\mathrm{Tot}}(i \to j) = \frac{1}{2k_i^2(2S_i + 1)} \sum_{\Lambda S \pi} \sum_{\ell_i m_{\ell_i} \ell_j m_{\ell_j}} (2S + 1) \left| T_{ji}^{\Delta} \right|^2, \quad (11.106)$$

in units of πa_0^2.

11.1.7 Illustrative Examples: N_2, O_2, N_2O, H_3^+

In this section we present four illustrative examples of electron–molecule collision calculations using non-adiabatic R-matrix theory and computer programs.

11.1.7.1 Resonances in Electron Collisions with N_2

Resonances have been observed in low-energy electron collisions with nitrogen molecules by many workers including Schulz [834, 837], Heideman et al. [451], Golden and Nakano [388], Andrick and Ehrhardt [19], Ehrhardt and Willmann [286], Kennerly [529] and Allan [10]. In early theoretical work by Herzenberg and Mandl [461], mentioned in Sect. 11.1.1, it was pointed out that resonances play a crucial role in vibrational excitation and dissociative attachment and these authors extended the Kapur–Peierls [521] resonance formalism, originally developed for resonant collisions in nuclear physics, to treat resonances in electron–molecule collisions.

The analysis of resonances in vibrational excitation of molecules by slow electrons was reviewed by Herzenberg [460] and a "boomerang" model was developed for resonant e^-–N_2 collisions by Herzenberg et al. [108, 274, 459] in which the lifetime of the resonance is such that the nuclei only have time for a single vibrational cycle before the colliding electron departs, after exchanging energy with the vibrational motion of the nuclei. However, this model, while presenting a convincing physical picture of the resonant process, involves parameters and does not describe the non-resonant background.

An ab initio non-adiabatic R-matrix theory of electron–molecule collisions, which enables resonant vibrational excitation and dissociative attachment cross sections to be calculated, was introduced by Schneider et al. [829] and is described in Sect. 11.1.4. The first application of this theory to resonant vibrational excitation of N_2 was made by Schneider et al. [830] who obtained good agreement with vibrational excitation measurements of Ehrhardt and Willmann [286]. More recently this theory has been extended and applied to N_2 by Morgan [659] and by Gillan et al. [373, 374], where in the work of Morgan cross sections were obtained for electron impact excitation of vibrational levels up to $v = 19$ for incident electron energies in the range 1–7 eV. In the calculations by Morgan, the N_2 target was represented at each internuclear separation by an SCF wave function, and target polarization effects were taken into account by including in the second expansion in (11.12) all terms describing two-particle-one-hole excitations. The hole was in one of the N_2 bound-state orbitals and the two particles occupied all possible combinations of virtual orbitals allowed by the symmetry of the state. In this calculation, a total of 7 σ_g, 7 σ_u, 3 π_u and 3 π_g orbitals were used.

We compare the total cross section calculations of Morgan [659], obtained by summing the cross sections over all vibrational states, with the absolute measurements of Kennerly [529] in Fig. 11.6. We see that the cross section is dominated by

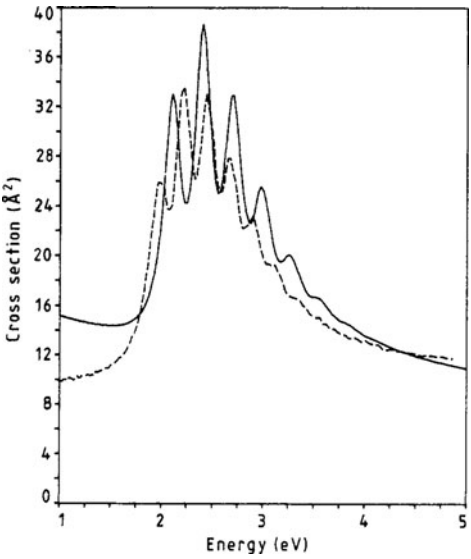

Fig. 11.6 Total cross sections for electron collisions with N_2. *Full curve*: *R*-matrix calculations by Morgan [659]; *broken curve*: experiment by Kennerly [529] (Fig. 1 from [659])

peaks in the energy range from 2 to 4 eV, which are found to be due to a low-energy $^2\Pi_g\ N_2^-$ shape resonance. The overall agreement between theory and experiment is satisfactory. However, the theoretical positions of the peaks are shifted slightly to higher energies and are more widely spaced than experiment, which can be attributed to a small difference between the theoretical N_2 ground state potential energy curve and experiment. A more significant discrepancy between theory and experiment occurs at low energies below the resonance region where the theoretical cross section is too high. This discrepancy in the total cross section may be due to inaccurate representation of the target polarization in the theoretical model and would probably be removed if the polarization effect is represented by the inclusion of polarized pseudostates in the *R*-matrix expansion.

Morgan also compared the results of individual vibrational excitation cross sections for $\sigma(0 \rightarrow v)$ for $v = 1$–19 with relative experimental measurements by Allan [10]. The experimental features of all the cross sections were well reproduced by the theory, particularly in the substructure of the lower energy peaks, although again the peaks in the cross sections are shifted slightly to higher energies and are more widely spaced than experiment.

In conclusion, the results obtained by Schneider et al. [830], Gillan et al. [373, 374] and Morgan [659] demonstrate that reliable results for resonant low-energy vibrational excitations in e–N_2 collisions can be obtained using the non-adiabatic *R*-matrix theory, described in Sect. 11.1.4, which treats the fixed-nuclei electron collision problem using the static exchange plus polarization approximation together with a non-adiabatic treatment of the nuclear motion.

11.1.7.2 Electron Collisions with O_2

A detailed knowledge of low-energy electron molecular oxygen collision cross sections is of importance in understanding a wide range of processes occurring in the earth's upper atmosphere, in gaseous discharges and in laboratory plasmas. Much experimental and theoretical effort has therefore been given over many years both to measure and to calculate the low-energy vibrational and electronic excitation cross sections and to determine the corresponding resonance structure. We show in Fig. 11.7 the low-energy potential energy curves of O_2 and the corresponding curves of O_2^-, which control the low-energy collision processes, calculated by Noble et al. [691]. The nine O_2 target potential energy curves shown in Fig. 11.7 have the assignments

$$1\pi_u^4 1\pi_g^2 \quad X^3\Sigma_g^-, \quad a\,^1\Delta_g, \quad b\,^1\Sigma_g^+ \tag{11.107}$$

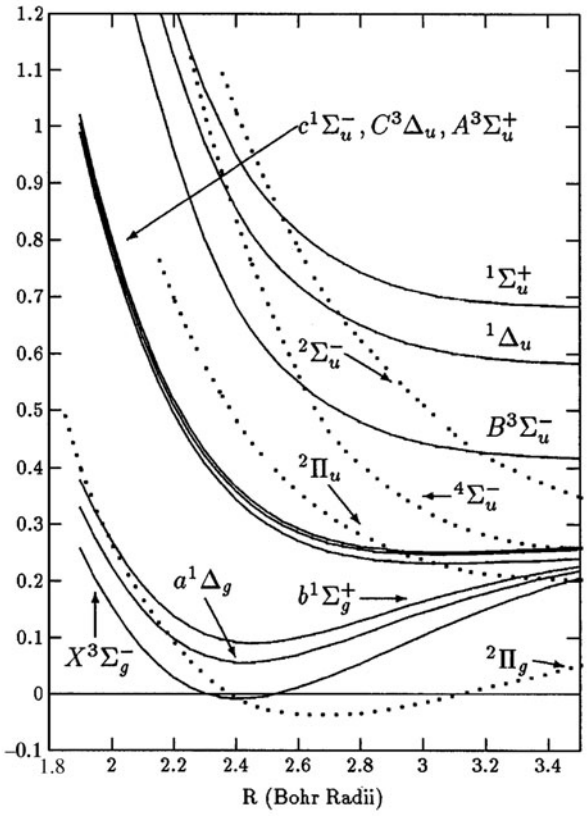

Fig. 11.7 Calculated potential energy curves in Rydbergs for O_2 target states (*full curves*) and for O_2^- resonance states (*dotted curves*) (Fig. 1 from [691])

and

$$1\pi_u^3 1\pi_g^3 \;\; c\,{}^1\Sigma_u^-, \;\; C^3\Delta_u, \;\; A^3\Sigma_u^+, \;\; B^3\Sigma_u^-, \;\; {}^1\Delta_u, \;\; {}^1\Sigma_u^+ \tag{11.108}$$

and the four O_2^- resonance curves shown in Fig. 11.7 have the assignments

$$1\pi_u^4 1\pi_g^3\,{}^2\Pi_g, \;\; 1\pi_u^3 1\pi_g^4\,{}^2\Pi_u, \;\; 1\pi_u^4 1\pi_g^2\,{}^3\Sigma_g^- 3\sigma_u\,{}^4\Sigma_u^-, \;\; 1\pi_u^4 1\pi_g^2\,{}^3\Sigma_g^- 3\sigma_u\,{}^2\Sigma_u^-. \tag{11.109}$$

In early electronic excitation R-matrix calculations by Noble and Burke [688] only the three lowest target states of O_2, given in (11.107), were included in the R-matrix expansion. However, in the later work by Noble and Burke [689], Higgins et al. [471, 472] and Noble et al. [691] all nine target states given in (11.107) and (11.108) and shown in Fig. 11.7 were included in the R-matrix expansion. In these 9-state calculations, each state was represented by a configuration interaction expansion, including up to 20 basis functions, which yielded relative excitation energies for the three lowest target states accurate to about 0.2 eV, and relative excitation energies for the three target states which lie approximately 6 eV above the ground state accurate to about 0.1 eV.

It was found in the 9-state calculations [471, 689] that the $X^3\Sigma_g^- \rightarrow a\,{}^1\Delta_g$ and $X^3\Sigma_g^- \rightarrow b\,{}^1\Sigma_g^+$ electronic excitation cross sections were dominated by the ${}^2\Pi_g$ and ${}^2\Pi_u$ resonances from threshold to 15 eV and were in good agreement with experiments by Middleton et al. [650]. In addition, it was found in the calculations by Noble et al. [691] that the ${}^4\Sigma_u^-$ resonance and, to a lesser extent, the ${}^2\Sigma_u^-$ resonance dominate the vibrational excitation cross sections in the O_2 $X^3\Sigma_g^-$ ground state in the incident electron energy range 0–14 eV. We compare these R-matrix calculations for vibrational excitation from the $v = 0$ to the $v' = 1, 2, 3, 4$ states in the $X^3\Sigma_g^-$ ground state with experiments reported by Noble et al. [691] and Shyn and Sweeney [875] in Fig. 11.8. The peak in the cross section near 11 eV arises mainly from the ${}^4\Sigma_u^-$ shape resonance where the scattered electron is temporarily captured into the $3\sigma_u$ orbital while the O_2 target remains unexcited in its $X^3\Sigma_g^-$ ground state. There is also a significant contribution from the ${}^2\Sigma_u^-$ shape resonance above about 10 eV where similar arguments apply. However, the contribution from the ${}^2\Pi_u$ resonance is small and only plays a significant role at the lowest energies. We also note from Fig. 11.8 that the peak in the experimental cross section occurs at a slightly lower energy and is larger than the theoretical predictions. The most likely cause of this discrepancy is the inadequate representation of the ground state polarization in the 9-state model. Representing the full polarizability by the inclusion of pseudostates in the expansion, as discussed in Sects. 2.2.2 and 6.2, would further improve the agreement between theory and experiment. However, we see that there is good overall agreement between the 9-state R-matrix calculations and experiment in this energy range.

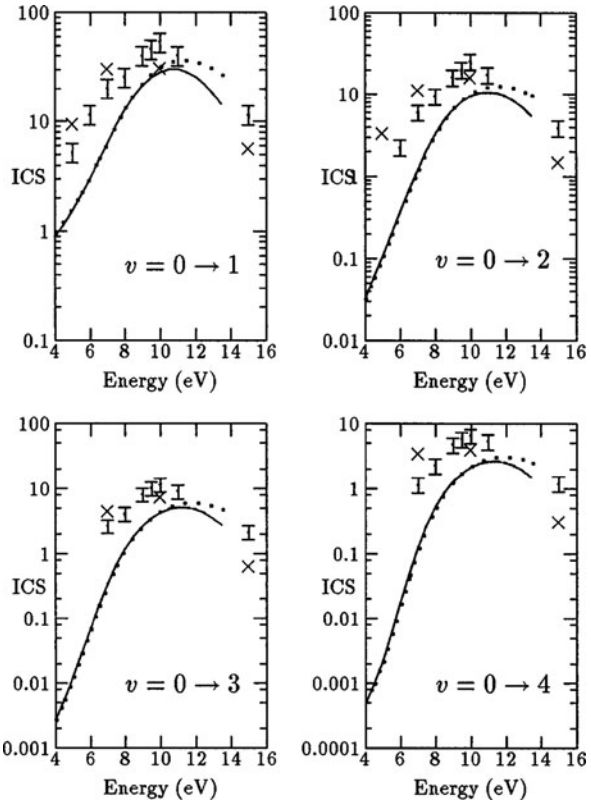

Fig. 11.8 Total vibrational excitation cross sections in 10^{-18} cm^2 from the $v = 0$ to the $v' = 1, 2, 3, 4$ states for e^-–O_2 collisions in the $X^3\Sigma_g^-$ ground electronic state. *Solid line*: *R*-matrix calculations including only the $^4\Sigma_u^-$ total symmetry; *dotted line*: including in addition the $^2\Sigma_u^-$ total symmetry; *vertical lines including error bars*: experiments reported by Noble et al. [691]; *crosses*: experiments by Shyn and Sweeney [875] (Fig. 2 from [691])

11.1.7.3 Electron Collisions with N_2O

Nitrous oxide is of considerable interest because of its role in a number of important processes and applications. For example, it has been found to be of considerable importance in the chemistry of the upper atmosphere where it plays a major role in the destruction of the ozone layer, discussed for example by Wayn [957]. In addition, N_2O lasers are used in medical applications and the gas is widely used as an anaesthetic.

There have been a number of experimental measurements of both total and differential electron–N_2O collision cross sections. Of particular interest in our comparison with the *R*-matrix calculations are total cross section measurements by Szmytkowski et al. [901, 902]. There have been two calculations, using independent polyatomic *R*-matrix computer programs, carried out by Morgan et al. [661] and by Sarpal et al. [814]. In the calculations by Morgan et al. two models were considered: a static-exchange (SE) model and a static-exchange-plus-polarization (SEP) model. In the SE model the N_2O target ground state was included in the first expansion in (11.12) and the second term in (11.12) was restricted to have the same form as the first, but with the additional electron occupying one of the virtual orbitals from the self-consistent-field (SCF) basis used to construct the target ground state. In the SEP model, the second term in (11.12) was constructed by allowing

one target electron to be excited from the target ground-state wave function into a virtual orbital, but the N-electron target part of the wave function was restricted to have the same spin symmetry as the target wave function used in the first term of (11.12). In the calculations by Sarpal et al. additional configurations were added in their SEP model to treat correlation effects in the states corresponding to the lower R-matrix poles.

We compare the SE and SEP integrated total cross section calculation results by Morgan et al. [661] with the experiments of Szmytkowski et al. [901, 902] in Fig. 11.9. The SE calculations of Morgan et al. [661] and Sarpal et al. [814] gave very similar results. Both calculations found a low-energy $^2\Pi$ shape resonance just below 4 eV which can be seen to have a major effect on the total cross section. However, the two SEP calculations produced somewhat different results. The SEP calculations of Morgan et al. found the $^2\Pi$ shape resonance at about 2 eV, close to but slightly lower than the experiments of Szmytkowski et al. However the Sarpal et al. calculations placed the SEP resonance at 0.8 eV. It is clear that the difference between the two SEP calculations is due to the difference in their treatment of the second L^2 term in the R-matrix expansion (11.12). A lack of balance between configuration interaction effects included in the first term in (11.12), representing electron correlation in the target, and configuration interaction effects included in the second term in (11.12), representing target polarization, can lead to errors in the location and width of the resonance.

Finally, we note that differential cross section results were also reported by Morgan et al. [661] over a range of energies from 5 to 10 eV. These were found to be in good agreement with experiments by Johnstone and Newell [507] except for some discrepancies at small and large scattering angles.

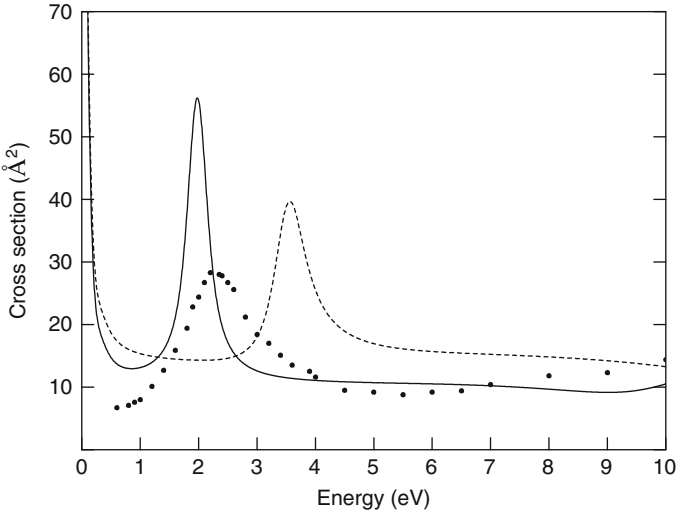

Fig. 11.9 Integrated total cross section for electron–N_2O collisions. *Full curve*: SEP model of Morgan et al. [661]; *broken curve*: SE model of Morgan et al. [661]; *full circles*: experiment by Szmytkowski et al. [901, 902] (Fig. 1 from [661])

11.1.7.4 Electron Collisions with H_3^+

Finally, we consider intermediate-energy electron–H_3^+ collision calculations by Gorfinkiel and Tennyson [404, 405] using a molecular extension of the *R*-matrix with pseudostates (M-RMPS) method discussed in Sect. 6.2. This work is particularly interesting since H_3^+, which is the simplest polyatomic molecular ion, is the dominant ion in low-temperature hydrogen plasmas. It also plays a fundamental role in interstellar chemistry and has been observed in planetary aurora and diffuse interstellar media where significant populations of energetic electrons are to be found. We have also mentioned in Sect. 3.3.4 that detailed dissociative recombination calculations have been carried out for this ion, combining multichannel quantum defect theory with a hyperspherical coordinate representation of the nuclear motion.

In the *R*-matrix calculations [404] two approximations have been considered. The first corresponds to an earlier calculation by Faure and Tennyson [312] where the lowest four target electronic states of H_3^+, X^1A_1', $^3E'$, $^1E'$ and $^3A_2''$ in D_{3h} symmetry were included in the *R*-matrix expansion. However, since the polyatomic *R*-matrix program uses D_{2h} or lower symmetry, the calculation was carried out using the C_{2v} point group. In this point group the doubly degenerate E' states split into A_1 and B_2 states yielding a 6-state *R*-matrix calculation corresponding to the X^1A_1,

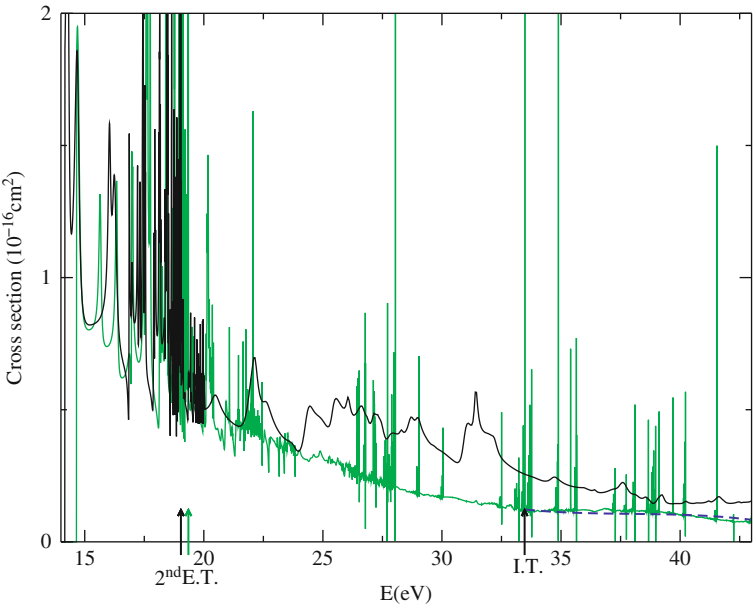

Fig. 11.10 Total cross section for electron impact excitation of the first excited electronic $^3E'$ state in H_3^+ from the X^1A_1' ground state at low and intermediate energies. *Dark full line*: 6-state calculation with no pseudostates; *light full line*: 64-state M-RMPS calculation; *dashed line*: fit to 64-state calculation above the ionization threshold, denoted by I.T. The *arrows* indicate the second excited threshold E.T. in each calculation and the I.T (Fig. 1 from [404])

$^3A_1$, $^3B_2$, $^1A_1$, $^1B_2$ and $^3B_1$ target states. In the second calculation, by Gorfinkiel and Tennyson, a further 58 pseudostates were included in the R-matrix expansion giving in total a 64-state M-RMPS calculation.

The total cross sections for electron impact excitation of the first excited electronic $^3E'$ state from the X^1A_1' ground state in the 6-state and 64-state approximations are presented in Fig. 11.10. We see that these two approximations are in good agreement at energies below about 20 eV. However, at energies above 20.78 eV, the energy of the highest target eigenstate included in the expansion, the M-RMPS calculation results in much reduced excitation cross sections due to loss of flux into the pseudostates. We also observe that the 6-state calculation exhibits more pronounced pseudoresonance structure at intermediate energies than the 64-state calculation which is close to a fully converged solution. In conclusion, this calculation shows that cross sections for electron collisions with simple polyatomic molecules can now be accurately calculated at both low and intermediate energies.

11.2 Positron Collisions with Molecules

In this section we consider briefly the extension of R-matrix theory to treat positron–molecule collisions and we present two illustrative examples of recent calculations. We commence in Sect. 11.2.1 by summarizing the extensions of R-matrix theory of positron collisions with atoms and ions given in Chap. 7 and R-matrix theory of electron collisions with molecules given in Sect. 11.1 of this chapter to enable positron–molecule collision processes to be accurately determined. We then consider the advances that have been made in recent years in positron–molecule collision calculations using R-matrix computer programs. Finally, in Sect. 11.2.2, we discuss the results of two recent positron–molecule collision calculations. Reviews of earlier positron–molecule collision theory and calculations have been given by Armour [22], Armour and Humberston [23] and Surko et al. [898].

11.2.1 R-Matrix Theory and Calculations

In collisions of positrons with molecules the following are the most significant processes that can occur:

$$
\begin{aligned}
e^+ + AB_{iv} &\rightarrow AB_{iv} + e^+ && \text{elastic scattering} \\
&\rightarrow AB_{i'v'} + e^+ && \text{vibrational and electronic excitation} \\
&\rightarrow AB^+_{i'v'} + e^- + e^+ && \text{ionization} \\
&\rightarrow AB^+_{i'v'} + Ps && \text{positronium formation} \\
&\rightarrow A_{i'} + B_{i'} + e^+ && \text{dissociation,}
\end{aligned}
\tag{11.110}
$$

which we see correspond to a combination of processes listed in (7.1) and (11.37). As in (11.37), we have not included the rotational quantum number j in (11.110) since rotational transitions can usually be included adiabatically.

The main difference between electron–molecule collision processes listed in (11.37) and positron–molecule collision processes listed in (11.110) is positronium formation where a positronium atom is formed leaving the residual molecular ion in its ground or an excited state. As pointed out in our discussion of positron collisions with atoms and ions in Sect. 7.1, the additional complexity of using antisymmetrized wave functions in electron collisions is replaced by the greater importance of including correlation (or polarization) effects due to the strong attraction between the positron and the electrons in positron collisions. While these effects can be represented by including additional correlation terms in the expansion of the positron collision wave function at low energies, it is clear that in order to calculate positronium formation cross sections, positronium formation channels must be included in the wave function expansion as in (7.13). Indeed, we observed in our discussion of positron collisions with atoms and ions in Chap. 7 that the inclusion of positronium formation channels in the wave function expansion is found to be necessary to obtain accurate positron–atom collision cross sections over a wide energy range as well as enabling positronium formation cross sections to be determined. We will see in our discussion of recent positron–molecule collision calculations in Sect. 11.2.2 that positronium formation channels should also be included in this case as well in order to obtain accurate collision cross sections for neutral molecules.

Before discussing in more detail two recent positron–molecule collision calculations in Sect. 11.2.2, we first summarize some important calculations that have been carried out in recent years using R-matrix theory. In practice most of these calculations have been based on expansions (11.11) and (11.12) in the internal region where, as discussed above, the antisymmetrization operator in (11.12) is omitted and additional quadratically integrable functions are included in the second expansion in (11.12) to allow for short-range positron–electron polarization effects.

In the first application of R-matrix theory to positron–molecule collisions, Tennyson [914] carried out low-energy calculations for e^+–H_2 and e^+–N_2 collisions using a modification of the diatomic electron–molecule computer program based on Slater-type orbitals [144, 528, 690]. In the case of e^+–H_2 good agreement was obtained with the Kohn variational calculation by Armour [21] provided that sufficient orbitals were included in the second expansion in (11.12) to represent important short-range polarization effects. In a later calculation by Tennyson and Morgan [919], these calculations were extended to low-energy e^+–CO collisions where, as well as elastic collision cross sections, rotationally inelastic and momentum transfer cross sections were obtained. The calculations were carried out using a number of different models representing the polarization and it was found that the computed total and momentum transfer cross sections varied widely between the different models employed. In a further important study of e^+–HF collisions, Danby and Tennyson [246] obtained strong evidence for a bound state of the e^+–HF system. Also, in e^+–H_2 collision calculations by Danby and Tennyson [247], results were presented for energies below the positronium formation threshold for a variety

of target representations. In addition two pseudostates were included in the expansion to account for polarization. Results were calculated for several symmetries and total and differential cross sections obtained. Danby and Tennyson [248] also extended the earlier work on e^+–HF collisions to determine vibrationally resolved e^+–N_2 collision cross sections using the adiabatic theory of Chase [217], discussed in Sect. 11.1.3, and the non-adiabatic R-matrix theory of Schneider et al. [829] and Gillan et al. [373], discussed in Sect. 11.1.4. Calculations were carried out in the fixed-nuclei approximation with up to 22 polarized pseudostates and for 12 internuclear separations, including the ground state and 10 polarized pseudostates. Cross sections were obtained for Σ_g^+, Σ_u^+, Π_g, Π_u, Δ_g and Δ_u symmetries for vibrational transitions $v = 0 \rightarrow 0$, $v = 0 \rightarrow 1$ and $v = 0 \rightarrow 2$ and it was found that non-adiabatic effects are significant for the $v = 0 \rightarrow 1$ cross section and dominate the $v = 0 \rightarrow 2$ cross section.

Finally, we mention more recent R-matrix calculations for positron collisions with polyatomic molecules. Baluja et al. [49] considered low-energy positron collisions with water, Franz et al. [339] considered low-energy positron collisions with carbon dioxide and Franz et al. [340] considered low-energy positron collisions with acetylene. In each case the R-matrix results were compared with other theoretical approaches and conclusions drawn concerning the accuracy and validity of the methods adopted. We consider the results of two of these calculations in Sect. 11.2.2.

11.2.2 Illustrative Examples: H_2O, CO_2

In this section we discuss in greater detail the R-matrix calculations by Baluja et al. [49] who considered positron collisions with water and by Franz et al. [339] who considered positron collisions with carbon dioxide. The role of target polarization effects in the CO_2 calculation is of crucial importance and methods for its inclusion are examined.

11.2.2.1 Positron Collisions with H_2O

We consider first the R-matrix calculations by Baluja et al. [49] who reported differential, integral and momentum transfer cross sections for vibrationally elastic and rotationally inelastic collisions of positrons with water at energies below 10 eV. The water molecule was described by an ab initio multicentre wave function and the calculations were carried out using a reprogrammed version of the electron–polyatomic molecule computer program (Morgan et al. [661, 662]) which uses Gaussian-type orbitals (GTOs). In the internal region the calculations were based on expansions (11.11) and (11.12) where the antisymmetrization operator in (11.12) was omitted. The H_2O ground state wave function was retained in the first expansion in (11.12), and quadratically integrable functions were included in the second expansion in (11.12) to relax orthogonality between the target and continuum orbitals and to allow for short-range polarization effects. In the external region the positron

moves in the long-range potential defined by the multipole moments of the target. For strongly dipolar molecules, such as water, it is also necessary to correct for the truncated partial wave expansion used in the calculation and this was achieved using the Born approximation.

The calculations were performed at the equilibrium geometry of the molecule and three independent models were used to represent the polarization effects. In the first "static" model the target was frozen in its ground state and the positron allowed to occupy all target and continuum orbitals with the appropriate symmetry. In the second "static + polarization" model, polarization effects were included by augmenting the target in the static model with 125 singlet excited states and the positron was allowed to occupy all target and continuum orbitals with the appropriate symmetry. Finally, in the third "natural orbital or NO" model polarization effects were introduced, as in electron–atom and electron–molecule collisions, by retaining four polarized pseudostates in expansion (11.12).

In Fig. 11.11 we compare rotationally summed elastic cross sections for positron collisions with water as a function of energy, calculated by Baluja et al. [49] for the different models discussed above. Also shown in this figure are cross sections calculated by Gianturco et al. [371] using a single-centre expansion where the static potential term in the positron–water interaction was augmented by a polarization potential determined from a homogeneous electron gas model. It can be seen that the dominant nature of the dipole moment of the water means that the results are

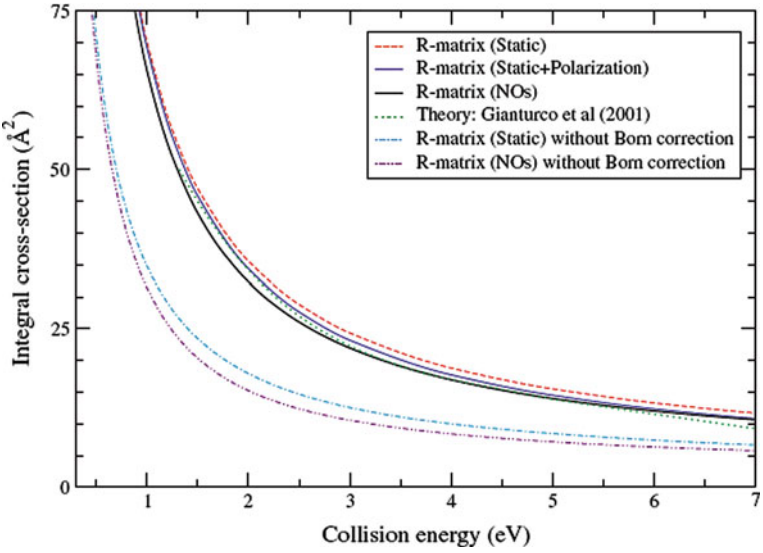

Fig. 11.11 *R*-matrix calculations of elastic (rotationally summed) integral cross sections for positron collisions with water as a function of the collision energy for three *R*-matrix models discussed in the text. Also shown are single-centre results calculated by Gianturco et al. [371] and results obtained without the Born correction which lie well below the other cross sections shown in the figure (Fig. 2 from [49])

rather insensitive to the degrees of polarization included in the model. Thus we see that the static, static + polarization and NO models all give similar results, which are also very similar to the results obtained by Gianturco et al. [371]. However, including the Born correction leads to a very significant increase in the calculated cross sections, particularly at low energies.

The elastic scattering results were also compared with several experiments and although there is considerable scatter in these experiments due to the importance of forward scattering, there is reasonable agreement between the best NO model and the most recent measurements by Zecca et al. [1004].

In conclusion, we see that once the Born correction is included to allow for the high partial waves contribution to the cross section arising from the large dipole moment of water, there is little difference between the integral cross sections obtained from the various models considered. The results obtained in this calculation are therefore expected to provide a realistic estimate of the positron–water elastic (rotationally summed) cross section below the positronium formation threshold.

11.2.2.2 Positron Collisions with CO_2

As our second example we consider the R-matrix calculations of positron collisions with carbon dioxide by Franz et al. [339] who reported differential and integral cross sections for positron collision energies below 8 eV. In this calculation particular attention was given to the inclusion of target polarization which plays a more important role than in positron collisions with polar molecules, such as water, discussed in our previous example.

In these calculations the multicentre polyatomic computer program using Gaussian-type orbitals (GTOs), adopted in the previous example, was used to describe the collision in a static-plus-polarization (SP) model based on expansions (11.11) and (11.12) without the antisymmetrization operator. In this model configuration space for the electrons was built up from the Hartree–Fock ground state by including all single-electron excitations into the virtual target molecular orbitals. Also the positron was allowed to occupy all target molecular orbitals as well as a set of single-centred diffuse Gaussian orbitals which were used to represent the continuum in the R-matrix internal region. In addition, in order to model polarization effects which were not fully described in this SP model, the electron–positron attraction integrals were scaled by an empirically adjusted enhancement factor f which increased the effect of target polarization on the collision cross section. Finally, in all the calculations reported the effect of the target quadrupole moment Q and the long-range polarizabilities α_0 and α_2 in (11.6) were included in the R-matrix expansion in the internal region, where the values $\alpha_0 = 15.608\ a_0^3$ and $\alpha_2 = 14.910\ a_0^3$, a_0 being the atomic unit of length, were calculated using density functional theory.

In Fig. 11.12 we compare the integral cross section for positron collisions with carbon dioxide calculated by Franz et al. [339] with experiment. The figure also shows the unscaled and the scaled R-matrix results as the polarization enhancement factor f is increased. The best agreement between theory and experiment is

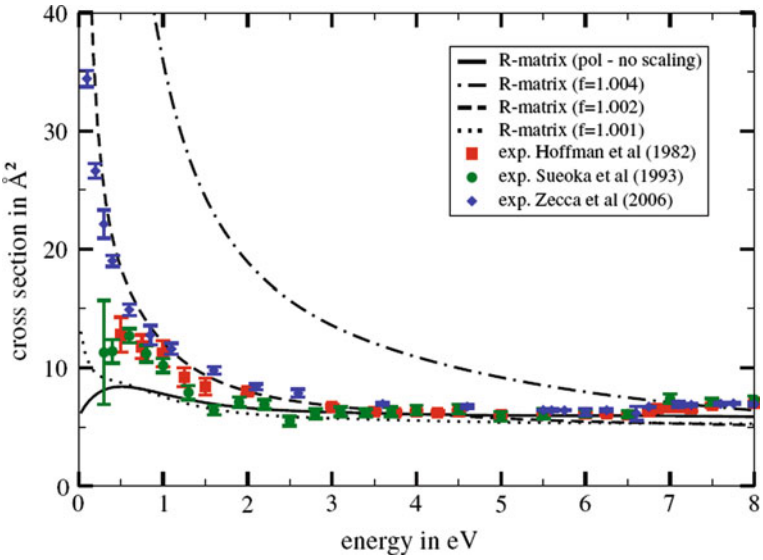

Fig. 11.12 Integral cross section for positron collisions with carbon dioxide showing the R-matrix results by Franz et al. [339] with no scaling and as the polarization enhancement factor f is increased. The experimental results are from Hoffman et al. [475], Sueoka and Hamada [893] and Zecca et al. [1005] (Fig. 1 from [339])

obtained with an enhancement factor $f = 1.002$, i.e. an enhancement of 0.2%. We see that without any scaling ($f = 1$) the calculated cross section is too low at incident positron energies below about 3 eV, but agrees well with experiment at higher energies. By using the enhancement factor the failure to fully describe the effect of molecular polarization at low energies is corrected, while maintaining the good agreement at higher energies.

Also in Fig. 11.13 we compare differential cross section (DCS) R-matrix calculations by Franz et al. [339] at 6.75 eV with experimental measurements by Przybyla et al. [760] where, since these measurements were not absolute, they have been scaled to give approximate agreement with theory. Also in this figure we have plotted single-centre calculations by Gianturco and Paioletti [370] at 7 eV, who used a local parameter-free correlation–polarization potential. In the absence of any scaling the R-matrix calculation shows a maximum in the forward direction and almost no oscillatory structure, while introducing a scaling factor $f = 1.002$ introduces oscillations in the DCS as a function of the scattering angle. However, while some oscillatory behaviour can be seen in the experimental data, the overall agreement between theory and experiment in the DCS remains unsatisfactory.

In conclusion, this calculation shows that in order to obtain agreement with experiment at low energies a scaling factor has to be introduced in order to fully represent the polarization of the molecule in positron–molecule collisions. As discussed in Sect. 11.2.1, it is clear that in order to represent the very strong attraction between the positron and the target electrons in a completely ab initio theory, positronium formation channels must be included in the expansion of the wave function, in anal-

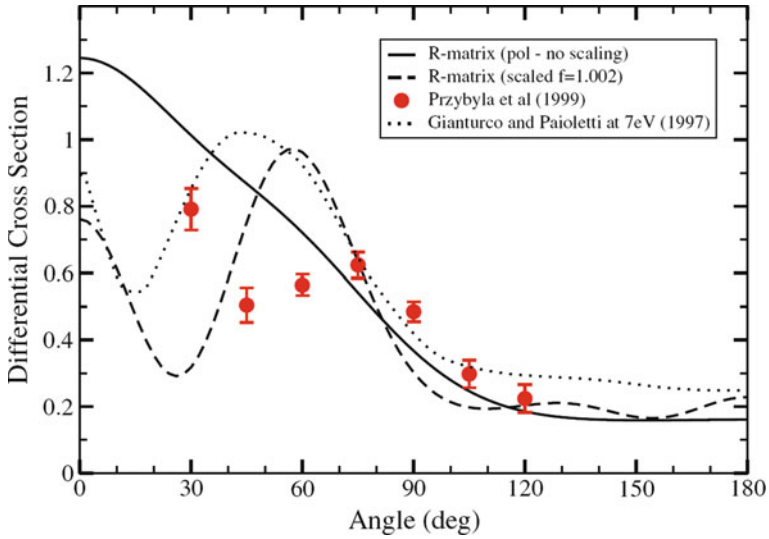

Fig. 11.13 Differential cross section in $Å^2/sr$ for positron collisions with carbon dioxide at 6.75 eV showing R-matrix results by Franz et al. [339] with no scaling and results with an enhancement factor $f = 1.002$, compared with measurements by Przybyla et al. [760] and single-centre calculations by Gianturco and Paioletti [370] at 7 eV (Fig. 5 from [339])

ogy with expansion (7.13) adopted in positron collisions with atoms and atomic ions. As pointed out by Franz et al. [339] this development, which is now under active consideration, is considerably more demanding for positron collisions with polyatomic molecules.

11.3 Molecular Multiphoton Processes

In this section we extend our discussion of R-matrix–Floquet theory of atomic multiphoton processes, considered in Chap. 9, to the interaction of intense laser fields with diatomic molecules. In Sect. 11.3.1 we consider R-matrix–Floquet theory of multiphoton ionization of a general diatomic molecule by an intense laser field. Then in Sect. 11.3.2 we illustrate this theory by considering its application to multiphoton ionization of H_2.

11.3.1 Molecular R-Matrix–Floquet Theory

We consider the following molecular multiphoton ionization process

$$n\mathrm{h}\nu + AB_i \rightarrow AB_j^+ + \mathrm{e}^-, \tag{11.111}$$

where AB_i is the initial electronic state of the diatomic molecule and AB_j^+ is the final electronic state of the molecular ion. We observe that, as in atomic R-matrix–Floquet theory considered in Sect. 9.1, laser-assisted electron–molecule collisions and harmonic generation can be treated by a straightforward extension of the theory presented in that section. The molecule, which in the present analysis contains $N+1$ electrons and is composed of two nuclei labelled A and B with nuclear charge numbers Z_A and Z_B, respectively, is immersed in an intense laser field with polarization direction $\hat{\boldsymbol{\epsilon}}$ as illustrated in Fig. 11.14. As in our discussion of electron–molecule collisions in Sect. 11.1.2, we treat the molecule in the fixed-nuclei approximation.

Following the theoretical developments given by Colgan et al. [187, 222–224], we proceed as in Sect. 9.1.1 by treating the laser field classically, using the dipole approximation and assuming it to be monochromatic, monomode, linearly polarized and spatially homogeneous. The corresponding electric field vector can then be written as

$$\boldsymbol{\mathcal{E}}(t) = \hat{\boldsymbol{\epsilon}}\mathcal{E}_0 \cos\omega t, \tag{11.112}$$

where $\hat{\boldsymbol{\epsilon}}$ is a unit vector along the laser polarization direction and ω is the angular frequency. The corresponding vector potential $\mathbf{A}(t)$ then satisfies

$$\mathbf{A}(t) = \hat{\boldsymbol{\epsilon}}A_0 \sin\omega t, \tag{11.113}$$

where $A_0 = -\mathrm{c}\mathcal{E}_0/\omega$ and where we have adopted the Coulomb gauge such that $\mathrm{div}\ \mathbf{A} = 0$. In Fig. 11.14 we have introduced two cartesian coordinate systems. First, a molecular fixed coordinate system (x, y, z) where the z-axis is chosen to lie along the internuclear axis from A to B. Second, a laser field fixed coordinate system (x', y', z'), where the z'-axis is chosen to lie along the laser field polarization direction $\hat{\boldsymbol{\epsilon}}$. The origins of both these coordinate systems are chosen to be the centre of gravity of the molecule, labelled G, and we introduce the Euler angles (α, β, γ), defined in Appendix B.5, which transform the (x, y, z) coordinate system into the (x', y', z') coordinate system. Also, the vector distances between A, B and G and

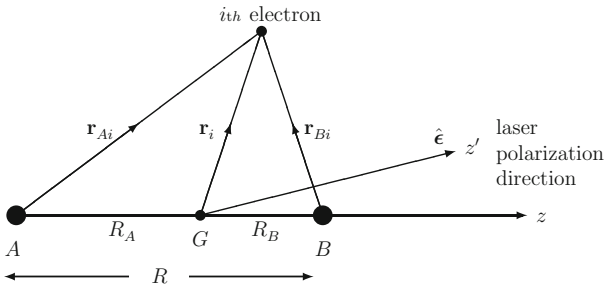

Fig. 11.14 Molecular frame of reference for multiphoton ionization of a diatomic molecule by a laser with polarization direction $\hat{\boldsymbol{\epsilon}}$, where the nuclei at A and B have nuclear charge numbers Z_A and Z_B and G is the centre of gravity of the molecule

the ith electron are given by $\mathbf{r}_{Ai}$, $\mathbf{r}_{Bi}$ and $\mathbf{r}_i$, respectively, and the corresponding distances of the two nuclei from G are R_A and R_B, where $R = R_A + R_B$ is the internuclear separation.

Neglecting relativistic effects, the molecular system in the presence of the laser field is described by the time-dependent Schrödinger equation

$$\left[H_{N+1} + \frac{1}{\mathrm{c}}\mathbf{A}(t)\cdot\mathbf{P}_{N+1} + \frac{N+1}{2\mathrm{c}^2}\mathbf{A}^2(t)\right]\widetilde{\Psi}(\mathbf{X}_{N+1}, t) = \mathrm{i}\frac{\partial}{\partial t}\widetilde{\Psi}(\mathbf{X}_{N+1}, t), \tag{11.114}$$

where H_{N+1} is the non-relativistic fixed-nuclei Hamiltonian of the $(N+1)$-electron molecular system in the absence of the laser field defined by (11.10) and where

$$\mathbf{P}_{N+1} = \sum_{i=1}^{N+1}\mathbf{p}_i \tag{11.115}$$

is the total electron momentum operator. Also, as in Chap. 9, the tilde on the time-dependent wave function $\widetilde{\Psi}$ in (11.114) and later equations distinguishes it from time-independent wave functions Ψ which we consider later in our analysis.

In order to solve (11.114) using R-matrix–Floquet theory we proceed, as in atomic multiphoton processes considered in Sect. 9.1.1 and in electron–molecule collisions considered in Sect. 11.1.2, by partitioning configuration space into three regions illustrated in Fig. 11.15, where the same criteria for defining the boundaries a_0 and a_p between the three regions, described in our discussion of Figs. 9.1 and 11.2, are adopted. We assume that the laser electric field vector defined by (11.112) has constant amplitude $\mathcal{E}_0$ and angular frequency ω so that we can represent the wave function in each region by a Floquet–Fourier expansion [325, 874] as follows:

$$\widetilde{\Psi}(\mathbf{X}_{N+1}, t) = \exp(-\mathrm{i}Et)\sum_{n=-\infty}^{\infty}\exp(-\mathrm{i}n\omega t)\Psi_n(\mathbf{X}_{N+1}). \tag{11.116}$$

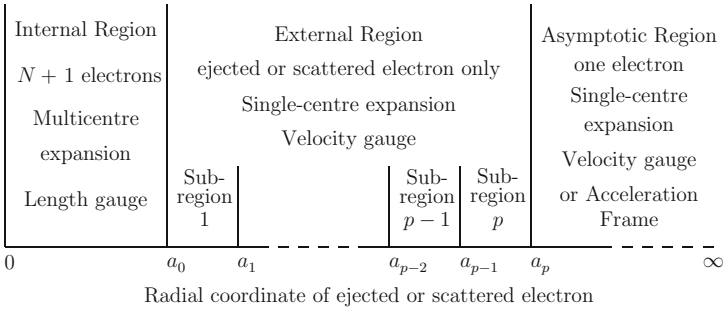

Fig. 11.15 Partitioning of configuration space in R-matrix–Floquet theory of molecular multiphoton processes

After substituting (11.116) into (11.114), we obtain an infinite set of coupled time-independent equations for the functions Ψ_n. The solutions of these equations in each region are then matched on the boundaries a_0 and a_p between the regions using the R-matrix. Finally, as described in Sect. 9.1.1, it is convenient and appropriate to use the length gauge to describe the laser–molecule interaction in the internal region and the velocity gauge to describe this interaction in the external and asymptotic regions. However, as discussed in Sects. 9.1.5 and 9.1.6, it is sometimes advantageous to adopt the acceleration frame in the asymptotic region. We now consider the solution in each of the three regions in turn.

11.3.1.1 Internal Region Solution

Following our analysis in Sect. 9.1.2, we transform (11.114) in the internal region to the dipole length gauge defined by the unitary transformation

$$\widetilde{\Psi}(\mathbf{X}_{N+1}, t) = \exp\left[-\frac{\mathrm{i}}{\mathrm{c}}\mathbf{A}(t)\cdot\mathbf{R}_{N+1}\right]\widetilde{\Psi}^{\mathbf{L}}(\mathbf{X}_{N+1}, t), \tag{11.117}$$

where

$$\mathbf{R}_{N+1} = \sum_{i=1}^{N+1}\mathbf{r}_i \tag{11.118}$$

and where the boldface superscript $\mathbf{L}$ in (11.117) and later equations indicates that the functions are defined in the dipole length gauge. Substituting (11.117) into (11.114) we find that $\widetilde{\Psi}^{\mathbf{L}}$ satisfies the time-dependent Schrödinger equation

$$(H_{N+1} + \mathcal{E}(t)\cdot\mathbf{R}_{N+1})\,\widetilde{\Psi}^{\mathbf{L}}(\mathbf{X}_{N+1}, t) = \mathrm{i}\frac{\partial}{\partial t}\widetilde{\Psi}^{\mathbf{L}}(\mathbf{X}_{N+1}, t). \tag{11.119}$$

We solve this equation by introducing the Floquet–Fourier expansion

$$\widetilde{\Psi}^{\mathbf{L}}(\mathbf{X}_{N+1}, t) = \exp(-\mathrm{i}Et)\sum_{n=-\infty}^{\infty}\exp(-\mathrm{i}n\omega t)\Psi_n^{\mathbf{L}}(\mathbf{X}_{N+1}), \tag{11.120}$$

where E is the quasi-energy of the corresponding stationary state. Substituting this expansion into (11.119) and equating the coefficient of $\exp[-\mathrm{i}(E + n\omega)t]$ to zero yields the infinite set of coupled time-independent equations

$$(H_{N+1} - E - n\omega)\Psi_n^{\mathbf{L}} + D_{N+1}(\Psi_{n-1}^{\mathbf{L}} + \Psi_{n+1}^{\mathbf{L}}) = 0, \tag{11.121}$$

where the dipole length operator

$$D_{N+1} = \frac{1}{2}\mathcal{E}_0\hat{\boldsymbol{\epsilon}}\cdot\mathbf{R}_{N+1} = \frac{1}{2}\mathcal{E}_0\sum_{i=1}^{N+1}z_i'. \tag{11.122}$$

In (11.122), z_i' is the z-coordinate of the ith electron in the (x', y', z') coordinate system defined in our discussion of Fig. 11.14. The calculation of the matrix elements of D_{N+1} between the molecular states referred to the molecular fixed coordinate system (x, y, z) requires D_{N+1} to be transformed from the (x', y', z') coordinate system to the (x, y, z) coordinate system. This transformation can be expressed in terms of Wigner rotation matrices using (B.91) which can be written here as

$$Y_{\ell m}(\theta', \phi') = \sum_{m'} D^{\ell}_{m'm}(\alpha, \beta, \gamma) Y_{\ell m'}(\theta, \phi), \tag{11.123}$$

where $Y_{\ell m}(\theta', \phi')$ and $Y_{\ell m'}(\theta, \phi)$ are spherical harmonics defined by (B.32) which are referred to the (x', y', z') and (x, y, z) coordinate systems, respectively. Using (11.123), and noting from (B.54) that

$$z' = r' \cos\theta' = (4\pi/3)^{1/2} r' Y_{10}(\theta', \phi'), \tag{11.124}$$

we find that

$$D_{N+1} = \frac{1}{2}\mathcal{E}_0 \left(\frac{4\pi}{3}\right)^{1/2} \sum_{i=1}^{N+1} r_i \sum_{m=-1}^{+1} D^{1}_{m0}(\alpha, \beta, \gamma) Y_{1\,m}(\theta_i, \phi_i), \tag{11.125}$$

where we note that if the Fano–Racah phase convention is adopted, see Appendix B.4, then the spherical harmonic $Y_{1\,m}(\theta_i, \phi_i)$ in (11.125) would be replaced by $-\mathrm{i}\mathcal{Y}_{1m}(\theta_i, \phi_i)$ according to (B.64). Having determined D_{N+1} we can then rewrite (11.121) as an infinite-dimensional matrix equation in photon space with the form

$$\left(\mathbf{H}_{\mathrm{F}}^{\mathbf{L}} - E\mathbf{I}\right) \boldsymbol{\Psi}^{\mathbf{L}} = 0, \tag{11.126}$$

where $\mathbf{H}_{\mathrm{F}}^{\mathbf{L}}$ is the Floquet Hamiltonian which is an infinite-dimensional tridiagonal matrix, with the form given by (9.16), $\boldsymbol{\Psi}^{\mathbf{L}}$ is a column vector with components $\ldots, \Psi^{\mathbf{L}}_{n-1}, \Psi^{\mathbf{L}}_{n}, \Psi^{\mathbf{L}}_{n+1}, \ldots$ and $\mathbf{I}$ is a unit matrix operator.

In order to solve (11.126) in the internal region in the fixed-nuclei approximation, we expand the solution vector $\boldsymbol{\Psi}^{\mathbf{L}}$, in analogy with (11.11) and (9.17), as follows:

$$\boldsymbol{\Psi}^{\mathbf{L}\delta}_{jE}(\mathbf{X}_{N+1}; R) = \sum_{k} \boldsymbol{\psi}^{\mathbf{L}\delta}_{k}(\mathbf{X}_{N+1}; R) A^{\mathbf{L}\delta}_{kj}(E). \tag{11.127}$$

In this equation and the following equations, we introduce a superscript δ which represents the quantum numbers conserved by the laser–molecule interaction process, in a similar way to the introduction of the superscript γ in (9.17). Also, as in (11.11) and (9.17), j labels the linearly independent solutions of (11.126), $\boldsymbol{\psi}^{\mathbf{L}\delta}_{k}$ are energy-independent basis functions and $A^{\mathbf{L}\delta}_{kj}(E)$ are energy-dependent expansion coefficients, which depend on the asymptotic boundary conditions satisfied by the

solutions $\boldsymbol{\Psi}_{jE}^{\mathbf{L}\delta}$ at the energy E. Following (9.20), we expand each Floquet–Fourier component of the vector basis functions $\boldsymbol{\psi}_{k}^{\mathbf{L}\delta}$ in a close coupling with pseudostates expansion given by

$$\psi_{nk}^{\mathbf{L}\delta}(\mathbf{X}_{N+1};\, R) = \mathcal{A} \sum_{\Delta ij} \overline{\Phi}_{n\Delta i}^{\delta}(\mathbf{X}_N;\, \hat{\mathbf{r}}_{N+1}\sigma_{N+1}) r_{N+1}^{-1} u_{n\Delta ij}^{0}(r_{N+1}) a_{n\Delta ijk}^{\mathbf{L}\delta}$$

$$+ \sum_{\Delta i} \chi_{n\Delta i}^{\delta}(\mathbf{X}_{N+1}) b_{n\Delta ik}^{\mathbf{L}\delta}, \quad k = 1, \ldots, n_t, \tag{11.128}$$

for each fixed internuclear separation R, where n_t is the total number of terms retained in the expansion. Also in (11.128), the summation over Δ goes over the molecular symmetries not conserved by the laser interaction, the channel functions $\overline{\Phi}_{n\Delta i}^{\delta}$ and quadratically integrable functions $\chi_{n\Delta i}^{\delta}$ are constructed from STOs or GTOs centred on the nuclei which vanish by the boundary $r = a_0$ of the internal region and finally the continuum basis orbitals $u_{n\Delta ij}^{0}$ are represented by numerical basis functions centred on G in Fig. 11.14 which are non-vanishing on the boundary $r = a_0$ of the internal region.

The coefficients $a_{n\Delta ijk}^{\mathbf{L}\delta}$ and $b_{n\Delta ik}^{\mathbf{L}\delta}$ in (11.128) are determined by diagonalizing the operator $\mathbf{H}_{\mathrm{F}}^{\mathbf{L}} + \boldsymbol{\mathcal{L}}_{N+1}$ in this basis over the internal region as follows

$$\langle \boldsymbol{\psi}_{k}^{\mathbf{L}\delta} | \mathbf{H}_{\mathrm{F}}^{\mathbf{L}} + \boldsymbol{\mathcal{L}}_{N+1} | \boldsymbol{\psi}_{k'}^{\mathbf{L}\delta} \rangle_{\mathrm{int}} = \mathbf{E}_{k}^{\mathbf{L}\delta} \delta_{kk'}, \quad k,\ k' = 1, \ldots, n_t, \tag{11.129}$$

where $\mathbf{E}_{k}^{\mathbf{L}\delta}$ is a diagonal matrix in photon space. Also in (11.129), $\boldsymbol{\mathcal{L}}_{N+1}$ is a Bloch operator which is diagonal in photon space and is chosen so that $\mathbf{H}_{\mathrm{F}}^{\mathbf{L}} + \boldsymbol{\mathcal{L}}_{N+1}$ is hermitian in the internal region in the basis of quadratically integrable functions satisfying arbitrary boundary conditions at $r = a_0$. We can write this operator as

$$\boldsymbol{\mathcal{L}}_{N+1} = \sum_{i=1}^{N+1} \frac{1}{2} \delta(r_i - a_0) \left(\frac{\mathrm{d}}{\mathrm{d}r_i} - \frac{b_0 - 1}{r_i} \right) \mathbf{I}, \tag{11.130}$$

where $\mathbf{I}$ is a unit matrix in photon space and b_0 is an arbitrary constant which is often set equal to zero. We note that $\boldsymbol{\mathcal{L}}_{N+1}$ has the same single-centre form as the Bloch matrix (9.22) adopted in atomic R-matrix–Floquet theory, since only the continuum basis orbitals $u_{n\Delta ij}^{0}(r)$ in expansion (11.128), which are centred on the centre of gravity G in Fig. 11.14, are non-zero on the boundary $r = a_0$. These calculations can be performed using standard molecular structure program packages used to diagonalize $H_{N+1} + \mathcal{L}_{N+1}$ in (11.13), extended to calculate the matrix elements of the dipole length operator D_{N+1} defined by (11.125).

We can now solve (11.126) in the internal region in the usual way by rewriting it as

$$\left(\mathbf{H}_{\mathrm{F}}^{\mathbf{L}} + \boldsymbol{\mathcal{L}}_{N+1} - E\mathbf{I} \right) \boldsymbol{\Psi}_{jE}^{\mathbf{L}\delta} = \boldsymbol{\mathcal{L}}_{N+1} \boldsymbol{\Psi}_{jE}^{\mathbf{L}\delta}, \tag{11.131}$$

which has the formal solution

$$\boldsymbol{\Psi}_{jE}^{\mathbf{L}\delta} = \left(\mathbf{H}_{\mathrm{F}}^{\mathbf{L}} + \boldsymbol{\mathcal{L}}_{N+1} - E\mathbf{I}\right)^{-1} \boldsymbol{\mathcal{L}}_{N+1} \boldsymbol{\Psi}_{jE}^{\mathbf{L}\delta}. \tag{11.132}$$

Using the spectral representation of $\mathbf{H}_{\mathrm{F}}^{\mathbf{L}} + \boldsymbol{\mathcal{L}}_{N+1}$ given by (11.129), we can rewrite (11.132) in the form

$$|\boldsymbol{\Psi}_{jE}^{\mathbf{L}\delta}\rangle = \sum_k |\boldsymbol{\psi}_k^{\mathbf{L}\delta}\rangle \frac{1}{\mathbf{E}_k^{\mathbf{L}\delta} - E\mathbf{I}} \langle \boldsymbol{\psi}_k^{\mathbf{L}\delta} | \boldsymbol{\mathcal{L}}_{N+1} | \boldsymbol{\Psi}_{jE}^{\mathbf{L}\delta}\rangle. \tag{11.133}$$

Projecting this equation onto the channel functions $\overline{\Phi}_{n\Delta i}^{\delta}$ and onto the nth component in photon space and evaluating on the boundary $r = a_0$ yields

$$F_{n\Delta ij}^{\mathbf{L}\delta}(a_0) = \sum_{n'\Delta'i'} R_{n\Delta in'\Delta'i'}^{\mathbf{L}\delta}(E) \left(a_0 \frac{\mathrm{d}F_{n'\Delta'i'j}^{\mathbf{L}\delta}}{\mathrm{d}r} - b_0 F_{n'\Delta'i'j}^{\mathbf{L}\delta} \right)_{r=a_0}, \tag{11.134}$$

where we have introduced the R-matrix $R_{n\Delta in'\Delta'i'}^{\mathbf{L}\delta}(E)$ in the length gauge by

$$R_{n\Delta in'\Delta'i'}^{\mathbf{L}\delta}(E) = \frac{1}{2a_0} \sum_{k=1}^{n_t} \frac{w_{n\Delta ik}^{\mathbf{L}\delta} w_{n'\Delta'i'k}^{\mathbf{L}\delta}}{E_k^{\mathbf{L}\delta} - E}, \tag{11.135}$$

the reduced radial wave functions $F_{n\Delta ij}^{\mathbf{L}\delta}(r)$ by

$$F_{n\Delta ij}^{\mathbf{L}\delta}(r) = \langle r_{N+1}^{-1} \overline{\Phi}_{n\Delta i}^{\delta} | \Psi_{njE}^{\mathbf{L}\delta} \rangle', \tag{11.136}$$

and the surface amplitudes $w_{n\Delta ik}^{\mathbf{L}\delta}$ by

$$w_{n\Delta ik}^{\mathbf{L}\delta} = \langle r_{N+1}^{-1} \overline{\Phi}_{n\Delta i}^{\delta} | \psi_{nk}^{\mathbf{L}\delta} \rangle'_{r_{N+1}=a_0} = \sum_j u_{n\Delta ij}^0(a_0) a_{n\Delta ijk}^{\mathbf{L}\delta}. \tag{11.137}$$

As in (9.28) and (9.29), the primes on the Dirac brackets in (11.136) and (11.137) mean that the integrations are carried out over the space and spin coordinates of all $N+1$ electrons in the internal region except the radial coordinate r_{N+1} of the ejected or scattered electron. Also $\Psi_{njE}^{\mathbf{L}\delta}$ in (11.136) are the components of the solution vector $\boldsymbol{\Psi}_{jE}^{\mathbf{L}\delta}$ defined by (11.127). If necessary, a Buttle correction to the R-matrix is added to the summation in (11.135) as discussed in Sect. 5.3.2. The R-matrix then provides the boundary condition at $r = a_0$ for solving (11.114) in the external region.

11.3.1.2 External Region Solution

In the external region, defined in Fig. 11.15, the ejected or scattered electron, with radial coordinate $a_0 \leq r_{N+1} \leq a_p$, is described using the velocity gauge, while the remaining N electrons, with radial coordinates $r_i \leq a_0$, $i = 1, \ldots, N$, are described using the length gauge. We proceed, as in Sect. 9.1.3 describing atomic R-matrix–Floquet theory, by reducing the time-dependent Schrödinger equation (11.114) using a Floquet–Fourier expansion to yield the following infinite set of coupled time-independent equations:

$$\left(H_{N+1} - E^{\mathbf{V}} - n\omega\right) \Psi_n^{\mathbf{V}} + D_N \left(\Psi_{n-1}^{\mathbf{V}} + \Psi_{n+1}^{\mathbf{V}}\right) + P_{N+1} \left(\Psi_{n-1}^{\mathbf{V}} - \Psi_{n+1}^{\mathbf{V}}\right) = 0, \tag{11.138}$$

where in analogy with (11.125) the dipole length operator D_N is now defined by

$$D_N = \frac{1}{2}\mathcal{E}_0 \left(\frac{4\pi}{3}\right)^{1/2} \sum_{i=1}^{N} r_i \sum_{m=-1}^{+1} D_{m0}^{1}(\alpha, \beta, \gamma) Y_{1\,m}(\theta_i, \phi_i), \tag{11.139}$$

where $Y_{1\,m}(\theta_i, \phi_i)$ is replaced by $-\mathrm{i}\mathcal{Y}_{1m}(\theta_i, \phi_i)$ if the Fano–Racah phase convention is adopted. Also the dipole velocity operator P_{N+1} is defined by

$$P_{N+1} = \mathrm{i}\frac{A_0}{2\mathrm{c}} \hat{\boldsymbol{\epsilon}} \cdot \mathbf{p}_{N+1}. \tag{11.140}$$

As in Sect. 9.1.3, we rewrite (11.138) in matrix form as

$$\left(\mathbf{H}_{\mathrm{F}}^{\mathbf{V}} - E^{\mathbf{V}}\mathbf{I}\right) \boldsymbol{\Psi}^{\mathbf{V}} = 0, \tag{11.141}$$

where $\mathbf{H}_{\mathrm{F}}^{\mathbf{V}}$ is the Floquet Hamiltonian which is an infinite-dimensional tridiagonal matrix operator in photon space.

In order to solve (11.141) we introduce the following single-centre close coupling expansion for the components $\Psi_n^{\mathbf{V}\delta}$ of the total wave function at energy E for each set of conserved quantum numbers denoted by δ, which has the same general form as (9.37)

$$\Psi_{njE}^{\mathbf{V}\delta}(\mathbf{X}_{N+1}) = \sum_{\Delta i} \overline{\Phi}_{n\Delta i}^{\delta}(\mathbf{X}_N; \hat{\mathbf{r}}_{N+1}\sigma_{N+1}) r_{N+1}^{-1} F_{n\Delta ij}^{\mathbf{V}\delta}(r_{N+1}), \quad r_{N+1} \geq a_0, \tag{11.142}$$

where the channel functions $\overline{\Phi}_{n\Delta i}^{\delta}$, retained in this expansion, are the same as those retained in the internal region expansion (11.128) and the multicentre quadratically integrable functions $\chi_{n\Delta i}^{\delta}$ in (11.128), which are confined to the internal region, are now omitted. Also, as in (11.127), j labels the linearly independent solutions of (11.141). Substituting expansion (11.142) into (11.141) and projecting onto the channel functions $\overline{\Phi}_{n\Delta i}^{\delta}$ and onto the nth component of the wave function in photon

space then yields the following set of coupled second-order differential equations:

$$\left(\frac{\mathrm{d}^2}{\mathrm{d}r^2} - \frac{\ell_i(\ell_i+1)}{r^2} + \frac{2(Z-N)}{r} + k_{ni}^2\right) F_{n\Delta ij}^{\mathbf{V}\delta}(r)$$

$$= 2\sum_{n'\Delta' i'} W_{n\Delta in'\Delta' i'}^{\mathbf{V}\delta}(r) F_{n'\Delta' i'j}^{\mathbf{V}\delta}(r), \quad r \geq a_0. \tag{11.143}$$

In this equation, ℓ_i is the orbital angular momentum of the ejected or scattered electron, Z is the sum of the nuclear charge numbers which, for the diatomic molecule illustrated in Fig. 11.14, is given by

$$Z = Z_A + Z_B, \tag{11.144}$$

and

$$k_{ni}^2 = 2\left(E^{\mathbf{V}} - \overline{e}_i - n\omega\right), \tag{11.145}$$

where the channel energies $\overline{e}_i$ are defined by (11.24). Finally in (11.143), $W_{n\Delta in'\Delta' i'}^{\mathbf{V}\delta}(r)$ is the long-range potential matrix coupling the channels. Following our discussion of atomic multiphoton processes considered in Sect. 9.1.3, this potential can be written in matrix notation as

$$\mathbf{W}^{\mathbf{V}\delta} = \mathbf{V}^{E\delta} + \mathbf{V}^{D\delta} + \mathbf{V}^{P\delta}, \tag{11.146}$$

where, as in (9.41), $\mathbf{V}^{E\delta}$, $\mathbf{V}^{D\delta}$ and $\mathbf{V}^{P\delta}$ arise, respectively, from the H_{N+1}, D_N and P_{N+1} terms in (11.138). We derive explicit expressions for the matrix elements corresponding to $\mathbf{V}^{E\gamma}$, $\mathbf{V}^{D\gamma}$ and $\mathbf{V}^{P\gamma}$ which arise in atomic R-matrix–Floquet theory in Appendix D.2 and a similar procedure can be used in the case of the matrix elements arising in (11.146).

In order to solve (11.143) in the external region, the boundary condition satisfied by the functions $F_{n\Delta ij}^{\mathbf{V}\delta}(r)$ at $r = a_0$ can be determined from the R-matrix in the length gauge, defined by (11.135), using the same procedure adopted in our discussion of atomic multiphoton processes, considered in Sect. 9.1.3. Finally, the coupled second-order differential equations (11.143) have the same form as the corresponding equations (9.38) obtained in our discussion of atomic multiphoton processes. Hence the same procedure considered in Sect. 9.1.3 can be used to propagate the R-matrix across the external region from $r = a_0$ to a_p.

11.3.1.3 Asymptotic Region Solution

In the asymptotic region, shown in Fig. 11.15, the ejected or scattered electron with radial coordinate $r_{N+1} \geq a_p$ can be described either in the velocity gauge or in the acceleration frame, while the remaining N electrons with radial coordinates

$r_i \leq a_0$, $i = 1, \ldots, N$, are described in the length gauge. In both cases the collision process is described, after using a Floquet–Fourier expansion, by a single-centre expansion and the corresponding solution can be obtained as in atomic R-matrix–Floquet theory considered in Sects. 9.1.4, 9.1.5 and 9.1.6. In the case of multiphoton ionization, which has been of most experimental interest, the coupled differential equations, which can be written in the same form as (9.61), are usually solved in the velocity gauge. After reducing these equations to the form given by (9.79), the solution is then determined by an asymptotic expansion as described in Appendix F.2. The required outgoing wave solution is then determined by an iterative procedure yielding the complex quasi-energy E^{V} which can be written as (9.95), where Γ is the total multiphoton ionization rate. In the case of laser-assisted electron–molecule collisions, the solution in the velocity gauge can be transformed to the acceleration frame, as described in Sect. 9.1.5 or 9.1.6, where the asymptotic form of the solution is defined, yielding the S-matrix and the collision cross sections in the fixed-nuclei approximation.

11.3.2 Illustrative Example: H_2

We conclude our discussion of molecular multiphoton processes by considering the application of molecular R-matrix–Floquet theory to multiphoton ionization of H_2 by Colgan et al. [223, 224]. We also note that two-photon double-electron ionization calculations of H_2 have been carried out by Colgan et al. [226] using the time-dependent close coupling method reviewed by Pindzola et al. [740]. In the R-matrix calculations by Colgan et al. [223, 224] the following process was considered:

$$n\mathrm{h}\nu + \mathrm{H}_2 \rightarrow \mathrm{H}_2^+ + \mathrm{e}^-, \tag{11.147}$$

where the molecule was assumed to be aligned along the linearly polarized laser field direction and the fixed-nuclei approximation was adopted, in which the motion of the ejected and target electrons was calculated in the laser field and in the field of the nuclei which were fixed in space. Two target states of the residual H_2^+ ion were retained in the R-matrix expansion (11.128), corresponding to the $1\sigma_{\mathrm{g}}\, \mathrm{X}\, ^2\Sigma_{\mathrm{g}}^+$ ground state and the $1\sigma_{\mathrm{u}}\, ^2\Sigma_{\mathrm{u}}^+$ first excited state. These states were represented by LCAO–MO–SCF wave functions, which were constructed from a 1s-2s-2p STO σ basis which had been adopted by Tennyson et al. [921] in a study of electron collisions with H_2^+. Also, the continuum orbitals $u^0_{n\Delta ij}(r)$ in (11.128) were represented by numerical basis functions obtained using a Schmidt orthogonalization procedure (Tennyson et al. [922]), and the quadratically integrable functions $\chi^{\delta}_{n\Delta i}$ in (11.128) were included to ensure completeness within the two-target state model.

The calculations were carried out for a number of fixed internuclear separations R, ranging from 1.0 to 2.6 a.u., where the potential energy curves for the system are illustrated in Fig. 11.16. Also shown in this figure are the Rydberg bound states converging to the $H_2^+(\mathrm{X}\, ^2\Sigma_{\mathrm{g}}^+)$ ground state and doubly excited states converging

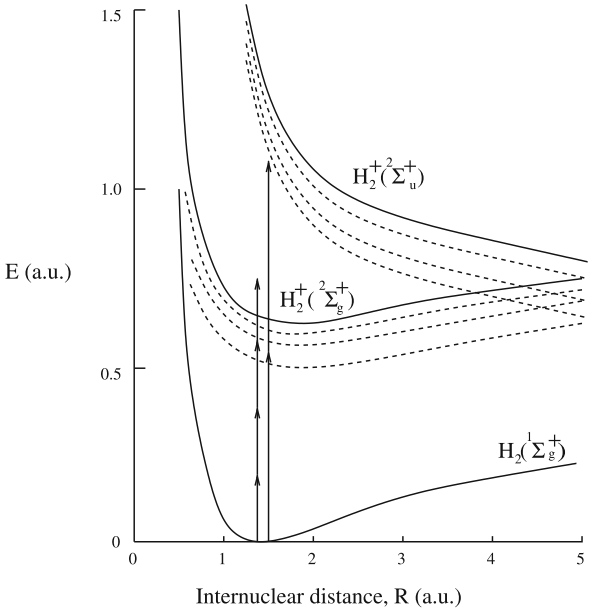

Fig. 11.16 Potential energy curves of H_2 and H_2^+. The *broken curves* represent Rydberg bound states converging to the $H_2^+(X\,^2\Sigma_g^+)$ ground state and doubly excited states converging to the $H_2^+(\,^2\Sigma_u^+)$ first excited state. Two- and four-photon processes are illustrated by *vertical lines* (Fig. 1 from [224])

to the $H_2^+(\,^2\Sigma_u^+)$ first excited state. Multiphoton ionization rates were obtained corresponding to one-photon, two-photon and four-photon ionization. In addition, calculations were carried out using both a one-state approximation, i.e. where just the $H_2^+(X\,^2\Sigma_g^+)$ ground state was included in the R-matrix expansion, and using a two-state approximation, where the $H_2^+(X\,^2\Sigma_g^+)$ ground state and the $H_2^+(\,^2\Sigma_u^+)$ first excited electronic state were included in the expansion. The results of the four-photon ionization rates, calculated using both the one-state approximation and the two-state approximation at the equilibrium internuclear separation of 1.4 a.u., are presented in Fig. 11.17. These calculations were carried out at three laser intensities 10^{13}, 3×10^{13} and 10^{14} W/cm^2 for a range of frequencies, which included the fundamental KrF laser frequency and the third harmonic of the Ti:Sapphire laser frequency, which are indicated by arrows in this figure. We see that the multiphoton ionization rates are dominated by resonance-enhanced multiphoton ionization (REMPI) peaks, where the first three photons excite a Rydberg bound state of the H_2 molecule and the fourth photon ionizes this state, as shown in Fig. 11.16. Due to the ponderomotive shift of the ionization threshold and the associated Rydberg states, these peaks go in and out of resonance as the laser intensity is increased, as discussed in Sect. 9.2.1. The good agreement between the results obtained using the one-state and two-state approximations indicates that the two-state results are close to convergence at the laser intensities and the low ejected electron energies considered in these calculations. Calculations were also carried out by Colgan et al. [224] which showed that the positions of the REMPI peaks are strongly dependent on the internuclear separation. This suggests that the population in different $H_2^+(X\,^2\Sigma_g^+)$ vibrational states can be controlled by varying the laser intensity and frequency. In

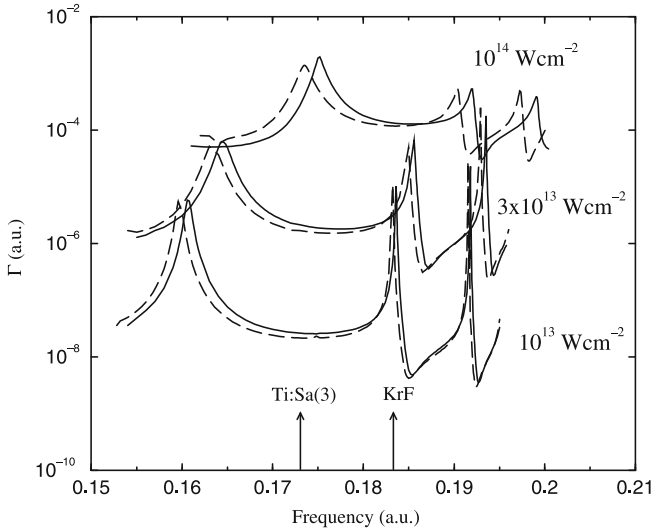

Fig. 11.17 Four-photon ionization rates in H_2, calculated at the equilibrium internuclear separation of 1.4 a.u. for three laser intensities as a function of laser frequency. The *full curves* and *broken curves* give the results obtained in the one- and two-state approximations, respectively. The frequencies of the KrF laser and the third harmonic of the Ti:Sapphire laser are indicated by *arrows* (Fig. 9 from [224])

addition, the probability of dissociation via the $H_2^+(\,^2\Sigma_u^+)$ repulsive state, illustrated in Fig. 11.16, will also depend strongly on the laser parameters. However, a full understanding of these processes will require the inclusion of the nuclear motion using non-adiabatic R-matrix theory of molecular multiphoton ionization, analogous to non-adiabatic R-matrix theory of electron–molecule collisions, discussed in Sect. 11.1.4.

In conclusion, we have seen that R-matrix–Floquet theory of multiphoton ionization of H_2 in the fixed-nuclei approximation yields interesting and important results. The extension of non-adiabatic R-matrix theory to include nuclear motion and to consider more complex multi-electron molecules are important objectives for future work in this field. Also, the extension of R-matrix theory and computer programs to treat the interaction of ultra-short laser pulses with molecules, using an extension of time-dependent R-matrix theory discussed in Chap. 10, is under active consideration.

Chapter 12
Electron Interactions in Solids

In this chapter we consider two extensions of R-matrix theory which describe interactions of electrons in solids. In Sect. 12.1 we consider an extension of R-matrix theory by Michiels et al. [648, 649] and Jones et al. [511] which describes low-energy electron collisions with transition metal oxides. This theory enables recent electron energy loss spectroscopy (EELS) experiments to be analysed and we show that calculations using this theory are in reasonable agreement with electron spin-flip measurements of Müller et al. [670] and with spin-averaged differential cross section measurements by Gorschlüter and Merz [406]. We also note that work has been initiated by Higgins et al. [186, 469] extending R-matrix theory to describe low-energy electron collisions with surface adsorbates.

In Sect. 12.2, we consider an extension of R-matrix theory which describes electron transport in two-dimensional semiconductor devices in the presence of an external field. This extension was introduced by Jayasekera et al. [500, 501], in an analysis of experiments by Goel et al. [384], which showed that R-matrix theory could be used to describe the transmission of electrons in four-terminal devices. Further developments and applications to solid-state devices have also been made by Jayasekera et al. [502].

We conclude this introduction by observing that a closely related "embedding method" of solving Schrödinger's equation for solid-state systems, in which space is divided into sub-regions, has been considered by Inglesfield [491]. For example, in the study of surfaces using the embedding method a surface potential is derived which can be added to Schrödinger's equation for a limited region of space embedded in an extended bulk substrate. This potential, which is energy dependent and non-local, is added to the Hamiltonian for the surface region and is determined from the Green's function for the bulk substrate. The embedding method was reviewed by Inglesfield [492] who considered two surface applications of the method. The first was the study of Rydberg series of electron states bound by the image potential [674], and the second was the study of Xe adsorbed on the surface of Ag [220]. Inglesfield also discussed a quite different application of the embedding method to the problem of electrons confined by a hard wall potential [234]. He then considered its relation to the R-matrix method, where the links with the R-matrix method are not just in the division of space into two or more regions but also in the mathematical structure of the method.

P.G. Burke, *R-Matrix Theory of Atomic Collisions*, Springer Series on Atomic, Optical, and Plasma Physics 61, DOI 10.1007/978-3-642-15931-2_12,

12.1 Electron Collisions with Transition Metal Oxides

In this section we consider an extension of R-matrix theory by Michiels et al. [648, 649] and Jones et al. [511] which describes electron transport in transition metal oxides using electron energy loss spectroscopy (EELS) experiments.

12.1.1 Introduction

Low-energy electron collision experiments with solid-state targets provide an important probe of the electronic structure of solids, yielding information on the momentum and energy transfer associated with excitations (see, for example, Fuggle and Inglesfield [354]). At high incident electron energies this process can be described in the Born approximation by a dielectric loss function. However, recently there has been increasing interest in low-energy EELS (LE-EELS) in which incident electrons, with energy typically in the range 20–100 eV, excite non-dipole-allowed transitions including electron exchange effects which can give rise to multiplicity-changing transitions. These LE-EELS experiments, which show a wealth of angle, spin polarization and energy-dependent structure (Fromme et al. [352, 353] and Gorschlüter and Merz [406]), have been used to study the localized 3d–3d excitations in transition metal compounds, such as NiO and CoO, and also the even more localized 4f–4f excitations in rare earth metals, such as Gd (Matthew et al. [646] and Porter et al. [750]). However, while the energy loss spectra, measured in this way, can be described by parametrized crystal field models, the R-matrix approach described in this section is one of the first ab initio procedures which can explain the energy loss spectra and their dependence on incident energy, angle of scattering and spin polarization.

12.1.2 R-Matrix Theory

The generalization of R-matrix theory to describe low-energy electron collisions with transition metal oxides was made by Michiels et al. [648, 649] and Jones et al. [511] where the localized 3d–3d excitations in the transition metal compound NiO were studied. Following Jones et al. [511] we now briefly describe how R-matrix theory of electron collisions with atoms and atomic ions, discussed in Chap. 5, can be extended to describe the electronic transitions of Ni^{2+} ions which are situated in a crystal field. In contrast to electron collisions with a free Ni^{2+} ion, which can be treated using R-matrix theory presented in Chap. 5, we will see that the crystal field potential has a strong effect on the interaction between the scattered electron and the target ion.

We consider first the target states of the Ni^{2+} ion in an octahedral crystal field, where we limit our discussion to states associated with 3d–3d excitation, although other transitions can be treated by a straightforward extension of the theory

considered here. The Ni^{2+} $3d^8$ configuration gives rise to the following five terms in the spherical environment of the free ion

$$^1S^e,\ ^3P^e,\ ^1D^e,\ ^3F^e,\ ^1G^e, \tag{12.1}$$

where $^3F^e$ is the ground term. Also the crystal field potential has the form [894]

$$V_C(r,\theta,\phi) = \left(\frac{7}{12}\right)^{1/2} \beta r^4 \left[Y_{40}(\theta,\phi) + \left(\frac{5}{14}\right)^{1/2} [Y_{44}(\theta,\phi) + Y_{4-4}(\theta,\phi)] \right] + V_M, \tag{12.2}$$

where the Madelung potential V_M is the electrostatic shift at the origin due to the neighbouring ions which is fitted to Hartree–Fock band structure calculations [929]. This potential splits the 5 spherical terms into 11 target states as follows

$$\begin{aligned}
^1S^e &\rightarrow\ ^1A_{1g} \\
^3P^e &\rightarrow\ ^3T_{1g} \\
^1D^e &\rightarrow\ ^1E_g + {}^1T_{2g} \\
^3F^e &\rightarrow\ ^3A_{2g} + {}^3T_{1g} + {}^3T_{2g} \\
^1G^e &\rightarrow\ ^1A_{1g} + {}^1E_g + {}^1T_{1g} + {}^1T_{2g},
\end{aligned} \tag{12.3}$$

where the labelling of the states on the right corresponds to the irreducible representations of the octahedral O_h symmetry group [928]. These states are determined as linear combinations of the five spherical states, determined by a Hartree–Fock calculation of Ni^{2+}.

Having determined the target states, we are now in a position to construct the configuration interaction basis in the internal region, corresponding to expansion (5.6) in electron collisions with atoms and atomic ions. The channel functions are formed by coupling the target states, having symmetries defined by (12.3), with the spin–angle function of the scattered electron. The angular functions, which are appropriate to cubic symmetry are constructed from spherical harmonics, as follows

$$X^{p\mu}_{h\ell}(\theta_{N+1},\phi_{N+1}) = \sum_m Y_{\ell m}(\theta_{N+1},\phi_{N+1}) b^{p\mu}_{h\ell m}, \tag{12.4}$$

where p denotes the irreducible representation (IR) and μ its component. Also h labels the different possible linear combinations of the spherical harmonics with angular momentum ℓ that transform according to the pth IR. The radial continuum basis orbitals $u^0_{ij}(r)$ in (5.6) representing the scattered electron are chosen to satisfy a zero-order differential equation corresponding to (5.75). The additional quadratically integrable functions, which are included in (5.6), come from the $3d^9$ configuration of Ni^+ with spherical $^2D^e$ symmetry which splits into ^2E_g and $^2T_{2g}$ symmetries in the octahedral crystal field. Finally, the coefficients corresponding to

a_{ijk}^{Γ} and b_{ik}^{Γ} in (5.6) are obtained by diagonalizing the $(N+1)$-electron crystal field Hamiltonian and Bloch operator $H_{N+1}^{\mathrm{CF}} + \mathcal{L}_{N+1}$ in the internal region where

$$H_{N+1}^{\mathrm{CF}} = H_{N+1} + V_{N+1}^{\mathrm{C}}, \tag{12.5}$$

and where $\mathcal{L}_{N+1}$ is the Bloch operator, defined by (5.8). Also in (12.5), H_{N+1} is the non-relativistic Hamiltonian in the absence of the crystal field defined by (5.3) and

$$V_{N+1}^{\mathrm{C}} = \sum_{i=1}^{N+1} V_{\mathrm{C}}(r_i, \theta_i, \phi_i), \tag{12.6}$$

where V_{C} is the crystal field potential defined by (12.2).

The radius a_0 of the internal region in Fig. 5.1 should, in principle, extend further out than the distance between neighbouring atoms in the crystal. Typically, for electron collisions with Ni^{2+} ions in free space $a_0 \sim 7$ a.u. However, in a solid-state environment the scattered electron "feels" the full Coulomb potential of the ion over a much shorter distance, typically the atomic sphere radius, and beyond this radius it interacts predominantly with the neighbouring atoms. This corresponds to the muffin-tin or atomic sphere approximation that is frequently made in band structure calculations (e.g. Gonis [390]). The atomic sphere radius of Ni^{2+} in NiO is taken to be 2.58 a.u. from conventional band structure calculations, and the scattering amplitude is determined at this radius. In a full multiple-scattering calculation, scattering by all the atomic spheres would be included. However, the calculations carried out so far use a single-scattering approximation taking a constant potential outside the atomic sphere radius.

In order to determine the scattering amplitude at the smaller radius, the internal region calculation is first carried out using a radius $a_0 = 7$ a.u. The R-matrix on this boundary is then propagated backwards from $r = 7$ a.u. to $r = 2.58$ a.u., using the propagator equation (E.28), where the Green's function in this equation is calculated using the same one-electron Hamiltonian used to calculate the radial continuum basis functions $u_{ij}^{0}(r)$ in (5.6). Given the R-matrix on the boundary $r = 2.58$ a.u., the corresponding K-matrix and S-matrix can be determined by fitting to an asymptotic region solution as in Sect. 5.1.4. Hence the differential and total cross sections for transitions between the target states defined by (12.3) can be calculated. Results from this calculation are presented in Sect. 12.1.3, where this model is compared with experiment.

12.1.3 Illustrative Example

In this section we illustrate the theory described in Sect. 12.1.2 by comparing R-matrix LE-EELS calculations for NiO, carried out by Jones et al. [511], with experiment. We show in Fig. 12.1 calculations of the spin-flip spectra of electrons scattered by NiO compared with experimental data obtained by Müller et al. [670].

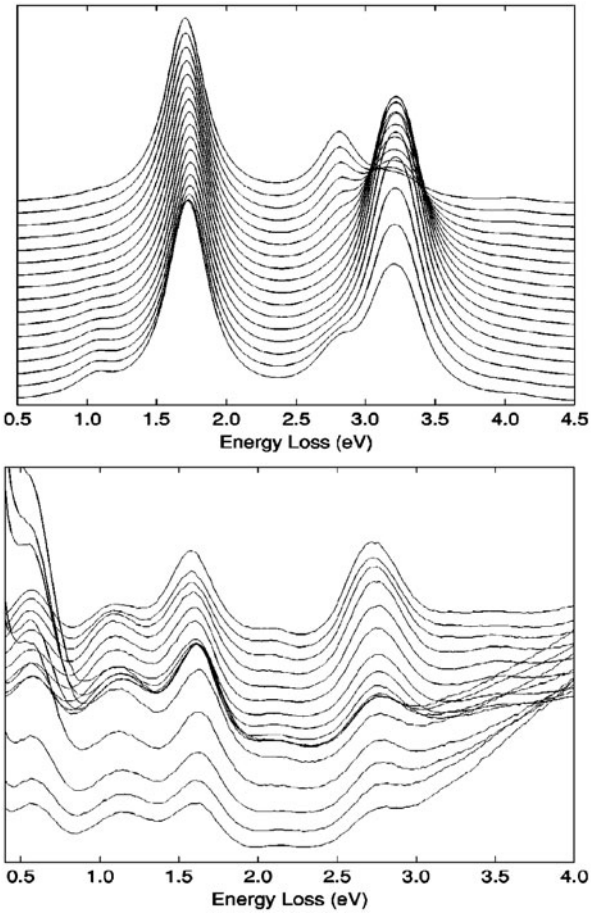

Fig. 12.1 Comparison of calculated spin-flip spectra (*top*) with experimental data (*bottom*) for electrons scattered from NiO as a function of scattering angle α and energy loss. The scattering angles are in the range $73^\circ \leq \alpha \leq 123^\circ$ in intervals of 3.125° with 73° being the lowest line (Figs. 13 and 14 from [511])

In this experiment, the energy loss of polarized electrons incident at an angle of 45° to the normal to the surface with an incident energy of 33 eV and undergoing a spin-flip was measured for 17 scattering angles α in the range $73^\circ \leq \alpha \leq 123^\circ$ at an interval of 3.125°. (The scattering angle α is related to the angle to the normal θ_f by $\theta_f = 135^\circ - \alpha$.) In the theoretical model the elastic peak is ignored as is the 0.6 eV loss peak, which is due to a surface excitation. The small 1.05 eV loss peak is due to $^3T_{2g}$ excitation and the big peak at 1.7 eV is due to two overlapping transitions ^1E_g (1.70 eV) and $^3T_{1g}$ (1.75 eV). The 3.2 eV loss peak is due to two overlapping transitions $^3T_{1g}$ (3.13. eV) and $^1T_{1g}$ (3.28 eV) and appears to be too narrow due to the contributing states being closer together than the experiment. It also lies slightly above experiment. Most significantly, at 2.7 eV we see a small shoulder at $\alpha = 73^\circ$ that increases and becomes dominant at 123°. This peak is of interest as it is a combination of two triplet–singlet excitations to the $^1A_{1g}$ (2.80 eV) and $^1T_{2g}$ (2.70 eV) states for which spin-flip dominates. Overall these results, taken together

with comparisons made with spin-averaged differential cross section measurements by Gorschlüter and Merz [406], show good agreement with experiment.

In conclusion, we have shown that the single inelastic scattering approximation, adopted in the above theory, provides an overall understanding of the main features of the experiment. However, a complete R-matrix theory of LE-EELS must also include a treatment of multiple-elastic scattering events that occur before and after the inelastic scattering event. In order to do this Jones et al. [511] suggested that the results from the theory of diffuse low-energy electron diffraction (LEED), used to treat an additional scatterer by Pendry et al. [725, 807], could be used with the further simplification that the cross section for inelastic scattering is small compared with elastic scattering, so that we need to only consider a single inelastic scattering with no multiple events. Jones et al. [511] also pointed out that it is possible to include the damping of the propagating electrons due to the mean free path effects in the electron gas, in this multiple-scattering formalism. The inclusion of multiple scattering and damping in the R-matrix formalism is thus a challenge for future work on LE-EELS from NiO and other transition metal oxides.

12.2 Electron Transport in Semiconductor Devices

In this section we consider a recent extension of R-matrix theory which describes electron transport in two-dimensional semiconductor devices in the presence of an external magnetic field perpendicular to the device. This theory was introduced by Jayasekera et al. [500, 501] in an analysis of experiments by Goel et al. [384] who observed significant bend resistance in InSb four-terminal devices. The theory has enabled the transmission coefficients in these devices to be calculated, and further developments and applications have been made to solid-state devices by Jayasekera et al. [502].

12.2.1 Introduction

Modern experiments can fabricate two-dimensional semiconductor devices in which the mean free path of an electron is larger than the size of the device. As a result, the electron transport properties of these devices have been of interest both theoretically and experimentally for several years. Studies of magnetotransport have led to many advances, such as the quantum Hall effect [724], as well as to applied devices, such as magnetic field sensors and spin-based devices.

We consider a two-dimensional device illustrated in Fig. 12.2 which consists of a rectangular internal region and four leads which has been used in a negative bend resistance (NBR) experiment by Goel et al. [384], analysed by Jayasekera et al. [500, 501]. In this experiment, a current is injected from lead 2 to lead 3 (I_{23}) in Fig. 12.2 and the voltage, V_{14}, between leads 1 and 4 is measured. The bend

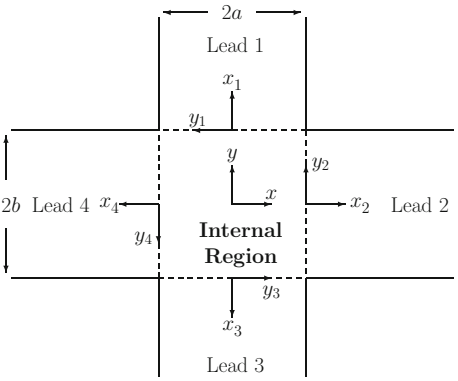

Fig. 12.2 Schematic diagram of a four-terminal two-dimensional junction device. It consists of an internal region and an external region made up of four leads, where the *dashed lines* indicate the boundary between the internal region and the external region and where a magnetic field B is applied perpendicular to the plane of the device. A local coordinate system (x,y) is introduced in the internal region, and local coordinate systems (x_p, y_p), $p = 1, \ldots, 4$, are introduced in each lead, where $x_p = 0$, $p = 1, \ldots, 4$, is where the pth lead meets the internal region. Finally, in the rectangular internal region the coordinates x and y satisfy $-a \leq x \leq a$ and $-b \leq y \leq b$

resistance is defined as $R_B = V_{14}/I_{23}$. If the electron transport is ballistic, charges tend to go forward into lead 4 giving a negative bend resistance. When an external magnetic field is applied perpendicular to the device electrons tend to deflect into lead 3 which suppresses the bend resistance. The bend resistance therefore decreases as a function of the applied magnetic field.

12.2.2 R-Matrix Theory

We now consider the generalization of R-matrix theory to describe the transport of electrons through a two-dimensional device in the presence of an applied perpendicular magnetic field B as illustrated in Fig. 12.2. In this analysis we assume that the electron transport is ballistic and we model the transport using a single-electron picture. We commence from the time-independent Schrödinger equation

$$H\Psi_j = E\Psi_j, \tag{12.7}$$

where Ψ_j is the two-dimensional wave function describing the scattered electron and j labels the linearly independent solutions of (12.7). Also in (12.7), E is the total collision energy and the Hamiltonian H is given by

$$H = \frac{1}{2\mathrm{m}^*}(\mathbf{P} - \mathrm{e}\mathbf{A})^2 + V, \tag{12.8}$$

where m^* is the effective mass of the electron and $\mathbf{A}$ is the vector potential. We observe that for devices made of InSb the electron has a small effective mass $\mathrm{m}^* = 0.0139\mathrm{m}$, where m is the free electron mass. We also note that the potential V in (12.8) is set zero in the calculations undertaken, although this is not essential in the R-matrix formalism.

In order to solve (12.7) in the internal region in Fig. 12.2 it is convenient to transform this equation so that the Hamiltonian is dimensionless [500]. We measure the lengths in terms of a characteristic length in the device; typically the width of the input lead, $w_0 = 2b$, is chosen. We measure the energies in terms of $E_0 = \hbar^2/\mathrm{m}^* w_0^2$ and define $\mathcal{E} = E/E_0$. Also a quantity $l_B^2 = \hbar/\mathrm{e}B$ is introduced, where l_B, which has the dimension of length, is called the "magnetic length" and is the average radius of the lowest Landau level of the system. Finally we define the dimensionless magnetic field $\mathcal{B} = w_0^2/l_B^2$. The Schrödinger equation (12.7) then becomes

$$\left[-\frac{1}{2}\left(\frac{\partial^2}{\partial x^2}+\frac{\partial^2}{\partial y^2}\right)+\mathrm{i}\mathcal{B}\left(\mathcal{A}_x\frac{\partial}{\partial x}+\mathcal{A}_y\frac{\partial}{\partial y}\right)+\frac{\mathcal{B}^2}{2}\left(\mathcal{A}_x^2+\mathcal{A}_y^2\right)\right]\Psi_j=\mathcal{E}\Psi_j, \tag{12.9}$$

where x and y are dimensionless coordinates and $\boldsymbol{\mathcal{A}}$ is the dimensionless vector potential.

In the following discussion of the solution in the internal region we will consider the general solution of (12.9). However, as discussed by Jayasekera et al. [500, 501] different gauges can be used in the solution. In the symmetric gauge we have $\mathbf{A}^{\mathrm{sym}} = (-y/2, x/2, 0)$ and in the asymmetric gauge $\mathbf{A}^{\mathrm{asym}} = (-y, 0, 0)$. While both gauges produce the same magnetic field the choice of gauge is important when the problem is solved approximately. We have to choose the gauge such that the solution will satisfy the boundary conditions of the system and the use of the appropriate gauge will give faster convergence. We will see when we discuss the solution in the external region that the asymmetric gauge is used. Finally, for future reference we rewrite (12.9) as follows

$$\mathcal{H}\Psi_j = \mathcal{E}\Psi_j, \tag{12.10}$$

and we consider in turn the solutions of this equation in the internal and external regions in Fig. 12.2.

12.2.2.1 Internal Region Solution

We consider first the solution of (12.10) in the internal region defined in Fig. 12.2. Following our discussion of electron–atom collisions in Sect. 5.1.2, we expand the

wave function Ψ_j in terms of energy-independent basis functions ψ_k which we write here as

$$\Psi_j(x, y) = \sum_k \psi_k(x, y) A_{kj}(\mathcal{E}), \tag{12.11}$$

where $A_{kj}(\mathcal{E})$ are energy-dependent expansion coefficients, which depend on boundary conditions satisfied by the wave function Ψ_j at the energy $\mathcal{E}$. We then expand the basis functions ψ_k in terms of non-orthogonal energy-independent functions $\phi_i(x, y)$ as follows

$$\psi_k(x, y) = \sum_{i=1}^{n} \phi_i(x, y) a_{ik}. \tag{12.12}$$

Finally, we determine the coefficients a_{ik} in (12.12) by diagonalizing $\mathcal{H} + \mathcal{L}$ in this basis giving

$$\langle \psi_k | \mathcal{H} + \mathcal{L} | \psi_{k'} \rangle_{\text{int}} = \mathcal{E}_k \delta_{kk'}, \tag{12.13}$$

where $\mathcal{H}$ is defined by (12.9) and (12.10) and $\mathcal{L}$ is a Bloch operator which ensures $\mathcal{H} + \mathcal{L}$ is hermitian in the internal region, where the integration in this equation is carried out over this region.

The Bloch operator $\mathcal{L}$ in (12.13) has four components. The first two correspond to the kinetic energy terms in (12.9) and the second two to the magnetic field terms involving $\mathcal{B}$ in (12.9). The remaining terms in (12.9) involving $\mathcal{B}^2$ are hermitian in the internal region. We consider first the kinetic energy terms in (12.9). We find that

$$-\frac{1}{2}\left(\frac{\partial^2}{\partial x^2} + \frac{\partial^2}{\partial y^2}\right) + L_x + L_y \tag{12.14}$$

is hermitian in the internal region where

$$L_x = \frac{1}{2}\left[\delta(x - a)\frac{\partial}{\partial x} - \delta(x + a)\frac{\partial}{\partial x}\right] \tag{12.15}$$

and

$$L_y = \frac{1}{2}\left[\delta(y - b)\frac{\partial}{\partial y} - \delta(y + b)\frac{\partial}{\partial y}\right]. \tag{12.16}$$

Next we consider the magnetic field terms in (12.9). We find that

$$\mathrm{i}\mathcal{B}\left(\mathcal{A}_x\frac{\partial}{\partial x}+\mathcal{A}_y\frac{\partial}{\partial y}\right)+\mathcal{L}_x+\mathcal{L}_y \tag{12.17}$$

is hermitian in the internal region where

$$\mathcal{L}_x=-\frac{1}{2}\mathrm{i}\mathcal{B}\mathcal{A}_x\left[\delta(x-a)-\delta(x+a)\right] \tag{12.18}$$

and

$$\mathcal{L}_y=-\frac{1}{2}\mathrm{i}\mathcal{B}\mathcal{A}_y\left[\delta(y-b)-\delta(y+b)\right]. \tag{12.19}$$

It follows that the Bloch operator $\mathcal{L}$ in (12.13) is defined by

$$\mathcal{L}=L_x+L_y+\mathcal{L}_x+\mathcal{L}_y, \tag{12.20}$$

where the boundaries of the internal region in the above definitions of the Bloch operators L_x, L_y, $\mathcal{L}_x$ and $\mathcal{L}_y$ correspond to $x=\pm a$ and $y=\pm b$ in Fig. 12.2.

We can now solve (12.10) in the internal region by including the Bloch operator $\mathcal{L}$, defined by (12.20), on both sides of this equation giving

$$(\mathcal{H}+\mathcal{L}-\mathcal{E})\,\Psi_j=\mathcal{L}\Psi_j. \tag{12.21}$$

This equation has the formal solution in the internal region

$$\Psi_j=(\mathcal{H}+\mathcal{L}-\mathcal{E})^{-1}\,\mathcal{L}\Psi_j, \tag{12.22}$$

where the spectral representation of the Green's function $(\mathcal{H}+\mathcal{L}-\mathcal{E})^{-1}$ can be obtained in terms of the energy-independent basis functions ψ_k defined by (12.12) and (12.13). Equation (12.22) then becomes

$$|\Psi_j\rangle=\sum_{k=1}^{n}|\psi_k\rangle\frac{1}{\mathcal{E}_k-\mathcal{E}}\langle\psi_k|\mathcal{L}|\Psi_j\rangle. \tag{12.23}$$

Equation (12.23) can now be evaluated on the four boundaries between the internal and the external regions in Fig. 12.2 and hence enables an R-matrix to be defined which relates the wave functions to the normal derivatives on these boundaries. By projecting this equation onto the transverse eigenfunctions for each lead in the external region, the transmission amplitudes between the leads can be determined. It has been found by Jayasekera et al. [500] that expanding the wave function ψ_k in (12.12) in terms of functions ϕ_i which are non-orthogonal and which satisfy

arbitrary boundary conditions avoids the use of a Buttle correction, required when homogeneous boundary conditions are used (see Sect. 5.3.2), and improves the convergence.

12.2.2.2 External Region Solution

We consider next the solution of (12.10) in the external region defined in Fig. 12.2. As in the internal region we assume that the leads are rectangular. For each lead we define a local coordinate system (x_p, y_p) as in Fig. 12.2, where y_p is the transverse coordinate and x_p is the longitudinal coordinate in the pth lead. In the absence of a magnetic field, the transverse confining potential is an infinite square well with $V = 0$ in the lead. The transverse lead eigenfunctions are therefore sine functions. However, these functions are not applicable if a magnetic field is present, so we seek transverse functions $f_{p\nu_p}(y_p)$ and wave numbers $k_{p\nu_p}$ in the pth lead, where ν_p is the transverse quantum number. Following [501] we choose the asymmetric gauge to describe the vector potential where $\mathbf{A} = (-By_p, 0, 0)$, which we note is different for different leads. Also, as in (12.9), we measure the length in terms of the width $w_0 = 2b$ of the input lead and we define $\mathcal{E} = E/E_0$, $l_B^2 = \hbar/eB$ and the dimensionless magnetic field $\mathcal{B} = w_0^2/l_B^2$. The Schrödinger equation in the pth lead then becomes

$$\left[-\frac{1}{2}\frac{\mathrm{d}^2}{\mathrm{d}y_p^2} + \frac{1}{2}\left(k_{p\nu_p}^2 + y_p\mathcal{B}\right)^2\right] f_{p\nu_p}(y_p) = \mathcal{E} f_{p\nu_p}(y_p). \tag{12.24}$$

This equation is then solved numerically for the transverse functions $f_{p\nu_p}(y_p)$, as discussed by Tamura and Ando [912], and the collision wave function in the pth lead is expanded in terms of these functions as

$$\Psi_{jE}(x_p, y_p) = \sum_{\nu_p} \tau_{p\nu_p} \exp(\mathrm{i}k_{p\nu_p}x_p) f_{p\nu_p}(y_p). \tag{12.25}$$

The transmission amplitudes $\tau_{p\nu_p}$ in (12.25) can then be determined by substituting the expression (12.25) for the collision wave functions for each lead into the internal region solution (12.23) evaluated on the boundary between the internal and the external regions. This enables the flux J_p in the pth lead to be determined using the result

$$\begin{aligned} J_p \sim \int \mathrm{d}y_p \Bigg[&\Psi_{jE}^*(x_p, y_p)\left(-\mathrm{i}\frac{\mathrm{d}}{\mathrm{d}x_p} - A_{x_p}\right)\Psi_{jE}(x_p, y_p) \\ &+ \Psi_{jE}(x_p, y_p)\left(\mathrm{i}\frac{\mathrm{d}}{\mathrm{d}x_p} - A_{x_p}\right)\Psi_{jE}^*(x_p, y_p)\Bigg]. \end{aligned} \tag{12.26}$$

Finally, from the resulting transmission amplitudes $\tau_{p\nu_p}$, we can calculate the transmission coefficients $T_{ij} = J_i/J_j$, where J_i and J_j are calculated using (12.26).

In comparing this analysis with that adopted in electron collisions with atoms, ions and molecules we observe that in the present analysis the external and asymptotic regions required in electron collisions are combined into one external region. This is because we have been able to match the solution on the outer boundary of the internal region directly with a linear combination of asymptotic solutions defined by (12.25). Of course, this simplification is compensated for by the more complicated nature of the boundary between the internal and the external regions in semiconductor devices, as illustrated in Fig. 12.2.

12.2.3 Illustrative Example

We consider calculations of transmission coefficients carried out by Jayasekera et al. [501] for a four-terminal symmetric square device consisting of a sample of InSb with an electron concentration 1.90×10^{11} cm^{-2} which is slightly less than the experimental value. The Fermi energy at this concentration is 32.7 meV, which equals 60 in the units E_0 used in this calculation. The width of the internal region in this device $w = 2a = 2b$, illustrated in Fig. 12.2, is 0.1 μm.

We show the transmission coefficients calculated for this device in Fig. 12.3. At zero magnetic field, shown in Fig. 12.3a, T_{12} and T_{32} lie on top of one another and T_{42} is always larger than the transmission coefficients for the sidearms. Therefore, more electrons accumulate in the forward lead than in the sidearms giving a negative bend resistance. However, as shown in Fig. 12.3b, we see that in the presence of a magnetic field, electrons are more likely to be deflected into the sidearms. Thus we see that at some energies the transmission coefficient T_{32} is larger than the forward

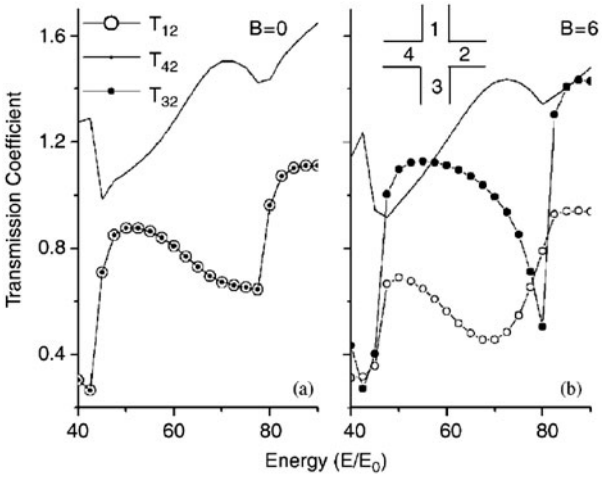

Fig. 12.3 Transmission coefficients for electrons injected into the four-terminal square device shown in Fig. 12.2. (**a**) shows the transmission coefficients at zero magnetic field. (**b**) shows the transmission coefficients when $\mathcal{B} = w_0^2/l_B^2 = 6$ (Fig. 2 from [501])

transmission coefficient T_{42}. In this case fewer electrons accumulate in lead 4, and the negative bend resistance (NBR), discussed in Sect. 12.2.1, is suppressed. The sign and magnitude of the bend resistance R_B depend on the ratio of these transmission coefficients.

Finally, we mention that R-matrix theory methods have also been used to calculate the cooling properties of several two-dimensional devices by Jayasekera et al. [502]. It is thus clear from the work reported in this section that R-matrix theory methods play an important role in the analyses of electron transport in semiconductor devices.

Part III
Appendices

Appendix A
Clebsch–Gordan and Racah Coefficients

In this appendix we summarize the formulae describing the coupling of two or more angular momenta required in our analysis of atomic, molecular and optical collision processes. This leads to the introduction of Clebsch–Gordan coefficients, Racah coefficients, 6-j symbols, 9-j symbols as well as higher order $3n$-j symbols. For a detailed discussion of these topics reference should be made to specialized monographs on angular momentum by Wigner [965, 967], Biedenharn et al. [106], Rose [797], Edmonds [284], Fano and Racah [308] and Brink and Satchler [139] and to the reprint volume by Biedenharn and van Dam [107].

A.1 Clebsch–Gordan Coefficients

Let us consider two independent quantum systems, or parts of a single system, with angular momenta denoted by the angular momentum operators $\mathbf{J_1}$ and $\mathbf{J_2}$. For example, $\mathbf{J_1}$ and $\mathbf{J_2}$ may be the orbital and spin angular momentum operators of a single particle or they may be the orbital angular momentum operators of two different particles. The Cartesian components of these operators satisfy the commutation relations (with $\hbar = 1$)

$$[J_{1x}, J_{1y}] = \mathrm{i}J_{1z}, \quad [J_{1y}, J_{1z}] = \mathrm{i}J_{1x}, \quad [J_{1z}, J_{1x}] = \mathrm{i}J_{1y}, \tag{A.1}$$

$$[\mathbf{J}_1^2, J_{1z}] = 0 \tag{A.2}$$

and

$$[J_{2x}, J_{2y}] = \mathrm{i}J_{2z}, \quad [J_{2y}, J_{2z}] = \mathrm{i}J_{2x}, \quad [J_{2z}, J_{2x}] = \mathrm{i}J_{2y}, \tag{A.3}$$

$$[\mathbf{J}_2^2, J_{2z}] = 0, \tag{A.4}$$

and they commute with each other so that

$$[\mathbf{J}_1, \mathbf{J}_2] = 0. \tag{A.5}$$

P.G. Burke, *R-Matrix Theory of Atomic Collisions*, Springer Series on Atomic, Optical, and Plasma Physics 61, DOI 10.1007/978-3-642-15931-2_13,

We denote by $\psi_{j_1 m_1}(1)$ and $\psi_{j_2 m_2}(2)$ the simultaneous angular momentum eigenfunctions of these quantum systems which satisfy

$$\mathbf{J}_1^2 \psi_{j_1 m_1}(1) = j_1(j_1+1)\psi_{j_1 m_1}(1), \quad J_{1z}\psi_{j_1 m_1}(1) = m_1 \psi_{j_1 m_1}(1), \tag{A.6}$$

where

$$m_1 = -j_1, -j_1+1, \ldots, j_1, \tag{A.7}$$

and

$$\mathbf{J}_2^2 \psi_{j_2 m_2}(2) = j_2(j_2+1)\psi_{j_2 m_2}(2)\ , \quad J_{2z}\psi_{j_2 m_2}(2) = m_2 \psi_{j_2 m_2}(2), \tag{A.8}$$

where

$$m_2 = -j_2, -j_2+1, \ldots, j_2. \tag{A.9}$$

Simultaneous eigenfunctions of the operators $\mathbf{J}_1^2$, J_{1z}, $\mathbf{J}_2^2$ and J_{2z} are then given by the product $\psi_{j_1 m_1}(1)\psi_{j_2 m_2}(2)$. We now define the total angular momentum operator of the two systems by

$$\mathbf{J} = \mathbf{J}_1 + \mathbf{J}_2, \tag{A.10}$$

and the z-component of this total angular momentum operator by

$$J_z = J_{1z} + J_{2z}. \tag{A.11}$$

The operators $\mathbf{J}_1^2, \mathbf{J}_2^2, \mathbf{J}^2$ and J_z form a set of commuting operators. Let us denote by $\psi_{j_1 j_2 jm}(1,2)$ the coupled eigenfunctions which are simultaneous eigenfunctions of the operators $\mathbf{J}_1^2, \mathbf{J}_2^2, \mathbf{J}^2$ and J_z. These simultaneous eigenfunctions satisfy

$$\begin{aligned} \mathbf{J}^2 \psi_{j_1 j_2 jm}(1,2) &= j(j+1)\psi_{j_1 j_2 jm}(1,2), \\ J_z \psi_{j_1 j_2 jm}(1,2) &= m\psi_{j_1 j_2 jm}(1,2), \end{aligned} \tag{A.12}$$

where

$$j = |j_1 - j_2|,\ |j_1 - j_2|+1, \ldots, j_1 + j_2, \tag{A.13}$$

and

$$m = -j, -j+1, \ldots, j. \tag{A.14}$$

The $(2j_1+1)(2j_2+1)$ simultaneous eigenfunctions $\psi_{j_1 j_2 jm}(1,2)$ of the operators $\mathbf{J}_1^2$, $\mathbf{J}_2^2$, $\mathbf{J}^2$ and J_z are related to the $(2j_1+1)(2j_2+1)$ product

eigenfunctions $\psi_{j_1 m_1}(1)\psi_{j_2 m_2}(2)$ of the operators $\mathbf{J}_1^2$, J_{1z}, $\mathbf{J}_2^2$ and J_{2z} by the unitary transformation

$$\psi_{j_1 j_2 jm}(1,2) = \sum_{m_1 m_2} (j_1 m_1 j_2 m_2 | jm)\psi_{j_1 m_1}(1)\psi_{j_2 m_2}(2). \tag{A.15}$$

The expansion coefficients $(j_1 m_1 j_2 m_2 | jm)$ in this transformation are called vector coupling or Clebsch–Gordan coefficients. These coefficients vanish unless (A.13) and (A.14) are satisfied and

$$m = m_1 + m_2. \tag{A.16}$$

To define these coefficients unambiguously, the relative phases of the eigenfunctions $\psi_{j_1 m_1}(1)\psi_{j_2 m_2}(2)$ and $\psi_{j_1 j_2 jm}(1,2)$ must be specified. We adopt here the phase convention of Condon and Shortley [227] where

$$(j_1 j_1 j_2 j_2 | j_1 + j_2 \; j_1 + j_2) = 1. \tag{A.17}$$

With this choice of phase the Clebsch–Gordan coefficients are real and satisfy the orthogonality relations

$$\sum_{m_1 m_2} (j_1 m_1 j_2 m_2 | jm)(j_1 m_1 j_2 m_2 | j' m') = \delta_{jj'}\delta_{mm'}, \tag{A.18}$$

which reduces to a single summation since (A.16) is satisfied, and

$$\sum_{jm} (j_1 m_1 j_2 m_2 | jm)(j_1 m_1' j_2 m_2' | jm) = \delta_{m_1 m_1'}\delta_{m_2 m_2'}. \tag{A.19}$$

Using (A.19) we can invert (A.15) to yield

$$\psi_{j_1 m_1}(1)\psi_{j_2 m_2}(2) = \sum_{j} (j_1 m_1 j_2 m_2 | jm)\psi_{j_1 j_2 jm}(1,2). \tag{A.20}$$

The Clebsch–Gordan coefficients satisfy the following symmetry relations

$$(j_1 m_1 j_2 m_2 | jm) = (-1)^{j_1 + j_2 - j}(j_1 - m_1 j_2 - m_2 | j - m), \tag{A.21}$$

$$= (-1)^{j_1 + j_2 - j}(j_2 m_2 j_1 m_1 | jm), \tag{A.22}$$

$$= (-1)^{j_1 - m_1}\left(\frac{2j+1}{2j_2+1}\right)^{1/2}(j_1 m_1 j - m | j_2 - m_2), \tag{A.23}$$

$$= (-1)^{j_2+m_2}\left(\frac{2j+1}{2j_1+1}\right)^{1/2}(j\,-mj_2m_2|j_1-m_1), \tag{A.24}$$

$$= (-1)^{j_1-m_1}\left(\frac{2j+1}{2j_2+1}\right)^{1/2}(jmj_1-m_1|j_2m_2), \tag{A.25}$$

$$= (-1)^{j_2+m_2}\left(\frac{2j+1}{2j_1+1}\right)^{1/2}(j_2-m_2jm|j_1m_1). \tag{A.26}$$

The Clebsch–Gordan coefficients also satisfy

$$(j_10j_20|j0) = 0, \quad \text{unless } j_1+j_2+j \text{ is even}, \tag{A.27}$$

and

$$(j_1m_100|jm) = \delta_{j_1j}\delta_{m_1m}. \tag{A.28}$$

Equation (A.27) gives rise to the parity selection rule in applications.

The symmetry relations satisfied by the Clebsch–Gordan coefficients can be simplified by introducing the 3-j symbols defined by Wigner [967]. These are defined by

$$\begin{pmatrix} j_1 & j_2 & j_3 \\ m_1 & m_2 & m_3 \end{pmatrix} = (-1)^{j_1-j_2-m_3}(2j_3+1)^{-1/2}(j_1m_1j_2m_2|j_3-m_3). \tag{A.29}$$

The 3-j symbols are invariant under an even permutation of the columns, while an odd permutation is equivalent to multiplication by $(-1)^{j_1+j_2+j_3}$. Thus

$$\begin{aligned}(-1)^{j_1+j_2+j_3}\begin{pmatrix} j_1 & j_2 & j_3 \\ m_1 & m_2 & m_3 \end{pmatrix} &= \begin{pmatrix} j_2 & j_1 & j_3 \\ m_2 & m_1 & m_3 \end{pmatrix} = \begin{pmatrix} j_1 & j_3 & j_2 \\ m_1 & m_3 & m_2 \end{pmatrix} \\ &= \begin{pmatrix} j_3 & j_2 & j_1 \\ m_3 & m_2 & m_1 \end{pmatrix}. \end{aligned} \tag{A.30}$$

Also the analogue of (A.21) is

$$\begin{pmatrix} j_1 & j_2 & j_3 \\ m_1 & m_2 & m_3 \end{pmatrix} = (-1)^{j_1+j_2+j_3}\begin{pmatrix} j_1 & j_2 & j_3 \\ -m_1 & -m_2 & -m_3 \end{pmatrix}. \tag{A.31}$$

The orthogonality relations satisfied by the 3-j symbols are

$$\sum_{m_1m_2}\begin{pmatrix} j_1 & j_2 & j_3 \\ m_1 & m_2 & m_3 \end{pmatrix}\begin{pmatrix} j_1 & j_2 & j_3' \\ m_1 & m_2 & m_3' \end{pmatrix} = (2j_3+1)^{-1}\delta_{j_3j_3'}\delta_{m_3m_3'} \tag{A.32}$$

and

$$\sum_{j_3 m_3} (2j_3+1) \begin{pmatrix} j_1 & j_2 & j_3 \\ m_1 & m_2 & m_3 \end{pmatrix} \begin{pmatrix} j_1 & j_2 & j_3 \\ m_1' & m_2' & m_3 \end{pmatrix} = \delta_{m_1 m_1'} \delta_{m_2 m_2'}. \tag{A.33}$$

We conclude this section by giving the following closed expression for the Clebsch–Gordan coefficients (see Wigner [965])

$$\begin{aligned} &(j_1 m_1 j_2 m_2 | j m) \\ &= \left[\frac{(2j+1)(j+j_1-j_2)!(j-j_1+j_2)!(j_1+j_2-j)!(j+m)!(j-m)!}{(j_1+j_2+j+1)!(j_1-m_1)!(j_1+m_1)!(j_2-m_2)!(j_2+m_2)!} \right] \\ &\times \sum_{\kappa} (-1)^{\kappa+j_2+m_2} \frac{(j_2+j_3+m_1-\kappa)!(j_1-m_1+\kappa)!}{\kappa!(j-j_1+j_2-\kappa)!(j+m-\kappa)!(\kappa+j_1-j_2-m)!} \\ &\times \delta_{m,m_1+m_2}, \end{aligned} \tag{A.34}$$

where the summation is over all integral values of κ such that none of the factorial arguments is negative. The explicit values of the Clebsch–Gordan coefficients when $j_2 = 1/2$ and $j_2 = 1$ are given in Tables A.1 and A.2, respectively.

Table A.1 Clebsch–Gordan coefficients $(j_1\ m - m_2\ \frac{1}{2}\ m_2 | j\ m)$

j	$m_2 = 1/2$	$m_2 = -1/2$
$j_1 + \frac{1}{2}$	$\left[\frac{j_1+m+\frac{1}{2}}{2j_1+1}\right]^{1/2}$	$\left[\frac{j_1-m+\frac{1}{2}}{2j_1+1}\right]^{1/2}$
$j_1 - \frac{1}{2}$	$-\left[\frac{j_1-m+\frac{1}{2}}{2j_1+1}\right]^{1/2}$	$\left[\frac{j_1+m+\frac{1}{2}}{2j_1+1}\right]^{1/2}$

Table A.2 Clebsch–Gordan coefficients $(j_1\ m - m_2\ 1\ m_2 | j\ m)$

j	$m_2 = 1$	$m_2 = 0$	$m_2 = -1$
$j_1 + 1$	$\left[\frac{(j_1+m)(j_1+m+1)}{(2j_1+1)(2j_1+2)}\right]^{1/2}$	$\left[\frac{(j_1-m+1)(j_1+m+1)}{(2j_1+1)(j_1+1)}\right]^{1/2}$	$\left[\frac{(j_1-m)(j_1-m+1)}{(2j_1+1)(2j_1+2)}\right]^{1/2}$
j_1	$-\left[\frac{(j_1+m)(j_1-m+1)}{2j_1(j_1+1)}\right]^{1/2}$	$\frac{m}{[j_1(j_1+1)]^{1/2}}$	$\left[\frac{(j_1-m)(j_1+m+1)}{2j_1(j_1+1)}\right]^{1/2}$
$j_1 - 1$	$\left[\frac{(j_1-m)(j_1-m+1)}{2j_1(2j_1+1)}\right]^{1/2}$	$-\left[\frac{(j_1-m)(j_1+m)}{j_1(2j_1+1)}\right]^{1/2}$	$\left[\frac{(j_1+m+1)(j_1+m)}{2j_1(2j_1+1)}\right]^{1/2}$

A.2 Racah Coefficients

We now consider three independent quantum systems, or parts of a single system, with angular momenta denoted by the operators $\mathbf{J}_1$, $\mathbf{J}_2$ and $\mathbf{J}_3$. We can write the total angular momentum operator $\mathbf{J}$ as

$$\mathbf{J} = \mathbf{J}_1 + \mathbf{J}_2 + \mathbf{J}_3. \tag{A.35}$$

However, there is no unique way of carrying out this addition. For example, we can first couple the angular momentum eigenfunctions $\psi_{j_1 m_1}(1)$ and $\psi_{j_2 m_2}(2)$ belonging to $\mathbf{J}_1$ and $\mathbf{J}_2$ to form eigenfunctions of $\mathbf{J_{12}} = \mathbf{J}_1 + \mathbf{J}_2$ according to

$$\psi_{j_1 j_2 j_{12} m_{12}}(1,2) = \sum_{m_1 m_2} (j_1 m_1 j_2 m_2 | j_{12} m_{12}) \psi_{j_1 m_1}(1) \psi_{j_2 m_2}(2) \ . \tag{A.36}$$

These eigenfunctions can then be coupled with the angular momentum eigenfunctions $\psi_{j_3 m_3}(3)$ belonging to $\mathbf{J}_3$ to form eigenfunctions of $\mathbf{J}$ according to

$$\psi_{jm}(j_{12}) = \sum_{m_{12} m_3} (j_{12} m_{12} j_3 m_3 | jm) \psi_{j_1 j_2 j_{12} m_{12}}(1,2) \psi_{j_3 m_3}(3). \tag{A.37}$$

Alternatively, we can first couple $\psi_{j_2 m_2}(2)$ and $\psi_{j_3 m_3}(3)$ to form eigenfunctions of $\mathbf{J_{23}} = \mathbf{J}_2 + \mathbf{J}_3$ according to

$$\psi_{j_2 j_3 j_{23} m_{23}}(2,3) = \sum_{m_2 m_3} (j_2 m_2 j_3 m_3 | j_{23} m_{23}) \psi_{j_2 m_2}(2) \psi_{j_3 m_3}(3) \tag{A.38}$$

and then couple these eigenfunctions with $\psi_{j_1 m_1}(1)$ to form eigenfunctions of $\mathbf{J}$ according to

$$\psi_{jm}(j_{23}) = \sum_{m_1 m_{23}} (j_1 m_1 j_{23} m_{23} | jm) \psi_{j_1 m_1}(1) \psi_{j_2 m_2}(2) \psi_{j_2 j_3 j_{23} m_{23}}(2,3). \tag{A.39}$$

Finally, we can first couple $\psi_{j_1 m_1}(1)$ and $\psi_{j_3 m_3}(3)$ to form eigenfunctions of $\mathbf{J_{13}} = \mathbf{J}_1 + \mathbf{J}_3$ and then couple the resultant eigenfunctions with $\psi_{j_2 m_2}(2)$ to form eigenfunctions of $\mathbf{J}$.

These three representations of the eigenfunctions of $\mathbf{J}$ are related by unitary transformations. For example, we can write

$$\psi_{jm}(j_{12}) = \sum_{j_{23}} R(j_{23}, j_{12}) \psi_{jm}(j_{23}). \tag{A.40}$$

The Racah coefficients W are then defined by the equation (Racah [764–767])

$$R(j_{23}, j_{12}) = [(2j_{23}+1)(2j_{12}+1)]^{1/2} W(j_1 j_2 j j_3; j_{12} j_{23}). \tag{A.41}$$

We can derive a relation between the Racah coefficients and the Clebsch – Gordan coefficients by expressing $\psi_{jm}(j_{12})$ and $\psi_{jm}(j_{23})$ in terms of $\psi_{j_1m_1}(1)$, $\psi_{j_2m_2}(2)$ and $\psi_{j_3m_3}(3)$. Equations (A.36) and (A.37) yield

$$\psi_{jm}(j_{12}) = \sum_{m_1 m_{12}} (j_1 m_1 j_2 m_{12} - m_1 | j_{12} m_{12})(j_{12} m_{12} j_3 m - m_{12} | jm) \times \psi_{j_1 m_1}(1) \psi_{j_2 m_{12} - m_1}(2) \psi_{j_3 m - m_{12}}(3) \tag{A.42}$$

and (A.38) and (A.39) yield

$$\psi_{jm}(j_{23}) = \sum_{m_2 m_{23}} (j_2 m_2 j_3 m_{23} - m_2 | j_{23} m_{23})(j_1 m - m_{23} j_{23} m_{23} | jm) \times \psi_{j_1 m - m_{23}}(1) \psi_{j_2 m_2}(2) \psi_{j_3 m_{23} - m_2}(3). \tag{A.43}$$

Substituting (A.42) and (A.43) into (A.40) and using (A.41) gives

$$\sum_f [(2e+1)(2f+1)]^{1/2} W(abcd; ef)(b\beta d\delta | f\beta + \delta)(a\alpha f\beta + \delta | c\alpha + \beta + \delta) = (a\alpha b\beta | e\alpha + \beta)(e\alpha + \beta d\delta | c\alpha + \beta + \delta). \tag{A.44}$$

Using the properties of the Clebsch–Gordan coefficients given by (A.18) and (A.19) and by (A.21), (A.22), (A.23), (A.24), (A.25) and (A.26) we obtain the following additional relations

$$[(2e+1)(2f+1)]^{1/2} W(abcd; ef)(a\alpha f\beta + \delta | c\alpha + \beta + \delta) = \sum_\beta (a\alpha b\beta | e\alpha + \beta)(e\alpha + \beta d\delta | c\alpha + \beta + \delta)(b\beta d\delta | f\beta + \delta), \tag{A.45}$$

where $\beta + \delta$ is a fixed parameter, and

$$[(2e+1)(2f+1)]^{1/2} W(abcd; ef) = \sum_{\alpha\beta} (a\alpha b\beta | e\alpha + \beta)(e\alpha + \beta d\delta | c\alpha + \beta + \delta)(b\beta d\delta | f\beta + \delta) \times (a\alpha f\beta + \delta | c\alpha + \beta + \delta), \tag{A.46}$$

where $\alpha + \beta + \delta$ is a fixed parameter.

It follows from the above definitions that the six angular momenta in $W(abcd; ef)$ satisfy the following four triangular relations

$$\Delta(abe), \quad \Delta(cde), \quad \Delta(acf), \quad \Delta(bdf), \tag{A.47}$$

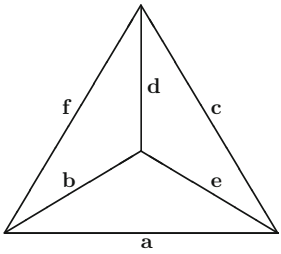

Fig. A.1 Tetrahedron illustrating the triangular relations satisfied by the arguments of the Racah coefficient $W(abcd; ef)$

where, for example, the notation $\Delta(abe)$ means that the three angular momenta a, b and e form the sides of a triangle. These four triangular relations can be combined by representing the six angular momenta by the sides of a tetrahedron as illustrated in Fig. A.1.

The Racah coefficients satisfy certain symmetry relations under the 24 possible permutations of the 6 arguments which preserve the 4 triangular relations. These symmetry relations, which result in at most a change of phase, are given by

$$W(abcd; ef) = W(badc; ef) = W(cdab; ef) = W(acbd; fe) \tag{A.48}$$

and

$$W(abcd; ef) = (-1)^{e+f-a-d} W(ebcf; ad) = (-1)^{e+f-b-c} W(aefd; bc) \tag{A.49}$$

together with the symmetry relations which can be obtained by applying the above symmetry relations more than once.

The Racah coefficients also satisfy the orthogonality relation

$$\sum_e (2e+1)(2f+1) W(abcd; ef) W(abcd; eg) = \delta_{fg} \tag{A.50}$$

and the sum rules

$$\sum_e (-1)^{a+b-e} (2e+1) W(abcd; ef) W(bacd; eg) = W(agfb; dc) \tag{A.51}$$

and

$$\begin{aligned} &\sum_g (2g+1) W(a'gdc; ac') W(bgec'; b'c) W(a'gfb; ab') \\ &\quad = W(adbe; cf) W(a'db'e; c'f). \end{aligned} \tag{A.52}$$

Hence when there is a sum over a product of several Racah coefficients it is often possible to reduce the number of terms in the product. Finally, if one of the

arguments of the Racah coefficient is zero we can use the symmetry relations and the following result

$$W(abcd;0f) = \frac{(-1)^{f-b-d}\delta_{ab}\delta_{cd}}{[(2b+1)(2d+1)]^{1/2}} \tag{A.53}$$

to simplify the expression.

A.3 6-j Symbols

The symmetry relations satisfied by the Racah coefficients can be simplified using the 6-j symbols introduced by Wigner [967] which are defined by

$$\begin{Bmatrix} j_1 & j_2 & j_3 \\ j_4 & j_5 & j_6 \end{Bmatrix} = (-1)^{j_1+j_2+j_4+j_5} W(j_1 j_2 j_5 j_4; j_3 j_6). \tag{A.54}$$

The 6-j symbols are invariant under any permutation of the three columns, i.e.

$$\begin{aligned} \begin{Bmatrix} j_1 & j_2 & j_3 \\ j_4 & j_5 & j_6 \end{Bmatrix} &= \begin{Bmatrix} j_2 & j_3 & j_1 \\ j_5 & j_6 & j_4 \end{Bmatrix} = \begin{Bmatrix} j_3 & j_1 & j_2 \\ j_6 & j_4 & j_5 \end{Bmatrix} = \begin{Bmatrix} j_2 & j_1 & j_3 \\ j_5 & j_4 & j_6 \end{Bmatrix} \\ &= \begin{Bmatrix} j_1 & j_3 & j_2 \\ j_4 & j_6 & j_5 \end{Bmatrix} = \begin{Bmatrix} j_3 & j_2 & j_1 \\ j_6 & j_5 & j_4 \end{Bmatrix}. \end{aligned} \tag{A.55}$$

They are also invariant under interchange of the upper and lower arguments in each of any two columns, i.e.

$$\begin{Bmatrix} j_1 & j_2 & j_3 \\ j_4 & j_5 & j_6 \end{Bmatrix} = \begin{Bmatrix} j_1 & j_5 & j_6 \\ j_4 & j_2 & j_3 \end{Bmatrix} = \begin{Bmatrix} j_4 & j_2 & j_6 \\ j_1 & j_5 & j_3 \end{Bmatrix} = \begin{Bmatrix} j_4 & j_5 & j_3 \\ j_1 & j_2 & j_6 \end{Bmatrix}. \tag{A.56}$$

A.4 9-j Symbols

In many applications we need to transform between two coupling schemes involving four angular momenta. This occurs, for example, in the transformation from jj-coupling to LS-coupling for two particles possessing both orbital and spin angular momenta. In this example the total angular momentum vector of the first particle is given by

$$\mathbf{j_1} = \boldsymbol{\ell}_1 + \mathbf{s_1} \tag{A.57}$$

and of the second particle is given by

$$\mathbf{j_2} = \boldsymbol{\ell}_2 + \mathbf{s_2}. \tag{A.58}$$

The total angular momentum of the two-particle system in jj-coupling is then given by

$$\mathbf{J} = \mathbf{j_1} + \mathbf{j_2}. \tag{A.59}$$

Alternatively, the total orbital angular momentum vector of the two particles is given by

$$\mathbf{L} = \boldsymbol{\ell}_1 + \boldsymbol{\ell}_2, \tag{A.60}$$

and the total spin angular momentum vector is given by

$$\mathbf{S} = \mathbf{s_1} + \mathbf{s_2}. \tag{A.61}$$

The total angular momentum of the two-particle system in LS coupling is then given by

$$\mathbf{J} = \mathbf{L} + \mathbf{S}. \tag{A.62}$$

The transformation between these coupling schemes is related to the 9-j symbol introduced by Wigner [967] by the following equation

$$\begin{aligned} &< (\ell_1 s_1) j_1, (\ell_2 s_2) j_2; JM | (\ell_1 \ell_2) L, (s_1 s_2) S; JM > \\ &\quad = [(2j_1+1)(2j_2+1)(2L+1)(2S+1)]^{1/2} \begin{Bmatrix} \ell_1 & s_1 & j_1 \\ \ell_2 & s_2 & j_2 \\ L & S & J \end{Bmatrix}, \end{aligned} \tag{A.63}$$

which is independent of the total magnetic quantum number M. The 9-j symbol in the curly bracket in this equation can be written as the sum over products of three 6-j symbols by expressing the bra vector in (A.63) in terms of the ket vector in (A.63) through repeated use of the recoupling transformation defined by (A.40) and (A.41). We obtain in the general case

$$\begin{aligned} \begin{Bmatrix} j_1 & j_2 & j_{12} \\ j_3 & j_4 & j_{34} \\ j_{13} & j_{24} & j \end{Bmatrix} &= \sum_{\kappa} (-1)^{2\kappa} (2\kappa+1) \begin{Bmatrix} j_1 & j_3 & j_{13} \\ j_{24} & j & \kappa \end{Bmatrix} \begin{Bmatrix} j_2 & j_4 & j_{24} \\ j_3 & \kappa & j_{34} \end{Bmatrix} \\ &\quad \times \begin{Bmatrix} j_{12} & j_{34} & j \\ \kappa & j_1 & j_2 \end{Bmatrix}. \end{aligned} \tag{A.64}$$

An even permutation of the rows or columns of the 9-j symbol leaves it unchanged as does the transposition obtained by interchanging rows and columns. An odd permutation of the rows or columns causes the 9-j symbol to be multiplied by the factor

$$f = (-1)^{j_1+j_2+j_{12}+j_3+j_4+j_{34}+j_{13}+j_{24}+j}. \tag{A.65}$$

The 9-j symbols satisfy the orthogonality relation

$$\sum_{j_{12}j_{34}} (2j_{12}+1)(2j_{34}+1)(2j_{13}+1)(2j_{24}+1) \begin{Bmatrix} j_1 & j_2 & j_{12} \\ j_3 & j_4 & j_{34} \\ j_{13} & j_{24} & j \end{Bmatrix} \begin{Bmatrix} j_1 & j_2 & j_{12} \\ j_3 & j_4 & j_{34} \\ j'_{13} & j'_{24} & j \end{Bmatrix}$$
$$= \delta_{j_{13}j'_{13}} \delta_{j_{24}j'_{24}} \tag{A.66}$$

and the sum rule

$$\sum_{j_{13}j_{23}} (-1)^{2j_2+j_{24}+j_{23}-j_{34}} (2j_{13}+1)(2j_{24}+1) \begin{Bmatrix} j_1 & j_2 & j_{12} \\ j_3 & j_4 & j_{34} \\ j_{13} & j_{24} & j \end{Bmatrix} \begin{Bmatrix} j_1 & j_3 & j_{13} \\ j_4 & j_2 & j_{24} \\ j_{14} & j_{23} & j \end{Bmatrix}$$
$$= \begin{Bmatrix} j_1 & j_2 & j_{12} \\ j_4 & j_3 & j_{34} \\ j_{14} & j_{23} & j \end{Bmatrix}. \tag{A.67}$$

When one of the arguments of the 9-j symbol is zero we can use the symmetry relations and the following result

$$\begin{Bmatrix} a & b & e \\ c & d & e \\ f & f & 0 \end{Bmatrix} = \frac{(-1)^{b+c+e+f}}{[(2e+1)(2f+1)]^{1/2}} \begin{Bmatrix} a & b & e \\ d & c & f \end{Bmatrix} \tag{A.68}$$

to reduce the 9-j symbol to a 6-j symbol times a factor.

A.5 Higher Order $3n$-j Symbols

We conclude this appendix by noting that in the theory of electron and photon interactions with complex atoms and ions with many open shells, it is often necessary to consider the recoupling of more than four angular momenta. For example, in the case of recoupling five angular momenta, 12-j symbols arise whose properties have been discussed by Jahn and Hope [498] and by Ord-Smith [708]. However, we will not discuss these higher order $3n$-j symbols further here but remark that in practical calculations they can be evaluated in terms of sums over products of Racah coefficients by repeated use of (A.40) and (A.41), and general computer programs have been written for this purpose by Shapiro [870], Burke [154] and Bar-Shalom and Klapisch [56].

Appendix B
Legendre Polynomials and Related Functions

In this appendix we first summarize formulae for Legendre polynomials, associated Legendre functions and spherical harmonics, which are required in defining the eigenfunctions of the orbital angular momentum operator. We then consider the phase of the spherical harmonics and its relation to the time-reversal operation, and we review two phase conventions that have been used in applications, referred to as the Condon–Shortley and the Fano–Racah phase conventions. Finally, we consider the transformation properties of wave functions under rotations of the axis of quantization in which we introduce and define Euler angles and Wigner rotation matrices. For a detailed discussion of spherical harmonics reference should be made to Hobson [474].

B.1 Legendre Polynomials

Let x be a real variable such that $-1 \leq x \leq 1$. In physical problems the variable x is usually the cosine of an angle θ so that $x = \cos\theta$. Legendre polynomials of degree ℓ are then defined by Rodrigue's formula

$$P_\ell(x) = \frac{1}{2^\ell \ell!}\frac{\mathrm{d}^\ell}{\mathrm{d}x^\ell}(x^2-1)^\ell, \quad \ell = 0, 1, 2, \ldots. \tag{B.1}$$

An equivalent definition of $P_\ell(x)$ is given in terms of a generating function, namely

$$F(x, y) = (1 - 2xy + y^2)^{-1/2} = \sum_{\ell=0}^{\infty} P_\ell(x) y^\ell, \tag{B.2}$$

where this relation has a meaning only when the summation converges, which occurs when $|x| \leq 1$ and $|y| < 1$. By differentiating (B.2) with respect to x we obtain the following useful relation

$$(1 - 2xy + y^2)^{-3/2} = \sum_{\ell=1}^{\infty} P'_\ell(x) y^{\ell-1}, \tag{B.3}$$

P.G. Burke, *R-Matrix Theory of Atomic Collisions*, Springer Series on Atomic, Optical, and Plasma Physics 61, DOI 10.1007/978-3-642-15931-2_14,

where $P'_\ell(x) = \mathrm{d}P_\ell(x)/\mathrm{d}x$.

The Legendre polynomials satisfy the following differential equation

$$\left[(1-x^2)\frac{\mathrm{d}^2}{\mathrm{d}x^2} - 2x\frac{\mathrm{d}}{\mathrm{d}x} + \ell(\ell+1)\right] P_\ell(x) = 0 \tag{B.4}$$

and recurrence relations

$$(\ell+1)P_{\ell+1} - (2\ell+1)xP_\ell + \ell P_{\ell-1} = 0, \tag{B.5}$$

$$P'_{\ell+1} - xP'_\ell = (\ell+1)P_\ell, \tag{B.6}$$

$$P'_{\ell+1} - P'_{\ell-1} = (2\ell+1)P_\ell, \tag{B.7}$$

$$(x^2-1)P'_\ell = \ell x P_\ell - \ell P_{\ell-1}. \tag{B.8}$$

These recurrence relations are valid for the case $\ell = 0$ if we define $P_{-1}(x) = 0$.

The Legendre polynomials also satisfy the orthogonality relation

$$\int_{-1}^{+1} P_\ell(x)P_{\ell'}(x)\mathrm{d}x = \frac{2}{2\ell+1}\delta_{\ell\ell'} \tag{B.9}$$

and the closure relation

$$\frac{1}{2}\sum_{\ell=0}^{\infty}(2\ell+1)P_\ell(x)P_\ell(x') = \delta(x-x'). \tag{B.10}$$

They have parity $(-1)^\ell$ so that

$$P_\ell(-x) = (-1)^\ell P_\ell(x) \tag{B.11}$$

and satisfy the boundary conditions

$$P_\ell(1) = 1, \quad P_\ell(-1) = (-1)^\ell, \tag{B.12}$$

with ℓ zeros in the interval $-1 < x < 1$. Explicit expressions for the first few Legendre polynomials are

$$P_0(x) = 1,$$

$$P_1(x) = x,$$

$$P_2(x) = \frac{1}{2}(3x^2-1),$$

$$P_3(x) = \frac{1}{2}(5x^3-3x),$$

$$P_4(x) = \frac{1}{8}(35x^4 - 30x^2 + 3),$$

$$P_5(x) = \frac{1}{8}(63x^5 - 70x^3 + 15x),$$

$$P_6(x) = \frac{1}{16}(231x^6 - 315x^4 + 105x^2 - 5),$$

$$P_7(x) = \frac{1}{16}(429x^7 - 693x^5 + 315x^3 - 35x). \tag{B.13}$$

Explicit values for the higher order polynomials are usually calculated using the recurrence relation (B.5).

B.2 Associated Legendre Functions

The associated Legendre functions $P_\ell^m(x)$ are defined over the interval $-1 \le x \le 1$ by the relation

$$P_\ell^m(x) = (1 - x^2)^{m/2} \frac{\mathrm{d}^m}{\mathrm{d}x^m} P_\ell(x), \quad 0 \le m \le \ell. \tag{B.14}$$

They are seen to be the product of the function $(1 - x^2)^{m/2}$ and a polynomial of degree $(\ell - m)$ and parity $(-1)^{\ell - m}$, having $\ell - m$ zeros in the interval $-1 \le x \le 1$. As with the Legendre polynomials, a generating function can be defined for the associated Legendre functions. It is given by

$$\frac{(2m)!(1 - x^2)^{m/2}}{2^m m!(1 - 2xy + y^2)^{m+1/2}} = \sum_{\ell=0}^{\infty} P_{\ell+m}^m(x) y^\ell. \tag{B.15}$$

The associated Legendre functions satisfy the differential equation

$$\left[(1 - x^2)\frac{\mathrm{d}^2}{\mathrm{d}x^2} - 2x\frac{\mathrm{d}}{\mathrm{d}x} + \ell(\ell + 1) - \frac{m^2}{1 - x^2}\right] P_\ell^m(x) = 0 \tag{B.16}$$

and the recurrence relations

$$(\ell - m + 1)P_{\ell+1}^m - (2\ell + 1)xP_\ell^m + (\ell + m)P_{\ell-1}^m = 0, \quad 0 \le m \le \ell - 1, \tag{B.17}$$

$$P_\ell^{m+1} - \frac{2mx}{(1 - x^2)^{1/2}} P_\ell^m + (\ell + m)(\ell - m + 1)P_\ell^{m-1} = 0, \quad 0 \le m \le \ell - 1, \tag{B.18}$$

$$(2\ell + 1)(1 - x^2)^{1/2} P_\ell^m = P_{\ell+1}^{m+1} - P_{\ell-1}^{m+1}, \quad 0 \le m \le \ell - 2, \tag{B.19}$$

$$(2\ell+1)(1-x^2)^{1/2}P_\ell^m = (\ell+m)(\ell+m-1)P_{\ell-1}^{m-1} - (\ell-m+1)$$

$$\times(\ell-m+2)P_{\ell+1}^{m-1}, \quad 0 \le m \le \ell, \tag{B.20}$$

$$(1-x^2)\frac{\mathrm{d}P_\ell^m}{\mathrm{d}x} = (\ell+1)xP_\ell^m - (\ell-m+1)P_{\ell+1}^m, \quad 0 \le m \le \ell, \tag{B.21}$$

$$= -\ell x P_\ell^m + (\ell+m)P_{\ell-1}^m, \quad 0 \le m \le \ell-1. \tag{B.22}$$

The associated Legendre functions also satisfy the orthogonality relations

$$\int_{-1}^{+1} P_\ell^m(x)P_{\ell'}^m(x)\mathrm{d}x = \frac{2(\ell+m)!}{(2\ell+1)(\ell-m)!}\delta_{\ell\ell'} \tag{B.23}$$

and have the values

$$P_\ell^m(1) = P_\ell^m(-1) = 0, \quad m \neq 0, \tag{B.24}$$

and

$$P_\ell^m(0) = (-1)^s\frac{(2s+2m)!}{2^\ell s!(s+m)!}, \quad \ell-m = 2s,$$

$$= 0, \quad \ell-m = 2s+1. \tag{B.25}$$

Explicit expressions for the first few associated Legendre functions are

$$P_1^1(x) = (1-x^2)^{1/2},$$

$$P_2^1(x) = 3x(1-x^2)^{1/2},$$

$$P_2^2(x) = 3(1-x^2),$$

$$P_3^1(x) = \frac{3}{2}(5x^2-1)(1-x^2)^{1/2},$$

$$P_3^2(x) = 15x(1-x^2),$$

$$P_3^3(x) = 15(1-x^2)^{3/2},$$

$$P_4^1(x) = \frac{5}{2}(7x^3-3x)(1-x^2)^{1/2},$$

$$P_4^2(x) = \frac{15}{2}(7x^2-1)(1-x^2),$$

$$P_4^3(x) = 105x(1-x^2)^{3/2},$$

$$P_4^4(x) = 105(1-x^2)^2. \tag{B.26}$$

B.3 Spherical Harmonics

The spherical harmonics $Y_{\ell m}(\theta, \phi)$ are simultaneous eigenfunctions of $\boldsymbol{\ell}^2$ and ℓ_z, where in quantum theory $\boldsymbol{\ell} = -\mathrm{i}(\mathbf{r} \times \boldsymbol{\nabla})$ (with $\hbar = 1$) is the orbital angular momentum operator of a particle and ℓ_z is its z-component. Thus

$$\boldsymbol{\ell}^2 Y_{\ell m}(\theta, \phi) = \ell(\ell + 1) Y_{\ell m}(\theta, \phi), \quad \ell = 0, 1, 2, \ldots, \tag{B.27}$$

$$\ell_z Y_{\ell m}(\theta, \phi) = m Y_{\ell m}(\theta, \phi), \quad m = -\ell, -\ell + 1, \ldots, \ell, \tag{B.28}$$

where, using spherical polar coordinates θ and ϕ,

$$\boldsymbol{\ell}^2 = -\left[\frac{1}{\sin\theta}\frac{\partial}{\partial\theta}\left(\sin\theta\frac{\partial}{\partial\theta}\right) + \frac{1}{\sin^2\theta}\frac{\partial^2}{\partial\phi^2}\right] \tag{B.29}$$

and

$$\ell_z = -\mathrm{i}\frac{\partial}{\partial\phi}. \tag{B.30}$$

The Laplacian ∇^2 can be written in terms of $\boldsymbol{\ell}^2$ as follows

$$\nabla^2 = \frac{1}{r^2}\frac{\partial}{\partial r}r^2\frac{\partial}{\partial r} - \frac{1}{r^2}\boldsymbol{\ell}^2, \tag{B.31}$$

where the kinetic energy of a particle of unit mass is $-\frac{1}{2}\nabla^2$.

The spherical harmonics are defined in terms of the associated Legendre functions by

$$Y_{\ell m}(\theta, \phi) = (-1)^m \left[\frac{(2\ell + 1)(\ell - m)!}{4\pi(\ell + m)!}\right]^{1/2} P_\ell^m(\cos\theta)\exp(\mathrm{i}m\phi), \quad m \geq 0, \tag{B.32}$$

where those with $m < 0$ can be obtained from the following important property

$$Y^*_{\ell m}(\theta, \phi) = (-1)^m Y_{\ell -m}(\theta, \phi). \tag{B.33}$$

In these and later equations $*$ corresponds to complex conjugation, and we have adopted the phase convention of Condon and Shortley [227] here and in the rest of this section. It follows from (B.32) and (B.33) that the spherical harmonics $Y_{\ell m}(\theta, \phi)$ have parity $(-1)^\ell$, so that under a reflection in the origin, such that $(\theta, \phi) \to (\pi - \theta, \phi + \pi)$, we have

$$Y_{\ell m}(\pi - \theta, \phi + \pi) = (-1)^\ell Y_{\ell m}(\theta, \phi). \tag{B.34}$$

The spherical harmonics satisfy the orthonormality relation

$$\int_0^{2\pi}\int_0^{\pi} Y^*_{\ell' m'}(\theta,\phi)Y_{\ell m}(\theta,\phi)\sin\theta \mathrm{d}\theta\mathrm{d}\phi = \delta_{\ell\ell'}\delta_{mm'} \tag{B.35}$$

and the closure relation

$$\sum_{\ell=0}^{\infty}\sum_{m=-\ell}^{+\ell} Y^*_{\ell m}(\theta,\phi)Y_{\ell m}(\theta',\phi') = \delta(\Omega-\Omega'), \tag{B.36}$$

where

$$\delta(\Omega-\Omega') = \frac{\delta(\theta-\theta')\delta(\phi-\phi')}{\sin\theta}. \tag{B.37}$$

They also satisfy the following product relation

$$Y_{\ell_1 m_1}(\theta,\phi)Y_{\ell_2 m_2}(\theta,\phi) = \sum_{\ell=|\ell_1-\ell_2|}^{\ell_1+\ell_2}\left[\frac{(2\ell_1+1)(2\ell_2+1)}{4\pi(2\ell+1)}\right]^{1/2}(\ell_1 m_1 \ell_2 m_2|\ell m_1+m_2)$$

$$\times\,(\ell_1 0\ell_2 0|\ell 0)Y_{\ell m_1+m_2}(\theta,\phi), \tag{B.38}$$

where $(\ell_1 m_1 \ell_2 m_2|\ell m_1+m_2)$ are Clebsch–Gordan coefficients defined in Appendix A. Using the result that $Y_{10}(\theta,\phi) = (3/4\pi)^{1/2}\cos\theta$, (B.38) yields the recurrence relation

$$\cos\theta\; Y_{\ell m}(\theta,\phi) = \left[\frac{(\ell+m+1)(\ell-m+1)}{(2\ell+1)(2\ell+3)}\right]^{1/2} Y_{\ell+1 m}(\theta,\phi)$$

$$+\left[\frac{(\ell+m)(\ell-m)}{(2\ell-1)(2\ell+1)}\right]^{1/2} Y_{\ell-1 m}(\theta,\phi). \tag{B.39}$$

Another useful relation which follows from (B.21) and (B.22) is

$$\sin\theta\frac{\partial}{\partial\theta}Y_{\ell m}(\theta,\phi) = \ell\left[\frac{(\ell+m+1)(\ell-m+1)}{(2\ell+1)(2\ell+3)}\right]^{1/2} Y_{\ell+1 m}(\theta,\phi)$$

$$-(\ell+1)\left[\frac{(\ell+m)(\ell-m)}{(2\ell-1)(2\ell+1)}\right]^{1/2} Y_{\ell-1 m}(\theta,\phi). \tag{B.40}$$

Other recurrence relations can be obtained by introducing the shift operators

$$\ell_\pm = \ell_x \pm \mathrm{i}\ell_y = \exp(\pm\mathrm{i}\phi)\left(\pm\frac{\partial}{\partial\theta} + \mathrm{i}\cot\theta\frac{\partial}{\partial\phi}\right). \tag{B.41}$$

We find that

$$\ell_{\pm} Y_{\ell m}(\theta, \phi) = [(\ell \mp m)(\ell \pm m + 1)]^{1/2} Y_{\ell m \pm 1}(\theta, \phi), \tag{B.42}$$

$$\ell_{+} Y_{\ell \ell}(\theta, \phi) = 0, \tag{B.43}$$

$$\ell_{-} Y_{\ell -\ell}(\theta, \phi) = 0. \tag{B.44}$$

The orthonormality relation (B.35) and the product relation (B.38) enable the following integral over three spherical harmonics to be evaluated

$$\int_0^{2\pi} \int_0^{\pi} Y^*_{\ell_3 m_3}(\theta, \phi) Y_{\ell_1 m_1}(\theta, \phi) Y_{\ell_2 m_2}(\theta, \phi) \sin\theta \mathrm{d}\theta \mathrm{d}\phi$$

$$= \left[\frac{(2\ell_1 + 1)(2\ell_2 + 1)}{4\pi(2\ell_3 + 1)} \right]^{1/2} (\ell_1 m_1 \ell_2 m_2 | \ell_3 m_3)(\ell_1 0 \ell_2 0 | \ell_3 0). \tag{B.45}$$

Another important relation is the spherical harmonic addition theorem

$$Y_{\ell 0}(\theta, 0) = \left(\frac{4\pi}{2\ell + 1} \right)^{1/2} \sum_{m=-\ell}^{+\ell} Y^*_{\ell m}(\theta_1, \phi_1) Y_{\ell m}(\theta_2, \phi_2), \tag{B.46}$$

where (θ_1, ϕ_1) and (θ_2, ϕ_2) are the spherical polar angles of two vectors $\mathbf{r_1}$ and $\mathbf{r_2}$ and θ is the angle between these vectors. Using the result that

$$Y_{\ell 0}(\theta, \phi) = \left(\frac{2\ell + 1}{4\pi} \right)^{1/2} P_{\ell}(\cos\theta), \tag{B.47}$$

the addition theorem can be written as

$$P_{\ell}(\cos\theta) = \frac{4\pi}{2\ell + 1} \sum_{m=-\ell}^{+\ell} Y^*_{\ell m}(\theta_1, \phi_1) Y_{\ell m}(\theta_2, \phi_2). \tag{B.48}$$

A further useful formula can be derived from the generating function satisfied by the Legendre polynomials, (B.2), which we write here as

$$\frac{1}{|\mathbf{r_1} - \mathbf{r_2}|} = \sum_{\ell=0}^{\infty} \frac{r_<^{\ell}}{r_>^{\ell+1}} P_{\ell}(\cos\theta), \tag{B.49}$$

where θ is the angle between the vectors $\mathbf{r_1}$ and $\mathbf{r_2}$ and $r_<$ is the smaller and $r_>$ is the larger of r_1 and r_2. Using (B.48) we can write (B.49) as

$$\frac{1}{|\mathbf{r_1} - \mathbf{r_2}|} = \sum_{\ell=0}^{\infty} \sum_{m=-\ell}^{+\ell} \frac{4\pi}{2\ell + 1} \frac{r_<^{\ell}}{r_>^{\ell+1}} Y^*_{\ell m}(\theta_1, \phi_1) Y_{\ell m}(\theta_2, \phi_2). \tag{B.50}$$

Also we have

$$\frac{\exp(\mathrm{i}k|\mathbf{r_1}-\mathbf{r_2}|)}{|\mathbf{r_1}-\mathbf{r_2}|} = \mathrm{i}k\sum_{\ell=0}^{\infty}(2\ell+1)\,j_\ell(kr_<)h_\ell^{(1)}(kr_>)P_\ell(\cos\theta), \tag{B.51}$$

where j_ℓ and $h_\ell^{(1)}$ are, respectively, spherical Bessel and spherical Hankel functions of the first kind (see Appendix C). Finally, the plane wave $\exp(\mathrm{i}\mathbf{k}\cdot\mathbf{r})$ can be expanded in spherical harmonics as

$$\exp(\mathrm{i}\mathbf{k}\cdot\mathbf{r}) = 4\pi\sum_{\ell=0}^{\infty}\sum_{m=-\ell}^{+\ell}\mathrm{i}^\ell\, j_\ell(kr)Y^*_{\ell m}(\theta_k,\phi_k)Y_{\ell m}(\theta,\phi), \tag{B.52}$$

where (θ_k,ϕ_k) and (θ,ϕ) are the spherical polar angles of the two vectors $\mathbf{k}$ and $\mathbf{r}$, respectively. If we use the addition theorem (B.48) and choose the z-axis to coincide with the direction of $\mathbf{k}$ then (B.52) reduces to the partial wave expansion

$$\exp(\mathrm{i}\mathbf{k}\cdot\mathbf{r}) = \sum_{\ell=0}^{\infty}(2\ell+1)\mathrm{i}^\ell\, j_\ell(kr)P_\ell(\cos\theta). \tag{B.53}$$

Explicit expressions for the first few spherical harmonics are

$$\begin{aligned}
Y_{00}(\theta,\phi) &= \left(\frac{1}{4\pi}\right)^{1/2},\\
Y_{10}(\theta,\phi) &= \left(\frac{3}{4\pi}\right)^{1/2}\cos\theta,\\
Y_{1\pm1}(\theta,\phi) &= \mp\left(\frac{3}{8\pi}\right)^{1/2}\sin\theta\exp(\pm\mathrm{i}\phi),\\
Y_{20}(\theta,\phi) &= \left(\frac{5}{16\pi}\right)^{1/2}(3\cos^2\theta-1),\\
Y_{2\pm1}(\theta,\phi) &= \mp\left(\frac{15}{8\pi}\right)^{1/2}\sin\theta\cos\theta\exp(\pm\mathrm{i}\phi),\\
Y_{2\pm2}(\theta,\phi) &= \left(\frac{15}{32\pi}\right)^{1/2}\sin^2\theta\exp(\pm2\mathrm{i}\phi),\\
Y_{30}(\theta,\phi) &= \left(\frac{7}{16\pi}\right)^{1/2}(5\cos^3\theta-3\cos\theta),\\
Y_{3\pm1}(\theta,\phi) &= \mp\left(\frac{21}{64\pi}\right)^{1/2}\sin\theta(5\cos^2\theta-1)\exp(\pm\mathrm{i}\phi),
\end{aligned}$$

$$Y_{3\pm2}(\theta,\phi) = \left(\frac{105}{32\pi}\right)^{1/2} \sin^2\theta\cos\theta\exp(\pm 2\mathrm{i}\phi),$$
$$Y_{3\pm3}(\theta,\phi) = \mp\left(\frac{35}{64\pi}\right)^{1/2} \sin^3\theta\exp(\pm 3\mathrm{i}\phi). \tag{B.54}$$

It follows that we can write the first-order ($\ell = 1$) spherical harmonics in terms of the Cartesian coordinates x, y and z as

$$Y_{1m}(\theta,\phi) = \left(\frac{3}{4\pi}\right)^{1/2} \frac{1}{r} \begin{cases} -\frac{1}{\sqrt{2}}(x+\mathrm{i}y), & m=1, \\ z, & m=0, \\ -\frac{1}{\sqrt{2}}(x-\mathrm{i}y), & m=-1. \end{cases} \tag{B.55}$$

Finally, we find it convenient to define two-particle angular functions $Y_{\ell_1\ell_2LM_L}(\hat{\mathbf{r}}_1,\hat{\mathbf{r}}_2)$ which are simultaneous eigenfunctions of the square of the total orbital angular momentum operator $\mathbf{L}^2$ and its z-component L_z of two particles labelled 1 and 2, where

$$\mathbf{L} = \boldsymbol{\ell}_1 + \boldsymbol{\ell}_2 \quad \text{and} \quad L_z = \ell_{1z} + \ell_{2z}. \tag{B.56}$$

It follows from (A.15) that these eigenfunctions are defined by

$$Y_{\ell_1\ell_2LM_L}(\hat{\mathbf{r}}_1,\hat{\mathbf{r}}_2) = \sum_{m_1m_2} (\ell_1m_1\ell_2m_2|LM_L) Y_{\ell_1m_1}(\theta_1,\phi_1) Y_{\ell_2m_2}(\theta_2,\phi_2), \tag{B.57}$$

which can be inverted using (A.19) giving

$$Y_{\ell_1m_1}(\theta_1,\phi_1) Y_{\ell_2m_2}(\theta_2,\phi_2) = \sum_{L} (\ell_1m_1\ell_2m_2|LM_L) Y_{\ell_1\ell_2LM_L}(\hat{\mathbf{r}}_1,\hat{\mathbf{r}}_2). \tag{B.58}$$

Also, it follows from the symmetry relation (A.22) satisfied by the Clebsch–Gordan coefficient in (B.57) that these eigenfunctions satisfy

$$Y_{\ell_1\ell_2LM_L}(\hat{\mathbf{r}}_1,\hat{\mathbf{r}}_2) = (-1)^{\ell_1+\ell_2-L} Y_{\ell_2\ell_1LM_L}(\hat{\mathbf{r}}_2,\hat{\mathbf{r}}_1). \tag{B.59}$$

In addition, it follows from the orthonormality relation (B.35) satisfied by the spherical harmonics that

$$\int\int Y^*_{\ell_1\ell_2LM_L}(\hat{\mathbf{r}}_1,\hat{\mathbf{r}}_2) Y_{\ell_1'\ell_2'L'M_{L'}}(\hat{\mathbf{r}}_1,\hat{\mathbf{r}}_2)\mathrm{d}\hat{\mathbf{r}}_1\mathrm{d}\hat{\mathbf{r}}_2 = \delta_{\ell_1\ell_1'}\delta_{\ell_2\ell_2'}\delta_{LL'}\delta_{M_LM_{L'}}, \tag{B.60}$$

where in this and the above equations we have written $\hat{\mathbf{r}}_1 \equiv (\theta_1,\phi_1)$ and $\hat{\mathbf{r}}_2 \equiv (\theta_2,\phi_2)$ for notational simplicity. These two-particle angular functions are important

in the quantum theory of two-electron systems, such as electron collisions with atomic hydrogen or with atoms containing one active electron as in the alkali metal atoms.

B.4 Phase of Spherical Harmonics

The phase of the spherical harmonics $Y_{\ell m}(\theta, \phi)$, defined by (B.32) and (B.33), corresponds to that adopted by Condon and Shortley [227] and is referred to in this monograph as the "Condon–Shortley phase convention". However, it was pointed out by Huby [477] that a careful choice of this phase has to be made in proving the equality of a matrix element to its complex conjugate by means of the time-reversal operation. In particular, the functions used in the vector addition of angular momenta must be defined in such a way that the operation of time reversal gives the same form of the result before and after vector addition. Although the principles involved are well known, an inconsistency in the choice of phase has led to discrepancies in some results. This was discussed by Breit [134] in the context of the Wigner and Eisenbud [972] R-matrix theory of nuclear reactions.

Let us consider the application of the time-reversal operator K (Wigner [966]) on an angular momentum eigenstate ψ_{jm}. We have

$$K\psi_{jm} = \alpha(j)\mathrm{i}^{2m}\psi_{j\,-m}, \tag{B.61}$$

where $\alpha(j)$ can be varied by multiplying the eigenstates by an arbitrary phase factor which is independent of m. It is desirable to choose $\alpha(j)$ so that the form of (B.61) is invariant under the vector addition of angular momenta defined by (A.15). Hence we require that if $\psi_{j_1 m_1}(1)$ and $\psi_{j_2 m_2}(2)$ in (A.15) conform to (B.61) then $\psi_{j_1 j_2 jm}(1, 2)$ should do likewise. It is found that when we use the conventional real representation of the Clebsch–Gordan coefficients $(j_1 m_1 j_2 m_2 | jm)$, this requirement is satisfied by taking

$$\alpha(j) = \mathrm{i}^{-2j} \tag{B.62}$$

so that (B.61) becomes

$$K\psi_{jm} = (-1)^{j-m}\psi_{j\,-m}. \tag{B.63}$$

In the case when ψ_{jm} represents a spherical harmonic, we must adopt a new definition for the phase of this quantity defined by

$$\mathcal{Y}_{\ell m}(\theta, \phi) = \mathrm{i}^{\ell} Y_{\ell m}(\theta, \phi), \tag{B.64}$$

where $Y_{\ell m}(\theta, \phi)$ is the spherical harmonic defined by (B.32) and (B.33). It then follows from (B.33) and (B.64) that

$$\mathcal{Y}^*_{\ell m}(\theta, \phi) = (-1)^{\ell+m}\mathcal{Y}_{\ell -m}(\theta, \phi). \tag{B.65}$$

This modified phase convention for the spherical harmonics $\mathcal{Y}_{\ell m}(\theta, \phi)$ was adopted by Fano and Racah [308], and it was used by Fano [302] in his analysis of the interaction between configurations with several open shells. Following this work, this convention was adopted by Hibbert [462, 464] in a general computer program for atomic structure calculations and by Burke et al. [178], Berrington et al. [95, 98, 102] and Scott and Taylor [844] in their general computer program for atomic continuum calculations using the R-matrix method. In this monograph this phase convention will be referred to as the "Fano–Racah phase convention".

In practice, the modifications which have to be made to the formulae given in Appendix B.3 due to the adoption of the Fano–Racah phase convention are small. However, care has to be taken to ensure that the same phase convention is used consistently throughout the analysis and calculation of any given process. As an example, we derive in Appendix D.1 explicit expressions for the long-range multipole potential coefficients in non-relativistic electron collisions with atoms and ions using both the Fano–Racah and the Condon–Shortley phase conventions. We give below formulae obtained using spherical harmonics satisfying the Fano–Racah phase convention.

We observe first that the spherical harmonics defined by (B.64) satisfy the usual orthonormality relation given by (B.35), which can be written as

$$\int_0^{2\pi} \int_0^{\pi} \mathcal{Y}^*_{\ell' m'}(\theta, \phi) \mathcal{Y}_{\ell m}(\theta, \phi) \sin\theta \mathrm{d}\theta \mathrm{d}\phi = \delta_{\ell\ell'} \delta_{mm'}. \tag{B.66}$$

However, the expression for the product of two spherical harmonics given by (B.38) now becomes

$$\begin{aligned} \mathcal{Y}_{\ell_1 m_1}(\theta, \phi) \mathcal{Y}_{\ell_2 m_2}(\theta, \phi) = \sum_{\ell} \mathrm{i}^{\ell_1 + \ell_2 - \ell} \left[\frac{(2\ell_1 + 1)(2\ell_2 + 1)}{4\pi(2\ell + 1)} \right]^{1/2} \\ \times (\ell_1 m_1 \ell_2 m_2 | \ell m_1 + m_2) \\ \times (\ell_1 0 \ell_2 0 | \ell 0) \mathcal{Y}_{\ell m_1 + m_2}(\theta, \phi). \end{aligned} \tag{B.67}$$

Using the result that $\mathcal{Y}_{10}(\theta, \phi) = \mathrm{i}(3/4\pi)^{1/2} \cos\theta$, (B.67) then reduces to

$$\cos\theta \mathcal{Y}_{\ell m}(\theta, \phi) = \sum_{\ell'} \mathrm{i}^{\ell - \ell'} \left[\frac{2\ell + 1}{2\ell' + 1} \right]^{1/2} (10\ell m | \ell' m)(10\ell 0 | \ell' 0) \mathcal{Y}_{\ell' m}(\theta, \phi). \tag{B.68}$$

In addition it follows from (B.40), by comparing with (B.39) and after using (B.68), that

$$\begin{aligned} \sin\theta \frac{\partial}{\partial\theta} \mathcal{Y}_{\ell m}(\theta, \phi) = \sum_{\ell'} \mathrm{i}^{\ell - \ell'} f(\ell, \ell') \left[\frac{2\ell + 1}{2\ell' + 1} \right]^{1/2} (10\ell m | \ell' m) \\ \times (10\ell 0 | \ell' 0) \mathcal{Y}_{\ell' m}(\theta, \phi), \end{aligned} \tag{B.69}$$

where

$$f(\ell,\ell') = \begin{cases} \ell, & \ell' = \ell+1 \\ -\ell-1, & \ell' = \ell-1. \end{cases} \tag{B.70}$$

Also we find that the integral over three spherical harmonics given by (B.45) reduces to

$$\int_0^{2\pi}\int_0^{\pi} \mathcal{Y}^*_{\ell_3 m_3}(\theta,\phi)\mathcal{Y}_{\ell_1 m_1}(\theta,\phi)\mathcal{Y}_{\ell_2 m_2}(\theta,\phi)\sin\theta \mathrm{d}\theta\mathrm{d}\phi$$

$$= \mathrm{i}^{\ell_1+\ell_2-\ell_3}\left[\frac{(2\ell_1+1)(2\ell_2+1)}{4\pi(2\ell_3+1)}\right]^{1/2}(\ell_1 m_1 \ell_2 m_2|\ell_3 m_3)(\ell_1 0\ell_2 0|\ell_3 0), \tag{B.71}$$

where the factor $\mathrm{i}^{\ell_1+\ell_2-\ell_3}$ is real since, from (A.27), the Clebsch–Gordan coefficient $(\ell_1 0\ell_2 0|\ell_3 0)$ vanishes unless $\ell_1+\ell_2-\ell_3$ is even.

The matrix element of the momentum operator $\hat{\boldsymbol{\epsilon}}\cdot\mathbf{p}$, which occurs in our discussion of multiphoton processes in intense laser fields in Chaps. 9 and 10, can be obtained from (B.68) and (B.69). If we take the z-axis to lie along the laser polarization direction $\hat{\boldsymbol{\epsilon}}$ then

$$\hat{\boldsymbol{\epsilon}}\cdot\mathbf{p} = -\mathrm{i}\frac{\partial}{\partial z} = -\mathrm{i}\left(\cos\theta\frac{\partial}{\partial r} - \frac{\sin\theta}{r}\frac{\partial}{\partial\theta}\right). \tag{B.72}$$

Using (B.68) and (B.69) we then obtain the following expression for the matrix elements

$$\langle \mathcal{Y}_{\ell m}(\theta,\phi)|\hat{\boldsymbol{\epsilon}}\cdot\mathbf{p}|\mathcal{Y}_{\ell' m'}(\theta,\phi)\rangle = \mathrm{i}^{\ell'-\ell-1}\left[\frac{2\ell'+1}{2\ell+1}\right]^{1/2}(10\ell' m'|\ell m)$$

$$\times\,(10\ell' 0|\ell 0)\left(\frac{\mathrm{d}}{\mathrm{d}r} - \frac{f(\ell',\ell)}{r}\right)\delta_{mm'}, \tag{B.73}$$

where $f(\ell',\ell)$ is defined by (B.70), with ℓ and ℓ' interchanged. Also, in our evaluation of the matrix elements which occur in multiphoton processes, discussed in Chaps. 9 and 10 and Appendix D, see, for example, (9.44) and (D.40), it is necessary to determine the angular integrals which arise in the following matrix element

$$M = \langle r^{-1}f(r)\mathcal{Y}_{\ell m}(\theta,\phi)|\hat{\boldsymbol{\epsilon}}\cdot\mathbf{p}|r^{-1}g(r)\mathcal{Y}_{\ell' m'}(\theta,\phi)\rangle. \tag{B.74}$$

After separating the radial and angular integrals in (B.74) we can rewrite this equation as

$$M = \langle r^{-2}f(r)|M_{\mathrm{ang}}|g(r)\rangle, \tag{B.75}$$

where the angular matrix element $M_{\rm ang}$ is defined by

$$M_{\rm ang} = \mathrm{i}^{\ell'-\ell-1}\left[\frac{2\ell'+1}{2\ell+1}\right]^{1/2}(10\ell' m'|\ell m)(10\ell' 0|\ell 0)$$

$$\times\left(\frac{\mathrm{d}}{\mathrm{d}r} - \frac{f(\ell',\ell)}{r} - \frac{1}{r}\right)\delta_{mm'}. \tag{B.76}$$

Comparing (B.76) with the angular matrix element defined by (B.73), we see that the additional factor $-1/r$, which occurs in (B.76), arises from the operation of $\hat{\boldsymbol{\epsilon}}\cdot\mathbf{p}$ on the radial wave function $r^{-1}g(r)$ in (B.74). The angular matrix element $M_{\rm ang}$ then operates on the reduced radial wave function $g(r)$ in (B.75).

Finally, we note that the expansions of the Legendre polynomial and the plane wave, given by (B.48) and (B.52), respectively, can be rewritten in terms of spherical harmonics, defined using the Fano–Racah phase convention as

$$P_\ell(\cos\theta) = \frac{4\pi}{2\ell+1}\sum_{m=-\ell}^{+\ell}\mathcal{Y}^*_{\ell m}(\theta_1,\phi_1)\mathcal{Y}_{\ell m}(\theta_2,\phi_2) \tag{B.77}$$

and

$$\exp(\mathrm{i}\mathbf{k}\cdot\mathbf{r}) = 4\pi\sum_{\ell=0}^{\infty}\sum_{m=-\ell}^{+\ell}\mathrm{i}^\ell j_\ell(kr)\mathcal{Y}^*_{\ell m}(\theta_k,\phi_k)\mathcal{Y}_{\ell m}(\theta,\phi). \tag{B.78}$$

Also, the simultaneous eigenfunctions of the square of the total orbital angular momentum operator $\mathbf{L}^2$ and its z-component L_z of two particles labelled 1 and 2, defined earlier by (B.57), are now given by

$$\mathcal{Y}_{\ell_1\ell_2 LM_L}(\hat{\mathbf{r}}_1,\hat{\mathbf{r}}_2) = \sum_{m_1 m_2}(\ell_1 m_1 \ell_2 m_2|LM_L)\mathcal{Y}_{\ell_1 m_1}(\theta_1,\phi_1)\mathcal{Y}_{\ell_2 m_2}(\theta_2,\phi_2), \tag{B.79}$$

where, as before, these eigenfunctions satisfy the symmetry relation

$$\mathcal{Y}_{\ell_1\ell_2 LM_L}(\hat{\mathbf{r}}_1,\hat{\mathbf{r}}_2) = (-1)^{\ell_1+\ell_2-L}\mathcal{Y}_{\ell_2\ell_1 LM_L}(\hat{\mathbf{r}}_2,\hat{\mathbf{r}}_1) \tag{B.80}$$

and the orthogonality relation

$$\int\int \mathcal{Y}^*_{\ell_1\ell_2 LM_L}(\hat{\mathbf{r}}_1,\hat{\mathbf{r}}_2)\mathcal{Y}_{\ell_1'\ell_2' L'M_{L'}}(\hat{\mathbf{r}}_1,\hat{\mathbf{r}}_2)\mathrm{d}\hat{\mathbf{r}}_1\mathrm{d}\hat{\mathbf{r}}_2 = \delta_{\ell_1\ell_1'}\delta_{\ell_2\ell_2'}\delta_{LL'}\delta_{M_L M_{L'}}. \tag{B.81}$$

B.5 Transformation Under Rotations

In Appendix A.1 we considered a quantum system described by a set of wave functions ψ_{jm} which were simultaneous eigenfunctions of the total angular momentum operator squared $\mathbf{J}^2$ and its z-component J_z belonging to the eigenvalues $j(j+1)$ and m, respectively. In this appendix we consider how these functions transform under rotations of the axis of quantization with the physical system fixed in space. An important example of the need for this development arises in electron–molecule collisions, which we consider in Chap. 11, where the transformation of the collision wave function from the molecular to the laboratory frame of reference is required in the calculation of the scattering amplitudes and cross sections.

We specify a general rotation by three Euler angles α, β and γ. We adopt a right-handed coordinate system, as used by Rose [797], Edmonds [284] and Fano and Racah [308]. The Euler angles are defined by the following three rotations which are performed successively, as illustrated in Fig. B.1:

i. A rotation about the z-axis through an angle α $(0 \leq \alpha < 2\pi)$ giving the new coordinate axes x', y', z', as illustrated in Fig. B.1 (i).
ii. A rotation about the new y'-axis through an angle β $(0 \leq \beta < \pi)$ giving the new coordinate axes x'', y'', z'', as illustrated in Fig. B.1 (ii).
iii. A rotation about the new z''-axis through an angle γ $(0 \leq \gamma < 2\pi)$ giving the final coordinate axes x''', y''', z''', as illustrated in Fig. B.1 (iii).

The Euler angles α, β, γ are each defined by a positive or zero right-hand screw rotation.

We now consider the effect on the wave function of a particle due to a rotation of the coordinate system through the Euler angles α, β, γ. The wave function $\psi(x, y, z)$ in the original coordinate system is related to the wave function

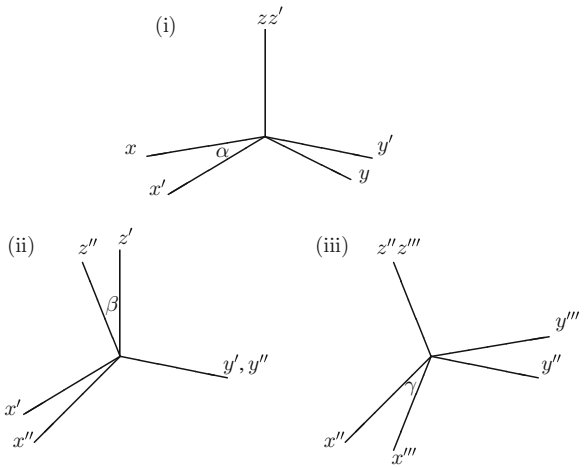

Fig. B.1 Right-handed coordinate system showing the Euler angles α, β, γ

$\psi'(x', y', z')$ in the rotated coordinate system by the product of three unitary operators as follows:

$$\psi' = R(\alpha, \beta, \gamma)\psi = R_\gamma R_\beta R_\alpha \psi, \tag{B.82}$$

where the operators R_α, R_β and R_γ correspond to successive rotations about the z-, y'- and z''-axes, respectively. For an infinitesimal rotation $\mathrm{d}\theta$ about the z-axis we find that

$$R\psi(x, y, z) = (1 - \mathrm{i}\mathrm{d}\theta J_z)\psi(x, y, z), \tag{B.83}$$

where the angular momentum operator J_z, introduced in this equation, and the corresponding angular momentum operators J_x and J_y, obtained by infinitesimal rotations about the x- and y-axes, respectively, are defined by

$$J_x = -\mathrm{i}\left(y\frac{\partial}{\partial z} - z\frac{\partial}{\partial y}\right), \tag{B.84}$$

$$J_y = -\mathrm{i}\left(z\frac{\partial}{\partial x} - x\frac{\partial}{\partial z}\right), \tag{B.85}$$

$$J_z = -\mathrm{i}\left(x\frac{\partial}{\partial y} - y\frac{\partial}{\partial x}\right). \tag{B.86}$$

It follows from (B.83) that a finite rotation about the z-axis can be written as

$$R\psi = \exp(-\mathrm{i}\theta J_z)\psi. \tag{B.87}$$

Hence, the sequence of rotations defined by the Euler angles α, β, γ in (B.82) are represented by the operator

$$R(\alpha, \beta, \gamma) = \exp(-\mathrm{i}\gamma J_{z''})\ \exp(-\mathrm{i}\beta J_{y'})\ \exp(-\mathrm{i}\alpha J_z), \tag{B.88}$$

where J_z, $J_{y'}$ and $J_{z''}$ are the components of $\mathbf{J}$ along the z-, y'- and z''-axes, respectively, in Fig. B.1. We can also show that the operator $R(\alpha, \beta, \gamma)$ in (B.88) can be expressed in terms of rotations made in the *original* coordinate system by the equation

$$R(\alpha, \beta, \gamma) = \exp(-\mathrm{i}\alpha J_z)\ \exp(-\mathrm{i}\beta J_y)\ \exp(-\mathrm{i}\gamma J_z), \tag{B.89}$$

which correspond to a rotation γ about the z-axis, followed by a rotation β about the y-axis and finally a rotation α about the z-axis. We observe that since the above equations have been obtained using the commutation relations satisfied by the orbital angular momentum operators, defined by (B.84), (B.85) and (B.86), they

are valid for general angular momentum operators satisfying these commutation relations.

The matrix elements of the rotation operator $R(\alpha, \beta, \gamma)$ in (B.82) are defined by the equation

$$D^j_{m'm}(\alpha, \beta, \gamma) = \langle \psi_{jm'} | R(\alpha, \beta, \gamma) | \psi_{jm} \rangle, \tag{B.90}$$

where j is a conserved quantum number since $\mathbf{J}^2$ commutes with each term in the expression for $R(\alpha, \beta, \gamma)$ defined by (B.89). Also when ψ in (B.82) is taken to be ψ_{jm} we obtain

$$R(\alpha, \beta, \gamma)\psi_{jm} = \sum_{m'} D^j_{m'm}(\alpha, \beta, \gamma)\psi_{jm'}. \tag{B.91}$$

The quantities $D^j_{m'm}(\alpha, \beta, \gamma)$ in (B.90) and (B.91) are known as Wigner rotation matrices.

In order to obtain an explicit expression for $D^j_{m'm}(\alpha, \beta, \gamma)$ we substitute (B.89) into (B.90) giving

$$D^j_{m'm}(\alpha, \beta, \gamma) = \langle \psi_{jm'} | \exp(-\mathrm{i}\alpha J_z)\ \exp(-\mathrm{i}\beta J_y)\ \exp(-\mathrm{i}\gamma J_z) | \psi_{jm} \rangle. \tag{B.92}$$

It follows from (A.6) that $J_z\psi_{jm} = m\psi_{jm}$, and hence (B.92) can be written as

$$D^j_{m'm}(\alpha, \beta, \gamma) = \exp(-\mathrm{i}m'\alpha)\, d^j_{m'm}(\beta)\ \exp(-\mathrm{i}m\gamma), \tag{B.93}$$

where the reduced rotation matrix $d^j_{m'm}(\beta)$ is defined by

$$d^j_{m'm}(\beta) = \langle \psi_{jm'} | \exp(-\mathrm{i}\beta J_y) | \psi_{jm} \rangle. \tag{B.94}$$

Using the Condon–Shortley phase convention, discussed in Appendix B.4, the reduced rotation matrices are real and are defined by

$$d^j_{m'm}(\beta) = \sum_t (-1)^{t+m'-m} \frac{[(j+m)!(j-m)!(j+m')!(j-m')!]^{1/2}}{(j-m'-t)!(j+m-t)!(t+m'-m)!t!} \times \left(\cos\tfrac{1}{2}\beta\right)^{2j+m-m'-2t} \left(\sin\tfrac{1}{2}\beta\right)^{m'-m+2t}, \tag{B.95}$$

where the summation is over all integer values of t such that the arguments of the factorials are greater than or equal to zero.

We can show that the reduced rotation matrix satisfies the following symmetry relations:

$$d^j_{m'm}(\beta) = d^j_{mm'}(-\beta), \tag{B.96}$$

$$d^j_{m'm}(\beta) = (-1)^{m'-m} d^j_{mm'}(\beta), \tag{B.97}$$

$$d^j_{m'm}(\beta) = (-1)^{m'-m} d^j_{-m'-m}(\beta). \tag{B.98}$$

We can also show that the rotation matrices satisfy the following symmetry relations:

$$D^j_{m'm}(-\gamma, -\beta, -\alpha) = D^{j*}_{mm'}(\alpha, \beta, \gamma), \tag{B.99}$$

$$D^j_{m'm}(\alpha, \beta, \gamma) = (-1)^{m'-m} D^{j*}_{-m'-m}(\alpha, \beta, \gamma). \tag{B.100}$$

They also satisfy the orthonormality relations

$$\sum_m D^{j*}_{m'm}(\alpha, \beta, \gamma) D^j_{m''m}(\alpha, \beta, \gamma) = \delta_{m'm''}, \tag{B.101}$$

$$\sum_m D^j_{mm'}(\alpha, \beta, \gamma) D^j_{mm''}(\alpha, \beta, \gamma) = \delta_{m'm''}. \tag{B.102}$$

These equations follow from (B.91), which corresponds to a unitary transformation from one set of orthogonal eigenfunctions ψ_{jm} to another set of orthogonal eigenfunctions $R(\alpha, \beta, \gamma)\psi_{jm}$, obtained by rotating the coordinate axes. Explicit values for the reduced rotation matrices $d^j_{m'm}$ are given in Tables B.1, B.2 and B.3 for $j = 1/2$, 1 and $3/2$, respectively.

Table B.1 Reduced rotation matrices $d^j_{m'm}$ for $j = \frac{1}{2}$

m'	$m = \frac{1}{2}$	$m = -\frac{1}{2}$
$\frac{1}{2}$	$\cos\frac{1}{2}\beta$	$-\sin\frac{1}{2}\beta$
$-\frac{1}{2}$	$\sin\frac{1}{2}\beta$	$\cos\frac{1}{2}\beta$

Table B.2 Reduced rotation matrices $d^j_{m'm}$ for $j = 1$

m'	$m = 1$	$m = 0$	$m = -1$
1	$\cos^2\frac{1}{2}\beta$	$-\frac{1}{\sqrt{2}}\sin\beta$	$\sin^2\frac{1}{2}\beta$
0	$\frac{1}{\sqrt{2}}\sin\beta$	$\cos\beta$	$-\frac{1}{\sqrt{2}}\sin\beta$
-1	$\sin^2\frac{1}{2}\beta$	$\frac{1}{\sqrt{2}}\sin\beta$	$\cos^2\frac{1}{2}\beta$

Table B.3 Reduced rotation matrices $d^{j}_{m'm}$ for $j = \frac{3}{2}$ where $p = 3\sin^2(\frac{1}{2}\beta) - 2$ and $q = 3\cos^2(\frac{1}{2}\beta) - 2$

m'	$m = \frac{3}{2}$	$m = \frac{1}{2}$	$m = -\frac{1}{2}$	$m = -\frac{3}{2}$
$\frac{3}{2}$	$\cos^3\frac{1}{2}\beta$	$-\sqrt{3}\cos^2\frac{1}{2}\beta\sin\frac{1}{2}\beta$	$\sqrt{3}\cos\frac{1}{2}\beta\sin^2\frac{1}{2}\beta$	$-\sin^3\frac{1}{2}\beta$
$\frac{1}{2}$	$\sqrt{3}\cos^2\frac{1}{2}\beta\sin\frac{1}{2}\beta$	$q\cos\frac{1}{2}\beta$	$p\sin\frac{1}{2}\beta$	$\sqrt{3}\cos\frac{1}{2}\beta\sin^2\frac{1}{2}\beta$
$-\frac{1}{2}$	$\sqrt{3}\cos\frac{1}{2}\beta\sin^2\frac{1}{2}\beta$	$-p\sin\frac{1}{2}\beta$	$q\cos\frac{1}{2}\beta$	$-\sqrt{3}\cos^2\frac{1}{2}\beta\sin\frac{1}{2}\beta$
$-\frac{3}{2}$	$\sin^3\frac{1}{2}\beta$	$\sqrt{3}\cos\frac{1}{2}\beta\sin^2\frac{1}{2}\beta$	$\sqrt{3}\cos^2\frac{1}{2}\beta\sin\frac{1}{2}\beta$	$\cos^3\frac{1}{2}\beta$

The spherical harmonics discussed in Appendix B.3 correspond to a particular example of functions satisfying (B.91). We can write (B.91) in this case as

$$Y_{\ell m}(\theta', \phi') = \sum_{m'} D^{\ell}_{m'm}(\alpha, \beta, \gamma) Y_{\ell m'}(\theta, \phi). \tag{B.103}$$

If $m = 0$ we find, using (B.47) and the spherical harmonic addition theorem (B.48), that

$$D^{\ell}_{m0}(\alpha, \beta, 0) = \left(\frac{4\pi}{2\ell + 1}\right)^{1/2} Y^{*}_{\ell m}(\beta, \alpha). \tag{B.104}$$

The rotation matrices also satisfy the following orthogonality relation

$$\int_0^{2\pi}\int_0^{\pi}\int_0^{2\pi} D^{j'*}_{m'n'}(\alpha, \beta, \gamma) D^{j}_{mn}(\alpha, \beta, \gamma) \mathrm{d}\alpha \sin\beta \mathrm{d}\beta \mathrm{d}\gamma = \frac{8\pi^2}{2j + 1}\delta_{jj'}\delta_{mm'}\delta_{nn'}, \tag{B.105}$$

which reduces to (B.35) satisfied by the spherical harmonics when $n = n' = 0$.

We conclude this appendix by observing that the Wigner rotation matrices are eigenfunctions of the total angular momentum operator of a rigid body whose orientation is specified by the Euler angles (α, β, γ) and which has two of its principal moments of inertia equal. The rotational kinetic operator of this body, which corresponds to a symmetric top molecule, is given by

$$T_R = \frac{1}{2I_1}(\ell_1^2 + \ell_2^2) + \frac{1}{2I_2}\ell_3^2, \tag{B.106}$$

where ℓ_1^2, ℓ_2^2 and ℓ_3^2 are the squares of the components of the angular momentum operator along the principal axes of inertia which are fixed in the body. The normalized eigenfunctions belonging to this operator are

$$\phi_{LKM}(\alpha, \beta, \gamma) = \left(\frac{2L+1}{8\pi^2}\right)^{1/2} D^{L^*}_{KM}(\alpha, \beta, \gamma), \tag{B.107}$$

where both K and M can assume integral values which go over the range $-L$ to L. The corresponding eigenenergies $E(L, K)$ of the rotational kinetic energy operator can be obtained by writing (B.106) as

$$T_R = \frac{1}{2I_1}\boldsymbol{\ell}^2 + \frac{1}{2}\left(\frac{1}{I_2} - \frac{1}{I_1}\right)\ell_3^2, \tag{B.108}$$

where $\boldsymbol{\ell}^2 = \ell_1^2 + \ell_2^2 + \ell_3^2$. Hence the eigenenergies are given by

$$E(L, K) = \frac{1}{2I_1}L(L+1) + \frac{1}{2}\left(\frac{1}{I_2} - \frac{1}{I_1}\right)K^2. \tag{B.109}$$

The rotational eigenfunctions of a general polyatomic molecule are described by the asymmetric top wave function

$$\psi_{LK\lambda}(\alpha, \beta, \gamma) = \left(\frac{2L+1}{8\pi^2}\right)^{1/2} \sum_M a_{LM\lambda} D^{L^*}_{KM}(\alpha, \beta, \gamma), \tag{B.110}$$

where the coefficients $a_{LM\lambda}$ can be obtained by diagonalizing the rotational kinetic energy operator

$$T_R = \frac{\ell_1^2}{2I_1} + \frac{\ell_2^2}{2I_2} + \frac{\ell_3^2}{2I_3} \tag{B.111}$$

in the basis of the symmetric top eigenfunctions $\phi_{LKM}(\alpha, \beta, \gamma)$ defined by (B.107). These coefficients have been given by King et al. [535, 536] and the rotational eigenfunctions and eigenfunctions of polyatomic molecules have been discussed by Herzberg [457].

Appendix C
Bessel Functions and Related Functions

In this appendix we summarize the properties of Bessel functions, spherical Bessel functions and related functions. These functions are required in the solution of the radial Schrödinger equation and in the derivation of formulae for scattering amplitudes and cross sections. They are also important in the discussion of other topics in this monograph including multiphoton processes. For more complete presentations of their properties, reference should be made to specialized monographs on mathematical functions such as Abramowitz and Stegun [1], Watson [956] and Whittaker and Watson [964].

C.1 Bessel Functions

We commence by considering the solution of Bessel's equation

$$z^2\frac{\mathrm{d}^2y}{\mathrm{d}z^2}+z\frac{\mathrm{d}y}{\mathrm{d}z}+(z^2-\nu^2)y=0, \tag{C.1}$$

where ν is a parameter. In general, Bessel functions of order ν are defined by the following power series expansion solution of (C.1):

$$J_\nu(z)=\sum_{s=0}^{\infty}\frac{(-1)^s}{s!\Gamma(s+\nu+1)}\left(\frac{z}{2}\right)^{2s+\nu}, \quad |\arg z|<\pi, \tag{C.2}$$

where Γ is the Gamma function. $J_\nu(z)$ are also called Bessel functions of the first kind. Further solutions of (C.1) can be obtained by replacing ν by $-\nu$ in (C.2) giving

$$J_{-\nu}(z)=\sum_{s=0}^{\infty}\frac{(-1)^s}{s!\Gamma(s-\nu+1)}\left(\frac{z}{2}\right)^{2s-\nu}, \quad |\arg z|<\pi. \tag{C.3}$$

Equations (C.2) and (C.3) define two linearly independent solutions of Bessel's equation except when ν is an integer n. In this case $J_n(z)$ and $J_{-n}(z)$ are not linearly independent but are related by

$$J_{-n}(z)=(-1)^nJ_n(z). \tag{C.4}$$

P.G. Burke, *R-Matrix Theory of Atomic Collisions*, Springer Series on Atomic, Optical, and Plasma Physics 61, DOI 10.1007/978-3-642-15931-2_15,

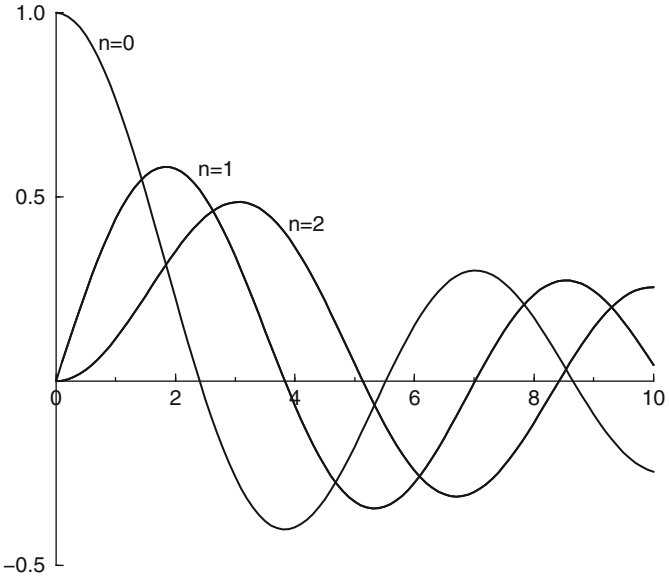

Fig. C.1 Bessel functions $J_n(x)$ for $n = 0$, 1 and 2 and $0 \le x \le 10$

The Bessel functions $J_0(x)$, $J_1(x)$ and $J_2(x)$ are illustrated in Fig. C.1 for small real arguments x.

Other important solutions of Bessel's equation are Neumann functions

$$N_\nu(z) = \frac{1}{\sin(\nu\pi)}[\cos(\nu\pi)J_\nu(z) - J_{-\nu}(z)], \quad \nu \neq 0,\ \pm 1,\ \pm 2,\ \ |\arg z| < \pi, \tag{C.5}$$

which are also called Bessel functions of the second kind and are sometimes denoted by $Y_\nu(z)$, and Hankel functions

$$H_\nu^{(1)}(z) = J_\nu(z) + \mathrm{i}N_\nu(z), \tag{C.6}$$

$$H_\nu^{(2)}(z) = J_\nu(z) - \mathrm{i}N_\nu(z), \tag{C.7}$$

which are also called Bessel functions of the third kind. When ν is an integer n, the linearly independent solutions corresponding to $J_n(z)$ are defined by

$$N_n(z) = \lim_{\nu \to n} N_\nu(z), \quad n = 0,\ \pm 1,\ \pm 2,\ \ |\arg z| < \pi. \tag{C.8}$$

The function pairs $\{J_\nu(z), N_\nu(z)\}$ and $\{H_\nu^{(1)}(z), H_\nu^{(2)}(z)\}$ are linearly independent solutions of Bessel's equation (C.1) for all values of ν. We can also define Bessel

functions of the first kind $J_n(z)$ for integral n in terms of a generating function $\exp[(z/2)(t-1/t)]$. We expand this generating function in a Laurent series as

$$\exp\left[\frac{z}{2}\left(t-\frac{1}{t}\right)\right]=\sum_{n=-\infty}^{\infty}J_n(z)t^n,\quad t\neq 0. \tag{C.9}$$

Expanding the exponential on the left-hand side of this equation and equating the coefficients of t^n, for $n\geq 0$, then yields the power series solution for $J_n(z)$ given by (C.2).

An integral representation for $J_n(z)$ can be derived from (C.9) by multiplying this equation by t^{-n-1} and integrating in a counter-clockwise sense in the complex plane about the point $t=0$. We obtain

$$J_n(z)=\frac{1}{2\pi \mathrm{i}}\oint t^{-n-1}\exp\left[\frac{z}{2}\left(t-\frac{1}{t}\right)\right]\mathrm{d}t. \tag{C.10}$$

This equation can be written in a more usual form by replacing t by $2s/z$. Equation (C.10) then becomes

$$J_n(z)=\frac{1}{2\pi \mathrm{i}}\left(\frac{z}{2}\right)^n\oint s^{-n-1}\exp\left[s-\frac{z^2}{2s}\right]\mathrm{d}s. \tag{C.11}$$

It can be shown that (C.2) and (C.11) are equivalent definitions of $J_n(z)$ for both integral and non-integral values of n. However, for non-integral n the argument of the integral in (C.11) is a multivalued function. Hence care has to be taken in the choice of the contour of integration which must enclose the origin. Reference should be made to Watson [956] and Whittaker and Watson [964] which discuss the choice of this contour.

We can transform (C.10) when n is a positive integer or zero by taking the contour of integration to be the circle $|t|=1$ with $t=\exp(\mathrm{i}\theta)$. In this way (C.10) reduces to Bessel's integral

$$\begin{aligned}J_n(z)&=\frac{1}{\pi}\int_0^{\pi}\cos(n\theta-z\sin\theta)\mathrm{d}\theta,\\&=\frac{\mathrm{i}^{-n}}{\pi}\int_0^{\pi}\exp(\mathrm{i}z\cos\theta)\cos(n\theta)\mathrm{d}\theta,\quad n=0,\ 1,\ 2.\end{aligned} \tag{C.12}$$

If $C_\nu(z)$ denotes $J_\nu(z)$, $N_\nu(z)$, $H_\nu^{(1)}(z)$ or $H_\nu^{(2)}(z)$ then we can show that the following recurrence relations for $C_\nu(z)$ and its derivative $C'_\nu(z)=\mathrm{d}C_\nu/\mathrm{d}z$ are satisfied for ν real or complex

$$C_{\nu-1}(z)+C_{\nu+1}(z)=\frac{2\nu}{z}C_\nu(z), \tag{C.13}$$

$$C_{\nu-1}(z)-C_{\nu+1}(z)=2C'_\nu(z), \tag{C.14}$$

$$C_{\nu-1}(z) - \frac{\nu}{z} C_\nu(z) = C'_\nu(z), \tag{C.15}$$

$$-C_{\nu+1}(z) + \frac{\nu}{z} C_\nu(z) = C'_\nu(z). \tag{C.16}$$

When ν is fixed and $z \to 0$, we have

$$J_\nu(z) \underset{z\to 0}{\sim} \frac{(z/2)^\nu}{\Gamma(\nu+1)}, \quad \nu \neq -1,\ -2,\ -3, \tag{C.17}$$

$$N_0(z) \underset{z\to 0}{\sim} \frac{2}{\pi} \ln z, \tag{C.18}$$

$$N_\nu(z) \underset{z\to 0}{\sim} -\frac{\Gamma(\nu)}{\pi} \left(\frac{z}{2}\right)^{-\nu}, \quad \mathrm{Re}\,\nu > 0. \tag{C.19}$$

Also, when ν is fixed and $|z| \to \infty$ we have the asymptotic expressions

$$J_\nu(z) \underset{|z|\to\infty}{\sim} \left(\frac{2}{\pi z}\right)^{1/2} \cos\left(z - \frac{1}{2}\nu\pi - \frac{1}{4}\pi\right), \quad |\arg z| < \pi, \tag{C.20}$$

$$N_\nu(z) \underset{|z|\to\infty}{\sim} \left(\frac{2}{\pi z}\right)^{1/2} \sin\left(z - \frac{1}{2}\nu\pi - \frac{1}{4}\pi\right), \quad |\arg z| < \pi, \tag{C.21}$$

$$H_\nu^{(1)}(z) \underset{|z|\to\infty}{\sim} \left(\frac{2}{\pi z}\right)^{1/2} \exp\left[\mathrm{i}\left(z - \frac{1}{2}\nu\pi - \frac{1}{4}\pi\right)\right], -\pi < \arg z < 2\pi, \tag{C.22}$$

$$H_\nu^{(2)}(z) \underset{|z|\to\infty}{\sim} \left(\frac{2}{\pi z}\right)^{1/2} \exp\left[-\mathrm{i}\left(z - \frac{1}{2}\nu\pi - \frac{1}{4}\pi\right)\right], -2\pi < \arg z < \pi. \tag{C.23}$$

C.2 Spherical Bessel Functions

When the order ν of the Bessel functions is half an odd integer, then $J_\nu(z)$ takes a simple form which is related to the trigonometric functions. Let us make the substitution

$$y(z) = z^{1/2} w(z), \tag{C.24}$$

in (C.1). Then we find that $w(z)$ satisfies the equation

$$\frac{\mathrm{d}^2 w}{\mathrm{d}z^2} + \frac{2}{z}\frac{\mathrm{d}w}{\mathrm{d}z} + \left[1 - \frac{\ell(\ell+1)}{z^2}\right] w = 0, \tag{C.25}$$

where we have written

$$\nu = \ell + \frac{1}{2}, \tag{C.26}$$

with $\ell = 0, 1, 2, \ldots$.

Particular solutions of (C.25) are spherical Bessel functions

$$j_\ell(z) = \left(\frac{\pi}{2z}\right)^{1/2} J_{\ell+\frac{1}{2}}(z), \tag{C.27}$$

which are also called spherical Bessel functions of the first kind, and spherical Neumann functions

$$n_\ell(z) = \left(\frac{\pi}{2z}\right)^{1/2} N_{\ell+\frac{1}{2}}(z), \tag{C.28}$$

which are also called spherical Bessel functions of the second kind. We see from (C.5) that when ℓ is an integer (C.28) reduces to

$$n_\ell(z) = (-1)^{\ell+1}\left(\frac{\pi}{2z}\right)^{1/2} J_{-\ell-\frac{1}{2}}(z). \tag{C.29}$$

When ℓ is non-integral or complex, which occurs in some applications, it is convenient to define the spherical Bessel function of the second kind by

$$n_\ell(z) = -\frac{1}{\cos \ell\pi}\left(\frac{\pi}{2z}\right)^{1/2} J_{-\ell-\frac{1}{2}}(z), \tag{C.30}$$

which reduces to (C.29) when ℓ is an integer. This definition is obtained from (C.5) by omitting the $J_{\ell+\frac{1}{2}}(z)$ component, yielding simpler analytic properties in the complex z-plane in the neighbourhood of $z = 0$. Linearly independent solutions of spherical Bessel's equation (C.25) for non-integral or complex ℓ are thus usually defined in terms of (C.27) and (C.30). Finally, other solutions of (C.25) are spherical Hankel functions of the first and second kind

$$h_\ell^{(1)}(z) = j_\ell(z) + \mathrm{i}n_\ell(z) = \left(\frac{\pi}{2z}\right)^{1/2} H^{(1)}_{\ell+\frac{1}{2}}(z), \tag{C.31}$$

$$h_\ell^{(2)}(z) = j_\ell(z) - \mathrm{i}n_\ell(z) = \left(\frac{\pi}{2z}\right)^{1/2} H^{(2)}_{\ell+\frac{1}{2}}(z), \tag{C.32}$$

which are also called spherical Bessel functions of the third kind.

It follows from (C.27) and (C.28) that spherical Bessel functions of the first kind are defined by the power series

$$j_\ell(z) = 2^\ell \sum_{s=0}^{\infty} \frac{(-1)^s (s+\ell)!}{s!(2s+2\ell+1)!} z^{2s+\ell}, \tag{C.33}$$

and spherical Bessel functions of the second kind are defined by the power series

$$n_\ell(z) = \frac{(-1)^{\ell+1}}{2^\ell} \sum_{s=0}^{\infty} \frac{(-1)^s (s-\ell)!}{s!(2s-2\ell)!} z^{2s-\ell-1}, \tag{C.34}$$

where negative factorials in expansion (C.34) are avoided by using the identity

$$\frac{(s-\ell)!}{(2s-2\ell)!} = \frac{(-1)^{\ell-s}(2\ell-2s)!}{(\ell-s)!}, \quad s < \ell. \tag{C.35}$$

Written out explicitly, the power series for $j_\ell(z)$ and $n_\ell(z)$ are

$$j_\ell(z) = \frac{z^\ell}{(2\ell+1)!!}\left[1 - \frac{z^2/2}{1!(2\ell+3)} + \frac{(z^2/2)^2}{2!(2\ell+3)(2\ell+5)} - \cdots\right], \tag{C.36}$$

$$n_\ell(z) = -\frac{(2\ell-1)!!}{z^{\ell+1}}\left[1 - \frac{z^2/2}{1!(1-2\ell)} + \frac{(z^2/2)^2}{2!(1-2\ell)(3-2\ell)} - \cdots\right]. \tag{C.37}$$

Hence for fixed ℓ and $z \to 0$ we see that

$$j_\ell(z) \underset{z\to 0}{\sim} \frac{z^\ell}{(2\ell+1)!!}, \tag{C.38}$$

$$n_\ell(z) \underset{z\to 0}{\sim} -\frac{(2\ell-1)!!}{z^{\ell+1}}, \tag{C.39}$$

which are important in deriving the threshold behaviour of collision processes.

The first few spherical Bessel, Neumann and Hankel functions are given explicitly by

$$\begin{aligned}
j_0(z) &= \frac{\sin z}{z}, \\
j_1(z) &= \frac{\sin z}{z^2} - \frac{\cos z}{z}, \\
j_2(z) &= \left(\frac{3}{z^3} - \frac{1}{z}\right)\sin z - \frac{3}{z^2}\cos z,
\end{aligned} \tag{C.40}$$

$$\begin{aligned}
n_0(z) &= -\frac{\cos z}{z}, \\
n_1(z) &= -\frac{\cos z}{z^2} - \frac{\sin z}{z}, \\
n_2(z) &= -\left(\frac{3}{z^3} + \frac{1}{z}\right)\cos z - \frac{3}{z^2}\sin z,
\end{aligned} \tag{C.41}$$

$$\begin{aligned}
h_0^{(1)}(z) &= -\frac{\mathrm{i}}{z}\exp(\mathrm{i}z), \\
h_1^{(1)}(z) &= -\left(\frac{\mathrm{i}}{z^2} + \frac{1}{z}\right)\exp(\mathrm{i}z),
\end{aligned} \tag{C.42}$$

$$h_0^{(2)}(z) = \frac{\mathrm{i}}{z}\exp(-\mathrm{i}z),$$
$$h_1^{(2)}(z) = \left(\frac{\mathrm{i}}{z^2} - \frac{1}{z}\right)\exp(-\mathrm{i}z). \tag{C.43}$$

Also, when ℓ is an integer and $z \gg \ell(\ell+1)/2$ we have the asymptotic expressions

$$j_\ell(z) \underset{|z|\to\infty}{\sim} \frac{1}{z}\sin\left(z - \frac{1}{2}\ell\pi\right), \tag{C.44}$$
$$n_\ell(z) \underset{|z|\to\infty}{\sim} -\frac{1}{z}\cos\left(z - \frac{1}{2}\ell\pi\right), \tag{C.45}$$
$$h_\ell^{(1)}(z) \underset{|z|\to\infty}{\sim} -\frac{\mathrm{i}}{z}\exp\left[\mathrm{i}\left(z - \frac{1}{2}\ell\pi\right)\right], \tag{C.46}$$
$$h_\ell^{(2)}(z) \underset{|z|\to\infty}{\sim} \frac{\mathrm{i}}{z}\exp\left[-\mathrm{i}\left(z - \frac{1}{2}\ell\pi\right)\right]. \tag{C.47}$$

When ℓ is not an integer, then (C.44) is still valid but $n_\ell(z)$ defined by (C.30) has the modified asymptotic expression

$$n_\ell(z) \underset{|z|\to\infty}{\sim} -\frac{1}{z\cos\ell\pi}\cos(z + \tfrac{1}{2}\ell\pi), \tag{C.48}$$

which reduces to (C.45) when ℓ is an integer. When ℓ is not an integer (C.46) and (C.47) are also modified.

If $f_\ell(z)$ denotes $j_\ell(z)$, $n_\ell(z)$, $h_\ell^{(1)}(z)$ or $h_\ell^{(2)}(z)$ then the following recurrence relations for $f_\ell(z)$ and its derivative $f'_\ell(z) = \mathrm{d}f_\ell/\mathrm{d}z$ are satisfied when $\ell > 0$:

$$f_{\ell-1}(z) + f_{\ell+1}(z) = \frac{2\ell+1}{z}f_\ell(z), \tag{C.49}$$
$$\ell f_{\ell-1}(z) - (\ell+1)f_{\ell+1}(z) = (2\ell+1)f'_\ell(z), \tag{C.50}$$
$$f_{\ell-1}(z) - \frac{\ell+1}{z}f_\ell(z) = f'_\ell(z), \tag{C.51}$$
$$-f_{\ell+1}(z) + \frac{\ell}{z}f_\ell(z) = f'_\ell(z). \tag{C.52}$$

Finally, spherical Bessel and Neumann functions satisfy the orthonormality relations

$$\int_0^\infty j_\ell(kr)j_\ell(k'r)r^2\mathrm{d}r = \frac{\pi}{2k^2}\delta(k-k'), \tag{C.53}$$

$$\int_0^\infty n_\ell(kr)n_\ell(k'r)r^2\mathrm{d}r = \frac{\pi}{2k^2}\delta(k-k'), \tag{C.54}$$

which are useful when normalizing the scattering solutions of the radial Schrödinger equation.

Appendix D
Applications of Angular Momentum Algebra

In this appendix we consider four applications of the angular momentum algebra theory described in Appendices A and B. In these applications we obtain explicit expressions for quantities that occur in the main body of this monograph. We first derive expressions for the long-range multipole potential coefficients, which arise in our discussion of both non-relativistic and relativistic electron–atom and electron–ion collisions. We then derive expressions for the long-range multipole potentials which arise in R-matrix–Floquet theory and in time-dependent R-matrix theory of multiphoton processes. Finally, we obtain an expression for the atomic differential photoionization cross section.

In these applications it is important to adopt a consistent phase convention throughout the analysis, although the final physical observables will not depend on the phase convention chosen. We have pointed out in Appendix B.4 that two phase conventions for spherical harmonics have been used in applications, referred to as the Condon–Shortley and the Fano–Racah phase conventions. In this appendix we adopt the Fano–Racah phase convention which has been used in many applications of R-matrix theory. However, in order to illustrate the importance of adopting a consistent phase convention in the analysis, we also derive explicit expressions in Appendix D.1.1 for the long-range multipole potential coefficients in non-relativistic electron collisions with atoms and ions when the Condon–Shortley phase convention is adopted.

D.1 Long-Range Electron–Atom Potential Coefficients

D.1.1 Non-relativistic Collisions

In this section we derive explicit expressions for the long-range multipole potential coefficients in non-relativistic electron collisions with atoms and ions using both the Fano–Racah and the Condon–Shortley phase conventions. We consider first the expression obtained using the Fano–Racah phase convention.

P.G. Burke, *R-Matrix Theory of Atomic Collisions*, Springer Series on Atomic, Optical, and Plasma Physics 61, DOI 10.1007/978-3-642-15931-2_16,

We have shown in Sect. 5.1.3 that the long-range local potential completely describes the electron–target interaction beyond some radius a_0 where the non-local exchange and correlation potentials are negligible. This enables R-matrix propagator methods to be used to solve the resultant coupled differential equations (5.29) in this external region. We also note that the long-range potential coefficients are used in the development of asymptotic expansion methods for solving these equations, described in Appendix F.1.

In the absence of relativistic effects, the long-range potential coefficients $\alpha^{\Gamma}_{ii'\lambda}$ in (2.73) and (5.30) are defined by the equation

$$\alpha^{\Gamma}_{ii'\lambda} = \langle r_{N+1}^{-1} \overline{\Phi}_i^{\Gamma}(\mathbf{X}_N; \hat{\mathbf{r}}_{N+1}\sigma_{N+1}) \left| \sum_{k=1}^{N} r_k^{\lambda} P_\lambda(\cos\theta_{kN+1}) \right| \times r_{N+1}^{-1} \overline{\Phi}_{i'}^{\Gamma}(\mathbf{X}_N; \hat{\mathbf{r}}_{N+1}\sigma_{N+1}) \rangle', \tag{D.1}$$

where the integration in this equation is carried out over all the $(N + 1)$-electron space and spin coordinates except the radial coordinate of the $(N + 1)$th or scattered electron. We expand $P_\lambda(\cos\theta_{kN+1})$ in (D.1) in terms of spherical harmonics satisfying the Fano–Racah phase convention, using (B.77) which we rewrite here as

$$P_\lambda(\cos\theta_{kN+1}) = \frac{4\pi}{2\lambda+1} \sum_{m=-\lambda}^{+\lambda} \mathcal{Y}_{\lambda m}(\theta_k, \phi_k) \mathcal{Y}^*_{\lambda m}(\theta_{N+1}, \phi_{N+1}), \tag{D.2}$$

and we define the channel functions $\overline{\Phi}_i^{\Gamma}$ in (D.1) as follows

$$\begin{aligned} \overline{\Phi}_i^{\Gamma}(\mathbf{X}_N; \hat{\mathbf{r}}_{N+1}\sigma_{N+1}) = \sum_{M_{L_i} m_{\ell_i}} \sum_{M_{S_i} m_i} & (L_i M_{L_i} \ell_i m_{\ell_i} | L M_L) \\ & \times (S_i M_{S_i} \tfrac{1}{2} m_i | S M_S) \Phi_i^{\mathrm{FR}}(\mathbf{X}_N) \\ & \times \mathcal{Y}_{\ell_i m_{\ell_i}}(\theta_{N+1}, \phi_{N+1}) \chi_{\frac{1}{2} m_i}(\sigma_{N+1}) \end{aligned} \tag{D.3}$$

and an analogous expression for $\overline{\Phi}_{i'}^{\Gamma}$. We also introduce the tensor operators

$$M^{\mathrm{FR}}_{\lambda m} = \left(\frac{4\pi}{2\lambda+1} \right)^{1/2} \sum_{k=1}^{N} r_k^{\lambda} \mathcal{Y}_{\lambda m}(\theta_k, \phi_k) \tag{D.4}$$

and

$$C^{\mathrm{FR}}_{\lambda m} = \left(\frac{4\pi}{2\lambda+1} \right)^{1/2} \mathcal{Y}_{\lambda m}(\theta_{N+1}, \phi_{N+1}). \tag{D.5}$$

Substituting these results into (D.1) and carrying out the summations over the spin magnetic quantum numbers, which yield $\delta_{S_i S_{i'}}$, then gives

$$\begin{aligned}\left(\alpha^{\Gamma}_{ii'\lambda}\right)^{\mathrm{FR}} = \sum_{m} \sum_{M_{L_i} m_{\ell_i}} \sum_{M_{L_{i'}} m_{\ell_{i'}}} & \langle \Phi_i^{\mathrm{FR}}(\mathbf{X}_N) | M^{\mathrm{FR}}_{\lambda m} | \Phi_{i'}^{\mathrm{FR}}(\mathbf{X}_N) \rangle \\ & \times \langle \mathcal{Y}_{\ell_i m_{\ell_i}}(\theta_{N+1}, \phi_{N+1}) | C^{\mathrm{FR}*}_{\lambda m} | \mathcal{Y}_{\ell_{i'} m_{\ell_{i'}}}(\theta_{N+1}, \phi_{N+1}) \rangle \\ & \times (L_i M_{L_i} \ell_i m_{\ell_i} | L M_L)(L_{i'} M_{L_{i'}} \ell_{i'} m_{\ell_{i'}} | L M_L) \delta_{S_i S_{i'}}. \end{aligned} \tag{D.6}$$

The integration over the scattered electron angular coordinates $\hat{\mathbf{r}}_{N+1}$ in (D.6) can be carried out using (B.71) yielding

$$\begin{aligned} & \langle \mathcal{Y}_{\ell_i m_{\ell_i}}(\theta_{N+1}, \phi_{N+1}) | C^{\mathrm{FR}*}_{\lambda m} | \mathcal{Y}_{\ell_{i'} m_{\ell_{i'}}}(\theta_{N+1}, \phi_{N+1}) \rangle \\ & \quad = \mathrm{i}^{\ell_{i'} - \ell_i - \lambda} (-1)^m \left[\frac{2\ell_{i'} + 1}{2\ell_i + 1} \right]^{1/2} (\lambda - m \ell_{i'} m_{\ell_{i'}} | \ell_i m_{\ell_i})(\lambda 0 \ell_{i'} 0 | \ell_i 0). \end{aligned} \tag{D.7}$$

In order to carry out the summation over the orbital magnetic quantum numbers, we introduce the reduced multipole moments of the target expressed as $\langle \alpha_i L_i S_i \pi_i || M^{\mathrm{FR}}_{\lambda} || \alpha_{i'} L_{i'} S_{i'} \pi_{i'} \rangle$ which are defined by the equation

$$\begin{aligned} \langle \Phi_i^{\mathrm{FR}}(\mathbf{X}_N) | M^{\mathrm{FR}}_{\lambda m} | \Phi_{i'}^{\mathrm{FR}}(\mathbf{X}_N) \rangle = (2L_i + 1)^{-1/2} & (L_{i'} M_{L_{i'}} \lambda m | L_i M_{L_i}) \\ & \times \langle \alpha_i L_i S_i \pi_i || M^{\mathrm{FR}}_{\lambda} || \alpha_{i'} L_{i'} S_{i'} \pi_{i'} \rangle. \end{aligned} \tag{D.8}$$

This result follows from the Wigner–Eckart theorem (Wigner [965], Eckart [282]) which states that the dependence of the matrix element $\langle \Phi_i | M_{\lambda m} | \Phi_{i'} \rangle$ on the magnetic quantum numbers M_{L_i}, $M_{L_{i'}}$ and m is entirely contained in the Clebsch–Gordan coefficient $(L_{i'} M_{L_{i'}} \lambda m | L_i M_{L_i})$. The reduced multipole moments of the target thus depend on the detailed atomic structure of the target states but not on their magnetic quantum numbers.

We now collect together the terms involving the orbital magnetic quantum numbers from (D.6), (D.7) and (D.8). We define the summation

$$\begin{aligned} S = \sum_{m} \sum_{M_{L_i} m_{\ell_i}} \sum_{M_{L_{i'}} m_{\ell_{i'}}} & (-1)^m (L_i M_{L_i} \ell_i m_{\ell_i} | L M_L)(L_{i'} M_{L_{i'}} \ell_{i'} m_{\ell_{i'}} | L M_L) \\ & \times (\lambda - m \ell_{i'} m_{\ell_{i'}} | \ell_i m_{\ell_i})(L_{i'} M_{L_{i'}} \lambda m | L_i M_{L_i}). \end{aligned} \tag{D.9}$$

This summation can be evaluated using the symmetry property of the Clebsch–Gordan coefficient

$$(\lambda - m \ell_{i'} m_{\ell_{i'}} | \ell_i m_{\ell_i}) = (-1)^{\ell_i - \ell_{i'} + m} \left[\frac{2\ell_i + 1}{2\ell_{i'} + 1} \right]^{1/2} (\lambda m \ell_i m_{\ell_i} | \ell_{i'} m_{\ell_{i'}}), \tag{D.10}$$

which follows from (A.21) and (A.23) and the definition of the Racah coefficient given by (A.46). We then obtain

$$S = (-1)^{\ell_i-\lambda-L+L_i}\,[(2\ell_i+1)(2L_i+1)]^{1/2}\,W(L_iL_{i'}\ell_i\ell_{i'};\lambda L), \tag{D.11}$$

where we have also used the symmetry properties of the Racah coefficients given by (A.48) and (A.49). Using this result, we find that the expression given by (D.6) for the long-range potential coefficients reduces to

$$\begin{aligned}\left(\alpha^{\Gamma}_{ii'\lambda}\right)^{\mathrm{FR}} &= \mathrm{i}^{\ell_i+\ell_{i'}-\lambda}(-1)^{L_i-L}(2\ell_i+1)^{1/2}(\ell_i0\lambda0|\ell_{i'}0)\,W(L_iL_{i'}\ell_i\ell_{i'};\lambda L)\\ &\quad\times\langle\alpha_iL_iS_i\pi_i||M^{\mathrm{FR}}_{\lambda}||\alpha_{i'}L_{i'}S_{i'}\pi_{i'}\rangle\delta_{S_iS_{i'}},\end{aligned} \tag{D.12}$$

where we note that the term $\mathrm{i}^{\ell_i+\ell_{i'}-\lambda} = \pm1$, since it follows from (A.27) that $(\ell_i0\lambda0|\ell_{i'}0) = 0$ unless $\ell_i+\ell_{i'}-\lambda$ is even. It also follows from (D.12) that $\alpha^{\Gamma}_{ii'\lambda}$ is real and from (D.1) that $\alpha^{\Gamma}_{ii'\lambda}$ is symmetric so that $\alpha^{\Gamma}_{ii'\lambda} = \alpha^{\Gamma}_{i'i\lambda}$.

We next derive an explicit expression for the long-range potential coefficients when we adopt the Condon–Shortley phase convention. We again commence from (D.1), but we now expand $P_\lambda(\cos\theta_{kN+1})$ in terms of spherical harmonics using (B.48) which we rewrite here as

$$P_\lambda(\cos\theta_{kN+1}) = \frac{4\pi}{2\lambda+1}\sum_{m=-\lambda}^{+\lambda} Y_{\lambda m}(\theta_k,\phi_k)Y^*_{\lambda m}(\theta_{N+1},\phi_{N+1}), \tag{D.13}$$

and we define the channel function $\overline{\Phi}^{\Gamma}_i$ in (D.1) as follows

$$\begin{aligned}\overline{\Phi}^{\Gamma}_i(\mathbf{X}_N;\hat{\mathbf{r}}_{N+1}\sigma_{N+1}) &= \sum_{M_{L_i}m_{\ell_i}}\sum_{M_{S_i}m_i}(L_iM_{L_i}\ell_im_{\ell_i}|LM_L)\\ &\quad\times(S_iM_{S_i}\tfrac{1}{2}m_i|SM_S)\Phi^{\mathrm{CS}}_i(\mathbf{X}_N)\\ &\quad\times Y_{\ell_im_{\ell_i}}(\theta_{N+1},\phi_{N+1})\chi_{\frac{1}{2}m_i}(\sigma_{N+1}),\end{aligned} \tag{D.14}$$

and an analogous equation for $\overline{\Phi}^{\Gamma}_{i'}$. We also introduce the tensor operators

$$M^{\mathrm{CS}}_{\lambda m} = \left(\frac{4\pi}{2\lambda+1}\right)^{1/2}\sum_{k=1}^{N} r_k^{\lambda}Y_{\lambda m}(\theta_k,\phi_k) \tag{D.15}$$

and

$$C^{\mathrm{CS}}_{\lambda m} = \left(\frac{4\pi}{2\lambda+1}\right)^{1/2} Y_{\lambda m}(\theta_{N+1},\phi_{N+1}). \tag{D.16}$$

Substituting these results into (D.1) and carrying out the summations over the spin magnetic quantum numbers then give

$$\left(\alpha^{\Gamma}_{ii'\lambda}\right)^{\mathrm{CS}} = \sum_{m} \sum_{M_{L_i} m_{\ell_i}} \sum_{M_{L_{i'}} m_{\ell_{i'}}} \langle \Phi_i^{\mathrm{CS}}(\mathbf{X}_N) | M^{\mathrm{CS}}_{\lambda m} | \Phi_{i'}^{\mathrm{CS}}(\mathbf{X}_N) \rangle$$
$$\times \langle Y_{\ell_i m_{\ell_i}}(\theta_{N+1}, \phi_{N+1}) | C^{\mathrm{CS}*}_{\lambda m} | Y_{\ell_{i'} m_{\ell_{i'}}}(\theta_{N+1}, \phi_{N+1}) \rangle$$
$$\times (L_i M_{L_i} \ell_i m_{\ell_i} | L M_L)(L_{i'} M_{L_{i'}} \ell_{i'} m_{\ell_{i'}} | L M_L) \delta_{S_i S_{i'}}. \quad \text{(D.17)}$$

The integration over the scattered electron angular coordinates $\hat{\mathbf{r}}_{N+1}$ in (D.17) can be carried out using (B.45) yielding

$$\langle Y_{\ell_i m_{\ell_i}}(\theta_{N+1}, \phi_{N+1}) | C^{\mathrm{CS}*}_{\lambda m} | Y_{\ell_{i'} m_{\ell_{i'}}}(\theta_{N+1}, \phi_{N+1}) \rangle$$
$$= (-1)^m \left[\frac{2\ell_{i'} + 1}{2\ell_i + 1} \right]^{1/2} (\lambda\, -m \ell_{i'} m_{\ell_{i'}} | \ell_i m_{\ell_i})(\lambda 0 \ell_{i'} 0 | \ell_i 0), \quad \text{(D.18)}$$

and we introduce the reduced multipole moments of the target by the equation

$$\langle \Phi_i^{\mathrm{CS}}(\mathbf{X}_N) | M^{\mathrm{CS}}_{\lambda m} | \Phi_{i'}^{\mathrm{CS}}(\mathbf{X}_N) \rangle = (2L_i + 1)^{-1/2} (L_{i'} M_{L_{i'}} \lambda m | L_i M_{L_i})$$
$$\times \langle \alpha_i L_i S_i \pi_i || M^{\mathrm{CS}}_{\lambda} || \alpha_{i'} L_{i'} S_{i'} \pi_{i'} \rangle. \quad \text{(D.19)}$$

Substituting (D.18) and (D.19) into (D.17) and collecting terms involving the orbital magnetic quantum numbers then yield the following summation

$$S = \sum_{m} \sum_{M_{L_i} m_{\ell_i}} \sum_{M_{L_{i'}} m_{\ell_{i'}}} (-1)^m (L_i M_{L_i} \ell_i m_{\ell_i} | L M_L)(L_{i'} M_{L_{i'}} \ell_{i'} m_{\ell_{i'}} | L M_L)$$
$$\times (\lambda\, -m \ell_{i'} m_{\ell_{i'}} | \ell_i m_{\ell_i})(L_{i'} M_{L_{i'}} \lambda m | L_i M_{L_i}), \quad \text{(D.20)}$$

which is the same as (D.9) and can thus be evaluated yielding (D.11). Substituting this result into (D.17) then gives the following expression for the long-range potential coefficients using the Condon–Shortley phase convention

$$\left(\alpha^{\Gamma}_{ii'\lambda}\right)^{\mathrm{CS}} = (-1)^{L_i + \ell_i - L} (2\ell_i + 1)^{1/2} (\ell_i 0 \lambda 0 | \ell_{i'} 0) W(L_i L_{i'} \ell_i \ell_{i'}; \lambda L)$$
$$\times \langle \alpha_i L_i S_i \pi_i || M^{\mathrm{CS}}_{\lambda} || \alpha_{i'} L_{i'} S_{i'} \pi_{i'} \rangle \delta_{S_i S_{i'}}. \quad \text{(D.21)}$$

Comparing this result with (D.12) we see that the Condon–Shortley reduced multipole matrix element is replaced by the equivalent Fano–Racah matrix element and the overall phase factor is modified, although in both cases $\alpha^{\Gamma}_{ii'\lambda}$ is real and symmetric. Hence, as pointed out in the introduction to this appendix, a consistent

phase convention must be adopted throughout the analysis in order to obtain correct results for the physical observables.

D.1.2 Inclusion of Relativistic Effects

The above analysis has to be extended as the nuclear charge number Z increases and relativistic effects start to play an important role in low- and intermediate-energy electron collisions with atoms and atomic ions. In this section we derive explicit expressions for the long-range potential coefficients, using the Fano–Racah phase convention, when relativistic effects can be accurately described by the Breit–Pauli Hamiltonian discussed in Sect. 5.4.2.

We commence by deriving an expression for the long-range potential coefficients when relativistic effects in the target can be neglected. Adopting the pair-coupling scheme, defined by (5.116), we obtain the following expression for the long-range potential coefficients $\alpha^{J\pi}_{ii'\lambda}$ in terms of the long-range potential coefficients, $\alpha^{\Gamma}_{ii'\lambda}$ defined by (D.1) in the absence of relativistic effects,

$$\begin{aligned}\alpha^{J\pi}_{ii'\lambda} = &\sum_{LS}\langle[(L_iS_i)J_i,\ell_i]K_i\tfrac{1}{2};JM_J|(L_i\ell_i)L,(S_i\tfrac{1}{2})S;JM_J\rangle\\ &\times\alpha^{\Gamma}_{ii'\lambda}\langle(L_{i'}\ell_{i'})L,(S_{i'}\tfrac{1}{2})S;JM_J|[(L_{i'}S_{i'})J_{i'},\ell_{i'}]K_{i'}\tfrac{1}{2};JM_J\rangle. \quad \text{(D.22)}\end{aligned}$$

We see that the transformation in this equation has the same form as the transformation of the K-matrix defined by (5.119). We can carry out the summation over L and S in (D.22) using the expression for the recoupling coefficients in terms of Racah coefficients given by (5.118) and for the long-range potential coefficient $\alpha^{\Gamma}_{ii'\lambda}$ given by (D.12). After using the orthogonality relation and the sum rule satisfied by the Racah coefficients, given by (A.50) and (A.52), we find that (D.22) reduces to

$$\begin{aligned}\alpha^{J\pi}_{ii'\lambda} = &\,\mathrm{i}^{\ell_i+\ell_{i'}-\lambda}(-1)^{L_{i'}+S_i-K_i-\lambda}\,[(2\ell_i+1)(2J_i+1)(2J_{i'}+1)]^{1/2}\\ &\times(\ell_i0\lambda0|\ell_{i'}0)W(\ell_iJ_i\ell_{i'}J_{i'};K_i\lambda)W(L_iJ_iL_{i'}J_{i'};S_i\lambda)\\ &\times\langle\alpha_iL_iS_i\pi_i||M^{\mathrm{FR}}_{\lambda}||\alpha_{i'}L_{i'}S_{i'}\pi_{i'}\rangle\delta_{S_iS_{i'}}\delta_{K_iK_{i'}}. \quad \text{(D.23)}\end{aligned}$$

This equation can be further simplified by introducing the following reduced multipole moments corresponding to the fine-structure levels of the target

$$\begin{aligned}&\langle\alpha_iL_iS_iJ_i\pi_i||M^{\mathrm{FR}}_{\lambda}||\alpha_{i'}L_{i'}S_{i'}J_{i'}\pi_{i'}\rangle\\ &\quad=(-1)^{L_{i'}+\overline{S}_i-\lambda}\,[(2J_i+1)(2J_{i'}+1)]^{1/2}\,W(L_iJ_iL_{i'}J_{i'};S_i\lambda)\\ &\qquad\times\langle\alpha_iL_iS_i\pi_i||M^{\mathrm{FR}}_{\lambda}||\alpha_{i'}L_{i'}S_{i'}\pi_{i'}\rangle\delta_{S_iS_{i'}}, \quad \text{(D.24)}\end{aligned}$$

where the reduced multipole moment on the right-hand side of this equation is defined by (D.8). The expression (D.23) for the long-range potential coefficients then becomes

$$\alpha_{ii'\lambda}^{J\pi} = \mathrm{i}^{\ell_i+\ell_{i'}-\lambda}(-1)^{-\overline{K}_i}(2\ell_i+1)^{1/2}(\ell_i 0\lambda 0|\ell_{i'}0)W(\ell_i J_i \ell_{i'} J_{i'}; K_i\lambda) \times \langle \alpha_i L_i S_i J_i \pi_i || M_\lambda^{\mathrm{FR}} || \alpha_{i'} L_{i'} S_{i'} J_{i'} \pi_{i'} \rangle \delta_{K_i K_{i'}}. \tag{D.25}$$

In (D.24) and (D.25) we have introduced the quantities $\overline{S}_i$ and $\overline{K}_i$ which are the integral parts of S_i and K_i, respectively, so that $\overline{S}_i - \overline{K}_i = S_i - K_i$. This ensures that the transformed reduced multipole moments of the target $\langle \alpha_i L_i S_i J_i \pi_i || M_\lambda^{\mathrm{FR}} || \alpha_{i'} L_{i'} S_{i'} J_{i'} \pi_{i'} \rangle$ defined by (D.24) are real. It follows from (D.24) and (D.25) that the long-range potential coefficients are diagonal in the quantum numbers S_i and K_i.

When relativistic effects in the target are important then the long-range potential coefficients must be transformed using the term-coupling coefficients $f(\Delta_i J_i \pi_i; \alpha_i L_i S_i \pi_i)$ defined by (5.122). The transformed long-range potential coefficients are then given by

$$\alpha_{\mu\mu'\lambda}^{J\pi} = \sum_{\alpha_i L_i S_i} \sum_{\alpha_{i'} L_{i'} S_{i'}} f(\Delta_i J_i \pi_i; \alpha_i L_i S_i \pi_i) \alpha_{ii'\lambda}^{J\pi} f(\Delta_{i'} J_{i'} \pi_{i'}; \alpha_{i'} L_{i'} S_{i'} \pi_{i'}), \tag{D.26}$$

where the channel subscripts μ and μ' on the coefficients $\alpha_{\mu\mu'\lambda}^{J\pi}$ are defined by

$$\mu \equiv \Delta_i \; J_i \; \ell_i \; K_i \; \tfrac{1}{2}, \quad \mu' \equiv \Delta_{i'} \; J_{i'} \; \ell_{i'} \; K_{i'} \; \tfrac{1}{2}. \tag{D.27}$$

The summation over S_i and $S_{i'}$ in (D.26) means that the transformed long-range potential coefficients are no longer diagonal in the spin quantum number S_i. However, it follows from (D.25) and (D.26) that these coefficients are still diagonal in the quantum number K_i. This conservation rule follows from the definition of the pair-coupling scheme given by (5.116). Since the total angular momentum quantum number J is conserved, and since the spin s_i of the scattered electron is also conserved in the external region, where electron exchange effects are zero, then the quantum number K_i is also conserved. As discussed in Sect. 5.4.2, conservation of K_i results in the coupled second-order differential equations, describing the radial motion of the scattered electron in the external and asymptotic regions, sub-dividing into two uncoupled sets of equations with considerable saving in computational effort.

In conclusion, we see from (D.12), (D.25) and (D.26) that the problem of calculating the long-range potential coefficients has been separated into two distinct parts: first, the calculation of the Clebsch–Gordan and Racah coefficients which depend on the target orbital angular momenta, the total angular momentum and λ and second, the calculation of the reduced multipole moments of the target which involves the detailed atomic structure of the target states.

D.2 *R*-Matrix–Floquet Multiphoton Potential

As our second application of angular momentum algebra theory, we derive explicit expressions for the long-range potential which arises in R-matrix–Floquet theory of atomic multiphoton processes, discussed in Sect. 9.1, where in this analysis and in later examples discussed in this appendix we adopt the Fano–Racah phase convention discussed in Appendix B.4. We have shown in Sect. 9.1.3 that this potential is defined by (9.41) as follows

$$\mathbf{W}^{\mathrm{V}\gamma} = \mathbf{V}^{E\gamma} + \mathbf{V}^{D\gamma} + \mathbf{V}^{P\gamma}. \tag{D.28}$$

We consider these three terms successively below.

First, $\mathbf{V}^{E\gamma}$ arises from the electron–electron and electron–nuclear potential terms in the Hamiltonian H_{N+1} defined by (5.3). Its matrix elements are defined by (9.42) as follows

$$V^{E\gamma}_{nLin'L'i'} = \langle r^{-1}_{N+1}\overline{\Phi}^{\gamma}_{nLi}(\mathbf{X}_N; \hat{\mathbf{r}}_{N+1}\sigma_{N+1}) \left| \sum_{j=1}^{N} \frac{1}{r_{jN+1}} - \frac{N}{r_{N+1}} \right| \times r^{-1}_{N+1}\overline{\Phi}^{\gamma}_{n'L'i'}(\mathbf{X}_N; \hat{\mathbf{r}}_{N+1}\sigma_{N+1})\rangle' \delta_{nn'}, \tag{D.29}$$

where the integration in this equation is carried out over all the $(N + 1)$-electron space and spin coordinates except the radial coordinate of the $(N + 1)$th electron. Also the term $-N/r_{N+1}$ is included so that the long-range Coulomb interaction experienced by the ejected or scattered electron is completely included on the left-hand side of (9.38). Using expansion (B.49) for the $1/r_{jN+1}$ terms in (D.29) we obtain

$$V^{E\gamma}_{nLin'L'i'}(r) = \sum_{\lambda=1}^{\lambda_{\max}} \alpha^{\gamma}_{ii'\lambda} r^{-\lambda-1} \delta_{nn'}\delta_{LL'}, \quad r \geq a_0, \tag{D.30}$$

which is the same as the long-range potential arising in electron collisions with atoms and atomic ions defined by (2.73) and (2.74). An explicit expression for the real coefficients $\alpha^{\gamma}_{ii'\lambda}$ has been derived in Appendix D.1.1 and is given by (D.12) using the Fano–Racah phase convention, where we observe that in these expressions the total orbital angular momentum $L = L'$ is conserved. The potential $\mathbf{V}(r)$ in (9.61) is then given in terms of $\mathbf{V}^{E\gamma}$ by

$$\mathbf{V}(r) = -\frac{\boldsymbol{\ell}(\boldsymbol{\ell} + \mathbf{I})}{r^2} + \frac{2(Z - N)}{r}\mathbf{I} - 2\mathbf{V}^{E\gamma}(r), \tag{D.31}$$

where the first two terms on the right-hand side of this equation are diagonal matrices.

Next, the $\mathbf{V}^{D\gamma}$ term in (D.28) arises from the dipole length operator D_N in (9.34) which we write here using the Fano–Racah phase convention as

$$D_N = \frac{1}{2}\mathcal{E}_0 \sum_{i=1}^{N} z_i = -\mathrm{i}\mathcal{D}_N = -\frac{\mathrm{i}}{2}\left(\frac{4\pi}{3}\right)^{1/2} \mathcal{E}_0 \sum_{i=1}^{N} r_i \mathcal{Y}_{10}(\theta_i, \phi_i), \tag{D.32}$$

where we have taken the z-axis to lie along the laser polarization direction $\hat{\boldsymbol{\epsilon}}$. The matrix elements of D_N, defined by (9.43), are then given by

$$\begin{aligned} V^{D\gamma}_{nLin'L'i'} = \langle r_{N+1}^{-1} \overline{\Phi}^{\gamma}_{nLi}(\mathbf{X}_N; \hat{\mathbf{r}}_{N+1}\sigma_{N+1}) \,|D_N|\, r_{N+1}^{-1} \\ \times \overline{\Phi}^{\gamma}_{n'L'i'}(\mathbf{X}_N; \hat{\mathbf{r}}_{N+1}\sigma_{N+1})\rangle' \left(\delta_{nn'-1} + \delta_{nn'+1}\right). \end{aligned} \tag{D.33}$$

We expand the channel functions $\overline{\Phi}^{\gamma}_{nLi}$ and $\overline{\Phi}^{\gamma}_{n'L'i'}$ in terms of the residual atom or ion states Φ_i and $\Phi_{i'}$ by an equation analogous to (D.3). The summation over the orbital magnetic quantum numbers in (D.33) can then be carried out by introducing the reduced dipole matrix elements of the target $\langle \alpha_i L_i S_i \pi_i || \mathcal{D}_N || \alpha_{i'} L_{i'} S_{i'} \pi_{i'} \rangle$, in analogy with (D.8). That is, we write

$$\begin{aligned} \langle \Phi_i(\mathbf{X}_N) | \mathcal{D}_N | \Phi_{i'}(\mathbf{X}_N) \rangle = (2L_i + 1)^{-1/2} (L_{i'} M_{L_{i'}} 10 | L_i M_{L_i}) \\ \times \langle \alpha_i L_i S_i \pi_i || \mathcal{D}_N || \alpha_{i'} L_{i'} S_{i'} \pi_{i'} \rangle. \end{aligned} \tag{D.34}$$

Following the angular momentum algebra procedure adopted in the simplification of $\alpha^{\gamma}_{ii'\lambda}$ defined by (D.6) we find that (D.33) reduces to

$$\begin{aligned} V^{D\gamma}_{nLin'L'i'} = -\mathrm{i}(-1)^{L_{i'}+\ell_i+L+L'+M_L+1} (\delta_{nn'-1} + \delta_{nn'+1}) \\ \times \left[\frac{(2L+1)(2L'+1)}{3}\right]^{1/2} (LM_L L' - M_{L'} | 10) W(LL_i L' L_{i'}; \ell_i 1) \\ \times \langle \alpha_i L_i S_i \pi_i || \mathcal{D}_N || \alpha_{i'} L_{i'} S_{i'} \pi_{i'} \rangle \delta_{\ell_i \ell_{i'}} \delta_{m_{\ell_i} m_{\ell_{i'}}} \delta_{M_L M_{L'}} \delta_{M_{L_i} M_{L_{i'}}} \\ \times \delta_{S_i S_{i'}} \delta_{M_{S_i} M_{S_{i'}}} \delta_{SS'} \delta_{M_S M_{S'}} \delta_{m_i m_{i'}}. \end{aligned} \tag{D.35}$$

We see that the $\mathbf{V}^{D\gamma}$ term is independent of the radial coordinate r of the ejected or scattered electron and connects channels where

$$n = n' \pm 1, \quad L_i = L_{i'}, L_{i'} \pm 1, \quad \ell_i = \ell_{i'}, \quad L = L', L' \pm 1, \quad M_L = M_{L'} \tag{D.36}$$

and also where the spin quantum numbers are conserved.

The symmetry properties of $\mathbf{V}^{D\gamma}$ follow immediately from the symmetry relations satisfied by the Clebsch–Gordan and Racah coefficients in (D.35)

and the following symmetry property of the reduced matrix element in this equation

$$\langle \alpha_i L_i S_i \pi_i || \mathcal{D}_N || \alpha_{i'} L_{i'} S_{i'} \pi_{i'} \rangle = \langle \alpha_{i'} L_{i'} S_{i'} \pi_{i'} || \mathcal{D}_N || \alpha_i L_i S_i \pi_i \rangle. \tag{D.37}$$

Also, this reduced matrix element can be shown to be real. Hence it follows that

$$\left(\mathbf{V}^{D\gamma}\right)^{\mathrm{T}} = -\mathbf{V}^{D\gamma} \quad \text{and} \quad \left(\mathbf{V}^{D\gamma}\right)^{\dagger} = \mathbf{V}^{D\gamma} \tag{D.38}$$

so that $\mathbf{V}^{D\gamma}$ is pure imaginary, antisymmetric, hermitian and independent of r. We also note that the potential $\mathbf{D}$ in (9.61) is given in terms of $\mathbf{V}^{D\gamma}$ by

$$\mathbf{D} = -2\mathbf{V}^{D\gamma}. \tag{D.39}$$

We observe that if instead of using the Fano–Racah phase convention for the spherical harmonics we had used the Condon–Shortley phase convention then $\mathbf{V}^{D\gamma}$ would have been real, symmetric and hermitian.

Finally, the $\mathbf{V}^{P\gamma}$ term in (D.28) arises from the dipole velocity operator P_{N+1} defined by (9.35). Its matrix elements are defined by (9.44) as follows:

$$\begin{aligned} V^{P\gamma}_{nLin'L'i'} = \langle r^{-1}_{N+1} \overline{\Phi}^{\gamma}_{nLi}(\mathbf{X}_N; \hat{\mathbf{r}}_{N+1}\sigma_{N+1}) \left| \mathrm{i}\frac{A_0}{2\mathrm{c}} \hat{\boldsymbol{\epsilon}} \cdot \mathbf{p}_{N+1} \right| r^{-1}_{N+1} \\ \times \overline{\Phi}^{\gamma}_{n'L'i'}(\mathbf{X}_N; \hat{\mathbf{r}}_{N+1}\sigma_{N+1}) \rangle' \left(\delta_{nn'+1} - \delta_{nn'-1}\right). \end{aligned} \tag{D.40}$$

In order to evaluate this expression we again take the z-axis to lie along the laser polarization direction $\hat{\boldsymbol{\epsilon}}$ so that $\hat{\boldsymbol{\epsilon}} \cdot \mathbf{p}$ is defined by (B.72). Also, we remember that the channel functions $\overline{\Phi}^{\gamma}_i$ are defined by (D.3) using the Fano–Racah phase convention and the matrix elements of $\hat{\boldsymbol{\epsilon}} \cdot \mathbf{p}$ in a spherical harmonic basis are given by (B.73). We then find after some angular momentum algebra that (D.40) reduces to

$$\begin{aligned} V^{P\gamma}_{nLin'L'i'} = {} & \frac{A_0}{2\mathrm{c}} (\delta_{nn'+1} - \delta_{nn'-1}) \mathrm{i}^{\ell_{i'} - \ell_i} (-1)^{\ell_i + L - L_i} [(2\ell_i + 1)(2L + 1)]^{1/2} \\ & \times (\ell_i 010 | \ell_{i'} 0)(L M_L 10 | L' M_L) W(L \ell_i L' \ell_{i'}; L_i 1) \\ & \times \left(\frac{\mathrm{d}}{\mathrm{d}r} - \frac{f(\ell_{i'}, \ell_i)}{r} - \frac{1}{r} \right) \delta_{SS'} \delta_{M_S M_{S'}} \delta_{M_L M_{L'}} \delta_{L_i L_{i'}} \delta_{M_{L_i} M_{L_{i'}}} \\ & \times \delta_{S_i S_{i'}} \delta_{M_{S_i} M_{S_{i'}}} \delta_{m_{\ell_i} m_{\ell_{i'}}} \delta_{m_i m_{i'}}, \end{aligned} \tag{D.41}$$

where $f(\ell_{i'}, \ell_i)$ is defined by (B.70) with the primed and unprimed quantities interchanged. In addition, following our analysis of (B.74), we observe that the $1/r$ term

in the brackets in (D.41) arises from the operation of $\hat{\boldsymbol{\epsilon}} \cdot \mathbf{p}_{N+1}$ in (D.40) on the radial wave function $r^{-1} F^{\mathbf{V}\gamma}_{nLij}(r)$, where the reduced radial wave function $F^{\mathbf{V}\gamma}_{nLij}(r)$ satisfies (9.38). Hence we find that $V^{E\gamma}_{nLin'L'i'}$ defined by (9.42), operates, as required, on the reduced radial wave function $F^{\mathbf{V}\gamma}_{nLij}(r)$ in (9.38).

The symmetry properties of $\mathbf{V}^{P\gamma}$ follow immediately from (D.41) and (B.70). Since $\ell_i = \ell_{i'} \pm 1$ in (D.41) then $\mathrm{i}^{\ell_{i'} - \ell_i} = \mp \mathrm{i}$, and since all other terms in this equation are real then $\mathbf{V}^{P\gamma}$ is pure imaginary. The potentials $\mathbf{P}$ and $\mathbf{Q}$ in (9.61) are defined in terms of $\mathbf{V}^{P\gamma}$ by

$$\mathbf{P}\frac{\mathrm{d}}{\mathrm{d}r} + \mathbf{Q}\frac{1}{r} = -2\mathbf{V}^{P\gamma}. \tag{D.42}$$

It then follows from (D.41) and (D.42) that $\mathbf{P}$ and $\mathbf{Q}$ are pure imaginary and independent of the radial coordinate r. It follows from the symmetry properties of the Clebsch–Gordan and Racah coefficients, given in Appendix A, and the symmetry of the function $f(\ell_{i'}, \ell_i)$, defined by (B.70), that

$$\mathbf{P}^{\mathrm{T}} = \mathbf{P} \quad \text{and} \quad \mathbf{Q}^{\mathrm{T}} = -\mathbf{Q}, \tag{D.43}$$

where $\mathbf{P}^{\mathrm{T}}$ and $\mathbf{Q}^{\mathrm{T}}$ are the transposes of $\mathbf{P}$ and $\mathbf{Q}$. Hence it follows that

$$\mathbf{P}^{\dagger} = -\mathbf{P} \quad \text{and} \quad \mathbf{Q}^{\dagger} = \mathbf{Q}, \tag{D.44}$$

where $\mathbf{P}^{\dagger}$ and $\mathbf{Q}^{\dagger}$ are the hermitian conjugates of $\mathbf{P}$ and $\mathbf{Q}$, respectively, so that $\mathbf{P}$ is antihermitian and $\mathbf{Q}$ is hermitian.

If instead of using the Fano–Racah phase convention for the spherical harmonics we had used the Condon–Shortley phase convention then both $\mathbf{P}$ and $\mathbf{Q}$ would have been real but (D.44) would still have been satisfied. In both cases it follows from (D.41) and (D.42) that the diagonal elements of $\mathbf{P}$ and $\mathbf{Q}$ are zero.

D.3 Time-Dependent Multiphoton Potential

As our third application of angular momentum algebra theory we derive explicit expressions for the long-range potential that arises in time-dependent R-matrix theory of atomic multiphoton processes, discussed in Sect. 10.1, using the Fano–Racah phase convention. We have shown in Sect. 10.1.3 that this potential is defined by (10.53) as follows:

$$\mathbf{W}^{\gamma} = \mathbf{V}^{E\gamma} + \mathbf{V}^{D\gamma} + \mathbf{V}^{P\gamma}, \tag{D.45}$$

where in the following analysis we will assume that the dipole velocity gauge is adopted. We now consider the three terms in (D.45) successively below.

First, $\mathbf{V}^{E\gamma}$ arises from the electron–electron and electron–nuclear potential terms in the Hamiltonian H_{N+1} defined by (5.3). Its matrix elements are given, in analogy with (D.29), by

$$V_{ii'}^{E\gamma} = \langle r_{N+1}^{-1} \overline{\Phi}_i^{\gamma}(\mathbf{X}_N; \hat{\mathbf{r}}_{N+1}\sigma_{N+1}) \left| \sum_{j=1}^{N} \frac{1}{r_{jN+1}} - \frac{N}{r_{N+1}} \right| \times r_{N+1}^{-1} \overline{\Phi}_{i'}^{\gamma}(\mathbf{X}_N; \hat{\mathbf{r}}_{N+1}\sigma_{N+1}) \rangle', \tag{D.46}$$

where the integration in this equation is carried out over all the $(N + 1)$-electron space and spin coordinates except the radial coordinate of the $(N + 1)$th electron. Following our analysis in Appendix D.2, see (D.30), we obtain the following expression for this potential:

$$V_{ii'}^{E\gamma}(r) = \sum_{\lambda=1}^{\lambda_{\max}} \alpha_{ii'\lambda}^{\gamma} r^{-\lambda-1}, \quad r \geq a_0, \tag{D.47}$$

which is the same as the long-range potential arising in electron collisions with atoms and atomic ions defined by (2.73) and (2.74). The potential $\mathbf{V}(r)$ in (10.55) is then given in terms of $\mathbf{V}^{E\gamma}$ by

$$\mathbf{V}(r) = -\frac{\boldsymbol{\ell}(\boldsymbol{\ell} + \mathbf{I})}{r^2} + \frac{2(Z - N)}{r}\mathbf{I} - 2\mathbf{V}^{E\gamma}(r), \tag{D.48}$$

where the first two terms on the right-hand side of this equation are diagonal matrices.

The $\mathbf{V}^{D\gamma}$ and $\mathbf{V}^{P\gamma}$ terms in (D.45) arise from the dipole velocity operator term $\mathrm{c}^{-1}\mathbf{A}(t) \cdot \mathbf{P}_{N+1}$, which when $t = t_{m+\frac{1}{2}}$, can be written as

$$P = \frac{1}{\mathrm{c}} \sum_{i=1}^{N+1} \mathbf{A}(t_{m+\frac{1}{2}}) \cdot \mathbf{p}_i = P_N + P_{N+1}, \tag{D.49}$$

where P_N arises from the laser interaction with the residual ion containing N electrons, defined by

$$P_N = \frac{1}{\mathrm{c}} \sum_{i=1}^{N} \mathbf{A}(t_{m+\frac{1}{2}}) \cdot \mathbf{p}_i, \tag{D.50}$$

and P_{N+1} arises from the laser interaction with the ejected or scattered electron, defined by

$$P_{N+1} = \frac{1}{\mathrm{c}} \mathbf{A}(t_{m+\frac{1}{2}}) \cdot \mathbf{p}_{N+1}. \tag{D.51}$$

We now consider the contribution to the potential from P_N and P_{N+1} in turn.

The matrix elements of the potential $\mathbf{V}^{D\gamma}$ in (D.45), which corresponds to the interaction of the laser with the residual ion, are given by

$$V_{ii'}^{D\gamma} = \langle r_{N+1}^{-1}\overline{\Phi}_i^{\gamma}(\mathbf{X}_N;\hat{\mathbf{r}}_{N+1}\sigma_{N+1})\,|P_N|\,r_{N+1}^{-1}\overline{\Phi}_{i'}^{\gamma}(\mathbf{X}_N;\hat{\mathbf{r}}_{N+1}\sigma_{N+1})\rangle', \tag{D.52}$$

where, taking the z-axis to lie along the laser polarization direction $\hat{\boldsymbol{\epsilon}}$, we can write

$$P_N = -\frac{\mathrm{i}}{\mathrm{c}}A(t_{m+\frac{1}{2}})\sum_{j=1}^{N}\left(\cos\theta_j\frac{\partial}{\partial r_j} - \frac{\sin\theta_j}{r_j}\frac{\partial}{\partial\theta_j}\right), \tag{D.53}$$

which follows from (B.72). Hence we can write

$$V_{ii'}^{D\gamma} = V_{ii'}^{D_1\gamma} + V_{ii'}^{D_2\gamma}, \tag{D.54}$$

where

$$V_{ii'}^{D_1\gamma} = -\frac{\mathrm{i}}{\mathrm{c}}A(t_{m+\frac{1}{2}})\langle r_{N+1}^{-1}\overline{\Phi}_i^{\gamma}(\mathbf{X}_N;\hat{\mathbf{r}}_{N+1}\sigma_{N+1})\left|\sum_{j=1}^{N}\cos\theta_j\frac{\partial}{\partial r_j}\right| \times r_{N+1}^{-1}\overline{\Phi}_{i'}^{\gamma}(\mathbf{X}_N;\hat{\mathbf{r}}_{N+1}\sigma_{N+1})\rangle' \tag{D.55}$$

and

$$V_{ii'}^{D_2\gamma} = \frac{\mathrm{i}}{\mathrm{c}}A(t_{m+\frac{1}{2}})\langle r_{N+1}^{-1}\overline{\Phi}_i^{\gamma}(\mathbf{X}_N;\hat{\mathbf{r}}_{N+1}\sigma_{N+1})\left|\sum_{j=1}^{N}\frac{\sin\theta_j}{r_j}\frac{\partial}{\partial\theta_j}\right| \times r_{N+1}^{-1}\overline{\Phi}_{i'}^{\gamma}(\mathbf{X}_N;\hat{\mathbf{r}}_{N+1}\sigma_{N+1})\rangle'. \tag{D.56}$$

In order to evaluate $V_{ii'}^{D_1\gamma}$, defined by (D.55), we expand the channel functions $\overline{\Phi}_i^{\gamma}$ and $\overline{\Phi}_{i'}^{\gamma}$ in terms of the residual atom or ion states Φ_i and $\Phi_{i'}$ using (D.3) with Γ replaced by γ. Also, it follows from (B.54) and (B.64) that

$$\cos\theta = -\mathrm{i}\left(\frac{4\pi}{3}\right)^{1/2}\mathcal{Y}_{10}(\theta,\phi), \tag{D.57}$$

and we define the reduced matrix element $\langle\alpha_i L_i S_i\pi_i||P_N^{(1)}||\alpha_{i'}L_{i'}S_{i'}\pi_{i'}\rangle$, in analogy with (D.34), as

$$\langle\Phi_i(\mathbf{X}_N)\left|\sum_{j=1}^{N}\mathcal{Y}_{10}(\theta_j,\phi_j)\frac{\partial}{\partial r_j}\right|\Phi_{i'}(\mathbf{X}_N)\rangle = (2L_i+1)^{-1/2}(L_{i'}M_{L_{i'}}10|L_iM_{L_i})\langle\alpha_iL_iS_i\pi_i||P_N^{(1)}||\alpha_{i'}L_{i'}S_{i'}\pi_{i'}\rangle. \tag{D.58}$$

In order to evaluate $V_{ii'}^{D_2\gamma}$, defined by (D.56), we again expand the channel functions $\overline{\Phi}_i^{\gamma}$ and $\overline{\Phi}_{i'}^{\gamma}$ in terms of the residual atom or ion states Φ_i and $\Phi_{i'}$ using (D.3) with Γ replaced by γ. Also, it follows from (B.40) and (B.64) that

$$\sin\theta\frac{\partial}{\partial\theta}Y_{\ell m}(\theta,\phi) = -\mathrm{i}a(\ell,m)\mathcal{Y}_{\ell+1m}(\theta,\phi) - \mathrm{i}b(\ell,m)\mathcal{Y}_{\ell-1m}(\theta,\phi), \tag{D.59}$$

where

$$a(\ell,m) = \ell\left[\frac{(\ell+m+1)(\ell-m+1)}{(2\ell+1)(2\ell+3)}\right]^{1/2} \tag{D.60}$$

and

$$b(\ell,m) = (\ell+1)\left[\frac{(\ell+m)(\ell-m)}{(2\ell-1)(2\ell+1)}\right]^{1/2}, \tag{D.61}$$

and where we have included the operation of $\sin\theta\partial/\partial\theta$ in (D.56) on the angular function $\mathcal{Y}_{\ell m}(\theta,\phi)$ in $\overline{\Phi}_{i'}^{\gamma}$. Hence we see that the operation of $\sin\theta\partial/\partial\theta$ in (D.56) modifies the orbital angular momenta of the residual ion by ±1 while leaving the magnetic quantum numbers unaltered. It follows that we can define the reduced matrix element $\langle\alpha_i L_i S_i \pi_i||P_N^{(2)}||\alpha_{i'}L_{i'}S_{i'}\pi_{i'}\rangle$ by

$$\begin{aligned}
&\langle\Phi_i(\mathbf{X}_N)\left|-\sum_{j=1}^{N}\frac{\sin\theta_j}{r_j}\frac{\partial}{\partial\theta_j}\right|\Phi_{i'}(\mathbf{X}_N)\rangle \\
&= -\mathrm{i}\left(\frac{4\pi}{3}\right)^{1/2}(2L_i+1)^{-1/2}\sum_{L_{i''}}(L_{i''}M_{L_{i'}}10|L_iM_{L_i}) \\
&\quad\times\langle\alpha_i L_i S_i\pi_i||P_N^{(2)}||\alpha_{i'}L_{i''}S_{i'}\pi_{i'}\rangle,
\end{aligned} \tag{D.62}$$

where, by comparing this result with (D.58), we see that there is an additional summation over $L_{i''}$, corresponding to the terms on the right-hand side of (D.59). Also, we have included the factor $-\mathrm{i}(4\pi/3)^{1/2}$ in (D.62) which corresponds to the factor in (D.57) used to transform (D.55). We then obtain after some angular momentum algebra that the matrix elements of $V_{ii'}^{D\gamma}$, defined by (D.54), (D.55) and (D.56), can be written in terms of the reduced matrix elements, defined by (D.58) and (D.62), as follows:

$$V_{ii'}^{D\gamma} = \frac{1}{\mathrm{c}}\left(\frac{4\pi}{3}\right)^{1/2} A(t_{m+\frac{1}{2}})(-1)^{L'+\ell_i}(2L+1)^{1/2}(LM_L10|L'M_L)$$
$$\times \sum_{L_{i''}}\Big[W(LL_iL'L_{i''};\ell_i 1)\langle\alpha_i L_i S_i\pi_i||P_N^{(1)}||\alpha_{i'}L_{i''}S_{i'}\pi_{i'}\rangle(-1)^{L_{i''}}\delta_{L_{i'}L_{i''}}$$
$$+ W(LL_iL'L_{i''};\ell_i 1)\langle\alpha_i L_i S_i\pi_i||P_N^{(2)}||\alpha_{i'}L_{i''}S_{i'}\pi_{i'}\rangle(-1)^{L_{i''}}\Big]$$
$$\times \delta_{M_LM_{L'}}\delta_{M_{L_i}M_{L_{i'}}}\delta_{SS'}\delta_{M_SM_{S'}}\delta_{S_iS_{i'}}\delta_{M_{S_i}M_{S_{i'}}}\delta_{\ell_i\ell_{i'}}\delta_{m_{\ell_i}m_{\ell_{i'}}}\delta_{m_im_{i'}}. \quad \text{(D.63)}$$

We see that $V_{ii'}^{D\gamma}$ is independent of the radial coordinate of the ejected or scattered electron and connects channels where

$$L = L', \quad L' \pm 1, \quad M_L = M_{L'}, \quad \text{(D.64)}$$

and where the spin quantum numbers are conserved. The reduced matrix elements in (D.63) can be shown to be antisymmetric and hence $\mathbf{V}^{D\gamma}$ is real, symmetric, hermitian and independent of r. We also note that the potential $\mathbf{D}$ in (10.55) is given in terms of $\mathbf{V}^{D\gamma}$ by

$$\mathbf{D} = -2\mathbf{V}^{D\gamma}. \quad \text{(D.65)}$$

Finally, we consider the matrix elements of $\mathbf{V}^{P\gamma}$ in (D.45), corresponding to the interaction of the laser with the ejected or scattered electron. In this case the matrix elements are given by

$$V_{ii'}^{P\gamma} = \langle r_{N+1}^{-1}\overline{\Phi}_i^{\gamma}(\mathbf{X}_N;\hat{\mathbf{r}}_{N+1}\sigma_{N+1})\,|P_{N+1}|\,r_{N+1}^{-1}\overline{\Phi}_{i'}^{\gamma}(\mathbf{X}_N;\hat{\mathbf{r}}_{N+1}\sigma_{N+1})\rangle', \quad \text{(D.66)}$$

where P_{N+1} is defined by (D.51). After taking the z-axis to lie along the laser polarization direction $\hat{\boldsymbol{\epsilon}}$, we can write

$$P_{N+1} = -\frac{\mathrm{i}}{\mathrm{c}}A(t_{m+\frac{1}{2}})\left(\cos\theta_{N+1}\frac{\partial}{\partial r_{N+1}} - \frac{\sin\theta_{N+1}}{r_{N+1}}\frac{\partial}{\partial\theta_{N+1}}\right). \quad \text{(D.67)}$$

We then expand the channel functions $\overline{\Phi}_i^{\gamma}$ and $\overline{\Phi}_{i'}^{\gamma}$ in (D.66) in terms of the residual atom or ion states Φ_i and $\Phi_{i'}$ using (D.3) with Γ replaced by γ, and we use (B.72) and (B.73) to write

$$\langle\mathcal{Y}_{\ell m}(\theta,\phi)|P_{N+1}|\mathcal{Y}_{\ell'm'}(\theta,\phi)\rangle$$
$$= \frac{1}{\mathrm{c}}A(t_{m+\frac{1}{2}})\mathrm{i}^{\ell'-\ell-1}\left[\frac{2\ell'+1}{2\ell+1}\right](10\ell'm|\ell m)(10\ell'0|\ell 0)\left(\frac{\mathrm{d}}{\mathrm{d}r_{N+1}} - \frac{f(\ell',\ell)}{r_{N+1}}\right)$$
$$\times \delta_{mm'}, \quad \text{(D.68)}$$

where $f(\ell', \ell)$ is defined by (B.70) with the primed and unprimed quantities interchanged. Using these results we then obtain after some angular momentum algebra that (D.66) reduces to

$$V_{ii'}^{P\gamma} = -\frac{\mathrm{i}}{\mathrm{c}} A(t_{m+\frac{1}{2}}) \mathrm{i}^{\ell_i' - \ell_i} (-1)^{\ell_i + L - L_i} \left[(2\ell_i + 1)(2L + 1)\right]^{1/2}$$
$$\times (\ell_i 010|\ell_{i'} 0)(LM_L 10|L'M_L) W(L\ell_i L'\ell_{i'}; L_i 1) \left(\frac{\mathrm{d}}{\mathrm{d}r} - \frac{f(\ell_{i'}, \ell_i)}{r} - \frac{1}{r} \right)$$
$$\times \delta_{SS'} \delta_{M_S M_{S'}} \delta_{M_L M_{L'}} \delta_{L_i L_i'} \delta_{M_{L_i} M_{L_{i'}}} \delta_{S_i S_{i'}} \delta_{M_{S_i} M_{S_{i'}}} \delta_{m_i m_{i'}} \delta_{m_{\ell_i} m_{\ell_{i'}}}. \tag{D.69}$$

We see that (D.69) has a similar form to (D.41), which arises in R-matrix–Floquet theory in Chap. 9. Also, it follows from the Clebsch–Gordan coefficients that the potential $V_{ii'}^{P\gamma}$ connects channels where

$$\ell_i = \ell_{i'} \pm 1, \quad L = L', \ L' \pm 1. \tag{D.70}$$

By comparing $\mathbf{V}^{P\gamma}$ with the potentials in (10.55) we find that

$$\mathbf{P} \frac{\mathrm{d}}{\mathrm{d}r} + \mathbf{Q} \frac{1}{r} = -2\mathbf{V}^{P\gamma}. \tag{D.71}$$

Also both $\mathbf{P}$ and $\mathbf{Q}$ are real since the factor $\mathrm{i}^{\ell_i' - \ell_i + 1}$ in (D.69) is real. In addition, it can be shown from (D.69) that $\mathbf{P}$ is antisymmetric, and hence antihermitian and $\mathbf{Q}$ is symmetric and hence hermitian so that

$$\mathbf{P}^{\mathrm{T}} = -\mathbf{P} \quad \text{and} \quad \mathbf{Q}^{\mathrm{T}} = \mathbf{Q}. \tag{D.72}$$

D.4 Atomic Photoionization Cross Section

In our final application of angular momentum algebra theory we derive an explicit expression for the differential photoionization cross section given in Sect. 8.1.1 by (8.43) and (8.44). In that section we obtained the following result for the differential cross section for photoionization of an unpolarized atom or ion by a polarized photon beam, see (8.41),

$$\frac{\mathrm{d}\sigma_{ij}^{V,L}}{\mathrm{d}\Omega} = \frac{A_{V,L}}{(2L+1)(2S+1)} \sum_{M_L M_S} \sum_{M_{L'} M_{S'}} \sum_{m_j'} |\langle \Psi_{jE}^- | D_\mu | \Psi_{iB} \rangle|^2, \tag{D.73}$$

where $A_{V,L}$ is a constant defined by (8.42) and where we write $\langle \Psi_{jE}^- | D_\mu | \Psi_{iB} \rangle$ in terms of the reduced matrix element $\langle \alpha_j' L_j' S_j' \ell_j' L' S' || D || \alpha_i L S \rangle$, defined by (8.38) as follows, see (8.40),

$$\langle \Psi_{jE}^{-}|D_\mu|\Psi_{iB}\rangle = \sum_{\ell'_j m_{\ell'_j}} \sum_{L'S'} (L'_j M_{L'_j} \ell'_j m_{\ell'_j}|L'M_{L'})(S'_j M_{S'_j} \tfrac{1}{2} m'_j|S'M_{S'})$$
$$\times (LM_L 1\mu|L'M_{L'})(2L'+1)^{-1/2}(-\mathrm{i})^{\ell'_j} \exp(\mathrm{i}\sigma_{\ell'_j}) \mathcal{Y}_{\ell'_j m_{\ell'_j}}(\theta_k, \phi_k)$$
$$\times \langle \alpha'_j L'_j S'_j \ell'_j L'S'||D||\alpha_i LS\rangle \delta_{SS'} \delta_{M_S M_{S'}}. \tag{D.74}$$

We now substitute (D.74) into (D.73) yielding

$$\frac{\mathrm{d}\sigma_{ij}^{V,L}}{\mathrm{d}\Omega} = \frac{A_{V,L}}{(2L+1)(2S+1)}$$
$$\times \sum_{M_L M_S} \sum_{M_{L'} M_{S'}} \sum_{\ell'_j m_{\ell'_j} L'} \sum_{\ell''_j m_{\ell''_j} L''} \sum_{m'_j} [(2L'+1)(2L''+1)]^{-1/2}$$
$$\times \mathrm{i}^{\ell'_j - \ell''_j} \exp(-\mathrm{i}\sigma_{\ell'_j} + \mathrm{i}\sigma_{\ell''_j}) \mathcal{Y}^*_{\ell'_j m_{\ell'_j}}(\theta_k, \phi_k) \mathcal{Y}_{\ell''_j m_{\ell''_j}}(\theta_k, \phi_k)$$
$$\times (L'_j M_{L'_j} \ell'_j m_{\ell'_j}|L'M_{L'})(L'_j M_{L'_j} \ell''_j m_{\ell''_j}|L''M_{L''})(S'_j M_{S'_j} \tfrac{1}{2} m'_j|SM_S)$$
$$\times (S'_j M_{S'_j} \tfrac{1}{2} m'_j|SM_S)(LM_L 1\mu|L'M_{L'})(LM_L 1\mu|L''M_{L''})$$
$$\times \langle \alpha'_j L'_j S'_j \ell'_j L'S||D||\alpha_i LS\rangle^* \langle \alpha'_j L'_j S'_j \ell''_j L''S||D||\alpha_i LS\rangle. \tag{D.75}$$

In order to simplify (D.75) we first observe from (A.16), satisfied by the Clebsch–Gordan coefficients, that

$$M_{L'} = M_{L''} \quad \text{and} \quad m_{\ell'_j} = m_{\ell''_j}. \tag{D.76}$$

Also, the summation over the spin magnetic quantum numbers M_S, $M_{S'}$ and m'_j in (D.75) can be carried out using (A.18) yielding a factor $(2S+1)$. We then use the following result satisfied by the Fano–Racah spherical harmonics:

$$\mathcal{Y}^*_{\ell'_j m_{\ell'_j}}(\theta_k, \phi_k) \mathcal{Y}_{\ell''_j m_{\ell''_j}}(\theta_k, \phi_k)$$
$$= \mathrm{i}^{-\ell'_j + \ell''_j} (-1)^{m_{\ell'_j}} \sum_{\ell} (4\pi)^{-1} [(2\ell'_j+1)(2\ell''_j+1)]^{1/2} (\ell'_j - m_{\ell'_j} \ell''_j m_{\ell''_j}|\ell 0)$$
$$\times (\ell'_j 0 \ell''_j 0|\ell 0) P_\ell(\cos\theta_k), \tag{D.77}$$

which follows from (B.33), (B.38), (B.47) and (B.64). We also use (A.45) and the symmetry relations given by (A.21), (A.22), (A.23), (A.24), (A.25), and (A.26) to carry out the following summations over Clebsch–Gordan coefficients in (D.75):

$$\sum_{m_{\ell'_j}} (-1)^{m_{\ell'_j}} (L'_j M_{L'_j} \ell'_j m_{\ell'_j} | L' M_{L'}) (L'_j M_{L'_j} \ell''_j m_{\ell'_j} | L'' M_{L''}) (\ell'_j - m_{\ell'_j} \ell''_j m_{\ell'_j} | \ell 0)$$

$$= (-1)^{L'_j + M_{L'}} [(2L'+1)(2L''+1)]^{1/2} (L' M_{L'} L'' - M_{L'} | \ell 0)$$

$$\times W(L' \ell'_j L'' \ell''_j; L'_j \ell) \tag{D.78}$$

and

$$\sum_{M_L M_{L'}} (-1)^{M_{L'}} (L M_L 1 \mu | L' M_{L'}) (L M_L 1 \mu | L'' M_{L'}) (L' M_{L'} L'' - M_{L'} | \ell 0)$$

$$= (-1)^{L+\mu} [(2L'+1)(2L''+1)]^{1/2} (1 - \mu 1 \mu | \ell 0) W(1L'1L''; L\ell). \tag{D.79}$$

Using (D.76), (D.77) and (D.78) we find that (D.75) can be rewritten in the form

$$\frac{\mathrm{d}\sigma_{ij}^{V,L}}{\mathrm{d}\Omega} = \frac{A_{V,L}}{4\pi(2L+1)} \sum_{\ell} A_\ell(\mu) P_\ell(\cos\theta_k), \tag{D.80}$$

where

$$A_\ell(\mu) = \sum_{L' L'' \ell'_j \ell''_j} (-1)^{L + L'_j + \mu} \exp(-\mathrm{i}\sigma_{\ell'_j} + \mathrm{i}\sigma_{\ell''_j}) \left[(2\ell'_j + 1)(2\ell''_j + 1)\right]^{1/2}$$

$$\times \left[(2L'+1)(2L''+1)\right]^{1/2} (1 - \mu 1 \mu | \ell 0) (\ell'_j 0 \ell''_j 0 | \ell 0)$$

$$\times W(L' \ell'_j L'' \ell''_j; L'_j \ell) W(1L'1L''; L\ell)$$

$$\times \langle \alpha'_j L'_j S'_j \ell'_j L' S || D || \alpha_i L S \rangle^* \langle \alpha'_j L'_j S'_j \ell''_j L'' S || D || \alpha_i L S \rangle. \tag{D.81}$$

This result for the differential photoionization cross section was used in Sect. 8.1.1 to obtain expressions for the integrated photoionization cross section and the asymmetry parameter.

Appendix E
Propagator Methods

In this appendix we describe R-matrix and log-derivative propagator methods that have been used to solve the coupled second-order differential equations which arise in R-matrix theory of atomic, molecular and optical collision processes in the external region. This generalizes and extends our discussion of propagator methods in potential scattering in Sect. 4.5.

R-matrix propagator methods were introduced by Light and Walker [594] and log-derivative methods were introduced by Gordon [402] and Johnson [506] in order to solve the coupled differential equations that arise in atom–molecule reactive and non-reactive collisions. Further developments including applications to atomic, molecular and optical collision processes were made by many workers including Stechel et al. [885], Schneider and Walker [827], Light et al. [595], Schneider and Taylor [828], Baluja et al. [47], Mrugala and Secrest [668], Alexander and Manolopoulos [8, 9], Burke and Burke [172] and Sunderland et al. [896]. In Appendices E.1, E.2 and E.3 we illustrate these methods by considering the solution of coupled homogeneous second-order differential equations which arise in the external region in electron–atom and electron–ion collisions, discussed in Chaps. 5 and 6. We also observe that these methods are applicable in R-matrix theory of positron collisions with atoms and ions considered in Chap. 7, in R-matrix theory of atomic photoionization processes considered in Chap. 8, in R-matrix–Floquet theory of multiphoton processes considered in Chap. 9 and in R-matrix theory of molecular collision processes considered in Chap. 11. In Appendix E.4, we generalize the R-matrix propagator method to solve the coupled inhomogeneous differential equations which arise in time-dependent R-matrix theory of atomic multiphoton processes considered in Chap. 10. In Appendix E.5 we derive an R-matrix propagator method for coupled inhomogeneous differential equations containing a first derivative term, which arise in atomic multiphoton processes when the interaction of the scattered or ejected electron with the laser field is treated in the velocity gauge. Finally, in Appendix E.6 we extend R-matrix propagator methods to treat channels which are strongly coupled in the internal R-matrix region but which separate in the external and asymptotic regions into two or more sets of channels which are uncoupled, although channels within each set remain strongly coupled. This occurs, for example, in positron collisions with atoms and ions leading to positronium

P.G. Burke, *R-Matrix Theory of Atomic Collisions*, Springer Series on Atomic, Optical, and Plasma Physics 61, DOI 10.1007/978-3-642-15931-2_17,

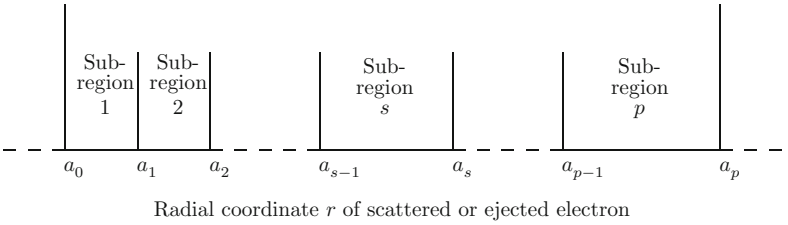

Fig. E.1 Partitioning of configuration space into p sub-regions in R-matrix and log-derivative propagator methods

formation, considered in Chap. 7, and in electron collisions with molecules leading to dissociative attachment, considered in Chap. 11.

The R-matrix and log-derivative propagator methods discussed in Appendices E.1, E.2, E.3, E.4 and E.5 commence by dividing the external region of interest $a_0 \leq r \leq a_p$ into p sub-regions, which may be of unequal length, as illustrated in Fig. E.1. Equations are then derived in each sub-region which enable the R-matrix, or log-derivative matrix, and the wave function, to be propagated from $r = a_0$ across each of the p sub-regions to $r = a_p$. Equations are also derived to enable inward propagation of the R-matrix, or log-derivative matrix, and the wave function from $r = a_p$ to a_0. The R-matrix or log-derivative matrix at $r = a_p$ can then be fitted to an asymptotic expansion enabling the K-matrix, S-matrix, cross sections and other observables to be determined, while the wave function can be used in the calculation of various matrix elements required in the analysis of collision processes.

We conclude this introduction by noting that the propagator methods discussed in this appendix have been incorporated in computer programs that have been widely used to obtain results reported in the main body of this monograph. In particular, the Light–Walker and BBM propagator methods, discussed in Sects. E.1 and E.3, have been incorporated in the FARM and PFARM programs written by Burke and Noble [191] and by Sunderland et al. [896] respectively, which are discussed in Sect. 5.1.1.

E.1 Light–Walker Propagator Method

We consider first the solution of the homogeneous coupled second-order differential equations (5.29) that arise using the R-matrix propagator method introduced by Light and Walker [594]. As discussed in the introduction to this appendix, this method and the methods discussed in Appendices E.2 and E.3 are applicable to a number of collision processes considered in this monograph.

We commence by rewriting (5.29) in matrix form as follows:

$$\left(\mathbf{I}\frac{\mathrm{d}^2}{\mathrm{d}r^2} + \mathbf{V}(r) + \mathbf{k}^2\right)\mathbf{F}(r) = 0, \tag{E.1}$$

where $\mathbf{I}$ in this and later equations in this appendix is the unit matrix, $\mathbf{V}(r)$ is the potential matrix, which includes the angular momentum, electron–target nucleus and electron–electron potential terms in (5.29) and is real and symmetric and hence hermitian, and $\mathbf{k}^2$ is a real diagonal matrix of wave numbers squared. We rewrite (E.1) as

$$\left(-\frac{1}{2}\mathbf{I}\frac{\mathrm{d}^2}{\mathrm{d}r^2} + \boldsymbol{\mathcal{V}}(r) - E\mathbf{I}\right)\mathbf{F}(r) = 0, \tag{E.2}$$

where the effective potential matrix $\boldsymbol{\mathcal{V}}(r)$ is defined by

$$\boldsymbol{\mathcal{V}}(r) = -\frac{1}{2}\left[\mathbf{V}(r) + \mathbf{k}^2\right] + E\mathbf{I}. \tag{E.3}$$

Also in (E.2) and (E.3) E is the total energy which we have explicitly separated out in (E.2) and which can be measured from any fixed position, for example, from the lowest target threshold so that $E = k_1^2/2$. In this way the potential matrix $\boldsymbol{\mathcal{V}}(r)$ is independent of the value of E.

The basic assumption made in the Light–Walker propagator method is that the potential matrix $\mathbf{V}(r)$, and hence $\boldsymbol{\mathcal{V}}(r)$, is a slowly varying function of r such that it can be accurately represented by a constant matrix in each sub-region in Fig. E.1 without the number of sub-regions p becoming excessively large. Hence in each sub-region we assume that $\boldsymbol{\mathcal{V}}(r)$, defined by (E.3), can be accurately represented by a constant matrix as follows:

$$\boldsymbol{\mathcal{V}}(r) = \boldsymbol{\mathcal{V}}_s, \quad a_{s-1} \le r \le a_s, \quad s = 1, \ldots, p, \tag{E.4}$$

where $\boldsymbol{\mathcal{V}}_s$ is real and symmetric.

In order to solve (E.2) in the sth sub-region we diagonalize $\boldsymbol{\mathcal{V}}_s$ by an orthogonal transformation matrix $\mathbf{O}_s$, which is independent of the total energy E, so that

$$\mathbf{O}_s^{\mathrm{T}}\boldsymbol{\mathcal{V}}_s\mathbf{O}_s = \boldsymbol{\nu}_s^2, \quad s = 1, \ldots, p, \tag{E.5}$$

and we introduce a transformed radial wave function $\boldsymbol{\mathcal{F}}_s(r)$ by

$$\boldsymbol{\mathcal{F}}_s(r) = \mathbf{O}_s^{\mathrm{T}}\mathbf{F}(r), \quad s = 1, \ldots, p. \tag{E.6}$$

Equation (E.2) can then be rewritten in the sth sub-region as

$$-\frac{1}{2}\left(\mathbf{I}\frac{\mathrm{d}^2}{\mathrm{d}r^2} + \boldsymbol{\lambda}_s^2\right)\boldsymbol{\mathcal{F}}_s(r) = 0, \quad a_{s-1} \le r \le a_s, \quad s = 1, \ldots, p, \tag{E.7}$$

where we have introduced the real diagonal matrix

$$\boldsymbol{\lambda}_s^2 = -2\boldsymbol{\nu}_s^2 + 2E\mathbf{I}, \quad s = 1, \ldots, p, \tag{E.8}$$

which depends on the total energy E. We then define the diagonal matrix operator

$$\mathbf{L}_s = -\frac{1}{2}\left(\mathbf{I}\frac{\mathrm{d}^2}{\mathrm{d}r^2} + \boldsymbol{\lambda}_s^2\right) \tag{E.9}$$

and we introduce the diagonal Bloch operator

$$\boldsymbol{\mathcal{L}}_s = \frac{1}{2}\mathbf{I}\left[\delta(r-a_s)\frac{\mathrm{d}}{\mathrm{d}r} - \delta(r-a_{s-1})\frac{\mathrm{d}}{\mathrm{d}r}\right], \tag{E.10}$$

where we take the arbitrary constant b_0, included in the usual definition of the Bloch operator defined by (4.31), to be zero. It follows that the diagonal matrix operator $\mathbf{L}_s + \boldsymbol{\mathcal{L}}_s$ is hermitian over the sth sub-region in the space of functions satisfying arbitrary boundary conditions at $r = a_{s-1}$ and a_s. We can then rewrite (E.7) as

$$(\mathbf{L}_s + \boldsymbol{\mathcal{L}}_s)\boldsymbol{\mathcal{F}}_s(r) = \boldsymbol{\mathcal{L}}_s\boldsymbol{\mathcal{F}}_s(r), \tag{E.11}$$

which has the formal solution in the sth sub-region

$$\boldsymbol{\mathcal{F}}_s(r) = (\mathbf{L}_s + \boldsymbol{\mathcal{L}}_s)^{-1}\boldsymbol{\mathcal{L}}_s\boldsymbol{\mathcal{F}}_s(r). \tag{E.12}$$

We now define the diagonal Green's function $\boldsymbol{\mathcal{G}}_s(r, r')$ as the solution of the equation

$$(\mathbf{L}_s + \boldsymbol{\mathcal{L}}_s)\boldsymbol{\mathcal{G}}_s(r, r') = \frac{1}{2}\mathbf{I}\delta(r-r'). \tag{E.13}$$

By integrating (E.13) across the singularities at $r = a_{s-1}$ and a_s we find that $\boldsymbol{\mathcal{G}}_s(r, r')$ satisfies the boundary conditions

$$\left.\frac{\mathrm{d}\boldsymbol{\mathcal{G}}_s(r, r')}{\mathrm{d}r}\right|_{r=a_{s-1}} = \left.\frac{\mathrm{d}\boldsymbol{\mathcal{G}}_s(r, r')}{\mathrm{d}r}\right|_{r=a_s} = 0, \quad a_{s-1} < r' < a_s. \tag{E.14}$$

Also, by integrating (E.13) across the singularity at $r = r'$ we obtain

$$\lim_{\epsilon\to 0+}\left[\left.\frac{\mathrm{d}\boldsymbol{\mathcal{G}}_s(r, r')}{\mathrm{d}r}\right|_{r=r'+\epsilon} - \left.\frac{\mathrm{d}\boldsymbol{\mathcal{G}}_s(r, r')}{\mathrm{d}r}\right|_{r=r'-\epsilon}\right] = -\mathbf{I}. \tag{E.15}$$

It follows from (E.13), (E.14) and (E.15) that when the ith element of the diagonal matrix $\boldsymbol{\lambda}_s^2$ defined by (E.8) satisfies $\lambda_{is}^2 \geq 0$, then the corresponding diagonal elements of Green's function are given by

$$\mathcal{G}_{is}(r, r') = -\frac{\cos\lambda_{is}(r'-a_s)\cos\lambda_{is}(r-a_{s-1})}{\lambda_{is}\sin\lambda_{is}(a_s-a_{s-1})}, \quad a_{s-1} \leq r \leq r', \tag{E.16}$$

and

$$\mathcal{G}_{is}(r,r') = -\frac{\cos\lambda_{is}(r-a_s)\cos\lambda_{is}(r'-a_{s-1})}{\lambda_{is}\sin\lambda_{is}(a_s-a_{s-1})}, \quad r' \le r \le a_s. \tag{E.17}$$

Also when $\lambda_{is}^2 < 0$, then the corresponding diagonal elements of Green's function are given by

$$\mathcal{G}_{is}(r,r') = -\frac{\cosh\mu_{is}(r'-a_s)\cosh\mu_{is}(r-a_{s-1})}{\mu_{is}\sinh\mu_{is}(a_s-a_{s-1})}, \quad a_{s-1} \le r \le r' \tag{E.18}$$

and

$$\mathcal{G}_{is}(r,r') = -\frac{\cosh\mu_{is}(r-a_s)\cosh\mu_{is}(r'-a_{s-1})}{\mu_{is}\sinh\mu_{is}(a_s-a_{s-1})}, \quad r' \le r \le a_s, \tag{E.19}$$

where in (E.18) and (E.19) we have written $\mu_{is}^2 = -\lambda_{is}^2$.

We can now rewrite (E.12) explicitly in terms of the Green's function $\boldsymbol{\mathcal{G}}_s(r,r')$ as follows:

$$\boldsymbol{\mathcal{F}}_s(r) = 2\int_{a_{s-1}}^{a_s} \boldsymbol{\mathcal{G}}_s(r,r')\boldsymbol{\mathcal{L}}_s\boldsymbol{\mathcal{F}}_s(r')\mathrm{d}r', \quad a_{s-1} \le r \le a_s. \tag{E.20}$$

Remembering that the functions $\boldsymbol{\mathcal{F}}_s(r)$ are defined in terms of the original functions $\mathbf{F}(r)$ by (E.6) then it follows from (E.20) that

$$\mathbf{F}(r) = 2\int_{a_{s-1}}^{a_s} \mathbf{G}_s(r,r')\boldsymbol{\mathcal{L}}_s\mathbf{F}(r')\mathrm{d}r', \quad a_{s-1} \le r \le a_s, \tag{E.21}$$

where the Green's function $\mathbf{G}_s(r,r')$ is defined by

$$\mathbf{G}_s(r,r') = \mathbf{O}_s\boldsymbol{\mathcal{G}}_s(r,r')\mathbf{O}_s^{\mathrm{T}}. \tag{E.22}$$

Evaluating (E.21) at $r = a_{s-1}$ and a_s and using (E.10) for the Bloch operator $\boldsymbol{\mathcal{L}}_s$ then yields the equations

$$\mathbf{F}(a_{s-1}) = \mathbf{G}_s(a_{s-1},a_s)\left.\frac{\mathrm{d}\mathbf{F}}{\mathrm{d}r}\right|_{r=a_s} - \mathbf{G}_s(a_{s-1},a_{s-1})\left.\frac{\mathrm{d}\mathbf{F}}{\mathrm{d}r}\right|_{r=a_{s-1}} \tag{E.23}$$

and

$$\mathbf{F}(a_s) = \mathbf{G}_s(a_s,a_s)\left.\frac{\mathrm{d}\mathbf{F}}{\mathrm{d}r}\right|_{r=a_s} - \mathbf{G}_s(a_s,a_{s-1})\left.\frac{\mathrm{d}\mathbf{F}}{\mathrm{d}r}\right|_{r=a_{s-1}}. \tag{E.24}$$

Following (5.32) it is convenient to define the R-matrices at $r = a_{s-1}$ and a_s by the equations

$$\mathbf{F}(a_{s-1}) = \mathbf{R}_{s-1} a_{s-1} \left.\frac{\mathrm{d}\mathbf{F}}{\mathrm{d}r}\right|_{r=a_{s-1}} \tag{E.25}$$

and

$$\mathbf{F}(a_s) = \mathbf{R}_s a_s \left.\frac{\mathrm{d}\mathbf{F}}{\mathrm{d}r}\right|_{r=a_s}, \tag{E.26}$$

where the arbitrary constant b_0 in the usual definition of the R-matrix is set zero. We then find that (E.23) and (E.24) yield the propagation equations

$$\begin{aligned} a_s \mathbf{R}_s = {} & \mathbf{G}_s(a_s, a_s) - \mathbf{G}_s(a_s, a_{s-1}) \left[\mathbf{G}_s(a_{s-1}, a_{s-1}) + a_{s-1}\mathbf{R}_{s-1}\right]^{-1} \\ & \times \mathbf{G}_s(a_{s-1}, a_s) \end{aligned} \tag{E.27}$$

and

$$\begin{aligned} a_{s-1} \mathbf{R}_{s-1} = {} & -\mathbf{G}_s(a_{s-1}, a_{s-1}) + \mathbf{G}_s(a_{s-1}, a_s) \left[\mathbf{G}_s(a_s, a_s) - a_s\mathbf{R}_s\right]^{-1} \\ & \times \mathbf{G}_s(a_s, a_{s-1}). \end{aligned} \tag{E.28}$$

Equations (E.27), for $s = 1, \ldots, p$, enable the R-matrix $\mathbf{R}_0$ at $r = a_0$ to be propagated outwards across the p sub-regions to yield the R-matrix $\mathbf{R}_p$ at $r = a_p$. In a similar way (E.28), for $s = p, \ldots, 1$, enable the R-matrix $\mathbf{R}_p$ at $r = a_p$ to be propagated inwards across the p sub-regions to yield the R-matrix $\mathbf{R}_0$ at $r = a_0$.

Having determined the R-matrix on the boundaries $r = a_s$ of the p sub-regions we can propagate the reduced radial wave function $\mathbf{F}(a_s)$ across these sub-regions using (E.23), (E.24), (E.25) and (E.26). We obtain the following equations for outward and inward propagation of the wave function:

$$\mathbf{F}(a_s) = a_s \mathbf{R}_s \left[\mathbf{G}_s(a_s, a_s) - a_s\mathbf{R}_s\right]^{-1} \mathbf{G}_s(a_s, a_{s-1})\, a_{s-1}^{-1}\, \mathbf{R}_{s-1}^{-1}\, \mathbf{F}(a_{s-1}) \tag{E.29}$$

and

$$\begin{aligned} \mathbf{F}(a_{s-1}) = {} & a_{s-1} \mathbf{R}_{s-1} \left[\mathbf{G}_s(a_{s-1}, a_{s-1}) + a_{s-1}\mathbf{R}_{s-1}\right]^{-1} \mathbf{G}_s(a_{s-1}, a_s) \\ & \times a_s^{-1}\, \mathbf{R}_s^{-1}\, \mathbf{F}(a_s). \end{aligned} \tag{E.30}$$

The wave function is often required in the calculation of matrix elements such as occur in the study of photoionization processes discussed in Chap. 8.

The computational effort in this method involves diagonalizing the matrix $\boldsymbol{\mathcal{V}}_s$ in each sub-region according to (E.5), calculating Green's functions using (E.16), (E.17), (E.18), (E.19) and (E.22) and then propagating the R-matrix across the sub-regions using (E.27) or (E.28). We note that only a single diagonalization is required in each sub-region for all energies E in (E.2) considered.

E.2 Log-Derivative Propagator Method

In this section we consider the solution of the coupled second-order differential equations (E.1) using the log-derivative propagator method introduced by Gordon [402] and Johnson [506]. This method, combined with a linear reference equation using an Airy function basis, has been developed by many workers including Mrugala and Secrest [668] and Alexander and Manolopoulos [8, 9]. It has had wide use in the computational study of atom–atom and atom–molecule collisions and has recently been developed and applied as an efficient method for solving the coupled differential equations that arise in the R-matrix external region.

Following our discussion of the R-matrix propagator method in Appendix E.1, we consider the solution of the coupled second-order differential equations (E.1) which we rewrite in the form

$$\left(\mathbf{I}\frac{\mathrm{d}^2}{\mathrm{d}r^2} + \mathbf{W}(r)\right)\mathbf{F}(r) = 0, \tag{E.31}$$

where $\mathbf{W}(r)$ includes the potential matrix $\mathbf{V}(r)$ and $\mathbf{k}^2$ and is real and symmetric. We consider the propagation of the log-derivative matrix defined by

$$\mathbf{Y}(r) = \frac{\mathrm{d}\mathbf{F}}{\mathrm{d}r}\mathbf{F}(r)^{-1}, \tag{E.32}$$

where we observe that $\mathbf{Y}(r)$ is related to the R-matrix by

$$\mathbf{Y}(r) = r^{-1}\mathbf{R}(r)^{-1} \tag{E.33}$$

and the R-matrix is defined by (E.26) with a_s replaced by r. We note that the log-derivative matrix is r^{-1} times the inverse of the R-matrix.

Following the procedure adopted in Sect. E.1 we sub-divide the external region $a_0 \le r \le a_p$ into p sub-regions, as illustrated in Fig. E.1, and we consider the propagation of the log-derivative matrix across these sub-regions. In order to solve (E.31) in the sth sub-region we introduce an orthogonal transformation $\mathbf{O}_s$ which diagonalizes $\mathbf{W}(r)$ at the mid-point $r = a_{s-\frac{1}{2}}$ of this sub-region where

$$a_{s-\frac{1}{2}} = \frac{1}{2}(a_{s-1} + a_s), \quad s = 1, \ldots, p. \tag{E.34}$$

Hence $\mathbf{O}_s$ is defined by the equation

$$\mathbf{O}_s\mathbf{W}_s\mathbf{O}_s^{\mathrm{T}} = \widetilde{\mathbf{k}}^2, \quad s = 1, \ldots, p, \tag{E.35}$$

where $\widetilde{\mathbf{k}}^2$ is diagonal,

$$\mathbf{W}_s = \mathbf{W}(a_{s-\frac{1}{2}}), \quad s = 1, \ldots, p, \tag{E.36}$$

and $\mathbf{O}_s$ is independent of r in each sub-region. It follows that the solution $\mathbf{F}(r)$ of (E.31), its derivative $\mathbf{F}'(r)$ and the corresponding log-derivative matrix are transformed in each sub-region as follows:

$$\widetilde{\mathbf{F}}_s(r) = \mathbf{O}_s\mathbf{F}(r), \quad \widetilde{\mathbf{F}}'_s(r) = \mathbf{O}_s\mathbf{F}'(r), \quad \widetilde{\mathbf{Y}}_s(r) = \mathbf{O}_s\mathbf{Y}(r)\mathbf{O}_s^{\mathrm{T}}, \quad s = 1, \ldots, p. \tag{E.37}$$

We now rewrite (E.31) in each sub-region by expanding $\mathbf{W}(r)$ about the mid-point $r = a_{s-\frac{1}{2}}$. Equation (E.31) then becomes

$$\left(\mathbf{I}\frac{\mathrm{d}^2}{\mathrm{d}r^2} + \mathbf{W}_s + (r - a_{s-\frac{1}{2}})\mathbf{W}'_s + \frac{1}{2}(r - a_{s-\frac{1}{2}})^2\mathbf{W}''_s + \cdots\right)\mathbf{F}(r) = 0, \tag{E.38}$$

where $\mathbf{W}'_s$ equals $\mathrm{d}\mathbf{W}/\mathrm{d}r$ and $\mathbf{W}''_s$ equals $\mathrm{d}^2\mathbf{W}/\mathrm{d}r^2$ both evaluated at $r = a_{s-\frac{1}{2}}$. After multiplying (E.38) on the left by $\mathbf{O}_s$ we then obtain

$$\left(\mathbf{I}\frac{\mathrm{d}^2}{\mathrm{d}r^2} + \widetilde{\mathbf{k}}_s^2 + (r - a_{s-\frac{1}{2}})\widetilde{\mathbf{W}}'_s + \frac{1}{2}(r - a_{s-\frac{1}{2}})^2\widetilde{\mathbf{W}}''_s + \cdots\right)\widetilde{\mathbf{F}}_s(r) = 0, \tag{E.39}$$

where

$$\widetilde{\mathbf{W}}'_s = \mathbf{O}_s\mathbf{W}'_s\mathbf{O}_s^{\mathrm{T}}, \quad \widetilde{\mathbf{W}}''_s = \mathbf{O}_s\mathbf{W}''_s\mathbf{O}_s^{\mathrm{T}}, \ldots. \tag{E.40}$$

It follows that the potential functions $\widetilde{\mathbf{W}}'_s$, $\widetilde{\mathbf{W}}''_s, \ldots$ are independent of r in each sub-region but are different in each sub-region.

In order to propagate the solution of (E.31), or equivalently (E.39), across the sth sub-region we consider the "imbedding-type" matrix propagator defined by

$$\begin{bmatrix} \widetilde{\mathbf{F}}'_s(a_{s-1}) \\ \widetilde{\mathbf{F}}'_s(a_s) \end{bmatrix} = \begin{bmatrix} \mathbf{G}_{11}^s & \mathbf{G}_{12}^s \\ \mathbf{G}_{21}^s & \mathbf{G}_{22}^s \end{bmatrix} \begin{bmatrix} -\widetilde{\mathbf{F}}_s(a_{s-1}) \\ \widetilde{\mathbf{F}}_s(a_s) \end{bmatrix}. \tag{E.41}$$

Introducing the transformed log-derivative matrix on the boundaries of the sth sub-region by

$$\widetilde{\mathbf{Y}}_s(a_{s-1}) = \widetilde{\mathbf{F}}'_s(a_{s-1})\widetilde{\mathbf{F}}_s^{-1}(a_{s-1}) \tag{E.42}$$

and

$$\widetilde{\mathbf{Y}}_s(a_s) = \widetilde{\mathbf{F}}'_s(a_s)\widetilde{\mathbf{F}}_s^{-1}(a_s) \tag{E.43}$$

we find that (E.41) yields the following log-derivative propagation equation:

$$\widetilde{\mathbf{Y}}_s(a_s) = \mathbf{G}_{22}^s - \mathbf{G}_{21}^s\left[\mathbf{G}_{11}^s + \widetilde{\mathbf{Y}}_s(a_{s-1})\right]^{-1}\mathbf{G}_{12}^s. \tag{E.44}$$

We see that this propagator has the same general form as the propagator (E.27) for the R-matrix.

We also consider the "Cauchy" matrix propagator defined by

$$\begin{bmatrix} \widetilde{\mathbf{F}}_s(a_s) \\ \widetilde{\mathbf{F}}'_s(a_s) \end{bmatrix} = \begin{bmatrix} \mathbf{C}^s_{11} & \mathbf{C}^s_{12} \\ \mathbf{C}^s_{21} & \mathbf{C}^s_{22} \end{bmatrix} \begin{bmatrix} \widetilde{\mathbf{F}}_s(a_{s-1}) \\ \widetilde{\mathbf{F}}'_s(a_{s-1}) \end{bmatrix}, \tag{E.45}$$

which we can show yields the same log-derivative propagator relation as (E.44) if the matrices $\mathbf{G}^s_{ij}$ in (E.41) and $\mathbf{C}^s_{ij}$ in (E.45) are related by the equations

$$\begin{aligned} \mathbf{G}^s_{11} &= \left(\mathbf{C}^s_{12}\right)^{-1} \mathbf{C}^s_{11}, \\ \mathbf{G}^s_{12} &= \left(\mathbf{C}^s_{12}\right)^{-1}, \\ \mathbf{G}^s_{21} &= \mathbf{C}^s_{22} \left(\mathbf{C}^s_{12}\right)^{-1} \mathbf{C}^s_{11} - \mathbf{C}^s_{21}, \\ \mathbf{G}^s_{22} &= \mathbf{C}^s_{22} \left(\mathbf{C}^s_{12}\right)^{-1}. \end{aligned} \tag{E.46}$$

If the off-diagonal elements of the matrices $\widetilde{\mathbf{W}}'_s$, $\widetilde{\mathbf{W}}''_s$ and higher order derivative terms in (E.39) are neglected, then the Cauchy matrices $\mathbf{C}^s_{11}$, $\mathbf{C}^s_{12}$, $\mathbf{C}^s_{21}$ and $\mathbf{C}^s_{22}$ in (E.45) and (E.46) are diagonal. We can then express the diagonal elements of the Cauchy matrices in terms of any two linearly independent solutions of the corresponding uncoupled equations, called the "reference equations", which are defined by

$$\begin{aligned} &\left[\frac{\mathrm{d}^2}{\mathrm{d}r^2} + \left(\widetilde{\mathbf{k}}^2_s\right)_{ii} + (r - a_{s-\frac{1}{2}}) \left(\widetilde{\mathbf{W}}'_s\right)_{ii} + \frac{1}{2}(r - a_{s-\frac{1}{2}})^2 \left(\widetilde{\mathbf{W}}''_s\right)_{ii} + \cdots \right] u^s_i(r) \\ &= 0, \quad i = 1, \ldots, n, \end{aligned} \tag{E.47}$$

where n is the number of coupled channels. If we introduce the following two linearly independent solutions of (E.47)

$$f^s_i(r), \quad g^s_i(r), \quad i = 1, \ldots, n, \tag{E.48}$$

and we denote the corresponding r-independent Wronskian in the sth sub-region by

$$w^s_i = f^s_i(r) g^{s\prime}_i(r) - f^{s\prime}_i(r) g^s_i(r), \quad i = 1, \ldots, n, \tag{E.49}$$

then the non-zero diagonal elements of the Cauchy matrices are given by the equations

$$\left(\mathbf{C}^s_{11}\right)_{ii} = \left[f^s_i(a_s) g^{s\prime}_i(a_{s-1}) - f^{s\prime}_i(a_{s-1}) g^s_i(a_s)\right] \left(w^s_i\right)^{-1}, \quad i = 1, \ldots, n, \tag{E.50}$$

$$\left(\mathbf{C}^s_{12}\right)_{ii} = \left[f^s_i(a_{s-1}) g^s_i(a_s) - f^s_i(a_s) g^s_i(a_{s-1})\right] \left(w^s_i\right)^{-1}, \quad i = 1, \ldots, n, \tag{E.51}$$

$$\left(\mathbf{C}^s_{21}\right)_{ii} = \left[f^{s\prime}_i(a_s) g^{s\prime}_i(a_{s-1}) - f^{s\prime}_i(a_{s-1}) g^{s\prime}_i(a_s)\right] \left(w^s_i\right)^{-1}, \quad i = 1, \ldots, n, \tag{E.52}$$

$$\left(\mathbf{C}^s_{22}\right)_{ii} = \left[f^s_i(a_{s-1})g^{s\prime}_i(a_s) - f^{s\prime}_i(a_s)g^s_i(a_{s-1})\right]\left(w^s_i\right)^{-1}, \quad i = 1, \ldots, n. \tag{E.53}$$

We can also show that the non-zero diagonal elements of the Cauchy matrices are related by the equation

$$\left(\mathbf{C}^s_{11}\right)_{ii}\left(\mathbf{C}^s_{22}\right)_{ii} - \left(\mathbf{C}^s_{12}\right)_{ii}\left(\mathbf{C}^s_{21}\right)_{ii} = 1, \quad i = 1, \ldots, n. \tag{E.54}$$

It then follows that the diagonal elements of the imbedding matrices defined by (E.41), corresponding to the reference equations (E.47), are defined in terms of the diagonal elements of the Cauchy matrices by

$$\left(\mathbf{G}^s_{11}\right)_{ii} = \left(\mathbf{C}^s_{12}\right)^{-1}_{ii}\left(\mathbf{C}^s_{11}\right)_{ii}, \quad i = 1, \ldots, n, \tag{E.55}$$

$$\left(\mathbf{G}^s_{12}\right)_{ii} = \left(\mathbf{C}^s_{12}\right)^{-1}_{ii}, \quad i = 1, \ldots, n, \tag{E.56}$$

$$\left(\mathbf{G}^s_{21}\right)_{ii} = \left(\mathbf{C}^s_{12}\right)^{-1}_{ii}, \quad i = 1, \ldots, n, \tag{E.57}$$

$$\left(\mathbf{G}^s_{22}\right)_{ii} = \left(\mathbf{C}^s_{22}\right)_{ii}\left(\mathbf{C}^s_{12}\right)^{-1}_{ii}, \quad i = 1, \ldots, n. \tag{E.58}$$

These equations enable the transformed log-derivative matrix $\widetilde{\mathbf{Y}}_s(r)$ to be propagated across the sth sub-region from $r = a_{s-1}$ to a_s using (E.44), where the Cauchy matrices are defined in terms of the two linearly independent solutions of the reference equations (E.47).

We now consider the linearly independent solutions of the reference equations (E.47). In practice, second and higher order derivative terms in these equations are small and can be neglected and the resultant equations reduce to the following linear reference equation with the general form

$$\left(\frac{\mathrm{d}^2}{\mathrm{d}x^2} - x\right) y(x) = 0. \tag{E.59}$$

The reference solutions of this equation are "Airy functions" $Ai(x)$ and $Bi(x)$ with the Wronskian

$$w(x) = Ai(x)Bi'(x) - Ai'(x)Bi(x) = \pi^{-1}. \tag{E.60}$$

These functions, which are related to Bessel functions of order $\pm 1/3$, have been discussed by Abramowitz and Stegun [1] and their present role as solutions of the linear reference equation has been considered by many authors including Gordon [402] and Alexander and Manolopoulos [9]. In the latter work explicit expressions are obtained for the imbedding propagator in terms of Airy functions, where it is found convenient to represent the Airy functions for both positive and negative arguments in terms of their moduli and phases. In this way both classically allowed and classically forbidden regions can be accurately treated.

Having propagated the log-derivative matrix across the sth sub-region, as described above, it is then necessary to transform this matrix at $r = a_s$ in order to initiate the propagation outwards across the $(s+1)$th sub-region. We remember from (E.37) that the transformation to the local basis in the sth sub-region is defined by the orthogonal matrix $\mathbf{O}_s$ and the transformation to the local basis in the $(s+1)$th sub-region is defined by the orthogonal matrix $\mathbf{O}_{s+1}$. Hence it is necessary to transform the log-derivative matrix on the boundary $r = a_s$ between the two regions by the orthogonal transformation

$$\widetilde{\mathbf{Y}}_{s+1}(a_s) = \mathbf{P}_s \widetilde{\mathbf{Y}}_s(a_s) \mathbf{P}_s^{\mathrm{T}}, \tag{E.61}$$

where

$$\mathbf{P}_s = \mathbf{O}_{s+1} \mathbf{O}_s^{\mathrm{T}}. \tag{E.62}$$

In this way the log-derivative matrix $\mathbf{Y}(r)$ can be propagated outwards across the p sub-regions in Fig. E.1 from $r = a_0$ to a_p.

We can also propagate the log-derivative matrix $\mathbf{Y}(r)$ backwards across the p sub-regions in Fig. E.1 from $r = a_p$ to a_0. By inverting (E.44) we find that

$$\widetilde{\mathbf{Y}}_s(a_{s-1}) = -\mathbf{G}_{11}^s + \mathbf{G}_{12}^s \left[\mathbf{G}_{22}^s - \widetilde{\mathbf{Y}}_s(a_s)\right]^{-1} \mathbf{G}_{21}^s, \tag{E.63}$$

which we see has the same general form as propagator (E.28) for the R-matrix. As before, the diagonal elements of the imbedding matrices, defined by (E.41), can be expressed in terms of the diagonal elements of the Cauchy matrices by (E.55), (E.56), (E.57) and (E.58) enabling backward propagation to be carried out.

E.3 BBM Propagator Method

The BBM propagator method, introduced by Baluja et al. [47], like the Light–Walker propagator method discussed in Sect. E.1, commences from (E.1) which is again solved by sub-dividing the external region $a_0 \le r \le a_p$ into p sub-regions, as illustrated in Fig. E.1. We now rewrite (E.1) in the sth sub-region as

$$(\mathbf{H} + \mathcal{L}_s - E\mathbf{I})\,\mathbf{F}(r) = \mathcal{L}_s \mathbf{F}(r), \tag{E.64}$$

where

$$\mathbf{H} = -\frac{1}{2}\left(\mathbf{I}\frac{\mathrm{d}^2}{\mathrm{d}r^2} + \mathbf{V}(r) + \mathbf{k}^2\right) + E\mathbf{I}, \tag{E.65}$$

and, as in (E.3), the total energy E can conveniently be measured from the lowest target threshold. Also, the Bloch operator $\mathcal{L}_s$, defined by (E.10), is such that the

operator $\mathbf{H}+\boldsymbol{\mathcal{L}}_s$ is hermitian over the sth sub-region in the space of functions satisfying arbitrary boundary conditions at $r=a_{s-1}$ and $r=a_s$. Equation (E.64) then has the formal solution in the sth sub-region

$$\mathbf{F}(r)=(\mathbf{H}+\boldsymbol{\mathcal{L}}_s-E\mathbf{I})^{-1}\,\boldsymbol{\mathcal{L}}_s\mathbf{F}(r). \tag{E.66}$$

A spectral representation of the Green's function $(\mathbf{H}+\boldsymbol{\mathcal{L}}_s-E\mathbf{I})^{-1}$ in (E.66) is obtained by introducing an orthonormal basis $v_j^s(r),\ j=1,\ldots,m$, in each channel $i=1,\ldots,n$ in the sth sub-region. This basis is often chosen to be orthonormal shifted Legendre polynomials defined by

$$v_j^s(r)=\left(\frac{2j-1}{a_s-a_{s-1}}\right)^{1/2}P_{j-1}(x),\quad j=1,\ldots,m, \tag{E.67}$$

where

$$x=\frac{2}{a_s-a_{s-1}}\left(r-\frac{a_{s-1}+a_s}{2}\right), \tag{E.68}$$

and $P_{j-1}(x)$ in (E.67) are Legendre polynomials of degree $j-1$ which are defined in Appendix B.1. However, members of other complete bases, such as B-splines discussed in Sect. 4.4.7, have also been used in the sub-regions.

Having chosen the basis $v_j^s(r)$, we define the functions $u_{ik}^s(r)$ as follows:

$$u_{ik}^s(r)=\sum_{j=1}^{m}v_j^s(r)a_{ijk}^s,\quad a_{s-1}\le r\le a_s,\quad i=1,\ldots,n,\quad k=1,\ldots,nm, \tag{E.69}$$

where n is the number of coupled channels and the coefficients a_{ijk}^s are determined by diagonalizing the operator $\mathbf{H}+\boldsymbol{\mathcal{L}}_s$ in the sth sub-region so that

$$\int_{a_{s-1}}^{a_s}\mathbf{u}_k^{s\mathrm{T}}(r)\,(\mathbf{H}+\boldsymbol{\mathcal{L}}_s)\,\mathbf{u}_{k'}^s(r)\mathrm{d}r=E_k^s\delta_{kk'},\quad k,\ k'=1,\ldots,nm. \tag{E.70}$$

In this equation, $\mathbf{u}_k^s(r)$ is a column vector whose elements are $u_{ik}^s(r),\ i=1,\ldots,n$. Equation (E.66) can then be written in the sth sub-region as

$$\mathbf{F}(r)=\int_{a_{s-1}}^{a_s}\sum_{k=1}^{nm}\frac{\mathbf{u}_k^s(r)\mathbf{u}_k^{s\mathrm{T}}(r')}{E_k^s-E}\boldsymbol{\mathcal{L}}_s\mathbf{F}(r')\mathrm{d}r',\quad a_{s-1}\le r\le a_s, \tag{E.71}$$

which can be rewritten as

$$\mathbf{F}(r)=2\int_{a_{s-1}}^{a_s}\mathbf{G}_s(r,r')\boldsymbol{\mathcal{L}}_s\mathbf{F}(r')\mathrm{d}r',\quad a_{s-1}\le r\le a_s, \tag{E.72}$$

where the Green's function $\mathbf{G}_s(r, r')$ in the sth sub-region is defined by

$$\mathbf{G}_s(r, r') = \frac{1}{2} \sum_{k=1}^{nm} \frac{\mathbf{u}_k^s(r) \mathbf{u}_k^{s\mathrm{T}}(r')}{E_k^s - E}. \tag{E.73}$$

Evaluating (E.72) at $r = a_{s-1}$ and a_s and using (E.10) for the Bloch operator $\mathcal{L}_s$ then yields (E.23) and (E.24), obtained using the Light–Walker propagator method. After defining the R-matrices by (E.25) and (E.26), the outward and inward propagation equations for the R-matrix are again given by (E.27) and (E.28), respectively, and the outward and inward propagation equations for the wave function are given by (E.29) and (E.30), respectively. We observe that, as in the Light–Walker and log-derivative propagator methods, a single diagonalization in each sub-region enables the Green's function to be calculated from (E.73) for all energies E considered.

In comparing the Light–Walker, log-derivative and BBM propagator methods we observe that, in general, the Light–Walker and log-derivative methods require a larger number of sub-regions than the BBM method to obtain the same accuracy. However, in each sub-region the Light–Walker and log-derivative methods diagonalize a matrix of order n whereas the BBM method diagonalizes one of order nm, where n is the number of coupled channels and m is the number of basis functions retained in each channel in the BBM method. Hence the BBM method is particularly useful in resonance regions, for example, in electron–ion collisions at low energies where the cross sections have to be calculated at a very large number of energy values to accurately represent the resonance structure. In this case the matrix diagonalization time is often small compared with the R-matrix propagation time. The BBM method is also appropriate if the potential $\mathbf{V}(r)$ in (E.1) is rapidly varying with r so that a prohibitively large number of sub-regions have to be used in the Light–Walker and log-derivative methods to obtain accurate results. On the other hand, the Light–Walker and log-derivative methods are usually preferred when results at only a few energies are required. This occurs, for example, in electron–atom and electron–ion collisions at energies above the resonance energy region where the cross sections are varying smoothly with energy. However, we observe that in the calculation of time-dependent multiphoton processes, discussed in Chap. 10, where the outward and inward propagations in the external region are only carried out at a single energy for each time step, the BBM method has been found to be efficient. In this case, the Green's function in (E.66) is determined in each sub-region by solving a set of linear simultaneous equations, rather than diagonalizing a matrix, as discussed in Sect. 4.4.4. This approach is discussed further in Appendix E.4.

Finally, we remark that the Light–Walker, log-derivative and BBM propagator methods can on occasions be combined with advantage. For example, the BBM method can be used at distances close to $r = a_0$ in Fig. E.1 where the potential $\mathbf{V}(r)$ in (E.65) is varying most rapidly, and the Light–Walker or log-derivative method used further out where the potential becomes a slowly varying function of distance.

E.4 Propagation of Driven Equations

In this section we derive an R-matrix propagator method for solving coupled inhomogeneous (driven) second-order differential equations. This method was introduced by Schneider and Taylor [828] for the direct calculation of transition matrix elements which arise in photoionization or photodissociation. We consider here the solution of coupled inhomogeneous differential equations which arise in time-dependent R-matrix theory of atomic multiphoton processes in the external region, discussed in Sects. 10.1.3 and 10.1.4. This method generalizes R-matrix propagator methods for solving coupled homogeneous second-order differential equations described in Appendices E.1 and E.3.

We consider the solution of the coupled inhomogeneous second-order differential equations (10.63) which we rewrite here as

$$\left(\mathbf{I}\frac{\mathrm{d}^2}{\mathrm{d}r^2} + \mathbf{V}(r) + \mathbf{k}^2\right)\mathbf{F}(r) = \boldsymbol{\phi}(r), \tag{E.74}$$

where we note that this equation can be obtained from (E.1) by including the inhomogeneous term $\boldsymbol{\phi}(r)$ on the right-hand side. Following our discussion in Appendices E.1 and E.3 we rewrite (E.74) in the form

$$(\mathbf{H} - E\mathbf{I})\,\mathbf{F}(r) = \boldsymbol{\theta}(r), \tag{E.75}$$

where

$$\mathbf{H} = -\frac{1}{2}\left(\mathbf{I}\frac{\mathrm{d}^2}{\mathrm{d}r^2} + \mathbf{V}(r) + \mathbf{k}^2\right) + E\mathbf{I} \tag{E.76}$$

and

$$\boldsymbol{\theta}(r) = -\frac{1}{2}\boldsymbol{\phi}(r). \tag{E.77}$$

As in (E.2) and (E.64) the total energy E in (E.75) and (E.76) can conveniently be measured from the lowest target threshold.

We now consider the propagation of the R-matrix corresponding to (E.75) across the p sub-regions illustrated in Fig. E.1. We rewrite (E.75) in the sth sub-region as follows:

$$(\mathbf{H} + \boldsymbol{\mathcal{L}}_s - E\mathbf{I})\,\mathbf{F}(r) = \boldsymbol{\mathcal{L}}_s\mathbf{F}(r) + \boldsymbol{\theta}(r), \tag{E.78}$$

where the Bloch operator $\boldsymbol{\mathcal{L}}_s$ is defined by (E.10). It follows that the operator $\mathbf{H}+\boldsymbol{\mathcal{L}}_s$ is hermitian over the sth sub-region in the space of functions satisfying arbitrary boundary conditions at $r = a_{s-1}$ and a_s. Equation (E.78) then has the formal solution in the sth sub-region

$$\mathbf{F}(r) = (\mathbf{H} + \boldsymbol{\mathcal{L}}_s - E\mathbf{I})^{-1}\left[\boldsymbol{\mathcal{L}}_s\mathbf{F}(r) + \boldsymbol{\theta}(r)\right]. \tag{E.79}$$

The Green's function in this equation is defined as the solution of the following equation in the sth sub-region

$$(\mathbf{H} + \boldsymbol{\mathcal{L}}_s - E\mathbf{I})\,\mathbf{G}_s(r, r') = \frac{1}{2}\mathbf{I}\delta(r - r'). \tag{E.80}$$

We can then rewrite (E.79) as

$$\mathbf{F}(r) = 2\int_{a_{s-1}}^{a_s} \mathbf{G}_s(r, r')\boldsymbol{\mathcal{L}}_s\mathbf{F}(r')\mathrm{d}r' + \mathbf{J}(r), \quad a_{s-1} \le r \le a_s, \tag{E.81}$$

where

$$\mathbf{J}(r) = 2\int_{a_{s-1}}^{a_s} \mathbf{G}_s(r, r')\boldsymbol{\theta}(r')\mathrm{d}r', \quad a_{s-1} \le r \le a_s. \tag{E.82}$$

Evaluating (E.81) at $r = a_{s-1}$ and a_s and using (E.10) for the Bloch operator $\boldsymbol{\mathcal{L}}_s$ then yields the equations

$$\mathbf{F}(a_{s-1}) = \mathbf{G}_s(a_{s-1}, a_s)\left.\frac{\mathrm{d}\mathbf{F}}{\mathrm{d}r}\right|_{r=a_s} - \mathbf{G}_s(a_{s-1}, a_{s-1})\left.\frac{\mathrm{d}\mathbf{F}}{\mathrm{d}r}\right|_{r=a_{s-1}} + \mathbf{J}(a_{s-1}) \tag{E.83}$$

and

$$\mathbf{F}(a_s) = \mathbf{G}_s(a_s, a_s)\left.\frac{\mathrm{d}\mathbf{F}}{\mathrm{d}r}\right|_{r=a_s} - \mathbf{G}_s(a_s, a_{s-1})\left.\frac{\mathrm{d}\mathbf{F}}{\mathrm{d}r}\right|_{r=a_{s-1}} + \mathbf{J}(a_s). \tag{E.84}$$

We see that these equations only differ from (E.23) and (E.24), obtained by solving the homogeneous equation (E.1), by the presence of the inhomogeneous terms $\mathbf{J}(a_{s-1})$ and $\mathbf{J}(a_s)$ on the right-hand sides.

In order to determine the inward and outward propagation equations for the R-matrix, we define R-matrices at $r = a_{s-1}$ and a_s as follows:

$$\mathbf{F}(a_{s-1}) = \mathbf{R}_{s-1}a_{s-1}\left.\frac{\mathrm{d}\mathbf{F}}{\mathrm{d}r}\right|_{r=a_{s-1}} + \mathbf{Z}(a_{s-1}) \tag{E.85}$$

and

$$\mathbf{F}(a_s) = \mathbf{R}_s a_s\left.\frac{\mathrm{d}\mathbf{F}}{\mathrm{d}r}\right|_{r=a_s} + \mathbf{Z}(a_s). \tag{E.86}$$

The inhomogeneous terms $\mathbf{Z}(a_{s-1})$ and $\mathbf{Z}(a_s)$, which we have introduced in (E.85) and (E.86), are required to represent the effect of the inhomogeneous terms $\mathbf{J}(a_{s-1})$ and $\mathbf{J}(a_s)$ in (E.83) and (E.84). If these inhomogeneous terms are not included, then (E.85) and (E.86) reduce to the usual definition of the R-matrix, given by (E.25)

and (E.26). In the application to time-dependent atomic multiphoton processes the R-matrix $\mathbf{R}_s$ and the matrix $\mathbf{Z}(a_s)$ are given on the boundary $r = a_0$ of the internal region by (10.71) and (10.72).

Substituting $\mathbf{F}(a_{s-1})$ and $\mathbf{F}(a_s)$, given by (E.85) and (E.86), into (E.83) and (E.84) yields the following outward propagation equations for the R-matrix $\mathbf{R}_s$ and for the inhomogeneous term $\mathbf{Z}(a_s)$

$$a_s\mathbf{R}_s = \mathbf{G}_s(a_s, a_s) - \mathbf{G}_s(a_s, a_{s-1})\left[\mathbf{G}_s(a_{s-1}, a_{s-1}) + a_{s-1}\mathbf{R}_{s-1}\right]^{-1} \times \mathbf{G}_s(a_{s-1}, a_s) \tag{E.87}$$

and

$$\mathbf{Z}(a_s) = \mathbf{J}(a_s) + \mathbf{G}_s(a_s, a_{s-1})\left[\mathbf{G}_s(a_{s-1}, a_{s-1}) + a_{s-1}\mathbf{R}_{s-1}\right]^{-1} \times \left[\mathbf{Z}(a_{s-1}) - \mathbf{J}(a_{s-1})\right]. \tag{E.88}$$

We can invert these equations to give the following inward propagation equations:

$$a_{s-1}\mathbf{R}_{s-1} = -\mathbf{G}_s(a_{s-1}, a_{s-1}) + \mathbf{G}_s(a_{s-1}, a_s)\left[\mathbf{G}_s(a_s, a_s) - a_s\mathbf{R}_s\right]^{-1} \times \mathbf{G}_s(a_s, a_{s-1}) \tag{E.89}$$

and

$$\mathbf{Z}(a_{s-1}) = \mathbf{J}(a_{s-1}) + \mathbf{G}_s(a_{s-1}, a_s)\left[\mathbf{G}_s(a_s, a_s) - a_s\mathbf{R}_s\right]^{-1} \times \left[\mathbf{Z}(a_s) - \mathbf{J}(a_s)\right]. \tag{E.90}$$

Equations (E.87) and (E.89) are identical to the corresponding equations (E.27) and (E.28) which arise in the propagation of the R-matrix corresponding to the homogeneous equation (E.1). However, we also have to propagate the inhomogeneous term $\mathbf{Z}(a_s)$ using (E.88) and (E.90) in order to relate the solution to its derivative using (E.85) and (E.86).

Having determined the R-matrix $\mathbf{R}_s$ and the inhomogeneous term $\mathbf{Z}(a_s)$ on the boundaries $r = a_s$, $s = 0, \ldots, p$, of the p sub-regions we can then propagate the wave function $\mathbf{F}(a_s)$ across these sub-regions using (E.83) to (E.86). We obtain the following equations for outward and inward propagation of the wave function:

$$\mathbf{F}(a_s) = a_s\mathbf{R}_s\left[\mathbf{G}_s(a_s, a_s) - a_s\mathbf{R}_s\right]^{-1}\Big\{\mathbf{G}_s(a_s, a_{s-1})a_{s-1}^{-1}\mathbf{R}_{s-1}^{-1} \times \left[\mathbf{F}(a_{s-1}) - \mathbf{Z}(a_{s-1})\right] + \mathbf{G}_s(a_s, a_s)a_s^{-1}\mathbf{R}_s^{-1}\mathbf{Z}(a_s) - \mathbf{J}(a_s)\Big\} \tag{E.91}$$

and

$$\mathbf{F}(a_{s-1}) = a_{s-1}\mathbf{R}_{s-1}\left[\mathbf{G}_s(a_{s-1}, a_{s-1}) + a_{s-1}\mathbf{R}_{s-1}\right]^{-1}\{\mathbf{G}_s(a_{s-1}, a_s) \times a_s^{-1}\mathbf{R}_s^{-1}\left[\mathbf{F}(a_s) - \mathbf{Z}(a_s)\right] + \mathbf{G}_s(a_{s-1}, a_{s-1})a_{s-1}^{-1}\mathbf{R}_{s-1}^{-1}\mathbf{Z}(a_{s-1}) + \mathbf{J}(a_{s-1})\}. \tag{E.92}$$

Equations (E.91) and (E.92) reduce to (E.29) and (E.30) obtained by solving the homogeneous equation (E.1) when the inhomogeneous terms $\mathbf{J}(a_s)$, $\mathbf{J}(a_{s-1})$, $\mathbf{Z}(a_s)$ and $\mathbf{Z}(a_{s-1})$ are absent.

The Green's functions in (E.87), (E.88), (E.89), (E.90), (E.91) and (E.92), which are solutions of (E.79), can be calculated using, for example, the Light–Walker method discussed in Appendix E.1 or the BBM method discussed in Appendix E.3. In both cases the calculation can use either matrix diagonalization or the solution of linear simultaneous equations. In the Light–Walker method this involves diagonalizing matrices or solving linear equations of order n, while in the BBM method it involves diagonalizing matrices or solving linear equations of order nm, where n is the number of coupled channels and m is the number of basis functions retained in each channel. However, we observed in our study of multiphoton processes using time-dependent theory in Chap. 10 that the outward and inward propagations in the external region are carried out at a single energy $E = 2\mathrm{i}\Delta t^{-1}$ at each time step, where Δt is the small time interval used in the propagation. An efficient method for diagonalizing the Hamiltonian matrix when using either the Light–Walker or the BBM propagator would then be the Jacobi iterative procedure discussed in Sect. 10.1.4, which commences from the solution at the previous time step. However, the procedure that has been adopted by van der Hart et al. [937, 938] and by Lysaght et al. [603–606] in their time-dependent multiphoton ionization studies of neon and argon atoms, discussed in Sect. 10.2, uses a basis of B-splines in the BBM method and determines the Green's functions by solving linear simultaneous equations in each sub-region as discussed in Sect. 4.4.4, which has proved to be very effective in practice.

E.5 Propagator Method with First-Order Derivative

We have seen in our discussion of atomic multiphoton processes in Chaps. 9 and 10 that the coupled second-order differential equations describing the radial motion of the scattered or ejected electron contain a first-order derivative term when the interaction of this electron with the laser field is treated in the velocity gauge. Also, we have seen in Sects. 1.6, 4.6 and 5.5.3 that the coupled first-order Dirac equations can be reduced to a second-order differential equation with a first-order derivative term. Although we showed in Sect. 9.1.3 that this first-order derivative term can be eliminated by a unitary transformation, enabling propagator methods described previously in this appendix to be used, a propagator method that can be applied directly

to the solution of differential equations containing a first-order derivative term was developed by Burke and Burke [172]. We now consider the solution of the coupled inhomogeneous differential equations (10.55) which arise in time-dependent R-matrix theory of atomic multiphoton processes, discussed in Chap. 10. However, the method can also be applied to the coupled homogeneous equations (9.61), obtained in R-matrix-Floquet theory, by omitting the inhomogeneous term in the following analysis.

We rewrite (10.55) in the following general form:

$$(\mathbf{H} - E\mathbf{I})\,\mathbf{F}(r) = \boldsymbol{\theta}(r), \tag{E.93}$$

where

$$\mathbf{H} - E\mathbf{I} = -\frac{1}{2}\left(\mathbf{I}\frac{\mathrm{d}^2}{\mathrm{d}r^2} + \mathbf{P}\frac{\mathrm{d}}{\mathrm{d}r} + \mathbf{W}(r) + \mathbf{k}^2\right), \tag{E.94}$$

where we find it convenient to measure the energy E in (E.93) and (E.94) from the lowest target threshold so that the operator $\mathbf{H}$ is independent of the value of E. Also in (E.94), $\mathbf{P}$ is an antihermitian matrix and $\mathbf{W}(r)$ is a hermitian matrix which represents the remaining potential terms in (10.55).

We now consider the propagation of the R-matrix and solution of the coupled inhomogeneous second-order differential equations (E.93) across the p sub-regions illustrated in Fig. E.1. We introduce the Bloch operators $\boldsymbol{\mathcal{L}}_{1s}$ and $\boldsymbol{\mathcal{L}}_{2s}$ defined by the equations

$$\boldsymbol{\mathcal{L}}_{1s} = \frac{1}{2}\mathbf{I}\left[\delta(r - a_s)\frac{\mathrm{d}}{\mathrm{d}r} - \delta(r - a_{s-1})\frac{\mathrm{d}}{\mathrm{d}r}\right] \tag{E.95}$$

and

$$\boldsymbol{\mathcal{L}}_{2s} = \frac{1}{4}\mathbf{P}\left[\delta(r - a_s) - \delta(r - a_{s-1})\right], \tag{E.96}$$

which are such that $-\frac{1}{2}\mathbf{I}\mathrm{d}^2/\mathrm{d}r^2 + \boldsymbol{\mathcal{L}}_{1s}$ and $-\frac{1}{2}\mathbf{P}\mathrm{d}/\mathrm{d}r + \boldsymbol{\mathcal{L}}_{2s}$ are both hermitian in the sth sub-region $a_{s-1} \le r \le a_s$, in the space of functions satisfying arbitrary boundary conditions at $r = a_{s-1}$ and a_s. It follows that $\mathbf{H} + \boldsymbol{\mathcal{L}}_{1s} + \boldsymbol{\mathcal{L}}_{2s}$ is hermitian in this sub-region. We can then rewrite (E.93) in the sth sub-region as

$$(\mathbf{H} + \boldsymbol{\mathcal{L}}_{1s} + \boldsymbol{\mathcal{L}}_{2s} - E\mathbf{I})\,\mathbf{F}(r) = (\boldsymbol{\mathcal{L}}_{1s} + \boldsymbol{\mathcal{L}}_{2s})\,\mathbf{F}(r) + \boldsymbol{\theta}(r), \tag{E.97}$$

which has the formal solution

$$\mathbf{F}(r) = (\mathbf{H} + \boldsymbol{\mathcal{L}}_{1s} + \boldsymbol{\mathcal{L}}_{2s} - E\mathbf{I})^{-1}\,[(\boldsymbol{\mathcal{L}}_{1s} + \boldsymbol{\mathcal{L}}_{2s})\,\mathbf{F}(r) + \boldsymbol{\theta}(r)]. \tag{E.98}$$

The Green's function in this equation is defined as the solution of the following equation in the sth sub-region:

$$(\mathbf{H} + \boldsymbol{\mathcal{L}}_{1s} + \boldsymbol{\mathcal{L}}_{2s} - E\mathbf{I})\,\mathbf{G}_s(r, r') = \frac{1}{2}\mathbf{I}\delta(r - r'). \tag{E.99}$$

We can then rewrite (E.98) as

$$\mathbf{F}(r) = 2\int_{a_{s-1}}^{a_s} \mathbf{G}_s(r, r')(\boldsymbol{\mathcal{L}}_{1s} + \boldsymbol{\mathcal{L}}_{2s})\mathbf{F}(r')\mathrm{d}r' + \mathbf{J}(r), \quad a_{s-1} \le r \le a_s, \tag{E.100}$$

where

$$\mathbf{J}(r) = 2\int_{a_{s-1}}^{a_s} \mathbf{G}_s(r, r')\boldsymbol{\theta}(r')\mathrm{d}r', \quad a_{s-1} \le r \le a_s. \tag{E.101}$$

Evaluating (E.100) at $r = a_{s-1}$ and a_s and using (E.95) and (E.96) for the Bloch operators $\boldsymbol{\mathcal{L}}_{1s}$ and $\boldsymbol{\mathcal{L}}_{2s}$ then yield the equations

$$\begin{aligned}\mathbf{F}(a_{s-1}) = \mathbf{G}_s(a_{s-1}, a_s)\left(\frac{\mathrm{d}\mathbf{F}}{\mathrm{d}r} + \frac{1}{2}\mathbf{P}\mathbf{F}\right)_{r=a_s} - \mathbf{G}_s(a_{s-1}, a_{s-1}) \\ \times \left(\frac{\mathrm{d}\mathbf{F}}{\mathrm{d}r} + \frac{1}{2}\mathbf{P}\mathbf{F}\right)_{r=a_{s-1}} + \mathbf{J}(a_{s-1})\end{aligned} \tag{E.102}$$

and

$$\begin{aligned}\mathbf{F}(a_s) = \mathbf{G}_s(a_s, a_s)\left(\frac{\mathrm{d}\mathbf{F}}{\mathrm{d}r} + \frac{1}{2}\mathbf{P}\mathbf{F}\right)_{r=a_s} - \mathbf{G}_s(a_s, a_{s-1}) \\ \times \left(\frac{\mathrm{d}\mathbf{F}}{\mathrm{d}r} + \frac{1}{2}\mathbf{P}\mathbf{F}\right)_{r=a_{s-1}} + \mathbf{J}(a_s).\end{aligned} \tag{E.103}$$

We see that these equations only differ from (E.83) and (E.84) by the generalization of the differential operator $\mathrm{d}\mathbf{F}/\mathrm{d}r$. We now define the R-matrices at $r = a_{s-1}$ and a_s by the equations

$$\mathbf{F}(a_{s-1}) = \mathbf{R}_{s-1}a_{s-1}\left(\frac{\mathrm{d}\mathbf{F}}{\mathrm{d}r} + \frac{1}{2}\mathbf{P}\mathbf{F}\right)_{r=a_{s-1}} + \mathbf{T}(a_{s-1}) \tag{E.104}$$

and

$$\mathbf{F}(a_s) = \mathbf{R}_s a_s\left(\frac{\mathrm{d}\mathbf{F}}{\mathrm{d}r} + \frac{1}{2}\mathbf{P}\mathbf{F}\right)_{r=a_s} + \mathbf{T}(a_s), \tag{E.105}$$

where the inhomogeneous terms $\mathbf{T}(a_{s-1})$ and $\mathbf{T}(a_s)$, which we have introduced in (E.104) and (E.105), represent the effect of the inhomogeneous terms $\mathbf{J}(a_{s-1})$ and $\mathbf{J}(a_s)$ in (E.102) and (E.103), respectively. We see that in time-dependent multiphoton theory the R-matrix $\mathbf{R}_s$ and the matrix $\mathbf{T}(a_s)$ for $s = 0$ are given on the boundary $r = a_0$ of the internal region by (10.37) and (10.42), respectively.

Following our discussion leading to (E.87), (E.88), (E.89) and (E.90) we obtain the following outward propagation equations for $\mathbf{R}_s$ and $\mathbf{T}(a_s)$:

$$\begin{aligned}a_s\mathbf{R}_s = \mathbf{G}_s(a_s, a_s) - \mathbf{G}_s(a_s, a_{s-1})\left[\mathbf{G}_s(a_{s-1}, a_{s-1}) + a_{s-1}\mathbf{R}_{s-1}\right]^{-1} \\ \times \mathbf{G}_s(a_{s-1}, a_s)\end{aligned} \tag{E.106}$$

and

$$\mathbf{T}(a_s) = \mathbf{J}(a_s) + \mathbf{G}_s(a_s, a_{s-1}) \left[\mathbf{G}_s(a_{s-1}, a_{s-1}) + a_{s-1}\mathbf{R}_{s-1}\right]^{-1} \times \left[\mathbf{T}(a_{s-1}) - \mathbf{J}(a_{s-1})\right]. \tag{E.107}$$

These equations can be inverted to give the following inward propagation equations for $\mathbf{R}_s$ and $\mathbf{T}(a_s)$:

$$a_{s-1}\mathbf{R}_{s-1} = -\mathbf{G}_s(a_{s-1}, a_{s-1}) + \mathbf{G}_s(a_{s-1}, a_s) \left[\mathbf{G}_s(a_s, a_s) - a_s\mathbf{R}_s\right]^{-1} \times \mathbf{G}_s(a_s, a_{s-1}) \tag{E.108}$$

and

$$\mathbf{T}(a_{s-1}) = \mathbf{J}(a_{s-1}) + \mathbf{G}_s(a_{s-1}, a_s) \left[\mathbf{G}_s(a_s, a_s) - a_s\mathbf{R}_s\right]^{-1} \times \left[\mathbf{T}(a_s) - \mathbf{J}(a_s)\right]. \tag{E.109}$$

Finally we obtain the following outward and inward propagation equations for the wave function

$$\mathbf{F}(a_s) = a_s\mathbf{R}_s \left[\mathbf{G}_s(a_s, a_s) - a_s\mathbf{R}_s\right]^{-1} \Big\{\mathbf{G}_s(a_s, a_{s-1})a_{s-1}^{-1}\mathbf{R}_{s-1}^{-1} \times \left[\mathbf{F}(a_{s-1}) - \mathbf{T}(a_{s-1})\right] + \mathbf{G}_s(a_s, a_s)a_s^{-1}\mathbf{R}_s^{-1}\mathbf{T}(a_s) - \mathbf{J}(a_s)\Big\} \tag{E.110}$$

and

$$\mathbf{F}(a_{s-1}) = a_{s-1}\mathbf{R}_{s-1} \left[\mathbf{G}_s(a_{s-1}, a_{s-1}) + a_{s-1}\mathbf{R}_{s-1}\right]^{-1} \Big\{\mathbf{G}_s(a_{s-1}, a_s)a_s^{-1}\mathbf{R}_s^{-1} \times \left[\mathbf{F}(a_s) - \mathbf{T}(a_s)\right] + \mathbf{G}_s(a_{s-1}, a_{s-1})a_{s-1}^{-1}\mathbf{R}_{s-1}^{-1}\mathbf{T}(a_{s-1}) + \mathbf{J}(a_{s-1})\Big\}. \tag{E.111}$$

We conclude by observing that, as in Appendix E.4, the Green's functions in the above equations which are solutions of (E.99) can be calculated using either the Light–Walker or the BBM propagator method.

E.6 Propagation of Sets of Uncoupled Channels

In this section we extend the propagator methods discussed in the previous sections of this appendix to treat channels which are strongly coupled in the internal R-matrix region but which separate in the external and asymptotic regions into two or more sets of channels, where channels in different sets are uncoupled although channels within each set remain strongly coupled. This arises in positron collisions with atoms and ions which we considered in Chap. 7. In this case the positron–atom

collision channels and positronium–ion collision channels are strongly coupled in the internal region but separate into two sets of uncoupled channels in the external and asymptotic regions. It also arises in electron collisions with molecules which we considered in Chap. 11. In this case the electron–molecule collision channels and molecular dissociation channels are strongly coupled in the internal region but separate into two sets of uncoupled channels in the external and asymptotic regions. We also observe that in the case of positron–molecule collisions, separation into three sets of uncoupled channels in the external and asymptotic regions is possible, corresponding to positron–molecule collision channels, positronium–molecular ion collision channels and molecular dissociation channels which can be analysed by an extension of the analysis presented in this section.

Channel decoupling also arises in low-energy electron collisions with atoms and ions, considered in Chap. 5. In this case electron exchange couples target states with different spins in the internal region, but target states with different spins are not coupled in the external and asymptotic regions where electron exchange effects vanish. A similar decoupling effect, discussed in Sect. 5.4.2, occurs in low-energy electron collisions with heavy atoms and ions where relativistic effects are important. In this case the channels that are strongly coupled by relativistic effects in the internal region divide into two uncoupled sets depending on the quantum number K_i in the external region.

We consider two sets of channels which are strongly coupled in the internal region and which separate into two sets of uncoupled channels in the external and asymptotic regions, which is the situation that occurs most often in applications, although the theory can be extended in a straightforward way to treat separation into three or more sets of uncoupled channels. We assume that the reduced radial wave functions in the first set of coupled channels satisfy the following set of n_1 coupled second-order differential equations in the external and asymptotic regions:

$$\left(\mathbf{I}_1 \frac{\mathrm{d}^2}{\mathrm{d}r^2} + \mathbf{V}_1(r) + \mathbf{k}_1^2\right) \mathbf{F}_1(r) = 0, \quad r \geq a_0, \tag{E.112}$$

and we assume that the reduced radial wave functions in the second set of coupled channels satisfy the following set of n_2 coupled second-order differential equations in the external and asymptotic regions:

$$\left(\mathbf{I}_2 \frac{\mathrm{d}^2}{\mathrm{d}R^2} + \mathbf{V}_2(R) + \mathbf{k}_2^2\right) \mathbf{F}_2(R) = 0, \quad R \geq A_0, \tag{E.113}$$

where in (E.112) and (E.113) $\mathbf{I}_1$ and $\mathbf{I}_2$ are unit matrices with dimensions $n_1 \times n_1$ and $n_2 \times n_2$, respectively, and we define $n = n_1 + n_2$. We subdivide the external region, where $r \geq a_0$ and $R \geq A_0$, into sub-regions as follows:

$$a_{s-1} \leq r \leq a_s, \quad s = 1, \ldots, p \tag{E.114}$$

and

$$A_{t-1} \leq R \leq A_t, \quad t = 1, \ldots, q. \tag{E.115}$$

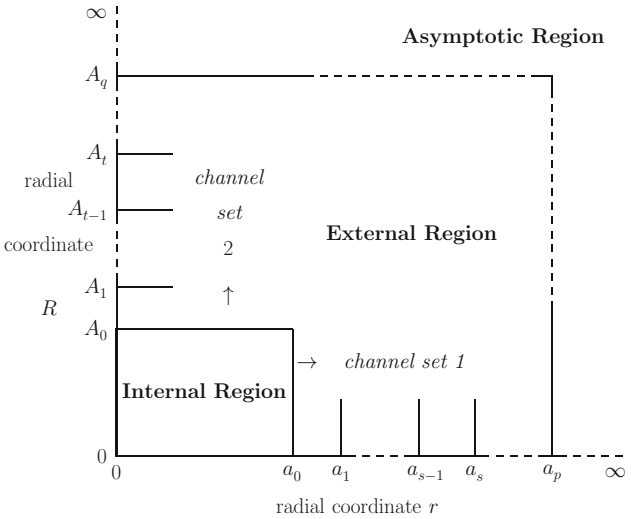

Fig. E.2 Partitioning of configuration space into sub-regions in R-matrix theory for two sets of channels which are strongly coupled in the internal region but uncoupled in the external and asymptotic regions

We illustrate this partitioning of configuration space in Fig. E.2.

As a result of the calculation in the internal region and the propagation of the resultant R-matrix in the external region from $r = a_0$ to a_s and from $R = A_0$ to A_t we assume that the functions $\mathbf{F}_1$ and $\mathbf{F}_2$ are related to the derivatives $\mathbf{F}'_1 \equiv \mathrm{d}\mathbf{F}_1/\mathrm{d}r$ and $\mathbf{F}'_2 \equiv \mathrm{d}\mathbf{F}_2/\mathrm{d}R$ by the equations

$$\mathbf{F}_1(s,t) = \mathbf{R}_{11}(s,t)a_s\mathbf{F}'_1(s,t) + \mathbf{R}_{12}(s,t)A_t\mathbf{F}'_2(s,t) \tag{E.116}$$

and

$$\mathbf{F}_2(s,t) = \mathbf{R}_{21}(s,t)a_s\mathbf{F}'_1(s,t) + \mathbf{R}_{22}(s,t)A_t\mathbf{F}'_2(s,t), \tag{E.117}$$

where the notation adopted in these equations recognizes that the functions and derivatives as well as the R-matrix sub-matrices $\mathbf{R}_{11}$, $\mathbf{R}_{12}$, $\mathbf{R}_{21}$ and $\mathbf{R}_{22}$ depend on both radial distances $r = a_s$ and $R = A_t$. We can write (E.116) and (E.117) using the following compact matrix notation:

$$\mathbf{F}(s,t) = \mathbf{R}(s,t)\boldsymbol{\rho}(s,t)\mathbf{F}'(s,t), \tag{E.118}$$

where the n-dimensional functions and derivatives $\mathbf{F}$ and $\mathbf{F}'$ are defined by

$$\mathbf{F}(s,t) = \begin{bmatrix} \mathbf{F}_1(s,t) \\ \mathbf{F}_2(s,t) \end{bmatrix}, \quad \mathbf{F}'(s,t) = \begin{bmatrix} \mathbf{F}'_1(s,t) \\ \mathbf{F}'_2(s,t) \end{bmatrix}, \tag{E.119}$$

and the $n \times n$-dimensional matrices $\mathbf{R}$ and $\boldsymbol{\rho}$ are defined by

$$\mathbf{R}(s,t) = \begin{bmatrix} \mathbf{R}_{11}(s,t) & \mathbf{R}_{12}(s,t) \\ \mathbf{R}_{21}(s,t) & \mathbf{R}_{22}(s,t) \end{bmatrix}, \quad \boldsymbol{\rho}(s,t) = \begin{bmatrix} \mathbf{I}_1 a_s & \mathbf{O} \\ \mathbf{O} & \mathbf{I}_2 A_t \end{bmatrix}. \tag{E.120}$$

We now consider the propagation of the R-matrix $\mathbf{R}(s-1,t-1)$ from the boundaries $r = a_{s-1}$ and $R = A_{t-1}$ to the boundaries $r = a_s$ and $R = A_t$ to yield the R-matrix $\mathbf{R}(s,t)$. Since (E.112) and (E.113) are not coupled in the external region then (E.23) and (E.24) can be applied independently to $\mathbf{F}_1$ and $\mathbf{F}_2$. Hence we obtain

$$\begin{aligned} \mathbf{F}(s-1,t-1) = {} & \mathbf{G}_{st}(s-1,t-1;s,t)\mathbf{F}'(s,t) - \mathbf{G}_{st}(s-1,t-1;s-1,t-1) \\ & \times \mathbf{F}'(s-1,t-1) \end{aligned} \tag{E.121}$$

and

$$\mathbf{F}(s,t) = \mathbf{G}_{st}(s,t;s,t)\mathbf{F}'(s,t) - \mathbf{G}_{st}(s,t;s-1,t-1)\mathbf{F}'(s-1,t-1), \tag{E.122}$$

where the $n \times n$-dimensional Green's function matrix has the following block diagonal form:

$$\mathbf{G}_{st}(s,t;s',t') = \begin{bmatrix} \mathbf{G}_{1s}(s,s') & \mathbf{O} \\ \mathbf{O} & \mathbf{G}_{2t}(t,t') \end{bmatrix}. \tag{E.123}$$

The Green's functions $\mathbf{G}_{1s}$ and $\mathbf{G}_{2t}$ correspond to (E.112) and (E.113), respectively, and can be calculated using either the Light–Walker or the BBM propagator method discussed in Sects. E.1 and E.3, respectively. Using (E.121) and (E.122) we find that the R-matrix $\mathbf{R}(s,t)$ is related to the R-matrix $\mathbf{R}(s-1,t-1)$, using a straightforward generalization of (E.27), by

$$\begin{aligned} \mathbf{R}(s,t)\boldsymbol{\rho}(s,t) = {} & \mathbf{G}_{st}(s,t;s,t) - \mathbf{G}_{st}(s,t;s-1,t-1) \\ & \times \left[\mathbf{G}_{st}(s-1,t-1;s-1,t-1) + \mathbf{R}(s-1,t-1)\right. \\ & \times \left.\boldsymbol{\rho}(s-1,t-1)\right]^{-1} \mathbf{G}_{st}(s-1,t-1;s,t), \end{aligned} \tag{E.124}$$

and similarly $\mathbf{R}(s-1,t-1)$ is related to $\mathbf{R}(s,t)$, using a straightforward generalization of (E.28), by

$$\begin{aligned} & \mathbf{R}(s-1,t-1)\boldsymbol{\rho}(s-1,t-1) \\ & = -\mathbf{G}_{st}(s-1,t-1;s-1,t-1) + \mathbf{G}_{st}(s-1,t-1;s,t) \\ & \quad \times \left[\mathbf{G}_{st}(s,t;s,t) - \mathbf{R}(s,t)\boldsymbol{\rho}(s,t)\right]^{-1} \mathbf{G}_{st}(s,t;s-1,t-1). \end{aligned} \tag{E.125}$$

Having determined the R-matrix on the boundaries of the sub-regions using (E.124) or (E.125) we can propagate the wave functions across the sub-regions, using straightforward generalizations of (E.29) and (E.30), given by

$$\begin{aligned} \mathbf{F}(s,t) = {} & \mathbf{R}(s,t)\boldsymbol{\rho}(s,t)\left[\mathbf{G}_{st}(s,t;s,t) - \mathbf{R}(s,t)\boldsymbol{\rho}(s,t)\right]^{-1} \mathbf{G}_{st}(s,t;s-1,t-1) \\ & \times \boldsymbol{\rho}^{-1}(s-1,t-1)\mathbf{R}^{-1}(s-1,t-1)\mathbf{F}(s-1,t-1) \end{aligned} \tag{E.126}$$

and

$$\mathbf{F}(s-1,t-1) = \mathbf{R}(s-1,t-1)\boldsymbol{\rho}(s-1,t-1)\,[\mathbf{G}_{st}(s-1,t-1;s-1,t-1) + \mathbf{R}(s-1,t-1)\boldsymbol{\rho}(s-1,t-1)]^{-1}\,\mathbf{G}_{st}(s-1,t-1;s,t) \times \boldsymbol{\rho}^{-1}(s,t)\mathbf{R}^{-1}(s,t)\mathbf{F}(s,t). \tag{E.127}$$

We see that (E.124), (E.125), (E.126) and (E.127) have the same form as the propagator equations (E.27), (E.28), (E.29) and (E.30). However, for the same total number of channels n, (E.124), (E.125), (E.126) and (E.127) take less time to solve since the Green's function matrix defined by (E.123) is block diagonal. This feature of the equations was used by Sunderland et al. [896] to develop an efficient parallel algorithm which was used to propagate the R-matrix for electron collisions with light atoms and atomic ions, where the coupled equations describing the collision in the external region decouple for different target spins.

In certain situations it will not be necessary nor appropriate to propagate the R-matrix and wave functions corresponding to (E.112) and (E.113) over the same number of steps in the external region. This will occur, for example, in electron–molecule collisions leading to dissociative attachment when the collision processes corresponding to (E.112) and (E.113) are very different in the external region. We will therefore derive a procedure for propagating the R-matrix and wave function when the value of r corresponding to (E.112) is propagated through one step from $r = a_{s-1}$ to a_s while the value of R corresponding to (E.113) remains fixed at $R = A_t$. That is we will propagate the R-matrix $\mathbf{R}(s-1,t)$, defined by the equation

$$\mathbf{F}(s-1,t) = \mathbf{R}(s-1,t)\boldsymbol{\rho}(s-1,t)\mathbf{F}'(s-1,t), \tag{E.128}$$

forward one step to yield the R-matrix $\mathbf{R}(s,t)$, defined by (E.118).

The equations corresponding to propagation of $\mathbf{F}_1$ through one step from $r = a_{s-1}$ to a_s keeping the radial coordinate R fixed at A_t are given by (E.23) and (E.24) which we can rewrite using our present notation as

$$\mathbf{F}_1(s-1,t) = \mathbf{G}_{1s}(s-1,s)\mathbf{F}'_1(s,t) - \mathbf{G}_{1s}(s-1,s-1)\mathbf{F}'_1(s-1,t) \tag{E.129}$$

and

$$\mathbf{F}_1(s,t) = \mathbf{G}_{1s}(s,s)\mathbf{F}'_1(s,t) - \mathbf{G}_{1s}(s,s-1)\mathbf{F}'_1(s-1,t). \tag{E.130}$$

We then eliminate $\mathbf{F}_1(s-1,t)$ and $\mathbf{F}'_1(s-1,t)$ from (E.128) using (E.129) and (E.130) and write the resultant equation in the form of (E.118). We find that the R-matrix $\mathbf{R}(s,t)$ has the components

$$\mathbf{R}_{11}(s,t)a_s = \mathbf{G}_{1s}(s,s) - \mathbf{G}_{1s}(s,s-1)\,[\mathbf{G}_{1s}(s-1,s-1) + \mathbf{R}_{11}(s-1,t)a_{s-1}]^{-1}\,\mathbf{G}_{1s}(s-1,s), \tag{E.131}$$

$$\mathbf{R}_{12}(s,t)A_t = \mathbf{G}_{1s}(s,s-1)\left[\mathbf{G}_{1s}(s-1,s-1)+\mathbf{R}_{11}(s-1,t)a_{s-1}\right]^{-1} \times \mathbf{R}_{12}(s-1,t)A_t, \tag{E.132}$$

$$\mathbf{R}_{21}(s,t)a_s = \mathbf{R}_{21}(s-1,t)a_{s-1}\left[\mathbf{G}_{1s}(s-1,s-1)+\mathbf{R}_{11}(s-1,t)a_{s-1}\right]^{-1} \times \mathbf{G}_{1s}(s-1,s), \tag{E.133}$$

$$\mathbf{R}_{22}(s,t)A_t = \mathbf{R}_{22}(s-1,t)A_t - \mathbf{R}_{21}(s-1,t)a_{s-1}\left[\mathbf{G}_{1s}(s-1,s-1) + \mathbf{R}_{11}(s-1,t)a_{s-1}\right]^{-1}\mathbf{R}_{12}(s-1,t)A_t. \tag{E.134}$$

On the other hand, if we eliminate $\mathbf{F}_1(s,t)$ and $\mathbf{F}_1'(s,t)$ from (E.118) using (E.129) and (E.130) and write the resultant equation in the form of (E.128) we find that the resultant R-matrix $\mathbf{R}(s-1,t)$ has the components

$$\mathbf{R}_{11}(s-1,t)a_{s-1} = -\mathbf{G}_{1s}(s-1,s-1)+\mathbf{G}_{1s}(s-1,s) \times \left[\mathbf{G}_{1s}(s,s)-\mathbf{R}_{11}(s,t)a_s\right]^{-1}\mathbf{G}_{1s}(s,s-1), \tag{E.135}$$

$$\mathbf{R}_{12}(s-1,t)A_t = \mathbf{G}_{1s}(s-1,s)\left[\mathbf{G}_{1s}(s,s)-\mathbf{R}_{11}(s,t)a_s\right]^{-1}\mathbf{R}_{12}(s,t)A_t, \tag{E.136}$$

$$\mathbf{R}_{21}(s-1,t)a_{s-1} = \mathbf{R}_{21}(s,t)a_s\left[\mathbf{G}_{1s}(s,s)-\mathbf{R}_{11}(s,t)a_s\right]^{-1}\mathbf{G}_{1s}(s,s-1), \tag{E.137}$$

$$\mathbf{R}_{22}(s-1,t)A_t = \mathbf{R}_{22}(s,t)A_t + \mathbf{R}_{21}(s,t)a_s\left[\mathbf{G}_{1s}(s,s)-\mathbf{R}_{11}(s,t)a_s\right]^{-1} \times \mathbf{R}_{12}(s,t)A_t. \tag{E.138}$$

Equations (E.131), (E.132), (E.133) and (E.134) describe the outward propagation of the R-matrix from $r = a_{s-1}$ to a_s, while (E.135), (E.136), (E.137) and (E.138) describe the inward propagation of the R-matrix from $r = a_s$ to $r = a_{s-1}$, in both cases keeping the radial coordinate R fixed at A_t.

Having determined the R-matrix on the boundaries of the sub-regions using either (E.131), (E.132), (E.133) and (E.134) or (E.135), (E.136), (E.137) and (E.138), we can derive equations which enable the wave function to be propagated either outwards or inwards across the sub-regions. We first write (E.118) in terms of its matrix components and solve the resultant equations for $\mathbf{F}_1'(s,t)$ and $\mathbf{F}_2'(s,t)$ giving

$$\mathbf{F}_1'(s,t) = \left[\mathbf{I}_1 - \mathbf{R}_{11}^{-1}(s,t)\mathbf{R}_{12}(s,t)\mathbf{R}_{22}^{-1}(s,t)\mathbf{R}_{21}(s,t)\right]^{-1} a_s^{-1} \times \left[\mathbf{R}_{11}^{-1}(s,t)\mathbf{F}_1(s,t) - \mathbf{R}_{11}^{-1}(s,t)\mathbf{R}_{12}(s,t) \times \mathbf{R}_{22}^{-1}(s,t)\mathbf{F}_2(s,t)\right] \tag{E.139}$$

and

$$\mathbf{F}_2'(s,t) = \left[\mathbf{I}_2 - \mathbf{R}_{22}^{-1}(s,t)\mathbf{R}_{21}(s,t)\mathbf{R}_{11}^{-1}(s,t)\mathbf{R}_{12}(s,t)\right]^{-1} A_t^{-1} \times \left[\mathbf{R}_{22}^{-1}(s,t)\mathbf{F}_2(s,t) - \mathbf{R}_{22}^{-1}(s,t)\mathbf{R}_{21}(s,t) \times \mathbf{R}_{11}^{-1}(s,t)\mathbf{F}_1(s,t)\right]. \tag{E.140}$$

We then write (E.128) in terms of its matrix components and solve the resultant equations for $\mathbf{F}_1'(s-1,t)$ and $\mathbf{F}_2'(s-1,t)$ giving

$$\mathbf{F}_1'(s-1,t) = \left[\mathbf{I}_1 - \mathbf{R}_{11}^{-1}(s-1,t)\mathbf{R}_{12}(s-1,t)\mathbf{R}_{22}^{-1}(s-1,t)\mathbf{R}_{21}(s-1,t)\right]^{-1} \times a_{s-1}^{-1}\left[\mathbf{R}_{11}^{-1}(s-1,t)\mathbf{F}_1(s-1,t) - \mathbf{R}_{11}^{-1}(s-1,t) \times \mathbf{R}_{12}(s-1,t)\mathbf{R}_{22}^{-1}(s-1,t)\mathbf{F}_2(s-1,t)\right] \tag{E.141}$$

and

$$\mathbf{F}_2'(s-1,t) = \left[\mathbf{I}_2 - \mathbf{R}_{22}^{-1}(s-1,t)\mathbf{R}_{21}(s-1,t)\mathbf{R}_{11}^{-1}(s-1,t)\mathbf{R}_{12}(s-1,t)\right]^{-1} \times A_t^{-1}\left[\mathbf{R}_{22}^{-1}(s-1,t)\mathbf{F}_2(s-1,t) - \mathbf{R}_{22}^{-1}(s-1,t) \times \mathbf{R}_{21}(s-1,t)\mathbf{R}_{11}^{-1}(s-1,t)\mathbf{F}_1(s-1,t)\right]. \tag{E.142}$$

The required propagation equations for the wave functions can then be obtained from the six matrix equations (E.129), (E.130), (E.139), (E.140), (E.141) and (E.142), which are linear homogeneous equations in the following four functions and four derivatives:

$$\begin{aligned} &\mathbf{F}_1(s-1,t), \quad \mathbf{F}_1(s,t), \quad \mathbf{F}_2(s-1,t), \quad \mathbf{F}_2(s,t), \\ &\mathbf{F}_1'(s-1,t), \quad \mathbf{F}_1'(s,t), \quad \mathbf{F}_2'(s-1,t), \quad \mathbf{F}_2'(s,t), \end{aligned} \tag{E.143}$$

where we see that the coefficients in these six matrix equations are defined in terms of Green's functions and R-matrices which can be determined using either the Light–Walker or the BBM propagator method. We proceed by eliminating the four derivative functions on the second row of (E.143) from these six matrix equations yielding two linear homogeneous matrix equations relating the four functions on the first row of (E.143), which can be written in the following form:

$$\begin{aligned} \mathbf{F}_1(s,t) &= \mathbf{A}_{11}\mathbf{F}_1(s-1,t) + \mathbf{A}_{12}\mathbf{F}_2(s-1,t) \\ \mathbf{F}_2(s,t) &= \mathbf{A}_{21}\mathbf{F}_1(s-1,t) + \mathbf{A}_{22}\mathbf{F}_2(s-1,t), \end{aligned} \tag{E.144}$$

where the matrices $\mathbf{A}_{11}$, $\mathbf{A}_{12}$, $\mathbf{A}_{21}$ and $\mathbf{A}_{22}$ are determined in terms of Green's functions and R-matrices. Equations (E.144) then enable the functions $\mathbf{F}_1(r, R)$ and $\mathbf{F}_2(r, R)$ to be propagated outwards from $r = a_{s-1}$ and $R = A_t$ to $r = a_s$ and $R = A_t$. In a similar way, we can derive two linear equations which enable the functions $\mathbf{F}_1(r, R)$ and $\mathbf{F}_2(r, R)$ to be propagated inwards from $r = a_s$ and $R = A_t$ to $r = a_{s-1}$ and $R = A_t$. In both the outward and inward propagations we observe that, although we are only propagating the radial coordinate r corresponding to the first set of channels in Fig. E.2, the functions $\mathbf{F}_2$ corresponding to the second set of channels in Fig. E.2 will also be modified.

Finally, the above procedure can be extended to propagate the functions $\mathbf{F}_1$ and $\mathbf{F}_2$ outwards and inwards by a range of steps in the r and R variables depending on the physical process under consideration. Also, we again observe that the computational effort required for propagating the R-matrix and the wave function is reduced from that required if all $n = n_1 + n_2$ channels are coupled in the external region since the inversions involve sub-matrices whose dimensions are n_1 and n_2 rather than n.

Appendix F
Asymptotic Expansions

In this appendix we describe asymptotic expansion methods which have been developed and applied in the study of electron, positron and multiphoton collision processes. We consider first asymptotic expansion solutions of the coupled second-order differential equations which arise in the study of electron and positron collisions with atoms, ions and molecules. We then consider asymptotic expansion solutions of the coupled second-order differential equations which arise in R-matrix–Floquet theory of multiphoton ionization and laser-assisted electron–atom and electron–ion collisions when the velocity gauge is adopted in the asymptotic region.

F.1 Electron and Positron Collisions

In this section we consider asymptotic expansion solutions of the coupled second-order differential equations which arise in electron collisions with atoms, ions and molecules, considered in Chaps. 5, 6 and 11 and in positron collisions with atoms, ions and molecules, considered in Chaps. 7 and 11. In the external and asymptotic regions, defined, for example, in Sect. 5.1.1, these coupled differential equations take the following general form:

$$\left(\frac{\mathrm{d}^2}{\mathrm{d}r^2} - \frac{\ell_i(\ell_i+1)}{r^2} + \frac{2(Z-N)}{r} + k_i^2\right) F_i(r) = 2\sum_{i'=1}^{n} V_{ii'}(r) F_{i'}(r), \quad i = 1, \ldots, n, \ r \geq a_0, \tag{F.1}$$

where the potential matrix $V_{ii'}(r)$ can be written as a summation in inverse powers of r as follows:

$$V_{ii'}(r) = \sum_{\lambda=1}^{\lambda_{\max}} \alpha_{ii'\lambda} r^{-\lambda-1}, \quad i, \ i' = 1, \ldots, n, \quad r \geq a_0, \tag{F.2}$$

P.G. Burke, *R-Matrix Theory of Atomic Collisions*, Springer Series on Atomic, Optical, and Plasma Physics 61, DOI 10.1007/978-3-642-15931-2_18,

where a general expression for the long-range potential coefficients $\alpha_{ii'\lambda}$, which occur in electron collisions with atoms and atomic ions, has been derived in Appendix D.1.

We commence by describing the asymptotic expansion method introduced by Burke and Schey [160] in their study of electron–hydrogen atom collisions, which was later generalized by Burke et al. [174] and Burke and Seaton [164] to treat electron–atom and electron–ion collisions. We assume in this derivation that the channels in (F.1) are ordered as follows:

$$k_1^2 \geq k_2^2 \geq \cdots \geq k_n^2 \tag{F.3}$$

so that n_a open channels, with $k_i^2 \geq 0$, occur first and $n_b = n - n_a$ closed channels, with $k_i^2 < 0$, occur last in this list. We first define n_a asymptotic solutions of (F.1) for $r \geq a_p$ in Fig. 5.1, satisfying outgoing wave boundary conditions by the equation

$$u_{ij}(r) = \exp(\mathrm{i}\theta_j) \sum_{s=0}^{\infty} c_{ij}^s r^{-s}, \quad i = 1, \ldots, n, \quad j = 1, \ldots, n_a, \tag{F.4}$$

where n_a is the number of open channels and θ_j is defined by, see (2.82),

$$\theta_j = k_j r - \frac{1}{2}\ell_j \pi - \eta_j \ln 2k_j r + \sigma_{\ell_j}, \quad j = 1, \ldots, n_a, \tag{F.5}$$

where

$$\eta_j = -\frac{Z - N}{k_j} = -\frac{z}{k_j}, \quad j = 1, \ldots, n_a \tag{F.6}$$

and

$$\sigma_{\ell_j} = \arg(\ell_j + 1 + \mathrm{i}\eta_j), \quad j = 1, \ldots, n_a. \tag{F.7}$$

We then substitute the outgoing wave expansion (F.4) for $F_i(r)$ into (F.1) and replace the potential matrix $V_{ii'}(r)$ by expansion (F.2). Equating the coefficient of $r^{-s}\exp(\mathrm{i}\theta_j)$ to zero then yields the following recurrence relations for the expansion coefficients c_{ij}^s in (F.4)

$$(k_i^2 - k_j^2)c_{ij}^s - 2\mathrm{i}k_j(s-1)c_{ij}^{s-1} + [(s-1)(s-2) - \eta_j^2 + \mathrm{i}\eta_j(2s-3)]c_{ij}^{s-2}$$

$$-\ell_i(\ell_i+1)c_{ij}^{s-2} - 2\sum_{i'=1}^{n}\sum_{\lambda=1}^{\lambda_{\max}} \alpha_{ii'\lambda} c_{i'j}^{s-\lambda-1} = 0, \quad i = 1, \ldots, n, \quad j = 1, \ldots, n_a. \tag{F.8}$$

We then determine n_a solutions for each $j = 1, \ldots, n_a$ by setting

$$c_{ij}^0 = \delta_{ij}, \quad i = 1, \ldots, n, \quad j = 1, \ldots, n_a \tag{F.9}$$

and

$$c_{ij}^s = 0, \quad s < 0, \quad i = 1, \ldots, n, \quad j = 1, \ldots, n_a. \tag{F.10}$$

The recurrence relations (F.8) then enable us to determine the remaining coefficients

$$c_{ij}^s, \quad 1 < s \leq s_{\max}, \quad i = 1, \ldots, n, \quad j = 1, \ldots, n_a, \tag{F.11}$$

where $s_{\max}$ is some suitably chosen maximum value of the expansion index s in expansion (F.4) which may depend on i and j. This enables us to obtain n_a linearly independent solutions of (F.1) satisfying the outgoing wave boundary conditions (F.4).

In a similar way, we define n_a asymptotic solutions of (F.1) satisfying ingoing wave boundary conditions by the equation

$$u_{ij+n_a}(r) = \exp(-\mathrm{i}\theta_j) \sum_{s=0}^{\infty} c_{ij+n_a}^s r^{-s}, \quad i = 1, \ldots, n, \quad j = 1, \ldots, n_a, \tag{F.12}$$

where the coefficients $c_{ij+n_a}^s$ satisfy recurrence relations obtained from (F.8) by replacing k_j by $-k_j$. We then determine n_a solutions for each $j = 1, \ldots, n_a$ by setting

$$c_{ij+n_a}^0 = \delta_{ij}, \quad i = 1, \ldots, n, \quad j = 1, \ldots, n_a \tag{F.13}$$

and

$$c_{ij+n_a}^s = 0, \quad s < 0, \quad i = 1, \ldots, n, \quad j = 1, \ldots, n_a. \tag{F.14}$$

The recurrence relations (F.8) then enable us to determine the remaining coefficients

$$c_{ij+n_a}^s, \quad 1 < s \leq s_{\max}, \quad i = 1, \ldots, n, \quad j = 1, \ldots, n_a. \tag{F.15}$$

We can then obtain n_a linearly independent solutions of (F.1) satisfying the ingoing wave boundary conditions (F.12). It follows that we have determined $2n_a$ solutions of (F.1) which satisfy the outgoing and ingoing wave boundary conditions

$$\begin{aligned} u_{ij}(r) &\underset{r\to\infty}{\sim} \exp(\mathrm{i}\theta_j)\delta_{ij}, \quad i = 1, \ldots, n, \quad j = 1, \ldots, n_a, \\ u_{ij+n_a}(r) &\underset{r\to\infty}{\sim} \exp(-\mathrm{i}\theta_j)\delta_{ij}, \quad i = 1, \ldots, n, \quad j = 1, \ldots, n_a. \end{aligned} \tag{F.16}$$

In order to define the K-matrix in Sect. 5.1.4 we also need solutions satisfying sine and cosine asymptotic boundary conditions. These are defined in terms of the outgoing and ingoing wave solutions as follows:

$$\begin{aligned} v_{ij}(r) &= \frac{1}{2\mathrm{i}}\left[u_{ij}(r) - u_{ij+n_a}(r)\right] \\ &\underset{r\to\infty}{\sim} \sin\theta_i\delta_{ij}, \quad i = 1,\ldots,n, \quad j = 1,\ldots,n_a, \\ v_{ij+n_a}(r) &= \frac{1}{2}\left[u_{ij}(r) + u_{ij+n_a}(r)\right] \\ &\underset{r\to\infty}{\sim} \cos\theta_i\delta_{ij}, \quad i = 1,\ldots,n, \quad j = 1,\ldots,n_a. \end{aligned} \tag{F.17}$$

If n_b channels are closed, we must also define n_b solutions of (F.1) satisfying decaying wave boundary conditions by the equation

$$u_{ij+n_a}(r) = \exp(-\phi_j)\sum_{s=0}^{\infty} c^s_{ij+n_a} r^{-s}, \quad i = 1,\ldots,n, \quad j = n_a+1,\ldots,n, \tag{F.18}$$

where ϕ_j is defined by

$$\phi_j = |k_j|r - \frac{z}{|k_j|}\ln(2|k_j|r), \quad j = n_a+1,\ldots,n. \tag{F.19}$$

The coefficient $c^s_{ij+n_a}$ in (F.18) satisfy recurrence relations obtained from (F.8) by setting

$$k_j = \mathrm{i}\kappa_j, \quad j = n_a+1,\ldots,n, \tag{F.20}$$

where in the closed channels k_j is positive imaginary. Hence we obtain the recurrence relations

$$\begin{aligned} &(k_i^2 - k_j^2)c^s_{ij} + 2\kappa_j(s-1)c^{s-1}_{ij} + \left[(s-1)(s-2) + \frac{z^2}{\kappa_j^2} - \frac{z}{\kappa_j}(2s-3)\right]c^{s-2}_{ij} \\ &-\ell_i(\ell_i+1)c^{s-2}_{ij} - 2\sum_{i'=1}^{n}\sum_{\lambda=1}^{\lambda_{\max}}\alpha_{ii'\lambda}c^{s-\lambda-1}_{i'j} = 0, \quad i = 1,\ldots,n, \\ &\qquad\qquad j = n_a+1,\ldots,n. \end{aligned} \tag{F.21}$$

We then determine n_b solutions for each $j = n_a+1,\ldots,n$ by setting

$$c^0_{ij+n_a} = \delta_{ij} \quad i = 1,\ldots,n, \quad j = n_a+1,\ldots,n, \tag{F.22}$$

and

$$c^s_{ij+n_a} = 0, \quad s < 0, \quad i = 1,\ldots,n, \quad j = n_a+1,\ldots,n. \tag{F.23}$$

This enables the n_b decaying wave solutions to be calculated by determining the remaining coefficients from the recurrence relations. It follows that the $n_b = n - n_a$ solutions of (F.1) defined in this way satisfy the boundary conditions

$$v_{ij+n_a}(r) = u_{ij+n_a}(r) \underset{r\to\infty}{\sim} \exp(-\phi_j)\delta_{ij}, \quad i = 1,\ldots,n, \quad j = n_a+1,\ldots,n. \tag{F.24}$$

The $n+n_a$ asymptotic solutions defined by (F.17) and (F.24) are the complete set of solutions which enable the K-matrix to be determined from the R-matrix at $r = a_p$, as discussed in Sect. 5.1.4. Since expansions (F.4), (F.12) and (F.18) are asymptotic (see, for example, Whittaker and Watson [964]) their accuracy is limited by the value of r at which they are evaluated, and for each r there is an optimum number of terms $s_{\max}+1$ which can be included in the expansions for the highest accuracy to be obtained. In practice, there are several circumstances where the required accuracy can only be obtained by taking very large values for the radius a_p in Fig. 5.1 where the expansions are evaluated. These circumstances are as follows:

i. when one of the coefficients $(k_i^2 - k_j^2)$ multiplying one of the first terms in (F.8) or (F.21) is very small. This occurs when two almost degenerate channels are coupled by the long-range potential matrix. This becomes increasingly likely as the complexity of the target atom or ion increases, necessitating the inclusion of many channel functions in the expansion of the total wave function to obtain accurate results. However, if the channels are degenerate, which occurs, for example, in electron scattering by H-like ions, or when several angular momenta are coupled to a single target state, then the corresponding coefficients in (F.8) or (F.21) vanish and this difficulty does not arise. In practice, it is often convenient to adjust the energies of the channels that are almost degenerate making them exactly degenerate, so avoiding this cause of the rapid divergence of the asymptotic expansion;
ii. when one of the coefficients $2k_j(s-1)$ or $2\kappa_j(s-1)$ multiplying one of the second terms in (F.8) or (F.21) is very small and the corresponding first term in (F.8) or (F.21) vanishes. This occurs when the momentum k_j or κ_j of the scattered electron in the relevant channel is small and hence the channel energy is close to threshold. Again this becomes increasingly likely as the complexity of the target increases and hence the thresholds become increasingly dense in the energy region of interest;
iii. when the value of η_j or one or more of the orbital angular momenta ℓ_i in (F.8) or (F.21) are large;
iv. when one or more of the long-range multipole moment coefficients $\alpha_{ii'\lambda}$ in (F.8) or (F.21) are large.

Several procedures have been suggested to overcome these difficulties which lead to a rapid divergence of the asymptotic expansions. Norcross and Seaton [694] and Norcross [693] suggested that the terms $\exp(\pm i\theta_j)$ and $\exp(-\phi_j)$ in expansions (F.4), (F.12) and (F.18) should be replaced by appropriate Coulomb functions calculated using an iterated WKB approximation. This leads to values of the radius a_p which remain finite in the limit k_j or κ_j tends to zero. However, expansions (F.4), (F.12) and (F.18) become more accurate than the iterated WKB approximation as the energy moves away from threshold and are more easy to apply. We therefore

limit our discussion here to considering extensions of expansions (F.4), (F.12) and (F.18) suggested by Gailitis [356] which overcome some of the above-mentioned difficulties and are relatively easy to apply.

Gailitis [356] replaced the asymptotic expansion (F.4) by the asymptotic expansion

$$u_{ij}(r) = \left[G_{\ell_j}(\eta_j, k_j r) + \mathrm{i}F_{\ell_j}(\eta_j, k_j r)\right] \sum_{s=0}^{\infty} d_{ij}^s r^{-s}, \quad i = 1, \ldots, n, \quad j = 1, \ldots, n_a, \tag{F.25}$$

where $F_{\ell_j}(\eta_j, k_j r)$ and $G_{\ell_j}(\eta_j, k_j r)$ are the regular and irregular Coulomb wave functions which are defined by (1.58) and (1.59). These functions have been carefully studied by many workers (e.g. Abramowitz and Stegun [1]), and algorithms and computer programs have been developed by Barnett [53], Seaton [862] and Noble [686] to accurately calculate these functions for all relevant values of ℓ_j, η_j and $k_j r$. Hence, in order to apply expansion (F.25), it is only necessary to derive recurrence relations for the coefficients d_{ij}^s.

In order to obtain these recurrence relations, we first derive an asymptotic expansion for the Coulomb wave functions in (F.25). We write

$$G_{\ell_j}(\eta_j, k_j r) + \mathrm{i}F_{\ell_j}(\eta_j, k_j r) = \exp(\mathrm{i}\theta_j) \sum_{s=0}^{\infty} b_j^s r^{-s}, \tag{F.26}$$

where θ_j is defined by (F.5). Substituting expansion (F.26) into the Coulomb wave equation (1.56) and equating the coefficient of $r^{-s}\exp(\mathrm{i}\theta_j)$ to zero gives the recurrence relations

$$2\mathrm{i}k_j s b_j^s - [s(s-1) - \eta_j^2 + \mathrm{i}\eta_j(2s-1) - \ell_j(\ell_j+1)]b_j^{s-1} = 0. \tag{F.27}$$

It follows that if we set

$$b_j^0 = 1, \quad b_j^s = 0, \quad s < 0, \tag{F.28}$$

then the recurrence relations (F.27) enable us to determine the remaining coefficients

$$b_j^s, \quad 1 < s \leq s_{\max}, \tag{F.29}$$

where again $s_{\max}$ is some suitably chosen maximum value of s in expansion (F.26). We now substitute (F.26) into (F.25) to yield

$$u_{ij}(r) = \exp(\mathrm{i}\theta_j) \sum_{s=0}^{\infty} \sum_{s'=0}^{\infty} b_j^s d_{ij}^{s'} r^{-s-s'}. \tag{F.30}$$

Comparing this expansion with expansion (F.4) we find the following relation between the expansion coefficients

$$c_{ij}^{s} = \sum_{s'=0}^{s} b_j^{s-s'} d_{ij}^{s'}. \tag{F.31}$$

Remembering from (F.28) that $b_j^0 = 1$ and re-arranging (F.31) we obtain the following recurrence relations for the coefficients d_{ij}^s

$$d_{ij}^{s} = c_{ij}^{s} - \sum_{s'=0}^{s-1} b_j^{s-s'} d_{ij}^{s'}, \quad s = 0,\ 1, \ldots. \tag{F.32}$$

Since we can determine the coefficients c_{ij}^s for $s \geq 0$ from the recurrence relations (F.8) and (F.10), and we can determine the coefficients b_j^s for $s \geq 0$ from the recurrence relations (F.27) and (F.28), (F.32) can be solved to yield the coefficients d_{ij}^s for $s \geq 0$. In a similar way we can determine asymptotic expansions satisfying ingoing wave boundary conditions defined by (F.12).

Gailitis [356] also considered two further expansions with the form

$$u_{ij}(r) = R_{\ell_j}(r) \sum_{s=0}^{\infty} \alpha_{ij}^{s} r^{-s} + \dot{R}_{\ell_j}(r) \sum_{s=0}^{\infty} \beta_{ij}^{s} r^{-s} \tag{F.33}$$

with

$$\dot{R}_{\ell_j}(r) = \frac{1}{k_j} \frac{\mathrm{d}R_{\ell_j}}{\mathrm{d}r} \tag{F.34}$$

and

$$u_{ij}(r) = R_{\ell_j}(r) \sum_{s=0}^{\infty} \gamma_{ij}^{s} r^{-s} + R_{\ell_j+1}(r) \sum_{s=0}^{\infty} \delta_{ij}^{s} r^{-s}. \tag{F.35}$$

In (F.33) and (F.35) we may use any solution of the Coulomb wave equation (1.56) as the function $R_{\ell_j}(r)$. Recurrence relations can then be derived for the coefficients α_{ij}^s and β_{ij}^s and for the coefficients γ_{ij}^s and δ_{ij}^s which have a similar form to (F.8) and (F.21). However, expansion (F.25) has the most acceptable form, since it contains only Coulomb functions for the channels under investigation, and has therefore been most widely used.

The advantage of the asymptotic expansions proposed by Gailitis compared with expansions (F.4), (F.12) and (F.18) can be easily seen. By examining (F.8) we see that the radius a_p where the asymptotic expansion gives an accurate result depends on, amongst other factors, the value of $\eta_j = -z/k_j$. If either z becomes large or k_j becomes small then the asymptotic expansion diverges rapidly for small a_p. By including the Coulomb wave function exactly in (F.25), (F.33) and (F.35) this cause

of rapid divergence is removed. The Gailitis expansion also avoids the divergence problems that arise when the orbital angular momentum ℓ_i becomes large.

In spite of these advantages, the expansions proposed by Gailitis can still diverge rapidly when two or more channels which are strongly coupled by the long-range potential are almost degenerate or when the channel energy lies very close to a threshold. These difficulties can be partially alleviated by rewriting the asymptotic expansion as a continued fraction as suggested by Noble and Nesbet [687], corresponding to the use of Padé approximants (e.g. see the monograph by Baker and Gammel [42]). However, difficulties still arise as the complexity of the target increases giving rise to many closely coupled channels. Hence large values of a_p often have to be used to obtain accurate results in such situations.

F.2 Multiphoton Processes

In this section we derive asymptotic expansion solutions of the coupled second-order differential equations (9.79) which arise in R-matrix–Floquet theory of multiphoton ionization and laser-assisted electron–atom and electron–ion collisions when the velocity gauge is adopted in the asymptotic region. These equations, first discussed by Dörr et al. [264], which we assume are n in number, take the following general form

$$\left(\frac{\mathrm{d}^2}{\mathrm{d}r^2} + 2\mathrm{i}\mathbf{d}\frac{\mathrm{d}}{\mathrm{d}r} + \mathbf{W}(r)\right)\mathbf{G}(r) = 0, \tag{F.36}$$

where $\mathbf{d}$ is a real, diagonal matrix and $\mathbf{W}(r)$ is a potential matrix, which following (9.82) can be written as a summation in inverse powers of r as

$$\mathbf{W}(r) = \sum_{\lambda=0}^{\lambda_{\max}} \mathbf{W}_\lambda r^{-\lambda}. \tag{F.37}$$

In (F.37) $\lambda_{\max}$ is determined by the angular momentum triangular relations satisfied by the potential $\mathbf{V}(r)$ in (9.61). We find that $\mathbf{W}_0$ is hermitian if the energy $E^{\mathbf{V}}$ in (9.62) is real, corresponding to laser-assisted electron–atom collisions, and is non-hermitian if $E^{\mathbf{V}}$ is complex, corresponding to multiphoton ionization. Also, the matrices $\mathbf{W}_\lambda$, $\lambda \geq 1$, do not depend on $E^{\mathbf{V}}$ and are hermitian.

We now define $2n$ linearly independent solutions of (F.36), for $r \geq a_p$ in Fig. 9.1, satisfying the following asymptotic expansion

$$\mathbf{G}_j(r) = \sum_{s=0}^{\infty} r^{-s} \exp\left(\mathrm{i}p_j r + \mathrm{i}\frac{Z_j}{p_j}\ln 2p_j r\right)\mathbf{A}_j^s, \quad j = 1, \ldots, 2n, \tag{F.38}$$

where the vector coefficients $\mathbf{A}_j^s$ for $s \geq 1$, each of which has n components, can be determined from recurrence relations which we derive below. Also, we will see that

the effective momenta p_j and effective charge numbers Z_j in (F.38) are determined from the requirement that the recurrence relations are self-consistent.

Substituting expansion (F.38) into (F.36) and equating the coefficients of the terms $r^{-s}\exp[\mathrm{i}p_j r + \mathrm{i}Z_j \ln(2p_j r)/p_j]$ to zero gives the following recurrence relations:

$$\left[-p_j^2 - 2\mathbf{d}p_j + \mathbf{W}_0\right]\mathbf{A}_j^s + \left[-2(\mathbf{d}+p_j)\frac{Z_j}{p_j} - 2\mathrm{i}(\mathbf{d}+p_j)(s-1) + \mathbf{W}_1\right]\mathbf{A}_j^{s-1} + \left[(s-1)(s-2) - \mathrm{i}\frac{Z_j}{p_j}(2s-3) - \frac{Z_j^2}{p_j^2} + \mathbf{W}_2\right]\mathbf{A}_j^{s-2} + \sum_{\lambda=3}^{\lambda_{\max}} \mathbf{W}_\lambda \mathbf{A}_j^{s-\lambda} = 0, \quad s = 0,\ 1,\ 2, \ldots, \quad j = 1, \ldots, 2n, \tag{F.39}$$

where we set

$$\mathbf{A}_j^s = 0, \quad s < 0, \quad j = 1, \ldots, 2n. \tag{F.40}$$

We now consider the solution of the recurrence relations (F.39) for $s = 0, 1, 2, \ldots$ in turn.

We consider first the solution of (F.39) when $s = 0$. In this case (F.39) reduces to n coupled equations for the n components of $\mathbf{A}_j^0$

$$\left[p_j^2 + 2\mathbf{d}p_j - \mathbf{W}_0\right]\mathbf{A}_j^0 = 0, \quad j = 1, \ldots, 2n, \tag{F.41}$$

which we rewrite as

$$\mathbf{L}_j \mathbf{A}_j^0 = 0, \quad j = 1, \ldots, 2n, \tag{F.42}$$

defining the $n \times n$-dimensional matrix $\mathbf{L}_j$. Equations (F.42) are a set of n linear simultaneous equations for each j which will have non-trivial solutions when

$$\det \mathbf{L}_j = 0. \tag{F.43}$$

Expanding the determinant of $\mathbf{L}_j$ then yields an algebraic equation of order $2n$ in p_j which will, in general, have $2n$ solutions

$$p_j, \quad j = 1, \ldots, 2n. \tag{F.44}$$

If $\mathbf{W}_0$ in (F.41) is hermitian, corresponding to laser-assisted electron–atom collisions, then the solutions p_j of (F.43) occur in real pairs or in complex conjugate pairs p_j and p_j^* or in some combination of real and complex conjugate pairs. On the other hand, if $\mathbf{W}_0$ is non-hermitian, corresponding to multiphoton ionization, the

solutions p_j of (F.43) will in general be complex with no special relation between the $2n$ values.

Having determined the $n \times n$-dimensional matrices $\mathbf{L}_j,\ j = 1, \ldots, 2n$, we now determine the corresponding eigenvalues and eigenvectors defined by

$$\mathbf{L}_j \mathbf{y}_{ij} = \lambda_{ij} \mathbf{y}_{ij}, \quad i = 1, \ldots, n, \tag{F.45}$$

where this equation and the following analysis are repeated for each $j = 1, \ldots, 2n$. Equation (F.45) defines a complete set of n eigenvalues $\lambda_{ij},\ i = 1, \ldots, n$, and n eigenvectors $\mathbf{y}_{ij},\ i = 1, \ldots, n$, for each j. It follows from (F.43) that one of these eigenvalues must be zero. We order the n eigenvalues and the corresponding eigenvectors so that the equation with the zero eigenvalue occurs first. Hence

$$\mathbf{L}_j \mathbf{y}_{1j} = 0, \tag{F.46}$$

where $\lambda_{1j} = 0$. By comparing (F.42) and (F.46) we see that the required solutions $\mathbf{A}_j^0$ of (F.42) are the eigensolutions $\mathbf{y}_{1j}$ corresponding to the zero eigenvalue of $\mathbf{L}_j$. We will also see that in order to solve the recurrence relations (F.39) for $s \geq 1$ we will need to determine the complete set of n eigenvalues and eigenvectors of $\mathbf{L}_j$ for each $j = 1, \ldots, 2n$.

In order to determine the n eigenvalues and eigenvectors of $\mathbf{L}_j$, we observe that if $\mathbf{W}_0$ is hermitian and p_j is real then the corresponding matrix $\mathbf{L}_j$ will be hermitian so that $\mathbf{L}_j = \mathbf{L}_j^\dagger$. Hence in this case, the eigenvectors $\mathbf{y}_{ij}$ of $\mathbf{L}_j$, defined by (F.45), belong to real eigenvalues $\lambda_{ij},\ i = 1, \ldots, n$. Taking the hermitian conjugate of (F.45) then gives

$$\mathbf{y}_{ij}^\dagger \mathbf{L}_j = \lambda_{ij} \mathbf{y}_{ij}^\dagger, \quad i = 1, \ldots, n. \tag{F.47}$$

It follows that when $\mathbf{L}_j$ is hermitian the right eigenvectors of $\mathbf{L}_j$ defined by (F.45) and the left eigenvectors of $\mathbf{L}_j$ defined by (F.47) are identical and can be chosen to satisfy the orthonormality relation

$$\mathbf{y}_{ij}^\dagger \mathbf{y}_{kj} = \delta_{ik}, \quad i,\ k = 1, \ldots, n. \tag{F.48}$$

On the other hand, if $\mathbf{W}_0$ is not hermitian or p_j is not real then $\mathbf{L}_j$ will not be hermitian. The eigenvalues λ_{ij} of $\mathbf{L}_j$ will then in general be complex, except the first λ_{1j} defined by (F.46) which is zero. If the eigenvalues of $\mathbf{L}_j$ are written as

$$\lambda_{1j},\ \lambda_{2j}, \ldots, \lambda_{nj}, \tag{F.49}$$

then the corresponding eigenvalues of $\mathbf{L}_j^\dagger$ are

$$\lambda_{1j}^*,\ \lambda_{2j}^*, \ldots,\ \lambda_{nj}^*. \tag{F.50}$$

The right eigenvectors $\mathbf{y}_{ij}$ of $\mathbf{L}_j$ belonging to the eigenvalues λ_{ij} are then defined by (F.45), and the left eigenvectors $\mathbf{x}_{ij}$ of $\mathbf{L}_j^\dagger$ belonging to the eigenvalues λ_{ij}^* are defined by

$$\mathbf{L}_j^\dagger \mathbf{x}_{ij} = \lambda_{ij}^* \mathbf{x}_{ij}, \quad i = 1, \ldots, n. \tag{F.51}$$

We now multiply (F.45) on the left by $\mathbf{x}_{kj}^\dagger$ and multiply the hermitian conjugate of (F.51) on the right by $\mathbf{y}_{kj}$. We then find after subtracting these results that

$$(\lambda_{ij} - \lambda_{kj})\mathbf{x}_{kj}^\dagger \mathbf{y}_{ij} = 0, \quad i,\ k = 1, \ldots, n. \tag{F.52}$$

Hence the eigenvectors of $\mathbf{L}_j$ and $\mathbf{L}_j^\dagger$ belonging to different pairs of eigenvalues, given by (F.49) and (F.50), are orthogonal. Also, if two or more eigenvalues in (F.49) and hence in (F.50) are identical, then the corresponding eigenvectors belonging to these eigenvalues can be chosen to be orthogonal.

Finally, if $\mathbf{U}_j$ is the $n \times n$-dimensional matrix whose columns are the n left eigenvectors $\mathbf{x}_{ij}$, $i = 1, \ldots, n$, and $\mathbf{V}_j$ is the $n \times n$-dimensional matrix whose columns are the n right eigenvectors $\mathbf{y}_{ij}$, $i = 1, \ldots, n$, then it follows from the above analysis that

$$\mathbf{U}_j^\dagger \mathbf{L}_j \mathbf{V}_j = \mathbf{\Lambda}_j, \tag{F.53}$$

where $\mathbf{\Lambda}_j$ is a diagonal matrix with diagonal elements λ_{ij}, $i = 1, \ldots, n$.

We consider next the solution of (F.39) when $s = 1$. In this case the recurrence relations (F.39) reduce to

$$\left[-p_j^2 - 2\mathbf{d}p_j + \mathbf{W}_0\right]\mathbf{A}_j^1 + \left[-2(\mathbf{d} + p_j)\frac{Z_j}{p_j} + \mathbf{W}_1\right]\mathbf{A}_j^0 = 0, \quad j = 1, \ldots, 2n, \tag{F.54}$$

which is a set of n linear simultaneous equations for the n components of the vector $\mathbf{A}_j^1$, $j = 1, \ldots, 2n$. We rewrite these equations as

$$\mathbf{L}_j \mathbf{A}_j^1 = \mathbf{M}_j \mathbf{A}_j^0, \tag{F.55}$$

where $\mathbf{L}_j$ is defined by (F.41) and (F.42) and

$$\mathbf{M}_j = -2(\mathbf{d} + p_j)\frac{Z_j}{p_j} + \mathbf{W}_1, \tag{F.56}$$

and where these equations and the following analysis are repeated for each $j = 1, \ldots, 2n$. In order to solve (F.55) we expand $\mathbf{A}_j^1$ in terms of the complete set of right eigenvectors of $\mathbf{L}_j$, defined by (F.45), as follows:

$$\mathbf{A}_j^1 = \sum_{i=1}^{n} \mathbf{y}_{ij} c_{ij}^1. \tag{F.57}$$

Substituting expansion (F.57) into (F.55) then gives

$$\sum_{i=2}^{n} \mathbf{L}_j \mathbf{y}_{ij} c_{ij}^1 = \mathbf{M}_j \mathbf{A}_j^0, \tag{F.58}$$

where we have used (F.46) to eliminate the $i = 1$ term in this expansion. We then project this expansion onto the n left eigenvectors $\mathbf{x}_{kj},\ k = 1, \ldots, n$ of $\mathbf{L}_j$, defined by (F.51), giving

$$\sum_{i=2}^{n} \mathbf{x}_{kj}^\dagger \mathbf{L}_j \mathbf{y}_{ij} c_{ij}^1 = \mathbf{x}_{kj}^\dagger \mathbf{M}_j \mathbf{A}_j^0, \quad k = 1, \ldots, n. \tag{F.59}$$

This is a set of n linear simultaneous equations in $n - 1$ coefficients $c_{ij}^1,\ i = 2, \ldots, n$, and the effective charge number Z_j in $\mathbf{M}_j$ defined by (F.56). In order to solve these equations we observe that since the first eigenvalue λ_{1j} of $\mathbf{L}_j$ is zero, it follows from (F.51) that

$$\mathbf{x}_{1j}^\dagger \mathbf{L}_j = 0. \tag{F.60}$$

Hence the left-hand side of the first equation in (F.59) corresponding to $k = 1$ is zero. It follows that the right-hand side of the first equation in (F.59) is zero, i.e.

$$\mathbf{x}_{1j}^\dagger \mathbf{M}_j \mathbf{A}_j^0 = 0, \tag{F.61}$$

which enables Z_j, which is the only unknown in this equation, to be determined. Using this value of Z_j the remaining $n - 1$ equations in (F.59) corresponding to $k = 2, \ldots, n$ can be solved to yield the coefficients $c_{ij}^1,\ i = 2, \ldots, n$.

It follows from this analysis that we have determined all the components of $\mathbf{A}_j^1$, defined by (F.57), except the component $\mathbf{y}_{1j}$ with coefficient c_{1j}^1. This component will be determined below by considering the recurrence relation (F.39) when $s = 2$.

We consider next the solution of (F.39) when $s = 2$. In this case the recurrence relations (F.39) reduce to

$$\left[-p_j^2 - 2\mathbf{d}p_j + \mathbf{W}_0\right]\mathbf{A}_j^2 + \left[-2(\mathbf{d} + p_j)\frac{Z_j}{p_j} - 2\mathrm{i}(\mathbf{d} + p_j) + \mathbf{W}_1\right]\mathbf{A}_j^1$$
$$+ \left[-\mathrm{i}\frac{Z_j}{p_j} - \frac{Z_j^2}{p_j^2} + \mathbf{W}_2\right]\mathbf{A}_j^0 = 0, \quad j = 1, \ldots, 2n, \tag{F.62}$$

which is a set of n linear simultaneous equations for $\mathbf{A}_j^2,\ j = 1, \ldots, 2n$. In analogy with (F.57) we expand $\mathbf{A}_j^2$ as follows:

$$\mathbf{A}_j^2 = \sum_{i=1}^{n} \mathbf{y}_{ij} c_{ij}^2, \tag{F.63}$$

where this equation and the following analysis is repeated for each $j = 1, \ldots, 2n$. We then project (F.62) onto the first left eigenvector $\mathbf{x}_{1j}$ of $\mathbf{L}_j$ and use the result that

$$\mathbf{x}_{1j}^\dagger \left[-p_j^2 - 2\mathbf{d} p_j + \mathbf{W}_0 \right] = -\mathbf{x}_{1j}^\dagger \mathbf{L}_j = 0, \tag{F.64}$$

which follows from (F.60). We obtain

$$\sum_{i=1}^{n} \mathbf{x}_{1j}^\dagger \left[-2(\mathbf{d} + p_j) - 2\mathrm{i}(\mathbf{d} + p_j) + \mathbf{W}_1 \right] \mathbf{y}_{ij} c_{ij}^1 = \mathbf{x}_{1j}^\dagger \left[\mathrm{i}\frac{Z_j}{p_j} + \frac{Z_j^2}{p_j^2} - \mathbf{W}_2 \right] \mathbf{A}_j^0. \tag{F.65}$$

Since we have calculated the coefficients $c_{ij}^1,\ i = 2, \ldots, n$, by solving (F.59), the only unknown in (F.65) is c_{1j}^1 which can now be determined. Hence all the terms on the right-hand side of (F.57) have been calculated and $\mathbf{A}_j^1$ is now known.

We next project (F.62) onto the left eigenvectors $\mathbf{x}_{kj},\ k = 2, \ldots, n$ giving

$$\sum_{i=2}^{n} \mathbf{x}_{kj}^\dagger \mathbf{L}_j \mathbf{y}_{ij} c_{ij}^2 = \mathbf{x}_{kj}^\dagger \left[-2(\mathbf{d} + p_j) - 2\mathrm{i}(\mathbf{d} + p_j) + \mathbf{W}_1 \right] \mathbf{A}_j^1 + \mathbf{x}_{kj}^\dagger \left[-\mathrm{i}\frac{Z_j}{p_j} - \frac{Z_j^2}{p_j^2} + \mathbf{W}_2 \right] \mathbf{A}_j^0, \quad k = 2, \ldots, n. \tag{F.66}$$

This is a set of $n - 1$ linear simultaneous equations in $n - 1$ coefficients c_{ij}^2, $i = 2, \ldots, n$, which can be solved to yield the values of these coefficients. Hence we have determined all the components of $\mathbf{A}_j^2$, defined by (F.63), except the component $\mathbf{y}_{1j}$ with coefficient c_{1j}^2. This component can be determined by considering the recurrence relation (F.39) when $s = 3$ in a similar way to our determination of c_{1j}^1 considered above.

We consider last the solution of (F.39) when $s \geq 3$. In this case we expand $\mathbf{A}_j^s$ as follows:

$$\mathbf{A}_j^s = \sum_{i=1}^{n} \mathbf{y}_{ij} c_{ij}^s, \tag{F.67}$$

where this equation and the following analysis is repeated for each $j = 1, \ldots, 2n$. We project (F.39) onto $\mathbf{x}_{1j}$ yielding the expansion coefficient c_{ij}^{s-1}, and we project (F.39) onto $\mathbf{x}_{kj}$, $k = 2, \ldots, n$, yielding $n - 1$ linear simultaneous equations whose solution yields c_{kj}^{s}, $k = 2, \ldots, n$.

In summary the recurrence relations (F.39) enable the coefficients $\mathbf{A}_j^s$, $0 \leq s \leq s_{\max}$ to be determined, where $s_{\max}$ is some suitably chosen maximum value of the expansion index s in (F.38), yielding $\mathbf{G}_j(r)$ on the boundary $r = a_p$. This procedure is repeated for each $j = 1, \ldots, 2n$ yielding the complete set of $2n$ solutions of the coupled second-order differential equations (F.36). Appropriate linear combinations of these solutions yield the physically required solutions corresponding to laser-assisted electron–atom collisions or multiphoton ionization, as discussed in Sect. 9.1.4.

Finally we observe that, as discussed in Sect. F.1, since expansion (F.38) is asymptotic, its accuracy is limited by the value of $r = a_p$ at which it is evaluated. For each a_p there is a related number of terms $s_{\max}$ which should be retained in the expansion to obtain the maximum accuracy. This difficulty can be partially alleviated by rewriting the asymptotic expansion as a continued fraction, as mentioned in Sect. F.1. However, in general, if higher accuracy is required then the coupled second-order differential equations (9.61) must be integrated out to a larger value of a_p as described in Sect. 9.1.3.

References

1. M. Abramowitz, I.A. Stegun (eds.), *Handbook of Mathematical Functions* (Dover Publications, New York, NY, 1965)
2. K.M. Aggarwal, K.A. Berrington, P.G. Burke, A.E. Kingston, A. Pathak, J. Phys. B At. Mol. Opt. Phys. **24**, 1385 (1991)
3. K.M. Aggarwal, F.P. Keenan, A.Z. Msezane, J. Phys. B At. Mol. Opt. Phys. **34**, L757 (2001)
4. P. Agostini, L.F. DiMauro, Rep. Prog. Phys. **67**, 813 (2004)
5. K. Aiba, A. Igarashi, I. Shimamura, J. Phys. B At. Mol. Opt. Phys. **40**, F9 (2007)
6. S. Ait-Tahar, I.P. Grant, P.H. Norrington, Phys. Rev. A **54**, 3984 (1996)
7. A.I. Akhiezer, V.B. Berestetsky, *Quantum Electrodynamics* (Interscience, New York, NY, 1965)
8. M.H. Alexander, J. Chem. Phys. **81**, 4510 (1984)
9. M.H. Alexander, D.E. Manolopoulos, J. Chem. Phys. **86**, 2044 (1987)
10. M. Allan, J. Phys. B At. Mol. Phys. **18**, 4511 (1985)
11. M. Allan, J. Phys. B At. Mol. Opt. Phys. **25**, 1559 (1992)
12. M. Allan, K. Franz, H. Hotop, O. Zatsarinny, K. Bartschat, J. Phys. B At. Mol. Opt. Phys. **39**, L139 (2006)
13. D.C.S. Allison, P.G. Burke, W.D. Robb, J. Phys. B At. Mol. Phys. **5**, 55 (1972)
14. D.C.S. Allison, P.G. Burke, W.D. Robb, J. Phys. B At. Mol. Phys. **5**, 1431 (1972)
15. P.L. Altick, J. Phys. B At. Mol. Phys. **18**, 1841 (1985)
16. M.V. Ammosov, N.B. Delone, V.P. Krainov, Sov. Phys. JETP **64**, 1191 (1986)
17. N. Andersen, K. Bartschat, J. Phys. B At. Mol. Opt. Phys. **37**, 3809 (2004)
18. H. Anderson, C.P. Ballance, N.R. Badnell, H.P. Summers, J. Phys. B At. Mol. Opt. Phys. **33**, 1255, **35**, 1613 (2000)
19. D. Andrick, H. Ehrhardt, Zeits. f. Phys. **192**, 99 (1966)
20. S. Armitage, D.E. Leslie, A.J. Garner, G. Laricchia, Phys. Rev. Lett. **89**, 173402 (2002)
21. E.A.G. Armour, J. Phys. B At. Mol. Phys. **18**, 3361 (1985)
22. E.A.G. Armour, Phys. Rep. **169**, 1 (1988)
23. E.A.G. Armour, J.W. Humberston, Phys. Rep. **204**, 165 (1991)
24. R.L. Armstead, Phys. Rev. **171**, 91 (1968)
25. W.E. Arnoldi, Q. Appl. Math. **9**, 17 (1951)
26. A.M. Arthurs, A. Dalgarno, Proc. R. Soc. A **256**, 540 (1960)
27. L. Avaldi, R. Camilloni, R. Multari, G. Stefani, O. Robaux, R.J. Tweed, G.N. Vien, J. Phys. B At. Mol. Opt. Phys. **31**, 2981 (1998)
28. M. Aymar, C.H. Greene, E. Luc-Koenig, Rev. Mod. Phys. **68**, 1015 (1996)
29. H. Bachau, E. Cormier, P. Decleva, J.E. Hansen, F. Martin, Rep. Prog. Phys. **64**, 1815 (2001)
30. N.R. Badnell, J. Phys. B At. Mol. Opt. Phys. **19**, 3827 (1986)
31. N.R. Badnell, J. Phys. B At. Mol. Opt. Phys. **30**, 1 (1997)
32. N.R.Badnell, J. Phys. B At. Mol. Opt. Phys. **41**, 175202 (2008)
33. N.R. Badnell, T.W. Gorczyca, J. Phys. B At. Mol. Opt. Phys. **30**, 2011 (1997)

P.G. Burke, *R-Matrix Theory of Atomic Collisions*, Springer Series on Atomic, Optical, and Plasma Physics 61, DOI 10.1007/978-3-642-15931-2,

34. N.R. Badnell, D.C. Griffin, J. Phys. B At. Mol. Opt. Phys. **32**, 2267 (1999)
35. N.R. Badnell, M.J. Seaton, J. Phys. B At. Mol. Opt. Phys. **36**, 4367 (2003)
36. N.R. Badnell, T.W. Gorczyca, A.D. Price, J. Phys. B At. Mol. Opt. Phys. **31**, L239 (1998)
37. N.R. Badnell, K.A. Berrington, H.P. Summers, M.G. O'Mullane, A.D. Whiteford, C.P. Ballance, J. Phys. B At. Mol. Opt. Phys. **37**, 4589 (2004)
38. N.R. Badnell, M.A. Bautista, K. Butler, F. Delahaye, C. Mendoza, P. Palmeri, C.J. Zeippen, M.J. Seaton, Mon. Not. R. Astron. Soc. **360**, 458 (2005)
39. M. Baertschy, T.N. Rescigno, W.A. Isaacs, X. Lin, C.W. McCurdy, Phys. Rev. A **63**, 022712 (2001)
40. M. Baertschy, T.N. Rescigno, W.A. Isaacs, X. Lin, C.W. McCurdy, Phys. Rev. A. **64**, 022709 (2001)
41. J.N. Bahcall, Astrophys. J. **153**, 679 (1968)
42. G.A. Baker Jr., J.L. Gammel (eds.) *The Padé Approximant in Theoretical Physics* (Academic Press, New York, NY and London, 1970)
43. C.P. Ballance, D.C. Griffin, J. Phys. B At. Mol. Opt. Phys. **37**, 2943 (2004)
44. C.P. Ballance, D.C. Griffin, J. Phys. B At. Mol. Opt. Phys. **39**, 3617 (2006)
45. C.P. Ballance, N.R. Badnell, E.S. Smyth, J. Phys. B At. Mol. Opt. Phys. **36**, 3707 (2003)
46. K.L. Baluja, P.G. Burke, A.E. Kingston, J. Phys. B At. Mol. Phys. **13**, L543 (1980)
47. K.L. Baluja, P.G. Burke, L.A. Morgan, Comput. Phys. Commun. **27**, 299 (1982)
48. K.L. Baluja, A. Hibbert, M. Mohan, J. Phys. B At. Mol. Phys. **19**, 3613 (1986)
49. K.L. Baluja, R. Zhang, J. Franz, J. Tennyson, J. Phys. B At. Mol. Opt. Phys. **40**, 3515 (2007)
50. A.D. Bandrauk (ed.) *Molecules in Laser Fields* (Dekker, New York, NY, 1994)
51. A.D. Bandrauk, E.E. Aubanel, J.-J. Gauthier, in *Molecules in Laser Fields*, ed. by A.D. Bandrauk (Dekker, New York, NY, 1994), p. 109
52. V. Bargmann, Rev. Mod. Phys. **21**, 488 (1949)
53. A.R. Barnett, Comput. Phys. Commun. **21**, 297 (1980)
54. R.F. Barrett, L.C. Biedenharn, M. Danos, P. Delsanto, W. Greiner, H.G. Wahsweiler, Rev. Mod. Phys. **45**, 44 (1973)
55. R.F. Barrett, B.A. Robson, W. Tobocman, Rev. Mod. Phys. **55**, 155 (1983)
56. A. Bar-Shalom, M. Klapisch, Comput. Phys. Commun. **50**, 375 (1988)
57. P.L. Bartlett, PhD Thesis, Murdoch University, Perth, Western Australia, 2005
58. P.L. Bartlett, J. Phys. B At. Mol. Opt. Phys. **39**, R379 (2006)
59. P.L. Bartlett, A.T. Stelbovics, Phys. Rev. Lett. **93**, 233201 (2004)
60. P.L. Bartlett, A.T. Stelbovics, Phys. Rev. A **69**, 040701 (R) (2004)
61. P.L. Bartlett, A.T. Stelbovics, I. Bray, J. Phys. B At. Mol. Opt. Phys. **37**, L69 (2004)
62. K. Bartschat, Comput. Phys. Commun. **75**, 219 (1993)
63. K. Bartschat, Phys. Rev. A **71**, 032718 (2005)
64. K. Bartschat, P.G. Burke, Comput. Phys. Commun. **41**, 75 (1986)
65. K. Bartschat, P.G. Burke, J. Phys. B At. Mol. Phys. **20**, 3191 (1987)
66. K. Bartschat, P.G. Burke, J. Phys. B At. Mol. Opt. Phys. **21**, 2969 (1988)
67. K. Bartschat, I. Bray, J. Phys. B At. Mol. Opt. Phys. **29**, L577 (1996)
68. K. Bartschat, A.N. Grum-Grzhimailo, J. Phys. B At. Mol. Opt. Phys. **35**, 5035 (2002)
69. K. Bartschat, R.H.G. Reid, P.G. Burke, H.P. Summers, J. Phys. B At. Mol. Opt. Phys. **23**, L721 (1990)
70. K. Bartschat, E.T. Hudson, M.P. Scott, P.G. Burke, V.M. Burke, J. Phys. B At. Mol. Opt. Phys. **29**, 115 (1996)
71. K. Bartschat, E.T. Hudson, M.P. Scott, P.G. Burke, V.M. Burke, Phys. Rev. A **54**, R998 (1996)
72. K. Bartschat, I. Bray, P.G. Burke, M.P. Scott, J. Phys. B At. Mol. Opt. Phys. **29**, 5493 (1996)
73. D.R. Bates, Planet. Space Sci. **9**, 77 (1962)
74. D.R. Bates, H.S.W. Massey, Philos. Trans. R. Soc. A **239**, 269 (1943)
75. D.R. Bates, A. Damgaard, Philos. Trans. R. Soc. A **242**, 101 (1949)
76. D.R. Bates, A. Dalgarno, in *Atomic and Molecular Processes*, ed. by D.R. Bates (Academic Press, New York, NY and London, 1962), p. 245

77. D.R. Bates, A. Fundaminsky, J.W. Leech, H.S.W. Massey, Philos. Trans. R. Soc. A **243**, 93 (1950)
78. M.A. Bautista, A.K. Pradhan, Astron. Astrophys. Suppl. **115**, 551 (1996)
79. M.A. Bautista, A.K. Pradhan, Astrophys. J. **492**, 650 (1998)
80. D. Baye, Nucl. Phys. A **627**, 305 (1997)
81. D. Baye, P.-H. Heenen, J. Phys. A Math. Gen. **19**, 2041 (1986)
82. D. Baye, M. Hesse, J.-M. Sparenberg, M. Vincke, J. Phys. B At. Mol. Opt. Phys. **31**, 3439 (1998)
83. I. Baz, Sov. Phys. JETP **9**, 1256 (1959)
84. A. Becker, F.H.M. Faisal, J. Phys. B At. Mol. Opt. Phys. **32**, L335 (1999)
85. W. Becker, S. Long, J.K. McIver, Phys. Rev. A **41**, 4112 (1990)
86. W. Becker, S. Long, J.K. McIver, Phys. Rev. A **50**, 1540 (1994)
87. K.L. Bell, P.G. Burke, A.E. Kingston, J. Phys. B At. Mol. Phys. **10**, 3117 (1977)
88. R.H. Bell, M.J. Seaton, J. Phys. B At. Mol. Phys. **18**, 1589 (1985)
89. O. Bely, Proc. Phys. Soc. **88**, 833 (1966)
90. M. Bentley, J. Phys. B At. Mol. Opt. Phys. **27**, 637 (1994)
91. R.O. Berger, L. Spruch, Phys. Rev. **138**, B1106 (1965)
92. K.A. Berrington, M.J. Seaton, J. Phys. B At. Mol. Phys. **18**, 2587 (1985)
93. K.A. Berrington, A.E. Kingston, J. Phys. B At. Mol. Phys. **20**, 6631 (1987)
94. K.A. Berrington, C.P. Ballance, J. Phys. B At. Mol. Opt. Phys. **35**, 2275 (2002)
95. K.A. Berrington, P.G. Burke, J.-J. Chang, A.T. Chivers, W.D. Robb, K.T. Taylor, Comput. Phys. Commun. **8**, 149 (1974)
96. K.A. Berrington, P.G. Burke, A.L. Sinfailam, J. Phys. B At. Mol. Phys. **8**, 1459 (1975)
97. K.A. Berrington, P.G. Burke, P.L. Dufton, A.E. Kingston, J. Phys. B At. Mol. Phys. **10**, 1465 (1977)
98. K.A. Berrington, P.G. Burke, M. Le Dourneuf, W.D. Robb, K.T. Taylor, Vo Ky Lan, Comput. Phys. Commun. **14**, 367 (1978)
99. K.A. Berrington, P.G. Burke, L.C.G. Freitas, A.E. Kingston, J. Phys. B At. Mol. Phys. **18**, 4135 (1985)
100. K.A. Berrington, P.G. Burke, K. Butler, M.J. Seaton, P.J. Storey, K.T. Taylor, Yu Yan, J. Phys. B At. Mol. Phys. **20**, 6379 (1987)
101. K.A. Berrington, P.G. Burke, A. Hibbert, M. Mohan, K.L. Baluja, J. Phys. B At. Mol. Opt. Phys. **21**, 339 (1988)
102. K.A. Berrington, W.B. Eissner, P.H. Norrington, Comput. Phys. Commun. **92**, 290 (1995)
103. K.A. Berrington, C.P. Ballance, D.C. Griffin, N.R. Badnell, J. Phys. B At. Mol. Opt. Phys. **38**, 1667 (2005)
104. H.A. Bethe, Phys. Rev. **76**, 38 (1949)
105. H.A. Bethe, E.E. Salpeter, *Quantum Mechanics of One- and Two-Electron Atoms* (Springer, Berlin, Göttingen, Heidelberg, 1957)
106. L.C. Biedenharn, J.M. Blatt, M.E. Rose, Rev. Mod. Phys. **24**, 249 (1952)
107. L.C. Biedenharn, H. van Dam, (eds.) *Quantum Theory of Angular Momentum* (Academic Press, New York, NY and London, 1965)
108. D.T. Birtwistle, A. Herzenberg, J. Phys. B At. Mol. Phys. **4**, 53 (1971)
109. P.K. Biswas, S.K. Adhikari, Phys. Rev. A **59**, 363 (1999)
110. J.D. Bjorken, S.D. Drell, *Relativistic Quantum Mechanics* (McGraw-Hill Book Co., New York, NY, 1964)
111. J.E. Blackwood, C.P. Campbell, M.T. McAlinden, H.R.J. Walters, Phys. Rev. A **60**, 4454 (1999)
112. J.E. Blackwood, M.T. McAlinden, H.R.J. Walters, Phys. Rev. A **65**, 030502 (2002)
113. J.E. Blackwood, M.T. McAlinden, H.R.J. Walters, Phys. Rev. A **65**, 032517 (2002)
114. J.E. Blackwood, M.T. McAlinden, H.R.J. Walters, J. Phys. B At. Mol. Opt. Phys. **35**, 2661 (2002)
115. J.M. Blatt, J.D. Jackson, Phys. Rev. **76**, 18 (1949)

116. J.M. Blatt, L.C. Biedenharn, Rev. Mod. Phys. **24**, 258 (1952)
117. J.M. Blatt, V.F. Weisskopf, *Theoretical Nuclear Physics* (Wiley, New York, NY, 1952)
118. C. Bloch, Nucl. Phys. **4**, 503 (1957)
119. K. Blum, *Density Matrix Theory and Applications*, 2nd edn. (Plenum Press, New York, NY and London, 1996)
120. K. Blum, P.G. Burke, J. Phys. B At. Mol. Phys. **8**, L410 (1975)
121. D. Bohm, *Quantum Theory* (Prentice-Hall, New York, NY, 1951), pp. 257–263
122. J. Bömmels, K. Franz, T.H. Hoffmann, A. Gopalan, O. Zatsarinny, K. Bartschat, M.-W. Ruf, H. Hotop, Phys. Rev. A **71**, 012704 (2005)
123. B.H. Bransden, *Atomic Collision Theory*, 2nd edn. (Benjamin/Cummins Publishing Company Inc., Reading, Mass., 1983)
124. S.J. Brawley, J. Beale, S. Armitage, D.E. Leslie, A. Kover, G. Laricchia, Nucl. Instrum. Methods B. **266**, 497 (2008)
125. I. Bray, J. Phys. B At. Mol. Phys. **28**, L247 (1995)
126. I. Bray, A.T. Stelbovics, Phys. Rev. Lett. **69**, 53 (1992)
127. I. Bray, A.T. Stelbovics, Phys. Rev. A **46**, 6996 (1992)
128. I. Bray, A.T. Stelbovics, Phys. Rev. Lett. **70**, 746 (1993)
129. I. Bray, A.T. Stelbovics, Adv. At. Mol. Opt. Phys. **35**, 209 (1995)
130. I. Bray, D.V. Fursa, A.S. Kheifets, A.T. Stelbovics, J. Phys. B At. Mol. Opt. Phys. **35**, R117 (2002)
131. G. Breit, Phys. Rev. **34**, 553 (1929)
132. G. Breit, Phys. Rev. **36**, 383 (1930)
133. G. Breit, Phys. Rev. **39**, 616 (1932)
134. G. Breit, in *Handbuch der Physik*, vol. 41/1, ed. by S. Flügge (Springer, Berlin, Göttingen, Heidelberg, 1959), p. 107
135. G. Breit, E.P. Wigner, Phys. Rev. **48**, 918 (1936)
136. G. Breit, H.A. Bethe, Phys. Rev. **93**, 888 (1954)
137. J.A. Brenig, R. Haag, Fortschr. Physik **7**, 183 (1959)
138. J.P. Briand, L. de Billy, P. Charles, S. Essabaa, P. Briand, J.-P. Desclaux, S. Bliman, C. Ristori, Phys. Rev. Lett. **65**, 159 (1990)
139. D.M. Brink, G.R. Satchler, *Angular Momentum*, 2nd edn. (Clarendon Press, Oxford, 1968)
140. G.E. Brown, Rev. Mod. Phys. **31**, 893 (1959)
141. J.N.H. Brunt, G.C. King, F.H. Read, J. Phys. B At. Mol. Phys. **9**, 2195 (1976)
142. J.N.H. Brunt, G.C. King, F.H. Read, J. Phys. B At. Mol. Phys. **10**, 3781 (1977)
143. R.A. Buckingham, *Numerical Methods* (Pitman & Sons, London, 1962), p. 255
144. B.D. Buckley, P.G. Burke, Vo Ky Lan, Comput. Phys. Commun. **17**, 175 (1979)
145. S.J. Buckman, C.W. Clark, Rev. Mod. Phys. **66**, 539 (1994)
146. S.J. Buckman, P. Hammond, F.H. Read, G.C. King, J. Phys. B At. Mol. Phys. **16**, 4039 (1983)
147. A. Burgess, Astrophys. J. **139**, 776 (1964)
148. A. Burgess, Ann. d'Astrophysique. **28**, 774 (1965)
149. A. Burgess, J. Phys. B At. Mol. Phys. **7**, L364 (1974)
150. A. Burgess, M.J. Seaton, Mon. Not. R. Astron. Soc. **127**, 355 (1964)
151. P.G. Burke, Adv. Phys. **14**, 521 (1965)
152. P.G. Burke, *Atomic and Molecular Collisions* (HMSO, London, 1967)
153. P.G. Burke, Adv. At. Mol. Phys. **4**, 173 (1968)
154. P.G. Burke, Comput. Phys. Commun. **1**, 241 (1969)
155. P.G. Burke, in *Computational Physics* (Inst. Phys. and Phys. Soc., London, 1970), p. 9
156. P.G. Burke, Comm. At. Mol. Phys. **4**, 157 (1973)
157. P.G. Burke, Comput. Phys. Commun. **6**, 288 (1974)
158. P.G. Burke, *Potential Scattering in Atomic Physics* (Plenum Press, New York, NY and London, 1977)
159. P.G. Burke, in *Atomic, Molecular and Optical Physics Handbook*, ed. by G.W.F. Drake (Springer Science & Business Media, New York, NY, 2006), p. 705

160. P.G. Burke, H.M. Schey, Phys. Rev. **126**, 147 (1962)
161. P.G. Burke, K. Smith, Rev. Mod. Phys. **24**, 458 (1962)
162. P.G. Burke, A.J. Taylor, Proc. Phys. Soc. **88**, 549 (1966)
163. P.G. Burke, T.G. Webb, J. Phys. B At. Mol. Phys. **3**, L131 (1970)
164. P.G. Burke, M.J. Seaton, in *Methods in Computational Physics*, vol 10, ed. by B. Alder, S. Fernbach, M. Rotenberg (Academic Press, New York, NY and London, 1971), p. 1
165. P.G. Burke, J.F.B. Mitchell, J. Phys. B At. Mol. Phys. **6**, 320 (1973)
166. P.G. Burke, J.F.B. Mitchell, J. Phys. B At. Mol. Phys. **7**, 665 (1974)
167. P.G. Burke, W.D. Robb, Adv. At. Mol. Phys. **11**, 143 (1975)
168. P.G. Burke, K.T. Taylor, J. Phys. B At. Mol. Phys. **8**, 2620 (1975)
169. P.G. Burke, M.J. Seaton, J. Phys. B At. Mol. Phys. **17**, L683 (1984)
170. P.G. Burke, K.A. Berrington, *Atomic and Molecular Processes: An R-Matrix Approach* (Inst. Phys. Publishing, Bristol and Philadelphia, PA, 1993)
171. P.G. Burke, C.J. Joachain, *Theory of Electron-Atom Collisions Part 1, Potential Scattering* (Plenum Press, New York, NY and London, 1995)
172. P.G. Burke, V.M. Burke, J. Phys. B At. Mol. Opt. Phys. **30**, L383 (1997)
173. P.G. Burke, J. Tennyson, Mol. Phys. **103**, 2537 (2005)
174. P.G. Burke, D.D. McVicar, K. Smith, Proc. Phys. Soc. **83**, 397 (1964)
175. P.G. Burke, J.W. Cooper, S. Ormond, Phys. Rev. Lett. **17**, 345 (1966)
176. P.G. Burke, J.W. Cooper, S. Ormond, Phys. Rev. **183**, 245 (1969)
177. P.G. Burke, D.F. Gallaher, S. Geltman, J. Phys. B At. Mol. Phys. **2**, 1142 (1969)
178. P.G. Burke, A. Hibbert, W.D. Robb, J. Phys. B At. Mol. Phys. **4**, 153 (1971)
179. P.G. Burke, N. Chandra, F.A. Gianturco, J. Phys. B At. Mol. Phys. **5**, 2212 (1972)
180. P.G. Burke, I. Mackey, I. Shimamura, J. Phys. B At. Mol. Phys. **10**, 2497 (1977)
181. P.G. Burke, K.A. Berrington, C.V. Sukumar, J. Phys. B At. Mol. Phys. **14**, 289 (1981)
182. P.G. Burke, C.J. Noble, M.P. Scott, Proc. R. Soc. A **410**, 289 (1987)
183. P.G. Burke, P. Francken, C.J. Joachain, Europhys. Lett. **13**, 617 (1990)
184. P.G. Burke, P. Francken, C.J. Joachain, J. Phys. B At. Mol. Opt. Phys. **24**, 761 (1991)
185. P.G. Burke, V.M. Burke, K.M. Dunseath, J. Phys. B At. Mol. Opt. Phys. **27**, 5341 (1994)
186. P.G. Burke, K. Higgins, J.E. Inglesfield, Philos. Trans. R. Soc. A **357**, 1143 (1999)
187. P.G. Burke, J. Colgan, D.H. Glass, K. Higgins, J. Phys. B At. Mol. Opt. Phys. **33**, 143 (2000)
188. P.G. Burke, C.J. Noble, A.G. Sunderland, V.M. Burke, Phys. Scr. T **100**, 55 (2002)
189. P.G. Burke, C.J. Noble, V.M. Burke, Adv. At. Mol. Opt. Phys. **54**, 237 (2007)
190. V.M. Burke, M.J. Seaton, J. Phys. B At. Mol. Phys. **19**, L527 (1986)
191. V.M. Burke, C.J. Noble, Comput. Phys. Commun. **85**, 471 (1995)
192. V.M. Burke, P.G. Burke, N.S. Scott, Comput. Phys. Commun. **69**, 76 (1992)
193. V.M. Burke, C.J. Noble, V. Faro-Maza, A. Maniopoulou, N.S. Scott, Comput. Phys. Commun. **180**, 2450 (2009)
194. K. Burnett, V.C. Reed, P.L. Knight, J. Phys. B At. Mol. Opt. Phys. **26**, 561 (1993)
195. P.J.A. Buttle, Phys. Rev. **160**, 719 (1967)
196. F.W. Byron, C.J. Joachain, B. Piraux, J. Phys. B At. Mol. Phys. **19**, 1201 (1986)
197. J. Callaway, Phys. Rev. A **32**, 775 (1985)
198. J. Callaway, J.W. Wooten, Phys. Rev. A **9**, 1924 (1974)
199. J. Callaway, J.W. Wooten, Phys. Rev. A **11**, 1118 (1975)
200. J. Callaway, K. Unnikrishnan, J. Phys. B At. Mol. Opt. Phys. **26**, L419 (1993)
201. C.P. Campbell, M.T. McAlinden, F.G.R.S. MacDonald, H.R.J. Walters, Phys. Rev. Lett. **80**, 5097 (1998)
202. C.P. Campbell, M.T. McAlinden, A.A. Kernoghan, H.R.J. Walters, Nucl. Instrum. Methods B **143**, 41 (1998)
203. G.D. Carse, D.W. Walker, J. Phys. B At. Mol. Phys. **6**, 2529 (1973)
204. C.M. Cassidy, C.A. Ramsbottom, M.P. Scott, P.G. Burke, Astron. Astrophys. **513**, A55 (2010)
205. L. Castillejo, I.C. Percival, M.J. Seaton, Proc. R. Soc. A **254**, 259 (1960)
206. L. Celenza, W. Tobocman, Phys. Rev. **174**, 1115 (1968)

207. N. Chandra, A. Temkin, Phys. Rev. A **13**, 188 (1976)
208. N. Chandra, A. Temkin, Phys. Rev. A **14**, 507 (1976)
209. S. Chandrasekhar, Astrophys. J. **102**, 223 (1945)
210. E.S. Chang, U. Fano, Phys. Rev. A **6**, 173 (1972)
211. J.-J. Chang, J. Phys. B At. Mol. Phys. **8**, 2327 (1975)
212. J.-J. Chang, J. Phys. B At. Mol. Phys. **10**, 3195 (1977)
213. J.-J. Chang, J. Phys. B At. Mol. Phys. **10**, 3335 (1977)
214. D. Charlo, M. Tereo-Dunseath, K.M. Dunseath, J.-M. Launay, J. Phys. B At. Mol. Opt. Phys. **31**, L539 (1998)
215. M. Charlton, G. Laricchia, J. Phys. B At. Mol. Opt. Phys. **23**, 1045 (1990)
216. M. Charlton, G. Laricchia, Comm. At. Mol. Phys. **26**, 253 (1991)
217. D.M. Chase, Phys. Rev. **104**, 838 (1956)
218. S.-I. Chu, Adv. At. Mol. Phys. **21**, 197 (1985)
219. C.W. Clark, K.T. Taylor, J. Phys. B At. Mol. Phys. **15**, 1175 (1982)
220. S. Clarke, M. Nekovee, P.K. de Boer, J.E. Inglesfield, J. Phys. Condens. Matter. **10**, 7777 (1998)
221. J. Colgan, M.S. Pindzola, Phys. Rev. A **74**, 012713 (2006)
222. J. Colgan, D.H. Glass, K. Higgins, P.G. Burke, Comput. Phys. Commun. **114**, 27 (1998)
223. J. Colgan, D.H. Glass, K. Higgins, P.G. Burke, in *Multiphoton Processes*, ed. by L.F. DiMauro, K.C. Kulander (American Institute of Physics Proceedings 525,Melville, NY, 2000), p. 427
224. J. Colgan, D.H. Glass, K. Higgins, P.G. Burke, J. Phys. B At. Mol. Opt. Phys. **34**, 2089 (2001)
225. J. Colgan, M.S. Pindzola, F.J. Robicheaux, D.C. Griffin, M. Baertschy, Phys. Rev. A **65**, 042721 (2002)
226. J. Colgan, M.S. Pindzola, F. Robicheaux, J. Phys. B At. Mol. Opt. Phys. **41**, 121002 (2008)
227. E.U. Condon, G.H. Shortley, *The Theory of Atomic Spectra* (Cambridge University Press, Cambridge, UK, 1935)
228. J.W. Cook, K.R. Nicolas, Astrophys. J. **229**, 1163 (1979)
229. J.N. Cooper, E.A.G. Armour, M. Plummer, J. Phys. A Math. Theor. **42**, 095207 (2009)
230. J.W. Cooper, U. Fano, F. Prats, Phys. Rev. Lett. **10**, 518 (1963)
231. P.B. Corkum, Phys. Rev. Lett. **71**, 1994 (1993)
232. C. Corliss, J. Sugar, J. Phys. Chem. Ref. Data **11**(1), 135 (1982)
233. R.D. Cowan, *The Theory of Atomic Structure and Spectra* (University of California Press, Berkeley, CA, 1981)
234. S. Crampin, M. Nekovee, J.E. Inglesfield, Phys. Rev. B **51**, 7318 (1995)
235. D.H. Crandall, R.A. Phaneuf, B.E. Hasselquist, D.C. Gregory, J. Phys. B At. Mol. Phys. **12**, L249 (1979)
236. D.S.F. Crothers, J. Phys. B At. Mol. Phys. **19**, 463 (1986)
237. D.S.F. Crothers, *Semiclassical Dynamics and Relaxation* (Springer Science & Business Media, New York, NY, 2008), p. 129
238. D.M. Crowe, X.Q. Guo, M.S. Lubell, J. Slevin, M. Emminyan, J. Phys. B At. Mol. Opt. Phys. **23**, L352 (1990)
239. S. Cvejanović, F.H. Read, J. Phys. B At. Mol. Phys. **7**, 1814 (1974)
240. S. Cvejanović, J. Jureta, M. Minić, D. Cvejanović, J. Phys. B At. Mol. Opt. Phys. **25**, 4337 (1992)
241. A. Cyr, O. Latinne, P.G. Burke, J. Phys. B At. Mol. Opt. Phys. **30**, 659 (1997)
242. A. Dalgarno, A.E. Kingston, Proc. R. Soc. A **259**, 424 (1960)
243. A. Dalgarno, W.D. Davison, Adv. At. Mol. Phys. **2**, 1 (1966)
244. R. Damburg, R. Peterkop, Proc. Phys. Soc. **80**, 1073 (1962)
245. R. Damburg, E. Karule, Proc. Phys. Soc. **90**, 637 (1967)
246. G. Danby, J. Tennyson, Phys. Rev. Lett. **61**, 2737 (1988)
247. G. Danby, J. Tennyson, J. Phys. B At. Mol. Opt. Phys. **23**, 1005 (1990); Corrigendum, J. Phys. B At. Mol. Opt. Phys. **23**, 2471s

248. G. Danby, J. Tennyson, J. Phys. B At. Mol. Opt. Phys. **24**, 3517 (1991)
249. M. Danos, W. Greiner, Phys. Rev. **146**, 708 (1966)
250. A. Dasgupta, A.K. Bhatia, Phys. Rev. A **30**, 1241 (1984)
251. P.C.W. Davies, M.J. Seaton, J. Phys. B At. Mol. Phys. **2**, 757 (1969)
252. H.C. Day, A.S. Fearnside, R.M. Potvliege, Phys. Rev. A **56**, 2447 (1997)
253. H.C. Day, B. Piraux, R.M. Potvliege, Phys. Rev. A **61**, 031402(R) (2000)
254. C. de Boor, *A Practical Guide to Splines* (Springer, New York, NY, 1978)
255. P.M. Dehmer, W.A. Chupka, J. Chem. Phys. **65**, 2243 (1976)
256. D. Delande, A. Bommier, J.C. Gay, Phys. Rev. Lett. **66**, 141 (1991)
257. L.M. Delves, Nucl. Phys. **9**, 391 (1959)
258. L.M. Delves, Nucl. Phys. **20**, 275 (1960)
259. Yu.N., Demkov, *Variational Principles in the Theory of Collisions* (Pergamon Press, London, 1963)
260. Yu.N. Demkov, A.M. Ermolaev, Sov. Phys. JETP **9**, 633 (1959)
261. A.S. Dickinson, P.R. Certain, J. Chem. Phys. **49**, 4209 (1968)
262. S. Diehl, D. Cubaynes, E.T. Kennedy, F.J. Wuilleumier, J.-M. Bizau, L. Journel, L. VoKy, P. Faucher, A. Hibbert, C. Blancard, N. Berrah, T.J. Morgan, J. Bozek, A.S. Schlachter, J. Phys. B At. Mol. Opt. Phys. **30**, L595 (1997)
263. P.A.M. Dirac, *The Principles of Quantum Mechanics*, 3rd edn. (Clarendon Press, Oxford, 1947)
264. M. Dörr, M. Terao-Dunseath, J. Purvis, C.J. Noble, P.G. Burke, C.J. Joachain, J. Phys. B At. Mol. Opt. Phys. **25**, 2809 (1992)
265. W. Domcke, Phys. Rep. **208** (2), 97 (1991)
266. G. Doolen, G. McCartor, F.A. McDonald, J. Nuttall, Phys. Rev. A **4**, 108 (1971)
267. S.F. dos Santos, V. Kokoouline, C.H. Greene, J. Chem. Phys. **127**, 124309 (2007)
268. N.A. Doughty, M.J. Seaton, V.B. Sheory, J. Phys. B At. Mol. Phys. **1**, 802 (1968)
269. M. Drescher, M. Hentschel, R. Kienberger, M. Ulberacker, V. Yakovlev, A. Scrinzi, Th. Westerwalbesloh, U. Kleineberg, U. Heinzmann, F. Krausz, Nature **419**, 803 (2002)
270. S.I. Drozdov, Sov. Phys. JETP **1**, 591 (1955)
271. S.I. Drozdov, Sov. Phys. JETP **3**, 759 (1956)
272. J. Dubau, J. Phys. B At. Mol. Phys. **11**, 4095 (1978)
273. J. Dubau, J. Wells, J. Phys. B At. Mol. Phys. **6**, 1452 (1973)
274. L. Dubé, A. Herzenberg, Phys. Rev. A **20**, 194 (1979)
275. K.M. Dunseath, M. Terao-Dunseath, J. Phys. B At. Mol. Opt. Phys. **37**, 1305 (2004)
276. K.M. Dunseath, M. Terao-Dunseath, Phys. Rev. A **73**, 053407 (2006)
277. K.M. Dunseath, M. Le Dourneuf, M. Terao-Dunseath, J.-M. Launay, Phys. Rev. A **54**, 561 (1996)
278. K.M. Dunseath, M. Terao-Dunseath, G. Bourhis, Phys. Rev. A **72**, 033410 (2005)
279. K.G. Dyall, I.P. Grant, C.T. Johnson, F.A. Parpia, E.P. Plummer, Comput. Phys. Commun. **55**, 425 (1989)
280. J.H. Eberly, Q. Su, J. Javanainen, Phys. Rev. Lett. **62**, 881 (1989)
281. J.H. Eberly, Q. Su, J. Javanainen, J. Opt. Soc. Am. B **6**, 1289 (1989)
282. C. Eckart, Rev. Mod. Phys. **2**, 305 (1930)
283. R.J. Eden, J.R. Taylor, Phys. Rev. **133**, B1575 (1964)
284. A.R. Edmonds, *Angular Momentum in Quantum Mechanics* (Princeton University Press, Princeton, NJ1, 1957)
285. H. Ehrhardt, K. Willman, Zeits. f. Phys. **203**, 1 (1967)
286. H. Ehrhardt, K. Willman, Zeits. f. Phys. **204**, 462 (1967)
287. H. Ehrhardt, L. Langhams, F. Linder, Zeits. f. Phys. **214**, 179 (1968)
288. L. Eisenbud, Dissertation, Princeton University, unpublished, 1948
289. W. Eissner, M.J. Seaton, J. Phys. B At. Mol. Phys. **5**, 2187 (1972)
290. W. Eissner, M. Jones, H. Nussbaumer, Comput. Phys. Commun. **8**, 270 (1974)
291. W. Eissner, M.E. Galavis, C. Mendoza, C.J. Zeippen, Astron. Astrophys. Suppl. **137**, 165 (1999)

292. I.I. Fabrikant, J. Phys. B At. Mol. Phys. **18**, 1873 (1985)
293. I.I. Fabrikant, Zeits. Phys. D **3**, 401 (1986)
294. I.I. Fabrikant, Comm. At. Mol. Phys. **24**, 37 (1990)
295. I.I. Fabrikant, Phys. Rev. A **43**, 3478 (1991)
296. I.I. Fabrikant, J. Phys. B At. Mol. Opt. Phys. **38**, 1745 (2005)
297. I.I. Fabrikant, H. Hotop, Phys. Rev. A **63**, 022706 (2001)
298. Y. Fang, K. Bartschat, J. Phys. B At. Mol. Opt. Phys. **34**, L19 (2001)
299. Y. Fang, K. Bartschat, J. Phys. B At. Mol. Opt. Phys. **34**, 2745 (2001)
300. Y. Fang, K. Bartschat, Phys. Rev. A **64**, 020701(R) (2001)
301. U. Fano, Phys. Rev. **124**, 1866 (1961)
302. U. Fano, Phys. Rev. **140**, A67 (1965)
303. U. Fano, Phys. Rev. A **2**, 353 (1970)
304. U. Fano, J. Phys. B At. Mol. Phys. **7**, L401 (1974)
305. U. Fano, Comm. At. Mol. Phys. **10**, 223 (1981)
306. U. Fano, Comm. At. Mol. Phys. **13**, 157 (1983)
307. U. Fano, Rep. Prog. Phys. **46**, 97 (1983)
308. U. Fano, G. Racah, *Irreducible Tensorial Sets* (Academic Press, New York, NY, 1959)
309. U. Fano, F. Prats, Proc. Natl. Acad. Sci. India A **33**, 553 (1963)
310. U. Fano, D. Dill, Phys. Rev. A **6**, 185 (1972)
311. U. Fano, C.M. Lee, Phys. Rev. Lett. **31**, 1573 (1973)
312. A. Faure, J. Tennyson, J. Phys. B At. Mol. Opt. Phys. **35**, 1865 (2002)
313. A. Faure, J.D. Gorfinkiel, L.A. Morgan, J. Tennyson, Comput. Phys. Commun. **144**, 224 (2002)
314. H. Faxén, J. Holtsmark, Zeits. f. Phys. **45**, 307 (1927)
315. J.M. Feagin, J. Phys. B At. Mol. Phys. **17**, 2433 (1984)
316. E. Feenberg, Phys. Rev. **40**, 40 (1932)
317. J. Feist, S. Nagele, R. Pazourek, E. Persson, B.I. Schneider, L.A. Collins, J. Burgdörfer, Phys. Rev. A **77**, 043420 (2008)
318. L. Feng, H.W. van der Hart, Phys. Rev. A **66**, 031402 (2002)
319. L. Feng, H.W. van der Hart, J. Phys. B At. Mol. Opt. Phys. **36**, L1 (2003)
320. H. Feshbach, Ann. Phys. (N.Y.) **5**, 357 (1958)
321. H. Feshbach, Ann. Phys. (N.Y.) **19**, 287 (1962)
322. H. Feshbach, C.F. Porter, V.F. Weisskopf, Phys. Rev. **96**, 448 (1954)
323. J.P. Fisk, Phys. Rev. **49**, 167 (1936)
324. G.D. Fletcher, M.J. Alguard, T.J. Gay, P.F. Wainwright, M.S. Lubell, W. Raith, V.W. Hughes, Phys. Rev. A **31**, 2854 (1985)
325. G. Floquet, Ann. Ec. Norm. **13**(2), 47 (1883)
326. V.A. Fock, Kgl. Norske Videnskab. Selskaba. Forh. **31**, 138 (1958)
327. W.C. Fon, K.A. Berrington, J. Phys. B At. Mol. Phys. **14**, 323 (1981)
328. W.C. Fon, P.G. Burke, A.E. Kingston, J. Phys. B At. Mol. Phys. **11**, 521 (1978)
329. W.C. Fon, K.A. Berrington, A. Hibbert, J. Phys. B At. Mol. Phys. **14**, 307 (1981)
330. W.C. Fon, K.A. Berrington, P.G. Burke, A. Hibbert, J. Phys. B At. Mol. Phys. **16**, 307 (1983)
331. W.C. Fon, K.A. Berrington, A. Hibbert, J. Phys. B At. Mol. Phys. **17**, 3279 (1984)
332. W.C. Fon, K.A. Berrington, P.G. Burke, A.E. Kingston, J. Phys. B At. Mol. Opt. Phys. **22**, 3939 (1989)
333. W.C. Fon, K.P. Lim, P.M.J. Sawey, J. Phys. B At. Mol. Opt. Phys. **26**, 305 (1993)
334. W.C. Fon, K.P. Lim, K. Ratnavelu, P.M.J. Sawey, Phys. Rev. A **50**, 4802 (1994)
335. W.C. Fon, T.G. Lee, K.P. Lim, K.A. Berrington, J. Phys. B At. Mol. Opt. Phys. **28**, 4129 (1995)
336. L. Fonda, R.G. Newton, Ann. Phys. (N.Y.) **7**, 133 (1959)
337. L. Fonda, R.G. Newton, Ann. Phys. (N.Y.) **9**, 416 (1960)
338. R. Frahm, K. Liang, G. Williams (eds.), *Synchrotron Radiation News* **20**(6) (Taylor and Francis Group, Boca Raton, FL, 2007)

339. J. Franz, K.L. Baluja, R. Zhang, J. Tennyson, Nucl. Instrum. Methods B **266**, 419 (2008)
340. J. Franz, F.A. Gianturco, K.L. Baluja, J. Tennyson, R. Carey, R. Monturo, R.R. Lucchese, T. Stoecklin, P. Nicholas, T.L. Gibson, Nucl. Instrum. Methods B **266**, 425 (2008)
341. L.C.G. Freitas, K.A. Berrington, P.G. Burke, A. Hibbert, A.E. Kingston, A.L. Sinfailam, J. Phys. B At. Mol. Phys. **17**, L303 (1984)
342. F.L. Friedman, V.F. Weisskopf, in *Niels Bohr and the Development of Physics*, ed. by W. Pauli, L. Rosenfeld, V. Weisskopf (Pergamon Press, London, 1955), p. 134
343. C.E. Fröberg, Rev. Mod. Phys. **27**, 399 (1955)
344. C. Froese Fischer, Comput. Phys. Commun. **1**, 151 (1969)
345. C. Froese Fischer, Comput. Phys. Commun. **4**, 107 (1972)
346. C. Froese Fischer, *The Hartree Fock Method for Atoms* (Wiley, New York, NY, London, Sydney, Toronto, ON, 1977)
347. C. Froese Fischer, Comput. Phys. Commun. **14**, 145 (1978)
348. C. Froese Fischer, Comput. Phys. Commun. **64** , 369 (1991)
349. C. Froese Fischer, T. Brage, P. Jönsson, *Computational Atomic Structure an MCHF Approach* (Institute of Physics Publishing, Bristol and Philadelphia, PA, 1997)
350. C. Froese Fischer, G. Tachiev, G. Gaigalas, M.R. Godefroid, Comput. Phys. Commun. **176**, 559 (2007)
351. A.M. Frolov, V.H. Smith Jr., Phys. Rev. A **55**, 2662 (1997)
352. B. Fromme, M. Schmitt, E. Kister, A. Gorschlüter, H. Merz, Phys. Rev. B **50**, 1874 (1994)
353. B. Fromme, M. Möller, Th. Anschütz, C. Bethe, E. Kister, Phys. Rev. Lett. **77**, 1548 (1996)
354. J.C. Fuggle, J.E. Inglesfield, in *Unoccupied Electronic States*, ed. by J.C. Fuggle, J.E. Inglesfield (Springer, Berlin, 1992)
355. D.V. Fursa, I. Bray, Phys. Rev. A **52**, 1279 (1995)
356. M. Gailitis, J. Phys. B At. Mol. Phys. **9**, 843 (1976)
357. M. Gailitis, Sov. Phys. JETP, **17**, 1328 (1963)
358. M. Gailitis, R. Damburg, Sov. Phys. JETP, **17**, 1107 (1963)
359. M. Gailitis, R. Damburg, Proc. Phys. Soc. **82**, 192 (1963)
360. H. Gao, Ch. Jungen, C.H. Greene, Phys. Rev. A **47**, 4877 (1993)
361. G. Gamow, Zeits. f. Phys. **51**, 204 (1928)
362. A.J. Garner, G. Laricchia, Özen, A., J. Phys. B At. Mol. Opt. Phys. **29**, 5961 (1996)
363. A.J. Garner, A. Özen, G. Laricchia, Nucl. Instrum. Methods B **143**, 155 (1998)
364. A.J. Garner, A. Özen, G. Laricchia, J. Phys. B At. Mol. Opt. Phys. **33**, 1149 (2000)
365. M. Gavrila, (ed.) Adv. At. Mol. Opt. Phys. Suppl. 1, *Atoms in Intense Laser Fields* (Academic Press, New York, NY, 1992)
366. R. Gębarowski, P.G. Burke, K.T. Taylor, M. Dörr, M. Bensaid, C.J. Joachain, J. Phys. B At. Mol. Opt. Phys. **30**, 1837 (1997)
367. R. Gębarowski, K.T. Taylor, P.G. Burke, J. Phys. B At. Mol. Opt. Phys. **30**, 2505 (1997)
368. S. Geltman, P.G. Burke, J. Phys. B At. Mol. Phys. **3**, 1062 (1970)
369. F.A. Gianturco, A. Jain, Phys. Rep. **143**, 347 (1986)
370. F.A. Gianturco, P. Paioletti, Phys. Rev. A **55**, 3491 (1997)
371. F.A. Gianturco, T. Mukherjee, A. Occhigrossi, Phys. Rev. A **64**, 032715 (2001)
372. S.J. Gilbert, C. Kurz, R.G. Greeves, C.M. Surko, Appl. Phys. Lett., **70**, 1944 (1997)
373. C.J. Gillan, O. Nagy, P.G. Burke, L.A. Morgan, C.J. Noble, J. Phys. B At. Mol. Phys. **20**, 4585 (1987)
374. C.J. Gillan, C.J. Noble, P.G. Burke, J. Phys. B At. Mol. Opt. Phys. **21**, L53 (1988)
375. C.J. Gillan, J. Tennyson, P.G. Burke, in *Computational Methods for Electron-Molecule Collisions*, ed. by W.M. Huo, F.A. Gianturco (Plenum Press, New York, NY, 1995), p. 239
376. A. Giusti, J. Phys. B At. Mol. Opt. Phys. **13**, 3867 (1980)
377. A. Giusti-Suzor, Ch. Jungen, J. Chem. Phys. **80**, 986 (1984)
378. A. Giusti-Suzor, F.H. Mies, L.F. DiMauro, E. Charron, B. Yang, J. Phys. B At. Mol. Opt. Phys. **28**, 309 (1995)
379. D.H. Glass, P.G. Burke, J. Phys. B At. Mol. Opt. Phys. **33**, 407 (2000)

380. D.H. Glass, P.G. Burke, H.W. van der Hart, C.J. Noble, J. Phys. B At. Mol. Opt. Phys. **30**, 3801 (1997)
381. R. Glass, A. Hibbert, Comput. Phys. Commun. **11**, 125 (1976)
382. R. Glass, A. Hibbert, Comput. Phys. Commun. **16**, 19 (1978)
383. R. Glass, A. Hibbert, Comput. Phys. Commun. **35**, c 368 (1984)
384. N. Goel, S.J. Chung, M.B. Santos, K. Suzuki, S. Miyashita, Y. Hirayama, Physica E **21**, 761 (2004)
385. G. Goertzel, Phys. Rev. **73**, 1463 (1948)
386. A. Goldberg, H.M. Schey, J.L. Schwartz, Am. J. Phys. **35**, 117 (1967)
387. M.L. Goldberger, K.M. Watson, *Collision Theory* (Wiley, New York, NY, 1964)
388. D.E. Golden, H. Nakano, Phys. Rev. **144**, 71 (1966)
389. G.H. Golub, C.F. Van Loan, *Matrix Computations*, 2nd edn. Chap. 8 (John Hopkins University Press, Baltimore, MD and London, 1989)
390. A. Gonis, *Green Functions for Ordered and Disordered Systems* (North-Holland, Amsterdam, 1992)
391. T.W. Gorczyca, Phys. Rev. A **61**, 024702 (2000)
392. T.W. Gorczyca, N.R. Badnell, J. Phys. B At. Mol. Opt. Phys. **29**, L283 (1996)
393. T.W. Gorczyca, N.R. Badnell, Phys. Rev. Lett. **79**, 2783 (1997)
394. T.W. Gorczyca, N.R. Badnell, J. Phys. B At. Mol. Opt. Phys. **30**, 3897 (1997)
395. T.W. Gorczyca, F. Robicheaux, Phys. Rev. A **60**, 1216 (1999)
396. T.W. Gorczyca, B.M. McLaughlin, J. Phys. B At. Mol. Opt. Phys. **33**, L859 (2000)
397. T.W. Gorczyca, F. Robicheaux, M.S. Pindzola, N.R. Badnell, Phys. Rev. A **52**, 3852 (1995)
398. T.W. Gorczyca, F. Robicheaux, M.S. Pindzola, D.C. Griffin, N.R. Badnell, Phys. Rev. A **52**, 3877 (1995)
399. T.W. Gorczyca, F. Robicheaux, M.S. Pindzola, N.R. Badnell, Phys. Rev. A **54**, 2107 (1996)
400. T.W. Gorczyca, N.R. Badnell, D.W. Savin, Phys. Rev. A **65**, 062707 (2002)
401. T.W. Gorczyca, O. Zatsarinny, H.-L. Zhou, S.T. Manson, Z. Felfli, A.Z. Msezane, Phys. Rev. A **68**, 050703(R) (2003)
402. R.G. Gordon, in *Methods in Computational Physics*, vol. 10, ed. by B. Alder, S. Fernbach, M. Rotenberg (Academic Press, New York, NY and London, 1971), pp. 81–109
403. W. Gordon, Zeits. f. Phys. **48**, 180 (1928)
404. J.D. Gorfinkiel, J. Tennyson, J. Phys. B At. Mol. Opt. Phys. **37**, L343 (2004)
405. J.D. Gorfinkiel, J. Tennyson, J. Phys. B At. Mol. Opt. Phys. **38**, 1607 (2005)
406. A. Gorschlüter, H. Merz, Phys. Rev. B **49**, 17293 (1994)
407. E. Goulielmakis, M. Uiberacker, R. Kienberger, A. Baltuska, V. Yakovlev, A. Scrinzi, Th. Westerwalbesloh, U. Kleineberg, U. Heinzmann, M. Drescher, F. Krausz, Science **305**, 1267 (2004)
408. I.P. Grant, Adv. Phys. **19**, 747 (1970)
409. I.P. Grant, Comput. Phys. Commun. **17**, 149 (1979)
410. I.P. Grant, in *Atomic, Molecular and Optical Physics Handbook*, ed. by G.W.F. Drake (Springer Science & Business Media, New York, NY, 2006), p. 325
411. I.P. Grant, *Relativistic Quantum Theory of Atoms and Molecules* (Springer Science & Business Media, New York, NY, 2007)
412. I.P. Grant, J. Phys. B At. Mol. Opt. Phys. **41**, 055002 (2008)
413. I.P. Grant, N.C. Pyper, J. Phys. B At. Mol. Phys. **9**, 761 (1976)
414. I.P. Grant, B.J. McKenzie, J. Phys. B At. Mol. Phys. **13**, 2671 (1980)
415. I.P. Grant, B.J. McKenzie, P.H. Norrington, D.F. Mayers, N.C. Pyper, Comput. Phys. Commun. **21**, 207 (1980)
416. C.H. Greene, Phys. Rev. A **23**, 661 (1981)
417. C.H. Greene, Phys. Rev. A **28**, 2209 (1983)
418. C.H. Greene, Phys. Rev. A **32**, 1880 (1985)
419. C.H. Greene, A.R.P. Rau, Phys. Rev. Lett. **48**, 533 (1982)

420. C.H. Greene, A.R.P. Rau, J. Phys. B At. Mol. Phys. **16**, 99 (1983)
421. C.H. Greene, Ch. Jungen, Adv. At. Mol. Phys. **21**, 51 (1985)
422. C.H. Greene, L. Kim, Phys. Rev. A **38**, 5953 (1988)
423. G.F. Gribakin, H.R.J. Walters (eds.), *Positron and Positronium Physics*, in Nucl. Instrum. Methods Phys. Res. B **266** (2008)
424. D.C. Griffin, C.P. Ballance, J. Phys. B At. Mol. Opt. Phys. **42**, 235201 (2009)
425. D.C. Griffin, M.S. Pindzola, N.R. Badnell, Phys. Rev. A **47**, 2871 (1993)
426. D.C. Griffin, N.R. Badnell, M.S. Pindzola, J. Phys. B At. Mol. Opt. Phys. **31**, 3713 (1998)
427. D.C. Griffin, N.R. Badnell, M.S. Pindzola, J.A. Shaw, J. Phys. B At. Mol. Opt. Phys. **32**, 2139, 4129 (1999)
428. F. Grossman, *Theoretical Femtosecond Physics* (Springer, Berlin and Heidelberg, 2008)
429. X. Guan, O. Zatsarinny, K. Bartschat, B.I. Schneider, J. Feist, C.J. Noble, Phys. Rev. A **76**, 053411 (2007)
430. X. Guan, K. Bartschat, B.I. Schneider, Phys. Rev. A **77**, 043421 (2008)
431. X. Guan, C.J. Noble, O. Zatsarinny, K. Bartschat, B.I. Schneider, Phys. Rev. A **78**, 053402 (2008)
432. X. Guan, O. Zatsarinny, C.J. Noble, K. Bartschat, B.I. Schneider, J. Phys. B At. Mol. Opt. Phys. **42**, 134015 (2009)
433. X. Guan, C.J. Noble, O. Zatsarinny, K. Bartschat, B.I. Schneider, Comput. Phys. Commun. **180**, 2401 (2009)
434. S.L. Haan, V.L. Jacobs, Phys. Rev. A **40**, 80 (1989)
435. Y. Hahn, Adv. At. Mol. Phys. **21**, 123 (1985)
436. Y. Hahn, Rep. Prog. Phys. **60**, 691 (1997)
437. Y. Hahn, K.J. LaGattuta, Phys. Rep. **166**, 195 (1988)
438. M.H. Halley, D. Delande, K.T. Taylor, J. Phys. B At. Mol. Opt. Phys. **25**, L525 (1992)
439. M.H. Halley, D. Delande, K.T. Taylor, J. Phys. B At. Mol. Opt. Phys. **26**, 1775 (1993)
440. F.S. Ham, Solid State Phys. **1**, 217 (1955)
441. D.O. Harris, G.G. Engerholm, W.D. Gwinn, J. Chem. Phys. **43**, 1515 (1965)
442. F.E. Harris, H.H. Michels, J. Chem. Phys. **43**, 5165 (1965)
443. D.R. Hartree, Proc. Camb. Philos. Soc. **24**, 426 (1928)
444. D.R. Hartree, *Numerical Analysis* (Clarendon Press, Oxford, 1952), p. 194
445. D.R. Hartree, *The Calculation of Atomic Structures* (Wiley, New York, NY, 1957)
446. A.U. Hazi, Phys. Rev. A **19**, 920 (1979)
447. M.H. Hebb, D.H. Menzel, Astrophys. J. **92**, 408 (1940)
448. D.W.O. Heddle, R.G.W. Keesing, A. Parkin, Proc. R. Soc. A **352**, 419 (1977)
449. J.W. Heggarty, Parallel R-matrix computation, PhD Thesis, Queen's University Belfast, 1999
450. J.W. Heggarty, M.P. Scott, N.S. Scott, P.G. Burke, Comput. Phys. Commun. **114**, 195 (1998)
451. H.G.M. Heideman, C.E. Kuyatt, G.E. Chamberlain, J. Chem. Phys. **44**, 355 (1966)
452. W. Heisenberg, Z. Naturforsch **1**, 608 (1946)
453. W.C. Henneberger, Phys. Rev. Lett. **21**, 838 (1968)
454. R.J.W. Henry, L. Lipsky, Phys. Rev. **153**, 51 (1967)
455. R.J.W. Henry, P.G. Burke, A.-L. Sinfailam, Phys. Rev. **178**, 218 (1969)
456. M. Hentschel, R. Kienberger, Ch. Spielmann, G.A. Reider, N. Milosovic, T. Brabec, P. Corkum, U. Heinzmann, M. Drescher, F. Krausz, Nature **414**, 509 (2001)
457. G. Herzberg, *Molecular Spectra and Molecular Structure II Infrared and Raman Spectra of Polyatomic Molecules* (D. Van Nostrand Company Inc. Princeton, NJ and London, 1945)
458. G. Herzberg, Phys. Rev. Lett. **23**, 1081 (1969)
459. A. Herzenberg, J. Phys. B At. Mol. Phys. **1**, 548 (1968)
460. A. Herzenberg, in *Electron–Molecule Collisions*, ed. by I. Shimamura and K. Takayanagi (Plenum Press, New York, NY and London, 1984), p. 191
461. A. Herzenberg, F. Mandl, Proc. R. Soc. A **270**, 48 (1962)
462. A. Hibbert, Comput. Phys. Commun. **1**, 359 (1969)
463. A. Hibbert, Comput. Phys. Commun. **2**, 180 (1971)

464. A. Hibbert, Comput. Phys. Commun. **9**, 141 (1975)
465. A. Hibbert, Rep. Prog. Phys. **38**, 1217 (1975)
466. A. Hibbert, C. Froese Fischer, Comput. Phys. Commun. **64**, 417 (1991)
467. K. Higgins, P.G. Burke, J. Phys. B At. Mol. Opt. Phys. **24**, L343 (1991)
468. K. Higgins, P.G. Burke, J. Phys. B At. Mol. Opt. Phys. **26**, 4269 (1993)
469. K. Higgins, P.G. Burke, in *New Directions in Atomic Physics*, ed. by C.T. Whelan, R.M. Dreizler, J.H. Macek, H.R.J. Walters (Kluwer Academic/Plenum Publishers, New York, NY, 1999), p. 217
470. K. Higgins, P.G. Burke, H.R.J. Walters, J. Phys. B At. Mol. Opt. Phys. **23**, 1345 (1990)
471. K. Higgins, C.J. Noble, P.G. Burke, J. Phys. B At. Mol. Opt. Phys. **27**, 3203 (1994)
472. K. Higgins, C.J. Gillan, P.G. Burke, C.J. Noble, J. Phys. B At. Mol. Opt. Phys. **28**, 3391 (1995)
473. T.-S. Ho, S.-I. Chu, Chem. Phys. Lett. **141**, 315 (1987)
474. E.W. Hobson, *The Theory of Spherical and Ellipsoidal Harmonics* (Cambridge University Press, Cambridge, UK, 1931)
475. K.R. Hoffman, M.S. Dababneh, Y.-F. Hsieh, W.E. Kauppila, V. Pol, J.H. Smart, T.S. Stein, Phys. Rev. A **25**, 1393 (1982)
476. H. Hotop, M.-W. Ruf, M. Allan, I.I. Fabrikant, Adv. At. Mol. Opt. Phys. **49**, 85 (2003)
477. R. Huby, Proc. Phys. Soc. A **67**, 1103 (1954)
478. E.T. Hudson, K. Bartschat, M.P. Scott, P.G. Burke, V.M. Burke, J. Phys. B At. Mol. Opt. Phys. **29**, 5513 (1996)
479. M.M. Hull, G. Breit, in *Handbuch der Physik*, vol. 41/1, ed. by S. Flügge (Springer, Berlin, Göttingen, Heidelberg, 1959), p. 408
480. L. Hulthén, Kgl. Fysiogr. Sallsk. Lund Förh. **14**, 21 (1944)
481. L. Hulthén, Arkiv. Mat. Ast. Fys. **35A**, 25 (1948)
482. D.G. Hummer, K.A. Berrington, W. Eissner, A.K. Pradhan, H.E. Saraph, J.A. Tully, Astron. Astrophys. **279**, 298 (1993)
483. W.M. Huo, in *Computational Methods for Electron–Molecule Collisions*, ed. by W.M. Huo, F.A. Gianturco (Plenum Press, New York, NY, 1995), p. 327
484. E.A. Hylleraas, B. Undheim, Z. Phys. **65**, 759 (1930)
485. A. Igarashi, I. Toshima, Phys. Rev. A **50**, 232 (1994)
486. A. Igarashi, I. Shimamura, Phys. Rev. A **56**, 4733 (1997)
487. A. Igarashi, I. Shimamura, Phys. Rev. A **70**, 012706 (2004)
488. A. Igarashi, I. Shimamura, J. Phys. B At. Mol. Opt. Phys. **37**, 4221 (2004)
489. C.A. Iglesias, F.J. Rogers, Astrophys. J. **464**, 943 (1996)
490. C.A. Iglesias, F.J. Rogers, B.G. Wilson, Astrophys. J. **322**, L45 (1987)
491. J.E. Inglesfield, J. Phys. C Solid State Phys. **14**, 3795 (1981)
492. J.E. Inglesfield, in *Supercomputing Collision Processes and Applications,* ed. by K.L. Bell, K.A. Berrington, D.S.F. Crothers, A. Hibbert, K.T. Taylor (Kluwer Academic/Plenum Publishers, New York, NY, 1999), p. 183
493. C. Iu, G.R. Welch, M.M. Kash, K. Hsu, D. Kleppner, Phys. Rev. Lett. **63**, 1136 (1989)
494. C. Iu, G.R. Welch, M.M. Kash, D. Kleppner, D. Delande, J.-C. Gay, Phys. Rev. Lett. **66**, 145 (1991)
495. J.L. Jackson, Phys. Rev. **83**, 301 (1951)
496. V.L. Jacobs, E. Behar, J. Quant. Spectrosc. Radiat. Transf. **65**, 317 (2000)
497. H. Jacubowicz, D.L. Moores, J. Phys. B At. Mol. Phys. **14**, 3733 (1981)
498. H.A. Jahn, J. Hope, Phys. Rev. **93** 318 (1954)
499. J.M. Jauch, F. Rohrlich, *The Theory of Photons and Electrons* (Addison-Wesley, Cambridge, MA, 1955)
500. T. Jayasekera, M.A. Morrison, K. Mullen, Phys. Rev. B **74**, 0235308 (2006)
501. T. Jayasekera, N. Goel, M.A. Morrison, K. Mullen, Physica E **34**, 584 (2006)
502. T. Jayasekera, K. Mullen, M.A. Morrison, Phys. Rev. B **75**, 035314 (2007)
503. C.J. Joachain, *Quantum Collision Theory*, 3rd edn. (North Holland, Amsterdam, 1983)
504. C.J. Joachain, M. Dörr, N.J. Kylstra, Adv. At. Mol. Opt. Phys. **42**, 225 (2000)

505. S. Johansson, Phys. Scr. **18**, 217 (1978)
506. B.R. Johnson, J. Comput. Phys. **13**, 445 (1973)
507. W.M. Johnstone, W.R. Newell, J. Phys. B At. Mol. Opt. Phys. **26**, 129 (1993)
508. G.O. Jones, M. Charlton, J. Slevin, G. Laricchia, Á. Kövér, M.R. Poulsen, S. Nic Chormaic, J. Phys. B At. Mol. Opt. Phys. **26**, L483 (1993)
509. M. Jones, J. Phys. B At. Mol. Phys. **3**, 1571 (1970)
510. M. Jones, Philos. Trans. R. Soc. **277**, 587 (1975)
511. P. Jones, J.E. Inglesfield, J.J.M. Michiels, C.J. Noble, V.M. Burke, P.G. Burke, Phys. Rev. B **62**, 13508 (2000)
512. S. Jones, D.H. Madison, Phys. Rev. A **62**, 042701 (2000)
513. S. Jones, D.H. Madison, Phys. Rev. A **65**, 052727 (2002)
514. P. Jönsson, X. He, C. Froese Fischer, I.P. Grant, Comput. Phys. Commun. **177** , 597 (2007)
515. R. Jost, Helv. Phys. Acta. **20**, 256 (1947)
516. Ch. Jungen, Phys. Rev. Lett. **53**, 2394 (1984)
517. Ch. Jungen, O. Atabek, J. Chem. Phys. **66**, 5584 (1977)
518. Ch. Jungen, D. Dill, J. Chem. Phys. **73**, 3338 (1980)
519. Ch. Jungen, S.C. Ross, Phys. Rev. A **55**, R2503 (1997)
520. B.R. Junker, Adv. At. Mol. Phys. **18**, 207 (1982)
521. P.L. Kapur, R.E. Peierls, Proc. R. Soc. A **166**, 277 (1938)
522. D. Kato, S. Watanabe, Phys. Rev. Lett. **74**, 2443 (1995)
523. D. Kato, S. Watanabe, J. Phys. B At. Mol. Opt. Phys. **29**, L779 (1996)
524. D. Kato, S. Watanabe, Phys. Rev. A **56**, 3687 (1997)
525. T. Kato, Progr. Theor. Phys. **6**, 295, 394 (1951)
526. A.K. Kazansky, V.N. Ostrovsky, J. Phys. B At. Mol. Opt. Phys. **27**, 447 (1994)
527. F.P. Keenan, A. Hibbert, P.G. Burke, K.A. Berrington, Astrophys. J. **332**, 539 (1988)
528. J. Kendrick, B.D. Buckley, An adaptation of the ALCHEMY atomic and molecular integrals packages for R-matrix electron-molecular collisions, Daresbury Laboratory Technical Memorandum, DL/SCI/TM18T, 1980
529. R.E. Kennerly, Phys. Rev. A **21**, 1876 (1980)
530. R.E. Kennerly, R.A. Bonham, Phys. Rev. A **17**, 1844 (1978)
531. A.A. Kernoghan, Positron scattering by atomic hydrogen and alkali metals, PhD Thesis, Queen's University Belfast
532. A.A. Kernoghan, D.J.R. Robinson, M.T. McAlinden, H.R.J. Walters, J. Phys. B At. Mol. Opt. Phys. **29**, 2089 (1996)
533. M.A. Khakoo, J. Wrkich, M. Larsen, G. Kleiban, I. Kanik, S. Trajmar, M.J. Brunger, P.J.O. Teubner, A. Crowe, C.J. Fontes, R.E.H. Clark, V. Zeman, K. Bartschat, D.H. Madison, R. Srivastava, A.D. Stauffer, Phys. Rev. A **65**, 062711 (2002)
534. G. Kilgus, J. Berger, P. Blatt, M. Grieser, D. Habs, B. Hochadel, E. Jaeschke, D. Krämer, R. Neumann, G. Neureither, W. Ott, D. Schwalm, M. Steck, R. Stokstad, E. Szmola, A. Wolf, R. Schuch, A. Müller, M. Wagner, Phys. Rev. Lett. **64**, 737 (1990)
535. G.W. King, R.M. Hainer, P.C. Cross, J. Chem. Phys. **11**, 27 (1943)
536. G.W. King, R.M. Hainer, P.C. Cross, J. Chem. Phys. **17**, 826 (1949)
537. H. Klar, J. Phys. B At. Mol. Phys. **14**, 3255 (1981)
538. H. Klar, W. Schlecht, J. Phys. B At. Mol. Phys. **9**, 1669 (1976)
539. B.A. Kniehl, A.A. Penin, Phys. Rev. Lett. **85**, 1210 (2000)
540. P.L. Knight, Comm. At. Mol. Phys. **15**, 193 (1984)
541. P.L. Knight, M.A. Lauder, B.J. Dalton, Phys. Rep. **190**, 1 (1990)
542. W. Kohn, Phys. Rev. **74**, 1763 (1948)
543. V. Kokoouline, C.H. Greene, Phys. Rev. Lett. **90**, 133201 (2003)
544. V. Kokoouline, C.H. Greene, Phys. Rev. A **68**, 012703 (2003)
545. V. Kokoouline, C.H. Greene, Phys. Rev. A **72**, 022712 (2005)
546. V. Kokoouline, F. Masnou-Seeuws, Phys. Rev. A **73**, 012702 (2006)
547. H.A. Kramers, *Collected Scientific Papers* (North Holland, Amsterdam, 1956), p. 272
548. J.L. Krause, K.J. Schafer, K.C. Kulander, Phys. Rev. Lett. **68**, 3535 (1992)

549. J.L. Krause, K.J. Schafer, K.C. Kulander, Phys. Rev. A **45**, 4998 (1992)
550. N.M. Kroll, K.M. Watson, Phys. Rev. A **8**, 804 (1973)
551. T.S. Kuhn, J.A. van Vleck, Phys. Rev. **79**, 382 (1950)
552. K.C. Kulander, B.W. Shore, Phys. Rev. Lett. **62**, 524 (1989)
553. K.C. Kulander, B.W. Shore, J. Opt. Soc. Am. B **7**, 502 (1990)
554. K.C. Kulander, K.J. Schafer, J.L. Krause, in Adv. At. Mol. Opt. Phys. Suppl. 1, *Atoms in Intense Laser Fields*, ed. by M. Gavrila (Academic Press, New York, 1992), p. 247
555. K.C. Kulander, K.J. Shafer, J.L. Krause, in *Super-Intense Laser–Atom Physics*, ed. by B. Piraux, A. L'Huillier, K. Rzazewski (Plenum Press, New York, NY, 1993), p. 95
556. M. Kurka, A. Rudenko, L. Foucar, K.U. Kühnel, Y.H. Jiang, Th. Ergler, T. Havermeier, M. Smolarski, S. Schössler, K. Cole, M. Schöffler, R. Dörner, M. Gensch, S. Düsterer, R. Treusch, S. Fritzsche, A.N. Grum-Grzhimailo, E.V. Gryzlova, N.M. Kabachnik, C.D. Schröter, R. Moshammer, J. Ullrich, J. Phys. B At. Mol. Opt. Phys. **42**, 141002 (2009)
557. N.J. Kylstra, C.J. Joachain, Phys. Rev. A **57**, 412 (1998)
558. K.J. LaGattuta, Phys. Rev. A **36**, 4662 (1987)
559. K.J. LaGattuta, Phys. Rev. A **38**, 1820 (1988)
560. K. Laghdas, R.H.G. Reid, C.J. Joachain, P.G. Burke, J. Phys. B At. Mol. Opt. Phys. **28**, 4811 (1995)
561. K. Laghdas, R.H.G. Reid, C.J. Joachain, P.G. Burke, J. Phys. B At. Mol. Opt. Phys. **32**, 1439 (1999)
562. G. Lagmago Kamta, A.F. Starace, Phys. Rev. Lett. **86**, 5687 (2001)
563. C. Lanczos, J. Res. Natl. Bur. Stand. **45**, 255 (1950)
564. M. Landtman, C. Laughlin, Y.-T. Shen, J.E. Hansen, J. Phys. B At. Mol. Opt. Phys. **26**, 1081 (1993)
565. A.M. Lane, J. Phys. B At. Mol. Phys. **19**, 253 (1986)
566. A.M. Lane, R.G. Thomas, Rev. Mod. Phys. **30**, 257 (1958)
567. A.M. Lane, D. Robson, Phys. Rev. **151**, 774 (1966)
568. A.M. Lane, D. Robson, Phys. Rev. **178**, 1715 (1969)
569. A.M. Lane, D. Robson, Phys. Rev. **185**, 1403 (1969)
570. M. Lange, J. Matsumoto, S. Buckman, O. Zatsarinny, K. Bartschat, I. Bray, D.V. Fursa, J. Phys. B At. Mol. Opt. Phys. **39**, 4179 (2006)
571. P.W. Langhoff, Chem. Phys. Lett. **22**, 60 (1973)
572. P.W. Langhoff, W.P. Reinhardt, Chem. Phys. Lett. **24**, 495 (1974)
573. L. Lapidus, J.H. Seinfeld, *Numerical Solution of Ordinary Differential Equations* (Academic Press, New York, NY, London, 1971)
574. G. Laricchia, Nucl. Instrum. Methods B **99**, 363 (1995)
575. G. Laricchia, Hyperfine Interact. **100**, 71 (1996)
576. G. Laricchia, in *New Directions in Atomic Physics*, ed. by C.T. Whelan, R.M. Dreizler, J.H. Macek, H.R.J. Walters (Kluwer Academic/Plenum Publishers, New York, NY, Boston, MA, Dordrecht, London, Moscow, 1999), p. 245
577. G. Laricchia, M. Charlton, T.C. Griffith, F.M. Jacobson, in *Positron (Electron)–Gas Scattering*, ed. by W.E. Kaupila, T.S. Stein, J.M. Wadehra (World Scientific, Singapore, 1986), p. 303
578. G. Laricchia, M. Charlton, S.A. Davies, C.D. Beling, T.C. Griffith, J. Phys. B At. Mol. Phys. **20**, L99 (1987)
579. G. Laricchia, N. Zafar, M. Charlton, T.C. Griffith, Hyperfine Interact. **73**, 133 (1992)
580. G. Laricchia, S. Armitage, D.E. Leslie, Nucl. Instrum. Methods B **221**, 60 (2004)
581. O. Latinne, N.J. Kylstra, M. Dörr, J. Purvis, M. Terao-Dunseath, C.J. Joachain, P.G. Burke, Phys. Rev. Lett. **74**, 46 (1995)
582. E.G. Layton, J. Phys. B At. Mol. Opt. Phys. **26**, 2501 (1993)
583. E.G. Layton, E. Stade, J. Phys. B At. Mol. Opt. Phys. **26**, L489 (1993)
584. M. Le Dourneuf, J.-M. Launay, P.G. Burke, J. Phys. B At. Mol. Opt. Phys. **23**, L559 (1990)
585. C.M. Lee, Phys. Rev. A **10**, 584 (1974)

586. H. Le Rouzo, G. Raşeev, Phys. Rev. A **29**, 1214 (1984)
587. N. Levinson, K. Dan. Vidensk. Selsk. Mat.-Fys. Medd. **25**, 9 (1949)
588. B.R. Levy, J.B. Keller, J. Math. Phys. **4**, 54 (1963)
589. M. Lewenstein, P. Balcou, M.Yu. Ivanov, A. L'Huillier, P.B. Corkum, Phys. Rev. A **49**, 2117 (1994)
590. A. L'Huillier, P. Balcou, Phys. Rev. Lett. **70**, 774 (1993)
591. A. L'Huillier, K.J. Schafer, K.C. Kulander, J. Phys. B At. Mol. Opt. Phys. **24**, 3315 (1991)
592. A. L'Huillier, L.-A. Lombré, G. Mainfray, C. Manus, in Adv. At. Mol. Opt. Phys. Suppl. 1, *Atoms in Intense Laser Fields*, ed. by M. Gavrila (Academic Press, New York, NY, 1992), p. 139
593. D.A. Liberman, B.I. Bennett, Phys. Rev. B **42**, 2475 (1990)
594. J.C. Light, R.B. Walker, J. Chem. Phys. **65**, 4272 (1976)
595. J.C. Light, R.B. Walker, E.B. Stechel, T.G. Schmalz, Comput. Phys. Commun. **17**, 89 (1979)
596. J.C. Light, I.P. Hamilton, J.V. Lill, J. Chem. Phys. **82**, 1400 (1985)
597. J.V. Lill, G.A. Parker, J.C. Light, Chem. Phys. Lett. **89**, 483 (1982)
598. C.D. Lin, Phys. Rev. A **10**, 1986 (1974)
599. C.D. Lin, Phys. Rev. A **25**, 76 (1982)
600. B.A. Lippmann, J. Schwinger, Phys. Rev. **79**, 459 (1950)
601. B.A. Lippmann, H.M. Schey, Phys. Rev. **121**, 1112 (1961)
602. K.T. Lu, F.S. Tomkins, W.R.S. Garton, Proc. R. Soc. A **362**, 421 (1978)
603. M.A. Lysaght, P.G. Burke, H.W. van der Hart, Phys. Rev. Lett. **101**, 253001 (2008)
604. M.A. Lysaght, P.G. Burke, H.W. van der Hart, Phys. Rev. A **79**, 053411 (2009)
605. M.A. Lysaght, P.G. Burke, H.W. van der Hart, 2009, Phys. Rev. Lett. **102**, 193001 (2009)
606. M.A. Lysaght, S. Hutchinson, H.W. van der Hart, New J. Phys. **11**, 093014 (2009)
607. M.T. McAlinden, A.A. Kernoghan, H.R.J. Walters, Hyperfine Interact. **89**, 161 (1994)
608. M.T. McAlinden, A.A. Kernoghan, H.R.J. Walters, J. Phys. B At. Mol. Opt. Phys. **27**, L625 (1994)
609. M.T. McAlinden, A.A. Kernoghan, H.R.J. Walters, J. Phys. B At. Mol. Opt. Phys. **29**, 555 (1996)
610. M.T. McAlinden, A.A. Kernoghan, H.R.J. Walters, J. Phys. B: At. Mol. Opt. Phys. **29**, 3971 (1996)
611. M.T. McAlinden, A.A. Kernoghan, H.R.J. Walters, J. Phys. B At. Mol. Opt. Phys. **30**, 1543 (1997)
612. I.E. McCarthy, A.T. Stelbovics, Phys. Rev. A **22**, 502 (1980)
613. I.E. McCarthy, A.T. Stelbovics, J. Phys. B At. Mol. Phys. **16**, 1233 (1983)
614. C.W. McCurdy, T.N. Rescigno, Phys. Rev. A **39**, 4487 (1989)
615. C.W. McCurdy, M. Baertschy, T.N. Rescigno, J. Phys. B At. Mol. Opt. Phys. **37**, R137 (2004)
616. F.A. McDonald, J. Nuttall, Phys. Rev. Lett. **23**, 361 (1969)
617. R.P. McEachran, A.D. Stauffer, J. Phys. B At. Mol. Phys. **16**, 4023 (1983)
618. J.H. Macek, Phys. Rev. **160**, 170 (1967)
619. J. Macek, J. Phys. B At. Mol. Phys. **1**, 831 (1968)
620. J. Macek, Phys. Rev. A **2**, 1101 (1970)
621. J.H. Macek, P.G. Burke, Proc. Phys. Soc. **92**, 351 (1967)
622. J.H. Macek, S.Yu. Ovchinnikov, Phys. Rev. A **54**, 544 (1976)
623. C. McKenna, H.W. van der Hart, J. Phys. B At. Mol. Opt. Phys. **36**, 1627 (2003)
624. C. McKenna, H.W. van der Hart, J. Phys. B At. Mol. Opt. Phys. **37**, 457 (2004)
625. B.J. McKenzie, I.P. Grant, P.H. Norrington, Comput. Phys. Commun. **21**, 233 (1980)
626. J.J. Macklin, J.D. Kmetec, C.L. Gordon, Phys. Rev. Lett. **70**, 766 (1993)
627. A. McPherson, G. Gibson, H. Jara, U. Johann, T.S. Luk, I.A. McIntyre, K. Boyer, C.K. Rhodes, J. Opt. Soc. Am. B **4**, 595 (1987)
628. D.H. Madison, R.V. Calhoun, W.N. Shelton, Phys. Rev. A **16**, 552 (1977)
629. D.H. Madison, I. Bray, I.E. McCarthy, J. Phys. B At. Mol. Opt. Phys. **24**, 3861 (1991)

630. C. Mahaux, H.A. Weidenmüller, *Shell-Model Approach to Nuclear Reactions* (North Holland, Amsterdam, London, 1969)
631. L. Malegat, J. Phys. B At. Mol. Opt. Phys. **27**, L691 (1994)
632. A. Maquet, S.-I. Chu, W.P. Reinhardt, Phys. Rev. A **27**, 2946 (1983)
633. P.J. Marchalant, K. Bartschat, J. Phys. B At. Mol. Opt. Phys. **30**, 4373 (1997)
634. P.J. Marchalant, K. Bartschat, Phys. Rev. A **56**, R1697 (1997)
635. P.J. Marchalant, C.T. Whelan, H.R.J. Walters, J. Phys. B At. Mol. Opt. Phys. **31**, 1141 (1998)
636. P.J. Marchalant, J. Rasch, C.T. Whelan, D.H. Madison, H.R.J. Walters, J. Phys. B At. Mol. Opt. Phys. **32**, L705 (1999)
637. P.J. Marchalant, B. Rouvellou, J. Rasch, S. Rioual, C.T. Whelan, A. Pochat, D.H. Madison, H.R.J. Walters, J. Phys. B At. Mol. Opt. Phys. **33**, L749 (2000)
638. P.De A.P. Martins, M.J. Seaton, J. Phys. B At. Mol. Phys. **2**, 333 (1969)
639. N.J. Mason, Rep. Prog. Phys. **56**, 1275 (1993)
640. N.J. Mason, W.R. Newell, J. Phys. B At. Mol. Phys. **20**, L323 (1987)
641. N.J. Mason, W.R. Newell, J. Phys. B At. Mol. Phys. **22**, 777 (1987)
642. H.S.W. Massey, C.B.O. Mohr, Proc. R. Soc. A **136**, 289 (1932)
643. H.S.W. Massey, C.B.O. Mohr, Proc. R. Soc. A **139**, 187 (1933)
644. H.S.W. Massey, D.R. Bates, Rep. Prog. Phys. **9**, 62 (1942)
645. H.S.W. Massey, R.O. Ridley, Proc. Phys. Soc. A **69**, 658 (1956)
646. J.A.D. Matthew, W.A. Henle, M.G. Ramsey, F.P. Netzer, Phys. Rev. B **43**, 4897 (1991)
647. J. Mauritsson, P. Johnsson, E. Mansten, M. Swoboda, T. Ruchon, A. L'Huillier, K.J. Schafer, Phys. Rev. Lett. **100**, 073003 (2008)
648. J.J.M. Michiels, J.E. Inglesfield, C.J. Noble, V.M. Burke, P.G. Burke, Phys. Rev. Lett. **78**, 2851 (1997)
649. J.J.M. Michiels, J.E. Inglesfield, C.J. Noble, V.M. Burke, P.G. Burke, J. Phys. Condens. Matter **9**, L543 (1997)
650. A.G. Middleton, M.J. Brunger, P.J.O. Teubner, M.W.B. Anderson, C.J. Noble, G. Wöste, K. Blum, P.G. Burke, C. Fullerton, J. Phys. B At. Mol. Opt. Phys. **27**, 4057 (1994)
651. W.H. Miller, Comm. At. Mol. Phys. **22**, 115 (1988)
652. G.V. Mil'nikov, H. Nakamura, J. Phys. B At. Mol. Opt. Phys. **34**, L791 (2001)
653. D.M. Mitnik, M.S. Pindzola, D.C. Griffin, N.R. Badnell, J. Phys. B At. Mol. Opt. Phys. **32**, L479 (1999)
654. D.M. Mitnik, D.C. Griffin, N.R. Badnell, J. Phys. B At. Mol. Opt. Phys. **34**, 4455 (2001)
655. D.M. Mitnik, D.C. Griffin, C.P. Ballance, N.R. Badnell, J. Phys. B At. Mol. Opt. Phys. **36**, 717 (2003)
656. B.L. Moiseiwitsch, *Variational Principles* (Interscience, New York, NY, 1966)
657. D.L. Moores, Proc. Phys. Soc. **88**, 843 (1966)
658. D.L. Moores, Proc. Phys. Soc. **91**, 830 (1967)
659. L.A. Morgan, J. Phys. B At. Mol. Phys. **19**, L439 (1986)
660. L.A. Morgan, in *Computational Methods for Electron-Molecule Collisions*, ed. by W.M. Huo, F.A. Gianturco (Plenum Press, New York, NY, 1995), p. 277
661. L.A. Morgan, C.J. Gillan, J. Tennyson, X. Chen, J. Phys. B At. Mol. Opt. Phys. **30**, 4087 (1997)
662. L.A. Morgan, J. Tennyson, C.J. Gillan, Comput. Phys. Commun. **114**, 120 (1998)
663. M.A. Morrison, Adv. At. Mol. Phys. **24**, 51 (1987)
664. P.M. Morse, H. Feshbach, *Methods of Theoretical Physics* (McGraw-Hill, New York, NY, 1953)
665. N.F. Mott, H.S.W. Massey, *The Theory of Atomic Collisions*, 1st edn. (Clarendon Press, Oxford, 1933).
666. N.F. Mott, H.S.W. Massey, *The Theory of Atomic Collisions*, 3rd edn. (Clarendon Press, Oxford, 1965)
667. L. Mouret, K.M. Dunseath, M. Terao-Dunseath, J.-M. Launay, J. Phys. B At. Mol. Opt. Phys. **36**, L39 (2003)

668. F. Mrugala, D. Secrest, J. Chem. Phys. **78**, 5954 (1983)
669. A. Müller, G. Hofmann, K. Tinschert, E. Satzborn, Phys. Rev. Lett. **61**, 1352 (1988)
670. F. Müller, P. Steiner, Th. Straub, D. Reinicke, S. Palm, R. de Masi, S. Hüfner, Surf. Sci. **442**, 485 (1999)
671. S.N. Nahar, A.K. Pradhan, Phys. Rev. A **44**, 2935 (1991)
672. S.N. Nahar, A.K. Pradhan, Phys. Rev. Lett. **68**, 1488 (1992)
673. S.N. Nahar, A.K. Pradhan, Phys. Rev. A **49**, 1816 (1994)
674. M. Nekovee, J.E. Inglesfield, Europhys. Lett. **19**, 535 (1992)
675. R.K. Nesbet, Phys. Rev. **175**, 134 (1968)
676. R.K. Nesbet, Phys. Rev. **179**, 60 (1969)
677. R.K. Nesbet, Phys. Rev. A **20**, 58 (1979)
678. R.K. Nesbet, *Variational Methods in Electron-Atom Scattering Theory* (Plenum Press, New York, NY and London, 1980)
679. R.K. Nesbet, S. Mazevet, M.A. Morrison, Phys. Rev. A **64**, 034702 (2001)
680. B.M. Nestmann, S.D. Peyerimhoff, J. Phys. B At. Mol. Opt. Phys. **23**, L773 (1990)
681. B.M. Nestmann, R.K. Nesbet, S.D. Peyerimhoff, J. Phys. B At. Mol. Opt. Phys. **24**, 5133 (1991)
682. B.M. Nestmann, K. Pfingst, S.D. Peyerimhoff, J. Phys. B At. Mol. Opt. Phys. **27**, 2297 (1994)
683. G.G. Newton, *Scattering Theory of Waves and Particles* (McGraw-Hill Inc., New York, NY, 1966)
684. K.R. Nicolas, PhD Thesis, University of Maryland, 1977
685. L.A.A. Nikolopoulos, J.S. Parker, K.T. Taylor, Phys. Rev. A **78**, 063420 (2008)
686. C.J. Noble, Comput. Phys. Commun. **159**, 55 (2004)
687. C.J. Noble, R.K. Nesbet, Comput. Phys. Commun. **33**, 399 (1984)
688. C.J. Noble, P.G. Burke, J. Phys. B At. Mol. Phys. **19**, L35 (1986)
689. C.J. Noble, P.G. Burke, Phys. Rev. Lett. **68**, 2011 (1992)
690. C.J. Noble, P.G. Burke, S. Salvini, J. Phys. B At. Mol. Phys. **15**, 3779 (1982)
691. C.J. Noble, K. Higgins, P. Duddy, P.G. Burke, P.J.O. Teubner, A.G. Middleton, M.J. Brunger, Phys. Rev. Lett. **76**, 3534 (1996)
692. D.W. Norcross, J. Phys. B At. Mol. Phys. **2**, 1300 (1969)
693. D.W. Norcross, Comput. Phys. Commun. **6**, 257 (1974)
694. D.W. Norcross, M.J. Seaton, J. Phys. B At. Mol. Phys. **2**, 731 (1969)
695. D.W. Norcross, M.J. Seaton, J. Phys. B At. Mol. Phys. **3**, 579 (1970)
696. P.H. Norrington, I.P. Grant, J. Phys. B At. Mol. Phys. **14**, L261 (1981)
697. P.H. Norrington, I.P. Grant, J. Phys. B At. Mol. Phys. **20**, 4869 (1987)
698. P.H. Norrington, I.P. Grant, available online at http://www.am.qub.ac.uk/DARC/
699. H. Nussbaumer, P.J. Storey, Astron. Astrophys. A **89**, 308 (1980)
700. H.M. Nussenzveig, Nucl. Phys. **11**, 499 (1959)
701. R.S. Oberoi, R.K. Nesbet, Phys. Rev. A **8**, 215 (1973)
702. R.S. Oberoi, R.K. Nesbet, Phys. Rev. A **9**, 2804 (1974)
703. P.E. O'Mahony, K.T. Taylor, Phys. Rev. Lett. **57**, 2931 (1986)
704. T.F. O'Malley, L. Spruch, L. Rosenberg, J. Math. Phys. **2**, 491 (1961)
705. T.F. O'Malley, P.G. Burke, K.A. Berrington, J. Phys. B At. Mol. Phys. **12**, 953 (1979)
706. Opacity Project Team, *The Opacity Project*, vol. 1 (Institute of Physics Publishing, Bristol, 1995)
707. Opacity Project Team, *The Opacity Project*, vol. 2 (Institute of Physics Publishing, Bristol, 1997)
708. R.J. Ord-Smith, Phys. Rev. **94**, 1227 (1954)
709. D.E. Osterbrock, *Astrophysics of Gaseous Nebulae and Active Galactic Nuclei* (University Science Books, Sausalito, CA, 1989)
710. D.H. Oza, Phys. Rev. A **30**, 1101 (1984)
711. D.H. Oza, J. Callaway, Phys. Rev. A **27**, 2840 (1983)

712. T.J. Park, J.C. Light, J. Chem. Phys. **85**, 5870 (1986)
713. J. Parker, K.T. Taylor, C.W. Clark, S. Blodgett-Ford, J. Phys. B At. Mol. Opt. Phys. **29**, L33 (1996)
714. J.S. Parker, E.S. Smyth, K.T. Taylor, J. Phys. B At. Mol. Opt. Phys. **31**, L571 (1998)
715. J.S. Parker, D.H. Glass, L.R. Moore, E.S. Smyth, K.T. Taylor, P.G. Burke, J. Phys. B At. Mol. Opt. Phys. **33**, L239 (2000)
716. J.S. Parker, L.R. Moore, K.J. Meharg, D. Dundas, K.T. Taylor, J. Phys. B At. Mol. Opt. Phys. **34**, L69 (2001)
717. J.S. Parker, B.J.S. Doherty, K.T. Taylor, K.D. Schultz, C.I. Blaga, L.F. DiMauro, Phys. Rev. Lett. **96**, 133001 (2006)
718. F.A. Parpia, C. Froese Fischer, I.P. Grant, Comput. Phys. Commun. **94**, 249 (1996)
719. F.A. Parpia, C. Froese Fischer, I.P. Grant, Comput. Phys. Commun. **175**, 745 (2006)
720. A. Pathak, A.E. Kingston, K.A. Berrington, J. Phys. B At. Mol. Opt. Phys. **21**, 2939 (1988)
721. A. Pathak, P.G. Burke, K.A. Berrington, J. Phys. B At. Mol. Opt. Phys. **22**, 2759 (1989)
722. P.M. Paul, E.S. Toma, P. Breger, G. Mullot, F. Augé, Ph. Balcou, H.G. Muller, P. Agostini, Science **292**, 1689 (2001)
723. W. Pauli, Zeits. f. Phys. **43**, 601 (1927)
724. F.M. Peeters, Phys. Rev. Lett. **61**, 589 (1987)
725. J.B. Pendry, D.K. Saldin, Surf. Sci. **145**, 33 (1984)
726. I.C. Percival, M.J. Seaton, Proc. Camb. Philos. Soc. **53**, 654 (1957)
727. A.M. Perelomov, V.S. Popov, M.V. Terent'ev, Sov. Phys. JETP, **23**, 924 (1966)
728. R. Peterkop, J. Phys. B At. Mol. Phys. **4**, 513 (1971)
729. R.K. Peterkop, *Theory of Ionization of Atoms by Electron Impact* (Colorado Associated University Press, Boulder, CO, 1977)
730. R. Peterkop, J. Phys. B At. Mol. Phys. **16**, L587 (1983)
731. T. Pfeifer, C. Spielmann, G. Gerber, Rep. Prog. Phys. **69**, 443 (2006)
732. K. Pfingst, B.M. Nestmann, S.D. Peyerimhoff, J. Phys. B At. Mol. Opt. Phys. **27**, 2283 (1994)
733. K. Pfingst, B.M. Nestmann, S.D. Peyerimhoff, in *Computational Methods for Electron-Molecule Collisions*, ed. by W.M. Huo, F.A. Gianturco (Plenum Press, New York, NY, 1995), p. 293
734. R.A. Phaneuf, C.C. Havener, G.H. Dunn, A. Müller, Rep. Prog. Phys. **62**, 1143 (1999)
735. F. Pichou, A. Huetz, G. Joyez, M. Landau, J. Phys. B At. Mol. Phys. **11**, 3683 (1978)
736. M.S. Pindzola, D.R. Schultz, Phys. Rev. A **53**, 1525 (1996)
737. M.S. Pindzola, F. Robicheaux, Phys. Rev. A **54**, 2142 (1996)
738. M.S. Pindzola, F. Robicheaux, Phys. Rev. A **57**, 318 (1998)
739. M.S. Pindzola, G.J. Bottrell, C. Botcher, J. Opt. Soc. Am. B **7**, 659 (1990)
740. M.S. Pindzola, F. Robicheaux, S.D. Loch, J.C. Berengut, T. Topcu, J. Colgan, M. Foster, D.C. Griffin, C.P. Ballance, D.R. Schultz, T. Minami, N.R. Badnell, M.C. Witthoeft, D.R. Plante, D.M. Mitnik, J.A. Ludlow, U. Klieman, J. Phys. B At. Mol. Opt. Phys. **40**, R39 (2007)
741. B. Piraux, R. Shakeshaft, Phys. Rev. A **49**, 3903 (1994)
742. M. Plummer, J.F. McCann, J. Phys. B At. Mol. Opt. Phys. **29**, 4625 (1996)
743. M. Plummer, C.J. Noble, J. Phys. B At. Mol. Opt. Phys. **32**, L345 (1999)
744. M. Plummer, C.J. Noble, J. Phys. B At. Mol. Opt. Phys. **33**, L807 (2000)
745. M. Plummer, C.J. Noble, J. Phys. B At. Mol. Opt. Phys. **35**, L51 (2002)
746. M. Plummer, C.J. Noble, J. Phys. B At. Mol. Opt. Phys. **36**, L219 (2003)
747. R. Poet, J. Phys. B At. Mol. Phys. **11**, 3081 (1978)
748. R. Poet, J. Phys. B At. Mol. Phys. **13**, 2995 (1980)
749. H. Poincaré, Acta. Math. **4**, 201 (1884)
750. S.J. Porter, J.A.D. Matthew, R.J. Leggott, Phys. Rev. B **50**, 2638 (1994)
751. J.H. Posthumus, *Molecules and Clusters in Intense Laser Fields* (Cambridge University Press, Cambridge, UK, 2001)
752. R.M. Potvliege, R. Shakeshaft, Phys. Rev. A **38**, 4597 (1988)

753. R.M. Potvliege, R. Shakeshaft, Phys. Rev. A **40**, 3061 (1989)
754. A.K. Pradhan, M.J. Seaton, J. Phys. B At. Mol. Phys. **18**, 1631 (1985)
755. A.K. Pradhan, K.A. Berrington, J. Phys. B At. Mol. Opt. Phys. **26**, 157 (1993)
756. A.K. Pradhan, H.L. Zhang, J. Phys. B At. Mol. Opt. Phys. **30**, L571 (1997)
757. W.H. Press, S.A. Teukolsky, W.T. Vetterling, B.P. Flannery, *Numerical Recipes in Fortran. The Art of Scientific Computing*, 2nd edn. (Cambridge University Press, Cambridge, UK, 1992)
758. S.G. Preston, A. Sanpera, M. Zepf, W.J. Blyth, C.G. Smith, J.S. Wark, M.H. Key, K. Burnett, N. Nakai, D. Neely, A.A. Offenberger, Phys. Rev. A **53**, R31 (1996)
759. M. Protopapas, C.H. Keitel, P.L. Knight, Rep. Prog. Phys. **60**, 389 (1997)
760. D.A. Przybyla, W. Addo-Asah, W.E. Kauppila, C.K. Kwan, T.S. Stein, Phys. Rev. A **60**, 359 (1999)
761. L. Quigley, K. Berrington, J. Phys. B At. Mol. Opt. Phys. **29**, 4529 (1996)
762. L. Quigley, K. Berrington, J. Pelan, Comput. Phys. Commun. **114**, 225 (1998)
763. I. Rabadán, J. Tennyson, J. Phys. B At. Mol. Opt. Phys. **32**, 4753 (1999)
764. G. Racah, Phys. Rev. **61**, 186 (1942)
765. G. Racah, Phys. Rev. **62**, 438 (1942)
766. G. Racah, Phys. Rev. **63**, 367 (1943)
767. G. Racah, Phys. Rev. **76**, 1352 (1949)
768. A. Raeker, K. Bartschat, R.H.G. Reid, J. Phys. B At. Mol. Opt. Phys. **27**, 3129 (1994)
769. C.A. Ramsbottom, Atom. Data Nucl. Data Tables **95**, 910 (2009)
770. C.A. Ramsbottom, M.P. Scott, K.L. Bell, F.P. Keenan, B.M. McLaughlin, A.G. Sunderland, V.M. Burke, C.J. Noble, P.G. Burke, J. Phys. B At. Mol. Opt. Phys. **35**, 3451 (2002)
771. C.A. Ramsbottom, C.J. Noble, V.M. Burke, M.P. Scott, P.G. Burke, J. Phys. B At. Mol. Opt. Phys. **37**, 3601 (2004)
772. C.A. Ramsbottom, C.J. Noble, V.M. Burke, M.P. Scott, R. Kisielius, P.G. Burke, J. Phys. B At. Mol. Opt. Phys. **38**, 2999 (2005)
773. C.A. Ramsbottom, C.E. Hudson, P.H. Norrington, M.P. Scott, Astron. Astrophys. **475**, 765 (2007)
774. G. Raşeev, H. Le Rouzo, Phys. Rev. A **27**, 268 (1983)
775. J. Rao, K.T. Taylor, J. Phys. B At. Mol. Opt. Phys. **30**, 3627 (1997)
776. A.R.P. Rau, Phys. Rev. A **4**, 207 (1971)
777. A.R.P. Rau, J. Phys. B At. Mol. Phys. **9**, L283 (1976)
778. A.R.P. Rau, Phys. Rep. **110**, 369 (1984)
779. J.W.S. Rayleigh, *The Theory of Sound*, 1st edn. (Macmillan and Co., London, 1877)
780. F.H. Read, J. Phys. B At. Mol. Phys. **17**, 3965 (1984)
781. F.H. Read, in *Electron Impact Ionization*, ed. by G.H. Dunn, T. Mark (Springer, New York, NY, 1984), p. 42
782. R.H.G. Reid, K. Bartschat, P.G. Burke, J. Phys. B At. Mol. Opt. Phys. **25**, 3175 (1992)
783. R.H.G. Reid, K. Bartschat, A. Raeker, J. Phys. B At. Mol. Opt. Phys. **31**, 563 (1998)
784. R.H.G. Reid, K. Bartschat, A. Raeker, J. Phys. B At. Mol. Opt. Phys. **33**, 5261 (2000)
785. W.P. Reinhardt, Comput. Phys. Commun. **17**, 1 (1979)
786. W.P. Reinhardt, Ann. Rev. Phys. Chem. **33**, 223 (1982)
787. T.N. Rescigno, W.P. Reinhardt, Phys. Rev. A **10**, 158 (1974)
788. T.N. Rescigno, C.W. McCurdy, A.E. Orel, B.H. Lengsfield, in *Computational Methods for Electron-Molecule Collisions*, ed by W.M. Huo, F.A. Gianturco (Plenum Press, New York, NY, 1995), p. 1
789. T.N. Rescigno, M. Baertschy, D. Byrum, C.W. McCurdy, Phys. Rev. A **55**, 4253 (1997)
790. T.N. Rescigno, M. Baertschy, W.A. Isaacs, C.W. McCurdy, Science, **286**, 2474 (1999)
791. W.D. Robb, Comput. Phys. Commun. **1**, 457 (1970)
792. W.D. Robb, PhD Thesis, Queen's University Belast, 1971
793. W.D. Robb, J. Phys. B At. Mol. Phys. **6**, 945 (1973)
794. F. Robicheaux, T.W. Gorczyca, M.S. Pindzola, N.R. Badnell, Phys. Rev. A **52** 1319 (1995)

795. D. Robson, A.M. Lane, Phys. Rev. **161**, 982 (1967)
796. K. Rohr, F. Linder, J. Phys. B At. Mol. Phys. **9**, 2521 (1976)
797. M.E. Rose, *Elementary Theory of Angular Momentum* (Wiley, New York, NY, London, 1957)
798. M.H. Ross, G.L. Shaw, Ann. Phys. (New York) **13**, 147 (1961)
799. M. Rotenberg, Ann. Phys. N.Y. **19**, 262 (1962)
800. S.L. Rubinow, Phys. Rev. **98**, 183 (1955)
801. A. Rudenko, K. Zrost, B. Feuarstein, V.L.B. de Jesus, C.D. Schröter, R. Moshammer, J. Ullrich, Phys. Rev. Lett. **93**, 253001 (2004)
802. E. Rutherford, Philos. Mag. **21**, 669 (1911)
803. Y. Saad, *Iterative Methods for Sparse Linear Systems*, 2nd edn. (SIAM, Philadelphia, PA, 2003)
804. H.R. Sadeghpour, J.L. Bohn, M.J. Cavagnero, B.D. Esry, I.I. Fabrikant, J.H. Macek, A.R.P. Rau, J. Phys. B At. Mol. Opt. Phys. **33**, R93 (2000)
805. H.P. Saha, Phys. Rev. A **39**, 5048 (1989); ibid **40**, 6111
806. K. Sakimoto, M. Terao, K.A. Berrington, Phys. Rev. A **42**, 291 (1990)
807. D.K. Saldin, J.B. Pendry, M.A. Van Hove, G.A. Somorjai, Phys. Rev. B **31**, 1216 (1985)
808. S.A. Salvini, Comput. Phys. Commun. **27**, 25 (1982)
809. G. Sansone, E. Benedetti, F. Calegari, C. Vozzi, L. Avaldi, R. Flammini, L. Poletto, P. Villoresi, C. Altucci, R. Velotta, S. Stagira, S. De Silvestri, M. Nisoli, Science **314**, 443 (2006)
810. H.E. Saraph, Comput. Phys. Commun. **3**, 256 (1972)
811. H.E. Saraph, Comput. Phys. Commun. **15**, 247 (1978)
812. H.E. Saraph, P.J. Storey, K.T. Taylor, J. Phys. B At. Mol. Opt. Phys. **25**, 4409 (1992)
813. B.K. Sarpal, J. Tennyson, L.A. Morgan, J. Phys. B At. Mol. Opt. Phys. **27**, 5943 (1994)
814. B.K. Sarpal, K. Pfingst, B.M. Nestmann, S.D. Peyerimhoff, J. Phys. B At. Mol. Opt. Phys. **29**, 857 (1996)
815. P.M.J. Sawey, K.A. Berrington, P.G. Burke, A.E. Kingston, J. Phys. B At. Mol. Opt. Phys. **23**, 4321 (1990)
816. K.J. Schafer, B. Yang, L.F. DiMauro, K.C. Kulander, Phys. Rev. Lett. **70**, 1599 (1993)
817. L.I. Schiff, *Quantum Mechanics* (McGraw-Hill, New York, NY, Toronto, ON, London, 1949)
818. L. Schlessinger, Phys. Rev. **171**, 1523 (1968)
819. L. Schlessinger, C. Schwartz, Phys. Rev. Lett. **16**, 1173 (1966)
820. L. Schlessinger, G.L. Payne, Phys. Rev. A **10**, 1559 (1974)
821. B.I. Schneider, Chem. Phys. Lett. **31** 237 (1975)
822. B.I. Schneider, Phys. Rev. A **11**, 1957 (1975)
823. B.I. Schneider, Phys. Rev. A **14**, 1923 (1976)
824. B.I. Schneider, Phys. Rev. A **24**, 1 (1981)
825. B.I. Schneider, in *Computational Methods for Electron-Molecule Collisions*, ed. by W.M. Huo, F.A. Gianturco (Plenum Press, New York, NY, 1995), p. 213
826. B.I. Schneider, P.J. Hay, Phys. Rev. A **13**, 2049 (1976)
827. B.I. Schneider, R.B. Walker, J. Chem. Phys. **70**, 2466 (1979)
828. B.I. Schneider, H.S. Taylor, J. Chem. Phys. **77**, 379 (1982)
829. B.I. Schneider, M. Le Dourneuf, P.G. Burke, J. Phys. B At. Mol. Phys. **12**, L365 (1979)
830. B.I. Schneider, M. Le Dourneuf, Vo Ky Lan, Phys. Rev. Lett. **43**, 1926 (1979)
831. I.J. Schoenberg, Q. Appl. Math. **4**, 45 (1946)
832. T.T. Scholz, J. Phys. B At. Mol. Opt. Phys. **24**, 2127 (1991)
833. A. Schramm, I.I. Fabrikant, J.M. Weber, E. Leber, M.-W. Ruf, H. Hotop, J. Phys. B At. Mol. Opt. Phys. **32**, 2153 (1999)
834. G.J. Schulz, Phys. Rev. **125**, 229 (1962)
835. G.J. Schulz, Phys. Rev. Lett. **10**, 104 (1963)
836. G.J. Schulz, Phys. Rev. Lett. **13**, 583 (1964)
837. G.J. Schulz, Phys. Rev. **135**, A988 (1964)
838. C. Schwartz, Phys. Rev. **124**, 1468 (1961)
839. C. Schwartz, Ann. Phys. (N.Y.) **16**, 36 (1961)

840. R. Schwienhorst, A. Raeker, R.H.G. Reid, K. Bartschat, J. Phys. B At. Mol. Opt. Phys. **28**, 4651 (1995)
841. J. Schwinger, Unpublished lecture notes, Harvard University, Phys. Rev. **72**, 742 (1947)
842. M.P. Scott, H. Teng, P.G. Burke, J. Phys. B At. Mol. Opt. Phys. **33**, L63 (2000)
843. N.S. Scott, P.G. Burke, J. Phys. B At. Mol. Phys. **13**, 4299 (1980)
844. N.S. Scott, K.T. Taylor, Comput. Phys. Commun. **25**, 347 (1982)
845. N.S. Scott, M.P. Scott, P.G. Burke, T. Stitt, V. Faro-Maza, C. Denis, A., Maniopoulou, Comput. Phys. Commun. **180**, 2424 (2009)
846. A. Scrinzi, B. Piraux, Phys. Rev. A **58**, 1310 (1998)
847. A. Scrinzi, M.Yu. Ivanov, R. Kienberger, D.M. Villeneuve, J. Phys. B At. Mol. Opt. Phys. **39**, R1 (2006)
848. M.J. Seaton, Philos. Trans. R. Soc. A **245**, 469 (1953)
849. M.J. Seaton, Proc. R. Soc. A **231**, 37 (1955)
850. M.J. Seaton, in *The Airglow and Aurora*, ed. by E.B. Armstrong, A. Dalgarno (Pergamon Press, Oxford, 1955)
851. M.J. Seaton, C.R. Acad. Sci. Paris **240**, 1317 (1955)
852. M.J. Seaton, Mon. Not. R. Astron. Soc. **118**, 504 (1958)
853. M.J. Seaton, Observatory **82**, 111 (1962)
854. M.J. Seaton, Proc. Phys. Soc. **88**, 801 (1966)
855. M.J. Seaton, Proc. Phys. Soc. **88**, 815 (1966)
856. M.J. Seaton, J. Phys. B At. Mol. Phys. **2**, 5 (1969)
857. M.J. Seaton, Adv. At. Mol. Phys. **11**, 83 (1975)
858. M.J. Seaton, J. Phys. B At. Mol. Phys. **11**, 4067 (1978)
859. M.J. Seaton, Rep. Prog. Phys. **46**, 167 (1983)
860. M.J. Seaton, J. Phys. B At. Mol. Phys. **18**, 2111 (1985)
861. M.J. Seaton, J. Phys. B At. Mol. Phys. **20**, 6363 (1987)
862. M.J. Seaton, Comput. Phys. Commun. **146**, 225, 250, 254 (2002)
863. M.J. Seaton, Mon. Not. R. Astron. Soc. **362**, L1 (2005)
864. M.J. Seaton, P.J. Storey, in *Atomic Processes and Applications*, ed. by P.G. Burke, B.L. Moiseiwitsch (North-Holland Publishing Co., Amsterdam, New York, NY, Oxford, 1976), p. 133
865. M.J. Seaton, N.R. Badnell, Mon. Not. R. Astron. Soc. **354**, 457 (2004)
866. M.J. Seaton, Y. Yan, D. Mihalas, A.K. Pradhan, Mon. Not. R. Astron. Soc. **266**, 805 (1994)
867. I. Seipp, K.T. Taylor, J. Phys. B At. Mol. Opt. Phys. **27**, 2785 (1994)
868. I. Seipp, K.T. Taylor, W. Schweizer, J. Phys. B At. Mol. Opt. Phys. **29**, 1 (1996)
869. M.B. Shah, D.S. Elliott, H.B. Gilbody, J. Phys. B At. Mol. Phys. **20**, 3501 (1987)
870. J. Shapiro, Comput. Phys. Commun. **1**, 207 (1969)
871. N. Sherman, Phys. Rev. **103**, 1601 (1956)
872. I. Shimamura, J. Phys. B At. Mol. Phys. **10**, 2597 (1977)
873. I. Shimamura, J.F. McCann, A. Igarashi, J. Phys. B At. Mol. Opt. Phys. **39**, 1847 (2006)
874. J.H. Shirley, Phys. Rev. B **138**, 979 (1965)
875. T.W. Shyn, C.J. Sweeney, Phys. Rev. A **48**, 1214 (1993)
876. A.J.F. Siegert, Phys. Rev. **56**, 750 (1939)
877. B. Simon, Phys. Lett. **71A**, 211 (1979)
878. H.A. Slim, A.T. Stelbovics, J. Phys. B At. Mol. Phys. **20**, L211 (1987)
879. H.A. Slim, A.T. Stelbovics, J. Phys. B At. Mol. Opt. Phys. **21**, 1519 (1988)
880. I.H. Sloan, Proc. R. Soc. A **281**, 151 (1964)
881. F.T. Smith, Phys. Rev. **118**, 349 (1960)
882. F.T. Smith, Phys. Rev. **120**, 1058 (1960)
883. F.T. Smith, J. Math. Phys. **3**, 735 (1962)
884. D. Spence, Phys. Rev. A **11**, 1539 (1975)
885. E.B. Stechel, R.B. Walker, J.C. Light, J. Chem. Phys. **69**, 3518 (1978)
886. M. Stepanović, M. Minić, D. Cvejanović, J. Jureta, J. Kurepa, S. Cvejanović, O. Zatsarinny, K. Bartschat, J. Phys. B At. Mol. Opt. Phys. **39**, 1547 (2006)

887. J.A. Stephans, C.H. Greene, J. Chem. Phys. **103**, 5470 (1995)
888. G.D. Stevens, C.-H. Iu, T. Bergeman, H.J. Metcalf, I. Seipp, K.T. Taylor, D. Delande, Phys. Rev. A **53**, 1349 (1996)
889. D.T. Stibbe, J. Tennyson, J. Phys. B At. Mol. Opt. Phys. **29**, 4267 (1996)
890. H.C. Stier, Zeits. f. Phys. **76**, 439 (1932)
891. D. Strickland, G. Mourou, Opt. Commun. **56**, 219 (1985)
892. E.C.G. Stückelberg, Helv. Phys. Acta. **5**, 369 (1932)
893. O. Sueoka, A. Hamada, J. Phys. Soc. Jpn. **62**, 2669 (1993)
894. S. Sugano, Y. Tanabe, H. Kamimura, *Multiplets of Transition-Metal Ions in Crystals* (Academic Press, New York, NY, 1970)
895. H.P. Summers, Adv. At. Mol. Opt. Phys. **33**, 275 (1994)
896. A.G. Sunderland, C.J. Noble, V.M. Burke, P.G. Burke, Comput. Phys. Commun. **145**, 311 (2002)
897. C.M. Surko, F.A. Gianturco (eds.), *New Directions in Antimatter Chemistry and Physics* (Kluwer, Dordrecht, 2001)
898. C.M. Surko, G.F. Gribakin, S.J. Buckman, J. Phys. B At. Mol. Opt. Phys. **38**, R57 (2005)
899. P. Swan, Proc. R. Soc. A **228**, 10 (1954)
900. G. Szegö, *Orthogonal Polynomials* (Am. Math. Soc., Providence, RI, 1967)
901. Cz. Szmytkowski, K. Maciag, G. Karwasz, Chem. Phys. Lett. **107**, 481 (1984)
902. Cz. Szmytkowski, K. Maciag, G. Karwasz, D. Filipović, J. Phys. B At. Mol. Opt. Phys. **22**, 525 (1989)
903. R. Szmytkowski, Phys. Rev. A **57**, 4351 (1998)
904. R. Szmytkowski, J. Math. Phys. **39**, 5231 (1998)
905. R. Szmytkowski, Phys. Rev. A **63**, 062704 (2001)
906. R. Szmytkowski, J. Math. Phys. **42**, 4606 (2001)
907. R. Szmytkowski, J. Hinze, J. Phys. B At. Mol. Opt. Phys. **29**, 761 (1996); Erratum, J. Phys. B At. Mol. Opt. Phys. **29**, 3800
908. R. Szmytkowski, J. Hinze, J. Phys. A Math. Gen. **29**, 6125 (1996)
909. I.G. Tamm, Sh. Eksper. i. Teor. Fiz. **14**, 21 (1944)
910. I.G. Tamm, Sh. Eksper. i. Teor. Fiz. **18**, 337 (1948)
911. I.G. Tamm, Sh. Eksper. i. Teor. Fiz. **19**, 74 (1949)
912. H. Tamura, T. Ando, Phys. Rev. B **44**, 1992 (1991)
913. G. Temple, Proc. R. Soc. A **121**, 673 (1928)
914. J. Tennyson, J. Phys. B At. Mol. Phys. **19**, 4255 (1986)
915. J. Tennyson, J. Phys. B At. Mol. Opt. Phys. **29**, 1817 (1996)
916. J. Tennyson, J. Phys. B At. Mol. Opt. Phys. **37**, 1061 (2004)
917. J. Tennyson, Phys. Rep. **491**, 29 (2010)
918. J. Tennyson, C.J. Noble, Comput. Phys. Commun. **33**, 421 (1984)
919. J. Tennyson, L.A. Morgan, J. Phys. B At. Mol. Phys. **20**, L641 (1987)
920. J. Tennyson, L.A. Morgan, Philos. Trans. R. Soc. A **357**, 1161 (1999)
921. J. Tennyson, C.J. Noble, S. Salvini, J. Phys. B At. Mol. Phys. **17**, 905 (1984)
922. J. Tennyson, P.G. Burke, K.A. Berrington, Comput. Phys. Commun. **47**, 207 (1987)
923. M. Terao, P.G. Burke, J. Phys. B At. Mol. Opt. Phys. **23**, 1815 (1990)
924. M. Terao-Dunseath, K.M. Dunseath, J. Phys. B At. Mol. Opt. Phys. **35**, 125 (2002)
925. M. Terao-Dunseath, K.M. Dunseath, D. Charlo, A. Hibbert, R.J. Allan, J. Phys. B At. Mol. Opt. Phys. **34**, L263 (2001)
926. U. Thumm, D.W. Norcross, Phys. Rev. A **45**, 6349 (1992)
927. U. Thumm, D.W. Norcross, Phys. Rev. A **47**, 305 (1993)
928. M. Tinkham, *Group Theory and Quantum Mechanics* (McGraw-Hill Book Company, New York, NY, and London, 1964)
929. M.D. Towler, N.L. Allan, N.M. Harrison, V.R. Saunders, W.C. Mackrodt, E. Aprà, Phys. Rev. B **50**, 5041 (1994)
930. H.W. van der Hart, J. Phys. B At. Mol. Opt. Phys. **30**, 453 (1997)

931. H.W. van der Hart, J. Phys. B At. Mol. Opt. Phys. **34**, L147 (2001)
932. H.W. van der Hart, Phys. Rev. Lett. **95**, 153001 (2005)
933. H.W. van der Hart, Phys. Rev. A **73**, 023417 (2006)
934. H.W. van der Hart, K. Burnett, Phys. Rev. A **62**, 013407 (2000)
935. H.W. van der Hart, L. Feng, J. Phys. B At. Mol. Opt. Phys. **34**, L601 (2001)
936. H.W. van der Hart, B.J.S. Doherty, J.S. Parker, K.T. Taylor, J. Phys. B At. Mol. Opt. Phys. **38**, L207 (2005)
937. H.W. van der Hart, M.A. Lysaght, P.G. Burke, Phys. Rev. A **76**, 043405 (2007)
938. H.W. van der Hart, M.A. Lysaght, P.G. Burke, Phys. Rev. A **77**, 065401 (2008)
939. E.G. Vincke, L. Malegat, D. Baye, J. Phys. B At. Mol. Opt. Phys. **26**, 811 (1993)
940. I. Vinkalns, M. Gailitis, *Abstracts 5th International Conference on the Physics of Electronic and Atomic Collisions* (Nauka, Leningrad, 1967), p. 648
941. Vo Ky Lan, M. Le Dourneuf, P.G. Burke, J. Phys. B At. Mol. Phys. **9**, 1065 (1976)
942. B. Wallbank, J.K. Holmes, Phys. Rev. A **48**, R2515 (1993)
943. B. Wallbank, J.K. Holmes, J. Phys. B At. Mol. Opt. Phys. **27**, 1221 (1994)
944. B. Wallbank, J.K. Holmes, J. Phys. B At. Mol. Opt. Phys. **27**, 5405 (1994)
945. B. Wallbank, J.K. Holmes, A. Weingartshofer, J. Phys. B At. Mol. Opt. Phys. **23**, 2997 (1990)
946. B. Wallbank, N. Djurić, O. Woitke, S. Zhou, G.H. Dunn, A.C.H. Smith, M.E. Bannister, Phys. Rev. A **56**, 3714 (1997)
947. B. Wallbank, J.K. Holmes, L. LeBranc, A. Weingartshofer, Zeits. Phys. D **10**, 467 (1998)
948. H.R.J. Walters, Phys. Rep. **116**, 1 (1984)
949. H.R.J. Walters, in *New Directions in Atomic Physics*, ed. by C.T. Whelan, R.M. Dreizler, J.H. Macek, H.R.J. Walters (Kluwer Academic/Plenum Publishers, New York, NY, Boston, MA, Dordrecht, London, Moscow, 1999), p. 105
950. H.R.J. Walters, J.E. Blackwood, in *New Directions in Antimatter Chemistry and Physics*, ed. by C.M. Surko, F.A. Gianturco (Kluwer, Dordrecht, 2001), p. 173
951. H.R.J. Walters, A.A. Kernoghan, M.T. McAlinden, C.P. Campbell, in *Photon and Electron Collisions with Atoms and Molecules*, ed. by P.G. Burke, C.J. Joachain (Plenum, New York, NY, 1997), p. 313
952. H.R.J. Walters, A.C.H. Yu, S. Sahoo, S. Gilmore, Nucl. Instrum. Methods B **221**, 149 (2004)
953. H.R.J. Walters, S. Sahoo, S. Gilmore, Nucl. Instrum. Methods B **233**, 78 (2005)
954. G.H. Wannier, Phys. Rev. **90**, 817 (1953)
955. G.H. Wannier, Phys. Rev. **100**, 1180 (1955)
956. G.N. Watson, *A Treatise on the Theory of Bessel Functions*, 2nd edn. (Cambridge University Press, Cambridge, UK, 1944)
957. R.P. Wayn, *Chemistry of Atmospheres*, 2nd edn. (Oxford Science Publications, Oxford, 1991)
958. V. Weisskopf, E. Wigner, Zeits. f. Phys. **63**, 54 (1930)
959. V. Weisskopf, E. Wigner, Zeits. f. Phys. **65**, 18 (1930)
960. J.A. Wheeler, Phys. Rev. **52**, 1083 (1937)
961. J.A. Wheeler, Phys. Rev. **52**, 1107 (1937)
962. J.A. Wheeler, Ann. N.Y. Acad. Sci. **48**, 219 (1946)
963. A.D. Whiteford, N.R. Badnell, C.P. Ballance, M.G. O'Mullane, H.P. Summers, A.L. Thomas, J. Phys. B At. Mol. Opt. Phys. **34**, 3179 (2001)
964. E.T. Whittaker, G.N. Watson, *A Course of Modern Analysis*, 4th edn. (Cambridge University Press, Cambridge, UK, 1927)
965. E.P. Wigner, *Gruppentheorie und ihre Anwendung auf die Quantenmeckanik der Atomspectren* (Friedrich Vieweg und Sohn, Braunschweig, 1931) Revised and translated edition by J.J. Griffin (Academic Press, New York, NY and London, 1959)
966. E.P. Wigner, Göttingen Nachr. **31**, 546 (1932)
967. E.P. Wigner, Unpublished 1940 manuscript reproduced in *Quantum Theory of Angular Momentum*, ed. by L.C. Biedenharn, H. van Dam (Academic Press, New York, NY and London, 1965), p. 87

968. E.P. Wigner, Phys. Rev. **70**, 15 (1946)
969. E.P. Wigner, Phys. Rev. **70**, 606 (1946)
970. E.P. Wigner, Phys. Rev. **73**, 1002 (1948)
971. E.P. Wigner, Phys. Rev. **98**, 145 (1955)
972. E.P. Wigner, L. Eisenbud, Phys. Rev. **72**, 29 (1947)
973. W.J. Wijesundra, I.P. Grant, P.H. Norrington, F.A. Parpia, J. Phys. B At. Mol. Opt. Phys. **24**, 1017 (1991)
974. W.J. Wijesundra, F.A. Parpia, I.P. Grant, P.H. Norrington, J. Phys. B At. Mol. Opt. Phys. **24**, 1803 (1991)
975. W.J. Wijesundra, I.P. Grant, P.H. Norrington, in *Many-Body Atomic Physics*, ed. by J.J. Boyle, M.S. Pindzola (Cambridge University Press, Cambridge, UK, 1998), p. 325
976. J.H. Wilkinson, *The Algebraic Eigenvalue Problem* (Clarendon Press, Oxford, 1965)
977. J.F. Williams, J. Phys. B At. Mol. Phys. **7**, L56 (1974)
978. J.F. Williams, J. Phys. B At. Mol. Phys. **8**, 1683 (1975)
979. J.F. Williams, J. Phys. B At. Mol. Phys. **8**, 2191 (1975)
980. J.F. Williams, J. Phys. B At. Mol. Opt. Phys. **21**, 2107 (1988)
981. J.R. Winick, W.P. Reinhardt, Phys. Rev. A **18**, 910 (1978)
982. J.R. Winick, W.P. Reinhardt, Phys. Rev. A **18**, 925 (1978)
983. C.N. Yang, Phys. Rev. **74**, 764 (1948)
984. F.L. Yost, J. Wheeler, G. Breit, Phys. Rev. **49**, 174 (1936)
985. I.G. Young, P.H. Norrington, Comput. Phys. Commun. **83**, 215 (1994)
986. S.M. Younger, J. Quant. Spectrosc. Radiat. Transf. **26**, 329 (1981)
987. Yu Yan, M.J. Seaton, J. Phys. B At. Mol. Phys. **18**, 2577 (1985)
988. N. Zafar, G. Laricchia, M. Charlton, T.C. Griffith, J. Phys. B At. Mol. Opt. Phys. **24**, 4661 (1991)
989. N. Zafar, G. Laricchia, M. Charlton, Hyperfine Interact. **89**, 243 (1994)
990. N. Zafar, G. Laricchia, M. Charlton, A. Garner, Phys. Rev. Lett. **76**, 1595 (1996)
991. O. Zatsarinny, Comput. Phys. Commun. **98**, 235 (1996)
992. O. Zatsarinny, Comput. Phys. Commun. **174**, 273 (2006)
993. O. Zatsarinny, C. Froese Fischer, Comput. Phys. Commun. **124**, 247 (2000)
994. O. Zatsarinny, C. Froese Fischer, J. Phys. B At. Mol. Opt. Phys. **33**, 313 (2000)
995. O. Zatsarinny, S.S. Tayal, J. Phys. B At. Mol. Opt. Phys. **34**, 1299 (2001)
996. O. Zatsarinny, S.S. Tayal, J. Phys. B At. Mol. Opt. Phys. **34**, 3383 (2001)
997. O. Zatsarinny, S.S. Tayal, J. Phys. B At. Mol. Opt. Phys. **35**, 2493 (2002)
998. O. Zatsarinny, K. Bartschat, J. Phys. B At. Mol. Opt. Phys. **37**, 2173 (2004)
999. O. Zatsarinny, K. Bartschat, J. Phys. B At. Mol. Opt. Phys. **37**, 4693 (2004)
1000. O. Zatsarinny, K. Bartschat, Phys. Rev. A **71**, 022716 (2005)
1001. O. Zatsarinny, K. Bartschat, Phys. Rev. A **72**, 020702 (2005)
1002. O. Zatsarinny, T.W. Gorczyca, C. Froese Fischer, J. Phys. B At. Mol. Opt. Phys. **35**, 4161 (2002)
1003. O. Zatsarinny, K. Bartschat, S.S. Tayal, J. Phys. B At. Mol. Opt. Phys. **39**, 1237 (2006)
1004. A. Zecca, D. Sanyal, M. Chakrabarti, M.J. Brunger, J. Phys. B At. Mol. Opt. Phys. **39**, 1597 (2006)
1005. A. Zecca, C. Perazzolli, N. Moser, D. Sanyal, M. Chakrabarti, M.J. Brunger, Phys. Rev. A **74**, 012707 (2006)
1006. H.L. Zhang, A.K. Pradhan, J. Phys. B At. Mol. Opt. Phys. **28**, L285 (1995)
1007. H.L. Zhang, A.K. Pradhan, Astron. Astrophys. **293**, 953 (1995)
1008. H.L. Zhang, S.N. Nahar, A.K. Pradhan, J. Phys. B At. Mol. Opt. Phys. **32**, 1459 (1999)
1009. H.L. Zhang, S.N. Nahar, A.K. Pradhan, Phys. Rev. A **64**, 032719 (2001)
1010. S. Zhou, H. Li, W.E. Kauppila, C.K. Kwan, T.S. Stein, Phys. Rev. A **55**, 361 (1997)

Index

T

Springer Series on

ATOMIC, OPTICAL, AND PLASMA PHYSICS